

Государственное образовательное учреждение
высшего профессионального образования
**«Томский государственный университет
систем управления и радиоэлектроники»**

ТЕМАТИЧЕСКИЙ РЕФЕРАТИВНЫЙ СБОРНИК № 4-2/2

**“Radar Remote Sensing”
(«Дистанционное зондирование в радиолокации»)**

Публикации в трудах конференций

Источник: *Digital Library IEEEExplore*

Язык: *английский*

Глубина поиска: *2007 – 2008 гг.*

Дата формирования: *март 2011 г.*

Составитель: *В.И. Карнышев*

Томск – 2011

ТЕМАТИЧЕСКИЙ РЕФЕРАТИВНЫЙ СБОРНИК № 4-2/2

"Radar Remote Sensing"

(«Дистанционное зондирование в радиолокации»)

Публикации в трудах конференций

"SAR Image Filtering Via Learned Dictionaries and Sparse Representations"

In the last decade there has been a growing interest in the study of sparse representation of signals. In particular, many new multiscale image representations in a geometric space have been proposed (Curvelets, Ridgelets, Contourlets, etc.). Instead of using a fixed transformation, an alternative approach is to build a sparse dictionary from the signal itself. In the present work, we propose a novel approach for speckle noise reduction in SAR images using a sparse and redundant representation over trained dictionaries. In this approach, an adaptive dictionary composed of image patches (called atoms) is learned from the image so that it constitutes a sparse representation of the image content. This learning process, called K-SVD, is efficiently performed using an Orthogonal Matching Pursuit (OMP) and a Singular Value Decomposition (SVD). This new approach is effective in removing white additive Gaussian noise despite the fact that elements of the dictionary are learned from the noisy image, the algorithm is converging toward meaningful atoms that are already showing a reduction in noise level. [C1664]

"Statistical Similarity Measure for Oil Slick Detection in SAR Image"

Spaceborne Synthetic Aperture Radar (SAR) is well adapted to detect ocean pollution independently from daily or weather condition. As it is sensitive to surface roughness, the presence of oil film on the sea surface decreases the backscattering of the sea surface resulting in a dark feature patches in SAR images. In fact, oil slicks have specific impact on ocean wave spectra. Initial wave spectra may be characterized by three kinds of waves, big, medium and small, which correspond physically to gravity and gravity-capillary waves. The increase of viscosity due to the presence of oil damps gravity-capillary waves. This induces a damping of the backscattering to the sensor, but also a damping of the energy of the wave spectra, then it modifies the sea surface roughness observed by the sensor. Thus, local detection of wave spectra modification may be achieved by a appropriated texture analysis of the original SAR image. In this paper, the texture analysis is based on measure of similarity between a local probability density function (pdf) of clean water and the local pdf of the zone to be inspected. The local distribution is estimated in the neighbourhood of each pixel, through a sliding window, and compared to the reference one by using the Kullback-Leibler (KL) distance between distributions. An efficient strategy has been adopted in order to perform pdf estimation through a non-parametric approach. [C1665]

"Comparison of Three Unsupervised Segmentation Algorithms for SAR Data in Urban Areas"

This paper presents a preliminary comparison of mean shift segmentation, efficient graph-based segmentation and normalized cuts for segmenting meter-resolution SAR data in urban areas. The small patches generated by these bottom-up segmentation algorithms provide spatial support for object detection. We evaluate their performances on ground truth data by varying their parameters. In order to obtain better spatial support, we apply multiple segmentations to a single segmentation of each algorithm. The multiple segmentations are representative samplings of the entire segmentation space. The experimental results demonstrate that the three algorithms are promising for SAR image segmentation, and that the multiple segmentations improves the abilities of providing spatial support. [C1666]

"Change Detection for Traffic Monitoring in Terrasar-X Imagery"

In this paper the changes occurring in two images acquired at two different time moments are analyzed. In particular the interest is in the changes of filling grade of car-parks or even detecting stopped vehicles on the congested or jammed roads. As input to the change detection processor can serve two repeat-pass single channel images acquired by any airborne or space borne SAR satellite sensor. Each channel is focused, calibrated and processed to a single look slant range complex SAR image. The proposed change detection approach is based on the combination of various techniques: co-registration of two SAR images by interferometric SAR processor, removal of the flat Earth phase, channel balancing, calculating of a coherent or

incoherent difference of two images and finally image post-processing and analysis. First experiments on TerraSAR-X imagery show promising results. [C1667]

"Extending Airborne SAR-ATI Algorithms to the RADARSAT-2 Moving Object Detection Experiment (MODEX)"

SAR-ATI algorithms, which have been developed and validated for airborne SAR data, are now being extended to the RADARSAT-2 Moving Object Detection Experiment (MODEX). Starting from a unified geometry model, specific airborne and spaceborne SAR-ATI features are discussed. Some of the very first MODEX results are presented. [C1668]

"SAR Image Despeckling in the Undecimated Contourlet Domain: A Comparison of Lmmse and Map Approaches"

In this paper, we propose an extension of two despeckling algorithms, proposed to denoise SAR images and based on the undecimated separable wavelet transform, to work with the nonsubsampling contourlet transform (NSCT). The NSCT is a powerful and versatile nonseparable transform that allows a multiresolution and directional representation to be achieved. The SAR signal is modeled as affected by a multiplicative noise. The noise-free NSCT coefficients are estimated from the observed ones according to either the maximum-a-posteriori (MAP) or the linear minimum mean square error (LMMSE) criterion. The results show that the proposed de-speckling algorithms highly benefit from the fact of working into a multiresolution and multidirectional domain. [C1669]

"Target Detection in Multiple-Viewing Through-the-Wall Radar Imaging"

We present a constant-false alarm rate detection scheme for use in Through-the-Wall Radar Imaging. We consider multiple-viewing scenarios with an arbitrary number of vantage points. Classical detection theory is used to fuse the obtained radar images to one reference image. By doing so, clutter and noise artifacts which are strongly represented in the individual images are reduced and targets of interest are more clearly visible. [C1670]

"Statistical Analysis of the Electromagnetic Field Scattered by the Ocean Surface in Various Weather Conditions: A Numerical Study in L-Band"

In this paper, we present a simulation of the radar cross section (backscattering configuration) for different wind speed conditions. More precisely, we highlight the fact that the numerical estimation using a Monte Carlo and a Method of Moment can provide more statistical information than asymptotic approaches. And we show that a statistical contrast criterion (for instance the T-value) can quantify the observability of the sea surface roughness (different weather conditions). Finally, we explain how to optimize this observability when two polarizations are measured using a linear discriminant analysis. [C1671]

"Validation of QSCAT-1 Geophysical Model Function Using Seawinds Level 2 and Buoy Data"

Geophysical model function (GMF) is the basis and prerequisite for the ocean surface wind vector retrieval with scatterometers. Among many operational models, the Qscat-1 model was specifically developed for SeaWinds scatterometer and is being applied to its operational wind retrieval. This paper is to validate the accuracy of the Qscat-1 model by using some SeaWinds Level 2 data and corresponding buoy data. First, a comparison between L2B and co-located buoy wind speed was made to analyze the systematic bias between them, and then a new geophysical model function was established using the match-ups of the L2A and buoy data to further evaluate the accuracy of the Qscat-1 model. The analytical and modeling results indicate that there may be some systematic error in the Qscat-1 model. [C1672]

"A Spaceborne Radar for Directional Wave Spectrum Estimation: First Performance Simulations"

SWIM is a Ku-band radar designed for wave directional spectrum estimation. This radar operates at six incidence angles (0deg to 10deg) with complete azimuth scanning. This paper presents the simulation tool developed for defining SWIM design and evaluating SWIM performance. The simulation tool is an end-to-end simulator, i.e. from the sea surface to the estimated wave spectrum. Some simulations are discussed, showing that the preliminary design of SWIM will fulfill the scientific requirements. [C1673]

"SeaWinds Hurricane Wind Retrievals and Comparisons with H* Wind Surface Winds Analyses"

This paper describes recent developments of an improved geophysical ocean wind vector retrieval algorithm that

uses both active and passive measurements from QuikSCAT. This algorithm results in significant improvements in wind vector measurements in hurricanes and better rain-flagging of severely rain contaminated areas than does NASA's standard wind vector product (L2B). By using a combined active/passive approach, we are able to infer wind estimates in the presence of light to moderate rain using the SeaWinds scatterometer. Rain effects (attenuation and volume scattering) are determined passively and then used to correct the measured ocean sigma-0 at 12.5 km wind vector cell resolution. Wind retrievals are performed using an improved geophysical model function (GMF) tuned for extreme wind events. These ocean vector wind retrievals, known as Q-Winds, are compared with surface winds products from the NOAA Hurricane Research Division's H*Wind Analysis System, which assimilates near-simultaneous measurements from in-situ and remote sensors, such as, the Stepped Frequency Microwave Radiometer (SFMR), GPS dropsondes, and flight-level inertial navigation winds. Comparisons to H*Wind are presented for Q-Winds and the SeaWinds Project's new L2B-12.5 km ocean vector winds products. [C1674]

"Radar Monitoring of Wetland Hydrology: Dynamic Information for the Assessment of Ecosystem Services"

Synthetic aperture radar (SAR) data can improve the ability to map and monitor forested wetlands. Forested wetland maps were developed using multiple incidence angle ENVISAT ASAR (C-HH) for the Tuckahoe River Watershed, Maryland. These maps were compared with U.S. Fish and Wildlife Service National Wetlands Inventory (NWI) and Natural Resources Conservation Service (NRCS) Soil Survey Geographic Database (SSURGO) maps. Radar derived wetland maps and NWI maps showed a high level of agreement (88%). The radar derived wetland maps and SSURGO demonstrated a lower level of agreement (54%), primarily due to a greater estimate of hydric soils by SSURGO than forested wetlands by the SAR derived maps. [C1675]

"Performance Assessment of GNSS-R Space Based Scatterometry by Means of Delay-Doppler Map"

This paper presents a preliminary analysis of the performance of space based GNSS-R scatterometry. In particular, this paper focuses on the characterisation of the processed delay-Doppler Map (DDM) with respect to the sea surface state as well as to the antenna pattern. The analyses are conducted on simulated waveforms; therefore characterization of models for sea state and scattering description and related assumptions adopted for the simulations are carefully addressed and described. All the analyses have been performed considering the currently broadcasted L1-band GPS C/A code signal. [C1676]

"System design and performance simulation of a spaceborne Ku-band rotation fan-beam scatterometer"

A spaceborne Ku-band rotation fan-beam scatterometer (RFSCAT) for sea surface wind field measurement is introduced. The system will be operated in Ku-band frequency so that the dimension of its antenna can be shortened enough for a small satellite platform. Then a simulation method is adopted to analyze the performance of this system. The results show that the proposed scatterometer has a good performance in wind retrieval. [C1677]

"Monitoring Inundation Dynamics in ParanГrBŸ River, Argentina, by C and L Band SAR"

This paper analyses the SAR response of wetland ecosystems under different environmental conditions and at two different frequencies. We exploited the opportunity of observing the same inundation phenomena by two currently available SAR systems, such as ENVISAT ASAR (C band) and ALOS PALSAR (L band). The results obtained for C band are similar to the ones reported previously in the same area. Increasing water level in marshes is characterized by an increase and then a decrease in the backscattering coefficient of vegetation. An increase when water level changes the soil from saturated to flooded condition and a decrease when the water covers the vegetation. The new ALOS PALSAR L band results shows that in marshes, the increase in water level is seen as a decrease in the backscattering coefficient, since the reduction of emerged biomass reduces the available matter for the wave to interact with. [C1678]

"A New Cross-Calibrated, Multi-Satellite Ocean Surface Wind Product"

A new set of cross-calibrated, multi-satellite ocean surface wind data sets is introduced. The principal data set covers the global ocean for the period beginning in 1987 with six-hour and 25-km resolution and is produced by combining all ocean surface wind speed observations from SSM/I, AMSR-E, and TMI, and all ocean surface wind vector observations from QuikSCAT and SeaWinds. An enhanced variational analysis method (VAM) performs quality control and combines these data with available conventional ship and buoy data and ECMWF

analyses. The VAM analyses fit the data used very closely. Comparisons with withheld WindSat observations are very good. [C1679]

"A Ku-Band Active/Passive Wind Vector Retrieval Over the Ocean"

This work investigates the design of an innovative conical scanning Ku-band (13.4 GHz) scatterometer/radiometer for measuring ocean vector winds. The sensor design is based upon actual measurements obtained by the SeaWinds scatterometer and the Advanced Microwave Scanning Radiometer (AMSR), which operated simultaneously on JAXA's Advanced Earth Observing Satellite-II (ADEOS-II) during 2003. This new design combines the conventional forward and aft-looking two-beam microwave scatterometer (SeaWinds) measurements with simultaneous linearly polarized passive microwave brightness temperatures. The unique aspect of this remote sensing technique is that it operates at a single microwave frequency, and it combines vertical and horizontal polarized microwave brightness temperatures with the scatterometer normalized cross sections to retrieve unambiguous ocean wind vectors. This technique has the potential to significantly improve the Ocean Vector Winds retrievals for future conical-scanning microwave scatterometers. [C1680]

"The European GMES Sentinel-1 Radar Mission"

The ESA Sentinels constitute the first series of operational satellites responding to the Earth observation needs of the EU-ESA Global Monitoring for Environment and Security (GMES) programme. The GMES space component relies on existing and planned space assets as well as on new complementary developments by ESA. This paper describes the Sentinel-1 mission, an imaging synthetic aperture radar (SAR) satellite constellation at C-band. It provides an overview of the mission requirements, its applications and the preliminary technical concept for the system. [C1681]

"Electromagnetic Modelling for Information Extraction from High Resolution SAR Images of Urban Areas"

Analysis, interpretation and feature extraction concerning High Resolution (HR) Synthetic Aperture Radar (SAR) images of urban areas urgently require support of sound and appropriate electromagnetic modelling. The modelling takes into consideration the radar geometry and the (geometric and electromagnetic) scene parameters but also the novelty brought by high resolution. In this paper, this way of developing suitable electromagnetic modelling for HR SAR images of urban areas is shown to be successful as able to interpret and retrieve, from these scenarios, new and interesting details that will certainly represent the main actor of next generation of applications for urban areas with SAR sensors. [C1682]

"Automated Information Extraction from TerraSAR-X Data: The Content Map"

While typical remote sensing imaging instruments produce more and more data, what we miss today are reliable tools for automated information extraction from these images. In the following, we propose a so-called Content Map, a novel Earth Observation value adding product. Basically, it comprises several class files and a viewer showing the different classes of land use and objects contained in the corresponding image data. In order to avoid processing delays, the class files have to be generated in an unsupervised mode as a real time product; thus, interactive user interactions have to be limited to training and testing intervals. As typical examples we use image data of the German TerraSAR-X mission that produces SAR image data in a variety of different modes. [C1683]

"Optimized Multilooking for Robust SAR Image Indexing"

Compared to conventional optical images, the classification of remote sensing SAR images represents a rather difficult task. As a rule, the various SAR imaging and product options, the high dynamic range of SAR images, and the presence of speckle noise prevent us from obtaining robust classification results. In the following, we try to circumvent these difficulties by proper pre-processing and despeckling of high resolution SAR images. Our approach aims at adapting the radiometry and the resolution of the scenes to the optimal target recognition capabilities of a classification algorithm. To this end, we have to apply systematic adaptations that provide optimized multilooking of our input data. Then these adapted data can be fed into a scene classification system. [C1684]

"Stepped-Frequency Radar System in Gating Mode: An Experiment as a New Helicopter-Borne GPR System for Geological Applications"

Ground-penetrating radar (GPR) has become a useful tool in solving different geophysical tasks in environmental geology, glaciology, archaeology, mineral exploration and the detection of near-surface objects. The large variety

of handheld GPR devices, even for harsh field conditions, is an effective tool for surveying small areas. A GPR system installed in a helicopter is an effective method to survey large areas with high data density. Large areas, even in inaccessible regions, may be surveyed within a short time and even under limited logistic demands. The high agility of a helicopter allows increasing the data density in areas of special interest. Using ground penetration radar for geological applications, fine resolution of near-surface structures is necessary. Stepped-frequency radar technology offers an attractive alternative to the classical pulse radar systems with operational advantages for airborne applications such as, for instance, reduced interference with other on-board systems.

[C1685]

"Moving Target Relative Speed Estimation in the Presence of Strong Stationary Surrounding Using a Single Antenna UWB SAR System"

This paper investigates how relative speed estimation of moving targets in synthetic aperture radar (SAR) images is affected by strong stationary surrounding clutter. The result extends previous work by estimating moving target relative speed under the influence of clutter and Gaussian noise. The results obtained show that good estimates can be obtained even in situations with relatively high clutter and noise, i.e. SNR and SCR lower than 10 dB.

[C1686]

"Moving Target Detection by Focusing for Frequency Domain Algorithms in UWB Low Frequency SAR"

Moving target detection at low radar frequencies is associated with long integration time and has to handle azimuth focusing for reliable detection. The detection by focusing in which time-domain is the basis for the focusing approach has been proposed and successfully experimented in reality. The main objective of this paper is to apply and evaluate the detection method for frequency-domain algorithms. Range Migration Algorithm (RM) is chosen as a candidate for this study due to the accuracy of the algorithm with very wide integration angles. The simulated SAR data, which is used in this study, is based on the parameters of a airborne UWB low frequency system such as CARABASII. [C1687]

"Texture Feature Selection for Buried Mine Detection in Airborne Multispectral Imagery"

In this paper, a methodology for the detection of buried mines in airborne multispectral imagery is explored. The approach is based on utilizing the color texture information in the buried mine signatures, which is extracted using the cross-co-occurrence texture features. A systematic two-stage approach, using Bhattacharya coefficient-based analysis and principal feature analysis, is developed for the selection of a small subset of discriminatory features. Detection results from actual airborne data from two different sites are presented. The performances are compiled for four different feature-based detectors, and are compared with the conventional multiband RX anomaly detector, to validate the feature selection approach and demonstrate buried mine detection performance based on texture features. [C1688]

"High-Resolution ASCAT Scatterometer Winds Near the Coast"

The Advanced Scatterometer, ASCAT, on MetOp-A was launched on 19 October 2006 as the third wind scatterometer currently in space joining up with the ERS-2 and the SeaWinds scatterometers. Scatterometers measure the radar backscatter from wind-generated cm-size gravity-capillary waves and provide high-resolution wind vector fields over the sea with high quality. In this paper we show progress in high resolution processing and its verification and in processing closer to the coast. [C1689]

"Validation of NOAA's Near Real-Time Ascat Ocean Vector Winds"

The ASCAT, launched on board MetOp-A satellite on October 19th 2006, is a C-band scatterometer operating at 5.255 GHz using fan-beam antennae to measure near surface vector wind over the world's ocean. NOAA produces near-real-time ASCAT wind product at 50 and 25 km resolutions. These wind data are validated against global wind field model and satellite observation from QuikSCAT. The results show ASCAT wind speed retrievals perform well for low to moderate wind speed under most weather conditions, but are underestimated for wind speeds ≥ 15 m/s. The standard deviation wind direction errors are well below 20 degrees for wind speed ≥ 5 m/s. [C1690]

"Global Observations of Precipitation Using Satellite Passive Millimeter-Wave Sensors"

This paper reviews main results from recently published papers and recent research being presented at IGARSS 2008. This work starts with developing and validating a global model, MM5/TBSCAT/F(Г,В), that simulates ground-truth and predicts millimeter-wave radiances consistent with those coincidentally observed by AMSU

aboard NOAA satellites. Sensitivity studies of the assumptions in the model further encourage its use as ground truth for development of global millimeter-wave precipitation retrieval methods. MM5/TBSCAT/F(Г,В) was then used to (1) study appropriate specifications for geostationary microwave sounders and their retrieval accuracies, (2) evaluate the ability of ATMS to retrieve precipitation, and (3) develop a series of precipitation retrieval algorithms, AMSU/MM5, where the latest version is able to estimate surface precipitation rates over snow-covered land and sea ice consistent with CLOUDSAT observed radar reflectivity profiles, provided that the atmosphere is not too cold to permit retrievals. [C1691]

"All Data are Useful, but not All Data are Used! What'S Going on Here?"

Issues limiting the use of modern data streams are described and possible approaches are outlined. Data assimilation system constraints and limitations are listed; a taxonomy of the various errors involved is given; and the difficulty of showing positive impacts for new or currently unused data is discussed. Improvements may come from creative, parsimonious representations of the principal errors; adaptively selecting or pre-processing the data; and questioning the basic assumptions made in current operational data assimilation systems. Examples given from the perspective of satellite scatterometry and IR retrievals illustrate problems of general interest. [C1692]

"The Orfeus Project (Optimised Radar for Finding Every Utility in the Street)"

The ORFEUS (Optimised Radar for Finding Every Utility in the Street) project addresses the requirement for advanced technologies for locating, maintaining and rehabilitating buried infrastructures and, in particular, it fulfils the requirement for locating buried assets, including the use of trenchless techniques for deploying pipes and cables in an urban environment. The aim of this project is to develop two radars. The first operates on the surface for planning deployment activities; the second (a bore-head GPR) will be installed in the drilling head of horizontal directional drilling (HDD) equipment so that they may avoid collision and possible damage to existing cables and other infrastructure. [C1693]

"GPR Imaging Using Compressed Measurements"

A new data acquisition and imaging method exploiting the sparsity of the target space is presented for ground penetrating radar (GPR) imaging. Sparsity is enforced by solving a convex lscr1 minimization problem which uses a very small number of random measurements. The method can greatly reduce the data acquisition time while producing sparse target space images. Simulation and experimental data results are provided to show that the method has excellent resolution and is robust to noise and random spatial sampling. [C1694]

"A Study on the Characteristics of the Sedimentary Environments by Using SAR Data in the Ganghwa Tidal Flat"

The Ganghwa tidal flat is located on the west coast of Korea. This area is covered by the sand, mud and mixed(sandy / muddy) sediments. The grain-size in the tidal flat is coarser to the seaward and finer to the eastern flat. The objectives of this study are to characterize the sedimentary environments based on the analysis of correlation between SAR data and factors of sedimentation. Therefore, we compared the backscattering coefficients and the coherence of JERS-1, ENVISAT, ERS-2 and ALOS images of SAR data. In the results of our analysis, we found a relationship between the backscattering coefficient and in-situ sediment grain-size. The backscattering coefficients appeared to be high in the region containing more of sand fraction because of the coarser grain-size and rougher surface. The coarse grain-size was more affected by the tide than the fine grain-size since the coarser grain-size has the smaller viscosity. Therefore the coherence is lower in the sand dominant area. [C1695]

"Integration of Spatial Chaotic Model and Type-2 Fuzzy Sets to Coastline Detection in SAR Images"

Coastline detection in SAR images suffers from the presence of speckle effect and the strong signal return from a wind-roughened and/or wave-modulated sea. It has already been recognized that ocean areas in SAR images are almost always much more homogeneous in grey levels than land areas. Therefore, features reflecting the roughness of an image can be very useful for ocean-land separation. To represent its geometric property, an SAR signal is modeled by a spatial chaotic model (SCM) and characterized by its fractal dimension. The differential box-counting (DBC) technique is adopted to estimate fractal dimension in this paper. Observations provided by SAR sensors are uncertain due to changing illumination conditions at different locations. Besides, the selection of window size Mand grid size s in DBC provides an additional degree of uncertainty. Both the uncertainty involved in the measurements and the uncertainty involved in the selection of Mand s motivate us of

integrating type-2 fuzzy sets with the SCM to achieve an appropriate selection of the threshold for ocean-land segmentation. The proposed approach is applied to an SAR image for coastline detection as a demonstration. The final result shows that the coastline detected coincide very well with the true situation when it is overlaid on the original image. Besides, the detected coastline also agrees very well with the terrestrial measurements.

[C1696]

"Comparison of Ship Detectability Using SAR Polarization Data: Envisat ASAR AP Mode"

Preliminary results are reported on ship detection using coherence images computed from cross-correlating images of multi-look-processed dual-polarization data of ENVISAT ASAR. The traditional techniques of ship detection by radars such as CFAR (Constant False Alarm Rate) rely on the amplitude data, and therefore the detection tends to become difficult when the amplitudes of ships images are at similar level as the mean amplitude of surrounding sea clutter. The proposed method utilizes the property that the multi-look images of ships are correlated with each other. Because the inter-look images of sea surface are covered by uncorrelated speckle, cross-correlation of multi-look images yields the different degrees of coherence between the images and water. The polarimetric information of ships, land and intertidal zone are first compared based on the cross-correlation between HH and HV. In the next step, we examine the technique when the dual-polarization data are split into two multi-look images. [C1697]

"Simulation Study on the Optimal Conditions for Shallow Water Bathymetry Observation by SAR"

Based on the analytical expression derived from the high frequency ocean spectrum balance equation but not surface wave action balance equation, continuity equation and the first order Bragg backscattering theory, a simulating model for the shallow water bathymetry SAR relative normalized radar backscattering cross-section has been developed. The relationship between SAR relative normalized radar backscattering cross-section and currents, winds, wave length, incidence angle and the polarization has been simulated and the optimal conditions for shallow water bathymetry by SAR was also analyzed, the conclusion was given in the last section. Valuable help for the study on SAR shallow water bathymetry surveys will be provided from this paper. [C1698]

"SAR Traffic Monitoring Using Time-Frequency Analysis for Detection and Parameter Estimation"

In the paper a ground moving target indication (GMTI) algorithm operating on preprocessed range-compressed SAR data is presented. For preprocessing range cell migration correction for stationary targets in most practical cases is sufficient. Moving target signal detection and extraction, adaptive range cell migration correction, position and across as well as along-track velocity estimation is then performed without a priori knowledge by using matched filter banks and the fractional Fourier transform. The proposed algorithm is able to cope with multi-component linear frequency modulated signals as they arise in real traffic scenarios containing a number of moving road vehicles. [C1699]

"Low Frequency Sea and Ice Sheet Impulse Responses Acquired by the Global Ice Sheet Mapping Orbiter (GISMO) Demonstrator"

A study of sea and ice sheet surface impulse responses measured at 150 MHz is reported. The presence of both coherent and noncoherent returns is observed due to the low frequency of observation, and attempts to interpret the observed wave-forms are presented. Further analysis using a Monte Carlo simulation of one dimensional surface impulse responses suggests that the physical optics theory should be applicable for modeling the observed waveforms so that they can be used in sensing ice sheet surface properties. [C1700]

"Toward an Operational Method for Refined Snow Characterization Using Dual-Polarization C-Band SAR Data"

This paper presents a method to characterize snow cover at a massif scale using dual-polarization C-band SAR data. It is demonstrated that it is crucial to exactly model the distribution of liquid water inside the snowpack in order to perform accurate snow characterization at C-band. Consequently, the key point of this new method consists in using a multi-layer meteorological snow model. Based on a validated multi-layer EM backscattering model, SAR data and snow profiles estimated by the weather model can be combined. An adequate spatial reorganization of these snow profiles leads to a refined snow characterization. Accurate snow monitoring like Liquid Water Content is presented, opening the way for a new operational method. [C1701]

"Seafloor and Land Cover Classification Through Airborne Lidar and Hyperspectral Data Fusion"

In 2007 the Joint Airborne Lidar Bathymetry Technical Center of Expertise (JALBTCX) collected concurrent bathymetric lidar and hyperspectral imagery in Hilo Bay, Hawaii. The data were collected using the Compact

Hydrographic Airborne Rapid Total Survey (CHARTS) system. CHARTS is JALBTCX in-house survey capability that includes a SHOALS-3000 lidar instrument integrated with a CASI-1500 hyperspectral imager. CHARTS collects either 20-kHz topographic lidar data and 3-kHz bathymetric lidar data, each concurrent with digital RGB and hyperspectral imagery. Optech International's Rapid Environmental Assessment (REA) Processor is designed to integrate the bathymetric lidar and hyperspectral data streams, creating a product suite that includes maps of water depth, bottom reflectance, water column volume reflectance, $a+bb$ (a measure of water column attenuation) derived from the bathymetric lidar data, spectral color-balanced mosaics of seafloor reflectance, spectral water column parameters, and seafloor and landcover classifications. This paper will demonstrate the capability of Optech REA on the production dataset from Hilo Bay. [C1702]

"Retrieval of 3-D Water Vapor Field Using a Network of Scanning Compact Microwave Radiometers"

Quantitative precipitation forecasting is currently limited by the paucity of observations of thermodynamic variables in the troposphere, including water vapor. Specifically, measurements of 3-D water vapor fields are needed at sub-meso-gamma scales in pre-storm conditions. This can be achieved using a network of remote sensors to retrieve the water vapor field with high spatial and temporal resolution. Such measurements may be used for assimilation into and validation of numerical weather prediction (NWP) models. Conventional measurements of water vapor density profiles are obtained using in-situ probes on-board weather balloons, including radiosondes. Remote sensing techniques to retrieve moisture profiles include ground-based networks receiving Global Navigation Satellite Systems (GNSS) signals, including GPS, and GPS receivers aboard the COSMIC satellite constellation for atmospheric occultation. These methods provide measurements with high vertical resolution but with coarse horizontal resolution. Differential Absorption Lidars (DIAL) can retrieve water vapor with comparable resolution to that of radiosonde observations. However, these lidars are expensive, and their operation is limited to clear-sky conditions due to the high opacity of clouds at optical wavelengths. Inversion of brightness temperatures measured by upward-looking, ground-based microwave radiometers allows the estimation of vertical profiles with high temporal resolution in both clear and cloudy conditions. However, assimilation of retrieved 3-D water vapor fields with improved spatial coverage into NWP models in pre-storm conditions has the potential for substantial impact on numerical weather prediction of convective storm activity. Measurements using a network of multi-frequency microwave radiometers can provide the necessary information to retrieve the 3-D distribution of water vapor in the troposphere. [C1703]

"S-Method-Based Approach for Image Formation, Motion Compensation, and Image Enhancement of Moving Targets in ISAR and SAR"

In this paper, we present the S-method-based approach to real-time motion compensation, image formation and image enhancement of moving targets in ISAR and SAR. This approach performs better than the Fourier transform by drastically improving images of fast, maneuvering targets. These advantages are a result of the S-method's ability to automatically compensate for quadratic and all even higher-order terms in phase. Thus, targets with constant acceleration will undergo full motion compensation and their point-scatterers will each be localized. It should be noted that the source of the quadratic term can come from not only acceleration, but also non-uniform rotational motion and the cosine term in wide-angle imaging. The method is also computationally simple, requiring only slight modifications to the existing Fourier transform-based algorithm. [C1704]

"Localization of Inanimate Moving Targets Using Dual-Frequency Synthetic Aperture Radar and Time-Frequency Analysis"

An important task in urban sensing applications is to accurately localize moving and vibrating targets in the presence of significant background clutter. A dual-frequency CW radar, which estimates the range of a target based on the phase difference between two closely spaced frequencies, has been shown to be a cost-effective approach for range estimation of a moving target. Previous work has shown that the use of Fourier transform and time-frequency analysis techniques provides an estimate of Doppler signature and enhanced signal-to-noise ratio (SNR), thereby enabling the range estimation of moving targets and significantly improving the estimation accuracy. In this paper, we consider the combined use of these technologies with a synthetic aperture array for the localization of inanimate moving targets. The synthetic array aperture provides the capability of high-resolution spatial localization of inanimate moving targets, as well as determining the orientation of the rotation or vibration. [C1705]

"Estimating Surface Water Speeds using Time-Frequency Analysis"

Joint Time-Frequency Analysis (JTFA) can estimate the speed of moving targets in Synthetic Aperture Radar (SAR) images. These targets are usually solid targets. JTFA estimation of water surface speeds is more difficult

since the returns are generated by Bragg scattering epochs that are randomly distributed in the radar's footprint in both time and space. The spectral characterization of these returns depends strongly on the geometry of the collection, which also affects the techniques needed to estimate the speeds. A novel phase differencing technique is presented to measure the frequency offset caused by the range motion of the surface water. JTFA is applied after extensive filtering to extract the motion induced component of the phase signal. [C1706]

"Estimation of Surface Velocity from Infrared Image Using the Global Optimal Solution to an Inverse Model"

We address the problem of obtaining ocean surface velocities from sequences of thermal (AVHRR) space-borne images by inverting the heat conservation equation (including sources of surface heat fluxes and vertical entrainment). We demonstrate the utility of the technique by deriving surface velocities from actual AVHRR images from one day. Typical formulations of this tracer inversion problem yield too few equations at each pixel, which is often remedied by imposing additional constraints (e.g., horizontal divergence, vorticity, and energy). In contrast, we propose an alternate strategy to convert the under-determined equation set to an over-determined one. We divide the image scene into many sub-arrays, and define velocities and sources within each sub-array using bilinear expressions in terms of the corner points (called knots). In turn, all velocities and sources on the knots can be determined by seeking an optimum solution to these linear equations over the large-scale, which we call the Global Optimal Solution (QOS). We test the accuracy of the GOS by contaminating the model output with up to 10% white noise, but find that filtering the data with a Gaussian convolution filter yields velocities nearly indistinguishable from those without the added noise. Application of the technique to a sequence of five NOAA AVHRR images yields a velocity field, which we compare with that from a Coastal Ocean Dynamics Radar (CODAR) array. We find that the GOS velocities generally agree more closely with those from the CODAR than they do with those from the MCC. Specifically, the root mean square error obtained by differencing GOS and CODAR velocities is smaller than that from the similar calculation with MCC velocities. The magnitude of the complex correlation between GOS and CODAR is larger than that between MCC and CODAR. The phase of the complex correlation indicates that both MCC and GOS on average yield velocity vectors biased in the clockwise direction relative to the CODAR vectors for the period examined. [C1707]

"An Improved Two-Scale Model for the Ocean Surface Bistatic Scattering"

Remote sensing applications require developing accurate models to predict radar bistatic scattering from rough surfaces. In this context, an improved two-scale model (TSM) is proposed for electromagnetic bistatic scattering from sea surface. The simplest TSM combines the first order small perturbation method (SPM1) with Kirchhoff Approximation. We add the second order SPM contribution to SPM1 to develop an improved TSM. The calculations are made by assuming the surface-height spectrum of Elfouhaily et al. for fully developed seas. In backscattering configuration the numerical results are compared with the published experimental data and SSA. The new TSM results are in good agreement with the experimental data specially, in cross-polarization. Finally, we use the new TSM to predict the sea scattering in bistatic configuration and compare the results with SSA. [C1708]

"A Study on Geophysical Model Function Modeling with Water Surface Temperature as One of the Input Parameters"

Geophysical model function is the basis for the wind vector retrieval with scatterometer and a number of models have been developed to operationally retrieve the ocean surface wind in the past three decades. However, none of the operational models ever took the water surface temperature into account in its modeling, which is considered to have some effect on the ocean backscattering, and in turn on the model accuracy. Taking Sea Winds as an example, this paper attempts to develop new geophysical model functions with surface temperature to be taken into account by using its level 2A data and corresponding buoy data. For contrast, two independent models are established for the ocean water and fresh water respectively. The modeling results and analysis indicate that some effect of the surface temperature on backscatter were found for both types of water, but with a larger extent of the temperature effect for fresh water. [C1709]

"Polarimetric Scattering Mechanisms of Ocean Surface from Wave Breaking or at Large Incident Angles"

Polarimetric scattering mechanisms of ocean surface are important for improving ocean surface scattering model and detecting objects on the ocean surface, especially at large incidence angles and wave breaking. We proposed polarimetric parameters technique to analyze the scattering mechanisms of ocean surface. Lacks of the related data, we only analyzed the variances of polarimetric parameters with incidence angles for C, L and P-band at low ocean state. The results show the polarimetric parameters are different at different incidence

angles and different radar work bands. It further indicates that the same ocean surface will present different scattering mechanisms at different radar work conditions. [C1710]

"Dependency of NRCS of Ocean Surface on Wind Direction Using an Airborne Dual-Frequency Polarimetric SAR Observation"

The normalized radar cross section (NRCS) of ocean surface is measured from three directions of illumination by an air-borne dual-frequency synthetic aperture radar (SAR) in the L- and X-bands, and the dependency of the NRCS and the polarization ratio on the relative wind direction is analyzed. In the X-band, the dependencies of the NRCSs in the parallel polarizations are different each other. The NRCS in the X-band HH polarization has difference between the up- and down-wind conditions, though that in the VV polarization the NRCSs for the up- and down-wind conditions are almost same. The dependency of the NRCS in the L-band is smaller than that of the X-band. The polarization ratio in the X-band shows the dependency on the wind direction with difference between the up- and down-wind conditions, though that in the L-band is not apparent. The results suggest the possibility of ocean wind measurement by the polarimetric SAR in the X-band. [C1711]

"Preliminary Polarimetric Measurements of Ruffled Water Surface Radar Backscattering Coefficients and Brightness Temperatures Angular Dependences at 15GHz"

In this paper preliminary results of smooth and waved water surface radar backscattering coefficient and brightness temperature angular dependences at 15 GHz are represented. The results were obtained by combined radar-radiometer system moving along a quarter circle shaped measuring platform of 7 m of radius. [C1712]

"Monitoring of Surface Ocean Circulation in the Gulf of Lions (North-West Mediterranean Sea) Using WERA HF Radars"

This paper presents the main results obtained by a long term experiment using HF radars which was conducted in the eastern part of the Gulf of Lions. The analysis focuses on statistical observations of the North Current, a large scale current vein occurring in the North of the Western Mediterranean, of current motions at diurnal and quasi-inertial periods and of submeso-mesoscale eddies. The study uses high resolution modellings of wind and current fields. [C1713]

"Ocean Surface Observation by C-Band Polarimetric Weather Radar in Okinawa Island"

We apply a C-band multi-parameter weather radar in the Okinawa Island to non-weather measurements. Its full-polarimetric and Doppler velocity measurement capability would be very powerful tool for observing land and ocean surface properties, if the target area is located appropriately to the radar. Located at the top of a mountain in the middle of the island, the radar has good view of its surrounding ocean. We make the radar observe ocean surfaces, in different wind conditions. The results show that the radar cross-section is larger when the wind speed is larger, and relatively smaller in the downwind side of the island, as expected. Cross-polarization components HV show similar dependency on wind conditions to HH and VV components. Measured Doppler velocities also show azimuth variation depending on the wind speed and direction. [C1714]

"SAR Measurement of Ocean Surface Wind Using A Physics Model"

Results of ocean surface wind speed retrieval from C-band ENVISAT ASAR images using a physics wind model are shown. The physics model is based on the radar backscatter theory in which the radar cross section is calculated considering the contribution of both Bragg scattering or resonance and specular reflection from the sea surface. The wind speeds retrieved from VV- or HH-polarized ASAR images using the physics model were compared to both buoy measurements in Hong Kong coastal waters and that retrieved using the empirical C-band algorithms (CMOD4, CMOD5, CMOD_IRR2). The results show the feasibility of the physics model for ocean surface wind speed retrieval from both VV and HH-polarized ASAR images at moderate wind condition. [C1715]

"A Parametric Algorithm to Retrieve Ocean Wave Spectra from Interferometric Synthetic Aperture Radar"

A new ocean wave retrieval method for the along-track interferometric synthetic aperture radar (ATI-SAR) phase image is presented. The new algorithm, named parametric retrieval algorithm (PRA), uses the full nonlinear mapping relations as proposed by He and W. Alpers (2003). It differs from previous retrieval algorithms in that it does not require apriori information on the sea state and also calibration of the ATI-SAR phase image. The

advantage of PRA is that it jointly retrieves information of wave parameters and wind speed. The method has been validated by collocating two X-band HH-polarized ATI-SAR phase image and one C-band HH-polarized ATI-SAR phase image spectra with spectral buoy measurements. The wave parameters and wind speed estimated from PRA are in agreement well with buoy observations. The proposed method can be employed by future satellite missions such as TerraSAR. [C1716]

"Remotely Monitoring Great Lakes Coastal Wetlands with Multi-Sensor, Multi-Temporal SAR and Multi-Spectral Data"

Wetland monitoring in the Great Lakes coastal areas is needed for assessment of overall health of the Great Lakes basin. Methods were developed that were robust yet cost-efficient and implementable. The methods rely on satellite imagery for mapping wetland type, adjacent land use, wetland extent and inundation extent. The best method for mapping wetland type and adjacent land use was a fusion of data from multiple SAR sensors (JERS, ERS, Radarsat-I) and Landsat. This data fusion allows for the unique SAR and optical/IR information to be integrated for improved mapping capabilities. [C1717]

"Extraction of Wind and Wave Information Using SAR Images"

This study is a preliminary research to extract the oceanic information such as ocean wind and wave using SAR images. The CMOD4, CMOD-IFR2, and polarization ratio (PR) models are used to estimate the magnitude of wind and the SAR-wave spectrum analysis and inter-look cross-spectra methods provides the wave information related to amplitude and direction of the ocean wave over a square-km sized area. [C1718]

"Monitoring of Coastal Vessels Using Surface Wave HF Radars: Multiple Frequency, Multiple Site and Multiple Antenna Considerations"

Marine situational awareness is a key factor in coastal activities, e.g. national security (terrorism, drug smuggling, etc.) and environmental protection (marine protected areas, fishery monitoring and regulation, oil spills, etc.). HF surface wave radar is a strong candidate to become a component of any large area, vessel-monitoring network. We discuss estimating the primary metrics for assessing performance for ship tracking radars (probabilities of detection P_d and false alarm P_{fa}) and their variation with parameters, such as range, azimuth and frequency, and number of observing modes. We discuss several design options for an HF radar, ship monitoring system, such as multiple or single frequency, multiple or single sites or method of target bearing determination (MUSIC or real aperture antenna) and present a model of the SNR for ship detection by HF radar and as well as observational examples of ship detection with single and multifrequency HF radars. Finally we suggest future experiments and draw conclusions. [C1719]

"Simulation Study on the Effect of Wind Direction on SAR Imaging Shallow Water Bathymetry"

A simulation model of SAR imaging of shallow water bathymetry has been developed according to SAR imaging mechanism of shallow water bathymetry and based on the software toolkit M4S. According to the simulation results of shallow water bathymetry and based on the analysis of shallow water bathymetry ERS-2 SAR images off the west south of Jilong Island, the relationship between the sea surface wind direction and SAR imaging shallow water bathymetry has been improved. The results showed that, the expression of SAR imaging shallow water bathymetry is mainly affected by the sea surface wind direction. When the wind direction is parallel or adverse to the current component in the direction of shallow water bathymetry, dark streaks or bright streaks appear on SAR images. Under crosswind, the bright and dark streaks are alternant. And the adverse wind direction is better for SAR imaging of shallow water bathymetry. [C1720]

"Estimation of Ocean Current Velocity in Coastal Area Using Radarsat-1 SAR Images and HF-Radar Data"

This paper presents the results of the surface current velocity estimation using 6 Radarsat-1 SAR images and high frequency (HF) radar data acquired in west coastal area near Incheon, Korea. We extracted the surface velocity from SAR images based on the Doppler shift approach in which the azimuth frequency shift is related to the motion of surface target in the radar direction. The extracted SAR current velocities were statistically compared with the current velocities from the HF-radar data. The corrected SAR current velocity inherits the average of HF-radar while maintaining high-resolution mature of the original SAR data. [C1721]

"Normalized Coherency Matrix Estimation Under the SIRV Model. Alpine Glacier Polsar Data Analysis"

This paper presents an application of the recent advances in the field of Spherically Invariant Random Vectors modelling. We propose the use of the Fixed Point (FP) estimator for deriving normalized polarimetric coherency matrices in compound Gaussian clutter. The main advantages of the FP estimator are that it does not require any "a priori" information about the probability density function of the texture and it can be directly applied on adaptive neighborhoods. Interesting results are obtained when coupling this FP estimator with an adaptive spatial support driven on the scalar span information. The proposed method is tested with both simulated POLSAR data and high resolution POLSAR data acquired over the French Alps. [C1722]

"Deformations occurring in the city of Auckland, New Zealand as mapped by the differential synthetic aperture radar"

Auckland is the largest city in New Zealand with a current population of more than one million. It is situated on a basaltic volcanic field with a total area of 360 square km and which consists of over 50 individual largely monogenetic volcanoes. The most recent and largest eruption occurred 600 years ago, and was witnessed by local inhabitants. It is anticipated that the chance of reawakening of a dormant volcano is very low; however, a new volcano could be created at any time in a new location within the field. In order to study ground deformations in the Auckland region twenty six ENVISAT ASAR images (Track 151, Frame 6442, IS2, VV) were acquired, spanning the period from 18 July 2003 to 9 November 2007. Over a hundred differential interferograms with perpendicular baselines of less than 500 meters were calculated and analyzed. Stacking, Small Baseline Subset and Permanent Scatterers processing algorithms were used to determine spatial and temporal patterns of surface deformation as well as average rates. A number of localized deformation regions were consistently observed by all three techniques. Three regions of subsidence are believed to be caused by groundwater extraction. The nature of uplifts is currently unclear, but a linear feature paralleling the regional tectonic fabric may be related to a hidden fault. The observed temporal deformation pattern is noisy but appears to be close to linear. [C1723]

"Remote sensing analysis of ongoing deformation in Hazara Kashmir Syntaxis in Northern Pakistan"

Hazara Kashmir Syntaxis (HKS) is a complex tec-tonic feature in North Western Himalayan Fold and Thrust Belt. Himalayan Frontal thrust starts from the core of the Syntaxis while other faults like Kotil thrust, Riasi thrust and Tanda fault runs along NS directed Jehlum Fault. Seismicity is distributed along all the parts of the Syntaxis i.e. in the core and along the outer loop but decreases southward. The Kangra (1905) and Kashmir Earthquake (2005) are major outputs of the ongoing deformation process and thus gave motivation for this study. This study focuses Kunhar, Kishanganga, Jehlum and Poonch River and their automatically extracted tributaries. The drainage pattern of these rivers is controlled by different tectonic and climatologically changes in the region. Digital elevation models (DEMs) are used for drainage network extraction as it provides elevation information for the land surface throughout the catchment of the area. Drainage network has been extracted from Shuttle radar digital elevation data (SRTM-DEM). Rivers are sensitive to changes in tectonic deformation, adjusting over different periods of time depending on the physical properties of the host rocks, climatic effects and tectonic activity. Thus, the drainage system of a region records the evolution of tectonic deformation. The stream profile analysis of these four rivers provides information about absolute uplift condition in the region. This analysis provides us with different indices and they can later provide us several maps which, integrated in a GIS, allows a better interpretation of the results. We apply fractal analysis to these four rivers and try to study the rigidity of the areas from where they are passing. This is later confirmed with the steepness and concavity indices of the areas to identify the spatial distribution of the different rock types. We can separate various tectonic units and their deformation using knickpoints, concavity and steepness indices and their fractal behavior. [C1724]

"Ground deformation measurement with radar interferometry in Exupýry"

The Exupery project funded by the German Federal Ministry of Education and Research is a multidisciplinary project aiming at setting-up an Early Response System (VFRS) for Volcanic Activity. The core of the system builds on established volcanic monitoring techniques such as seismicity, ground deformation, and remote sensing tools for gas measurements. A major novelty of this mobile system is the attempt of a direct inclusion of satellite based observations to deduce ground deformation, to detect hazardous gas emissions and to monitor thermal activity. Within the project, the study group at the Technical University of Munich and at the German Aerospace Center DLR is responsible for ground deformation measurements with satellite observations. Millimetric subsidence or uplift can be retrieved from SAR images by using interferometric techniques. The multi-frequency SAR data-set used for the test sites include three different sorts of band data, X-, C- and L-Band, respectively. Azores (Portugal) and Stromboli (Italy) were chosen for the test sites. The volcanic movements were measured with the differential phases and the measurement accuracy will be compared with on site measurements including GPS and ground based DInSAR measurements later for field campaign in Azores. The estimated

deformation will be then incorporated into geophysical stress models to initialize, calibrate and, ultimately, improve the models. Our presentation gives a short overview of the Exupery project and presents first results from multi-wavelength InSAR data and different processing techniques such as PSI. [C1725]

"Ground-based radar remote sensing of explosive volcanic ash eruptions: Numerical models and quantitative applications"

Microphysical and dynamical features of volcanic clouds, due to Plinian eruptions, can be quantitatively monitored by using ground-based microwave weather radars. In order to illustrate the potential of this microwave active remote sensing technique, the case study of the eruption of Augustine volcano in Alaska in January 2006 is described and analyzed. Volume data, acquired by a NEXRAD WSR-88D S-band ground-based weather radar, are processed to automatically classify and estimate eruptive cloud particles concentration. In this study we use the plume model ATHAM to investigate processes leading to particle aggregation in the eruption column. The interactions of hydrometeors and volcanic ash within the eruption column that lead to aggregate formation are simulated for the first time within a rising eruption column. A sensitivity analysis is carried out to evaluate the impact of aggregate particles on microwave radar reflectivity. The ash retrieval physical algorithm is based on the backscattering microphysical model of volcanic cloud particles, used within a Bayesian classification and optimal regression algorithm. The evolution of the Augustine eruption is discussed in terms of radar measurements and products, pointing out the unique features, the current limitations and future improvements of radar remote sensing of volcanic plumes. [C1726]

"Requirements for an L-band SAR-mission for global monitoring of tectonic activities"

SAR interferometry is a well established technology for mapping tectonic activities from space. In this study a mission concept is investigated that provides a global monitoring capability of geo-tectonic threads. Due to the requirement of long-time interferometric coherence of the mapped surfaces an L-band system is proposed. Four scenarios are defined and the respective product requirements are given for each of them: tectonics/earthquakes, tectonics/volcanoes, landslides, and urban subsidence. [C1727]

"Study of scattering coefficient of flooded soil, semi dry soil and natural dry soil at CJ, X and Ku band of microwave frequencies"

The soil is one of the natural earth material which is produced by withering of rocks. The soil is characterized by its physical and electrical parameters. The physical parameters include the texture, temperature, surface roughness. The electrical parameters are dielectric constant, emissivity and scattering coefficient. The emissivity and scattering coefficient are function of dielectric constant of the soil and also function of sensor parameters like polarization, angle of incidence and frequency of operation. In this study, the scattering coefficient is measured for different conditions of the soil which include flooded, semi dry and natural dry soil at CJ, X and Ku band of microwave frequencies using ground based scatterometer which can be used for study of different terrains and other geophysical parameters. The scatterometer used in this experiment consists of components like gun oscillator, directional coupler, horn antenna and power meter as receiver. The soil is a mixture of sand, silt and clay with air pores. The natural soil is having some percentage of moisture content. In present case, the percentage moisture of natural dry soil is around 2.17% and semi dry soil having 7.2% of moisture content by weight. The flooded soil is fully saturated with water and has a 3 mm to 5 mm layer of water above the soil surface. Here, the scattering coefficients obtained for incidence angle from 20deg to 60deg with 5deg intervals at CJ (5.2 GHz), X (11.22 GHz) and Ku (12.83GHz) band of microwave frequencies for V-H and V-V polarization for different soil surfaces have been presented. The methodology of measurement along with experimental setup and estimation of scattering coefficients at CJ, X and Ku band of microwave frequencies for V-H and V-V polarization for different soil surface have been presented. This study will provide inputs for microwave remote sensing applications. [C1728]

"Definition of the deformation pattern of Sicily (Italy) through DInSAR techniques and studies on its integration with geodetic data"

A complete study of the deformation pattern of Sicily is planned, in the framework of the project Г, BiExtension and enhancement of the volcanic and seismic monitoring systems of Sicily Г, Bi, according the agreement among the National Department of Civil Defense (DPC), Sicilian regional government and National Institute of Geophysics and Volcanology (INGV). In this study, it is also planned a research aimed at implementing a new technique to integrate GPS vector displacements and DInSAR Interferograms. [C1729]

"Recent advances of POL-SAR, POL-IN-SAR & RP-POL-IN-SAR imagery for remotely sensing

natural habitats: Desert and wetlands remote sensing"

Land cover monitoring is one of the most potential applications of Polarimetric Synthetic Aperture Radar (POLSAR) sensing and so is Repeat-Pass Polarimetric-Interferometric SAR (RP-DIFF-POL-IN-SAR) stress-change assessment for air/high-altitude/spaceborne SAR sensor deployment. Provided fully polarimetric SAR information can be made available, a plethora of novel POLSAR matrix decomposition methods can be implemented for recovering rather precise scattering contributions from isolated and distributed scattering scenarios, and so can rather exact environmental changes from consecutive repeat-pass observations. With the recent launches of the fully polarimetric satellites JAXA-ALOS (PAL-SAR-L), the DLR TerraSAR-X and RADARSAT-2 (C), a new era in space imaging of the terrestrial terrain and ocean surfaces has arrived providing unforeseen advantages. Whereas in the past, POLSAR applications were focused mainly on information product gathering for agriculture, forestry and the fisheries, little emphasis was placed on demonstrating its full capacity also for the assessment of natural habitats and especially wetlands. Therefore, it is essential to demonstrate how seasonal changes and features of vegetation in natural habitats, shallow vegetated lakes and wetlands can be recovered, provided fully polarimetric SAR image data takes can be made available for full polarimetric scattering matrix acquisition for which the standard symmetry condition $HV=VH$ may not necessarily be sufficient. [C1730]

"Recent advances in RP-POL-IN-SAR Hazard monitoring of tectonic stress and land-slides"

Worldwide, medium- to short-term earthquake prediction is becoming ever more essential for safeguarding man due to an un-abating population increase, but hitherto there have been no verifiable methods of reliable earthquake prediction developed-except for a few isolated examples of earthquake prediction in China and in Greece. This dilemma is a result of previous and still current approaches to earthquake prediction which are squarely based on the measurement of crustal movements, observable only after a tectonic stress-change discharge (earthquake) has occurred. The prediction models were derived from past histories of measurements, mainly carried out during the past 30-40 years, although initiated soon after the San Francisco Earthquake of 1906. During the past decade it was proved and shown that it is not possible to derive reliable models for earthquake predictions from crustal movement measurements alone, and that an entirely new approach must be taken and rigorously pursued over years and decades to come. In support of this conclusion, there have been reported throughout the history of man anecdotal historical up to scientifically verifiable earthquake precursor or "seismo-genic" signatures of various kind-biological, geological, geo-chemical and especially a rather large plethora of diverse electromagnetic ones on ground, in air and space, denoted as "seismo-electromagnetic" signatures. The existence of all of these signatures can no longer be denied even by the fiercest seismological expert opponents; and it is absolutely high noon that those signatures be more rigorously assessed in order to develop a strategy for designing and carrying out controlled "seismo-genic" and "seismo-electromagnetic" studies on how to set up world-wide a network of measurement sites for conducting a holistic set of measurements for providing an improved understanding on why and how such precursor signatures are generated, and how and where they may best be observed subject to the rather poor signal-to-noise ratio (SNR), requiring much improved digital instrumentation as time goes on due to the ever increasing man-made electromagnetic noise generation. A number of pilot studies had been initiated, had been supported for a few years, and then aborted because of the high operating costs involved, the poor SNR making signal detection tedious if not impossible with the current state of the art in instrumentation, and because earthquakes don't appear upon demand. For example such major studies as the USGS/NSF NEHER Program of the early 1990s after the Loma Prieta M 7 earthquake of 1987; in Japan the ERSFP after the Kobe Earthquake of 1995; in Greece the ongoing electro-potential methods of Varatsov; in China, and in various regions as well as independent states of the former Soviet Union. There exists a rather large number of fiercely competing groups in Russia coming up with their own diversified yet highly incomplete modeling approaches seeking support from the West for unfortunately all too low-cost scientific mercenary services. No clear picture has evolved and should not be expected; and a much wider internationally coordinated investigation is required, which may well last for several decades before a unified approach and with it a solution to this vital problem may be found-if ever. In this overview a systematic analysis of main historical records, a summary of pertinent "seismo-genic" as well as observed "seismo-electromagnetic" effects and modern ground-based to air- and space-borne metrological signature investigations are presented. Specifically, remote sensing techniques not yet conceived but in urgent need-such as the remote sensing of the groundwater table-for advancing our understanding of this highly interdisciplinary complicated geophysical problem are being identified, and input is sought from participants for possible active future involvement. [C1731]

"SAR Imaging Simulation for an Inhomogeneous Undulated Lunar Surface Based on Triangulated Irregular Network"

Based on the statistics of the lunar cratered terrain, e.g. population, dimension and shape of craters, the terrain feature of cratered lunar surface is numerically generated. According to inhomogeneous distribution of the lunar

surface slope, the triangulated irregular network is employed to make the digital elevation of lunar surface model. The Kirchhoff approximation of rough surface scattering is then applied to simulation of lunar surface scattering. The synthetic aperture radar (SAR) image for comprehensive cratered lunar surfaces is numerically generated. Making use of the digital elevation and Clementine UVVIS data at Apollo 15 landing site as the ground truth, an SAR image at Apollo 15 landing site is simulated. [C1732]

"Volcano monitoring via fractal modeling of lava flows"

In this paper use is made of fractal models for the development of a processing chain devoted to volcano monitoring. In particular, we present new models for the characterization of microwave images of fractal surfaces and we show how these models can account for the presence of different types of lava flows on these images. The imaged surfaces are modeled as fractional Brownian motion (fBm) stochastic processes. First of all, we show how the radar image relevant to an fBm can be linked to an associated fractional Gaussian noise (fGn) process. Different types of lava flow surfaces are simulated and their image spectra are analyzed and compared. Finally, a case study is presented. The area of interest is the Vesuvio volcano close to Naples, Italy. Simulated results, showing the possibility to discriminate different types of lava, are provided. [C1733]

"Photogrammetric and LIDAR surveys on the Sciara del Fuoco to monitor the 2007 Stromboli eruption"

Focused on the Stromboli Island, this research investigates whether airborne remote sensing systems, such as those based on digital photogrammetry and laser scanner sensors, can be adopted to monitor slope deformation and lava emplacement processes in active volcanic areas. Thanks to the capability of extracting accurate topographic data and working on flexible time schedule these methods can be used to constrain the regular and more frequent measurements derived from satellite observations. In this work we present an application dedicated to the monitoring of Stromboli volcanic edifice useful to obtain quantitative data on the geometry of deformation features and the displaced (failures and landslides) and emplaced (lava flows) volumes. In particular, we focused on the capability of extracting average effusion rates from volume measurements that can be used to validate or integrate satellite derived estimates are often affected by biases which are not easily detectable. Since 2001 a number of airborne remote sensing surveys, namely Digital Photogrammetry (DP) and Airborne Laser Scanning (ALS), were carried out on Stromboli volcano to obtain high resolution digital terrain models (DEM) and orthophotos characterized by sub-meter spatial resolution and time schedule suitable for monitoring the morphological evolution of the surface during the quiescent phases. During the last two effusive eruptions (2002-2003 and 2007) the surface modifications, suffered by the Sciara del Fuoco slope and by the crater area as a consequence of effusive activity, were quantified and controlled using the same methodologies. This work is mainly focused on the 2007 eruption but also accounts for analogies and differences with the 2002-2003 event being based on a multi-temporal quantitative analysis of the data collected from 2001 to 2007. The 2007 eruption involved the Sciara del Fuoco slope from the 27th February until the 2nd April: five flows produced a compound lava field including a lava delta on the shoreline and discharging most of the lava into the sea. The comparison of the 2007 DEMs with a pre-eruption surface (2006 LIDAR survey) allowed evaluating the total lava volume emplaced on the slope while two syn-eruption DEMs were used to calculate the average effusion rates through the eruption. Finally hypothesis on the lava discharge and slope instability mechanisms, which appear strongly connected, are formulated. [C1734]

"Satellite remote sensing of volcanic activity in New Zealand"

Mt Ruapehu is New Zealand's most active volcano. In 2007, the volcano produced a large lahar following a crater lake dam wall breach, in addition to a minor eruption and small associated lahars. Here, satellite remote sensing and image processing is used to extract the path of the major lahar, and to compare the results achieved through classification of ASTER visible and near infra-red imagery to those derived from ALOS-PALSAR L-band synthetic aperture RADAR data. This study also details how remote sensing can be used to derive temperature values useful for monitoring volcanic activity. Eleven ASTER thermal images were acquired to extract the temperature of the crater lake and a linear correlation coefficient (r^2) of 0.94 was achieved when compared to field survey. The results herein demonstrate the utility of satellite remote sensing for mapping and monitoring volcanic activity in New Zealand. [C1735]

"DInSAR, GPS and gravity observation results in La Palma, Canary islands"

We review several results from geodetic observations carried out in La Palma Island during the period 1992-2007. A gravity survey was done for structural studies, and InSAR and GPS observations techniques were applied to study the existence of deformation areas in the Island. Gravity anomalies have been inverted using a non-linear three-dimensional gravity inversion approach to obtain the geometry of the anomalous bodies. The

main structural feature is a large high density body interpreted as a dense intrusive plutonic body and the Pliocene-age uplifted seamount. An elongated minimum is detected below the Cumbre Vieja according to the rift structure. InSAR results show two areas of subsidence, a mild long wavelength signal on the western part of Cumbre Vieja and clear subsidence located on the Teneguia volcano where the last eruption took place in 1971. A GPS network composed by 26 stations covering the island has been defined. Vertical displacements determined by comparing the GPS coordinates obtained in 2007 and in 1994 are consistent with the InSAR results. From the comparison of 2006 and 2007 coordinates we conclude that more time span is needed to obtain clearly significant displacements, but observed trends are also consistent with InSAR results. All the observed significant displacements are at stations located outside of the large high density central body. [C1736]

"Roughness effect of the soil of Alwar on passive and active microwave remote sensing"

Real and imaginary parts of complex permittivity (ϵ_{siv}' and ϵ_{siv}'') of soil of Alwar have been determined at a single microwave frequency 9.78 GHz. In view of passive microwave remote sensing horizontal components of emissivity for bare and smooth soil surfaces along with various rough surfaces are determined using the emissivity model. The radar backscattering coefficient of soil surfaces with different small level roughness is calculated by small perturbation model. It is observed that both the emissivity and backscattering coefficient increases with increasing roughness of soil surface. Thus, the active microwave remote sensing is very sensitive for roughness of soil surfaces in comparison to passive microwave remote sensing. Directional dependence of the detection of microwaves at the sensor is also strongly related to roughness of soil. [C1737]

"Detection of Deep Convective Clouds Using AMSU-B and GOES-9 Data"

Methods to detect the deep convective clouds using NOAA-16/AMSU-B and GOES-9 data are provided, and a series of algorithms of detection and discrimination are presented and tested, which include the microwave brightness temperatures detection from the two window channels, water vapor channel microwave brightness differences identification based on the AMSU-B data, infrared brightness thresholds detection of cloud top temperatures, the water vapor and infrared window temperature differences determination, and the classification of cumulonimbus clouds correlating with deep convective clouds with infrared/water vapor spectral features. By detecting and analyzing deep convective clouds in the images on 16 June in 2004, the techniques are investigated, and by matching surface conventional data the results of various methods are validated. The results show that microwave brightness temperatures from window channels can discriminate deep convective clouds efficiently, differences between three water vapor channels can identify the deep convective clouds well and depend on the thresholds less. The GOES-9 different infrared brightness thresholds are given the detection regions are more or less. The water vapor and infrared window temperature differences determination areas are smaller. The stepwise cluster can identify cumulonimbus clouds correlating with deep convective clouds applying with infrared/water vapor spectral features, the detection areas are coincident with AMSU-B detection areas, and the surface conventional data can validate the results, which include hazards weather and cumulonimbus clouds. [C1738]

"Antenna technologies for microwave sensors: A review"

Summary form only given. There has been a rapid technological growth in the field of antennas for space-borne, air-borne and ground based microwave sensors of passive as well as active types. The performance of the sensors largely depend on the radiation characteristics of the multifunctional antenna system. The development of these antenna systems pose a very challenging task in achieving the stringent performance in terms of various antenna parameters like beam efficiency, beam shape, gain, sidelobe level and cross-polarisation etc. Innovative design techniques are prerequisite for achieving the required gain, sidelobe level, polarization isolation and bandwidth specifications in the smallest aperture size consistent with mass limitations and ease of manufacturing. Various antenna technologies for passive as well as active microwave sensors like Radiometer, Millimeter wave Sounder, Scatterometer, Precipitation Radar, Altimeter, Synthetic Aperture Radar etc have been reviewed in this paper. This paper will elaborate the salient features of the advanced antenna systems developed for various microwave remote sensing missions of ISRO. This paper will also address requirement of future mission of ISRO. [C1739]

"Microwave remote sensing using space borne sensors"

Microwaves are part of radio spectrum the frequency bands in the range of 3 GHz to 30 GHz are characterized as microwave. This part of spectrum has unique capabilities for microwave remote sensing. The microwaves can be used for remote sensing of objects in day as well as in night. They have all weather capability because microwaves can penetrate clouds. The soil moisture can be determined using microwave sensors. The microwaves can penetrate vegetation as well as soil and so they can give information about the objects which

are under vegetation and under ground. The microwaves can penetrate dry snow and so one can detect buried objects under snow. There are two types of microwave sensors which can be used for microwave remote sensing. They are (i) passive sensors and (ii) active sensors. The Radiometers are passive sensors where as the scatterometer, altimeter, real aperture radar and synthetic aperture radar are part of active sensors. The microwave remote sensing using these sensors (both passive and active) can be done from different platforms. The platforms which can be used are ground based (on towers) platforms, Airborne platforms and Space borne platforms. The first microwave passive sensors were put on Nimbus satellites. These sensors were radiometers for study of oceans, atmosphere and land. The first synthetic aperture Radar system operating in L-band was placed in SEASAT in year 1978. Later at different times various passive and active sensors were put by American Agency NASA, Russian Space Agency, Indian Space Agency (ISRO), European Space Agency ESA, and Japanese Space Agency NASDA. The passive sensors were having coarser resolution where as resolution of the active sensors was finer than that of passive sensors. The latest passive sensors which are being used for different applications are SSM/I radiometers and AMSR-E providing data at different microwave frequencies. The space borne active sensors are RADARSAT-2 of Canada and Oceansat-2 of India. In future the active microwave sensors will be put in spaceborne RISAT satellite in India and cosmoSkymed of USSR. All these space borne sensors will provide very useful data for operational applications. The applications of these sensors are in agriculture, soil moisture estimation, flood mapping, geology/ geomorphology forestry, snow cover and glaciers, oceanography, Topography, Terrain and oil spill detection. The sensors have to be calibrated and all these applications have to be validated. From the data obtained from sensors the data products have to be generated. In this talk the evolution of the space borne sensors will be presented and the operational, quasi operational applications will be discussed. [C1740]

"Recent advances in microwave multi-modal SAR remote sensing of the terrestrial covers"

Land cover monitoring is one of the most potential applications of Polarimetric Synthetic Aperture Radar (POLSAR) sensing and so is Repeat-Pass Polarimetric-Interferometric SAR (RP-DIFF-POL-INSAR) stress-change assessment by air/high-altitude/space-borne SAR sensor deployment. Provided fully polarimetric SAR information can be made available, a plethora of novel POLSAR matrix decomposition methods can be implemented for recovering rather precise scattering contributions from isolated and distributed scattering scenarios, and so can rather exact environmental changes from consecutive repeat-pass observations at 1 m resolution from air and from space. With the recent launches of the fully polarimetric satellites JAXA-ALOS (PAL-SAR-L-Band), the DLR TerraSAR-X (X-Band) and of RADARSAT-2 (C-Band), a new era in space imaging of the terrestrial terrain and ocean surfaces has arrived providing unforeseen advantages. Whereas in the past, POLSAR applications were focused mainly on information product gathering for agriculture, forestry and the fisheries, little emphasis was placed on demonstrating its full capacity also for the assessment of natural habitats and especially wetlands and desert regions. Specifically, we are now able to demonstrate how seasonal changes and features of vegetation in natural habitats, shallow vegetated lakes and wetlands & deserts can be recovered under worst weather conditions and at day and during night at most distant and often inaccessible hidden sites, where for example migrant birds rest. Land cover monitoring is one of the most potential applications of Polarimetric Synthetic Aperture Radar (POLSAR) sensing and so is Repeat-Pass Polarimetric-Interferometric SAR (RP-DIFF-POL-INSAR) stress-change assessment by air/high-altitude/space-borne SAR sensor deployment. Provided fully polarimetric SAR information can be made available, a plethora of novel POLSAR matrix decomposition methods can be implemented for recovering rather precise scattering contributions from isolated and distributed scattering scenarios, and so can rather exact environmental changes from consecutive repeat-pass observations at 1 m resolution from air and from space. It is essential to emphasize that fully polarimetric SAR image data sets are strictly required for optimal information extraction and compacted or hybrid quasi-polarimetric SAR imaging will fail to discover intricate detailed feature characteristics and parameters.

[C1741]

"Research in the Spaceborne Meteorological Radar Equation"

This paper starts from the general radar meteorological equation and derives a new form which is suitable for spaceborne usage. Preliminary research has been done in the four main factors of the equation, which are phased array antenna gain, the scattering of deformed raindrop, the atmosphere attenuation and low sidelobe level of antenna. The results are helpful to improve the remote sensing precision of spaceborne precipitation radar. [C1742]

"A new digital signal processor for Doppler radar cardiopulmonary monitoring system"

Remote sensing and monitoring of cardiopulmonary activities based on direct conversion Doppler radar shows promise in medical and security applications. For accurate sensing, demodulation of the quadrature outputs of a direct-conversion Doppler radar is a great challenge. A digital signal processor based on Kalman filtering and

principal component combining of quadrature channels is suggested. Rate detection ability and success ratio is evaluated and compared with other techniques. This radar sensor system achieves good detection accuracy in increased noise power level. [C1743]

"Basics of microwave radar & SAR polarimetry and its applications"

The development of radar polarimetry and radar interferometry is advancing rapidly, and these novel radar technologies are revamping "synthetic aperture radar imaging" decisively. In this exposition the successive advancements are sketched; beginning with the fundamental formulations and high-lighting the salient points of these diverse remote sensing techniques. Whereas with radar polarimetry the textural fine-structure, target-orientation and shape, symmetries and material constituents can be recovered with considerable improvements above that of standard 'amplitude-only polarization radar'; with radar interferometry the spatial (in depth) structure can be explored. In 'polarimetric-interferometric synthetic aperture radar (POL-IN-SAR) imaging' it is possible to recover such co-registered textural plus spatial properties simultaneously. This includes the extraction of 'digital elevation maps (DEM)' from either 'fully polarimetric (scattering matrix)' or interferometric (dual antenna) SAR image data takes' with the additional benefit of obtaining co-registered three-dimensional 'POL-IN-DEM' information. Extra-wide-band POL-IN-SAR imaging-when applied to 'repeat-pass image overlay interferometry'-provides differential background validation and measurement, stress assessment, and environmental stress-change monitoring capabilities with hitherto unattained accuracy, which are essential tools for improved global biomass estimation. More recently, by applying multiple parallel repeat-pass EWB-POL-D(RP)-IN-SAR imaging along stacked (altitudinal) or displaced (horizontal) flight-lines will result in 'tomographic (multi-interferometric) polarimetric SAR stereo- imaging', including foliage and ground penetrating capabilities. It is shown that the accelerated advancement of these modern 'EWB-POL-D(RP)-IN- SAR' imaging techniques is of direct relevance and of paramount priority to wide-area dynamic homeland security surveillance and local-to-global environmental groundtruth measurement and validation, stress assessment, and stress-change monitoring of the terrestrial and planetary covers. [C1744]

"LOS PALSAR data analysis of snow cover area in Himalayan region using four component scattering decomposition technique"

Snow cover is the important parameter for hydrological modeling and climate change modeling. Land use/cover classification is one of the most important applications of polarimetric synthetic aperture radar (POLSAR) sensing. Hence, the application of radar polarimetry is one of the best remote sensing techniques to classify snow cover terrain. In this paper, PALSAR data have been analyzed of snow cover area in Himalayan region based on three and four component scattering mechanism model. This study shows the implementation problem of four-component decomposition model in Himalayan terrain. Finally, supervised Wishart classifier has been used for snow cover and other land feature classification. The over all accuracy was measured to be 74.12 % without speckle noise reduction. [C1745]

"Multifractal analysis of SAR images for unsupervised classification"

In present paper an attempt has been made for unsupervised classification of SAR images based on the surface roughness using multifractal technique. Surface roughness is measured with the help of fractal dimension (D), which lies in the range 2.0 and 3.0. Based on roughness values, i.e., D, various land classes are grouped in different classes. The D values are estimated for a number of local window sizes and thus the window size is very important for classification. The window size is optimized for best classification and in present case it is 9times9. The K-means classifier has been used for this procedure which clusters various land classes according to D values. Although fractal dimension is able to provide the roughness values for various land classes, it can not uniquely identify all classes. In order to remove this discrepancy, the multifractal analysis has been performed. The multifractal dimension has been estimated as 5 generalized dimensions providing 5 multifractal images and then these images are classified. The overall classification accuracy using fractal dimension alone comes to be nearly 60% while it increases to 67% with multifractal images. [C1746]

"Microwave sensitivity analysis of soil texture at C-band with bistatic scatterometer for remote sensing"

The main aim of this paper is to check the microwave response on soil texture in specular direction. For this purpose, an indigenous bistatic scatterometer has been assembled at C-band which has facility to change incidence angle from 25deg to 70deg and can take observation in both like polarization (i.e., HH and VV-polarization). Four fields has been prepared with different soil texture (i.e., sand, silt and clay), mainly sand percentage is changed more in comparison to other soil constituents. Moisture and roughness effect on soil texture is also observed. It is observed that sand has a strong influence in specular scattering in case of HH-

polarization and this effect is observable for wide range of moisture value. It is noticed that roughness effect is dominant than texture effect. To minimize the roughness effect on texture, polarization analysis has been carried out and it is found that copolarization may be quite helpful to minimize the roughness effect. This type of study will be helpful in near future to design the bistatic radar system for soil parameter monitoring and especially will be helpful for cartwheel satellite system. [C1747]

"Snow density estimation using polarimetric ASAR data"

Remote sensing of radar polarimetry has great potential to determine the extent and properties of snow cover. Availability of spaceborne sensor dual polarimetric C-band data of ENVISAT-ASAR can enhance the accuracy in measurement of snow physical parameters as compared to single fixed polarization data measurement. This study shows that the capability of C-band SAR data for estimating dry snow density over snow covered rugged terrain in Himalayan region. The study area lies in Beas, Chandra and Bhaga catchments of Himachal state (India). For this investigation, the main assumptions are that the snow is dry and at C-band, total backscattering coefficient comes from snowpack and snow ground interface. An algorithm for estimating snow density has been developed based on snow volume scattering and snow-ground scattering components. Snow density estimation algorithm requires HH and VV polarization combination data. The radar backscattering coefficients of both HH and VV polarization and incidence angle are given as input to the developed algorithm. Finally, the algorithm gives the snow dielectric constant which can further be related to snow density using Looyengapsilas semi empirical formula. Comparison was done between algorithm estimated snow density and field value of snow density in the study region. The mean absolute error between estimated and measured snow density was 21.3 kg/m³. [C1748]

"Investigation of SAR compression technique for point target"

The essence of remote sensing resides in the acquisition of information about remote targets for further processing. Synthetic Aperture Radar (SAR) has evolved as a powerful tool that accomplishes the necessities of remote sensing plus some additional characteristics such as day-night all-weather operation and good resolution. These characteristics make SAR a very attractive tool in remote sensing but a very expensive operation from the point of view of computational processing and storage costs. Based on advances in signal processing and image processing, for example, fast Fourier Transform (FFT), correlation and convolution techniques, an environment for SAR processing has been developed and constitute the work reported in this paper. The environment includes implementation of one of the SAR algorithms meant for Point target. A MATLAB based environment is presented for signal processing. Special attention is given to the development of algorithm for image formation from raw data. [C1749]

"Design and development of multi-frequency comb generator for space borne microwave active sensors"

An integral part of space borne active remote sensors like scatterometer is the Frequency Generator unit (FG) which caters to the requirement of coherent, highly stable, multiple frequency signals required for the operation of the payload right from clock generation, LO signals to linear frequency transmit signal. At the heart of FG is a comb generator which simultaneously generates some of the required frequencies. This paper presents the design and development of an active frequency multiplier designed using BJT device, with multi frequency output. The comb-generator like active multiplier generates X5, X10 and X17 multiplies of the input frequency simultaneously. Desired signal at 250 MHz, 500 MHz and 850 MHz are generated using a 50 MHz input from a stable crystal source. It features a low input power and low added phase noise. Size of the designed hybrid MIC on 25 mil substrate is 33.5 times 12.7 mm. It also offers rejection to adjacent harmonics to ease the design of subsequent filters. This paper discusses the topology selection, its merits and demerits. It is followed by simulation techniques and critical issues addressed during design. Finally it shows the measured results of the comb generator which has successfully passed through environmental stress screening. [C1750]

"Measurement of soil moisture using microwave radiometer"

The science of microwaves owes its origin to the development of radar. Microwaves are part of electromagnetic spectrum. This field became vitally important as man reached out to space. Frequency range of these waves are from 3 GHz to 30 GHz. Microwaves have unique capabilities in remote sensing. The field of microwaves remote sensing has come to a stage of rapid growth. Microwaves can penetrate clouds and so the sensors can operate in all weather conditions. They are sensitive to the presence of moisture in the soil as well as in vegetation or any another material which absorbs moisture. Microwave sensors are of two types: active sensors and passive sensors. Passive sensors have been used for soil studies for the determination of moisture content, oceanographic application to determine winds over the ocean surface and water vapor content in atmosphere as

well as liquid water content in clouds. Soils are composed of solids, liquids and gases mix in variable proportions. Soil texture depends upon the size of the particle and structure of soil depends on the way particles are arranged. Soil has physical as well as electrical properties. Colour, texture, grain soil etc. comprised the physical properties where the electrical properties include dielectric constant, conductivity and permeability. Dielectric constant is the primary electrical property which is used to estimate emissivity and brightness temperature of soil. Emissivity is an important parameter for microwave remote sensing, which provides information about soils. All substances at a finite absolute temperature radiate electromagnetic energy. Emissivity is the ratio of energy emitted by object to black body maintained at same physical temperature. Emissivity is a function of physical and electrical parameters of the object and electrical parameter of sensors. These are the moisture content in the object surface type (smooth or rough), dielectric constant (ϵ), angle of incidence, polarization. Emissivity can be--obtained from the measured dielectric constant (ϵ) using the available models. The emissivity can be measured by instrument radiometer, which is highly sensitive receiver. Radiometers are passive microwave sensor, which collects the incoming radiations, amplify as well as process the signal, and gives the output, which is linearly related to incoming radiation collected by antenna. The electromagnetic radiations are measured by passive remote sensor in the form of brightness temperature. The radiometer system used here consists of LNBC, receiver and power meter. The LNBC (low noise block down converter) converts the signal to a lower frequency and sends them out to the cable connector, which is connected to satellite receiver via co-axial cable. LNBC have input frequency range 10.75 to 12.75 GHz and noise temperature of 35 degK. The receiver output is connected to microwave power meter. The power monitored is related to incoming EM radiations. The radiometer is calibrated using liquid nitrogen and sky as the targets. Then the EM radiations emitted by dry and wet soil are measured at different look angles (10deg to 60deg) with step of 5deg. The measured power is converted into brightness temperature and the brightness temperature is co-related to soil moisture. In the paper the relation between soil moisture and brightness, temperature is presented. This provides input for determination of soil moisture using passive sensors. [C1751]

"A decade of applying Differential SAR Interferometry on Mount Etna volcano: Analysis at different time and space scales"

Through the last decade, the Differential SAR Interferometry (DInSAR) was more and more applied to measure ground deformation on Mt. Etna, allowing to investigate ground deformation pattern both at broad and local scales. In this paper a few significant results of the experiences carried out at the Remote Sensing Laboratory of the INGV, Section of Catania, are discussed. Many of them are relevant to the most recent eruptive events of this volcano. [C1752]

"Systematic InSAR monitoring of African active volcanic zones: What we have learned in three years, or an harvest beyond our expectations"

We present here a brief overview of some findings and preliminary results obtained after almost three years of systematic monitoring of active volcanic areas in Africa by means of differential synthetic aperture radar interferometry (InSAR). With a database rich of more than 400 SAR scenes of Fogo (Cape Verde), Ol Doinyo Lengai (Tanzania), Nyiragongo-Nyamulagira (DR of Congo) and Mount Cameroon volcanoes, we processed more than 2000 interferograms among which we could detect significant and major geophysical processes: the first dyking event ever captured geodetically in a continental rift (Lake Natron; Northern Tanzania), the co-eruptive deformations of the Lengai, Nyiragongo and Nyamulagira volcanoes, the co-seismic displacements associated to the mb 6.1 February 3rd 2008 Bukavu earthquake as well as the identification of atmospheric induced phase delays over Fogo and Mount Cameroon volcanoes to be attributed to the seasonal oscillations of the inter-tropical convergence zone (ITCZ). These results have been reached given the abundance of data that increases the chances to capture unpredictable events, and capture them with the most favorable interferometric conditions as possible (e.g. in terms of geometrical and temporal baselines that minimized the vegetation-induced decorrelation). They provided strong scientific material as well as tools for hazard assessment. [C1753]

"Support to Aviation for Volcanic Ash Avoidance (SAVAA)"

Volcanic ash is a known hazard to aviation. Currently there are several satellite-based measurements that can detect volcanic substances, notably ash and SO₂ gas, and these have been used in an ad hoc way to provide information to Volcanic Ash Advisory Centres (VAACs) and then to aviation to assist averting danger. While these data have been extremely useful, they lack quantitative value and all the data (except for the recent CALIPSO lidar measurements) lack height information- thought to be critical for aviation. A new project initiated by the European Space Agency (ESA) has been established to support aviation by supplying quantitative and timely satellite-based products and to fill the gaps in knowledge regarding the avoidance of hazardous volcanic clouds. The aims and implementation of the project -Г,ВїSupport to Aviation for Volcanic Ash Avoidance (SAVAA)Г,Вїare described here. The main outcomes of the 3 year project will be the completion of a

demonstration system-VAS3 that will be able to ingest satellite data and meteorological wind fields, compute the injection height profile of volcanic emissions to produce a range of analysis fields (products) that can be swiftly provided to support aviation avoid hazardous volcanic clouds. [C1754]

"Eruptive cycles inferred from ground deformation at Piton de La Fournaise—a case study for the Globvolcano project"

Due to its high eruptive activity, Piton de La Fournaise is an ideal case study to follow ground deformation associated with eruptive activity. Ground deformation is monitored in the field by the Volcanological Observatory of Piton de La Fournaise. GPS data reveal the presence of two time scales of ground deformation: (1) large short-term displacements (up to 20 mm d⁻¹) monitored a few min to hours prior each eruption (2) and since 2000, small long-term ground displacements recorded during pre-eruptive unrests (0.4–0.7 mm d⁻¹ of summit inflation) and after major distal eruptions (0.3–1.3 mm d⁻¹ of summit deflation). The large GPS dataset available to follow the eruptive cycles is particularly useful to validate the remote sensing data as shown by the Globvolcano project. The good correlation between GPS and PSInSAR data recorded during pre-eruptive unrest periods allowed us to validate the ground deformation mapping using PSInSAR data at Piton de La Fournaise. The combination of PSInSAR and GPS data, in the future, will give us complementary data to investigate the ground deformation associated with eruptive cycles on a larger space scale and thus better constrain the deformation sources. [C1755]

"InSAR time series investigation of land subsidence due to groundwater overexploitation in Tehran, Iran"

Land surface deformation associated with groundwater overexploitation is a serious challenge for plain aquifers of Iran, particularly in semiarid and arid region. In the Greater Tehran area, the capital of Iran with a population of 14 million people, ground-water discharge has exceeded natural recharge over the last decades, causing significant drawdown of groundwater level and land subsidence. In this study we use 46 Envisat ASAR data acquired in descending and ascending orbits between 2003 and 2007 to examine in detail the spatio-temporal pattern of land subsidence in Tehran. [C1756]

"SBAS-DInSAR GRID processing on-demand: A case study"

We present the results of the first experiment to plug the Small Baseline Subset (SBAS) DInSAR algorithm into a GRID-based system; the key idea is to combine the robustness of the exploited advanced interferometric SAR approach with the high computing capability provided by a GRID environment. In particular, we have exploited the low-resolution SBAS algorithm and we benefited of the availability of the ESA Grid Processing-on-demand environment. The presented results, carried out on ENVISAT data, provide an overview of the main characteristics of the implemented SBAS-GRID processing solution. [C1757]

"Surface deformation analysis of the Mauna Loa and Kīlauea volcanoes, Hawai'i, based on InSAR displacement time series"

We investigate the deformation of Mauna Loa and Kīlauea volcanoes, Hawai'i, by exploiting the advanced differential Synthetic Aperture Radar Interferometry (InSAR) technique referred to as the Small Baseline Subset (SBAS) algorithm. In particular, we present time series of line-of-sight (LOS) displacements derived from SAR data acquired by the ASAR instrument, on board the ENVISAT satellite, from the ascending (track 93) and descending (track 429) orbits between 2003 and 2008. For each coherent pixel of the radar images we compute time-dependent surface displacements as well as the average LOS deformation rate. Our results quantify, in space and time, the complex deformation of Mauna Loa and Kīlauea volcanoes. The derived InSAR measurements are compared to continuous GPS data to assess the quality of the SBAS-InSAR products. [C1758]

"Microwave Soil Moisture Retrieval Under Trees"

During 2007 a field experiment was conducted with a goal of optimizing microwave soil moisture retrieval algorithms for small to medium deciduous trees. After initial field checkout in Fall 2006, the ComRAD microwave truck instrument system was deployed to a test site with several stands of deciduous paulownia trees. A joint effort of NASA/GSFC and George Washington University, ComRAD consists of a quad-polarized 1.25 GHz radar and a dual-polarized 1.4 GHz radiometer sharing the same antenna. ComRAD can function as a ground-based instrument simulator for L band space missions such as SMOS, SMAP, and Aquarius. In the current study, ComRAD acquired data from April to November 2007 to monitor the seasonal difference in microwave response to soil moisture under deciduous trees. To conclude the three-year planned field measurement effort, ComRAD will deploy to a natural coniferous pine tree site in 2008. [C1759]

"Wide-Area, Planning Level Archaeological Surveys Using SAR and Multispectral Images"

Archaeological sites vary greatly in terms of type, size, and material composition. They have in common only that they humanly caused perturbations of what would otherwise be a landscape ordered by natural causes. Protocols are presented in this paper for detecting archaeological sites that can be characterized generally as positive as opposed to normative, in the way that these two terms are used in the philosophy of science. Positive statements are defined in the philosophy of science as those that are (a) falsifiable and (b) made in the attempt to describe reality. Normative statements, in contrast, describe how things ought to be or are assumed to be. The multi-parameter statistical difference signature development presented in this paper rests upon protocols that test the statement that sensed data recorded at archaeological sites are significantly different from sensed data taken from surrounding landscapes, which is both falsifiable and verifiable. The object of this testing is to find which types of data sensed at archaeological sites are most different from data sensed at surrounding areas. It would seem that previous automated signature development protocols are essentially normative, in that they have the object of finding areas that are similar to idealized models of archaeological sites. The application of this approach to the seven steps of the multi-parameter statistical difference signature development protocols is presented. [C1760]

"Physic and Experimental Issues on High Resolution SAR Imaging of Urban Area"

Here are presented issues about building or urban area high resolution imaging using synthetic aperture radar (SAR). Promises of circular imaging are assessed. Indeed, this acquisition mode, though available only to airborne sensors, has the potential to solve shadow and overlay problem through rotation of the slant range projecting direction. It has also an intrinsic elevation dependency that would allow "along track stereo" reconstruction. This is illustrated from several recent circular/spotlight acquisitions over urban areas. [C1761]

"Polarization Dependence of L-Band Measurements Over the Ocean on Surface Wind at 23-25 Incidence Angles"

Polarization dependence of L-band measurements over the ocean on surface wind is investigated for the incidence angle ranging from 23 to 25 degrees, by using the Phased-Array L-band Synthetic Aperture Radar (PALSAR) onboard the Advanced Land Observing Satellite (ALOS) and MetOp/ASCAT wind vectors. Polarization ratio (VV/HH) shows clear incidence angle and wind speed dependencies. It increases with increasing incidence angle and decreases with wind speed, ranging from 1.8 dB at 2 m/s wind to 0.5 dB at strong wind >12 m/s. These dependences are in good quantitative agreement with the Resonant Curvature Approximation (RCA) model proposed by Mouche et al. (2007). Although relative wind direction dependency of the polarization ratio is not so significant, downwind values are larger than cross- and upwind values at strong winds >12 m/s. [C1762]

"ALOS emergency observations by JAXA for monitoring earthquakes and volcanic eruptions in 2008"

In 2008, many disasters occurred in different places around the world. Remote sensing technique contributed significantly to observing and monitoring those disasters that occurred in remote locations. The ALOS satellite has observed the entire world using three sensors since its launch, thus providing important results soon after disasters strike. By comparing optical images or SAR amplitude images acquired before and after the disaster, we can identify surface changes associated with earthquakes or volcanic eruptions. Such information helps us evaluate risks of second disasters. InSAR observation detected crustal deformation associated with earthquakes, and the geodetic information helped us to understand fault mechanisms. [C1763]

"Palsar Calval and Generation of the Continent Scale Mosaic Products for Kyoto and Carbon Projects"

ALOS/PALSAR has been on the orbit since January 24 2006. After the initial calibration phase, the PALSAR has been being used as the calibrated instrument for the land monitoring. Using the calibration target data of the corner reflectors and the distributed target, it has been confirmed that the PALSAR is well stabilized and calibrated. One of the two major themes that the PALSAR can contribute to, the forest monitoring, is being progressed. The creation of the 50-meter orthorectified multi polarization mosaic, the major part of the providing products, is being generated at Kyoto and Carbon project. Here, the JAXA's contribution, the generation of the Asia SAR mosaic data, is in progress. This paper introduces the PALSAR CALVAL updated information and the quality of the PALSAR ortho-mosaic. [C1764]

"Polarimetric PALSAR System Model Assessment and Calibration"

Polarimetric PALSAR system parameters are assessed using data sets collected over various calibration sites. The data collected over the Amazonian forest permits validating the zero Faraday rotation hypotheses near the equator. The analysis of the Amazonian forest data and the response of the corner reflectors deployed during the PALSAR acquisitions lead to the conclusion that the antenna is highly isolated (better than -35 dB). These results are confirmed using data collected over the Sweden and Ottawa calibration sites. The 5-m height trihedrals deployed in the Sweden calibration site by the Chalmers University of technology permits accurate measurement of antenna parameters, and detection of 2-3 degree Faraday rotation during day acquisition, whereas no Faraday rotation was noted during night acquisition. Small Faraday rotation angles (2-3 degree) have been measured using acquisitions over the DLR Oberpfaffenhofen and the Ottawa calibration sites. The presence of small but still significant Faraday rotation (2-3 degree) induces a CR return at the cross-polarization HV and VH that should not be interpreted as the actual antenna cross-talk. PALSAR antenna is highly isolated (better than -35 dB), and diagonal antenna distortion matrices (with zero cross-talk terms) can be used for accurate calibration of PALSAR polarimetric data. [C1765]

"Land subsidence monitoring using InSAR time series, case study: Mashhad, Iran (2004-2007)"

Interferometric Synthetic Aperture (InSAR) observations acquired by the Envisat satellite in a descending orbit during 2004-2007 are used to study land subsidence caused by groundwater over-exploitation in Mashhad Valley, northeast of Iran. Motagh et al (GJI 2006) presented a preliminary analysis of the subsidence in this area using a few interferograms covering the 2003-2005 periods. This paper utilizes ENVISAT data to retrieve the temporal evolution of the surface deformation in Mashhad. [C1766]

"A Scalability Study on Multicore Cluster Systems of an AFRL Radar Frequency Tomography Imaging Code Written in MATLAB(r) for Parallel Execution Using Star-P(r)"

The Radar Signal Processing Technology Branch of the air force research laboratory (AFRL), Sensors Directorate (Kevin Magde, Principal Investigator) is investigating development of radar frequency (RF) tomography technology for sensing applications. In conjunction with the recent arrival of a remote test facility, the quantity of collected input test data will increase, and the computational requirements will significantly increase. As the team's work involves frequent algorithmic modifications, the team focuses its research writing programs in high-level languages such as MATLAB. Applications are currently running on the team's own small SGI Altix system and exploit parallelism via Interactive Supercomputing, Inc.'s Star-Preg product. Anticipating increased computational requirements, the team would like to use department of defense (DoD) high performance computing modernization programs (HPCMP) major shared resource center (MSRC) systems for some of their work and seeks recommendations moving forward. The team is also interested in processing data at a field location when it is being collected in an effort to improve productivity. This study examines the scalability of example research RF tomography Star-P/MATLAB codes on the Arizona State University Fulton high performance computing Saguaro system, which is an Intel multicore Xeon cluster with an InfiniBand interconnect; this type of system can be found at DoD HPCMP MSRCs. The study provides direction toward shortening the development cycle time for RF tomography imaging experiments, in addition to providing guidance for future computing purchases. [C1767]

"A point target reference spectrum based on Loffeld's bistatic formula (LBF) for hybrid configurations"

This paper concentrates on the focusing for hybrid bistatic SAR configurations, consisting of a space borne/airborne carrier configuration with considerable differences in velocities and altitudes of transmitter and receiver. Therefore the direct implementation of a bistatic SAR focusing algorithm based on Loffeld's bistatic formulae (LBF) cannot be readily applied. An extension of the bistatic point target reference spectrum, based on LBF is derived. Simulated focusing results verify the proposed approach. [C1768]

"Mapping Water Basins in the Eastern Sahara by SRTM Data"

RTM (~90 m) data and Radarsat-1 images of northern Sudan were processed for exploring potential groundwater accumulation sites in the region. Data analysis unveiled three extensive ancient river courses named as Howar, El-Qaab and Arbain. These eastward flowing rivers, which are now partly hidden beneath the sand, are extinct tributaries of the Nile Valley hydro-system. The main channels of these rivers were mapped from Radar data and compared with those delineated by the GIS hydrologic routines. The beds of these river courses, which are now void of moisture, must have hosted a great volume of surface water in the past and played a significant role in recharging the sandstone groundwater aquifers in the region. An ongoing data investigation will provide additional information as to the specific nature of these ancient rivers that will help in future water prospecting in the region. [C1769]

"Reconfigurable L-band radar"

The reconfigurable L-band radar is an ongoing development at NASA/GSFC that exploits the capability inherently in phased array radar systems with a state-of-the-art data acquisition and real-time processor in order to enable multi-mode measurement techniques in a single radar architecture. The development leverages on the L-band imaging scatterometer, a radar system designed for the development and testing of new radar techniques; and the custom-built DBSAR processor, a highly reconfigurable, high speed data acquisition and processing system. The radar modes currently implemented include scatterometer, synthetic aperture radar, and altimetry; and plans to add new modes such as radiometry and bi-static GNSS signals are being formulated. This development is aimed at enhancing the radar remote sensing capabilities for airborne and spaceborne applications in support of Earth Science and planetary exploration. This paper describes the design of the radar and processor systems, explains the operational modes, and discusses preliminary measurements and future plans. [C1770]

"Synthetic Digital Correlation for Combined Polarimetric Microwave Remote Sensing"

Combined passive and active microwave remote sensing can provide complementary information and enhance performance of the retrieval of parameters. In consideration of the combination of passive and active microwave polarimeters in an identical system, an active polarimetric matrix consisting of six parameters is combined with the format of the passive polarimetric parameters matrix which is known as the Stokes vector. A synthetic digital correlation method is designed to perform combined measurements of the two types of parameter matrixes, and to achieve cost saving using shared subsystems and hardware. Performances of the design are analyzed including measurement sensitivities, relative errors, and dynamic range. [C1771]

"On-board SAR compression system based on back-propagation neural network"

Synthetic aperture radar (SAR) is a coherent active and high-resolution microwave imaging system with diverse applications in remote sensing. A significant characteristic of this system is the generation of a large amount of data that involves major problems related to on-board data storage. The near future SAR satellite missions planned would be pushing downlink data bandwidth to prohibitive levels. Given the unprecedented volume of data that will be generated by future high-resolution SAR satellites, the use of innovative data compression techniques will be essential if economically feasible. It is proposed to first pre-process the raw data and then to apply a suitable compression technique like back-propagation neural network whose on-board implementation would be efficient both in terms of speed and power. [C1772]

"Monitoring of bridges using coherent radar: Detection of longitudinal and torsional modes"

A microwave sensor for remote detection of structural displacements is experimented as geotechnical instrument for dynamic and static testing of bridges. The results of a number of validation campaigns are reported: a highway bridge forced by vehicular traffic, a railways bridge, and a pedestrian bridge. Furthermore, in this paper the authors present a novel development of the technique that allows to detect torsional movements too. [C1773]

"Obstacle Based Concept for Compact Mode-Preserving Waveguide Transitions for High-Precision Radar Level Measurements"

This contribution deals with a concept for the realization of compact mode-preserving waveguide transitions. For radar distance measurements, the cross-section of a single-moded waveguide is enlarged to an overmoded circular waveguide. In order to obtain a mostly monomode signal propagation within the waveguide, a parabolic waveguide transition in combination with a centrically mounted metallic obstacle is investigated. In comparison to the same transition without obstacle, a significant improvement in terms of the fundamental H₁₁ mode preservation can be achieved over a wide frequency range from 8.5 to 10.5 GHz. Radar measurements are presented that prove the capability of such a concept providing submillimeter distance accuracy without any need of modifying the applied conventional free-space signal processing algorithms. [C1774]

"Radarsat-2 Moving Object Detection Experiment (MODEX)"

This paper presents an overview of various detection and estimation algorithms that have been implemented in the RADARSAT-2 MODEX Processor as well as experimental plans for the validation and demonstration of the space-based GMTI mode. Preliminary RADARSAT-2 GMTI results are also presented. [C1775]

"Acquisition of reflected GPS signals for remote sensing applications"

Reflected GPS (Global Positioning System) signals, known as multipath signals are one of the contributing factors in error sources during navigation and are therefore mitigated during position and velocity calculations. However, they can be utilized in various remote-sensing applications as they contain valuable information regarding the reflecting surface. One of the major challenges for the practical realization of any remote sensing system based on GNSS (Global Navigation Satellite System) signals is the reception of weak reflected signals owing to their appalling signal to noise ratio. This paper describes the detection and acquisition of reflected GPS signals using a custom made LHCP (Left Hand Circularly Polarized) high gain helical antenna and a two-channel GPS front end and data capturing device intended for the simultaneous acquisition of direct and reflected GPS signals. Details of some initial experiments are presented. [C1776]

"Foreign Objects Debris Detection (FOD) on Airport Runways Using a Broadband 78 GHz Sensor"

This paper describes a compact broadband (73-80 GHz) mm-Wave front-end used for FOD detection application. The design philosophy of our system is to have several low-profile, low-cost mm-Wave sensors placed along the runway. Tests were conducted on the small airport of Aix Les Milles (south of France). High sensitivity and simultaneous objects detection capabilities were shown. Even very small objects like nuts were seen. The extension of the actual detection range is needed in order to go from 110 m (in the most favourable case) to 500 m. [C1777]

"Twelve Years of Radarsat-1 Calibration: Operations Experience and Lessons Learned"

This paper examines the calibration performance of the RADARSAT-1 products since spacecraft commissioning in 1996, and briefly reassesses the calibration ground systems and methodologies in the light of the mission's twelve-year calibration experience and data record. Choices made in the design, deployment and implementation of the RADARSAT-1 calibration plan are retrospectively explored in the context of successor missions, and more specifically RADARSAT-2, which was declared operational on April 25 2008. Preparations at the Canadian Space Agency calibration monitoring activities for RADARSAT-2 are also presented. [C1778]

"Initial Evaluation of Radarsat-2 for Operational Sea Ice Monitoring"

Environment Canada's Canadian Ice Service (CIS) is responsible for the daily monitoring of Canadian coastal waters for ice and icebergs, and the presence of oil-based pollution. The routine provision of information on floating ice conditions promotes safe and efficient maritime operations and protects Canada's environment by providing reliable and timely information to marine users in Canadian waters. The CIS relies on a suite of both airborne and satellite sensors to operationally monitor ice in Canadian coastal and inland waterways. Satellite SAR, primarily from RADARSAT-1 and Envisat ASAR, are the primary satellite datasets used by the CIS for monitoring. On December 14, 2007, RADARSAT-1's successor, RADARSAT-2 was successfully launched. In the winter and spring of 2008, the CIS will be performing an evaluation of the performance of RADARSAT-2 in support of its ice operations. In this work, we will provide a preliminary assessment of the use of this new SAR sensor for monitoring sea ice conditions. Its performance will be compared against RADARSAT-1 and the utility of the new advanced SAR modes (e.g. ScanSAR dual-polarization) for operational ice monitoring will be reviewed based on images collected to date. Preliminary recommendations on mode selection will also be made to assist those interested in using this new platform for ice monitoring. [C1779]

"Back propagation neural network approach for SAR raw data compression"

Synthetic aperture radar (SAR) is a coherent active and high-resolution microwave imaging system with diverse applications in remote sensing. A significant characteristic of this system is the generation of a large amount of data that involves major problems related to on-board data storage. The near future SAR satellite missions planned would be pushing downlink data bandwidth to prohibitive levels. Given the unprecedented volume of data that will be generated by future high-resolution SAR satellites, the use of innovative data compression techniques will be essential if economically feasible. It is proposed to first pre-process the raw data and then to apply a suitable compression technique like back-propagation neural network whose on-board implementation would be efficient both in terms of speed and power. [C1780]

"Lidar Network for Monitoring Asian Dust and Air Pollution Aerosols"

Network observations of Asian dust and air pollution aerosols are being performed in the East Asian region using automated two-wavelength (1064 nm, 532 nm) polarization (532 nm) lidars. At present, the lidars are continuously operated at 20 locations including cooperative observation sites, in Japan, Korea, China, Mongolia and Thailand. The data from the network are transferred to the data center and processed automatically to derive the extinction coefficients for Asian dust and spherical aerosol. (An iterative backward integration method with an assumption of the lidar ratio and the method using the depolarization ratio for estimating the contributions of

non-spherical and spherical aerosols are used in the data processing.) The data from the network are used in various studies including validation/assimilation of dust transport models and the climatological studies of aerosols and clouds. [C1781]

"Model Based SAR Tomography of Forested Areas"

In this paper a technique is described for the tomographic characterization of forested areas through multiple SAR observations. This technique is based on a model of the second order statistics of the multi baseline, multi polarimetric, data which accounts for the presence of multiple distributed targets within the system resolution cell. The results of an experiment performed on a real P-band, multi-baseline, fully polarimetric data set relative to the forested site of Remningstorp, Sweden, are reported. Such results show the feasibility of performing a model based tomographic analysis of forests, resulting in a characterization of both the ground and the canopy in terms of elevation, spatial structure, and scattered power. [C1782]

"Multi-baseline coherence optimisation in partial and compact polarimetric modes"

Modern space-borne SAR sensors, like ALOS-PALSAR, TerraSAR-X and Radarsat-2 all provide at least a "partial polarimetric mode", acquiring only 2 of the 4 elements of the Sinclair matrix, like for example HH and HV or VV and VH. In addition, it has been demonstrated that with certain so-called "compact PolSAR" single-transmit dual-receive techniques one can obtain an estimation of the fully polarimetric information. Such systems are attractive in terms of reduction of pulse repetition frequency, data rate, and complexity and are currently very popular. However, they do not acquire complete information pertaining to the full polarisation state of the target and, as a consequence also coherence optimisation suffers from the reduced configuration space. In this paper, the potential of the different partial polarimetric setups for coherence optimisation is evaluated both theoretically and experimentally and compared to the capabilities of a fully polarimetric system. It will be analysed to which extent partial polarimetric system can improve the derivation of interferometric information from partly decorrelated surfaces, in particular of vegetated or even forested areas. Special attention is paid to the constrained coherence optimisation of multi-baseline setups, important for modern DInSAR techniques like PS analysis and continuous DInSAR monitoring in general. All experimental analyses will be performed using fully polarimetric multi-baseline data sets. For proper comparison, partial polarimetric information is derived from these by matrix transformations according to the respective transmit / receive configuration. [C1783]

"Analysis of Saharan Dust Observations by Calipso in the Context of CRAM"

Since its first collection of lidar data in June of 2006, the Cloud Aerosol Lidar with Orthogonal Polarization (CALIOP) lidar instrument aboard CALIPSO has observed numerous Saharan dust events in Western Africa and the Atlantic, predominantly during the boreal summer months of late May through early September. A tremendous amount of data is currently available from which to begin analysis. With CALIOP's sensitivity to polarization at 532 nm, such dust layers are easily identified by significant amounts of depolarization relative to other aerosol types due to the non-sphericity of dust particles. Dust aerosols represent an interesting basis upon which to examine the performance of the CRAM technique, and in particular its dust model, due to the fact that dust is distinctly identifiable from depolarization. The results from this analysis aim to demonstrate the capability of aerosol modeling as a solution to the retrieval problem, where independent verification of aerosol type (i.e., from 532 nm depolarization and known dust transport paths) may be made to facilitate the investigation. [C1784]

"Polinsar at Low Frequency and Ionospheric Effects"

Global warming is now known to be the major environmental issue mankind will have to face in the next decade. Monitoring of vegetation and biomass is clearly an essential piece of information required at all levels ranging from the scientific studies to understand and forecast, to the political actors and government leaders responsible for drafting remediation policies and evaluating their impact. Microwave remote sensing with the low-frequency SAR technique can provide a useful characterization of forest (spatial coverage, species, density, height...) at a global scale, relying on the all-weather imaging capabilities of SAR linked with the significant penetration of the low-frequency EM wave in the canopy. The published techniques for forest characterization from low frequency SAR data include radiometry inversion, polarimetric inversion based on the anisotropy parameters and PolInSAR Random Volume Over Ground inversion. In this paper, we will more specifically concentrate on the PolInSAR technique and the impact of ionospheric effect on this inversion. PolInSAR at low frequency can be envisioned with two radar platforms flying in formation or as a repeat pass mission. The second alternative is more plausible given the cost and the size of a low frequency SAR instrument. However the two cases will be discussed in the paper. [C1785]

"Image Formation Algorithm for Topside Ionosphere Sounding with Spaceborne HF-SAR System"

The exploration of ionosphere is significant for satellite communication and navigation etc. Spaceborne HF-SAR is utilized for the observation of topside ionosphere, in order to acquire higher spatial resolution, global scale ionospheric electron density map and irregularities distribution. The operation mode and system parameters are introduced. The echo signal of spaceborne HF-SAR has long synthetic aperture time, large range migration, and small depth of focus due to the low carrier frequency. Considering these characteristics of spaceborne HF-SAR, a two dimension time-frequency domain correlation image formation algorithm is presented. The effectiveness of the algorithm is validated by computer simulation results. [C1786]

"Using Combined 532 NM HSRL and 1064 NM Elastic-Scatter Lidar Observations to Verify and Update CRAM Dual-Wavelength Aerosol Retrieval Models"

The widely employed Fernald lidar equation solution relation retrieves aerosol backscatter versus height for an assumed aerosol extinction-to-backscatter ratio, S_a , and known system calibration factor, C , at a given wavelength, subject to the constraint/assumption that S_a is spatially constant over the solution layer (height range). At 532 nm, the calibration factor may be estimated fairly accurately by Rayleigh (molecular) normalization in high-altitude, clean-air regions. For elevated aerosol layers embedded in clean air, the direct transmittance approach may be used to estimate the optical depth of the layer, thereby giving an auxiliary input that permits S_a to be determined as a part of the solution. Otherwise, S_a must be specified based on models or determined through use of some other constraining information. The retrieval at 1064 nm is more problematic because the molecular scatter contribution is much weaker, typically making it difficult to either calibrate by molecular normalization or to accurately estimate the transmittance of an elevated aerosol layer, particularly for the weak signals from satellite lidar or eye-safe airborne lidar. As such, aerosol retrievals from dual-wavelength satellite lidars such as those onboard ICESat and CALIPSO have largely been limited to 532 nm retrievals using a table look-up approach to select assumed S_a values based on climatological/geographically determined models. Dual-wavelength retrievals using a Constrained Ratio Aerosol Model-fit (CRAM) retrieval method, employing AERONET based model ratio parameters, have also been obtained with some success for a few satellite lidar data sets. [C1787]

"Forest Spatial Structure Enhancing Non-Gaussian Texture in Airborne L-Band PolSAR Images"

In this paper, results of texture analyses over coniferous forests using airborne L-band POLSAR data are shown. Interestingly, field experiments have disclosed existence of patch-like sparse areas in a forest division where low order parameters of the K-distribution are calculated in the texture analyses. In order to validate that the observed non-Gaussian texture is related to existence of the patch-like sparse forests, the two-component decomposition method is applied. It is successfully revealed that there is spotted high contribution of ground (double-bounce or direct) scattering in the highly textured forest division. Furthermore, difference of the ground contribution between polarization channels could encourage our understanding of polarimetric variation of the forest texture. [C1788]

"Towards Complex-Valued Neural Algorithms for Forest Parameters Estimation from Polinsar Data"

We discuss the development and application of a Complex-Valued Neural Network (CVNN) algorithm for retrieving forest biomass from polarimetric interferometric SAR data. After discussing some features of the net and of the training procedures, we analyze the performance of the algorithm in inverting combinations of simulated radar backscattering at different polarization states. The CVNN performance is compared with that of other retrieval algorithms. [C1789]

"W-band 2-D Scanning Fully Polarimetric Radiometer System for Remote Sensing Applications"

In this paper, we present the design and calibration of the fully polarimetric radiometer at 94 GHz. For stable and high sensible Stokes parameters measurements, we applied a wideband analog correlator and a total power type receiver with a periodic calibration. To perform the fully polarimetric calibration, a calibration standard was designed and tested. Using the calibration standard, the calibration gain-offset was estimated and evaluated. The measured sensitivities with the integration time of 10 ms are approximately 1.26 K and 1.27 K in the horizontal and vertical channels, respectively. Other performances of the developed system and the calibration are also described and discussed. [C1790]

"Robust vegetation height Extraction using maximum likelihood estimation for Dual-baseline PolInSAR"

Polarimetric SAR interferometry technique has been widely used for parameters extraction of the earth's surface vegetation. In this paper, based on the two layers Random Volume over Ground model, we present a vegetation

height inversion algorithm for dual-baseline PolInSAR data. The method obtained the ground and volume scattering component respectively by using the theory of Freeman polarimetric decomposition. Then the maximum likelihood estimation of the covariance matrix was used to construct the vegetation height for dual-baseline PolInSAR. The proposed algorithm overcomes the restriction of traditional maximum likelihood estimation method which required the parameters of ground scattering to be known. Finally, the experimental results of L-band PolInSAR simulated data show that the algorithm improves the effect of height estimation compare to the coherence method. [C1791]

"A Public Database of Simulated Multidimensional SAR Data for Techniques Validation"

This paper presents a new benchmark for techniques validation based on a multidimensional database of simulated data. By exploiting a SAR simulator of complex targets, series of numerical simulations may be run for specific sets of observation conditions and the results made public. Targets are in principle focused on urban structures, despite any other type of man-made targets may be considered. User interaction has allowed to fix the range of values for some design parameters according to the experience gained with real data. Multi-baseline polarimetric SAR interferometry and SAR tomography are the techniques for which this benchmark has been initially conceived, despite other research areas may also benefit, as multi-temporal or multi-frequency analysis. With the resulting amount of images, an adequate testing set can become available for multidimensional methods, which validation with real imagery is difficult. [C1792]

"Extraction of Forest Biophysical Parameters Using Polarimetric SAR"

There is a continual pressing need for the ability to produce accurate, quick and cost-effective forest inventories to assist with forest management and the development of ecological models. Canada Space Agency's recently launched Radarsat-2 offers the ability to significantly advance this field with its multi-temporal and fully polarimetric C-band SAR capabilities. To explore the usefulness of C-band fully polarimetric data for modeling forest biophysical parameters, Convair-580 polarimetric C-band SAR data have been acquired over the Petawawa Research Forest in Ontario, Canada. An inventory of more than 1600 forest stands with information on species, age, canopy closure, height, stocking, basal area and volume have been obtained in order to determine which SAR parameters are most related to each of these biophysical parameters. The VV polarization, target anisotropy, ratios of the radar cross-section measurements and the order parameter of the K-distributed SAR clutter were found to consistently produce the strongest relationships. [C1793]

"Analysis and Correction of Speckle Noise Effects on Polinsar Data Based on Coherent Modeling"

PolInSAR data is a good example of a high dimensional SAR data. A blind filtering of these data does not make use of possible constraints imposed by the scattering process. In this paper it is shown that the scattering over forested areas induces some constraints on the data that can be fruitfully exploited to improve the final filtering, with consequent improved quantitative estimation process. [C1794]

"Quantifying and Correcting Ionospheric Effects on P-Band SAR Images"

Faraday rotation and scintillation will seriously affect P-band SAR images if methods are not used to deal with them. There are published methods for correcting Faraday rotation when polarimetric data are available, but less is known about scintillation. Scintillation is unlikely to present a problem if data acquisitions at low and mid latitudes avoid the post-sunset equatorial region, but correction procedures are likely to be needed in the auroral zones. Such correction is possible using autofocus methods; this is demonstrated using the Phase Gradient Algorithm applied to SAR imagery seriously affected by simulated scintillation. [C1795]

"Modeling and Interpretation of the Multitemporal and Multibaseline Polinsar Coherence"

This paper focuses on the physical understanding of the polarimetric interferometric SAR (PolInSAR) coherence, and on the accurate utilization of this coherence for vegetation parameter inversion. A polarimetric interferometric vegetation model presented here provides the possibility to estimate parameters related to ground topography, vegetation, and surface scattering. In particular, one can estimate such vegetation characteristics as the main orientation, the degree of orientation randomness and the effective shape of the particles, together with structural parameters like the ground height and the depths of vegetation layers. The polarimetric model is based on the Freeman's three component decomposition, which is extended to consider vegetation orientation. To enhance polarimetry, a complementary interferometric coherence model is presented. The model and the parameter inversion method are tested on accurate electromagnetic simulations of real forests. Parameter inversion performance is evaluated for single-baseline and multibaseline data. [C1796]

"Temporal Decorrelation Studies for Vegetation Parameter Estimation with Space-Borne Radars"

The SAR/InSAR component of the NASA DesdynI mission for measuring vertical vegetation structure from space consists of four possible approaches. These include the use of radar backscatter to estimate biomass, to employ PolInSAR relative phase for measuring the vertical extent, the use of interferometric phase and a ground reference, or the use of interferometric correlation magnitude alone. Temporal decorrelation is a significant contributor to decorrelation of interferometric echoes and is not always separable from volumetric decorrelation hence contributing to uncertainties in vegetation parameter estimates obtained using just correlation magnitude. In this text we analyze data that is close to the best case scenario for isolating temporal decorrelation. With almost zero baseline and a repeat pass of one day, SIR-C data over the eastern US serves as our case study of temporal decorrelation. [C1797]

"SAR Derived Wind Fields of Mesoscale Cyclones"

In this study we show how satellite images taken by space-borne radar sensors can be used to determine mesoscale high resolution wind fields in synergy with cloud parameters from optical data. The aim of this study is to use Synthetic Aperture Radar (SAR) and Medium Resolution Imaging Spectrometer (MERIS) onboard the ENVironmental SATellite (ENVISAT) in synergy to analyse severe weather systems. We investigated the fine scale structure of a severe weather case on Nov 1, 2006 over the North Sea using satellite data. The satellite data are compared with numerical model results of the German Weather Service "Lokal Modell", LM and the High Resolution Limited Area Model, HIRLAM. LM and HIRLAM show differences in mesoscale turbulent behaviour. Maximum wind speeds of up to 25 m/s are measured by SAR and are confirmed by the models. Significant differences are observed in the location of the maxima. Due to the high resolution ENVISAT ASAR measurements provide very detailed information on small scale atmospheric features, which seem to be not well captured by the analyzed numerical models in particular in coastal areas.. [C1798]

"Analysis of Temporal Decorrelation in Dual-Baseline Polinsar Vegetation Parameter Estimation"

Vegetation parameters can be estimated using the single-baseline polarimetric synthetic aperture radar interferometry (POLinSAR) data based on the random volume over ground (RVoG) model. Temporal decorrelation, which is the coherence loss due to scene changes within the time between radar data acquisitions, will decrease the estimation accuracy and needs to be compensated. The RVoG+VTD model is a simple model incorporating a temporal decorrelation term into the RVoG model. The inversion of RVoG+VTD model can not perform due to the limited number of single-baseline POLinSAR observables. Dual-baseline POLinSAR approach provides more observables and hence can be used to invert the model. This paper introduces and analyzes the dual-baseline inversion procedure of RVoG+VTD model and validates them using simulated data. [C1799]

"Detection of Single and Multiple Scatterers in Multibaseline Multitemporal SAR Data"

This work is focused on the detection of single and multiple scatterers in multiview/multitemporal SAR data in order to locate and monitor a high number of ground structures with low signal misinterpretation. This issue is addressed here by combining amplitude and phase data, differently from common techniques for the detection of single scatterers which rely on phase coherence measures. Experiments with real satellite C-band data are presented with both full resolution and multilook processing. [C1800]

"3D Tomographic and Differential Tomographic Response to Partially Coherent Scenes"

Much interest is continuing to grow in advanced SAR methods for full 3D imaging of volumetric scatterers, in particular forests. Multibaseline SAR tomographic elevation beam forming is a promising technique in this framework. In this paper, the effect of temporal decorrelation during the repeat pass multibaseline acquisition on the advanced adaptive elevation beam forming tomography is analyzed, using a simple temporal decorrelation model. Also, the response of the recently introduced differential tomography technique, producing "space-time" signatures of scattering phenomena in the SAR cell, is investigated in the same conditions. Finally, first analyses of tomography robust to some temporal decorrelation phenomena through differential tomographic processing are carried out for simulated temporal decorrelating volumetric scatterers. Preliminary differential tomography results with real L-band forest data are also presented. [C1801]

"SAR Coherence Tomography for Boreal Forest with Aid of Laser Measurements"

In this paper we evaluate X- and L-band SAR coherence tomography in boreal forest with the help of detailed digital terrain and canopy height models, produced by laser scanning. Polarimetric coherence tomography (PCT) needs accurate estimates of ground phase and tree height. Supplemental accurate elevation models allow us to

evaluate the performance of PCT in normal case when initial values are derived from RVoG model inversion and provides opportunity to use PCT for nonpolarimetric data. The work is based on E-SAR L-band and X-band measurements in Finland. Our results show that with accurate elevation and tree height information single polarization X-band coherence tomography is feasible and works well. Accurate ground elevation information improves also the performance of fully polarimetric repeat pass L-band PCT. The laser DEM provides better ground phase estimate than RVoG model inversion in the presence of temporal decorrelation. Our results show that accurate ground phase estimation is more critical for successful coherence tomography than other parameters. [C1802]

"Analysis of Atmospheric Propagation Effects in TerraSAR-X Images"

TerraSAR-X, the first civil German synthetic aperture radar (SAR) satellite has been successfully launched in 2007, June 15th. After 4.5 days the first processed image has been obtained. The overall quality of the image was outstanding, however, suspicious features could be identified which showed precipitation related signatures. These rain-cell signatures motivated a further in-depth study of the physical background of the related propagation effects. During the commissioning phase, a total of 12000 scenes have been investigated for potential propagation effects and about 100 scenes have revealed atmospheric effects to a visible extent. An interesting case of a data acquisition over New York will be presented which shows typical rain-cell signatures and the SAR image will be compared with weather-radar data acquired nearly simultaneously (within the same minute). Furthermore, in this contribution we discuss the influence of the atmosphere (troposphere) on the external calibration (XCAL) of TerraSAR-X. By acquiring simultaneous weather-radar data over the test-site and the SAR-acquisition it was possible to improve the absolute calibration constant by 0.15 dB. [C1803]

"Mapping the Ionosphere Using L-Band SAR Data"

The influence of the ionosphere on spaceborne SAR signals can be significant, especially approaching wavelengths at L-band or larger. By measuring these effects and inverting the underlying physical model, these effects can be used to measure and map aspects of the ionosphere. ALOS PALSAR data is employed to demonstrate this capability. Single-pol data is used to determine second-order gradients of the ionospheric Total Electron Content (TEC) (the second derivative of intensity). Dual-pol can yield lateral TEC variations in homogeneous areas. Finally, Faraday rotation measurements from full-pol data can be used to create 2-D maps of the absolute TEC. [C1804]

"Overview of Wind Lidar Techniques and Current Related Developments at the Technical University of Catalonia"

The Lidar group in the Technical University of Catalonia is actively working in wind lidar techniques. An extensive review of such techniques is presented. A special emphasis is made on the direct Doppler technique and the direct motion technique with a lines-of-sight scanning pattern. Current developments are also mentioned. [C1805]

"Initial Assessment of the Applicability of TerraSAR-X for Repeat-Track Interferometry"

In our contribution we present an initial assessment of the applicability of TerraSAR-X for repeat-track interferometry. A series of TerraSAR-X repeat observation in stripmap mode over an test site that includes different land use classes as well as fast and slow deformation phenomena was selected for our investigation. From our investigation we conclude that long-term interferograms can mainly be interpreted over urban areas. For forested areas and for denser agricultural vegetation such as fully grown crops the coherence levels are very low even for 11 day intervals. For sparse vegetation as present in late winter the coherence is high, over many fields even over several 11-day cycles. The high spatial resolution is ideal to measure localized deformation patterns. For slow deformation at larger scale confusion with atmospheric effects is strong. Multi-temporal approaches can be used to resolve the deformation and atmospheric phase components if sufficient numbers of observations are available. [C1806]

"RADARSAT ScanSAR Wind Retrieval and Rain Effects on ScanSAR Measurements Under Hurricane Conditions"

RADARSAT-1 ScanSAR SWA images of Hurricane Katrina are used to retrieve surface wind vectors over the ocean. Collocated H*wind wind directions are used as the wind direction while the wind speed is derived from SAR sigma_{deg} by inversion of a C-band HH-polarization Geophysical Model Function (GMF) that is derived from the VV-polarization GMF, CMOD5, using a polarization ratio model. Because existing polarization models do not fit the ScanSAR SWA data well, a recalibration model is proposed to "recalibrate" the ScanSAR SWA images.

Validated with collocated H*wind wind speed estimates, the mean difference between SAR-retrieved and H*wind speed is small and the root mean square (RMS) error is below 4 m/s. Rain effects on the ScanSAR measurements are analyzed for an incidence angle range of 22deg to 23.6deg using collocated ground-based Doppler weather radar (NEXRAD) rain measurements. [C1807]

"Gaussian model adaptive time domain filter (GMAT) for weather radars"

This paper presents an adaptive time domain filter for ground clutter filtering and signal parameter estimation for dual-polarization capable weather radars. The auto-covariance function of radar signal can be expressed as a sum of auto-covariance functions of the clutter, precipitation and noise that follow Gaussian forms. The filter matrix is designed such as when it is applied to the time series data, clutter component in the signal will be transformed to noise (i.e. the auto-covariance matrix is diagonal). However, weather echoes overlap clutter are also suppressed. An interpolation procedure then is used to recover the transformed part of the weather. The proposed design overcomes limitations of current spectral processing method caused by finite length of the data. A unique filter can be designed to use for both H and V channels for dual-pol parameter estimation. This way ensures the correlation between the two channels and minimizes estimate errors. In addition, the filter can be directly extended for staggered PRT 2/3 sampling scheme. The filter performance analysis was done using simulated time series radar data and CSU-CHILL measurements. [C1808]

"Automatic Detection and Classification of Buried Objects in GPR Images Using Genetic Algorithms and Support Vector Machines"

This work presents a novel pattern recognition approach for the automatic analysis of ground penetrating radar (GPR) images. The developed system comprises pre-processing, segmentation, object detection and material recognition stages. Object detection is done using an innovative unsupervised strategy based on genetic algorithms (GA) that allows to localize linear/hyperbolic patterns in GPR images. Object material recognition is approached as a classification issue, which is solved by means of a support vector machine (SVM) classifier. Results on synthetic images show that the proposed system exhibits promising performances both in terms of object detection and material recognition. [C1809]

"Singular Unit Restoration Based on Complex-Valued Markov Random Field Model for InSAR Interferograms"

The complex-valued Markov random field (CMRF) model is a powerful basis in complex-amplitude image processing. In this paper, we propose a method to reduce singular points (SPs) included in interferograms based on the CMRF model by focusing on the local pixel-value correlation. We deal with the SP-forming four pixels as a set, namely the singular unit (SU), in the CMRF-based compensation of data values distorted in electromagnetic-wave propagation with interference. We find that the method reduces the SP number with less processing distortion. [C1810]

"High Resolution Remote Sensing Image Analysis with Exogenous Data: A Generic Framework"

With the recent (or in the very next future) availability of high resolution optical and radar satellite sensors, the need of multi-sensor image processing systems able to assist human operators in scene interpretation is more and more crucial. This paper focuses on remote sensing image understanding with exogenous data, in the framework of cartographic applications. We propose a processing chain for cartographic database creation/update using high resolution (metric and submetric) optical and/or radar remote sensing images. [C1811]

"Inferring Deformation Fields from Multidate Satellite Images"

We focus on a geophysical application of image processing: the measurement of high resolution ground deformation from two optical satellite images taken at different dates. Disparity maps estimated from image pairs usually lack quantitative error estimates. This is a major issue for measuring physical parameters, such as ground deformation or topography variations. Thus, we propose a new method to infer the disparity map. We adopt a probabilistic approach, treating all parameters as random variables, which provides a rigorous framework for parameter estimation and uncertainty evaluation. We start by defining a generative model of the data given all model variables. This forward model consists of warping the scene using B-Splines and applying a spatially adaptive radiometric change map. Then we use Bayesian inference to invert and recover the a posteriori probability density function (pdf) of the disparity map. The method is validated on multidate SPOT 5 imagery related to the Bam earthquake (Iran), showing results compatible with INSAR measurements. [C1812]

"Fourier Array Processing for Buried Victims Detection Using Ultra Wide Band Radar with

Uncalibrated Sensors"

The purpose of this paper is to propose a new way to detect victims buried in or under layers of rubble or debris in case of disasters such as earthquakes, fires or terrorist attacks. The method is based on Fourier processing and principal component analysis (PCA). It utilizes a moving array of sensors arranged in the line of motion. It combines the speed and robustness of Fourier-based processing with a capability of space-time adaptive processing (STAP) to detect objects moving at extremely low velocities. The concept is demonstrated on several experiments carried out using an ultra wide band (UWB) ground penetrating radar (GPR). A fast, yet robust and extremely sensitive technique is being tested to achieve detection of the slightest motion (such as breathing) of a subject using uncalibrated sensors. [C1813]

"Characterization of Backscatter by Surface Features in L-Band Active Microwave Remote Sensing of Soil Moisture"

Satellite-based remote sensing of soil moisture is generally conducted with active (radar) and passive (radiometer) microwave measurements. During active microwave remote sensing the backscattering from the target i.e, the soil surface is adversely affected by the overlaying vegetation, consequently, sending degraded signal back to the radar sensor. This phenomena greatly compromise with the quality of soil moisture measurements. The proposed research presents an algorithm that averts usage of theoretical and empirical backscattering models. The algorithm uses Soil-Vegetation-Atmosphere-Transfer model for soil moisture estimation that is used to quantify the backscattering components of radar signals. The algorithm has simple and valid assumptions that convert the total radar backscattering equations for a particular temporal scale into a set of simple linear systems. The algorithm reasonably estimates the stochastic surface roughness and vegetation backscattering components. [C1814]

"Analysis of Valid Ranges in Soil Inversion Models Based on the Cloude-Pottier Decomposition"

In this paper we improve the valid range analysis method in soil inversion models, using entropy/alpha space in the Cloude-Pottier decomposition theory. The ranges in data where inversion models can be applied are called the valid ranges of the inversion models. The improved valid ranges are considered more accurate through the Integral Equation Method (IEM) simulations. General method used to find out valid ranges of inversion models is the Normalized Difference Vegetation Index (NDVI), which shows the areas where the vegetation over soil is not too heavy for inversion models to apply. The proposed method introduces entropy/alpha parameters to the analysis of valid ranges, because these two parameters are closely related to target scattering mechanisms. Experiment results with fully polarimetric AIRSAR data show that the effectiveness of inversion models is increased by adding entropy/alpha space analysis. [C1815]

"An Adaptive Method for the Construction of Digital Terrain Model from Lidar Data"

To generate a DTM, measurements from above-ground features such as buildings, vehicles, and vegetation have to be classified and removed, which is nontrivial. The above-ground features present great challenges in conjunction with varying slopes of the ground. In this paper, we present a method to remove above-ground LiDAR measurements and generate DTMs by using adaptive window size according to the local gradients. Iterative construction measurements are performed until difference between two iterations are minimum. In our experiments, we apply our method to the LiDAR data acquired from the downtown region of New Orleans. It was demonstrated that the adaptive window method can remove most of the above-ground points effectively. [C1816]

"Automatic Point Target Detection for Interactive Visual Analysis of SAR Images"

Point target analysis is an important tool to analyze the quality of SAR images. To permit interactive visual analysis, visualization applications need to automatically detect point targets in a SAR image and estimate associated quality measurements such as the peak sidelobe ratio (PSLR). This task is computationally expensive. In this paper, we propose methods for automatic point target detection that work on hierarchical data structures and process the image data on the graphics processing unit (GPU) to allow interactive use. For each detected point target in the currently visualized area of the image, the visualization application can then display color-coded quality measurements, thus providing the user with an overview of the point targets in the scene as well as an immediate impression of the SAR image quality. Detailed point target analysis results can be displayed on demand. [C1817]

"Non-Parameter Correlation Analysis in Polarimetric Signature and its Application to Change Detection in Polarimetric SAR"

Gonradsen et al. developed a change detection method with multilook fully polarimetric Synthetic Aperture Radar

(SAR) data. The method is based on complex Wishart distribution supposition limits the applicable scope of test statistic, especially when only polarimetric diversity (the texture and speckle statistics depend on polarization) and not radiometric diversity. On the other hand, the polarization signature has the capability of representation of the polarimetric diversity. A new test statistic for equality of two polarization signature is proposed in this paper. Without statistical distribution hypothesis, it can give the associated asymptotic probability measure as the Conradsen's method just by non-parameter correlation analysis. Some experiments have been done in this paper with ALOS-PALSAR data by two different algorithms. It has been shown that the new method is effective. [C1818]

"Classification of Lidar Data Using Standard Deviation of Elevation and Characteristic Point Features"

A simple classification scheme is proposed for LiDAR data from a mixed urban area. The basic classifications are urban, low, high, and other vegetation, and water. Standard deviation of elevation within a grid cell, point return number, number of returns per pulse, and point return intensity are used to classify each point individually. Additional classifications are based on the average elevation of the basic classes. The scheme classifies up to three-quarters of data points. [C1819]

"SAR Target Recognition Based on MRF and Gabor Wavelet Feature Extraction"

This paper presents a method for synthetic aperture radar (SAR) target recognition based on Markov random field (MRF) segmentation and Gabor wavelet transform feature extraction. ICM algorithm which based on Markov random field is used to segment a SAR target chip into target and background two fields and generate a two-value figure. Gabor wavelet transform is applied to extract feature vectors from the two-value figure. The method is verified by recognizing three-class targets in MSTAR database. The highest average probability of correct classification arrives at 93.11%, which indicates that the approach proposed in this paper is an effective method for SAR target recognition. [C1820]

"Texture Analysis and its Application for Single-Band SAR Thematic Information Extraction"

In this paper single-band and single-polarization Radarsat-1 SAR image is used to evaluate image classification with textural analysis. Firstly, the statistic information of sample were analyzed using semivariogram to determine the optimum parameters for textural extraction; Then four textures such as Homogeneity, Mean, Angle Second Moment and Entropy had been calculated based on GLCM, and the image data were processed using Support Vector Machine classification. The results show that the water and settlement areas are extracted accurately with accuracy 99.34% and 82.54%, and the SVM method has better extension ability for SAR image classification; Assisting with textural information, the image classification based on SVM has a obvious enhancement to original SAR, especially for some complex objects such as settlement areas (about increasing accuracy 18%). [C1821]

"Extended Subspace Method for Remote Sensing Image Classification"

This study proposes an extended subspace method (ESM) in feature extraction and dimension-reduction problems for land cover classification of hyperspectral and multi-spectral remote sensing images. The main idea of our method is to use a multiple similarity method (MSM) onto an averaged learning subspace method (ALSM) and makes use of fidelity value criteria in the selection of the optimal subspace dimensions. This method is compared with the support vector machine (SVM) method using Compact Airborne Spectrographic Imager-2 (CASI-2) hyperspectral remote sensing data. Experimental results show that ESM is a valid and effective alternative to other pattern recognition approaches for the classification of remote sensing data. [C1822]

"Super-Resolution of Polarimetric SAR Images Based on Target Decomposition and Polarimetric Spatial Correlation"

Polarimetric SAR (PolSAR) is becoming more and more popular in remote sensing research area. Super-resolution processing of PolSAR image is usually desired for PolSAR image applications, such as image interpretation and target detection. Usually in a PolSAR image, each resolution contains several different scattering mechanisms. If these mechanisms can be allocated to different parts in one resolution cell, the details of the images can be enhanced, which means the resolution of the images is improved. In this paper, a new super-resolution algorithm for PolSAR image processing is proposed, in which target decomposition and polarimetric spatial correlation are both taken into consideration. Results of ESAR L-band full polarized images have validated the effectiveness of the proposed method. [C1823]

"A New Method to Retrieve Soil Moisture at Bare Soil Surface Using ERS Scatterometer Data"

ERS wind scatterometer provides capability of the multiple angles by their three different look antennas, In this study, we evaluate whether the multi-incidence angle observations can help on improving surface soil moisture estimations. With the theoretical surface backscattering model-the advanced integral equation Model (AIEM), we first simulated a surface backscattering database with a wide range of surface roughness and soil moisture properties at different incident angles. Then, a parameterized surface backscattering model is developed using the simulated database. The newly developed simple model has the roughness function that can be described by a single combined roughness parameter from the commonly used surface roughness descriptors (RMS height and correlation length). This makes it possible to be used as an inversion model. We will demonstrate this simple model development, its accuracy, and inversion test by using the ground measurements from the Intensive Observation Period (IOP'98) field campaign in 1998 of the Global Energy and Water Experiment (GEWEX) Asian Monsoon Experiment Tibet (GAME/Tibet). [C1824]

"An Airborne Remote Sensing Experiment for Catchment-Scale Water Cycle Study in a Typical Inland River Basin of China"

A simultaneous airborne, satellite and ground based remote sensing experiment which is aiming to improve the observability, understanding, and predictability of hydrological and related ecological processes at catchmental scale is implemented in a typical inland river basin of northwest China. The experiment is composed of the cold region, forest, and arid region hydrological experiments as well as a hydro/meteorological elements and Doppler radar precipitation observation experiment. Airborne microwave radiometers at L, K and Ka bands, hyperspectral imager, thermal imager, and lidar are used. Various satellite data are collected. Based on these observations, the remote sensing retrieval models and algorithms of water cycle variables can be developed or improved, and a catchment-scale land/hydrological data assimilation system is going to be developed. [C1825]

"Surface Roughness Classification with Multipolarized C-Band SAR Data"

In this paper, we propose a methodology to classify surface roughness in agricultural fields with multipolarisation C-band SAR data. This information can help constraining the inversion of the Integrate Equation Model for soil moisture retrieving. Also, it could support annual surveys on agricultural practices. [C1826]

"Potential of C-Band Multipolarized and Polarimetric SAR for Soil Drainage Classification and Mapping"

Among the various soil properties, drainage is the most important one for land productivity as well as the environmental management. Classification and mapping of regional and local soil drainage conditions and hydrologic soil groups are often required as input in many hydrological models used for assessing soil degradation processes and soil vulnerability to environmental losses under intensive agricultural production. The objective of this study was to evaluate the capability of high resolution SAR remote sensing data for mapping soil drainage. Backscattering coefficients (HH, VH, VV, RR, LL, psi45deg and psi135deg) extracted from CV-580 SAR were analyzed as function of drainage classes according to the land use (bare soil, annual crops). The multipolarization data showed a maximum of difference of 2 dB between drainage classes. Discriminant analysis performed after applying principal component analysis (PCA) showed overall classification accuracy of 60% for drainage classes. Only the poorly drained class was clearly discriminated (73-97%) under agricultural fields. Introducing the polarimetric parameters (mean alpha_ angle, entropy (H), and anisotropy (A)) in the general discriminant classification, the soil drainage classification accuracy was improved particularly by the anisotropy parameter. The study demonstrated the potential of C-band multipolarized and polarimetric SAR for soil drainage classification and mapping. However, the high spatial resolution of the CV-580 showed high variability of scattering mechanisms associated to the fall acquisition period, where many crop fields were harvested but some corn fields being not. Spring acquisition near seeding of RADARSAT-2 (launched on December 14, 2007) imagery, should give better classification results. [C1827]

"High Wind and Power Density Over Global Oceans"

Spacebased scatterometer measures ocean surface roughness, which is in equilibrium with surface stress (momentum flux). Under general conditions, the variation of stress is reflected in the variation of winds. Eight years of QuikSCAT data are used to give a good representation of the probability distribution and power density of wind speed over global oceans and to provide useful applications. For hurricane-scale winds (> 35 m/s), present scatterometer measurements are not sensitive to increase in winds. Although strong efforts have been made to adjust the model functions for retrieving winds under moderate wind to the strong wind conditions and to improve the sensor design to retrieve strong winds, such effort is likely to be limited by the natural process of turbulent transport. Surface stress does not increase with wind in hurricane-scale winds due to flow separation. [C1828]

"High-Velocity Wind Measurements Using Synthetic Aperture Radar"

The change in accuracy of synthetic aperture radar (SAR) near-surface wind measurements as a function of increasing wind speed is assessed by matching satellite SAR measurements with wintertime buoy measurements in the Bering Sea. For wind speeds less than 15 m/s, SAR-buoy wind speed comparisons show biases less than 1 m/s with standard deviations less than 2.5 m/s. For wind speeds from 15 to 25 m/s, SAR wind measurements have a positive bias above 2 m/s and somewhat more scatter when compared to buoy winds. For winds larger than 25 m/s, the accuracy of SAR winds is not well known. Very few buoy matches are available. Comparisons of SAR winds with hurricane model winds and aircraft measurements are still in a preliminary stage, but indicate that improved algorithms are needed. [C1829]

"Rain and Wind Estimation from Seawinds in Hurricanes at Ultra High Resolution"

A Bayesian method for estimating wind and rain in hurricanes from SeaWinds at ultra-high resolution is developed. We use a hurricane model to generate prior distributions for the wind speed, wind direction, and rain rate. The rain prior is derived from data from the Tropical Rainfall Measuring Mission Precipitation Radar (TRMM-PR). The new method reduces the variability of the standard simultaneous wind and rain estimates while preserving meso-scale detail. [C1830]

"Scatterometer-Derived Wind Fields for Mid-Latitude Storms"

Data from several satellite passes can be combined to produce surface vector wind fields for the bulk of the storm. A wide range of gridding techniques and assumptions can be used to produce these gridded wind fields, each with substantial strengths and weaknesses. For example, numerical weather prediction (NWP) tools can be used to assimilate the satellite data, and to advect information to a common time. However, such models tend to have rather poor boundary-layer physics, and imposed physical assumptions rarely work well for severe weather. These problems are much worse in the tropics than in mid-latitudes; however, they remain a serious problem for warm core seclusions (mid-latitude storms with a core that is warm relative to its surroundings), which are extremely powerful storms. Another problem with these storms is that they tend to translate very rapidly and change their structure on short time scales compared to NWP output. These rapid changes hamper traditional objective analysis techniques, greatly limiting the time window for which data can be usefully assimilated. Data from adjacent scatterometer passes (less than two hours difference) have been used with some success in the representation of patterns for wind speed and direction. Spatial derivative of wind vectors are often of more interest for ocean and atmospheric dynamics. In this study, the vorticity field (the curl of the winds) is investigated in the context of warm core seclusions. The vorticity is calculated in the individual swaths (prior to regridding), and in the gridded product. [C1831]

"Active and Passive Microwave Sensors as a Tool to Monitor Soil Moisture Over Winter"

The present case study focuses on monitoring the wetness state of the experimental Bibeschbach catchment (10.8 km²), located within the Alzette river basin in the Grand-Duchy of Luxemburg over the last three winters (2005-2008). The objectives of this study are (1) to retrieve soil moisture from spaceborne active and passive microwave sensors, namely AMSR-E and ERS-2 SAR, (2) to compare the remote sensing-derived estimates of basin-averaged soil moisture with ground measurements that are performed throughout the catchment. [C1832]

"KU-Band Sensitivity to Soil Moisture. An Evaluation Study for Monitoring Temporal Soil Moisture Change Detection Over the NAFE06 Study Area"

The combination of radiometer and radar observations is a very promising technique for spatial disaggregation of soil moisture. The enhanced QuikSCAT sigma-0 product (2.225 km) offers a possibility for overcoming the temporal and spatial limitations of the available radar systems. The current study investigates QuikSCAT sensitivity to soil moisture and its capability to accurately monitor and capture change in soil moisture. The research was undertaken for the National Airborne Field Experiment area located in the Murrumbidgee catchment, SE Australia. Validation of the temporal change detection analysis was undertaken using an airborne soil moisture product derived from the Polarimetric L-band Multibeam Radiometer (PLMR). The main propose of the PLMR use was to assess accuracy in terms of spatial patterns distribution. The results reveal expected temporal variability and adequate response of the active sensor to change in meteorological conditions. The presence of irrigation and standing water (rice fields) in the region challenges the spatial agreement throughout the study area. [C1833]

"Soil Moisture Change Retrieval Using S-Band Radar Data During SGP99 and SMEX02"

HJ-1C will be launched at the end of 2008, it is a component of HJ satellites which are developed in China. HJ-1C SAR has a frequency of S-band (3.2 GHz), VV single polarization, and incident angle range from 25deg-47deg. Soil moisture retrieval using L- and C-band radar has been widely studied, but little attention was paid to S-band data. For the application of HJ-1C SAR, in this paper, the available data of S-band radar data by PALS (Passive and Active L- and S-band sensor) from SGP99 and SMEX02 experiments was used to study the potential of soil moisture change retrieval using S-band single polarization radar. [C1834]

"Error Estimation of Soil Moisture Derived from Active and Passive Microwave Satellite Observations and Model Data"

Triple collocation error estimation is a powerful tool to simultaneously estimate the error structure and calibrate a set of independent observations. In this study, we use this technique to estimate the errors of a passive microwave (TRMM-TMI) derived, an active microwave (ERS-2 scatterometer) derived and a modelled (ERA-Interim reanalysis) soil moisture data sets. [C1835]

"SAR Remote Sensing Data for Subsurface Targets Detection and Lop Nur Lake Evolution and Extinction Study"

This paper presents the observation from SAR images of the dried Lop Nur Lake in Xinjiang of west China. Lop Nur Lake is one of the driest places in the world and finally lost its last drop of water in 1972. It is well known for its "human ear shape" feature in optical remote sensing images. Likewise, the "ear" feature is shown in synthetic aperture radar (SAR) images, and is even larger because of the penetration effect. The universal existence of lacustrine deposit with high water content and salinity are undetectable by previous remote sensing images in Lop Nur Lake. We have made some laboratory experiments about subsurface soils and developed an improved dielectric model for moist saline soil at microwave bands. A field trip was conducted from October 25 to November 8, 2006 to validate the image interpretation results. As an important indicator for environment degradation and climate change study in arid region, Lop Nur does need long-term and overall research to answer many scientific questions. [C1836]

"Calibration of IEM Model for the Soil Moisture Mapping of Non-Inundated Paddy Fields Using ALOS/PALSAR Data"

This paper reports calibration of model parameters to estimate soil moisture of non-inundated paddy fields using SAR (synthetic aperture radar) data. The IEM (Integral Equation Method) model, theoretical model to represent surface scattering in the microwave region, was examined. Surface roughness parameters (standard deviation of surface height, autocorrelation function of the surface height, and autocorrelation length) are important parameters for microwave backscattering. However, the surface roughness of the paddy fields was found to change, and the autocorrelation length is quite difficult to accurately measure on the surface. Therefore, the two parameters, standard deviation of surface height, and autocorrelation length, were calibrated with actual soil moisture. As a result, it was found that the objective function to minimize the sum of residuals between estimated soil moisture and actual soil moisture produced the most optimal estimation results. In this case, the root mean square of errors between the estimated volumetric soil moisture and the actual soil moisture used for the calibration was 9.4%. This can be acceptable to consider the fluctuation of the surface roughness parameters during the non-inundated season. [C1837]

"Preliminary Polarimetric Measurements of Bare and Vegetated Soils Radar Backscattering Coefficients and Brightness Temperatures Angular Dependences at 15GHz"

In this paper preliminary results of bare soil and soil vegetation radar backscattering coefficient and brightness temperature angular dependences at 15 GHz are represented. The results were obtained by combined radar-radiometer system moving along a quarter circle shaped measuring platform of 7 m of radius. [C1838]

"A New Method for Identification and Analysis of Persistent Scatterers in Series of SAR Images"

Synthetic aperture radar (SAR) interferometry is a powerful technology for measuring slow terrain movements. The extraction of this information is a complex task, because the phase of the signal is measured only modulo 2π and is affected by noise and systematic terms. The persistent scatterer (PS) approach brought important advances in the solution of this problem. In this work, we present a new method, named persistent scatterer pairs (PSP) method, for the identification and the analysis of PS in series of full resolution SAR images. The problems coming from orbital and atmosphere phase artifacts are effectively overcome by exploiting their spatial correlation, without using model based interpolations or fits, which can be advantageous when the atmospheric artifacts or the displacement to be retrieved are not very well described by the models used in the standard PS

approach. Moreover, the proposed method does not need a preprocessing to calibrate the data and is insensitive to the density of PS candidates, it is able to identify PS in natural terrains and PS characterized by non linear movements, is computationally efficient and highly parallelizable. The results obtained on real ERS SAR data confirm the validity of the proposed approach. [C1839]

"TerraSAR-X Calibration Results"

TerraSAR-X is a satellite mission for scientific and commercial applications operating a highly flexible X-band SAR instrument with a multitude of different operation modes. As product quality is of crucial importance, the success or failure of the mission depends essentially on the method of calibrating TerraSAR-X in an efficient way during commissioning the entire system in a restricted time. Only then, product quality and the correct operation of the SAR system can be ensured. The paper describes the method of calibrating TerraSAR-X and final results derived from all calibration procedures. [C1840]

"TerraSAR-X Payload Data Processing: Results from Commissioning and Early Operational Phase"

TerraSAR-X, the first national German radar satellite, was launched in June 2007. It carries an X-band high-resolution synthetic aperture radar instrument featuring Stripmap, ScanSAR and, particularly, Spotlight imaging in a variety of different polarization modes. The mission completed its commissioning phase (CP) in December 2007, the provision of the SAR products for both the scientific and commercial user community was started in January 2008. One central TerraSAR-X element on ground is the pay-load ground segment PGS. From the beginning of the mission, PGS was nominally operated. About ten thousand data takes were already acquired and processed in 2007, not only for SAR verification and calibration purposes, but also for the operational ground segment validation. This paper provides the commissioning and early operational phase results from the SAR payload data processing perspective addressing data reception and SAR processing. Specifically the tuning and adjustment of the TerraSAR-X multi-mode SAR processor TMSP to meet the in-orbit data characteristics and to optimize the SAR focusing results is addressed. Relevant issues are the high-bandwidth chirp replica processing, side lobe suppression, Doppler frequency determination, processor normalization and phase-preservation. [C1841]

"A Novel Strategy for Radar Imaging Based on Compressive Sensing"

This paper aims at introducing the recent theory of compressive sensing to radar imaging systems in order to retrieve the imaged scene with better resolution and a reduced amount of collected samples. As a result of the application of the alternative imaging technique proposed, the use of matched filtering is avoided and the effect of its sidelobes in the images is drastically diminished. Furthermore, the amount of data to be stacked in the sensor and then downlinked to the ground station is meaningfully lower. This permits a more efficient management of resources. [C1842]

"TerraSAR-X Instrument, SAR System Performance & Command Generation"

The paper presents selected results from the TerraSAR-X Commissioning Phase from instrument performance, SAR system performance and command generation. [C1843]

"Thermal Noise Analysis on the Resistive Vee Dipole Antenna for Ground-Penetrating Radar Applications"

Thermal noise characteristics of a resistively-loaded vee dipole (RVD) are numerically analyzed using a commercial method of moments software. The RVD analyzed in this paper is loaded with 28 chip resistors. The resistors are loaded such that the resistors with higher values are placed farther from the drive point than the resistors with lower values. The results show that the resistors with lower values contribute more to the total noise power accepted by a 200 Ohm feed line though the resistors with lower values generate smaller noise voltage. [C1844]

"Subsurface Sensing of Near Surface Object Using Cavity Backed Slot (CBS) Antenna"

This paper presents a novel cavity backed slot (CBS) antenna for subsurface sensing applications. The CBS antenna is designed to be "matched" in the two-half-space configuration (one half space air; and the other ground) over a relatively wide frequency band. As a result, when attached onto ground surface, it is able to efficiently couple microwave power into and out of the ground. In this study, CBS antennas with operating frequency range [8.5 GHz, 13.6 GHz] are designed to detect objects buried in sand. Data acquisition is carried out using a sandpit with size (125 cm times 100 cm times 80 cm) as the test bed. One transmitting CBS

antenna is fixed at the center of the sandpit and one receiving antenna is physically moved along a rectangular grid (i.e., multi-static measurement). An inverse synthetic aperture radar (ISAR) algorithm is adopted for inverse processing. A 4-inch-diameter metallic sphere is used as calibration target; and three targets are tested, including a 3-inch-diameter metallic sphere, a T-shaped copper target, and a landmine simulant. Imaging results are presented and compared with those obtained using horn antennas (which are not "matched" to the air-ground interface). Better signal-to-clutter ratios are demonstrated by the proposed CBS antennas. [C1845]

"TerraSAR-X Commissioning Phase Execution and Results"

The paper summarizes the results of the TerraSAR-X commissioning phase. The overall schedule and the planning tool are presented. The strategy for data take (DT) command generation and a statistic about all acquired data takes are discussed. An overview about the characterization/verification results is provided. [C1846]

"Soil Moisture Retrieval Using an L-Band Synthetic Aperture Radiometer During the Soil Moisture Experiments 2003 (SMEX03) and 2004 (SMEX04)"

Soil moisture retrievals made using data from the airborne L-band microwave radiometer, 2D-STAR, over a wide range of land cover types are presented. The 2D-STAR was flown over six regional-scale sites during Soil Moisture Experiments in 2003 and 2004. Four sites located in Alabama, Georgia, Arizona, and Sonora were selected for this work. Land cover types included bare soil, bare soil with gravelly surface, shrub, crop field, and forest. Topographic conditions varied from flat or gently rolling plains to high-relief hilly or mountainous area. Results indicate fairly good soil moisture retrieval performance of the 2D-STAR over the various land cover types and moisture conditions (overall RSME=0.22 m³/m³). The 2D-STAR also showed improved soil moisture retrieval over a C- and X-band microwave instrument (PSR-C/X) for densely vegetated areas and gravelly soil surfaces. [C1847]

"Combined Passive and Active Soil Moisture Observations During CLASIC"

An important issue in advancing higher spatial resolution and better accuracy in soil moisture remote sensing is the integration of active and passive observations. In an effort to address these questions an airborne passive/active L-band system (PALS) was flown as part of CLASIC in Oklahoma over the Little Washita (rangeland and winter wheat) and Fort Cobb watersheds (irrigated agriculture and winter wheat). A total of 11 flight days were flown during the field campaign over each watershed. Extensive ground observations (soil moisture, soil temperature, vegetation) were made concurrent with the PALS observations. These flights were complemented by the acquisition of ALOS PALSAR data. Inter-comparison of radar observations indicated comparative calibration and possibly linear scaling. Extremely wet conditions were encountered during the field experiment. Initial results show the potential of combining passive and active PALS observations. Over the sampling sites PALS radiometer estimated soil moisture was in closer agreement over the Fort Cobb (SEE=0.048 m³/m³) than over the Little Washita watershed (SEE=0.067 m³/m³). [C1848]

"Passive and Active L-Band System and Observations during the 2007 CLASIC Campaign"

This article describes the upgraded PALS instrument and the characteristics of data acquired from the Cloud Land Atmospheric Interaction Campaign (CLASIC) 2007. The data acquired over lake passes were used to remove the radiometer calibration bias. The calibrated radiometer data showed significant consistency with the L-band land emission model for soil surfaces published in the literature. We observed significant temporal (days) changes of a few dB in the radar data. The change of radar backscatter appeared to correlate well with the change of in situ soil moisture or the soil moisture data derived from the PALS dual-polarized brightness temperatures. The radar vegetation index also correlated well with the vegetation opacity estimated from the radiometer data. The preliminary analyses suggest complementary information contained in the surface emissivity and backscatter signatures for the retrieval of soil moisture and vegetation water content. [C1849]

"Enhancement of Along-Track Interferometry for Ground Moving Target Indication"

Along-Track Interferometry (ATI) for the indication of moving targets with two channel Synthetic Aperture Radar (SAR) shows a low detection probability for a small number of looks. This paper proposes an enhancement called Better ATI (BATI). It is characterized by a constant parameter added to the interferometric SAR image before determining its phase. Statistical analysis shows that the new technique significantly outperforms ATI, is comparable to Displaced Phase Center Antenna (DPCA) for homogeneous terrain and may outperform DPCA in heterogeneous terrain. The theoretical results are confirmed successfully with experimental data. [C1850]

"Volume Coherence Estimation for Random Forest Height Retrieval Based on Polinsar Data"

The volume coherence is an important parameter in the two-layer model for random forest height retrieval. Though it is "invisible" from the observation, it can be estimated from the data. Considering the argument range of the coherences for all the possible polarizations, six polarizations can be obtained for each scattering cell. The volume coherence can be estimated more reasonably and the ground phase center can be determined more accurately. It benefits to improve the height retrieval accuracy by this model. The proposed method is validated by using L-band single-baseline polarimetric interferometric SAR data collected with the DLR Experimental SAR system. [C1851]

"Investigation of a New Multifunctional High Performance SAR System Concept Exploiting MIMO Technology"

In this paper, we introduce an innovative system concept for synthetic aperture radar (SAR) and investigate the performance. Based on multiple-input multiple-output (MIMO) configuration, a versatile SAR operation can be feasible, for instance interferometric and full polarimetric SAR operation over a wide area simultaneously. For this purpose the space-time coding (STC) and digital beamforming (DBF) are key elements of the proposed MIMO SAR concept. A waveform diversity gain is obtained from the STC scheme, applied on transmit and DBF on receive provides array gain and improved noise performance for each multiple SAR images. In this paper, using a simple transmit diversity technique, well known as Alamouti scheme, the complete processing topology is introduced. The performance is investigated from a system point of view. [C1852]

"On the Use of Dual-Polarized SAR Data for Oil Spill Observation"

In this paper a novel approach for oil spill observation, based on partially polarimetric Synthetic Aperture Radar (SAR) data, is proposed. A model which relates the co-polarized phase difference (CPD) to the sea surface scattering mechanism with and without slicks is developed. Experiments accomplished over multi-look complex (MLC) C-Band SAR data, show that the CPD approach is useful both to observe oil spills and to distinguish between oil spills and biogenic slicks. [C1853]

"Dual Sensor ALIS for Humanitarian Demining and its Evaluation Test in Mine Fields in Croatia"

More than 60 courtiers are still suffered from land mines. ALIS is a hand-held dual-sensor developed for humanitarian demining, which has been developed at Tohoku University, Japan since 2002. The dual-sensor ALIS is equipped with a metal detector and a GPR (Ground Penetrating Radar). A unique and novel sensor tracking system, which can record the GPR and Metal detector signal with their acquired locations, is equipped in ALIS. Due to its sensor location information, we can reconstruct buried land mine images in 3D space after data acquisition. IN addition, we found that the image reconstruction or migration processing drastically increases the quality of the image of the buried objects. ALIS evaluation test was conducted in Croatia in October 2007. Then a half-year evaluation test of ALIS in QC test in Croatia was held during December 2007 and April 2008. In this test, we could obtain fruitful experience in various soil and environmental conditions in Croatia. [C1854]

"High Bandwidth Spotlight SAR Interferometry with TerraSAR-X"

TerraSAR-X data are operationally available to the public since January 2008. This paper shows selected TerraSAR-X interferometric examples with an emphasis on challenges introduced by the high resolution in spotlight mode and with 300 MHz. [C1855]

"High Resolution Interferometric Stacking with TerraSAR-X"

The German radar satellite TerraSAR-X was launched in June 2007. Radar interferometry (InSAR) is supposed to be one of the major applications of this sensor. It allows the three-dimensional mapping of the Earth's surface (InSAR) or even its displacement effects using differential interferometry (D-InSAR) or the more advanced persistent scatterer interferometry (PSI). All InSAR-applications are well-supported by the sensor, the SAR-processor and the mission design. DLRs operational interferometric system PSI-GENESIS has been adapted to cope with the new sensor and the innovative acquisition modes. Interferometric example applications could be shown already in the early stage of the six months commissioning phase. In this paper, recent processing examples and an update on the interferometric characteristic are presented. [C1856]

"Precise Orbit and Baseline Determination for TerraSAR-X and TanDEM-X"

TerraSAR-X (TSX), the recent German radar satellite launched on June 15, 2007, carries as primary instrument a synthetic aperture radar (SAR) sensor. The GFZ German Research Centre for Goesciences and the Center for

Space Research (CSR) at the University of Texas in Austin, USA, provided the Tracking, Occultation and Ranging Category A instrument package (TOR) to the TSX mission to enhance the quality of the scientific SAR products and to collect occultation measurements for atmospheric/ionospheric sounding. The TOR consists of a precise dual frequency GPS flight receiver (Integrated GPS and Occultation Receiver-IGOR) and a Laser retro-reflector (LRR) that supports Satellite Laser Ranging (SLR) observations from the Earth's surface. Also the CHAMP and GRACE satellites are equipped with the LRR originally developed for CHAMP by GFZ. TanDEM-X (TDX), a twin to TSX, to be launched in September 2009 will fly with TSX in a tandem orbit configuration. Its compatible SAR system enables bistatic application for the derivation of digital elevation models (DEMs). For TDX, GFZ again supplies the TOR payload. The IGORs on both satellites will become the key to the continuous determination of the baseline (the distance of the two individual SAR antennae) with millimeter accuracies. In this paper, we concentrate on results gained so far for TSX precise orbit determination (POD) and on the status of our preparations for precise baseline determination (PBD) for the tandem mission. [C1857]

"A Regularization Approach for InSAR and Optical Data Fusion"

This paper investigates the joint use of interferometric SAR and optical data for 3D reconstruction. A framework for phase filtering constrained by the discontinuities of the optical image is presented. First, both the amplitude and the interferometric phase are projected in a 3D coordinate system. The problem is then expressed as the regularization of the amplitude and phase images with the introduction as prior knowledge of the edges detected on the optical image. We define the regularized elevation in the framework of Markov random fields (MRF) and derive a smoothness prior that both preserves sharp boundaries (based on total variation minimization) and is driven by the structures present in the optical image. We apply a recent graph-cut based algorithm to perform fast regularization of the elevation field. First results on a real pair of optical and InSAR images are presented. [C1858]

"Performance Prediction for Low-SNR Lidar Sensors"

Technological advances in the performance of small micro-lasers and photo-detector sensitivity have recently enabled the development of experimental airborne lidar systems with low signal-to-noise ratios (SNR). These systems show the potential to perform highly accurate topographic and bathymetric mapping. There is a need to build up a modeling capability in order to aid in future system and mission design. A numerical sensor model has been developed to predict measurement performance from low SNR lidar systems. Both optical and signal processing components are considered, along with other factors including atmospheric effects and surface conditions. [C1859]

"Robust Extraction of Exterior Building Boundaries from Topographic Lidar Data"

Methods for generating accurate building models from lidar data have received considerable attention in the recent literature. Many of the proposed techniques examine the data to define dominant planes in the structure, then intersect these planes to determine the location of internal edges and vertices. However, since most airborne lidar datasets are collected from near-nadir orientations, there are usually very few data points that lie on vertical surfaces. As such, it is usually difficult to determine the planes corresponding to exterior walls using data points on these walls. However, if we assume that exterior walls are oriented directly under the outer boundary of the roof structure, we may identify the geometry of these walls by modeling the 2D shape of the building exterior. This paper presents a robust approach for extracting this exterior boundary directly from the lidar data. [C1860]

"3D Organization of 2D Urban Imagery"

Working with New York data as a representative and instructive example, we fuse aerial lidar imagery with satellite pictures and Geographic Information System (GIS) layers to form a comprehensive 3D urban map. Digital photographs are then mathematically inserted into this detailed world space. Reconstruction of the photos' view frusta yields their cameras' locations and pointing directions which may have been apriori unknown. It also enables knowledge to be projected from the urban map onto georegistered image planes. For instance, absolute geolocations can be assigned to individual pixels, and GIS annotations can be transferred from 3D to 2D. Moreover, such information propagates among all images whose view frusta intercept the same urban map location. We demonstrate how many imagery exploitation challenges (e.g. identify all photos containing some stationary ground target, quantify match between two pictures) become mathematically tractable once a 3D framework for analyzing 2D images is adopted. Finally, we close by briefly discussing future applications of this work to photo-based querying of urban knowledge databases. [C1861]

"Compensation of Faraday Rotation in Multi-Polarization Scatterometry"

The effects of Faraday rotation on spaceborne polarimetric scatterometers are discussed. A method of exploiting an estimate of the Faraday rotation angle to retrieve co-cross polarization is outlined. [C1862]

"Validation of Coarse Resolution Microwave Soil Moisture Products"

The strong relationship between soil moisture content and the soil dielectric constant offers a direct way of measuring soil moisture with microwave sensors. Global coarse-resolution soil moisture datasets are currently retrieved from active microwave spaceborne instruments (AMI onboard ERS and ASCAT on Metop-A) and in the near future from dedicated passive microwave satellite sensors (SMOS). This article summarizes recent soil moisture research activities and briefly discusses the strategies for validation and cross-comparison of remotely sensed soil moisture datasets. Special attention is given to the first validation of the soil moisture data from the ASCAT instrument on Metop-A in relation to the absolute and relative calibrations of the instrument. A first assessment of the quality of the ASCAT surface soil moisture is given by studies of stable targets and the spatial and temporal extent of recent extreme drought and rainfall events. [C1863]

"Hierarchical Methods for Landmine Detection with Wideband Electro-Magnetic Induction and Ground Penetrating Radar Multi-Sensor Systems"

A variety of algorithms are presented and employed in a hierarchical fashion to discriminate both anti-tank (AT) and anti-personnel (AP) landmines using data collected from wideband electromagnetic induction (WEMI) and ground penetrating radar (GPR) sensors mounted on a robotic platform. The two new algorithms for WEMI are based on the In-phase vs. Quadrature plot (the Argand diagram) of the complex measurement obtained at a single spatial location. The angle prototype match method uses the sequence of angles as a feature vector. Prototypes are constructed from these feature vectors and used to assign mine confidence to a test sample. The angle model based KNN method uses a two parameter model; where the parameters are fit to the In-phase and Quadrature data. For the GPR data, the Linear Prediction Processing and Spectral Features are calculated. All four features from WEMI and GPR are used in a Hierarchical Mixture of Experts model to increase the landmine detection rate. The EM algorithm is used to estimate the parameters of the hierarchical mixture. Instead of a two way mine/non-mine decision, the HME structure is trained to make a five way decision which aids in the detection of the low metal anti personnel mines. [C1864]

"The Effect of Rain on Satellite Sensor Estimates of Surface Roughness Conditions and on the Air-Sea Momentum Flux"

Changes in the sea surface roughness from the combined effects of wind and rain, on scales of tens of kilometers, are being studied using the QuikSCAT scatterometer (NRCS) and simultaneous NEXRAD three-dimensional measurements of rain. The studies of air-sea interaction, related to surface fluxes. The results to be presented were acquired during a significant rain event in the Gulf of Mexico, to the east of Corpus Christi, and just south of Houston, TX in May 2005. Preliminary results in NRCS caused by rain, relative to that in nearby regions with negligible rain shows distinct characteristics. Three regions with different wind speeds (4-6, 6-8 and 8-10 m/s) show definitive variation of this total NRCS with respect to wind magnitude, satellite-relative wind direction, polarization and rainrate. Relative changes are stronger in the lower wind region for both polarizations, with H-pol providing a more definitive signature. At higher wind speeds (e.g. 10 m/s) the relative splash induced increases in NRCS are still significant, and show distinct differences between polarizations. [C1865]

"Very Shallow Water Bathymetry Retrieval from Hyperspectral Imagery at the Virginia Coast Reserve (VCR'07) Multi-Sensor Campaign"

A number of institutions, including the Naval Research Laboratory (NRL), have developed look up tables for remote retrieval of bathymetry and in-water optical properties from hyperspectral imagery (HSI) [6]. For bathymetry retrieval, the lower limit is the very shallow water case (here defined as < 2m), a depth zone which is not well resolved by many existing bathymetric LIDAR sensors, such as SHOALS [4]. The ability to rapidly model these shallow water depths from HSI directly has potential benefits for combined HSI/LIDAR systems such as the Compact Hydrographic Airborne Rapid Total Survey (CHARTS) [10]. In this study, we focused on the validation of a near infra-red feature, corresponding to a local minimum in absorption (and therefore a local peak in reflectance), which can be correlated directly to bathymetry with a high degree of confidence. Compared to other VNIR wavelengths, this particular near-IR feature corresponds to a peak in the correlation with depth in this very shallow water regime, and this is a spectral range where reflectance depends primarily on water depth (water absorption) and bottom type, with suspended constituents playing a secondary role. [C1866]

"Comparison of Aviris and AISA Airborne Hyperspectral Sensing for Above-Ground Forest Carbon

Mapping"

Monitoring of the 418 million ha of forests in Canada is needed to ensure the sustainable development of these forests. Hyperspectral sensing can provide mapping of forest species, forest health, and above-ground biomass. Airborne two-meter AISA hyperspectral and LIDAR data were acquired by the University of Victoria (UVic) over the Greater Victoria Watershed District (GVWD) test site and compared to NASA's AVIRIS data that had been acquired in the summer of 2002 at 4 m spatial resolution. Tree heights derived from LIDAR data, and allometric equations were used to provide independent ground estimates of biomass. Between-sensor calibration calibrated the AISA data to the same basis as the AVIRIS data. The calibrated reflectance data were used to generate forest species classifications, and biomass estimates for the test site. Average classification accuracies exceeded 89% in mapping major forest species. These products were used to create a map of above-ground carbon for the forested portion of the GVWD test site. [C1867]

"Subarctic Boreal Forest Albedo Estimation Using Envisat ASAR for BRDF Determination"

Surface albedo estimates based on optical and microwave satellite data were compared to corresponding ground based values in a Subarctic boreal forest test site. The ground based albedo values were derived from radiation measurements carried out at the forest floor using an albedo model and measured global and diffuse radiation data. The use of both optical and microwave satellite data turned out to produce more accurate surface albedo estimates than using only optical satellite data. The relative accuracy of the optical/microwave based near infrared and broad band albedo estimation was better than 10% for clear sky cases. The inclusion of microwave data improved the satellite based surface albedo estimation accuracy. [C1868]

"Detection of Ionospheric Structures with L-Band Synthetic Aperture Radars"

Numerical simulations of low-latitude ionospheric instabilities show the formation of plasma density structures can be detected by synthetic aperture radar (SAR) radio signals. At L-band, the phase front distortions produced by propagation through plasma "bubbles" should provide measurable changes in both the complex-amplitude and polarization waves from orbiting satellite radars. The diffraction pattern from scattered ground SAR signals can be detected by orbiting receivers. Based on reciprocity, ground radars at Kwajalein Atoll are being used to determine the feasibility of space-based detection of ionospheric density structures. This new measurement technique can provide a global data base of ionospheric data for space-weather models that predict the effects of the ionosphere on radio systems. [C1869]

"A Vegetation Correction Methodology Applied for Soil Moisture Retrieval from C-Band Radar Observations"

This research presents a methodology to correct backscatter (σ^0) observations for vegetation effects. The proposed methodology is based on the concept that the ratio between the surface scattering over the total amount of scattering ($\sigma^0_{\text{surface}}/\sigma^0_{\text{total}}$) is affected only by the vegetation and can be described as a function of the vegetation water content. The data set used in this study was collected at USDA's Optimizing Production Inputs for Economic and Environmental Enhancement (OPE3) experimental site in Beltsville, Maryland (USA) over a corn growth cycle in 2002 and includes C-band (4.75 GHz) HH- and VV-polarized observations acquired at incidence angles of 15, 35 and 55 degrees. During this period the corn crops reached peak biomass of 6.6 kg m⁻² and a soil moisture range varying from 0.02 to 0.26 cm³cm⁻³. The results show that through application of the proposed vegetation correction methodology the soil moisture retrieval accuracy can be improved from 0.033 to 0.032 cm³cm⁻³, 0.049 to 0.033 cm³cm⁻³, and 0.079 to 0.047 cm³cm⁻³ at incidence angles of 15, 35 and 55 degrees, respectively. [C1870]

"Inversion Algorithm for Soil Moisture Retrieval from Polarimetric Backscattering Coefficients of Vegetation Canopies"

This paper presents soil moisture retrieval from measured polarimetric backscattering coefficients of a vegetated surface. Based on the analysis of the quite complicate first-order radiative transfer scattering model for vegetated surfaces, a simplified scattering model is proposed for an inversion algorithm. Extraction of the surface-scatter component from the total scattering of a vegetation canopy is addressed using the simplified model, and also using the three-component decomposition technique. The back-scattering coefficients are measured with a polarimetric L-band scatterometer during two months as well as the biomasses, leaf moisture contents, and soil moisture contents. Then the measurement data are used to estimate the model parameters for vv-, hh-, and vh-polarizations. The scattering model for tall-grass-covered surfaces is inverted to retrieve the soil moisture content from the measurements using a genetic algorithm. The retrieved soil moisture contents agree quite well with the in-situ measured soil moisture data. [C1871]

"The Impact of the Ionosphere on Interferometric SAR Processing"

The impact of ionospheric propagation effects on the signal properties of SAR systems is significant and increases with decreasing carrier frequency. Besides polarimetric applications, also interferometric SAR processing can be significantly affected. Relative range shifts, internal image deformations, range and azimuth blurring, and interferometric phase errors are the most significant effects to be considered. In this paper we provide the theoretical background for ionospheric effects on InSAR. We quantify expected magnitudes of the respective effects for various existing SAR sensors and discuss methods for their detection and correction. Real data examples, mainly stemming from the ALOS PALSAR mission, are presented to verify the derived theory.

[C1872]

"Status Report on the TerraSAR-X Mission"

TerraSAR-X is Germany's first national remote sensing satellite being implemented in a public-private partnership between the German Aerospace Centre (DLR) and EADS Astrium GmbH. TerraSAR-X was launched on June 15th, 2007 and will supply high-quality radar data for purposes of scientific observation of the Earth for a period of at least five years. At the same time it is designed to satisfy the steadily growing demand of the private sector for remote sensing data in the commercial market [1].

[C1873]

"Rapid Land Mapping by TerraSAR-X VHR Data"

This work is devoted to the definition and application of a processing chain for rapid mapping using TerraSAR-X data. The approach is based on a quick extraction of spatial features such as linear and textural elements of the scene, and their combination with the original SAR data. The suitability of such procedure for an operative use is proved by the results shown on a simulated and two real TerraSAR-X data sets.

[C1874]

"Discovery of Anomalous Stripes Over the Amazon by the PALSAR onboard ALOS satellite"

We discovered anomalous stripes over the large area of Amazon when the region was scanned by the radar (PALSAR) onboard ALOS satellite. The stripes appeared on the local midnight along the geomagnetic field line with a typical characteristic width of 600 m.

[C1875]

"From EARLINET-ASOS Raman-Lidar Signals to Microphysical Aerosol Properties Via Advanced Regularizing Software"

Knowledge on the aerosol distribution in the Earth's atmosphere is not sufficient to calculate or even estimate the impact of aerosols on global and regional climate. One of the techniques to gain more knowledge in this field is advanced lidar remote sensing. Indeed, there are several problems connected with the retrieval of microphysical parameters of the aerosol from the data gained by Raman lidar measurements. The calculation can be reduced to two basic steps; in the first step, the aerosol extinction and backscatter profiles have to be extracted from the Raman signals, then those profiles are used for the retrieval of the microphysical properties. In the framework of the EARLINET-ASOS project, new algorithms for both of these parts of the problem are being developed with the long-term goal of being used for a continuous data evaluation of the data produced by the EARLINET stations.

[C1876]

"On the Minimum Number of Tracks for SAR Tomography"

The main drawback of SAR Tomography (SARTom) is the considerable number of tracks required to achieve the 3-dimensional (3D) representation of a viewed scene. The key point concerns the trade-off between the vertical resolution and the control on ambiguities phenomena. This paper deals with the problem of the determination of the minimum number of required tracks when super-resolution subspace methods are applied. The results are validated on real data acquired in L-band by the E-SAR system of the German Aerospace Centre.

[C1877]

"Combining Time-Domain Back-Projection and Capon Beamforming for Tomographic SAR Processing"

Various tomographic processing methods have been investigated in recent years. The quality of the focused tomographic image is usually limited by several factors. In particular, Fourier-based focusing methods are susceptible to irregular and sparse sampling, two problems that are unavoidable in case of multi-pass, multi-baseline SAR data acquired by an airborne system. Neither time-domain back-projection (TDBP) processing, although providing a very accurate processing framework, is able to overcome the problem of ambiguous target detection in the tomographic image. In this paper, a possible extension of the TDBP approach to multi-looking based tomographic focusing methods like standard beamforming and Capon beamforming is discussed.

Preliminary results obtained with a simulated and a real airborne tomographic P-band data set are shown.

[C1878]

"Backscatter Lidar Measurement in the Atmospheric Boundary Layer: Data Analysis and Interpretation Capabilities"

In this presentation we summarize analysis approaches of the backscatter lidar signal, providing the following parameters in the Atmospheric Boundary Layer (ABL): the aerosol backscatter coefficient and the mixing layer height. These ABL parameters are important in the atmospheric studies and air quality control. The application of the discussed approaches will be illustrated by examples of backscatter lidar measurements above Neuchatel, Switzerland (47.0degN; 6.95degE, 485 m asl), one of the stations in EARLINET. [C1879]

"Surface Parameter Estimation Over Periodic Surfaces Using a Time-Frequency Approach"

The aim of this paper is to analyze the feasibility of soil moisture retrieval over rough periodic surfaces. For this kind of fields, the Bragg phenomenon effect appears and the inversion algorithms are shown to be no more valid. Using a time-frequency approach and a new random periodic surface scattering model, a polarimetric analysis allows to show that the use of alpha1polarimetric parameter is important for the inversion since it is quasi insensitive to this phenomenon. Thus, the alpha1inversion method is proposed that provides some encouraging results. [C1880]

"The European Aerosol Research Lidar Network (EARLINET): An Overview"

The European Aerosol Research Lidar NETWORK (EARLINET) is the first aerosol lidar network on a continental scale with the main goal to provide a comprehensive, quantitative, and statistically significant database for the aerosol distribution over Europe. Next, we present EARLINET along with the main network activities. [C1881]

"Earlinet Approach to Optimisation of Individual Network Instruments with the Aim of Homogenisation of Aerosol Data Products and Increased Data Coverage"

The European Aerosol Research Lidar NETWORK (EARLINET) is an aerosol lidar network on a continental scale. EARLINET is now a leading network in quality-controlled quantitative aerosol profiling performing a schedule of routine measurements and presently consists of 28 stations distributed over Europe. The construction of an unbiased spatio-temporal database of vertical profiles of aerosol optical properties on a regional scale for climate and air quality research is the main objective of EARLINET and is accomplished through application of Raman lidars. One of the tasks in the EC-funded project EARLINET-ASOS is to optimize individual instruments with the aim of homogenization of aerosol data products over the network and increased data coverage by automation. This task is approached by selection of optimal solutions existing in the pool of individual stations. This is done for components, subsystems as well as for system integration. In system integration emphasis lies on automation to reduce the amount of manpower needed, to improve temporal coverage, and to make performance independent from individual operators. The procedure to perform these tasks is outlined and the set of tools enabling the assessment of performance under development is described. [C1882]

"Context-Dependent Multi-Sensor Fusion for Landmine Detection"

We present a novel method for fusing the results of multiple landmine detection algorithms that use different types of features, different classification methods, and different sensors. The proposed fusion method, called context-dependent multi-sensor fusion (CDMSF) is motivated by the fact that the relative performance of different detectors can vary significantly depending on the sensor, mine type, geographical site, soil and weather conditions, and burial depth. The training part of CDMSF has two components: context extraction and algorithm fusion. In context extraction, the features used by the different algorithms are combined and used to partition the feature space into groups of similar signatures, or contexts. The algorithm fusion component assigns an aggregation weight to each detector in each context based on its relative performance within the context. Results on ground penetrating radar (GPR) and wideband electromagnetic induction (WEMI) data collections show that the proposed method can identify meaningful and coherent clusters and that different expert algorithms can be identified for the different contexts. Our initial experiments have also indicated that the context-dependent fusion outperforms all individual detectors. [C1883]

"Data Fusion Study Between Polarimetric SAR, Hyperspectral and Lidar Data for Forest Information"

ALOS PALSAR L-band quad-pol data were acquired over our study area on Vancouver Island in British Columbia in the summer of 2007. The site has significant topographic relief and high biomass in this temperate

coastal rainforest. Our emphasis was on integration and fusion techniques of polarimetric SAR, hyperspectral and LIDAR data for useful forest information extraction. The polarimetric SAR techniques and analysis methods studied in this project drew on the work of other researchers. The Jong-Sen Lee algorithm for polarization compensation for terrain azimuth slope variations was implemented and tested. The Shane Cloude decomposition method, with basic types of scattering analysis for reducing sensitivity to topography effects was examined and applied. In this study, the hyperspectral data was used for providing high spectral resolution information, such as major forest species and land-cover characterization, and the LIDAR data were utilized to generate information related to vertical structure of both the underlying topography and the forest structure. The combination of these data sources and techniques provided an opportunity to examine the potential capabilities of polarimetric SAR and the synergy of the fused data for forest classification. [C1884]

"Scattering type phase for wetland classification using C-band polarimetric SAR"

The Touzi decomposition is investigated for wetland characterization. Like the Cloude alpha scattering type, the magnitude alpha of the symmetric scattering is not effective for vegetation type discrimination. The phase Phi of the symmetric scattering type has to be used for enhanced characterization of wetland vegetation species. A new tool is introduced for assessment of the scattering type phase coherence, and the phase of the dominant scattering type is shown to be very promising for wetland target classification. The unique information provided by Phi for enhanced wetland class discrimination is demonstrated using Convair-580 polarimetric C-band SAR data collected over the Mer Bleue wetland in the East of Ottawa, Canada. The use of Phi makes possible the discrimination of shrub bog from sedges fen, and permits even the discrimination between conifer dominated treed bog from upland deciduous forest under leafy conditions. [C1885]

"Seasonal Change Monitoring of Wetlands by Using Airborne and Satellite PolSAR Sensing"

This paper presents a simple water area classification technique based on POLSAR image analysis and investigates the seasonal change of the true water area in wetland by making use of the satellite ALOS/PALSAR data, in addition to the air-borne Pi-SAR data. We here utilize the scattering power decomposition method in the image analysis, and verify that the double-bounce scattering, which can be considered as a true water area classification marker, is observed from the wetland and the surrounding emerged plants for both the airborne and satellite POLSAR data sets, even though the resolution and the incident angle are quite different. The dependency of the polarimetric scattering feature on the variation of the incident angle is also investigated by the polarimetric scattering analysis for a simplified emergent-water boundary model by using the finite-difference time-domain (FDTD) method. It is resultantly confirmed that the double-bounce scattering is utilized as a useful marker for the distinction of the true water area of the wetland even for small incident angle case. [C1886]

"A Novel Protocol for Accuracy Assessment in Classification of Very High Resolution Multispectral and SAR Images"

This paper presents a novel protocol for the accuracy assessment of thematic maps obtained by the classification of very high resolution images. As the thematic accuracy alone is not sufficient to adequately characterize the geometrical properties of classification maps, we propose a novel protocol that is based on the analysis of two families of indexes: (i) the traditional thematic accuracy indexes, and (ii) a set of geometric indexes that characterize different geometric properties of the objects recognized in the map. These indexes can be used in the training phase of a classifier for identifying the parameters values that optimize classification results on the basis of a multi-objective criterion. Experimental results obtained on Quickbird images show the effectiveness of the proposed protocol in selecting classification maps characterized by better tradeoff between thematic and geometric accuracy with respect to standard accuracy measures. [C1887]

"Quantifying Surface Reflectivity for Spaceborne Lidar Missions"

Spaceborne lidar missions are being studied to estimate atmospheric concentrations of CO₂, water vapour and O₃, as well as for measuring surface biophysical properties. Lidar instruments typically observe the highest possible surface reflectance due to observing in the retroreflection peak (the so-called 'hotspot'), where shadowing on the surface is minimised. The likely range of observed reflectance will determine the required dynamic range and desired signal-to-noise ratio (SNR) of such an instrument, but it is difficult to predict this range a priori. A method is presented for estimating lidar surface reflectance over a range of vegetated surface types using multi-angle, multi-spectral reflectance data. The approach is validated using radiative transfer simulations of highly detailed 3D vegetation canopy models. The method is particularly useful for testing proposed lidar instrument configurations. [C1888]

"A Preprocessing Method for Automatic Break Lines Detection"

We present a preprocessing method for automatic break line detection. Our method is given a set of edges (break lines and non-break lines) we eliminate the non-break line edges leaving only those with higher probability of being break lines. Our method is based on fusing IR images and LiDAR cloud points. In the first step, we apply the Canny edge detection algorithm to the IR images (producing a superset of break lines). Then we project the LiDAR points onto a 2-D plane, ignoring the set of points that are greater than a selected threshold (different elevation thresholds have been selected), which allows the footprints of some elevated structures to appear clearly in the set of projected points. Those structures that appear in both LiDAR points and IR images are used as references for registration of LiDAR cloud points with the IR images. After registration, we eliminate all the edges that appear in flat areas, which is achieved by applying a 3D filter to the LiDAR points.

[C1889]

"Fourier Error Analysis of Ray Tracing on a Geospatial Polygonal Model"

This paper demonstrates that the error associated with ray tracing photorealistic polygonal models of Light Detection and Ranging (LIDAR) scan data is negligible for many applications. In some cases, the standard deviation of error is actually reduced by ray tracing to points on a polygonal model between LIDAR data rather than capturing more data from a scanner. Numerical analyses on the sources of error were performed using Fourier analysis, Taylor expansion, and a statistical model of LIDAR data. Ray tracing was then used to calculate the intersection of each polygon at a point of interest, allowing 3D data to be quantified at any location in between LIDAR points. Actual acquired from a LIDAR scanner and modeled data are then compared to the ray traced values. Results show that many data types have sufficiently low spectral content, allowing accurate representation of 3D data acquired from a LIDAR scanner as a polygonal model. [C1890]

"Dynamic Phenomena in the Coastal Waters of the North-Eastern Black Sea Retrieved from Satellite Data"

Our paper discusses satellite observations data for the north-eastern Black Sea. Our study is based on remote sensing satellite data obtained by ERS-2 SAR, Envisat ASAR, Terra and Aqua MODIS, and NOAA AVHRR instruments. The data from different sensors was analyzed jointly to investigate coastal water circulation and in particular the occurrence, evolution and drift of vortical structures. One result of our investigation included a discovery of surface manifestations of non-tidal internal waves generated in the vicinities of sea eddy structures. Another finding was a seasonal variability of vortex structures in the coastal zone. [C1891]

"Advanced Land Observing Satellite PALSAR Observations of the Oceanic Dynamic Phenomena in the Coastal Zone"

Satellite SAR is a valuable tool providing all-weather data on the mesoscale and fine-scale features of phenomena and processes both in the open ocean and in the coastal zones. Analysis of C-band ERS-1/2 SAR and Envisat ASAR ocean images allowed selecting the areas for detailed study with L-band ALOS PALSAR data. The Kuroshio-Oyashio confluence zone, Soya Warm Current, Okhotsk Sea shelf, the Kuril Straits, Pacific Ocean east of Kamchatka, Peter the Great and Toyama Bays in the Japan Sea, Taiwan Strait and several areas in the East- and South-China Seas are among them. A rather remarkable assemblage of oceanic dynamic phenomena such as currents, coastal fronts, eddies, internal waves, river plumes, etc. were evident in the PALSAR images. The detailed study was carried out for the images with well-defined imprints of oceanic dynamic, for which ancillary data consisting of Terra and Aqua MODIS and NOAA AVHRR images, QuikSCAT-derived wind fields, ocean color, surface analysis maps, bathymetry maps, etc. were available. [C1892]

"Statistical Models for Landmine Detection in Ground Penetrating Radar: Applications to Synthetic Data Generation and Pre-Screening"

As ground penetrating radar phenomenology continues to improve, more advanced statistical signal processing approaches become applicable to subsurface inference in GPR data. Despite the wide body of literature exploring the applications of various approaches to processing GPR data, statistical modeling of realistic soil responses is a difficult task, and the algorithms developed for real-time fielded GPR processing are rarely directly motivated by statistical models of GPR data. In this work, we present a tractable spatial statistical model for volumetric GPR data which can be used to motivate the application of various signal processing approaches to solving problems of interest in GPR data like pre-screening, feature extraction, and air/ground response tracking. [C1893]

"The Influence of Air Density on Scatterometer Retrievals of Surface Turbulent Stress"

There has long been speculation that scatterometers respond to surface stress rather than wind; however, all

previous efforts to demonstrate this suggestion have had negative results. Previous efforts have focused on wave-related changes in stress. Herein, the dependence of stress on near surface air density is examined. The biases expected for such a dependency are found in data similar to those used to calibrate the QuikSCAT (QSCAT) scatterometer. [C1894]

"Recent Advances in POL-SAR & POL-IN-SAR Imaging of Natural Habitats and Wetland Remote Sensing"

Land cover monitoring is one of the most potential applications of Polarimetric Synthetic Aperture Radar (POLSAR) sensing and so is Repeat-Pass Polarimetric-Interferometric SAR (RP-DIFF-POL-IN-SAR) stress-change assessment for air/high-altitude/space-borne SAR sensor deployment. Provided fully polarimetric SAR information can be made available, a plethora of novel POLSAR matrix decomposition methods can be implemented for recovering rather precise scattering contributions from isolated and distributed scattering scenarios, and so can rather exact environmental changes from consecutive repeat-pass observations. With the recent launches of the fully polarimetric satellites JAXA-ALOS (PAL-SAR-L), the DLR TerraSAR-X and RADARSAT-2 (C), a new era in space imaging of the terrestrial terrain and ocean surfaces has arrived providing unforeseen advantages. Whereas in the past, POLSAR applications were focused mainly on information product gathering for agriculture, forestry and the fisheries, little emphasis was placed on demonstrating its full capacity also for the assessment of natural habitats and especially wetlands. Therefore, it is essential to demonstrate how seasonal changes and features of vegetation in natural habitats, shallow vegetated lakes and wetlands can be recovered, provided fully polarimetric SAR image data takes can be made available for full polarimetric scattering matrix acquisition for which the standard symmetry condition $HV=VH$ may not necessarily be sufficient. [C1895]

"The Detection and Mitigation of RFI with the Aquarius L-Band Scatterometer"

The Aquarius sea-surface salinity mission includes an L-band scatterometer to sense sea-surface roughness. This radar is subject to radio-frequency interference (RFI) in its passband from 1258 to 1262 MHz, a region also allocated for terrestrial radio location. Due to its received-power sensitivity requirements, the expected RFI environment poses significant challenges. We present the results of a study evaluating the severity of terrestrial RFI sources on the operation of the Aquarius scatterometer, and propose a scheme to both detect and remove problematic RFI signals in the ocean backscatter measurements. The detection scheme utilizes the digital sampling of the ambient input power to detect outliers from the receiver noise floor which are statistically significant, and flags nearby radar echoes as potentially contaminated by RFI. This detection strategy, developed to meet tight budget and data downlink requirements, has been implemented and tested in hardware, and shows great promise for the detection and global mapping of L-band RFI sources. [C1896]

"Cross-Validation of Wind Products from Seawinds and AMSR on ADEOS-II"

The Advanced Earth Observing Satellite-II (ADEOS-II), which carried a microwave radiometer, AMSR, and microwave scatterometer, SeaWinds, provided us with unique opportunity to validate wind products from the both sensors. Two examples of the cross-validation of wind observations by spaceborne active and passive microwave sensors are presented in this paper. These examples clearly exhibited importance of the sensor synergy of the active and passive microwave sensors, and demonstrated needs of future missions with a combination of microwave scatterometer and radiometer onboard the same satellite to achieve simultaneous observation. [C1897]

"Volcanic Deformation Mapping using PSInSARTM: Piton de la Fournaise, Stromboli and Vulcano test sites for the Globvolcano project"

This presentation focuses on the results of the application of the Permanent Scatterers Technique (PSInSAR_{T,Bi}, an advanced InSAR technique capable of measuring millimetre scale displacements of individual radar targets on the ground) as a method for measuring deformation in volcanic area within the Globvolcano project. In this project, T.R.E. takes part as a service provider for the Deformation Mapping products. Three cases of PSInSAR_{T,Bi} application are presented: Piton de la Fournaise (Reunion Island), Stromboli and Vulcano (Eolie, Italy). More than 200 ENVISAT ASAR scenes have been processed to estimate the velocity field of the volcanoes surface, as a consequence of the magmatic camera evolution; time series of displacement have been extracted and, whenever possible, ascending and descending geometry dataset have been jointly exploited in order to produce vertical and easting displacement maps. The test cases presented will give the opportunity to describe the enhancement applied to the PSInSAR_{T,Bi} processing chain, required to make the algorithm capable to cope with the complex volcanic deformation dynamics (abrupt changes, non-linear motion) and to allow their representation through a web interface for a quick browsing of the results provided to the users. [C1898]

"Remote sensing image fusion based on fast discrete curvelet transform"

Wavelet transform has the good characteristic of spatial and frequency locality, but it isn't suitable for describing the signals, which have high dimensional singularities. Curvelet is one of new multiscale transform theories, which possess directionality and anisotropy, and it breaks some inherent limitations of wavelet in representing directions of edges in image. So when the curvelet transform is applied in image fusion, the characteristics of original images are taken better and implemented more easily. This paper tries fast discrete curvelet transform (FDCT) for image fusion of SAR (synthetic aperture radar) image and TM (thematic mapper) image. Then, visual result and statistical parameters are used to evaluate the result. The experimental results indicate that the FDCT-based fusion method can provide more detailed spatial information and simultaneously, preserves the richer spectral content than the conventional approach, such as the discrete wavelet transform (DWT) and the intensity-hue-saturation (IHS) transform. [C1899]

"The Mid-Atlantic Regional Coastal Ocean Observing System: Serving coast guard needs in the mid-atlantic bight"

The mid-atlantic regional coastal ocean observing system (MARCOOS) will implement an end-to-end regional ocean data acquisition, management, modeling and product generation system to satisfy user needs as defined by the middle atlantic coastal ocean observing regional association (MACOORA). MARCOOS will leverage extensive existing regional assets to augment federal backbone products in response to the MACOORA regional themes of maritime safety and ecological decision making. Regional products enabled by MARCOOS will in turn support the development of even higher resolution products at the sub-regional level, including supporting local MACOORA needs for Coastal Inundation and Water Quality. Through MARCOOS, regional scale observations from a network of HF-Radars, satellites, glider AUVs, and an array of meteorological stations will feed 4 operational numerical modeling systems. The HF radar network provides near realtime surface current observations along 1000 km of coastline with varying coverage from the coast out to the shelf break. The primary goal is to operate the regional system in a coordinated way to guarantee the delivery of quality ocean current and wave data. In this paper we present MARCOOS with an emphasis on the HF Radar network. Particular attention is placed on the setup, operation, and application of the network. Quality control metrics based on comparisons with coast guard deployed surface drifters (SLDMBs) have a specific focus to quantifying the uncertainty in the HF radar surface current estimates as applied to search and rescue observations. These metrics will be used to ensure that quality data is going to the coast guard and that this information is properly incorporated into existing search planning tools. [C1900]

"Remote sensing of coastal ecosystems"

Advances in sensor design and data analysis techniques are now making remote sensing systems practical and attractive for coastal ecosystem research and management. Multispectral and hyperspectral imagers are available for mapping coastal land cover and concentrations of organic/inorganic suspended particles and dissolved substances in coastal waters. Thermal infrared scanners can map sea surface temperatures accurately and chart coastal currents, while microwave radiometers can measure ocean salinity, soil moisture and other hydrologic parameters. Radar imagers, scatterometers and altimeters provide information on ocean waves, ocean winds, sea surface height and coastal currents. Using airborne LIDARs one can produce bathymetric maps, even in moderately turbid coastal waters. Since coastal ecosystems have high spatial complexity and temporal variability, they frequently have to be observed from both, satellite and aircraft, in order to obtain the required spatial, spectral and temporal resolutions. A reliable field data collection approach using ships, buoys, and field instruments with a valid sampling scheme is required to calibrate and validate the remotely sensed information. This paper presents a brief overview of recent advances in coastal remote sensing. [C1901]

"Multi-photo combined adjustment with airborne SAR images based on a few ground control points"

This paper introduces an ortho-rectification method of airborne SAR images which is multi-photo combined adjustment method in the circumstances of a few Ground Control Points (GCPs). Multi-photo combined adjustment model and adjustment conditions are given, and the number and distribution of GCPs, pass points is analyzed in this paper. Two adjustment experiments have been done with one-meter resolution airborne SAR images in Chengdu study site. In the two experiments, the GCPs and the Pass Points are distributed rationally in each image. The two experimental results show that the coordinate accuracy of Pass Points is feasible for 1:10 000 scale ortho-image making and topographic map updating. Compared with traditional ortho-rectification, which needs more than six GCPs in single image, this method reduces ground control work dramatically. [C1902]

"Road tracking by Parallel Angular Texture Signature"

Road tracking is a promising technique to increase the efficiency of road mapping. In this paper, a new semi-automatic road tracker, parallel angular texture signature (PATS) is presented. The tracker is object-oriented in some sense, because it makes best use of the texture signature of road primitives on high-resolution remotely sensed imagery. Our tracker uses parabola to model the road trajectory and predict the position of next road centreline point. It employs parallel angular texture signature (PATS) to get the moving direction of current road centreline point, and it will move on one predefined step along the direction to reach a new position, and then it uses curvature change to verify the newly added road point. We also build compactness of Angular Texture Signature polygon to check whether the parallel angular texture signature (PATS) is suitable for tracking. Extensive experiments demonstrate that the proposed tracker reliably extracts ribbon roads from high resolution optical imagery even in very complex scenes. [C1903]

"Object-oriented classification of polarimetric SAR imagery based on Statistical Region Merging and Support Vector Machine"

This paper presents a new object-oriented classification method based on statistical region merging (SRM) for segmentation and support vector machine (SVM) for classification where polarimetric synthetic aperture radar (PolSAR) data are used. The proposed approach makes use of polarimetric information of PolSAR data, and takes advantage of SRM and SVM. The SRM segmentation method not only considers spectral, shape, scale information, but also has the ability to cope with significant noise corruption, handle occlusions. The SVM used for classification takes its advantages of solving sparse sampling, non-linear, high-dimensional, and global optimum problems comparing with other classifiers. It is thus expected that the input vectors of SVM will include fully polarimetric information for image classification. A test image, acquired by the Jet Propulsion Laboratory Airborne SAR (AIRSAR) system, is used to demonstrate the advantages of the proposed method. It is shown that the proposed approach outperforms the traditional pixel-based SVM classification method for land cover classification with PolSAR data, and the integration of SRM and SVM makes the proposed algorithm an attractive and alternative method for polarimetric SAR classification. [C1904]

"Ground truth extraction from LiDAR data for image orthorectification"

The availability of high accuracy GCPs (ground control points) and DEMs (digital elevation models) becomes the key issue for successful implementation of an image orthorectification project. It is a very difficult task for collecting a large number of high quality GCPs by using traditional methods to meet all the requirements for digital photogrammetric and orthorectification process. Airborne light detection and ranging (LiDAR)-also referred to as airborne laser scanning (ALS), provides an alternative for high-density and high-accuracy three-dimensional terrain point data acquisition. One of the appealing features in the LiDAR output is the direct availability of three dimensional coordinates of points and intensity data in object space. With LiDAR data, high-accuracy and high-resolution intensity image, hillshade DSM (digital surface model) image, and DEM can be generated. Due to high planimetric accuracy characteristics of LiDAR data, ground truth can be extracted from these LiDAR-derived products (e.g., hillshade image and intensity image). This study investigated the feasibility of using LiDAR-derived hillshade DSM image and intensity image to extract ground truth for aerial image orthorectification. Two sets of GCPs were extracted from hillshade image and intensity image separately, and then were used as the inputs for aerial triangulation processing. LiDAR- derived DEM was then employed for differential rectification to produce the final orthoimage. The assessment of the planimetric accuracy of orthorectified images by using different set of GCPs was conducted by comparing the coordinates of some checking points from orthoimages and correspondent GPS surveyed coordinates. [C1905]

"Ship detection over single-look complex SAR images"

Synthetic aperture radar (SAR) ship detection is an important application in the context of environment and security monitoring. Ship detection techniques are generally based on statistically significant contrast between the ship and the local ocean background. Typically, high resolution (few tenths of meters) SAR images need to be considered. Such images are heavily affected by the presence of the speckle, and, for this reason, many ship detection algorithms employ constant false alarm rate (CFAR) algorithms. In this study, a different approach is proposed. The speckle is not mitigated but considered as a source of information. The ship is considered as a dominant scatterer responsible for a strong and coherent backscatter signal. Hence, the different behavior of the speckle statistics in presence of a dominant scatterer exploited. A new simple and very effective filtering technique, which is able to process high resolution SAR images, has been conceived and implemented. Experiments, accomplished over C-band Single Look Complex ERS 1/2 SAR images, show the effectiveness of this new approach for ship detection. [C1906]

"Polarimetric signature for oil spill observation"

Synthetic aperture radar (SAR) oil spill observation is not at all an easy task since the presence of many natural phenomena and surfactants call for complex and time-consuming classification techniques, generally based on the use of ancillary external data. In this study, polarization diversity is employed to assist oil spill observation techniques. The polarization signature, commonly used for land application, is firstly read in terms of a sea surface scattering mechanism with and without surface slicks. Experiments, accomplished over multilook complex (MLC) C-band SIR-C/X-SAR data, show that the polarization signature can be useful both for observing oil spills and for distinguishing between oil spills and biogenic look-alikes. [C1907]

"EASI Modelling Algorithms for Aerosol-Cloud Distribution Analysis"

Algorithms to distinguish between clouds and aerosols are important in the environmental and remote sensing study. The colour-modulated image from cloud aerosol lidar and infrared pathfinder satellite observation (CALIPSO) has been analysed in this study. CALIPSO is currently obtaining global aerosol and cloud measurements from space. We study the possibility to apply EASI modelling algorithms to differentiate aerosols and clouds in the CALIPSO image. This image processing method has shown good outcome for visualization analysis. [C1908]

"Detection of oil spills on SAR images, identification of polluters and forecast of the slicks trajectory"

SAR images from the Estonian coastal area were analyzed to identify oil spills. Slicks were detected on five images in February and March 2008. The analysis showed that the slicks occurred on the ship track. Seatrack Web model (SMHI) that includes ship automatic identification (AIS) data provides a possibility to identify the polluters. In two cases the hindcast model together with AIS information system enabled to detect the possible polluters. [C1909]

"Recent advances in ferrybox monitoring on board Finnmaid ferry"

Finnish Institute of Marine Research (FIMR) as a founding member of Alg@line consortium has been a forerunner in the field of monitoring research using commercial ferries. In 1992 FIMR started continuous measurements on board the ferry Finnjet, crossing the Baltic Sea Proper, using unattended recording and sampling system. During the spring of 2007 the ferrybox monitoring system was reinstalled in a new ferry Finnmaid providing real time observed data transmission with satellite connection. Chlorophyll-a (Chla) still remains the principal monitoring parameter. However, the distribution of cyanobacteria cannot be evaluated using Chla in vivo fluorescence, as most of their Chla is located in the poorly-fluorescing photosystem I. Instead, phycocyanin (PC) fluorescence is used in the detection of cyanobacterial blooms in 2005-07. PC fluorescence shows a linear relation to the biomass of the bloom forming filamentous cyanobacteria. During blooms of filamentous cyanobacteria the variability in Chla concentrations is better explained by PC fluorescence than by Chla fluorescence. Additionally, Chla records have been applied in validation of MODIS satellite monitoring for the water quality. [C1910]

"Seatrack Web forecasts and backtracking of oil spills-an efficient tool to find illegal spills using AIS"

Seatrack Web is a fully operational oil drift forecasting system. It covers the Baltic Sea and part of the North Sea. The system is available over the Internet and has the latest weather and ocean forecasts, thus giving the user the best possible decision tool in an oil combating situation. The drift model calculates the three-dimensional movements of substances or objects at sea, including sinking, stranding and turbulent dispersion. For oils, the evaporation, emulsification and wave-induced vertical dispersion are also calculated. Seatrack Web is the HELCOM system for forecasting of oil drift, and the primary users are oil combating authorities in the countries surrounding the Baltic Sea. It has been in operation since the early 1990s. The system now includes several new features, where a coupling to an AIS (Automatic Identification System) ship track data base is the most important. When finding a spill in the sea, it is possible to make a backtracking calculation with the system. The result shows every hour the location of the oil back in time. Adding AIS data to those oiled areas shows clearly which ships have been close to the oil during the whole calculation period. The system then fetches new ship tracks in space and time depending on the changing positions of the oil. A large number of possible ships are often found, and those can then be deleted successively after analyses and more information about the circumstances. The first year of experience with using AIS in Seatrack Web have led to many suggestions for improvement. It now, for instance, works faster to identify the suspected ships and it is also easier to ignore irrelevant ships. One valuable new feature is that if AIS data are missing it is possible to take those data from

the log book and fill in so the ship track will be completed, thus having correct information when analysing the situation. During 2008 satellite information will be shown in the map, which simplifies the identification of illegal polluters even further. The satellite image can also show an ongoing release of a spill, by showing a ship connected to the oil while releasing it. Two radar satellites will be used, RADARSAT 1 and ENVISAT. A case with all information included can also be saved to show as evidence in court at later occasions as animation or special pictures. [C1911]

"Possibilities of identification of oil films using radar probing of the sea surface"

A brief review of experiments on damping of short wind waves due to surfactant (monomolecular) and oil films carried out at the Institute of Applied Physics RAS using radar and optical methods is given. The damping degree of wind waves (spectral contrast) in film slicks is analyzed in a wide (decimeter-centimetre-scale) wavelength range of wind waves at different wind speeds and physical characteristics of films. A simple local balance model of the wind wave spectrum is developed to describe the film effect on short wind waves. Differences in the spectral contrasts for film slicks and for some "look-alikes", in particular, for wind depression areas (WDA) are revealed: the spectral contrast for film slicks increases with surface wave number, while for WDA the contrast is practically constant for decimeter-centimeter-scale wind waves. The specific behaviour of the spectral contrast can be used as a slick "spectral signature". [C1912]

"Detecting ground deformation with Permanent scatterer of Suzhou region"

Permanent scatterer interferometry is one of the latest developments in radar interferometric processing. It is achieved by the analysis of the interferometric phase of the individual point targets that are discrete and temporarily stable natural reflectors or permanent scatterers in long temporal series of interferometric SAR images with one master image. The wrapped phase of a point in differential interferogram can be decomposed to uncompensated topography, target motion in the time between the acquisitions, object scattering phase related to the path length traveled in the resolution cell, the atmospheric phase accounting for signal delays, the phase caused by imprecise orbit data and additive noise term. Based on this principle, it could bypass the problem of geometrical and temporal decorrelation. Furthermore, by using a large amount of data, atmospheric signal is estimated and corrected for. This paper addresses the how we use the PS-InSAR technology and Differential Interferogram procedure to estimate the velocity of deformation of Suzhou region in the time span 1992-2002. The main processing is done with the GAMMA software. [C1913]

"Registration of remote sensing images based on Gaussian fitting"

Image registration is one of the critical techniques in multi-sensor image fusion. Classical image registration method using similarity measures can only find Registration Control Point (RCP) on discrete points on images, which makes it difficult to get higher registration precision. This paper presents an image registration method based on Gaussian fitting matching, which takes two dimensional Gaussian fit matching on measurement matrix produced by classical search method of image RCPs. This method has the potential of getting more accurate position of RCPs. Experiment shows that using our method can obtain higher registration accuracy than that of classical method. [C1914]

"Correlation processing of noise-like signals from coherent radar"

The paper is devoted to an algorithm for processing of a like-noise signal that corresponds to volume scatterers in turbulent steams. The algorithm is based on properties of the signal correlation functions and as the experiments showed the algorithm provides gain in signal-to-noise ratio more than 20 dB. [C1915]

"Distributed Collaborative Adaptive Sensor networks for remote sensing applications"

Enabled by a dense network of Doppler weather radars with overlapping coverage, Distributed Collaborative Adaptive Sensing (DCAS) represents a new paradigm in remote sensing. Rather than each radar periodically sampling its surroundings with sit-and-spin volume coverage patterns as with today's NEXRAD weather radars, DCAS is an end-user driven approach that targets sensitivity when and where the needs of its end-users are greatest. The advantage is that by adaptively allocating sensitivity, higher quality measurements are possible due to the ability to dwell longer in volumes where echoes are weak, sample faster in volumes with rapidly evolving dynamics, and obtain multi-Doppler looks for high accuracy wind field retrieval. This paper describes the multiuser, multi-attribute utilities-based approach being used to coordinate the scanning activities of the weather radars in the first prototype DCAS system being fielded by the National Science Foundation sponsored Engineering Research Center for Collaborative Adaptive Sensing of the Atmosphere (CASA- ERC). [C1916]

"Classification algorithms for weather radar"

Theory, measurements, and signal processing applying to the radar remote sensing of weather objects are considered. Algorithms for hydrometeor type and turbulence intensity recognition are developed and analyzed. Particularly, fuzzy logic and neural network approaches are applied for weather radar signal processing. [C1917]

"X-band opacity of a tropical tree canopy and its relation to intercepted rain, eddy fluxes and other meteorological variables"

During summer and autumn 2007, we deployed a 11 GHz microwave radiometer in an experimental tree plantation in Sardinilla, Panama, in the vicinity of the Panama Canal. With this instrument, we determined the opacity of the tree canopy. A collocated eddy-covariance flux tower measured water vapor and carbon dioxide fluxes as well as other meteorological variables such as photosynthetically active radiation (PAR), vapor pressure deficit (VPD) and rain. We observed a pronounced diurnal cycle of the opacity during dry periods and a close relation of the opacity to canopy intercepted rain during rainy periods. The diurnal opacity cycle shows a strong correlation with PAR, VPD and the water vapor flux. [C1918]

"Radiometric observations of vines from the green period to the withering"

The SMOS REFLEX 2006 field experiment aimed to monitor changes in the L-band (1.4 GHz) emission of vineyards as a function of the plants development. The experiment site was the Valencia Anchor Station, which has been selected as a calibration/validation site for the ESA's Soil Moisture and Ocean Salinity (SMOS) mission. This paper presents SMOS REFLEX 2006 and shows the temporal variation of the emissivity. The daily emission decreases from dusk till dawn and then increases again in the daylight hours. This oscillation in the emissivity has a peak to peak variation up to 0.05 (~ 15 K in brightness temperature). Emissivity decreases with time, especially at H-polarisation, due to the increase in the vegetation water content before harvest, and to the increase in soil moisture due to rain events after harvest. The contribution of soil to the measured emissivity is larger after harvest and at incidence angles smaller than 55deg. In this case, an increase in the rock-fraction decreases the mean range of emissivity up to 68%. [C1919]

"CFAR robust detection of moving target in presence of fluctuating background"

The paper describes the techniques for the autonomous detection of moving targets by processing a sequence of sensor imageries in remote sensing applications. Two detection algorithms, which do not need a matrix inversion, are developed by extension of Hotelling's principal-component method showing excellent performance and robustness. The detection of small, barely discernible, moving objects in presence of correlated fluctuating background and unknown background intensity are presented and tested experimentally. [C1920]

"A dual-frequency dual-polarized planar airborne array antenna"

A new dual-frequency dual-polarized array antenna for airborne applications is presented. Two planar arrays with ultra-thin substrates are integrated to provide a simultaneous operation of S-band and X-band. The ultra-thin array can be easily placed on the aircraft fuselage due to its lightweight and conformal structure, and will be useful for the use of wireless communications, radar, remote sensing, and surveillance. [C1921]

"Recent investigations in sensing through the wall radar modeling"

This paper presents radar imaging simulations for sensing through the wall (STTW) applications. One area of investigation is the synthetic aperture radar (SAR) image of a human body as compared to that of common furniture objects. Another topic analyzes the advantages of using a cross-polarization radar configuration in detecting humans inside rooms and buildings. The electromagnetic scattering models were performed using the Finite Difference Time Domain (FDTD) technique. [C1922]

"GA optimized reconfigurable frequency selective surfaces for passive standoff detection of chemical agents"

In this paper we present a new class of reconfigurable frequency selective surfaces (FSS) for the remote passive detection of chemical agents. The frequency selective surface is composed of a periodic tiled pixelized pattern on a thin dielectric substrate. The pixelized pattern consists of squares of either metallic patches or chemoresistive patches. In the absence of an analyte, the chemoresistive patches have a high impedance and in the presence of an analyte they have a low impedance. The FSS is designed to provide a sharp narrowband reflection resonance that shifts down in frequency with exposure to the analyte. The geometry of the FSS is selected via a Genetic Algorithm (GA) [1]. [C1923]

"Polarization filtering enhancement of buried landmine"

Here the optimum polarization of antenna for buried landmines detection in soil surface clutter is investigated theoretically to enhance radar target back scattered power. An expression of the Mueller matrix from this fractal surface is obtained. The optimum polarization to reduce clutter is given. Then, the variations are found of power density of buried landmines with polarization state, and the optimum polarization is given to increase power density. In the end, the paper researches the polarization filtering enhancement of buried landmines in soil surface clutter. [C1924]

"Building segmentation for densely built urban regions using aerial LIDAR data"

We present a novel building segmentation system for densely built areas, containing thousands of buildings per square kilometer. We employ solely sparse LIDAR (Light/Laser Detection Ranging) 3D data, captured from an aerial platform, with resolution less than one point per square meter. The goal of our work is to create segmented and delineated buildings as well as structures on top of buildings without requiring scanning for the sides of buildings. Building segmentation is a critical component in many applications such as 3D visualization, robot navigation and cartography. LIDAR has emerged in recent years as a more robust alternative to 2D imagery because it acquires 3D structure directly, without the shortcomings of stereo in un-textured regions and at depth discontinuities. Our main technical contributions in this paper are: (i) a ground segmentation algorithm which can handle both rural regions, and heavily urbanized areas, where the ground is 20% or less of the data, (ii) a building segmentation technique, which is robust to buildings in close proximity to each other, sparse measurements and nearby structured vegetation clutter, and (iii) an algorithm for estimating the orientation of a boundary contour of a building, based on minimizing the number of vertices in a rectilinear approximation to the building outline, which can cope with significant quantization noise in the outline measurements. We have applied the proposed building segmentation system to several urban regions with areas of hundreds of square kilometers each, obtaining average segmentation speeds of less than three minutes per km² on a standard Pentium processor. Extensive qualitative results obtained by overlaying the 3D segmented regions onto 2D imagery indicate accurate performance of our system. [C1925]

"Automatic registration of aerial imagery with untextured 3D LiDAR models"

A fast 3D model reconstruction methodology is desirable in many applications such as urban planning, training, and simulations. In this paper, we develop an automated algorithm for texture mapping oblique aerial images onto a 3D model generated from airborne light detection and ranging (LiDAR) data. Our proposed system consists of two steps. In the first step, we combine vanishing points and global positioning system aided inertial system readings to roughly estimate the extrinsic parameters of a calibrated camera. In the second step, we refine the coarse estimate of the first step by applying a series of processing steps. Specifically, We extract 2D corners corresponding to orthogonal 3D structural corners as features from both images and the untextured 3D LiDAR model. The correspondence between an image and the 3D model is then performed using Hough transform and generalized M-estimator sample consensus. The resulting 2D corner matches are used in Lowe's algorithm to refine camera parameters obtained earlier. Our system achieves 91% correct pose recovery rate for 90 images over the downtown Berkeley area, and overall 61% accuracy rate for 358 images over the residential, downtown and campus portions of the city of Berkeley. [C1926]

"Post-doppler space-time filtering for suppressing moving target signals in multi-channel SAR data"

Synthetic aperture radar (SAR) as a method for ground imaging by using a single antenna or a sensor array has widely found attraction for remote sensing applications and reconnaissance tasks. Independent of the particular sensor but inherent to the SAR processing, moving objects in the observed scene will be imaged at wrong positions and can appear in a smeared fashion. To avoid these disturbing artifacts in the image, a joint spatial-spectral filtering approach is proposed in this paper that allows to suppress signal contributions from moving targets in multi-channel radar data. Results obtained with experimental data from an airborne system show the potential for a practical application of the presented method. [C1927]

"Comparison of two configurations of a four-reflector beam-waveguide for a large space communication facility"

In this paper we perform full-wave two-dimensional (2-D) simulation and performance comparison of the E-polarized beam wave guidance and scattering by two variations of a typical fragment of quasioptical feeding circuit of a deep-space communication antenna. The fragments are similar and consist of a chain of four finite-size reflectors and mirrors with varied position of the second pair. The feed beam generated by the aperture of a corrugated horn is simulated with the incident complex-source-point (CSP) field. Numerical solution is obtained

from the coupled singular integral equations (IEs) discretized using new quadrature formulas of interpolation type that take full account of the IE kernel singularity and the edge behaviour. [C1928]

"On realization of the transition radiation antenna"

Consideration is given to the possibility of realization of the transition radiation antenna. The radiation is formed by relativistic point charge scattering on a metal surface. A plane disk is proposed to be used as a reflector. For the spectrum of a point charge field $0 \text{ Hz} \leq f \leq 1 \text{ THz}$ the disk diameter should not exceed 1 m. The discrete character of radiation formation is marked. The antenna is a UWB antenna of a low-level power and can be used in the space-based systems. [C1929]

"Coherent scattering from distributed targets"

Based on the formulation for coherent backscattering from distributed targets previously published by the first author, this paper presents a unified formalism for incorporating the small amplitude, the small slope, the physical optics as well as a "two-scale model" approximation into analyses of backscattering by irregular air-dielectric interfaces. The distinguishing feature of this approach is that it takes explicit account of the antenna radiation properties and provides a direct means of numerically assessing the effects of spatial coherence of the surface irregularities on the receiver response. In particular, this leads to a generalization of the normalized backscattering cross-section which becomes dependent on both the antenna radiation properties and surface scattering characteristics. Numerical results obtained under the small amplitude approximation show that spatial coherence of the surface irregularities can lead to significant deviations from the classical Bragg scattering formula. [C1930]

"Dual band reconfigurable slot antenna with high frequency ratio"

In this paper, a design of compact dual band reconfigurable slot antenna is presented. The dual band operation is realised by effectively changing the slot electrical length using solid state shunt switches. Two resonant frequencies are obtained with the frequency ratio of 2:1. Although the ratio is high, good matching is achieved on both resonant frequencies without the need for a reconfigurable matching network. Also, radiation pattern, polarisation and efficiency remain reasonable similar at both frequencies. Computation results are confirmed with the experimental results. [C1931]

"Remote monitoring of human cardiorespiratory system parameters by radar and its applications"

The diagnostic monitoring of humans (as well as their detection behind of the opaque obstacles), by means of radar have called bio-radiolocation. As an illustration ultra-wideband (UWB) radar in medicine and in psychophysiology for remote measuring of patient's heart activity and respiration is shown. The measuring method is described and practical results of tests are cited. New technical decisions on hardware and software which allow obtaining reliable physiological data at the monitoring of back-and-forth motion of objects are considered. This paper considers various applications of the bio-radiolocation. [C1932]

"Integrated hardware reduction schemes for retrodirective array architectures"

This paper will present and review a few recent developments in retrodirective array architectures that integrate schemes for hardware reduction. The proposed systems offer simplified architectures for retrodirective array application that can lead to low-cost solutions for various communication scenarios. First, the flexibility of the retrodirective architecture is discussed with simple integration into sparse arrays. Combination of a sparse array with a switching network allows a single phase conjugator to be shared by four radiating elements within a six element aperture. Finally, an example of a conformal sparse retrodirective array is presented in a potential mobile platform application that is known to have limited hardware requirements. [C1933]

"Reconfigurable reflectarrays based on RF MEMS technology"

Innovative and high-performance antenna systems are required by the increasing demand of bandwidth and service quality in modern communication systems, as well as in a number of industrial applications. At the same time, new technologies and devices are emerging to comply with such specifications. Thanks to their inherent low costs and high performance, RF-MEMS can potentially bring in completely new classes of tuneable devices and circuits for RF applications. This paper focuses on the possible use of RF-MEMS in beam scanning antennas and particularly in reconfigurable reflectarrays. After reviewing some of the basic principles of such systems, two projects recently carried out in the framework of the AMICOM Network of Excellence are described. Besides the general features of these antennas, currently under test, the innovative single wafer architecture and the relevant packaging issues are specifically addressed. [C1934]

"A compact highly sensitive radiometer for thermal sounding of atmosphere in 5 MM band"

Design and characteristics of a compact highly sensitive direct detection MMIC radiometer of 5 MM wave band with a goal of atmosphere temperature profile determination are presented. The radiometer has bandwidth 56.6 plusmn 0.25 GHz and fluctuation sensitivity 35 mK/Hz^{1/2}/65 mK/Hz^{1/2} in a "total power" modulation mode. The radiometer was successfully used for atmospheric temperature profile measurements with the thermal sounder MTP-5. Average deviation of a measured atmospheric temperature profile from the temperature profile constructed according to 11 probes was 0.2 C-0.4 C, average mutual difference of two devices was equal to or less than 0.2 C. [C1935]

"Interactive-mode X-band direction-finder"

The compact broad-band direction-finder is presented in this paper. The bearing features and the operation algorithm of the system using the "null-amplitude" technique are described in detail. Based on the results of model experiments the sensitivity and resolving capacity of the direction-finder prototype are evaluated. The problems of bearing more than one SHF sources are discussed. [C1936]

"PaRaDe-PAssive RADar DEmonstrator family development at Warsaw University of Technology"

The paper presents a family of passive coherent location (PCL) radar demonstrators, called PaRaDe (passive radar demonstrator), which were developed at Warsaw University of Technology. The systems exploit commercial FM radio transmitters as illuminators of opportunity in order to detect and track airborne targets. In the paper, the details of demonstrator systems are described and the results obtained in tests are presented. [C1937]

"Coherent multilateration systems"

Passive coherent location systems using "transmitters of opportunity" like radio or TV broadcasters, GSM base stations, satellite communication and GNSS signals has reached a substantial attention in the last years. In this paper the coherent location system, based on bistatic radar principle with multiple non-cooperative transmitters is described and various aspects of signal processing and signal parameters are discussed. [C1938]

"Status of advanced scattering distortion system analysis for nav aids and radar-examples of A380 and wind turbines"

Modern systems, e.g. navigation, landing, radar and communication systems, rely on the physics of antennas and propagation. Their electrical performance is determined by the intended radiation and by the scattering of distorting objects. The scattering analysis is an integral part of the system simulations. The modeling of the antennas, the environment, the distorting objects and of the system itself are the basic steps of the simulation process. This paper describes the aspects of state-of-the art system simulations by evaluating actual examples, such as the new A380 with respect to the landing system ILS and wind turbines WT to radar systems, in particular to weather radar. [C1939]

"Material parameter measurements for microwave anti reflection coating development"

The main steps for characterization and measurement of microwave absorbent materials in the 1-10 GHz range is introduced. The coaxial reflection-transmission type of material parameter measurement is analyzed in detail and the main measurement error is corrected. The microscopic material particle parameter measurement concept is also presented using different mixing rule laws to determine the material parameters of the single particles from the macroscopic parameters. Two dimensional FDTD simulations have been used to model the behavior of mixed electric and magnetic type of material. [C1940]

"Analysis of generalized polarimetric measurement equations for Stokes polarimetry techniques"

We study the errors variances for some popular strategies of Stokes vector measurement. It was shown that the errors of the Stokes parameters measurement are non-uniformly distributed for different measurement strategies. This fact can be used in optimization of the polarization parameters measurement. [C1941]

"Fusion of Multi-band SAR Images Based on Nonsubsampled Contourlet and PCNN"

In this paper, a new fusion rule based on pulse coupled neural network (PCNN) and the clarity of images is proposed for multi-band synthetic aperture radar (SAR) images fusion. After the nonsubsampled Contourlet transform (NSCT) of the registered SAR images, we can get a flexible multiscale, multidirectional and shift-

invariant representation of images. Then the linking strength of each neuron in PCNN is determined by the clarity of images, and new fire mapping images are obtained for each decomposed subband image taking part in the fusion. Experimental results show that the new fusion rule outperforms some classical rules, and after the inverse NSCT, the obtained fusion image can preserve much information of textures and edges of images than its counterparts. [C1942]

"Synchronised data acquisition for sensor data fusion in airborne surveying"

An existing facility for data acquisition in aerial surveys is presented. It contains a laser radar, an infrared camera and a video camera. The system supports synchronisation of sensor data, even when the sensor does not inherently offer that feature. This allows data from different sensors to be merged and processed together. The necessary temporal referencing is achieved by specialised hardware implemented in a field programmable gate array, which also serves to acquire data from the IR camera. The usefulness of FPGAs for this purpose is demonstrated. The possibilities FPGAs offer are shown up, and future extension of the system are presented. [C1943]

"Application of generalized partial volume estimation for mutual information based registration of high resolution SAR and optical imagery"

Mutual information (MI) has proven its effectiveness for automated multimodal image registration for numerous remote sensing applications like image fusion. We analyze MI performance with respect to joint histogram bin size and the employed joint histogramming technique. The affect of generalized partial volume estimation (GPVE) utilizing B-spline kernels with different histogram bin sizes on MI performance has been thoroughly explored for registration of high resolution SAR (TerraSAR-X) and optical (IKONOS-2) satellite images. Our experiments highlight possibility of an inconsistent MI behavior with different joint histogram bin size which gets reduced with an increase in order of B-spline kernel employed in GPVE. In general, bin size reduction and/or increasing B-spline order have a smoothing affect on MI surfaces and even the lowest order B-spline with a suitable histogram bin size can achieve same pixel level accuracy as achieved by the higher order kernels more consistently. [C1944]

"Underwater motion and physiological sensing using UHF doppler radar"

The feasibility of Doppler radar measurement of physiological data from fish is demonstrated with a simple radar system. Detected motion includes body movement (locomotion), fin movement and other signals, such as gill movement. A video reference provides verification of the measured quantities for body and fin motion. The technology demonstrated in this experiment is expected to form the basis for systems that accurately sense gill and heart motion from moving fish in their natural environment. [C1945]

"Using LIDAR doppler velocity data and chaotic oscillatory-based neural network for the forecast of meso-scale wind field"

Current research based on various approaches including the use of numerical prediction models, statistical models and machine learning models have provided some encouraging results in the area of long-term weather forecasting. But at the level of meso-scale and even micro-scale severe weather phenomena (involving very short-term chaotic perturbations) such as turbulence and wind shear phenomena, these approaches have not been so successful. This paper focuses on the use of chaotic oscillatory-based neural networks for the study of a meso-scale weather phenomenon, namely, wind shear, a challenging and complex meteorological phenomena which has a vital impact on aviation safety. Using LIDAR data collected at the Hong Kong International Airport via the Hong Kong Observatory, we are able to forecast the Doppler velocities with reasonable accuracy and validate our prediction model. Preliminary results are promising and provide room for further research into its potential for application in aviation forecasting. [C1946]

"A Real Time Simulation of Flood Hazard"

Kuala Lumpur city is located at the confluence of two rivers and are flood prone area. With rapid development and uncontrolled town planning, the city had experience several major flash flood incidents and have caused tremendous damage to country. This research describes a study made to model and simulate the flash flood incident that struck Kuala Lumpur on 10 June 2007 using 3D computer graphic and fluid simulation techniques. The aim is to examine the stability and effectiveness of this approach as a solution tool for environmental hazard studies. Particle-based method used to model the fluid objects using MAYA software. Light detection and ranging (LIDAR) data and remote sensing imagery were used to model the study area. The main contribution of this study is the introduction of this approach to enhance realistic visualization for environmental studies thus

enable better planning and countermeasures created to prevent the disaster. [C1947]

"Multi-frequency polarimetric radar earth observations"

The air-borne multi-frequency polarimetric SAR IdquoIMARCrduo allows radar earth observation measurements at 4 frequency bands (X,L,P and VHF) and utilizes a complete set of different linear polarizations: VV, HH, VH and HV. Theoretical and experimental feasibilities have been carried out in recent years. System capabilities and potential applications have been demonstrated. Operational usage in a wide range of applications is expected. However, from our research it became obvious that despite interesting data can be collected the major limitation of full and reliable utilization in various applications comes from the mismatch between available electro-magnetic models and the description of the actual earth surface and sub-surface during the SAR measurement campaigns. Applications are foreseen in hydrology and in classifying vegetation, snow, ice and frozen soils, and in sub-surface sensing for locating artificial and natural objects, as well as different natural anomalies. New and more advanced electro-magnetic modeling is needed in order to exploit all IMARC potentials. In the framework of a large multi-national activity an integrated software package will be developed in which new and more-advanced vegetation surface and sub-surface scattering models are included. [C1948]

"Noise-robust data fusion on a pixel level"

In present paper there was done analysis of possibility to use local correlation at pixel level data fusion in order to increase effectiveness of multilevel information fusion method. [C1949]

"Design and fabrication of a 100 GHz channel-drop filter"

We have designed and are fabricating a novel passive mm-wave spectrometer based on a photonic band gap (PBG) channel-drop filter (CDF). There is a need for a compact, wide-band, versatile and configurable mm-wave spectrometer for applications in mm-wave communications, radio astronomy, and radar receivers for remote sensing and nonproliferation. The CDF spectrometer was designed to operate in the frequency range of 90-130 GHz. We have manufactured a single proof-of-principle channel-drop filter. The manufacturing process involved etching the rods on a silicon wafer and then bonding them to metallic plates. The initial testing results for the filter will be presented here. Research is also underway to explore alternative configurations of the CDF, including one with metallic rods. [C1950]

"Multispectral Land Cover Classification Using Averaged Learning Subspace Method"

For the excellent appearances of Subspace methods in dimension reduction and classification, it is useful to introduce them into classification for multispectral remotely sensed data. This paper presents the first utilization of averaged learning subspace method (ALSM) for land cover classification using Landsat TM image. In particular, a comparative study was made about the classification performances of ALSM and maximum likelihood classification (MLC). ALSM yielded higher classification accuracies than MLC; the overall accuracy of the former algorithm was 99.00% while that of MLC was only 94.99%. The comparison of the classification performance in terms of training set size shows that ALSM outperformed MLC. [C1951]

"SAR Image Compression Based on Bandelet Network"

Finding efficient geometric representations of images is a central issue in improving the efficiency of image compression. Bandelet provides an efficient way for image representation based on geometric regularity. However, a degeneration of performance will appear in high ratio compression for all the transformation based compression approaches. Moreover, Bandelet is time consuming and lacks of flexibility. In this paper, we construct a Bandelet network for image compression based on discrete Bandelet frame, in which the Bandelet basis is adopted as the activation function in the hidden layer of a feed-forward neural network. The Bandelet basis can provide an efficient representation of image. Moreover, neural networks based methods is more flexible and can achieve high compression ratio with its parallel implementation structure, when compared with transformation based image compression approaches. The construction and the leaning of the Bandelet network are addressed. Experiment results show that it can provide a potential way for SAR image compression. [C1952]

"A texture based approach for ocean surface wind detection in SAR images"

The radar backscattering on the sea surface is used for wind direction estimation. Current approaches at this problem are based on spectral methods which have limited spatial resolutions. Recent Image Processing methods use features extracted from local histograms of the image gradient direction. Here we report an alternative image processing approach which is based on the idea of extracting the preferred orientation of the textural patterns rather than the preferred orientation of the energy variation. Our method is based on a

multichannel filtering approach which decomposes the input image over a set of matched filters. We also use a regularization operator for the detected orientations based on non linear diffusion. Experimental results are reported on synthetic images and real images. [C1953]

"Application of artificial neural computation in topeX waveform data: A case study in water ratio regression"

Using the TOPEX radar altimeter for land cover studies has been of great interest due to the TOPEX near global coverage and its consistent availability of waveform data for about one and a half decades from 1992 to 2005. However, the complexity of the TOPEX Sensor Data Records (SDRs) makes the recognition of the radar echoes particularly difficult. In this paper, artificial neural computation as one of the most powerful algorithms in pattern recognition is investigated for water ratio assessment over Lake of the Woods area using TOPEX reflected radar signals. Results demonstrate that neural networks have the capability in identifying water proportion from the TOPEX radar information, controlling the predicted errors in a reasonable range. [C1954]

"2-8 GHz FMCW radar for estimating snow depth on antarctic sea ice"

This paper presents the development and initial results from a prototype airborne Frequency Modulated Continuous Wave (FMCW) snow thickness radar operating at 2-8 GHz. The FMCW radar was constructed at the Center for Remote Sensing of Ice Sheets (CReSIS), Kansas University (USA), and is the product of a collaborative effort between Kansas University, the University of Tasmania (Australia) and the Australian Antarctic Division. This radar was successfully tested in a laboratory, and then deployed on a helicopter during the Australian-led Sea Ice Physics and Ecosystem Experiment (SIPEX) research cruise to the East Antarctic pack ice zone in September-October 2007. Approximately twenty hours of airborne radar data were collected and time-stamped with GPS data for accurate geolocation. Coincident data from a scanning laser altimeter, as well as digital photography, enable a multi-dimensional view of the sample areas, and are important for interpreting the radar signatures. The data obtained provide a multi-dimensional view of the snow and sea ice surface. [C1955]

"A new separation method for Micro-Doppler information of a target with rotating parts"

The classical range-Doppler algorithm canpsilat obtain clear ISAR image of a target with rotating parts. In spectrogram, the micro-Doppler information of the rotor blades is represented as the sinusoidal frequency modulation, whereas the information of main body is depicted as the form of straight lines. So the extraction of micro-Doppler is transformed to the separation of the sinusoids and straight lines. Based on this idea, a simple method of spectrogram cancellation is proposed, which can quickly achieve the purpose of separation and get clear ISAR image of main body. The effectiveness of the algorithm is proved by the simulation results. [C1956]

"Multi year sea ice concentration mapping using passive and active microwave satellite data"

Though changes of the full ice cover in the Arctic are well described due to availability for processing SMMR/SSM/I passive microwave data, changes of the composition of the Arctic ice cover, in terms of ice types still need to be quantified, at least for winter season. Algorithms for mapping multiyear ice concentrations based on passive microwave data suffer from a number of problems. In this paper, those problems are described and it has been shown that QuikSCAT scatterometer data can add complimentary information to that available from passive microwave, which can assist in fixing the boundary between first-year and multiyear ice and in removing erroneously classified by passive microwave algorithm multiyear ice in the ice edge area. [C1957]

"Using Airborne Hydrographic LiDAR To Support Mapping of California's Waters"

A specialist team comprising academic, industry and government members is underway in a program that will ultimately lead to mapping of all 14,500 km² of California's state waters from MHHW out to the three-nautical-mile boundary. The technical and scientific team is lead by California State Coastal Conservancy through a contract with California State University Monterey Bay (CSUMB), and includes principle investigators from the seafloor mapping Lab of CSUMB, Fugro Pelagos, Inc; the US geological survey's coastal and marine geology program; and moss landing marine Labs' center for habitat studies. The data acquisition program includes a seafloor mapping component that incorporates the latest multibeam echosounding and airborne LiDAR bathymetry technologies and a ground truth component that includes video transects and sampling. This presentation describes the comprehensive and high-resolution seafloor-mapping program, with a focus on integrating the airborne LIDAR component with the multibeam data. The airborne bathymetric LiDAR sensor is capable of providing beach and bluff topography, digital aerial imagery, nearshore bathymetry and nearshore seabed laser reflectance imagery. All LiDAR data will be integrated with deeper water acoustic data and ground truth data to ultimately support a three-tier level of data processing and analyses. The Tier 1 and Tier 2 products specified as

requirements include a minimum of nine GIS data layers (ESRI compatible) with FGDC compliant metadata files. Two tier 3 interpretation example products are also being created: 1) an updated 1:100,000 essential fish habitat (EFH) interpretation map, and 2) a 1:24,000 geological quad map. The first portion of the California coast to be mapped extends from Punta Arena north of the golden gate, southward to Punta del Aflo Nuevo. This area was identified as a high priority during a workshop attended by statewide stakeholders. This ground-breaking program is funded by the California- Ocean Protection Council through the California State Coastal Conservancy. The program manager was the Monterey Bay Sanctuary Foundation, working in collaboration with NOAA's National Marine Sanctuary Program. This presentation includes sections on the various technologies used, examples of results obtained to date, notes on planning the statewide mapping program, and a report on current program status. This major integrated mapping program along 1800 km of shoreline is establishing standards that can be applied to new regional coastal and offshore mapping for the management of marine resources. [C1958]

"High-Resolution Inverse Synthetic Aperture Radar Imaging Based on the Shooting and Bouncing Ray Method"

This paper concerns the simulation of inverse synthetic aperture radar (ISAR) image for radar targets based on the shooting and bouncing ray (SBR) method. Contrary to the conventional approach where the ISAR image is obtained by inverse Fourier transforming to the scattering field, we adopt a newly-developed method [8], where the Fourier transformation has been merged into the SBR algorithm. Such a method has been improved and used in the imaging of real-size aircraft. High resolution two-dimensional ISAR images have been obtained. Hence such a method is considered as a general tool for the characterization of large and complex targets. [C1959]

"Z-R Relationship from the Particle Size and Velocity (Parsivel) Optical Disdrometer and its Application in Estimating Areal Rainfall"

In order to improve the precision of Radar rainfall estimates, the Parsivel was used for observation of rain drop spectra over Leizhou Peninsula from July to August, 2007. A total of 18070 size distributions were analyzed and the Z-R relationship of convective precipitation and mixtures of convective and stratocumulus cumulogenitus precipitation were obtained. These Z-R values were used for estimating areal rainfall and then compared with observations from automatic weather station. Cases with convective and mixtures of convective and stratocumulus cumulogenitus precipitation were selected for the evaluation. The precipitation studies were also used to evaluate the precision of the PARSIVEL measurements as compared to the rainfall data of automatic weather station. [C1960]

"Ocean Observing System in the East China Sea"

With the enforcement of the Basic Act on Ocean Policy, on July 20, 2007 of the original Marine Day, Japan should give the highest priority to the Exclusive Economic Zone (EEZ) in the East China Sea in the management of the Japanese EEZ. This paper describes the state of ocean observing system in the East China Sea present and future. [C1961]

"Development of Coherent, Expandable, Reconfigurable Instrument Node (ERIN) for Web Sensor Applications"

Microwave radars operating over the L-band microwave spectrum are often used as sensors for estimation of vegetation biomass, land surface topography and surface deformation, surface soil moisture, and polar ice sheets thickness. Monitoring of these parameters is essential for gauging the Earth's ecosystem. Because of restriction on the mass and size of a radar sensor that can be deployed on a small aircraft/spacecraft, the surface resolution with which these essential earth parameters can be improved using this technology by forming interferometric baselines between nodes. The expandable reconfigurable instrument node (ERIN) will provide a semi-closed loop system solution for a variety of sensors. The ERIN baselines a reconfigurable processing technology with required memory to allow on-board processing of science data. Standardized interfaces are provided to allow for interfacing to attitude control instrumentation such as global positioning systems (GPS) and inertial measurement units (IMU). A communications device will be added to the node that would allow for node-to-node communications. [C1962]

"Image fusion of radar and optical remote sensing data for land cover classification"

The aim of this paper is to propose a new unsupervised land cover classification method based on probabilistic fusion theory. This method combines two different Besag Markovian auto models: a Markovian Gamma auto

model that characterizes the radar texture data and a Gaussian Markov Random Field auto model to characterize the optical spectral data. An optimal Markovian neighborhood order is also applied in order to improve the speckle texture modeling. [C1963]

"A Monostatic Ocean Scattering Cross Section for the Case of Surface Wave Radar Operating from a Floating Barge"

An understanding of the parameters affecting the high frequency surface wave radar (HFSWR) cross sections of the ocean surface is essential to employing such formulations in remote sensing models. Available techniques to date have not explicitly included the effect of antenna motion on the ocean clutter spectra derived from HF Doppler radar data. Here, a model, which assumes the incident radiation to be a simple pulse and accounts for the fact that there may be antenna motion in the radar look direction, is presented. Simulations indicate that the motion of the antennas may give rise to additional, significant spectral content which cannot be ignored when the Doppler spectra are used for ocean parameter estimation. [C1964]

"Practical Algorithms for Gathering Stored Correlated Data in a Network"

Many sensing systems remotely monitor/measure an environment at several sites, and then report these observations to a central site. We propose and investigate several practical algorithms for joint routing and compression of data files as they are forward from remote nodes to a central site, with the goal of minimizing the communication cost incurred. Our algorithms are practical in that they do not assume that nodes have a priori information about the correlation structure (and resulting compression gains) of the individual measurements at a given sensor or among multiple sensors. Instead, this correlation structure is learned as pieces of the files are routed and jointly compressed on their way to the sink, and routes are adaptively changed as the nodes learn more about the correlation structure of the data. [C1965]

"Three-dimensional Microwave Tomography: Waveform diversity and distributed sensors for detecting and imaging buried objects with suppressed electromagnetic interference"

Microwave tomographic techniques are described in this paper for developing high-resolution images of buried targets using 3D RF CAT Scans with frequency, angular, and polarization diversity and distributed sensors. Surface-contact sensors are used to collect the tomographic data for relay to a circling UAV and transmission to a remote control site (using layered sensing). 3D imaging algorithms have been developed to detect, image, and characterize buried targets. Distributed transmitters and receivers significantly increase unwanted mutual coupling and EM emissions (EMI) that interfere with signal reception, but also increase image resolution. For Ground Penetration (GPEN), reduced mutual coupling and EMI, and improved signal-to-noise ratios (SNR), can be achieved by embedding the transmitter/receiver sensors underground. Simple surface SAR experiments have been performed to detect deep mine shafts at the Zinc Corporation of America. 2D sensor data have been used to validate the 3D processing algorithms. Scale-model lab tests in the DETECT Chamber at AFRL have also been performed to optimize the tomographic images. In addition, WIPL-D models have been used to simulate the embedded and diverse/distributed sensors and to verify the significant enhancement in the received SNR for GPEN obtained by burying the radiating ring under the surface. [C1966]

"Detection and velocity estimation of moving vehicles in high-resolution spaceborne synthetic aperture radar data"

Automatic estimation of traffic parameters has evolved to an important topic of research. Current and upcoming SAR satellite missions offer new possibilities for traffic monitoring and control from space as an alternative to conventional traffic data acquisition. In this paper a detection approach is presented which evaluates simultaneously the effects moving objects suffer from in the SAR focusing process. Information about the measured signal and the expected signal are utilized in the detection framework. Analyses of the proposed technique are done with real spaceborne SAR data. [C1967]

"Compact Digital Receiver Development for Radar Based Remote Sensing"

This paper is the first of a series of publications that discusses the design and implementation of an inexpensive, nearly all-digital FPGA-based radar receiver which can be used in a variety of applications including single/dual-polarization weather radar, sidelobe cancellation, a subarray module for a digital beam-forming phased-array radar, and other applications where a compact, low-power, low-cost receiver is needed. The design of the receiver includes a minimal analog RF front-end followed by an analog-to-digital converter utilizing a bandpass sampling technique which allows the FPGA to produce baseband in-phase (I) and quadrature (Q) signals without the use of multipliers or look-up tables. The primary difference between the efforts of others and the efforts here

is the use of single or multiple frequency channels in the receiver. The efforts of others have had applications in multi-channel military radars and in software defined radios that receive a variety of information. Here, only one frequency channel is needed for environmental observations, which provides a unique impetus to facilitate low-cost, low-power designs by leveraging software defined radio techniques. [C1968]

"An aperture synthesis radiometer at millimeter wave band"

Synthetic aperture radiometer has the potential to meet the spatial resolution requirement of passive microwave remote sensing from space. A one-dimensional prototype of aperture synthesis radiometer at millimeter wave band is introduced in this paper. It contains 16 antenna elements, 16 receiving channels, 16 ADCs, and image reconstruction part. Error correction is made in the image reconstruction. Experiment results show the radiometer can give good images of natural scenes. [C1969]

"An overlapped subaperture polar format algorithm based on sub-chirp signals"

In this work, a 2-D subaperture polar format algorithm (PFA) based on stepped-chirp signal is proposed. Instead of traditional pulse synthesis preprocessing, the presented method integrates the pulse synthesis process into the range subaperture processing. Meanwhile, due to the multi-resolution property of subaperture processing, this algorithm is able to compensate the space-variant phase error caused by the radar motion during the pulse cluster. Point target simulation has validated the presented algorithm. [C1970]

"FPGA based radar image enhanced: A robust evolutionary controlled filter approach"

In this work, we implemented the robust evolutionary controlled (REC) filter in a FPGA platform. Due unknown a priori statistical information, we replace the Optimal Wiener Filter by its rough approximation referred to as REC filter. The evolution of the filter is controlled by changing/choosing the vector of the controlled parameters gamma. Such a control provides additional degrees of freedom of the filter. We report and discuss some implementation results in the Xilinx Virtex-II Pro XC2VP30 FPGA related to enhancement of the uncertain real-world RS imagery, these are indicative of the significantly increased performance efficiency gained with the developed approach. [C1971]

"A High Altitude Airborne Wind Mapping Radar"

Through the NASA Instrument Incubator Program (IIP), NASA, the University of Massachusetts and remote sensing solutions have teamed to design and develop a dual wavelength, dual beam conically scanning Doppler radar for deployment on the NASA Global Hawk platform and other high altitude aircraft. This system is to map the tropospheric, atmospheric, and surface wind fields in and around tropical cyclones by using cloud particles and precipitation as tracers. The design has been completed and the instrument is now being fabricated. To realize this system, innovations in antenna design, transmitter design and measurement processing were required. This paper shall present these innovations and outline the expected performance of this novel system. [C1972]

"Dual-RiverSonde Measurements of Two-Dimensional River Flow Patterns"

Two-dimensional river flow patterns have been measured using a pair of RiverSondes in two experiments in the Sacramento-San Joaquin River Delta system of central California during April and October 2007. An experiment was conducted at Walnut Grove, California in order to explore the use of dual RiverSondes to measure flow patterns at a location which is important in the study of juvenile fish migration. The data available during the first experiment were limited by low wind, so a second experiment was conducted at Threemile Slough where wind conditions and surface turbulence historically have resulted in abundant data. Both experiments included ADCP near-surface velocity measurements from either manned or unmanned boats. Both experiments showed good comparisons between the RiverSonde and ADCP measurements. The flow conditions at both locations are dominated by tidal effects, with partial flow reversal at Walnut Grove and complete flow reversal at Threemile Slough. Both systems showed complex flow patterns during the flow reversals. Quantitative comparisons between the RiverSondes and an ADCP on a manned boat at Walnut Grove showed mean differences of 4.5 cm/s in the u (eastward) and 7.6 cm/s in the v (northward) components, and RMS differences of 14.7 cm/s in the u component and 21.0 cm/s in the v component. Quantitative comparisons between the RiverSondes and ADCPs on autonomous survey vessels at Threemile Slough showed mean differences of 0.007 cm/s in the u component and 0.5 cm/s in the v component, and RMS differences of 7.9 cm/s in the u component and 13.5 cm/s in the v component after obvious outliers were removed. [C1973]

"Simulator Implementation of an Inverse Synthetic Aperture Radar System for an Extended Naval

"Target in a Three Dimensional Synthetic Environment"

The construction steps regarding a computer simulator implementation for an extended naval target as viewed by an ISAR system is presented in this paper. The analysis involves the build up of the associated conceptual model, the explanation of the applied modelling approach and the depiction of the utilised data exchange standard. Finally the verification, validation and quality focus issues of the simulator are discussed. [C1974]

"Enhancements of an Adaptive Neighborhood Speckle Filtering Algorithm to Improve Analysis of Polarimetric SAR Imagery"

Image noise often hinders the analysis and understanding of most remote sensing imagery. Synthetic aperture radar (SAR) images, in particular, suffer from a phenomenon known as speckle. Speckle is the result of the coherent sum of scattering mechanisms within a resolution cell and is typically modeled as multiplicative noise. Numerous approaches have been taken to reduce speckle, the most promising of which are adaptive and statistically based. These algorithms typically take advantage of the statistics of speckle or the multi-scale image structure to detect regions of similarity. Several of these algorithms also take advantage of the multi-channel nature of polarimetric SAR to improve the region detection. This work presents two enhancements to such an algorithm with an application toward polarimetric parameter estimation and change detection and presents results using the Japanese satellite-based Phased Array L-band Synthetic Aperture Radar (PALSAR) system. [C1975]

"Surface current and wave validation of a nested regional HF radar Network in the Mid-Atlantic Bight"

The National High Frequency Surface Current Mapping Radar Network is being developed as a backbone system within the Integrated Ocean Observing System (IOOS). Of the core variables recognized in the IOOS Development Plan, two can be measured by high frequency radar (HFR): ocean surface currents and ocean surface waves. Rutgers University operates a nested multi-frequency network of HF radar systems along the coast of New Jersey. The network provides near real-time current observations with varying coverage from the coast to the shelf break. This is a subset of the larger regional coverage of the 26-site Mid-Atlantic HF Radar Consortium. The primary goal of this consortium is to operate the regional system in a coordinated way to guarantee the delivery of quality ocean current and wave data. In this paper we present the validation of both wave and current observations measured with this nested network. Particular emphasis is placed on surface current comparisons with Coast Guard deployed surface drifters (SLDMBs) and nearshore wave comparisons with moorings. The Coast Guard comparisons have a specific focus on quantifying the uncertainty in the HF radar surface current estimates as applied to search and rescue operations. These metrics will be used to ensure that quality data is going to the Coast Guard and that this information is properly incorporated into existing search planning tools. The nearshore measurements focus on algorithm development projects to incorporate shallow water effects into the estimates of nearshore waves. [C1976]

"A conceptual design for simultaneous measurements of 3D surface wave field and ocean surface current vector using the InSAR technology"

The radial velocity measured by a conventional along-track interferometric synthetic aperture radar (ATI) is contributed by all three orthogonal velocity components of the ocean surface current, of which the oscillatory orbital velocity of surface waves is frequently a dominant term. Mathematically, three simultaneous radial velocity measurements from different incident or azimuthal angles are needed to yield the unique solution of the ocean surface current. The 3D solution for sidelooking ATI is presented. If only two measurements are available, the error of the two horizontal velocity components caused by assuming zero vertical velocity is quantified. A conceptual design of integrating cross-track (XT) and along-track (AT) interferometry is presented. The XT phase data give the surface wave topography, from which the 3D wave-induced current field can be calculated. The wave contribution in the ATI phase data can then be removed to recover the mean component of the ocean surface current while maintaining the SAR resolution. By taking a zigzag path, both horizontal components of the surface current and the 3D wave field can be resolved from a single sensor on a single platform. [C1977]

"Current Measurements in Coastal Waters and Rivers by TerraSAR-X Along-Track InSAR"

As discussed by several authors during the last 20 years, the along-track interferometric synthetic aperture radar (along-track InSAR) is a promising instrument for direct high-resolution surface current measurements from air- or spaceborne platforms. After theoretical studies, airborne InSAR experiments, and a demonstration of current measurements from space with data from the Shuttle Radar Topography Mission, the new German satellite TerraSAR-X will be the first to offer along-track InSAR capabilities during a period of several years. We summarize results of two recent studies on current measuring capabilities of TerraSAR-X in coastal waters and

rivers. [C1978]

"Marine Doppler Radar Surface Current Measurements in the Surf Zone"

This paper presents a comparison of microwave radar surface velocity estimates to the estimates derived from video observations in the surf zone. The data presented here were collected during the Nearshore Canyon Experiment (NCEX) in the fall of 2003. The radar estimates are inferred from the Doppler shift of the backscattered radiation while video velocity estimates were produced using particle image velocimetry (PIV) technique. Comparisons of longshore velocity estimates show high spatial correlation within the central surf zone. The comparisons of the near cross-shore velocity shows the importance of bore velocity removal while showing high spatial correlation when the bias is removed. Both alongshore and cross-shore velocity estimates display discrepancies in the breaker and the swash zones. [C1979]

"Millimeter Wave Technology for Moon and Mars Exploration"

The new vision for the moon exploration calls for a return to the moon in a series of missions that start with robotic. Many of the large-scale features, such as steep crater walls and large boulders, are insurmountable obstacles to the rover. Thus, the development of systems for the guidance of rovers is a crucial issue. In this paper a radio frequency (RF) multifunctional payload for the support of rover operations on the lunar surface is presented. Since the dimensions of Radio-Frequency devices is strictly correlated with the wavelength, the use of higher frequency allows to obtain payload with small dimensions. The instruments proposed in this paper operates in the W-band (75-110 GHz). After an introduction explaining the reasons that could make such a payload successful, the navigation requirements are evaluated on the basis of the expected rover characteristics. Then, the payload functional scheme is presented and its performance and physical features are shown. [C1980]

"Models and Signal Processing for Millimeter-Wave LFM CW SAR Imaging"

In remote sensing applications, there is a special interest in lightweight, cost effective, and high resolution imaging sensors. The combination of linearly frequency modulated continuous wave (LFMCW) technology and synthetic aperture radar (SAR) technique can lead to such a sensor. As such, this paper concentrates on the models and signal processing of millimeter-wave (mmW) LFM CW SAR for high-resolution imaging, which includes two main parts. In the first part, the system models and useful relations for mmW LFM CW SAR imaging are provided, and an image formation algorithm that takes into account the special characteristics of CW (continuous wave) SAR is investigated. The second part focuses on the impact of LFM CW waveform errors on SAR imagery. The allowable magnitudes of phase error for each category are quantified, and an effective compensation technique for compensating possible frequency nonlinearity errors in LFM CW signals is presented. Thus the novel combination of mmW LFM CW and SAR can pave the way for the development of a small, lightweight, and high resolution imaging sensor. [C1981]

"Baseline Estimation in Distributed Spaceborne Interferometry SAR Systems"

Distributed spaceborne interferometry SAR (DS-InSAR) is the synthesis of distributed SAR including bi- and multi-static SAR techniques and interferometry techniques, which has addressed some of the limitations in conventional InSAR and subsequently has opened many new remote sensing applications. Compared to conventional InSAR, DS-InSAR has the technical challenge of baseline estimation, because the baseline between the transmitter and receiver must be known precisely during data recording. As such, this paper concentrates on the baseline estimation for DS-InSAR systems. The spatial baseline of DS-InSAR is described in many aspects, and an equation to determine the optimal spatial baseline is derived. Moreover, a high precision ranging technique is proposed to resolve the baseline estimation for high resolution spaceborne DS-InSAR systems. [C1982]

"A wireless network based on the combination of Zigbee and GPRS"

Due to its low-power consumption, low-cost, self-organization and powerful ability to route data, ZigBee, an emerging wireless network technology, has plenty of applications; GPRS (general packet radio service) network, a convenient way to access Internet, covers widely nowadays. This paper combines GPRS and ZigBee to establish a multi-mode network structure which employs GPRS as the data transmission device in the wide-area while ZigBee in the local area. This kind of network structure, providing a simple way to setup wireless network between terminal equipment, remote devices and personal stuff, will make the data servicing people freely. [C1983]

"The radon transform for the tomography of vegetated areas"

The tomography of vegetated areas has recently gained interest in the radar framework due to the many, relevant related applications. However, obtaining three-dimensional reconstructions of large vegetated regions is currently of difficult reach due to the need of acquiring and processing large amounts of data. On the other side, new acquisition configurations (e.g., bistatic or multistatic), allowing to enlarge the amount of data at one's disposal, are currently analyzed and stimulate the introduction of accurate and fast reconstruction algorithms, capable to flexibly deal with the available information. To this end, in this paper, we present a new approach for the tomographic reconstruction of vegetated areas employing a scattering model based on the Radon transform. In this way, imaging the cross-sectional areas of the regions of interest can be obtained by an FFT-based, filtered backprojection algorithm. The performance and potentiality of the approach are pointed out by numerical examples. [C1984]

"A new DEM reconstruction method based on an accurate flattening algorithm in interferometric SAR"

This paper presents a new approach to reconstruct digital elevation model (DEM) without compensating the flat earth phase back to the unwrapped interferometry in the interferometric synthetic aperture radar (InSAR). The new approach is based on an accurate flattening algorithm called model-spectrum algorithm which combines the advantages of classic algorithms. The experimental results show that the new algorithm has a better performance than the conventional ones. Based on this novel algorithm, DEM reconstruction can be implemented by a quasi-linear scaling after phase unwrapping. There is no need to add the flat earth phase back to the flattened interferogram, which avoids complex geometrical conversion as what is done in the conventional algorithms. [C1985]

"A 410GHz CMOS Push-Push Oscillator with an On-Chip Patch Antenna"

The uses of terahertz systems (300 GHz to 3 THz) in radars, remote sensing, advanced imaging, and bio-agent and chemical detection have been extensively studied. A compact and low-cost signal source is a key circuit block of terahertz systems. Traditionally, the circuits have been built using highly optimized III-V technologies. With the advances of CMOS, it has become realistic to consider terahertz circuits in CMOS. This paper reports a signal source operating near 410 GHz that is fabricated using low-leakage transistors in a 6 M 45 nm digital CMOS technology. [C1986]

"Deployments of microwave and millimeterwave radiometers in the Arctic"

Measurement of water vapor and cloud liquid during very cold (-20 to -40 Deg. C) and dry (precipitable water vapor < 5 mm) conditions is a very important, but difficult task. Starting in 1999, three radiometric experiments were conducted at the U. S. Department of Energypsilas Atmospheric Radiation Measurement (ARM) Programpsilas North Slope of Alaska (NSA) field site near Barrow, Alaska. Principal results from the first two experiments are summarized. Most recently, the Radiative Heating in Underexplored Bands Campaign (RHUBC) was conducted in February-March 2007. The millimeter- and submillimeter-wave channels of the ground-based scanning radiometer (GSR) are very sensitive to low water vapor and cloud contents and allow for accurate observations in the extremely dry and cold conditions typical of the Arctic. Moreover, window channels (e.g., at 90 and 340 GHz, both with horizontal and vertical polarizations) show a high sensitivity to Artic clouds over an extended range of liquid water path (LWP). For RHUBC, during conditions when the precipitable water vapor (PWV) was less than 2 mm, these radiometers were supplemented by frequent Vaisala RS92 radiosonde observations at the ARM site. In this paper, representative PWV and LWP retrievals from the GSR and several ARM instruments are compared. Based on comparisons with 87 RS92 RAOB launches, GSR PWV retrievals achieved almost unprecedented accuracy of 0.1 mm, or about 6 % of the mean PWV during the operating period. [C1987]

"High precision and high resolution global precipitation map from satellite data"

The five year research project, IdquoThe Global Satellite Mapping of Precipitation (GSMaP)rdquo sponsored by Japan Science and Technology Agency(JST) ended in March 2008. The research project aimed at developing microwave radiometer rain rate retrieval algorithms based on the reliable physical models of precipitations and producing high precision and high resolution global precipitation maps only from the satellite data. This paper reviews the research activities of GSMaP. [C1988]

"Estimation of canopy attenuation for active/passive microwave soil moisture retrieval algorithms"

This paper discusses the importance of the proper characterization of scattering and attenuation in trees needed for accurate retrieval of soil moisture in the presence of trees. Emphasis is placed on determining an accurate estimation of the propagation properties of a vegetation canopy using the complex frequency correlation function

(FCF). A new technique for determining the canopy attenuation that uses the measured stepped frequency radar backscatter response is proposed. It makes use of the details found in a transient solution where the canopy (volume scattering) and the tree-ground (double interaction) effects appear at different times. The proposed technique is based on separating the backscattering sources within a forest canopy in the time response. The technique has been used with L band data collected over deciduous trees to verify that the algorithm results match the simulated data. [C1989]

"Perturbative solution for the scattering from multilayered structure with rough boundaries"

The objective of this paper is to investigate analytically the fully polarimetric electromagnetic wave scattering and emission from a three-dimensional layered structure with N-rough interfaces in the framework of SPM method. Assuming that deviations and slopes-with respect to the reference mean plane-exhibited by rough interfaces are small enough, we firstly perform a perturbative expansion of the fields in the rough-interfaces layered structure, following the classical scheme employed to deal with a rough surface. Subsequently, by using effectively the concept of generalized reflection/transmission coefficients, the unknown expansion coefficients of scattered wave propagating upward in the upper half-space are derived via a recursive method. This approach can be also applied to the evaluation of the second-order contribution, opening the way to the accurate calculation of thermal emission from complex layered structure. [C1990]

"On the reduction of the systematic error in imaging radiometry by aperture synthesis: a new approach for the SMOS space mission"

The SMOS mission is a European Space Agency project aimed at global monitoring of surface Soil Moisture and Ocean Salinity from radiometric L-band observations. This work is concerned with the reduction of the systematic error (or bias) in the reconstruction of radiometric brightness temperature maps from SMOS interferometric measurements. A recent and efficient method has been proposed for reducing this error. However, a residual bias still persists. A new approach for reducing this bias down to residual values less than 0.1 K is presented here and illustrated with numerical simulations. [C1991]

"Remote Sensing"

First Page of the Article [C1992]

"The development of Doppler sonar technology at SIO"

Development of acoustic techniques for the remote sensing of ocean velocity has been progressing at Scripps for the past 34 years. While many scientifically productive systems have been created, there have also been numerous technical surprises and well explored dead-ends. Here, the development of both coherent and incoherent backscatter systems at SIO is reviewed, with an emphasis on the real-world problems encountered. [C1993]

"On the use of microwave sounder data for high-temporal rainfall maps based on microwave radiometers"

In this study, we have been developing rainfall retrievals for the Advanced Microwave Sounding Unit (AMSU) based on the Global Satellite Mapping of Precipitation (GSMaP) microwave radiometer algorithm to produce microwave-based rain maps at high-temporal resolution. The GSMaP-retrieved rainfall from the AMSU is compared to NOAA standard algorithm retrieved data using the Tropical Rainfall Measuring Mission (TRMM) data as the reference. [C1994]

"Air-sea interaction monitoring by remote and contact measurements: The results of the CAPMOS'05 and CAPMOS'07 experiments on an oceanographic platform in the Black Sea"

The paper presents the results of the experiments CAPMOSpsila05 and CAPMOSpsila07 performed on an offshore oceanographic platform in the Black Sea. The platform equipped with contact and remote sensors is located approximately 600 m to the south of Crimea coast, Ukraine. The experiments aimed at air-sea interaction monitoring were carried out by an international research team during summer months in 2005 and 2007. Spectral parameters of wind and waves were estimated from direct and remote measurements. A comparison with known spectrum models was performed. [C1995]

"Dynamics of short waves spectrum measured by remote and contact sensors from an oceanographic platform"

The paper presents the results of the experiment CAPMOSpsila05 performed on an offshore oceanographic platform in the Black Sea. Microwave radiometer measurements were applied for gravity-capillary wave spectrum retrieval using the original techniques. The spectrum components evolution under unstable wind conditions was investigated. It was demonstrated that the spectral components in the vicinity of the curvature maximum are the most sensitive to the wind velocity variations. [C1996]

"Neural-Network based algorithm for ice concentration retrievals from satellite passive microwave data"

Present algorithms for observing the multiyear ice cover are not accurate in multiyear fraction calculations, which is a significant disadvantage of the present system of global ice monitoring considering the fact that multiyear ice is one of the key indicators of changes in the Arctic climate. In this research regionally differing Neural Networks (NN)-based algorithms for total and multiyear Arctic sea ice concentration retrievals from Special Sensor Microwave Imager (SSM/I) data are developed using closed scheme of the numerical experiment. Era-40 Reanalysis data on atmospheric parameter profiles and sea ice temperature are used for the numerical integration of the radiation transfer of the microwave emission in the Atmosphere-Ocean-Ice System. The data on cloud liquid water content and cloud boundaries are modeled basing on the results of Arctic SHEBA experiment. Numerical values for first year and multiyear ice emissivities are taken from published experimental data. The calculated radiometer brightness temperature values are used for NN-based theoretical algorithm development. New weather filter is defined. The algorithms are validated for stable winter conditions using collocated SSM/I data and Synthetic Aperture Radar (SAR) images, classified by an ice expert. [C1997]

"An anisotropic ocean surface emissivity model based on WindSat polarimetric brightness observations"

{no data available} [C1998]

"On the correlation of area-extensive measurement of fractional area whitecap coverage with microwave brightness temperatures"

On August 21, 2007, while mounted in a U.S. Navy P3 aircraft, the Naval Research Laboratorypsilas Airborne Polarimetric Microwave Imaging Radiometer (APMIR) and the University of Washingtonpsilas FoamCam recorded microwave and video images of the sea surface in the Gulf of Mexico as a function of distance from the eye of Hurricane Dean. From a working altitude of 6.1 km, the FoamCam sea surface optical imagery determined sea state, including presence of whitecaps, while APMIR measured the ocean surface brightness temperature at bands from 6.6 GHz to 37 GHz. The specific brightness temperatures measured were 6.6 VH, 6.8 VH, 7.2 VH, 10.7 V and full polarimetric data at 19.35 and 37 GHz. Collocated nearly cotemporaneous data from both SSM/I and WindSat satellite radiometer overpasses were available, as were oceanographic and meteorological data from National Buoy Data Center buoys. As an initial result from the analysis of these datasets, this paper provides a comparison of the APMIR-measured brightness temperatures with those measured by SSM/I and WindSat. The APMIR data and the surface video imagery is also used to investigate the relationship between linearly polarized microwave brightness temperatures and whitecap coverage. Future analysis directions for this data are discussed at the end of the paper. [C1999]

"Combined passive and active microwave retrieval of falling snow during the 2003 Wakasa Bay field experiment"

The present research describes a novel snowfall retrieval algorithm using combined radar and radiometer observations of cold-cloud precipitation. The algorithm retrieves a 1-D vertical distribution of precipitation rate, particle size, particle density, and cloud liquid water content using aircraft-or satellite-based co-located dual-wavelength radar and passive microwave radiometer observations. The 2003 Wakasa Bay field experiment over the Sea of Japan provided high-resolution observations of snowfall using aircraft-based instruments compatible with the present technique. The dual-frequency APR-2 radar operated at 13.4 and 35.6 GHz, while the co-located the MIR radiometer made cross-track observed brightness temperatures at 89, 150, 220, 183.3plusmn1, 183.3plusmn3, 183.3plusmn7, 220 and 340 GHz. The techniques described here are being developed with an eye toward the upcoming Global Precipitation Measurement Mission (GPM). Parameterizations based on these retrievals are already being used to identify and communicate the key characteristics of cold-cloud precipitation to the larger remote sensing and climate modeling community. [C2000]

"High-resolution spectral radiometer imaging system"

A high-resolution spectral radiometer imaging system developed at DLR combines high-resolution aperture

synthesis imaging with spectral sensing. The frequency range of 1.4 to 7 GHz allows a high penetration depth in order to extract information about the surface and material of observed objects. The aperture synthesis principal can produce a high resolution snapshot image with a highly thinned array without mechanical movement of a antenna system. Another advantage of that combination, i.e. a higher spatial resolution at higher frequencies and a higher penetration at lower frequencies, can enhance the overall imaging capability using combined processing for the image reconstruction. In this paper the experimental system ANSAS is presented, the setup and receiver assembly is outlined, and some imaging results using the developed electronics on a two-elements interferometer shows the capabilities of the concept. [C2001]

"Investigation into the utility of using CFAR cluster size information in target track association"

During CFAR processing of low-resolution-radar data (e.g. from yacht navigation systems), the target is represented by a cluster of range-azimuth cells. The centroid is usually passed to the tracking system, however information on the size of the cluster, and therefore extent of location error is available from the CFAR. The main hypothesis of this paper is "would the use of the cluster bounding-box 'corners' allow better plot-to-track associations when compared to using the region centroid alone?". [C2002]

"An Experimental Study of the Lowest Troposphere Layers at 10 GHz-First Results"

In this paper an extensive innovative experiment for combined, both local and remote sensing of the troposphere is introduced. The experiment is based on a unique set of mutually linked, time-space dependent, synchronized radio-electrical and radio-meteorological measurements. The first results for first two months of operation are presented and discussed as well. [C2003]

"Terrain-based navigation: Trajectory recovery from LiDAR data"

The need for complementary technologies to support navigation in GPS-challenged environment is rapidly growing in both outdoor and indoor environments. Remote sensing/mapping sensor performance continues to advance resulting in better spatial and temporal resolution of the acquired geospatial data, which, combined with the increasing hardware performance, can be available real-time or near real-time, and thus could be utilized in forming or improving the navigation solution. Terrain-based navigation has been used for a number of years to navigate airborne platforms, but the continuous exchange of precise geolocation information between the imaging and navigation modules to improve the overall error calibration is a novel idea, which should significantly increase the systems fault tolerance in a variety of situations. The typical navigation solutions for airborne mapping systems are currently based on a GPS or integrated GPS/IMU systems, supporting usually a single imaging sensor, with no feedback between the sensory data processing filters. Most of the research in terrain-based navigation proposes the use of optical measurements from airborne imagery, although the concept of exploring LiDAR-based terrain navigation has also been reported. This paper is concerned with obtaining navigation data from LiDAR, and investigates the feasibility of the airborne trajectory recovery method based on LiDAR data using reference terrain surface models. If GPS signals are lost, the coordinates of LiDAR points can still be computed using the inertial-only solution, however, with errors growing in time. If reference surface data exists, they can be used to recover the LiDAR sensor trajectory by surface matching as long as the IMU drift is under a certain threshold. To assess the performance of the proposed method both simulated LiDAR data were used and an analysis of the feasibility of the method is provided. [C2004]

"Performance Assessment of IHS Fusion for Remote Sensing Images Based on Multiple Attribute Decision Making"

Base on the traditional IHS (Intensity-Hue-Saturation) fusion and weighted IHS fusion algorithm, the adaptive weighted IHS information fusion based on local mean is discussed in this paper. Because the advantages and disadvantages of fusion algorithm have direct influences on the effect of remote sensing information fusion, the multiple attribute decision making method is proposed for assessing fusion algorithm. Finally, the effects of the different fusion IHS algorithm for remote sensing images are assessed using the decision making method for comparing the fusion effect. It proves that the proposed multi-attribute decision-making approach performs quite well for assessing the fusion algorithms. [C2005]

"Texture Analysis on Weather Radar Images of Severe Convective Precipitation in the Arid Area of Ningxia"

Using the Yinchuan new generation radar volume scan data of severe convective precipitation in 2004-2005, composite reflectivity images in polar coordinate were projected into the coordinate of x-y. 51 cases were studied with gray level co-occurrence matrix and the parameters of angle second moment, contrast, correlation, entropy

and inverse difference moment. Results show that, there are obvious differences of texture between the remote sense images of precipitation in Ningxia and south China. In the radar images of severe convective precipitation in climate arid region in north-mid part of Ningxia, the texture is not as distinct as in south China, and the definition is not very clear, the texture is weaker and thinner, the images are smoother and stable than that of south China, the features indicate that the clouds of severe convective precipitation in the climate arid region in north-mid part of Ningxia are homogeneous. [C2006]

"Application of Ridgelet Transform to Wave Direction Estimation"

To extract wave direction from sea surface images, a new method is proposed, which is based on ridgelet transform. Due to the linear feature of sea wave images, this method first provides a pre-processing to take a disk shape area from the middle of the wave image. Then the wave direction which has an associated ± 180 degree ambiguity is calculated using ridgelet transform. Meanwhile, a timestack image is collected from successive frames in specific orientation to track the wave propagation. Furthermore, the timestack is processed by ridgelet transform to find the forward wave direction. Lastly, the wave direction without degree ambiguity is determined effectively. The experiment results show the validity and feasibility of the method and good accuracy is achieved. [C2007]

"Adaptive Balancing of Edge Extraction in LADAR-Referenced Navigation over Plain Area"

Although high-resolution remote sensing (RS) images can supplement the reference map's deficiency in LADAR (Laser Radar) referenced navigation system over plain area, their different imaging modes still leave great errors' introduction into the positioning process. As positioning is commonly accomplished by matching the edges extracted as the obvious terrain characteristics, exploring automatic procedure for balancing mutual information is an important step to improve the system's performance. To solve this issue, this paper explores the criterion of edge-points ratio (EPR) based on wavelet multi-scale analysis extraction method, and then appropriate measures are applied for different conditions. EPR at various decomposition layer works as the key circle for adaptive balancing, and so related edge-distribution characteristics can be used individually, such as close-contour or line. [C2008]

"FLORAD: Micro-satellite flower constellation of millimeter-wave radiometers for atmospheric remote sensing"

Requirements and preliminary specifications to design a micro-satellite flower constellation, named FLORAD, of millimeter-wave (MMW) radiometers for atmospheric observations are here introduced. The FLORAD small-mission scientific objectives are aimed at the retrieval of thermo-dynamical and hydrological properties of the atmosphere. Radiometer specifications and inversion algorithms are briefly discussed, pointing out the trade-off between performances and complexity for low-cost low-weight micro-satellite platforms. In order to fulfill the goal of a short revisit time for meteorological monitoring and now casting purposes, a flower constellation (FC) of micro-satellites is proposed due to its design flexibility. [C2009]

"Combined airborne radio-instruments for ocean and land studies (CAROLS)"

The CAROLS, L band radiometer, is built and designed as a copy of EMIRAD II radiometer of DTU team. It is a Correlation radiometer with direct sampling and fully polarimetric (i.e 4 Stockes). It will be used in conjunction with other airborne instruments (in particular the C-Band scatterometer (STORM) and IEEC GPS system, Infrared CIMEL radiometer, one visible camera), in coordination with in situ field campaigns for SMOS CAL/VAL. The instruments are implemented on board the French research airplane ATR42. A validation campaign with four flights was made over south west of France, Hourtin Lake and Bay of Biscay (Atlantic Ocean) in September 2007. In order to qualify the radiometer data, different types of aircraft movements were realized: circle flights, wing and nose wags. Simultaneously to flights, different ground measurements were made over continental surfaces and ocean. First results show a good quality of data over ocean surfaces. For continental surfaces, important Radio-Frequency Interferences (RFI) were observed over a large part of the studied region. [C2010]

"A compact airborne G-band (183 GHz) water Vapor Radiometer and retrievals of liquid cloud parameters from coincident radiometer and millimeter wave radar measurements"

ProSensing Inc. has developed a G-band (183 GHz, 1.5 mm wavelength) water Vapor Radiometer (GVR) for measuring low concentrations of atmospheric water vapor and liquid water. Using four double sideband receiver channels, the instrument measures brightness temperature at 183.31 \pm 1, \pm 3, \pm 7 and \pm 14 GHz. An airborne version of the instrument, packaged and wired to operate from a standard PMS probe canister, was successfully tested onboard the National Research Council of Canada Convair-580 aircraft during the Canadian CloudSat and

CALIPSO validation flights (C3VP) through the winter of 2006-07. The Zenith G-band radiometer brightness temperature data collected with the GVR were complemented with co-located cloud reflectivity measurements with the NRC W and X-band (NAWX) radar system and in situ probes. By flying the aircraft in a stepped and porpoising ascent/descent patterns, liquid cloud water content was estimated from the GVR retrieved liquid water path. The effective radius and number density of liquid clouds were then estimated by combining the liquid water content with the W-band radar reflectivity factor (Z) and by applying a small correction factor, based on the characteristic drop size distribution shape of the observed cloud. [C2011]

"The Aquarius/SAC-D mission and status of the Aquarius instrument"

The Aquarius/SAC-D mission is a partnership between the USA (NASA) and Argentina (CONAE). The observatory consists of Aquarius, an L-band radiometer/radar combination being developed under NASA's Earth System Science Pathfinder (ESSP) program to map the surface salinity field of the oceans from space, together with the SAC-D bus and several instruments provided by CONAE and its partners. The Aquarius instrument is currently in I&T at NASA/JPL. The mission is scheduled for launch in May, 2010. [C2012]

"Microwave characteristics of organized mesoscale convection over the ocean"

Fields of AMSR-E brightness temperatures TBs of organized mesoscale convection over the ocean are analyzed together with MODIS visible images, Envisat ASAR images and QuikSCAT-derived wind fields. Cloud liquid water content Q and water vapor content V are estimated for the areas with mesoscale convection and for individual large cells. Models describing distribution of wind speed and direction, water vapor and cloud water in convective rolls, open and closed cells were suggested to simulate TBs and imprints of convective cells on SAR images. Computed passive microwave and radar pattern are in a good agreement with satellite measurements and can be used for retrieval algorithm advancement, estimation of effects of spatial smoothing, etc. [C2013]

"Microwave radiometry of land, vegetation and water bodies: More than 30 years of modeling, conducting experiments and practical applications"

In this paper an overview of the activities concerning microwave radiometry of land, vegetation and water bodies carried out for more than 30 years by Anatolij Shutko and his research group is given. In particular, the experiments carried out for validating the electromagnetic models, the results achieved during these years and the practical applications derived from this research are here described. [C2014]

"Simultaneous multi-sensor data for global information management system"

An international consortium of specialists from the Netherlands, Russia, Bulgaria, United States and Australia has developed and demonstrated a new airborne multi-sensor system that is ready for implementation in environmental remote sensing. The airborne multi-sensor system consists of several cameras and produces (underground) soil moisture data, ground temperature data, digital elevation models, and high resolution orthophotos. All sensors are mounted on board one single light aircraft and are operated simultaneously to produce a wide range of critical information at a time that is then processed into an information monitoring system (IMS). The international team has demonstrated the benefits of the system in a show case project in Bulgaria in the summer of 2007, and the results are presented in this paper. [C2015]

"Sentinel-1, the GMES radar mission"

The ESA Sentinels constitute the first series of operational satellites responding to the Earth Observation needs of the EU-ESA Global Monitoring for Environment and Security (GMES) programme. The GMES space component relies on existing and planned space assets as well as on new complementary developments by ESA. This paper describes the Sentinel-1 mission, an imaging synthetic aperture radar (SAR) satellite constellation at C-band. It provides an overview of the mission requirements, its applications and the preliminary technical concept for the system. [C2016]

"Current interferometry results in Canada"

A number of groups are currently active in radar interferometry in Canada, including government institutions, universities and industry. This paper will present a survey of interferometry applications in Canada, and illustrate recent results. In the airborne radar domain, early research with the Canada Centre for Remote Sensing (CCRS) Convair-580, has led to successful commercial programs at MacDonald Dettwiler (MDA) and Intermap Technologies. MDA has built three single-pass interferometers that are in operational use in the Amazon basin, and Intermap have built five systems that are producing DEMs with 1-m vertical accuracy. On the satellite front, RADARSAT-1 data has been used for repeat pass mapping in the Canadian Arctic. A number of subsidence and

landslide sites are being continually monitored with the permanent scatterers technique. A 3-satellite constellation, the RADARSAT constellation mission, will support future InSAR applications. [C2017]

"Mars north polar cup subsurface materials property estimation using GPR SHallow RADar data"

Since September 2006 SHARAD (SHallow RADar) is mapping the distribution of water, liquid and solid, in the upper portions of the Martian crust, the SHallow RADar (SHARAD) is active. Upon the instrument data acquisition an appropriate processing has to be performed to discriminate the Martian subsurface echo from the surface one. The detected subsurface signal is then processed with a dual frequencies techniques in order to estimate the materials loss property. Using the system parameters the surface material dielectric constant can be evaluated. Finally, using a data inversion procedure the subsurface material property of the Mars subsurface are estimated by taking into account the geometric clutter contribution. [C2018]

"Airborne Ku-band polarimetric radar remote sensing of terrestrial snow cover"

Preliminary analyses of the POLSCAT data acquired from the CLPX-II in winter 2006-2007 are described in this paper. The data showed the response of the Ku-band radar echoes to snowpack changes for various types of background vegetation. We observed about 0.2 to 0.4 dB increases in backscatter for every 1 cm SWE accumulation for sage brush and agricultural fields. The co-polarized VV and HH radar responses are similar, while the cross-polarized (VH or HV) echoes showed greater response to the change of SWE. The data also showed the impact of surface hoar growth and freeze/thaw cycles, which created large snow grain sizes and ice lenses, respectively, and consequently increased the radar signals by a few dBs. [C2019]

"A two dimension overlapped subaperture polar format algorithm based on stepped-chirp signal"

In this work, a 2-D subaperture polar format algorithm (PFA) based on stepped-chirp signal is proposed. Instead of traditional pulse synthesis preprocessing, the presented method integrates the pulse synthesis process into the range subaperture processing. Meanwhile, due to the multi-resolution property of subaperture processing, this algorithm is able to compensate the space-variant phase error caused by the radar motion during the period of a pulse cluster. Point target simulation has validated the presented algorithm. [C2020]

"Water/land segmentation in SAR images using level sets"

This paper presents a method for the separation between land and water in SAR amplitude images. The proposed technique uses region based level sets and adopts a mixture of log-normal densities as the probabilistic model for the pixel intensities in both the water and the land regions. The expectation-maximization (EM) algorithm is used to estimate the probability density functions in each region. Experimental results with real SAR data are provided to illustrate the performance of the proposed algorithm. [C2021]

"Terrain modeling from lidar data: Hierarchical K-means filtering and Markovian regularization"

Lidar 3D point cloud corresponds to the terrestrial topography, including true ground and objects belonging either to vegetated areas or to human made features. This paper deals with DTM (digital terrain model) production. First step filtering data into ground and off-ground points is based on a multi-resolution coarse-to-fine approach. The K-means algorithm is used in a hierarchical way that provides robust data filtering. The number of cluster splits is used to automatically qualify the filtering reliability. This point is rarely treated in previous works. Secondly, a regularization process over ground points generates an accurate DTM on a regular grid. The fine DTM is processed with ground points without using classical interpolation algorithms. In fact, a Markovian regularization minimizes a global energy that confronts the terrain regularity and the goodness of fit to the data. It also depends on the filtering reliability. Conclusive results are presented on vegetated and mountainous areas and provide realistic terrain models. [C2022]

"Descriptive experiment design unified with worst-case performance optimization-adapted regularization for high-resolution radar/SAR imaging"

This paper considers the problem of high-resolution imaging of the environment formalized in terms of a nonlinear ill-posed inverse problem of nonparametric estimation of the power spatial spectrum pattern (SSP) of the wavefield scattered from an extended remotely sensed scene (referred to as the scene image) via processing the discrete measurements of a finite number of independent realizations of the observed degraded radar data signals (one realization of the trajectory signal in the case of SAR). The model-level uncertainties are associated with unknown statistics of perturbations of the signal formation operator (SFO) in turbulent environment. The system-level uncertainties are attributed to the imperfect array calibration, finite dimensionality of measurements, uncontrolled antenna vibrations and random carrier trajectory deviations in the case of SAR. An effective method

for SSP reconstruction is therefore proposed by incorporating into the minimum risk (MR) nonparametric spectral estimation strategy the experiment design-motivated constraints of SSP observability/identifiability for the finite-dimensional range continuous-to-discrete SFO algorithmically coupled with descriptive experiment design regularization (DEDR) and unified with worst-case statistical performance optimization approach. The MR objective functional is constrained by this information, and the robust DEDR reconstruction operator applicable to the scenarios with the low-rank uncertain estimated data correlation matrices is found. We also show how this algorithm may be considered generalization of the robust MVDR and the regularized inverse spatial filtering techniques. The efficiency of the developed technique is illustrated via numerical simulations. [C2023]

"Recent advances in Polarimetric SAR Interferometry for forest parameter estimation"

Polarimetric SAR Interferometry (Pol-InSAR) is a radar remote sensing technique that, based on the coherent combination of SAR interferometry and radar polarimetry, provides sensitivity to the vertical distribution of different scattering processes and makes the inversion of forest structure parameters possible. In this paper we present the main scientific results achieved in actual airborne campaigns, discuss the potential and limitations of the different inversion scenarios (based on different frequencies, temporal and spatial baselines) and draw the conclusions. [C2024]

"Advances in SAR Polarimetry applications exploiting polarimetric spaceborne sensors"

The SAR Polarimetry represents an active area of research in Radar Remote Sensing. This interest is clearly supported by the fact that nowadays there exists a non negligible quantity of launched Polarimetric SAR Spaceborne sensors. The aim of this communication is to present the current state of the art in SAR Polarimetry ranging from theory to applications, with special emphasis in the analysis of data provided by the new Polarimetric Spaceborne SAR sensors. A review of the current status of the PolSARpro v3.0 Software (Polarimetric SAR Data Processing and Educational Toolbox), developed under contract to ESA by a consortium comprising I.E.T.R at the University of Rennes 1, AELc, DLR-HR and Dr mark Williams from Adelaide is also made. The objective of this toolbox is to provide Educational Software that offers a tool for self-education in the field of Polarimetric SAR data analysis at University level and a comprehensive suite of functions for the scientific exploitation of fully and partially polarimetric multi-data sets and the development of applications for such data. [C2025]

"Multiple scattering of HF skywave radar signals: Physics, interpretation and exploitation"

HF radar signals rely on the ionosphere to achieve over-the-horizon surveillance, but this is obtained at the expense of subjecting the signals to a diverse range of scattering and modulation phenomena. Many of these effects are associated with multiple scattering, both in the ionosphere and near the earth's surface. This paper reviews a variety of multiple scattering phenomena and shows how an understanding of the physics enables the radar echoes to be interpreted so as to extract information about targets and the environment. Particular attention is focussed on (i) scattering from small scale plasma irregularities, which can be used to classify propagation modes and thus improve target tracking, and (ii) scattering from the sea surface, which can be exploited for optimising radar ship detection performance as well as a range of remote sensing applications. [C2026]

"Subsurface sounding in Northern hemisphere for Mars by MARSIS: Mars express mission"

The MARSIS observations are optimized during periods when the pericenter of the orbit is near or below zero degrees sun elevation (Idquonightsiderdquo) and the nightside phase, the last of the primary MEX mission, occurs on March-July 2005, in the northern latitude of MARS regions. This paper provides a description of the modeling approach and of the expected performance of the MARSIS radar in the northern hemisphere of Mars. Few models, suitable for a preliminary analysis of the MARSIS instruments are reported. The knowledge of these performance, evaluated according to the model used for the surface and subsurface of the Martian crust, are necessary in order to decide, during the planning activity of the mission, the radar operative mode. In addition the model utilized are an effective tool for the simulator that has to perform the radar equation inversion in order to evaluate, by the radar returns, the surface and subsurface dielectric characteristics. Few simulation results of the surface characteristics are reported and a radar gram is shown, as an example, in order to state the preliminary criteria for the radar equation inversion. [C2027]

"Real-time autonomous disturbance detection and monitoring system with L-band UAVSAR"

We developed an autonomous disturbance detection and monitoring system with imaging radar that combines the unique capabilities of imaging radar with high throughput onboard processing technology and onboard automated response capability based on specific science algorithms. This smart sensor development leverages

off recently developed technologies in real-time onboard synthetic aperture radar (SAR) processor and onboard automated response software as well as science algorithms previously developed for radar remote sensing applications. In this project, we use a high rate data interface to ingest NASAs UAVSAR data and compute SAR imagery in real-time complete with motion compensation and antenna beam steering capabilities. NASAs UAVSAR is a compact, L-band 80 MHz bandwidth, fully polarimetric radar. It is designed for repeat-pass InSAR and has had engineering flights in 2007 and successful science data collections in 2008. The fidelity of the onboard SAR processor is tuned by implementing polarimetric calibration capabilities. Science algorithms are implemented for detecting and monitoring fire disturbances over the US forests. We additionally developed artificial intelligence for decision-making, and adapted existing onboard activity re-planning and execution software to interface with the UAVSAR radar controller. The product of this development is a prototype closed loop smart sensor. [C2028]

"The German satellite mission TerraSAR-X"

TerraSAR-X is Germanys first national remote sensing satellite being implemented in a public-private partnership between the German Aerospace Centre (DLR) and EADS Astrium GmbH. TerraSAR-X was launched on June 15th, 2007 and will supply high-quality radar data for purposes of scientific observation of the Earth for a period of at least five years. At the same time it is designed to satisfy the steadily growing demand of the private sector for remote sensing data in the commercial market (Werninghaus et al., 2007) sigma. [C2029]

"Decision Fusion for Reliable Flood Mapping Using Remote Sensing Images"

Flood extent mapping is a basic tool for flood damage assessment, which can be done by digital classification techniques using satellite imageries, including the data recorded by radar and optical sensors. However, converting the data into the information we need is not a straightforward task. One of the great challenges involved in the data interpretation is to separate the permanent water bodies and flooding regions, including both the fully inundated areas and the wet areas where trees and houses are partly covered with water. This paper adopts the decision fusion technique to combine the mapping results from radar data and the NDVI data derived from optical data. An improved capacity in terms of identifying the permanent or semi-permanent water bodies from flood inundated areas has been achieved. Computer software tools Multispec and Matlab were used. [C2030]

"The fractal analysis of radar images of tropical cyclones"

The questions of fractal processing data of remote sensing are considered. The analysis of radar images has allowed the selection of characteristic zones of tropical cyclones. [C2031]

"Providing basic data for the wood segment of GEOUA-information service system "leskosmos" (Forest-UA)"

On the stage of elaboration of Forest-UA system, as a wood segment of GEOUA national program, the following remote sensing principles should be realized: synchronous remote and necessary field measurements of the surface and meteorological parameters; repeated observations in order to estimate changeability of the surface reflective properties and increase detection reliability; using apriori information about the surface reflective properties from contrasting schemes. [C2032]

"Analysis of relative permits depending on signal-noise ratio at the use of optimal on minimum error average square in signal processing algorithms"

Presented in this paper is comparative analysis regarding the resolution of CO and MSK algorithms of radar mapping at the side looking. The analysis displays that at $q \geq 0$ MSK algorithm has better resolution than SF, but its signalnoise ratio at the output is worse. [C2033]

"Experimental investigations of flat reflector influence on the signal in Fresnel zone"

The experimental results of the flat reflector size and rotation angle influence on radar meter signal characteristics in Fresnel zone are presented. [C2034]

"Organization of computer experiment for Radar research"

In this report some questions of organization of computer experiment with using different methods of its realization and computer laboratories (problem-oriented software based on system modelling of Radar) for research and designing of Radar and its elements are considered. [C2035]

"Hybrid Algorithms for Electromagnetic Detection Satellites Scheduling"

Electromagnetic detection satellite (EDS) is a type of Earth observation Satellites (EOSs). The Information collected by EDSs is very important in some application domain, such as industry, science and military. The scheduling of EDSs is a complex combinatorial optimization problem. Current research mainly focuses on the scheduling of imaging satellites and SAR satellites, little work on the scheduling of EDSs for its specific requirements. Considering the specific constrains of EDSs, we established a MultiSatellites scheduling model and proposed a scheduling algorithm based on genetic algorithm. A hybrid algorithm incorporated with genetic algorithm and stochastic climbing algorithm was constructed to improve the scheduling algorithm. To deal with some specific constrains, a punish function method was introduced. We have conducted some experiments to validate correctness and practicability of our scheduling algorithms. [C2036]

"Modelling of SAR transceiver as a complex system"

The system of embedded control of APAR parameters was considered by the example of radar remote sensing of the Earth. [C2037]

"A novel electrowetting approach for optical phased arrays invited talk-EOSS"

The University of Cincinnati has launched a broad program in electrowetting optics for displays, beam steering, retroreflectors, and adaptive camouflage. In this talk, we will review the operational basics of electrowetting micropisms, and the challenges/outlook pertaining to use as fixed-pitch and wide-angle optical phased array. [C2038]

"A hierarchical boosting algorithm based on feature selection for Synthetic Aperture Radar image retrieval"

A hierarchical boosting algorithm based on feature selection is proposed for Synthetic Aperture Radar (SAR) image retrieval here. Motivated by Joint Boost and Shared feature frameworks, category combinations are adopted as the training and classification set of a hierarchical boosting-based classification frameworkpsilas middle layer. It has superiorities over the classical method which combines Boosting algorithm with many features as inputs. Meanwhile, different from the Joint Boost scheme, our method separates feature selection from training and retrieval processes. Thus more flexible feature selecting schemes can be used, e.g. nonlinear separating plane can be obtained. Some typical features such as Gabor, Edge Orientation Histogram, gray-level co-occurrence matrix, Grey Histogram and Tamura are used as the candidates of the input and statistics-based selecting method is used as the feature selection scheme. The experiments are carried on the KTH_TIPS and SAR image datasets and the results reveal our algorithmspsilas efficient performances and superiorities. [C2039]

"Azimuth signal processing for near-space high-resolution and wide-swath SAR imaging"

Near-space defined as the space region between 20 km and 100 km can offer many capabilities that are not accessible for satellites and airplanes. By placing transmitter/receiver inside near-space platforms, many functions that are currently performed with satellites or airplanes could be performed much more cheaply and with greater operational unity. It appears that near-space can provide a satisfied solution to high-resolution and wide-swath (HRWS) SAR imaging. Inspired by these promising advantages, this paper describes the concept of near-space HRWS SAR for remote sensing applications. A multiple-beam based azimuth ambiguity suppression technique is presented. The system concepts, signal models, and corresponding azimuth signal processing algorithms are provided. An example near-space HRWS SAR system is conceptually designed. [C2040]

"Snail Identification Based on Fourier Transformation"

Based on the monitoring of satellite remote sensing images, a lot of big progresses have been made in environment analysis and researches about the Schistosoma snail breeding ground and the distribution of snails in marshland. This paper focuses on the identification of the Schistosoma snail individual goals. Based on the image segmentation by maximum inter-variance, the objects, including snails, are segmented from the background. The radius functions of the typical snails are calculated by scanning the boundary of the object with 8-neighborhood following method. By matching the waveform of Fourier transformation, the snail targets are identified. In the laboratory environment, the recognizing rate can reach over 90% and it has robust in rotation, scaling and translation. [C2041]

"Use doppler radars for studying turbulence of air weights in storm clouds"

The method of estimation of the turbulent pulsations of the air weights velocity in the storm clouds by the spectrums of the scattered signals is produced in this project. Using the first moment of the characteristics of the scattered signal spectrum one can estimate shifted characteristics of the air stream, and using the second moment one can estimate velocity spread of the scatterers strictly connected with the dispersion of the stream fluctuations inside the cloud. [C2042]

"Title page"

The following topics are dealt with: radioengineering research; integrated microwave devices; solid state device CAD/CAM; O-type and DRO microwave devices; M-type devices and gyrodevices; broadband wireless access systems; superwideband radio systems; information resources and networks; microwave antennas; SHF-devices materials and technology; nanoelectronics and nanotechnology; very high power microwave electronics; EM and radiation resistance of materials; microwave measurements; materials measurement; objects and media parameters gauges; medical and ecological applications; radioastronomy and atmosphere research; radar and remote sensing. [C2043]

"Wind map retrieval from SAR data for offshore wind turbines positioning"

The feasibility study for the selection of the optimal site for offshore wind farms is usually made by in situ measurements. This methodology suffers from point information that is not sufficient for this purpose, because it is needed a dense spatial wind information. Remote sensing overcomes this problem by using the high capability to cover periodically wide areas in one acquisition. From this point of view satellite synthetic aperture radar (SAR) wind mapping can be a useful tool in selecting optimal sites and may therefore increase the cost-effectiveness of planning wind farms. In this paper an overview on the physical backscattering mechanisms that models the wind signatures in SAR images is illustrated. Several strategies to derive wind map are described and some results using CMOD algorithm are shown. [C2044]

"Electromagnetic modelling of ship classification in OTHR"

Because of the Faraday rotation effect in the ionosphere, the elliptical polarization high frequency electromagnetic wave is used to simulate the sky wave to illuminate the ship targets. The half space FDTD method is utilized to model the ship targets on ocean which have the similar structures. The backscattered instantaneous polarization information of the targets can help to classify targets. The computer simulation results show this method not only can classify them, but also can distinguish the targets motion direction. [C2045]

"Digital beamforming for near-space wide-swath SAR imaging"

Inspired by recent advances in near-space technology and synthetic aperture radar (SAR) technique, this paper presents one digital beamforming-based near-space wide-swath imaging technique. Near-space defined as the space region between 20 km and 100 km, which is above storms and not constrained by orbital mechanics like satellite or high fuel consumption like airplane. These advantages make many new capabilities that are not accessible to current spaceborne or airborne SAR being possible for near-space SAR. This also offers an opportunity to design new SAR imaging technique. This paper deals with conceptual design, as opposed to technological implementation. Multiple beams in azimuth are used to suppress the possible azimuth ambiguities for near-space high-resolution and wide-swath SAR imaging. An example near-space wide-swath SAR is conceptually designed. Simulation results show that the combination of digital beamforming technology and near-space platform can provide a promising solution for remote sensing applications. [C2046]

"Architecture of vision enhancement system for maritime search and rescue"

Because of the limitation of physiological characteristics of human eyes, it is necessary to develop vision enhancement system for maritime search and rescue (SAR-VES), which is intended to improve the poor searching performance of human vision at sea. A system with its framework architecture, which integrate the imaging systems of visible light, infrared, radar and satellite remote sensing, is proposed in this paper to compensate the weakness of the human observation in the maritime search and rescue environment. The system will promote the sensitivity and the detection rate of targets, especially small ones, at sea. It will help improve the safety of life at sea and reduce economical losses in marine accidents. [C2047]

"Doppler radar sensing system of respiration and heart rate"

In this paper, Doppler radar system is designed, which is composed of oscillator, mixer, LNA, and antennas. The idea of this paper is using reverse circular polarization for bio-detection Doppler radar to selectively receive signals reflected from highly conductive body surfaces. To improve isolation property between transmitter and

receiver, we use the bistatic system using LHCP and RHCP antennas. The budget of system is analyzed and the experimental results are discussed. [C2048]

"Classification for polarimetric SAR images based on subaperture decomposition"

In this paper, a novel method, which combines subaperture decomposition with H/ α /Wishart classifier, is introduced to classify polarimetric synthetic radar (SAR) images. We use H/ α plane to initially classify the full-resolution polarimetric SAR image. The initial classification map defines training sets for classification based on coherency matrices of subapertures and wishart distribution. The classified results are then used to define training sets for the next iteration. The convergence of this kind of iteration is much faster than using full-resolution images. And the interpretation of this method is more easily. Results show that the method provides a significant performance improvement with respect to the approaches based on full-resolution images. [C2049]

"A new method of camouflage jamming against ISAR based on compensating modulation"

It is quite significant in the military field that an effective jamming can be executed against inverse synthetic aperture radar (ISAR) successfully. However, ISAR has a well anti-jamming capability, which is stronger than that of conventional radar due to its special imaging approach. Camouflage jamming with many particular advantages becomes a very effective and important jamming approach nowadays. However, it is a novel and important technologic approach that an effective camouflage jamming can be carried out against ISAR. A new method of camouflage jamming is proposed in the paper, based on principle of ISAR imaging. The compensating modulation can be employed for the ISAR signals received by jamming device to achieve camouflage jamming, based on the phase relationship between ISAR signals received by jamming device and the real returned signals of targets. The feasibility and effectiveness of the methods are verified by simulation results. [C2050]

"Range sidelobes suppression for HF surface wave radar with discontinuous spectra"

In order to improve the anti-interference performance, the high-frequency surface wave radar uses several discontinuous clear frequency bands for transmission. Spectral discontinuity causes high range sidelobes which influence detecting and identifying the targets. A novel modified CLEAN algorithm is proposed to remove the sidelobes interferences of the equivalent matched processing result of the received signals. The simulation results show that the method can not only suppress the range sidelobes efficiently but also enhance the range resolution greatly. [C2051]

"Automated procedure for InSAR data inversion using Finite Element Method"

Source inversions performed using different kind of static deformation data, such as GPS displacements, DInSAR imagery, levelling and EDM measurements, suggest that slip on fault is usually not uniform and is better modeled as a distribution of dislocation sources. To this aim, we developed an automated procedure for geodetic data inversion to estimate slip distribution along the fault interfaces. Finite Element Models are used to compute synthetic Green's functions for static displacement. FEM-generated synthetic Green's functions are combined with inverse methods to estimate slip distributions that explain the observed ground deformation. [C2052]

"Surface deformation studies of Tenerife Island, Spain from joint GPS-DInSAR observations"

This work presents results for the three-dimensional displacement field at Tenerife Island calculated from campaign GPS and ascending and descending ENVISAT DInSAR interferograms. The goal of this work is to provide an example of the flexibility of the technique by fusing together new varieties of geodetic data, and to observe surface deformations and study precursors of potential activity in volcanic regions. Interferometric processing of ENVISAT data was performed with GAMMA software. All possible combinations were used to create interferograms and then stacking was used to increase signal-to-noise ratio. Decorrelated areas were widely observed, particularly for interferograms with large perpendicular baseline and large time span. Tropospheric signal was also observed which significantly complicated the interpretation. Subsidence signal was observed in the NW part of the island and around Mount Teide and agreed in some regions with campaign GPS data. It is expected that the technique will provide better results when more high quality DInSAR and GPS data is available. [C2053]

"Preliminary results of lava flow mapping using remote sensing in Piton de la Fournaise, La Réunion island"

The use of remote sensing is more and more incontrovertible in volcanic monitoring, especially in INSAR and

thermal studies. A comprehensive database of high-resolution multispectral and multitemporal optical satellite imagery exists for Piton de la Fournaise, the active volcano on La Reunion Island. This database, however, remains relatively underexploited in volcanological studies of Piton de la Fournaise. Using a large image data set including SPOT 5 and 4, ASTER and aerial photography, we performed cartography of recent lava flows. Different methods were applied for each sensor in order to extract and map lava flow contours and surface morphology. These methods include photo interpretation as well as fusion of thermal band and optical images. In addition we performed several tests with specific software combining object and spectral based techniques. Subsequently, a simple statistical comparison between different perimeters and areas mapped allowed us to determine a precision ratio. Results show that difficulties in extracting contours arise when the study area is a complex lava flow field where the different lava flows overlap, or have a similar textural and radiometric characteristics. [C2054]

"GlobVolcano project overview"

The GlobVolcano project is part of the ESA DUE programme. The project aims at demonstrating EO-based services to support the Volcanological Observatories and other mandate users (e.g. Civil Protection authorities, scientific communities of volcanoes) in their monitoring activities. During the project a worldwide selection of user organizations will cooperate with the GlobVolcano team in order to harmonize user's requirements and to evaluate the EO-based services. The "Osservatorio Vesuviano" of Naples (INGV-Italy) coordinates the communications between the project and the User Community. IPGP of Paris is responsible for the scientific coordination and the validation activities. The project activities are split in two phases. During the first phase (completed in June 2008) the service infrastructure and interface to the users have been developed. Prototype EO-based information products have been generated and validated. Service provision on pre-operational basis will take place during the second phase. [C2055]

"Proceedings of the 2008 second workshop on USE of remote sensing techniques for monitoring volcanoes and seismogenic areas USEReST 2008"

The following topics dealt with: volcanic SO₂ emission monitoring; Global Ozone Monitoring Experiment; GOME-2 satellite; geophysics-geodesy coupled model; active faults; microwave interferometric sensor; space analysis; time analysis; active volcano deformation; data acquisition; data product generation; volcanic crisis; seismic hazard assessment; Vrancea area; Romania; Europe; Interferometric Synthetic Aperture Radar; InSAR data; finite element method; Tenerife Island; Spain; Global Positioning System; GPS-DInSAR observation; Robust Satellite Technique; RST assessment; volcanic ash plume identification; volcanic ash tracking; lava flow mapping; Piton de la Fournaise; La Reunion island; volcanic deformation mapping; Permanent Scatterer InSAR; PSInSAR; Globvolcano project; landscape response monitoring; tectonic forcing; central Badakhshan-Hindukush-Pamir Region; lava flow fractal modeling; volcanic plumes trajectory matching; volcanic plume dispersion modeling; thermal anomaly monitoring; gravity observation; La Palma; Canary Island; New Zealand; hot spot detection; photogrammetric survey; light detection and ranging; LIDAR survey; Sciara del Fuoco; Stromboli eruption monitoring; ground deformation measurement; radar interferometry; Hazara Kashmir Syntaxis; northern Pakistan; Auckland; differential synthetic aperture radar; DSAR; ground-based radar remote sensing; volcanic ash eruptions; numerical model; quantitative application; Sicily Island; Italy; surface deformation pattern; L-band mission; global tectonic activities monitoring; Kalman Filter; earthquake prediction; seismogenic layer monitoring; Advanced Land Observing Satellite; ALOS observation; JAXA mission; earthquake monitoring; AD 2008; Support for Aviation for Volcanic Ash Avoidance; SAVAA; MSG satellite; Spinning Enhanced Visible and Infrared Imager; MSG-SEVIRI measurement; AD 2006 11 24; Mt. Etna eruption; African active volcanic zone; Italian Space Agency; Agenzia Spaziale Italiana; Sistema-- Rischio Vulcanico; ASI-SRV optical sensor data processing modules; seismogenic areas; ASI Pilot Project; volcanic risk monitoring; Earth observation; EO Data; Mauna Loa; Kilauea volcanoes; Hawaii; land subsidence investigation; groundwater overexploitation; Tehran; Iran; and with AD 2004 to 2007. [C2056]

"Coupling geophysical modelling and geodesy to unravel the physics of active faults"

The major requirements of seismic hazard assessment must address mainly the information about the expected location, time and magnitude of the impending strong earthquakes, as well as the scenarios ground motion associated with the possible future seismic events. While the quick notification of seismic events, appears nowadays pretty well established, thanks to the development of regional and local seismic networks, in terms of prevention more and more importance is devoted to studies of the inter- and pre- seismic earthquake cycle. To improve the intra seismic and pre-seismic information, which may lead to an effective mitigation of seismic risk, we are proposing an innovative approach, that combines Earth Observation data (GPS and SAR) and new advanced approaches in seismological and geophysical data analysis. The employed EO data are the observations acquired by means of SAR sensors, treated by Differential Interferometric techniques, the data

observation acquired by permanent GPS stations or Γ, Bi ad-hoc Γ, Bi campaigns of the observations done over earthquake prone area. The aim is to combine the geophysical modelling of the faults with the surface displacement measured with the two mentioned techniques. In particular, application of the DInSAR techniques, using a stacking of interferograms, makes it possible, under the classical interferometric constraints (coherence, baseline, etc.), to retrieve a vertical displacements map, referred to a temporal interval, over areas where seismic fault system are localized. The displacements fields coming from GPS/DInSAR and other additional information, constitute the input for the geophysical model which shall indicate whether the fault is in a Γ, Bi critical situation Γ, Bi . [C2057]

"Microwave interferometric sensors as a tool for space and time analysis of active volcano deformations: The Stromboli case"

A Ground Based SAR Interferometer (GB-InSAR) was installed at Stromboli volcano (Italy) in February 2003 to continuously monitor the behaviour of the morphological depression known as Sciara del Fuoco, SdF, with alerting purposes. This was decided as a consequence of the collapse of a large landslide from the NW slope of the SdF and the subsequent tsunami occurred on December 2002. The GB-In SAR system, working at Ku band, was set up on the stable right flank of the SdF; it has been continuously working and during this last five years has permitted to follow the temporal and spatial evolution of the mass movement in the SdF and the crater. Interferometric maps have permitted to assess the deformation field over a large portion of the target area and to characterize different processes. The system allowed to observe in particular two main events occurred on 5 April 2003 (a major explosion) and on 27 February 2007 (beginning of the effusive phase) respectively. The potential of the use of DInSAR from satellite platforms working at C band to understand the dynamic of the whole volcano has been also investigated. Different images acquired from the ERS2, RADARSAT and ENVISAT satellites before and after the 2003 collapse of the landslide, and before and after the 2007 event, have been interferometrically processed as well. Notwithstanding the restricted number of available images, the ground deformation occurred on the island due to the volcanic activity has been obtained with spatial and temporal characteristics complementary to those ones provided by GB-InSAR. [C2058]

"Dynamic Range Compression and Pseudo-color Presentation Based on Retinex for SAR Images"

Synthetic Aperture Radar (SAR) can provide all-time and all-weather surveying of the earth. It is a very important data source for remote sensing. While SAR images often display in gray scale and usually are coded in 16 bits, it is necessary to propose an efficient method to generate pseudo-color SAR images to ease the interpretation difficulty. Considering combining the dynamic range compression and pseudo-color coding, a method based on Retinex is proposed in the paper. Experiments indicate that the proposed method can generate acceptable pseudo-color images. Analysis indicates that the proposed method can be improved further. [C2059]

"Experimental verification of COSMO-SkyMed SAR capabilities"

COSMO-SkyMed is the Italian Remote Sensing programme which foresees the utilization of a constellation of four SAR Satellites in Low Earth Orbit, dedicated to the management, control and exploitation of Earth resources for civil and defence applications. The program is completely funded by the Italian Government, mainly through the Italian Ministry of Research (MIUR) and the Ministry of Defence (I-AD). Thales Alenia Space Italia is responsible for the design, development and verification of the complete constellation. Satellites will take SAR images of the Earth in the X-band for a variety of government, commercial and scientific users, providing data with unprecedented quality in terms of numbers of images, resolution and accuracy. Following the canonical space qualification and acceptance processes customers and Thales Alenia Space Italia decided to pursue an end-to-end experimental verification of the SAR instrument in order to provide evidence of its capabilities. With respect to the classical approach for the on-ground verification of space-borne SAR which is done through the verification by parts and the final analytical compilation, it was decided to set-up an outdoor verification Test able to exploit all radar functionalities and performance in an integrated approach i.e. radar electronics, antenna and calibrated targets all together. In this paper they are described the test-set-up and the results of the experimental verification campaign made through the qualification hardware of the SAR. [C2060]

"Arctic sea ice mapping with satellite radars"

Drastic reduction of Arctic sea ice in recent years demands ice monitoring over various spatial and temporal scales. Sea ice backscatter signatures from field measurements and from model analyses are obtained at L-band and C-band frequencies. Based on these signatures, capabilities for Arctic sea ice mapping are determined for current and future satellite active microwave sensors including synthetic aperture radars (SAR) and scatterometers. This study includes L-band and C-band radars such as the ERS (European Remote Sensing),

Envisat (Environmental Satellite), RADARSAT-1 and 2, ALOS (Advanced Land Observing Satellite), and DESDynI (Deformation, Ecosystem Structure, and Dynamics of Ice) SARs with resolutions from 10 to 100 m, and the SMAP (Soil Moisture Active-Passive) scatterometer with resolutions from 1 to 10 km. [C2061]

"Ground-based multi-channel synthetic-aperture radar for mapping the ice-bed interface"

An 8-channel ground-based radar has been developed and used to image the ice-bed interface under the icesheet near Summit Camp, Greenland. This radar, which chirps from 120 to 300 MHz, was developed to demonstrate the feasibility of using radar to characterize the basal conditions (topography, roughness, and presence of liquid water) thus enabling improved modeling of ice-sheet dynamics. Using a basal contour map from the dataset processed in depth-sounding mode to establish the elevation level, the data were SAR processed to produce 15-look images with 30-m resolution. A SAR mosaic covering a 6.25-km by 25-km area reveals for the first time regions of relative roughness as well as a wide, smooth valley beneath the 3.2-km thick ice sheet. [C2062]

"Portable temperate ice depth sounder radar (TIDSoR)"

Glaciers in several parts of the world are reported to be retreating and thinning rapidly over the last decade. Radar instruments can be used to provide information on the internal and basal conditions of large and small ice masses. Radars operating in the lower part of the HF spectrum are required for sounding temperate glaciers. Also, low-frequency sounders are useful for measuring thickness of fast-flowing glaciers in Greenland and Antarctica. This is due to the composition, attenuation, and back-scattering from large pockets of water present in temperate ice. We are developing a dual-frequency temperate-ice-depth sounder radar (TIDSoR) for determining ice thickness and basal conditions. The most significant features of this novel sensor are its portability as well as its low-power consumption. The system operates at 7.7 MHz and 14.0 MHz with 1 MHz bandwidth and 20 W of output peak power. The radar will be installed in a small aircraft such a DCH-6 (Twin Otter) or carried in a backpack for surface-based measurements. In the first case, the radar will be supported by the airplane power supply and in its backpack configuration by a compact 12 VDC power supply. TIDSoR is expected to be deployed during the summer 2008 for surface-based observations. In this paper, we discuss our design considerations and current progress towards the development of this radar. [C2063]

"ERS Differential SAR Interferometry: A powerful tool for surface deformation analysis"

We investigate the key role played by the European Remote Sensing satellites ERS-1 and ERS-2 to demonstrate the revolutionary nature of the Differential Synthetic Aperture Radar Interferometry (DInSAR) technique to investigate surface displacements over large temporal and spatial scales. The presented analysis starts with a short overview of the basic principles of DInSAR, followed by the presentation of a number of successful applications based on exploiting ERS data; in particular, several results focused on seismic deformations, volcanic activities and land subsidence, are shown. Subsequently, the analysis is dedicated to introduce the recently developed advanced DInSAR algorithms. In this case the emphasis is given on discussing the approaches that allows analyzing time sequences of ERS SAR data to produce deformation time series. The main aspects related to these advanced DInSAR algorithms are discussed first, followed by the presentation of key results obtained by processing long time series of ERS data. [C2064]

"Monitoring water defense structures using radar interferometry"

Monitoring the safety of water defense systems is crucial for life in low-lying countries such as the Netherlands. Conventional monitoring of structures such as dams and dikes is often limited to visual inspection, with additional in situ measurements if deemed necessary. Here we show that advanced satellite radar technology can be used to obtain weekly updates on dike stability for a significant part of all dikes in the Netherlands. Applying a supervised classification of potential coherent scatterers, it is possible to provide a dense sampling of line structures such as water defense systems. Such observations can be used to assess structural stability of the water defense systems, leading to improved hazard assessment in relation to flooding risk. This may have a significant impact on safety assessment and hazard mitigation in the Netherlands. [C2065]

"Advanced synthetic aperture radar based on digital beamforming and waveform diversity"

This paper introduces innovative SAR system concepts for the acquisition of high resolution radar images with wide swath coverage from spaceborne platforms. The new concepts rely on the combination of advanced multi-channel SAR front-end architectures with novel operational modes. The architectures differ regarding their implementation complexity and it is shown that even a low number of channels is already well suited to significantly improve the imaging performance and to overcome fundamental limitations inherent to classical SAR systems. The more advanced concepts employ a multidimensional encoding of the transmitted waveforms to

further improve the performance and to enable a new class of hybrid SAR imaging modes that are well suited to satisfy hitherto incompatible user requirements for frequent monitoring and detailed mapping. Implementation specific issues will be discussed and examples demonstrate the potential of the new techniques for different remote sensing applications. [C2066]

"Analysis of antenna pointing errors on SAR image quality"

Antenna beam pointing accuracy and stability are key issues for obtaining reliable and high quality remote sensing data in space-borne SAR sensors. A wide set of causes, related to technological aspects and environmental conditions acting at both bus and payload level, contribute to misalign the actual antenna bore sight from the theoretical direction. Even very small error angles on the yaw, pitch and roll axes directly reflect on antenna pointing, impacting on key image quality parameters such as resolution, swath width, signal to ambiguity ratio. Particularly, two major types of errors can be considered: time invariant (static) errors and time-variant (dynamic) errors. The different SAR image quality parameters show different sensitivity to mispointing and therefore are affected in different ways by satellite attitude. In this paper we analyze the effects of static and dynamic errors and we predict their impact of the most relevant SAR image quality parameters, by assuming as reference a generic X-band SAR mission. [C2067]

"COSMO-SkyMed: Calibration & validation resources and activities"

COSMO-SkyMed is the largest Italian investment in Space Systems for Earth Observation, commissioned and funded by Italian Space Agency (ASI) and Italian Ministry of Defense (MoD). It consists of a constellation of Low Earth Orbit mid-sized satellites, each carrying a multi-mode high resolution Synthetic Aperture Radar (SAR) instrument operating at X-band and a full featured Global Ground Segment to properly exploit space capabilities. In the framework of COSMO SkyMed mission, the CALVAL represents the system element that performs the calibration activities and the assessment of the image quality. In this paper main characteristics, driving requirements, technical choices and CALVAL first results are described. [C2068]

"Maximum likelihood estimation of the forest stem volume from VHF SAR data at the individual tree level"

An algorithm based on the exact maximum likelihood (ML) estimator for retrieving the mean stem volume of mature forest stands on relatively flat ground is presented. A VHF-band forest backscatter model at the individual tree level is used to derive the algorithm. The model interprets the tree trunk volume as a random variable and employs a concept of random forest reflection coefficient to characterize fluctuations of radar returns from individual trees. The algorithm is derived under the condition that both the trunk volume and forest reflection coefficient are non-random constant values. Performance (normalized standard deviation and bias) of the algorithm is analyzed by means of Monte-Carlo simulation for various scenarios in terms of statistical distributions for the trunk volume and forest reflection coefficient. It is shown that the algorithm exhibits robustness to the distributions and provides nearly unbiased and accurate stem volume estimation over a wide range of the variances of distributions. A computationally efficient algorithm based on the approximate maximum-likelihood (AML) estimator is also derived. It is shown that the performance of this algorithm is close to that of the ML-based one when the signal-to-noise ratio (SNR) is about 6 dB and perfectly coincides with that for SNRges8 dB. The asymptotic performance of the ML-based algorithm in the infinite SNR limit is numerically evaluated. Simulation results have shown that both of the algorithms almost attain the asymptotic performance at physically realizable SNR. [C2069]

"Analysis of sea state parameters and ocean currents from temporal sequences of marine radar images of the sea surface"

This work uses ordinary X-band marine radars to extract directional wave spectra and their related sea state parameters, as well as speed and direction of ocean surface currents, including tidal information. The used method analyzes the structure in frequency and wave number vector of the image spectra derived from temporal sequences of marine radar images of the sea surface acquired by a marine radar system. The presented data and the related results were measured from a research platform located in the North Sea. In addition, the work presents some comparisons between sea state parameters derived from the marine radar analysis and the equivalent sea state parameter obtained from in-situ wave sensor records. [C2070]

"Multipolar SAR ATR: Experiments with the GTRI dataset"

Multipolar radar data is a rich source of information. Even though multipolar synthetic aperture radar (SAR) images have been used extensively for remote sensing applications, the use of the same for airborne radar

systems has been limited. With the release of the GTRI turn table multipolar data in public domain, the scopes to experiment with real multipolar data has increased. The current work reports the experiments done with the GTRI dataset to examine the effect of using multipolar data for SAR based target classification. The results indicate that multipolar data may give better classification performance and may also be useful to make the classifier less sensitive to minor variations between the training and test target images. [C2071]

"Preliminary performance analysis and design for a distributed P-band synthetic aperture radar"

This paper focuses on a new concept for spaceborne P-band radar implementation, that is distributed SAR based on formation flying. This approach can in principle allow to overcome physical constraints that limit the performance of monolithic SARs, leading in the P-band case to huge antennas and hard swath/resolution trade-offs. The proposed SAR is based on a larger transmitting satellite and a set of light-weight receiving-only platforms. This architecture also allows for multi-mission capabilities. In particular, in the P-band case forests observation and biomass estimation can be in theory combined with interferometric ice sounding. Payload concept is clarified, and a preliminary performance analysis in terms of ambiguity and coverage is proposed. [C2072]

"Development of a polarimetric CFAR detector using Markov Chains"

The paper proposes a novel constant false alarm rate (CFAR) detector using Markov chain models, an innovative new technique that will utilize the finer resolution of RADARSAT-2 to yield improved detection performance for higher-resolution objects. The Markov chain based CFAR detector extends traditional PDF based CFAR detection to first-order Markov chain model by considering both correlation between neighboring pixels and PDF information in CFAR detection. With the additional correlation information, the proposed approach results in advancing the performance of conventional CFAR detectors. Our both analytical and experimental results both show that the new Markov chain CFAR detector can improve the conventional PDF CFAR detector about 30% in terms of detection probability gain and about 2.84 dB in terms of signal-to-clutter ratio gain. [C2073]

"Performance measurements of the radar "in situ""

Method of implementation and the radar system oriented set of tests have particular interest in maintaining current radar net (primary/secondary-military/civilian) at the peak of their operational capabilities. This work is traditionally shared between the radar operational personal and the original radar manufacturer (OEM) engineers. The shortcomings of these methods are known, because the level of test or technical check is determined by built in test equipments (BITE) of the radar, and their supplementary tools; the original equipment manufacturer site visits are seldom, expensive and sometimes profit oriented. Because it is difficult to track the safety feature changes of the SSR system and/or ECCM performance levels over a longer period-it is therefore very hard to get an objective picture of the radar performances on a regular basis. However to get the maximum available information regularly regarding a radar under test within a minimum required downtime one has to implement a comprehensive set of tests which complement each other and maintain the data/results. The evaluation of the test results should be based on the scientifically proven criteria and their syntheses. This kind of activity sounds quite interesting for radar experts; however they lack the impetus to gain the attention by the radar scientific community. This paper intends to give the momentum to introduce a practical realisation of the system performance check (SPC) applied for ground-based radars. [C2074]

"Spectral estimation by the model of Autoregressive Moving Average and its resolution power"

This work addresses the problem of stochastic modelling of short time series. Questions of autoregressive spectral analysis and autoregressive moving average spectral analysis and its application in the tasks of signal processing of informational measuring systems are considered. Autoregressive and autoregressive moving average spectral methods as well as by discrete Fourier transform are given. [C2075]

"Radar pulse trains classification"

The paper presents on the base of theoretical approach of time-frequency analysis and time-frequency representation optimizations, classification results of real radar signals. The results show, that applying class-dependent methodology it is possible to achieve acceptable classification level on the base of few intercepted pulses. [C2076]

"Nonparametric method for estimating spoken language sound multivariate probability density function"

In the paper a new approach for estimating of the spoken language sound multivariate probability density is suggested. It is based on the use of a projection of a random process to the set of random variables, with the probability density defined as a product of two-dimensional densities. The estimates of two-dimensional probability densities are obtained with the help of filtering of the two-dimensional empirical characteristic function. Therefore, we are suggesting a nonparametric estimate of the characteristic function. On the basis of these estimates nonparametric algorithms of sound classification are constructed. [C2077]

"Modification of Newton-Kantorovich iteration procedure for piecewise-constant real permittivity profile reconstruction"

General Newton-Kantorovich method and its new modification for piecewise-constant real permittivity profile reconstruction on the basis of multifrequency reflectometry data are described. The method of spectral analysis based on the chain-fraction approximation is proposed to be used as stage of modified Newton-Kantorovich method and is also described. Some results of numerical simulation are presented. [C2078]

"Edge-preserving piecewise-constant image restoration via method of minimum of extension"

Problem of edge-preserving piecewise-constant image restoration is considered in the paper. Algorithm based on solution of nonlinear nonquadratic regularization problem is developed and discussed in the paper. Nonenergy measure of signal in the form of time duration of signal or spatial extension of image is introduced and used afterwards as a nonquadratic regularization term. Proposed approach is investigated through numerical simulations for one-dimensional signals and images, and compared to results given by standard Tikhonov regularization scheme. Results of application of developed algorithm for filtration of noisy aerospace images are given. [C2079]

"Microwave Fourier-holography approach improvement via minimum duration amplitude multifrequency data extrapolation"

The problem of restoration improvement of complex multifrequency reflection coefficient data of layered dielectric structure from scalar amplitude data measurements is considered. It is proposed to use extrapolated amplitude multifrequency data in the framework of developed Fourier-holography approach, making it easier to extract informative segment of data, which corresponds to structure, in the time domain. Extrapolation is carried through special nonquadratic regularization procedure based on method of minimum of duration. Results of numerical simulations and experimental data processing are given. [C2080]

"The CLEAN type algorithms for radar signal processing"

A new class of signal processing algorithm based on CLEAN methods primary introduced in radio-astronomy is presented in the paper. The classical radar signal processing is based on match filtering concept, which is optimal in mean square sense in case, when single target echo is detected against white or colour Gaussian noise. Such approach was effective when pulse radar have been widely used. The introduction of pulse-compression technique changes significantly the signal model, but still the match filter have been widely. The introduction of continuous wave radars, and especially noise and passive radars changed dramatically the situation. In such radars all echoes are superimposed and interfere with each other and the simple model no longer fits to that case. The straightforward solution-use of inverse problem mathematical solutions such as solving the set of nonlinear equations to find all echoes in received signal-is usually computationally ineffective and often numerically not stable, so suboptimal methods are being developed to improve detections of weak signals in CW radars. One of possible solution is to use concept of CLEAN technique an remove all strong echoes from received signal. When only weak signals and white noise remains in is possible to use matched filter concept without significant loses of radar sensitivity. In the paper several techniques for radar signal processing utilizing CLEAN concept are shown. [C2081]

"Recent researches in the field of weather radar at the National Aviation University"

An overview and analysis of weather radar methods and systems are presented based on the developments and researches fulfilled in the National Aviation University in Kiev, Ukraine during the last decade. Functional, methodical, and technological aspects of weather radar are analyzed. Airborne weather radar is considered as multifunctional avionic system and the instrument to obtain qualitative and quantitative information about the dangerous weather during the flight. Directions of further development of "weather radar" as both an electronic system and a field of science & engineering are discussed. [C2082]

"2-D analysis and synthesis of dielectric lens antennas with boundary integral equations"

At first, we study the electromagnetic performance of 2-D models of hemielliptic dielectric lens antennas (DLAs) with the aid of an advanced numerical algorithm. It is based on the Muller boundary integral equations (MBIE) discretized with the trigonometric Galerkin scheme. Then this solver, combined with an in-house genetic-type optimizer, is applied to the synthesis of the lens profile aimed at the improvement of the lens off-axis radiation properties. The results obtained highlight the interplay between the focusing and resonance mechanisms in the behaviour of compact dielectric lenses. Furthermore, it is demonstrated that the lens shaping enables one to improve the performance of switched-beam DLAs typically used in base stations for indoor communication systems. [C2083]

"Quasi-loop antenna for SAW RFID device"

The quasi-loop antenna for surface acoustic wave (SAW) radio frequency identification (RFID) device has been presented in the paper. It operates at frequency 433 MHz that is commonly used for RFID (ISO 18000-7). The main advantage of the solution is antenna feeding elements elimination as a result of precise SAW and antenna input admittance design. For this reason the whole system is very small and low cost. [C2084]

"Multivariate algorithms for dangerous turbulence detection in weather formations"

This paper briefly describes methodologies of turbulence detection and classification. Proposed methods based on neural network approach. One method provides multivariate analysis of measured variables. Another one based on spectrum shape analysis. These methods are very flexible and allow reduction of calculation time and can be successfully implemented for warning purposes in airborne systems. [C2085]

"Weather radar-recent developments and trends"

Recent developments in weather radar technology are discussed and results obtained with the NOAA/NSSL polarimetric Doppler research radar are shown. These include mitigation of range velocity ambiguities via systematic phase coding of transmitted signal and staggered PRT technique. Reduction of errors and faster volume scans is possible by decorrelation transformation (whitening) of oversampled signals in range. Spectral processing of polarimetric variables brings a new dimension whereby it is possible to adaptively recognize ground clutter and filter it as well as to estimate winds by separating passive wind tracers (such as insects) from migrating birds. [C2086]

"The estimate of instantaneous power of polarization spectrum components in polarimetric weather radar"

New approach to use polarimetry for turbulence intensity estimate is proposed. It is based on estimation of the energetic characteristics of turbulent polarization spectrum. Such approach can increase the informativity of weather radar systems relatively to obtaining information about factors that are the origin of changing polarization of reflected signal. [C2087]

"Use of spectral differential reflectivity at remote sensing of precipitation"

Recent advances in the radar system design allow to perform Doppler and polarimetric measurements simultaneously. This paper considers behavior of a Doppler-polarimetric parameter-spectral differential reflectivity and its characteristics. Slope of differential reflectivity which is connected with turbulence intensity in rain zone is considered using real data processing. [C2088]

"An automatic approach to lossy compression of images corrupted by Poisson noise"

Lossy compression of images corrupted by Poisson noise is considered. Peculiarities on noisy images are discussed. An automatic approach in selection of a parameter that controls compression ratio (CR) is proposed. It is demonstrated how to reach optimal operation point (OOP), i.e., such CR that provides minimal peak signal-to-noise ratio (PSNR) calculated between compressed and noise free images without having an actual noise-free image. A provided CR is of about 6...16 and it depends upon image complexity. [C2089]

"Amplification of space charge waves of millimeter wave range in transversely inhomogeneous n-GaN Films"

Amplification of space charge waves (SCW) due to the negative differential conductivity in n-GaN films placed onto a semi-infinite substrate is investigated theoretically. A general case of transverse inhomogeneous films is considered. The diffusion-drift equations for volume electron concentration were used jointly with the Poisson equation for the electric field. The transverse inhomogeneity results in a decrease of the electron mobility near

the surfaces of the film due to surface scattering and, correspondingly, to some decrease of spatial increments of amplification. It is demonstrated that the non-uniform doping can compensate an influence of the surfaces on the spatial increments. It is possible to observe an amplification of SCW in n-GaN films of submicron thicknesses at high frequencies f ges 100 GHz. Also, due to amplification, high (~ 10 kV/cm) output electric fields of the short wave part of the millimeter wave range can be obtained. [C2090]

"Simulation of electromagnetic wave propagation through dielectric waveguide with p-i-n control element"

Simulation of the electromagnetic wave interaction with a p-i-n control element in a dielectric waveguide is presented. The problem has been solved numerically. Our simulation gives the coefficient of propagation like a function of basic parameters of a p-i-n structure. The investigation has demonstrated an efficiency of the control element in a dielectric waveguide in mm wave range. [C2091]

"Microwave oscillations in a cavity with dispersive double negative medium"

Microwave oscillations excited by a wideband current pulse in a cavity filled with double negative dispersive medium and bounded by a closed perfectly conducting surface is studied. Some features of eigenfrequencies of such electromagnetic system are presented. Transient field evolution is shown. [C2092]

"Quasi-optical sapphire resonators for millimeter wave impedance characterization of high-TC superconducting thin films"

A number of whispering gallery mode (WGM) dielectric resonators or quasi-optical dielectric resonators (QDR) are proposed by authors for high-temperature superconducting film surface resistance measurement in millimeter wavelength range. Results of comparing advantages and disadvantages of the resonators of three types are presented. The resonators were made of single crystal sapphire in the forms of cylindrical disk, truncated cone and hemisphere with a purpose of work in Ka-band. The peculiarities of resonance frequency spectra, field distribution and interaction of microwave field with the sample under test are considered. In authorspsila opinion each of the resonators has own niche for application. [C2093]

"Wide range Time of Flight camera for outdoor surveillance"

This paper presents the application of the time of flight (ToF) cameras to outdoor surveillance. The applications of ToF camera were limited to its non ambiguity distance range, less than 10 meters. We present the problems and the solution for extending the distance use of ToF cameras beyond the non ambiguity range. The distance ambiguity can be solved by measuring the distance with two different frequencies. The needed contrast range of the amplitude image increases with the square of the distance. The efficient use of ToF cameras for outdoor surveillances imposes not only the increase of the illuminating power but also to increase the accuracy of the distance and amplitude images. The ambiguity of the measured distance can be effectively solved if the multiple reflections inside the camera body are reduced. [C2094]

"Availability analysis of the multilateration surveillance system in Kiev (Boryspil) airport"

In this paper application of multilateration (MLAT) systems for vehicles localisation is considered. Deployments of such system require special algorithms to be developed and implemented. Analysis of multilateration system deployment is done for Boryspil airport in Kiev, Ukraine. With the help of calculation algorithms, different cases of target position inside the airport area are considered and brief analysis of detection is done. The simulation scheme is developed in order to obtain maximum accuracy of target localization. [C2095]

"Microwave study of ferroelectrics in waveguide"

Peculiar feature of ferroelectrics is high dielectric permittivity ϵ_{psiv} which sometimes is accompanied by very big loss tangent tandelta . This is a reason of difficulties to obtain accurate characterization despite of variety of techniques available. This report is devoted to the selection of proper waveguide method for specific cases of bulk or film materials investigation to obtain reliable data of their ϵ_{psiv} and tandelta . [C2096]

"Quantum interference in transistors"

We consider adiabatic charge transport through transistor based on quantum dot caused by two periodically changing external perturbations. Both the magnitude and the sign of the transmitted charge are extremely sensitive to the configuration of the transistor and to the magnetic field. We find the correlation function characterizing the random value of this pumped charge for arbitrary strength of perturbation. In contrast to

previous theoretical and experimental claims, the charge is found not to have any symmetry with respect to the inversion of magnetic field. At strong pumping perturbation, the variance of the charge, $\langle Q^2 \rangle$ is found to be proportional to the length of the contour in parametric space. [C2097]

"Comparisons of 3 dimensional temperature distributions of mm and IR images"

The temperature distributions of many objects are measured with both a thermal camera and mm wave imaging system working at 8 mm to show the difference between thermal and mm wave images. mm waves penetrate to many materials including clothes, cloud and plastics, makes the distributions different from the thermal wave. The distributions plotted as a 3 dimensional form enhance the difference between the distributions more. [C2098]

"Microwave multifrequency radar images of electrodynamic objects"

The results of microwave measurements for some objects combining multifrequency measurements and transversal scanning is presented. Longitudinal distance dependencies of reflectivity have been obtained by synthesis from multifrequency data. The multifrequency measurements and synthesis have been done in real-time. The measurements in free space were carried out by the apparatus using measuring modules of scalar reflectometer of series P2 (R2). The combination of data in longitudinal and transversal directions produced radio images of some metal structures. [C2099]

"High-temperature superconductor-films microstrip band-pass filters for extreme working conditions"

The microwave microstrip band-pass filters (BPF) for 1.7 GHz manufactured on the basis of normal metal (Cu) thin films, Au/YBCO bilayer films and pure YBCO thin films are investigated. Features of the BPF-construction on the basis of YBCO films are described. The designed high-temperature superconductor (HTS) BPF has electrodynamic characteristics (passband-loss, steepness of transition area from the pass-band to the stop-band etc.), which are inaccessible for normal metal film filters. The influence of moisture, storage in real atmosphere, temperature shocks on electrodynamic characteristics of the microwave HTS BPF with a narrow passband has been investigated. The characteristics of the designed HTS BPF in the hermetic housing were stable after 5 cycles of rapid cooling and heating (300 K down to 77 K and up to 300 K) and more than a year of usage. The designed construction of hermetic housings ensures safety of YBCO films in microwave devices for extreme operation regimes in satellite and cellular communication systems. [C2100]

"Hybrid oscillations in composite resonators with uniaxial hexaferrites"

The coupled oscillations are theoretically and experimentally investigated in the composite solid-state resonators (ferrite-dielectric structure). The experiments have been conducted for barium ferrite ($\text{BaFe}_{12}\text{O}_{19}$) and strontium hexagallate ($\text{SrGa}_{12}\text{O}_{19}$) plates in the saturation region. The calculation is carried out for the first four magnetostatic modes of ferrite plate. The obtained results do correlate with theoretical calculations. [C2101]

"System-in-a-package technology for 3D integration of radar modules"

3D thin-film technology including substrate vias and integrated passives is used as a platform for heterogeneous integration of high frequency wireless systems and radar. The features of the technology are first described and next demonstrated with an integrated Doppler radar operating in the Ku band. [C2102]

"High-speed photodiodes for microwave and millimeter-wave systems"

The high-speed InGaAs/InP p-i-n photodiodes for microwave generation and frequency up-conversion in microwave and millimeter-wave systems is discussed. Based on numerical simulation study of maximal output microwave power with appropriate optical-to-microwave conversion loss for InGaAsP/InP partially depleted absorber photodiodes in frequency range from 10 to 60 GHz are presented. The design and operation regime peculiarities of InGaAs/InP p-i-n photodiode as optoelectronic up-converter in radio-over-fiber system are provided. [C2103]

"Radar determination of probable icing-in-flight"

This paper summarizes recent works done in NAU in the field of development of icing detection algorithm, based on remote sensing of clouds and precipitation. Conditions of aircraft icing are described. Backscattering of microwaves on water droplets and ice crystals of different shapes is considered as function of polarization, antenna elevation, size distribution of scatterers and other factors. Polarization parameters of scattered signal are

calculated for hazardous and non-hazardous cases. Icing detection algorithm is proposed. [C2104]

"Regional analytical algorithm of sea chlorophyll concentrations retrieving from sea reflectance"

The method of chlorophyll concentration calculation using remote sensed ocean reflectance is proposed. This method can take into account the regional features of investigated basin, so it allows to avoid some errors caused by standard methods application. Phytoplankton pigment concentrations were retrieved from satellite and contact data using the method proposed, showing good correlation with biological data. Pigment absorption spectra were also calculated, providing information about not only chlorophyll, but many auxiliary phytoplankton pigments. [C2105]

"Using ASTER imagery for massive sulphide deposits exploration"

This study aims at exploiting multi-spectral data, acquired from ASTER, satellite to explore areas of hydrothermal alteration and Gossan including massive Sulphide deposits. Auger sulphide is a good source of raw materials such as economic copper, silver, gold and zinc. Major steps involved in the analysis of ASTER satellite data have been discussed using ERDAS Imagine Software. The extent of interdependence among spectral regions, hydrothermal alteration and Gossan has been studied through digital image analysis and classification. The visual interpretation techniques have been employed to identify and earmark hydrothermal alteration and Gossan zones on the satellite image for carrying out subsequent supervised image classification. Imagery Analysis was supported by the color composite, developed by exposing bands 4, 6 & 9 with Red, Green and Blue radiations respectively, to make iron-rich cap or Gossan and hydrothermal alteration zones prominent. The Gossan-laden regions appeared in Red color while the hydrothermal alteration zones took color range from reddish green to light green. Image enhancement has also been achieved through the application of image ratioing techniques and an improved color composite was developed by exposing results of band ratios of band 5 & band 7, band 5 & band 4, and band 2 & band 1 with Red, Green and Blue radiations respectively. Resultantly, the combination of visual interpretation, previous knowledge of the landcover and digital image processing techniques applied on the ASTER Satellite imagery in multi-spectral mode, has proved beneficial in studying hydrothermal alteration zones and Gossan in the Nuqrah area. [C2106]

"Remote sensing for systems of active impact on clouds"

The problem of remote sensing for of active impact on clouds is considered. The main peculiarities of climate in Ukraine and methods of active impact are discussed. It was shown that climate in Ukraine requires using of such methods for mainly two reasons: protection of agriculture crops (defence against hail) and stimulation of precipitation. Therefore the remote measurement of clouds parameters is of great importance that requires the complex methods, including passive and active sensing. In the paper the various approaches are discussed. [C2107]

"Bandwidth suppression in MM-Wave photonic structure with magnetic "defect""

In this paper an effect of bandwidth suppression in magneto-photonic structure is described and illustrated by different ferrites as a "defect" plate. The theoretical explanation and analysis are given. Possible applications of such structures are suggested. [C2108]

"Computation method of mutual impact coefficient of the quarter-wave wire antennas placed on airplane wire-grid model"

The method of currents distribution on electrodynamic body wire-grid model calculation is developed to solve some problems of electromagnetic compatibility. On the base of currents distribution found, a mutual impact coefficient for the case of two antennas, mounted on Antonov-148-100 and Antonov-70 type aircrafts is obtained. [C2109]

"Design and performance assessment of an airborne ice sounding radar front-end"

The paper describes the design and experimental performance assessment of the RF front-end of an airborne P-band ice sounding radar. The ice sounder design features newly developed components at a centre frequency of 435 MHz, such as, antenna 20% bandwidth at RL < 13 dB, compact high power in-phase and out-of-phase power dividers with a relative bandwidth of 20% and more than 75 W CW power handling, high power SPDT PIN switch with 90 W CW power handling and a 70 W CW high efficiency LDMOS power amplifier with >60% power-added efficiency. The system comprises also a digital signal generator, a digital front-end and a control unit. The system was functionally tested in March 2008 and had a first successful proof-of-concept campaign in Greenland in May 2008. [C2110]

"Mathematical modeling of the cardiac electrical signals formation"

The mathematical model of the myocardium muscular fibers as a nonlinear inertial element is developed and investigated in paper. [C2111]

"Application of microwave radiation in incinerator"

The construction of stove for food productspsila incinerating (making ash) by microwave energy at frequency of 2450 MHz is offered. The construction of irradiation structure that distributes the energy of electromagnetic field from magnetron on four equal parts is offered too. The calculation of the electromagnetic fields in a stove at given location of vessels with the explored product is conducted. [C2112]

"Electromagnetic energy application for soil infectious diseases sterilization"

New ecologically safe biophysical method of sterilization of pathogenic microorganisms that are contained in agricultural soils has been developed. Researches of suppression with the help of electromagnetic fields of ultrahigh frequency of pathogenic microflora and soil sterilization with simultaneous correlation between the species of microorganisms have been carried out. [C2113]

"Multi-switch Satellite Digital System (MSDS)"

In this paper we developed multi-switch satellite digital system (MSDS). MSDS provides eight output lines from three input lines. The MSDS system is suitable for airport hotels where many users can use different satellites (Hotbird, Nilesat, Cirius ... etc) using only single fixed dish with three low noise blocks (LNB), instead of using three fixed dishes with three LNBs. This system can be modified to be suitable for n number of users. [C2114]

"The effect of amplitude fades on a forward transmission system using a DS CDMA"

In this paper, we a study the effect of using pseudorandom sequence spread spectrum signal (Gold sequence) on the generation and detection process of a DS CDMA system with fade amplitudes. The forward transmission in the IS-95 system is assigned to individual base stations using orthogonal (Hadamard) sequences to each of them. The use of pilot-aided Rake receiver gives a conditional bit error probability that does not depend on the number of users and the effect of fade amplitudes decreases the probability of error. This phenomenon can be compensated by increasing the normalized energy per one user. [C2115]

"Noise modeling for global satellite aeronavigation systems"

This paper describes implementation of Neiman method for random process with desired distribution parameters modeling. The models of noise created by Neiman method are used in noise recognition and classification system for global positioning system (GPS). [C2116]

"Organization of software for dynamic scenes visualization and analysis in real-time geoinformation complexes"

In the paper the structure of program environment for real-time geoinformation complexes on the base of object-oriented approach is proposed. The method of geometric range searching that uses moving objects representation on the screen data, for real-time geoinformation complexes is described and its effectiveness are compared with Bentley trees, exhaustive and moving points search methods. Formulas for determination, which of these methods is the most effective for a given character of the dynamic scenes analysis, are deduced. [C2117]

"More efficient ATR system using the decision fusion between HRR and video imaginary"

One of the most important methods to improve automatic target recognition (ATR) function is to use fusion techniques. In this paper we propose an application using an improved version of Sugeno's fuzzy integral to increase the target recognition performance based on high-resolution radar (HRR) and video imaginary. In order to confirm the broached theoretical aspects, a real database was used. [C2118]

"Remote sensing of urban areas from polarimetric SAR data using Time-Frequency and spectral analysis methods"

This article presents two complementary approaches for the study of urban areas using polarimetric and interferometric SAR (POL-inSAR) data. A multidimensional linear Time-Frequency (TF) decomposition is used to

analyze the intrinsic polarimetric behavior of different components of an urban area. A TF signal model, adapted to the case of urban areas, is proposed and studied using relevant statistical descriptors. A TF classification procedure is introduced to retrieve building location and characterize their polarimetric response, and applied to fully polarimetric SAR data acquired by the E-SAR sensor at L-band. Multiple POL-inSAR signals, acquired from different positions, are used to estimate the height of buildings using the interferometry principle. High-performance array signal processing techniques are adapted to the case multi-baseline POL-InSAR (MBPI) observations, in order to enhance the height estimation of scatterers by calculating optimal polarization combinations and determining their scattering characteristics. These multidimensional spectral estimation methods are shown to resolve the building layover problem by extracting and analyzing two components within one azimuth-range resolution cell. [C2119]

"High-accuracy Doppler measurements for airborne SAR imaging"

In this paper, we demonstrate several novel promising techniques and applications of accurate Doppler measurements for airborne SAR imaging. A technique for estimation of the antenna beam orientation angles from Doppler centroid measurements is described. This technique provides an effective clutter-lock. The estimated angles can be used for correction of geometric distortions in SAR images. A multi-look contrast optimization autofocus technique is proposed for an accurate estimation of the Doppler rate via the estimation of the aircraft acceleration. Novel method for retrieving 3D topography of Earth surfaces by using a conventional squint-mode SAR is described. The method is based on high-resolution Doppler centroid measurements with a sub-Hertz accuracy. Experimental results prove the efficiency of these methods. [C2120]

"Multilook technique for dominant scatterer removal in SAR images"

In the paper a multilook method of dominant scatterer removal for SAR image enhancement is presented. Sidelobes produced by very strong scatterers in range and cross-range dimension form a characteristic cross-shaped pattern centred on dominant scatterer. The presence of these sidelobes decreases the overall image quality and can mask weak scatterers close to the strong one. The proposed method is an expanded version of algorithm based on adaptive removal of modelled strong scatterer echoes from raw radar data. The use of multilook technique gives much better results of dasiacleaningspsila the signal. Like in the raw radar signal is reprocessed after removal, and strong scatterers are then added to the final image. The multilook cleaning method has been successfully tested using raw radar data. [C2121]

"Analysis of the parameters of asymmetrical dual feeding full wave dipole antenna"

Analysis of the parameters of asymmetrical dual feeding full wave dipole antenna is presented. Initially, the current distribution was measured, followed by the measurement of parameters of antenna like gain, radiation patterns and input impedance. Based on these observations one equation for current distribution were eventually formulated. This equation was then used to compute the values of the same parameters of the antenna. [C2122]

"Test results of a compact smooth-walled spline-profile horn at 30-38 GHz for radio astronomy application"

A compact smooth-walled spline-profile horn covering the 30-38 GHz frequency band (8 mm radioastronomy band) has been optimized, manufactured and tested. A maximum aperture size was limited by the array application. The measured 3 dB-beamwidths are 40deg/37deg/38deg in the H/E/45deg-planes. The measured sidelobe level is less than -30 dB/-23 dB/-25 dB in H/E/45deg-planes and the maximum gain is 13.8 dBi. The measured cross-polarization level is less than -20 dB at the top of the band. The results of the trial observations at the RATAN-600 radio telescope with the horn are given. The antenna measurement and test results are in good agreement with simulation. We consider using such a horn as an efficient feed of a multi-beam receiving array for a radio telescope. [C2123]

"Monopole antenna with plug-shape ground plane"

Computational modelling of the plug-shape ground plane antenna with different geometrical parameters is carried out. The input reflection coefficient, near-field distributions, and radiation patterns of antenna operating both in the dual-band mode and the wide frequency band are determined. Based on the near-field distributions of this antenna the configuration and mutual arrangement of antenna elements are chosen in order to shape the mono-beam radiation pattern. [C2124]

"Near-field measurements in the microwave and millimetre ranges"

The multi-functional set-up for measuring the near-field distributions in the inductive ($0 < R < \lambda/2\pi$) and

radiating ($R < 2D^2/\lambda$) regions in the frequency range 6 GHz-150 GHz is presented. Dynamic range of the measured SHF signals and the evaluation precision of their relative radiation power are 60 dB and 0.1 dB, respectively. The accuracy of the phase measurements does not exceed $\pm 20^\circ$. The point-to-point accuracy of the positioner is ± 0.005 mm. Performance capabilities of the available facilities are demonstrated by the results of manifold experiments. [C2125]

"Target tracking using radar and direction finder"

At the radar systems, traditional target tracking algorithms are based on the radar measurements termed as plots. In this paper we consider a plot as a vector, which contains measurements of azimuth angle, slant range and sometimes elevation angle. These data are quite sufficient to estimate the target position. Direction finder is a device, which measure only azimuth angle termed as bearing; bearings is considered as another imported source of information nonetheless traditional tracking algorithms based on the plots. This work presents the concept of uniform using plots and bearings as sources of information for tracking systems. Modifications of Kalman filter equations enabling the use bearings, for tracking are presented. The key idea includes the concept of a precision matrix being the reverse of a covariance matrix. The bearing may be used as a plot, in which the precision of distance measurement is zero. Thus a bearing is a plot defined in a singular precision matrix. The precision matrix easily enables the description of this type of measurement. In addition estimators formulae using the precision matrix are much simpler. [C2126]

"An adaptive Kalman filter for radar tracking application"

An adaptive Kalman filter for manoeuvring targets tracking is developed. The approach is based on adding a scale factor to the process noise, therefore the noise level can be adapted depend on the manoeuvres of the tracking targets. At each epoch a time-average of the sum of the diagonal elements of the covariance matrix for the innovation is computed and compared with the value from dynamic and observable models, if the difference is larger than a predetermined threshold, the scale factor will be set to update the level of the process noise. Some computer simulations are carried out to compare the performance of the adaptive algorithm and the conventional Kalman filter. [C2127]

"Global stability analysis and stabilization of power amplifiers"

Power amplifiers often exhibit undesired behavior from certain input power value which cannot be predicted with a small-signal stability analysis. Among the commonly observed undesired phenomena are spurious oscillations, frequency divisions, hysteresis or chaos. In this contribution, simulation tools are presented, enabling an in-depth study of the origin and characteristics of these phenomena. The developed global stability analysis and stabilization tools have enabled an efficient suppression of the undesired behavior in a switching-mode power amplifier, with minimum degradation of the amplifier performance, in terms of drain efficiency and output power. [C2128]

"Procedures to improve the performances of a Sfcw radar used for landmine detection"

In the last decades a lot of research has been done to develop different types of ground penetrating radars to be used for antipersonnel landmine detection, archaeological investigations, search for underground pipes etc. They have to provide a resolution comparable with the dimension of the smallest landmine and the needed penetration for each application. To comply with high resolution requirement a ultra wide band system is required and it can be manufactured to work either in time domain or in frequency domain. In this paper two procedures to improve downrange and cross range resolution of stepped frequency continuous wave (SFCW) radar are described. The two procedures are applied to experimental data collected with SFCW radar and the improvements in the radar performances are described in the paper. [C2129]

"New difference Doppler centroid estimation method with high space resolution"

In this paper a new, phase-based method of Doppler centroid estimation is proposed. This method allows attaining both high precision and fine space resolution. It is based on the measurement of difference between corresponding points of two synthetic aperture radar images processed with different pre-assigned centroid values. Both theoretical background, and results application of the method to real synthetic aperture radar data are given in the paper. [C2130]

"The Coherent MapDrift technique robustness to low SNR SAR data"

Most of known autofocus techniques properly focusing synthetic aperture radar (SAR) images for high signal to noise ratio (SNR) data include many strong prominent points. This paper presents advantages of using the

coherent MapDrift (CMD) technique for precise estimation of radar platform flight parameters, even for low SNR SAR data. To show the advantages, the CMD has been compared with the classical MapDrift (MD) method using the Monte Carlo technique for forward velocity estimation. The Monte Carlo technique has been applied for different SNR levels. The achieved results show, that CMD is characterized by better accuracy of estimated radar platform velocity parameter when compared to traditional MD. Moreover, CMD is characterized by lower standard deviation (STD) and bias of estimated radar platform velocity parameter. The final results lead to the conclusion that even for low SNR SAR data, it is possible to obtain a fully focused image by using the novel CMD technique. [C2131]

"Advances in millimetre wave FMCW radar"

This paper addresses some of the recent advances in frequency modulated continuous wave (FMCW) radar at millimetre wave frequencies. It describes a coherent radar architecture incorporating direct digital synthesis (DDS) and, in particular, the choice of stable local oscillator (STALO). Consideration is given to phase noise, sweep linearity and the benefits of coherency. Examples of radar performance, including the measurement of sub-micron displacements are given and some example applications are described. [C2132]

"3D Imaging of Ground based SAR Data"

Ground-based SAR systems play a key role in active microwave remote sensing in many areas of environmental risk monitoring. Real time capability and flexibility make ground-based SAR suitable for monitoring in emergency cases, such as sudden landslide or volcanic activities. In this work we propose a 3D SAR imaging, for a ground-based stepped frequency radar, based on a tomographic technique. This method allows separate scattering mechanisms associated at target interfering in the same resolution cell. [C2133]

"A Comparison between Fast Factorized Backprojection and Frequency-Domain Algorithms in UWB Lowfrequency SAR"

Two frequency-domain algorithms chirp scaling (CS) with the advantage of simplification and range migration (RM) with the advantage of accuracy are candidates for a comparative study to the time-domain algorithm Fast factorized backprojection (FFBP) with reference to a UWB system are presented in this paper. The comparison is based on UWB SAR image quality measurements such as spatial resolution, Integrated Sidelobe Ratio (ISLR), peak sidelobe ratio (PSLR) and processing time connected to computational cost. The simulated SAR data, which is used in this study, is based on the parameters of the airborne UWB low frequency CARABAS-II system. [C2134]

"Radar Signal Level Fusion Imaging"

In this paper, we consider bandwidth fusion to improve the range resolution. We propose a method based on spectral estimation and amplitude-phase error model to compensate for the lack of mutual coherent between radar subbands. Then we consider two-dimensional fusion to improve the range and cross-range resolution. A new algorithm, called EMEMP, is developed to resolve the poles mismatch occurred in traditional fusion method based on modified Root-Music. By simulations, good performance of these methods will be show. [C2135]

"Land Cover Characterization and Classification using Polarimetric ALOS PALSAR"

In this study, the Touzi and Cloude-Pottier decompositions are compared for land cover characterization using ALOS/PALSAR polarimetric data collected at September, 4, 2006, over the Weinan region of Shanxi Province in China, the most useful parameters are combined for land cover classification. The classification results are assessed and validated using Landsat TM image of Weinan area acquired at August, 9, 2006. [C2136]

"Synthetic Aperture Radar Image Processing using the Supervised Textural-Neural Network Classification Algorithm"

Synthetic Aperture Radar (SAR) satellite images have proven to be a successful tool for identifying oil slicks. Natural oil seeps can be detected as elongated, radar-dark slicks in SAR images. Use of SAR images for seep detection is enhanced by a Texture Classifying Neural Network Algorithm (TCNNA), which delineates areas where layers of floating oil suppress Bragg scattering. The effect is strongly influenced by wind strength and sea state. A multi orientation Leung-Malik filter bank [1] is used to identify slick shapes under projection of edges. By integrating ancillary data consisting of the incidence angle, descriptors of texture and environmental variables, considerable accuracy were added to the classification ability to discriminate false targets from oil slicks and look-alike pixels. The reliability of the TCNNA is measured after processing 71 images containing oil slicks. [C2137]

"A Nonlinear Refined Extended Chirp Scaling Algorithm for Spaceborne ScanSAR"

In this paper, a new nonlinear Refined Extended Chirp Scaling (RECS) imaging algorithm is proposed for spaceborne ScanSAR with large cell migration to resolve the effects of residual cubic phase error in the deducing of the traditional RECS algorithm. The algorithm achieves cubic phase error correction of RECS by nonlinear filter to improve the spaceborne ScanSAR image qualities. The full derivation and the realizing approach of the algorithm are presented. And the algorithm is verified with simulations. [C2138]

"Along-Track Resolution Enhancement Forwide-Bandwidth, Low-Frequency SAR by Accounting for the Wavelength Change over the Bandwidth"

Common methods for processing SAR data, such as the Range-Doppler Algorithm (RDA) and the Chirp Scaling Algorithm (CSA), make certain approximations about the SAR signal. As the transmit frequency drops, the bandwidth grows, and the beamwidth increases, the approximations miss important factors required to precisely process the data. This paper shows that the approximations correspond to keeping lower order terms of the expansion of the SAR transfer function. We demonstrate the limits for focusing low frequency SAR data with these approximations. Previous methods for correcting the approximation errors are shown and a new method for including an arbitrary number of terms in processing the data is discussed. The concepts presented are verified using simulated SAR data. [C2139]

"Oil Spill Identification based on Textural Information of SAR Image"

Oil spill pollution is a major environmental threat for many countries in the world, which can cause serious damage to marine environment. Synthetic aperture radar (SAR) has become a valuable tool for marine oil spill monitoring, because of its all-weather and all-day capabilities. However, interpretation of marine SAR imagery is often ambiguous, and some other look-alike features often pose a fundamental challenge to the identification of oil spills and make the discrimination between oil spills and the look-alikes become a necessary procedure. In this paper, co-occurrence matrix method is employed to extract textural features of marine SAR image first, then these features are analyzed and optimized, and then support machine vector (SVM) method is used to identify oil spills in SAR images. Experiments on several SAR images show that method proposed in this paper can improve the detection and identification of oil spill in SAR images. [C2140]

"Study on the Geometric Distortion Correction Algorithm for Circular-Scanning SAR Imaging"

The images generated by a circular-scanning synthetic aperture radar (SAR) can provide precise guiding information though image-matching post-processing, which necessitates their high precision in geometry. However, due to the irregular motion of the radar platform and the circular scanning antenna beam, the inevitable geometric distortion in the focused images is necessarily to be corrected. In this paper, a two-dimensional geometric distortion correction algorithm based on projection transformation between the scatterers and the images is presented, in condition of focusing the subimages using linear range-Doppler algorithm. The geometric distortion in any subimage obtained at any squint angle within 360 degrees can be effectively corrected. The point-target simulation results are provided to demonstrate the validity of the proposed method. [C2141]

"A New Interference Elimination Method for Multi-Satellite SAR System"

Multi-channel interference elimination technology for Small-Satellites-Borne Distributed Synthetic Aperture Radar (SSBD-SAR) system is discussed in this paper. On the basis of analyzing the spacial difference of jamming signals and the SAR echo signals, we apply the multi-channel interference elimination technology to the SSBD-SAR system. The simulation results testify that this technique can effectively eliminate the jamming signals from the fixed jammer in the SAR observation scenario. [C2142]

"Precise Simulation of Spaceborne Synthetic Aperture Radar and Its Evaluation"

Simulation technique becomes increasingly important with the development of Synthetic Aperture Radar (SAR). It can be applied for many purposes such as testing different imaging algorithms and validating different SAR system design parameters[1]. For improving the precision of simulator determination of the location (mainly refers to latitude) of satellite which illuminates the fixed scene center is reconsidered in this paper. As attitude of satellite strongly affects Doppler parameters, determination of attitude is also discussed for simulated system approaching real system. Although attitude determination based on Doppler centroid was studied in many articles[2][3], this paper utilizes the information about the footprint shape of beam, and develops the equations relating yaw, pitch and especially roll to slant range and Doppler shift of echo data. We can get the attitude of

satellite by solving these equations. Then for validating and evaluating the simulated system, this paper describes a novel approach which involves imaging combination of real and simulated echo data. Doppler parameters adopted in imaging algorithm before and after combining are identical. Effect of focalizing simulated echo data indicates whether the simulated system is acceptable, and relative error of geometric distortion which appears in the SAR image reflects the approaching degree of simulated system to real system. Test was conducted by generating simulated data for RADARSAT-1, the result shows the precision of location and attitude determination and validation of this evaluation approach. [C2143]

"Adaptive Subaperture Approach for Spotlight SAR Azimuth Processing"

This paper presents an improved step transform subaperture approach for spotlight Synthetic Aperture Radar (SAR). The step transform algorithm will obtain desired high azimuth resolution only if the linear FM rate and the sampling rate of the SAR signal satisfy a certain constraint. In order to obtain a high quality image, the minimum entropy autofocus using an adaptive order polynomial model is extended and applied before the coherent summation step in this paper. The extended autofocus processing not only compensates quadratic and higher order phase errors but also shifts the coarse-resolution response functions to their correct positions. The simulation results of 1-dimension and 2-dimension are given, and the validity of this algorithm is demonstrated. [C2144]

"A New LASAR Fast 3-D Imaging Method via Wavelet Approximation"

In this paper, we present a fast 3-D imaging method for linear antenna synthetic aperture radar (LASAR). The basic idea of this technique is to consider the 3-D SAR imaging problem as tracing a surface in the observation region, since a great deal of 3-D image region contains no scatterer (such as atmosphere) or is shadowed by the other scatterers. The steps of the fast 3-D imaging method includes: Initiation, prediction, searching and recursion. Finally, some numerical experiments are presented to demonstrate the feasibility of this method. And we find that the computational cost of the fast 3-D imaging method varies according to the fluctuation of ground, and is about a dozen of times larger than that of 2-D BP algorithm. [C2145]

"Airborne Spotlight SAR Imaging with Super High Resolution based on Back-Projection and Autofocus Algorithm"

In this paper, we consider the super resolution millimeter wave spotlight SAR imaging problem through the simulation under the given Strap-down Inertial Navigation System/Global Positioning System (SINS/GPS) and introduce the Phase Gradient Algorithm (PGA) into the Back-Projection (BP) for SAR focusing. The imaging results indicate that it is feasible to obtain super high resolution imagery at the millimeter wave using the SINS/GPS. [C2146]

"Thematic Applications of ERS-ENVISAT Cross-Interferometry"

ERS-ENVISAT cross-interferometry is a unique tool for a number of applications since it combines a short repeat-pass interval (28 minutes) with a long perpendicular baseline (2 km). Temporal decorrelation effects are limited and the sensitivity to topographic features is strongly enhanced. The short repeat-pass also allows monitoring of fast-moving displacements. In this paper we show a number of examples on Digital Elevation Map (DEM) generation in flat areas, crop height retrieval and displacement monitoring using data from the recent tandem mission dedicated to ERS-ENVISAT interferometric acquisitions. The examples demonstrate the feasibility of the applications, highlighting at the same time some limitations, which are due primarily to the very specific configuration of the interferometric system. [C2147]

"A Novel Method of InSAR Processing Performance Evaluation based on Ideal Interferometric Factors"

An algorithm for interferometric phase simulation is presented, which is applicable to spaceborne Interferometric synthetic aperture radar (InSAR). Not only the ideal interferometric phase but also the ideal interferometric factors are generated in this algorithm. A novel method for InSAR performance evaluation was proposed, which is based on ideal interferometric factors. With this method, the errors of each step of InSAR processing can be isolated and analyzed. Furthermore, performance of InSAR processing algorithm can be evaluated. [C2148]

"Evaluation of TerraSAR-X Observations for Wetland InSAR Application"

This paper assesses the potential of using space-borne X-band SAR data for monitoring water level changes over wetlands. Our analysis is based on four TerraSAR-X (TSX) observations acquired over the south Florida every 11 day repeat cycle between 2008/04/25 and 2008/05/28. Interferometric processing of the data shows a

high level coherence (> 0.35) over both wetland and urban regions maintaining interferometric phase in all three interferograms spanning 11 days. Surprisingly phase is maintained over some of the wetlands even in 33 days spanning interferogram. The high interferometric coherence level suggests that a significant part of the X-band scattered signal interact with lower sections of the vegetation (trunks and branches), because scattering from wind moving canopies cannot support such high coherence level. Our analysis indicates that the high spatial resolution with 11 repeat orbit TSX data suitable for wetland InSAR application. [C2149]

"Effect of the Unwrapping Process on the Correlations Among InSAR Differences for the Same Area"

Differences among SAR interferograms (InSAR) represent an important tool for the measurement of natural and man-induced surface deformations. If not important terrain movements are observed during the considered time interval, largest differences are mostly interpreted in terms of atmospheric effects. Otherwise, smaller differences can be interpreted in terms of interseismic terrain landslides or other generic land cover or ground surface changes. In particular, significant correlations among InSAR differences and/or with the topography are reported in previous papers. In some cases, these are interpreted in terms of atmospheric or geological mechanisms. In this paper, a relationship between the unwrapping process and the correlations among InSAR and InSAR differences is observed. It is concluded that these correlations can be, at least partially, of non-geophysical origin, driven by computational procedures. [C2150]

"Trajectory Optimization of Sparse LASAR 3-D SAR Via Lagrange Multiplier Method"

This paper discusses the antenna phase centre trajectory (APCT) design for the sparse linear array 3-D imaging SAR (LASAR). Firstly, we introduce the signal model of the sparse LASAR. Based on the model, we discuss the 3-D ambiguity function (AF) of the sparse LASAR, and reveal the relationship between the 3-D AF and the system parameters. Finally, the distribution of the pseudo-random APCF is optimized by the Lagrange multiplier method under the minimum variance criterion, and we find that when the pseudo random APCF obeys the parabolic distribution, the cross-range 2-D AF attains optimal, which has both good mainlobe and sidelobe performance. [C2151]

"Phase Unwrapping using 2D-Kalman Filter-Potential and Limitations"

In the SAR community there are many methods offered for solving the problem of unwrapping the phase obtained from a noisy interferometric SAR (InSAR) image [2-5]. Generally a Kalman filter is a powerful tool to obtain accurate model based estimates out of different sources of information. All the given information is fused in an efficient way and also the noise is cancelled optimally. Because of this a Kalman filter based data fusion approach to unwrap and simultaneously filter the phases of interferometric SAR images is developed. The data fusion concept exploits phase information, extracted from the complex interferogram rather than from the phase image and fuses that information with phase slope information extracted from the power spectral density of the interferogram. The paper explains a Kalman filter method for phase unwrapping purposes and discusses the pros and cons of this approach. [C2152]

"InSAR Phase Unwrapping by Means of a Particle Filter"

This work presents a phase unwrapping (PU) algorithm for SAR interferometry based on a particle filter (PF). This PU algorithm performs simultaneously noise filtering and phase unwrapping. The formulation of this technique provides independence from noise statistics and is not constrained by the non-linearity of the problem. Results show a significant improvement with respect to conventional PU algorithms in some situations. [C2153]

"Heavy-Tailed Rayleigh Distribution: A New Tool for the Modeling of SAR Amplitude Images"

In order to model the synthetic aperture radar (SAR) amplitude images as the heavy-tailed Rayleigh distribution, we focus our attention on two questions in this paper. First, based on the negative-order moments, we propose the logarithmic moment estimator and the iterative logarithmic moment estimator to accurately estimate the parameters of the heavy-tailed Rayleigh distribution. Second, we use the asymptotic series to evaluate the density function of heavy-tailed Rayleigh distribution, and propose an efficient three-step method suitable for real-time calculation based on interpolating polynomial fit. SAR image modeling experiments demonstrate that the heavy-tailed Rayleigh distribution reflects the high peak and heavy tail of SAR amplitude images, so it is an accurate tool for the modeling of SAR amplitude images. [C2154]

"Automatic Range-Migration Correction in SAR Imaging"

A new technique is presented for range-migration correction in SAR imaging. In the range-Doppler domain, the

samples at a Doppler frequency constitute a Doppler slice. Different Doppler slices have similar envelopes. Based on this similarity, the Doppler slices are shifted and aligned in range to correct range migration. The technique applies even if the prior knowledge about the relative motion between the radar and the target is unavailable. [C2155]

"Imaging Experiments from Phase-Corrupted Airborne L-SAR Data"

For the lack of high precision inertial measurement system, the experimental airborne L-band SAR system was badly affected by random phase error induced by motion instability. The resultant SAR images derived from the L-SAR system were out of focus by conventional SAR signal processing and imaging method. It is necessary to estimate and correct phase errors for high precision SAR imaging. As a prospective scheme to refocus these images, the phase gradient autofocus (PGA) algorithm was tested in the SAR imaging processing. The effectiveness of PGA algorithm was tested not only for isolated point scatter scene, but also for various distributed-object scenes to verify its performance. Particularly, a near-range scene, a mid-range scene, and a far-range scene were tested. Comparisons between images before refocusing and after PGA refocusing were made. [C2156]

"Automatic Target Recognition by Means of Polarimetric ISAR Images and Neural Networks"

Inverse Synthetic Aperture Radar (ISAR) images are often used for classifying and recognising targets. Moreover the use of a fully polarimetric ISAR image enhances classification capabilities. In this paper, the authors propose a novel ATR technique based on the use of fully polarimetric ISAR images and Neural Networks. In order to reduce the amount of data processed by the classifier, the brightest scattering centres are first extracted by means of the Pol-CLEAN technique and then their scattering matrices are decomposed using Cameron's decomposition. The proposed ATR algorithm is finally tested on real data. [C2157]

"Application of Independent Component Analysis on ERS SAR Interferograms for the Elimination of Spurious Artifacts"

The Interferometric Synthetic Aperture Radar (InSAR) phase shifts can be considered as overlapping contributions from different phenomena. Based on this, the new 'InSAR-ICA' technique has recently been developed for deriving the nominal topographical and surface deformation components. The InSAR-ICA's innovation is its capability to reach good performance by minimal or null non-SAR data, even in case of very few SAR interferograms available for the observational area. Therefore, it allows the SAR monitoring of unreachable areas and in case of no availability of meteorological data that are sufficiently simultaneous to SAR acquisition times for the atmospheric corrections. In this paper, a summary description of the InSAR-ICA technique is given, with specific references to the usefulness of its application on mountainous areas. [C2158]

"Extraction of Area Averaged Urban Parameters from POLSAR Measurement"

By using data analysis using full-polarimetric measurement results, we can estimate area-averaged urban parameters which can not be observed from simple HH, HV and VV pseudo-color map due to insufficiency of spatial resolution of POLSAR. For example, estimation of urban buildings density or building orientation is reported. In the above estimation, we analyzed air-borne Pi-SAR and satellite-borne PALSAR data as POLSAR observations measured over Tokyo area. For evaluation of the estimated results, we adopt high-resolution optical observation data from QuickBird and 1/2500 POLYGON map surveyed by Tokyo Metropolitan Office. [C2159]

"Analysis of Simulated Polarimetric SAR Images Generated by a Multilayer Electromagnetic Scattering Model"

The evaluation of a polarimetric SAR image, which is generated by means of computation of far electric field scattered by multilayer structure, is carried out. The image analysis consists on the study of statistical properties of amplitude data and the investigation of the information gathered by α and σ angles derived from the standard Cloude-Pottier's target decomposition and the orientation angle induced by azimuthal terrain slope. The discriminatory power capability of these three angle features is assessed through a simple threshold polarimetric classification procedure. The results show that the simulation process is working properly and that the SAR return is extremely sensitive to scatter local orientation. [C2160]

"Adaptive SAR Despeckling using a Proximity Measure to Boundary"

In this paper, a SAR-despeckling approach of adaptive iteration based a Bayesian model using the lognormal distribution for image intensity and a Gibbs random field (GRF) for image texture is proposed for noise removal of the images that are corrupted by multiplicative speckle noise. When the image intensity is logarithmically

transformed, the speckle noise is approximately Gaussian additive noise, and it tends to a normal probability much faster than the intensity distribution. The MRF is incorporated into digital image analysis by viewing pixel types as states of molecules in a lattice-like physical system. The iterative approach based on MRF is very effective for the inner areas of regions in the observed scene, but may result in yielding false reconstruction around the boundaries due to using wrong information of adjacent regions with different characteristics. The proposed method suggests an adaptive approach using variable parameters depending on the location of reconstructed area, that is, how near to the boundary. The proximity of boundary is estimated by the statistics based on edge value, standard deviation, entropy, and the 4th moment of intensity distribution. [C2161]

"Monte Carlo Simulation of Altimeter Pulse Returns and Electromagnetic Bias"

The electromagnetic bias is a critical error term in sea surface height estimation from satellite radar altimetry. While the electromagnetic bias has been studied extensively, most studies are based on low-order hydrodynamic and electromagnetic models. This paper proposes an alternate approach for electromagnetic bias studies by employing a Monte Carlo procedure with numerical non-linear hydrodynamic simulations coupled with numerical methods for electromagnetic scattering from the sea surface. A deterministic set of sea surface profiles and the corresponding altimeter pulse returns are produced in the simulation. The coupled electromagnetic/hydrodynamic methods can be chosen to tradeoff varying levels of physical fidelity with computational efficiency. The approach allows studies of the impact of various physical effects on the electromagnetic bias. Clear evidence of the electromagnetic bias can be observed in the simulated pulse returns in terms of a shift in the pulse return time. [C2162]

"Automatic Model Inversion of Multi-Temporal C-band Coherence and Backscatter Measurements for Forest Stem Volume Retrieval"

Retrieval of forest stem volume from synthetic aperture (SAR) backscatter and interferometric SAR (InSAR) coherence is generally performed using a model-based approach, where in situ measurements are necessary to estimate the unknown model parameters. Problems arise when in situ data are either not available or of low quality or the observables present spatial variations. In this work we present three approaches for automatic modeling and inversion of forest backscatter and coherence to retrieve forest stem volume. The three approaches exploit statistical distributions of the observables to obtain estimates for the unknowns in the model. Results shows remarkable agreement with those obtained by means of traditional modeling approaches based on in situ data. [C2163]

"A Soil Moisture Smart Sensor Web using Data Assimilation and Optimal Control: Formulation and First Laboratory Demonstration"

We have developed a new concept for a smart sensor web technology for measurements of soil moisture that include spaceborne and in-situ assets. The objective of the technology is to enable a guided/adaptive sampling strategy for the in-situ sensor network to meet the measurement validation objectives of the spaceborne sensors with respect to resolution and accuracy. One potential application is the Soil Moisture Active/Passive (SMAP) mission. The science measurements considered are the surface-to-depth profiles of soil moisture estimated from satellite radars and radiometers, with calibration and validation using in-situ sensors. Installing an in-situ network to sample the field for all ranges of variability is impractical. However, a sparser but smarter network can provide the validation estimates by operating in a guided fashion with guidance from its own sparse measurements. The feedback and control take place in the context of a dynamic data assimilation system subject to energy and accuracy constraints. The overall design of the smart sensor web including the control architecture, assimilation framework, and actuation hardware are presented in this paper. We also present results of initial numerical and laboratory demonstrations of the sensor web concept, which includes a small number of soil moisture. [C2164]

"An Empirical Study of Breaking Wave Contribution to Radar Backscatter from the Ocean Surface at Low Grazing Angle"

The anomaly of radar sea spikes, defined here as the non-Bragg scattering events with backscattering cross section of horizontal polarization exceeding that of vertical polarization, has been associated with steep wave features possibly going through wave breaking process. This property is employed for remote detection of breaking waves. The results are used to quantify the effect of wave breaking on radar returns. Large increase due to breaking is found in the Doppler velocities of both polarizations (about 50% faster with breaking). The effect of breaking on the backscattering cross section is much stronger for the horizontal polarization (with 15 to 20 dB enhancement) and relatively small in the vertical polarization (on the order of 0.5 dB fluctuations). The presence of swell reduces the impact of breaking waves on radar return in comparison to the scattering from wind seas. [C2165]

"The UMass X-Pol Mobile Doppler Radar: Description, Recent Observations, and New System Developments"

Accurate detection and forecasting of severe storms has driven radar tornado probing as an important research topic that has added significantly to the understanding and prediction of severe weather phenomena. The need for close range observation, coupled with the fact that significant information is buried at low altitudes, has made mobile Doppler radars an important tool in the characterization of severe storms and related weather phenomena. The UMass XPol radar is one such truck mounted dual-polarized Doppler radar operating at 9.41 GHz. This paper documents the existing mobile radar system and presents close range, high resolution observations of Doppler velocity, reflectivity, differential reflectivity and cross-polarization correlation coefficient of a variety of storms observed during 2007. Additionally, the architecture of a planned pulse compression system upgrade is described. [C2166]

"Calibration of the UMass Advanced Multi-Frequency Radar (AMFR)"

In this paper the calibration of the University of Massachusetts Advanced Multi-Frequency Radar (AMFR) is discussed in detail. The calibration is performed primarily through the use of an internal calibration path, and is confirmed through cross-calibration with another calibrated radar. Additionally, the performance of AMFR during the 2007 Canadian CloudSat/CALIPSO Validation Project (C3VP) is demonstrated with respect to calibration and instrument stability. It is shown that the calibration during the C3VP experiment was accurate to within 1.5 dB when compared with a C-band weather radar operated by Environment Canada. [C2167]

"Considerations in Pulse Compression Design for Weather Radars"

Pulse compression is a useful technique for weather radar, as an enabling technology to facilitate use of low-power solid state transmitters. It also has the benefit of improving the dynamic range and range resolution of the radar, permitting rapid scanning of a volume. The nonlinear FMPulse waveform described produces the low sidelobe levels required for weather radar applications, while remaining Doppler-tolerant within the range of radial velocities expected for weather radar (plusmn100 m/s). Traditional pulse compression waveforms must be modified to reduce their range sidelobes to levels suitable for use in weather radar. The use of pulse compression involves some changes to the methods used during radar calibration, and places some restrictions on the design and implementation of the RF and IF components of the radar. [C2168]

"Experimental Performance Investigation of Digital Beamforming on Synthetic Aperture Radar"

In this paper, we present the experimental results of a Digital Beam Forming (DBF) Synthetic Aperture Radar (SAR) performance on the purpose of the High-Resolution Wide-Swath (HRWS) SAR concept. A ground-based SAR system successfully demonstrated the DBF SAR operation. The demonstrator acquired SAR raw data with very dense spatial sampling rate in order to obtain various sampling rates. We evaluate DBF performance with respect to the image quality factor with two different types of the beam former, a fixed-beam former and an adaptive beam former. The results show that an adaptive DBF algorithm offers a wide range of the selection of the pulse repetition frequency (PRF). In addition we evaluate the noise performance compared to a reference mono-static SAR system on the same condition on single target experiment. [C2169]

"Achieving HRWS Images with Space-borne Bistatic SAR with Multiple Phase Centers"

An algorithm for achieving High-resolution wide-swath (HRWS) images in bistatic space-borne SAR with multiple phase centers is presented. Based on the analysis of the correlation of echos from all phase centers, a signal model is built that all echoes combined form a periodically nonuniform undersampled signal. Then the echoes with Doppler ambiguities are reconstructed to unambiguous uniform samplings which can be processed with conventional imaging algorithms. Simulation trials prove that the approach is valid and robust. [C2170]

"Analysis of C-band Polarimetric Signatures of Arctic Lead Ice using Data from AIRSAR and RADARSAT-1"

In December 2004 the JPL airborne synthetic aperture radar (AIRSAR) flown on the NASA DC-8 acquired fully polarimetric data in the Beaufort Sea at C, L and P-band. This work presents the backscatter coefficients (σ_{HH} , σ_{VV} , σ_{HV}), copolarized ratios (σ_{HH}/σ_{VV}) and copolarized phase differences (ϕ_{HH-VV}) at C-band from different young sea-ice types formed in recently frozen leads. Two weeks of RADARSAT-1 imagery from the same region as the AIRSAR data were used in order to identify when and where leads were formed and to estimate the age of the newly formed ice contained within the leads. A known empirical relationship based on freezing degree days was used to estimate the sea-ice thickness. The results

indicate that some of the identified thin ice types have characteristic signatures. [C2171]

"Semi-Automated Extraction of Human Settlement Extent in HR SAR Images"

In this paper a novel method, based on autocorrelation indexes and gray-level co-occurrence matrix, for the extraction of urban areas in high resolution SAR images, is presented. It strongly reduces human interpreters' intervention thanks to a high degree of automation within the processing chain and allows a fast and accurate generation of built-up area maps, which can be employed for land mapping and support in relief operations. [C2172]

"Evaluation of Distributed Collaborative Adaptive Sensing in a Four-Node Radar Network: Integrated Project 1"

A dense weather radar network is an emerging concept advanced by the Engineering Research Center for Collaborative Adaptive Sensing of the Atmosphere (CASA). A major goal of CASA is to develop an entirely new paradigm, referred to as Distributed Collaborative Adaptive Sensing (DCAS), for improving the coverage of the lowest portion of the atmosphere through coordinated scanning of low-power, short-range, networked radars. The CASA enterprise designs, develops, and deploys system-level test beds to integrate underlying scientific and technical advances and demonstrate the potential to observe, understand, predict and respond to hazardous atmospheric phenomena-with end users involved from the outset. The first one of DCAS test-beds was deployed in south-west Oklahoma, named as Integrated Project 1 (IP1). It is an end-to-end system of a network of four, low-power, short-range, dual polarization, Doppler radar units, aimed at severe weather and hazardous wind sensing. In this paper, a number of aspects in developing a DCAS radar network for these specific applications are reviewed. [C2173]

"Meteorological Command & Control: Architecture and Performance Evaluation"

IP1 is a prototype CASA radar sensor network located in southwestern Oklahoma whose goal is to detect severe weather in the lower part of the atmosphere. At the center of this system's control loop is its Meteorological Command and Control (MC&C). In this paper, we presented the overall control architecture for the IP1 network and highlight new features that have recently been added to the MC&C. We also present an analysis of the MC&C performance based on measurement data from a 5-day operation period. In addition, we introduce a distributed version of the MC&C. [C2174]

"User Evaluations of Adaptive Scanning Patterns in the CASA Spring Experiment 2007"

The Engineering Research Center for Collaborative Adaptive Sensing of the Atmosphere (CASA) is creating a new paradigm for weather observation based on low cost, densely spaced networks of X-band radars. These networks adapt their scanning strategy based on the evolving weather and user needs for data. This paper presents the results of an evaluation by National Weather Service forecasters and academic researchers of the dynamically reconfigurable radar scanning patterns that operated in CASA's prototype test bed in southwest Oklahoma in spring 2007. The evaluation demonstrates that a pilot group of users were satisfied overall with CASA's scanning patterns. The evaluation also uncovered needed improvements to the scanning strategy that have been subsequently implemented. Through this iterative cycle of design, implementation, evaluation, we have demonstrated the flexibility of the system architecture and our ability to modify existing and add new capabilities to increase the benefits of CASA radar systems. [C2175]

"Simulation of Improved Bandwidth Conformal Bow-Tie Antennas for Remote Sensing Printed on Multi-Scale Triangular-Patch High-Impedance Ground Planes"

Two low-profile bow-tie antenna designs are presented, printed conformally on high-impedance ground planes (HIGPs). The HIGPs were constructed using two different scale triangular patch mushroom elements which allow for a suitable platform for the active bow-tie antenna. The multiscale nature of the HIGP was utilized to further increase the frequency band-gap of the surface waves, and to enhance the properties of the low-profile bow-tie. The bandwidth of the bow-tie on the HIGP is evaluated and compared with perfect-electric-conductor (PEC) and perfect-magnetic-conductor (PMC) ground planes. [C2176]

"Compromise and Trade-Off between Signal-to-Noise Ratio and Number of Independent Samples for Radar Scatterometers with Pulse Compression"

It is well known, that the backscattering radiometric accuracy of radar scatterometers for ocean surface wind and precipitation measurements is decided by the signal-to-noise ratio and number of independent samples for non-coherent average. For sea wind scatterometers and meteorological radars, pulse compression can be employed

to improve the range resolution and increase the number of independent numbers. But for airborne and spaceborne scatterometers, the peak power of the transmitter and the pulse length are usually decided by the platform capability, orbit parameter and observation geometry. As a result, compromise and trade-off between the signal-to-noise ratio (SNR) for measurement of each resolution cell and the total number of independent samples of each pulse are usually required. In this paper, based on the radiometric accuracy model, an optimization scheme for design of the independent samples numbers and the corresponding system bandwidth are presented. Based on the presented optimization scheme, the bandwidth of a Ku-band rotating fan-beam radar scatterometer for sea surface wind measurement is design. Simulation validates the optimization and design results. [C2177]

"Wave Parameters Estimated from Scatterometer Data"

A new model is proposed to estimate significant wave heights from ERS-1/2 scatterometer data. We find that the relationship between wave parameters and the radar backscattering cross section is similar to that between the radar backscattering cross section and wind. The model for the relation between significant wave height and the radar cross section is obtained by a neural network algorithm. When the average wave period is less than 7s, the root mean square of significant wave height retrieved from ERS-1/2 data is 0.51 m. When the average wave period is more than 7 s, it is 0.72 m. [C2178]

"Fractal based Modeling of Altimeter Data"

This paper presents a new systematic simulation procedure to compute the altimeter signal return, thus showing the correlation of the signal return shape with height, slope, sub-surface layers and different scales of roughness of the surface of interest. For the first time, and as appropriate to natural surfaces, the scene is fully modelled by means of the fractal geometry. By observing the results presented in this paper, it appears that an advanced processing of altimeter data is possible. [C2179]

"Analysis of 3D-SAR based on Angle Compression Principle"

This paper presented the 3D-SAR based on angle compression principle which could, in contrast to conventional single-channel 2D-SAR, create the real 3D resolution cells to avoid geometric distortions. Except for conventional side-looking mode, 3D-SAR system herein can be operated in downward-looking mode which can avoid shadowing effects. The angle compression principle and the angular ambiguity problem are analyzed in this paper. The analytic expression of angle compression and the condition which should be satisfied to avoid angular ambiguity are also derived in this part. The demonstration of the feasibility of the 3D-SAR based on angle compression principle and the angular ambiguity problem are given by simulation in the last part of this paper. [C2180]

"Towards the Virtual Remote Sensing Laboratory: Intelligent Experiment Design Paradigm"

We address the unified intelligent descriptive experiment design regularization (DEDR) methodology for (near) real time formation/enhancement/reconstruction/post-processing of the remote sensing (RS) imagery acquired with different thinned stationary multi-sensor arrays and/or synthetic aperture radar and present the elaborated "Virtual RS Laboratory" (VRSL) software that provides the end-user with efficient computational tools to perform numerical simulations of different collaborative RS imaging problems in the context of the proposed intelligent experiment design paradigm. Computer simulation examples are reported to illustrate the usefulness of the elaborated VRSL for system-level and algorithmic-level optimization of high-resolution image formation, enhancement, fusion and post-processing tasks performed with the real-world RS imagery. [C2181]

"SAR Image Simulation of Man-Made Scenes based on Computer Graphics"

To enhance the computational efficiency and authenticity of Synthetic Aperture Radar (SAR) image simulation of man-made scenes, computer graphics (CG) method was introduced into imaging geometry simulation, graphical electromagnetic computing (GRECO) was used for the interested target scattering calculation. With these two methods, the targets' characteristics will be visualized in simulated image, such as shadow, foreshortening, layover and simple scattering property. The simulated SAR images can be used for target recognition, target detection, system verification and other researches. [C2182]

"Simulation of Spaceborne Microwave Radiometer Measurements of Snow Cover using In-Situ Data and Emission Models"

In this paper, three different models for the extinction coefficient of snow are compared by simulating the brightness temperature of snow-covered ground with HUT snow emission model. The input in-situ data set was

measured in Sodankyla, Finland during winter 2006-2007. The simulation results are compared with AMSR-E measurements. All the extinction coefficient models are developed for dry snow. Thus, in addition to the whole winter time series, the dry snow periods are studied. Since all the three models calculate extinction coefficient from snow grain size, the effect of grain size is studied by minimizing the simulation error using grain size as optimization parameter. [C2183]

"System Design of Cloud Profiling Radar for Earthcare"

European and Japanese space agencies plan to launch a satellite called EarthCARE (Earth Clouds, Aerosols and Radiation Explorer). The Cloud Profiling Radar (CPR), which will be the first millimeter-wave Doppler radar in space, is installed on this satellite as a main sensor to observe clouds. This paper describes the outline of the system design of EarthCARE CPR. [C2184]

"A Ka-band Interferometer for Cryospheric Applications-Instrument Description and First Results"

Characterization of the Earth's oceanic and cryospheric topography is among NASA's strategic goals for the next decade. An effective technique for achieving such measurements is radar interferometry. For this technology, use of mm-wave frequencies (Ku- and Ka-band) is appealing due to the proportional size of the space borne structure to the observing wavelength and minimal snow penetration. At such high frequencies, achieving stability in instrument performance and the mechanical deployment structure for accurate measurements is an engineering challenge. To address this, the Microwave Remote Sensing Laboratory at the University of Massachusetts is developing a high performance Ku- and Ka-band interferometer as a prototype for a space borne instrument. The interferometer will be used in a scaled-down ground-based configuration. This paper presents an instrument description of the Ka-band interferometer (the down-converter in particular) and first results from its performance evaluation. [C2185]

"The Thinned Array Time Division Multiple Phase Center Aperture Synthesis and Application"

Three-dimensional imaging radar based on thinned array is investigated in the paper. The multiple phase center aperture synthesis method in time division mode is used to eliminate the high side lobes of thinned array. Using simulated annealing algorithm to optimize the location of antennas, so as to minimize the number of antennas used. Combined with motion compensation, the synthesized phase centers both in quantity and distribution are coincident with a full array. For the cross-track array length is far smaller than the scene width, three-dimensional imaging method is employed with sub-aperture imaging along cross-track. The simulation results denote the validity of the method proposed in the paper. [C2186]

"Implementation of Pulse Compression on an Airborne Scatterometer"

The pulse compression scheme implemented on the Imaging Wind and Rain Airborne Profiler (IWRAP) is described. Developed at the UMASS Microwave Remote Sensing Laboratory (MIRSL), IWRAP is a dual-band (C and Ku) conically scanning Doppler scatterometer designed to map the atmospheric boundary layer wind fields, ocean surface wind fields, and precipitation within tropical cyclones. IWRAP has previously been deployed using a pulsed transmit waveform with a peak transmit power of 80 watts. This limits the average transmit power and sensitivity for the system which affects the more distant range gates (especially at Ku-band). As a result, IWRAP could operate only at lower altitudes (approx. 5000 ft) causing safety concerns and limiting the missions for which it can be deployed. Increasing sensitivity was achieved by converting IWRAP to a pulse compression radar system. Pulse compression is a technique that combines the increased energy of a longer pulse with the high resolution of a short pulse by implementing a frequency modulated (FM) "chirped" transmit wave-form. This method requires advanced signal processing, in which the received signal is passed through a matched filter to compress the pulse on the receiving end. A system with various chirp/filtering schemes which UMASS has recently developed will be discussed in this paper. [C2187]

"Digital Beamforming for a 3D MIMO SAR-Improvements through Frequency and Waveform Diversity"

The 3D imaging and nadir looking ARTINO (Airborne Radar for Three-dimensional Imaging and Nadir Observation) principle uses a sparse MIMO antenna array distributed over the whole wings of an airplane. The adaption of the ARTINO principle to high and fast flying airplanes with large wings requires new concepts to deal with PRF limitations. In this paper, an extension of the ARTINO principle is presented based on two different strategies namely the frequency diversity and the waveform diversity. Both concepts allow the implementation of the ARTINO principle to arbitrary airborne platforms. [C2188]

"Ultra Wide Swath Imaging with Multi-Channel ScanSAR"

Multi-channel synthetic aperture radar (SAR) systems enable high-resolution wide-swath imagery thus overcoming the inherent limitation of conventional SAR. A possible realization based on the combination of multi-aperture SAR signal reconstruction in azimuth with digital beamforming on receive in elevation is given in [1]. The present paper turns focus to advanced concepts for the imaging of even wider swaths while still providing high azimuth resolution [2]. In this regard, the operation of multi-channel SAR systems in burst modes like ScanSAR or TOPS is introduced and aspects of applying the multi-aperture reconstruction algorithm to burst mode data are analyzed. The influence of the digital processing network on performance parameters as signal-to-noise-ratio and azimuth ambiguity-to-signal-ratio in multi-channel burst mode systems is considered and embedded in the design example of a ScanSAR system that allows for the imaging of a 400 km wide swath with a geometric resolution of 5 m. Finally, first results for a multi-channel TOPS system are presented and an optimized TOPS processing approach is introduced. [C2189]

"Surface Subsidence Monitoring with Coherent Point Target SAR Interferometry"

In this paper, an improved approach for surface subsidence monitoring with SAR interferometry by using coherent point target is presented. A joint criterion of amplitude dispersion index and high spectral correlation criterion are proposed for coherent point target identification, which enable a flexible target selection in case of small or large volume of SAR data. Further more, in order to avoid the decorrelation caused by long temporal or spatial baseline, interferogram stack are generated from the combination of those images with a small baseline. For subsidence rate calculation, a spatial and temporal regression is exploited to unwrap the differential phase of each coherent point target and a linear model is adopted for the estimation of deformation parameters. Case studies in two different test sites demonstrate the advantage and limitations of the algorithm. [C2190]

"Understanding Phytoplankton Variability Throughout Spencer Gulf, South Australia, via Satellite Derived Chlorophyll-A"

MODIS chlorophyll-a imagery was analysed to better understand the dynamics of phytoplankton in Spencer Gulf, South Australia. MODIS chlorophyll-a was validated against in situ chlorophyll-a measurements to assess the performance of MODIS algorithms in this shallow coastal body of water. Monthly mean chlorophyll-a imagery was then used to study the broad-scale seasonal variability in chlorophyll-a throughout Spencer Gulf and surrounding waters. Validation showed a slight overestimation in chlorophyll-a via MODIS when concentrations were low, and also likely coastal influences upon the measurements. The validation was less than conclusive with MODIS measurements explaining just 46% of the variation in the field data. The monthly image sequences identified significant differences in seasonal chlorophyll-a characteristics between different locations within the gulf. Elevated chlorophyll-a concentrations were also observed near the southern bluefin tuna aquaculture zone during winter compared to nearby waters of southern Spencer Gulf. [C2191]

"Modeling Atmospheric Effects of InSAR Measurements based on Meris and GPS observations"

Atmospheric water vapor is a major limitation for high precision interferometric synthetic aperture radar (InSAR) applications due to its significant impact on microwave signals. Temporal variability of the atmosphere delay can be estimated directly from GPS data, but spatial variations of water-vapor-induced distortions cannot easily be separated by the sparse network of GPS observations in the imaged area. The primary objective of this work is to build a hybrid model combining the GPS and Medium Resolution Imaging Spectrometer (MERIS) water vapor measurements for correcting the atmosphere effects on InSAR measurements. Moreover, a comparison between MERIS and GPS water vapor products was performed using data covering Beijing from January 2004 to February 2007. MERIS water vapor values appeared to be slightly greater than GPS values. However, MERIS water vapor agreed well with GPS water vapor retrievals under Beijing's conditions with a RMS error of 2.38 mm. [C2192]

"Integrated Retrieval of Surface and Atmospheric Parameters over the Arctic from AMSR-E Satellite Microwave Radiometer Data using Inverse Methods"

We present a method for the retrieval of atmospheric and surface parameters (namely, surface wind speed, total water vapor, cloud liquid water, surface temperature, ice concentration, multiyear ice fraction) over the Arctic Ocean from brightness temperature measurements by the spaceborne microwave radiometer AMSR-E (Advanced Microwave Scanning Radiometer for EOS) on the satellite Aqua. We use an inverse method, with a forward model based on a fast radiative transfer for AMSR-E over open ocean which we have extended by including the possibility of ice-covered or partly ice-covered sea, using new data on sea ice emissivity at AMSR-E frequencies. The method performs reasonably well and can even retrieve cloud liquid water over ice, and ice concentration in the marginal ice zone in cloudy and humid conditions. [C2193]

"Comparison of Surface Roughness Parameters of Tidal Flat Estimated from AIRSAR and ALOS Observations"

Tidal flats form a unique ecosystem, playing important roles in the environmental assessment of coastal zones. This study aims to derive surface characteristics of tidal flats from fully polarimetric SAR data sets. The microwave surface scattering models were employed to measure the surface roughness on tidal flats from air-borne and space-borne polarimetric SAR data, such as NASA/JPL AIRSAR and ALOS PALSAR. Surface roughness parameters were estimated from the circular polarization coherence and co-polarized scattering elements. Recent changes in coastal wetlands will be continually monitored by using the PALSAR data sets together with other newly developed space-borne SAR systems, such as RADARSAT-2 and TerraSAR-X. [C2194]

"Very High Resolution Interferogram Acquisition Campaign and Analysis"

The ONERA RAMSES system is a flexible SAR system in constant evolution, developed mainly as a test bench for new technologies and to provide specific data for TDRI (Target Detection, Recognition and Identification) algorithm evaluation. It is flown on a Transall C160 platform operated by the CEV (Centre d'Essais en Vol). This paper presents the multi-pass interferometric acquisitions in very high resolution acquired over Salon de Provence, in south of France. The interferometric and coherence information capabilities are analyzed for this resolution. [C2195]

"Analysis of Flood Inundated Area using Hydrological Model and Radarsat SAR Imagery"

A flood resulting from climate changes recently has brought about tremendous damage to the people and property. For restoration and to establish the countermeasure, various investigations into the flood-inundated area have been underway. Among the investigation measures commonly adopted in South Korea are on-site survey and indirect investigation using flood outflow model. However, with such methods, it's difficult to obtain a quick outcome as well as require verification for reliability. SAR that provides data irrespective of weather conditions and enables to perform rapid and precise investigation has been used since 1990s for flood monitoring. This study as basic research in preparation for launching KOMPSAT-5 in 2010 to use SAR sensor for water resources development is intended to compare the existing method to identify flood inundated area with that using SAR image, and measures to make use of SAR image. [C2196]

"Two-Dimensional Flow Patterns Observed at Threemile Slough Using Two RiverSondes"

Two-dimensional river flow patterns were measured using a pair of RiverSondes in an experiment at Threemile Slough in the Sacramento-San Joaquin River Delta system of central California during October 2007. An earlier experiment at Walnut Grove in April 2007, on the migration path of juvenile fish, revealed complex flow patterns during periods of tidally-induced flow reversals, but data there were limited by low winds. Consequently, a follow-on experiment was conducted at Threemile Slough where wind conditions and surface turbulence historically have resulted in abundant data from a single RiverSonde. The experiment at Threemile Slough included ADCP near-surface velocity measurements from unmanned survey vessels. Quantitative comparisons between the RiverSondes and the ADCPs showed mean differences of 0.007 cm/s in the cross-channel component and 0.5 cm/s in the along-channel component, and RMS differences of 7.9 cm/s in the cross-channel component and 13.5 cm/s in the along-channel component after obvious outliers were removed. Interpolation and integration of the velocity vectors revealed complex trajectories of simulated particles during times of flow reversal and smooth trajectories during the remainder of the tidal cycle. [C2197]

"Weather Radar Network Design"

The Engineering Research Center for Collaborative Adaptive Sensing of the Atmosphere (CASA) is investigating the use of dense networks of short-range radars for weather sensing. A first test-bed of this new paradigm is currently deployed in southwest Oklahoma. The potential benefits of closely deployed, overlapping, short-range weather radars are easy to see intuitively amounting to a greater ability to measure at lower beam heights (mitigating the effects of the Earth curvature), an increased spatial and temporal resolution in the measurements, and the capability of optimally and adaptively tasking the individual radars according to the meteorological scene. In this paper formulations for radar network design are provided, with various parameters such as number of radars with overlapping coverage, network coverage area, number of radars in a network, and number of elemental cells in a network, and applied to the design of a radar network based on system specifications such as detection sensitivity, beam size, minimum beam height, and overlapping coverage. [C2198]

"Capabilities of Full-Polarimetric PALSAR/ALOS for Snow Extent Mapping"

Snow classification using full-polarimetric PALSAR data is investigated in this paper. It is first demonstrated that dry snowpack over frozen ground slightly affects polarimetric signature at L-band. Given the fact that PALSAR data do not permit the use of a simplistic threshold-based method, a refined method for Snow Covered Area mapping is outlined. A supervised Support Vector Machine approach is used showing fairly good results within the framework of a three-classes classification (dry snow over frozen ground, wet snow and no snow). [C2199]

"The Radiation Behavior Analysis of Thin Snow Cover based on Field Measurements by a Multi-Frequency Microwave Radiometer"

In this paper, we mainly studied of microwave emission behavior of shallow snow cover with the field experiments over Huabei Plain, China., The evaluation of microwave emission character over snow surface was using the data collected by a ground-based multi-frequency and dualpolarization microwave radiometer (RPG-8CH-DP) at 10.7 GHz, 18.7GHz and 36.5 GHz, with the incidence angles ranging from 20deg to 60deg. Through analysis of the observation brightness temperature, we found that the radiation behavior of thin snow cover is very different from that of deep snow, especially during melting and refreezing period of thin snow cover. One is that the emission over shallow snow surface increased as frequencies increase. Secondly, at the same frequency, when shallow snow was melt in diurnal refreezing-thaw cycle, the emission would decrease. These two emission behavior were caused by the attenuation of snow cover was weak than the increment of emission from the underground snow surface. From this study, it has been shown that the ground-based microwave radiometry provides a useful tool to investigate the radiation characteristics of thin snow cover and snow type identification. It also helps to evaluate snow emission models and develop retrieval algorithms of snow characteristics from space-borne microwave radiometer data. [C2200]

"Scalable Multifunction Dense Radar Network"

This paper discusses an approach to evaluating network topologies of scalable, low power, solid-state phased array radars that improve the coverage of the lower troposphere (<3 km), which is absent in coverage available with current weather sensing networks. [C2201]

"Mie versus Point Matching Algorithm for Radar Rain Properties Retrieval"

This contribution compares retrieval algorithms after Mie (quick, but neglecting the real shape of rain drops) and after Oguchi (slower, but more exact) for radar forward scattering and backscatter at frequencies of 10 and 35 GHz. The retrieved quantities were drop size distribution (DSD), rain rate and attenuation (e.g. of microwave link). Measurements of drop size distributions over one year in the Czech Republic served as reference. The simulation shows that the simple Mie algorithm can be used on a good accuracy level. [C2202]

"Networked Waveform System for Range Velocity Ambiguity Mitigation"

A networked waveform system is developed to overcome the fundamental limitation of a single pulsed Doppler radar in resolving ambiguities. The networked radar system uses the principle that the underlying intrinsic properties of the precipitation medium remain consistent in a network. The ambiguity in range and velocity is resolved by jointly processing the measurements from all the radars in the network. In this paper results for networked waveform system are shown for simulated data as well as data collected with first generation CASA (The Center for Collaborative Adaptive Sensing of the Atmosphere, an engineering research center established by the National Science Foundation) radars deployed in Oklahoma. [C2203]

"A Novel Solid-State, Dual-Polarized, Dual Wavelength Precipitation Doppler Radar/Radiometer"

The economic wealth and daily lives of United States citizens and people of all nations are affected by precipitation. Accurate quantitative precipitation measurements locally and on a global scale are needed to improve our ability to forecast and our understanding of these events. Efficient resource mobilization to minimize the impact of devastating precipitation events demands accurate and timely mapping of these event as they occur. To help address these needs, Remote Sensing Solutions, working with NASA, is developing a novel solid-state, dual-polarized, dual-wavelength precipitation Doppler radar/radiometer system. The innovations necessary to realize this unique and powerful system are described and the performance presented. [C2204]

"Experiences Developing OAIS-RM Recommended Submission Agreements"

The National Environmental Satellite, Data, and Information Service (NESDIS) under the National Oceanic and Atmospheric Administration (NOAA) is responsible for the collection, archival, and dissemination of environmental

data collected by a variety of in situ and remote sensing observing systems operated by NOAA and by a number of its partners, e.g., National Aeronautics and Space Administration (NASA). To prepare for large increases in its data holdings, the NESDIS Office of Systems Development (OSD), has been developing the Comprehensive Large Array-data Stewardship System (CLASS). CLASS currently provides data acquisition, storage, access, and dissemination at three distinct locations: the NOAA Satellite Operations Facility (NSOF) in Suitland, Maryland; the National Climatic Data Center (NCDC) in Asheville, North Carolina; and the National Geophysical Data Center (NGDC) in Boulder, Colorado. CLASS currently holds data from Polar-orbiting Operational Environmental Satellite (POES), Geo-stationary Operational Environmental Satellite (GOES), Defense Meteorological Satellite Program (DMSP), and Initial Joint Polar-Orbiting Operational Satellite System (IJPS) satellites and derived products. Planned future data campaigns will add data from the Next Generation Weather Radar (NEXRAD) system, as well as the National Polar-orbiting Operational Environmental Satellite System (NPOESS), NPOESS Preparatory Project (NPP), Earth Observing System Moderate-resolution Imaging Spectroradiometer (EOS/MODIS), and GOES-R series satellite systems. CLASS has adopted the recommendations of the Open Archival Information System Reference Model (OAIS-RM) and has developed processes around these recommendations. The recommendation with the most impact on the way that CLASS conducts business is the development of Submission Agreements between the Producers and the Archive.

[C2205]

"Integration of Spatial Chaotic Model and Type-2 Fuzzy Sets for SAR Images Change Detection"

It is very difficult to perform change detection in SAR images, because speckle noise contaminates the images in nature. Speckle, which results from coherent energy imaging, is indeed a chaotic phenomenon. As a result, an SAR signal can be modeled by a spatial chaotic system and characterized by its fractal dimension. The differential box-counting (DBC) technique is adopted to estimate fractal dimension in this paper. Based on the spatial chaotic model (SCM), a simplified SAR image change detection procedure is proposed. Observations provided by SAR sensors are uncertain due to changing illumination conditions at different acquiring time. Besides, the selection of window size M and grid size s in DBC provides an additional degree of uncertainty. Both the uncertainty involved in the measurements and the uncertainty involved in the selection of M and s motivate us of integrating type-2 fuzzy sets with the SCM to achieve a better performance. The proposed approach is applied to multitemporal polarimetric SAR images for change detections as demonstrations. The change detection results of using the original SCM method and the proposed approach are compared. The effects of misregistration for different change detection approaches are also presented. Simulation results suggest that the proposed approach is more tolerant to misregistration and offers better results of detecting changes when speckle noise is present. [C2206]

"Change Detection with Multi-Polarization SAR Imagery"

In this paper, change detection with multi-polarization SAR imagery is focused. Based on the polarimetric statistic distribution, a polarimetric test statistic is applied to evaluate the equality of two areas in two pass polarimetric SAR images. And then, in order to find out the 'real' changed area, a constant false alarms rate (P_{fa}) is given to determine a threshold for change detection. Moreover, a majority processing considering the context information of a given target is preferred to improving the final accuracy of the change detection. Finally, the proposed method was tested with the multitemporal Envisat-ASAR's alternative polarization SAR data. Experiments are performed to validate efficiency of the method presented in the paper. [C2207]

"Monitoring of Oil Spills in the North Caspian Sea using SAR Imagery and Multi-Sensor Satellite Data"

Since may 2007 the regular operational satellite monitoring of the north Caspian sea was set up and carried out. The purpose of the project is to monitor the ecological situation (namely, oil spills) particularly around the oil-rig offshore exploration platforms operating in Russian and Kazakhstan sectors, as well in the overall area of the North Caspian sea. The used data set includes RADARSAT and ENVISAT SAR, ENVISAT MERIS imagery and meteorological data available in Internet. The methodology of monitoring includes expert analysis of the SAR images, extraction of oil spills and oil spill-alikes, comparison with weather data and oil dynamics from a series of images using the geo-informational approach developed by authors. It was shown that the spaceborne radar is the valuable source of information while performing the off-shore oil and gas exploration activities. [C2208]

"The Impact of Adaptive Speckle Filtering on Multi-Channel SAR Change Detection"

One of the most promising applications of synthetic aperture radar (SAR) imagery is change detection. However, the success of change detection algorithms is highly dependent on the type of change being detected. With the advent of multi-channel SAR systems (multi-frequency and/or polarimetric) new algorithms to improve change

detection are being developed to take advantage of the additional information. However, these algorithms are still hindered by the speckle phenomena of radar imaging. Adaptive neighborhood filtering techniques have been shown to be effective to reduce speckle, but the impact on change detection has not been explored. The research presented explores the impact of an adaptive filtering algorithm on the probability of detection for synthesized changes. [C2209]

"Design and Analysis of UWB TEM Horn Antenna for Ground Penetrating Radar Applications"

A TEM horn antenna is usually applied to the air-launching GPR system. Traditionally, the variation of characteristic impedance of a TEM horn antenna is usually set to range from 50 Ω (characteristic impedance of a coaxial cable) to 376.7 Ω (free space wave impedance). However, a difference regularly exists between transmission-line wave characteristic impedance and free space wave impedance. In this paper, we demonstrate that there is no significant difference of performance with the different aperture impedance of the antenna. In addition, the simulated and experimental results both show that the performance of the designed TEM horn antenna matching with impedance of 200 Ω is better than that with free space impedance of 376.7 Ω . For fully understandings, a discussion is provided to explain the possible reasons. At the final aspects of this research, the other components, such as transmitter, receiver, and control units, would work with the TEM horn antennas to complete an air-launching GPR system. [C2210]

"A BPM Two-Scale Contrast Model"

This paper describes a new two-scale polarimetric contrast model based on the Boundary Perturbation Model (BPM). The damping of the short gravity-capillary surface waves by small slicks is modelled by the Marangoni damping coefficient. The surface slick is supposed to modify both the short wave part of the sea surface spectrum intensity and the wind input. The model has been validated over SIR-C/X-SAR Multi Look Complex (MLC) L- and C-band Synthetic Aperture Radar (SAR) data. [C2211]

"Interferometric Data Fusion for Topographic Profile Reconstruction"

Topographic profile reconstruction and ground surface change detection are actually being measured by SAR and differential SAR interferometry. The deal is how topography is estimated from interferometry especially the relative sensitivity of measured radar phase to topography and changes in topography. The objective of this paper is to combine several DEM (Digital Elevation Model) resulting from different interferometric processing by taking into account the coherence information in order to improve the topographic profile accuracy. For that purpose different conjunctive operators are used in data fusion processing. The resulted digital elevation models are evaluated using Mean Square Error (MSE) according to a local reference DEM. [C2212]

"A Markov Random Field Model-based Fusion Approach to Segmentation of SAR and Optical Images"

In this paper, a data fusion approach to the segmentation of SAR and optical images in Markov random field (MRF) framework is proposed. In the joint segmentation scheme based on an MRF model defined on a region adjacency graph (RAG), a fusion rule made on local features of source images is developed for appropriately measuring the feature saliency and incorporating the source reliability of each data source to weigh the source influence in the segmentation procedure. A specific scheme for segmentation of a set of Landsat Thematic Mapper (TM) images and a synthetic aperture radar (SAR) image is presented in detail. Comparative analysis of the proposed segmentation approach against several conventional segmentation approaches carried out on synthetic and real datasets confirms the effectiveness of the proposed approach. [C2213]

"Approximation Error in Differential SAR Interferometry"

Two approximations are used in "Three-pass" D-InSAR (Differential SAR Interferometry). First, in this paper, the error caused by the approximations is deduced and defined as First-order Approximation Error. Then, the characteristics of First-order Approximation Error are discussed in theory and proved by two experiments. In the end, three viable and effective methods are put forward to correct approximation error. [C2214]

"Land Cover Segmentation of ALOS Polarimetric SAR Data"

Image segmentation is a basic step of any segment-based classification method. Various segmentation approaches of polarimetric SAR data, such as region growing and splitmerge to name a few, have been proposed recently. This paper describes the development of a new segmentation approach that improves the polarimetric SAR data analysis by including information from the backscattering behavior of objects in the Freeman-Durden analysis images. This method is based on the main scattering mechanism that appears in

each image pixel and the second most important scattering mechanism that might have been contributed significantly in the scattering process. Further segmentation is performed based on the calculated histograms of sub-regions. The state-of-art ALOS polarimetric SAR data are used in this study. The study area is located in the south of the United Kingdom and includes the city of Minehead. [C2215]

"Integration of RADARSAT-2 Dual and Quad Polarization Data into Pipeline Third Party Encroachment Monitoring"

Mechanical damage incurred from unauthorized third-party activities remains a leading cause of oil and gas pipeline failure, indicating the need for effective strategies to monitor encroachment over extensive sections of pipeline right-of-ways (ROWs). The purposes of the work discussed in this paper are to evaluate the use of polarimetric spaceborne synthetic aperture radar (SAR) for detecting vehicle targets and discriminating them from false alarms and to lay the foundation for integrating RADARSAT-2 products into the existing encroachment management system (EMS). RADARSAT-2 simulated products were created from Convair-580 imagery collected over Calgary, Canada. Results show that target detection is better for higher resolution data, but discrimination of targets from false alarms is better for dual and quad polarization data due to the increased feature set available that captures more of the scattering behavior. Overall, the Ultra Fine HH and dualpolarization Fine HH/HV or quad-polarization Fine are the recommended modes for an EMS using RADARSAT-2. [C2216]

"A study on the classification of urban region using Hyper-spectrum data at AVIRIS"

The purpose of this study is to improve accuracy of land cover classification in urban area. This study used Quick bird and airborne hyper spectrum sensor AVIRIS. Land cover survey was attempted at residential area. There were houses, road, pond, park and vegetations. There were many kinds of vegetations, broad leave trees as Ash, Elm, Willow, Maple, Cotton tree, Needle leave trees as Pine, Tsuga, Spruce. In the study in the past, about Quick Bird analysis, supervised classification (Maximum likelihood algorithm) was executed with some supervisors obtained from field study. 6categories were classified. The results show that with Quick Bird analysis, distribution of vegetation is comprehended well, but timber species are not comprehended well. About AVIRIS analysis, SAM (Spectral Angle Mapper classification) was executed with some supervisors obtained from field study. About broad leave trees, there were five species which spectrums were classified to categories. About grass, 3 categories were classified with conditions of land coverage condition. The accuracies of classification were 26% to 84%. It is confirmed that better results were obtained with AVIRIS. In this study, the classification of the material was tried. There were many kinds of roof materials at residential area, for example, Onix black, Shasta white, Desert tan, Siera gray, Terra cotta, Tile, Wood, Concrete, Asphalt. About AVIRIS analysis using measured spectrums, 7categories were classified. Target area was 2residential areas and Site of university. Target area size was 360 m by 360 m. The accuracies of classification were 44.4% to 100%. [C2217]

"Analysis of Temporal Land Cover Change using the ESA Rolling Archives"

In order to test the potential of the ESA Rolling Archives for the study of temporal land cover change, an area in the Western part of Switzerland has been selected. During the period of 29 September 2007 to 18 May 2008, a total of 21 ENVISAT scenes of the region of interest in Wide Swath mode (WSM) have been downloaded from the ESA ftp server. Though the spatial resolution of data acquired is rather modest (150 m), the fact that the temporal resolution (approximately an image every 10 days) is high makes this type of data very valuable. Change detection techniques have been applied to this dataset and interesting results have been obtained for the analysis and monitoring of land cover changes over forestry and agricultural areas. [C2218]

"A Permanent Scatterers Method for Analysis of Deformation over Permafrost Regions of Qinghai-Tibetan Plateau"

The surface displacement by seasonally freezing bulge and thawing subsidence are main hazards for engineering construction in permafrost regions, especially for the Qinghai-Tibet railway. One of the main problems is how to monitor the frozen ground's displacement in the process of construction and protection of the Qinghai-Tibetan railway. The technology of PS (Permanent Scatterers) has been successfully use to detecting the long time subsidence at urban area. For detecting the subsidence of the frozen earth on Qinghai-Tibet Plateau, this paper extended the capability of the technology of Permanent Scatterers to investigate deformation phenomena in vegetated area. The paper analyzes interferometric phase model, and presents an improved PS-InSAR algorithms for separating different components in interferometric phase. The proposed technique is implemented by using ENVISAT ASAR images to detect the deformation over permafrost region of Qinghai-Tibet Plateau. The results are in concordance with results provided by a traditional ground levelling, which encourages future development for use permanent scatterers method to analyze deformation of the frozen earth on Qinghai-Tibet Plateau. [C2219]

"Correlation between the NRCS and the Wind Speed over Sea in Both Monostatic and Bistatic Configurations"

In this paper, we study and analyze the correlation between the NRCS and the wind speed over the sea surface in both monostatic and bistatic configurations. In our investigation we paid special attention to particular behavior in this correlation. The NRCS numerical calculations were made by using the first order of the Small Slope Approximation (SSA) scattering model and by assuming the Elfouhaily et al. surface-height spectrum for fully developed seas. [C2220]

"Microwave Subsurface Crosswell Imaging using Finite Difference Frequency Domain Modeling"

We have developed a new algorithm for electromagnetic inverse scattering problem in inhomogeneous media using finite difference frequency domain (FDFD) forward modeling, referred as FDFD-based inversion method. The key issue of this method is to build a linear expression for the inverse problem from the FDFD forward modeling by using the Born approximation. An important advantage of this matrix-based method is that there is no need to specify a Green's function. This inversion algorithm is applied to microwave subsurface object detection using cross well radar. The new method is compared with the conventional inversion using Green function-based Born Approximation (GFBA). This EM scattering inverse algorithm is easily implemented and is robust to the heterogeneity of background. Numerical experiments are presented for a two dimensional borehole geometry for buried object detection in soil. [C2221]

"Layered Subsurface Radar Profiling with Combined ESPRIT and SVA Algorithms"

In this paper, a high-performance profiling algorithm with the combination of ESPRIT and SVA (Spatially Invariant Apodization) was proposed. In the algorithm, SVA is firstly used to reduce the sidelobes of compressed pulses, because they could mask the weak signals reflected from subsequent subsurfaces, and ESPRIT is then used to get super-resolution profiling. Detailed simulations for one four-layer geometry with comparison of the results obtained by FFT plus ESPRIT and by SVA plus ESPRIT were presented to show the efficiency of the proposed algorithm. [C2222]

"Polarimetric Characterization of Magnetic Flat Dipole Embedded in Multilayer Structures"

The scattering properties of an embedded planar magnetic dipole are addressed in this paper. In order to obtain the scattered fields the method of moments in spectral domain is applied. The dipole scattering is characterized by the radar cross section (RCS), the polarimetric response and the alpha-angle from Cloude-Pottier's target decomposition theorem. The results point out that alpha-angle is the most sensible parameter to variations on incident angles. The RCS is influenced by the incident angles and by the geometrical dipole area. The incident angles have also influence over polarimetric response, showing its use and interpretation must be done with extremely care. [C2223]

"Forward Propagation over Thick Oil Spills on Sea Surfaces for a Coastal Coherent Radar"

The Ament model is a practical and fast means to evaluate the forward radar propagation over the sea surface in coastal environment. Based on the Rayleigh roughness parameter, it calculates the total coherent power received by an on-board antenna. Here, by extending the Rayleigh roughness parameter to the case of a rough layer, the Ament model extended to the case of rough layers (in which the two rough surfaces are uncorrelated) is presented. This new model is applied to the case of thick oil spills on the sea surface, for which numerical simulations are presented in order to study the possibility of detecting this pollution. [C2224]

"Modeling of Height Spectrum and Radar Cross Section of Oil Slicks on Sea Surfaces"

The influence of oil pollution over sea surfaces on the height spectrum of rough surfaces is studied. An oil slick covering the sea damps the capillarity waves of the surface height spectrum and reduces the root mean square slope of the surfaces. These modifications have an influence on the normalized radar cross section (NRCS) of contaminated seas. The bistatic NRCS of the contaminated sea surface is then presented by comparison with a clean sea: results from a benchmark numerical model are presented and compared with a new semi-empirical approach using asymptotic models, like the weighted curvature approximation. [C2225]

"Bistatic Scattering from a Sea-Like One-Dimensional Rough Surface with the Perturbation Theory in HF-VHF Band"

We investigate the scattering of waves from a rough surface. From the analytical theory of rough surface green's

function based on the extension of the diagram method of Bass, Fuks and Ito, with the smoothing approximation, numerical results are presented for a sea spectrum and compared with a benchmark method by considering a one-dimensional perfectly-conducting gaussian rough surface. The effects of multiple scattering due to the surface roughness are incorporated systematically into the solution through an effective surface impedance. In addition, bistatic scattering coefficients are presented with the first- and second-orders conventional small perturbation method. This study will be useful for remote sensing of the ocean surface, especially when the transmitter is close to the surface. [C2226]

"Biophysical Estimation of Paddy Rice with Canopy Scattering Model and ALOS/PALSAR Imagery in Southeast China"

Rice is a major food supply in southeast China. With increased population and urbanization, reliable rice mapping is critical to meet the socioeconomic need in this region. A 1st-order radiative transfer model was developed in this study to simulate L-band scattering properties of paddy rice and to relate it to biophysical estimation. The simulated HH backscatter in sample fields matched with the variation of PALSAR observations although the simulated backscatter coefficients were around 3dB lower than image-extracted values. HH backscatter was more sensitive to rice's structural variation than VV and therefore, was more useful in rice modeling and bio-mapping studies. [C2227]

"Very Large Baseline Interferometry based On Distributed SAR Satellites For High Resolution DEM"

The high resolution distributed SAR satellites provide the chance to derive DEMs with submeter accuracy (HRTI-4) on local or even regional scale, which can be called Very Large Baseline Interferometry (VLBI). This paper presented a survey of the signal processing flow chart for VLBI. Performance prediction and analysis were based on error contributions as absolute phase estimation error and baseline measurement error, and so on. The simulation experimental results assure the effectiveness of the processing techniques. [C2228]

"Using Small Baseline SAR Interferometry to Investigate Land Subsidence Induced by Underground Coal Mining"

This work presents the application of SAR interferometry for coal mining induced land subsidence investigation and monitoring. Since mining subsidence characterized with, e. g., high rate, relatively small extent and significant nonlinear temporal evolution, it requires a dense spatial sample and a temporal frequent measurement. For SAR data processing, a small baseline interferogram strategy is adopted and the SAR data pairs with a small spatial baseline and short time span are combined to generate differential interferograms with good coherence, and consequently to measure the subsidence and derive the temporal evolution process. We use the available ENVISAT ASAR data acquired from 2004 to 2005 for analyzing the subsidence of Kailuan coal field. The InSAR derived subsidence is compared with the result from the classical mining subsidence prediction model and the result shows a good agreement. For operational purpose, the relation between InSAR parameter and the deformation spatial-temporal pattern are discussed. [C2229]

"The Imaging Wind and Rain Airborne Profiler (IWRAP) Data Archive"

The Microwave Remote Sensing Laboratory (MIRSL) at the University of Massachusetts developed and operates the Imaging Wind and Rain Airborne Profiler (IWRAP). With support from NASA, NOAA, and ONR, UMass has collaborated with NOAA-NESDIS and NOAA-AOC to operate the instrument aboard the NOAA WP-3D "Hurricane Hunter" aircraft since the 2002 hurricane season and for four winter experiments sampling high-latitude storms. The goals of these experiments have been to characterize storm boundary layers and to develop improved retrievals for space-based scatterometers, specifically, NASA SeaWinds Scatterometer on QuikSCAT and Advanced Scatterometer (ASCAT) which was developed by ESA on behalf of EUMETSAT. IWRAP is a conically-scanning, dual-frequency (C- and Ku-band) coherent radar with dual-polarization capability. The incidence angles are nominally: 30, 35, 40, and 50 degrees. At times, the instrument has been configured to address specific scientific and engineering problems. Examples include: C-band measurements of high incidence angle backscatter for ASCAT validation, and C-band horizontal polarization measurements to develop a high wind speed geophysical model function (GMF). Independent measurements of surface wind speed and column integrated rain rate are made coincidentally with the UMass Simultaneous Frequency Radiometer (USFMR) and AOC Stepped Frequency Microwave Radiometer (SFMR). Since 2005, IWRAP has operated in a raw data mode, recording individual radar pulses to enable the separation of near surface backscatter contributions (i.e. surface scattering versus volume scattering). The intensity of tropical cyclones ranged from tropical storm to category five hurricane, and high-latitude storms with up to hurricane force winds. Currently, we are post-processing and standardizing IWRAP raw data collected since 2005. This effort is intended to expand the utility

of IWRAP and (USFMR/SFMR) measurements beyond the scope of the initially proposed research projects by making a standardized dataset available to the larger scatterometer community as well as the hurricane and high-latitude storms research communities. We provide an overview of IWRAP, the data it has collected, describe the processing effort, give the current status, and outline a schedule of data availability. [C2230]

"An Ocean Wave Spectrum Derived from Polarimetric Microwave Radiometer Data"

This paper presents a detailed analysis of a simplified Two-Scale Model for ocean surface polarimetric microwave emission, and investigates the extent to which varying ocean surface length scales contribute to brightness temperature zeroth and second azimuth harmonics. The Two-Scale Model can be expressed as a weighting function $M_{0,2}$ multiply ocean surface curvature spectrum $C_{0,2}$. This implies a simple way to investigate the effect of curvature spectrum on ocean emission. It is found that ocean waves with wavelengths both comparable to and much greater than the electromagnetic wavelength can contribute to these harmonics, depending on the value of the ocean surface spectrum in these length scales. An ocean wave spectrum was derived from polarimetric microwave radiometer data according to constrained linear least-squares method. [C2231]

"Analysis of SAR Images in the Framework of Scale Mixture of Gaussian Models"

In this paper we present the normal variance-mean mixture model as a framework for analyzing SAR data. The complex envelope of the echo signal is considered as a double stochastic circular Gaussian variable, in which both the variance and the mean are linearly scaled by a stochastic scaling factor Z . We then derive the generalized K amplitude model, and indicate how its parameters can be estimated from data. Some preliminary results show that this model represents the amplitude of SAR data well. [C2232]

"The High Resolution Radar Image Simulation of Target on Rough Surface"

The high frequency method can deal with the metal material structure and get a good result. The other method should be used to describe the process of the shadow in the radar image. These shadows are important feature in the radar image. The stability of the shadow contour makes it helpful for the recognition process of the target body. Deterministic and statistical methods play different parts in the radar image simulation. The ray tracing techniques is constructed to describe whole simulation process. Corresponding to the MSTAR image, X band image is simulated under the same imaging condition. Comparing with the same attitude's images, the shadow contour looks similar; and the target part is well coincident too. [C2233]

"InSAR Coherence Measurement Techniques for Snow Cover Mapping in Himalayan Region"

Snow cover area is a very important parameter for snowmelt runoff modeling and forecasting. Snow cover information is also useful for managing transportation and avalanche forecasting. Our study area includes Gangotri glacier region, Siachen glacier region and Beaskund glacier region in the North-West Himalayas of India. Our previous studies discuss the capability of several algorithms for optical sensor as well as SAR to map the snow cover area in Himalayan regions. In recent years, the SAR interferometry has provided number of attractive applications in landuse/landcover mapping. This study discusses the capability of both backscattering ratio techniques and InSAR coherence measurement techniques for snow cover mapping in Himalayan region with repeat passes data of ERS12 and ENVISAT-ASAR. By analyzing the several pairs of ENVISAT repeat passes ASAR images for the study area, we find that the coherence measurement from bare soil, bare rock and vegetation are high and snow covered area and glacier area have very low coherence except in one day difference image. [C2234]

"The H/A/Alpha Polarimetric Decomposition Theorem and Complex Wishart Distribution for Snow Cover Monitoring"

This study discusses the capability of full polarimetric L-band ALOS PALSAR data for snow classification. In this study, Polarimetric decomposition and the complex Wishart classifier are applied on ALOS-PALSAR data. Optical (ALOS-AVNIR) data within six days difference was used for visual interpretation of snow and non-snow classes. Application of Entropy-Anisotropy-Alpha-Wishart classifier for training samples gives better classification results. To reduce speckle effects and to improve classification results, the refined Lee filter was applied on the covariance matrix several times, each time increasing the size of the moving window. Over all classification accuracy were observed 75.61%, 91.46%, 94.91%, 96.19%, 97.16% and 98.37% using different window sizes 1times1 (without filtered image), 3times3, 5times5, 7times7, 9times9 and 11times11 respectively for refined lee speckle filter. It is observed that classification accuracy increases as size of the filter window increases for speckle reduction. Polarization signatures of various features have also been generated using polarization synthesis techniques and signatures are represented in 3-D plot. [C2235]

"Spaceborne InSAR Technique for Study of Himalayan Glaciers using ENVISAT ASAR and ERS Data"

An endeavor is made for the study of movement of Himalayan glaciers using Spaceborne InSAR technique, which is based on preserving the coherence between two acquisitions of the same scene. Gangotri, Siachen, Bara Shigri and Patsio are major glaciers in the Himalayan region, which are showing retreat, and their respective tributary glaciers completely disconnected from main body of glaciers. ERS-1/2 observations show high correlation on glacier area and hence movement of Siachen and Gangotri glacier are measured. Information about dynamism of glaciated terrain can be retrieved by counting differential interferograms. Displacement of Gangotri glacier in the radar look direction has been observed as 8.4 cm represented by 3 fringes. Siachen glacier exhibits a displacement of 22 cm represented by 8 fringes. ERS-1/2 tandem data over all these glaciers show highest correlation over glacier areas but ENVISAT ASAR data shows coherence loss over glacier area due to decorrelation. Coherence loss is usual phenomena in glaciated terrain as repeativity of sensor is high (35 days for ENVISAT). Among all these, Siachen glacier shows highest coherence and then Gangotri, respectively. A tandem pair of ERS-1&2 acquired on April 1 and 2, 1996 in descending pass over Siachen shows high coherence than the ascending pair acquired on May 2 and 3, 1996. It is due to change in climate between two acquisitions at glacier locations. A systematic monitoring of dynamism of Himalayan glaciers can be done using Permanent Scatterer Interferometric SAR (PSInSAR) if we place a corner reflector on the glaciers. [C2236]

"Observations of Small Deviations in Glacier Velocity Measurements"

As part of the international IPY project GLACIODYN (the dynamic response of Arctic glaciers to global warming) the velocity of the Kronebreen glacier at Svalbard was measured testing an interferometric radar with high range and high temporal resolution. The measurements were performed at a distance of approximately 4 km from the glacier using a FMCW interferometric radar at 5.65 GHz with a range resolution of 1 m. The velocity of the glacier measured with the interferometric radar corresponds well with results from other measurement methods such as photogrammetry. The high temporal sampling rate of the interferometric radar measurements revealed a high frequency small forward/backward movement in the glacier that were superimposed on the average glacier flow velocity. These small movements are in the order of up to a couple of mm and occur frequently, approximately from every second to every 10 second. The paper presents the measurement set-up and results. [C2237]

"The Glacier Identification using SAR Interferometric and Polarimetric Information in Qinghai-Tibetan Plateau"

For climatological and hydrological investigations, the areas covered by glacier and their spatial variability are important parameters, particularly in Qinghai-Tibetan Plateau. A interferometric SAR technique not only can produce a high-resolution digital elevation models but also can identify the surface object with coherence coefficients. This property of SAR polarimetry is particularly useful in classification. In this paper we analyze to demonstrate the method and result for the glacier identification integrated intensity of backscattering from Envisat/ASAR images, coherence coefficients of repeat pass interferometry from ASAR and ALOS/PalSAR, and full polarimetric SAR from PalSAR. [C2238]

"Estimation the Movement of Glacier IN Qinhai-Tibetan Plateau Using Satellite Radar Interferometry"

The movement parameter of glacier is the very important factor of the glacier changes. And now, mainly two types of methods have been used for the estimation of glacier movement: differential synthetic aperture radar interferometry (D-InSAR) and Image matching (mainly used for optical data). Although the main potential of D-InSAR for glacier movement estimation has been shown in several case studies, its successful application is often limited by decorrelation. Due to the backscattering characteristic change of the individual scatters on glacier surface, the coherence of glacier surface will be entirely missing for the long temporal baseline (such as 35 days or more). In this paper, we present a novel method to monitor the movement of the whole glacier. According to glacier dynamics theory the glacier's movement is mainly affected by two factors, its gravity and pressures of the firm. The direct consequence of the whole glacier movement is that caused the deformation of the earth surface around the glacier. So we use the motion result extracted by D-InSAR of the earth's surface near the terminus of glacier to deduce the movement of the whole glacier. [C2239]

"Digital elevation models by a GBSAR interferometer for monitoring glaciers: the case study of Belvedere Glacier"

Belvedere Glacier, east face of the Mount Rosa, has experienced drastic changes in flow regime and morphology in the last years. Within the activities of the European project GALAHAD a Ground Based SAR (GB-SAR) interferometer was employed for the first time on this glacier. In the present work it is reported how the sensor capability of generating digital elevation models (DEMs) was exploited in order to retrieve information about the occurred surface changes. In particular, in this case study, the DEM obtained by the radar on summer 2007 was compared with two previous DEMs from other sources: one relative to summer 2005 and the other to summer 1995. Significant differences in the ice surface height have appeared from the comparison reflecting both the extraordinary surge type movement occurred in 2003-2004 and afterwards the overall reduction of the ice mass. [C2240]

"Development of Grounding Line Database using ERS-1/2 Data by InSAR Technique"

We have a plan to build the ocean-continent boundary database at Antarctica mainly to apply InSAR analysis technique using ERS-1 and ERS-2 tandem mission data. This database shows the snapshot of the state of Antarctic ice shelves and ice sheet in 1995-1996, when the tandem mission operated. The ocean-continent boundary data consist of grounding line and coast line, both which have vector property, and these vector data are stored by ESRI shape format (SHP), which is the world's standard vector format. This database will be expected to be used for ice mass flux study at Antarctica and is opened public on internet in this year to contribute the International Polar Year (IPY) activities and anyone can access this database freely through web browser. [C2241]

"Integral Representation of the Electromagnetic Field for the Description of the Main Mechanisms Appearing in Forested Area for Monostatic Radar Configurations"

In this paper, an electromagnetic scattering model based on the electric field integral representation is used to separate the scattering mechanisms involved in the interaction of an electromagnetic field with forested areas. This model is used to examine the different coupling effects between the main scatterers (trunks and branches) and those between the scatterers and the ground. [C2242]

"Decomposition of Polarimetric Scattering of Paddy Rice"

This paper reports the effects of the probability distribution of the target shape to the results of four-component decomposition. The four-component decomposition method decomposes polarimetric microwave data into four components, i.e. surface scattering, double bounce scattering, volume scattering and helix scattering. Prior to the present research, three dimensional structure of the rice was measured and modeled. The model was used to calculate the probability density function of the rice leaves at a viewpoint of arbitrary zenith and azimuth angles. With this probability density function, a covariance matrix of volume scattering for the rice was developed. This covariance matrix was embedded in the four-component decomposition, and it was applied for the polarimetric X-band scattering data of rice, measured in an anechoic radio wave chamber in Niigata Univ. during September 25 to 26, 2007. It was found that the proposed four-component decomposition produced more volume scattering and less surface scattering than the results produced by the standard four-component analysis. As a result, it is concluded that the probability distribution to the target shape should be considered. [C2243]

"Conjunctive Radar and Laser Altimetry Data Processing to Measure Snow Thickness"

Sea ice is generally covered with snow. Information about snow thickness is essential to estimate sea-ice thickness from freeboard measurements and to model ocean-ice-atmosphere interactions. This paper discusses an algorithm to measure snow thickness by processing of coincident radar and the laser altimetry data. Radar return is dominated by the reflected signal from the snow-ice interface whereas laser return by the snow-air interface. Radar data are processed to obtain an accurate estimate of range to the snow-ice interface using aircraft trajectory derived from differential Global Positioning system (GPS) and Inertial Navigation System (INS). Laser data are processed to obtain range to the snow-air interface. The snow cover thickness is estimated from the difference in the radar and laser range estimates. The snow-thickness estimates obtained from radar and laser altimeter are comparing with the in situ snow thickness data collected over the Chukchi and Beaufort lines. [C2244]

"A Study on Sea Ice Observation in the Sea Okhotsk by Polarimetric SAR"

Since polarimetric SAR data are powerful tools to derive scattering mechanism of the observation target, it is expected to give us more detailed information in sea ice monitoring. Electro-Magnetic (EM) measurement for sea ice was conducted during the Soya cruise period in February, 2004. Pi-SAR/L-band polarimetric data simultaneously acquired during the ship cruise were compared with the sea ice thickness and the surface roughness derived by EM measurement. RR-LL coherence is related to sea ice surface roughness in lower

incidence angle, while VV to HH backscattering ratio in higher incidence angle is also related to sea ice thickness. [C2245]

"Sea Ice SAR Feature Extraction by Non-Negative Matrix and Tensor Factorization"

We have studied the feature extraction from sea ice SAR images based on non-negative factorization methods. The methods reported here are the sparseness-constrained non-negative matrix factorization (SC-NMF) and Non-negative tensor factorization (NTF). The studies performed show that these methods can be used to extract meaningful features from SAR images and that they can be used in sea ice SAR classification. [C2246]

"Comparison Between Envisat SAR and 3-D Laser Scanner Statistics for the Baltic Sea Ice"

Airborne laser scanner (ALS) measurements along with a nearly coincident ENVISAT APP image were acquired in the Baltic Sea in March 2005 under cold conditions. The ALS data were processed to ice freeboard data. The data is analyzed using non-overlapping windows with a resolution of 300 m. First, a correlation analysis between different freeboard statistics and sigmadeg is performed. Then, using a nonlinear regression model the dependence between the mean sigmadeg and the mean freeboard is studied. The inversion from sigmadeg to freeboard obtained in this manner gave surprising good results. The whole SAR image (only HH polarization) was inverted using the same technique and the resulting freeboard histogram is discussed. Finally, the factors contributing to the results are shortly reviewed. [C2247]

"Evaluating ALOS-PALSAR for Ice Monitoring-What Can L-band do for the North American Ice Service?"

The Canadian Ice Service (CIS), the U.S. National Ice Center (NIC), and the International Ice Patrol (IIP), partners in the North American Ice Service (NAIS), have individually and jointly used airborne and spaceborne synthetic aperture radar data extensively for almost three decades in their daily ice monitoring operations. SAR's unique ability to penetrate clouds and weather make these data invaluable to the NAIS' efficient environmental stewardship and safe operation in Canadian and U.S. waters. Since 1992, solely C-Band satellite radar has been in use as operational SAR missions such as ERS 1 & 2, RADARSAT-1, and Envisat ASAR have selected it as the band of choice. With the launch of RADARSAT-2 on December 2007 and approved plans for Sentinel-1, the NAIS intends to continue utilizing C-Band data in its daily operations. However, it is important to understand the unique and complementary capabilities of other SAR bands. The January 2006 launch of the JAXA ALOS satellite and present availability of L-band SAR data from its PALSAR instrument provides a unique opportunity to assess L-band data for application to ice monitoring. ALOS/PALSAR availability also provides the potential for examining the synergies between L-Band data and C-Band data available from the current and planned C-Band missions. The existing literature suggests that the use of different frequencies could be advantageous in certain ice conditions, which is of interest to the NAIS because of the vastness of the geographical area monitored annually and the associated variations in ice regimes and conditions. This paper summarizes the preliminary results of a NAIS evaluation of near-coincident C-Band (RADARSAT-1) and L-Band data sets collected in various ice regimes. Through both quantitative and qualitative analysis we attempt to identify the unique and complementary sea ice information PALSAR can provide. In doing so, we identify the role these data could play in the NAIS' operational programs, both in a complementary role to existing C-Band SARs and its potential as a contingency platform. This work will also help us better understand the potential for future possible multi-frequency SAR platforms. [C2248]

"Predistortion Arithmetic on Low Sidelobe Pulse Compression Signal for Spaceborne Weather Radar"

Pulse compression with very low sidelobes is one of challenges in the design of spaceborne weather radar. To detect the weak echoes of clouds occurring near the strong echoes of sea surface, sidelobe performance below -60 db is needed in the pulse compression system. To achieve such low sidelobes, high SNR and linearity are required in the radar system. But in spaceborne radar system, the transmitter often works at saturation point to get high output power and high efficiency. So a successive over relaxation (SOR) iterative method of digital predistortion is applied here to ensure the sidelobe performance and high efficiency of PA. A test system based on RFLPA, ESG and VSA is carried out to verify and optimize the predistortion arithmetic. [C2249]

"A TSVM Based Semi-Supervised Approach to SAR Image Segmentation"

Image segmentation is a fundamental issue in image processing. Segmentation of synthetic aperture radar (SAR) images is extremely difficult on account of intrinsic multiplicative speckle noises. Due to the ambiguities of SAR images, labeled instances are difficult and time-consuming to obtain while unlabeled data are abundant. In

this paper, a new semi-supervised approach based on transductive support vector machine (TSVM) is proposed to segment SAR images, it is robust to noises and is effective when dealing with low numbers of high-dimensional samples, moreover, it could efficiently make use of unlabeled data to reduce human labor and improve precision. Segmentation results are also compared to SVM and TSVM trained by using different samples and parameters. Experimental results demonstrate that the proposed method is very promising. [C2250]

"SIFT Based Automatic Tie-Point Extraction for Multitemporal SAR Images"

Tie-point extraction is the key step of coregistration of multitemporal images. In this paper, Scale invariant feature transformation (SIFT) is applied to extract tie-points from multitemporal SAR images. A histogram-based preprocessing method and the optimization of SIFT parameters are proposed for increasing the number of correct tie-points. We explore the performance of SIFT algorithm on different topographic ENVISAT SAR images. The experimental results show that these methods are robust to speckle noise and can markedly improve the performance of SIFT on SAR images. [C2251]

"Study on Point Spread Function of Optical Synthetic Aperture"

Optical synthetic aperture has extensive application in the space exploration and earth observation with technology progress in aviation and spaceflight fields. Using a sparse array of smaller apertures, one can synthesize an aperture with the resolution of the equivalent filled aperture while reducing the size and weight of system. The point spread function of optical synthetic aperture has an important influence on optical synthetic aperture imaging. The point spread function under different fill factor and piston errors are given by calculating. [C2252]

"Ocean Surface Currents Determination from X-Band Radar Image Sequences"

An algorithm for retrieving ocean surface currents using nautical radar-image sequences is presented in this paper. The image sequences are acquired by common marine X-Band radar. With the Fast Fourier Transformation the image sequences are transformed to the wave number frequency domain and produce a three dimensional image power spectrum. In the absence of the sensor's velocity and the near surface current the spectral energy in this three-dimensional wave number frequency space will lie on a shell defined by the dispersion relationship. Any deviation from the expected dispersion relationship can be interpreted as a current induced Doppler shift of the wave frequency. A weighted least squares curve fitting technique is used to determine the surface current. For validation of the algorithm, the surface current derived from the inverted radar data sets and from ground truth data are compared. It is shown that the radar-retrieved surface currents are within the accuracy of the conventional instrumentation. [C2253]

"Improving PWF Method of Despeckle in Polarimetric SAR Image by Fusion Based on Nonsampled Contourlet Transform"

A novel and efficient improving PWF method of speckle reduction in polarimetric SAR image by fusion based on nonsampled contourlet transform is proposed. First, the three complex elements (HH, HV, and VV) of the polarimetric scattering matrix were decorrelated to form a new elements matrix. Then we show that the sub-band decompositions of the three elements using nonsampled contourlet transform, and fusion factor is applied to the decomposed directional high-frequency coefficients to create new sub-band coefficients. Finally, we process and reconstruct multi-resolution contourlet coefficients according to the PWF method. Experimental results show that compared with PWF de-speckling algorithm, the proposed algorithm can achieve an excellent balance between suppresses speckle effectively and preserves image details, and the significant information of original image like textures and contour details is well maintained. [C2254]

"Optimal Mismatch Network in Active Radar Reflector"

The use of mismatch network to modulate the retransmitted signal of an active radar reflector (ARR) can separate the reflected ARR signal from background signals effectively. The effect of separation depends on the characteristics of the mismatch network. In order to achieve the best separation between the reflected ARR signal and background signals, we need to make optimization design of mismatch network. This paper gives out an optimal mismatch network, which is modeled as weighting functions. Based on the loss of signal noise rate (SNR), the optimal weighting coefficients can be solved. Simulation experiments with compression of line frequency modulate (LFM) signals were carried out. The results prove that the mismatch network could separate the reflected ARR signal from background signals effectively. The optimal weighting coefficients were solved with certain SNR conditions. [C2255]

"A ZigBee Based Mesh Network for Home Control System"

The current development and the application status of the home network are introduced briefly, then, a two-tier architecture of home control system (HCS) based on ZigBee multi-hop mesh network is presented. In addition to the basic data acquisition and processing functions, the gateway which has been designed and fabricated supports ZigBee based wireless access interface, Bluetooth based local interface and GPRS based remote interface. The hardware architecture and protocol software, as well as the communication control method are proposed in detail. Under the constructed test environment, the performance results show that the proposed scheme is more convenient for home control services, and except the gateway, all of the router nodes in the system work on sleep mode at most of the time, which will improve the lifetime of the whole system efficiently.

[C2256]

"Evaluation of a 35-GHz Radar for Cloud and Precipitation Research in SCHeREX-Experiment"

HMBQ radar is the first millimeter-wavelength (8mm) cloud radar with Doppler and polarization in China. Several new techniques like coherence accumulation, polarization and pulsating compressive had been applied in this radar. The minimum effective radar reflectivity factor of water cloud that is measured by this radar at a range of 10 km is estimated to be -40dBz. During May to September in 2008, HMBQ radar was situated in DongGuan, GuangDong Province for the SCHeREX experiment to observe clouds and obtained much valuable information. Some examples of cloud structures are presented in the experiment, also presented here is the liquid water content retrieved by this radar.

[C2257]

"Numerical Study for Backscattering Enhancement of Concrete Specimens with FRP-TriCR Buried and Its Compatibility with Infrared Camouflage"

Lower electromagnetic backscattering from concrete pavement as its smooth surface results the much darker image feature when exposures to imaging radar when compared with rough surface such as vegetation. In this paper, exploratory research on radar cross-section enhancement of concrete specimens with composite scatterer consisted of fiberglass reinforced plastics and trihedral corner reflector (FRP-TriCR) buried is presented.

Scattering properties of concrete specimen, corner reflector, concrete specimen mixed with corner reflectors and with FRP-TriCR buried are numerical simulation based on the model of finite difference-time domain (FD-TD) in lossy dielectric with perfect matched layer (PML) in z-direction and period boundary conditions(PBC) in x,y-direction. In the conditions of given incident wave and dielectric coefficient of concrete specimen, the monostatic RCS of concrete specimen with FRP-TriCR buried is -5.6 dBsm and the average is -10.6 dBsm when theta is 30 to 60 degree, which increase much when compared to concrete specimen mixed trihedral corner reflector (monostatic RCS is -12.3 dBsm, the average is -15.8 dBsm from theta = 30 to theta = 60 degree). It is much more important that FRP-TriCR scatterer is independence of moisture of concrete. On the other hand, the transmission characteristic of infrared radiation has been changed because of cavity structure, which is possible for compatibility for camouflage.

[C2258]

"Monitoring Land Subsidence by Using Multi-temporal Differential SAR Interferometry: A Use Case in Jiaxing, China"

Decorrelation caused by temporal change and SAR imaging geometry prevents conventional SAR interferometry from monitoring land surface subsidence precisely. In addition, conventional methods don't deal with phase delay which caused by atmosphere. It negatively influences the accuracy of differential synthetic aperture radar interferometry (D-InSAR) for small-scale deformation monitoring. In this paper, a multi-temporal D-InSAR method was used to extract the surface deformation of Jiaxing, China, automatically. At first, terrain phase has been subtracted from multi-temporal interferograms by using digital elevation model (DEM) data. Then, the amplitude dispersion and phase stability analysis were combined to select stable high coherent pixels, which connected by Delaunay triangulation to form a spatial network, as reliable unwrap object. After spatial and temporal correlation analysis, the terrain error is corrected and the atmospheric delay phase and residual noise phase are removed. At last, the surface deformation map stack was created to generate land subsidence velocity map. The result has been proved to be reliable by comparing the ground monitoring data.

[C2259]

"Validation of Two Soil Moisture Products from ERS Scatterometer Data over East China"

In this study, two soil wetness products- Surface Soil Moisture (SSM) and Soil Water Index (SWI), derived from ERS (European Remote Sensing) scatterometer data are validated based on the in situ measurements in north and east China. Results indicate that the soil wetness climatology in the ERS products is similar distributed with the observations, showing wet status in the northeast and southeast, while dry status in the northwest of the concerned domain. Moreover, the SSM and SWI have the ability to represent the principal characteristics of the spatial distributions for the soil moisture anomalies during transitional seasons. Regions of high variability for the

soil moisture include northeast China, the middle-lower reaches of the Yellow River and the Yellow-Huaihe River Basin in April; while a band of high variability is found along the semi-arid regions in October. [C2260]

"Research and Application on Network Update of Land Survey Spatial Data Based on Embedded GIS and GPS"

This paper studies the methods and strategies of the network update of the land survey spatial data based on embedded terminal equipment and server and application of multi-level distributed heterogeneous land spatial database. Web services network model has been used to do the design and implementation work of embedded system of land survey data update. The main procedure of spatial data real-time network update method in this article includes: web services network asynchronous transmission, wireless transmission based on GPRS, spatial data real-time updating, layer-grid index by applying the model of setting many levels and blocks, interactive operations between spatial data and attribute, location services and automatic acquisition based on GPS. [C2261]

"A Study of Drop-Size Distribution in Precipitation Cloud from Wind Profile Radar"

Author retrieves the raindrop size distribution in precipitation, by separating two distinct return signals from clear-air and from precipitation, based on the return signal spectrum density derived from the wind profile radar, and on the relationship between the terminal velocity and the diameter of descending raindrops. Further retrieval of precipitating cloud data at different heights has resulted in the raindrop size distribution indicating a basic match with the distribution of M-P distribution. The reflectivity value derived from wind profile radar is in agreement with that from Doppler weather radar. Calculating the water content in the clouds at different heights through a raindrop size distribution reveals that is close to the water content observed by the Weather Doppler Radar. [C2262]

"Modeling and Implementation Of Wireless Embedded System For Intelligent Transport System Application"

Intelligent transport system (ITS) deals with the remote sensing as well as access to the Internet and multimedia on the move. There is a need for a system that supports both remote sensing and communication aspects with simple and reconfigurable hardware. In the present work MATLAB/SIMULINK based modeling of such a system is done based on DSSS. Hardware realization of this model is achieved through the signal wave software defined radio (SDR). From the simulation results two empirical formulae are developed for target detection. [C2263]

"Automated image registration to 3-D scene models"

This paper develops a technique for the registration of multi-sensor/multi-modality images to 3-D models utilizing the keyhole markup language (KML) encoding standard. Given the recent advancements in visualization of geographic information utilizing such software tools as Google earth, microsoft virtual earth, and NASA's Worldwind, it is becoming increasingly necessary to understand and utilize the capabilities of these impressive software tools in the field of remote sensing. [C2264]

"Propagation environments of radiowave information systems"

Radio systems are in contact with the channels of information transmission in high-tech information times tightly more and more. The channel becomes an important part of radio systems, which is known as the radiowave propagation environment. Digital grid data can not only reflect the continuous visibilities of different part of the radiowave environmental parameters, but can achieve the propagation forecasts and generate the necessary visual maps for any regions. Based on the radiowave space grid environmental information data from advanced remote sensing instruments and radiowave environment station networks, as well as the management and application of space-time information which is expressed by radiowave environment grid data, the radiowave environment observation and security system is realized with comprehensive observation system, abundant data acquisition methods, integrated earth space, and real-time information capacity that can be used in radar, communication, monitoring and control, navigation and other electronic information systems, and integrated security systems, etc. [C2265]

"Road-surface abstraction using ladar sensing"

Propose a road-surface abstraction algorithm which suitable for structured and semi-structured road environments. Algorithm uses fuzzy cluster method which based on maximum entropy theory to cluster ladar points that belong to a scan line. After fitting clustered data linearly, one can abstract straight lines that belong to road-surface by their location and slope angle. We can acquire a current referenced horizontal by comparing

several continuous ladar scan lines and then the algorithm abstracts obstacles on road-surface area. Experiments show our algorithm works well in spite of the road-boundary's shape is regular or not, and free from the impact of complex texture or irregular illumination of the road. [C2266]

"Passive Bistatic Radar (PBR) using FM radio illuminators of opportunity"

We present a system characterisation of a passive bistatic radar (PBR). The system under investigation exploits dasiailluminators of opportunitypsila, which in this case are commercial, non-cooperative, VHF FM broadcast transmissions. The PBR under investigation demonstrates the detection of large passenger-jet aircraft in the airspace over greater London. FM based PBRs such as the type examined here have been shown to be effective at remote sensing of auroral turbulence, density irregularities in the E-region and F-region of the ionosphere and meteor trails. Detection of aircraft is an important step in attempting to remotely sense outer-atmospheric phenomena as aircraft scattered power is of a comparable magnitude and similar Doppler frequency to the natural phenomena described. This paper also analyses the merits of FM broadcast transmissions for use as radar signals. A system characterisation with performance predictions is presented. The results show that target detections have been achieved to ranges in excess of 70 km (bistatic range). Multiple broadcast channels from two different transmitters of opportunity enhance the case for deciding whether or not targets are present. Air-truth data provided by a mode S/ADS-B IFF receiver is used for comparison with the 2-D bistatic results. [C2267]

"HF passive bistatic radar potential and applications for remote sensing"

Passive radar is briefly discussed before the concept of HF passive bistatic radar is introduced using a sky-wave illumination path and surface-wave reception path. The HF passive radar under construction at UCL is described briefly. The signal processing required to reveal targets is presented followed by a comparison of analogue and digital illuminators of opportunity and their potential to detect targets. Finally the signal to interference ratio for the HF specific case is presented and conclusions are drawn on the need for interference cancellation. [C2268]

"Beach soil moisture measurement with a land reflected GPS bistatic radar technique"

In this work we investigate the potential for sensing beach soil moisture with the L band GPS bistatic radar concept. Characterisation of sediment surface (properties like humidity) is indeed important to better understand morphodynamic activity of intertidal part of beaches. In our approach we compare the direct GPS Signal to Noise Ratio with the reflected one in order to measure the soil moisture. We use a bit grabber to digitize and store the GPS L1 carrier (1.5 Ghz) samples. In this context the signal processing is off-line. In this work we proposed a model of the received signal after demodulation and demultiplexing. We deduce from this model a MAP estimate of the navigation message and of the signal SNR. In our case the signal model is a piecewise stationary process with change instants at bit edge position. We present preliminary SNR measurement with this technique for the discrimination of water and humid sand. [C2269]

"Internal Wave Detection and Parameter Estimation from SAR Images Based on a Novel Radon Transform Method"

The potential of using satellite imagery for studying oceanic internal waves have long recognized by the oceanographers and remote sensing researchers. A great deal can be learnt about internal waves from satellite data if the grey tone patterns of the Synthetic aperture radar images can be confirmed to correspond to the trough and crest patterns of internal waves. In this paper, a new solution of internal wave detection and parameter estimation in SAR ocean image is presented. It improves the traditional Radon transform through normalize the Radon coefficients in an ellipse region and thus detect the inconspicuous lines in ocean background. Making use of the idea of glide windows we use the proposed transform to detect the internal wave region, and then we can estimate the internal wave parameters, named the wave direction and the wavelength, simply through dealing with the Radon coefficients. The experiment results on simulation and real SAR images shows that the proposed method can detect the internal wave region automatically and correctly, and the parameter estimated is corresponding with the real observation. [C2270]

"Synthesizing Large-Scale Virtual Terrain from Image Atlas"

In this paper, a novel algorithm to synthesize large-scale virtual terrain from a set of images is presented based on digital image processing technologies and radial weighted blending method. The algorithm first creates standardized terrain-blocks from the images, and then smoothes the blocks by employing fast Fourier transform (FFT) and butter worth low-pass filter. A radial-weighted defined on each block, which is used to synthesize four local neighboring blocks to a single blended area, is subsequently constructed for each block. As a result, a complete and smooth large-scale terrain can be obtained by blending operator with the radial-weights. The

algorithm also provides user a tool of controlling terrain by adjusting several parameters. Experiments show that our algorithm can generate terrains with various scales and styles, fast and effectively. [C2271]

"Radar Echo Characteristics of Convective and Stratiform Mixed Clouds during Their Formation in a Mountainous Region"

The mixture of convective and stratiform clouds is an important precipitation system and also a major object for weather modification studies. To investigate the forming process, we studied 48 such clouds precipitation processes happened in GuiZhou province during 2005 and 2006 using Doppler radar echo images and other data. Convective and stratiform mixed clouds are primarily formed in two ways: 1) merging and expansion of convective clouds and 2) convective cells embedded in stratiform clouds. The merging type mixture was found in 85% of the cases while the embedded convection made up the remaining 15%. [C2272]

"The Turbulent Wake Detection and Beam Estimation of a Ship in SAR Images"

Synthetic aperture radar (SAR) images of sea surface often reveal ship wakes, which appear in the form of bright and dark streaks. The bright streaks are always attributed to the Kelvin wake and bright narrow V-wake, and the dark ones are always to the turbulent wake. In some SAR images the Kelvin wakes and the bright V-wakes are distinct and there are plenty of papers have discussed on the detection of them. But in some other SAR images the turbulent wakes are more obvious. The present work deals with the turbulent wakes of the ships, proposed a method called ellipse normalize-Radon transform to detect the dark lines of the turbulent wake. Once the turbulent wake is detected, the ship beam is estimated by a semi-empirical relation between the ship and the width of the turbulent wake in SAR images and the ship beam developed by Greory Zilman. The experiment results demonstrate that this algorithm's robustness in the presence of noise, as well as its ability to detect the turbulent wake and estimate the beam of a ship. [C2273]

"Research on scattering and imaging simulation from the object and randomly rough surface"

Research progress on electromagnetic (EM) scattering and imaging simulation from the volumetric object and randomly rough surface in Fudan University is briefly reported in this paper. [C2274]

"0.18um CMOS receiver front-end for non-invasive cardiopulmonary monitoring"

In this paper, the results of simulation a receiver front-end for CW Doppler radar remote vital sign sensing is designed and simulated integrated on a chip by 0.18 um CMOS technology. This receiver has low power consumption (10 mW with 1.8 V) and low flicker noise performance. Whole CW Doppler radar system for cardiopulmonary monitoring will be implemented on PCB and experimented. [C2275]

"Radar altimeter echo simulation based on PO method"

Radar altimeter as one of the most important microwave sensors has been playing an important role since later 1970s in ocean environment monitoring, ocean science research and global climate change study, etc. Recently, SAR altimeters have been designed to improve the spatial resolution along the satellite track. Synthetic aperture processing inherently can give a high spatial resolution in the along track direction by combining of several pulses. This paper overviews the development of radar remote sensing. Also, the physical optics method is discussed and the process of electromagnetic simulation of radar altimeter working in burst mode with chirp waveforms over land surfaces is described. [C2276]

"Measuring the Microwave Backscattering Coefficient of Paddy Rice Using FM-CW Ground-Based Scatterometer"

An experiment to measure microwave backscattering coefficients of paddy rice was carried out with FM-CW ground-based scatterometer at L-band, S-band, C-band, X- band. This paper introduces scatterometers that were adopted in the experiments and the measuring technique in detail, analyzes the data which were obtained under the different wave band and different polarized condition, and discusses the factors that affect emphatically the backscattering coefficient of scatterometer parameters: incidence angle, polarization, wave length. [C2277]

"Shallow water height mapping with interferometric synthetic aperture sonar"

Height mapping of shallow water areas is an important task for many commercial and scientific applications like river navigability, infrastructure maintenance or natural resource monitoring. The use of an autonomous boat presents several advantages that ease the use of synthetic aperture images to create three-dimensional topographic maps through interferometric techniques. Sample data obtained during test trials illustrate how

synthetic aperture can be used to generate imagery and bathymetry data. [C2278]

"The MODENA project: Modeling and simulation of the maritime environment remotely sensed by radar"

This paper describes the goals of the MODENA project, aiming at a fine description of the maritime environment by means of electromagnetic sensors. The main steps of the project go through a modeling of the ocean surface, the man-made objects on the surface as well as of the interaction between the electromagnetic waves with this surface and the objects. The project is scheduled to last 4.5 years. The final objective consists of providing a view of the dynamic simulation of the ocean surface and moving objects following a script and constrained by the selected radar parameters (frequency, polarization, speed and altitude of the carrier, etc). We will discuss the different parts of the project and present the actual state of development achieved by the partners and the expected results. [C2279]

"Retrospective and prospective views of the Ocean Observing System in the Gulf of Maine"

The Gulf of Maine Ocean Observing System (GoMOOS) is a comprehensive prototype integrated coastal ocean observing system that was established in the summer of 2001. Its current configuration includes eleven solar-powered buoy-monitored locations with physical and optical sensors, four shore-based long-range HF radar systems for surface current measurement, operational circulation and wave models, satellite observations, inshore nutrient monitoring, and hourly web-delivery of data. It serves a broad array of real-time oceanographic and marine meteorological data and data products to scientists, state and federal regulators, the National Weather Service, both the US and Canadian Coast Guards, the National Data Buoy Center, educators, regional natural resource managers, the Gulf of Maine fishing and maritime industries, local airports and airlines, sailors, and the general public. The ocean observing system that can be thought of as consisting of four major subsystems: the data acquisition subsystem; the data handling, processing, and archiving subsystem; the system of numerical nowcast and forecast models; and a web-based data distribution/presentation subsystem. [C2280]

"Surveillance of Canada's high Arctic"

The Canadian Arctic is fast becoming an area of increasing strategic and economic importance to Canadians and its federal and territorial governments. As a result, the Canadian Forces (CF) need to be more aware of activities in this area; particularly in the navigable passages. However, due to the large expanse, low population density, and lack of extensive infrastructure in the Canadian Arctic, this is a difficult task. Presently, information is primarily limited to that gathered from RADARSAT, by over-flights carried out by the CF's Maritime Patrol Aircraft, to ground patrols carried out by the Canadian Rangers or the Army, and patrols by the Canadian Coast Guard or Canadian Navy. To improve the ability of the CF to obtain an Operational Picture (OP) for the high Arctic, Defence Research and Development Canada (DRDC) started a four year Technology Demonstration (TD) project in April 2007 to investigate and demonstrate technologies that could be used to monitor and surveil the waters of the high Arctic. This paper discusses the various technologies that will be investigated, developed and demonstrated, and presents the program of work that has been proposed and which we are in the process of realizing. [C2281]

"2003-2008 Ice Sheet Elevation Change on the Lake Vostok, Antarctica, From ICESat"

This paper estimate the recently trend of ice sheet elevation change in the Lake Vostok region of the east Antarctica using the time series of the ground track crossover from the ICESat (ice cloud and land elevation satellite) laser altimetry, and adopt several methods to improve the processing of the crossover elevation change time series, utilize the more crossover points from the whole ICESat laser operation periods dataset. The elevation change rate we got is -1.36 ± 0.09 cm per year from 2003 to 2008 in the Lake Vostok region. The result shows we can get an accuracy cm-level elevation change rate in the flat interior region of the Antarctica, which provided a useful approach to detect the whole polar ice sheet mass balance. [C2282]

"Oil Spill emergency response mapping for coastal area using SAR imagery and GIS"

Oil spill disaster is unexpected accident occurs through failures in operations, transportations, ship accidents, human errors or due to other disasters such as flood and earthquake. Most of oil spills happen in coastal and sea environment that make the emergency response for the accident much difficult and complicate. Intricate operations involve through complexity of sea and coastal conditions, especially in bad weather where the access to the accident site is difficult. Management of such event needs an organized contribution, covering all procedures of disaster operation from monitoring and detection to mitigation and relief. This paper presents methods of SAR image and GIS technology applications for oil spill management in coastal area. The developed

framework is based on automatic detecting and mapping of oil spills in SAR image and provision of oil spill location and extent map which includes information about the spill thicknesses and geographic references such as major towns and features along the coastal area. The output from SAR image processing then transferred into oil spill trajectory simulation model to simulate the next destinations of oil spill. Oil spill trajectory predicts the movement, spreading, and coastal impact of oil spill in the marine environment. The output vectors from trajectory simulation used as input data for creating other disaster products including oil spill risk map, affected area map and emergency response map. Each product demonstrates the results from various analyses aspects, include situational analysis, risk analysis, damage analysis, and emergency response analysis using satellite SAR image in GIS and image analysis software. All the models and applications are described and depicted.

[C2283]

"Convective clouds modelling and tracking by an airborne radar"

A method for modelling and tracking convective clouds within radar images is described. Clouds are non-rigid heterogeneous objects; a good representation of the weather scene is performed by extracting skeletal lines of the 2-dimensional grayscale pictures. Skeletons are reduced to sets of segments within a graph structure and tracked among successive pictures by means of relaxation labelling processes. We present preliminary results of our method on airborne weather radar data. The conventional morphological skeleton constraint -i.e., to be centered in relation to the object boundaries- is here replaced by attachment to the gray levels local maxima. The resulting skeletal line is forced to go through each intense convective cell, and links neighboring ones into a global structure. Moreover, each feature point can be labelled and enriched by meteorological information. Such pattern is particularly suitable for weather nowcasting, since the user (for example, an aircraft's crew) is specially interested in the convective cells evolution. [C2284]

"LIDAR technique for remote gas analysis in solid scattering media"

LIDAR techniques are used to measure gases in solid scattering media remotely, by analyzing the differential absorption observed in the multiple scattering light. The gas exchange (O₂/N₂) in polystyrene foam is monitored.

[C2285]

"Microwave imaging systems: Achievements and improvement prospects"

There is considered the methodology of constructing the microwave radar systems for 24 -hour and all-weather remote monitoring with information possibilities not yielding to the optical ones. The analysis of the achieved technical characteristics has been made, and the main ways for further improvement of the microwave imaging systems have been defined. [C2286]

"Sparse antenna array geometry synthesis for remote sensing systems"

In this paper approach of sparse antenna array geometry construction based on combining prime sub-geometry are proposed. [C2287]

"Difference patterns from continuous line sources"

Sum and difference patterns are produced from two arrays or from one array with dual excitations. Sum patterns are useful for range detection of moving targets and the difference patterns are useful to determine angular tracking accuracy. Some works are available in literature on such patterns from different arrays .In the present work, an attempt is made to produce difference patterns from continuous line source of different lengths. The patterns are presented in sin-thetas domain. [C2288]

"High frequency (HF) radar cross sections of the ocean surface incorporating a continuous wave frequency modulated source"

Frequency modulated continuous wave (FMCW) is often employed in practical HF radar ocean surface remote sensing systems. The first- and second-order monostatic cross sections of the ocean surface in the context of high frequency ground wave radar operation are derived for a dipole source with an FMCW waveform. The Fourier coefficients of the rough ocean surface are described as zero-mean Gaussian random variables. The electric field equations for the reception of vertically polarized radiation scattered from ocean surfaces are obtained. Illustrative comparisons of the cross sections between the pulsed and FMCW waveforms are presented and their properties are addressed. [C2289]

"Autonomy based modeling for the simulation of ocean remote sensing"

This article presents the simulation structure for the MODENA project [1] and illustrates what should become an original dynamical model for the reflectivity map of the sea surface. From our point of view, MODENA challenges to find accurate models for simulating dynamically interaction between sea state, sonar, radar and ship, while keeping physical coherency during the whole observation scenario (several tens of minutes), including human participation in this virtual reality system. To deal with such a complexity, as it is impossible and inappropriate to compute dynamically hydrodynamic, electromagnetic and acoustic equations on an accurate grid of points or mesh, MODENA simulation structure aims to use an autonomy based approach: the model of each phenomenon (wave, breaking, group, ship, wind, stream, transmitter, receiver...) involved in the simulation is seen as an autonomous entity, including an autonomy of time, space and scale. These models are combined and animated using enaction-based multi-agents simulation. In such simulation, computer activity is optimised at places where and when interaction occurs within relevant scale, according to chosen models. Furthermore, to add new phenomena or to modify existing models do not make previous work obsolete, as one has only to characterise interactions of new phenomena with previously defined models. This modeling approach facilitates interaction between research teams involved in the MODENA project, as the whole simulation results from the set of autonomized models developed by each team in parallel. Such a virtual laboratory should help for example to better distinguish the signal of breaking from the signal of small boats, in the dynamical signature of sea-states.

[C2290]

"Measurements of the effect of rain-induced sea surface roughness on the QuikSCAT scatterometer radar cross section and wind stress"

Changes in the sea surface roughness from the combined effects of wind and rain, on scales of tens of kilometers, are being studied using the QuikSCAT scatterometer (NRCS) and simultaneous NEXRAD three-dimensional measurements of rain. The studies of air-sea interaction, related to surface fluxes. The results to be presented were acquired during a significant rain event in the Gulf of Mexico, to the east of Corpus Christi, and just south of Houston, TX in May 2005. Preliminary results in NRCS caused by rain, relative to that in nearby regions with negligible rain shows distinct characteristics. Three regions with different wind speeds (4-6, 6-8 and 8-10 m/s) show definitive variation of this total NRCS with respect to wind magnitude, satellite-relative wind direction, polarization and rainrate. Relative changes are stronger in the lower wind region for both polarizations, with H-pol providing a more definitive signature. At higher wind speeds (e.g. 10 m/s) the relative splash induced increases in NRCS are still significant, and show distinct differences between polarizations. [C2291]

"Performance Analysis and Improved Method for Airborne Three-Channel SAR/GMTI System"

A new antenna arrangement scheme and moving target detection method is presented after analyzing the shortcoming of conventional three-channel synthetic aperture radar (SAR) ground moving target indication (GMTI) methods. The shortcoming of conventional three-channel SAR/GMTI methods is that you cannot improve the performance of minimum detectable velocity, ambiguous speed and blind-velocities simultaneously to meet the requirements of the system. The improved method proposed in this paper solves the problem by rearranging the transmitting and receiving antennae without increasing the number of receiving channels. Theoretical analysis and simulation results show the validity of this scheme. [C2292]

"Soil Moisture Mapping in Typical Semi-Arid Regions of China by Using Envisat ASAR Data"

Both passive and active microwave sensors have long been used in retrieving the soil moisture, however, only the SAR can provide the high spatial resolution data (10 m~1 km) suitable for watershed scale hydrological studies. In this paper, we took a preliminary study on deriving the catchment scale soil moisture content and their spatial variations in a typical semi-arid rangeland located at the Loess Plateau of China with active microwave remotely sensed data. The Advanced Integral Equation Model (AIEM) was coupled with the Envisat ASAR images by using the simulated surface roughness information retrieved from the multi-angle (15deg a 31deg) ASAR data as constraining condition to estimate the surface soil moisture content within the studied watershed, the Jinhe River Basin. In general, the soil moisture map derived from this study shows high wetness in most part of the basin, which is in agreement with the actual rainy condition in the study region. [C2293]

"Long Term Analyses on Spatial and Temporal Evaluation of Snow Covers in Northern China by Using RS and Meteorological data"

Piling and melting of snow cover is a dynamic process which has important effect on the radiation balance, and water circulation over the land surface. Accurate information on snow depth is essential for the study of hydrology and climatology. However, it is almost impossible to obtain any long-term and annual variability characteristics of snow covers by means of conventional field observations. Passive microwave remote sensing has the advantage to penetrate the cloud, and its all-weather capability for snow cover monitoring makes it

superior to the optical sensor and near-infrared remote sensing techniques. By means of daily snow cover monitoring data derived from SMMR and SSM/I during the period from 1979 to 2005, snow depth and snow cover days over the northern China were quantitatively analyzed. Spatio-temporal variations of snow covers were evaluated in terms of spatial-temporal distribution and the significant level by the Mann-Kendall rank statistical test. The results suggested that the snow-cover periods became notably shorten and the snow depth turned to decrease obviously with the significant level of $\alpha < 0.01$ in the desert of northwest arid region under the significant warming trend. In contrast, the snow depth tended to increase notably with the significant level of $\alpha < 0.001$ in the northwest alpine region and Xiaoxing'an Mountain, where the climate tended to be much warm and humid at the same period. [C2294]

"Linking Geospatial Datasets with Different Scales by Conflation"

The comprehensive consistent administration of geographic data of different scales has been under scientific investigation for several years. A database which keeps datasets with different scales and links between corresponding geospatial features is called multiple representation database (MRDB). Linking datasets is motivated by the need for propagating updates from larger scale datasets to smaller scale ones in MRDB, which is the key step to build a MRDB. Because the data are captured by different organizations, one object of the landscape is stored in several datasets at different acquisition times, with different quality characteristics and in different scales. Crucial for linking is certainty of equivalence of different object representations. This paper introduces a general structure of a generic conflation approach for linking geospatial datasets with different scale in MRDB, discusses the topological algorithms used in data matching process in detail. [C2295]

"Mapping Paddy Rice Biomass Using ALOS/PALSAR Imagery"

Accurately estimating rice biomass and yield is important not only for rice cropping management, but also for quantitatively understanding carbon cycle in agricultural ecosystem. This study integrated a rice canopy scattering model with Genetic Algorithm Optimization Tool (GAOT) to simulate rice biophysical parameters and to estimate rice biomass from L-band, HH polarization mode ALOS/PALSAR radar imagery. Plant height and density, the two most determinant biophysical parameters related to rice biomass, could be retrieved with the error of less than 6 cm and 30/m², respectively. The simulated biomass was within adjusted residual of 200 g/m² of the measured value. The results demonstrated the potentials of new ALOS SAR data to mapping paddy rice biomass with the microwave canopy scattering model. [C2296]

"Quality Evaluation of Spatial Point-Cloud Data Collected by Vehicle-Borne Laser Scanner"

Vehicle-borne laser scanning is used to collect urban street and building data for various modeling and mapping applications. The quality of laser point-cloud data is important for regenerating 3D urban street scene. Quality evaluation includes spatial structure analysis and positioning accuracy analysis. In spatial structure analysis, we evaluate the quality of point-cloud data high or low by analyzing the objectspsila spatial structure projection at each of the three coordinate axis. In positioning accuracy analysis, comparing sign pointpsila 3D coordinates collected by laser scanner with the precise coordinates collected by Total Station, we get the point-cloudpsila positioning accuracy. A new sign point was also designed to overcome the difficulty of extracting sign points coordinates from point cloud data. After the evaluation, we make a suggestion about how to improve the data quality. [C2297]

"Design and Application of In-Vehicle Terminal for Car Network System Based on ARM9"

A kind of in-vehicle terminal for car network system based on ARM9 has been researched and designed in this paper. The main hardware module of the in-vehicle terminal is introduced in detail and the hardware architecture has been presented as well. The software module and its implementation of the terminal have been explained in detail, including CAN (controller area network) bus module, GPRS (general packet radio service) module, GPS (global positioning system) module. The software system of the in-vehicle terminal is implemented, and a kind of practical package format and flow chart between the in-vehicle and the server is put forward. The implementation of the system indicates that cars are directed and controlled well through the terminal. [C2298]

"Study on the Methods of InSAR Baseline Estimation"

Baseline is an important parameter of the process of InSAR (interferometric synthetic aperture radar), which directly influences the accuracy of the ultimate DEM generated. In this paper, firstly, the relationship between positioning and deformation measure accuracy and baseline error was analyzed. Secondly, three classical baseline estimation methods, which are the method based on precise orbit data, the method based on fast Fourier transform (FFT) and the method based on control points, were compared. Meanwhile, three combination projects of baseline estimation methods with higher accuracy were also studied. Finally, an experiment was done

with the ERS1/2 image pairs located in Shandong province, and the DEM generated by three combination methods and SRTM DEM were compared. According to that, the conclusions can be obtained as follows: The baseline between two images isn't a constant value, which is changed with the variation of coordinates of the images; The accuracy of DEM generated by the last combination project is improved about 50 m than that obtained by the method based on precise orbit data. Therefore, it is proved that the combination projects of baseline estimation methods proposed in this paper are available. [C2299]

"DGPS-Supported Flight Track Processing and Direct Geo-location from High Resolution Airborne SAR Images"

During the mapping task using high-resolution airborne SAR images, the effective using of DGPS data has important influence on the final accuracy and efficiency of surveying and mapping. This paper analyzed the imaging geometric characteristics of airborne SAR system, and, under the condition of space-constant PRF imaging technique, it put forward to a kind of flight track processing method for radar sensor position correction using iteration computation supported by DGPS data. And further, it discussed the data processing flow for direct geo-location application from airborne SAR images, and utilized the test dataset in Sichan area in China to testify the relative methods. The test results showed that the methods are reliable and effective, and it can improve the research on direct geo-location from airborne SAR images as a reference method. [C2300]

"Quad Polarimetry SAR Target Recognition Based on Parametric Statistics and Multidimensional Analysis"

Diverse parameters decomposed from quad-polarimetric SAR could become the important basis in target recognition, classification and other applications. During the target recognition, due to the sidedness of single parameter or two parameters decomposed by same algorithm, obvious differences exist among the results extracted by different parameters. In this paper, a parametric statistics and multidimensional analysis algorithm will be applied in target recognition from quad-polarimetric SAR image. The proposed algorithm looked the backscattering characters of land cover targets as the basis of analysis. Through parametric statistics, the dominant scattering mechanisms of every decomposing algorithm would be picked out such as volume scattering and sphere scattering of paddy. They become the data of multi dimensional analysis. In the multi-dimensional analysis, the target's location of parametric space will be the basis of target recognition. The application on land cover and land use by the proposed algorithm improved the monitoring capability of quad polarimetric SAR. [C2301]

"Land-Based Scatterometer Measurements and Retrieval of Surface Parameters Using Neural Networks"

In this study, a multi-band FM-CW land-based scatterometer is used to measure the backscattering coefficient of bare soil surface. And then combined with the neural network which can be simulated in any nonlinear problem in theory, and integrated equation model (IEM) which has a wide range of surface roughness, has realized all of the surface parameters inversion through the theoretical simulation and the experimental data, including dielectric constant, surface rms high and correlation length. The results have a better consistency with the actual measurement parameters, and the difference among different angles inversion results reflects the uneven characteristics of reality surface. Final shows that retrieval of multi-parameter using neural networks to be effective, at the same time that simultaneous measurement of backscattering coefficient and surface parameter is a effective means that study features of microwave scattering. [C2302]

"Analysis of Quantitative Estimation of Precipitation Using Different Algorithms with Doppler Radar Data"

By means of the Doppler radar measurements and automatic precipitation station data collected in the Linyi district, Shandong Province, improved genetic algorithm (IGA) and the optimization method (OM) were employed to determine the relation between radar echo intensity and precipitation intensity. The evaluation of the Z-R relation from IGA and OM are compared and analyzed with that of the empirical Z-R relation. The result show that IGA yielded the better estimations and was used to estimate the regional precipitation. For regional rainfall estimation, it is found from IGA that the spatial distribution were in good accordance with rain-gauge network, but the difference appeared in intense rainfall location centers, with the mean relative error of 43.8%. After adjustments by using rain-gauge networks, radar rainfall estimations were improved dramatically on precision, with the mean relative error of the average adjustment, rain-gauge adjustment, Kalman filter, 14.5%, 10.2% and 7.9% respectively. [C2303]

"Application of Back-Propagation Neural Network to Estimate Precipitation with Doppler Radar in Yishuhe Watershed of China"

By means of the Doppler radar measurements and automatic precipitation station data collected during four precipitation processes of 2005 in the Yishuhe Watershed, the back-propagation neural network (BPNN) based on BFGS algorithm is used to train and estimate the rainfall. Reflectivity (Z) and rain intensity (R) relation are determined by an improved window probability matching method and used to verify and evaluate the precision of BPNN. The results suggested that the precision from BPNN is higher than from Z-R relation, especially in intensified rainfall process. The hourly rainfall and total accumulations of BPNN is in good consistence with rain gauge observation in intensified process and exists some extent overestimation in medium intensified process. Rainfall estimation of Z-R relation would yield underestimation of different degree with the change of rainfall intensity, the more underestimation, the more intensified rainfall process. [C2304]

"Typical Ocean Features Detection in SAR Images"

Ocean features such as internal waves and eddies become visible on radar images because they are associated with a variable surface current which modulates the sea surface roughness and thus the backscattered radar power. This paper propose a new algorithm to detect typical ocean features namely the internal waves, the ocean fronts, the ocean eddies and the wind waves in the SAR images with two dimensional continuous wavelet. Experimental Results show that this method is very effective in the localization of various ocean features. [C2305]

"MAGIC: MAP-Guided Ice Classification system for operational analysis"

A map-guided ice classification (MAGIC) system that aims at effectively interpreting SAR sea ice images using the associated ice charts in an operational environment is presented. As an ongoing project, MAGIC version 1.0 has been developed using operational SAR image data from the Canadian ice service (CIS). MAGIC is intended to not only be used for SAR sea ice classification research and development, but also used for classification research of generic digital imagery using the available fundamental and advanced algorithms. At some point, we hope to make the system freely available. [C2306]

"Western Massachusetts Off-the-Grid Radar Technology Testbed"

Distributed networks of short-range radars offer the potential to observe winds and rainfall at high spatial resolution in volumes of the troposphere that are unobserved by today's longrange weather radars. One class of potential distributed radar network designs includes Off-the-Grid (OTG) weather radar networks. These are short-range radar nodes designed to be deployed as part of an ad-hoc network and to limit their reliance on existing infrastructure. Independence of the wired infrastructure (power or communications) would allow OTG networks to be deployed in specific regions where sensing needs are greatest, such as mountain valleys prone to flash-flooding, geographic regions where the infrastructure is susceptible to failure, and underdeveloped regions lacking urban infrastructure. This paper will present an OTG network testbed being deployed in Western Massachusetts to support experimentation with OTG nodes. This testbed will focus on the energy performance of the OTG network and the virtualization of the radar sensor. [C2307]

"Phase-Tilt Array Antenna Design for Dense Distributed Radar Networks for Weather Sensing"

This paper describes the design of a dual-polarized microstrip series-fed linear array as part of the phase-tilt active planar array antenna being designed for weather sensing for the CASA Engineering Research Center. The dual-polarized planar array antenna is composed of 64 linear array columns, each one formed by 32 aperture coupled patch antenna elements in cascade and excited by a 2 W solid state transmit and receive (TR) module. A straightforward synthesis method is used in order to achieve the desired amplitude and phase excitation of each linear array. Radiation patterns computed using method of moments (MoM) and measured in a compact range system are presented in order to validate the synthesis method proposed. [C2308]

"Development of Scan Strategy for Dual Doppler Retrieval in a Networked Radar System"

The NSF engineering research center for Collaborative and Adaptive Sensing of the Atmosphere has developed a networked weather radar test-bed to monitor and respond to severe thunderstorms and severe wind. For acquisition of radar reflectivity and other scalar fields, each radar is an independent unit and only the radar range equation is of primary concern. However, with respect to the acquisition of wind velocity, pairs or triplets of radar need to be considered as units and the perspective observation angles are of primary concern, besides the constraint in range. Multiple candidate pairs exist for most of the test-bed coverage and choice has to be made in scan strategy. In addition, the whole network is required to update the observations within a finite time period.

This further limits the number of sweeps depending on the sector width to be scanned. All these constraints are consolidated together in generating the scan strategy based on the best dual-Doppler pair. In this paper, the method to generate dual Doppler scan strategy is presented. The method is tested in field experiments for scan evaluation and the results are presented. [C2309]

"Real-time implementation of the network-based reflectivity retrieval for CASA"

The first generation testbed of the Center for Collaborative Adaptive Sensing of the Atmosphere (CASA-IP1) is currently operational in Oklahoma. The CASA-IP1 system is a radar network observing a weather event simultaneously by four radars. Within the CASA, a network-based reflectivity retrieval technique has been developed and evaluated extensively. This paper presents the evaluation of the network-based reflectivity retrieval by comparing retrieval results using CASA-IP1 data with WSR-88D observations. This paper also describes the design and implementation of an architectural framework for real-time processing of the network-based retrieval algorithm. Experimental results show that the implementation meets the real-time requirement of CASA. [C2310]

"Early Results using Single-Pass L-band Pol-InSAR"

The extraction of bio-and geophysical parameters by means of Pol-InSAR has gained a lot of interest in recent years. In particular, the exploitation of full quad-pol mode long wave-length (L-and P-band) data in combination with advanced theoretical models like the Random-Volume-over-Ground (RVoG) model has successfully been used to derive quantities like ground topography or tree height with impressive accuracy. However, to date all experiments (airborne and spaceborne) have been conducted in repeat-pass interferometry mode and thus, results have been suffering from two major limitations: temporal decorrelation and, in the airborne case, uncompensated motion errors. Both error sources can significantly reduce the usability of the acquired data, which is of importance especially if operational mapping of large areas is being considered. This paper reports about first experiments with a single-pass airborne L-band quad-pol interferometer that has been implemented on Intermap's TopoSAR platform. [C2311]

"Sar Interferometry For Estimating Above-Ground Biomass Of Savanna Woodlands In Belize"

Tropical savannas cover 20% of the Earth's land surface and are important ecosystems in the global Carbon cycle due to their high productivity. This paper evaluates the capability of different shortwave synthetic aperture radar interferometry (InSAR) data for estimating above-ground biomass of the woody vegetation in heterogeneous tropical savanna woodland in Belize, Central America. Single-pass InSAR data used are X-band (Intermap) and C-band (AIRSAR and SRTM). Results show that retrieved canopy heights from both X- and C-band InSAR are indicative of general patterns of tree height, but the details remain inaccurate due to the heterogeneity of the canopy. Scattering phase centers for C-band are generally higher than for X-band over sparse woodlands, whereas dense tropical forest areas yield higher X-band scattering phase centers. [C2312]

"Real-Time Refractivity Retrieval using the Magnetron-based CASA X-band Radar Network During the Spring 2008 Campaign"

A real-time refractivity retrieval platform for the CASA IP-1 [1] testbed is currently being developed at the University of Oklahoma. From our previous efforts in the 2007-2008 KTLX/KFDR refractivity experiment [2], a software module to produce refractivity products has been developed and is ported over to the IP-1 testbed this year. One of the challenges for refractivity using the IP-1 radars is the use of X-band systems, which results in more rapid phase wrapping across ranges. In this work, a theoretical explanation will be presented to show that X-band is not a limiting factor to refractivity retrieval. Another significant challenge is the use of magnetron-based transmitter, which changes the effective wavelength being applied for measuring the propagation phase. This question remains open but it will be shown that through the use of differential refractivity technique, scan-to-scan refractivity can still be useful in practice. [C2313]

"Classification of Polarimetric SAR Images using the Degree of Polarization and the Co-Polarized Phase Difference"

A new polarimetric SAR image classification technique based on the degree of polarization (DoP) and the co-polarized phase-difference (CPD) is presented in this paper. Since the DoP and the CPD of a scattered wave provide information on the randomness of the scattering and the type of scattering mechanisms, at first, the statistics of the DoP and CPD are examined with measured polarimetric SAR image data. Then, a DoP-CPD diagram with appropriate boundaries between six different classes is developed based on the SAR image. The classification results are compared with the existing Entropy-alpha diagram as well as the JPL-AirSAR

polarimetric data. The technique may have capability to classify an SAR image into six major classes; a bare surface, a village, a crown-layer short vegetation canopy, a trunk-layer short vegetation canopy, a crown-layer forest, and a trunk-dominated forest. [C2314]

"Analysis of WindSat Data over Arctic Sea Ice"

The radiation of the 3rd and 4th Stokes components emitted by Arctic sea ice and observed by the spaceborne fully polarimetric radiometer WindSat is investigated. Two types of analysis are carried out, spatial (maps of different quadrants of azimuth look angles) and temporal (time series of daily averages over small selected ranges of azimuth angles). The 3rd Stokes component at 37 GHz has shown the highest signal during early summer (Gt2 K). The next highest signals were observed at the 10.7 GHz 3rd and 4th Stokes components during the summer months (Gt1 K). The 37 GHz 4th Stokes component has shown the least variability (Lt1 K). The 10.7 GHz 4th Stokes component has higher signal at the ice edge, confirmed from the sea ice concentration maps derived from Advanced Microwave Scanning Radiometer (AMSR-E) data, and similar to signals observed over global coastlines. From the comparison with near surface air temperature of the European Center for Medium-Range Weather Forecasts (ECMWF) model data and Scanning Multichannel Microwave/Imager (SSM/I) NASA Team ice concentrations it was concluded that the microphysical processes during early melting in the topmost sea ice layers are responsible for the high 37 GHz 3rd Stokes signal. [C2315]

"TerraSAR-X/SPOT-5 Fused Images for Supervised Land Cover Classification"

This paper reports the study of supervised neural network algorithm for classification purposes. SPOT 5 and TerraSAR-X dataset are analyzed. Classification results are critically discussed and compared to ground truth map and unsupervised neural classification of the same area. The aim is to demonstrate the capability of neural networks in managing heterogeneous dataset and the accuracy improvement obtained by the use of the textural object based layers fused with the optical and radar data. [C2316]

"A Markov Chain CFAR Detector for Polarimetric Data using Adaptive Linear Discriminant Analysis"

The paper proposes a new Markov chain based CFAR detector for polarimetric data using adaptive linear discriminant analysis. The Markov Chain based CFAR detector extends traditional PDF based CFAR detection to first-order Markov chain model by considering both correlation between neighboring pixels and PDF information in CFAR detection. With the additional correlation information, the proposed approach results in advancing the performance of conventional CFAR detectors. Moreover, to take advantage of full polarizations of polarimetric data, the new polarimetric detector utilizes complementary features from full polarizations for target detection using adaptive Fisher linear discriminant analysis. Our experimental results both show the superiority of the new Markov chain polarimetric CFAR detector over conventional CFAR detectors. [C2317]

"Anisotropic Rotation Invariant Built-Up Presence Index: Applications to SAR Data"

The results shown in this paper highlight the usefulness of a recently proposed index to extract hints of built-up areas in remotely sensed images. The novelty of this work is in the application of the approach to a very different data set than the one for which the index was originally developed, i.e. SAR instead of optical data. Due to the different approaches (active vs. passive sensors), wavelengths (optical vs. microwave) and distortion/noise effects (additive vs. speckle noise), it is valuable to find out the advantages and limits of the index results on these new data sets. Moreover, due to the different geometry of acquisition for radar sensors, two different implementations of the same index are considered and compared, adding insights on the suitability of slant-range vs. ground-range analysis of SAR data for built-up area recognition. [C2318]

"Segmentation of Polarimetric SAR Data based on the Fisher Distribution for Texture Modeling"

The Polarimetric Synthetic Aperture Radar (PolSAR) covariance matrix is generally modeled by a complex Wishart distribution. For textured scenes, the product model is used and the texture component is often modeled by a Gamma distribution. In this paper, authors propose to use the Fisher distribution for texture modeling. From a Fisher distributed texture component, we derive the distribution of the complex covariance matrix and we propose to implement the KummerU distribution in a hierarchical segmentation and a hierarchical clustering algorithm. Segmentation and classification results are shown on synthetic images and on ESAR L-band PolSAR data over the Oberpfaffenhofen test-site. [C2319]

"Enhanced Military Target Discrimination using Active and Passive Polarimetric Imagery"

Surveillance operations often make use of electro-optic (EO) imaging systems to detect civilian and military targets. To increase the overall target detection performance, such active/passive EO sensors could exploit the

polarization of light as additional information to discriminate man made objects against different backgrounds. The target contrast enhancement obtained by analyzing the polarization of the reflected light from either a direct polarized laser source as encountered in active imagers, or from natural ambient illumination, can be used for such target discrimination scheme. This paper reports results from field experiments exploiting polarization-based imaging sensors to enhance the detection of man made objects. Active and passive polarimetric signatures of objects have been acquired at wavelengths in the near and long-wave infrared bands. Results demonstrate to what extent and under which illumination and environmental conditions the exploitation of active/passive polarimetric images is suitable to enable target discrimination. [C2320]

"Mobile X- to Ku-band Scatterometer in Support of the CoRe-H2O Mission"

Information on snow coverage, structure, and liquid water content are important for many applications including avalanche warning, numerical weather prognosis (NWP), and snow pack water storage estimate. Active microwave remote sensing from space has an excellent potential to address these needs. However, the current generation of C-band SAR satellite systems are not well suited for snow related applications because of the small impact of the dry snow cover on the backscattering signal at 5.3 GHz. In order to be more sensitive to snow properties the envisaged ESA CoReH2O mission proposes a dual-frequency radar operating at 9 and 18 GHz (X- and Ku-band). In support of this mission, a ground based 9 to 18 GHz scatterometer is being developed to help to address the lack of simultaneous backscatter information of snow in this frequency range. We are also preparing a dedicated field campaign in the Swiss Alps to evaluate the performance of the system and acquire first data. [C2321]

"ASCAT Scatterometer Ocean Calibration"

A new scatterometer, the so-called Advanced scatterometer (ASCAT), onboard MetOp-A satellite was successfully launched on October 19 2006. During the commissioning phase one of the main goals is to accurately calibrate the instrument. The radar backscatter has been calibrated using three ground-based transponders in February 2008. Calibration of the ASCAT retrieved winds over the ocean is done by comparing the backscatter measurement with backscatter values derived from collocated NWP winds. Using calibration corrections, ASCAT winds are produced routinely at KNMI since March 2007 as the first MetOp-A geophysical product. Ocean calibration results and scatterometer wind speed statistics show that the Ocean and Sea Ice Satellite Application Facility (OSISAF) wind product is of high quality. [C2322]

"Pulse Compression with Very Low Sidelobes in a Spaceborne Weather Radar"

Pulse compression with very low sidelobes is one of challenges in the design of spaceborne weather radar. To detect the weak echoes of clouds occurring near the strong echoes of sea surface, sidelobe performance below -60 db is needed in the pulse compression system. Based on the traditional ways of pulse compression, double Kaiser Windows are applied here for sidelobe suppression and the Peak Sidelobe Level (PSL) can reach -75 db. To avoid power and SNR loss, the time domain Kaiser Window weighted on transmitter was replaced by the frequency domain window weighted on receiver equally. A real time signal processor and digital predistortion method based on successive overrelaxation (SOR) arithmetic is carried out. It can be used for verifying the arithmetic and modifying the nonlinear and noise character of the system. [C2323]

"Retrieval of Reflected Direct Broadcast Satellite (DBS) Signals for Earth Science Applications"

This paper presents the results of a pilot study that provides an initial assessment of the applicability of reflected DBS signals for Earth remote sensing. The study uses off-the-shelf hardware and signals from a Dish Network satellite at 12 GHz (Ku-band) reflected from soil and water to characterize the power reflected from these surfaces. Power levels directly from the satellite are compared to the power levels obtained from reflections from the soil and water. It is shown that the power reflected from water reaches 54 % of the direct power. Conversely, the power reflected from the soil is shown to be within the noise floor of the off-the-shelf hardware. The high DBS reflected power from water, much stronger than that found in the already successful use of reflected GPS, gives rise to high expectations for oceanographic remote sensing applications. [C2324]

"Analysis of Antarctic Iceberg and Sea Ice Melting Patterns using QuikSCAT"

QuikSCAT tracking of Antarctic icebergs is discussed, and iceberg movement trends are illustrated. Iceberg melting factors are explored and a backscatter time-series is presented. Interactions between ice-berg and sea ice are examined using QuikSCAT data. To improve QuikSCAT sea ice mapping capability, a threshold algorithm to detect polynyas is developed. The 2006-2007 Antarctic ablation season is analyzed and correlations between polynya formation and sea ice melting are explored. General sea ice melting patterns are discussed, and statistics are derived from QuikSCAT's life mission and compared with SSM/I measurements. This study finds

that while average Antarctic sea ice coverage is increasing, minimum sea ice extent is decreasing. [C2325]

"Autonomous Registration of LiDAR Data to Single Aerial Image"

This paper proposes the use of phase correlation for the automatic registration of light detection and ranging (LiDAR) data and aerial imagery. First, buildings existent in the LiDAR data and aerial imagery are detected. Then the LiDAR data is interpolated to fixed point spacings, producing both a range image and a building binary mask. In the range image the pixel intensities correspond to the terrain's elevation and in the building mask the bright pixels correspond to buildings and dark pixels to everything else. A building binary mask is also produced from buildings detected in a corresponding aerial image. The Fourier transforms and the log polar Fourier transforms of both building binary masks are computed. Phase components are correlated and their peaks reveal the translation, rotation and scaling geometric transformation parameters. Results with real data are presented. [C2326]

"SWIM: A Multi-Incidence Beams Ku-band Real Aperture Radar for the Observation of the Ocean Wave Field Spectra"

The instrument SWIM (Surface Waves Investigation and Monitoring) on the CFOSAT (Chinese French Oceanographic Satellite) project aims at measuring the directional spectra of ocean waves on a 180 km wide swath. Orbiting on a 500 km sun-synchronous orbit, it provides with a global full coverage of the oceans between -80 and 80deg. It consists in a real aperture radar (RAR) operating in Ku-band (13.575 GHz) on 6 distinct beams pointing at incidence angles from 0deg (nadir) to 10deg, while scanning the whole azimuth angles (0-360deg). The nadir beam is similar to the one provided by a standard altimeter. Its main objective is to measure the significant wave height and wind speed (from the measurement of the radar cross section). Radar cross-sections are also estimated from 2 to 10deg off-nadir observations, then ensuring the access to profiles dependence with incidence and azimuth angles. Appropriate processes of observations at 4 to 10deg incidence provide with an estimate of the spectral properties of the local wave field. [C2327]

"Forest Vertical Structure Estimation using Coherence Tomography"

In this paper we introduce a new algorithm for radar estimation of the vertical structure of vegetated land surfaces. The algorithm is based on a low frequency 3-D image reconstruction using polarization coherence tomography or PCT. We first summarize the technique, present a new method for selecting the optimum interferometric baseline and then apply it to airborne P and X-Band data from the DLR E-SAR system. We conclude by assessing the potential of the technique for providing improved global and regional forestry products using space-borne radar remote sensing. [C2328]

"Compact Polarimetry Mode for a Low Frequency SAR in Space"

In spaceborne SAR, a single-polarisation on transmit has, over full polarisation, the vast advantage of a double swath due to SAR system design issues. Without getting into the technical details deserving by themselves a full paper, we can just mention the swath characteristics of ALOS PALSAR, reducing from 70km for dual-pol mode to 30 km for full-polarisation mode. The options chosen up to now for dual-pol system designs (or single-polarisation on transmit) rely on a linear polarisation on transmit, with two orthogonal polarisations on receive. In an earlier paper, we proposed a more pertinent alternative for the selection of the transmit polarisation leading to a better characterisation of the scattering mechanisms [1,2]. This mode is called the iquest/2 CP mode, in reference to the transmit polarisation being circular. At low frequency, where the ionosphere has a significant effect, the circular transmit polarisation is the only sensible option as it provides an effective constant polarisation as seen by the scattering surface. This is an essential condition for a meaningful multi-temporal analysis. In this paper, the analysis is pursued in more depth by including the effect of the ionosphere on the wave propagation, exploring both the POLSAR and PolInSAR applications and investigating procedure to estimate the Faraday rotation from the CP data. [C2329]

"Temporal Decorrelation for Forested Areas Observed in Spaceborne L-band SAR Interferometry"

Interferometric coherence from nine image pairs acquired by the Japanese satellite ALOS over a forest area in northern Sweden have been analyzed. Coherence levels for sparse and dense forest are compared. The results are in line with previous studies for JERS-1 and confirm that in most cases the temporal decorrelation is a severe problem for L-band SAR with repeat cycles on the order of six weeks. However, frozen conditions can give relatively high coherence for sparse forest and thereby allow good separation between dense and sparse forest. [C2330]

"Small Perturbation Method for Scattering From Rough Multilayers"

In this paper, we present an elegant closed form solution obtained applying perturbation theory to three-dimensional layered structures with an arbitrary number of rough interfaces. A general method has been developed to treat layered structures that can be described by small changes with respect to an idealized (unperturbed) structure, whose associated problem is exactly solvable. The final expression, beyond the compactness, allows us to directly prove that our formulation satisfies the reciprocity principle. [C2331]

"SAR Imaging Simulation for an Inhomogeneous Undulated Lunar Surface based on Triangulated Irregular Network"

Based on the statistics of the lunar cratered terrain, e.g. population, dimension and shape of craters, the terrain feature of cratered lunar surface is numerically generated. According to inhomogeneous distribution of the lunar surface slope, the triangulated irregular network is employed to make the digital elevation of lunar surface model. The Kirchhoff approximation of rough surface scattering is then applied to simulation of lunar surface scattering. The synthetic aperture radar (SAR) image for comprehensive cratered lunar surfaces is numerically generated. Making use of the digital elevation and Clementine UVVIS data at Apollo 15 landing site as the ground truth, an SAR image at Apollo 15 landing site is simulated. [C2332]

"Scattering from a Scatterer Near a Large Random Rough Surface with the Extended PILE Method"

In this paper, the scattering from two homogeneous scatterers embedded in a homogeneous medium is investigated by using an efficient rigorous method based on the method of moments, published by N. Dechamps and recently extended by G. Kubicki, and referred as to E-PILE (extended propagation-inside-layer-expansion). This method is applied for a circular cylinder near (above or below) a one-dimensional (1-D) rough surface, and for a stack of two 1-D rough surfaces separating homogeneous media. In addition, to decrease its complexity, the forward-backward spectral acceleration of Chou and Johnson is applied to calculate the local interactions on the rough surface(s). [C2333]

"Amplitude and Phase Statistics for Bistatic Scattering from Rough Surfaces"

In this paper we study the statistical characteristics of scattering from rough surfaces. By assuming normal-distributed and correlated real and imaginary scattering components, we derive analytical probability density functions (pdfs) for the amplitude and phase. The amplitude pdf is in the form of an infinite sum of modified Bessel functions while the phase pdf is expressed in terms of the error function. The analytical amplitude and phase distributions are verified by comparing with both the empirical distributions of simulated data and experimental measurements. Simulated data sets are derived from Monte Carlo simulations of bistatic scattering from ocean-like rough surfaces. Experimental data were collected from monostatic measurements conducted at a wind-roughened reservoir with an S-band polarimetric radar. These simulated and experimental results show that the amplitude and phase pdfs vary with wind speed, observation angle, and polarization. The TM wave is observed to have a wider amplitude distribution than a TE wave. The phase of the scattered field is not uniformly distributed, especially under the low wind condition. The analytical amplitude and phase distributions are in good agreement with the empirical distributions of both simulated and experimental data sets. [C2334]

"Comparison of Polarimetric Change Detection Methods on ALOS PALSAR Images over Finland"

Six polarimetric change detection indices were tested on L band ALOS PALSAR data over Kuortane, Finland. Tests included quantitative evaluation of change indices compared to reference change maps, and qualitative evaluation by visual inspection. Results suggest an additional accuracy using fully polarimetric data in change detection. Contrast Ratio and the Wishart test gave the best results among the tested indices. [C2335]

"Improvement of Earthquake Prediction by using Global Signal Elimination from Environmental Electromagnetic Signals"

Anomalous environmental electromagnetic (EM) radiation waves have been reported as the portents of earthquakes. We have been measuring the Extremely Low Frequency (ELF) range all over Japan. Our goal is to predict earthquakes using EM radiation waves. Previously, we proposed a method of detecting anomalous signals by focusing on linear prediction errors. However, this method also sensitively responds to earthquake-unrelated anomaly. For accurate earthquake-prediction, we should eliminate earthquake-unrelated signals. In this paper, we try to reduce false detection rate by global signal elimination using Non-negative Matrix Factorization (NMF) and evaluate the effectiveness of this method. [C2336]

"Validation of Multilayered Cloud Properties using A-Train Satellite Measurements"

Multilayered clouds are a common, very important component in the atmosphere, affecting both the radiation budget and hydrological cycles. Accurate characterization of the vertical and horizontal distribution of clouds and their properties is essential for simulating the role of clouds in weather and climate models. Several passive remote sensing methods for retrieving multilayered cloud properties have been developed, but have been difficult to validate due to the lack of observations from active sensors. The Cloud-Aerosol Lidar and Infrared Pathfinder Satellite Observations (CALIPSO) satellite and CloudSat launched in 2006 provide rich information about the vertical structure of clouds. In this study, the Aqua Moderate-Resolution Imaging Spectroradiometer (MODIS) cloud properties derived for the Clouds and the Earth's Radiant Energy System (CERES) Project merged with CALIPSO and CloudSat profile data are used to study an example set of multilayered clouds. Assuming that the lower-layer cloud properties (such as height, temperature, optical depth and liquid water path) are obtained from CloudSat, the properties of the upper cloud layer are retrieved from the multilayer cloud retrieval system (MCRS) and then validated using the observations from CALIPSO and CloudSat. [C2337]

"Development and Observation of the Ku-band Broad-Band Radar for Meteorological Application"

Hazardous weather such as severe storms, tornadoes and hurricanes are small scale weather phenomena whose detailed profiles are important practically and scientifically. Despite this, conventional radars cannot resolve them, because of their low resolution capability. In this study, we developed a new high resolution Ku-band Doppler radar with scanning capability for meteorological applications. With the new radar system design, the radar can accurately measure the radar reflectivity factor with the range resolution of 4 m and the time resolution of 1 min per 1 volume scan from the nearest range of 50 m to about 15 km for 10 W power using pulse compression technique. In this paper, the details of the system design and the signal processing algorithm are described. To demonstrate the accuracy of this system, the radar reflectivity measurements are compared with 2D-video disdrometer measurements. The initial observation results of spiral mode are also shown. [C2338]

"Investigation on Tree Height Retrieval with Polarimetric SAR Interferometry"

Polarimetric SAR interferometry (POLInSAR) has been widely applied in tree height retrieval. A refined algorithm of three-stage inversion process for polarimetric SAR interferometry is proposed in this paper. The refined algorithm focuses on resolving the ambiguity estimation of the volume coherence. The coherence region extraction algorithm is combined with the three stage inversion algorithm to obtain accurate estimate of volume decorrelation. According to the physical explanation of the scattering model of the forest area, we can conclude that the proposed algorithm can get more accurate inversion results. The proposed algorithm is applied to simulated coherent L-Band SAR data provided by ESA, and the validity of the modified algorithm is confirmed. [C2339]

"Understanding of the interaction of the radar response with the river ice cover"

The development of a theoretical model to describe the scattering mechanisms involved in the interaction of the radar signal with the fresh water ice is important, as it helps in river ice monitoring. The model used in this study is based on radiative transfer theory which is solved by Doubling Matrix Methods". This numerical method accounts for scattering effects due to the volume, boundaries, boundary-volume interactions and coupling between layers. Three ice types were formed on this river (Columnar ice, snow ice and frazil ice). This study focused mainly on two objectives. First, the understanding of the interaction of the radar signal with the different ice types formed in the river. Second, the determining the dominant scattering mechanism for the different ice types and radar configurations (frequencies and angles of incidence). [C2340]

"Combining Lidar and InSAR Observations over the Harvard and Duke Forests for Making Wide Area Maps of Vegetation Height"

In this paper, two data sets consisting of co-located full-waveform lidar and InSAR observations are discussed, one over the Duke Forest, near Durham, North Carolina, and the other, the Harvard Forest, located in Western Massachusetts. Data for the Duke forest consists of AIRSAR and GeoSAR (both airborne sensors) interferometric SAR observations spanning in frequency from X-band down to P-band, and data from the GSFC's SLICER instrument. For the Harvard Forest, spaceborne data from JAXA's ALOS/PALSAR mission is used in conjunction with GSFC's LVIS instrument. Early work with SLICER and GeoSAR data has used a lookup table approach for generating a table that correlates the InSAR observables of differential height between X-and P-band observations, and X-band correlation magnitude to lidar derived height. This table was then used for estimating heights over the remaining swath, where lidar data was not available. A similar technique can be used for spaceborne data, in this case, over the Harvard Forest. In this paper, the comparison between lidar

observations and the InSAR Duke observations are shown, and then followed by a preliminary treatment highlighting relationships in the ALOS/PALSAR Harvard data that can be exploited for similar purposes. [C2341]

"The Potential of Combined Lidar and SAR Data in Retrieving Forest Parameters using Model Analysis"

3D Lidar waveform and 3D radar backscatter models based on Radiative Transfer theory were used to simulate waveform and backscattering of various plots with different stand ages and structures, which were generated using forest growth model. The inversion models for estimating forest Above Ground Biomass (AGB) and Average Stand Height (ASH) were derived from the combined simulated database of large footprint Lidar waveforms and L-band polarimetric SAR backscattering using stepwise analysis method. The inversion procedures were then applied to NASA LVIS and ALOS PALSAR data to retrieve forest parameters for the study area. The study area is a 10km by 10km area located at International Paper's Northern Experiments Forest, Maine, USA, where field measurements that include stem coordinate, DBH, species and canopy position were recorded within a 200m by 150 m stand. Heights and AGB of total 7956 trees were estimated by applying species-specific allometric equations to stand measurements. AGB and height were then scaled up to the area according to the LVIS footprint size and location at 149 20m*20m plots, which were used to verify the inversion model developed using simulated database. The study concludes that Lidar waveform indices and SAR backscattering are complementary for forest parameters retrieving, which improved the limitation of signature saturation for regional biomass mapping using SAR data only. The comparison between inversed forest parameters and field measurements shows good consistency. [C2342]

"Automatic vehicle extraction from airborne LiDAR data of urban areas using morphological reconstruction"

In this paper, we address issues in traffic monitoring of urban areas using airborne LiDAR data. Our aim in this paper is to extract individual vehicles from common LiDAR data of urban areas, based on which the dynamical status of vehicles and other traffic-related parameters can be derived. A context-guiding bottom-up processing strategy is developed to accomplish the task. Ground level separation is first used to exclude the irrelevant objects and provide the "Region of Interest". The marker-controlled watershed transformation assisted by morphological reconstruction is then performed on the gridded and filled raster of ground level points to delineate the single vehicles. The evaluation of experimental results has shown that most vehicles can be correctly detected, whose delineated contours are accurate. [C2343]

"Combining AMSR-E and QuikSCAT image data to improve sea ice classification"

The benefits of augmenting AMSR-E image data with QuikSCAT image data for supervised sea ice classification in the Western Arctic region are investigated. Experiments compared the performance of a maximum likelihood classifier when used with the AMSR-E only data set against the combined data and examined the preferred number of features to use as well as the reliability of training data over time. Adding QuikSCAT often improves classifier accuracy in a statistically significant manner and never decreased it significantly when enough features are used. Combining these data sets is beneficial for sea ice mapping. Using all available features is recommended and training data from a specific date remains reliable within 30 days. [C2344]

"Streamline regularization for large discontinuous motion of sea ice"

Non-rigid motion has to sometimes contend with the presence of discontinuous structures when it is estimated under a non-topology preserving deformation. In this paper, we propose an algorithm that estimates large scale non-rigid motion in the presence of these discontinuous structures. We have developed a streamline regularization framework that uses particle streamlines to compute a plausible flow at discontinuities, thereby enabling us to predict the motion more accurately. To quantitatively validate the accuracy of our results, we applied the Wilcoxon Signed Rank Test, which shows an improvement in estimation accuracy using our proposed scheme. [C2345]

"Optimization algorithms in FMRF model-based segmentation for LIDAR data and co-registered bands"

In this paper, a fuzzy Markov random field (FMRF) model is used to segment land-objects into tree, grass, building, and road regions by fusing remotely sensed LIDAR data and co-registered color bands, i.e. scanned aerial color (RGB) photo and near infra-red (NIR) photo. An FMRF model is defined as a Markov random field (MRF) model in a fuzzy domain. Three optimization algorithms in the FMRF model, i.e. Lagrange multiplier (LM), iterated conditional mode (ICM), and simulated annealing (SA), are compared with respect to the computational

cost and segmentation accuracy. The results have shown that the FMRF model-based ICM algorithm balances the computational cost and segmentation accuracy in land-cover segmentation from LIDAR data and co-registered bands. [C2346]

"Applications for remote laser vibration sensing"

Laser vibrometry based on coherent detection techniques allows to measure vibration characteristics of objects due to the high Doppler resolution. Examples for applications in the field of defense and security such as target classification and identification including camouflaged or partly concealed targets as well as the detection of buried land mines are presented. [C2347]

"Automatic registration of inter-band and inter-sensor images using robust complex wavelet feature representations"

A robust method for registering inter-band and inter-sensor remote sensing images has been designed and implemented. The proposed method introduces noise-resilient and contrast invariant control point detection and control point matching schemes based on robust complex wavelet feature representations. Furthermore, an iterative refinement scheme is introduced for achieving improved control point pair localization and mapping function estimation between the images being registered. The registration accuracy of the proposed method was demonstrated on the registration of multi-spectral optical and synthetic aperture radar (SAR) images. The proposed method achieves better registration accuracy when compared with the state-of-the-art MSSD and ARRSI registration algorithms. [C2348]

"Extraction of building polygons from SAR images: Grouping and decision-level in the GESTALT System"

The GESTALT-system is a stratified architecture for challenging computer vision tasks. This contribution focuses on the 3rd and 4th layer of it-the grouping and decision layers. As example application building recognition from high resolution SAR-data is presented. The 3rd layer contains an assessment driven perceptual grouping process with any-time capability and flexible control. Important grouping principles such as good continuation and symmetry are utilized. A dynamic programming optimization is used in the final decision and post-processing layer to find closed polygons that describe the outlines of buildings. Further post processing includes polygon editing and consistency enforcement. [C2349]

"Phased Array Radar Polarimetry for Weather Sensing: Challenges and Opportunities"

It is becoming widely accepted that radar polarimetry provides accurate and informative weather measurements, while phased array technology can shorten data updating time. In this paper, a theory of phased array radar polarimetry is developed, and the relationship between the wave field at the radar antenna coordinate and that at the hydrometeors is established, along with the correction matrix to the scattering matrix. The challenges and opportunities for the weather sensing are discussed. [C2350]

"Ice Water Content Estimation in Clouds Using Radar Reflectivity and Dual-Frequency Ratio at 94 and 220 GHz"

Dual-frequency radar observables are simulated at 94 and 220 GHz frequencies for remote sensing of clouds. Their use in cloud ice water content and particle size estimation are evaluated. [C2351]

"Reflectivity and Differential Reflectivity Rainfall Algorithm Performance at X-band"

X-band weather radar systems present several advantages mainly related to their lower cost and smaller size relative to their S and C band counterparts. The main drawback of X-band is the attenuation suffered by the electromagnetic wave propagating through precipitation that reduces the reliability of rainfall estimates based on power measurements. Developments in dual-polarization techniques have provided solutions to mitigate this problem and have revived the interest on X-band radar systems for operational applications. Because of this growing interest, there is a need to evaluate the performance of X-band polarimetric radars for quantitative rainfall estimation. At X-band, attenuation affects any radar parameter based on backscatter power measurements such as Z_h , while differential attenuation affects parameters based on differential power measurement such as Z_{dr} . Consequently, Z_{band} and Z_{dr} must be corrected prior to use in quantitative applications such as rainfall estimation. However, correction procedures can introduce additional errors that impact on rain estimation and therefore must be applied with caution. When using the X-band rain algorithm based on Z_{band} and Z_{dr} , the biases due to attenuation and differential attenuation nearly cancel each other and result in a small bias of the estimated rainfall rate, so that correction of Z_{band} and Z_{dr} may not be needed. This paper investigates this

property of rain rainfall estimation based on X-band dual-polarization measurements. [C2352]

"Ground Scattering Analysis to Identify Targets for Refractivity Field Estimation"

Efforts to estimate the near-surface moisture field using weather radar returns from coherent ground targets has been successfully demonstrated in recent years. A very crucial step to make the moisture retrieval successful is the identification of appropriate targets. The estimation process also depends on adequate spatial distribution of these targets, so it is actually more important to have a good distribution than to have every target be extremely coherent. Presently, however, there is no fully automated technique to identify the targets. The currently accepted method is to manually examine phase difference scans that span approximately an hour to identify a time period where the phase gradient is approximately the same across all azimuths. Unfortunately, this is not simple and improper selection can have drastically different results. In order to design an algorithm to automate this process, one must first understand the phase behavior of ground reflections for this purpose. Previous analysis of ground returns were for the purpose of eliminating them, but the work presented here aims to identify suitable targets for refractivity estimation. [C2353]

"Requirements for Model-based Polarimetric Decompositions"

Several authors have proposed decompositions of measured polarimetric covariance matrices into the weighted sums of individual covariance matrices that represent known scattering models. In this paper we critically examine some minimum requirements that these model-based polarimetric scattering decompositions must satisfy. Starting with the definition of the covariance matrix, we show that a necessary requirement for these decompositions is that the eigenvalues of the individual covariance matrices must be non-negative. We then show with examples that this is not guaranteed for some of the proposed decompositions. Finally, we propose a method of decomposition that would ensure that the eigenvalues of the individual covariance matrices would be non-negative. [C2354]

"Effect of Forest Structure on Scattering Center Height from Model and SAR Data"

Modeling vegetation using coherent approaches has attained prominence over the past two decades. The distorted Born approximation has been known as one of the basic approaches used for coherent modeling of vegetation, in which each scatterer is illuminated by a mean field and the backscattered fields are added coherently. In some papers, Lindenmayer Systems (L-systems) were employed to generate accurate 3D tree structures. Although this method is found to be useful, it needs too many input parameters. Thus it is not suitable to retrieve forest parameters by model inversion. In this study the three-dimensional radar backscatter model of forest canopy constructed by Sun and Ranson in 1995 was modified to be a coherent model for simulation of InSAR signals. It provides a balance between the accuracy and feasibility of parameters' retrieval. The effects of incident wave length and forest stand structure on phase center heights were analyzed. The phase center heights were also compared with the phase center heights from PALSAR LHH InSAR data. It shows that the simpler coherent model described in this study gives acceptable results. [C2355]

"Radar Volume Backscatter from Spatially Extended Geophysical Targets in "Slice" Approach"

Assessment of the radar backscatter from spatially extended geophysical target (SEGT) is under consideration. The SEGT is any geophysical object which is, at least, semi transparent for radar illumination (cloud, rain, snowfall of the atmosphere, thick snow cover of a terrain). It consists of a multitude of point Rayleigh scatterers. The "slice" approach is applied, it means that particles located close to the wave front of the radar illumination produce the backscatter mainly coherently. This approach allows describing the contribution of the microphysical parameters of the scattering media to volume component of the radar cross section (RCS) more comprehensively than the incoherent approach. Known result of the incoherent approach based on summation of RCS from each scatterer takes place in particular case when the fluctuation of particle number within slices is pertaining to the Poisson law. [C2356]

"microASAR: A Small, Robust LFM-CW SAR for Operation on UAVs and Small Aircraft"

The Artemis microASAR is a flexible, robust SAR system built on the successful legacy of the BYU SAR and other BYU SAR systems. It is an LFM-CW SAR system designed for low-power operation on small, manned aircraft or UAVs. This paper describes the high-level methodology used in designing the microASAR system and contains a description of the hardware specifications. Performance projections are also calculated and presented. [C2357]

"Ray Tracing for Simulating Reflection Phenomena in SAR Images"

This paper presents an approach for using backward ray tracing for simulating radar reflectivity maps. After explaining the simulation concept which consists of three parts-modeling, sampling and image generation-two applications are presented for showing the performance of the simulator. At first reflection contributions like single or multiple bounce are simulated for a modeled building and compared to a real TerraSAR-X image. It shows how the capability of separating different bounce levels in different layers can support the interpretation of the SAR image. Afterwards reflection effects caused by quasi-perfect specular reflection are detected for another building model by means of geometrical analysis. This is thought as input for advanced Persistent Scatterer (PS) Analysis, since PS typically appear due to such reflection effects. [C2358]

"Radar Signature Analysis of Urban Structures"

Synthetic Aperture Radar (SAR) measurements of urban structures provide a challenge for data interpretation. In fact the basic mechanism of the reflection and scattering behavior has to be understood in very much detail. Theoretical models exist and can be used, but experimental data from a controlled environment are rather sparsely available. In this paper the construction of a well-defined wall structure is presented and corresponding radar measurements are illustrated. The results are discussed with respect to theoretical expectations. [C2359]

"Along Track Interferometry on Rhone River"

The Along Track Interferometry technique has been experimented on a RAMSES X band radar dataset. The concept behind ATI is to compare the phase of SAR images obtained from two receive antennas, separated in the along-track direction. This phase difference is coding the velocity of targets moving towards or away from the radar, within a mono-pass acquisition. Potential applications are numerous, nevertheless in this work we applied ATI technique to estimate river surface currents. The study areas were over the Rhone river at two locations, first one is near Beaucaire where the Rhone river has a large annual discharge rate and the second one is the Rhone estuary. This paper describes the RAMSES radar dataset that has been acquired in a dedicated flight and results obtained applying ATI technique. The surface velocity maps and profiles computed are promising, and are consistent with ground measurements that have been done simultaneously to the RAMSES radar data acquisitions. Such velocity maps could then constitute a support for hydrologists to drive numerical models and contribute to river discharge monitoring. [C2360]

"Joint Filtering of SAR Interferometric and Amplitude Data in Urban Areas by TV Minimization"

This paper investigates the use of a popular regularization model, the total variation minimization (TV), to filter SAR interferometric images (amplitude and phase data). This model is extensively used for its property of preserving edges and is therefore well adapted for urban areas. Using a TV model adapted to multi-dimensional data, we propose to do a joint filtering of phase and amplitude images. Due to the many local minima, the minimization of such a model is hard to perform. A new fast approximate discrete algorithm is presented. The filtering is applied in the framework of 3D reconstruction. Results on real images are presented. [C2361]

"4D SAR Focusing: A Tool for Improved Imaging and Monitoring of Urban Areas"

4D (space-velocity) SAR focusing is applied to real data acquired over urban areas to determine the position, in 3D, and the deformation velocity of single and double scatterers interfering, at high resolution, in the same azimuth-range pixel. We discuss the procedure required to identify the presence of stable single and double scatterers after the elevation-velocity focusing. Moreover we present a technique for the separation of time series associated with interfering scatterers to measure their possible non linear temporal deformations. [C2362]

"Change Detection for Bridges over Water in Airborne and Spaceborne SAR Data"

The main advantages of SAR are the capability of imaging large areas in short time and delivering data at any day time and under nearly all weather conditions. This is especially important for disaster management and continuous long term monitoring applications. Key elements of man-made infrastructure are bridges. Especially for bridges over water, the SAR specific side looking imaging geometry can lead to special characteristics in the image. In this paper, the possibilities of extracting bridge features like width and height from SAR data, especially for bridges over water, are discussed. The feature extraction is based on the segmentation of parallel lines in an image. An approach is presented to exploit this feature extraction for change detection. The investigations are supported by SAR simulations, and real airborne and spaceborne data are presented. [C2363]

"Comparison between SAR Atmospheric Phase Screens at 30' by Means of ERS and Envisat Data"

The permanent scatterers (PS) technique is able to estimate atmospheric artifacts that delay the SAR

interferometric phase over pointwise targets. In this work, for the first time, the atmospheric phase screen (APS) estimated with ERS data is compared to the APS retrieved with ENVISAT data at 30' time delay. The goal of the comparison is to add new insights to the phase delay that affects InSAR measurements. Preliminary but interesting real data results have been obtained over the city of Milan. [C2364]

"Laser Sounder for Global Measurement of CO₂ Concentrations in the Troposphere"

We report progress in assessing the feasibility of a new satellite-based laser-sounding instrument to measure CO₂ concentrations in the lower troposphere from space. [C2365]

"InSAR Monitoring of Permafrost Activity in the Lower Mackenzie Valley, Canada"

The region of interest is located approximately in the downstream part of the Mackenzie River, Canada. Our study focuses on guidelines to process RADARSAT-1 interferometric C-band data in a permafrost environment and monitor permafrost activity and landslide motion over 18 month period. From the interferometric method (D-InSAR) on ~100 interferograms, the main conclusions are (1) a high resolution Digital Elevation Models (DEM) and a shorter satellite revisit time intervals are essential to ensure InSAR processing accuracy for small deformations associated with permafrost activity; (2) the permafrost has sustained several changes over a year of monitoring (thaw starting during end of April-mid of May, and freezing around mid October). The deformation peak is reached in the summer time between mid of May and July (up to 15 plusmn 2 mm). This method will provide a guideline for In SAR monitoring of similar areas in permafrost environment. [C2366]

"Automatic Retrieval of Tectonic Parameters with Neural Networks and Sar Interferometry: An Assessment with Experimental Data"

A concurrent exploitation of the capabilities of neural networks and SAR interferometry is considered for the characterization of a seismic source and the estimation of its geometric parameters. This requires the generation of an appropriate number of synthetic interferograms necessary for the network training phase. After the training the network is ready to perform the inversion on new interferograms. The paper illustrates the assessment of such a methodology over a significant set of experimental data. [C2367]

"Construction of Satellite Derived PM_{2.5} Maps using the Relationship between AOD and PM_{2.5} at the Cabauw Experimental Site for Atmospheric Research (CESAR)-The Netherlands"

To acquire daily estimates of PM_{2.5} distributions based on satellite data one depends critically on a well established relation between AOD and ground level PM_{2.5}. In this study we aimed to experimentally establish the AOD-PM_{2.5} relationship for the Netherlands. For that purpose an experiment was set-up at the AERONET site Cabauw. The average PM_{2.5} concentration during this ten month study was 18 mug/ m³, which confirms that the Netherlands are characterized by a high PM burden. A first inspection of the AERONET level 1.5 (L1.5) AOD and PM_{2.5} data at Cabauw showed a low correlation between the two properties. However, after screening for cloud contamination in the AERONET L1.5 data, the correlation improved substantially. When also constraining the dataset to data points acquired around noon, the correlation between AOD and PM_{2.5} amounted to $R^2=0.6$ for situations with fair weather. This indicates that AOD data contain information about the temporal evolution of PM_{2.5}. We used lidar observations to detect residual cloud contamination in the AERONET L1.5 data. Comparison of our cloud-screened L1.5 with AERONET L2 data that became available near the end of the study showed favorable agreement. The final relation found for Cabauw is $PM_{2.5} = 124.5 \cdot AOD - 0.34$ (with PM_{2.5} in mug/m³) and is valid for fair weather conditions. The relationship determined between MODIS AOD and ground level PM_{2.5} at Cabauw is very similar to that based on the much larger dataset from the sun photometer data, after correcting for a systematic overestimation of the MODIS data of 0.05. We applied the relationship to a MODIS composite map to assess the PM_{2.5} distribution over the Netherlands for the first time based on MODIS data only. [C2368]

"PolSARpro v3.3: The Educational Toolbox for Polarimetric and Interferometric Polarimetric SAR Data Processing"

The objective of this paper is to make a review of the current status of the PolSARpro v3.3 Software (Polarimetric SAR Data Processing and Educational Toolbox), developed under contract to ESA by a consortium comprising I.E.T.R at the University of Rennes 1, AELc, DLR-HR and Dr mark Williams from Adelaide. The objective of this current project is to provide Educational Software that offers a tool for selfeducation in the field of Polarimetric SAR data analysis at University level and a comprehensive suite of functions for the scientific exploitation of fully and partially polarimetric multi-data sets and the development of applications for such data. The PolSARpro v3.3 Software establishes a foundation for the exploitation of Polarimetric techniques for

scientific developments and stimulates research and applications developments using PolSAR and PolInSAR data. [C2369]

"Leaf Area Index Estimation using Lidar and Forest Reflectance Modelling of Airborne Hyperspectral Data"

Insect-induced damages in forests are a major concern for timber production, landscape conservation and ecosystem research. Early detection methods based on remote sensing data can document the severity and spatial extent of ongoing attacks and might aid in designing mitigation measures or even prevention where necessary. In southeastern Norway, a large-scale insect defoliation of pine trees is ongoing. The larvae of the Pine sawfly *Neodiprion sertifer* create it with its mass attacks during their feeding on needles in June and July. In the winter before the attack, egg galleries are evident in the needles. This provides a test case for early detection methods and remote sensing techniques for monitoring forest health. In the context of an ongoing project on REMote sensing of FOREst health (REM-FOR) in Norway, we approach this problem by mapping leaf area index (LAI) before and after the attack in a test area (size around 20 km²). LAI is used as a proxy for the crown density, and decreasing trends not related to phenology (non-periodic) indicate defoliation. Estimates for effective LAI for two different years, 2005 and 2007, were derived using airborne laser scanning (LIDAR) calibrated with ground-based point measurements with the LAI-2000 Plant Canopy Analyzer (LI-CORreg, USA). These estimates are based on an application of the Beer-Lambert law and a threshold-based separation of laser reflections from the ground and from the canopy. We also obtained airborne high-resolution hyperspectral images (HySpexTM, Norsk Elektrooptikk, Norway) for the same reference years to investigate the spectral response of the affected forest. The set of two cameras deliver 330 different spectral channels in the wavelength range 400 to 1800 nm. The analysis might be done using advanced multivariate methods or spectral unmixing using spectral libraries. Here, it was performed using a physically-based model emphasizing geometrical and optical properties of canopies,-- the Forest Reflectance Model FRT. FRT was designed for the application to (managed) Northern European Forests and is based on conventional forest inventory data, species-dependent parametrized crown shapes, canopy LAI, needle clumping index, and needle optical properties. Here, however, we run the model in an inverse mode, by iteratively minimizing the discrepancy between measured and simulated reflectances, and predicting the LAI, keeping well-constrained parameters of the model (e.g. tree density, tree height, optical properties of needles) fixed while calibrating others (e.g. needle weight per tree, average shoot length, shoot self-shading). A set of 14 sample trees felled in 2005 further constrain the range of the calibrated parameters, excluding local model inversion minima with unrealistic parameter estimates. The LAI values predicted by the model are then compared to those obtained with airborne laser-scanning with a spatial resolution of 20 m times 20 m for the pine- dominated part of the scenes. In doing so, the spectra from each pixel (size 25 cm times 25 cm) were aggregated by calculating channel-wise median values. In effect, the modelling setup results in determining geometrical and optical properties of forest plots, trees and needles from hyperspectral images. The project data are complemented by images from a range of satellite-based sensors, including MODIS, SPOT, and Hyperion to cover larger regions and as a basis for operationalizing the approach for future insect attacks. [C2370]

"Spatial Classification of Hyperspectral Data of Dune Vegetation along the Belgian Coast"

This work evaluates a classification method, including spatial information, for dune vegetation along the Belgian coastline. The used method is a recursive supervised segmentation algorithm based on a tree-structured Markov Random Field. This technique describes a K-ary field as a sequence of binary Markov Random Fields, each of which is represented by a node in the tree. The obtained classification results were compared to results with the same data set, for a purely spectral classification and a spectral classification, followed by spatial smoothing. [C2371]

"Comparison between Multitemporal and Polarimetric SAR Data for Land Cover Classification"

The investigation focuses on the determination of the land cover type using SAR data, including single polarisation, dual polarisation and fully polarimetric data, at L-band. The analysed data set was acquired during the AgriSAR 2006 campaign by the airborne ESAR system over the Gormin agricultural site (Northeast Germany). The multitemporal acquisitions significantly improve the classification results for single and dual polarization configurations. The best results for the single and dual polarization configurations are better than for the polarimetric mode. Overall, the cross-polarisation configuration provides the best results. [C2372]

"Monitoring Sea Level by Radar Altimeter and CGPS in the North-Western Mediterranean"

Sea level is an environmental variable which is widely recognised as being important in many scientific disciplines as a control parameter for coastal dynamical processes or climate processes in the coupled

atmosphere-ocean systems, as well as engineering applications. A major source of sea-level data are the national networks of coastal tide gauges, in Spain belonging to different institutions as the Instituto Geografico Nacional (IGN), Puertos del Estado (PE), Instituto Hidrografico de la Marina (IHM), etc. Three Spanish sites for monitoring sea level are located in Ibiza island, l'Estartit and Barcelona. L'Estartit tide gauge is a classical floating tide gauge set up in l'Estartit harbour (NE Spain) in 1990. Data are taken in graphics registers from which each two hours the mean value is recorded in an electronic support and delivered to the Permanent Service for Mean Sea level (PSMSL). Periodic surveying campaigns along the year are carried out for monitoring possible vertical movement of the geodetic benchmark adjacent to the tide gauge. In the framework of a Spanish Space Project, the instrumentation of sea level measurements has been improved by providing the Barcelona site with a radar tide gauge and with a continuous GPS station nearby. The radar tide gauge is a Datamar 3000C device and a Thales Navigation Internet- Enabled GPS Continuous Geodetic Reference Station (iCGRS) with a choke ring antenna. It is intended that the overall system will constitute a CGPS Station of the ESEAS (European Sea Level) and TIGA (GPS Tide Gauge Benchmark Monitoring) networks. Puertos del Estado (Spanish Harbours) installed the tide gauge station at Ibiza harbour in January 2003. The station belongs to the REDMAR network, composed at this moment by 21 stations distributed along the whole Spanish waters, including also the Canary islands (<http://www.puertos.es>). The tide gauge also belongs to the ESEAS (European Sea Level) network. Also it has a radar tide gauge at Barcelona--harbour. A description of the actual infrastructure at Ibiza, l'Estartit and Barcelona is presented and its applications to sea level monitoring and altimeter calibration in support of the main CGPS at Ibiza harbour. Three Begur Cape experiences on radar altimeter calibration and marine geoid mapping were made on 1999, 2000 and 2002. One campaign was also made in June 2003 at the Ibiza island area. GPS buoys and GPS catamaran were used. We present a synthesis of the sea level results obtained from TOPEX/POSEIDON and JASON-1 altimeter calibration campaigns using the direct measurements from GPS buoys and the derived marine geoid. The main objective of the marine campaigns is to check the value of Ibiza Island as a permanent calibration site in the western Mediterranean Sea, to complement the Corsica site in the network of altimeter calibration sites. Now there is preparation for a new Ibiza/Cape of Begur altimeter calibration campaign after launch of JASON-2 at the Vanderbergh site scheduled on June 20, 2008. [C2373]

"Analysis and Processing of Spaceborne/Airborne Bistatic SAR Data"

This paper concentrates on the bistatic SAR (BiSAR) signal processing for the spaceborne/airborne hybrid bistatic configuration. A bistatic SAR experiment based on this hybrid configuration is being planned in cooperation with FGAN/FHR and DLR. Due to the extreme differences of the platform's velocities and altitudes, the spaceborne system works in the sliding spotlight mode, while the airborne system operates in the inverse sliding spotlight mode. In this paper, our previous work (i.e. ISFT) is applied to focus the hybrid bistatic SAR data based on the extended Loffeld's Bistatic Formula (ELBF). [C2374]

"Microwave Scattering Profiles of a Rice Sample by Means of Polarization Coherence Tomography"

In this work we have applied the polarization coherence tomography (PCT) to indoor data acquired on a rice sample. Different baselines, frequency bands and polarimetric channels have been used in order to analyze the potential of this technique for retrieving information about the vertical structure of such a specific crop and, additionally, these observations have been also used for studying the validity of the RVoG and OVoG models. Results obtained show that the PCT profiles exhibit no dependence on polarization, which is in agreement with the clustering effect observed on PolInSAR observables, i.e. coherences for different polarimetric channels are located very close one to another. In the dual-baseline case, the best profile reconstruction is obtained for the highest baseline ratio available (0.25deg and 1deg baselines) when the condition number of the inversion problem is improved by filtering out the fifth coefficient of the Legendre-Fourier expansion. Differences on the reconstructed profiles between linear and Pauli basis are negligible. The application of the triple-and four-baseline approaches without filtering out the last terms of the expansion leads to unstable results, whereas the filtered cases reveal that the contribution of a fourth baseline is null. [C2375]

"InSAR Phase Unwrapping based on a Combination of Markov Random Fields and Hypergeometric Phase Pdf Models"

In this paper, we propose a new Bayesian estimation-based algorithm for two dimensional phase unwrapping of discontinuous phase fields with noisy principal values. The proposed algorithm uses the Markov random field models to build the prior distribution, so the unwrapping problem became equivalent to a minimization of an energy function. Our main contribution in this work is to propose a modification to the classical quadratic potential function, which enforces a global smoothness condition, so that the phase jumps, which result from the phase discontinuities, contribution to the energy are mitigated. This was possible throw weighting the classical

quadratic potential function by the probability of occurrence of these jumps which decrease when they increase. Theoretically, this probability follows an hypergeometric distribution which can be approximated as a Gaussian one in order to make easier mathematical manipulations. An analytical expression for the minimization automate was derived. [C2376]

"Soil Moisture Estimation in time with D-InSAR"

This paper explores the potential to estimate soil moisture in the presence of vegetation using differential SAR interferometry and polarimetry. It is well known that a change in soil moisture changes the penetration depth of the electromagnetic wave, hence inducing an "artificial" change in the observed phase center. The presence of vegetation, or the vegetation vitality itself, can also affect the location of the observed phase center. Finally, a change in the polarimetric signature of the scatterer can also induce a phase center change. The purpose of this paper is to make a first study concerning the possibility to separate those contributions using differential SAR interferometry together with SAR polarimetry. Exemplary results are shown with data acquired by the airborne E-SAR system of DLR in the frame of the AGRISAR campaign. [C2377]

"Small Temporal Baseline Subset (STBAS): A New InSAR Technique for Multi-Temporal Monitoring Wetland's Water Level Changes"

Interferometric synthetic aperture radar (InSAR) techniques can successfully detect phase variations related to the water level changes in wetlands and produce high spatial resolution maps of water level changes. We present a new InSAR technique, termed small temporal baseline subset (STBAS), for monitoring not relative but absolute water levels and their variations with time (time series) using successive radar observations over wetlands. Our approach follows the small baseline subset (SBAS) used for monitoring displacement time series of solid earth surfaces. The new STBAS algorithm utilizes highly coherent interferometric phases obtained only with relatively short time difference regardless of spatial baseline. We tested the STBAS technique with two year long Radarsat-1 data acquired over a small section of the Everglades wetlands in south Florida (USA). Our study uses ground-based stage (water level) data for calibration and validation, which indicate a good fit between the InSAR the stage data. The new STBAS technique can transform relative wetland InSAR observations to absolute frame and generates both detailed maps of water levels, as well as water level time series for almost each pixel (50 m resolution). [C2378]

"A new bistatic-based sparse linear array 3D imaging SAR model"

A bistatic-based sparse linear array three dimensional (3D) imaging SAR (BSLASAR) is demonstrated and its resolution characteristic are analyzed in this paper. First, the principle of the BSLASAR is presented, the echo model is build and the imaging condition of BSLASAR is derived. The 3D BP (back projection) algorithm is introduced to focus the 3D SAR data. Then 3D PSF is analyzed, and the 3D spatial resolution expressions of BSLASAR are obtained. It is proved that the 2D horizontal PSF can be decomposed into two independent 1D PSF, the along track (AT) PSF and the cross track (CT) PSF, when the linear array direction is perpendicular to the AT direction. Compared to other configurations, this system inherits the advantages of conventional bistatic SAR and has these additional advantages: the receiver antenna phase center (APC) control precise is more flexibility than the curved SAR (CSAR), the hardware expenditure is saved and the couples between the elements are avoided. [C2379]

"An Approach for Mapping Frozen Soil of Agricultural Land under Snow Cover using RADARSAT-1 and RADARSAT-2"

A frozen soil map is a key tool to assess environmental impacts of agricultural practices on water quality, because the frost penetration in the ground has a direct impact on runoff and nutrient losses at spring melt in Eastern Canada. SAR images data have a great potential to provide this information due to there sensibility to the soil dielectric properties. The goal of this study is to develop a classification model by analyzing interactions between the different parameters resulting from insitu field data and SAR images under snow cover and to produce frozen soil maps at watershed scale. Two issues will be tackled, the mapping of frozen soil using RADARSAT-1 images and the polarimetric scattering mechanisms generated by frozen/unfrozen soil status. In this paper we present some initial results of polarimetric radar measurements using the C-band Convair-580 SAR. The analysis is addressing polarimetric signatures and entropy-alpha space distributions. [C2380]

"Simultaneous field experiments with PALSAR observations for soil moisture estimation"

We performed three field experiments with PALSAR/polarimetry observations in Ulaanbaatar/Mongolia, Arctic National Wildlife Region (ANWR/ Alaska)/US, and Sendai/Japan, to evaluate soil moisture models. The PALSAR

polarimetry observations with off-nadir angle of 21.5deg were done in May 4, 2007, Jul. 29, 2007, and Apr. 14, 2007 in each place. On the other hand, the field experiments were done for May 2-7, 2007, Jul. 28-Aug 4, 2007, and Apr. 14, 2007. The surface parameters derived from field measurements show large dynamic ranges, which are from 4% to 80% for soil moisture value, from 0.16 to 2.22 for surface roughness, and from 1.97 to 8.09 for correlation length. We applied SPM model, X-bragg model, and Oh model in this time. While some discrepancies are appeared, the SPM and Oh models show agreements with absolute/relative sigma0value in some degree. The X-bragg model shows moderate agreement in anisotropy-ks relation. [C2381]

"Analysis and Surface Parameter Retrieval from Multitemporal Airborne and Satellite Data During AGRISAR 2006"

Water and energy fluxes at the interface between the land surface and atmosphere are strongly depending on the surface soil moisture content which is highly variable in space and time. It has been shown in numerous studies that microwave remote sensing can provide spatially distributed patterns of surface soil moisture. In order to use remote sensing derived soil moisture information for practical applications as e.g. flood forecasting and water balance modeling in mesoscale areas, frequent large area coverage is a prerequisite. The present paper investigates the potential of using frequent microwave observations to retrieve information on surface soil moisture characteristics, as they will become available from the SENTINEL-1 mission. SAR data from the ESA AGRISAR 2006 campaign is used for that purpose. The paper first investigates the potential of using different models for the retrieval of surface soil moisture information using airborne data. An empirical parameter retrieval model is then applied for the retrieval as well as to ENVISAT ASAR satellite data to investigate the trade-off in spatial scale. The rms error of the retrieval results was found to be between 4 and 7 vol.%, which is consistent with previous findings. [C2382]

"Contribution of Multi-Frequency, Multi-Sensor, and Multi-Temporal Radar Data to Operational Annual Crop Mapping"

Information on agricultural land use (crop inventory) is needed by various organizations on an annual basis. To meet this operational requirement, Agriculture and Agri-Food Canada (AAFC) has carried out a multi-year (2004-2007), multi-sensor (Landsat TM, SPOT, RADARSAT-1, ASAR), and multi-site (five provinces: Ontario, Saskatchewan, Alberta, Manitoba, P.E.I.) research activity to develop a robust methodology to inventory crops across Canada's large and diverse agricultural landscapes. Results clearly demonstrated that multi-temporal satellite data can successfully classify crops for a variety of cropping systems across Canada. Overall accuracies of at least 85% were achieved. When available, multi-temporal (2 to 3 scenes acquired at different growth stages) optical data are ideal for crop classification. However due to cloud and haze interference, good optical data are not always obtainable. A SAR-optical combination offers a good alternative. This research has found that when only one optical image is available, the addition of two ASAR images acquired in VV/VH polarization will provide acceptable accuracies. Of particular interest is the observation that with the incorporation of radar, crop inventories can be delivered earlier in the growing season. [C2383]

"Pathfinder Advanced Radar Ice Sounder: PARIS"

The objective of the PARIS NASA Instrument Incubator Project was to demonstrate successful ice thickness sounding from a high-altitude airborne radar. This paper describes key features of the system, including the radar and the processing algorithm. Test flights over the ice sheets of Greenland produced good results. [C2384]

"A Multi-Functional Fiber Laser Lidar for Earth Science & Exploration"

A multi-pixel laser altimeter using pseudo-random-noise-modulated fiber lasers has been developed for Climate Change research and Exploration. The architecture supports a wide set of operational parameters (range resolution, range ambiguity interval, temporal update rate) without modifications to the hardware. These parameters can be changed dynamically, based on mission operational needs. The implementation is suitable for orbital and sub-orbital platforms and has reached TRL 6 having flown in a relevant environment over relevant terrain. We will present the status of the instrument development efforts, the results from the on-going field campaign, and notional implementations for Earth Science Decadal Missions and Exploration. [C2385]

"High-Altitude Imaging Wind and Rain Airborne Radar (HIWRAP)"

This paper describes the development of the High-Altitude Imaging Wind and Rain Airborne Profiler (HIWRAP) which is funded under the NASA Instrument Incubator Program (IIP). HIWRAP is a dual-frequency (Ka- and Ku-band), dual-beam (30deg and 40deg incidence angle), conical scan, Doppler radar system designed for operation on the high-altitude (65,000 ft) Global Hawk Unmanned Aerial System (UAS). It utilizes solid state

transmitters along with novel pulse compression scheme that will result in a system that is considerably more compact in size, lighter in weight, less power consumption, and ultimately cost significantly less than radars currently in use for precipitation and Doppler wind measurements. By combining measurements at Ku- and Ka-band, HIWRAP will be able to image winds by measuring volume backscattering from clouds and precipitation.

[C2386]

"Bistatic spaceborne-airborne experiment TerraSAR-X/F-SAR: data processing and results"

Following an original proposal by the authors to the TerraSAR-X (TSX) scientific coordination board, a spaceborne-airborne bistatic experiment was successfully performed early November 2007. TSX was used as transmitter and DLR's new airborne radar system, F-SAR, as receiver; due to the capability of the latter to acquire data quasi-continuously, no echo window synchronisation is needed. Monostatic data were also recorded during the acquisition. This paper includes description and results of the spaceborne-airborne bistatic experiment, with special focus on data processing and image comparison. Given the acquisition scenario, with two-channel sampling and transmitter and receiver clocks operating independently, data processing must necessarily follow a three-step strategy: 1) channel balancing, 2) data synchronisation and 3) bistatic SAR processing. Since neither absolute range nor Doppler references are available in the bistatic data set, synchronisation is done with the help of calibration targets on ground and based on the analysis of the acquired data compared to expected data. Due to the variant nature of the bistatic acquisition and the required precision for the processing, data are processed using a bistatic backprojection approach. [C2387]

"Optimizing the Individual Azimuth Contribution of Transmitter and Receiver Phase terms in Loffeld's Bistatic Formula (LBF) for Bistatic SAR Processing"

The individual azimuth contribution of transmitter and receiver phase terms has been optimized by weighting them unequally based on a weighting factor μ , in Loffeld's bistatic formula (LBF). Analytical results are verified with the simulations. [C2388]

"GPS/INS Integration for Footprint Chasing in Bistatic SAR Experiments"

The paper starts with a brief consideration of a novel bistatic SAR experiment and the requirements on attitude and position determination in SAR. GPS/INS integration strategies are summarized. To obtain an affordable system for the antenna pointing for footprint chasing, low-cost inertial measurement units are in the focus. By an observability analysis it is proven that additional redundant attitude information as it can be derived from a multi-antenna GPS receiver can remarkably aid the integration. [C2389]

"Multisource Image Classification Based on Parallel Minimum Classification Error Learning"

In this paper we present a parallel classification learning method, referred to as parallel minimum classification error (PMCE) learning, for supervised classification of multisource remote sensing images. The approach is based on the positive Boolean function (PBF) classifier scheme. The PBF implements the minimum classification error (MCE) as a criterion to improve classification performance. By evenly distributing both positive and negative samples of MCE learning modules to different PMCE learning nodes, PMCE outperforms the original one in terms of execution time. It fully utilizes the significant parallelism embedded in MCE learning of PBF to create a set of PMCE learning nodes implemented by using the message passing interface (MPI) library and the open multi-processing (OpenMP) application programming interface. A sophisticated hierarchical structure of hybrid PMCE, which combines cluster based MPI with multicore-based OpenMP, is proposed to demonstrate the flexibility of implementation of the proposed scheme. The effectiveness of the proposed PMCE is evaluated by fusing MODIS/ASTER airborne simulator (MASTER) hyperspectral images and the Airborne Synthetic Aperture Radar (AIRSAR) images for land cover classification during the Pacrim II campaign. The experimental results demonstrated that PMCE can improve the computational speed of PBF classification significantly. [C2390]

"Analysis of Polarimetric Surface Scattering in High Resolution SAR"

Statistical properties of rough surfaces can be affected by the spatial resolution of the radar sensor. This study aims to understand effects of the spatial resolution on the statistical description of surface roughness properties and on the surface scattering characteristics of polarimetric radar signal. A new expression for the surface autocovariance function and its corresponding roughness spectrum is proposed in order to characterize surface scattering. Results represent increases in the backscattering coefficients in accordance with decreases in the resolution cell size. Conventional continuous spectrum in the theoretical scattering model could underestimate the radar response in case of the surface defined by high correlation length. [C2391]

"Results from Microwave Radiometer Campaign of Seasonal Snow and Comparison with Emission Models"

Ground based multitemporal microwave radiometer to measurement snow covered terrain. Snow emission models and algorithms are developed for retrieving snow characteristics from space-borne radiometer data. Microwave radiometer measurements of snow cover was made at Kirkkonummi, southern Finland in AD 1985 01 to 04. Radiometer data include brightness temperatures at 1 GHz, 16.5 GHz and 37 GHz, vertical and horizontal polarization, continuous recording are done. The free-space systems were operated at 12 GHz 35, GHz and 18 GHz respectively. Daily data collection was conducted. Aluminium sheets cover the ground near observation tower, thus providing opportunity to observe microwave emission from snow alone. Ancillary data are also included like water equivalent, depth, temperature, layering, and surface roughness and grain size. The ground surface temperature are measured and vertical distribution of near-surface ground temperature also observed. Numerous homogeneous samples were taken from various depths. Dielectric and extinction properties of snow are measured. Snow extinction coefficients values and wetness values are also considered. TKK model; is a single-layer radiative transfer model. The Microwave Emission Model of Layered Snowpacks (MEMLS) model; is a radiative multiple-scattering model. . Experimental values were compared with snow emission models. [C2392]

"Reprocessing Altimeter Data Records along European Coasts: Lessons Learned from the Alticore Project"

A coastal-oriented processing strategy has been developed in the Northwestern part of the Mediterranean Sea and has showed that improved altimetry in the coastal ocean is feasible and could be extended to other regions. In this work, we will provide an overview of current capabilities and challenges of existing altimetry products in Black, Caspian, White and Barents seas, in the prospect of increasing the quantity and quality of data in these regions. With respect to the work done in the project called ALTICORE (ALTImetry for COastal REGions- www.alticore.eu), the obstacles limiting the use of the data and the possible areas of improvement are highlighted and discussed. [C2393]

"Basic Radar Altimetry Toolbox"

A NEW SET OF TOOLS FOR ALL ALTIMETRY USERS The field of satellite radar altimetry has matured to a point where it is now time to encourage a multimission approach and conceive an "all-altimeter" toolbox including a tutorial. Such an integrated approach and view is vital not only for assessing the current status of what offers altimeter products but also to show the system and consistency with the past. The Basic Radar Altimetry Toolbox (BRAT) is a collection of tools, tutorials and documents designed to facilitate the use of radar altimetry data for altimetry users, experienced as well as beginners, and particularly the users of the upcoming CryoSat mission. It is able to read most distributed radar altimetry data, from ERS-1 & 2, TOPEX/Poseidon, Geosat Follow-on, JASON-1, Envisat, and the future Cryosat missions, to perform some processing, data editing and statistic and to visualise the results. A version 2 is being developed with additional visualisation features such as waveform viewing. Also, a release for the MacOS is planned. As part of the Toolbox, a Radar Altimetry Tutorial gives general information about altimetry, the technique involved and its applications, as well as an overview of past, present and future missions, including information on how to access data and additional software and documentation. It also presents a series of data use cases, covering all uses of altimetry over ocean, cryosphere and land, showing the basic methods for some of the most frequent manners of using altimetry data. [C2394]

"Study of Atmospheric Correction in the Remote Sensing based on Multifunctional Raman/Mie Lidar System and Sunphotometer"

Obtaining high-accuracy optical property of atmosphere timely will lead to good results of atmospheric correction and real remote sensing image inversion. We have developed a multi-function Raman/Mie lidar system. Making use of this lidar, we can get the spatial distribution and the time evolution of many atmospheric parameters. In this paper, we studied the main factors affecting atmospheric correction, namely absorption and scattering by aerosols and several major atmospheric elements. Preliminary experimental results are described. These data are combined with sunphotometer data and another scanning Mie lidar data, integrated with the imagery from such as remote sensing of the Earth satellite to obtain the ground truth. [C2395]

"Overview of Research and Networking with Ground based Remote Sensing for Atmospheric Profiling at the Cabauw Experimental Site for Atmospheric Research (CESAR)-The Netherlands"

CESAR, the Cabauw Experimental Site for Atmospheric Research, is the Dutch focal point for collaboration on climate monitoring and atmospheric research and is situated on the KNMI meteorological research site near Cabauw in the Netherlands. CESAR addresses challenging topics in atmospheric research, especially the questions that are related to the interaction between clouds, aerosols and radiation and questions dealing with

land-atmosphere interaction. These topics are approached via process studies, model evaluations, climate monitoring, development of new experimental techniques and supporting activities for satellite missions. For each of these approaches, specific demands are put on the instrumentation, mode of operation and overall infrastructure. This paper gives an overview of CESAR that was recently augmented with a scanning drizzle radar (IDRA) and a multi-wavelength Raman lidar for aerosols, clouds and water vapor (CAELI). [C2396]

"Monitoring Fuel Moisture and Improving the Prediction of Wildfire Potential in Boreal Alaska with Satellite C-Band Imaging Radar"

Alaska currently relies on the Canadian Fire Weather Index (FWI) System for the assessment of the potential for wildfire and although it provides invaluable information it is designed as a single system which does not account for the varied fuel types and drying conditions (day length, permafrost, decomposition rate, and soil type) that occur across the North American boreal forest. Since 1999 research has been conducted to develop techniques for using Synthetic Aperture Radar to assess ground fuel moisture to improve the current fire danger prediction system in boreal Alaska. Research has been focused on recently burned forests using C-band satellite data. Analysis of the single channel SAR data resulted in two methods that can be used operationally, and a third time-series analysis method that is in need of further development but shows great promise in reducing the time-invariant confounding factors of surface roughness and aboveground biomass. Current and future research is focused on L-band PALSAR to expand to unburned areas, and the recently launched fully polarimetric Radarsat-II instrument. [C2397]

"Comparison of individual crowns among species in Japanese conifer plantations using airborne data for leaf-on and leaf-off conditions"

Japan is one of the most extensively forested countries in the world. We investigated seasonal process of conifer plantations using high-resolution optical airborne data based on an individual tree crown (ITC) approach. ITC information for the stand polygons was extracted automatically and compared to detailed field survey data. In comparison leaf on and leaf off image with selected from 4 representative plantations, accuracy of leaf off image was better than that of leaf on image. We found that this approach can be effectively applied to the management of dominant trees in conifer plantations without multiple layers or mixed high density stands in Japan. [C2398]

"Pasture Monitoring from Polarimetric TerraSAR-X Data"

Good pasture management and optimal feed use are key drivers of profitability for New Zealand's pastoral dairy and meat industries. Preliminary results are reported on a study to evaluate TerraSAR-X dual-polarisation radar imagery for estimation of pasture biomass. At the time of writing, 4 out of 36 images have been acquired and processed. Several linear models have been tested for field-measured pasture biomass in terms of co- and cross-polarisation backscatter. The best model is a linear regression using the HH and HV sum and difference, resulting in a residual standard error of 191.4 (kg/ha), with no evidence of a date effect. [C2399]

"Polarimetric SAR Data for Forest and Deforestation Mapping in Guizhou Province, Southwest of China"

Forestry inventory in southwest of China often suffers from the cloudy cover, and Synthetic Aperture Radar (SAR) can play an important role because of its all-weather and all-day capabilities. In this paper, we studied the potential of polarimetric SAR data for forest mapping in heavy cloud prone and rainy areas with polarimetric TerraSAR-X, Radarsat 2 data and how to improve the forestry classification accuracy through integration of SPOT 5 image and polarimetric SAR data. Field works were carried out in late August of 2007, and parameters were collected using a ground based Lidar and field measurements. For the high relief condition at the test site, a geometric correction strategy using two side looking direction SAR images and high resolution digital elevation model was proposed to overcome the geometric distortion of SAR image such as foreshortening, layover and shadow in hilly areas. Neural net method was suggested for classification of the SAR and SPOT images. [C2400]

"Retrieval of Aerosol Optical Properties based on Measurements of Lidar, Sun-Photometer, and CALIPSO at Wuhan, China"

Studying optical properties of atmospheric aerosol is important because aerosol affects people around the world significantly. These effects strongly depend on the physical and optical properties of aerosol particles. In this paper, we propose to use lidar, sun-photometer, and CALIPSO synchronously, then present combined retrieval to investigate the optical properties of aerosol. The observations were performed at Wuhan during the period of December 2007 to May 2008. The primary results show that the proposed method improved the precision of

aerosol optical depth effectively. Furthermore, long-term atmospheric and aerosol data could be obtained by consecutive observations. Also these data will be useful for future understanding about their environmental and climate effects. [C2401]

"Aerosol Character Comparison of CALIPSO and Sunphotometer in Hubei Province, China"

The stable aerosol retrieval algorithm needs a prior assumption of lidar ratio (the extinction-to-backscatter ratio), and the known aerosol type that is the prerequisite of this assumption, so how to identify the clouds and aerosol from lidar profile is fundamental to acquire atmospheric optical parameter. In this paper, we first employ the CloudSat to validate the CALIPSO's classificatory results, which is released in different versions, after choosing more accurate classification, then start retrieving. Second, sun-photometer is used for verifying the CALIPSO's calibration coefficient and supplies the day time records which are relatively more accurate. Finally, aerosol characteristic in Hubei province is analyzed. All the data will supply more available information for further climate change research. [C2402]

"SAR Image Fusion in Multi Sensor Context for Small Urban Area Detection"

The purpose of this work is to provide new fusion methods adapted to multi sensor SAR use for urban area segmentation. We explain first backscattering of radar signal from urban object and characterize variation due to sensors characteristics. Then, we propose two new data fusion methods suitable for radar images. The first one will use similar response to enhance quality of building backscattering and the second one will use two images to calibrate a statistical scheme based on the differences in backscattering from speckled area to urban area. We will show the results of our work applied on tropical areas. [C2403]

"Retrieval of Spectral Aerosol Optical Thickness over Land Surface from Multi-Wavelength Polarization Space-Borne Sensors"

Polarization space-borne sensor, just like POLDER (Polarization and Directionality of the Earth's Reflectances), is a new instrument devoted to the global observation of solar radiation reflected by the Earth surface-atmosphere system. It is necessary to acquire polarized information in retrieval of aerosol properties over land surface. Often the aerosol contribution is small compared to the surface, especially by covered vegetation. Atmospheric scattering is much more polarized than the surface reflectance. Using polarized information could solve the inverse problem of separating the surface and atmospheric scattering contributions. This paper presents retrieval of aerosols properties from multi-wavelength polarized measurements. The results suggest that it is feasible and possibility for discriminating the aerosol contribution from the surface in the aerosol retrieval procedure using multidirectional and multiwavelength polarization measurements. [C2404]

"Vertical Velocity Turbulence Observed with FMCW Radar"

Very fine space and time resolution observations of clear air reflectivity and vertical velocity were obtained in a day-time convective boundary layer by a frequency-modulated continuous-wave radar. Historically, most atmospheric FMCW radar investigations have focused on the extremely fine range resolution of which such radars are capable. When used in this mode, Doppler velocity information is usually lost due to the long integration time of the frequency sweep. That is, the effective pulse repetition frequency of the radar is so low that the Nyquist velocity interval is too narrow for useful measurements of atmospheric velocities. However, when configured for rapid profiling at the expense of either height coverage or spatial resolution, FMCW radars are capable of obtaining Doppler velocity timeseries from moderately sized resolution volumes at rates of several Hz. These are sufficient to resolve turbulent velocity variations in the inertial subrange down to timescales of approximately one second or less. [C2405]

"Planetary Boundary Layer Height and Wind Field Characterization by Means of a Lidar at the Teide Observatory in the Canary Islands"

A lidar field campaign was performed between 30th June and 4th July 2007 in the Teide Observatory in the Canarian island of Tenerife to characterize the atmosphere of this astrophysical observation site in terms of nocturnal boundary layer height and wind fields. The nocturnal boundary layer height was found lower than 810 m in all cases and the aerosol optical thickness lower than 0.005 and 0.03 at 1064 and 532 nm, respectively. Wind fields could hardly be retrieved because of faint signals and very weak wind velocities observed during the campaign. [C2406]

"Retrieval of Aerosol from Space-Borne Polarimetric Data in Beijing"

It is difficult to determinate the aerosol model when retrieving the aerosol over land surfaces. In this paper, from

the products of Aerosol RObotic NETwork (AERONET), the aerosol model in city area of Beijing was analyzed. Then, the aerosol properties were retrieved from polarized data of the Polarization and Anisotropy of Reflectances for Atmospheric Science coupled with Observations from a LIDAR (PARASOL), and validated by the AOD products of AERONET. The results show: (1) the aerosol model based on ground based observations in Beijing is different from standard aerosol model of POLDER; (2) the particular aerosol model over Beijing can improve the retrieval accuracy over Beijing. [C2407]

"Three-Dimensional Digitizing of Paddy Rice and Modeling for the Scattering Simulation"

In the present research, a model of three-dimensional (3D) structure of rice was developed. Three-dimensional position of rice leaves were measured along the edges of the leaves, and the position of stems were measured along the middle line. The measured data were contaminated by systematic error due to the device and random error due to the wind. The proposed methodology reduces such errors through the following steps. First, the positional data of the middle line of leaf was estimated from a pair of data measured at both leaf edges. Next, in xy-plane, principal component analysis (PCA) produced the first principal component, named as u-axis. Then, in uz-plane, a quadratic curve of the leaf was estimated by minimizing the sum of squared minimum distances between the points and the curve. The leaf width was modeled as a function of the leaf relative length to the full length. Finally, 3D structure of rice was modeled. The estimated length and area of rice leaves were compared with the measured data. It was revealed that the relative error of the estimated areas of all leaves per rice individual was -6.8%, which is acceptable for the analysis of microwave scattering. [C2408]

"The SIGRIS Project: A Remote Sensing System for Seismic Risk Management"

SIGRIS (Sistema di osservazione spaziale per la Gestione del Rischio Sismico) is a pilot project aiming to the realization of a system, based on satellite remote sensing data, for the seismic risk management. The project is funded by the Italian Space Agency (ASI). ASI is deeply interested in the development of new applications, using satellite data, dedicated to the monitoring and management of the natural hazards. SIGRIS is focused on providing the information services for mapping, monitoring, forecasting and awareness of seismic risk. The Earth Observation products are generated by using GPS data, optical and SAR (Synthetic Aperture Radar) images. This project deals with the data exploitation of the new Italian Earth Observation mission: COSMO-SkyMed, a constellation of four satellites equipped with an X-band high resolution SAR. [C2409]

"Field Surveys for Biomass Assessment in African Savanna Woodlands"

Most rural and some low-income urban households in southern Africa rely on fuelwood and charcoal to meet their domestic energy demands, targeting specific tree species for their calorific value. The lack of quantitative data on extractable standing woody biomass makes it difficult for energy planners to ascertain the sustainability of exploiting such resources. Large scale estimation of biomass using ground-based methods is both tedious and time-consuming. Optical remote sensing techniques are constrained by adverse atmospheric conditions such as clouds and haze, and in any case survey only the upper surface of the vegetation canopy. Recent advances in synthetic aperture radar (SAR) remote sensing and Global Positioning Systems (GPS) technologies coupled with geographic information systems (GIS) offer innovative ways to quantify and assess available woody biomass. Tree species heterogeneity in savanna woodlands requires training data with minimal target-to-image noise to distinguish tree vegetation on SAR imagery. The absolute positioning of trees is critical for correlating ground survey measurements with the corresponding aerial photography or satellite positions. The ground truth data is useful for calibrating and validating radar satellite imagery in biomass assessment surveys. GPS offers rapid methods of establishing both control and capturing field data. While Differential-GPS gives highly accurate ground positions, Electronic Distance Meter (EDM) surveying techniques are used to complement GPS measurements when field conditions are not favourable. GPS accuracy is degraded when receivers are operated under dense tree canopies. Connecting field surveys to national mapping systems or GPS networks allows easy integration of woodland spatial information with data from other sectors. This is constrained by the lack of common reference frameworks. In Africa, a unified African Reference Framework (AFREF) is still in its formative stages and network GPS is not yet fully developed. South Africa is the probably the only country that has a well developed GPS infrastructure. Although commercial GPS base stations are available, the required initial capital investment and annual maintenance charges often limit their use in developing countries. This paper proposes a method which combines rapid static DGPS, EDM topographic surveying and mobile GIS techniques to capture, compute and record absolute positions and vegetation parameters of preferred fuelwood tree species in African savanna woodlands. The proposed method will generate ground-truth data for preferred fuelwood species in selected case study villages under the VW Foundation Biofuels Modeling project, covering Zambia, Mozambique and South Africa. [C2410]

"TerraSAR-X Imaging for Unsupervised Land Cover Classification and Fire Mapping"

Since a few months TerraSAR-X has been acquiring X-band SAR images of the earth surface from space. This contribution reports on a study carried out to understand the main textural features of the X-band radar return from various kinds of surfaces and in particular to assess the potential of images acquired by X-band space borne radars in mapping fire scars and in classifying suburban/agricultural land cover. To this end, a novel unsupervised neural network algorithm, the Textural Self-Organizing Map (TexSOM), based on the textural features of the radar image, has been worked out and tested on areas in Greece and Italy. [C2411]

"Second-Order Motion Compensation in Bistatic Airborne SAR based on the Windowed Fourier-Transformation"

A crucial problem in most airborne Synthetic Aperture Radar (SAR) systems is the compensation of motion errors to prevent the image degradation. If these errors are not compensated, some undesired effects will appear, such as loss of geometric resolution and radiometric accuracy, reduction of image contrast, azimuth ambiguities and strong phase distortions. For the bistatic airborne SAR systems, the motion errors become more complex since two separate trajectory deviations contribute to these errors. This paper proposes an approach that will compensate the bistatic motion errors in the frequency domain. [C2412]

"Back and Forward Bistatic Interferometry"

This paper characterizes the interferometric phase for a fixed-receiver bistatic SAR system. Also, the expressions for the interferometric phase and image resolution cell are summarized. It will be distinguished between two particular acquisition geometries: back-scattering and forward-scattering. A bistatic interferometric chain has been implemented whose particularities are discussed. The theoretical developments are complemented with the comparison of the Digital Elevation Models (DEM) generated from the bistatic interferometric data acquired with our fixed receiver, named SABRINA (SAR Bistatic Receiver for INterferometric Applications) with a SRTM DEM and a Digital Terrain Model (DTM) from the Institut Cartografic de Catalunya (ICC). [C2413]

"Polarimetric BISAR Image Simulation and Analysis"

Employing three-dimensional mapping and projection algorithm (MPA), imaging simulation of bistatic SAR (BISAR) observation over complex scenario is developed. Based on the explicit expression of point target response of stripmap BISAR imaging, raw data is efficiently generated from the scattering map pre-calculated by MPA. Some examples of BISAR image simulation are studied. Polarimetric characteristics of BISAR image are then discussed. A transform of unified bistatic polar bases for BISAR image is proposed. Analysis of simulated images shows that the redefined parameters by the unified bistatic polar bases transform well describe different scattering mechanisms in BISAR imaging. It provides a primary tool for BISAR image interpretation and terrain classification. [C2414]

"Airborne Bistatic SAR Receiver with the Capability of Use Different Opportunity Transmitters"

This paper describes the design and construction of a bistatic SAR receiver suitable for airborne applications, using orbital SAR systems (ENVISAT, ERS-2, RADARSAT, TerraSAR-X among others) as opportunity transmitters. The challenge of this design is to reduce the required data throughput of the recorded data. This is achieved storing data only in the time intervals when scattered signal from the target area appears. The task of detecting this time intervals is performed in real time using a matched filter of the signal received directly from the SAR transmitter. [C2415]

"Predicting L-band Microwave Attenuation through Forest Canopy using Directional Structuring Elements and Airborne Lidar"

The L-band signals broadcast by GPS satellites are attenuated by vegetation, making it problematic, if not impossible, to predict the performance of the system in forested areas without some quantitative measure of the structure and density of the local forest canopy. Airborne laser swath mapping (ALSM) observations can be used to rapidly and remotely sample the structure and density of forested areas. We report here the results of a study performed to determine the attenuation of GPS signals in forests, by correlating changes in the signal-to-noise ratio (SNR) of the received GPS signals under different canopies, using three dimensional structure and density information about each canopy derived from ALSM observations. The results of this study verify that the loss of signal is strongly correlated with the local structure and density of the forest, and we demonstrate how the ALSM point cloud can be used to better predict the attenuation of the GPS signals. The results of this research also pertain to other modes of microwave transmission in forested areas, including satellite and cellular telephony, and the estimation of biomass from L-band radar. [C2416]

"Polarimetric Classification of Vegetation in Prairie Landscapes"

The successful launch and commissioning of several fully polarimetric synthetic aperture radar satellites has made possible the routine use of polarimetric imagery for the classification of and detection of change in the vegetated cover of our planet. In a precursor study for Radarsat 2 application development, three lines of airborne quad-pol SAR data were collected over Canadian Forces Base Shilo in southwestern Manitoba, Canada. Analysis of these data in comparison to classified Landsat imagery shows that a classification based purely on radar data can successfully reproduce the basic sense of the visible/infrared classification although detailed, arbitrary sub-classes are not well replicated. A critical dependency on incidence angle in the classification implies that it will be important to collect comparative imagery from space-borne radars at a constant incidence angle. [C2417]

"Development of Rice Yield Estimation Method based on Spaceborne Hyperspectral Data: Preliminary Study using Airborne Hyperspectral Data"

Bidirectional Reflectance Distribution Function (BRDF) would affect the data acquired by a future spaceborne hyperspectral sensor with pointing capability. BRDF of rice was measured by FieldSpec and an airborne hyperspectral sensor (AISA) in this study to improve estimate accuracy of rice yield and crude protein using BRDF correction. As a result, an error of reflectance caused by BRDF was corrected. In addition, this study confirmed that estimate accuracy of crude protein was unaffected by BRDF in range of AISA's FOV (22 degrees). [C2418]

"Extracting Tree Heights over Topography with Multi-Spectral Spaceborne Waveform Lidar"

It is generally agreed that the optimal footprint size for a spaceborne lidar is 30 m. Over topography such a large footprint can blur the canopy and ground signal together preventing information extraction. Multi-spectral lidar waveforms have been simulated with Monte-Carlo ray tracing over explicit geometric forest models. A method for using multi-spectral waveform lidar to distinguish ground from canopy returns has been tested over a range of ground slopes. The results are promising, with an initial error of +/-5 m for a signal level of only 5,000 photons with noise; an easily achievable figure. The inversion algorithms completely dominate inversion errors for all cases above 10,000 signal photons. [C2419]

"Atmospheric Compensation using a Geometrically-Compensated Empirical Line Method"

This paper presents a geometric extension to the well known Empirical Line Method (ELM) for atmospheric compensation, enabling improved results through the use of 3D scene geometry. Typically, this geometry is assumed to be known, either through direct measurement or analysis of other imagery such as lidar or photogrammetric products. However, when the scene geometry is unknown and only spectral information is available, in certain cases estimates of the surface orientation may be obtained directly from image brightness values. In this paper we derive a means to determine surface orientation estimates from a pair of brightness images, and then use this geometric information to improve the ELM solution. [C2420]

"Signal Processing Techniques for Feature Extraction and Classification using Small-Footprint Full-Waveform Airborne LIDAR"

Full-waveform digitizer hardware integration within discrete return LIDAR systems provides an enhanced capability to resolve vertical structure within the laser line of sight and potentially classify specific surfaces or objects. However, the subject of waveform signal processing as it applies to surface classification is fairly underdeveloped. This research includes the examination of LIDAR waveform pulse characteristics for known targets and vegetation types. Using these data, a number of signal processing techniques were investigated as precursors to classification engines without prior knowledge of surface slope, or obscuration density. Relevant waveform features were extracted using both Gaussian decomposition method and raw waveform features revealing surface classification distinctions. Preliminary results from this data set indicate that the total integrated waveform energy provides an efficient and rapid methodology for discrimination of vegetation from built surfaces. These results indicate that metrics derived from the full waveforms can be utilized to characterize and classify (to a limited degree) an environment without prior knowledge. [C2421]

"A Two-Stage Approach for Decomposition of ICESat Waveforms"

Decomposing a waveform into distinct components by fitting a mixture of Gaussians impacts the ultimate interpretation of the return waveform, because the resulting parameter estimates of the Gaussian mixture directly affect the understanding of vertical structure within laser footprints. Decomposing the waveform into a mixture of

Gaussians involves two related problems; (1) determining the number of Gaussian components in the waveform, and (2) estimating the parameters of each Gaussian component of the mixture. In this study, a two-stage approach is proposed and applied over three areas with different land cover characteristics. Experimental results indicate that the proposed two-stage approach typically fits Gaussian mixtures over received waveforms using fewer components, while the SSE value is smaller than that of the corresponding NASA GLA14 product. [C2422]

"A Semi-Decadal Multi-Sensor Gridded Data Record of Outgoing Longwave Radiation (OLR) from Aqua"

Launched on May 4, 2002, Aqua carries two well calibrated independent infrared (IR) instruments, Atmospheric Infrared Sounder (AIRS) and Moderate Resolution Imaging Spectro- radiometer (MODIS), which together could provide a precise decadal measurement across the IR electro- magnetic spectrum from 3.7 μm to 15 μm to form a fundamental climate data record. According to the National Academy of Science-Nation Research Council report, the notion of a fundamental climate data record (FCDR) is defined as "a time series of measurements of sufficient length and continuity to determine climate variability and change from sensor data (e.g., calibrated radiances, brightness temperatures (BT), radar backscatter) that have been improved and quality controlled over time." AIRS and MODIS have been continuously returning upwelling IR spectral radiance measurements while maintaining a nominal grid precision of $\sim 0.2\text{-}0.4$ K BT [2] with quality controlled calibration improvements for more than five years. Based on the Aqua senior Project Review of available flight fuel, power and orbital maneuvers, the assessed life span of the satellite Aqua is estimated to be 2013. AIRS and MODIS instrument teams also expect their passive radiometers to continue providing self-calibrating measurements with the same precision through the year 2013. With these assumptions, we show in this paper that with these two independent sensors on the same platform with on orbit relative validations, this data record would be of sufficient length and continuity to meet the FCDR definition to observe and determine the decadal variability of seasonal to interannual climate processes. In addition, NPOESS preparatory project will launch satellite systems carrying instruments similar to AIRS and MODIS which will enable production of an FCDR record for additional decades. [C2423]

"A Land-Cover Monitoring for Volcanoes by using ALOS-PALSAR Quad-Pol. Data"

We applied three-component (H//A) decomposition analysis and four-component (Ps, Pd, Pv and Pc) analysis to ALOS-PALSAR quad-polarized data of Izu-Oshima and Miyakejima volcanoes to monitor volcanic activities. The results demonstrated clear discrimination of forest, urban and volcanic deposit areas, indicating a high possibility of detecting land-cover changes at volcanoes by space-borne PolSAR observations. [C2424]

"River Ice Mapping from PolSAR Images"

This paper presents different mapping algorithms to discriminate river ice types using full-polarized C-band and dual-polarized X-band data. Field data are conjointly used with an electromagnetic river ice model to simulate backscattering response of river ice. Finally different classifications, proposed and tested, show encouraging results. [C2425]

"GB-SAR/PiSAR simultaneous experiment for a trial of flood area detection"

We performed a Ground Based SAR (GB-SAR) and PiSAR simultaneous experiment over a flood test site. In this site, one prefab was constructed in a baseball field of a Nihon University in Chiba, Japan. The PiSAR observations were done for three days with different soil moisture condition of $\sim 25\%$, $\sim 50\%$, and 100% . Some GB-SAR experiments have been also done in two of three days and the scattering process are examined. Preliminary experiment with GB-SAR showed that L-band σ_0 from a double scattering of ground-wall is increased for a few dB, when a reflectivity of the ground is assumed to be 1. These increase are also confirmed in the test site for both PiSAR and GB-SAR. Furthermore, high resolution GB-SAR images show double and single bounce scattering from a metal bar behind the wooden board of the prefab. We conclude that L-band SAR has a enough ability to detect a flooding area in urban site. [C2426]

"Recent Advances in RP-POL-In-SAR Hazard Monitoring of Tectonic Stress and Land-Slides"

Worldwide, medium- to short-term earthquake prediction is becoming ever more essential for safeguarding man due to an un-abating population increase, but hitherto there have been no verifiable methods of reliable earthquake prediction developed. This dilemma is a result of previous and still current approaches to earthquake prediction which are squarely based on the measurement of crustal movements, observable only after a tectonic stress-change discharge (earthquake) has occurred. During the past decades it was proved and shown that it is not possible to derive reliable models for earthquake predictions from crustal movement measurements alone, and that an entirely new approach must be taken and rigorously pursued over years and decades to come. In

support of this conclusion, there have been reported throughout the history of man anecdotal historical up to scientifically verifiable earthquake precursor or "seismo-genic" signatures of various kind-biological, geological, geo-chemical and especially a rather large plethora of diverse electromagnetic ones on ground, in air and space, denoted as "seismo-electromagnetic" signatures. Taiwan is one of the few regions where those phenomena may best be observed. In this overview a systematic analysis of main historical records, a summary of pertinent "seimogenic" as well as observed "seismo-electromagnetic" effects and modern ground-based to air- and space-borne metrological signature investigations are presented placing major emphasis on ongoing studies in Taiwan. [C2427]

"A High performance Communication Program for a GPS-based Vehicle Tracing Mobile Platform"

This paper describes the design and implementation of a high performance terminal communication program for a GPS-based vehicle-tracing mobile prototyping platform (GPSVTMPP). First we introduce the architecture and function of our mobile platform and analyze some bottlenecks. Then, we present detailed strategies and methods for how to use Microsoft's I/O Completion Port(IOCP) model to implement the Winsock 2 communication server program. We prove that this server program can improve the efficiency, flexibility and robustness of the single communication server, especially for large-scale communication. Finally, this paper summarizes the results of some application experiments and other results using this platform. [C2428]

"The Soil Moisture Active/Passive Mission (SMAP)"

The Soil Moisture Active/Passive (SMAP) mission will deliver global views of soil moisture content and its freeze/thaw state that are critical terrestrial water cycle state variables. Polarized measurements obtained with a shared antenna L-band radar and radiometer system will allow accurate estimation of soil moisture at hydrometeorological scale (10 km) and hydroclimatological scale (40 km) resolutions. The sensors will share a feed and a deployable light-weight mesh reflector that will make conical scans of the Earth surface at a constant look angle. The wide-swath (1000 km) measurements will allow global mapping of soil moisture and its freeze/thaw state with 2-3 days revisit. Freeze/thaw in boreal latitudes will be mapped using the radar at 3 km resolution with 1-2 days revisit. The synergy of active and passive measurements enables global soil moisture mapping with unprecedented resolution, sensitivity, area coverage, and revisit. This paper outlines the science objectives of the SMAP mission and provides an overview of the measurement approach and data products. [C2429]

"Deformation, Ecosystem Structure, and Dynamics of Ice (DESDynI)"

The National Research Council Earth Science Decadal Survey, Earth Science Applications from Space, recommends that DESDynI (Deformation, Ecosystem Structure, and Dynamics of Ice), an integrated L-band InSAR and multibeam Lidar mission, launch in the 2010-2013 timeframe. The mission will measure surface deformation for solid Earth and cryosphere objectives and vegetation structure for understanding the carbon cycle. InSAR has been used to study surface deformation of the solid Earth and cryosphere and more recently vegetation structure for estimates of biomass and ecosystem function. Lidar directly measures topography and vegetation structure and is used to estimate biomass and detect changes in surface elevation. The goal of DESDynI is to take advantage of the spatial continuity of InSAR and the precision and directness of Lidar. There are several issues related to the design of the DESDynI mission, including combining the two instruments into a single platform, optimizing the coverage and orbit for the two techniques, and carrying out the science modeling to define and maximize the scientific output of the mission. [C2430]

"Landslide Susceptibility Mapping using Remotely Sensed Soil Moisture"

Slope stability analysis using remotely sensed data is routinely conducted throughout the world. This study focuses on rainfall induced landslides and the use of AMSR-E and TRMM satellite data to develop susceptibility maps that can be used to forecast landslides. This research established the first relationships among soil moisture derived from AMSR-E, precipitation from TRMM and major landslide events, respectively, in California, U.S., Leyte, Philippines and, Dhading, Nepal. Each of the three study regions had slope movements when soil moisture was high and rainfall occurred and clearly indicates a strong relationship among landslide events, remotely sensed soil moisture and rainfall. A slope stability model is used to develop susceptibility maps for a California site under a range of conditions. Results suggest that the AMSR-E and TRMM satellite data, coupled with land-surface model estimates, are viable for enhancing rainfall induced slope stability analysis at regional or global scales. [C2431]

"Weibull Distribution for the Global Surface Current Speeds Obtained from Satellite Altimetry"

Near-real time ocean surface currents derived from satellite altimeter (JASON-1, GFO, ENVISAT) and

scatterometer (QSCAT) data on 1deg times 1deg resolution for world oceans (59.5deg S to 59.5deg N) are available online as "Ocean Surface Current Analyses-Real Time (OSCAR)". The probability distribution function (PDF) of the current speeds (w), constructed from global OSCAR data from 1992 to 2008, satisfies the two-parameter Weibull distribution reasonably well. Knowledge on PDF of w will improve the ensemble horizontal flux calculation, which contributes to the climate studies. [C2432]

"Space Altimetry from Nano-Satellites: Payload Feasibility, Missions and System Performances"

Thales Alenia Space is an industry world leader in high performance altimeters for ocean topography from space (Poseidon1 on TOPEX-Poseidon, Poseidon2 on Jason1, Poseidon3 on Jason2 and AltiKa on AltiKa/SARAL), and for ice topography from space (SIRAL1 and SIRAL2 on Cryosat). Thales Alenia Space is also involved on advanced altimeter concepts such as wide swath and high resolution altimetry (SWOT) for hydrology. CLS is dedicated to satellite environmental monitoring and security services. In this framework, CLS is involved in algorithms and products definition, data processing and CalVal for the altimetry missions developed in cooperation between US and France (TOPEX-Poseidon, Jason1/2), in US (GFO) and in Europe (ERS1-2, Envisat, Cryosat) and is currently involved in the definition and development of future missions (AltiKa, Sentinel3) and future wide swath altimetry concepts (SWOT). Altimetry satellites for space oceanography have seen continuous and tremendous reduction in size, mass, and program cost: TOPEX-Poseidon satellite mass is 2500 kg. Jason1/2 satellites mass is 500 kg. AltiKa microsatellite mass shall be around 150 kg. Is a further step in reduction of satellite mass (and cost) achievable? What kind of altimetry payload? Which (system) performances? Which payload and satellite technologies? For which (new) mission(s)? This paper addresses these points and shows the way of an additional step in innovative solutions opening to low cost constellation of altimetry satellites with new applications and services. [C2433]

"Development of a Parameterized Snow Scattering Model"

Snow monitoring at regional and continental scale is an important task in Cryosphere studies. Space-borne active microwave sensors are capable of delivering long-term, all-weather observations of snow at large scale and providing information on key snow parameters, such as snow water equivalent (SWE). However, the complexity of snowpack makes it difficult to model the microwave scattering and retrieve snow parameters. A computationally efficient snow scattering model with simple terms is desirable for studying microwave interactions with snow and developing inversion techniques. In this study, a parameterized dry snow scattering model for analyzing X-band and Ku-band snow measurements is developed. The parameterized model is built from the microwave signal database simulated from a wide range of snowpack conditions by a theoretical model, which accounts for multiple-scattering effects and has been well-validated. The parameterized model is simple and reliable, with RMSEs 0.20 dB, 0.24 dB and 0.43 dB for VV, HH and VH polarizations, respectively. [C2434]

"Scientific Preparations for CoRe-H2O, a Dual Frequency SAR Mission for Snow and Ice Observations"

The COld REGions Hydrology High-resolution Observatory (CoRe-H2O) satellite mission has been selected for scientific and technical studies within the ESA Earth Explorer Programme. The mission addresses the need for spatially detailed snow and ice observations in order to improve the representation of the cryosphere in climate models and to improve the knowledge and prediction of water cycle variability and changes. CoRe-H2O will observe the extent, water equivalent and melting state of the snow cover, accumulation and diagenetic facies of glaciers, and properties of sea ice and lake ice. The sensor is a dual frequency SAR, operating at 17 GHz and 9.6 GHz, VV and VH polarizations. This configuration enables the decomposition of the scattering signal for retrieving physical properties of snow and ice. Scientific preparation activities include experimental field campaigns, improvement of radar backscatter models, and the development of inversion algorithms. [C2435]

"POLSCAT Ku-band Radar Remote Sensing of Terrestrial Snow Cover"

Characteristics of the POLSCAT data acquired from five sets of aircraft flights in the winter months of 2006-2008 for the second Cold Land Processes Experiment (CLPX-II) in Colorado are described in this paper. The data showed the response of the Ku-band radar echoes to snowpack changes for various types of background vegetation in the study site in north central Colorado. We observed about 0.15 to 0.5 dB increases in backscatter for every 1 cm of snow water equivalent (SWE) accumulation for areas with short vegetation. Based on a simplified radiative transfer model, the change detection technique is used to convert the temporal change of radar backscatter into SWE accumulation for dry snow conditions. The resulting SWE accumulation estimates are consistent with the in-situ SWE measurements, with about 2 to 3 cm Root-Mean-Square (RMS) difference for regions with sagebrush or pasture. [C2436]

"Modeling Active Microwave Remote Sensing of Multilayer Dry Snow using Dense Media Radiative Transfer Theory"

In this paper, we model the backscattering coefficients of multi-layer dry snowpacks, based on Dense Media Radiative Transfer theory (DMRT) with the Quasicrystalline Approximation (QCA). The DMRT model accounts for adhesive aggregate effects, which leads to dense media Mie scattering by using a Sticky particle model. The same set of DMRT equations are used for modeling both active and passive remote sensing. The model is validated by using the Cold-Land Processes Field Experiment CLPX ground based polarimetric scatterometry observation at local-scale observation site (LSOS) and airborne polarimetric Ku-band scatterometer (POLSCAT) data at Fool-Creek, Fraser. The snow density profiles are from ground observation and grain sizes are fitting parameters. It shows that the co-polarization simulations are in good agreement with the data, the cross-polarization simulations are around 2 dB lower than ground based observation and 5 dB lower than airborne observation. With the same set of multi-layer snowpack profile, the QCA/DMRT model matched co-polarization backscattering coefficients and all 4 channels of brightness temperature observations simultaneously at LSOS. The cross-polarization simulation can be improved by 3-dimensional numerical solutions of Maxwell equations (NMM3D). Study at Fool-Creek shows that NMM3D/DMRT simulations can match both co-polarization and cross-polarization observations simultaneously. [C2437]

"Estimation of Terrain Slope Using a Compensation-Lambertian Method from Single-Pass Polsar Data"

In this paper, we introduce a new method of terrain slope estimation in the azimuth direction and the ground range direction using only one pass POLSAR data. This method is derived from the polarimetric SAR data compensation for terrain azimuth slopes variation [1] and the Lambertian backscattering model used in the radarclinometry [2]. The AIRSAR L-band POLSAR data are used to show the preliminary results of this method. The comparison of the proposed method and the digital elevation model (DEM) are given to show the effectiveness. The preconditions and limitation of this method are also discussed in this paper. [C2438]

"The use of the SHOALS waveforms to mapping habitat within the seamless benthoscape"

The Scanning Hydrographic Operational Airborne LiDAR Survey (SHOALS) consists of an ubiquitous topographic and bathymetric LiDAR system which provides high resolution measurements of emerged and immersed elevation. Besides, the return signals, i.e., waveforms, contain signatures of the benthic return for subtidal area and of the salt marsh cover for intertidal zone. This paper highlights the seamless classification of the coast from the upper marsh to the near-shore. The subtidal seafloor is characterized in applying a supervised classifier to 12 SHOALS-derived benthic variables, supporting by underwater image classification (78.6 %). The intertidal marsh is classified in respect to the combination of a synthetic Vegetation indice (based on Red and InfraRed) and the elevation (95.2 %). The merge of both classifications points out 16 classes with an overall accuracy of 86.9 %. [C2439]

"Dual-643 GHz and 874 GHz Airborne Radiometers for Ice Cloud Measurements"

In this paper, recently developed dual polarization 643 GHz and single polarization 874 GHz receivers for airborne CoSSIR, Compact Scanning Sub-millimeter wave Imaging Radiometer were utilized for ice cloud measurements. The results show that the brightness temperature map clearly demonstrates the recent advance in sub-millimeter wave radiometry for ice cloud sensing. The 874 GHz radiometer greatly improves the CoSSIR sensitivity to small ice particles. This implies that CoSSIR is able to pick up the measurements of ice clouds where the visible and inferred approaches left behind, i.e. saturated. The polarization measurement capability at 643 GHz can provide information on particle shapes, as well as improve the accuracy of the ice cloud parameters retrievals, e.g., ice water path and particle size. [C2440]

"Brightness temperature retrieval with scale-model antenna patterns of the aquarius l-band radiometer"

The Aquarius is a L-band passive/active instrument onboard a spacecraft due for launch in 2010, targeting sea surface salinity retrieval with an accuracy better than 0.2 psu. Measurement and retrieval of salinity by the Aquarius radiometer are simulated using a radiative transfer model. The cross-polarization coupling in the antenna pattern complicates the correction of the Faraday rotation effect in the ionosphere, causing errors in brightness temperature up to several Kelvin. The second-order correction for the Faraday effect is developed and reduces the retrieval error better than the required accuracy (~less 0.1 K). [C2441]

"Laser Intensity Used in Classification of Lidar Point Cloud Data"

LIDAR (Light Detection And Ranging) is a powerful remote sensing technology for the acquisition of terrain surface. The LIDAR system not only generates the 3D points cloud with irregular spacing, but also detects the laser impulse reflection data. The algorithms used for the LIDAR data are mostly used to deal with the 3D points cloud, produce the digital terrain model (DTM) and detect the objects, such as buildings. Usually, these objects must be classified as part of the extraction. In order to classify, other information besides the height information of points cloud is required, such as laser intensity information. However, few classification algorithms using intensity data have been deeply investigated. The laser intensity is different from material to material. The intensity of reflection on the same material is similar, while pulsed on different material is differ. Based on this theory, this paper provides a classification algorithm of airborne laser scanning altimetry data combined with the intensity of laser in detail. This paper proposes a classification algorithm for LiDAR points data by fusing height data and intensity data. Initially, the height data is used to generate the original terrain data after filtering. As a result, the terrain data and objects data are separated. Second, a filter algorithm is applied to the raw laser intensity of object points. Third, a histogram of filtered intensity is obtained. Fourth, the statistic result combined with the height information according to the pulse feature of laser intensity, is analyzed. [C2442]

"Simulations of Space-Based CO2 Measurements: Measurement Impacts on Mesoscale Transport Modeling"

We have developed an algorithm testbed designed for end-to-end simulation of atmospheric lidar measurements. The testbed provides a framework for the rapid prototype and development of trace gas remote sensing systems. It not only provides a means of simulating sensor performance during the design phase, but also provides a modular implementation that enables integrations algorithm tools with measured data from prototype/operational sensors. Further, the retrieved output parameters can be fed directly into data assimilation schemes in order to fully test the utility from an end-user perspective. This paper describes the application of this testbed to a LIDAR system designed to measure atmospheric carbon dioxide (CO2). We provide results of sensor simulation studies and show how assimilation of data from a satellite-based LIDAR system would enhance the regional modeling and simulation of sources and sinks of atmospheric CO2. [C2443]

"Space Borne Laser and Airborne Lidar Experiences at L'Estartit (Spain)"

One airborne calibration campaign with a Partenavia P-68 (ICC) carrying an Optech Lidar ALTM-3025 (ICC) was made on June 16, 2007, overflying l'Estartit harbour (about 6 km wide by 50 km long) and mapping with observe lidar strips of about 800 m. wide. The validation of this new technology LIDAR may be useful to fill coastal areas where satellite radar altimeters are not measuring due to the large footprint and the resulting gaps of about 20-40 km within the coastline. Measurements with a GPS Buoy were made during the experience and a GPS reference station was installed in Aiguablava. A DSM of l'Estartit harbour area was derived in the first results from the campaign. [C2444]

"Study on the Resolution of Laser Scanning Point Cloud"

Resolution governs the level of identifiable details within the scanned point clouds. It can be classified into angular, range and intensity resolution. The first one is as an indicator of resolution and is the focus of this paper. The main problem concerned is the impact of angular resolution by different scan range and angle. The function of calculating point density is proposed and confirmed through practice. We use a Leica HDS3000 laser scanner to do the field test and the grassplot, cement ground, wooden wall have been taken as the test samples, and then, compared each other. The analysis shows that it is feasible to estimate the point density and evaluate the level of details that can be resolved from the scanned point clouds on beforehand. [C2445]

"CR-Based SAR-Interferometry for Landslide Monitoring"

To monitor and detect the events of landslide, rock-fall along the banks of the Yangtze River in the Three Gorges area, the differential INSAR technique with corner reflectors (CR-INSAR) might be more effective than the conventional geological, and discrete GPS measurement techniques, conventional D-INSAR, as well as nature persistent scatteres method. Unfortunately, in most parts of the world, the correlation between radar acquisitions degrades with time due to vegetation, climatic condition, or other surface property changes. In those areas only a few persistent point scatterers or even no any one can be found out. The corner reflectors, duo to their design, provide a very clear and stable target response (both amplitude and phase) to the radar at any acquisition time. They don't suffer from de-correlation effects of conventional InSAR. Aside from the millimeter-lever measurement accuracy, the great benefit of this technique is the regular and remote monitoring and measuring without the need for repeated ground field visits and their associated costs. [C2446]

"Insar Analysis of Land Subsidence Caused by Groundwater Exploitation in Changping, Beijing,"

China"

Land subsidence in Changping, Beijing of China, has been an ongoing problem for the past four decades (since the later 1970s). We use permanent scatterers interferometric synthetic aperture radar (PS-InSAR) technique to detect and measure ground movement in this area. The detail information of deformation shows that spatial extent of subsidence is controlled by geologic structures (Huangzhuang-Gaoliying and Nankou-Sunhe faults) and thickness of Quaternary sediment. Comparing the subsidence line to the aggregate clay thickness of Changping area, both of them are mostly consistent. The locations of high-subsidence areas coincided with areas of heavy groundwater use and the clay mud layer, which is thicker than 50 m. [C2447]

"Using Remote Sensing for Mapping the Effects of Natural Hazards in New Zealand"

New Zealand is susceptible to numerous natural hazards on an annual basis that threaten properties, infrastructure, and lives. Remote sensing can be used as a means to provide both detailed and synoptic information to councils and emergency services, assisting with decision making in response to a hazard or disaster. This paper details a number of case studies undertaken in New Zealand to acquire and process remotely sensed data, with the ultimate goal of developing robust and effective procedures for providing spatial information of damages in the event of future natural disasters. [C2448]

"Land Subsidence Investigation Along Railway Using Permanent Scatterers SAR Interferometry"

Land subsidence is a common geohazards in many countries of the world, which cause damages for many urban areas and civil infrastructure. The development of spaceborne SAR interferometry provides an efficient tool for large spatial scale surface deformation monitoring with a high accuracy and precision. This paper presents a case study of land subsidence investigation along railway by using Permanent Scatterers SAR interferometry (PSI). Based upon the conventional InSAR techniques, PS-InSAR overcomes atmospheric delay anomalies and temporal and geometric decorrelation by exploiting the temporal and spatial characteristics of radar interferometric signatures collected from point-wise targets that preserve phase coherent over time. In this work, a linear model is adopted to retrieval land subsidence rate by using the differential phase series of the permanent scatterers. For the subsidence rate derivation along the railway, a buffer with a width of 10 km is set up and those PS within the buffer is interpolated to generate the subsidence map. The results archived using ENVISAT ASAR images acquired from 2003 to 2004 are validated with the precise leveling data and used to investigate the Jing-Jin railway in north china. [C2449]

"Combined Airborne Radio-instruments for Ocean and Land Studies (CAROLS)"

The CAROLS, L band radiometer, is built and designed as a copy of EMIRAD II radiometer of DTU team. It is a Correlation radiometer with direct sampling and fully polarimetric (i.e 4 Stockes). It will be used in conjunction with other airborne instruments (in particular the C-Band scatterometer (STORM) and IEEC GPS system, Infrared CIMEL radiometer, one visible camera), in coordination with in situ field campaigns for SMOS CAL/VAL. The instruments are implemented on board the French research airplane ATR42. A validation campaign with four flights was made over south west of France, Hourtin Lake and Bay of Biscay (Atlantic Ocean) in September 2007. In order to qualify the radiometer data, different types of aircraft movements were realized: circle flights, wing and nose wags. Simultaneously to flights, different ground measurements were made over continental surfaces and ocean. First results show a good quality of data over ocean surfaces. For continental surfaces, important Radio-Frequency Interferences (RFI) were observed over a large part of the studied region. [C2450]

"Carols Campaign, Scientific Data Analysis Results"

The CAROLS L-band radiometer, which is built and designed as a copy of DTU EMIRAD II instrument will be used in conjunction with other airborne instruments (in particular the C-band scatterometer STORM) in coordination with insitu field campaigns for future SMOS CAL/VAL activities. A validation campaign with four flights was made over the South West of France and the Bay of Biscay (Atlantic Ocean) in September 2007. Different instrumented sites over ocean and land surfaces were covered. Moreover, in order to qualify the radiometric data, different types of aircraft maneuvers were performed over the ocean: circle flights, wing and nose wags. We present in this paper the first analysis of the data quality using these ocean measurements. We show a very good sensitivity of both channels. [C2451]

"The Geomorphometry of Rainfall-Induced Landslides in Alishan Area Obtained by Airborne Lidar and Digital Photography"

For understanding the distribution of slope angles, OHM and roughness of the rainfall-induced landslides in Alishan Area of Central Taiwan, a survey was carried out with airborne Lidar and aerial digital camera to obtain

DEM and DSM of 1 m grid and color orthophotos of 50 cm grid. DEM, DSM and orthophotos are georeferenced and co-registered. The 106 landslide polygons derived from photo-interpretation are used for extracting slopes, OHM and roughness. Results show that the average slope angle of landslides is 41 degrees with a standard deviation of 14 degrees; average OHM is 4.4 m with a standard deviation of 6.3 m; average roughness is 2.05 m with a standard deviation of 2.56 m. It is also observed that scale effects are obvious for roughness but not for slope and OHM when the grid is larger than 40 m, which is the average dimension of landslides. These morphometric parameters can be further applied in the automation of landslide inventory. [C2452]

"Airborne Measurement of Snow Thickness over Sea Ice"

Snow cover on sea ice plays an important role in the climate of the polar regions. Snow on the sea ice reduces the heat exchange between the ocean and the atmosphere by its high albedo and low thermal conductivity. The lower the albedo, the less solar energy is reflected back into the atmosphere. Data on the extent and thickness of snow cover is needed to understand the condition and future behavior of sea ice. Remote sensing is a commonly used means of observing snow cover over sea ice. The advanced microwave scanning radiometer (AMSR-E) is one instrument for accomplishing this objective. To validate measurements made by AMSR-E, the University of Kansas developed an ultrawideband frequency-modulated continuouswave (FM-CW) airborne radar to measure snow thickness over sea ice. The University of Kansas tested their radar system on board the NASA P-3 aircraft during the NASA Arctic 2006 Field Campaign over the Alaskan coastal region. The objective of this field campaign was to acquire a comprehensive data set that will enable validation of the snow thickness retrieval algorithm AMSR-E passive microwave sensor measurements on board NASA's AQUA satellite. This paper contains the preliminary results of resolving the air/snow interface and the snow/ice interface. [C2453]

"Downscaling of Global Soil Moisture using Auxiliary Data"

Soil moisture is important to land surface modeling and climate modeling, which usually use soil moisture as a critical parameter. Derivation of soil moisture by radar remote sensing has theoretically and practically proven to be possible. However, radar-derived soil moisture is at coarse resolution, nominally about 25 kilometers, which does not satisfy the requirements of models using higher resolution grids. It is desirable to downscale the soil moisture to resolutions finer than 25 kilometers, especially 1 to 5 kilometers. In this study, derived parameters from MODIS have been used to derive the correlation between soil moisture and these parameters and downscale soil moisture. Six downscaling algorithms were proposed and compared. Geographically weighted regression (GWR) was used as the base model. Results showed that GWR performed well in downscaling. Further studies would look into more parameters for base models and higher-order polynomial regression for improving the accuracy of soil moisture downscaling. [C2454]

"Bayesian Estimation of Altimeter Echo Parameters"

This paper studies a Bayesian algorithm for estimating the parameters associated to Brown's model. The joint posterior distribution of the unknown parameter vector (amplitude, epoch and significant wave height) associated with this model is derived. This posterior is too complex to obtain closed form expressions of the minimum mean square error and the maximum a posteriori estimators. We propose to sample according to this distribution using an hybrid Metropolis within Gibbs algorithm. The simulated samples are then used to estimate the unknown parameters of Brown's model. The proposed strategy provides better estimations than the standard maximum likelihood estimator at the price of an increased computational cost. [C2455]

"Impact of Vegetation in the Retrieval of Snow Parameters from Backscattering Measurements at the X- and Ku-bands"

In preparation of the satellite mission CoReH2O, one of the six missions which has been selected for scientific and technical feasibility studies within the Earth Explorer Programme of the European Space Agency, experimental and theoretical studies started in order to investigate backscatter properties and improve the methods for retrieval of snow physical properties from SAR data. The aim of this paper is to investigate the impact of vegetation in the retrieval of snow parameters from backscattering measurements at the X- and Ku-bands. First the key vegetation types found in snow covered regions were identified on the basis of available global scale data base. A model able to simulating scattering from a vegetated snow-covered terrain was then developed and implemented. Lastly, a sensitivity analysis to vegetation parameters was conducted on sparse vegetation and coniferous forest. [C2456]

"Dual Polarization Detection of Ships and Icebergs-Recent Results with ENVISAT ASAR and Data Simulations of RADARSAT-2"

The RADARSAT-2 satellite is an advanced C-band synthetic aperture radar (SAR) with a variety of new modes including options for polarization combinations, resolution, and swath width. This paper examines the potential of multi polarization data for detecting and discriminating ship and iceberg targets. Data used in this study consist of well validated airborne Convair-580 SAR and spaceborne ASAR HH/HV and HH/VV. In total, the data set used for evaluating detection and discrimination consists of 901 validated iceberg and ship targets. Optimizing target detection is accomplished using receiver operator curves (ROC) as proposed by [6] and discrimination is conducted using a quadratic discriminant (QD) with feature selection based on sequential forward selection (SFS). In general it was found that detection and discrimination improve with more polarimetric information; however, HH/HV and VV/VH only had nominally less discrimination performance than the quad polarization modes evaluated. [C2457]

"A Real-Aperture Radar for Ground-Based Differential Interferometry"

Satellite interferometry has been used extensively for ground-motion monitoring with good success. In the case of landslides, for example, space-borne SAR interferometry has a good potential to get an overview on the slope stability. The role of a space-borne INSAR as an element in a landslide or rock fall warning system is constrained by the specific space-borne SAR imaging geometry, the typical multiple-week repeat-interval, and uncertainties in the data availability. Most of these limitations can be overcome with an in-situ radar imaging system. GAMMA has developed a portable radar interferometer that utilizes real-aperture antennas to obtain high azimuth resolution. Images are acquired line by line while rotating the transmitting and receiving antennas about a vertical axis. Phase differences between successive images acquired from the same location are used to determine line-of-sight displacements. The instrument operates at 17.2 GHz and has measurement sensitivity better than 1 mm. The instrument uses two receiving antennas with a short baseline to form an interferometer. Phase differences between simultaneous acquisitions by these antennas are used to calculate the precise look angle relative to the baseline, permitting derivation of the surface topography. Expected statistical noise in the height measurements is on the order of 1 meter. In this contribution the design, measurement principles and characteristics of GAMMA's Portable Radar Interferometer (GPRI) are presented. [C2458]

"Development of SAR-Based Snow-Covered Area Estimation Method for Boreal Forest Zone"

Development of an enhanced method for fractional snow-covered area (SCA) estimation for the boreal forest zone is presented. The TKK snow-covered area estimation method was developed and demonstrated for northern boreal forest zone using ERS, Envisat ASAR and Radarsat C-band synthetic aperture radar (SAR) data. The new enhanced approach for SCA estimation, presented here, merges the proven TKK SCA estimation method with several new innovations, enhancing its reliability and accuracy in operational use. The enhancements that form the new method include the weather station assimilation method presented earlier and a new reference data selection process. The SCA estimates acquired with the enhanced method are compared with optical satellite data-based (MODIS) SCA data. The results show a significant increase in accuracy when the enhanced SCA method is applied. Correlation between the radar-based and optical comparison data increases from 0.914 to 0.947 and RMS-error improves from 0.151 to 0.123 when the new method is employed. Additionally the SCA estimation method is adapted to produce SCA estimates in 5 km times 5 km spatial resolution. The analyses for the 5 km times 5 km method indicate poorer estimation accuracy than the nominal drainage-basin-based method. [C2459]

"GMTI Performance of a High Resolution Wide Swath SAR Operation Mode"

In this paper an operation mode for space-based SAR/GMTI is suggested which uses a rectangular antenna array and employs subpulse beamsteering on transmit in order to yield wide swath coverage. A signal modeling in range Doppler domain is introduced that is suitable for studying the SAR/GMTI performance. Simulation results are given. [C2460]

"PolInSAR for Forest Biomass Retrieval: PALSAR Observations and Model Analysis"

This paper presents a new approach to the exploitation of polarimetric and interferometric (POLINSAR) data for the quantitative estimation of the forest height and, in general, of forest parameters. Our procedure aims to match simulations from the coherent scattering model PolSARProSim and real measurables. First, a parametric model analysis is used to study the dependence of the interferometric coherence versus forest height, canopy density and terrain slope. Secondly, we show the separation of scattering phase centers on PALSAR data acquired over the Amazon forest. Finally, we perform a preliminary forest height inversion based on the sensitivity of coherence versus forest height. The same procedure can be applied to a compact polarimetric (CP) data-set. In this case, we introduce a full POLINSAR (FP) reconstruction algorithm based on symmetry properties of geophysical media. [C2461]

"Satellite Data Fusion Techniques for Terrain and Surficial Geological Mapping"

Increased satellite image data availability, with different spatial, spectral, and radiometric resolutions, present some challenges for image fusion techniques to be used in many application areas. In this study, we demonstrate an improved technique combining RADARSAT (SAR), Digital Elevation Model (DEM) and Landsat (ETM+) images with surficial geology data into two complementary composite image maps within Mackenzie Valley Pipeline Corridor, Canada. The method includes four processing steps. (1) The shaded relief derived from DEM was blended with SAR data to produce 3-D effect for terrain and geological structural interpretation. (2) Image fusion using a pan-sharpened IHS technique produced a higher resolution multi-spectral (MS) image. (3) The higher resolution MS image is blended with the SAR-DEM to produce an image terrain map. (4) Two complementary composites were then produced. The first image map contains of geomorphic features/surficial geology GIS layers, and 3D terrain information derived from the SAR-DEM image. The second image map is a composite of geomorphic features/surficial geology blended with the SAR-DEM-ETM+ image map. Integrated image maps generated in steps 1 and 3 provide standardized image base maps to display surficial geological and terrain information. [C2462]

"Smart Multi-Aperture Radar Techniques for Spaceborne Remote Sensing"

The paper deals with the performance of next generation SAR sensors, here referred to as SMART (Smart Multi Aperture Radar Techniques) equipped with digital beamforming capabilities. Apart from representing a technological jump, these sensors offer the flexibility of actually deciding on the (possibly hybrid) mode(s) of operation on-ground after the data have been acquired. The paper presents the performance of SMART system configurations and modes of operation for a digital beamforming SAR which covers a large swath with a high resolution. [C2463]

"Theoretical Model of SAR Altimeter over Water Surfaces"

This paper provides a brief overview of the objectives and methodology of the ESA funded project SAMOSA: "Development of SAR Altimetry Studies and Applications over Ocean, Coastal zones and Inland waters", and mainly concentrates on the development of a theoretical model for the mean return echo from a synthetic aperture radar (SAR) altimeter (also know as a delay doppler altimeter or DDA) observations over water surfaces, in the same spirit set by conventional altimeters. [C2464]

"Multistatic Scenarios for a GPS SAR System"

This paper presents research results in space-surface multistatic synthetic aperture radar (SS-MSAR) with non-cooperative GPS satellites. The effect of the system's geometry is investigated. We will show that in SS-MSAR, the spatial resolution depends on the geometry of the system, i.e. satellite-receiver-target positions relative to each other. General ambiguity function (GAF) and the point spread function (PSF) are defined in our case in a 3D case corresponding to our study. These criteria are then computed, and compared, for several scenarios including one (bistatic case) to three emitters (multistatic case). [C2465]

"Reflectivity and DEM Estimation from Multi-baseline Complex SAR Signals"

Multi-baseline interferometric Synthetic Aperture Radar (In-SAR) systems are used to obtain increased accuracy Digital Elevation Model (DEM) of the observed ground scene. The techniques which are commonly used exploit only the interferometric phase information, and are based on Maximum Likelihood (ML) estimation. Due to the difficulty of express the multi-baseline likelihood function in closed form, they adopt the statistical independence approximation of the interferometric phases. In this paper we present a method exploiting both amplitude and phase of the interferometric images, and allowing to express the multi-baseline likelihood function in closed form. It has also the advantage of correctly performing multi-baseline speckle reduction on the image intensity. [C2466]

"InSAR Monitoring of Landslides in Canada"

In this study we used differential and CTM InSAR techniques to monitor landslide slides at different geological sites in Canada. Our results show that InSAR measurements are providing new information on the deformation behaviour of complex landslide processes. [C2467]

"TanDEM-X: DEM Calibration Concept"

The TanDEM-X mission will derive a global digital elevation model (DEM) with satellite SAR interferometry. The aimed accuracies are an absolute height error of 10 m and a relative height error of 2 m for 90% of the data.

This requires a correction of the elevation heights after interferometric processing by residual systematic DEM errors. The estimation and correction of these errors is called DEM calibration. This paper gives an overview of the DEM calibration strategy within the TanDEM-X mission. First, the error sources and their influence on the DEM are determined by a functional description. Then, a strategy for a new block adjustment of DEMs is set up and evaluated with simulated and real DEMs. [C2468]

"TanDEM-X DEM Calibration and Processing Experiments with E-SAR"

The TanDEM-X mission has the goal to deliver a digital elevation model (DEM) that fulfils HRTI-3 quality requirements on a global scale. The interferometric height is determined by the phase difference between the two acquired images and the spatial geometry. Baseline errors intrinsic of the bi-static SAR configuration combined with errors and drifts of the radar instrument introduce phase inaccuracies in the interferogram. Therefore, an accurate calibration of the interferometric system parameters and independent height references are required. In order to validate the DEM calibration concept with real interferometric data, a measurement campaign was carried out with the experimental airborne radar system (E-SAR) of the German Aerospace Center (DLR) in Oberpfaffenhofen. This paper will present some of the various results from these interferometric experiments, stressing on the quality assessment of the ICESat GLAS14 elevation data, which will be a key aspect in a successful TanDEM-X DEM generation. [C2469]

"Automatic Forest Species Classification using Combined LIDAR Data and Optical Imagery"

Forest species classification is important for forest management and environment monitoring and protection. As the conventional methods are mainly based on the spectral signatures of forest canopies and the results are at stand level. With the high spatial resolution data, classification at individual tree level becomes achievable. The objective of this study is to develop a novel algorithm of tree crown segmentation for automatic classification at individual tree level. The approach uses the integrating laser scanning data with high spatial multispectral optical imagery. The automatic classification is composed of two stages: (1) tree crown segmentation, (2) species classification. The approach is applied to the test area consisting of both conifers and deciduous trees. The segmentation result shows good accuracy of crown delineation, and over 90% of the trees are segmented correctly. [C2470]

"Determining the optimum compromise between SAR data compression and radiometric performance -An approach based on the analysis of TerraSAR -X data-"

Data compression is crucial for modern synthetic aperture radar systems where high resolution or large coverage may result in huge amounts of raw data. Modern satellite systems, such as TerraSAR-X, give complete flexibility in choosing between various compression levels. This, however, results in additional effort to decide on the suitable compression level used, which may depend on the operation mode, polarization, scene backscatter, etc. The paper describes the approach used in the case of TerraSAR-X and shows the result of analyzing the data acquired during the commissioning phase. The methodology is considered novel in the sense that it combines SAR measured data analysis with theoretical, i.e. model based simulations, results and later combines theory and measured data to extract optimum compression levels. [C2471]

"Classification of Altimetric Signals using Linear Discriminant Analysis"

This paper addresses the problem of classifying altimetric waveforms backscattered from different kinds of surfaces including oceans, ices, deserts and forests. Appropriate features associated with altimetric radar waveforms are first introduced for this classification. These features are completed by radiometer temperatures and pre-processed using a linear discriminant analysis for dimensionality reduction. The classification of altimetric waveforms is finally achieved using the resulting pre-processed vector with reduced dimension. Different classification strategies are finally considered. These strategies are based on the nearest mean rule, the nearest neighbor method or on the multilayer perceptron. Various simulation results illustrate the performance of the proposed classifier. [C2472]

"TerraSAR-X: Complex Image Inversion for Feature Extraction"

In this paper we present two algorithms for information extraction from Single Look Complex (SLC) Synthetic Aperture Radar (SAR) images. The first algorithm is based on Tikhonov regularization with Total Variation (TV) and a Point-Based Feature (PBF) term. Based on the equivalence of Tikhonov and the Bayesian estimate, the second algorithm is a Maximum A Posteriori (MAP) estimation with a complex-valued Gauss-Markov Random Field (GMRF) in addition to the TV prior. The first algorithm produces a despeckled image preserving fine details and texture. The second algorithm gives a denoised image and in addition the estimated feature parameter vector θ . [C2473]

"Automatic Extraction of Water Bodies from TerraSAR-X Data"

Medium resolution SAR satellite data have been widely used for water and flood mapping in recent years. Since the beginning of 2008 high resolution radar data with up to one meter pixel spacing of the TerraSAR-X satellite are operationally available. The improved ground resolution of the system offers a high potential for water detection. However, image analysis gets more challenging due to the large amount of image objects that are visible in the data. Water body detection methods are reviewed with regard to their applicability for TerraSAR-X data. Flood detection approaches for rapid disaster mapping are presented in this paper. [C2474]

"Multi-Doppler Measurements of Atmospheric Rotors and Turbulent Mountain Waves"

Radar measurements of reflectivity and Doppler velocity for selected cases of rotors and turbulence associated with mountain waves from 2006 T-REX and NASA06 field campaigns are analyzed. The data were collected with the Wyoming Cloud Radar (WCR, <http://atmos.uwvo.edu/wcr>) on board the University of Wyoming King Air research aircraft (UWKA, <https://atmos.uwvo.edu/n2uw/>). The retrieval of single- Doppler vertical velocity at 30 m resolution above and below the aircraft and two-dimensional (2-D), high-resolution (on the order of 40x40 m) Dual-Doppler, vertical velocity fields below the aircraft are discussed. The results demonstrate complex dynamics occurring within mountain cap and roll/rotor clouds. Turbulent dynamics and small-scale vortices, without the presence of a larger-scale organized vortex, appear to be more prevalent below mountain wave crests at low levels. The analysis of radar data from consecutive passes during mountain wave events also suggests that while the terrain-induced waves exhibit both stationary and non-stationary behavior, there is a significant evolution in the turbulent dynamics under mountain wave crests and individual features/vortices have a variable life span (on the order of minutes to tens of minutes). The reflectivity fields reveal a disorganized and turbulent structure of the scatterers in the roll clouds. When scatterers are present below the roll cloud (e.g., due to precipitation) their distribution is highly non-uniform. Our radar data does not resolve the 3rd dimension (across these flight tracks) and thus some 2-D assumptions are made. The three-dimensionality of the terrain may influence the mountain wave structure and dynamics, but our assumptions are reasonable for flow structures generated by long mountain ranges. [C2475]

"Linear Inversion of PEC Scatterers"

The inverse scattering problems for Perfectly Electrical Conducting (PEC) objects is dealt with in the two dimensional case. A multifrequency multi-monostatic configuration is considered, where the illumination-observation domain is limited to one side of the investigation domain (i.e., only "reflection mode" data are disposable). Two direct linear models are considered and an inversion algorithm based on the Truncated Singular Value decomposition (TSVD) approach is proposed. The algorithm is applied to numerical and experimental data and results in the localization of the scatterers, in the case they are small with respect to the wavelength, or in the reconstruction of their shape otherwise. [C2476]

"Understanding the Distribution of Groundwater Resources using Synthetic Aperture Radar Data over Southwest Egypt"

Two NSF-funded studies (OISE-0417704; OISE-0513379) carried out by the author over SW Egypt (between 20-24.5degN and 25-32degE, in the East Oweinat and Tushka regions, respectively) used C-band Radarsat-1 SAR images and topographic data to understand groundwater distributions in the local aquifers that underlie the study areas. In these studies, areas with enhanced groundwater represent the best locations for groundwater development in order to address the water and food pressures that exist in the regions. In the East Oweinat area, small-scale agricultural development is already underway, while in Tushka there are plans for development in the near future. Radar waves are uniquely able to image beneath the desert sand in the eastern Sahara to reveal groundwater-related near-surface features, that is, the courses of ancient rivers and streams and faults and fractures. The depth of near-surface imaging for the datasets used is on the order of half a meter. The distribution of groundwater-recharge near-surface features was analyzed and the variation in groundwater storage was appraised. Three new areas have been identified as promising sites for agricultural development. [C2477]

"Combining CALIPSO and Meteosat Images to Study the Distribution of Atmospheric Dust"

The identification and tracking of atmospheric dust is important to many disciplines due to its impact on the climate and ecological system. Sensors on-board existing imaging satellites such as MSG and CALIPSO provide good horizontal and vertical resolution, respectively, and therefore the resolution of any dust products derived solely from one sensor will be limited in the same manner as the sensor. We propose a new method of

identifying dust distributions in the atmosphere using data from two separate satellite sources, the SEVIRI on-board MSG and the CALIPSO lidar. The approach employs a supervised classification method using texture data derived from a bank of Gabor filters. Once the dust has been identified, the SEVIRI data is augmented with vertical CALIPSO data to produce a 2D dust cloud top height distribution. [C2478]

"Change Detection with Misregistration Errors"

Bi-date change detection and image registration are based on local similarity measures. When applied to Synthetic Aperture Radar (SAR) observations, the first one is based on the comparison of the local probability density functions (pdf) of the 2 images, while the latter is based on correlation or mutual information (MI) measure. A specific implementation of MI has been found to be efficient in change detection from heterogeneous SAR images as well as for SAR image registration. This implementation may be splitted in 2 terms and that can be linked to the change detection part and to the registration one respectively. Hence a set of measures are proposed in order to perform similarity measure for change detection in homogeneous and heterogeneous SAR images that prevents from misregistration errors. This point of view has been applied to a set of Radarsat images and a pair of ERS images acquired in the frame of the International Charter Space and Major Disasters, corresponding to a lava flow and a flooding event. [C2479]

"An Adaptive Technique based on Similarity Measures for Change Detection in Very High Resolution SAR Images"

This paper presents a novel adaptive technique for change detection in very high geometrical resolution (VHR) Synthetic Aperture Radar (SAR) images that exploits information theoretical similarity measures for modeling the temporal evolution of probability density functions (pdfs). Image statistics for characterizing pdfs are adaptively estimated on a local basis by exploiting the spatial-context information of pixels on small homogeneous regions shared by multitemporal images (i.e., multitemporal "parcels"). The joint analysis of different orders statistics makes the method robust and suitable to the detection of both step changes of the backscattering and texture changes. The use of parcels allows one to model both complex objects in the investigated scene and borders of the changed areas and change details. Experimental results confirm the effectiveness of the proposed approach. [C2480]

"A DCT-based Change Detection Method for Multi-Temporal SAR Images"

This paper aims at effectively detecting the changes in multi-temporal synthetic aperture radar (SAR) images. Since pixel-based method does not sufficiently utilize the correlation between pixels, it usually may only be used in some specific applications. We propose a change detection method that is based upon discrete cosine transform (DCT) classification. It can utilize the correlation between pixels and eliminate unimportant or nuisance forms of changes. It generates a threshold automatically in DCT classification according to the relationship between DCT coefficient and pixel's gray level. In order to eliminate the block effect, we check pixels not only within the target block, but also inside the neighborhood window around the target block. Experimental results show that the proposed method outperforms some recently published pixel-based methods. [C2481]

"A Comparative Analysis of Tropospheric Water Vapor Measurements from MERIS and SAR"

Tropospheric water vapor delay is the main error source limiting the accuracy of SAR interferometric measurements. In persistent scatterer interferometry (PSI), the presence of atmospheric effects increases the required data amount for PSI immensely, limiting the reaction time and applicability of the technique. On ENVISAT, water vapor products derived from the optical sensor MERIS may be used to mitigate tropospheric effects in simultaneously acquired ASAR data. In this paper the atmospheric signals in MERIS and ASAR are compared, and methods for their optimal combination are suggested. [C2482]

"Bayesian DEM Reconstruction from SAR and Optical Data"

Interferometric SAR (InSAR) systems are able to estimate height profiles of the Earth surface. For the involved estimation problem, Maximum A Posteriori (MAP) statistical technique and Markov Random Field image models have been used, showing to be effective in case of multiple interferograms, obtained via different baselines/frequencies. In this paper, we are interested in the application of such estimation procedure in urban areas, where due to SAR geometry, many geometrical distortions appear. In particular, we focus on the layover problem. We present a procedure to manage layover areas, based on the optical and SAR data fusion. Moreover, we exploit the optical data to improve the a priori term of the MAP approach. We test the method on simulated data, showing the effectiveness of the method. [C2483]

"Time Series Analysis of Scansar Interferograms using the Small Baseline Subset Technique"

We generate a deformation time series by applying the Small Baseline Subset (SBAS) InSAR processing algorithm to ScanSAR (burst mode) data synthesized from ERS-1/2 stripmap SAR data. Careful selection of interferometric image pairs based on short spatial and temporal baselines mitigates higher levels of decorrelation observed in low-resolution ScanSAR data. We simulate burst mode data from 40 ERS-1/2 stripmap raw datasets over Phoenix, Arizona by omitting raw data lines. Interferograms are formed for varying amounts of burst overlap to reflect a realistic ScanSAR scenario and the effect of loss of resolution and coherence on accuracy of time series solution due to varying amounts of burst overlap is investigated. Comparison of ScanSAR SBAS results with stripmap SBAS results shows a mean error of 0.01-0.1 cm/year in velocity estimates and 0.4-2.1 cm error in displacements. [C2484]

"Multivariate AR Model based Support Vector Machine for Multispectral Remote Sensing Image Classification"

Time series statistical models such as autoregressive moving average (ARMA) were considered useful in describing the texture and contextual information of an remote sensing image. To simplify the computation, we use a two-dimensional (2-D) autoregressive (AR) model instead. In our previous research, the 2-D univariate time series based imaging model was derived mathematically to extract the features for further terrain segmentations. The effectiveness of the model was demonstrated in region segmentation of a multispectral image of the Lake Mulargias region in Italy. Due to the nature of remote sensing images such as SAR (synthetic aperture radar) and TM (Thermal Mapper) which are mostly in multi-spectral image stack format, a 2-D Multivariate Vector AR (ARV) time series model with pixel vectors of multiple elements (i.e. 15 elements in the case of TM+SAR remote sensing) are examined. The 2-D system parameter matrix and white noise error covariance matrix are estimated for further classifications. To compute the time series ARV system parameter matrix and estimate the error covariance matrix efficiently, a new method based on modern numerical analysis is developed by introducing the Schur complement matrix, the QR (orthogonal, upper triangular) matrix and the Cholesky factorizations in the ARV model formulation. As for pixel classification, the powerful Support Vector Machine (SVM) kernel based learning machine is applied in conjunction with the 2-D time series ARV model. The SVM is particularly suitable for the high dimensional vector measurement as the "curse of dimensionality" problem is avoided. [C2485]

"Analysis and Classification of high Arctic Glaciers with ASAR Data"

We apply a polarimetric classification scheme to Envisat Alternating Polarisation mode ASAR images and compare to ground truth data. By analysing images with a range of acquisition conditions and comparing the classification accuracy with the ground truth data, we investigate the influence of the acquisition conditions for glacier facies discrimination. We find that the main influence is the image swath angle, which affects the image pixel geometry. There was no obvious preference for the different polarisation channels, although the dual polarisation classifications were consistently better than single polarisation classifications. [C2486]

"Cross Comparison of ALOS PALSAR L-Band Retrieval Model Functions"

We make a systematic comparison of wind speed computed from the advanced land observing system (ALOS) phased array type L-band synthetic aperture radar (PALSAR) against wind speed analyses from an operational weather model. The standard deviation of the residual difference is very similar to results from C-band synthetic aperture radars (SARs) on Radarsat-2 and Envisat when compared against models, albeit with a systematic and easily removed bias. Results are limited to HH-polarization data. There is little available VV-polarization data over water. [C2487]

"Validation and Evaluation of QuikSCAT Ultra-High Resolution Wind Retrieval in the Gulf of Maine"

Researchers at Brigham Young University have created an experimental 2.5 km ultra-high resolution (UHR) wind product from the QuikSCAT scatterometer. This product adds to the standard 25 km and new 12.5 km resolution data provided by that satellite, and offers the potential for new access to coastal surface wind dynamics at the sub-mesoscale level. With its nineteen meteorological buoys, the Gulf of Maine provides an excellent test site for evaluating the UHR wind retrievals. Comparison with these buoys, mesoscale meteorological model winds, and standard QuikSCAT products throughout the month of October 2006 allows detailed investigation of UHR wind speed and direction. Even with a land contamination mask, the UHR product provides extended coverage near the coast. An additional ambiguity reselection routine improves wind direction agreement between the UHR winds and the other products. With this refinement, the ultra-high resolution winds show great promise in the coastal region. [C2488]

"Hybrid Neural Network Technique to Estimate Rainfall from TRMM Measurements"

Neural network is a nonparametric method to represent the relationship between radar measurements and rainfall rate. The relationship is derived directly from a dataset consisting of radar measurements and rain gauge measurements. Tropical Rainfall measuring Mission (TRMM) Precipitation Radar (PR) is known to be the first observation platform for mapping precipitation over the tropics. TRMM measured rainfall is important in order to study the precipitation distribution all over the globe in the tropics. TRMM ground validation is a critical important component in TRMM system. However, the ground sensing systems have quite different characterizations from TRMM in terms of resolution, scale, viewing aspect, and uncertainties in the sensing environments. In this paper a novel hybrid Neural Network model is presented to train ground radars for rainfall estimation using rain gage data and subsequently using the trained ground radar rainfall estimation to train TRMM PR based Neural networks. One year of ground data from Melbourne Florida and Houston Texas are used to demonstrate this hybrid approach. The performance of the rainfall product estimated from TRMM PR is compared against TRMM standard products. A direct gage comparison study is done to demonstrate the improvement brought in by the neural networks. [C2489]

"An Improved Oceanic Rainfall Retrieval Algorithm and Results from Seawinds"

This paper describes the development of an oceanic rainfall retrieval algorithm that combines both the simultaneous active (radar backscatter) and passive (microwave brightness temperatures) observations from the SeaWinds scatterometer on the QuikSCAT satellite. The retrieval algorithm is statistically based, and has been developed using collocated measurements from SeaWinds, the Tropical Rainfall Measuring Mission (TRMM) Microwave Imager (TMI) rain rates, and the National Center for Environmental Prediction (NCEP) wind fields. The rain is retrieved on a wind vector cell (WVC) measurement grid that has a spatial resolution of 25 km. Due to its broad swath coverage, SeaWinds affords additional independent sampling of the oceanic rainfall, which may contribute to NASA's future Global Precipitation Mission. Results emphasize the powerful rain detection capabilities of the SeaWinds retrieval algorithm. [C2490]

"Progress Toward Validation of Quikscat Ultra-High-Resolution Rain Rates using TRMM PR"

Although originally designed solely for wind retrieval, the QuikSCAT scatterometer has also proved to be a useful tool for rain retrieval. Resolution enhancement algorithms designed for QuikSCAT allow for ultra-high-resolution (UHR) (2.5 km) simultaneous wind and rain (SWR) retrieval. To enable SWR retrieval, we adjust the geophysical model function (GMF) to account for rain effects such as attenuation or increased backscatter due to increased surface roughness. Comparisons of a co-located data set show that QuikSCAT UHR SWR rain rates are comparable to those from Tropical Rainfall Measuring Mission Precipitation Radar (TRMM PR) but have higher variance. The noise level of the QuikSCAT rain estimates can be reduced by forming the reduced resolution rain rate estimates. As expected, rain estimates are significantly worse in regions where wind dominates the backscatter. [C2491]

"Lidar based Particulate Flux Measurements of Agricultural Field Operations"

In this paper, we discuss the potential of using remote sensing to map and track the evolution of emission plumes from agricultural facilities. Toward this approach, we utilize a multi-wavelength lidar (Aglite) that is real-time calibrated using a suite of standard point sensors. The Aglite lidar is a robust, agile, and easily operated system that displays emitted particulate distributions in a few seconds under most meteorological and diurnal conditions. Aglite uses three laser wavelengths in combination with information derived from an array of point sensors to distinguish between different types and sizes of particulate emissions. The resulting combination of point samplers and scanning lidar provides near real time measurements of facility operations which can be used to evaluate emission fluxes. [C2492]

"An Experiment of GB-SAR Interferometric Measurement of Target Displacement and Atmospheric Correction"

We made a ground-based synthetic aperture radar (GB-SAR) system and tested its interferometric SAR (InSAR) measurement on the displacement of a trihedral corner reflector with atmospheric correction in terms of humidity and range. The GB-SAR worked at C-band with the synthetic aperture length of 5 m. Fully-polarimetric images were obtained with resolutions of 25 cm in range and 0.32 degree in azimuth direction. Located 160 m away from the system, the reflector was moved from 1 mm to 40 mm toward the system during each acquisition. An atmospheric correction function was obtained in terms of humidity and range by analyzing the phase of several stationary targets. The result showed an atmospheric delay of 3 mm at 160 m range when humidity changed from 47% to 58%. After atmospheric correction, DInSAR error was less than 1 mm with the correlation coefficient

of 0.9999 when compared with the actual displacements. We concluded that atmospheric correction should be reinforced somehow for most spaceborne InSAR applications. [C2493]

"Scansar Differential Interferometry and Wet Delay Correction: Case Studies in Dangxiong, Tibet"

ScanSAR is a synthetic aperture radar (SAR), which has a very wide image swath. This provides a new option for interferometric applications. It makes the large scale deformation observation easier to implement. In this paper, we applied ScanSAR differential interferometry in Dangxiong, Tibet to observe the crust deformation there. However, the accuracy of ScanSAR interferometry is also affected by water vapour in the atmosphere. In our work, we tried to correct the wet delay using synchronous MERIS integrated water vapour products. In the end of this paper, the advantages and problems of ScanSAR interferometry are concluded. [C2494]

"Spaceborne Hyperspectral Image Generation based on Airborne Hyperspectral Image"

In order to support spaceborne hyperspectral sensor system design, an end-to-end simulation model for spaceborne hyperspectral image generation starting from the airborne image has been developed in this paper. Airborne image after being resampled both in the space and spectrum performs as the at-sensor radiance that is the input of the sensor model. Sensor model is the main part of proposed model. According to the sensor's imaging process, the simulation is divided into four sub-modules, which are optics, detector, electronics parts and system noise. Based on the theory of optical transfer function (OTF), each sub-module can be treated as a spatial filter and thus its simulation can be realized in the spatial frequency domain. Using parameters of spaceborne sensor Hyperion as well as the image acquired by Airborne Visible and Infrared Imaging Spectrometer (AVIRIS), the validity of the proposed model for sensor design and operation are also demonstrated in the paper. [C2495]

"Derivation of sub-footprint scale σ_0 observed by TRMM Precipitation Radar"

To derive the sub-footprint scale σ_0 from TRMM/PR observation datasets, a new formulation to calculate the sub-footprint σ_0 is devised. The sub-footprint scale σ_0 would be useful to, (1) relieve the underestimate of the path integrated attenuation (PIA) at off-nadir angle observations over land, and (2) examine the nonuniformity of rainfall. The PIA estimated from σ_0 of the standard product "2A21" tends to be biased toward small at off-nadir angle observations over land. Because 2-6 sub-footprint scale σ_0 exists within one instantaneous field of view (IFOV), σ_0 at the surface echo peak is likely unrepresentative for the IFOV especially for observations over land, depending on the surface conditions and the nonuniformity of rain. The underestimate of PIA can be relieved by averaging the subfootprint scale σ_0 over the IFOV (5 km by 5 km) for each angle bins. The effect of the unbiased PIA, estimated with the sub-footprint scale σ_0 , on the rain rate estimate is examined. The result shows about 10% increase of the rain rate at off-nadir angle observations over land. [C2496]

"Extraction of Building Heights from VHR SAR Imagery using an Iterative Simulation and Match Procedure"

The new spaceborne very high resolution (VHR) SAR sensors onboard the TerraSAR-X and COSMO-SkyMED satellites have a spatial resolution of up to 1 meter. In VHR SAR data, features from individual urban structures (like buildings) can be identified in their characteristic settings in urban settlement patterns. In this paper, we present a novel methodology for the height estimation for generic man made structures from single power SAR data. The proposed approach is based on the definition of a hypothesis on the height of the building and on the simulation of a SAR image for that hypothesis. Then a matching procedure is applied between the estimated and the actual SAR images in order to validate the height assumption. The process is iterated for different initial height assumptions until the matching function is satisfied and thus the building height is estimated. The efficiency and the properties of the proposed method are demonstrated for the height estimation of flat- and gable roof buildings from a VHR airborne SAR scene and for a pyramid in Giza (Egypt) from VHR TerraSAR-X SPOT beam data. [C2497]

"3D Urban Remote Sensing using Dual-baseline POL-InSAR Images at L-Band"

This paper generalizes a multibaseline interferometric SAR signal model to the polarimetric configuration. Based on this formulation, two high-performance array signal processing techniques are adapted to analyze multibaseline POL-InSAR observations. These new methods enhance the height estimation of scatterers by calculating optimal polarization combinations and allow the determination of their physical characteristics. Applying the algorithms to urban environments, the building layover problem is resolved by means of polarimetric dual-baseline InSAR measurements: Up to two components within one azimuth-range resolution cell are separated. The techniques are tested using dual-baseline Pol-InSAR data acquired by DLR's E-SAR system

over Dresden city. [C2498]

"Evaluation of the Effect of the Orbit Boost of the TRMM Satellite on the PR Rain Estimates"

The rainfall amount estimated by PR shows a decrease after the satellite altitude was changed from 350 to 402.5 km in August 2001 to extend its lifetime. The major causes of the changes in rain estimates by the orbit boost are (1) the sensitivity degradation by the increase of satellite altitude, (2) the increase of the range of surface clutter by the increase of the footprint size, and (3) the mismatch between the transmission and reception angles for one pulse in every 32 pulses. The decrease of the echo signal strength by the change of the satellite altitude from 350 km to 402.5 km is 1.21dB ($= 20\log(402.5/350)$). From a simulation result, we estimate a decrease of 0.50 % in the surface rainfall estimates by the sensitivity degradation. Because the heights of clutter free bottom have increased at the off-nadir by the increase of the footprint size from 4.3 km to 5.0 km, the sampling range bins for near-surface rain have raised and the PR misses low rain systems more often after the boost than before the boost. A beam mismatch correction is executed in the current 1B21 algorithm, but the correction algorithm still has a small problem and rain rate estimates near the surface in the second-half of the PR scan tend to be smaller than those in the first-half on average. The changes due to the second and third causes can be estimated by comparing the estimates at off-nadir bins with those at near-nadir bins with the assumption that rain rates at all range bins should be the same on average. We estimate that the estimated surface rain decreased by 2.47 % by the increase of the footprint size and by 2.93 % by the beam mismatch after the boost. In summary, it is necessary to add a 5.90 % ($= 0.50 + 2.47 + 2.93$ %) correction to compensate the biases in the surface rain estimates caused by the boost. [C2499]

"PALSAR SCANSAR SCANSAR Interferometry"

We have examined the capability of the PALSAR SCANSAR SCANSAR interferometry by observing the African forest and Sahara desert, both of which are separated 46 days in March and April of 2008. These two paths are well tuned for the orbital tube of 200 m and the beam synchronization of the transmission positions in 200 m to 500 m, we have succeeded the PALSAR SCANSAR SCANSAR interferometry and achieved the detection of the height information. We will report the results in this paper. [C2500]

"Bistatic Pol-InSAR Scenario and Evaluation by Forest Scattering Simulations"

This paper comes within the context of exploring the potential of bistatic Pol-InSAR. Numerical simulations are carried out by means of MIPERS, multistatic interferometric polarimetric electromagnetic model for remote sensing which has already proved many abilities. The latter involves an electro-magnetic coherent approach of a discrete natural media description and enables us to model Pol-InSAR observables over forests in the bistatic configuration. Taking into account bistatic SAR constraints in terms of resolution, critical base-line, SNR, range and height ambiguities, new configurations for Pol-InSAR applications are envisioned. [C2501]

"Low-Altitude Digital Photogrammetry Technique to Assess Ephemeral Gully Erosion"

Recent development in digital imaging makes it feasible to employ photogrammetry procedures to delineate landscape and erosion features. We evaluated the feasibility of using low-altitude photogrammetry to assess ephemeral gully erosion at agricultural fields. We tested an unmanned aerial vehicle (UAV) and a ground based technology to acquire low-altitude surface images to create digital elevation models (DEMs). Collaborators at Wuhan and Yangling in China also used the LIDAR technology on a steep slope for DEM acquisition. We found (1) current DEMs derived from airplane flights are not accurate enough to delineate ephemeral gully channels; (2) a ground-based LIDAR system is capable of generating an accurate DEM and gully channels at steep hillslopes; and (3) at gentle slope situations, low altitude photogrammetry has the potential for acquiring DEMs. Nevertheless, proper deployment of a camera at a suitable height to have sufficient aerial coverage while maintaining the resolution at the Z (elevation) scale to assess rill ephemeral gully development is still a challenge. [C2502]

"Performance Analysis of Multivariate Super-resolution Processing of Polarimetric Synthetic Aperture Radar Tomography"

In a previous paper, the authors developed a technique known as Vector Linear Prediction (VLP) which achieved super-resolution processing for polarimetric SAR tomography. In this paper, the performance of this multivariate super-resolution processing technique is investigated. Both simulations and field data are used to assess the limitations of this technique due to the loss of spatial and polarimetric coherence. The model assumes two scattering centers in each image pixel. The study shows that if one component remains linearly polarized, while the other is fully depolarized, then meaningful interferometric information can still be retrieved for the linearly

polarized scattering center. However, if the depolarized component is also spatially decorrelated (loss of spatial coherence), then the interferometric phase estimates of both components are prone to significant errors. The field data is used to verify and validate the observations obtained with the simulations. [C2503]

"Baltic Sea Ice Thickness Charts based on Thermodynamic Snow/Ice Model, C-band SAR Classification and Ice Motion Detection"

We have studied the estimation of the Baltic Sea ice thickness based on a thermodynamic ice model and SAR data to produce ice thickness charts (ITCs) for navigation. Our new algorithm, also taking into account the ice motion between successive SAR images, has shown promising results. [C2504]

"Comparison of Airborne Radar Altimeter and Ground-based Ku-band Radar Measurements on the Ice Cap Austfonna, Svalbard"

We compare data from the European Space Agency's (ESA) Airborne SAR/Interferometric Radar Altimeter System (ASIRAS) with ground-based Very High Bandwidth (VHB) stepped frequency radar measurements in the Ku-band. Using the VHB radar we have been able to pinpoint the major backscatter sources within the accumulation area. The ground-based and airborne waveforms show good agreement and we therefore find the ground-based measurements valuable for validation and interpretation of the airborne altimeter waveforms. The comparison shows that the surface and the Last year Summer Surface (LSS) can be tracked in the airborne data, but fails at lower elevations with snow depths less than ~1 m. For ground truth, i.e. snow depth, we use ground based radar profiles (800 MHz), snow pits, snow probing, and density retrieved from 7-12 m deep boreholes using a neutron probe. [C2505]

"The New ONERA Multispectral Airborne SAR System"

This paper provides an overview of the new airborne SAR system developed by the French Aerospace Lab ONERA over the last two years. This system, called SETHI, was developed according to the standard FAR25 applied to civil application. The main improvement compared to the previous ONERA airborne radar system RAMSES is that the antennas are located in two pods compatible with small aircrafts like the Falcon 20. This pod-based configuration allows the easy integration of any kind of payloads under the single certification of the pods by authorities. In the first section a quick introduction presents the aircraft configuration (cabin and pods) with an overview of SETHI development. The second section describes the SETHI concept with the installation on board the Falcon 20 cabin, the hardware development to control and command all ONERA racks, the pods with their control and command systems. The last section illustrates the validation campaign which took place in September 2007 at Ni circmes Garons Airport in France. [C2506]

"Building Detection from High Resolution PolSAR Data by combining Region and Edge Information"

We propose a three step method to extract buildings from the high-resolution PolSAR data, using both the region-based and edge-based information. Firstly, low-level detectors are employed to provide raw region and edge information of the scene. In the second step, improved region-based building detection results are achieved by fusion of label fields, meanwhile the building profile line segments are extracted under a line Markov random field framework. The last step gives the final building footprint estimates: initial rectangle buildings are defined from the building line segments; by optimizing a surface criterion, the final rectangles are retrieved to fit the region-based building detection results. The effectiveness of this method is demonstrated using the real full PolSAR data. [C2507]

"Geometrical and Topological Urban Areas Characterization using TerraSAR-X Data"

With the launch of the German TerraSAR-X system in June 2007, a new generation of high-resolution spaceborne synthetic aperture radar (SAR) data is available; which should facilitate the interpretation of urban environments. This article proposes a new automatic tool for geometric and topological urban areas characterization. Our approach is divided into three main steps. First, a bright linear structures detector is applied to extract the geometrical information. Then, a graph-based spatial characterization is used to model the topological relationships between the different detected bright pixels (nodes). Next, a classification by examining the profile of the distributions of the angles between neighboring nodes, is performed in order to label the linked structures. Evaluations of the proposed approach in characterizing the geometry and topology of urban areas were carried out using TerraSAR-X data over three different cities: Las Vegas in the United States, Paris in France and Cairo in Egypt. [C2508]

"Coherent Decomposition of Fully Polarimetric Radar Data"

This paper presents a coherent decomposition scheme for a few scattering matrix data. A simple model-fitting decomposition method is applied to retrieve scattering mechanism or identify scatterers based on the coherency matrix. The decomposition results are compared with some experimental data obtained by fully polarimetric FM-CW radar. It is shown the scattering mechanisms are well recovered and the orientation angles of wire scatterer are precisely measured. [C2509]

"Developing Aerosol Height Product from MODIS and Synergy of MODIS and CALIPSO Measurements for Global Application"

Aerosol vertical distribution is critical in many perspectives of atmospheric research. Lidar instrumentation is currently considered as the only means in providing the ground truths of aerosol vertical profiles. The MODIS normalized aerosol height index (NAHI) can be used routinely to estimate aerosol layer height with the same coverage of MODIS AOD, creating a virtual 3-D view of daily aerosol fields. The synergy of the wide-coverage MODIS aerosol height index and high-precision CALIPSO aerosol vertical profile enables us to constrain NAHI and also translate the estimated errors to the entire MODIS swath. [C2510]

"Polarimetric Scattering Analysis for Simplified Man-Made Structure Model on Rough and/or Inclined Ground Plane"

This paper analytically examines polarimetric scattering for a simplified man-made structure model, by utilizing the finite-difference time-domain (FDTD) method. The model considered here simulates a building in mountainous environment and is composed of a dielectric rectangular parallelepiped on finite rough and/or inclined plate. The statistical FDTD analysis on two polarimetric indices, the scattered power decomposition and the polarimetric correlation coefficient, with respect to squint angle change is carried out. It is found from the detailed analysis that the considered polarimetric indices are valid even when the surface of the ground plate has small roughness and gentle slope. This result contributes to the development of Polarimetric Synthetic Aperture Radar (POL-SAR) image analysis for detecting or classifying man-made residential houses in mountainous region. [C2511]

"Estimation of the Equivalent Number of Looks in Polarimetric SAR Imagery"

We present two new estimators for the equivalent number of looks (ENL) designed for polarimetric synthetic aperture radar data. These are the first known estimators to utilise the full multilook polarimetric covariance matrix, and both are derived from moments of the Wishart distribution. The first estimator is obtained from the second-order trace moment, which provides a multivariate generalisation of the conventional ENL definition. The second estimator is found from the log-determinant moment, and is also shown to be the maximum likelihood estimator. The latter estimator proves to have superior statistical properties to any other known ENL estimator. These properties are decisive for the good performance obtained with a proposed procedure for unsupervised estimation. We demonstrate on airborne AIRSAR data how a robust ENL estimate can be extracted from the distribution of small sample estimates collected over the whole scene. [C2512]

"Hybrid-Quad-Pol SAR"

Data products from a quadrature-polarized synthetic aperture radar (SAR) are fully characterized by Stokes parameters. It follows that choice of the polarization basis of either the transmitted or the received EM fields has no impact on the measurement potential of the system. Hence the polarization plan for a quad-pol SAR can be selected to optimize the radar's engineering performance. The logical conclusion is that an optimal quad-pol radar should transmit circular polarization, and receive orthogonal linear polarizations. This paper shows that there is no loss in SNR on any polarization combination in the quad-pol data products as a result of this architecture, which is a more robust result than is true for a hybrid-dual-pol radar, in which SNR preservation is true if and only if the output polarization basis is chosen to match the input (circular) basis. [C2513]

"Road Extraction and Network Building from Synthetic Aperture Radar Images using A-Priori Information"

This paper describes a method for the extraction of road networks from radar images. Three phases can be distinguished: (1) detection of road lines, (2) network building, and (3) network fusion. The method has been demonstrated on two radar images, one urban and one rural. Despite the differences, the procedure was able to cover a large part of both networks that was not obscured by trees. This was done using roughly the same parameters. Topology was preserved, and one of the networks was fused with a network from a 1: 50,000 digital map, and one extracted from a high-resolution optical image. However, the network extraction and merging process described in this paper can not be regarded as optimal. Additional rules and processing are required.

Useful input is expected from image analysts with respect to the procedure and results. [C2514]

"Image Registration of TerraSAR-X Data using Different Information Measures"

Image registration is known as an important part of generating Digital Elevation Models (DEM) with Interferometric SAR (InSAR) processing and is one of the critical preprocessing steps in remote sensing. It is used in the formation of 3-D models based on 2-D images taken at different view points as well as for mosaicking applications. The paper gives an overview of the information measures which can be used for automatic generation of reference points and finding the correspondences in the second image. The approach is validated with simulated and real image pairs originate from the TerraSAR-X satellite. Additionally to the classic correlation based methods, we will employ, compare and combine theoretical methods, based on information theory, such as mutual information, alignability in conjunction with automated bin size determination to achieve optimally. Considering the co-registration of single look complex SAR data, where correlation approaches are standard, the exploitation of similarity measures and transformation, based on information theory, is rather novel. Comparing these novel approaches with standard references with respect to quality and quantitative measures, will broaden the scientific understanding, and, furthermore, provide new insights concerning co-registration techniques for interferometric applications. [C2515]

"Simulation of Spaceborne Radar Observations of Precipitation: Application to GPM-DPR"

Global precipitation measurement (GPM) is poised to be the next generation precipitation observations from space after the TRMM mission. The GPM will carry a dual-frequency precipitation radar (DPR), operating at Ku-band, and Ka-band frequencies. Since spaceborne precipitation observations have never been done in Ka-band before, extensive research work on dual-frequency radar, including electromagnetic wave propagation characteristics from space and retrieval algorithms are essentially required in developing system design and instrument performance evaluations. This paper presents a simulation-based study of Ku-and Ka-band radar observation of precipitations. [C2516]

"Evaluation of a Statistical Fusion of Linear Features in SAR Data"

In this paper, we describe an extension of an automatic road extraction procedure developed for single SAR images towards multi-aspect SAR images. Extracted information from multi-aspect SAR images is not only redundant and complementary, in some cases even contradictory. Hence, multi-aspect SAR images require a careful selection within the fusion step. In this work, a fusion step based on probability theory is proposed. During fusion each extracted line primitive is assessed by means of Bayesian probability theory. The assessment is based on the attributes of the line primitive (i.e. length, straightness, etc), global context and sensor geometry. The fusion and its integration into the road extraction system are tested in a sub-urban SAR scene. [C2517]

"X-band InSAR Observations in New Orleans, Louisiana"

Understanding the effects of regional subsidence in New Orleans, Louisiana requires knowledge of a number of factors (coast-parallel normal growth faults, deltaic deposit system, fluid withdrawal, etc). High accuracy and spatially dense subsidence data that can be obtained by TerraSAR-X (TSX) InSAR analysis can help to separate these various subsidence processes. In this study we report first X-band InSAR result using TerraSAR-X to detect urban subsidence with high spatial resolution. Our results can be tested against other InSAR results that may be derived from ERS, ENVISAT, and RADARSAT-1 and RADARSAT-2. These comparisons will provide useful tests for the general applicability and accuracy of the new X-band space-borne SAR interferometry. [C2518]

"A Critical Analysis to Generate Change Detection Map using SAR Interferometry for Land Subsidence Monitoring of New Orleans City of USA"

Present paper aims to critically analyze and study the SAR interferometric RADARSAT-1 data for land subsidence monitoring system for New Orleans USA, using Differential SAR Interferometry (D-InSAR) approach. In Louisiana, areas along the coast are sinking as much as one inch a year, and New Orleans is among the worst affected area due to land subsidence. For mapping subsidence, 84 complex data sets from April 15, 2002 to March 15, 2007 were available. Out of this, we have chosen six sets of suitable differential interferometric pairs with approximately one year of temporal span and six interferometric pairs to provide DEM generation for the above differential pairs. In this paper, change detection due to surface deformation is identified using D-InSAR methodology and is compared with classical change detection approach using MRD (mean ratio detector). Results show that subsidence was widespread throughout New Orleans, with maximum subsidence near MRGO canal in period of March 01, 2005 to April 1, 2006. [C2519]

"Radar Backscattering Measurement of a Paddy Rice Field using Multi-frequency(L, C and X) and Full-polarization"

The objective of this study is to measure backscattering coefficients of paddy rice using L, C, X-bands scatterometer system with full polarization and various angles during a rice growth variables. The measurement was conducted at an experimental field located in National Institute of Agricultural Science and Technology (NIAST), Suwon, Korea. The rice cultivar was Japonica type, called Chuchung. The scatterometer system consists of dual-polarimetric square horn antennas, HP8720D vector network analyzer (20 MHz ~ 20 GHz), RF cables, and a personal computer that controls frequency, polarization and data storage. The backscattering coefficients were calculated by applying a radar equation for the measured at incidence angles between 20deg and 60deg for full polarization (HH, VV, HV, VH), respectively, and compared with rice growth data such as plant height, stem number, fresh and dry weight and LAI that were collected at time of each scatterometer measurement simultaneously. [C2520]

"Simulation of ASIRAS Multilooked Echoes for Snow Covered Sea Ice"

We have studied simulation of the ESA's ASIRAS (Airborne SAR/Interferometric Altimeter System) altimeter echoes for snow covered first-year sea ice. Simulated echoes can be used to investigate the relationships between the snow and ice characteristics and the measured echoes, and for the development of range retracking algorithms. Our results show that when snow cover is dry, the ice surface echo dominates. Snow cover properties have a large effect on the ice freeboard estimation from the ASIRAS data. [C2521]

"P-band Polarimetric Ice Sounder: Concept and First Results"

ESA has assigned the Technical University of Denmark to develop an airborne P-band ice sounding radar demonstrator. The intention is to obtain a better understanding of the electromagnetic properties of the Antarctic ice sheet at P-band and to test novel ice sounding techniques in preparation for a potential spaceborne ice sounding radar. The airborne system is a coherent, high-resolution and fully polarimetric radar. Aperture synthesis is applied in the along track direction and an experimental surface clutter suppression technique based on a multi-aperture antenna can be applied in the across track direction. In May 2008, a proof-of-concept campaign was organized in Greenland, where data were acquired over the ice sheet. The system proved capable of detecting the bedrock under 3 km thick ice and of mapping the internal ice layers down to a depth of at least 1.3 km. In this paper, the system concept is outlined and first results are presented. [C2522]

"A VHF Radar for Deployment on a UAV for Basal Imaging of Polar Ice"

A VHF-band radar is being developed to characterize polar ice sheets and their basal conditions from a UAV developed specifically for low-altitude polar operation. The radar's 195-MHz center frequency, 30-MHz bandwidth, and 200-W transmit power will map internal layers and ice thickness with a depth resolution of less than 3 m in ice, and image the ice-bed interface. To satisfy the mass and volume constraints of the UAV, a distributed architecture was developed employing transmit/receive modules mounted on each of the eight wing-mounted wide-bandwidth Vivaldi antennas. An eight-channel digital waveform generator will be used to create transmit waveforms to simultaneously measure ice thickness and map internal layers along the nadir track, and image ice-bed interface on the left and right sides of the platform in strip-map mode. [C2523]

"SAR Image Analysis to Estimate Freeze-Thawdates for a High Latitude Lake in Alaska"

This paper presents a novel method to estimate freeze-thaw dates of a small lake, with area 10 km², using SAR data from RADARSAT-1 remote sensing spacecraft. The algorithms analyze an annual time series of the difference in average backscatter, between the lake and the surrounding region, to estimate the day of occurrence of the respective lake ice event. The initial results obtained, using multi-year data from a northern high-latitude lake, are promising. The mean absolute error in estimating the thaw date is 0.7 days and for the freeze date it is 4 days. These results encourage further testing of these algorithms on lakes in other geographic regions. [C2524]

"Polarimetric Scattering Model Decomposition for Pol-InSAR Data"

This paper presents scattering model decomposition technique with Pol-InSAR datasets. The target model decomposition based on the scattering mechanisms corresponding to surface, double, and volume scattering, is one of the powerful tools to analyze and classify the ground surface conditions with fully polarimetric SAR data. However, we sometimes meet difficulty that the power of the decomposed component(s) becomes negative. This is caused by assumptions in the decomposition technique. When a Pol-InSAR dataset is available, additional observables can be obtained. These new observables will be available to resolve the difficulty of negative power

in the conventional decomposition technique. In this paper, we consider the scattering model decomposition technique with Pol-InSAR data, and propose some modifications for the decomposition. [C2525]

"Monitoring Changes in the Antarctic Ice Sheet from 1978 to 2007"

This paper presents a study distilling radar backscatter measurements made by three Ku-band scatterometers of the Antarctic ice sheet over a nearly thirty-year study period. Backscatter signature modeling techniques are used to compensate for observation geometry and operating frequency differences among the sensors. Findings of this study include large regions of both positive and negative change in average backscatter, particularly in regions of West Antarctica and along much of the coast. [C2526]

"Decadal Mass Balance of the Greenland and Antarctic Ice Sheets from High Resolution Elevation Change Analysis of ERS-2 and Envisat Radar Altimetry Measurements"

Here we measure fine-scale polar ice sheet elevation change and estimate decadal mass balance for the Greenland and Antarctic ice sheets from ERS-2 and ENVISat satellite radar altimeter data. The Greenland results show that moderate to slightly positive elevation change rates (ECRs) dominate the interior areas while large negative ECRs are observed for many coastal areas. In Antarctica, glaciers in the coastal areas of the West Antarctic Ice Sheet (WAIS) are experiencing rapid thinning. The strong thinning of some of these glaciers extends well into the interior of the continent. Over the East Antarctic Ice Sheet (EAIS), positive ECRs dominate the interior areas while some glaciers in coastal areas are experiencing thinning. The equivalent mass change for the GIS, EAIS, WAIS, and AIS over the period 1995-2006 is -20, 27, -53, and -26 Gt/yr, respectively. [C2527]

"Polarimetric Deformation Maps Retrieval of Urban Areas using Ground-Based SAR Acquisitions"

A one-year subsidence monitoring activity has been carried out by the Remote Sensing Laboratory (RSLab) of the Universitat Politècnica de Catalunya (UPC) using an X-band ground-based SAR sensor. The project aimed at studying the subsidence phenomenon induced by salt mining extraction of the past years in the village of Sallent (Spain). The polarimetric capability of the system allowed to gather zero-baseline POL-SAR data in the single-pass mode in 9 different days, from June 2006 to April 2007. The estimation of the linear component of deformation process obtained using each polarization channel separately is here compared with the result of a new approach exploiting the full knowledge of the scattering matrix at once. For this purpose, a coherence-based approach is employed. The higher amount information carried by polarimetric data is finally pointed out both in terms of number of reliable pixels selected within the scene and higher quality of the retrieved subsidence map. [C2528]

"Analysis of the Interaction of Aerosol Transport Layers on Local Air Quality"

In this paper, the usefulness of multi-wavelength lidar measurements to study the interaction of aerosols in the PBL with long range advected aerosol plumes is presented. Lidar's measurements are used to determine the plume angstrom exponent, which is used to differentiate smoke events from dust events, as well as partitioning the total aerosol optical depth obtained from a CIMEL sky radiometer between the PBL and the high altitude plumes. Furthermore, the correlation between the lidar derived PBL aerosol optical depth and surface PM_{2.5} is high, only if the optical depth from the upper level plumes is taken into account. In addition, the dynamic interaction of high altitude plumes interacting with the PBL result a dramatic rise in surface PM₁₀ concentrations without a corresponding dramatic rise in PM_{2.5} concentrations. These observations strongly suggest the deposition of large particulates into the PBL which is consistent with both lidar angstrom coefficient measurements and back-trajectory analysis. [C2529]

"Review of Polarimetric Indicators for Forest Characterisation over Several Sites"

Global warning is now known to be the major environmental issue mankind will have to face in the next decade. Monitoring of vegetation and biomass is clearly an essential piece of information required at all levels ranging from the scientific studies to understand and forecast, to the political world responsible for drafting remediation policies and evaluating their impact. Microwave remote sensing with the low-frequency SAR technique can provide a useful characterization of forest (spatial coverage, species, density, height...) at a global scale, relying on the all-weather imaging capabilities of SAR linked with the significant penetration of the low-frequency EM wave in the canopy. In this paper, we will review the potential polarimetric indicators and evaluate their performance over several types of forest. We will particularly focus on the impact of the topography and the influence of the weather conditions. [C2530]

"Agricultural Vegetation Parameter Estimation using Pol-SAR: Retrieval of Soil Moisture"

In this paper the focus is given to the soil moisture retrieval under a vegetation cover, exemplarily for two crop types winter wheat and rape. For this Pol-SAR data over a whole vegetation period were used acquired in the frame of the AGRISAR campaign in 2006 at L-band. The potentials and limitations over time are investigated by modifications of the model based Freeman decomposition in order to decompose the scattering contributions and to invert the surface and dihedral scattering component for soil moisture estimation. The applied decomposition approaches for agricultural land surfaces are suitable, but exhibit deficiencies in modeling the volume component, even though some improvements due to the modifications could be presented. In the end the soil moisture estimation does not perform constantly well over the whole acquisition period due to the complexity of the crop vegetation. [C2531]

"A New Superresolution SAR Imaging Algorithm based on Extrapolation"

In this paper, we present an extrapolation approach, which uses minimum weighted norm constraint and minimum variance spectrum estimation, for improving synthetic aperture radar (SAR) resolution. Minimum variance method is a robust high resolution method to estimate spectrum. Based on the theory of SAR imaging, the signal model of SAR imagery is analyzed to be feasible for using data extrapolation methods to improve the resolution of SAR image. The method is used to extrapolate the efficient bandwidth in phase history field and better results are obtained compared with adaptive weighted norm extrapolation (AWNE) method and traditional imaging method using simulated data and actual measured data. [C2532]

"Identification of Coherent Scatterers: Spectral Correlation vs. Multi-Chromatic Phase Analysis"

In recent years, attention has been devoted to the possibility of retrieving accurate phase information from stable targets in long SAR data series through Permanent Scatterers Interferometry (PSI), SBAS approach or equivalent methods. Recently, alternative methods for detecting stable targets on single images have been investigated. In particular, the availability of new SAR sensors provided with innovative features, including a wider transmitted bandwidth, allows to explore backscatter stability in the new dimension given by spectral diversity. The Multi-Chromatic Phase (MCP) approach, introduced in [2], uses images processed at range sub-bands and explores the phase trend of each pixel as a function of the different central carrier frequencies. In this paper we present the results of the application of this technique to point target detection. We compare the results with an alternative method proposed in [5] which identifies scatterers with stable spectral behavior. [C2533]

"Focusing SAR Data Acquired from Non-Linear Sensor Trajectories"

Standard focusing of SAR data assumes a straight recording track of the sensor platform. Small non-linearities of airborne platform tracks are corrected for during a motion compensation step while keeping the assumption of a linear flight path. In the following, the processing of SAR data from non-linear tracks is discussed as may originate from small aircraft or drones flying at low altitude. They fly not a straight track but one dependent on topography, influences of weather and wind, or dependent on the shape of dedicated areas of interest such as rivers or traffic routes. A time-domain back-projection based technique, is proposed and evaluated with the help of experimental data featuring a drop in height, a double bend, a 90-degree curve and a linear flight track. In order to assess the quality of the focused data, close-ups of amplitude images are compared and the coherence is evaluated. The experimental data was acquired by the German Aerospace Center's E-SAR L-band system. [C2534]

"Aircraft and in Situ Salinity and Ocean Color Measurements and Comparisons in the Gulf of Mexico"

We report here on aircraft measurements made in May, 2007, with the NRL STARRS (Salinity, Temperature and Roughness Remote Scanner), and optical multi-wavelength radiance and irradiance sensors (Satlantic OCR-507 at SEA-WIFS wavelength bands). These measurements were made in conjunction with in situ measurements of sea surface salinity (SSS), ocean color, and fluorescence in the Atchafalaya River outflow from the R/V Pelican. In this work we demonstrate the ability of the aircraft optical and L-Band measurements to (a) detect the location of salinity and color fronts as observed in the in situ measurements from the ship and (b) provide context for the in situ measurements by providing synoptic measurements over a wider area than the ship was able to cover. A multilinear regression for salinity, based on three of the optical channels, provides an excellent qualitative proxy for large scale salinity in the Atchafalaya plume region. We believe this is the first simultaneous use of L-Band and optical instruments to measure salinity from an aircraft. [C2535]

"Application of ALOS PALSAR and Landsat ETM+ Data for the Study of Periglacial Features and Permafrost within the South Shetland Islands, Western Antarctica"

This paper deals with the application of ALOS microwave and Landsat optical data in the study of glacial and periglacial features as well as morphostructural features in a selected area in Livingston Island which lies in the South Shetland Islands of the northern Antarctic Peninsula region. Polar Regions are key areas in the study of the Earth System having an important role in the understanding of the dynamics, reconstruction and monitoring of global natural processes. The main objective of this work is to study and map periglacial, including permafrost, glacial and geological structures by applying an integrated remote sensing approach in one of our study sites in Livingston Island (Byers Peninsula) for which extensive ground truth information exists from various field expeditions. [C2536]

"Velocities of Major Outlet Glaciers of the Patagonia Icefield Observed by TerraSAR-X"

The capabilities of TerraSAR-X data for feature tracking by amplitude correlation over glacier surfaces are investigated. Methodical aspects of the amplitude correlation approach are described. The TerraSAR-X based velocity fields are compared with former InSAR derived velocities and field measurements on three outlet glaciers on the South Patagonia ice field. [C2537]

"Radar Polar Decomposition for Natural Surfaces Cartography"

Illustrations of parameters obtained from polar decomposition derived from fully polarimetric data acquired by ALOS-PALSAR over the Mai-Ndombo lake, in the Democratic Republic of Congo are presented. Results show their complementarity to usual polarimetric indices, such as the entropy or the alpha parameters [C2538]

"Moving Targets Detection and Analysis on Multi-Look Polarimetric SAR Images using PWF Method"

The motion of moving targets causes distortions in SAR image, which present a challenge on image interpretation. Comparing to stationary targets' signatures, signatures of moving target are distorted from azimuth displacement to smearing beyond detectability. In this paper, a moving target detection algorithm is proposed based on polarimetric whitening filter (PWF) as well as time-frequency (TF) analysis. An experiment is implemented using multi-look X-band PolSAR image acquired by PiSAR. Both moving target and stationary target are included in the image. Results shows PWF method and time-frequency analysis could be used detect moving targets as respected. [C2539]

"Computation of Optimum Azimuth Sampling Time for Dual-Channel DPCA System based on Signal-to-Noise Ratio"

This paper starts on the flow of moving target detection in dual channel DPCA system. Firstly the output power density spectrum of moving target and noise in DPCA system is analyzed, and the output SNR is obtained. Then the effect of synthetic aperture time of moving target's echo and azimuth antenna pattern on output SNR in DPCA is discussed in detail. Based on this effect, the paper deduces the expression which describes the variation of output SNR against synthetic aperture time in Dual-Channel DPCA system, where azimuth pattern is Sinc function, and the synthetic aperture time for optimizing the ability of detecting the moving target is obtained. Further more, this method of acquiring the aperture time can be applied for other antenna patterns. It is testified by processed result of simulated data that the relationship between output SNR and synthetic aperture time fits the above conclusion in Dual-Channel DPCA system. [C2540]

"GMTI Performance Analysis for Circular Scanning SAR Equipped on Slow Platform"

The GMTI (Ground Moving Target Indication) performance for circular scanning SAR (Synthetic Aperture Radar) equipped on slow platform was analyzed in this paper. The characteristics of SAR equipped on slow platform and the GMTI application were described in the beginning, and the circular scanning mode was advanced to resolve the low azimuth imaging efficiency of the slow platform borne SAR. Then the range models of the stationary and moving targets based on circular scanning mode were built, and the Doppler frequency expressions were derived from the range models. The detectable velocities distribution areas were derived by separating the Doppler frequency of two kinds of targets. The quantitative computer simulations were given to demonstrate the detectable velocities area along with azimuth angle and pulse repetition frequency in the end. [C2541]

"A New Method of SAR Image Target Recognition based on AdaBoost Algorithm"

We propose a novel target recognition algorithm for classification of three types of ground vehicles in the moving and stationary target acquisition and recognition public release database. Algorithms that produce classifiers with large margins, such as support vector machines (SVMs), AdaBoost, etc. are receiving more and more attention in the literature. A real application of AdaBoost for synthetic aperture radar automatic target recognition is presented and the result is compared with conventional classifiers. And we also describe how AdaBoost algorithm can be used as a multiclass classification method as well as a feature fusion method. Results are presented to verify that, the performance of the recognition system is improved significantly, and the method presented in this paper is an effective method for SAR images feature fusion and target recognition. [C2542]

"Rain Impact on Sensitivity of Ka-band Scan-on-Receive Synthetic Aperture Radars"

This paper analytically analyses the radiometric performance of a spaceborne Ka-band SAR based on scan-on-receive Rx antenna beam. The analysis outlines the major limiting factors for the design of this instrument. The instrument radiometric sensitivity is evaluated considering a figure of merit that includes the signal-to-noise ratio and the signal-to-rain clutter ratio as well as. In the simulations, different rainfall rates are considered, and the instrument availability for given performance is evaluated. Potential instrument configurations and geometric options are traded-off in order to find the optimal configuration. The analyses show the scan-on-receive technique as a potential solution leading to spaceborne Ka-band synthetic aperture radars with sufficient availability. [C2543]

"Comparison of Atmospheric Phase Delay on ALOS PALSAR Interferogram and Cloud Distribution Pattern on Simultaneously Observed AVNIR-2 Images"

Tropospheric artifact is a serious problem for detecting crustal deformation using differential synthetic aperture radar interferometry (DInSAR) technique. Advanced Land Observing Satellite (ALOS) has capability for simultaneous observation between synthetic aperture radar, PALSAR and optical sensor, AVNIR-2. We compared ALOS PALSAR interferogram with simultaneously observed AVNIR-2 images. Nominal spatial resolution of AVNIR-2 is sufficient for valuation of PALSAR interferogram. Terra/Aqua MODIS images are compared with PALSAR interferogram and cloud top heights is estimated. Test site is Miyagi prefecture where one of the most active seismic zone in Japanese islands. AVNIR-2 images show the two types of clouds pattern that causes interferometric phase delay. The first is lee wave cloud which shows the presence of gravity waves. The second is thick cloud as cumulus which is formed by condensation of water vapor. An interferogram show combination of phase delays in a couple of data. Simultaneously observed AVNIR-2 image is possible to use for evaluation of PALSAR interferometric fringe patterns. [C2544]

"Doppler Parameter Estimation for Single-Channel SAR Moving Target based on a Novel Model in Complex Image Domain"

In order to characterize the signal of moving target in complex image domain (CID) of synthetic aperture radar (SAR), this paper deduces the model of moving target based on Range-Doppler imaging algorithm and stationary phase principle (SPP). In CID, the target approximately modeled as a linear frequency modulated signal (LFM), which has a great improvement in signal-clutter ratio (SCR), and distributes as mis-located segment in the 2D image. The center and slope of the segment is determined by the Doppler center and Doppler ambiguity integer. Meanwhile, the spreading length is jointly determined by the azimuth velocity and Doppler ambiguity integer. Furthermore, this paper derives the Cramer-Rao Bound (CRB) of parameter estimation in CID. At last, numeric experiments is made to approve the conclusion. [C2545]

"Moving Target Detection in along Track SAR Interferometry from In-Phase and Quadrature Components Data"

We show that using the in-phase and quadrature components of the two acquired images in AT-InSAR systems produces an increasing of the detection probability of ground moving targets for constant false alarm rates respect to the detection performance obtained with AT-InSAR conventional systems using only phase information. In this paper, we consider a Gaussian model for the moving target response. The improved performances of the proposed method respect to the interferometric phase approach are showed with numerical experiments on simulated data, and varying the signal to clutter ratio (SCR) and the target radial velocity. [C2546]

"Revealing Intra-Urban Features using Optical and SAR Images"

We developed a method for revealing the intra-urban features and estimating population density using remotely sensed imagery. Remotely sensed imagery has been widely used in urban studies. However, the moderate-

resolution optical data (e.g. Landsat) is often too coarse for delineating urban features, since urban areas are far more heterogeneous than most other land cover types. Therefore, we employed both optical and synthetic aperture radar images for estimating population density inside urban areas. This research indicated that the integrated features of the optical and SAR images can increase the accuracy for estimating population density.

[C2547]

"Imaging Geometry Analysis of 3D SAR using Linear Array Antennas"

Linear array antennas SAR has a resolving capability in the elevation direction, and can get the 3D image of the target. In this paper, we derive the signal model of 3D SAR using a linear array antenna, and get the 3D resolutions and 3D point spread function of array antenna SAR, at the same time the sampling space of array antennas is given. The variance of the resolution in the elevation direction with array antenna angle and referenced look angle is studied. The geometry to reach the best resolution in the elevation direction is analyzed. Meanwhile the resolution for horizontal and vertical antenna array are calculated and compared.

[C2548]

"Advanced Displacement Estimation for PSI using High Resolution SAR Data"

The Persistent Scatterer (PS) technique is a well known method for estimating object and/or surface deformation from space with high accuracy and high spatial coverage and sampling by analyzing estimation frameworks generated from stacks of interferograms [1]. It is especially suitable for urban areas which, in general, show a high density of PS to detect movements with a wide area deformation pattern as well as changes within small scales, e.g. subsidence of isolated buildings. The new high resolution class satellites like TerraSAR-X, Radarsat-2 or Cosmo-SkyMed put forth new potentials and challenges as the density of PS increases dramatically. As several PS can be found on one single object like a building or a bridge, a advanced motion estimation for this group of points can be introduced, accounting for the coupled movement. In this paper we show how the estimation can be carried out restricting the movement to certain models we employ in order to increase the accuracy of the displacement for the whole group of PS. The results obtained for the proposed estimation technique are based on simulated data to thoroughly investigate the potentials of this approach. They are the basis for real datasets available from TerraSAR-X. [C2549]

"A Flood Hazard Risk Assessment Map in Growing Urban Areas by Integrating Remote Sensing and DEM Data"

This article presents a new approach based on an integration of multi-attributes semantic partitions (MASP) coming from the three following attributes: an urban growth layer computed from a couple of ERS-SAR images - exploited as a vulnerability map-, a dispersion flow (DF) layer estimated from a linear DF model -used as a flood hazard map-, and a NDVI layer used as an urban/non-urban interpretation measure, in order to produce a flood risk (FR) map. Thus, input mono-attribute semantic partitions (imASP) are first defined from attributes, and their membership degree functions are built based on the fuzzy subset theory. Then imASP are selected to form MASP according to the degree of confidence given to each one to perform the flood risk (FR) and membership degrees of MASP are calculated to provide individual degrees of FR worsening (FRW). Lastly, the global degree of FRW is computed by aggregating previous individual degrees of MASP by using a fuzzy integral (FI) to achieve the resulting FR map. [C2550]

"Influence and Dependent Parameters of Terrain Undulation to Bistatic SAR Imaging"

As the Doppler history depends both on the transmit range and the receive range in bistatic SAR, those targets, who have the same bistatic range but different locations, will have different doppler history. So the unknown terrain undulation will cause defocusing in bistatic SAR imaging. This paper firstly analyzes which parameters in bistatic configuration affect the defocusing severely, and then shows the simulation results to testify the analysis. Besides, it points out the 3D imaging ability (though very weak) of bistatic SAR based on the defocusing phenomena. And Finally the 3D imaging results are also exhibited. [C2551]

"Compensation of the Range Variant Bistatic Deformation Term for LBF"

The range variant bistatic deformation term of LBF is analyzed. By linearizing the difference between the nearest ranges of transmitter and receiver, the range variant bistatic deformation term is approximated as the linear function of nearest ranges summation. Based on this, the new interpolation function is presented. Then the range variant bistatic deformation is compensated by interpolation, this processing is more efficient without blockwise in range blocks. The simulation results prove its effectiveness. [C2552]

"3-D Range Stacking Algorithm for Forward-Looking SAR 3-D Imaging"

In this paper, a three-dimensional (3-D) F-SAR imaging algorithm is introduced for Forwarding-looking SAR (F-SAR) data processing. The algorithm is the extension of the two-dimensional (2-D) range stacking algorithm (RSA) and allows the accurate image reconstruction without any interpolation and geometric correction. Then the spatial-varying and spatial-shift properties of the 3-D spread point function (PSF) of Forwarding-looking SAR are revealed with the analytical expression. Finally, the simulation experiment is performed to demonstrate the validity of the 3-D RSA. [C2553]

"Synchronization of Geo Spaceborne-Airborne Bistatic SAR"

This paper analyzes the synchronization of a bistatic synthetic aperture radar (SAR) system based upon a geostationary transmitter and small "receive-only" SAR systems mounted on airplanes or unmanned aerial vehicles (UAVs), namely GEO Spaceborne-Airborne Bistatic SAR. This paper will analyze and present our solution of the space synchronization, time synchronization, frequency synchronization and phase synchronization for the GEO Spaceborne-Airborne bistatic SAR respectively. It will first introduce the GEO Spaceborne-Airborne bistatic SAR system and geometry model briefly. Then possible solutions of the system synchronization will be discussed. It will introduce the synchronization scheme based on the direct path between the transmitter and receiver. It uses synchronization modules to realize the time and frequency synchronization. A mathematical model considering the time and frequency synchronization error is given and a phase error analysis is performed. Range and azimuth compressions of a single target are implemented by simulations. [C2554]

"Estimation Performance for Canonical Shape Features"

In this paper, we outline two parameter estimation schemes for discerning canonical shape parameters from bistatic and monostatic radar data collected over a non-linear flight path. We present initial results characterizing both optimal and sub-optimal estimation performance for location and size estimation of plates, dihedrals, and trihedrals. [C2555]

"Velocity Unfolding in Networked Radar System"

This paper presents an algorithm that derives the vector velocity estimate in a radar network environment considering the velocities that exceed the maximum unambiguous velocity of its observing sensor nodes. At first, an analytical derivation with underlying assumptions is presented and then simulation results are shown and discussed. This unfolding vector velocity algorithm is based on maximum likelihood theory operating on the first three weather radar spectral moments and can potentially provide a real time velocity detection of broader range of velocities than given by the nodal maximum unambiguous velocity. [C2556]

"Use of Vector Velocity Estimate Accuracy for Improved Resource Allocation in a Network of Doppler Radars"

To help optimize the real time scanning of an adaptive radar network, it is necessary to define a performance metric for weighing the competing scanning tasks. A point volume vector velocity estimation methodology can be used in this context to derive the confidence bounds of the vector velocity estimator that can, in turn, be utilized as a quality indicator in devising scanning strategies. This document presents the basic derivation of this estimation process and provides examples of processed weather moment data. [C2557]

"Sahelian-Grassland Parameter Estimation from Backscattered Radar Response"

In recent years a special emphasis has been placed on the retrieval of physical parameters from polarimetric radar at microwave frequencies in many research programs. In this paper, we adapted a technique based on an empirical model and a genetic algorithm, and verify its applicability for a complex class of vegetation within a wide temporal interval. This complex class of vegetation is Sahelian grassland which is mainly composed of annual grass and shrubs. The proposed retrieval algorithm is conformed of 3 main steps: (1) Identification of sensitive parameters, (2) Development of the empirical model, and (3) Implementation of a genetic algorithm for the inverse process. For this class of vegetation the sensitive parameters are: the soil moisture content m_s , the grass density D , and the grass moisture content m_v . When applying the retrieval algorithm to simulated radar responses, a great agreement (an error of 6% when estimating the soil moisture content, 13% for the grass density, and 18% for the grass moisture content in the adult-plant stage) is observed between input parameters and estimated ones. [C2558]

"Detection of Anomalous Environmental Electromagnetic Wave by Statistical Property in Magnetic

Field Azimuth"

Anomalous radiation of environmental electromagnetic waves is reported as a portent of earthquakes. Then, we are observing environmental electromagnetic waves of the ELF range all over Japan. We have been regarding the high amplitude in the observed signal as anomalous radiation. However, the observed signal contains a lot of low amplitude anomalies hidden by background noise. These anomalies also have the possibility with significant information of a portent of an earthquake. In this paper, we propose the method of detecting anomalous radiation using statistical property in magnetic field azimuth which doesn't depend on the amplitude level. Moreover, we show that an anomalous radiation is the portent of earthquakes by calculating an azimuthal cross-correlation among two or more observation sites. [C2559]

"Fusion of High Resolution Polarimetric SAR and Multi-Spectral Optical Data for Precision Viticulture"

In the follow-up of the BACCHUS project, aimed at establishing a reference high quality geographic information system for vineyards, an airborne SAR survey has been carried out in fall 2005 in the Frascati area, near Rome (Italy) to investigate on the potential of radar remote sensing in vineyard monitoring. This contribution reports the joint use of high resolution polarimetric SAR data and QuickBird optical data in order to evaluate the potential of remote sensing in vineyard detection and bio-physical parameters retrieval. [C2560]

"Comparison between the Kalman and the Non-Linear Least-Squares Estimators in Low Signal-to-Noise Ratio Lidar Inversion"

This work departs from previously published results of the authors and focus on joint estimation and time evolution of the atmospheric backscatter profile and a range-independent lidar ratio by means of 1) adaptive extended Kalman filtering (EKF) and 2) non-linear least-squares (NLSQ), under moderate-to-low signal-to-noise ratios ($SNR < 100$ at the starting sounding range). A Rayleigh/Mie atmosphere and a calibrated lidar system are considered. Performance parameters studied are data sufficiency, tracking of the optical parameter time fluctuations, inversion errors, power estimation, and noise impact. The EKF inversion solution is, in turn, compared with Klett's method as a reference. Finally, it is shown that the EKF outweighs the NLSQ in noisy environments. [C2561]

"Optimal Spectral Decomposition (OSD) for Remotely Sensed Ocean Data Assimilation"

Assimilation of remotely sensed ocean data (velocity, temperature, and salinity) into numerical model is of great importance in oceanic and climatic research. However, the data should be reconstructed (onto grids) before assimilation since the original datasets are usually noisy and sparse. This paper describes a recently developed optimal spectral decomposition (OSD) method for mapping and noise filtration with examples of reconstructing the data from the Argo profiling and trajectories, Ocean Surface Current Analyses-Real time (OSCAR), shore-based high-frequency (HF) Doppler radar (CODAR) and Global Temperature-Salinity Profile Program (GTSP). [C2562]

"Motion Compensation Processing of Airborne SAR Data"

This paper presents a motion compensation algorithm to focus high resolution SAR data taken from an airborne sensor. The basic idea is to fragment the sensor trajectory into smaller segments that can be modelled as linear or quadratic. The synthetic antenna is then considered as an array of smaller subarrays. The algorithm can easily adapt and trade efficiency for sensor path irregularity. In fact the algorithm is more efficient if the segments are longer. Experimental results with real airborne data confirm the correctness of the approach. [C2563]

"Combined Wavelet and Contourlet Denoising of SAR Images"

The nonsubsamped contourlet transform (NSCT) is a new image representation approach that has sparser representation at both spatial and directional resolution and thus captures smooth contours in images. On the other hand, wavelet transform has sparser representation of homogeneous areas. In this paper, three combinations of undecimated wavelet and nonsubsamped contourlet transforms will be used for denoising of SAR images. Two of the methods use the wavelet transform to denoise homogeneous areas and the nonsubsamped contourlet transform to denoise areas with edges. The segmentation between homogeneous areas and areas with edges is done by using total variation segmentation. The third method is a linear averaging of the two denoising methods. A thresholding in the wavelet and contourlet domain is done by non-linear functions which are adapted for each selected subband. The non-linear functions are based on sigmoid functions. Simulation results suggested that these denoising schemes achieve good and clean images. [C2564]

"Unsupervised Change Detection in SAR Image using Graph Cuts"

In this paper, we present an unsupervised change detection approach in temporal sets of SAR images. The change detection is represented as a task of energy minimization and the energy function is minimized using graph cuts. Neighboring pixels are taken into account in a priority sequence according to their distance from the center pixel, and the energy function is formed based on Markov Random Field (MRF) model. Graph cuts algorithm is employed for computing maximum a-posteriori (MAP) estimates of the MRF. Experiments results obtained on a SAR data set confirm the effectiveness of the proposed approach. The comparisons between graph cuts algorithm and iterated conditional modes (ICM) algorithm about the quality of change map and running time of energy minimization illustrate that graph cuts algorithm is a huge improvement over ICM. [C2565]

"Speckle Reduction of SAR Images in the Bandlet Domain"

Synthetic Aperture Radar (SAR) images are inherently affected by multiplicative speckle noise, which is due to the coherent nature of the scattering phenomenon. This paper deals with the speckle reduction using the bandlet transform combined with the adaptive sigmoid thresholding. The operation needs to provide multiscale transform. We use the Undecimated Discrete Wavelet Transform (UDWT) and apply the bandlet transform on each resulting scale. Numerical tests applied on Lena image contaminated with multiplicative noise show that our method provides improvement both in terms of image visual fidelity and in terms of Peak Signal-to-Noise Ratio (PSNR). Comparisons are made with the standard wavelet transform and the shift invariant discrete time wavelet transform. [C2566]

"Application of Spatial Spectrum Estimation Technique in Multibaseline SAR for Layover Solution"

Spatial spectrum estimation technique is applied to resolve layover effect with multi-baseline synthetic aperture radar (SAR) in the paper. Based on the signal model of multi-baseline SAR, the mathematical principle of layover solution with spectrum estimation is derived. The main steps of spatial spectrum estimation technique for layover solution in multi-baseline SAR are obtained. In order to deal with the spectrum ambiguity problem generated by FFT method under limited multi-baseline SAR data, we introduce the Yule-Walker method for spectrum estimation to resolve layover effect. We analyze the principle of Yule-Walker method for performance improvement, and give the processing steps using Yule-Walker method for layover solution in detail. The simulation results for layover solution with FFT method and Yule-Walker method are realized and compared. [C2567]

"Inversion of Backscatter Ionograms Optimization by using Simulated Annealing and Genetic Algorithms"

The Over-The-Horizon Radars (OTHR) use the refraction of the waves on the ionosphere to reach the targets over the horizon. In order to know the real position of the targets the actual ionospheric characteristics must be estimated. So an inversion method to obtain them has been developed. This inversion method is capable to obtain the parameters of a model of the electronic density profile from some measurements realized with the radar, the backscatter ionograms. To optimize the method two algorithms has been introduced: the simulated annealing and the genetic algorithm. [C2568]

"Region Feature Extraction Based on Improved Regularization Method in SAR Image"

The noise existed in Synthetic Aperture Radar (SAR) image weakens the detailed features of region of interest (ROI) such as target and shadow. It also leads to the serious performance reduction of subsequent target detection, classification and recognition. The conventional regularization method could enhance target features in SAR image; however, the high computation complexity limits the real-time application of it. An improved regularization method is introduced in this paper, which increases processing speed of region feature extraction for SAR image significantly. It is theoretically proved that, by optimizing SAR projection operator, computation complexity could be reduced from $O(M^3N^3)$ to $O(MN)$ without ability losing of the region-based feature enhancement. MSTAR SAR image data is employed for algorithm experiment. The result shows that our method can increase target-to-clutter ratio significantly while restraining the noise in ROI, and then extract target and shadow from background clutters in SAR image more accurately. [C2569]

"The Effects of Finite Resolution on Radar Images of Fractal Profiles"

In this paper a first step toward a complete model of the fractal imaging process is taken: for the sake of simplicity the mathematical details are here provided for a fractal profile with topological dimension equal to one. In particular, we show how the signal backscattered from a fractal profile modeled as a fractional Brownian

motion (fBm) stochastic process is strictly linked to an associated fractional Gaussian noise (fGn) process. We compute in closed form the power density spectrum of the received signal in the simplified hypothesis of a linear dependence of the backscattered signal on the profile derivative process. Our results apply to physical fBm processes, as dictated by the low-pass filtering introduced by both the incident electromagnetic field wavelength and the finite sensor resolution. In the last section a numerical study of the above mentioned is also provided.

[C2570]

"Speckle Filtering of Dual-Polarization and Polarimetric SAR Data based on Improved Sigma Filter"

The advancement of SAR technology with high resolution and multiple polarization data demands better and efficient speckle filtering algorithms. In this paper, we developed an effective speckle filtering algorithm for dual-pol and fully polarimetric high resolution data. The proposed algorithm is effective and computational efficient based on the improved sigma filter ALOS/PALSAR and JPL AIRSAR data were used for demonstration.

[C2571]

"Monitoring Crustal Deformation along the Xianshuihe Fault in the Eastern Tibetan Margin Area with Envisat ScanSAR Interferometry"

The Xianshuihe fault of Sichuan province, southwest China, is a highly active strike-slip fault approximately 350 km long. Previous studies have described up to 10-17 mm/yr of left-lateral slip on the Xianshuihe fault during the last decades, as indicated from geological criteria and GPS observations. The satellite InSAR observation is an alternative technique effectively used to measure the crustal deformation on the active fault. However, the conventional strip mode SAR imagery (i.e. ENVISAT/ASAR IM image) covers usually a 100 km wide stripe and will therefore not be sufficient for such large-scale deformation study. In this paper, we presented ScanSAR interferometry applied to ENVISAT/ASAR WSM data to produce about 400times400 km² deformation map over the Xianshuihe fault zone and the Garze-Yushu fault zone. The preliminary stacked deformation results of six WS-WS interferograms indicated a northeast-southwest deformation trend nearly perpendicular to the two fault zones and demonstrated the potential to monitor such wide-stretched deformation using ENVISAT WSS data.

[C2572]

"Classification of Polarimetric SAR Images using Radiometric and Texture Information"

Image segmentation and unsupervised classification are difficult problems. We propose to combine both. A clustering process is applied over segment mean values. Only large segments are considered. The clustering is composed of a mean-shift step and a hierarchical clustering step. The approach is applied on a 9-look polarimetric SAR image. Textured and non-textured image regions are considered. The K and Wishart distributions are used respectively. The obtained region groups constitute an important simplification of the image and a good initial classification map. Multiplying the class map by the image of scalar texture component produces an image almost identical to the original where speckle 'color' noise variation is filtered out.

[C2573]

"Turbo Speckle Filtering applied to PolSAR Data"

A new approach for speckle reduction in polarimetric synthetic aperture radar (PolSAR) images based on the turbo iterative principle is proposed. The turbo iterative algorithm shows high performances due to the propagation of the information between two complementary filters. One filter can boost up the results of the other by processing its residue image and retrieving valuable information in the noise subspace.

[C2574]

"A Tool to Query and Visualize the Complete SRTM Data Set Indexed by the Q-tree in an Open GIS"

Geospatial data are increasingly frequent and useful in Visualization, Virtual Reality and, of course, Geographic Information System (GIS) applications due to its realism. Most of the geospatial data sources are heterogeneous because they come from diverse satellites and the data are of different nature. Nevertheless, the Shuttle Radar Topographic Mission (SRTM) provided an unique source of uniform data of the almost entire Earth's surface. On the other hand, to make effective and efficient regional queries over these SRTM data, the indexing with a space partitioning data structure is needed, making easy the visualization of their results. This paper presents a tool to query and visualize the complete SRTM data set indexed by the Q-tree multidimensional index structure. The tool is totally integrated into the VTBUILDER, an open GIS, allowing the visual selection of rectangular and polygonal spatial query regions and the retrieval of the query results by using the multidimensional index. The query results of the selected regions can also be exported to files with two specific format types for their further analysis. Finally, the visualization takes place in both 2D and virtual 3D rendering for its visual analysis.

[C2575]

"Observation of Crude Oil Spill Off the West Coast of Korea using TerraSAR-X, ENVISAT ASAR

and ALOS PALSAR"

On December 7th, 2007, more than 10,000 tons of crude oil from a tanker leaked into the Yellow Sea off the west coast of Korean Peninsula. Several SAR images including TerraSAR-X, ENVISAT ASAR, RADARSAT-1, ERS-2 SAR and ALOS PALSAR were acquired over the contaminated area from oil spill. Observed dark patches in SAR images, due to the presence of oil slicks, were extracted using adaptive thresholding methods, and then classified based on field information. The damping ratio, which is a ratio between slick-free and slick-covered sea surface, was analyzed by the SAR radar frequencies and wind condition. With the acquired SAR images in temporal resolutions, the movement of oil slicks was monitored and traced. [C2576]

"Deformation Monitoring by Long Term D-InSAR Analysis in Three Gorges Area, China"

After the Three Gorges Dam began to function in China in 2003, the water level of the Yangtze River in Three Gorges area rose more than 100 meters. The impact of the man-made reservoir caused by the dam on the surroundings is becoming the object of several studies. In this paper we make use of two long term D-InSAR techniques, the quasi-permanent scatterer technique (QPS) and the Stanford Method for Persistent Scatterer (StaMPS), to measure the deformation trends in Badong, Three Gorges area, China. The results obtained by the two processing tools with the same focused and co-registered data sets are analyzed and compared. Two subsidence areas are identified by both techniques. However, since the QPS analysis is able to process partially coherent targets, many more points are extracted than in StaMPS, and more information can be retrieved. [C2577]

"Data Analysis System Design for Lidar Experimentation"

A Web-based Lidar Experimentation and Data Analysis System (LEDAS) was developed, with support from a National Science Foundation award, to support resource sharing of lidar equipment, datasets and data analysis routines and collaboration between members of the Connecticut State University System (CSUS) Lidar Collaboratory. The system allows users at different geographical locations to conduct remote sensing research and education over the Web through remote access and control of a single shared lidar system and Web-based data analysis. Users need not have any specialized instrumentation or software at their institutions, thereby making real remote sensing research available to students and faculty from institutions which may not have the internal budgets for such facilities. An original structure providing basic functionality was developed and implemented. This paper describes the second generation data analysis system which provides significant new enhancements and capabilities. [C2578]

"Analysis of Natural Scenes using Polarimetric and Interferometric SAR Data Statistics in Particular Configurations"

This paper introduces statistical tools for the analysis of POL-inSAR data acquired over natural environments. Maximum likelihood procedures are provided to test particular structures of POL-inSAR data presentations and to estimate relevant parameters. These particular configurations concern the stationarity of the separate POLSAR information between, the equality of the optimal POL-inSAR projection vectors and the presence of reflection symmetry. [C2579]

"Measuring and Modeling the NRCS of the Sea for Backscatter"

Recent ship-based measurements using a calibrated, coherent, dual-polarized, X-band radar illuminated the behavior of the normalized radar cross section of the sea, NRCS or s_0 , at incidence angles of 88deg to 89deg. For wind seas $s_0(VV)$ at these incidence angles behaves much like those at lower incidence angles while $s_0(HH)$ behaves very differently, being largest looking upwind and smallest looking downwind. Fits of a multiscale scattering model to these data and data at lower incidence angles show that over the range of incidence angles from 0deg to 89deg, $s_0(VV)$ is adequately explained by the model while $s_0(HH)$ is generally higher than the model predicts at incidence angles above about 45deg. Thus scattering phenomena exist on the ocean that affect HH backscatter very strongly at high incidence angles while impacting VV backscatter only slightly. We show that when the ocean surface is disturbed by currents $s_0(HH)$ can exceed $s_0(VV)$ by as much as 15 dB for long periods of time and over large spatial areas. We examine phenomena that might account for this behavior and how they might affect the wind sea case. [C2580]

"The Impact of Surface Scattering on Ocean Atmospheric Boundary Layer (ABL) Wind Profile Estimates from an Airborne Doppler Radar"

IWRAP, the Imaging Wind and Rain Airborne Profiler is a conically scanning dual-band (C and Ku), dual-polarized pencil-beam airborne Doppler radar that profiles the volume reflectivity and Doppler velocity from

precipitation. It also measures the ocean backscatter response especially during tropical and extra tropical cyclones. IWRAP is designed to measure troposphere winds and surface winds. Of particular importance to the storm forecasting and research community are the winds in the lower part of the hurricane boundary layer near the sea surface (lower ABL). The covariance data processing technique IWRAP traditionally employed assumes a uni-modal and symmetric Doppler spectrum and therefore, it alone is unable to account properly for the influence of the surface scattering on wind profiles in the lower ABL region. In this paper we compare covariance-based approaches and full-spectral approaches utilized to derive the true wind speed for atmospheric vertical profiles. Techniques for removal of the surface contamination and example of wind profiles retrieved from Hurricane Rita are presented. [C2581]

"Region-Based Classification of Multisensor Optical-SAR Images"

Multispectral and synthetic aperture radar (SAR) images are known to exhibit complementary properties: unlike optical sensors, SAR provides information about the soil roughness and moisture, and acquires useful data despite clouds and Sun-illumination conditions. However, the analysis of the resulting images turns out to be more difficult, as compared to the use of optical imagery, due to the noise-like speckle phenomenon. In order to exploit this complementarity for classification purposes, a criticality relies in the definition of accurate joint optical-SAR statistical models, due to the different physical natures of these two data typologies and to the corresponding differences in the related parametric models. In this paper, a region-based semiparametric classification technique is proposed for multisensor optical-SAR images. The method combines the tree-structured Markov random field approach to segmentation with the dependence tree approach to probability density estimation and with case-specific bivariate models for the distributions of optical and SAR data. A Bayesian decision rule is formulated at the segment level in order to incorporate spatial-contextual information and to gain robustness against noise. [C2582]

"Sediment Modeling based on Radar Observed Surface Hydrodynamics"

An integration method will be presented to combine a one dimensional bottom shear stress model based on hydrodynamic field observations with radar current data. The data acquired are the bathymetry, the surface current velocity, the grain size and vertical profiles of the current and water characteristics. The observation method used here was run fully operationally for the first time during an experiment in May 2006. We estimate the bottom shear stress from the surface current under the parametric approach that we have hydrographic conditions of a completely mixed water column. Several assumptions have to be made i.e. a hydrodynamical rough bottom and a homogeneous wind situation for each profile. As results we present area-wide maps of the bottom shear stress value and maps of the initiation of motion. [C2583]

"Evaluating the Potential of L Band PolSAR Data to Discriminate Deforestation Increment Areas in Amazon Rain Forest"

The main objective of this work is to evaluate the potential of L band PolSAR data to discriminate deforestation increment. In order to achieve this purpose, it was performed a coherent attributes exploratory analysis and a Maximum Likelihood-ICM (Iterated Conditional Modes) classification of R99B sensor L band PolSAR data. The PolSAR data classification obtained good agreement with PRODES Digital project reference map ($k=0,71$). This result might indicate that R99B L band PolSAR data have good potential to discriminate deforestation increment areas in Amazon Forest. [C2584]

"Alaskan Glaciology from Space"

Global totals of ice area and volume for mountain glaciers are small compared to the Antarctic and Greenland ice sheets, however, their present contribution to sea level rise (SLR) is on par with the ice sheets. Alaska Glaciers provide the largest contribution of all mountain glaciers to SLR. We discuss the use of spaceborne remote sensing techniques to study Alaska glacier contributions to sea level and suspected changes in ice velocity. Direct calculation of ice volume changes and rates of change on Kenai Peninsula glaciers are based on differences in USGS and SRTM DEMs and airborne Lidar profiles. A preliminary study of ice velocities on the Seward Glacier using L-band InSAR from PALSAR is presented. [C2585]

"Investigation of Atmospheric Gravity Waves and Rotors in the Marine Boundary Layer using Spaceborne Synthetic Aperture Radar Images"

Atmospheric gravity waves (AGWs) propagating in the marine boundary layer leave fingerprints on the ocean surface which are detectable by synthetic aperture radar (SAR). They are associated with a variable wind speed at the sea surface which modulates the small-scale sea surface roughness and thus the backscattered radar

power. We present 5 examples of SAR images acquired by the Advanced Synthetic Aperture Radar (ASAR) onboard the European Envisat satellite which show that spaceborne SAR images contain valuable information on the generation of AGWs and on the extent and shape of AGW fields. Furthermore, we show how quantitative information on the sea surface wind speed fluctuations induced by AGWs can be extracted from SAR images of the sea surface. [C2586]

"Subinertial Variations in the Soya Warm Current Revealed by HF Ocean Radars, Coastal Tide Gauges, and Bottom-Mounted ADCP"

Subinertial variations in the Soya Warm Current (SWC) are investigated using data obtained by high frequency (HF) ocean radars, coastal tide gauges, and a bottom-mounted acoustic Doppler current profiler (ADCP). The SWC exhibited subinertial variations with a period of 5-20 days. The surface transport by the SWC was significantly correlated with the sea level difference between the Sea of Japan and Sea of Okhotsk for both the seasonal and subinertial variations, indicating that the SWC is driven by the sea level difference between the two seas. The subinertial variations in the SWC were significantly correlated with the meridional wind stress component over the region. Sea level difference through the strait caused by wind-generated coastally trapped waves along the east coast of Sakhalin and west coast of Hokkaido are considered to be a possible mechanism causing the subinertial variations in the SWC. [C2587]

"A System for Automatic Identification of Oil Spill in ENVISAT ASAR Images"

An automatic oil spill identification system was introduced in this paper. It was designed to work independently to detect oil spills in ENVISAT ASAR level 1b images (of WS, IMP and APP mode). The absolute calibration, geometric correction without any GCPs, dark patches segmentation based on wind force levels, dark patches feature extraction, drift trend prediction and identification confidence evaluation are the essential components of the system. The system works well for its accuracy of 85% in discriminating between oil spills and look-alikes in the case of 60 scenes of examined images. [C2588]

"Effectiveness of 2D FDTD Ground Penetrating Radar Modeling for Bridge Deck Deterioration Evaluated by 3D FDTD"

Computational modeling is effectively analyzes the wave propagation and interaction within bridge structures, providing valuable information for sensor selection and placement. It provides a good basis for the inverse problem for defect detection and reconstruction. The finite difference time domain (FDTD) method can be used to model nondestructive wave based sensing using air-coupled ground penetrating radar (GPR). A full 3D model is able to capture all interactions but is limited by computational size and CPU time. In contrast, a 2D model is computationally fast and capable of studying a large computational region, but lacks a complete view of the problem. In this study, we propose to use the 2D FDTD model to simulate the GPR detection of bridge deck defects. The effectiveness of the 2D model is validated by comparison to a full 3D model. The bridge deck is a relatively uniform in the transverse direction so that the 2D longitudinal geometry analysis can therefore adequately capture most of the 3D scattering behavior. [C2589]

"Oil spill monitoring using multi-temporal SAR and microwave scatterometer data"

On the 7th of December 2007, the 146,000-ton oil tanker, Hebei Spirit, was wrecked and leaked more than 10,000 ton crude oil onto the sea off the west coast of the South Korea. In this paper, the monitoring of the oil spills in this pollution accident using multi-temporal Synthetic Aperture Radar (SAR) and microwave scatterometer (QSCAT and ASCAT) data was illustrated. The impact of this oil spill pollution on the China's marine environment was evaluated. The result shows the capability and the effectiveness of microwave remote sensing data in oil spill monitoring and forecasting. [C2590]

"On the Mathematical Formulation of the SAR Oil-Spill Observation Problem"

A novel approach to oil-spill classification, based on the paradigm of one-class classification, is proposed. Basically, a classifier is trained using only examples of oil-spills, instead of using oil-spills and look-alikes, as in two-class approaches. In addition, as a large number of candidate features have been considered in the literature, a feature selection algorithm, to objectively select the most effective subset, is proposed. Results on two case study datasets are reported to validate the proposed approach. [C2591]

"Traffic Spatial Measures and Interpretation of Road Network Using Aerial Remotely Sensed Data"

The most common measurement of usage in road network is vehicular traffic flow, which is defined as the number of vehicles passing a specific location along a road during a unit of time. Flow is often expressed as

AADT (the annual average daily traffic). Traditionally, the traffic vehicle flow is measured by using ground-based sensors, most common of which are inductive loop detectors and pneumatic tube detectors. The sampling rate of a detector depends on the application and the operating agency, typically ranging from under one minute to a full day. This paper presents methods for spatial measures and interpretation of roadway network from aerial remotely sensed image. First, this paper presents the interpretation of roadway network using co-registration between up-to-date aerial imagery and geospatial database, which is called image-to-GIS co-registration. The up-to-date aerial imagery and their extracted road network features are thought as reference data, and the early GIS data are co-registered onto aerial images after orthorectified in order to interpret the remotely sensed image; (2) the vehicles are detected based on the co-registered data; (3) Based on the co-registered data, and recognized vehicle, the measurement including vehicle density, headway are conducted, further to compute the flow rate; (4) the experimental results are compared with the results from the ground-based detection. Finally, some conclusions are drawn up. [C2592]

"Surface deformation retrieval of Yongcheng City(China) based on small baseline DInSAR technique"

In this paper, we apply small baseline DInSAR technique for the generation of surface deformation maps of the investigated area based on complex network. The technique estimates the linear deformation velocity in wide areas, not only in urban areas but also in suburban areas. The results presented in this study are obtained using 6 SAR data acquired by ENVISAT ASAR during 2004-2006. We compare the results with precise leveling data, which validate our results. [C2593]

"Optimization of Ground Penetrating Radar (GPR) Mixture Model in Road Pavement Density Data Analysis"

This paper presents an optimization of GPR mixture model based on the measurements and simulation results at frequency range of 1.7-2.6 GHz. The purpose is to get a most accurate relationship between attenuation and density for various road pavements densities. The proposed method is simple, fast, nondestructive and accurate way to determine the density of road pavement. Density is a one of the important parameter in order to determine the compressive strength of road pavement. In laboratory, a few of received signal strength and measured attenuation for nine road pavement slab samples were taken at four different frequencies. The GPR mixture model has been used to produce the predicted attenuation due to the pavement density. The calculation and selection of mixture model has been discussed thoroughly and only the best performance of GPR mixture model was selected for optimization. [C2594]

"Detection of Oil Slicks in SAR Images using Hierarchical MRF"

This study deals with hierarchical Markov Random Field (MRF) models and with their application for the segmentation of SAR images of oil spills, which are going to be segmented into three classes: denser oil, thinner oil and sea water. The proposed unsupervised scheme takes into account the variety of the laws in the distribution mixture of a SAR image in order to estimate MRF parameters. To obtain a more precise model of local and global characteristics of image content, a hierarchical model involving a pyramidal scheme is used. The main goal of this strongly filtered representation is to introduce a rough map which facilitates the detection in the upper high resolution level. The proposed segmentation procedure works as a sequential technique which combines communication between the different levels of the pyramid. Because of the noisy nature of the SAR images, a MRF scheme, which exploits its contextual analysis, is used. The investigation was carried out using an ERS-2/SAR image, collected on June 9 2000 over the South Adriatic Sea (orbit: 26858 frame: 451) and showing the presence of a large oil slick. From the full SAR scene, a subset, 1000times1500 pixel size, covering large part of the slick, was extracted to become our test image. Before applying the proposed scheme, the speckle noise was removed from the image by means of an adaptive filter. Using the proposed hierarchical MRF scheme, different segmentation experiments were carried out. The results of this study will be presented and discussed. [C2595]

"Retrieval of wind speed using an L-band synthetic aperture radar"

Retrieval of wind speed using L-band synthetic aperture radar (SAR) is both an old and new endeavor. Although the Seasat L-band SAR in 1978 was not well calibrated, early results indicated a strong relationship between observed SAR image intensity and wind speed. The JERS-1 L-band SAR had limited usefulness over the ocean. Most recent wind retrievals from spaceborne SARs have been at C-band for ERS-1/2, Radarsat, and Envisat. With the launch of the sophisticated multi-polarization Phased Array L-band Synthetic Aperture Radar (PALSAR) on the Advanced Land Observing Satellite (ALOS), we renew the investigation of wind retrieval from L-band. [C2596]

"Probability density function of ocean surface slopes from radar observations"

Airborne radar observations of the sea surface at C- Band and small incidence angles are used to investigate some properties of the surface slope probability density function (pdf). The method is based on the analysis of the variation of the radar cross-section with incidence angle, assuming that the backscatter can be described by the Geometrical Optics theory. First, we show that roughness properties with scales larger than 12 cm can be analyzed in our configuration (C-Band, incidence 7 to 16deg). The radar data are then analyzed in terms of filtered mean square slope under the assumption of a Gaussian slope pdf. Dependence with wind speed of the upwind and total mss are analyzed and compared to various published studies. Finally an analysis of the radar data under a non-Gaussian assumption for the slope pdf is proposed, by applying the compound model suggested by [1]. [C2597]

"Identification of oil spills based on ratio of alternating polarization images from ENVISAT"

We propose here a method to identify surface film in SAR images using the Alternating Polarization ratio images from ENVISAT. This ratio is lower in polluted areas than in non-polluted areas due to the difference in relative contributions of the non-Bragg scattering to the total radar signal. [C2598]

"Oil spill segmentation of SAR images via graph cuts"

Segmentation of dark patches in SAR images is an important step in any oil spill detection system. Segmentation methods used so far include 'adaptive image thresholding', 'hysteresis thresholding', 'edge detection' (see [1] and references therein) and entropy methods like the 'maximum descriptive length' technique [2]. This paper extends and generalizes a previously proposed Bayesian semi-supervised segmentation algorithm [3] oriented to oil spill detection using SAR images. In the base algorithm on which we build on, the data term is modeled by a finite mixture of Gamma distributions, with a given predefined number of components, for modeling each one of two classes (oil and water). To estimate the parameters of the class conditional densities, an expectation maximization (EM) algorithm was developed. The prior is an M- level logistic (MLL) Markov Random Field enforcing local continuity in a statistical sense. The methodology proposed in [3] assumes two classes and known smoothness parameter. The present work removes these restrictions. The smoothness parameter controlling the degree of homogeneity imposed on the scene is automatically estimated and the number of used classes is optional. To extend the algorithm to an optional number of classes, the so-called alpha-expansion algorithm [4] has been implemented. This algorithm is a graph-cut based technique that finds efficiently (polynomial complexity) the local minimum of the energy, (i.e, a labeling) within a known factor of the global minimum. In order to estimate the smoothness parameter of the MLL prior, two different techniques have been tested, namely the least squares (LS) fit and the coding method (CD) [5]. Semi-automatic estimation of the class parameters is also implemented. This represents an improvement over the base algorithm [3], where parameter estimation is performed on a supervised way by requesting user defined regions of interest representing the water and the oil. The effectiveness of the proposed approach is illustrated with simulated SAR images and real ERS and ENVISAT images. [C2599]

"A physically consistent stochastic model to observe oil spills and strong scatterers on SLC SAR images"

A speckle model to characterize low backscatter areas and areas with strong scatterers in marine SLC SAR images is presented. The model allows using high resolution speckled SAR images instead of dealing with multi-look SAR images where, at the expense of a poorer spatial resolution, the speckle is mitigated. The new approach is based on the use of the three parameters of the generalized K probability density function. This speckle model embodies the Rayleigh, the Rice and the K-distribution scattering scenes, which are descriptors of scenes dominated by Bragg scattering, scenes in which a dominant scatter is present and scenes with a non-Gaussian signal statistic, respectively. A large data-set of ERS 1/2 SLC SAR images, provided by the ESA under the Project C1P-2769, is employed. Results show the effectiveness of the approach. [C2600]

"The role of performance modelling in active phased array SAR"

Phased array antennas play an important role in many radar applications and their use has increased during recent years in space-based remote sensing applications. Their success is mainly due to high agility in reconfiguring pattern, quick steering capability along both elevation and azimuth axis, easy packaging on spacecraft, low sensitivity to T/R module failures, high achievable directivities. In the frame of SAR systems implementation and calibration activities, a SAR simulator is required to support engineering activities devoted to scenario definition, performance assessment, estimation of error effects on signal Tx/Rx/Cal chain. Such a tool shall also implement an electromagnetic antenna model which is required to predict antenna performance, in

terms of beam shape, directivity and sidelobe levels, with high accuracy and reliability, by keeping into account characterisation data provided at various levels (both pre-flight and in-flight), mutual coupling, VSWRs, insertion losses, amplitude and phase errors. This paper discusses preliminary results achieved by mean of a SAR simulator which implements a non-electromagnetic antenna model developed by Alcatel Alenia Space Italia for SAR instrument calibration and phased array antenna pattern prediction, which is based on array factor computation by mean of fast Fourier transform applied on the excitation matrix, where nominal excitation values are corrected on the base of near field pre-flight and in-flight measures. In particular, the predicted beam is achieved by matching together both information on antenna configuration (operative frequency, bandwidth, element spacing, number of T/R modules, TDLs, failures), data coming from near field measures (pre optimisation and post optimisation holograms) and in-flight telemetries. This paper presents the former results obtained by loading pre-flight measured data, and shows the high accuracy achieved in directivity computation, beam shape prediction and pointing angle-estimation, by comparing such results with those achieved by mean of an electromagnetic validated model. The tool, developed in Matlab, operates a correction of nominal antenna excitations by applying over them a pre-distortion array obtained by opportunely sampling the near field holograms acquired during pre-flight tests and correcting such information to compensate for probe to AUT distance. The effect of correction is evident both along azimuth and elevation cuts, even if the elevation pattern shows some discrepancies over far sidelobe regions. In any case, the general good matching toward validated analyses demonstrates the effectiveness of such approach which offers high accuracy even with low computational complexity. Furthermore, the model is designed to account for in-flight deviations from nominal behaviour, like those due to module failures or component degradation. The model loads calibration data and status telemetries and updates its database in order to predict the whole sets of beams in the most accurate way. As a project and analysis tool, the model also implements the possibility to cycle over independent variables to perform statistical analyses. In such way, the effects of frequency variations, graceful degradation, pointing deviations, amplitude/phase and random errors may be analysed and predicted in terms of expected values and variances. [C2601]

"Use of quikscat ku-band scatterometer data for retrieval of seasonal snow characteristics in Finland"

The feasibility of using scatterometer data from the spaceborne QuikScat instrument for retrieval of snow characteristics in Finland has been studied. QuikScat data for the winters of 1999-2000 through 2005-2006 have been used along with in situ data for 21 test sites. [C2602]

"Ship signatures in synthetic aperture radar imagery"

Ship signatures in synthetic aperture radar (SAR) imagery have been matched to Automatic Identification System (AIS) data to yield a large database of known ships for ship signature analysis. This paper focuses on ship radar cross section and ship length derived from the ship signature length. Cross-polarization is an attractive option for ship detection. [C2603]

"Comparison of geometric optics and diffraction effects in radar scattering from steep and breaking waves"

To address the issue of radar scattering from steep and breaking ocean waves, we developed an efficient and fast 2-D numerical full-wave approach to model both wave evolution and radar scattering from these waves. It enabled us to reproduce the main features of the temporal and polarization behavior of the radar signal such as sea spikes. In addition, to better understand the contribution of multiple scattering that might emerge from radar scattering on steep and breaking waves, we have modeled scattering using a ray-tracing approach that not only provides the ray picture but also supplies both the ray amplitude and the ray phase. This approach eliminates diffraction effects from consideration, leaving only geometric optics effects that include multiple reflections. As a result, angular dependencies of the scattering cross section based on the ray approach were calculated and compared with corresponding values from the full-wave approach. Generally, better agreement between these two approaches is obtained for forward scattering directions than for backscattering directions. Ray simulation for a backscattering direction does not reproduce the HH/W ratio with the spikes observed in the full-wave solution. This indicates that diffraction effects are critical for explaining important features of backscattering from breaking waves. The role of multiple reflections from the breaking wave profile in creating spikes with an anomalous HH/W ratio proved to be negligible. [C2604]

"The RADARSAT constellation payload design"

The Canadian Space Agency completed the definition phase of the RADARSAT Constellation, a constellation of three satellites that will ensure C-band data continuity with RADARSAT-2. The first satellite is scheduled to enter

in operation toward the end of the RADARSAT-2 mission, for a full implementation of the constellation in 2014-15. The RADARSAT Constellation is designed to improve significantly the availability of SAR data for main Canadian Government departments, the main applications areas being maritime surveillance, ecosystem monitoring and disaster management. An important constraint on the mission was to reduce significantly the cost of SAR data, which forced the use of new approaches in the payload design. The paper presents the initial payload design process and three techniques investigated to improve its performance. [C2605]

"The role of spatial interactions for prediction of the spectral structure of the atmospheric phase screen"

The atmospheric phase screen is one of the main error sources that affect the precise phase measurements in many fields of earth remote sensing. The atmospheric effects can be mitigated if a precise knowledge of the power spectral density of the process is available and if same sample observations can be retrieved on a sparse grid. At smaller scales, where interactions are no longer isotropic, the behaviour is not easily predicted by the ultimate dissipative behaviour of turbulence eddies. We start by assuming that the propagation of the electromagnetic wave in the lower atmosphere can be represented by a ray travelling in a layered medium where the refractive index is constant along each layer. In a turbulent atmosphere, the interaction among eddies induces a diffusion process that propagates with different rates in both vertical and horizontal direction with the final effect of ruling the number of effective layers in the atmosphere. In this way, the overall path travelled by the electromagnetic wave is governed by the accumulated number of such effective layers whose interactions play a primary role in our model. A good model for the interactions among different layers is the linear interaction model. The power spectrum of the process can be found by solving a differential equation with given initial conditions. It can be demonstrated that an asymptotic power law decay is found under binomial competitive interactions and that, at a smaller scale, the behaviour observed in the observed data is naturally induced by the interaction process itself. The model predictions have been tested using samples of the atmospheric phase screen extracted from Synthetic Aperture Radar interferograms. To this end, the model parameters have been estimated from the data set and the predicted spectrum has been compared with the measured one. [C2606]

"X-band backscatter from the ocean at low-grazing angles"

In 2005 and 2006, we mounted an X-band Doppler radar on ships that operated in the South China Sea and off the coast of New Jersey, respectively. The measurements were made only at W polarization in 2005 but at both HH and W polarization in 2006. On average, VV normalized radar cross sections, $\sigma_0(VV)$, behaved at grazing angles between 1 and 2 degrees in much the same manner that they do at higher grazing angles. In particular, they showed the second-harmonic dependence on the angle between the antenna-look direction and the wind direction that is characteristic of scatterometry. $\sigma_0(HH)$, on the other hand, showed little evidence of the second harmonic component, maximizing with the antenna looking into the wind and minimizing in the opposite direction. For both polarizations, σ_0 was generally well above that expected from Bragg scattering and the polarization ratio $\sigma_0(VV) / \sigma_0(HH)$ was much smaller. Surface signatures of internal waves (IWs) off the New Jersey coast were much weaker when the antennas looked in the direction of internal wave propagation than when they looked opposite this direction. Interestingly, for the nonlinear internal waves found in the South China Sea, the opposite phenomenon occurred: W signatures were stronger looking in the direction of IW propagation than opposite to it. [C2607]

"Qualitative approaches to rapidly identify completely submerged rice due to tropical cyclone using satellite data"

The objective of the present study is to identify completely submerged rice areas due to tropical cyclones using remotely sensed data. The Kendrapara district of Orissa state hit by a tropical cyclone on 30th October 1999 is considered as study area and for this area, pre event (October 11, 1999) visible- near IR image and pre (October 11, 1999) and post event (November 2, 1999 and November 4, 1999) Radarsat images were procured. The pre event IRS ID LISS III (resolution = 22 m) image of Kendrapara district was geometrically corrected and classified into several landuse and landcover classes. Supervised classification technique was used for landuse/landcover classification. This landuse/landcover map is assumed to be accurate and is used as a base map in the present study. Pre and post event Radarsat-SAR images were also geometrically corrected. Further preprocessing included speckle noise removal, data calibration and incidence angle adjustment. Based on literature, a threshold of -16.5 db (DN value =100) was chosen to classify each pixel in pre Radarsat-1 SAR image as water or non-water. The landuse/landcover map was used to identify the rice regions in the pre and post-event Radarsat images. Application of the threshold allows for the determination of the submerged rice areas. To determine the validity of a single threshold, water pixels in pre event Radarsat-1 SAR images were extracted corresponding to the base map. A histogram of these values suggests that a single value threshold approach may not be fully accurate. To overcome these limitations, two alternative approaches, namely image

histogram and change in db were formulated. For both approaches, the rice pixels in pre and post event Radarsat- SAR images were extracted corresponding to base map rice pixels. In case of image approach, a histogram was plotted for the DN values of the pre and post Radarsat-1 SAR rice pixels. This allows the qualitative identification of the submerged rice areas. Using change in db approach, pixel-to-pixel change in db in pre and post event Radarsat-1 SAR images in rice pixels was calculated. Analysis of these values allows for the identification of different effects of submergence on the rice area. This type of analysis will help policy makers in determining the extent of submergence and could serve as a tool for rapid assessment of damage and help expedite release of relief funds and aid proper allocation of funds to the affected areas/people. [C2608]

"Retrieving land cover information from MERIS and MODIS Data: a comparative study for landscape characterization in Portugal"

This is a preliminary study in the framework of an ongoing research work that aims at comparing the aptitude of MERIS and MODIS images for land cover mapping at regional scale. Overall and per class accuracies achieved with a Maximum Likelihood classification of MODIS and MERIS images acquired during August 2005, are used as a measurement of their adequacy for land cover characterization in Portugal. Attained results show that differences in spatial and spectral resolutions of used images do not produce overly disparities in land cover classes' discrimination. Still, the separation between such numerous land cover classes is hampered by landscape fragmentation of the territory at such spatial resolution. [C2609]

"Mapping and modelling the snowmelt and greening pattern in southern norway by combining microwave and optical remote sensing sensors"

Southern Norway has strong climatic gradients and is well suited for studying snow melt and greening patterns. In this study we combine snow cover maps with phenological maps for the early May period for the years 2004 and 2006. The snow cover area maps are based on both microwave (ASAR) and optical (MODIS) sensors. The phenological maps are based on NDVI thresholds from the MODIS sensor. The onset of growing season 2004 was among the earliest recorded over the last 30 years. On May 8, 2004 30% of the study area was covered by snow and 29% had unfolded leaves on trees. The onset of the growing season in 2006 was slightly later than average, and on May 4, 2006 64% of southern Norway was covered by snow and the phenophase of unfolded leaves had not started yet. [C2610]

"Bora events over the adriatic sea and black sea studied by multi-sensor satellite imagery"

Bora events over the Adriatic Sea and Black Sea are investigated by using synthetic aperture radar (SAR) images acquired by the Advanced Synthetic Aperture Radar (ASAR) onboard the Envisat satellite, optical and infrared images acquired by the MODIS sensor onboard the Terra satellite, and sea surface wind data acquired by the scatterometer onboard the Quikscat satellite. Quantitative information on the sea surface wind field is extracted from the ASAR images by using the CMOD4 wind scatterometer model. It is shown that SAR images yield information of the spatial structure of bora events over coastal waters with high spatial resolution that cannot be obtained by other spaceborne instruments. Furthermore, by using ASAR data in combination with MODIS data we are able to detect cyclonic atmospheric eddies, which are often generated by lateral wind shear associated with bora events. [C2611]

"Satellite eye for the galathea 3 ship expedition: global tour 2006-2007"

Satellite Eye for Galathea 3 (www.satelliteeye.dk) contains education at the internet for secondary and upper secondary schools and the public. The Galathea 3 ship expedition circumnavigated the globe starting from Denmark 11 August 2006, visiting Greenland, Azores, South Africa, Australia, Solomon Islands, New Zealand, Antarctica, Chile, Galapagos, the Caribbean, the Northeastern USA and finishing in Denmark 25 April 2007. During the entire expedition satellite images were ordered along the ship track, downloaded, processed, archived and used for education. The satellite images are displayed in Google Earth along with 10 minute observations of air and sea parameters observed at the ship (<http://galathea.oersted.dtu.dk>). This material forms basis for 9 running projects along the entire route and 24 site-specific cases. Observations from several science projects onboard will be used in the site-specific cases. One of the continuous study cases is chlorophyll observed from Envisat MERIS. As an example: in the upwelling zone near Namibia a very high level of chlorophyll was observed from MERIS. The ship route consequently was changed slightly the day after in order to traverse the area with the highest amount of chlorophyll. Chlorophyll observed onboard (in-situ) two days later show high amounts. In addition, in the science project on the carbon cycle a significant emission of CO₂ was observed. The students can use the data online in the classroom. Students from several classes were onboard for part of the expedition and these classes in particular used the Satellite Eye teaching material. In Google Earth satellite images of many themes are shown. These include sea ice, sea surface temperature, ocean wind, wave height,

sea surface level, ozone, clouds and radar images of ocean and land. Also high spatial resolution land cover mapping of the visited harbors and their surroundings are included. The case studies use the image processing software LEO Works developed through the ESA project EDUSPACE, the European Earth Observation web site for Secondary Schools (<http://www.eduspace.esa.int>). For each theme a thorough educational material has been developed in Danish and English. ESA has granted a large amount of Envisat as well as PROBA images and third mission data from SPOT and Landsat. Also data from NOAA, NASA, JAXA and QUICKBIRD were used. [C2612]

"Combined use of InSAR and ICESat / GLAS data for high accuracy DEM generation on Antarctica"

This study aims to use ICESat /GLAS data for correction of DEM made from Interferometric SAR data instead of traditional ground control points (GCPs) collected by ground survey. GLAS is a laser altimeter system and it can measure the earth surface topography with ultimate vertical accuracy (plusmn14 cm) and high spatial accuracy (plusmn15 m). Therefore, we can treat GLAS data for the reference of height and position on Antarctic ice sheet. We applied this method at south of Breivika. The elevation values derived by ERS-1/2 InSAR DEM have insufficient height accuracy compared to GLAS data due to insufficient baseline estimation, ice flow appeared in the fringe pattern, and difficulty of phase unwrapping, which is RMS plusmn284.0 m compared with GLAS data. After the correction of InSAR DEM using GLAS data, it improved to plusmn32.6 m. Next, we validated this result using the 28th JARE (Japanese Antarctic Research Expedition) GPS survey result. The RMS height difference between JARE GPS result and corrected InSAR DEM showed plusmn39.5 m. The result showed that our correction method works quite well and we can produce spatially dense and high accuracy DEM along with Antarctic coast line. The one remaining problem is how to reduce the effect of ice flow appeared in the fringe pattern. [C2613]

"Polarview@FIMR: WWW-based delivery of Baltic sea ice products to end-users"

Sea ice information for navigational purposes is essential in the Baltic Sea. Winter navigation is made possible by the use of icebreakers, ice-strengthened vessels and by restricting navigation. Thus the icebreakers need detailed ice information for route planning. The smoothness of traffic has been possible due to better ice monitoring, where use of Earth observation data has become more and more important. For this purpose the FIMR PolarView web pages have been set up and they contain information to aid navigation in the area of the Baltic Sea. One such future SAR-based product could be the ice motion estimated from successive SAR images. For this purpose an algorithm for the ice motion detection has been developed at FIMR. Also the presentation of the existing products will be developed, for an example also the animations of the SAR-based ice thickness charts and ice predictions will probably be available in near- real-time next winter. [C2614]

"SAR simulation of ocean scenes covered by oil slicks with arbitrary shapes"

The identification of oil slicks on the ocean surface from SAR data requires quantitative sound models accounting for the most important characteristics (ocean spectrum, slick viscosity, slick shape, and so on). In this paper we present the implementation of an innovative SAR raw signal and image simulator, which is able to reproduce images relative to ocean surfaces covered by oil slicks with arbitrary shapes. The attention is mainly focused on slicks with fractal contours. The fractal Weierstrass-Mandelbrot function is used to generate slicks with fixed fractal dimension. A box counting technique is employed to evaluate the fractal dimensions of the generated slicks and the corresponding SAR images. Radiometric properties of the area covered by oil are also estimated in order to show how the simulated data provide a powerful set for processing algorithms. [C2615]

"Extraction of forest parameters in a mire biotope using high-resolution digital surface models and airborne imagery"

The objective of this paper is to spatially predict tree/shrub genera using generalized linear models (GLM), color-infrared (CIR) aerial images, ADS40 images, digital surface models (DSMs) and field samples. The present study was carried out in the framework of the Swiss Mire Protection Program, where extraction of forest parameters for description of present state of a mire ecosystem and as indicators for changes are of high importance. In a first step, high-quality DSMs were automatically generated from CIR aerial images for two test sites, both located in the Pre-alpine zone of Central Switzerland. In a second step, tree layers were then generated combining canopy height models derived from the DSMs and LiDAR DTM with a fuzzy classification of CIR aerial images. In a third step, on the basis of these tree layers, fractional tree/shrub covers were generated using explanatory variables derived from the DSMs and logistic regression models. Then tree genera were predicted for the pixel values (tree/shrub probability > 0.3) of the fractional covers using a multinomial regression model and additional spectral information as provided by Leica ADS40 data for one test site and CIR aerial

images for the other test site. Overall, prediction of tree genera was less satisfactory when only using CIR aerial images. In contrary, up to six different tree genera were predicted with high accuracy using explanatory variables derived from ADS40 images. The study stresses the importance of high-resolution and high-quality DSMs and highlights the potential airborne remotes sensing data for ecological modeling purposes. [C2616]

"ComRAD active / passive microwave measurement of tree canopies"

The NASA/GSFC and George Washington University network analyzer-based multifrequency truck-mounted radar system has recently been upgraded with the addition of a dual-polarized 1.4 GHz total power radiometer. The system, now called ComRAD for Combined Radar/Radiometer, can function as a ground-based instrument simulator for L band space missions such as Hydros, Aquarius, and SMOS. In late summer 2006 ComRAD was deployed to the field to begin a series of coordinated active/passive L band measurements over small stands of deciduous and coniferous trees in order to improve our understanding of the microwave properties of trees and their effect on soil moisture retrieval algorithms. This paper describes the preliminary measurements obtained at the start of a three-year planned field measurement effort. [C2617]

"A statistical and theoretical study about radar sensitivity to crop growth from S to X band"

In this work, we show the correlation study carried out on the data collected on a maize field in the Swiss region named Central Plain, by the multifrequency RASAM scatterometer. This agricultural field was monitored over long periods, at a wide range of frequencies and observation angles, so that the correlation between backscattering and crop height, biomass and soil moisture could have been studied under several plant and observation conditions. Moreover, we describe some recent refinements applied to the vegetation scattering model developed at Tor Vergata University, and we evaluate the accuracy of extended comparisons between model outputs and RASAM signatures. The Tor Vergata model is finally applied to give a theoretical basis to the experimental correlation findings. [C2618]

"The use of ASAR data for class cover identification from small swatches"

In this work we address the problem of land cover classification in advanced synthetic aperture radar (ASAR) images. The derivation and assessment of texture features for ASAR image segmentation is investigated using full multidimensional co-occurrence matrices as features. Expansion of local patches in terms of Walsh functions helps identify the optimal distance for the calculation of the co-occurrence matrices. The defined distance agrees with the one chosen by performing exhaustive tests where many distances were tried and the best was chosen from the training data. The well known chi-square test of statistical significance has been used for classification. [C2619]

"Integration of first and last return LiDAR with hyperspectral data to characterize forested environments."

The fusion of active LiDAR and passive optical hyperspectral data allows us to characterize the forest environments in ways that have not been possible previously with only one data source. This paper describes an airborne platform configured to collect data from multiple sensors simultaneously. Data from the platform have been applied to describe forest environments both in terms to species and structure. Integration of the data yields information and characterization of forest environments than has been possible in the past. [C2620]

"Evaluation of ASAR and optical data synergy for high resolution land cover mapping in portugal"

This paper aims at presenting the usefulness of combining satellite optical data from the visible and infrared wavelengths with longer wavelength radar data for land cover mapping in Portugal. This is a ground-breaking study in a geographical region that does not experience continuous intra-annual dreadful atmospheric contamination that commonly justifies radar usage. In this study we exploit the ability of ASAR images as an extra input feature for land cover classification together with the most used satellite optical data, i.e. Landsat. The goal of this paper is three-fold: 1) compare single date classification of ASAR data with Landsat data for land cover mapping; 2) evaluate the usefulness of multi-temporal ASAR measurements for land cover classification improvement; and 3) to compare a final map accuracy assessment with the classification scores attained with training and test sample sets. We conclude that ASAR imagery does not individually improve overall classification accuracy, but their synergy with Landsat data or in a multi-temporal context show up specific advantages; statistically sound accuracy assessment of final map bends optimal classification accuracies attained with test sampling observations. [C2621]

"Emissivities of rough surface over layered media in microwave remote sensing of snow"

The rough surfaces in Greenland are exhibited as sastrugi. The roughness heights are less than 8 cm for much of the year except in late winter and spring, when they increase to 25 cm or less. Roughness profiles were also related to snow and firn ventilation. WindSat, launched in January 2003, was the first spaceborne polarimetric radiometer to measure all 4 elements of Stokes vector, viz., the vertical polarized brightness temperatures, the horizontal polarized brightness temperatures, and the real and imaginary part of the cross-correlations of the vertical and horizontal polarizations. It was shown by Tsang (1984, 1990) that azimuthal asymmetry will create nonzero third and fourth Stokes parameter in passive microwave remote sensing. Thus the third and fourth Stokes parameters contain information of the azimuthal structure. Usually the third and fourth Stokes parameters are quite small between 0.5 K to 1 K over land and less than plusmn2.5 K over ocean. However, measurements of third and Stokes parameters over Greenland show surprising values of 10 K for the third Stokes parameter and between -10 K and 20 K for the fourth Stokes parameter. In this paper, we use physically based electromagnetic model to study the passive polarimetric remote sensing of snow in Greenland by consider the scattering and emission from a random rough surface over multi-layered media. We consider the random rough surface varied in only one horizontal direction so that azimuthal asymmetry exists in the 3-D problem. Dyadic Green's functions of multilayered medium (Tsang et al., 2000) is used to formulate the surface integral equation so that the polarization dependence of emission and scattering is accounted for systematically. The surface integral equations are solved by using the method of moments in conjunction with fast numerical algorithms such as the multilevel UV method. Numerical results of brightness temperatures are illustrated for all four Stokes parameters to demonstrate the signatures of sastrugi in passive microwave remote sensing. To account for the large third and fourth Stokes parameters, we also consider the case of anisotropic scatterers in volume scattering. Full multiple volume scattering are studied with numerical solutions of the radiative transfer equations for non-spherical scatterers with preferred orientation. [C2622]

"Ground-based microwave interferometric measurements over a snow covered slope:an experimental data collection in Tyrol (Austria)"

This paper reports on some results obtained during an experimental campaign carried out for monitoring a snow covered alpine mountainside and based on the use of a ground based interferometer working at C band. The effect of the interaction between radar signal and a dry snow cover on interferometric phase has been investigated on the bases of a simple model, representing the snow cover as a homogeneous lossless dielectric layer over the soil. Measured differential phases have been converted into snow depth estimations and compared to ground truth data. Coherence behaviour has been also investigated to evaluate the effectiveness of the proposed technique. As previously documented from other researchers, the potential of the technique has been demonstrated but limits to its applicability were found to be analysed thoroughly. [C2623]

"Empirical SWE retrieval using airborne microwave and in situ snow measurements"

We examine the response of microwave brightness temperatures to snow water equivalent over a wide range of snowpack conditions observed during the Cold Land Processes Experiment (CLPX) in 2002 and 2003. Spatially intensive measurements of snow were collected over the CLPX study areas within the Colorado Rocky Mountains. The NOAA Earth System Research Laboratory's Polarimetric Scanning Radiometer (PSR) was operated to obtain coincident high-resolution (150-500 m) multiband microwave imagery of the snowpack. Together, a robust data set of over 2300 collocated in situ and remotely sensed observations were obtained for this analysis. For each point we modeled brightness temperatures using observed snow properties and the Helsinki University of Technology (HUT) snow emission model. Using observed and modeled data, we developed multiple regression algorithms to retrieve snow water equivalent (SWE). The algorithms use brightness temperature differences between 10.7, 18.7, and 21.5 GHz with 37 GHz and 89 GHz. Results show that the CLPX microwave data are consistent with a) historically established data and, b) after removal of cases with macro vegetation or possible wet snow, with theoretically derived curves for microwave dependence on SWE. [C2624]

"Deconvolution algorithms in image reconstruction for aperture synthesis radiometers"

In remote-sensing applications the inclusion of subgrid-scale variability in coarse resolution data still remains an elusive challenge. This paper is devoted to the development of an appropriate downscaling technique for future Aperture Synthesis Radiometer's images. A comparative study of different deconvolution algorithms has been performed and particular emphasis is made on the use of least-squares Lagrangian methods and Fourier Wiener filtering. Results show that with this technique it is feasible to improve the spatial resolution of brightness temperature images from the Spatial Sensor Microwave Imager (SSM/I) radiometer and from an upgraded version of the Soil Moisture and Ocean Salinity (SMOS) End-to-end Performance Simulator (SEPS). [C2625]

"Combination of one-class remote sensing image classifiers"

This paper presents simple but powerful combination methods of dedicated one-class classifiers (OCCs) for efficient remote sensing image classification. The mean and product combination rules are applied to the probabilistic outputs generated by OCCs, and the performance is illustrated in a urban monitoring application in which multi-sensor (optical and SAR) data and multi-source (spectral and contextual) features are available. Two OCCs are used as core parts: the classical mixture of Gaussians (MoG) and the support vector domain description (SVDD) classifier. The obtained results by combining SVDD classifier outputs show a clear improvement in the accuracy, and more robustness to high dimensional samples compared to both MoG and stacked approaches. [C2626]

"Speckle noise reduction in SAR imaging using lattice filters based subband decomposition"

A new speckle reduction algorithm based on lattice filters for SAR imaging is presented. In the new method, the subband decomposition of the speckled image is performed using lattice filters. The noisy image is decomposed into subband images using high-pass and low-pass filters having lattice structure, then a threshold value is estimated according to noise variance in each subband and soft-thresholding is applied on the subband images. The despeckled image is obtained from the thresholded subband images using the inverse lattice filter. The proposed speckle reduction method is applied to RADARSAT/SAR images. The performance of the proposed method has also been compared with median filtering, and discrete and stationary wavelet transform based speckle reduction methods. Results show that the proposed method may be used efficiently for speckle noise reduction in SAR images. [C2627]

"Overview of the active TerraSAR-X calibrators and first results"

This paper describes the development and system concept for an active and highly integrated, digitally controlled SAR system calibrator. For precise and high-quality SAR data, precise ground targets are necessary for external calibration of the SAR data. Compared to passive targets, active radar targets like transponders offer more features. The recording of the transmitted radar signals from the satellite becomes possible and allows additional data analysis and data correction. A total of 18 active transponder and receiver systems and 16 receiver only systems were fabricated for the TerraSAR-X calibration campaign in summer 2007 [1], [2], [3]. TerraSAR-X is the first German spaceborne X-band SAR satellite mission. [C2628]

"COSMO-SkyMed active calibrator: A sophisticated tool for SAR image calibration"

In the framework of the COSMO-SkyMed mission¹, Space Engineering has designed and manufactured four Active Calibrators (AC). An AC has a twofold function: 1) re-radiating the received radar signal with the required Radar Cross Section (RCS) and polarisation; 2) acquiring the received Synthetic Aperture Radar (SAR) pulses amplitude for successive elaboration. The AC will be used as a tool of the COSMO-SkyMed Calibration / Validation facility during the SAR commissioning phase to validate the on-board SAR and during the normal phase to maintain stable the image quality figures. The Active Calibrators will be operated together with a set of Passive Calibrators, characterised by a fixed RCS. The former ones have the great benefit of providing much higher RCS figures and recording capabilities than the latter ones. This paper describes the characteristics and performance of this Active Calibrator. [C2629]

"Transpolarizing surfaces for polarimetric SAR systems calibration"

A novel transpolarizing or crosspolarizing surface has been proposed to be applied in polarimetric SAR calibrating systems, like trihedrals, since they can not provide initially a crosspolar response. So the trans-surface has been designed and measured in an anechoic chamber, providing good results for normal incidence. [C2630]

"New polarimetric calibration proposal and its evaluation using ALOS PALSAR calibration campaign measurements"

We propose new polarimetric calibration algorithms using two reference targets: a polarization-preserving reflector and a polarization rotating one. In this method, iteration procedure is adopted for accuracy improvement in deriving transfer matrices of radar transmitting and receiving antennas, FR(Faraday rotation) matrix and actual scattering matrix of observed target. Availability of this method was evaluated by measured results obtained in calibration campaign of PALSAR(phased array type L-band synthetic aperture radar) boarded on ALOS(advanced land observing satellite). It is proved that the proposed method can derive each matrix component separately. [C2631]

"ALOS PALSAR Calibration and Validation Results from Sweden"

In 2006 calibration activities for ALOS PALSAR were conducted in Sweden. Four five-metre trihedral corner reflectors and three smaller dihedral reflectors were deployed and operated during eight months. 23 PALSAR scenes were acquired over the calibration site allowing an evaluation of the quality and temporal stability of the data. Results show that the co-polarized data have been stable during the whole calibration period with variations in the trihedral responses lower than 0.7 dB. The measured resolution in azimuth was 4.4 m and in slant range 4.7 m for single polarization images and 9.5 m for polarimetric data. For the cross-polarized data large variations in the dihedral responses were found. It is assumed that this is caused by a larger sensitivity to pointing errors. For the polarimetric data, estimation of Faraday rotation gave values ranging from 0.1deg to 3deg. [C2632]

"The value of SAR Multi-polarization data in delivering annual crop inventories"

The outcome of a multi-year project carried out across sites within Canada has been the development of a method to deliver crop inventories using the integration of SAR and optical satellite data. Although multi-temporal optical imagery can classify crops at the target accuracy, SAR data will be valuable in boosting accuracies and ensuring operational delivery of this annual inventory. [C2633]

"Error analysis of Envisat ASAR level 2 algorithm based on simulation technique"

In ESA's Envisat ASAR level 2 algorithm, it is assumed that the synthetic aperture radar (SAR) image cross spectra of mixed ocean waves were the summation of SAR image cross spectra of wind waves and that of swells. But our previous studies show that in addition to this, the cross spectra of mixed waves consist of an extra term (see the companion paper submitted to this symposium). Just this term leads to an inherent error of this algorithm which has not been considered yet. This paper presents an error analysis of Envisat ASAR level 2 algorithm for ocean wave spectra retrieval in different significant wave height, wavelength, wave direction and wave component conditions based on simulation technique. It shows that the inherent errors (1) change with above parameters, and are always positive which mean the retrieved ocean wave height are overestimated; (2) increase for larger significant wave height; (3) increase for smaller wavelength; (4) increases for smaller propagation angle respect to azimuth direction. (5) increase for more wind wave component. Therefore, Envisat ASAR level 2 algorithm only works in small wave height, or large wavelength, or large propagation angle, or few wind wave component conditions. [C2634]

"Bathymetric retrieval from manifold coordinate representations of hyperspectral imagery"

In this paper we examine the accuracy of manifold coordinate representations as a reduced representation of a hyperspectral look-up table for bathymetry retrieval. The approach is based on the extraction of a reduced dimensionality representation in manifold coordinates of a sufficiently large representative set of hyperspectral imagery [4]. The manifold coordinates are derived from a scalable version [4] of the isometric mapping (ISOMAP) algorithm [12] [11]. In the present work and in [5], these coordinates are used to establish an interpolating look-up table for bathymetric retrieval by associating the representative data with ground truth data, in this case from a LIDAR estimate in the representative area. The compression of look-up tables could also readily be applied to look-up tables generated by forward radiative transfer models [9]. In this paper, we analyze the approach using data acquired by the PHILLS [6] hyperspectral camera over the Indian River lagoon Florida in 2004. Within a few months of the PHILLS overflights, SHOALS LIDAR data was obtained for a portion of this lagoon, principally covering the beach zone and in some instances portions of contiguous river channels. [C2635]

"Generation of ENVISAT ASAR Mosaics accessible on-line"

This paper describes the routine generation of ASAR mosaics at ESRIN and their distribution via Web map servers. ASAR products are automatically collected from various processing sites to be geocoded and mosaicked on the GRID Processing on Demand system at ESRIN. New mosaics are automatically transferred to an OpenGIS Web map server where they can be directly visualized at full resolution by external users. The generation of mosaics involves several processing steps including antenna pattern correction and compensation of incidence angle depending on vegetation type. Several map projections are supported including polar stereographic projections (Arctic and Antarctic's) as well as Plate Carre acute projections (entire World). [C2636]

"ASAR instrument performance and product quality evolution"

ENVISAT ASAR is successfully operating since March 2002 and resulting ASAR products are operationally distributed to the user community since December 2002. This paper provides an update of the ASAR performance, from the instrument status to the product quality assessment. [C2637]

"A comparison of internal calibration schemes for spaceborne single-pass InSAR applications"

In this paper, first compared different receive channel schemes for InSAR application, then the main principal and technique of three practical internal calibration schemes are analyzed and compared, especially the famous SIR-C and X-SAR internal calibration system. Based on these different schemes, a new internal calibration scheme using microwave over fiber link is subscribed. [C2638]

"Differential absorption microwave radar measurements for remote sensing of atmospheric pressure"

The accuracy of numerical weather model predictions of the intensity and track of tropical storms may be improved by large spatial coverage and frequent sampling of sea surface barometry. The feasibility of a microwave radar operating at moderate to strong O₂ absorption bands in the frequency range of 50~56 GHz to remotely measure surface barometric pressure may provide such capability. At these radar wavelengths, the reflection of radar echoes from water surfaces is strongly attenuated by atmospheric column O₂. Because of the uniform mixture of O₂ gases within the atmosphere, the total atmospheric column O₂ is proportional to atmospheric path lengths and the total atmospheric column air, and thus, to surface barometric pressures. Recent research has developed a technique based on the use of a dual-frequency, O₂-band radar to overcome many of the difficulties associated with techniques requiring larger frequency separation. The ratio of reflected radar signals at multiple wavelengths are used to minimize the effect of microwave absorption by liquid water, water vapor in the atmosphere and the influences of sea surface reflection over the frequency of operation. Langley Research Center (LaRC) has developed a radar based on this measurement technique to estimate barometric pressure. This paper will present an overview of the differential absorption measurement concept and will discuss a radar instrument to verify the differential O₂ absorption measurement approach. Results of instrument functional testing and initial measurements will be presented. [C2639]

"Detection of May 2006 Saharan dust outbreak over Granada, Spain, by combination of active and passive remote sensing"

During May 2006 a severe Saharan dust outbreak affected the Iberian Peninsula. During this event that lasted almost a whole week a large amount of mineral particles were present in the atmospheric column. In this work we present some results on this particular event that has been monitored at Granada, Spain (37.16degN, 3.6degW and 680 m a.m.s.l.) using different types of instrumentation. To investigate the optical properties of atmospheric aerosols, we used a combination of passive and active remote sensing, including Lidar system and radiometers, together with in situ techniques to characterize the physical properties of the aerosol. Features of the mineral aerosol outbreak are discussed in combination with other external information sources like back trajectory analyses. Our analyses are based mainly on the information obtained on the columnar properties of the atmospheric aerosol, although considerations were done on the atmospheric aerosol characteristics at the surface boundary layer. [C2640]

"Sampling quantization analysis and results for FMCW SAR"

One of the advantages of Frequency Modulated Continuous Wave (FMCW) radars is the relative low required sampling frequency even when transmitting high bandwidths. This is a consequence of the inherent homodyne configuration of the radar front-end. A simple way to reduce further the data rate is to use few bits per sample. The paper analyzes the effects of low bit sampling in FMCW Synthetic Aperture Radar (SAR) data. A low number of bits used to sample the FMCW deramped signal could produce spurious peaks and intermodulation products of the sinusoidal signal. However, it is shown in the paper that, for typical value of signal to noise ratio in FMCW systems, white noise suppresses the spurious products. Simulation results and verifications on real data collected with the FMCW SAR system built at the Delft University of Technology are presented. [C2641]

"Determine the location of a thermal front in the Iroise Sea by using HF radar data and tide model results"

The Iroise Sea is a shallow sea, located on the North West European Shelf close to Western Brittany (France) and North of the Bay of Biscay. Due to strong gradients in the bathymetry close to the coast and strong local winds, tidal currents can reach up to 3.5 m/s during spring tide and induce a strong vertical mixing along the coast. During summer, solar radiation and thus warming of the sea surface, together with mixing along the coast, and thus colder temperatures in this area, leads to a formation of a thermal front, where the differences between the sea surface temperatures on both sides can reach up to 3degC. During the SURLITOP experiment, that took place from August to November 2005, two HF radar stations have been installed at the French coast. Both stations were working simultaneously at a working frequency of 12.4 MHz and a measurement cycle of 12 min.

The surface current fields processed from the radar data have been interpolated to a regular 2times2 km grid. For the same period, tide model simulations (MARS 2D) have been processed with the same temporal and spatial resolutions. Because the model has been run under barotropic conditions, the location of the front, which is induced by density gradients, can not be reproduced. In contrast to the model, the radar measures the total circulation including the baroclinic signal, so that the difference between radar data and model results can be exploited to find the location of the thermal front. To validate this result, satellite remote sensed sea surface temperature data have been used. The result is very promising, as the region of highest differences between radar data and model results coincide with the location of the thermal front. The location of the front itself can be determined by the narrowness of the isotherms. Also the structures of the front isotherms and the strongest gradients of the currents are very similar. Thus it is possible, to determine the location and dynamics of a thermal front by using HF radar data in combination with model results, if the model is working under barotropic conditions. [C2642]

"Exact electromagnetic modeling of the scattering of realistic sea surfaces for HFSWR applications"

As a long term objective we would like to define the required conditions to detect oil spills, using high frequency surface wave radar (HFSWR). Assuming that the presence of oil spills on the sea surface modifies the surface tension which in turn affects the dynamics of the sea, we would like to determine the minimal surface tension which makes this phenomenon observable on a Doppler spectrum. For this purpose we have developed a simulator based on a realistic modeling of the sea and of its temporal variation as well as on an exact modeling of the interactions between the electromagnetic waves and the environment. We have chosen to implement a full wave model called ELSEM3D, developed by ONERA. This tool is based on the method of moments (MoM) which can be accelerated by the fast multipole method (FMM). The issues of such a modeling are numerous: computational time due to the number of temporal realizations required to generate a Doppler spectrum and the dimension of the scene. In this paper, we will discuss the issues raised by this study and outline how we can overcome them. We will also present some simulated Doppler spectra for different sea states and radar configurations. [C2643]

"Validation of a backscatter model of a river ice covers using Radarsat-1 images"

Simultaneous microwave radar data and measurements field at some study sites on river ice were collected over the Athabasca River during winter 2006. These data will be employed to validate an electromagnetic model developed to simulate the backscatter of river ice cover. This model is based on radiative transfer theory which is solved by doubling matrix methods". This numerical method accounts for scattering effects due to the volume, boundaries, boundary-volume interactions and coupling between layers. Three ice types were formed on this river (columnar ice, snow ice and frazil ice). The measurements collected from the extracted ice cores included the ice thickness, ice type, ice densities, and size and form of the scatters embedded in the ice cover. These measurements will be used as inputs data for the model developed to its validation with the Radarsat-1 images and to understand the interaction of radar signal with the different ice types formed on the river. [C2644]

"Application of persistent scatterer InSAR and GIS for urban subsidence monitoring"

The purpose of this paper is to demonstrate the application of C-band ERS-1/2 and ENVISAT radar images to investigate the urban subsidence due to groundwater extraction. Cities in Australia without groundwater being over-extracted are compared to cities in Australia and China with groundwater being over-extracted. The persistent scatterer InSAR results are interpreted and compared to investigate the effect of groundwater extraction to urban subsidence. The GIS software is used to interpret the persistent scatterer InSAR results. The combined methods between persistent scatterer InSAR and GIS allow an integration of information from various sources and hence improve the efficiency for interpreting the data. A total of 15, 18 and 27 images of ERS-1/2 images acquired from August 1992-December 1996, April 1992-April 1997 and August 1992-July 2002 for Canberra, Sydney and Newcastle respectively are chosen to be investigated with persistent scatterer InSAR. Together with the above images, ten ERS-1/2 images from June 1992-December 1996 and nine ENVISAT images from December 2003-June 2006 acquired over Perth (Australia) and Northern China respectively are also chosen for similar investigation. The results show that the deformation rate from the cities with groundwater over-extracted, are significantly larger than the cities without groundwater over-extracted. The results have demonstrated the effect of groundwater extraction to urban subsidence. [C2645]

"Hurricane wind field estimation from seawinds at ultra high resolution"

Although SeaWinds was not originally designed to observe tropical cyclones, new higher resolution products resolve much of the horizontal structure of these storms. However, these higher resolution products (reported at 2.5 km) are inherently noisier than the standard 25 km products and the high rain rates often associated with

hurricanes corrupt the wind estimates. Fortunately, these storms have structure which can be exploited using a model. This paper develops a new procedure for hurricane wind field estimation from the SeaWinds instrument at ultra high resolution. We develop a simplified hurricane model to provide prior information to be used in maximum a posteriori probability (MAP) wind estimation. Using the hurricane model ameliorates the effects of rain and noise on the scatterometer measurements and directly provides useful hurricane parameters such as the eye center location and intensity. [C2646]

"The vertical distribution of Saharan dust over the western and central Mediterranean through dust modelling and lidar observations"

Aerosol extinction vertical profiles during Saharan dust events measured by two EARLINET lidar stations in the western and central Mediterranean during a two-year period (2001-2002) are compared to profiles forecasted by the dust regional atmospheric model (DREAM) that currently operates dust forecasts over the Mediterranean region. 35 Saharan dust cases were successfully captured in Barcelona (Spain) with a 1064 nm backscatter lidar and 45 Saharan dust cases in Naples (Italy) with a 351 nm Raman lidar. The objective of the present study is twofold: (1) to evaluate the skills of the model to forecast the dust vertical distribution in the Mediterranean basin and (2) to study the synoptic pattern dependence of the Saharan dust events over the western and central Mediterranean. The comparison between the modeled and the measured mean annual aerosol extinction vertical profiles shows a rather good agreement between model forecasts and lidar data. However, below 2000 m the extinction measured by the lidar systems is not captured by DREAM due to the significant influence of local anthropogenic aerosols in the boundary layer. The main synoptic patterns responsible for all the measured events of Saharan dust were identified and classified for both sites. It was found that the main synoptic situations in which the Saharan dust reaches the Mediterranean basin are anticyclonic systems located in North Africa (both for dust transport over the western and the central Mediterranean) and a low pressure system located in Portugal (for the western Mediterranean) and in central Europe (for the central Mediterranean). In the presence of low pressure, the altitude of the dust plume is higher in the western than in the central Mediterranean and this is probably related to geographical factors. [C2647]

"Examination of hygroscopic properties of aerosols using a combined multiwavelength elastic-Raman lidar"

Water vapor is an important greenhouse gas due to its high concentration in the atmosphere (parts per thousand) and its interaction with tropospheric aerosols particles. The upward convection of water vapor and aerosols due to intense heating of the ground leads to aggregation of water particles or ice on aerosols in the air forming different types of clouds at various altitudes. The condensation of water vapor on aerosols is affecting their size, shape, refractive index and chemical composition. The warming or cooling effect of the clouds hence formed are both possible depending on the cloud location, cover, composition and structure. The effect of these clouds on radiative global forcing and therefore on the short and long term global climate is of high interest in the scientific world. A major interest is manifested in obtaining accurate vertical water vapor profiles simultaneously with aerosol extinction and backscatter in the meteorological and remote sensing fields all around the globe in an effort to understand the hygroscopic properties of aerosols. In previous work, simultaneous measurements of RH with backscatter measurements from a surface nephelometer were used to probe the hygroscopic properties of aerosols. However, most of these measurements were not able to probe the high RH domain since such high RH is rare for surface altitudes. For this reason, experiments using a 355 nm Raman water vapor and aerosol lidar at the ARM site were used. Capable of providing simultaneous backscatter and RH profiles, and performing the experiments under low altitude cloud decks insured stable well mixed layers as well as probing RH profiles to above 95% which is required for the differentiation of different aerosol hygroscopic models. [C2648]

"Wavelet polarimetric SAR signature analysis of sea oil spills and look-alike features"

Marine dark features in SAR imagery related to oil spills, biogenic look-alikes and low wind areas are analyzed by means of the wavelet polarimetric signature (WASP) tool. The WASP encapsulates in a graph the dependency of the wavelet variance on dyadic scale and polarization state. Experiments on SIR-C/X-SAR C-band data showed the effectiveness of this analysis in characterizing textural features of the areas of study. [C2649]

"Distributed target detection in SAR images using improved chaos-based method"

Detection of distributed targets such as internal wave or ship wake on sea surface in Synthetic Aperture Radar (SAR) images is an important application of ocean microwave remote sensing. The chaotic characteristic of sea clutter gives some clues to targets detection on sea surface. Speckle, the inherent noise of SAR image, will

affect the predictive accuracy of sea clutter adversely and reduce the detection performance of radar. In order to apply the chaotic characteristic of sea clutter to targets detection in SAR images more effectively, an improved chaos-based detection method is proposed in this paper. First, speckle noise is suppressed by undecimated wavelet transform (UWT), and then targets are detected on the basis of the chaotic characteristic of sea clutter from the denoised SAR images. Experimental results prove that the method proposed in this paper is effective for the distributed targets detection in SAR ocean images. [C2650]

"Simulation of SAR image cross spectra from mixed ocean waves"

A 6-parameter frequency spectrum with two peaks and a cos-2s type spreading function is used to simulate the mixed waves. The spaceborne and airborne synthetic aperture radar (SAR) image cross spectra of mixed waves in different significant wave height, wave length, wave direction and wave component are then calculated by using Engen's nonlinear transformation formula. Analysis based on above simulation indicate that (1) the cross spectra of mixed waves dilate in range direction and shrink in azimuth direction (the so-called azimuth cutoff effect); (2) the cutoff effect increases for waves with larger wave height, or for waves with shorter wave length, or for waves propagating closer the azimuth direction, or for waves containing more wind wave component, or for spaceborne SAR; (3) the cross spectra split into two parts for waves propagating along range direction (the so-called double-peak phenomenon); (4) the direction ambiguity of ocean waves can be removed by using the imaginary part of cross spectra; (5) in addition to the contribution of wind wave part and swell part of the mixed waves, the cross spectra of mixed waves consist of an extra term which leads to an inherent error when using ESA's Envisat ASAR level 2 algorithm to retrieve ocean waves (see the companion paper submitted to this symposium). [C2651]

"Automatic recognition of coastal and oceanic environmental events with orbital radars"

An automatic classification procedure was developed able to identify different oceanic events, detectable in orbital radar images. The procedure was customized to be used in the southeastern Brazilian coast, since the classification training and test used examples extracted from 402 RADARSAT-1 images acquired in this region. Different sets of spectral, geometric and contextual (meteo-oceanographic and location) features of selected low backscatter patches were evaluated. Machine learning procedures (neural networks, decision trees and support vector machines) were used to induce classifiers to differentiate between seven classes, belonging to two categories. The classification procedure involves two steps: first the features area classified in one of two categories-oil spill or meteo- oceanographic phenomena. In the second step, the identification of tree classes of oil spills and four classes of meteo- oceanographic phenomena is done. The oil spill related classes are associated to operational exploration and production spills, ship releases and others. The meteo-oceanographic phenomena include biogenic oils and/or upwellings, algae blooms, low wind areas and rain cells. The models induced by support vector machines and neural networks achieved good results, allowing the operational implementation of the proposed procedures. [C2652]

"Extreme wind conditions in tropical cyclones observed from synthetic aperture radar images"

Both atmospheric and oceanic processes play an important role in the dynamics of tropical cyclones. Due to the relatively small amount of in situ data available for extreme events like hurricanes or typhoons remote sensing techniques play an important role in the measurement of the relevant geophysical parameters. In this paper some recent results on SAR observation of extreme wind conditions are summarized. The study is based on the use of ENVISAT ASAR wide swath images. The objective of this study is to investigate the performance of SAR to improve the existing model for the retrieval of information on wind field under extreme wind and wave conditions using information from a parametric Holland type model. [C2653]

"Measurement of extreme wave height by ERS-2 SAR and numerical wave model (WAM)"

The Synthetic Aperture Radar (SAR) onboard the European Satellite ERS-2 is operated in wave mode over the global oceans whenever no image mode data acquisition is requested. In the present paper new SAR algorithms to derive sea state at German Aerospace Center (DLR) are shortly introduced and used to determine SAR derived ocean parameters from wave mode data. Global Significant wave height statistics on a 3deg by 3deg grid derived by an empirical method (CWAVE) is presented in this paper for sea state analysis. A severe North Pacific storm that produced significant wave height above 10 m along the northern great circle shipping route is presented in the paper. The sea state generated is analyzed in more detail using the empirical method to derive significant wave height and compared to the ocean wave model WAM. [C2654]

"A case study on swell modulation caused by surface winds using spaceborne Synthetic Aperture Radar"

In an ERS-SAR image of the sea off Kii Peninsula on 30 March 1996, we found an atmospheric front formed by the sheltering effect of land topography and swell modulation in the sheltered/non-sheltered areas. From the SAR image, high-resolution wind speed and SAR-wave spectrum are retrieved. In the frequency range higher than the peak frequency, the SAR-spectra of the non-sheltered area have energy density higher than that of the sheltered area. The difference between the spectra of sheltered/non-sheltered areas is well explained by the simulated SAR spectra using the SAR-derived winds and a wind wave development formula suggest that the observed swell modulation is caused by the surface wind. This is a preliminary report and a full paper will appear elsewhere. [C2655]

"Wave measurements under the typhoon by 9.25MHz ocean radar"

National Institute of Information and Communications Technology (NICT) is developing 9.25 MHz ocean radar for measuring the sea surface currents and ocean waves on the offshore. This study clarifies the validity and accuracy of observing ocean waves, when the typhoon passed through the observation area, with 9.25 MHz ocean radar. In addition, we compare inversion algorithms for 9.25 MHz ocean radar wave measurements. This study compares the performance of two inversion techniques due to Kojima and Hashimoto, and Howell and Walsh. [C2656]

"Integrated satellite tracking of pollution: A new operational program"

The Canadian Ice Service (CIS) new operational program ISTOP (Integrated Satellite Tracking Of Pollution) is designed to effectively use SAR satellite imagery from Canada's Radarsat-1 as an aid in marine oil spill detection. [C2657]

"A FEXP model Short Range Dependence analysis for improving oil slicks and low-wind areas discrimination in sea SAR imagery"

Starting from a consideration of the Long Range Dependence (LRD) behavior of sea SAR image spectra, an overview is given of the LRD approaches currently being used to achieve reliable sea surface anomalies discrimination from high resolution sea SAR images. In this paper, the problem of SAR image analysis to discriminate oil slicks from low wind areas on the sea surface is addressed by employing fractional exponential (FEXP) models and short range dependence (SRD) parameters. The presented method demonstrated reliable results when applied to European remote sensing 2 (ERS-2) SAR precision images (PRI) and ERS-2 SAR ellipsoid geocoded images (GEC) of the Atlantic and the Pacific Oceans. [C2658]

"High resolution millimeterwave SAR for the remote sensing of wave patterns"

High resolution imaging of the ocean swell was performed using data collected with the polarimetric millimetre wave synthetic aperture radar MEMPHIS. The data, representative for a region off the south Spanish Atlantic coast in spring, have been evaluated using imaging and non-imaging statistical methods. The influence of high resolution processing on the clutter statistics for the Ka- and the W-band is discussed. [C2659]

"Multibaseline POL-InSAR analysis of urban scenes for 3D modeling and physical feature retrieval at L-band"

This paper generalizes a multibaseline interferometric SAR signal model taking polarization diversity into account. Based on this formulation, two high-performance spectral analysis techniques are extended to the multibaseline POL-InSAR configuration. These new algorithms enhance the height estimation of scatterers by calculating optimal polarization combinations and allow to determine their physical characteristics. Applying the methods to urban scenes, experimental results show the retrieval of building height and polarimetric properties by means of single-baseline polarimetric datasets. Dual-baseline observations permit the solution of the layover problem by separating two contributions within one resolution cell. The algorithms are tested using multibaseline Pol-InSAR data acquired by DLR's E-SAR system over Dresden city. [C2660]

"Uncertainty analysis in advanced differential interferometric SAR processing"

The DInSAR technique enables to determine with precision the surface displacements, using a combination of multiple interferograms. The DInSAR processing steps generate different kinds of errors, which propagate in the entire chain. This work is focused on a particular type of error generated during the DInSAR processing: the unwrapping related errors. The errors generated during the unwrapping process and the use of a procedure to automatically detect and correct them are presented in this work. By an iterative process and exploiting the SVD least squares method for outliers rejection, this procedure determines the phases values associated with each SAR image, starting from a stack of interferograms. It works on previously selected pixels and provides good

results with high observation redundancy. The effectiveness of the procedure is illustrated by using ERS SAR data acquired over Barcelona (Spain). [C2661]

"Increased export of grounded ice after the collapse of northern Larsen ice shelf, Antarctic Peninsula, observed by Envisat ASAR"

Time series of satellite radar image data of Envisat ASAR were used to study the retreat of ice shelves and glaciers at northern Larsen Ice Shelf, Antarctic Peninsula, up to March 2007. After the disintegration event in March 2002, the small remaining ice shelf section of Larsen B decreased further in area. The retreat of grounded glacier ice continued also. The glacier velocities above previous Larsen B increased further since 2004, but the acceleration has been smaller than in the first two years after the collapse in 2002. Ice export increased rapidly after the glaciers started to calve directly into the ocean. The sea level contribution due to discharge of grounded ice above the disintegrated ice shelf sections amounts to about 6% of the present glacier and ice sheet contribution to sea level rise. [C2662]

"ASAR parallel-track PS analysis in urban sites"

In this work we present a methodology for developing a Permanent Scatterers (PS) analysis jointly exploiting data acquired from parallel orbits to estimate height and deformation trend of multi-angle urban targets. The methodology allows applying the PS technique also in areas where the number of ASAR acquisitions per single track would prevent to get reliable estimates. Preliminary experimental results achieved in the Shanghai test site confirm the promising potential of the proposed methodology. [C2663]

"Surface deformation analysis of the Campi Flegrei caldera, Italy, by exploiting the ENVISAT ASAR data with the SBAS-DInSAR technique"

We have investigated the deformation affecting the Campi Flegrei caldera (Italy), from 2002 to the end of 2006, by analyzing ENVISAT ASAR IS-2 data. This study has been performed by exploiting the SBAS-DInSAR algorithm that allows us to detect earth surface displacements and to investigate their temporal evolution via the generation of deformation time series. The presented analysis highlighted the renewed volcanic activity that started on mid-2005; moreover, we have combined the ascending and descending data in order to separate the vertical and east-west components of the detected displacements. The obtained results have been confirmed by the leveling data collected by the Osservatorio Vesuviano. [C2664]

"Optimizing interferogram generation, pixel selection and data processing for high non-linear deformation monitoring with Orbital DInSAR"

A necessary step for every DInSAR technique is to properly select the data from which deformation information will be calculated. Two main processes must be done in this sense, the interferogram set creation and the quality pixel selection. In this paper we will present advances concerning both issues: a new method for selecting a high quality and reduced interferogram set solving an equivalent minimum spanning tree system and a pixel selection criterion based in region growing type algorithms. Furthermore, in order to avoid errors when dealing with highly non-linear deformation patterns, a temporal block differential processing is proposed. [C2665]

"A multi-scattering and multi-layer snow model and its validation"

Microwave scattering from snow is difficult to model due to the complexity and heterogeneity of natural snow. In this paper, we developed a multi-layer, multi-scattering model based on recent theoretical advances in snow and surface modeling. In the proposed multi-layer model, Matrix Doubling method is used to account for scattering from each snow layer; and Advanced Integral Equation Model (AIEM) is incorporated into the model to describe surface scattering. Comparisons were made between the model predictions and field observations from truck-mounted L- and Ku-band scatterometers (frequencies are 1.25 GHz and 15.5 GHz) at Local-Scale Observation Site (LSOS) of NASA Cold- land Processes Field Experiment (CLPX) during Third Intensive Observation Period (IOP3). It was found that model predictions were in good agreement with field observations with proper particle size selected. Analysis on scatterer shape, multiple scattering and snow stratification effects were also made based on model simulations. [C2666]

"Microwave remote sensing of alpine snow"

In the alpine zone snow is a dominant factor for more than half of the year and has strong influence on the ecosystem and economy. The knowledge of snow coverage, structure, liquid water content etc. is important and useful for many applications ranging from flood management to avalanche warning. Remote sensing from space has good potential to address these needs. Within ASSIST, Alpine Safety, Security and Information services and

Technologies, these topics are also of interest. Two snow related products were identified that can be produced on an operational base with the available satellite systems to be ingested into the ASSIST service. Avalanche maps, mapping the contours of avalanches, and snow cover maps, mapping the snow covered area. The produced products are in good agreement with validation data. Unfortunately the current available satellite systems (mainly c-band SAR that is applicable) are not very well suited for snow related applications due to the small influence of the dry snow on the microwave signal at C- band. To overcome this limitation the CoReH2O mission was designed. With its X- and Ku-band system and repeat rates of 3 and 15 days it has high potential for alpine snow applications. Additional microwave signature measurements at these frequencies with standardized and reproducible snow characterization information will be needed for model development and validation. Recent developments allow a more quantitative snow characterizations and will be considered in the SnowScat project in combination with traditional snow characterization methods. [C2667]

"Airborne Ku-band radar remote sensing of terrestrial snow cover"

Preliminary analyses of the POLSCAT data acquired from the CLPX-II in winter 2006-2007 are described in this paper. The data showed the response of the Ku-band radar echoes to snowpack changes for various types of background vegetation. We observed about 0.4 dB increase in backscatter for every 1 cm SWE accumulation for sage brush and agricultural fields. The data also showed the impact of surface hoar growth and freeze/thaw cycles, which created large snow grain sizes and ice lenses, respectively, and consequently increased the radar signals by a few dBs. [C2668]

"CoRe-H2 O-A dual frequency SAR mission for hydrology and climate research"

Taking into account the needs for improved, spatially detailed observations of snow and ice in climate research, hydrology, and glaciology, the satellite mission COld REgions Hydrology High-resolution Observatory, CoRe-H2O, was proposed to ESA. As payload a co- and cross-polarized Ku-band (17.2 GHz) and X-band (9.6 GHz) SAR was selected, because of its sensitivity to dry snow, thin sea ice, and the metamorphic state of snow, firn and ice on glaciers and ice caps. A cost-effective ScanSAR scheme with parabolic reflectors (each with multiple beams) is proposed fulfilling the requirements for swath width, spatial resolution and radiometry. The mission has been selected by ESA for further scientific and technical studies in the frame of the Earth Explorer Satellite Programme. [C2669]

"The SARALPS-2007 measurement campaign on Xand Ku-Band Backscatter of snow"

The retrieval of snow parameters, and snow water equivalent in particular, are key parameters in hydrology and climate research. Theory, ground-based signature research and analysis of spaceborne scatterometry suggests that the high- frequency combination of Ku- and X-band active microwave sensors is an excellent tool for the retrieval of snow physical properties. In order to validate this, a snow measurement campaign was carried out with the University of Cranfield's portable Ground-Based Synthetic Aperture Radar (GB-SAR) System during the winter of 2006/7 at two test-sites in the Austrian Alps close to Innsbruck. Fully polarimetric X-and Ku-band backscatter signatures were acquired over a range of incidence angles (~20deg-70deg), with the active sensor operating predominately in SAR mode, but occasionally also in InSAR mode. Microwave signatures and snow properties were measured on seven different dates. Detailed complementary meteorological and snow metamorphic conditions were also recorded. [C2670]

"Ship detection with the fuzzy c-mean clustering algorithm using fully polarimetric SAR"

A fuzzy c-mean clustering algorithm to detect ships is proposed using fully polarimetric SAR data. The algorithm is unsupervised. It does not need the statistical decision and the performance is not data specific, as often arises with CFAR methods. A distance measure, based on a complex Wishart distribution, is applied using the fuzzy c-means clustering algorithm. The algorithm makes use the statistical properties of polarimetric data, and takes advantage of a clustering algorithm. It is thus expected that the algorithm could include fully polarimetric backscattering information for ship detection. Its effectiveness is demonstrated by applying it to detect the targets in a set of AIRS AR data. [C2671]

"Characterizing the radiation fields in the atmosphere using a cloud-aerosol-radiation product from integrated CERES, MODIS, CALIPSO and CloudSat data"

CloudSat and CALIPSO cloud and aerosol information is convolved with CERES and MODIS cloud and radiation data to produce a merged 3-dimensional cloud and radiation dataset. [C2672]

"X-band extinction in boreal forest: Estimation by using E-SAR POLInSAR and HUTSCAT"

In this paper we study the extinction coefficient of boreal forest by utilizing airborne E-SAR X-band POLInSAR and HUTSCAT X-band profiling scatterometer measurements. By combining E-SAR VV-pol coherency with HUTSCAT tree height measurements we calculate forest extinction coefficients by RVoG model inversion and compare the results with extinction values obtained from HUTSCAT measurements. For retrieval of the extinction coefficient we propose robust RVoG model inversion procedure and discuss the model inversion conditions. Our results show, that extinction coefficient for boreal forest is quite low even for X-band, especially from nadir looking instruments. The extinction coefficient of forest canopy retrieved from HUTSCAT measurements is 0.15 dB/m and retrieved from E-SAR and HUTSCAT measurements is 0.9 dB/m. [C2673]

"Cloud Profiling Radar Performance Eastwood Im"

The Cloud Profiling Radar (CPR), the primary science instrument of the CloudSat Mission, is a 94-GHz nadir-looking radar that measures the power backscattered by clouds as a function of distance from the radar. This instrument has been acquiring global time series of vertical cloud structure at 500-m vertical resolution and 1.4-km horizontal resolution since June 2, 2006. In this paper an overview of the radar performance during the first year in flight is provided. [C2674]

"An investigation of PN sequences for multistatic SAR/InSAR applications"

This paper investigates the performance of pseudo-noise (PN) sequences as pulse compression waveforms in the radar imaging of distributed targets. Multiple transmitter schemes such as multi-static synthetic aperture radar (SAR) and multi-baseline interferometric SAR (InSAR) provide high resolution images for remote sensing applications at lower costs. PN sequences are a natural choice for such systems. The performance of different PN coding schemes such as the maximal length sequences (m-sequences), Gold sequences and shifted m-sequences are compared. [C2675]

"Obtaining a ship's speed and direction from its Kelvin wake spectrum using stochastic matched filtering"

The Kelvin wake of a ship is directly linked to the ship's speed, heading and hull shape. This wake can be visible in high resolution synthetic aperture radar images or optical images. Whenever it is possible, analyzing it can provide elements to identify the ship and track its course. We propose a strategy based on the generalized Radon Transform and the Stochastic Matched Filtering where the locus of the wake signature in the 2D spectrum of the image is to be detected. [C2676]

"Volume and double-bounce decorrelation effects in the OVoG model for Single-Tx PolInSAR"

The formulation of the complex interferometric coherence for the oriented volume over ground model (OVog) has been recently proposed for the case of dominant double-bounce mechanism from the ground when the interferometer is operated in single-transmit (bistatic) mode. This paper analyzes the two contributions to the total coherence function: the volume and the double-bounce terms. The study is performed by observing the model predictions of the coherence loci for several agricultural crop scenarios and with system parameters corresponding to the TanDEM-X mission. For low vegetation depths (up to 1 m) neither of the two contributions is negligible when the ground-to-volume ratio is low. However, when the backscattering returns from ground and vegetation are similar, i.e. ground-to-volume ratios around 0 dB, the volume decorrelation terms does not affect the coherence so much. As predicted by theory, higher vegetation layers yield an increase of the influence of the volume term and more differences between polarimetric channels. [C2677]

"Vertical profile reconstruction with Pol-InSAR data of a subpolar glacier"

The last decade has seen an increasing demand for accurate mapping and wide-coverage monitoring of glaciers and ice sheets in order to measure and predict their response to global climate change and their contribution to sea level rise. This in turn requires a more complete understanding of their properties including topography, accumulation rates and vertical profiles. One promising new technique for vertical profile reconstruction using polarimetric interferometric SAR (Pol-InSAR) data is polarization coherence tomography (PCT) and for the first time, PCT is adapted here to a glacier scenario. The inversion algorithm to reconstruct vertical ice profiles is applied to both simulated data to assess its accuracy and sensitivity to input parameters, and to airborne Pol-InSAR data at L- and P-band and InSAR data at X-band collected using DLR's E-SAR system over the Austfonna ice cap in Svalbard, Norway. [C2678]

"POLINSAR for FOPEN using flashlight mode images along circular trajectories"

The airborne radar system RAMSES collected data over the Sweden forest to investigate the capabilities of

detection at P-band and influences of different SAR parameters like resolution, central frequencies, and look angle. During this campaign, circular trajectories have been performed in order to analyze the presence of anisotropic scattering from the targets at P-band. We show the treatment of two circular trajectories using the Flashlight imaging mode and its ability to collect several SAR data with different look angles. The scope of this paper includes a general description of the operating mode of flashlight SAR images in the interferometric mode and the use of it for FOPEN purpose. The capabilities of detection of such polarimetric images have already been investigated, but without using the interferometric mode [1]. It had been shown that using circular trajectories at P-band was necessary to detect targets: first in our configuration detection was very difficult because the forest was very dense, secondly the targets were very sensitive to the orientation angle of the radar, which should not be the case at lower frequencies. Moreover, polarimetry and polarimetric interferometry are useful tools once the acquisition conditions ensure that detection is possible. Now, the full polarimetric and interferometric information are used in order to explore the potential of the POLINSAR circular mode to yield high detection rate. [C2679]

"Potential of forest height estimation using X band by means of two different inversion scenarios"

Polarimetric SAR interferometry (Pol-InSAR) is a powerful remote sensing method for forest height estimation by using the random volume over ground model (RVoG). At higher frequencies implementation of forest height estimation in X band is limited to less dense and low forest types where X band is able to penetrate through the volume to the ground. However, the penetration depth at X band is insufficient to cover all forest types. In the paper, forest height inversion at X band using two different approaches is demonstrated with focus on the impact of extinction on forest height estimation. [C2680]

"Compact PolInSAR for vegetation characterisation"

In this paper, we analyse the potential associated with a compact polarimetry (CP) P band spaceborne SAR system. Indeed, this architecture allows polarimetric acquisition without the usual reduction in swath. The CP data is shown to be almost equivalent to the full polarimetric data over extended targets, and the PolInSAR analysis can be performed without a significant loss of performance. [C2681]

"Polarimetric Calibration Experiment of ALOS PALSAR with Polarization-Selective Dihedrals"

Polarization-selective dihedrals are developed for polarimetric calibration of the PALSAR. The PALSAR is the first spaceborne polarimetric SAR boarded on the ALOS satellite launched in January 2006. This paper presents calibration experiments of PALSAR with the dihedrals in the ALOS initial calibration and validation phase. The reflectors are deployed in open fields of Tomakomai forest, to be imaged by not only the PALSAR but also the airborne polarimetric SAR, Pi-SAR. [C2682]

"Comments on hybrid-polarity SAR architecture"

Recent work on compact polarimetry is reviewed in the context of the fifty-year history of polarimetric diversity. One promising form of this genre is hybrid-polarity (CL-pol), in which a synthetic aperture radar (SAR) transmits circular polarization and receives on two orthogonal mutually-coherent linear polarizations. The CL-pol technique is compared and contrasted to alternative compact polarimetric schemes. Useful characteristics that are unique to the hybrid-polarity architecture are described, especially rotational invariance and polarimetric calibration. [C2683]

"Unsupervised classification of polarimetric SAR data using graph cut optimization"

The paper presents a new framework for the classification of polarimetric SAR data. The underlying model introduces cyclic conditional dependencies among the class labels assigned to neighboring observations as a mechanism to regulate the spatial homogeneity of classification results. Classification is posed as an inference problem, and is solved by coherently integrating expectation maximization and graph cut optimization. Results based on real SAR data are presented. [C2684]

"Application of bootstrap techniques for the estimation of Target Decomposition parameters in RADAR polarimetry"

The precise estimation of the eigenvalues of PolSAR responses is essential in the derivation of Target Decomposition parameters such as the Cloude-Pottier parameters (Entropy, Anisotropy and average angle Alpha). However, sample eigenvalues are strongly biased for small sample sizes leading to underestimated Entropy and overestimated Anisotropy values. In this paper, we investigate the use of a particular bootstrap technique for the correction of the bias. Bootstrap techniques are attractive because they can deal with very

small sample sizes under minimal assumptions on the signal distribution. Here, we are using the jackknife bias correction technique which has been successfully applied to various signal processing problems. Monte-Carlo simulations reveal that the jackknife bias correction directly applied on the Cloude-Pottier parameters lead to better bias reduction. [C2685]

"MERIT Erasmus Mundus: an opportunity for international cooperation in Remote Sensing education in Europe"

MERIT is a research-oriented Joint European Master on Information and Communication Technologies funded by the Erasmus Mundus program of the European Community. Its well funded scholarship scheme offers an outstanding opportunity for students, professors and researchers from non-European countries to participate in education programs (e.g remote sensing) in Europe. [C2686]

"Remote sensing information visualization using volume based objects in world wind"

Visualization of remotely-sensed meteorological data has traditionally consisted of two dimensional maps. However, the technological advancements in recent years have allowed data to be collected in new and unique ways and with greatly increased range and density. In particular, data are now collected at discrete locations within a volume, as opposed to points on a surface. The data volume, as opposed to an image, necessitates a different form of visualization. Unlike common techniques that stick on two dimensional maps, the main focus for the new techniques is showing the precipitation and other meteorological data in a more intuitive manner. This paper will introduce one of several possible ways to visualize a volume dataset. In this particular case rain intensity values gathered by NASA's TRMM satellite deliver a stereotypic volume dataset. [C2687]

"Dual-polarization and dual-frequency radar scattering from ice crystals"

Dual-polarization and dual-frequency radar observables are simulated at 3, 35, and 94 GHz frequencies for remote sensing of clouds. Their use in ice crystal classification, ice water content and particle size estimation are evaluated. [C2688]

"Cloud particle size measurements in Arctic clouds using lidar and radar data"

The ratio of the lidar and radar scattering cross section is sensitive to cloud particle size. High Spectral Resolution Lidar (HSRL) provides robustly calibrated scattering cross sections without the uncertainties introduced when conventional lidar data are corrected for attenuation. This paper explores the use of HSRL data and 35 GHz radar data for measuring particle size, particle phase, number density and the water content of Arctic clouds. [C2689]

"Impact of surface heterogeneity on surface soil moisture retrievals from passive microwave data"

Water and energy fluxes at the interface between the land surface and atmosphere are strongly depending on the surface soil moisture content which is highly variable in space and time. The sensitivity of active and passive microwave remote sensing data to surface soil moisture content has been investigated in numerous studies. Recent satellite borne mission concepts, as e.g. the SMOS mission, are dedicated to provide global soil moisture information with a temporal frequency of 1-3 days to capture the high temporal dynamics of surface soil moisture. Passive satellite microwave sensors have spatial resolutions in the order of tens of kilometres. The paper investigates the impact of land surface heterogeneity on soil moisture retrievals from L-band passive microwave data at different spatial scales between 1 km and 40 km. The impact of sensor noise and quality of ancillary information is explicitly considered. A synthetic study is conducted where brightness temperature observations are generated using simulated land surface conditions. The soil moisture retrieval uncertainties resulting from the heterogeneity within the image pixels as well as the uncertainties in the a priori knowledge of surface temperature data and due to sensor noise, is investigated. [C2690]

"The use of multidimensional copulas to describe amplitude distribution of polarimetric SAR data"

The paper focuses on a flexible model of multidimensional probability density function (pdf) dedicated to describe amplitude distribution of polarimetric SAR data. The model is based on the copula theory for characterizing the dependency between polarimetric channels (HH, VV, HV/VH or the target vector components). The benefit in using copula theory is to extend correlation concept to a wider dependence one, which may not be linear. From this point of view, the model is more flexible than the classical Wishart distribution. But it may include it. The other benefit in using the copula model is to separate the dependence concept from the shape of the marginal pdfs. Hence, this multidimensional characterization may be linked to classical 1D gamma pdf, or to a more flexible Pearson system of distributions. In the case of high resolution data, pdf shapes are becoming of heavy

tailed and the Fisher system of distributions seems to be an interesting alternative for such a model. Any parametric 1D model may be used. The paper mainly focuses on the model itself and more precisely on the technique required to construct such multidimensional dependence function. The difficulties arise for copula on 3D in which the dependency is not homogeneous between the components (the link between HH and VV may not be of the same behavior as the one between HH and HV). Illustrations are given on classification and despeckling. Classification will be performed by a stochastic estimation maximisation (SEM). Despeckling will be achieved by a maximum A posteriori technique. [C2691]

"Segmentation of polarimetric SAR data using contour information via spectral graph partitioning"

A new method for segmenting polarimetric Synthetic Aperture Radar (POLSAR) data is proposed. Image segmentation is formulated as a graph partitioning problem. Spectral graph partitioning-known to provide perceptually plausible image segmentation results using one or more cues (e.g., similarity, proximity, contour continuity)-is applied on POLSAR image data. The degree of similarities between pairs of pixels are calculated based on contour information. Graph partitioning is performed using the Multiclass Spectral Clustering method that minimizes the normalized cut cost function to ensure minimal similarity between partitions. The resulting segmentation is an approximation to the global optimal solution. C-band POLSAR data acquired by CV-580 are used for testing the performance. The results are found to closely agree with manual segmentations. [C2692]

"Multi-waveform radar for ice sheet measurements and classroom demonstration"

The Center for Remote Sensing of Ice Sheets (CReSIS), at the University of Kansas, is a Science and Technology Center established by the National Science Foundation (NSF) in 2005, with the mission of developing new technologies and computer models to measure and predict the response of sea level change to the mass balance of ice sheets in Greenland and Antarctica. As part of a senior undergraduate capstone design course we designed and simulated a wideband, push-broom, multi-waveform radar for fine-resolution airborne ice sheet surface elevation measurements. A prototype of this system was developed and its response was measured. The prototype will serve as a teaching tool and a design platform for the final instrumentation package to be used on an uncrewed aerial vehicle (UAV) being developed at the University of Kansas. In this paper we will present the objectives of the project, design details, simulation results, and testing results from experiments delay line and point targets. [C2693]

"Influence of mechanical antenna distortions on the performance of the HRWS SAR system"

High-Resolution Wide-Swath (HRWS) Synthetic Aperture Radar (SAR) is a multi-static spaceborne Radar. The performance of the Radar system is improved by the mean of DBF on receive in azimuth and in elevation. This requires an relieve antenna array with large number of elements. In this paper the performance of large antenna array under the influence of plane distortions is analyzed. Presented is the influence on the array factor of symmetrical, unsymmetrical and random mechanical distortion. The paper considers also the influence on the performance of the antenna distortion on the High-Resolution Wide-Swath (HRWS) Synthetic Aperture Radar (SAR) in elevation. [C2694]

"Performance analysis of bistatic SAR configurations"

In this work we analyze the properties of integration time and azimuth coverage of bistatic SAR configurations. The kinematics of antennas is modelled as a motion at a constant velocity along a linear path. Orbits can be at different heights above the ground and have crossing projections on a horizontal plane. Footprints on the reference ground plane move at different velocities. Performances of bistatic SAR configurations are compared to those of monostatic ones. [C2695]

"Elevation-dependent motion compensation for frequency-domain bistatic SAR image synthesis"

While numerically more efficient, frequency domain SAR image synthesis is less easily adaptable to the irregular real airborne trajectories than time-domain image synthesis. Trajectory nonlinearities have another consequence: The image focusing depends on the terrain elevation, hence motion compensation for irregular trajectories on mountainous areas must take into account terrain elevation data. Bistatic SAR processing is elevation-dependent even if the trajectory are perfectly linear (with the exception of the case where both aircrafts follow the same flight line). Terrain elevation can only be ignored at distance very large with respect to the elevation fluctuations, which is only the case in airborne bistatic SAR imaging when the area flown over is extremely flat. We describe here how the monostatic elevation-dependent motion compensation for omega-k algorithm is adapted to bistatic omega-k synthesis algorithm. [C2696]

"Translational variant bistatic SAR signal space-time feature and processing method"

In this paper, we discuss the translational-variant feature of translational-variant bistatic SAR configuration using the space Taylor's expansion in section II. In section III, a new translational-variant bistatic SAR imaging method is proposed, which uses scaled IFFT technique to eliminate the translational-variant feature of SAR space resolution. Finally, some numerical experiments are conducted to demonstrate the feasibility of this method and discuss the depth-of-focus of the scaled IFFT bistatic SAR imaging algorithms. [C2697]

"Performance analysis of a hybrid bistatic SAR system operating in the double sliding spotlight mode"

A bistatic synthetic aperture radar uses a separated transmitter and receiver flying on different platforms to achieve benefits like exploitation of additional information contained in the bistatic reflectivity of targets, reduced vulnerability for military applications, forward looking SAR imaging or increased RCS. A particular constellation, where the transmitter is in space and the receiver near or on the earth surface (e.g. aircraft, tower) is called a hybrid bistatic SAR system. Besides technical challenges, like the synchronization of transmitter and receiver, the overlap of the two antenna footprints is of vital importance. Due to the extreme platform velocity differences, SAR modes with flexible steering of the antenna beams are necessary. The sliding spotlight mode offers such a beam steering, where the antenna footprint velocity can be chosen slower or faster than the platform velocity. If both transmitter and receiver use this mode it is called double sliding spotlight mode, which will be investigated in this paper using the example of the satellite TerraSAR-X and the airborne SAR system PAMIR. Several aspects like the ground resolution, Doppler frequency and Doppler-bandwidth will be analyzed. [C2698]

"Development of web-based SAR processor for education"

Recently, synthetic aperture radar (SAR) processing algorithms have become more complicated due to the variety of observation modes of SAR sensors. Understanding the basics of the SAR processing technique is necessary to work out new approaches using the new sensing modes. A web-based SAR processor using Ajax technology is proposed for easy use in an educational computer system with various limitations. This paper presents the concept and the implementation method of this software and shows processing examples. [C2699]

"A low cost testbed for synthetic aperture techniques"

This paper describes a testbed for synthetic aperture techniques. The developed testbed uses only off-the-shelf components providing the students and the researchers with a low cost environment for development and testing of new algorithms. The applicability of the platform is demonstrated with acoustic images of point-like and extended targets. [C2700]

"Lidar education at Georgia Tech"

The lidar research team at the Georgia Tech Research Institute (GTRI) is developing an educational program with many components including academic classes, short courses, classroom teaching materials, hands-on laboratory demonstrations, and web-based resources. We are currently developing a textbook for introductory instruction on the basic principles of lidar systems. [C2701]

"Synchronization techniques for the bistatic spaceborne/airborne SAR experiment with TerraSAR-X and PAMIR"

The separation of transmitter and receiver makes bistatic SAR (synthetic aperture radar) systems preferable to conventional monostatic systems in several applications. However, this separation also leads to difficulties in image processing and in synchronization of the involved systems. For the upcoming hybrid bistatic SAR experiment with the TerraSAR-X satellite as transmitter and the airborne SAR/GMTI system PAMIR as receiver the synchronization issues are discussed in this paper and possible solutions are presented. [C2702]

"Vehicleborne bistatic synthetic aperture radar imaging"

A complete vehicleborne Bistatic Synthetic Aperture Radar (SAR) imaging experiment is presented in this paper. Some new technologies were used to solve synchronization problems. An algorithm named the Glide Window Echo CFAR was used to realize time synchronization and collect the echo. High stable local oscillator was employed to achieve frequency and phase synchronization, and the PRF was adjusted adaptively in the Data Acquisition Device in the receive station. Finally, the Range-Doppler algorithm with range migration correction was using to image the certain scene successfully. [C2703]

"Processing disdrometer raindrop spectra time series from various climatological regions using estimation and autoregressive methods"

A large data set of rain drop size distribution (RSD) measurements collected with Joss-Waldvogel (JWD) and 2D video disdrometers (2DVD) in UK, Athens, Japan and USA are analyzed. The objective of this work are manifold: i) show the differences of a wide climatological DSD-derived moments; ii) retrieve from this disdrometer data set the driving parameters of the normalized gamma RSD and perform a sensitivity analysis of these results by using different best-fitting techniques; iii) exploit the correlation structure of the estimated RSD parameters as input of a vector autoregressive stationary model in order to simulate time series (or horizontal profiles) of RSDs and, consequently, of either rain rate or path attenuation; iv) characterize the distribution of the inter-rain duration (or dry periods: DP) and rain duration (or wet periods: WP) to design a simple semi-Markov chain to represent the intermittency feature of rainfall process. The overall stochastic procedure to randomly synthesize (or generate) RSD time series is named Vector Autoregressive Raindrop Markov Synthesizer (VARMS) model. This stochastic RSD generation tool may find useful applications both in hydro-meteorology and radio-propagation. [C2704]

"Bistatic border effects modelling in forest scattering"

Simulating forest scattering by electromagnetic waves has been proposed with both coherent and incoherent models. However, to our best knowledge, most models consider a description of the forest as infinite in the horizontal plane and layered vertically. Such description is relevant in most cases, but fail when border effects are present near the boundaries: the shadowing effects as well as the reinforcement ones, which are present in true SAR images, are absent in the synthetic images. The purpose of this study is to present a coherent scattering model taking into account forest regions of finite extent and benefit from its polarimetric, interferometric and bistatic capabilities to bring out interesting outlooks about border effect in the bistatic case. [C2705]

"Comparison of similarity measures of multi-sensor images for change detection applications"

Change detection of remotely sensed images is a particularly challenging task when the available data come from different sensors. Indeed, many change indicators are based on radiometry measures, operating on their differences or ratios, that are no longer reliable when the data have been acquired by different instruments. For this reason, it is interesting to study the performance of those indicators that do not rely completely on radiometric values. A series of similarity measures for automatic change detection has been investigated and their general performance compared using optical and SAR images covering a period of about six years. We could observe that the considered change detection algorithms perform differently but that none of them permits an "absolute" measure of the changes independent of the sensor. Also the dimensions of the windows, for the estimation of the pixel statistics and of the similarity measure, affect the final results. [C2706]

"Mapping of wind-thrown forests using VHF/UHF SAR images"

SAR images from the Swedish airborne CARABAS-II and LORA systems have been visually analyzed over simulated wind-thrown forest at both single tree and stand level. In ideal conditions, the results show that LORA is more accurate than CARABAS-II at detecting wind-thrown trees, regardless of tree size and direction of the fallen trees relative to flight heading. Furthermore, the visible single trees in the LORA images appeared more distinct than in the CARABAS-II images, which could be explained by the high resolution in the LORA images. Based on visual interpretation, it is likely that the detection of wind-thrown forests could be improved using VHF/UHF SAR images acquired both prior to and after a storm event. [C2707]

"Analysis of airborne SAR data (L-band) for discrimination land use/land cover types in the Brazilian Amazon region"

The objective of this paper is to show the potential of multi-polarized mosaic-images from a MAPSAR (L-band) simulation campaign performed in the Amazon region (test site Tapajos) in order to discriminate land use/land cover classes. An Enhanced-Frost filter was used and the thematic discrimination was done by an algorithm for attribute extraction based on Bhattacharya distance. A comparison was made among the radiometric aspects of the SAR mosaic for 10 thematic classes obtained, converting these B-distances to JM distance values. This allowed to define which individual or multiple polarizations are more appropriate for the identification of thematic classes. [C2708]

"backscatter and interferometry for estimating above- ground biomass in tropical savanna woodland"

Tropical savannas cover 15% of the Earth's land surface and are important ecosystems in the global Carbon cycle due to their high productivity. SAR interferometry and backscatter are investigated for estimating biomass in a tropical savanna in Belize, Central America. Single-pass InSAR data used are C-band (AIRSAR) and X-band (Intermap); SAR backscatter data used are fully polarimetric L and P band (AIRSAR). Results show that both C-band and X-band InSAR show a clear trend in vegetation patterns although both underestimate vegetation heights due to the heterogeneity of the vegetation cover. The scattering phase centre is lowered more for the X-band due to larger ground- level contribution. High P and L-band backscatter values are observed for areas containing high biomass vegetation, but also for leafy palmetto that have relatively low biomass. [C2709]

"Conditional copula for change detection on heterogeneous SAR data"

A new preprocessing technique is presented in this paper to perform automatic change detection in multitemporal multimodal remotely sensed images, mainly synthetic aperture radar (SAR) ones. This technique is dedicated to the case where the two acquisitions, before and after an major disaster, are different for some reason (different sensor, modality of acquisition or climatic conditions). A measure, based on the local statistics of the images between the two dates, has proved to be a relevant change indicator. Nevertheless, the measure is valid when the two observations have been acquired with a similar point of view only. When the modalities of acquisition differ, local statistics tend to be too different, from one image to the other, to be relevant to the ground evolution without mixing to the normal changes. The technique, that overcomes this constraint, is based on the assumption that some dependence exists indeed between the two images. This dependence is modelled by the copula theory and used to perform an estimation of the local statistics that would have been observed if the modality of the first image had been similar to the other. It yields an estimation of local statistics of the first image, through the point of view of the latter. Then, usual comparison of those statistics may be applied to perform change detection. Some results are shown on a pair of ERS images and pairs of SPOT/ERS acquired before and after a flood. [C2710]

"Calibration and performance analysis of the PAU- RAD instrument"

This paper presents the calibration of the PAU-RAD instrument: a novel pseudo-correlation radiometer with digital beamforming, it consist on a Wilkinson power splitter and two receiving chains whose outputs are cross-correlated. To types of calibration are required: an internal hardware, relative calibration to perform the phase and an amplitude correction, and internal radiometric calibration. The simplified and unified calibration procedure is presented using internal well-known temperatures. [C2711]

"Detecting changes in polarimetric SAR data with content-based image retrieval"

In this study, we extended the potential of a Content- Based Image Retrieval (CBIR) system based on Self-Organizing Maps (SOMs), for the analysis of remote sensing data. A database was artificially created by splitting each image to be analyzed into small images (or imagelets). Content-based image retrieval was applied to fully polarimetric airborne SAR data, using a selection of polarimetric features. After training the system on this imagelet database, automatic queries could detect changes. Results were encouraging on airborne SAR data and may be more useful for spaceborne polarimetric data. [C2712]

"Large scale change detection techniques dedicated to flood monitoring using ENVISAT wide swath mode data"

Semi-automatic flood extraction procedures based on change detection techniques appear particularly adapted to plain flood monitoring and mapping. The change detector was specifically elaborated to analyse ENVISAT ASAR wide swath mode data pairs, which appear very well adapted to flood monitoring over wide areas. The algorithm is based on two analysis levels: an enhanced ratio for strong changes over large homogeneous and flat areas combined with a ratio calculated from the two raw images which aims to keep the raw data's thematic precision. Slope and aspect effects are also eliminated by the use of a digital elevation model during the processing. This change detection analysis was performed on 35 data pairs acquired within the framework of the flood DRAGON project. The first set of results is very promising and robust using HH polarization. Change detection between data with W polarization or with different polarization (HH versus W) has to be fully validated but results are promising. [C2713]

"Comparison and evaluation of polarimetric change detection techniques in aerial SAR data"

This article aims at providing a comparison of polarimetric change detection indices from a practical point of view. Six polarimetric change detection indices were tested on L band EMISAR data over Norway. Tests included quantitative evaluation of change maps compared to a ground truth of changes, and qualitative evaluation by visual inspection. Contrast ratio and the Wishart test gave the best results among the tested

indices. [C2714]

"Estimation of the bidirectional reflectance distribution function of subarctic boreal forest using C-band SAR"

Surface albedo is acknowledged as an important variable in climate research. Monitoring of Earth's surface albedo in a global scale is practical only with satellite observations. However, satellite-based albedo research in the boreal regions is hampered by continual cloud contamination in the optical wavelengths, as well as long periods of low sun elevation. As the surface albedo can be calculated from the Bidirectional Reflectance Distribution Function (BRDF) of an area, new methods to improve the accuracy of BRDF calculation and remove cloud contamination effects are needed to enhance the accuracy of future climate studies. This study explores the possibility of estimating the BRDF of boreal forest using C-band synthetic aperture radar (SAR) data. The principle of the estimation is based on the knowledge that the BRDF of boreal forests depends on structural parameters such as NDVI or LAI, and that similar structural information can be derived from SAR imagery. The results of the study show that the estimation of BRDF from C-band SAR is possible at least under certain conditions, the proposed estimation method yielded a coefficient of determination of 0.68 for the small-scale study area in Northern Finland. [C2715]

"Analysis of the temporal behavior of coherent scatterers (CSs) in ALOS PaISAR data"

Coherent scatterers (CSs) are scatterers detected by using spectral correlation properties and characterized by a deterministic scattering behavior. In this paper we investigate, for the first time, the temporal behavior of CSs using quad-pol data acquired by ALOS/PaISAR. In this sense, we can evaluate the stability of the deterministic scattering nature of individual scatterers. [C2716]

"InSAR monitoring of landslides on permafrost terrain in Canada"

In this study we used differential InSAR techniques to monitor landslide slide and permafrost activity at a site along the Mackenzie Valley Pipeline Corridor. Our results that motion are about 3 times more on exposed burnt slopes than the adjacent areas. The maximum activity is in September, probability related to gradual accumulated increases in soil temperatures. [C2717]

"Inversion algorithms comparison using L-band simulated polarimetric interferometric data for forest parameters estimation"

Polarimetric SAR interferometric data can provide estimates of forest biomass density. There are different approaches to deal with the inversion problem, such as neural networks and the traditional optimal estimation approach. This paper presents a study to evaluate their performance by means of quantitative indexes addressing both the computation time and the retrieval accuracy. Better forest parameters estimates have been obtained when neural networks algorithms were used. [C2718]

"Preliminary quantitative analysis of S-band FNCW radar data from atmospheric observation"

For more than three decades, S-band, frequency-modulated, continuous-wave (FMCW) radars have been used to study the structure and dynamics of the atmospheric boundary layer (ABL). With tremendous sensitivity and spatial resolution compared to their pulsed counterparts, these systems have been successfully applied to detection of clear-air turbulence in the lower atmosphere. In this study, data collected during field experiments by the University of Massachusetts' high-resolution S-band FMCW radar is used to illustrate and discuss system performance. S-band FMCW radar is sensitive to both Bragg scatterers (from spatial variations in radio refractive index of air) and Rayleigh scatterers (strong point-like echoes from nonatmospheric targets), and in the convective boundary layer Rayleigh echo appears to dominate the observed vertical profile of mean reflectivity. A postprocessing technique, which is based on single-lag covariance differences between the clear-air echo and Rayleigh echo, is applied to time-series of backscattered power to estimate clear-air component of the backscatter and remove the influence of Rayleigh scatter on the vertical profiles. The preliminary results of a quantitative analysis (mean and statistical distribution) of radar reflectivity are presented and compared with theoretical predictions about the convective ABL. [C2719]

"Modeling fractional shrub/tree cover and multi-temporal changes in mire ecosystems using high-resolution digital surface models and CIR aerial images"

The objective of this paper is to assess increase and decrease of forest area and estimate shrub encroachment between 1997 and 2002 in open mire land using CIR aerial images, DSMs derived from it and LiDAR data. The

present study was carried out in the framework of the Swiss Mire Protection Program, where changes of forested area are a key issue. The study area is located in the Pre-alpine zone of Central Switzerland. In a first step, high-quality DSMs were automatically generated from CIR aerial images of 1997 and 2002. This DSM generation is based on high accuracy, intelligent matching methods developed at ETHZ which are able to produce very dense and detailed DSMs that allow a good 3D modeling of both deciduous and coniferous trees and shrubs, and multi-temporal analysis of their growth pattern. In a second step, tree layers from both years were generated combining canopy height models derived from the DSMs and LiDAR DTM with a fuzzy classification of spectral information (NDVI) of CIR aerial images. In a third step, on the basis of these tree layers fractional tree/shrub covers were produced using explanatory variables derived from the DSMs in logistic regression models. Bias (due to different quality of input data) was estimated by analyzing the distribution of the fractional model differences. The corrected models reveal a general decrease of tree/shrub probability that indicates a decrease of forest and other wooded areas between 1997 and 2002. On the other side, the models also indicate real shrub encroachment and tree growth in open mire land. The study stresses the importance of high-resolution and high-quality DSMs and highlights the potential of fractional covers for ecological modeling. [C2720]

"Forest monitoring with JERS-1/SAR and ALOS/PALSAR"

JERS-1/SAR images taken in 1990's and ALOS/PALSAR images taken in 2000's are used and examined the deforestation status during ~14 years. Many trees had been fallen by a typhoon hit in 2004 in a test site, Tomakomai. There is also a plantation area and the site show active change during the term. The forest stands could be roughly classified for four types, forest stands, vacant, where almost all trees were carried out, and two types of transitional stands from a forest to a vacant. Many deforested areas are easily detected by using the difference of backscattering coefficients between two images, if fallen trees have been carried out from the stands. The change from the normal forest to the vacant stands causes 3.1dB decrease in the σ_{0HH} . On the other hands, transitional stands show almost same backscattering as the normal forest stands, although. Three-component scattering model shows surface scattering component accounts for 50% over the vacant stands, while volume scattering component accounts for ~60% over the forest stands. But the model doesn't show the clear difference between transitional forest site and normal forest. The temporal changes of the forest during 14 years are also examined for the plantation area. One stand show gradual increase of σ_0 and the values seem to be saturated around 17.4 tons/ha (~5 m in average height). [C2721]

"Detection of forest changes using ALOS PALSAR satellite images"

A controlled experiment has been performed to quantify the ability to detect clear-cuts using ALOS PALSAR data. The experiment consisted of 8 old spruce dominated stands, each with a size of about 1.5 ha, located at a test site in southern Sweden. Four of the stands were clear-felled and the remaining stands were left untreated for reference. A time series of PALSAR images was acquired prior to, during, and after treatment, including 7 fine beam single polarization (FBS, look angle 34.3deg, HH-polarization) SAR images. The results clearly show that the clear-felled stands could be separated from the reference stands. The drop in backscattering coefficient between the reference and the clear-felled stands was on average 2.1 dB. This implies that ALOS PALSAR data potentially can be used for large-scale mapping of changes in forest cover. [C2722]

"Vegetation modelling for height inversion using InSAR/Pol-InSAR data."

The random volume over ground model has been extensively used for forest height inversion using Pol-InSAR data. Two different forest models are proposed to better represent the forest structure for height inversion using Pol-InSAR. The first one takes into account a vertically varying mean extinction coefficient and the second one considers contributions localized in a finite height interval. [C2723]

"Spatial patterns of the canopy stress during 2005 drought in Amazonia"

In the last decades, the detection of drought occurrences and assessment of its severity using satellite data are becoming popular in disaster, desertification, crop production, phenology, land cover change and climate change studies. To detect the drought effects on different vegetation types, many methodologies have been developed, mostly relying on the use of vegetation indices. This communication reports the first attempt to assess the capability of MODIS NDVI, Enhanced Vegetation Index (EVI) and Normalized Difference Water Index (NDWI) from 2000 to 2006 time-series to detect the 2005 drought in Amazonia. To reach this objective, monthly composites of the MOD13A2 product were generated from period. Then, monthly anomalies were calculated, considering anomalous values when lower than -1 standard deviation (sd) or higher than 1 sd. Rainfall data provided by the Tropical Rainfall Measuring Mission (TRMM) was also acquired for the same time-series with the objective of supporting the understanding of vegetation response with the precipitation. Water deficit data

calculated based on the TRMM data were also used to guide the sampling scheme. A land cover map for South America updated with natural land cover changes detected by the Near Real Time Deforestation Detection Project (DETER) was used as a mask to avoid false anomalies in the Brazilian Amazon. In general, NDWI and EVI showed to be sensitive and consistent for the temporal series used. NDVI presented a high variability and though a difficult interpretation. Critical months in the NDWI and EVI series coincided with the months with higher water stress calculated based on the TRMM data. EVI also showed to detect changes in the canopy structure. These preliminary results suggest that this is a strong methodology to be used in the spatial analysis of the extent of the drought effects in the vegetation. Literfall data will be incorporate in this research for validation purposes. [C2724]

"Using MODIS and GLAS data to develop timber volume estimates in central Siberia"

Mapping of boreal forest's type, structure parameters and biomass are critical for understanding the boreal forest's significance in the carbon cycle, its response to and impact on global climate change. The biggest deficiency of the existing ground based forest inventories is the uncertainty in the inventory data, particularly in remote areas of Siberia where sampling is sparse, lacking, and often decades old. Remote sensing methods can overcome these problems. In this study, we used the moderate resolution imaging spectroradiometer (MODIS) and unique waveform data of the geoscience laser altimeter system (GLAS) and produced a map of timber volume for a 10degx12deg area in Central Siberia. Using these methods, the mean timber volume for the forested area in the total study area was 203 m³/ ha. The new remote sensing methods used in this study provide a truly independent estimate of forest structure, which is not dependent on traditional ground forest inventory methods. [C2725]

"Ku-band, polarimetric, combined, short pulse scatterometer-radiometer system for stationary fixed platform, vessel and airborne applications"

In this paper a Ku-band (~15 GHz), dual polarization, combined scatterometer-radiometer system is described. The system allows carry out polarimetric (vv, vh, hh, hv), simultaneous and coincident microwave active-passive measurements of the observed surface (soil, vegetation, snow and water surface) parameters. The originality of the developed system is in the spatial-temporal combination of microwave active and passive channels of observation and its possible application for short distance sensing (the minimum operational range for the scatterometer is ~6 m) from low altitude platforms under far field conditions for both radar and radiometric observations. [C2726]

"Two-dimensional synthetic aperture radiometry over land surface during soil moisture experiment in 2003 (SMEX03)"

Microwave radiometry at low frequencies (L-band, ~ 1.4 GHz) has been known as an optimal solution for remote- sensing of soil moisture. However, the antenna size required to achieve an appropriate resolution from space has limited the development of spaceborne L-band radiometers. This problem can be addressed by interferometric technology called aperture synthesis. The Soil Moisture and Ocean Salinity (SMOS) mission will apply this technique to monitor global-scale surface parameters in the near future. The first airborne experiment using an aircraft prototype of this approach, the Two-Dimensional Synthetic Aperture Radiometer (2D-STAR), was performed in the Soil Moisture Experiment in 2003 (SMEX03). The L-band brightness temperature data acquired in Alabama by the ID- STAR was compared with ground-based measurements of soil moisture and with C-band data collected by the Polarimetric Scanning Radiometer (PSR). Our results demonstrate a good response of the 2D-STAR brightness temperature to changes in surface wetness, both in agricultural and forest lands. The behavior of the horizontally polarized brightness temperature data with increasing view-angle over the forest area was noticeably different than over bare soil. The results from the comparison of 2D-STAR and PSR indicate a better response of the 2D-STAR to the surface wetness under both wet and dry conditions. Our results have important implications for the performance of the future SMOS mission. [C2727]

"Assessing pine barrens soil moisture regimes using Synthetic Aperture Radar (SAR) techniques"

The evaluation of soil moisture parameters within various soil regimes is somewhat difficult and challenging. Spatial and temporal invariability often complicates this process. The following study presents a format in which the spatial and temporal variations that govern upper surface (0-5 cm) soil moisture regimes within ecologically sensitive regions such as "Pine Barrens" can be studied. Based on in situ measurements, coupled with satellite derived analysis, radar backscatter, surface roughness, incidence angles, relative beam modes, and nominal area coverage, comparable soil moisture data between simulated and measured values within the upper surface (0-5 cm) soil moisture regime can be analyzed. [C2728]

"Return from insects in the clear-air convective boundary layer"

The Microwave Remote Sensing Laboratory (MIRSL) at the University of Massachusetts operated its S- band Frequency Modulated Continuous Wave (FMCW) radar during the International H2O Project (IHOP_2002) over the months of May and June 2002. The radar operates at very high spatial and temporal resolutions, 2.4 m and 5 s, respectively, which allows the segregation of scatter from different scattering mechanisms. Rayleigh scattering from particulate scatterers (i.e. dust and insects) dominated the return, however Bragg scattering from turbulence was also significant, especially at the top of the afternoon convective boundary layer (CBL). Scattering from insects was isolated using a 5x5 median high-pass filter. The majority of reflectivity measurements from particulate scatterers ranged from -30 dBZ to -10 dBZ, however intense point-scatterers (> 0 dBZ) skewed the distribution which resulted in mean values much greater than the median values. There is a strong diurnal signal in the backscatter: minima in the morning and at dusk and a maximum mid-afternoon and in the nocturnal boundary layer. The strong diurnal signal suggests that with targeted allocation of radar resources return from insects can be used to monitor the clear-air CBL of the central Great Plains of North America. [C2729]

"Atmospheric vertical profiles obtained by Lidar over Évora during CAPEX project"

CAPEX is a European project to investigate aerosol particles, radiation, cloud properties, precipitation and radioactivity over Portugal. During the campaign, carried out during the first fortnight June 2006 at Évora, Portugal (38deg34' N, 7deg54' W, 293 m a.s.l.), synoptic conditions favoured the arrival of air masses coming from Europe, Northern Africa and Mediterranean basin at several levels. In this study, two complex profiles, including layers coming from Europe and Sahara desert, are analyzed by a combination of Lidar and Cimel CE-318-4 data. Good agreements were found between them. [C2730]

"Usage of multitemporal filtering of SAR images for change detection"

A methodology for change detection of artificial features using multitemporal series of SAR data is presented. The methodology uses time averaging of data from ERS-2 and Envisat yielding improved radiometric quality which highly improves the photointerpretability. The methodology is tested in several scenarios in the context of security applications when data needs to be gathered during cloudy season when optical satellites are unable operate. The results have been validated with very high resolution optical data from summer season. [C2731]

"Accuracy comparison of Differential Interferometric Synthetic Aperture Radar using LiDAR Digital Elevation Model"

This paper describes about accuracy of differential interferometric synthetic aperture radar (DInSAR) using different resolutions of external digital elevation models from ERS-1/2, STRM, LiDAR. For DInSAR technique, external DEMs have to have correct surface information. Typical DInSAR processes used the space-borne SAR data such as SRTM, ERS-1/2, JERS, and RADARSAT. However, they did not remove the vegetation and non-terrain feature. It is the cause of errors in final result using non-correct DEM. For improved accuracy of DInSAR results, in this paper, LiDAR DEM which has high spatial resolution with removed non-terrain data is used and compare with other DEMs. [C2732]

"Change detections from sar images for damage estimation based on a spatial chaotic model"

Because of its all-weather and all-time characteristics, SAR images are particularly effective to monitor disaster events. When a disaster occurs, the image acquired from a SAR sensor changes dramatically. As a result, damage estimation for natural and human-made disasters from SAR images can be achieved by applying a change detection technique. Theoretically, SAR signals can be characterized as a chaotic phenomenon because that the scattering signals within a resolution cell are summed up coherently. Accordingly, SAR signal can be represented by a spatial chaotic model and characterized by its fractal dimension. In this paper, based on the spatial chaotic model, a simplified SAR image change detection procedure is proposed. The proposed method is then applied to estimate the flood-damage area caused by flooding events. Experimental results reveal that the proposed method is an effective and efficient tool for damage estimation from SAR images. [C2733]

"A method to retrieve soil moisture using ERS Scatterometer data"

Soil moisture is a key component in the hydrologic cycle and climate system. It is an important input parameter for many hydrologic and meteorological models. Taking the advantage of the multi-incident angles of the ERS Wind Scatterometer(WSC), a new soil moisture retrieving method, that significantly improves the surface backscattering presentation, is proposed in this study based on the Advanced Integral Equation Model (AIEM) and the Water-Cloud model. It utilizes the correlations in each backscattering components (bare soil and vegetation) for the simultaneous measurements of each incident angle pairs to reduce the effect of surface

roughness and vegetation scattering on soil moisture estimation. The result is validated by using the ground measurements from the Intensive Observation Period (IOP'98) field campaign in 1998 of GAME/Tibet in the end of this paper, and the time series of the estimated soil moisture shows a consistent trend with those sampled on the ground. [C2734]

"Modeling of soil roughness using terrestrial laser scanner for soil moisture retrieval"

The present work reports the bases of an ongoing research whose main objective is the development of a methodology to characterize surface roughness models using terrestrial laser scanning devices. The classical measurements take the profile as the valuable information on roughness variations but a brand new paradigm is applied here where an original three-dimensional, multi-scale framework leads towards an accurate characterization of patterns and roughness for different surfaces. Terrestrial laser scanners are able to provide a complete picture of the roughness properties over the spatial scale of a Synthetic Aperture Radar satellite resolution cell. The paper describes the methodology for measuring the roughness of different surfaces and analyzes parameters what can be used as ancillary data in soil moisture retrieval from satellite datasets. [C2735]

"Stratospheric ozone layer observations over tsukuba, Japan by NIES ozone DIAL."

The paper presents results from differential absorption lidar (DIAL) observations of the vertical profiles of ozone, aerosols, and temperature at the National Institute for Environmental Studies (NIES) in Tsukuba (36degN, 140degE), Japan. Currently, the lidar system uses 308/355 nm (DIAL) for lower stratospheric ozone measurements. The 355 nm is also used for aerosol measurements. The lidar system is a part of the International Network for the Detection of Atmospheric Composition Change (NDACC). The version 2 algorithm was used for accurate determination of ozone, aerosols, and temperature profiles. Methods for correcting systematic errors have been applied to the algorithm. Aerosol corrections have been applied to the temperature and ozone calculations. The mean vertical ozone profiles of the NIES ozone lidar were compared with those of SAGE II; they agreed well within a 5% relative difference in the 20- to 40-km altitude range and within 10% up to 45 km. The long-term variations of ozone obtained by the NIES ozone lidar also showed good agreement with those by the ozone sondes and SAGE II at 20 km, 25 km, 30 km, and 35 km. The temperatures retrieved from the NIES ozone lidar and those given by the National Center for Environmental Prediction (NCEP) agreed within 7 (K) in the 35- to 50-km range. [C2736]

"SHARAD design and operation"

This paper describes the operating principles and the design of the Mars shallow radar sounder (SHARAD), an HF sounding radar devoted to the mapping of sub-surface features of Mars and currently operational on board the NASA/JPL's Mars reconnaissance orbiter spacecraft. Compared to its predecessor MARSIS, currently operating from ESA's Mars Express, SHARAD is characterised by an higher carrier frequency (20 MHz vs a max of 5 MHz for MARSIS) and a much wider signal bandwidth (10 MHz vs 1 MHz of MARSIS). This allows SHARAD to achieve a finer range resolution (15 metres unweighted in free space) at the expenses of ground penetration, which makes the instrument ideal to probe the shallow subsurface layers (to depths of hundreds of meters) which cannot be resolved from the surface by the much far- reaching MARSIS. SHARAD uses a 85 usec chirp signal with a PRF of 700 Hz and a peak power of 10 W, and radiates by means of a 10 meters fiber foldable tube (FFT) dipole antenna, with a wide-band matching network in charge of impedance matching with the transceiver. The most challenging requirement (especially considering the large fractional bandwidth of the system) is the level of the range sidelobes, which shall be below -55 dBc after the 6th lobe, to allow proper detection of the weak subsurface echoes in presence of strong surface returns. On this side, the design takes advantage from the wide download bandwidth made available by the MRO Spacecraft to keep the on-board processing to a minimum level (basically, only a programmable coherent presuming), and leave most of the processing (range compression and synthetic aperture) on ground. In this way it is easy to use Tx chirps and Rx transfer functions characterised on- ground as reference for range correlation, with the range sidelobes limited, basically, only by the stability of the RF hardware. The limited amount of on-board processing also helped in limiting the complexity of the instrument design and, therefore, its mass and power consumption. SHARAD uses a very simple architecture, with the transmit chirp generated directly on the RF frequency (using a digital chirp generator) before being amplified to the transmit level by a class C amplifier. The receiver is even more essential, providing direct amplification of the received signal (with programmable gain and band filtering) to an A-to-D converter operated in downsampling mode by digitising the signal at 26.6 MHz rate. In this way, the complete 10 MHz signal bandwidth can be represented unambiguously with only an acceptable amount of oversampling (30%) minimising the required hardware. Instrument control and processing tasks are performed by the same AD-21020 DSP (with the help of a couple of FPGAs). The presuming can be varied from 1 to 32 in powers of two steps, and the resolution of science data can be selected to be 4, 6 or 8 bits, to allow optimisation of the data rate vs the operating scenarios. The receive window position can either be controlled in open loop,

using an a priori knowledge of S/C orbit and surface topography (which demonstrated to be a very robust approach) or in closed loop. [C2737]

"Study of ground surface displacement estimation using ALOS/PALSAR D-InSAR interferometry"

The area of Southwestern Ryukyu Arc and Eastern Taiwan are characterized by collision and subduction of the Philippine Sea Plate under the Eurasian Plate. Huatung Valley is a huge valley formed by plate motion and existing between the cities of Hualian and Taitung with approx. length of 130 km. Since 1998, Tokai University has started seismological activity measurements with Dahan institute of technology (DIT). DIT measuring GPS and electronic distance meter (EDM) data to monitor the crustal movement in the northern part of test area. We have performed a repeat-pass differential interferometric analysis using the ENVISAT/ASAR data in 2005 and 2006. In addition, we propose a crustal movement extraction using successful ALOS/PALSAR image pairs in 2007. [C2738]

"Evaluation of the interaction between SAR L-band signal and structural parameters of forest cover"

The objective of this paper is to evaluate the interaction between backscatter (sigmadeg) from polarimetric L-band SAR data (collected by the airborne sensor R99-B/SIPAM) and biophysical parameters of the primary forest and secondary succession sites. The area under study is located in the region of Tapajos (Brazil), where SAR data were collected in May 2005. Another approach under investigation is the evaluation of the contribution from basic backscatter mechanisms, using the Freeman-Durden decomposition technique, applied to complex SAR images, where the physiognomic-structural characteristics of the forest stands give a significant contribution. In brief, it was possible to verify that the variable "tree height" has better relations with the backscatter values, when compared to other biophysical variables, especially when the model also includes variations of the incidence angle of the stripes imaged. The decomposition technique showed that the volumetric scattering component has the strongest influence on the SAR response at primary and secondary tropical forests. [C2739]

"Parameter based SAR simulator for image quality evaluation"

A SAR simulator for image quality evaluation is presented. This simulator can be used for the estimation of SAR image quality performance from the simulated raw data and the verification of the SAR payload design parameter associated with the image quality parameters. Evaluation of SAR image quality is achieved by analyzing the error effect of system parameter using the developed simulator. [C2740]

"Robust forest height extraction using polarimetric SAR interferometry"

Recently, many researches have demonstrated that polarimetric SAR interferometry is the most promising technique for forest parameter extraction. In this paper, we present a robust forest height extraction technique based on reliable phase estimation. The more accurate interferometric phase estimation can be attained with the reliable ground phase and canopy phase using three-stage inversion process and ESPRIT technique, respectively. We show the validity of the method by applying it to L-band simulated polarimetric and interferometric SAR data. The experimental results are also provided to give the availability of this method. [C2741]

"Classification of satellite images applied to geological mapping (Douro Region-Northeastern Portugal)"

Optical and microwave remote sensing data, from the northeastern of Portugal, was used to the discrimination of lithologies outcropping in that region. Classification techniques was applied and from the results it can be concluded that the optical data performed a better discrimination that the radar data. In this last case, a texture analysis shows that the mean (with matrix of 5*5) gave the best results. [C2742]

"Recognizing salt-structures on the basis of geophysical and remote sensing data: the case of monte real salt-structure (onshore west-central portugal)"

Remote sensing data from Monte Real sub-basin (onshore West-Central Portugal), collected by the LANDSAT 7 ETM+, JERS-1 (SAR) and Envisat (ASAR) satellites, are used with the purpose to give new insights relatively to the Monte Real salt-structure. The recognized pattern of the diapir and of the structural lineaments is in agreement with the geophysical and geological data. [C2743]

"Structural lineaments in a volcanic island evaluated through remote sensing techniques The case of Santiago Island (Cape Verde)"

The remote sensing data (optical and radar) was used with the purpose of identify the structural lineaments that crosscut the geological formations that composed the bedrock of the south part of Santiago island (Cape Verde). Besides tectonics, this study also provided new insights to the understanding of the hydrogeological system of the volcanic island. [C2744]

"Ortho-rectification and terrain correction of polarimetric SAR data applied in the ALOS/Palsar context"

Methods for terrain correction of polarimetric SAR data were studied and developed. Ortho-rectification resampling and amplitude correction utilized Stokes matrix data. The Stokes matrix of thermal noise was subtracted before amplitude normalization. Application of an azimuth-slope correction algorithm resulted in slightly narrower distribution of orientation angles compared to input data. [C2745]

"Uplift rates from river profiles: methodology and case study, Oriente, Cuba"

The thrusting of the Cuban Oriente block onto the Bahamas platform and the transform movement between the Caribbean and North American plate cause oscillating uplift in the east of Cuba, manifesting itself in tilted blocks, coral reef terraces and rivers cutting deep into the bedrock. Objectives of this work are to identify active tectonic boundaries and derive relative uplift rates in Oriente using power-law scaling relation between channel slope and contributing drainage area to obtain a more detailed picture of the tectonic processes of the study area. Geomorphological interpretation and analysis of river profiles shows an inhomogeneous distribution of relative uplift rates within the Cuban Oriente block. This method allows for the estimation of deformation over large areas, the localization and the quantification of vertical displacements. [C2746]

"High resolution DSM generation from ALOS PRISM"

PRISM carried at ALOS satellite is expected to generate worldwide topographic data in respects of its high resolution and stereoscopic observation. The algorithms for generating digital surface model (DSM) and ortho-rectified image (ORI) have been developed for those objectives in Earth Observation Research Center / Japan Aerospace Exploration Agency (EORC / JAXA). During first one year following the successful ALOS launch, the capabilities of the algorithm have been widely tested. In this paper, the performance analysis intermediate results of DSM and corresponding ORI processing are described. First, the geometric model analysis of PRISM sensor is presented with the experimental results of the orientation processing. Then, the performance analysis of DSM and ORI generated with the PRISM geometric model is presented. The accuracy assessment results of generated DSM are presented from the comparison with high accuracy and high resolution reference DSM data sets of LiDAR DSM and Aerial Photo DSM. The accuracy assessment results of generated ORI are presented from the comparison with GCP. [C2747]

"Evaluation of accuracy in PS-based radar interferometry with simulated data"

This paper analyzes the relationship between the noise level in interferometric phases at permanent scatters (PS) and the accuracy in deformation measurements with the PS-based differential SAR interferometry (PS-DInSAR). The study is carried out based on interferograms that are simulated with parameters of 26 ERS-1/2 SAR scenes over Shanghai. The results show that in the cases of high phase signal to noise ratio (noise level lower than ± 0.5 rad), the accuracy of the deformation rates estimated with PS-DInSAR can be up to about ± 2 mm/a, and the accuracy of the estimated elevations is about ± 1 m. The accuracies decrease with the increase of the noise level of the phase data. When the noise level is ± 0.8 rad, the accuracy of deformation measurements decreases to ± 1 cm/a and that of elevation measurements decreases to ± 3 m. [C2748]

"Deformation monitoring over a large area via the ESD technique with data takes on adjacent tracks"

Enhanced spatial differences (ESD) is a new processing chain for monitoring ground deformations at small scale over wide areas. Core of the processing is the spatial differencing (SD) step that performs a quick preliminary estimation of the mean deformation velocity and residual topography via spatial differences. We show the results achieved by applying the ESD algorithm to data collected over adjacent tracks for ERS and ENVISAT. [C2749]

"Point target interferometry for natural and artificial scatterers"

The Coherent Targets Monitoring technique is providing superior ground deformation mapping compared with standard interferometry based on one pair of Master/Slave scenes. This is because using a larger data set it is possible to estimate and correct for additional phase error sources. Also the point targets detected as coherent targets are generally characterized by stronger signal that provides more accurate phase information than the clutter present in the rest of the scene. This paper reviews previous work in SAR noise estimation and shows the advantages of point targets versus distributed targets. Results from the Turtle Mountain/Frank Slide site show that the measured phase/deformation errors at the point target positions are within the estimated range. Corner reflectors with a high SNR are expected to improve the accuracy of the method. [C2750]

"Glacier displacement field estimation using airborne SAR interferometry"

This paper deals with the methodology in the processing of airborne SAR data to measure glacier displacement fields. The possibility to retrieve a 2D displacement map of the deformation in slant-range geometry with an airborne platform is discussed. A new extended multisquint approach is proposed to simultaneously estimate residual motion errors and the along-track displacement of the glacier, while the across-track displacement is obtained by means of differential interferometry. Experimental results are shown with data acquired by the Experimental SAR (E-SAR) of the German Aerospace Center over the Aletsch glacier in the Swiss Alps. [C2751]

"Persistent scatterer density improvement using adaptive deformation models"

Because the quality assessment of Persistent Scatterers (PS) is dependent on the deformation model chosen, PS may be falsely rejected due to model imperfections. To accept these PS, more advanced deformation models should be used. Two methods applying adaptive deformation models are proposed. The first is based on a sequential scheme of alternative hypothesis testing of extended deformation models within the integer least-squares framework. The second uses an iterative scheme of global deformation modeling based on previous PS results. Application of the techniques to a salt mining area in The Netherlands confirms the increase in the number of detected PS. [C2752]

"A bistatic SAR interferometric simulator for fixed receiver configurations"

Bistatic SAR systems are an emerging research field. In which context, the Universitat Politècnica de Catalunya is developing a ground based bistatic system using ESAs ENVISAT and ERS-2 as transmitters. In this paper we characterize the bistatic interferometric phase and the different sources of decorrelation. We will also present a bistatic interferometric simulator which is able to generate realistic synthetic bistatic interferograms. The simulator is validated with real data obtained with our bistatic acquisition system, named SABRINA. [C2753]

"Comparison between MARSIS & SHARAD results"

MARSIS (Mars advanced Radar for subsurface and ionosphere sounding) is a low frequency nadir looking sounding radar selected by ESA as a payload of the Mars Express mission, whose primary Scientific Objective is to map the distribution of water both solid and liquid, at global scale on the Martian crust. MARSIS is the first instrument to be able to detect what lies beneath the surface of Mars (up to about 5 km). MARSIS operates with a very high fractional bandwidth: 1 MHz bandwidth allows a vertical resolution of 150 m in vacuum which corresponds to 50-100 m in the subsurface, depending on the electromagnetic wave propagation speed in the crust. The center frequency of the pulses transmitted by MARSIS can be set to 1.8 MHz, 3 MHz, 4 MHz and 5 MHz. On day side operations, it operates only in 4 MHz and 5 MHz due to the ionosphere plasma frequencies of Mars cutting off all frequencies lower than 3 MHz. All the four carrier frequencies are available for subsurface sounding on night side. The Mars Shallow Radar Sounder (SHARAD), a facility instrument provided by the Italian Space Agency (ASI), is embarked on board the NASA Mars Reconnaissance Orbiter spacecraft. SHARAD began science operations on October 3rd 2006: it has been collecting data from surface and subsurface. This instrument penetrates to roughly half a kilometer below Mars' surface to search for information about underground layers of ice, rock and, perhaps, melted water. SHARAD operates with a center frequency of 20 MHz and 10 MHz bandwidth. These parameters allow vertical resolution on the order of 10-20 m. The carrier frequency of 20 MHz guarantees the capability of SHARAD to operate in day side as well as in night side. Both MARSIS and SHARAD use the principle of a Synthetic Aperture Radar (SAR) to achieve a fine along-track resolution. In particular, MARSIS is an unfocused SAR with best along-track resolution of 2 km; data coming from SHARAD can be processed with focusing algorithm (Chirp Scaling Algorithm), resulting in a best horizontal resolution of 300 m. This paper provides a comparison between MARSIS and SHARAD images in different zones of the Mars' surface. From the preliminary analysis it has been evident that MARSIS detects signals from subsurface interfaces at 3 km of depth, while the signals received by SHARAD in the same zone and at the same depth are much weaker compared with the background noise. However, SHARAD radar-grams show subsurface interfaces at 100-200 m of depth: these interesting targets can not be discriminated by MARSIS because of its coarse

vertical resolution. At the same time, SHARAD data add to MARSIS data scientific information about the upper portions of the crust of Mars. [C2754]

"Second-order motion compensation in bistatic airborne SAR based on a geometrical approach"

Common efficient SAR processing algorithms are based on nominal operational conditions. Unfortunately, due to atmospheric turbulences and maneuvering errors, these conditions are often violated in real SAR systems. Hence, a crucial problem in most airborne SAR systems is the compensation of motion errors; if not corrected, the image quality will considerably degrade. A first-order motion compensation (MoCo) technique was developed at our institute, based on a precise knowledge of the position and the velocity of the transmitter and the receiver. The problem arose while proceeding with our processing algorithm, since the reconstructed image was better focused but not completely focused. Our paper proposes a second-order MoCo technique that will considerably improve the reconstruction of the SAR image. While the first-order MoCo considered the range and azimuth times, the second-order MoCo approximation will consider the frequencies. Experiments with different sets of bistatic airborne SAR data are performed based on this solution, and some promising results are given. [C2755]

"Research on differential interferometry for spaceborne bistatic SAR"

Differential interferometry (D-InSAR) for spaceborne bistatic SAR is studied. According to advantages of the system, particularities and superiorities of D-InSAR based on spaceborne bistatic SAR are discussed first. Then, solid baseline is decomposed and the model of "three-pass" D-InSAR is established. Afterwards, the theory of data fusion is introduced to D-InSAR and a new method is put forward to avoid the max detection error. A simulation experiment accompanied by very good result is shown in the end. [C2756]

"Monitoring of mining induced land subsidence using L- and C-band SAR interferometry"

In this study, we applied InSAR technique to Zonguldak Hardcoal Basin in Republic of Turkey using JERS-1/SAR, RADARSAT and PALSAR data in order to monitor mining induced surface displacement. [C2757]

"Six years of land subsidence in shanghai revealed by JERS-1 SAR data"

Differential interferometric synthetic aperture radar (SAR) (DInSAR) has proven to be very useful in mapping and monitoring land subsidence in many regions of the world. Shanghai, China's largest city, is one of such areas suffering from land subsidence as a result of severe withdrawal of groundwater for different usages. DInSAR application in Shanghai with the C-band European Remote Sensing 1 & 2 (ERS-1/2) SAR data has been difficult mainly due to the problem of decorrelation of InSAR pairs with temporal baselines larger than 10 months. To overcome the coherence loss of C-band InSAR data, we used eight L-band Japanese Earth Resource Satellite (JERS-1) SAR data acquired during 2 October 1992 to 15 July 1998 to study land subsidence phenomenon in Shanghai. Three of the images were used to produce two separate digital elevation models (DEMs) of the study area to remove topographic fringes from the interferograms used for subsidence mapping. Six interferograms were used to generate 2 different time series of deformation maps over Shanghai. The cumulative subsidence map generated from each of the time series is in agreement with the land subsidence measurements of Shanghai city from 1990-1998, produced from other survey methods. [C2758]

"SAR images classification using case-based reasoning method"

In this paper, we investigate a case-based reasoning (CBR) method for the classification of multi-temporal SAR images with the aid of ancillary information. Our scheme for the problem of multi-temporal SAR images classification comprises four main steps, including SAR image processing, construction of case library, case-based classification and post-classification processing. During the construction of case library, we employ a spatial-temporal analysis technique to remove fake cases, which can guarantee cases with high confidence. In the implementation of case-based classification, we propose a similarity assessment and use it for the case-based matching. After that, we investigate an object-oriented post-classification method which takes the shape of land use region into account, as a result, it leads to a more meaningful classification, and the regenerate land use image or map can be easier compared and combined with usual GIS data. Multi-temporal ENVISAT ASAR images from 2004 to 2005 are used in our experiments, where their resolution are 12.5 times 12.5 m. The study site is located in Beijing, China. During our experiments, we use the land use map of 2004 to assist the construction of the case library. The results of our experiments indicate that the CBR method is very promising for the classification of multi-temporal SAR images, where the overall classification accuracy can reach up to 80%. [C2759]

"Combining modern techniques for urban 3D modelling"

This paper will give an insight into modern ways of buildings modelling considering the case of TU Delft's campus with the use of classic photogrammetry tools and terrestrial laser scanning data. In addition we will use airborne LIDAR (Light- Imaging Detection and Ranging) for generating of extrusion models. The used methods aim to obtain models which can be used in Geographical Information Systems supporting different level of details. The detail factor may vary from pure city models, which are only blocks containing no facade information, to more complex 3D models with facade information as a texture and/or geometry. In our paper we will make some comparisons using a building model and discuss upon its information type and the achieved accuracy. Further more we will show an application example for the extrusion models. [C2760]

"Application of random set-based clustering to landmine detection with hyperspectral imagery"

We apply a population-based classifier to Long Wave HyperSpectral Imagery (LWHSI) for the purposes of landmine detection. In LWHSI, there are many environmental factors that are correlated with groups of samples (pixels in an image) in sample populations (individual images). These factors greatly affect samples' values making it difficult for standard classification models to perform well on a consistent basis. Population-based classifiers capture information correlated with sample populations. We perform classification experiments over a range of LWHSI imagery and compare results between the population-based classifier and standard kNN. After analysis, we show that the use of population-correlated information in LWHSI greatly improves classification results and consistency. [C2761]

"The mega capture of the negro river, central amazonia, brazil: a novel feature revealed by SRTM data"

In Central Amazonia, Brazil, the Solimoes and Negro rivers converge to form the Amazonas, the largest river in the world. Interferometric-derived topographic data, generated during the Shuttle Radar Topography Mission (SRTM), indicate that the present-day lower course of the Negro River is the result of a mega fluvial capture governed by neotectonics. The data indicated that the ancient confluence of the Negro River with the Solimoes River was located where today is the mouth of Manacapuru River, 60 km west of the present location in the vicinity of the city of Manaus. [C2762]

"Urban land cover classification: potential of high and very-high resolution SAR imagery"

A comparative study on the complexity of the urban environments in SAR imagery at different spatial resolutions is presented. Two datasets have been considered, including the city of Rome, Italy imaged in decametric resolution and the Frascati area (Rome, Italy) acquired in very high spatial resolution (~2 m) at L-band in a fully polarimetric mode. The different characteristics of the radar sensors require careful managing of the corresponding product capabilities to maximize the various pieces of information contained in the variety of scattering mechanisms. [C2763]

"Correction of tropospheric water vapour effect on ASAR interferogram using synchronous MERIS data"

The water vapour in troposphere has been identified as one of the major errors in SAR interferograms, which can cause a spatial delay during two non-simultaneous acquisitions. The microwave-signal propagation path delay due to water vapour may reduce the reliability of deformation measurements. In this paper, it aims to assess the water vapour effect on interferograms, and apply synchronous MERIS data to reduce the effect on ASAR interferograms. Due to the co-existence of MERIS and ASAR on board of ENVISAT satellite, they can acquire data co-located in the same time and space. So it has a unique advantage to combine MERIS and ASAR data to reduce the tropospheric water vapour effect on ASAR interferograms. However, the method is not so well operational, and still existing some problems need to be further discussed, such as: how to deal with the cloud coverage over MERIS water vapour image; and how to register MERIS to ASAR from different reference systems, and so on. These will be discussed in this paper, and novel ideas are proposed to deal with them. The discussions are based on the application of the test site in the middle and lower reaches of Yangze River, southwest Hubei province, China. [C2764]

"Radar interferometry for 3-D mining deformation monitoring"

Geodetic information of terrain can be measured using remote sensing techniques such as photogrammetry, airborne laser scanner (ALS) and interferometric synthetic aperture radar (InSAR). They are considered to be relatively more cost-effective than and complementary to conventional ground-based surveying methods. Our previous studies demonstrated the capability of using differential InSAR for underground longwall mining subsidence monitoring in New South Wales, Australia. The mining subsidence (vertical surface deformation) was

measured using DInSAR with the assumption of negligible horizontal deformation. However, the ground surveying data shows that the underground mining activity may induce horizontal surface deformation. Therefore, both ascending and descending orbits and different swath modes of ENVISAT/ASAR data are used in this paper to quantify the vertical and horizontal vectors of mining deformation. [C2765]

"A stability analysis of the lambda estimator for solving the ambiguity problem in persistent scatterer interferometry"

Persistent Scatterer Interferometry is a well-known technique to obtain displacement rates in urban areas from a stack of SAR interferograms. Besides the original method introduced by A. Ferretti, C. Prati and F. Rocca in the late 1990's, which estimates the displacement rates and DEM corrections by an ensemble coherence maximization approach (periodogram) based on a common master image, several other algorithms have been introduced in the past few years. One of these approaches has been developed at DLR It incorporates the Least-squares AMBiguity Decorrelation Adjustment (LAMBDA) method that was originally developed for fast GPS double difference ambiguity estimation. In this paper different parameters are tested to investigate robustness and performance of this estimation method. At first the effects of a reduced number of observations and varying reference points on the estimation with LAMBDA are analyzed while in the second part a direct comparison between LAMBDA and ensemble coherence maximization (periodogram) is performed. [C2766]

"A wavelet based targets detection method for high resolution airborne SAR data"

A wavelet based automatic targets detection method for high resolution airborne SAR data is described in this article to receive faster and more accuracy detection. This method is based on the assumption that man-made objects are easily detectable at low resolution because their scattering is more persistent than that of natural objects. The algorithm involves an improved wavelet soft threshold filter (IWSTF) and a wavelet based RCCFAR detector. In order to retain the target feature, the wavelet soft threshold filter is improved by the strategy used in the enhanced Lee filter. Instead of using a global threshold, we adopted an adaptive threshold calculated according to the detail coefficients in each scale. To accelerate the RCCFAR detector, two RCCFAR detectors are used. One is first applied to the approximate coefficients to make a coarse detection. The other one is applied to the filtered images in those regions which are regarded as candidate targets. Performance of the algorithm is assessed by some high resolution airborne SAR image and it shows that the algorithm can effectively reduce false alarms caused by speckles. [C2767]

"Urban subsidence observed by InSAR in Tianjin Region"

In this paper, we present the results of D-InSAR technique and conventional leveling at selected area in Tianjin city, using 8 ENVISAT SAR images between 17 October 2003 and 17 February 2005. The D-InSAR results show that the subsidence rate reached over 5 cm/year (7 cm within 16 months) in highly sinking area, and it is consistent with leveling results. D-InSAR is able to provide more details of urban subsidence, and it is supplement to leveling surveys in those areas with sparse leveling benchmarks. [C2768]

"Surface signature of ocean convection in the greenland sea as detected by SAR and enhanced by statistical pattern analysis"

The aim of this work is to present a process to enhance the image feature of the surface signature produce by the SAR sensor of the convective chimney discovered in March 2001 in the Greenland Sea. The procedure developed to extract the feature is described and some examples of the results of this study are presented and discussed. [C2769]

"A simple implementation of multi-baseline INSAR"

Multi-baseline INSAR is a kind of technology that obtains terrain height information using multiple SAR images, therefore, it has a better performance than single-baseline INSAR. There are primarily two methods to increase the accuracy of terrain height estimation. One increases the quality of the interferometric absolute phase image by utilizing several single-look complex images. The other decreases the errors of the terrain height estimation through iterative ways. Integrating the former method and noise-immune phase unwrapping method, this paper presents a realistic method to implement multi-baseline INSAR. This method mainly includes two steps; the first one is about how to obtain multi-baseline interferometric absolute phase image whereas the second one is the unwrapping mechanism. Then, through simulation, the achieved results not only demonstrate the validity and practicability of the method, but also prove that the performance of the multi-baseline INSAR is much better than single-baseline INSAR. [C2770]

"Parameter inversion models based on PolInSAR images"

Polarimetric SAR Interferometry (PolInSAR) can be used for parameter inversion of ground. An appropriate model is of most importance for parameters inversion. This paper derives a series of random scattering model that can be used for parameter inversion of forestry area, such as RV, RVoG, OV and OVoG. These models can reveal the characteristics of forestry area as well as establish the relationship between observed data and parameters of test area. Finally, these scattering models are compared. [C2771]

"Modified phase history model for high resolution spaceborne bistatic SAR"

Recently bistatic synthetic aperture radar (SAR), especially spaceborne SARs, has attracted the attention of many radar researchers. Generally, the orbit of satellite for remote sensing purposes is an ellipse with small eccentricity, and the earth should be modeled as an ellipsoid. It is well known that a second-order relative motion model can be a good approximation to a monostatic spaceborne SAR. However, for bistatic cases, this phase history model mismatches the real relative motion between a satellite and a rotating earth, dissatisfying the imaging accuracy requirement, and it limits the available azimuth resolution. In order to use the well studied SAR imaging algorithms, we develop a new second-order phase history model for bistatic spaceborne SAR using the phase error fitting method based on the ephemeris data. The new model strengthens the applicability of the conventional second-order phase history model of spaceborne bistatic SAR significantly. [C2772]

"Multi-scale feature analysis method for bridge recognition in SAR images"

Target recognition is an important field in remote sensing image processing. This paper handles with the problem of bridge recognition in Synthetic Aperture Radar (SAR) images. Based on features of bridges, rivers and land in different spatial resolution SAR images, a method of multi-scale analysis is proposed. The original data is split into low and middle resolution level. The bridge candidates are located in low level by automatically detecting river. And regions of interesting (ROI) are obtained in middle one. So, bridges are recognized by analyzing those regions. The example results indicate that the processing speed can be greatly improved and the precision of recognition can also be ensured. [C2773]

"The propagation of orbital errors in the 3-Pass DInSAR processing"

Orbital satellite state vectors are required not only to determine the baseline parameters, the offset of coarse registration but also to remove the reference phase and geocode the data to WGS84 in the 3-pass DInSAR processing. The quality of orbit limited to the current value of around 5-10 cm plays an important role in determining the precise deformation maps. Orbit errors in the along-track, the across-track and the radial directions can be represented by a noise baseline vector which leads to a convenient way of interpreting orbit errors. Under this transformation, we build the relationship between the residual reference phase and orbit errors in a concise way from which the approximate orbit precision can be estimated based on the residual reference phase. The analyses of the characteristics and influence of orbit errors indicate that the precision of height and deformation is much more sensitive to errors in the across direction. A series of error propagating equations derived reveal the influence of orbital error on height is nearly 103 times higher than that on deformation, which is verified by processing the SAR data acquired by ERS-2 satellite over the site of the 1999 Chichi Taiwan earthquake with the ERS and DEOS orbits separately. [C2774]

"High resolution COSMO-SkyMed SAR images for oil spills automatic detection"

In recent decades SAR images have extensively been used for the observation and the characterization of the sea surface. A number of experiments have been carried out with airborne and spaceborne sensors. These show SAR's ability of detecting oil slicks and distinguishing them from similar oceanic features. A great amount of archived data is available in many spectral bands. In spite of this, nowadays C-band is the most widely used for the observation of the sea from a satellite. For this reason, in the last year we have developed OSAD (Oil Spill Automatic Detector), a system focusing on C-band. The availability of high resolution X-band images (supplied by COSMO-SkyMed satellites and managed by the Italian Space Agency) has encouraged further investigation aimed at extending the scope of this methodology to X band images with the final goal of employing it for detecting oil spills. X-SAR data (obtained from airplane multi-band experiments and from SIR-C X-SAR mission carried out by NASA's space shuttle in 1994) are analyzed in order to compare SAR images in different bands and spot locations contaminated by an oil slick. The COSMO- SkyMed constellation (supplying high spatial and temporal coverage of the Mediterranean basin) makes it possible to develop an operational oil spill survey system, particularly in protected areas and areas close to the coast. [C2775]

"High resolution COSMO/SkyMed SAR data analysis for civil protection from flooding events"

The paper focuses on the multiple roles and advantages of the use of remotely sensed, especially COSMO/SkyMed, imagery in the context of flooding-event prevention and management, describing a support system for civil protection from floods and some of the image processing and analysis techniques involved in. [C2776]

"Radar image segmentation using active contour"

A new method for texture image segmentation is proposed which has three advantageous. Firstly, it has excellent texture discrimination and low complexity, for uniform LBP/C (local binary patterns and pattern contrasts) operator which reduces the number of texture pattern to 23% is used to extract texture features from a texture image. Secondly, active contours without edges are improved so that the LBP/C histogram can be used to evolve the initial curve during the segmentation process. A multiple object texture image can be segmented, because the proposed model is expanded to multiphase segmentation by the hierarchical method which can avoid the problem due to the choice of initial conditions. Finally, the speed of image segmentation is higher, for AOS scheme is applied for the numerical solution of the proposed method. Experiments on both synthetic and remote sensing images show that the proposed method is more accurate and faster. [C2777]

"An improved model of HF-SAR for estimating surface current velocity"

With the requirement of surface current extraction by a single station of high frequency surface wave radar, high frequency SAR (HF-SAR) is proposed and proved to be theoretically feasible. However the old model of HF-SAR is not perfect enough and there are several drawbacks such as Bragg scattering not included, high computation burden and implementation difficulty. Thus in this paper we present an improved model of HF-SAR to overcome the previous drawbacks. For the improved model, Bragg frequency is introduced into the echo signal and an iterative approach to estimate parameters of chirp signals is adopted for velocity estimation algorithms. Also an implementation scheme of HF-SAR on the sea is proposed. Simulation results with the improved model show that the precision of surface current velocity estimation is high enough to meet practical requirements. [C2778]

"Internal wave parameters retrieval from SAR image: based on EMD filter and parameterized buoyancy frequency"

Synthetic aperture radar (SAR) is a most useful instrument of internal waves (IWs) observation and study for its high resolution and all-weather remote sensing capability. Generally by combining the IWs hydrodynamic model and SAR image of internal wave mechanism we can retrieve the wavelength, amplitude and phase speed of IWs from SAR image. The mostly used method for this retrieve is the two-layer KdV theory which uses a two density invariable ocean fluid layer to simulate the actually continues stratified ocean fluid profile. This approximation works well for most of the shallow water but sometimes it will cause a significant error especially when the ocean stratification is weak. We propose the retrieve method based on EMD filter and parameterized buoyancy frequency for this condition. [C2779]

"Uncertainty of the 2003 BAM Mw =6.4 earthquake fault model inverted from ENVISAT SAR interferometric data"

The authors collected several papers about Bam earthquake of 26thDec 2003 with 6.4-magnitude from 2004 to 2007. We found that up to now there exist two different conclusions that the seismic fault is one or two. Most of papers used SAR interferometry to constrain the surface deformation and invert the source parameters by linear or non-linear methods. This paper have re-processed the 3 pairs of interferograms by the 4 scenes European remote sensing satellite images (ENSAT-ASAR), including two coseismic pairs and one postseismic pair. The authors think there is much uncertainty of source model only based on the interferometry and correlation mapping because of error in the interferometric results and uncertainty of inversion methods. The paper analyzed how to influence the uncertainty of source model from errors of interferomegrams and present inversion methods. [C2780]

"Semiautomatic registration between ground-level panoramas and an orthorectified aerial image for building modeling"

Aerial imagery and ground-level imagery are two complementary data sources for architectural modeling. How to integrate them is a critical issue in creating complete, photo-realistic and large-scale urban models. We describe a semiautomatic approach of detecting feature correspondences between ground-level images and the building footprint in an orthorectified aerial image. The ground-level images are stitched into panoramas in order to obtain a wide camera field of view. Line segments are extracted from ground-level images. Their corresponding

segments on the building footprints are automatically detected through a voting process. Meanwhile the camera pose of the ground-level images is also obtained. Wrong correspondences are corrected through user interaction. Later, the height values of the building roof corners are computed and a piece-wise planar 3D model with photo-realistic facade and roof texture is then created. [C2781]

"Airborne MMW cross-track InSAR System Analysis"

An airborne MMW cross-track InSAR system is discussed. The system design is presented based on MMW solid transmitter, dual-channel receivers, low phase noise signal generator, gyro-stabilized mount, position and orientation system. The system's parameters are analyzed. A performance simulation result denotes that the elevation accuracy (0.5-1m) is possible for the MMW InSAR with 0.5m resolution. [C2782]

"Change detection methodology based on region classification fusion"

In this paper, several classification methods are presented and a fusion structure is included to improve the final classification performance. The definition of "layer" and the method to create it are then introduced. Based on "layer", a multiple level change detection algorithm is proposed, which gives the details of the changes in each region and is demonstrated to be an easy, effective and reliable method. Experimental results are provided using RADARSAT images, which have been registered with the automated registration algorithm of A.U.G. Signals that is currently available under the distributed processing system www.signalfusion.com. [C2783]

"Development of TanDEM-X DEM calibration concept"

The TanDEM-X mission [1] comprises two fully active synthetic aperture radar satellites operating in X-band. The primary goal of this mission is the derivation of a high-precision global Digital Elevation Model (DEM) according to HRTI level 3 quality [2]. This requires accurate calibration of the interferometric system parameters, where the interferometric height is determined by the phase difference between the two images and the spatial geometry. Content of this paper is the development of a general concept for this calibration, which has a key incidence on mission aspects like the data acquisition plan and the data take adjustment and mosaicing. [C2784]

"Multi-band SAR Images Fusion Using the EM Algorithm in Contourlet Domain"

Aimed at the fusion of multi-band Synthetic Aperture Radar(SAR) images, a new fused method using estimation theory in the contourlet transform domain is presented. Contourlet transform is a new "true" two-dimension presentation for images which provided a flexible multiresolution, anisotropy and directional expansion. The coefficients of contourlets can be accurately modeled by Gaussian mixture model. This approach is based on an image formation model which the contourlet coefficients of multi-band SAR images are described as the true scene corrupted by Gaussian mixture distortion. A set of iterative equations are developed using the Expectation Maximization(EM) algorithm to estimate the model parameters and produce the fused images. The efficiency of this approach is verified by fusing the Ku, X bands and L, Ku bands SAR images. Also, some statistical factors are employed for evaluating the objective quality of the fused result. [C2785]

"Pixel level image fusion based on ICA and wavelet transform"

Image fusion is the process of producing a single image from a set of input images with more complete information and has broad applications in many fields, such as computer vision, automatic object detection, image processing, and remote sensing. In this paper, a pixel level image fusion algorithm based on independent component analysis (ICA) and wavelet transform is proposed. Firstly, we use the 2D discrete wavelet transform in order to extract multiple subband images, and then apply ICA on the subband images to get ICA bases, at last fuse the image by the independent component bases. The results show that it gives promising results as compared to previous methods and performs considerably well across a variety of multi-sensor imaging data. [C2786]

"The fusion arithmetic of multi-resolution remote sense image based on a modified fast independent component analysis"

Independent Component Analysis (ICA) is an effective approach to the separation of blind signal, and has attracted broad attention and has been successfully used in many fields. The fundamental, target functions and practical algorithm of Independent Component Analysis are discussed. Then, by modifying the performance of FastICA algorithm are merged into one iteration of M-FastICA. The M-FastICA algorithm achieves the correspondent effect of FastICA. So the convergence of ICA will be accelerated. Finally, M-FastICA is applied to images fusion. The experiment results show that the modified algorithm reduces iterations with the correspondent fusion performance. [C2787]

"Data fusion of multiple polarimetric SAR images based on combined curvelet and wavelet transform"

Data fusion is a very effective technique which can be applied to many remote sensing areas such as battle awareness, monitoring of environmental surveillance and man-made target detection. In this paper, we test fusion of multiple polarization (HH, HV, VH and W) SAR images, which is performed using multiscale image fusion technique based on combined curvelet and wavelet transform. Curvelet transform provides a flexible multiresolution, anisotropy and directional expansion for SAR images. Compared with wavelets, it can afford more efficient presentation of image edges. The fusion approach exploits the advantages of both curvelet and wavelet in multiscale domain. The example result of four polarimetric SAR image fusion show that the proposed method has a good performance. [C2788]

"Near-space SAR: A revolutionary microwave remote sensing mission"

Inspired by the recent advances in near-space defined as the region between 20km and 100km, this paper proposed the concept of near-space SAR. To the author's knowledge, this is the first time that the near-space SAR is being proposed for microwave remote sensing missions. By placing the SAR's transmitter/receiver in the near-space platforms, many functions that are currently performed with the satellites or airplanes could be performed much more cheaply and with much greater operational unity. These advantages make near-space SAR attractive for a variety of remote sensing missions. In this paper, the potential and challenges of the near-space SAR, compared to current spaceborne SAR and airborne SAR, were detailed. Various near-space SAR configurations are introduced, and their potential for different applications such as passive imaging, high-resolution and wide-swath imaging, and inverse SAR imaging were investigated. It is shown that, the use of near-space SAR can lead to the solutions that are previously thought to be out of reach for remote sensing scientists and customers. [C2789]

"A validation method for bare soil surface parameters inverted by Oh empirical model using integral equation method"

A new method is developed to validate the parameter inversion results of the empirical models proposed by Oh et al. for bare soil surface. Oh et al. developed a series of empirical models for retrieving bare soil moisture and root mean square (rms) height, while Fung et al. proposed integral equation method (IEM) to provide the relationship between backscattering coefficient and surface parameters in a rather wide range of roughness and moisture conditions. The proposed validation method combines the empirical scattering model Oh and the theoretical scattering model IEM, which provides a method to show the accuracy of the inversion results. This method needs no ground truth measurement of surface in situ. [C2790]

"The SBAS-DInSAR technique as a tool for the observation of active volcanic areas: Results and future perspectives"

In this work we describe the application of the basic small Baseline subset (SBAS) technique, which exploits multilook interferograms, to a number of active volcanic areas. The use of such a technique reduces the amount of data to be processed and simplifies the analysis of geophysical phenomena occurring in extended areas (up to 100 km by 100 km). Moreover, it can be trivially extended in order to combine data acquired by different sensors with similar geometrical and electromagnetic characteristics, i.e., ERS and ENVISAT IS-2 mode, thus allowing an easy extension of the temporal observation window. The selected test sites for this study are Long Valley caldera, Mt. Etna and the Neapolitan Volcanic district (Mt. Vesuvio and Campi Flegrei caldera). Finally, we shortly analyze the implications of the use of forthcoming SAR sensors that operates in L-and X-bands. [C2791]

"Performance results of the SHARAD instrument"

SHARAD (SHAlow RADar) is a subsurface sounding radar provided by ASI as a Facility Instrument to NASA's 2005 Mars Reconnaissance Orbiter for the characterization of the upper part of the Martian crust. The design of the instrument reflect a balance of scientific requirements versus SHARAD mission and Hardware constraints. One of the most difficult point in SHARAD design was the choice of the radar wavelength, since longer wavelengths have the potential for deeper subsurface penetration at the expense of depth resolution. Shorter wavelengths enhance the ability to generate surface images and accurate profile. A radar sounder needs a system requirements for large dynamic range and precise sidelobe control. Very low range side-lobes are mandatory to allow detection of weak sub-surface echoes in presence of the strong surface return. The approach of limiting to the minimum the amount of processing performed on-board was selected in order to allow the pulse compression process (critical from the point of view of range side-lobes) to be performed on ground, using

the computed instrument Point-Target-Response (PTR) as correlation reference waveform. One of the main goal of this paper is to describe the design of the experiment design of SHARAD and the selection of the instrument parameters. An assessment of radar performance has been obtained by using both on-ground and on-flight measurements. Some preliminary results from the mars mission have been reported. [C2792]

"Bistatic SAR imaging: A novel approach using a stationary receiver"

This paper introduces a novel approach to bistatic radar imaging. The proposed technique utilizes a synthetic transmit aperture and a stationary receiver to create a high resolution, 2-D bistatic SAR image of a given target scene. The technique can also be used to generate 3-D SAR images simply by utilizing a second, coherent receiver; hence operating in an interferometric bistatic SAR mode. The new technique is validated through both indoor and outdoor experiments. [C2793]

"Position and orientation estimation of two airborne platforms towards each other"

The interest in bi- and multistatic radar has been growing over the last years as they offer various advantages. For instance the transmitter and receiver can easily be separated and therefore the survivability can be enhanced by deploying the transmitter further away from the scene. Bistatic radar can provide a cost effective solution as the transmitter and receiver can be built without the cost driving transmit/receive-modules. Beyond this, with large baselines it is likely to increase the signature from stealthy objects. Another interesting aspect of bistatic imaging radar is the reduced dynamic range of difficult imaging environments such as urban ones. However, besides the benefits of bi- and multistatic radar one has to solve several technical problems [1]-such as the synchronisation and determining the relative position and orientation of both platforms towards each other. This paper discusses a method which allows determining these two fundamental parameters of an airborne bistatic SAR system and presents first simulations result, which confirms the method. [C2794]

"Bistatic SAR interferometry using ENVISAT and a ground based receiver: Experimental results"

The Universitat Politecnica de Catalunya is developing a ground based bistatic system using ESA's ENVISAT and ERS-2 as transmitters. The spatial resolution of this configuration is similar to that of their monostatic counterpart, although foreshortening effects have a lesser impact. First single-pass interferometric images corresponding to a local test-site are presented and compared to a synthetic interferogram. [C2795]

"Experimental investigation of Digital Beamforming SAR Performance using a ground-based demonstrator"

Digital beamforming (DBF) technique is a promising technique for future synthetic aperture radar (SAR). In this paper, we present the preliminary experiment and results. The measurements were accomplished by a ground-based DBF SAR system for a single target. The system is evaluated by mono-static SAR operation first. Comparing between DBF SAR and mono-static SAR images the channel imbalance effect is investigated. Since the experiment provides the SAR raw data containing the system response, from this raw data we estimate the linear phase error due to the channel imbalance and compensate it. The reconstructed DBF SAR images show that the minimum variation of the phase between the receive channel is crucial to obtain the theoretical improvement factor. [C2796]

"Merging of the stereogrammetry and interferometry techniques as relative bandwidth grows. Illustration with VHF Carabas SAR images"

SAR interferometry, requires the sensor separation to be below a critical baseline above which the coherency is lost as the ground projected frequency ranges do not overlap (frequency band shifting of one sensor -the delta-k system- is not addressed here). Indeed, as critical baseline increases with both wavelength and bandwidth, low frequency and/or wide band SAR systems have less stringent constraint for interferometric coherence, which is especially worthy for airborne acquisitions. However, as mentioned in earlier publications, the number of fringes apparent on an interferogram is (roughly) limited to twice the inverse of the relative bandwidth. Hence, wide band interferometry requires range migration evaluating for maintaining coherency, this range migration evaluation is similar to a stereogrammetric measure. As relative bandwidth grows, the two techniques merge, which can be illustrated from FOI Carabas VHF SAR data (of which the relative bandwidth is 111%). [C2797]

"Evaluation of the Bistatic Range migration processor"

The bistatic image formation process is more complex than the monostatic one, because the bistatic range equation consists of the sum of two hyperbolas. Several bistatic SAR processors have been presented in the last years. One of them is the bistatic range migration processor, which will be evaluated in this paper not only with

regard to translational invariant configurations but also in view of variations from a model assumption. The bistatic range migration processor will be compared with a bistatic generic time domain SAR processor. The processing quality will mainly be evaluated by measuring the resolution and PSLR of point target responses. [C2798]

"Delay/Doppler altimeter data processing"

The ESA Cryosat-2 mission will mount a de- lay/Doppler radar altimeter (DDA), named SIRAL, for the study of the trends in Earth's continental and marine ice fields. A DDA has many advantages over a conventional altimeter, retrieving a better resolution in the along track direction as a result of coherent processing of the backscattering energy. This permits the extension of applications to ice sheet monitoring as well as coastal studies, maintaining necessary precision for the open ocean. Operational SIRAL data processing for the Cryosat-2 mission is based on the precise wavenumber domain approach, following the strategy developed and verified for the Cryosat-1 mission [1]. A novel way of processing, supported by the chirp zeta transform (CZT) is here presented. Basically the CZT allows the Doppler beam formation to be directed toward the output surface samples in a single stage, increasing the computational efficiency of the processing at the expense of a slightly lower accuracy. The more precise wavenumber domain approach can be used to validate the method. The SIRAL sensor parameters and simulated scenarios will be taken as models to derive experimental results. [C2799]

"Improvement of interferometric SAR coherence estimates by slope-adaptive range common-band filtering"

The accuracy of SAR interferometric coherence estimates depends on the precision of several processing steps. In particular decorrelation can occur if range common-band filtering does not perform optimally. Typically a planar surface is adopted which introduces additional decorrelation in case of sloped terrain. To take into account topographic variations a slope-adaptive range common-band filtering method has been developed. A DEM is used to simulate an unwrapped interferogram and the fringe rate is used as driver for the filter size in the range common-band filtering step. Tests with several spaceborne interferometric SAR datasets confirmed the robustness of the method. The improvement of the coherence increased for increasing perpendicular baseline. As a consequence, the fringe visibility also greatly improved. To quantify the improvement of the coherence estimates with the slope-adaptive range common-band filtering, we considered the variation of classification in forest mapping, i.e. an application in which accurate coherence estimates are needed. With improved coherence the classified forest stem volume agreed better with forest maps derived from other remote sensing datasets. [C2800]

"Polarimetric phase gradient autofocus"

In the past decade the use of fully polarimetric SAR (polSAR) systems has increased significantly due to their effectiveness in target classification and detection applications. While polSAR imagery has been extensively used to distinguish between different scattering mechanisms in a scene, there has been a lack of research in the exploitation of polarimetry to assist in image formation and in particular autofocus for fine resolution SAR. In this paper an extension of the phase gradient algorithm (PGA) for polSAR imaging is proposed and its effectiveness is tested on simulated and real data. [C2801]

"Space-based moving target positioning using radar with a switched aperture antenna"

Ground moving target indication (GMTI) by space based radar can effectively only be performed with a multi-aperture / multi-channel system or a satellite cluster [1]. To keep weight, power consumption, data rate and costs low, the technique of switching subapertures from pulse to pulse has been proposed. While the detection performance using STAP (space-time adaptive processing) has been analysed in several publications, the estimation performance and the mechanisms leading to good or bad aperture switching strategies, have not yet been treated sufficiently. In fact, aperture partitions well suited for detection must not necessarily be good for estimation. This paper is thought as a contribution to fill the knowledge gaps concerning repositioning algorithms and performance analysis. [C2802]

"Polarimetric feature fusion in GPR for landmine detection"

A polarimetric multi-feature framework for the detection of antipersonnel landmines with ground penetrating radar (GPR) is suggested. The features result from independently acquired and processed GPR measurements in co- and cross-polar configurations. The initial detection in the confidence maps is made independently after which the coordinates of the detected targets are co-located. The marginal feature distributions are normalized via Johnson's transform prior to the fusion process and a Maximum Likelihood based linear-quadratic classifier is

used as a fusion rule. The framework makes use of secondary data acquired from an open test site to train the classifier. The framework performance is illustrated on the data acquired over a specifically designed test- site. [C2803]

"Concept design of a near-space radar for tsunami detection"

Off-shore detection of tsunami waves is a critical component of an effective tsunami warning system (TWS). Even more critical is the off-shore detection of local tsunamis, namely tsunamis that strike coastal areas within minutes from the triggering quake. In this paper we propose a new concept for tsunami detection. NESTRAD (Near-Space Tsunami Radar) consists of a real aperture radar accommodated inside a stationary stratospheric airship providing continuous monitoring of tsunamigenic oceanic trenches. [C2804]

"Use of an application-specific dictionary for matching pursuits discrimination of landmines and clutter"

The HSTAMIDS handheld landmine detection system has been used in a number of humanitarian demining activities. Existing algorithms used with this system to assist human in discrimination process do a better job than the operator alone. However, they are unable to model mine and clutter signatures completely, leading to inaccurate mine confidence assignment. This paper presents a matching pursuits (MP) based landmine detection system using an application-specific dictionary. Prototypes for mine and clutter classes are built using MP decomposition of class members. A fuzzy K-nearest neighbor rule is used to assign confidence values for mine and clutter discrimination. The proposed algorithm is demonstrated on data acquired from three different landmines test sites. [C2805]

"Possibilistic multi-sensor fusion for humanitarian demining"

We propose a method for combining humanitarian mine detection sensors based on possibility theory. Firstly, different features are extracted from the sensor data. Possibility distributions are then derived from the features based on prior information. After that, the combination of possibility degrees is performed in two steps, on separate sensor level and between the sensors. Combination operators are chosen to account for the different characteristics of the sensors. The final decision is obtained by thresholding the fusion result. Promising results have been obtained on a set of real mines and non-dangerous objects. In particular a 100% mine recognition rate was achieved, with a limited number of false alarms. [C2806]

"Hand held dual sensor ALIS and its evaluation test in Cambodia"

Since 2002, we have developed a new hand-held land mine detection dual-sensor ALIS. ALIS is equipped with a metal detector and a GPR, and it has a sensor tracking system, which can record the GPR and Metal detector signal with its location. It makes possible to process the data afterwards, including migration. The migration processing drastically increases the quality of the image of the buried objects. ALIS uses two different GPR systems, namely VNA (Vector Network Analyzer) based GPR and an Impulse GPR VNA based GPR can provide better quality GPR images, although the impulse GPR is faster and light weight. ALIS evaluation tests were held in mine affected countries including Afghanistan, Croatia, Egypt and Cambodia. In the two-month evaluation test in Cambodia, ALIS worked without any problem. After some demonstrations and evaluation, we got many useful suggestions. Using these advises, we have modified the ALIS and it is now more easy to use. ALIS will be commercialized in 2007. [C2807]

"Feasibility of spaceborne bistatic radar missions for land applications"

This paper deals with a feasibility analysis of spaceborne bistatic missions for Earth Observation, with signals at microwave bands. The analysis, performed in the frame of a wider study financed by ESA, considers as input bistatic configurations, investigated in another paper, suitable for typical land applications i.e. soil moisture and vegetation biomass retrieval. Signal sources are GPS constellation and spaceborne SAR's. This analysis mainly encompasses the design of possible orbits implementing the desired bistatic configurations, and the characterization of the system performances. The latter are evaluated through several different parameters, grouped in two classes: target observation parameters, strictly related to the illuminator-target-receiver geometry at given epoch (e.g. signal to noise ratio, spatial resolution, observation angles) and system parameters such as: spatial coverage (measuring whether or not a point is accessible by the satellites in bistatic configuration), number of bistatic accesses to the target area, revisit time (indicating the delay between two successive bistatic acquisitions of the same area). [C2808]

"Phase and temporal synchronization in bistatic SAR systems using sources of opportunity"

This paper discusses temporal and phase synchronization in SABRINA, a bistatic system that uses ENVISAT and ERS-2 as transmitters of opportunity. Phase synchronization and pulse alignment is achieved using a dedicated channel that receives a clean signal directly from the satellite. It is studied how to temporally align the acquired data with the satellite orbit using the apparent range migration history. [C2809]

"Improvement of 3D radar backscatter model by matrix-doubling methods"

Radiative transfer models have been widely used to simulate the radar backscatter from forested areas. Most of these models are two dimensional. In order to take full account of spatial position of trees in a forest stand, a three-dimensional radar backscatter model of forest canopy was constructed by Guoqing Sun and Ranson in 1995[1]. The model takes into account only first-order scattering within tree crown and the double scattering between tree trunk (crown) and ground surface. The model predictions agree well with copolarized backscatter measurements, while it tends to underestimate the backscattering coefficients for cross-polarization, when there is strong volume scattering. In order to produce good estimations for cross-polarized component, the matrix-doubling method is employed in this paper to compute multiple-scattering within the crown. The comparison between the results of original model and that of modified model shows that the method is effective. The cross-polarization can be improved in different degrees according to the size and density of scatters within crown cell. [C2810]

"Measurements of the effect of rain-induced sea surface roughness on the satellite scatterometer radar cross section"

Radar measurements of the sea surface, with satellite scatterometers that operate at Ku-band, will be affected by the presence of rain through modification of the sea surface roughness by rain impacts. This is in addition to wind driven roughness, atmospheric reflectivity and attenuation that affect the measured normalized radar cross section (NRCS). Numerous surface-based studies, using ocean platforms and wind-wave tanks, have shown the increase in the total NRCS can be significant and strongly dependent on radar frequency, incidence angle, polarization and wind speed [1],[2],[3]. Herein is the first study combining satellite based Ku-band data with high-resolution 3-D volumetric rain measurements, from simultaneous collocated NEXRAD data. The results to be presented were acquired during a significant rain event in the Gulf of Mexico just south of Houston, TX in May 2005. They are directly applicable to questions that are important to the interpretation of satellite derived wind vector estimates in the presence of rain of varying intensity and spatial distribution. This project is developing techniques to correct scatterometer derived wind- vector estimates. The acquisition of new knowledge on rain-splash effects is a necessary part of this effort. [C2811]

"Bistatic scattering from bare soils: Sensitivity to soil moisture and surface roughness"

The sensitivity of bistatic scattering coefficient σ_{deg} to soil moisture (smc) is investigated on the whole upper half space by means of model simulations of the incoherent scattered fields. The achieved results, represented as maps of σ_{deg} as a function of azimuth and zenith angles, are evaluated by means of a quality index which takes into consideration the effect of roughness on smc measurement. [C2812]

"Design Considerations For An Atmospheric Imaging Radar"

This paper describes the design requirements, tradeoffs and simulations involved with the design specifications of an Atmospheric Imaging Radar (AIR). Design constraints are discussed including size and portability. Radar details include the range of meteorological targets detectable, maximum range, and other criteria needed for the weather radar equation. A dual pulse repetition time waveform is used to improve the maximum unambiguous velocity and range. The trade-offs in volume, sensitivity and pulse integration are described in the radar design. Calculations are made and initial plots showing at least 15 dBZ sensitivity at 10 km are shown for a radar that will image a cone 16.5deg wide and 40 km long. [C2813]

"Laser Technology Development at NASA Langley Research Center for Space based Applications"

In this paper, salient features of various laser based developmental efforts carried out at NASA Langley Research Center for coherent and direct detection LIDAR systems for land, airborne and space based platforms will be discussed. [C2814]

"Robust Road Extraction for High Resolution Satellite Images"

Automatic road extraction is a critical feature for an efficient use of remote sensing imagery in most contexts. This paper proposes a robust geometric method to provide a first step extraction level. These results can be used as an initialization for other algorithms or as a starting point for manual road extraction. Results of the

extraction are vectorized for GIS integration and for a better interaction with human experts that can refine the results. The algorithm is fast, has very few parameters and is only slightly affected by the image properties (resolution, noise). The algorithm is available in the open-source Orfeo toolbox. [C2815]

"Land Use Management Based on GPS Technology, and Satellite and Ground Remote Sensing Technologies"

The paper presents an overview of the GPS technology, satellite remote sensing technologies, ground remote sensing technologies, and GIS technologies applications to the land use management. The technological method, developed by the Centre for Geo-Information Technologies and Systems Novi Sad, aimed for but not restricted to agricultural land use management using GPS, satellite remote sensing, geo-radar sensing and GIS technologies is presented as a case study. [C2816]

"Collusion Attack-Resilient Hierarchical Encryption of JPEG 2000 Codestreams with Scalable Access Control"

This paper proposes a collusion attack-resilient method of encryption for access control of JPEG 2000 codestreams with hierarchical scalabilities. The proposed method generates one encryption key from one single key by multi-dimensional scanning to serve encryption keeping the scalability of codestreams. To avoid collusion attacks in which multiple users generate an illegal key from their own keys to overcome the access control, sufficient conditions are considered in this method. Moreover, a skip encryption is introduced to decrease the computational complexity and key management-and-de-livery cost of encryption. Simulation results show the effectiveness of the proposed method. [C2817]

"Unification of Descriptive Experiment Design and Worst-Case Performance Optimization-Adapted Regularization Paradigms for High-Resolution Reconstruction of Radar Imagery"

We address a new approach to solving radar imaging problems stated and treated as uncertain ill-conditioned inverse problems of nonparametric spatial power spectrum estimation via processing the finite number of independent observations of the degraded array data signals (one realization of the trajectory signal in the case of SAR). The idea is to adapt a statistically optimal minimum risk nonparametric power spectrum estimation approach to the radar imaging scenarios with model-level and system-level uncertainties. The proposed incorporation of the worst-case performance optimization-adapted robust regularization aggregated with the descriptive experiment design paradigm into the minimum risk nonparametric estimation strategy leads to a new unified doubly regularized minimum risk approach for robust adaptive high-resolution reconstructive imaging in the uncertain remote sensing scenarios. [C2818]

"Distributed/Embedded Sub-Surface Sensors for Imaging Buried Objects with Reduced Mutual Coupling and Suppressed Electromagnetic Emissions"

The proliferation of strategic subsurface sanctuaries has increased the need for enhanced remote sensing techniques providing for the accurate detection and identification of deeply buried objects. A new RF tomographic technique is proposed in this concept paper for developing RF CAT scans of buried objects using spectral, spatial/angular, and polarization diversity. This imaging technique uses an embedded ring of subsurface radiators, delivered by earth-penetrating non-explosive, electronic "e-bombs", as the source of strong underground radiated transmissions. Distributed surface-contact sensors are used to collect the tomographic data for relay to a circling UAV and transmission to a remote control site (using layered sensing). [C2819]

"Simultaneous Three-wavelength Depolarization Lidar Using a Coherent White Light Continuum"

In this paper, application of white light lidar system for the multi-wavelength depolarization measurement of clouds and aerosols will be presented. The new lidar system consisted of three depolarization channels at 450, 550 and 800 nm. The linear depolarization ratio ($\Delta = S/P$) at 450 nm can be seen to increase with increasing cloud depth due to the multiple scattering. [C2820]

"Efficient high-energy Raman laser for troposphere ozone lidar"

Summary form only given. The use of a folded cavity for Raman laser to obtain the efficient high-energy first Stokes generation is demonstrated in this report. Four types of cavities (linear cavity, two types of folded three-mirror cavities and folded four-mirror cavity) are investigated. Optical pulses with 15-16 ns duration and 0.6 mrad divergence are generated at pump pulse energy up to 135 mJ. The obtained first Stokes pulses are frequency doubled in DKDP crystal to produce 281 nm radiation needed as an online radiation for different absorption lidars

for ozone sounding in troposphere. [C2821]

"Remote Gas Detection in Solid Scattering Media using Differential Absorption Lidar"

Large-scale GASMAS (gas in scattering media absorption spectroscopy) measurement, which resemble multiple-scattering differential absorption lidar (DIAL) is discussed. Preliminary experiments have been performed and limitation and possibilities will be discussed. Potential future applications could include helicopter-born detection of snow avalanche victims (trapped carbon dioxide) or leaking snow-covered natural gas pipe lines. [C2822]

"Improving oil slick detection by SAR imagery using ancillary data"

The main trouble of oil spill detection systems based on synthetic aperture radar image is the discrimination of true oil slicks from other surface phenomena giving a similar signature. Most of these systems consist of three main stages: dark areas detection, features extraction and classification. The aim of this work is to improve the classification performance by using additional data in order to define a more accurate training set and identifying the features with the highest discrimination capability. It was used 27 ENVISAT ASAR images of the Prestige oil spill together with data from other sources and meteorological or oceanographic models. Results show that the radiometric features seem to work better in order to distinguish between oil slicks and look-alikes, and also that it is possible to identify as look-alikes using ancillary data up to 10% of the dark areas previously detected. [C2823]

"Genetic Algorithm and Region Growing Based Road Detection in SAR Images"

A new method for detecting roads in SAR images is presented in this paper. The method consists of four parts: preprocessing, Hough transform, genetic algorithm and region growing. In the preprocessing step, morphological operations are employed to remove many details in binarized SAR images. The Canny operator is applied to detect image edge, and small areas are deleted by using morphological area open operation. Hough transform is employed to extract lines. Genetic algorithm (GA) is used to search and connect road segments. Region growing approaches are utilized to extend road segments. The experimental results show that the proposed method can better detect roads in SAR images. [C2824]

"The Influence of Random motion Errors on Bistatic SAR Resolution"

In order to assess the quality of the system, this paper analyzes the effects of phase errors due to random motion on the resolution of airborne bistatic SAR. For zero mean random motion errors, an analytical result of RMS (root mean square) resolution is derived. Based on the derived model, Gaussian function is found to be the optimum weighting function on azimuth processing and the best achievable RMS resolution is obtained in closed form. [C2825]

"Heart Rate Analysis and Telemedicine: New concepts & Maths"

Our paper deals with some new aspects of ambulatory (Holter) ECG monitoring extending its indications and using for risk management purpose. Remote sensing consists of the transmittal of patient information, such as ECG, X-rays, or patient records, from a remote site to a collaborator in a distant site. Our earlier developed internet based ECG system was unique for on/off-line analysis of long-term ECG registrations. After the 5-year experience in a smaller region of Budapest, Hungary involving a municipal hospital and the surrounding outpatient cardiology departments and general practitioners, we decided to integrate into our new ECG equipment, the CardioClient the results. In the first clinical study of the four was a wavelet, non-linear heart rate analysis in sudden cardiac death patients using the Internet and the GPRS mobile communication. After the wavelet transformation by the Haar wavelet and the Daubechies 10-tap wavelet, the phase-space of the wavelet-coefficient standard deviation and the scale parameters showed an excellent separation in the scale-range of 3-6 between the two groups: in that region, the average scaling exponents was 0.14 ± 0.04 for Group-A, and 1.22 ± 0.27 for Group-B ($p < 0.001$). In the next study, we used the Internet database of long-term ambulatory, mobile, GPRS electrocardiograms for the risk stratification of patients through the cardiovascular continuum. From our ambulatory mobile GPRS ECG database the following a priori groups were defined after a 24 months follow-up: G1: N=227 patients (without manifest cardiovascular disease, clustered "boxes" based on the age, sex, cholesterol level, diabetes, hypertension); G2: N=89 patients (postinfarction group); G3: N=66 (patients with chronic heart failure) with (+) or without (-): all-cause death (acD), myocardial infarction (MI), malignant ventricular arrhythmia (MVA), sudden cardiac death (SCD). The actual vs. predicted values were analyzed with chi-square test. The best-significance levels ($p < 0.001$) were found with method in G1/MI+, G2/SCD+, G3/acD+, G3/SCD+ groups. In the third study a wavelet analysis of late potentials based on long-term, high-resolution, mobile, GPRS ECG data was performed. These pathological changes were also detected by the Haar and Daubechies_4 wavelets, but in a narrower space (110-128 ms and 180-240) and with lesser significance ($p < 0.01$). Late potentials were found in Group-A (N=21) in 18 cases with Morlet, 16 with

Haar, 19 with Daub-4 analysis, and in 15 cases using all the 3 waves; for Group-B the data were 5, 9, 8, 5, respectively. In the fourth clinical study the prognostic value of the nonlinear dynamicity measurement of atrial fibrillation waves detected by GPRS Internet long-term ECG monitoring were analyzed. The multivariate discriminant model selects the best parameters stepwise, the entry or removal based on the minimalization of the Wilks' lambda. Three variables remained finally: x_1 = CI mean-value at $\log r = -1.0$ (m9-14), x_2 = CI mean-value at $\log r = -0.5$ (m12-17), and x_3 = CD_cg. The Wilks' lambda was 0.011, chi-square 299.68, significancy: $p < 0.001$. [C2826]

"Multidimensional waveform encoding for spaceborne synthetic aperture radar systems"

This paper introduces the innovative concept of multidimensional waveform encoding for spaceborne synthetic aperture radar (SAR). The combination of this technique with digital beamforming on receive enables a new generation of SAR systems with improved performance and flexible imaging capabilities. Examples are high-resolution wide-swath radar imaging with compact antennas, enhanced sensitivity for applications like along-track interferometry and moving object indication, or the implementation of hybrid SAR imaging modes which are well suited to satisfy hitherto incompatible user requirements. Implementation specific issues will be discussed and performance examples demonstrate the potential of the new technique for different remote sensing applications. [C2827]

"Speckle Reduction for Remote Sensing Images Based on Nonsubsampled Contourlet"

Existing speckle reduction methods for remote sensing images such as SAR cannot capture image edge detail information and reduce noise effectively at the same time. The nonsubsampled contourlet (NSCT) is built upon nonsubsampled pyramids and nonsubsampled directional filter banks and provides a shift-invariant directional multiresolution image representation. Therefore, a speckle reduction model based on NSCT is presented. Firstly original image with speckle noise was transformed into with additive noise by means of homomorphism transform, and then the NSCT was implemented, finally threshold denoising method was adopted to separate the noise and signal. A comparison between the above NSCT denoising method and conventional methods was carried out on remote sensing images contaminated by multiplicative noise and SAR original image. The experimental results show that the performance of the NSCT is superior not only in speckle reduction but also in edge preservation. [C2828]

"Simulation Study of the SAR Imaging with the Virtual Remote Sensing Laboratory"

In this paper, we work with the virtual remote sensing laboratory (VRSL) developed in the CINVESTAV Telecommunication area, to do the simulation study of the synthetic aperture radar (SAR) imaging, which is the principal objective of this work. Also, we modified the so-called Mv parameter matrix, which is a degree of freedom implied in some reconstruction methods as the weighted constrained least squares (WCLS) and the proposed method called modified WCLS method (MWCLS) described in this paper. We include this proposed method and other characteristics in the first version of the VRSL. [C2829]

"Remote Probing of Sea Waters. Stages and Development; (to the 30-years Anniversary of Native Satellite Oceanology)"

Considered in this paper are the basic stages of creation of oceanographic space system <<Ocean -Sich>> and preceding researches. Possibilities of sea surface monitoring using Sich radar are analyzed. Results of the system exploitation are presented. [C2830]

"Test bed for Remote Environmental Monitoring in Northwestern China"

In this paper we design the heterogeneous network instead of homogeneous one to reduce the load of single node and as a result it could eliminate probability of wireless sensor network (WSN) overload. For wide feasibility in China northwestern area we choose the Global System for Mobile Communications (GSM) to transmit monitoring data to server and implement a protocol stack like TCP to get a reliable short message service (SMS) from local telecom provider. Finally we show some test result of this test bed and discuss about the next step. [C2831]

"Geometry and System Aspects of Spaceborne/Airborne Hybrid Bistatic SAR"

Spaceborne/airborne hybrid bi-static SAR is a new kind of remote sensor raised in recent years, whose development is still at an early stage for its great difficulty. Due to the high differences between satellites' and aircrafts' velocities and altitudes, there are remarkable differences between the hybrid system and systems which have the symmetrical structure, such as spaceborne bi-static SAR and airborne bi-static SAR. Three basic and

critical issues in the hybrid system are discussed, including geometry, Doppler properties and signal model. On the basis of the research work done in this paper, imaging algorithm of the hybrid system can be further designed in the next step. [C2832]

"Feasibility of Heart Rate Variability Measurement from Quadrature Doppler Radar Using Arctangent Demodulation with DC Offset Compensation"

This paper describes the experimental results of the beat-to-beat interval measurement from a quadrature Doppler radar system utilizing arctangent demodulation with DC offset compensation techniques. The comparison in SDNN and in RMSDD of both signals demonstrates the potential of using quadrature Doppler radar for HRV analysis. [C2833]

"Development of an imaging lidar for aerosol monitoring using a wide field-of-view, high-resolution telescope"

All-sky survey high resolution air-shower (Ashra) telescope has been developed to detect cosmic-ray particles. An imaging lidar system has been constructed by applying the Ashra telescope technique to atmospheric monitoring. The two-dimensional information on the aerosol distribution near the ground level can be obtained from the bistatic, imaging-lidar measurement. [C2834]

"Millimetre wave radar visualisation in mines"

This paper describes the development of millimetre-wave frequency modulated continuous wave radar visualization systems for mining applications. The implementations and performance verifications of the radar sensor for range and 3D profiling in underground and surface mines are presented in applications ranging from cavity, stope fill and ore-pass monitoring to dragline and rope shovel environmental mapping. [C2835]

"Joint influence of rain rate and turbulence on radar signal spectrum width"

This paper presents the developed model description and the calculation results of the joint influence that both rain intensity and turbulence produce on the spectrum width of the reflected signal in microwave frequency band. The model provides the possibility to calculate backscattered signal parameters at wide variety of the initial data. [C2836]

"Polarimetric approach to detection of probable aircraft icing zones. icing detection algorithms"

Aircraft icing is a dangerous meteorological phenomenon. Most important conditions for growing of ice coating on aircraft body or wings are presence of supercooled liquid water (SLW) drops, high humidity and negative temperature of air. Remote sensing of the clouds with the help of polarimetric radar can detect the SLW in cloud. It can be used to avoid dangerous situations during the flight. Mathematical simulation of microwave backscattering from ice crystals of different forms and water drops in rain and clouds have been done. Different icing detection algorithms are described and analyzed. [C2837]

"Digital beamforming and multidimensional waveform encoding for spaceborne radar remote sensing"

This paper describes an active electronically scanned array (AESA) FMCW radar with eight transceivers. Each transceiver has its own direct digital synthesizer (DDS) for signal generation which enables digital beamforming on transmit as well as on receive. The coherent operation of the eight transceivers and the capability to perform digital beam forming on transmit and receive is demonstrated. [C2838]

"Spectrum of rough sea surfaces covered in oil: consequences on the radar cross section"

This paper describes the influence of oil pollution over sea surfaces on the height spectrum of the rough surfaces. An oil slick damps the capillarity waves of the surface height spectrum, and reduces the RMS slope of the surface. These modified functions have then an influence on the radar cross section from contaminated sea surfaces. The impact of the contaminated sea surface on the bistatic radar cross section is then presented. [C2839]

"Joint influence of rain rate and turbulence on radar signal spectrum width"

This paper presents the developed model description and the calculation results of the joint influence that both rain intensity and turbulence produce on the spectrum width of the reflected signal in microwave frequency band.

The model provides the possibility to calculate backscattered signal parameters at wide variety of the initial data. [C2840]

"Statistical distribution for scattering mechanism of targets based on eigenvector decomposition in Polarimetric Radars"

In this paper a decomposition scheme for analysis and classification of statistical radar targets is presented. For this purpose eigenvector target decomposition (ETD) analysis method is used for calculating coherency eigenvalues. Also a simulation scheme is developed for calculating entropy, scattering mechanism for discrimination of several surface scattering objects within distributed targets. As results, radar image data set have been used for compare. [C2841]

"Polarimetric approach to detection of probable aircraft icing zones. Icing detection algorithms"

Aircraft icing is a dangerous meteorological phenomenon. Most important conditions for growing of ice coating on aircraft body or wings are presence of Supercooled Liquid Water (SLW) drops, high humidity and negative temperature of air. Remote sensing of the clouds with the help of polarimetric radar can detect the SLW in cloud. It can be used to avoid dangerous situations during the flight. Mathematical simulation of microwave backscattering from ice crystals of different forms and water drops in rain and clouds have been done. Different icing detection algorithms are described and analyzed. [C2842]

"Statistical distribution for scattering mechanism of targets based on eigenvector decomposition in polarimetric radars"

In this paper a decomposition scheme for analysis and classification of statistical radar targets is presented. For this purpose eigenvector target decomposition (ETD) analysis method is used for calculating coherency eigenvalues. Also a simulation scheme is developed for calculating Entropy, Scattering mechanism for discrimination of several surface scattering objects within distributed targets. As results, radar image data set have been used for compare. [C2843]

"Development of TanDEM-X DEM calibration concept"

The TanDEM-X mission (A. Moreira et al., 2004) comprises two fully active synthetic aperture radar satellites operating in X-band. The primary goal of this mission is the derivation of a high-precision global digital elevation model (DEM) according to HRTI level 3 quality. This requires accurate calibration of the interferometric system parameters, where the interferometric height is determined by the phase difference between the two images and the spatial geometry. Content of this paper is the development of a general concept for this calibration, which has a key incidence on mission aspects like the data acquisition plan and the data take adjustment and mosaicing. [C2844]

"Passive microwave remote sensing for security applications"

The security of persons or sensitive infrastructures is of increasing importance. Passive microwave remote sensing allows a daytime-independent non-destructive observation and examination of the objects of interest without artificial exposure under nearly all weather conditions. The penetration capability of microwaves enables the detection of hidden objects. Examples for various imaging experiments are shown. The experimental systems are used to investigate basic key parameters for the specific applications like suitable frequency band, required spatial resolution, sensitivity, and field of view. Systems close to real-time are under investigation and development. [C2845]

"Buoy and Radar Observation Network around Taiwan"

The coastal ocean monitoring center (COMC) was assigned by the government offices to establish an coastal ocean monitoring network around Taiwan. It is composed by data buoys, radars, tide stations and coastal weather stations. All field stations are operational and have real time data transmission function. The purpose of this paper is to present the frame of this observation network and show observation results especially during past typhoons. This paper focuses on the introduction of data buoy and radar systems. The hardware and analysis method of data buoy and radar system are presented in this study. [C2846]

"Monitoring Coastal Processes and Ocean Wave Directional Spectra Using a Marine Radar"

We discuss the application of microwave radars to remote sensing of ocean waves and currents in the coastal zone. A new X-band marine radar family (coherent and noncoherent) operating at 10-m scales can map

nearshore bathymetry, and measure ocean currents and wave spectra at distances out to a few kilometers. We present some examples of bathymetry experiments and recent empirical results in establishing the modulation transfer function that relates radar image spectra to ocean wave directional spectra, and allows such wave spectrum measurements. We discuss the plan for a real time operational system based on this technology.

[C2847]

"Recent Advancements of Multi-modal Radar & SAR Imaging"

Radar polarimetry radar interferometry and polarimetric SAR interferometry represent the current culmination in 'microwave remote sensing' technology. Whereas with radar polarimetry, the textural fine-structure, target orientation, symmetries and material constituents can be recovered with considerable improvement above that of standard 'amplitude-only' radar, by implementing 'radar interferometry', the spatial (in depth) structure can be explored. With polarimetric interferometric synthetic aperture, radar (POL-IN-SAR) imaging it is possible to recover such co-registered textural and spatial information from POL-IN-SAR digital image data sets simultaneously, including the extraction of digital elevation maps (DEM) from either polarimetric (scattering matrix) or interferometric (dual antenna) SAR systems. [C2848]

"Characterization of dust aerosols with dual wavelengths (532 nm/1064 nm) polarization lidar"

Asian dust over Suwon Korea in 2006 and 2007 has been measured with dual wavelengths (532 nm and 1064 nm) polarization lidar. The results of analysis showed that a ratio of particle depolarization ratio between 1064 nm and 532 nm are sensitive to mixing states of the dust and spherical aerosols. [C2849]

"Determination of the Melting Layer from Meteorological Radar Data in Malaysia"

A developed algorithm based on the vertical profile of radar reflectivity, has been applied to determine the boundaries of "the melting layer and its thickness. The average values of the melting layer heights are compared with ITU-R recommendations and other obtained results in tropical regions at 500 m resolution range. The results obtained showed lower values for heights of the melting layer. [C2850]

"Signal Detection Algorithms Based on Non-Parametric Estimates of Density Function"

This paper presents a novel approach to design radar signal detection algorithms that are applicable when a priori information is limited. The problem is formulated as testing hypothesis on the kind of density function. A novel method that allows to adopt permutation test in a practical algorithm is suggested and researched. The developed new adaptive algorithm is based on non-parametric kernel estimates of the density function. The results are useful for applications of signal detection in surveillance and remote sensing radar systems. [C2851]

"Development of an airborne ice sounding radar front-end"

This paper describes the design of an airborne P-band ice sounding radar. The ice sounder design features a microstrip antenna array with a relative operating bandwidth of 20%, compact RF components, a high efficiency high-power LDMOS power amplifier with >60% power-added efficiency across a relative bandwidth of 20% at a center frequency of 435 MHz, and a digital signal generation and acquisition unit. Furthermore, we demonstrate broadband performance of our left-handed/right-handed out-of-phase power dividers. In 2008 the first data acquisition campaign will take place in Greenland. [C2852]

"Electromagnetic scattering from multilayer rough surfaces with arbitrary dielectric profiles for remote sensing of subsurface soil moisture"

Radar remote sensing of soil moisture content at low frequencies requires an accurate scattering model of realistic soils, which often involves multilayer rough surfaces and inhomogeneous dielectric profiles. In this paper, a hybrid analytical/numerical solution to two-dimensional scattering from multilayer rough surfaces separated by arbitrary dielectric profiles based on the extended boundary condition method (EBCM) and scattering matrix technique is presented. The reflection and transmission matrices of a rough interface are constructed using EBCM. The inhomogeneous dielectric profile is modeled as a stack of piecewise homogeneous dielectric thin layers. The scattering matrices of an inhomogeneous dielectric profile are computed by recursively cascading reflection and transmission matrices of individual dielectric interfaces. The interactions between the rough interfaces and the inhomogeneous dielectric profile are accounted for by applying the generalized scattering matrix technique. The solution presented in this paper is for the two-dimensional scenario of multilayer rough surfaces. The technique can also be applied in three dimensions. In numerical simulations, the actual field-collected soil moisture data are used. In particular, the dielectric profiles during both dry and wet ground conditions are examined. The numerical simulations are performed to investigate both backscattering scattering

coefficients and co-polarized phase difference due to different subsurface roughness parameters and ground conditions. The results show that both backscattering coefficients and co-polarized phase difference at low frequencies are sensitive to the roughness of subsurface interfaces and deep soil moisture. Also, much larger depth sensitivity can be achieved using co-polarized phase difference than scattering coefficients. [C2853]

"VHF PortMap Sea Surface Radar Observations in a Shipping Channel"

A new sea surface radar system is described, which gives a spatial resolution of 100 m and operating ranges to up to 3 km. The deployment of the dual-radar system at the Lido Entrance to the Venice Lagoon gave current flow data in the channel and provided detail of a complex counter-flow at the end of the channel where it debouches into the Adriatic Sea. This circulating flow near the end of the channel is similar to that observed in wide-mouthed natural channels and is bringing turbid water into the channel. The presence of the circulation at the end of the channel has some consequences for sediment dynamics at the site. This deployment demonstrates the functionality of the PortMap radar in a busy shipping channel. [C2854]

"Feasibility of HRV measurement from single-channel doppler radar"

The single-channel Doppler radar system was evaluated for heart rate variability (HRV) measurement. Pearson PMCC, scatter plots, absolute differences, and mean were used and demonstrated good correlation between Doppler radar operating at different power levels and the finger pulse reference. Doppler radar may be of interest for heartbeat monitoring because of its remote sensing ability and shows good potential for HRV measurement. [C2855]

"A SAR processing algorithm for TOPS imaging mode based on extended chirp scaling"

This paper presents an efficient phase preserving processor for TOPS (Terrain Observation by Progressive Scans) imaging mode. TOPS has been proposed as a new wide swath imaging mode, which solves the problems of scalloping and azimuth-varying ambiguities introduced by the conventional ScanSAR mode by means of steering the antenna along the azimuth direction. An algorithm based on ECS (Extended Chirp Scaling) is proposed, which uses sub-apertures and a new azimuth scaling step. The proposed solution is also efficient in the sense that it allows selecting the final azimuth image spacing by means of azimuth scaling, hence easing the forthcoming mosaicking of the different sub swaths. Simulations with point targets are used to validate the processor. [C2856]

"A high resolution SAR sensor for space and airborne applications"

This paper discusses the general layout to achieve a flexible SAR radar design with the potential for extremely high resolutions. [C2857]

"An advanced airborne multisensor imaging system for fast mapping and change detection applications"

The advanced airborne multisensor imaging system (AAMIS) has been developed for a light fixed wing aircraft. It integrates a suite of state-of-the-art electro-optical (EO), thermal, hyperspectral, and Lidar imaging instrument packages for simultaneous active ranging and passive imaging that covers the electromagnetic (EM) spectrum of the visible and near infrared range and the long-wave infrared range. AAMIS has been tested for today's fast mapping and change detection needs. It demonstrates leading performance in providing comprehensive geometric and geophysical aerial image products with high spatial, spectral, radiometric, temporal and range resolutions. High resolution innovative data products collected by AAMIS sensors are presented. These include 3.5 cm resolution orthomosaics for a complete 15 km times 25 km large area coverage, 1 ft resolution hyperspectral images with contiguous 10 nm spectral resolution for the 410-820 nm range, 0.02 K resolution thermal images in a large 1 k by 1 k frame video format, and 20 cm range accuracy 3D Lidar mapping products. [C2858]

"A combined sensor system of digital camera with LiDAR"

In order to utilize the advantages of the high height accuracy of laser ranging and the good planimetric accuracy of processed digital camera imagery, the feasibility of a combined sensor system of LiDAR with digital camera using area or line array CCDs is first analyzed in this paper. The hardware composition of the combination system is given and the algorithm of integrally processing LiDAR points cloud and digital camera image is illustrated. Software development and availability for the processing at all stages of the work flow, is the key to the full utilization of such an integrated system. [C2859]

"A distributed approach to efficient time-domain SAR processing"

This paper presents a distributed approach for time-domain focusing, which significantly enhances the overall efficiency by distributing the computational load across a (potentially large) number of networked computers. The system described includes the so-called master, responsible for pre-processing, the distribution of fragments of raw-data data and the collection of processed image fragments. Fragments of raw-data are passed to so-called slaves, any number of which can be connected to the master, which are responsible for the focusing itself. Master and slave actively communicate over the network to organise the entire process in a scalable manner. In this way, time-domain processing can be accelerated by a factor that is virtually linear in the number of participating slaves. This paper summarises the current status of software development, realised in a platform-independent way using the IDL and Java languages. Additionally, some preliminary evaluations of performance, scalability and the required network infrastructure are given. Some examples of SAR data, acquired by the airborne sensor E-SAR of DLR, and processed with the system described are shown. [C2860]

"Effects of attitude error on spaceborne ScanSAR mosaic"

Attitude stability is a very important parameter for the platform design of scanning synthetic aperture radar (ScanSAR) satellite. In this paper, the effect of satellite attitude error on the Doppler parameters is derived in detail. And the effects of Doppler centroid frequency error on spaceborne ScanSAR mosaic in azimuth are analyzed, to provide a theoretical guideline for the design of spaceborne ScanSAR system, as verified by simulations. [C2861]

"Surface clutter analysis and ranging sidelobe level requirements for spaceborne meteorological radars"

Pulse compression techniques are very attractive in the development of new-generation spaceborne meteorological radars, because it has the advantages to reduce the transmit power requirements and improve the measurement precision by increasing incoherent average samples. Compared with TRMM, which employed a pulsed-CW signal, it is very important to analyze the effect of surface clutter from ranging sidelobes of the returned signal after pulse compression. In this paper, the effect of surface clutter with different antenna sidelobe levels and different ranging sidelobe levels are analyzed in details. Based on the analysis of surface clutter, the requirements for antenna sidelobe level and pulse compression range sidelobe level are proposed. [C2862]

"Scientific use of TerraSAR-X"

TerraSAR-X is a new German radar satellite scheduled to be launched in May, 2007. Its lifetime will be five years. It carries a high frequency X-band SAR sensor that can be operated in three different modes and various polarizations. The Spotlight-, Stripmap- and ScanSAR-modes provide high resolution images for detailed analysis as well as wide swath data whenever a larger coverage is required. These high geometric and radiometric resolutions together with the single, dual and quad-polarization capability are innovative and unique features with respect to space borne systems. Additionally several incidence angle combinations will be possible and double side access can be realized by satellite roll maneuvers. The satellite will be positioned in an 11 days repeat orbit. The revisit time in the very high resolution Spotlight mode is 2.5 days for 95% Earth's surface visible to TerraSAR-X. [C2863]

"Optimum design of antenna pattern for spaceborne SAR performance using improved NSGA-II"

Optimization of antenna array using in SAR system is considered in this study. A robust evolutionary algorithm, non-dominated sorting genetic algorithms (improved NSGA-II), is applied on a spaceborne SAR antenna pattern design. The system consists of two objective functions with two constraints. Pareto front are generated as a result of multi-objective optimization. After being validated by a test problem ZDT4, the algorithms were used to synthesis antenna radiation pattern. The good results with low ASR and high directivity are obtained. [C2864]

"Disaster monitoring and environmental alert in Taiwan by repeat-pass spaceborne SAR"

The prevailing complex geological and ecological conditions of Taiwan have drawn considerable attention from various geo-ecological communities because of their vulnerability to produce various natural hazards at different scales. Located in the tropical/subtropical zone of the Pacific Rim, its ecological and rugged mountainous properties are environmentally sensitive making monitoring and observations especially difficult because of the high population density. For example, in terms of natural hazard mitigation tectonically active regions are used for analyzing the cause of abundant risk events, such as earthquakes, landslides and land subsidence. In fact Taiwan is well suited as a test site for studying those geologically disastrous processes. Implementing novel techniques of space remote sensing has proved to be an effective means in recent years for greatly improving

our understanding of these phenomena. In this paper we report on the monitoring of such events using multi-modal polarimetric and/or interferometric SAR images at C and L band from ERS, JERS-1, RADARSAT-1, ENVISAT, and from the recent ALOS satellite. For crustal and surface deformation, we used radar image pairs with long temporal baselines and large areas of coverage for investigating deformation over Western Taiwan. Pre-seismic and co-seismic deformation patterns are spatial-temporally analyzed. The other topic deals with the coastline changes observed from a sequence of ERS-1/2 SAR images within the years of 1996 to 2005. Waterlines were extracted using multi-scale procedures of edge detection and were corrected with tidal motion data. Substantial analyses were carried out in conjunction with ground surveys and lidar mapping. The topographic feature changes due to large scale landslides triggered by torrential rains were also monitored. In addition, the SAR interferograms were used to analyze the deposition changes along the riverbeds and riverbanks for short-intervals using optimal baselines. Summary and remarks on the implementation of such multi-modal polarimetric and/or interferometric SAR imagery for environmental monitoring are provided. [C2865]

"Investigation of H.264 intra coding for SAR image"

In this paper we investigate the performance of H.264 intra coding for synthetic aperture radar (SAR) image. The results show that H.264 intra coding is a high performance coder for the SAR image. However, when the SAR image is despeckled, H.264 Intra coding is not so efficient than the wavelet based image coder, such as JPEG2000 and SPIHT. Then more efficient representation is needed when H.264 Intra Coding is used to code the despeckled SAR image. [C2866]

"Dyadic resolution multilook image generation by wavelet packet transform correlation of complex SAR signals"

We present a signal processing approach for generation of multilook SAR intensity images at dyadic scales of resolution. Orthogonal subband decomposition inherent in discrete wavelet packet transform is utilized in shift-invariant manner to produce multiresolution complex SAR images. The symmetry of detailed subband spectra is utilized in separating the disjoint spectra to produce multilook image. Analytical results and sample imagery of diffused reflection are presented. [C2867]

"The equivalence of Cameron's unit disc and Poincaré's sphere for symmetric scattering characterisation and classification"

Cameron's coherent target decomposition and classification is able to represent a symmetric scatterer onto a unit disc in the complex plane, and assign it to one of the six symmetrical elemental scatterer classes. Recently, Touzi et al. proposed a variation of Cameron's method by introducing a coherent analysis. Moreover the Poincaré's sphere, was used instead of the unit disc for representing symmetric scattering because it was considered a more suitable domain. The aim of this work is to demonstrate the equivalence of using Poincaré's sphere domain and Cameron's unit disc, in term of characterisation and classification of symmetric scattering types. [C2868]

"Reconstruction of the building objects from multi-aspect high-resolution SAR images"

In this paper, an approach to the automatic reconstruction of 3D simple building objects from multi-aspect metric-resolution SAR images is proposed. The edge detector of constant false alarm rate (CFAR) and a parallel Hough transform technique are first employed to extract the parallelogram-like image of the building walls in SAR image. A set of probability density functions is presented to describe the extracted random wall-images and their multi-aspect coherence. Then the maximum-likelihood estimation of object is derived from its multi-aspect object-images. A hybrid priority criterion is defined to evaluate the reliability of reconstruction result, based on which, an automatic reconstruction algorithm is further devised to match object-images of different aspects and finally reconstruct the building objects. Four-aspect Pi-SAR images over Sendai, Japan are adopted for reconstruction. The results show the fidelity of the whole process chain and the feasibility of 3D objects automatic reconstruction from multi-aspect SAR images. [C2869]

"Unsupervised land cover classification of SAR images by contour tracing"

The potentiality of synthetic aperture radar (SAR) images for land cover mapping is an important area of research. For single band, single polarized SAR images, information is available in the form of intensity and texture only. Land cover classification of SAR images requires exploitation of spatial relationship of pixels also, in addition to pixel level segmentation. SAR images can be segmented successfully if the regions with homogeneous intensity and texture areas can be identified and grouped together. So far, contour tracing has been used only in demarcating sea and land. Identifying contours in a domesticated area with a mixture of

water, urban and vegetation areas require complex analysis of the spatial distribution of pixels. In this paper, we have presented an unsupervised classification algorithm using maximum a posteriori (MAP) segmentation for SAR images in which SAR image is classified into monotone, texture and edge regions. Monotone and textured regions are labeled as land cover types like water, urban and vegetation areas using K-means classification. SAR image of the region with latitude varying from 77.86deg to 77.91deg and longitude varying between 29.89deg and 29.85deg of Haridwar region, India is considered for segmentation. We have compared the segmented image obtained by this methodology with the topographic map of the corresponding region. The water, urban and vegetation areas are clearly recognized with the proposed classification approach which represents a very good agreement with the original topographic sheet. [C2870]

"The analysis and compensation for the unwrapped phase error raised by the dynamic baseline of DSS-INSAR"

The DSS-INSAR (distributed small satellite INSAR) applies the interferometry to the carrier platform which is made up of small satellites flying in a certain formation. It aims to retrieve DEM (digital elevation map) with quite high precision globally. In fact, every small satellite in the flying formation is dynamically circling around a reference central point along a certain track. Therefore, the baselines generated by the flying satellites are also unstable. However, the stability of these baselines is very crucial to get elevation measurement with high precision. Therefore, it is valuable to analyze the influences of the above-mentioned baselines on unwrapped phases. This article demonstrates the errors of unwrapped phases introduced by dynamical baselines of DSS-INSAR and provides effective solutions to compensate those errors in detail. In the first beginning, this article deduces the relationship between the across-track baseline, the along-track baseline and the orbit elements, respectively. Then, it analyzes the unwrapped phase error introduced by the dynamical baseline of DSS-INSAR. Finally, it provides a very effective model which can be used to compensate the error. [C2871]

"A new method for Doppler centroid estimation for spaceborne SAR based on chirp scaling algorithm"

We introduce a new method to estimate the Doppler centroid accurately based on chirp scaling algorithm after investigating the performances of curvature factor C_s and the effective FM rate K_s regarding to Doppler ambiguity number (DAN) and finding that C_s and K_s will lose their functions if a wrong DAN is used and the generated image definition will be degraded. So relations between definition evaluation functions (such as entropy and variance) and the DAN can be used to find the correct DAN which makes the entropy minimum or the variance maximum. Radarsat raw data is used to test the proposed method and find that the performance of using variance is better than that of using entropy. [C2872]

"Region feature extraction based on improved regularization method in SAR image"

The noise existed in synthetic aperture radar (SAR) image weakens the detailed features of region of interest (ROI) such as target and shadow. It also leads to the serious performance reduction of subsequent target detection, classification and recognition. The conventional regularization method could enhance target features in SAR image; however, the high computation complexity limits the real-time application of it. An improved regularization method is introduced in this paper, which increases processing speed of region feature extraction for SAR image significantly. It is theoretically proved that, by optimizing SAR projection operator, computation complexity could be reduced from $O(M^3N^3)$ to $O(MN)$ without ability losing of the region-based feature enhancement. MSTAR SAR image data is employed for algorithm experiment. The result shows that our method can increase target-to-clutter ratio significantly while restraining the noise in ROI, and then extract target and shadow from background clutters in SAR image more accurately. [C2873]

"Fine micro-Doppler analysis in ISAR imaging"

In ISAR imaging, it's well known that rotating parts of a target such as wheels or rotors induce additional features in the Doppler frequency spectrum. These features are called micro-Doppler effect and appear as sidebands around the central Doppler frequency. They can provide valuable information about the structure and motion of the rotating parts and may be used for target identification. In this paper, we propose a fine analysis of the Doppler returned by reflectors of a rotating wheel. Thanks to the micro-Doppler signature we are able to extract information on its geometrical features (position, orientation). The method has been performed on simulated and experimental data and provides satisfactory results. [C2874]

"Spotlight-mode SAR data focusing using a modified wavenumber domain algorithm"

In this paper, a modified version of the wavenumber domain algorithm (MWDA) is analytically presented and

formulated. It is capable of processing the spotlight-mode SAR data. MWDA combines the high accurate focusing of the wavenumber domain algorithm (which is also called range migration algorithm) and the interpolation-free requirement. To avoid costly interpolation manipulation, the inverse scaled Fourier transform (ISFT) is substituted for Stolt mapping. The subaperture processing is used to circumvent the limitation that the pulse repetition frequency (PRF) is not high enough to sample the signal in azimuth. [C2875]

"Clutter analysis of high resolution millimeter-wave SAR-data in the spatial and wavelet domain"

This paper presents the analysis of high resolution millimeter SAR clutter data, measured in a joint Swiss-German flight campaign. The generalized Gaussian function and the Kolmogorov-Smirnov test are considered to test the hypothesis of Gaussian clutter process. 35 GHz and 94 GHz data are compared. The results are presented in the time and wavelet domain, as the wavelet domain is an import transform domain for the development of terrain classification, target recognition and data compression algorithms. [C2876]

"A velocity vector estimation algorithm tested on simulated SAR raw data"

This paper presents an improved method for estimating the velocity vector of a moving target from SAR raw data. The velocity estimate is carried out without a priori information by a recursive procedure coupling Along Track Interferometry (ATI) for the range component to the Impulse Reference Function (IRF) analysis for the azimuth component. To develop and test the estimation scheme, a dual channel SAR raw data simulator has been built and the retrieval algorithm has been implemented, taking into consideration the coupled effect of the two velocity components. Significant statistics have been generated by considering different targets and backgrounds, simulating scenes with constant backscatter, vehicles in a shrubs environment and ships at sea. [C2877]

"UAV based collision avoidance radar sensor"

In this paper, the critical requirement for obstacle awareness and avoidance is assessed with the compliance of the equivalent level of safety regulation, and then the collision avoidance radar sensor system is presented with the key design parameters for the requirement of the smart unmanned aerial vehicle in low-altitude flight. Based on the assessment of various sensors, small-sized radar sensor is selected for the suitable candidate due to the real-time range and range-rate acquisition capability of the stationary and moving aircraft even under all-weather environments. Through the performance analysis for the system requirement, the conceptual design result of radar sensor model is proposed with the range detection probability and collision avoidance mode is established based on the time-to-collision, which is analyzed by collision scenario. [C2878]

"ISAR imaging of helicopter"

Conventional envelope alignment method of ISAR imaging assumes that the target is a rigid body, and therefore, the correlation between one-dimensional range profiles at neighboring time slots gives a larger value compared to correlation between time separated range profiles. But this is not the case for targets such as helicopter which have rotating body parts. In this paper, an envelope alignment algorithm for helicopter target ISAR imaging is proposed. For every range profile, correlation with other range profiles are done, and the range profiles with larger correlation value are used to provide an initial estimate of the target motion parameters by polynomial fitting. Then the estimated parameters are averaged to get a better estimation. The position of the rotor signals are obtained by taking the difference of the range profiles in the slow time domain. The rotor signals are then suppressed by zero-force windowing technique. Simulation results have shown the effectiveness of this algorithm. [C2879]

"Frequency domain imaging algorithm for spaceborne/airborne hybrid bistatic SAR"

A frequency domain imaging algorithm for the hybrid spaceborne/airborne BSAR is presented. The key point of deriving the algorithm is the analytical evaluation of the system point target response's 2-D spectrum. To overcome the difficulty of resolving analytical solution for the stationary phase point, the spectrum's phase is approximated by two-order Taylor expanding around the point, which is not only in the neighborhood of the system's corresponding stationary phase point but also can be obtained analytically. Thus the approximated analytical spectrum is pretty close to the actual one. In the imaging algorithm, both range-dependent range cell migration and azimuth-dependent range cell migration are compensated in two steps: Inverse Scaled Fourier Transform which can be realized through the chirp z-transform and phase multiplication. The validity of the algorithm is demonstrated by experiment with the simulated data. [C2880]

"Shape from shading of SAR imagery in fourier space"

A new shape from shading technique is presented in this study. This technique is a further development of Pentland's linear shape from shading technique (1990). The equations and geometric modeling are extracted for SAR imagery. However, the modeling can be easily adapted for optical images as the geometric modeling is much simpler than SAR images due to the fact that the geometric transformation from 3D object space to 2D image space in optical imagery is modeled by a well-estimated orthogonal projection or perspective projection itself. This solution for shape from shading problem employs linear estimation of the reflectance model using Taylor expansion. As there are one known image intensity and two unknown surface gradients for every pixel, there is no direct solution. By using a global approach and solving all the image pixels at the same time, it is possible to estimate an answer and overcome the ambiguity problem in the incidence angle estimation. For this purpose, the Fourier transform of the expanded reflectance model will be taken and as the Fourier transform of the surface gradients is a linear function of the surface height, the number of equations and unknowns will be equal and the system is soluble. In the proposed algorithm, an iterative approach is used to improve the accuracy of the estimated surface height. Iteration starts with a low resolution digital terrain model (DTM) of the area for the initial guess of the surface gradients and based on the equation system in Fourier space, the iteration continues until a threshold is reached or the number of iterations exceeds a tolerance. The technique is tested on a Radarsat image from Death Valley area and the results are shown and validated with the available DTM of the area. Based on the results, it seems that the proposed method is sensitive to the noise. The noise problem should be carefully considered either during the reflectance modeling or during solving the problem in the Fourier space as a filtering problem. [C2881]

"The effect of polarization ratio on RADARSAT wind vector retrievals"

In this presentation, the polarization ratios were calculated from AIRSAR polarimetric SAR data and ENVISAT ASAR dual-polarization data; and their empirical CC parameters which depend on incidence angle were obtained. Five C band HH polarization RADARSAT-1 SAR images are used to validate these polarization ratios and we found that the empirical parameter $\alpha = 0.5$ is superior to other possible parameter α values. [C2882]

"Automobile-based Bistatic SAR processing and experimental results"

In recent years, the interest in bistatic synthetic aperture radar (SAR) has rapidly increased and many bistatic SAR models and processing methods are presented. But some technical problems of bistatic SAR, such as synchronization (in both time and frequency) and the imaging processing of bistatic raw data, have not been resolved sufficiently. To verify bistatic SAR system synchronization plan and imaging processing algorithm, the University of Electric Science and Technology of China (UESTC) developed an Automobile-Based Bistatic SAR system because of its convenience, and carried out a series of experiments. Comparing with airborne monostatic SAR imaging processing, some special problems should be considered. In this paper, we introduce the Automobile-based Bistatic SAR system and discuss the corresponding imaging processing method. [C2883]

"A multi-sensor approach and ranking analysis procedure for oil seeps detection in marine environments"

Accidents involving oil spills from petroleum exploration, production, and transportation facilities have stained the history of major companies. The implementation of monitoring systems as an aid to contingency planning is crucial to guarantee proper environmental performance in offshore activities. On the other hand, natural oil and gas seeps have historically provided invaluable information to oil explorers in frontier areas. The use of Synthetic Aperture Radar (SAR) orbital systems is commonly used for oil slicks detection in the marine environment. Such information can be applied to petroleum exploration (oil seeps detection) and environmental assessment (oil spills monitoring). In combination with SAR satellite images (RADARSAT-1 and ENVISAT ASAR), and essential meteorological and oceanographic data, the proposed technology enhances the detection of oil slicks in the ocean surface based on radar texture. [C2884]

"Bistatic SAR Raw Data Simulation for Ocean"

Bistatic SAR is a potential and effective tool for ocean remote sensing, and the simulation of bistatic SAR raw data from ocean surface plays a great role in the understanding of the mechanism of bistatic SAR ocean surface imaging. In this paper, a bistatic SAR raw data simulation model for ocean surface is presented, which includes bistatic scattering simulation and ocean echo data simulation. In our research, based on IEM scattering model, a stochastic multiscale scattering model is improved by applying the second order nonlinear modulation model, and the speckle noise and coherent time character of ocean surface are simulated in the SAR raw data simulation. [C2885]

"Kuroshio-induced cold eddy streets in the lee of isolated islands"

Cold eddy streets formed in the lee of isolated islands were investigated in relation to the Kuroshio current. Multi-temporal SAR images acquired over a one-month period revealed island wake patterns, such as meandering disturbances and eddy streets. These patterns corresponded to the Kuroshio path, indicating a Kuroshio-island interaction. We constructed high-spatial-resolution sea-surface temperature (SST) images for the time when the Kuroshio impinged on the islands by regressing the LANDSAT infrared images on the AVHRR-derived SST. The images revealed low-SST island wakes, some of which included cold eddy streets. A numerical simulation was performed to investigate their formation mechanism. The simulation qualitatively reproduced the cold eddy pattern, with eddy-driven mixing developing a mixed layer down to 100 m, causing the low-SST island wakes. The shedding frequency and distance of the model-produced eddies were close to those of the Karman vortex theory, suggesting that Karman-like cold eddy streets developed behind the islands when the Kuroshio passed. [C2886]

"High resolution SAR imaging along circular trajectories"

After a first series of full circle SAR acquisitions in L and P-bands during a 2004 joint FOI-ONERA campaign in Sweden, ONERA experimented in 2006 high resolution (15 cm) polarimetric, full circle acquisitions in France and Germany using its X-band sensor. In order to cope with narrower antenna pattern and aircraft attitude fluctuations, a steerable antenna was used. Furthermore, an experimental setup for retrieving high accuracy trajectory was installed. This paper describes the processing of this signals. [C2887]

"A quadtree algorithm for high squint SAR imaging"

In this paper, a quadtree algorithm is used for high squint SAR image reconstruction. It is very difficult for current SAR-imaging algorithms to be used directly in high-squint configurations. This is due to the large range-cell migration and the nonnegligible cubic-phase term in the signal. Every preceding problem is eliminated by using backprojection at the expense of substantially greater processing time. The quadtree image formation technique is a computationally efficient approximation to standard convolution backprojection algorithm. A quantitative analysis and simulations show that this algorithm can process the SAR data with a high squint angle. [C2888]

"A simulator for SAR sea surface waves imaging"

This paper describes a synthetic aperture radar (SAR) sea surface waves simulator. The simulator, based on the velocity bunching (VB) theory, has been developed and implemented modularly and its use can also assist microwave remote sensing courses. The present version of the software is run in classes at National Oceanographic Centre of Southampton (NOCS), UK and at the Universita di Napoli Parthenope, Italy. [C2889]

"Dielectric spectroscopic model for tussock and shrub tundra soils"

In this paper, the measured microwave dielectric data are presented for some soils collected in the tussock and shrub tundra area located on the North Slope, Alaska, near Toolik Lake, at N 68deg 38', W 149deg 35' with an elevation of 730 m. The measured samples represented the organic rich soil picked up from the middle and base of tussock, organic poor soil from the depth of 20 cm in the valley between tussocks, and organic rich soil from the depth of 20 cm in the shrub tundra site. The measurements were carried out in the range of frequencies from 0.5 to 16.0 GHz and temperatures from -30degC to +25degC. On the basis of that data, the spectroscopic model of complex dielectric constant was developed for the moist soils measured, using the methodology of the generalized refractive mixing dielectric model [1]. This model takes into account contributions from the organic/mineral contents of soil, soil ice, free liquid soil water, and bound soil water arising due to interaction of soil water molecules with the surface of organic/mineral and ice particles. The complex dielectric constants for all the types of soil water observed were shown to follow the Debye formulas, with a single relaxation frequency for every distinct type of soil water. The temperature dependences were obtained for the parameters of the generalized refractive mixing dielectric model, including the parameters of soil water Debye relaxation, that is, the low and high frequency limits of dielectric constant and relaxation time, as well as the ohmic conductivity relating to every component of the soil water. The previously unknown physical phenomenon of liquid soil water transformation into a transition type of bound water, instead of ice, was observed in the range of temperatures below -6degC, which appeared to arise in the organic rich soils studied. The results obtained can be considered as a substantial contribution to the soil dielectric database, to be employed in the physically based data processing algorithms for radar and radiometry remote sensing of the northern circumpolar region. [C2890]

"Scattering from 2D-dielectric random surfaces effect of roughness and moisture of seedbed surfaces upon the bistatic scattering coefficient"

We propose a statistical model to describe the seedbed surfaces and we study the roughness and moisture influence upon the backscattering coefficient and the scattering patterns by means of Monte-Carlo predictions. For each realization, the scattering amplitudes are obtained by the C method. [C2891]

"Closed form expressions for scattering matrix of simple targets in multilayer structures"

Scattering matrix of a simple target embedded in multilayer planar structure is derived. The structure is excited by an elliptically polarized plane wave incident at an oblique angle. The calculation of the electromagnetic fields is performed in spectral domain. The scattering matrix of a planar electric dipole printed on upper interface and surrounding by free-space is evaluated. The obtained results agree with those existing on the literature for normal incidence case. [C2892]

"A UAV avionics system to facilitate VHF depth sounding and SAR"

An avionics system for an autonomous UAV platform supporting VHF depth sounding and SAR is under development. The system is divided into navigation, communication, and data processing or logging. This design provides accurate position, velocity, acceleration, and attitude data. It supports over-the-horizon communication via an Iridium satellite link. The data collected by this system will allow for motion effects of the UAV to be compensated for, to enable SAR image formation. [C2893]

"Cassini RADAR: investigation of titan's surface parameters by means of Bayesian inversion technique and gravity-capillary waves modelling of liquid hydrocarbons surfaces"

During the first two years of the Cassini mission, a great amount of data dealing with Titan's surface has been collected. In particular, the analysis derived from the SAR imagery reflects the complex Titan's surface morphology. In fact, in the different Cassini radar images a certain number of areas with peculiar features has been identified, such as: dark and bright areas (Ta, T3), periodic structure ("sand dunes") and, above all, hydrocarbon lakes [2],[11]. The proof for the presence of hydrocarbons lakes on Titan has been obtained during the T16, the radar pass performed on Titan by the Cassini spacecraft on 22 July 2006 [12]. In this paper, the investigation of Titan's surface parameters (physical and morphological) has been carried out by the means of Bayesian inversion technique, and simulations of the wave motion for the hypothesized hydrocarbons liquid surfaces has been performed. [C2894]

"Pulse electromagnetic sounding of the petroleum- containing layered medium"

In this research, propagation of super wide-band pulse in a frequency dispersive medium representing the oil-saturated collector. The capability of their use for geonavigation in techniques of lateral drilling is discussed on the basis of the results of simulation obtained. The complex dielectric constant of oil-saturated rock was calculated on the basis of refraction mixing dielectric model, the oil, sodium chloride solution, methane, quartz and bentonite being contained in each layer. The thin cylindrical vibrator of finite dimensions was used as antenna, being excited by voltage the like one period sinus pulse of nanosecond duration. The time-domain structure of pulse propagation in a plane-layered medium was calculated. Attenuation of power flow pulse reflecting from oil-bearing bed was studied. The gain-frequency characteristic relating to each particular layer was analyzed proving the medium of petroleum collector to operate like a low-pass filter. [C2895]

"Study of millimeter-wave radar for helicopter assisted landing system"

This paper discusses the development of an algorithm used to simulate the effectiveness of millimeter-wave radar in imaging a rough terrain, for the purpose of helicopter assisted landing. Using an externally generated terrain and the physical optics approximation, the algorithm computes the backscatter response of the terrain when illuminated by a real aperture antenna. Results are presented from simulating terrains with different macroscopic features, such as a hump, ditch or a slope. It shown that operating at millimeter-wave, more specifically at W-Band frequencies, is ideal for such an application where a compact sensor is required to achieve high resolution imaging. [C2896]

"Polarimetric microwave emission from snow surfaces: 4th Stokes component analysis"

The effect of ice on polarimetric 4th Stokes component observations is investigated using WindSat data over Antarctica. The difference in the magnitude of the signal observed during (July 2003) and summer (February 2004) months are investigated using a second harmonic sine function of the azimuth look angle. The seasonal variations are further investigated by a time series of the 4th Stokes component for a location in Wilkes Land in east Antarctica and compared with a time series observed by the ERS scatterometer (ESCAT) from a previous work. The paper discusses the potential of a polarimetric radiometer in providing information about scattering

and thermal properties of a snow ice pack. [C2897]

"Validation of the soil dielectric spectroscopic models with input parameters based on soil composition"

In this paper, a comparative analysis of dielectric spectrum predictions for moist soils in the microwave band was carried out, regarding a well known and prevalent semiempirical dielectric model proposed in [1]-[3], on the one hand, and recently developed generalized refractive mixing dielectric model [5], on the other hand. The analysis is based on the measured dielectric data borrowed from [4], in which a set of soils measured includes all of grain-size distributions that are observed in nature, with measurements being performed over the range from 40 MHz to 17 GHz. In the case of the soil measured in [4] that has an intermediate position in terms of its texture parameters, input data for the semiempirical model were attained, using the texture and soil mineralogy data available in [4], and dielectric spectra predictions both for the dielectric constant and loss factor were calculated. Simultaneously, with the use of the dielectric data of [4], input parameters for the generalized refractive mixing dielectric model were derived, and dielectric predictions for the same moistures were calculated. Comparative analysis based on the measured data together with both predictions showed the semiempirical dielectric mixing model to generate dielectric constants and loss factors that have a noticeable bias relative to the measured ones, correlation coefficients being on the order of 0.93. At the same time, the GRMDM predictions appeared to correlate with the measured values with noticeably better accuracy both in the frequency and moisture domains. As a result, the ability to make accurate predictions for dielectric spectra with the use of the SDMM was shown to be doubted, regarding the moist soils, which falls out of the scope of soils measured and fitted to develop the SDMM in [1]-[3]. On the contrary, the GRMDM [5] has proved to be able to make predictions for the dielectric spectra of moist soils with the same error as that of initial dielectric measurements. [C2898]

"Semi-Analytic Mode Matching (SAMM) algorithm for efficient computation of nearfield scattering in lossy ground from borehole sources"

The 3D semi-analytic mode matching (SAMM) algorithm is used to determine nearfield scattering from underground targets in lossy soil, where the source is a dipole placed within a borehole in the ground. Scattering is described by moderately low-order superpositions of spherical modes placed at multiple user-specified coordinate scattering centers (CSCs); the mode coefficients are found numerically by least-squares fitting all boundary conditions at discrete points along the relevant interfaces while at the same time obeying radiation conditions. SAMM results are compared with a completely different method: the Half-Space Born Approximation (HSBA). Good agreement between methods serves as algorithm validation. [C2899]

"The C-SAR instrument for the GMES sentinel-1 mission"

The paper describes the C-SAR instrument for the GMES Sentinel-1 mission. After a brief introduction of the Sentinel-1 instrument requirements a design description of the overall C-SAR instrument as well as of its major subsystems (i.e. the SAR Antenna Subsystem (SAS) and the SES Electronic Subsystem (SES)), is given. The paper concludes with an overview on the predicted instrument performance. [C2900]

"SRAL SAR radar altimeter for sentinel-3 mission"

The SRAL SAR radar altimeter is the core instrument of the topography mission carried on board the Sentinel-3 satellite which is planned to be launched in 2012. A detailed overview of this instrument is given in this paper in terms of architecture, functions, modes and performances. [C2901]

"The contribution of the european space agency to the ALOS PRISM / commissioning phase"

The Advanced Land Observing Satellite (ALOS) was launched on Jan 24th, 2006 by a Japan Aerospace Exploration Agency (JAXA) H-IIA launcher. It carries three remote sensing instruments: Advanced Visible and Near Infrared Radiometer type-2 (AVNIR-2), Panchromatic Remote-sensing Instrument for Stereo Mapping (PRISM) and Phased Array Type L-band Synthetic Aperture Radar (PALSAR). Within the framework of European ALOS Data European Node (ADEN), European Space Research INstitute (ESRIN) as part of European Space Agency (ESA), teamed up with JAXA for contributing to ALOS commissioning phase plan. This paper summarizes the strategy that ESA adopted to define and implement a data verification plan for mission operated by foreign nation, classified as so called ESA Third Party Missions (TPM). The verification of ALOS optical data from PRISM / AVNIR-2 instruments activities had begun four months after satellite launch on March 2007. GAEL Consultant (French company) has supported ESA / ESRIN for designing and executing the plan. A team of principal investigator's has been put together to provide technical expertise. This paper includes a description of the verification plan and summarizes the methodologies that were used for radiometric, geometric

and image quality assessment. Preliminary results indicate that the radiometric calibration of the AVNIR-2 sensor agrees with Landsat 5 (L5) Thematic Mapper and the MEdium Resolution Imaging Spectrometer (MERIS) calibration to within 10%. The geometry accuracy of PRISM and AVNIR-2 product remains within specifications but some recommendations are provided to improve the quality of product. The preliminary results from the PRISM image quality assessment through computation of PRISM Modulation Transfer Function (MTF) raised few questions toward jpeg compression that degrades image. [C2902]

"Pol-dinSAR: polarimetric SAR differential interferometry using coherent scatterers"

We investigate the impact of polarimetry and polarimetric effects on the Differential Interferometry (DinSAR) technique for the coherent backscattering reciprocal case, with the aim to obtain better accuracy and to extract additional information about the scatterer. Emphasis is given to the effects of Faraday and scatterer line-of-sight (LOS) rotations, and to the determination of the intrinsic scatterer scattering mechanism. [C2903]

"Classification of stricken residential houses by the mid niigata prefecture earthquake based on POLSAR image analysis"

This report attempts to apply a hybrid classification technique based on POLSAR image analysis to detect the man-made residential houses in a local mountainous area stricken by the Mid Niigata Prefecture Earthquake. The present hybrid scheme includes the scattered power decomposition method based on physical scattering nature and the scattering feature extraction method using polarimetric correlation coefficient. From the results of the image analysis for actual POLSAR data, it is verified that the present hybrid scheme provides us accurate classification of the man-made targets even in the severe mountainous [C2904]

"Feature extraction of gable-roofed buildings from multi-aspect high-resolution InSAR data"

The achievable spatial resolution of state-of-the-art synthetic aperture radar (SAR) sensors enables the analysis of urban areas. The appearance of buildings in magnitude images is governed by effects of the inherent oblique scene illumination, such as layover, radar shadow and salient lines of bright scattering caused by direct reflection or multipath signal propagation. For example, in urban residential districts often salient pairs of parallel lines of bright magnitude are observed at locations of gable-roofed buildings. The first line (closer to sensor) is due to direct reflection of planar roof parts orientated toward the sensor. The second line can be related to signal caused by a dihedral corner reflector between ground and building wall. In this paper an approach is presented aiming at reconstruction of gable-roofed buildings by knowledge based analysis considering the mentioned SAR-specific effects. First, line and edge primitives are segmented and grouped to parallel line pair objects. Then for each of these objects geometrical and radiometrical features are extracted in the InSAR images. Based on the interferometric elevation data in the adjacent area of the primitives the projection from slant range into ground range geometry is done. After geocoding, building hypotheses are built from the fused set of extracted primitives from both aspect directions. The estimation of the building height is carried out by two complementing methods: One is based on the extracted geometric parameters and the other on interferometric height data. The reconstruction results are quantitatively assessed by using a high resolution LIDAR surface model as ground truth data. [C2905]

"Quantitative analysis of texture parameter estimation in SAR images"

This paper deals with the validation of a previously developed texture model for SAR data as well as its associated parameter estimation algorithm. The mentioned model is named the Anisotropic Gaussian Kernel (AGK) model and allows the description of the possibly nonstationary and anisotropic behaviour of texture on heterogeneous areas of SAR images. The parameter estimation performance is evaluated over simulated data. We also investigate about the validity of our model over experimental data, by means of dissimilarity measures. [C2906]

"Estimation of 3-D Water vapor distribution using a network of compact microwave radiometers"

Quantitative precipitation forecasting is limited by the paucity of observations of water vapor in the troposphere. In particular, severe storms have been observed to develop in regions of strong and rapidly evolving moisture gradients. Conventional measurements of water vapor density profiles are obtained using in-situ probes on-board weather balloons, including radiosondes. These in-situ profile measurements have high vertical resolution, but have severe limitations in both temporal and spatial sampling. Lidars use differential absorption techniques to estimate water vapor with comparable resolution to that of radiosonde observations. However, lidars are expensive, and their operation is limited to clear-sky conditions due to the high opacity of clouds at optical wavelengths. Inversion of brightness temperatures measured by upward-looking, ground-based microwave radiometers allows the estimation of vertical profiles with high temporal resolution in both clear and cloudy

conditions. However, assimilation of retrieved water vapor fields with improved spatial coverage has the potential for more substantial impacts on numerical weather prediction of convective storm initiation. Measurements using a network of multi-frequency microwave radiometers can provide information to retrieve the 3-D distribution of water vapor in the troposphere. [C2907]

"GAS: the Geostationary Atmospheric Sounder"

This paper presents the concept and initial breadboarding results of geostationary atmospheric sounder (GAS), which is being developed by Saab Space AB and Omnisys AB, Sweden, and funded by European Space Agency (ESA). GAS utilizes interferometric synthetic aperture radiometry to obtain desired spatial (30 km) and temporal (nowcasting) resolution for measurement of atmospheric temperature and humidity profiles under all weather conditions. These parameters are decisively important to meteorological and climate models at all time scales. [C2908]

"Synthetic Aperture PAU: a new instrument to test potential improvements for future SMOSops"

This paper describes some potential improvements that could be eventually implemented for future MIRAS (Microwave Imaging Radiometer by Aperture Synthesis) payloads of the follow-on missions of the ESA's SMOS (Soil Moisture and Ocean Salinity) mission. A ground-based instrument concept demonstrator has been designed and it is being implemented to validate these improvements. Both MIRAS and the (Synthetic Aperture Passive Advanced Unit, SA-PAU) are Y shaped arrays, but the receiver topology and the processing unit are significantly different. This paper identifies the elements in the MIRAS's design that could be improved and presents a new instrument (Synthetic Aperture PAU) that could be used to test some potential improvements for future SMOSops (SMOS operational system). [C2909]

"Polarimetric temporal information for urban deformation map retrieval"

In this work, a preliminary study on the use of polarimetric persistent scatterers for differential interferometric applications within an urban environment is presented. The PolSAR measurements campaign that the RSLab of UPC is carrying on in the village of Salient using an X-Band ground-based SAR sensor is first described. The work is then focused on the additional information the knowledge of full scattering matrix [S] may provide with respect to the single polarization approach. The problem of instability of the polarimetric signature of urban targets is also analyzed. Finally, a solution based on the search of repeated patterns in the long-temporal profile of pixels' polarimetric signature is briefly introduced. [C2910]

"Classification comparisons between dual-pol and quad-pol SAR imagery"

We present a study of the polarimetric information content of dual-pol imaging modes, e.g. (HH, HV) and (VV, VH), and compare these against full quad-pol datasets. We discuss classification accuracies for various dual-pol datasets over several terrain/vegetation types with respect to the full quad-pol classification. The linear polarization modes implemented on space borne SAR systems are of primary importance. However, we also consider novel dual-pol modes, e.g. transmitting a circular polarization and receiving both H and V polarizations, and the so-call compact polarimetry models based on dual-pol data. Our primary emphasis is the inter-comparisons amongst the various dual-pol and compact polarimetric modes. [C2911]

"Analysis of fully polarimetric SAR data based on the Cloude-Pottier decomposition and the complex Wishart classifier"

An estimation of the number of clusters is proposed for fully polarimetric SAR data analysis, and a corresponding unsupervised segmentation algorithm is also given based on the Cloude-Pottier decomposition and the complex Wishart clustering. The Monte-Carlo Cross-Validation (MCCV) is used to estimate the optimal number of clusters to reveal the inner structure of the data. Since it is a quantitative estimation of the classification performance, the MCCV algorithm also has the potential capability to perform the unsupervised segmentation validation. The effectiveness of the MCCV estimation and the segmentation algorithm is demonstrated using ESAR data acquired. [C2912]

"Analysis of non-Gaussian POLSAR data"

In this paper we present a generalised Wishart classifier derived from a non-Gaussian model for polarimetric synthetic aperture radar (POLSAR) data. Our starting point is to demonstrate that the scale mixture of Gaussian (SMoG) distribution model is suitable for modelling POLSAR data. We show that the distribution of the sample covariance matrix for the SMoG model is given as a generalisation of the Wishart distribution, and present this expression in integral form. We then derive the closed form solution for one particular SMoG distribution, known

as the multivariate K-distribution. Based on this new distribution, termed the K-Wishart distribution, we propose a Bayesian classification scheme, which can be used in both supervised and unsupervised mode. Modelling and classification is tested on airborne EMISAR data. [C2913]

"Investigations on the TOPSAR acquisition mode with TerraSAR-X"

The paper reports about investigations on the implementation of the recently proposed TOPSAR acquisition mode with TerraSAR-X. Differently from ScanSAR, TOPSAR mode allows a wide swath coverage with nearly uniform signal to noise ratio (SNR), therefore avoiding scalloping and azimuth dependent SNR. To achieve this goal the antenna beam is steered within the different swaths in the along-track direction. TerraSAR-X can electronically steer the azimuth beam; however, angle quantization is introduced because of the limited number of available azimuth beams per data take. The effects of the TerraSAR-X angle quantization of the antenna steering are analyzed resulting in a negligible distortion. The maximum azimuth steering angle of TerraSAR-X allows the implementation of TOPSAR with the same coverage and resolution as the nominal TerraSAR-X ScanSAR mode, four range subswaths with 16 m azimuth resolution and a total swath of 100 km. Finally, TerraSAR-X TOPSAR interferometry capability and the possibility of using an inverse TOPSAR configuration are discussed. [C2914]

"Tomographic processing of multi-baseline P-band SAR data for imaging of a forested area"

Recently, various attempts have been undertaken to obtain information about the structure of forested areas from multi-baseline synthetic aperture radar data. Tomographic processing of such data has been demonstrated but the quality of the focused tomographic image is limited by several factors. In particular Fourier-based focusing methods are susceptible to irregular and sparse sampling, two problems, that are unavoidable in case of multi-pass, multi-baseline SAR data acquired by an airborne system. We propose a tomographic focusing method based on the time-domain back-projection algorithm, which maintains the geometric relationship between the original sensor positions and the imaged target and is therefore able to cope with irregular sampling without introducing any approximations with respect to the geometry. We assess the tomographic focusing quality with the help of the impulse response of simulated point targets and an in-scene corner reflector. And, in particular, preliminary results obtained with the newly acquired P-band tomographic data set consisting of eleven flight tracks are presented. [C2915]

"Monitoring temperate glaciers by high resolution Pol-InSAR data: First analysis of Argentine E-SAR acquisitions and in-situ measurements"

This paper highlights the potential to measure temperate glacier velocities and surface characteristics by airborne interferometric and polarimetric SAR remote sensing. Indeed, a novel SAR airborne campaign took place in October 2006 over two Alpine glaciers. Simultaneously to the acquisition of repeat pass interferometric, polarimetric and multi-band data, in-situ measurements were carried out to provide useful information for the SAR synthesis, for backscattering analysis and for performance assessment. Analysis of the experimental data as well as early PolInSAR processing results regarding information extraction are presented. [C2916]

"Sub-band interferometry on polarimetric SAR dataset"

Complex SAR image spectral analysis has been shown to provide interesting information about the scattering media, highlighting differences in behavior between homogeneous areas with a fully-developed speckle and point scatterers potentially presenting a more coherent radar spectral response. In the line of previously published works by other groups dealing with coherent scatterers, we have studied the statistics of their occurrence as a function of several parameters like frequency, resolution or polarization. The first step of our procedure consists in selecting two or more sub-bands in the Doppler spectrum (in the azimuth direction) or in the distance direction. The sub-bands are subsequently frequency-shifted in order to provide a nonzero correlation. The resulting inter sub-band interferograms are explored to identify the points presenting a significant coherence and the relevance of the associated phase is investigated. The number of detected coherent scatterers, and the associated complex correlation coefficient is analyzed, with respect to the different polarizations, the width of the sub-bands and the distance between the sub-bands. Different polarimetric high resolution SAR datasets acquired with the ONERA airborne system RAMSES have been used. The large panel of RAMSES acquired datasets allows the exploration of the influence of frequency (P, L and X bands) and landscape. The theoretical approach will be detailed, and experimental results will be discussed. [C2917]

"Review of existing monographs and books on radar polarimetry and polarimetric SAR with the aim of justifying the need of updates"

Radar Polarimetry, Radar Interferometry and Polarimetric SAR Interferometry represent the current culmination in active 'Microwave Remote Sensing' technology, but we still need to progress considerably more in order to reach the limits of physical realizability. Whereas with radar polarimetry the textural fine-structure, target orientation, symmetries and material constituents can be recovered with considerable improvement above that of standard 'amplitude-only radar', by implementing 'radar interferometry' the spatial (in depth) structure can be explored. With Polarimetric Interferometric Synthetic Aperture Radar (POL-IN-SAR) imaging, it is possible to recover such co-registered textural and spatial information from POL-IN-SAR digital image data sets simultaneously, including the extraction of Digital Elevation Maps (DEM) from either Polarimetric (scattering matrix) or Interferometric (dual antenna) SAR systems. However, in order to further advance this promising technology, we require pertinent basic educational and advanced research texts plus application oriented books for the practicing engineering scientists and users. Hitherto there are not available satisfactory updated sets of basic books or application oriented handbooks. Therefore, in this paper a succinct review of the existing pertinent monographs, books and guides will be presented with the aim of identifying particular topics that still need to be covered. We do now require these urgently associated sets of revised and updated multi-lingual (English, Japanese, Korean, Chinese) books. [C2918]

"Evaluation and bias removal of multi-look effect on entropy/alpha/anisotropy"

Entropy, alpha and anisotropy ($H/\alpha/A$) of the polarimetric target decomposition has been an effective and popular tool for polarimetric SAR image analysis and geophysical parameter estimation. However, multi-look processing can severely affects the values of these parameters. In this paper, we evaluate the bias problem in $H/\alpha/A$ due to insufficient averaging. We found that the estimated bias is radar frequency dependent. A procedure for bias compensation is proposed. Data from L-band DLR/E-SAR and L-band JPL/AIRSAR, and X-band PI-SAR data are used for demonstration in this study. [C2919]

"Multidimensional speckle noise reduction in synthetic aperture radar images"

A new approach to filter speckle noise in multidimensional SAR data, based on the multiplicative-additive speckle noise model, is presented. This approach is based on processing the elements of the sample covariance matrix differently, according to the complex correlation coefficient. As it is demonstrated with experimental PolSAR data, the filter does not produce a loss of information, but an improvement of the capabilities to filter speckle noise. [C2920]

"Localizing metallic small spheres by a linear distributional approach"

The problem of determining the number and the locations of "small" metallic spheres from scattered far-field measurements under plane waves incidence is considered. The problem is formulated by neglecting the mutual scattering between the spheres and by representing their locations as the support of delta-functions. This allows to cast the problem as the inversion of a linear integral operator we tackle by means of a Truncated Singular Value Decomposition. The performance of the inversion scheme are analyzed for both the cases of a multi-view/single-frequency and a single-view/multi-frequency configuration by exploiting synthetic exact data. [C2921]

"Phase distortion modelling due to motion in wave scattering mechanism applied to SAR images analysis"

In SAR image processing, taking phase distortion in radar signals into account is equivalent to considering motion as information embedded in it. In the aim of doing this, a model based on Gaussian linear frequency modulation is introduced, adapted to quantification and estimation of phase distortion. This model is based on three parameters, the Doppler frequency modulation rate K , the analysis time T_a and the Doppler frequency f_d , and allows practically a local representation of any quasi-punctal target echo. [C2922]

"Spaceborne SAR raw signal simulation of ocean scene"

According to fractal ocean surface model, electromagnetic scattering model under Kirchhoff approximation and the raw signal simulation procedure of dynamic scene based on time domain, spaceborne synthetic aperture radar (SAR) raw signal of ocean scene is generated. The SAR images obtained from the echo of both simple cosine wave and complex fractal ocean surface are in accordance with the tilt modulation and the velocity bunching theoretically, and also with the statistical properties of real ocean SAR images, which validate the simulation procedure. The raw signal could be the input data of studying along-track InSAR (ATI) for ocean current measurements. [C2923]

"The extraction of ocean wind, wave, and current parameters using SAR imagery"

Recently satellite SAR techniques have become essential observation tools for various ocean phenomena such as wind, wave and current. The CMOD4 and CMOD-IFR2 models are used to calculate the magnitude of wind at SAR resolution with no directional information. Combination of the wave-SAR spectrum analysis and the inter-look cross-spectra techniques provides amplitude and direction of the ocean wave over a square-km sized imagette. The Doppler shift measurement of SAR image yields surface speed of the ocean current along the radar looking direction at imagette resolution. In this paper we report the development of a SAR Ocean Processor (SOP) incorporating all of these techniques. We have applied the SOP to several RADARSAT-1 images along the coast of Korean peninsula and compared the results with oceanographic data, which showed reliability of space-borne SAR based oceanographic research. [C2924]

"ISAR imaging of targets with moving parts using micro-doppler detection on the range profile image"

In ISAR imaging, most works have assumed the target to be a rigid body, a body without any rotating, vibrating or moving parts. The rotation of structures in a target, such as the rotor of a helicopter or the turret of a tank target, may induce frequency modulation on the returned signals and generate sidebands about the center frequency of the target's body Doppler frequency, known as the micro-Doppler phenomenon. In this paper we present a new method based on range grouping of the target's range profile for the separation of the rotating or moving parts from the target's body. The method is carried out on the Range Profile Image, different from other methods that do the separation at the signal level. [C2925]

"Combined wavelet and curvelet denoising of SAR images using TV segmentation"

Synthetic aperture radar (SAR) images are corrupted by speckle noise due to random interference of electromagnetic waves. The speckle degrades the quality of the images and makes interpretations, analysis and classifications of SAR images harder. Therefore, some speckle reduction is necessary prior to the processing of SAR images. The speckle noise can be modeled as multiplicative i.i.d. Rayleigh noise. The discrete curvelet transform is a new image representation approach that codes image edges more efficiently than the wavelet transform. On the other hand, wavelet transform codes homogeneous areas better than curvelet transform. In this paper, two combinations of time invariant wavelet and curvelet transforms will be used for denoising of SAR images. Both of the methods use the wavelet transform to denoise homogeneous areas and the curvelet transform to denoise areas with edges. The segmentation between homogeneous areas and areas with edges is done by using total variation segmentation. Simulation results suggested that these denoised schemas can achieve good and clean images. [C2926]

"Variational-based speckle noise removal of SAR imagery"

In this paper we present a variational method for synthetic aperture radar (SAR) speckle removal. Variational method is a newly developed technique for the removal of SAR's multiplicative noise. For an image, we could define an energy functional. The energy evolves as the original image changes, and the minimum energy corresponds to the speckle reduced result. Partial differential equation (PDE) technique is used to get the minimal solution. Our energy functional makes use of the statistical information of the multiplicative noise since it follows a Gamma law with mean $\mu = 1$ and variance $\sigma^2 = 1/M$ for M-look SAR. Our energy is a regularization term with two constraints. The regularization term is the integral for the norm of image gradient; two constraints are the mean of noise should be 1 and the variance of noise should be $1/M$. We use the method of Lagrange multipliers, Euler-Lagrange equation and heat flow method to obtain the minimizer of the energy. ERS Precision Image (PRI) data are to demonstrate our algorithm. Numerical result shows that the speckle reduced image preserves edges and point targets while smoothes homogenous regions in the original image. The algorithm is computationally efficient and easy to implement. [C2927]

"Parallel computation of synthetic SAR raw data"

For modern SAR data acquisition, bi- and multistatic SAR missions become increasingly important. Established methods for processing monostatic SAR signals need to be adapted to new algorithms for signal processing. In order to support the evolution and development of these new algorithms simulated SAR raw data of arbitrary bi- and multistatic SAR scenarios are essential. This paper refers to a modular SAR simulator, which is able to simulate complex bi- and multistatic SAR scenarios. It focuses on the geometrical simulation approach of the simulator and the computationally intensive synthesis of SAR raw data. The main part describes the parallel implementation of the radar lobe footprint scan and of the succeeding SAR raw data generation executed on a compute cluster. An example will be shown, which compares the simulation of the same SAR scenario on three different compute systems and their runtimes. [C2928]

"Three dimensional SAR image focusing from non-uniform samples"

Multiple SAR signals acquired along different orbits can be exploited for reconstructing a three dimensional (3-D) reflectivity profile of the scene along azimuth, range and elevation co-ordinates. For the 3-D image formation, the problem of the non-uniform spacing of the orbits has to be considered. In this paper we propose a technique based on two steps: 1) a preprocessing step, in which the samples of the multi-pass signal is computed on a grid which is uniform in the elevation direction, starting from its unevenly spaced samples; 2) a 3-D image focusing based on a simple 3-D convolution operator. The technique proposed has the main advantages of preserving numerical efficiency and allowing to easily include information on the signals bandwidth in the pre-processing step, in such a way to regularize the problem and obtain stable solutions. [C2929]

"Geological lineament and shoreline detection in SAR images"

In this paper, an algorithm for unsupervised detection of linear structures, in particular, the geological lineament and shoreline, as seen in Synthetic Aperture Radar (SAR) satellite images is proposed. Methodologies to extract linear features consist of three stages. First, the refined local statistics filter is used to remove the speckle noise on the raw image. The likelihood ratio edge detector and local non-maximal suppression are performed on the result images for edge enhancements and detection. In the second stage, mathematical morphology techniques are used to reconnect the fragmented lines and remove the uninterested patterns in the binary image which is produced by thresholding the enhanced image after edge detection. Spatial statistics including spatial mean and spreading coefficient of each cluster (object) in the binary image are calculated in order to simply classify their shapes. The clusters with large spreading coefficient will be remained and others will be removed. Finally, in the third stage, the edge features detected will be described by chain code method and polygonal approximation. The last stage contains many substeps such as edge thinning and curve pruning. [C2930]

"A multiprocessing framework for SAR image processing"

This paper introduces a framework developed for image processing of synthetic aperture radar (SAR) images. It encapsulates features of modern hardware architectures, including symmetric and asymmetric multiprocessing, within an easy and intuitive to use application programming interface (API). The multiprocessing part is designed for unified usage of different architectures reaching from multicore processors to cluster of workstations to grids of clusters. So an application using the framework can be ported from one architecture to another without any changes in the source code. The framework builds the bottom layer of the processing system developed for the German Aerospace Center's (DLR) new airborne SAR sensor, the F-SAR [1]. [C2931]

"Evaluation of the single and two data set STAP detection algorithms using measured data"

Traditional space time adaptive processors for radar target detection require a training data set which is usually drawn from adjacent range gates. Clutter heterogeneity, however, can severely limit the available training sample support and consequently degrade the detection performance. The SDS algorithms, on the other hand, overcome this problem by operating solely on the test data without recourse to training data. In this paper we evaluate both of these approaches, in particular the AMF and MLED, using the MCARM data set. We illustrate the performance degradation of the AMF that results from the clutter heterogeneity and the corresponding advantage of the MLED. We also show that a calibration step of the spatial steering vectors results in significant performance improvement of all of the algorithms considered here. [C2932]

"Application of 3D-SAR nearfield imaging algorithms to GPR data"

This contribution addresses the utilization of near field 3D-SAR imaging algorithms applied to radar data from an ultra wideband (UWB) ground penetrating radar (GPR) system. The measured data were collected at the test field of the multi sensor mine signature (MsMs) group at the European Joint Research Centre (JRC) in Ispra/IT. The layout of this test field was designed for the more difficult problem of detecting targets representing anti-personnel mines. The 3D-SAR imaging algorithms can be implemented in time-domain or frequency domain. This contribution focuses on the time-domain implementation. The influence of the quality of the 3D-SAR imaging algorithm on the performance of an automated detection process is evaluated. [C2933]

"Target recognition in SAR images with Support Vector Machines (SVM)"

This paper addresses object recognition problem in SAR images with SVM classifier; the work has been mainly focused on feature vector definition. Actually, each object is represented by a feature vector and SVM aims to estimate the best hyperplanes that separate classes in the feature space. Very robust definition of feature vector is proposed and tested on real data (MSTAR database). Confusion matrices prove that a very good recognition rate is reached, even for mixed incidence angles configuration. [C2934]

"Elimination of oil spill like structures from radar image using MODIS data"

Oil-spill detection from radar imagery is a complicated task in Estonian coastal sea where look-alikes caused by ice, upwelling events, cyanobacterial blooms may occur. We compared SAR image with the MODIS optical imagery and look-alikes caused by upwelling event and cyanobacterial bloom were detected from images of August 7, 2007. Analysis of MODIS imagery from years 2000-2006 showed that during the ice free period upwellings occur frequently in the Gulf of Finland and they are strongest during summertime stratification period. Cyanobacterial blooms occurred in July and August in Estonian coastal sea. Some ice cover is present in Estonian coastal sea every winter. [C2935]

"Measurement and analysis of depolarization generated by scattering over constructive obstacles at 5.8 GHz"

The interest on the scattering due to constructive obstacles appears in different knowledge areas, mainly radar theory and mobile communications. In radar terms, a target can be identified by means of its scattering pattern. Those patterns are also useful in radio communications, in order to obtain confident models for planning the deployment of networks. If co-polar scattering itself gives an important amount of knowledge, the definition of the obstacle is better done when cross-polar data is incorporated. In order to characterize the scattering patterns due to constructive walls, a measurement campaign has been developed, using an automated system, which integrates the mechanical movement to the vector network analyzer control. The aim of the campaign was to check the reflection behavior of different constructive materials. All the experimental work has been performed at the frequency band around 5.8 GHz. Materials considered are a metallic surface, used as a reference, a brick wall, and a chip wood panel. All sample sizes are large enough to ensure that the 3-dB illuminated area, an ellipse with a major axis of 80 cm, falls within the limits of the slabs, thus reducing any diffraction effects on the edges of the samples. As measurements were performed in co-polar and cross-polar polarizations, both co-polar scattering pattern analysis and depolarization index computations could be made. By means of cross-polar measurements, depolarization indexes can be extracted. This magnitude indicates the percentage of the incident wave that is reflected in the orthogonal polarization. The values obtained for the chip wood panel are between 2 and 3%, and those corresponding to the brick wall are clearly polarization-dependent, being 8% for parallel incidence and 0.4% for perpendicular incidence. [C2936]

"Steerable filter based multiscale registration method for JERS-1 SAR and ASTER images"

It is a challenging problem to automatically register the SAR and optical satellite images in remote sensing applications. In this paper, a novel intensity based multiscale registration method using steerable Simoncelli filters is proposed to register JERS-1 SAR and ASTER images. The mutual information is used as the similarity measure, and a hybrid search technique is used to do the parameter optimization. The experimental results showed that the proposed registration scheme is competent for JERS-1 SAR and ASTER images, though the robustness of this scheme should be verified further more. [C2937]

"Design of GMTI combining networks"

Multichannel radar systems are of choice for ground moving target indication (GMTI) since they allow for a joint space-time processing of the received data that enables an efficient suppression of ground clutter returns. The design of the receiving sensor group is driven by the performance specifications of the intended GMTI modus, which usually requires the sensor array to consist of a few hundred up to a few thousand elements. Though desirable, a full digital processing of all receiving channels is practically not feasible due to both hardware constraints and computational load. The formation of sub-arrays using a proper combining network before A/D conversion reduces the number of processing channels while maintaining the advantages of the full array. In this paper the impact of the combining network design on the GMTI performance of a simulated airborne multichannel radar system is investigated. [C2938]

"CAESAR-XInSAR: A new software for interferometric SAR processing"

In order to meet the need of the development in interferometric SAR, especially the development of Permanent Scatterers InSAR (PS-InSAR) in these years, we develop a new software called CAESAR-XInSAR at the Remote-Sensing Satellite Ground Station, CAS. Both conventional InSAR and PS-InSAR are considered in this system. It supports the interferometric processing from SAR SLC data to end products of DEM or surface deformation map. It is organized in different modules and developed in Visual C++ 6.0 environment on PC under windows operating system. It is currently at the stage of the development from scientific platform to operational system. In this paper, the organization and the modules of this system are described and the results from CAESAR-XInSAR are also processed in the end. [C2939]

"Relationship between antenna pointing stability and spaceborne ScanSAR scalloping calibration"

Based on uniform weighting antenna model, the Doppler center frequency error from instability of antenna pointing is derived in detail for spaceborne scanning synthetic aperture radar (ScanSAR) system. And the effects of Doppler center frequency error on image radiometric correction are analyzed. The basic precision of the antenna pointing stability is present for the offsets of ScanSAR image radiometric correction, which is verified by simulations. [C2940]

"Semi-automatic fast recognition of areas of interest for SAR image interpretation"

The framework of this study is focused on semiautomatic fast recognition of areas of interest for SAR images. The intended goal is to label regions in an image as fast as possible, into classes significant for a given application. The proposed approach defines the information extraction as a two-level procedure. First, a segmentation technique is applied to obtain an image partition in homogeneous regions, this property being of a crucial interest for the rest of the process. Then, several measures are computed over regions, considered at this level as "objects", in order to identify at which typical class of land-cover they can be attached. Among a large set of measures experimented, we will point out the most pertinent ones for the considered SAR images. In this paper, we focus more on "forest"/"field" areas extraction in SAR images, and show that the discrimination results obtained here are more precise than in a "classical" purely raster classification process. The proposed approach can be extended to discriminate other classes from high resolution SAR images. [C2941]

"Target separation in SAR image with the MUSIC algorithm"

The aim of this work is to exploit the MUSIC algorithm performance in order to enhance target separability in range and azimuth, i.e. achieve point targets separation inside a resolution cell. Simulations have been done in order to plan and check the feasibility of a super-resolution experiment that took place in September 2006 on the test site of Oberpfaffenhofen (Germany). The data set has been acquired with the E-SAR system of the DLR in X-band. The targets to be separated were seven small corner reflectors that have been placed in a way that their response falls in one or, at maximum, two resolution cells of the standard Fourier SAR image. A post-processing implementation of the MUSIC algorithm has been proposed allowing, in the already focused SAR image, to retrieve the targets geometry. Conditions and analysis of the results have been carried out. [C2942]

"Multi-track PS-InSAR datum connection"

InSAR data acquired from independent overlapping tracks can be exploited for a reliability assessment of the Persistent Scatterer InSAR (PS-InSAR) technique. This is obtained by means of the datum connection of multiple tracks, simultaneously evaluating the misclosures between multi-track PS-InSAR estimates. Due to a different viewing geometry, many of the detected PS will physically not be the same. However, their estimates may still refer to the same deformation signal. The existence of independent observations of the same deformation signal provides a powerful tool to increase the redundancy and evaluate the reliability. The datum connection can be subdivided in two steps. The first step consists of the conversion of PS locations to a common datum. Secondly, the PS-InSAR parameter estimates (velocities, displacements, heights) are connected. In stead of the conventional approach of separately geocoding each track, we propose the use of a common radar datum defined by the acquisition geometry of the 'master track'. Multi-track datum connection has been applied in the Groningen region, the Netherlands, which is affected by subsidence due to gas extraction with displacement rates up to 7 mm/year. The main reservoir is (partly) visible in 6 independent overlapping ERS tracks from 1992 (ascending and descending). Datum connection resulted in a consistent set of PS-InSAR deformation estimates. Additionally, the deformation signal was decomposed in horizontal and vertical movements, utilizing the different viewing geometries of the tracks. [C2943]

"Inland lake monitoring using low and medium resolution ENVISAT ASAR and optical data: Case study of Poyang Lake (Jiangxi, P.R. China)"

Poyang Lake, one of the most regularly flooded areas in China, can be considered as a key natural flood control and reduction element within the Changjiang middle basin. Within the Flood DRAGON Project, part of the MOST-ESA DRAGON Programme, Poyang Lake's water extent was monitored based on 64 ENVISAT low and medium resolution ASAR and MERIS Full Resolution data, over a two and half year period. It's the first time that such an amount of ENVISAT data was exploited in monitoring inland lake water extent variations. This original integration approach permitted: lake-surface variation analysis, yearly submersion-time estimation, and the recognition of three hydrological sub-systems. The results highlight the great potential of ENVISAT and more largely of Earth Observation Medium Resolution data in monitoring and managing large inland water bodies. This approach can be applied worldwide in a global climate change context. [C2944]

"Identification of inland fresh water wetland using SAR and ETM+ data"

The main aim of this paper was to explore the potential of SAR data, in combination with optical remote sensing data, in identifying inland fresh water wetland from crop, especially rice paddy. The test area is a part of Hongze Lake, the fourth biggest fresh water lake in China. It is one of important wetlands for migratory birds in China. Due to unreasonable exploitation of wetland resources, the lake is facing a great loss of wetland. In Hongze lake watershed, Jiangsu Provincial Sihong Hongze Lake wetland ecological reserve was established for the preserve of wetland ecosystem and rare species in the watershed. In the processing of the dataset, clustering algorithm ISODATA was employed firstly to generate initial classification results for sample selection. Then, 1500 samples were taken in total by using stratified random sampling. These samples were superimposed on the screen on top of rectified aerial images. The land cover class at each point was determined based on field investigation and visual interpretation. 900 samples of them were for training and the other for the assessment of classification accuracy. Attributes of samples such as the digital number values of six bands of ETM+(TM1-5, 7), texture, DEM and 4 components of principal components analysis of six bands of ETM + data, were fed into the CART (Classification and Regression Tree) algorithm for the generation of knowledge rules. Because the training observations were evenly distributed among classes, the class assignment at each terminal node was determined by the majority of per-class observations at that node. Then, decision tree classifier was applied to the imagery of ETM+ for the classification of landuse/cover in the whole study area. RADARSAT SAR C-band was classified into four classes: lowest backscatter, low backscatter, medium and high backscatter. The results from two data sources were combined by using rules. The results showed that the combination of the SAR data and the optical remotely sensed data have achieved the highest classification accuracy (92.3% of total classification accuracy). The results also confirmed the value of classification tree in the identification of fresh water wetland. It was illustrated that radar data was a good complementary data source for the identification of wetland. [C2945]

"Analysis of urban land use pattern based on high resolution radar imagery"

The actual process of rapid urbanization is associated with various ecological, social and economic changes in both the urban area and the adjacent natural environment. To keep up with the effects and impacts of this development, effective urban and regional planning requires accurate and up-to-date information on the urban dynamics. Recent studies have proven the applicability of high resolution optical satellite data for the acquisition of some of the requisite spatial and socio-economic information. Although radar data is more reliably available than optical imagery, high resolution radar imagery has barely been employed for urban applications so far. This fact is mainly due to a lack of civil space borne radar systems featuring a ground resolution which is suitable for the analysis of urban structures. Additionally significant difficulties concerning the interpretation of according data over highly structured urban areas occur. The german TerraSAR-X system will provide radar imagery with a spatial resolution comparable to actual high resolution optical platforms. This study investigates the potential use of high resolution radar data in the context of urban applications. Thereby a concept-that was developed on the basis of SAR data recorded by DLR's airborne E-SAR system-will be adapted to an analysis of TerraSAR-X imagery. It introduces a temporally and spatially robust approach towards an automated analysis of the urban structure. For that purpose data sets of single-polarised X-band imagery are analysed by means of an object-oriented classification. This study includes the development of an improved image segmentation procedure in order to create meaningful spatial entities. Moreover, it contains the definition and application of a rule base for the detection of built-up areas, the derivation of the urban land cover and the generation of additional value-added information related to the urban structure. [C2946]

"DEM estimation from multi-Baseline ENVISAT- ASAR interferometric data through maximum likelihood techniques"

In this paper, two techniques for estimating accurate height profiles of the ground, using multi-baselines interferometric synthetic aperture radar (In-SAR) data and an a-priori inaccurate digital elevation model (DEM) of the observed scene, are analyzed. The methods are both based on maximum likelihood (ML) estimation: the first estimates directly the quota of each pixel of the image, independently from the other pixels, while the latter estimates the parameters of the local planes which best approximate, in the ML sense, the height profile in a small neighborhood of each pixel. The inclusion of this contextual information allows improving the estimation accuracy. Results on simulated and real ENVISAT-ASAR data are presented. [C2947]

"Improving interferometric radar measurement accuracy using local meteorological data"

Permanent monitoring of potential rock-slide area can be done using interferometric radar measurements where the accuracy is limited by the variation of the velocity of light, i.e. variation of the refractive index. Using

differential interferometric measurements, the measurement accuracy can be very good if the distance between the reference and the potential rock-slide area is small. However, if the distance to the reference is large or if using a reference is not possible, the measured accuracy is dependent on the variation of the refractive index. Using meteorological data at the radar site, the refractive index can be estimated locally. The results show that the meteorological data can improve the interferometric radar measurement accuracy. [C2948]

"Uncertainty analysis of flood disaster assessment using radar imagery"

Flood is a paroxysmal natural disaster, which results in vast damage to economy in China every year. Precise loss evaluation is an effective method to alleviate the loss. The inundated area, on which loss evaluation is based, is the most fundamental element to evaluate the loss caused by floods, and is a critical step to control the precision of the loss evaluation. Satellite SAR imagery is broadly used in monitoring and evaluating flood disaster. Spatial resolutions of radar images and ground scale are crucial to the extraction of inundated area in the process of disaster monitoring. In order to calculate the error of the statistic of submerged areas in the process of remote sensing disaster monitoring using Radarsat imagery, we take the Airborne SAR image as ground truth data and calculate the error brought by radarsat data, we get the explicit error finally. By performing the test and precision appraisal of the remote sensing monitoring process aiming at the same study area and the same disaster event, and promotes the precision and credibility of remote sensing monitoring. [C2949]

"Semiautomatic reconstruction of building height and footprints from single satellite images"

Extraction of man-made structures from satellite images is one of the essential issues in remote sensing and many techniques were proposed for building extraction from high resolution satellite images. However, most of them rely stereo analysis or additional data sources such as LIDAR for retrieval of 3D building information. This paper proposes a semiautomatic approach that extracts 3D building information from single satellite images. In this approach, after measuring boundaries of a building roof we determine the building height by projecting building shadow onto the image space until the projected shadow matches the actual shadow. Then we extract building footprints by translating roof boundaries along the direction of vertical edges to the amount determined by the building height. To increase the level of automation, we devised a technique that adjusts the height so that the projected shadow matches the actual shadow and determine building height automatically. We also devised a technique to extract roof boundaries by clicking only two corner points. A panchromatic IKONOS image and Quickbird image over Deajeon area were used to test proposed algorithms and a IKONO stereo pair was used to get reference building heights. While building heights determined manually showed the accuracy of an RMS error of 1.66 m, the heights determined automatically showed an RMS error of 1.86 m. The results show that 3D building information can be extracted from single satellite images and that the automation approaches proposed in this paper worked. [C2950]

"Typhoon monitoring/operational forecasting and services 2005 in China"

Typhoons bring about serious damage to China. The forecasters of CMA predict typhoon track and rainfall intensity with numerical model, satellite imagines, radar data, automatic station data etc. There are 7 landfalling typhoons in China in 2005. Among these typhoons, Haitang has some characters of high intensity, strong wind, long maintenance over land etc. Its track and rainfall were predicted with numerical model successfully. Typhoon Matsa move towards northwest after landfall, overlapping with the astronomical tide forming strong storm surge. Warnings and disaster prevention and preparedness were in time but there was certain rainfall forecasting bias existed when Matsa move towards north and northeast. [C2951]

"Small scale surface deformation detection of the Gulf of Corinth (Hellas) using Permanent Scatterers technique"

The Permanent Scatterers (PS) technique, invented by Politecnico di Milano research team, is an approach that minimises the undesirable noise components in the classic InSAR technique, such as spatial and temporal decorrelations, signal delay due to tropospheric and ionospheric disturbances, orbital errors as well as topographical errors. This approach is suitable for the measurement of near vertical displacements of the order of ~1 mm per year. It exploits almost all of the available SAR interferometric data over an area and requires availability of natural and/or artificial permanent scatterers. In this study we describe the implementation of the PS technique, called PerSePHONE (Permanent Scatterers Project Held by the Observatory, National, of Hellas). Its development has been based on a number of algorithmic adaptations, as well as new approaches in PS candidate selection. An example of this implementation is shown for the case of the Corinth Rift area (Hellas). [C2952]

"SAR measurements of surface displacements at Augustine volcano, Alaska from 1992 to 2005"

Augustine volcano is an active stratovolcano located at the southwest of Anchorage, Alaska. Augustine volcano had experienced seven significantly explosive eruptions in 1812, 1883, 1908, 1935, 1963, 1976, and 1986, and a minor eruption in January 2006. We measured the surface displacements of the volcano by radar interferometry and GPS before and after the eruption in 2006. ERS-1/2, RADARSAT-1 and ENVISAT SAR data were used for the study. Multiple interferograms were stacked to reduce artifacts caused by different atmospheric conditions. Least square (LS) method was used to reduce atmospheric artifacts. Singular value decomposition (SVD) method was applied for retrieval of time sequential deformations. Satellite radar interferometry helps to understand the surface displacements system of Augustine volcano. [C2953]

"Offset Phase Estimation in Multi-Channel InSAR DEM Reconstruction"

Interferometric SAR (InSAR) systems are able to estimate height profiles of the Earth surface. For the involved estimation problem, Maximum A Posteriori (MAP) statistical technique and Markov Random Field image models have been used, showing to be effective in case of multiple interferograms, obtained via different baselines/frequencies. In this paper, we face the problem of unknown phase offsets presence affecting real interferograms, which makes impossible to retrieve correct height estimations. We present a procedure to estimate these offset values, based on statistical estimation and we test it both on simulated and real data, showing the effectiveness of the method. [C2954]

"DEM calibration concept for TanDEM-X"

The TanDEM-X mission [1] comprises two fully active synthetic aperture radar satellites operating in X-band. The primary goal of this mission is the derivation of a high-precision global Digital Elevation Model (DEM) according to HRTI level 3 quality [2]. This requires accurate calibration of the interferometric system parameters. Content of this paper is the development of a general concept for this calibration, which comprises the determination of instrument and baseline errors, an adjustment concept and the distribution of control points. This concept has a key incidence on mission aspects like the data acquisition plan and the data take adjustment procedure. [C2955]

"Investigation of creation methods of digital elevation model"

The investigation of the existing techniques of phase unwrapping has been carried out. [C2956]

"Statistical description of tropospheric delay for InSAR: Overview and a new model"

This paper focuses on statistical modeling of water vapor fluctuations for InSAR. The structure function and power spectral density approaches are reviewed, summarizing their assumptions and results. The linking equations between these modeling techniques are reported. A structure function model of zenith tropospheric propagation delay is then derived from a two-regime power spectral density function presented in literature. The novelty lies in the fact that a closed form expression is derived and a free model parameter is allowed, which may be tuned to available measurements or, in the absence of these, to atmospheric statistics. The latter approach is used to compare the derived model with previously published results. [C2957]

"Impact of SAR impulse response function in interferometric measurement"

The stable point network (SPN) is a persistent scatterer interferometric technique developed by ALTAMIRA INFORMATION in 2001. The technique makes use of both ERS SAR and/or ASAR differential phase measurements to generate long term terrain movement and precise height maps with the same resolution as the original SAR images. The algorithm is capable to use all the available phase information even in conditions of large baselines or platform instabilities giving place to large Doppler centroid variations. Such behaviour is handled by precise location estimate of the scatterer within the pixel and accurate elevation extraction which permits the exact location of the radar measurement in ground geometry. However not all the SPN interferometric measurements within a pixel have a direct correspondence in the real scene. Some points presented as measurement points may not be related to existing structures on ground but directly generated by the processing itself. For instance, several artifacts can be created in the Synthetic Aperture Radar images due to the signal acquisition system. Azimuth ambiguities are one of them. They may appear as strong targets in low backscattering areas like forest or water. Secondary lobes of strong targets are also an issue. Since low level signals can be masked by the side lobes of higher level signals. They cannot be handled like standard scatterers and present completely different geometric behaviour not related to their position in the radar image. This paper discusses the way to identify those artifacts and analyses their impact on SPN measurements compared to their reference points (centre of the main lobe). [C2958]

"Mixture model for the segmentation of the InSAR coherence map"

In this work, we classify the interferometric SAR (InSAR) coherence map into three classes using the Bayes' theorem. The segmentation procedure is performed using a mixture modelling of the coherence map. The multimodal density of the mixture comprises three component functions characterizing different land surface categories (lake, bare soil, urban ...). This work is an ameliorated segmentation approach of that published by the authors in R. Abdelfattah, et. al., (2006). We test the performance of the proposed mixture model on a dataset about regions with different geophysical characteristics and different time interval between the acquisitions. The results of this study could be used as a supervised learning step for an automatic land cover classification algorithm. This new method classifying the image considering the corresponding InSAR coherence map is particularly powerful for the detection of layover and shadow regions. [C2959]

"Development of a baseband signal ATI-SAR simulator for ground moving target indication"

Along-track SAR interferometry has long been used to measure ocean surface currents with small velocities. There is a significant potential to employ this technique to detect slow ground moving targets with small radar cross-sections. In this paper, we present the development of a baseband signal simulator on ground moving target indication with along-track SAR interferometry. We summarize current state-of-the-art along-track SAR interferometry techniques and algorithm developments for ground moving target detection, and consider the case of an airborne SAR operated in the stripmap mode. And then we propose to investigate and develop advanced techniques for potential civilian and military applications in Australia. [C2960]

"A multi-baseline InSAR DEM reconstruction approach without ground control points"

Distributed spaceborne interferometric synthetic aperture radar (DS-InSAR) system includes more than one baseline, so it is also called multi-baseline InSAR system. It offers additional observation information for the derivation of position and height of object, compared to the single-baseline InSAR system. Based on the additional information it offers, a new DEM reconstruction approach of multi-baseline InSAR system is proposed. At first, theory of the approach is introduced and DEM reconstruction equations are derived. Then, error sensitivity analysis is made by first order approximation of Taylor expanding, which is validated by Monte-Carlo simulation. The results show that theoretical error analysis formula can give support for analysis and design of the system directly and the DEM accuracy is very sensitive to the interferometric phase difference error. [C2961]

"Remote sensing of glacier by ground-based radar interferometry"

The Belvedere Glacier, east face of Monte Rosa, has been investigated for many decades because of a long history of outburst threatening the village of Macugnaga and, in the latest years, a surge-type evolution, responsible for the formation of a large depression at the foot of the east wall of Monte Rosa, which hosted a supraglacial lake named "Lago Effimero" in summer 2002. In this contribution, a Ground Based SAR (GB-SAR) interferometer was employed for determining the ice-flow velocity of the illuminated part of the Belvedere Glacier in order to enhance the understanding of ice flow mechanics and hopefully reduce the glacier hazard. The deformation field and the velocities measured by the GB-SAR sensor have been validated with data by more conventional ground-based measurements. [C2962]

"Image coregistration in SAR interferometry only by means of arithmetic operations"

An alternative interpolation technique for SAR image coregistration in interferometric processing is formulated and described. The proposed algorithm is based on the 1-D Farrow interpolator and, when combined with an adequate implementation, it involves a smaller computational burden than the conventional method and yields high accuracy. Basically, this technique enables to carry out the coregistration without resorting to a set of functional weights, and it only requires arithmetic operations and 2-D FFTs. This paper includes several results and comparisons that confirm its validity: the proposed technique is combined with two different polynomial interpolation procedures (Taylor and Chebyshev); bounds on its interpolation error in the 1-D and 2-D cases are derived; and, additionally, it is tested numerically with a synthetic image. [C2963]

"Introduction of a grid-based filter approach for InSAR phase filtering and unwrapping"

This work presents a phase unwrapping (PU) algorithm for SAR interferometry based on an approximate grid-based filter (GbF). This PU algorithm, which makes use of state space techniques, performs simultaneously noise filtering and phase unwrapping. The formulation of this technique provides independence from noise statistics and is not constrained by the non-linearity of the problem. Results obtained with synthetic and real data show a significant improvement with respect to conventional PU algorithms in some situations. [C2964]

"Error analysis of ICESat waveform processing by investigating overlapping pairs over Europe"

Full waveform laser altimetry is a recently developed method to obtain a complete vertical profile of the height of objects in the footprint as illuminated by a laser pulse. The richness of the signal also complicates the processing. One way to improve the processing strategy is to analyze differences of waveforms that should be very similar because they were obtained at approximately the same time and location. Such waveform pairs are still difficult to find. Here it is shown how to use the archive of ICESat space-borne altimetry data over Europe to determine a set of tenths of thousands of at least partial overlapping waveform pairs. The differences in the values of the waveform parameters, median energy, waveform extent, relative returned energy and intensity distribution are determined and discussed. As a case study, three typical pairs of almost perfectly overlapping waveforms are shown, where considerable differences are still occurring. In all three cases an explanation for these differences is found and discussed. Further analysis of the waveform pairs in this database is expected to considerably improve automatic processing of full waveform data. [C2965]

"Ground deformation retrieval of urban and suburb areas based on multi-baseline DInSAR algorithm: A case study in Cangzhou City (China)"

This paper aims at ground surface deformation retrieval in wide areas including urban and suburb areas based on multi-baseline DInSAR algorithm proposed by Mora. Several progresses are made in order to extract good results. Firstly, a new complex network is presented to restrain noise influence on delaunay triangular network. Secondly, Based on a model coherence function, linear deformation velocity increments and height error increments between neighboring high coherent points (HCPs) are resolved. In order to integrate increments in network, least squares adjustment method and error controlling method are used to obtain stable parameters estimation. At last, by Combining complex and delaunay networks, wide areas deformation is investigated, from center urban areas to suburb areas. The algorithm is performed to investigate the subsidence of CangZhou City, Hebei province (China) during the time of 1993-1997 by using 9 scenes of ERS SAR data. The experiment results show serious subsidence in the region and are validated by leveling data and groundwater wells data. [C2966]

"Enhancement of radar based DEMs using 3D techniques"

Digital elevation models may contain several errors, what causes uncertainty about the reliability of the data. Reliable use of elevation data requires that uncertainty associated with the data be accounted for and that the errors responsible for this uncertainty are identified, quantified and removed. Several studies have proposed assorted methods to detect and quantify, and also to remove different kinds of errors. However, these automatic procedures apply algorithms that are specialized in detecting errors with particular characteristics, producing good results only when the model contains predominantly these specific types of errors. In this context, this paper presents a methodology and a tool for enhancing digital elevation models, named DEMEditor. Visual interpretation plays an important role in this work, which exploits user's knowledge about the data in the decision-making process about areas to be enhanced in the digital elevation model. The background of the user allows the identification of any type of error, relieving the need for automatic detection algorithms that specialize in detecting errors with particular characteristics. [C2967]

"Dynamic persistent scatterers interferometry"

This paper presents the concept of Dynamic Persistent Scatterers Interferometry (PSI) processing, which enables the sequential estimation of parameters. The method is based on the Integer Least Squares (ILSQ) PSI concept and makes use of the estimation vector and corresponding variance-covariance matrix of the initial estimation epoch. In addition, the concept of multi-modal adaptive estimation and testing is applied. The algorithm systematically adds a new acquisition or set of acquisitions to an existing stack, updates the solution of the previous run, and analyzes whether the behavior of the (pre-) selected points fits the expected one. [C2968]

"An autofocus approach for residual motion errors with application to airborne repeat-pass SAR interferometry"

Airborne repeat-pass SAR data are very sensible to sub-wavelength deviations from the reference track. To enable repeat-pass interferometry a high-precision navigation system is needed. Due to the limit of accuracy of such systems, deviations in the order of centimeters remain between the nominal and the processed reference track causing mainly undesirable phase undulations and misregistration in the interferograms, referred as residual motion errors. Up to now only interferometric approaches, as multi-squint, are used to estimate those deviations to compensate for such residuals. In this paper we present for the first time the use of the Autofocus technique for residual motion errors. A very robust autofocus technique has to be used since the accuracy of the

estimated motion has to be at millimeter scale. Because we deal with low-altitude-strip- map mode data we propose a new robust autofocus technique based on the WLS (Weighted Least-Squares) phase estimation and Phase Curvature Autofocus (PCA) extended to the range- dependent case. We call this new technique WPCA (Weighted PCA). While the multi-squint approach is only able to estimate the baseline variation from coregistered images, the autofocus approach has the advantage of being able to estimate motion deviations independently for each image. Repeat-pass data of the E-SAR system of the German Aerospace Center (DLR) are used to demonstrate the performance of the proposed approach. [C2969]

"DEM alignment and registration in interferometric SAR processing and evaluation"

Interferometric synthetic aperture radar (InSAR) processing, if lacking high quality ground control points (GCPs), may produce large errors in the final DEM. Some kind of alignment or registration can reduce these errors. This paper evaluates the accuracy of InSAR processed digital elevation models (DEM), against a high resolution DEM. InSAR DEMs were aligned and least-squares registered with USGS, 1/3 arc second NED. The accuracy evaluations after registration show InSAR DEMs alignment and registration can eliminate DEM errors caused by lack of accurate GCPs. In some cases, this process improves the accuracy of the InSAR DEM even more efficiently than including GCPs into InSAR processing. [C2970]

"TerraSAR-X and TanDEM-X: Revolution in spaceborne radar"

Commercially available imagery is and will remain indispensable to civilian and military organizations gathering various types of geo-spatial information. Whether fulfilling international agreements, providing military contingents in international peacekeeping or humanitarian missions, or conducting joint technical exercises with other countries-a reliable access to timely, high resolution remote sensing data is an essential basis for well-informed decision making, particularly in time-critical situations. Today, organizations with those needs customarily resort to high resolution data acquired by optical sensors-often a lengthy operation. The radar satellite TerraSAR-X, and at a later stage together with TanDEM-X with its complementary near-real time data acquisition capabilities, offer a whole new approach to the use of space-borne datasets for mapping purposes in time- critical situations. [C2971]

"Verification of the TerraSAR-X system"

The paper discusses the areas covered by the TerraSAR-X Calibration/Verification-Plan. By means of a commissioning phase planning tool the data take requests required for characterization, calibration and verification are sequentially arranged. The status of the individual data takes is tracked from request planning to the final image analysis. All data take requests and results are supervised and summarized in a so-called verification matrix. In the end the paper gives an overview about the commissioning phase schedule and the repeat cycle based planning. [C2972]

"Advanced control and processing capabilities in the aquarius scatterometer flight electronics"

The Aquarius mission requirement for 0.1 dB scatterometer measurement stability has driven the radar's control and processing hardware design. Two new aspects of the flight electronics that contribute toward the overall stability will be discussed in this paper: 1) a high- rate radar timing mode for verifying performance on the ground, and 2) an onboard processor for flagging echoes corrupted by radio-frequency interference (RFI). [C2973]

"Genesis of a new NASA InSAR mission concept, and natural hazards applications"

The National Research Council's Decadal Survey for Earth Science identified InSAR (Interferometric Synthetic Aperture Radar) observations among the highest priorities for new NASA Earth missions. A system making observations required by the solid Earth, vegetation, and ice/climate science communities is recommended. In response, analyses are underway to evaluate efficient combinations of science objectives and mission/instrument scenarios. The InSAR component can be satisfied by a new radar instrument concept capitalizing on existing technology and hardware, including a large commercial mesh reflector antenna and transmit/receive modules developed for the UAVSAR airborne radar. This InSAR system satisfies key science objectives and addresses several shortcomings of existing InSAR capable satellites. To reduce temporal decorrelation, L-Band (23 cm) wavelength is used. A 300 km wide-swath scanSAR mode with 8 day repeat enhances study of ice dynamics, pre/post earthquake deformation, volcano monitoring, and other dynamic phenomena. With a minor orbit change, global biomass surveys are possible using multipolarization. Key challenges are involve scheduling to optimize conflicting observational requirements of various science communities served. [C2974]

"RadSTAR L-band imaging scatterometer- performance assessment"

L-band Imaging Scatterometer (LIS), developed at NASA/Goddard Space Flight Center as part of the RadSTAR initiative, is an airborne imaging radar that combines phased array technology and digital beam forming techniques for the measurement of important scientific parameters. The instrument operates at 1.26 GHz, horizontal polarization, and employs a real-time processor capable of synthesizing multiple beams over a scan range of +/-50 degrees. LIS was flight tested in May 2006 and in January 2007 on board of the NASA P3 aircraft over the Delmarva Peninsula, VA. In this paper we describe the RadSTAR system and present some preliminary analysis of the radar data collected during the test flights. [C2975]

"Research of influence of transients, non-equidistance of the taken readings, divergence of beams on characteristics of interferometric SAR"

There is under consideration a combined influence of the transients in the filters of the radar system selective circuits, non-equidistance of the taken readings and divergence of the beams at the distance up to the earth surface reflecting elements that is comparable with a synthetic antenna aperture value. There is taken into account influence of the above-mentioned factors on the resolution capability of the radar system for the earth remote sensing. The transients lead to swinging of the SAR antenna pattern; the other indicated factors result in widening of the synthetic antenna pattern. There are given the corresponding relationships and diagrams that make it possible to take into account the influence of the above-mentioned factors and determine the ways for reduction of the destructive factors influence on the synthetic antenna pattern. [C2976]

"Multiband CFAR detection of thermal anomalies using principal component analysis"

This paper deals with the problem of CFAR detection of thermal anomalies in multispectral satellite data. The goal is to extend the algorithm proposed in [1], and successfully applied to MODIS data from band 21, to the case of multiband investigation. A multiple-channel model has been designed, where data from MODIS bands 21 and 31 are projected into a new coordinates system by adopting the principal component analysis (PCA). A preliminary statistical analysis has been performed on both the principal components of data to verify that the Weibull distribution can be adopted for background. Subsequently, a Kendall test has been used to check the level of dependency of the projected data and it has shown that channels independence can be assumed with high significance level. After PCA, a CFAR detection is applied to projected data and thanks to data independence the single detections are combined with an AND rule. The outcome of the AND operation gives the thermal anomalies detected in both channels with an assigned overall probability of false alarm (PFA). The Multiband CFAR algorithm has been applied to a 256 x 256 MODIS image from bands 21 and 31 and results have been compared with those from NASA-DAAC MOD14. [C2977]

"Fusion of support vector machines for classifying SAR and multispectral imagery from agricultural areas"

A concept for classifying multisensor data sets, consisting of multispectral and SAR imagery is introduced. Each data source is separately classified by a support vector machine (SVM). In a decision fusion the outputs of the preliminary SVMs are used to determine the final class memberships. This fusion is performed by another SVM as well as two common voting schemes. The results are compared with well-known parametric and nonparametric classifier methods. The proposed SVM-based fusion approach outperforms all other concepts and significantly improves the results of a single SVM that is trained on the whole multisensor data set. [C2978]

"Detecting moving targets in dual-channel high resolution spaceborne SAR images with a compound detection scheme"

Traffic data acquisition from space has evolved to an important task over the last years. Future SAR satellite missions will provide high resolution dual-channel SAR data and therefore a possibility to collect traffic parameters of a large area from space. In this paper a detection approach for vehicles will be presented, which considers simultaneously the effects moving objects suffer from in the SAR image. The performance of the proposed detection scheme is analyzed using experimental airborne SAR data. [C2979]

"A new method for moving target indication and detection in multi-channel SAR data"

A new and fast algorithm for MTI/MTD processing is presented. This algorithm is based on a formation of SAR images from each channel and using these for separation between moving and stationary targets. First, the problem is described by means of a generalized model. Then, an inverse problem is formulated and some of its approximate solutions by means of the Fourier transform are given. The approximate solutions are used to show how one can resolve stationary targets and moving ones completely regardless their distribution in space or

reflectivity. The only criterion used is the velocity of a target. Further, it is shown how moving targets and stationary targets can be separated from processed, that is focused, SAR images. [C2980]

"Simulation of LIDAR-based aircraft wake vortex detection using a bi-gaussian spectral model"

A new spectral model of the return signal from a LIDAR Doppler wake vortex detector is proposed. It has been experimentally discovered during ground-based and flight test campaigns but suffered a lack of theoretical evidence. Using high resolution fluid simulations of wake vortices, we highlight the physical meaning of this model. Comparisons with the traditional single Gaussian model show the superiority of this new approach is consistent with previous experimental results. [C2981]

"Advanced D-InSAR techniques applied to a time series of airborne SAR data"

This paper presents airborne differential SAR results using a stack of 14 images, which were acquired by the experimental SAR (E-SAR) system of the German Aerospace Center during a time span of only two and a half hours. An advanced differential technique is used to retrieve the error in the digital elevation model and the temporal evolution of the deformation for every coherent pixel in the image. The two main limitations in airborne SAR processing are analyzed, namely the existence of residual motion errors (inaccuracies in the navigation system in the order of 1-5 cm), and the accommodation of the topography and the aperture during processing. The SAR focusing chain to process the data is also presented, together with the modifications in the differential processor to deal with the remaining baseline error. The detected deformation of a corner reflector and of several agricultural fields allows validating the proposed techniques. [C2982]

"X-band airborne differential interferometry over the Perugia area"

In this paper we show the results of an airborne differential SAR interferometry (DInSAR) experiment carried out over the Perugia area, center of Italy, by using the X-Band OrbiSAR system. Measurements on corner reflectors allowed us evaluating the system detection capability. [C2983]

"Coherent-stable scatterers detection in SAR multi-interferograms: Feature fuzzy fusion in Alpine glacier geophysical context"

SAR interferometry (InSAR) performs two acquisitions (spatially separated by the baseline) of the signal back-scattered by the resolution cell which contains height and/or displacement information. Repeat pass spaceborne interferometry provides multi-interferograms which can be used to extract such information either by combining the multi-temporal results of conventional interferometry or by a different approach based on specific targets: the coherent stable scatterers (CSS). In this paper a two-step approach is proposed to obtain specific features from multi-temporal InSAR data sets. The first step consists in extracting image attributes related to the useful information. The second step consists in merging the attributes using an interactive fuzzy fusion technique. The interactive fuzzy fusion is proposed to provide end-users with a simple and easily understandable tool for tuning the detection results. The method is applied on a data set of five co-registered ERS 1/2 tandems from the French Alps (the Mont-Blanc region), including two temperate glaciers: the Argentiére and the Mer-de-glace. The results illustrate how the end-user can combine the proposed attributes to detect the presence of CSS or distributed stable scatterers useful for multi-temporal analysis. [C2984]

"Unsupervised change detection by multichannel SAR data fusion"

In the contexts of environmental monitoring and disaster management, multichannel synthetic aperture radar (SAR) data present a good potential, thanks both to their insensitivity to atmospheric and Sun-illumination conditions, and to the improved discrimination capability they may provide as compared to single-channel SAR. In this paper an unsupervised contextual change-detection method is proposed for two-date multichannel SAR images, by adopting a data-fusion approach. Each SAR channel is modelled as a distinct information source and Markovian data fusion is used by introducing a suitable Markov random field model. The task of the estimation of the model parameters is addressed by combining the expectation-maximization algorithm with the recently proposed "method of log-cumulants." The proposed technique is experimentally validated on SIR-C/XSAR data. [C2985]

"Similarity measures between SAR and optic data"

With the development of remotely-sensed multisensor satellites like Pleiades Cosmo-Skymed that have the particularity of providing both SAR and optic data, new techniques in image processing are needed. These techniques must take into account the complementarities and differences in nature of these data. A preliminary operation for advanced techniques that use multisensor images such as fusion, classification, etc. is registration.

In the case of SAR and optic data, we can do automatic registration if we exactly know the sensor parameters and have a digital terrain model (DTM) or a digital elevation model (DEM) at our disposal. If we do not have an exact knowledge of these parameters, the registration becomes difficult. Another approach to achieve the automatic registration which does not need sensor parameters will rely on comparison measures between both data. In this paper, we present a comparison of several similarity measures between multisensor SAR and optic images used in matching algorithms. An evaluation of these measures for synthetic data based on their distributions is given. Then results on real images are analyzed. [C2986]

"Comparison of parameter estimation accuracy of distributed-target polarimetric calibration techniques"

The accuracy with which distributed-target polarimetric calibration algorithms estimate crosstalk and the ratio of Tx-to-Rx channel imbalance is compared. The algorithms investigated are minor variants of previously-published algorithms but rederived for notational and definitional consistency. Numerical simulations were used to assess the algorithms' performance in the absence of noise. Results indicate that the imbalance parameter is generally accurately-estimated but that crosstalk estimation accuracy varies greatly. [C2987]

"The problem of parameter estimation for spatially correlated polarimetric ground clutter at millimeterwave frequencies"

Most mathematical methods commonly used to estimate the parameters of a probability density function are based on the assumption of independent identically distributed (iid) data. However, the analysis of the reflectivity values of polarimetric ground clutter has shown that there may be a considerable amount of correlation depending on the type of clutter. For this analysis the estimated autocorrelation function, the Bartels test, and the runs up and down test for randomness are used. [C2988]

"A ship detection method for dual polarization SAR data based on whitening filtering"

Recently, as the rapid growing use of dual polarization spaceborne SAR data for ship detection, it seems necessary in practice for us to find a favorable detection algorithm, however, which is still scarce in literatures. In this paper, based on the application of the whitening filter, we proposed to design a dual polarization CFAR (Constant False Alarms Rate) detection method for ship detection, with the verification of its CFAR property. Preliminary detection results of real Envisat/ASAR Alternating Polarization (AP) mode data were shown in the last section to validate the detection method. [C2989]

"A neural approach to unsupervised classification of very-high resolution polarimetric SAR data"

Analysis of L-band polarimetric SAR data has not been extensively carried out for undulating, heterogeneous and fragmented landscapes, where classification can become quite challenging. This paper reports results of a study on the pixel-by-pixel unsupervised classification of very-high resolution polarimetric images by self-organizing neural networks. [C2990]

"Retrieval of fully polarimetric mueller matrix under Faraday rotation effect at P band in spaceborne polarimetric SAR observation"

Spaceborne microwave observation of subcanopy and subsurface requires the SAR (polarimetric synthetic aperture radar) technology at lower microwave frequencies, such as P band. However, SAR observation at P band is remarkably influenced by Faraday rotation (FR) effect through ionosphere. An example in this paper illustrates why the measured polarimetric data with FR at P band cannot be directly applied to terrain surface classification. We further present that the parameters u , v , H , a , A for terrain surface classification derived from the polarimetric data without FR, which are recovered from the data with FR, can be applied to the surface classification, even there is a plusmn $\pi/2$ ambiguity error unresolved. Based on gradual change of FR degree along geographical location, a method to eliminate the plusmn $\pi/2$ ambiguity error is designed. Thus, the polarimetric scattering vector and Mueller matrix without FR and plusmn $\pi/2$ ambiguity can be fully inverted from the measured polarimetric data with FR. [C2991]

"Signatures of polarimetric parameters and their implications on land cover classification"

Knowledge-based or rule-based classification schemes provide robust classification of normally a few major classes. In order to determine optimum polarimetric parameters for such classification schemes, a study has been performed, where the separability between different sets of major classes using many different polarimetric parameters has been investigated using airborne, C- and L-band polarimetric SAR data. [C2992]

"An approach to classify polarimetric P-band SAR images for land use and land cover mapping in the"

In this paper the potentiality of polarimetric P-band SAR data for Amazon tropical forest land cover mapping is assessed. The classifying approach is based on the Iterative Conditional Mode (ICM) algorithm, taking into account several specific distributions to SAR data. Distinct land cover classes are modeled considering different distributions. The results show that the P-band data is not capable to discriminate the nine classes initially used. However this capability improves significantly when classes having similar vegetation structure are grouped. The HV image is effective in differentiating primary and very old regeneration forest areas from other land cover classes, while W image increases the classification of bare soil and crop/pasture areas. The results show the importance of polarimetric information for the classification of several land use classes. [C2993]

"Polarimetric optical tools and decompositions applied to SAR images"

Radar polarimetry aims to determine the scattering properties of a target or scatterer. For this purpose, the scattering matrix can be analyzed and represented in several ways using various techniques to extract information about the scattering mechanisms. Polarimetry and ellipsometry are techniques which both study the properties of the polarization of the scattered waves but traditionally refer to different wavelengths: optical wavelengths for ellipsometry, and high-frequencies radio waves for radar polarimetry. This paper deals with natural targets in the general bistatic case, for which the 16 parameters of the Mueller matrix are independent. We try to answer the following questions: how to deduce the radar polarimetric parameters from the optical measurements of a Mueller ellipsometer? What are the polarimetric parameters traditionally devoted to optical images, and in which extent is it possible to apply and interpret them in the case of SAR images? [C2994]

"Design of FMCW millimeter-wave radar for helicopter assisted landing"

This paper discusses the design and construction of a compact, ultrafast, monostatic frequency modulated continuous wave (FMCW) millimeter-wave radar, operating at 94.75 GHz, intended to be used as a helicopter assisted landing sensor. A high speed direct digital synthesizer is used to generate the baseband FM signal. Custom transmitter/receiver baseband boards are designed to up/down-convert the frequency modulated (FM) signal to an appropriate IF before it can be connected to the W-band RF frontend. A high-gain lens horn antenna is used in the RF frontend, in conjunction with other waveguide-based W-band components. A Xilinx FPGA is used in the backend data processing, preferred over conventional DSPs because of its speed. The whole system is packaged in an aluminum casing, with dimensions of 9' x 11' x 11' and weighing under 20 lbs. [C2995]

"Degree of polarization for weather radars"

Future operational weather radars are likely to implement hybrid polarization, an operating mode that involves transmitting 45deg slant polarization and receiving the horizontal and vertical components of the backscattered field. In this work, the degree of polarization at slant send is theoretically considered and experimentally evaluated from fully polarimetric signatures in order to assess its potential for use in next generation operational weather radars. [C2996]

"Grecosar, a SAR simulator for complex targets: Application to urban environments."

This paper presents a preliminary study about the scattering properties of urban-like scatters based on simulated SAR images. A simple target performed by a box of gypsum located over a perfectly conducting flat plane is analyzed for different views in both ISAR and SAR fully-polarimetric modes. The results are analyzed with the Pauli decomposition theorem and they show that the scattering response of such a target is dominated by a strong scatter, which polarimetric behavior depends on the relative orientation of the target with respect to the radar. Tests with interferometry shows that the height of the box can be reasonably retrieved despite of model simplicity. [C2997]

"Focusing problems of subsurface imaging by a low-frequency SAR"

ONERA radar RAMSES was recently upgraded with low frequency band (P-band, 435 MHz). In P-band, frequencies penetrate through the ground and through forest canopy. Unfortunately, the formation of the subsurface radar images presents a number of new specific challenges that include algorithm validity, calibration methods, radio-frequency interference, and image focusing and analysis. This paper addresses the aspects of focusing images from an airborne low frequency SAR of buried targets in a lossy and dispersive soil. The hydrological model (Richards' equation) was used to model the multilayer case. [C2998]

"Experimental validation of a Kirchhoff based shape reconstruction algorithm in realistic conditions: a test case for buried pipes"

A two dimensional shape reconstruction algorithm is applied to experimental GPR in-situ measurement data. The reconstruction algorithm is based on the Kirchhoff approximation and is exploited to process data collected under a multimonostatic configuration by a pulsed GPR. Thus the need to pass from time domain measurements to frequency domain data suitable for the inversion algorithm is also addressed. [C2999]

"GPR missions on mars"

Recently in order to investigate the distribution of water, liquid and solid, in the upper portions of the crust of Mars planet two different instruments are active, the Mars Advanced Radar for Subsurface and Ionosphere Sounding (MARSIS) and SHAallow RADar (SHARAD). Both the instruments are a low frequency (1.8-5MHz for MARSIS and 20 MHz for SHARAD) Ground Penetrating Radar (GPR) in altimeter configuration which uses the synthetic aperture technique. The main differences between the two instruments are the spatial resolution (150 m vertical resolution, 5-10 Km along track resolution for MARSIS and 15 m vertical resolution, 300-500 m along track resolution for SHARAD) and the penetrating capability (about 5 Km for MARSIS and 1 Km for SHARAD). After the instrument data acquisition from the Martian surface an appropriate processing shall be performed in azimuth (unfocused for MARSIS and focused for SHARAD) and range dimension to produce the scientific final data. In this work will be presented an efficient procedure to detect the possible subsurface presence using the available surface topography data. After the performance evaluation of this technique an example of application will be presented on real SHARAD data [C3000]

"GPU-based framework for interactive visualization of SAR data"

Synthetic aperture radar data presents specific problems for interactive visualization. The high amount of multiplicative speckle noise has to be reduced. The high dynamic range of the amplitude data must be mapped to the lower dynamic range of display devices in a way that makes image features appropriately visible. In addition to interactive navigation in the data, it is desirable to allow interactive selection of despeckling and dynamic range reduction methods and adjustment of their parameters. Graphics processing units (GPUs) can be seen as ubiquitous parallel coprocessors with extreme computational power. In this paper, we propose a GPU-based framework for interactive visualization of SAR data. Data management techniques are used to make full use of the GPU. We reworked well-known despeckling and dynamic range reduction techniques for the GPU programming model and implemented them in our framework. Both navigation in large data sets and adjustment of processing parameters are fully interactive. [C3001]

"Active remote sensing applications to disaster management with implications to spectrum management"

Spaceborne active sensors have been used for years to study the Earth's surface and atmosphere. The intent of this paper is to present the unique types of active remote sensors and their characteristics that apply to disaster management; and to present a status of current frequency spectrum use and needs of spaceborne active sensors, along with any issues or concerns. [C3002]

"Properties of polarimetric sea clutter at 35 GHz"

The FGAN operated MEMPHIS radar was used to measure the backscatter behaviour of sea clutter at 35 GHz. The resulting fully polarimetric, carefully calibrated reflectivity data were analysed with respect to their temporal and spatial characteristics. Temporal decorrelation is fast, accordingly the polarimetric persistence is very low. As to spatial statistics, several well-known probability density functions like redistribution or log-normal are compared to each other. It is found that none of them is ideal. There is always a number of outliers that statistically behave differently. By eliminating them the goodness of the fit can be improved. [C3003]

"Bayesian classification of hydrometeors from polarimetric radars at S- and X- bands: algorithm design and experimental comparisons"

Dual-polarized weather radars are capable to detect and identify different classes of hydrometeors, within stratiform and convective storms exploiting polarimetric diversity. A model- supervised Bayesian method for hydrometeor classification (BRAHC), tuned for S- and X- band, is described in this study. The critical issue of X-band radar data processing is the path attenuation correction, usually negligible at S-band. During the IHOP experiment (Oklahoma, 2002) two dual-polarized radars, at S- and X- bands, were deployed and jointly operated with closely matched scanning strategies, giving the opportunity to perform experimental comparisons between coincident measurements at different frequencies. Results of hydrometeor classification and water content

estimates at S- and X- bands are discussed and the impact of path attenuation correction is quantitatively analyzed. [C3004]

"The dependence of polarimetric decomposition parameters on biophysical forest parameters, frequency and methodology"

The increasing availability of fully polarimetric SAR data provides a large potential for the assessment of biophysical forest parameters. Aiming at an inversion of polarimetric parameters into forest parameters, this study shows the sensitivity of polarimetric decomposition theorems (Pauli- and H-lambda decompositions) to biophysical forest parameters, especially forest density. Effects of non-biophysical parameters on the estimation of decomposition parameters are also shown. The investigations were carried out on fully polarimetric data at L-band (1.3 GHz) and P-band (350 MHz) acquired in 2003 in a preAlpine region in Switzerland with the German E-SAR (Experimental SAR) platform. [C3005]

"Bistatic foliage penetration modelling"

This paper aims at presenting a model able to study the impact of the target presence under vegetation and to assess the detection feasibility. In a first part the model is described. We will then get at the analysis of results for several set of radar configurations to illustrate the potentiality of detection by means of shadows. [C3006]

"Multi-look polar decomposition of polarimetric SAR images"

This paper focuses on the multi-look polar decomposition of SAR images. Standard polar decomposition is generally used in single look polarimetry to decompose a bi-static or mono-static polarimetric scattering matrix into a product of an Hermitian matrix (boost) and a unitary matrix (rotation). An extension of this use in the framework of multi-looked polarimetry is proposed here. This new approach consists in decomposing the scattering matrix into boost and rotation components before vectorisation, then in averaging to generate boost and rotation coherency matrices separately, with new inferred parameters; the boost and rotation entropies, and concurrent dominant scattering mechanisms (alpha boost and alpha rotation). This multi-look extension of polar decomposition may allow for the definition of a new classification strategy for remote sensing data. [C3007]

"Assimilating spaceborne radar and ground-based weather station data for operational snow-covered area estimation"

An enhanced method for snow-covered area (SCA) estimation for boreal forest zone is presented. The method combines TKK developed spaceborne radar-based SCA estimation with ground-based weather station observations. The purpose is to improve the reliability of SCA estimates near and after the end of snow-melt season. The SCA estimates acquired with the enhanced method are compared with optical satellite data-based (MODIS) SCA data. Investigations were carried out for snow-melt seasons of 2004-2006. The results show a significant increase in accuracy when the enhanced SCA method is applied. Correlation between the radar-based and optical reference data increases from 0.919 to 0.937 and RMS-error improves from 0.151 to 0.140 when the new method is employed. [C3008]

"Brightness temperature validation for SeaWinds radiometer using Advanced Microwave Scanning Radiometer on ADEOS-II"

After the launch of NASA's SeaWinds scatterometer in 1999, a radiometer function was implemented in the Science Ground Data Processing Systems to allow the measurement of the Earth's microwave brightness temperature. This paper presents the validation of the SeaWinds radiometer (SRad) ocean brightness temperatures using the Advanced Microwave Scanning Radiometer (AMSR) as a brightness temperature standard. Results are presented which compare collocated and simultaneously measured ocean brightness temperatures while operating on Japan's ADEOS-II satellite. [C3009]

"Calibration of SMOS geolocation biases"

The Soil Moisture and Ocean Salinity (SMOS) mission aims at observing two variables critical for a large scientific community, from biosphere dynamics to climate monitoring. The mission should also provide information on root zone soil moisture and vegetation and contribute to significant research in the field of the cryosphere. The original design, 2D interferometric radiometer at L-band, and principle of measurement makes SMOS a challenge at various technical levels. Moreover, stringent requirements on the estimated variables make the complete processing of SMOS data even more challenging. One of these requirements is concerned with the ability to accurately localize all the footprints of the instrument on the surface of the earth. Based on simulation and sensitivity studies with respect to the final retrieval of soil moisture, this accuracy requirement has been

established so that the localization error on each footprint presents a zero mean and a standard deviation of 400 m. This high accuracy is mainly due to the need for knowledge of open water within a footprint, not to bias soil moisture estimation. This accuracy is highly challenging and unprecedented for sensors of this class and resolution. The on board devices that will help characterize the geolocation of the SMOS products include stellar sensor and gyroscopes, which can achieve an accuracy consistent with the requirements in terms of standard deviation. But the overall localization budget is also contaminated by an important bias, due to the mechanical deployment of the instrument antenna arms after launch, and to the launch shift that impacts all the alignments on the satellite (mechanical shift of stellar sensor due to shocks and vibrations, moisture desorption in mechanical brackets...). The purpose of this study is to characterize these biases, obviously inaccessible to on ground measurement and expected not to evolve once in orbit, so that they can be accounted for in the ground processing prior to initiate the soil moisture retrieval. [C3010]

"New inversion algorithm for raman lidar without derivative of the inelastic signal"

A new algorithm for extracting the backscattering coefficient profiles from elastic and inelastic lidar signals is presented. It re-formulate the Raman lidar equation, provided by the interaction of the laser light with the atmospheric nitrogen, in order to obtain the exponential of the integral of the extinction coefficient at the elastic wavelength instead of the extinction coefficient profile, as it is traditionally made, assuming the usual wavelength-dependent relationship between the Raman and Elastic extinction coefficients, and then substitutes that quantity into the elastic lidar equation to obtain the backscattering profile. That circumvents the calculation of the derivative of the noisy inelastic lidar signal with the main advantage of the extraction of backscattering coefficient profiles, one of the final products, without requiring any smoothing or filtering of the original signals. Several examples of the new method applied to profiles obtained with the CIEMAT lidar system, located in Madrid (SPAIN), are analyzed and the results are compared with other algorithm calculations. In conclusion, an improvement of the reliability and accuracy of the retrieved data was observed in the cases analyzed. [C3011]

"Morphological tools for range-interval segmentation of elastic lidar signals"

This article presents a preliminary semi-automated range-interval segmentation toolset for the identification of: 1) the apparent range of full overlap, 2) the clear-sky level (i.e., the molecular level), and cloud layers (cloud-base, cloud-peak, and cloud-top range), and 3) apparent homogeneous extinction intervals. [C3012]

"Inversion of a layered rough surface model: maximizing the number of retrievable parameters for the design of future subsurface sensing radar systems"

We previously applied an optimization technique known as Simulated Annealing (SA) to the inverse problem associated with a 3D two-layer dielectric structure with slightly rough interfaces and showed that simulated annealing methods are capable of globally minimizing cost functions with many local minima [1]. Nonlinearity of the cost function is a major factor that decreases the performance of the inversion algorithm. With a fixed set of measurement and inversion parameters, as the number of unknown model parameters increases, the cost function nonlinearity becomes more severe, decreasing the efficiency of inversion and making the annealing process perform like an inefficient brute force search. The focus of this work is on strategies to choose the optimal set of measurement parameters for retrieval of the largest possible number of parameters of a layered dielectric structure. [C3013]

"Accuracy and resolution analysis of the pencil beam radar scatterometer onboard China's HY-2 satellite"

The Ku-band scatterometer onboard HY-2 (SCAT/HY-2) is a pencil-beam radar employing pulse compression techniques to ensure number of the independent measurement samples and the resulted precision of the backscattering coefficient for each resolution cell. In this paper, the system specifications of SCAT/HY-2 are introduced. The signal processing scheme, including pulse compression, resolution cell regroup and the area weighted incoherent average of the backscattered power, is presented and analyzed. Based on the analysis of the resolution cell after pulse compression processing, the radiometric accuracy and surface resolution of the SCAT/HY-2 for all the azimuth angles will be simulated. Simulation and analysis results shows that SCAT/HY-2 can satisfy the specification requirements of HY-2 satellite. [C3014]

"Polarimetric, combined, short pulse scatterometer-radiometer system at 5.6GHz"

In this paper a C-band (~5.6 GHz), dual polarization, combined scatterometer-radiometer system is described. The system allows carry out polarimetric (vv, vh, hh, hv), simultaneous and coincident microwave active-passive measurements of the observed surface (soil, vegetation, snow and water surface) parameters. The originality of

the developed system is in the spatial-temporal combination of microwave active and passive channels of observation and its possible application for short distance sensing (the minimum operational range for the scatterometer is ~6 m) from low altitude platforms under far field conditions for both radar and radiometric observations. [C3015]

"The effect of rain on retrieval of C- and Ku-band scatterometer surface winds during Hurricanes Lili (2002) and Isabel (2003)"

The Imaging Wind and Rain Airborne Profiler (IWRAP) and Simultaneous Frequency Microwave Radiometer have been flown aboard the NOAA WP-3D "Hurricane Hunter" aircraft for the past five (2002-2006) hurricane seasons. IWRAP is a conically scanning, high resolution C- and Ku-band Doppler radar that profiles from the aircraft to ocean at four incidence angles. The microwave return from the ocean is used to infer ocean surface vector winds via scatterometry. The UMass Simultaneous Frequency Microwave Radiometer (USFMR) is a C-band radiometer that measures integrated rainfall rate and ocean surface wind speed. The combination of these two instruments allows for the determination of the effect of rain on scatterometer derived surface vector winds. Our focus is on scatterometer retrievals at an incidence angle of 50deg during Hurricanes Lili (2002) and Isabel (2003). The measurements were carried out under the Coupled Boundary Layers and Air-Sea Transfer (CBLAST) program and are the highest resolution radar measurements of the lower atmospheric boundary layer in powerful hurricanes. The retrievals at C-band use the CMOD5 geophysical model function (GMF) while those at Ku-band use one which is a synthesis of the QSCAT- 1 GMF and one developed using IWRAP data. As has been reported, the effect of rain at Ku-band is a dramatic decrease, even for wind speeds greater than 20 m s⁻¹. The atmospheric attenuation dominates these results. At C-band the primary effect is a decrease in azimuthal modulation which is especially important at high wind speeds where this modulation decreases in the absence of rain. [C3016]

"Simultaneous wind and rain retrieval for ERS scatterometer measurements"

Using collocated ESCAT, TRMM PR, and ECMWF data, the effects of rain on the ESCAT wind-only retrieval has been evaluated. For high incidence angle measurements, the additional scattering of rain causes estimated wind speeds to appear higher than expected. It is also noted that the selected directions of the rain-corrupted wind vectors generally point along swath in heavy rain, regardless of the true wind. A simultaneous wind/rain retrieval method (SWRR) is developed using a simple wind/rain backscatter model. Validation shows that SWRR method significantly improves the wind vector estimates at high incidence angles in heavy rain cases. It also provides an estimate of the surface rain rate. [C3017]

"Frequency impact on the bistatic radar scattering from an ocean surface"

In this paper we study the frequency impact on the normalized bistatic cross section (NBCS) of the sea surface. Numerical simulations are presented and analyzed in the frequency range from 1 to 14 GHz (L- to Ku-band). We treat this problem with the unifying scattering model denoted small slope approximation (SSA). The computations were made assuming the surface-height spectrum of Elfouhaily et al. for fully developed seas. Numerical results are obtained and discussed in both forward and fully bistatic configurations for different sea states and polarizations. [C3018]

"Matching stereoscopic SAR images for radargrammetric applications"

The aim of this paper is to present our studies about extraction of 3D information from radar images. Several radargrammetric methods allow DEM (digital elevation model) generation from SAR images and we take a special interest to stereoscopic method. The main idea is to match image stereo pairs, to create a disparity map from one image to the other and to compute elevation thanks to the incidences angles. [C3019]

"P-sounder: an airborne P-band ice sounding radar"

This paper presents the top-level design of an airborne, P-band ice sounding radar under development at the Technical University of Denmark. The ice sounder is intended to provide more information on the electromagnetic properties of the Antarctic ice sheet at P-band. A secondary objective is to test new ice sounding techniques, e.g. polarimetry, synthetic aperture processing, and coherent clutter suppression. A system analysis involving ice scattering models confirms that it is feasible to detect the bedrock through 4 km of ice and to detect deep ice layers. The ice sounder design features a digital signal generator, a microstrip antenna array, a conventional RF-architecture with a central transmitter, four receivers, and internal calibration loops. In 2008 the first data acquisition campaign will take place in Greenland. [C3020]

"Potential of a C-band SAR mission with 12-day repeat cycle to derive ice surface velocity with interferometry and offset tracking"

The goal of this contribution is the assessment of the potential of a C-band SAR mission with repeat-pass interval of 12 days-as the intended European satellite system Sentinel-1-to derive ice surface velocity using SAR interferometry (InSAR) and offset-tracking. For this purpose we investigated ERS-1 SAR data acquired during the ice missions in 1992 and 1994 in 3-day repeat- orbits at Nordaustlandet in the northeast Svalbard archipelago. In 12-days winter InSAR pairs phase decorrelation is mainly observed in areas of high strain rates and, in certain cases, because of snow melting or redistribution through snowfall or wind. Velocity maps derived from these image pairs were found useful to enhance in regions of slow glacier flow the mapping of the surface ice-flow divides previously determined from optical imagery and topographic information. Range-azimuth offset-tracking investigations suggest that the expected error of this method is on the order of 50 m/year and that spatial coverage is generally satisfactory. Application of dual-azimuth offset- tracking, use of HH polarization and enhanced spatial resolution, feasible with Sentinel-1, could enhance the expected error. [C3021]

"An improved methodology to map Snow Cover by means of Landsat and MODIS imagery"

In this article we propose a methodology to determine snow cover by means of Landsat-7 ETM+ and Landsat-5 TM images, as well as an improvement in daily Snow Cover TERRA- MODIS product (MOD10A1), between 2002 and 2005. Both methodologies are based on a NDSI threshold > 0.4 . In the Landsat case, and although this threshold also selects water bodies, we have obtained optimal results using a mask of water bodies and generating a pre-boundary snow mask around the snow cover. Moreover, an important improvement in snow cover mapping in shadow cast areas by means of a hybrid classification has been obtained. Using these results as ground truth we have verified MODIS Snow Cover product using coincident dates. In the MODIS product, we have noted important commission errors in water bodies, forest covers and orographic shades because of the NDVI-NDSI filter applied to this product. In order to improve MODIS snow cover determination using MODIS images, we propose a hybrid methodology based on experience with Landsat images, which provide greater spatial resolution. [C3022]

"Diurnal SAR variability due to ice and snow air interface wetness overnight changes."

For a water content over 8%, the transmitted component of a SAR beam becomes negligible. The electromagnetic wave interaction with the interface discontinuity is then determined by the scattering efficiency of surface roughness rms and correlation height. It is illustrated by the difference of contrast observed on images acquired from a same scene one late in the afternoon after a warm day and the development of a wet interface, and the other, early in the morning after a cool night and growth of frost flower in place of the wet interface. The increased the rms height of newly formed crystals reduce the angle dependence of the backscattered signal and therefore the contrast on the scene, however, the increased volume scattering in snow covered areas seems to be the main factor causing a resolution difference on the ridge network between images recorded on morning and at the end of the afternoon. A detailed survey of the air-snow or air-ice interface of the snow cover and ice blocks surfaces. Surface wetness, snow wetness content and surface roughness are documented. Radar data measured on a variety of snow and ice interfaces are presented and analyzed. We show that the presence of a wet film on snow and ice surfaces produces an increased forward scattering whereas interfaces covered with newly crystallized ice display an enhanced backscattering. [C3023]

"Ice flow estimation of Shirase Glacier by using JERS-1/SAR image correlation"

We applied an image correlation method to the Japanese Earth Resources Satellite-1 (JERS-1) synthetic aperture radar (SAR) data obtained from 1996 to 1998. The obtained ice flow velocity was systematically larger on the western streamline than on the eastern streamline from the grounding line towards the downstream region. The differences were 0.28 km/a in 1996 and 0.33 km/a in 1998, which were significantly larger than the error estimate of 0.04 km/a. The ice flow direction was about 312deg at the grounding line and changed to 327deg at 10 km, 346deg at 20 km and 2deg at 30 km downstream from the grounding line. The total deflection attained 38deg towards east. [C3024]

"Estimation of forest stem volume using ALOS PALSAR satellite images"

A first evaluation of ALOS PALSAR data for forest stem volume estimation has been performed at a coniferous dominated test site in Sweden. In total, 7 Fine Beam Single polarization (FBS, look angle 34.3deg, HH-polarization) and 7 Polarimetric (PLR, look angle 21.5deg, HH-, HV-, VH-, and W- polarization) SAR images were used. In total, 56 forest stands with stem volume in the range of 45-650 m³ ha⁻¹ (average 325 m³ ha⁻¹) were analyzed by relating backscatter intensity to field data. The estimation accuracy of stem volume at stand level was calculated in terms of root mean square error (RMSE). For the best case investigated an RMSE of

30% was obtained using one of the FBS images acquired in the winter season. The corresponding RMSEs for the PLR images with HH-, HV-, VH-, and W-polarization were 65%, 65%, 62%, and 81%, respectively. The better results for FBS compared to PLR mode could be explained by particularly favorable weather conditions at image acquisition, or by the higher ground resolution in the FBS images, which makes small stands less sensitive to errors in geocoding. [C3025]

"Forest inventory applications using optical and RADARSAT-2 images in Mexico"

There is a need in Mexico for accurate and up to date forest inventories due to concerns related with sustainable development programs. Forest inventories in the past have been incomplete and are not useful at regional levels. The national forest inventory is scheduled to be updated soon -optical remote sensing techniques and traditional field surveying are envisaged. There are no operational applications of radar remote sensing for forest management within government agencies or academic institutions in the country. Forest land cover is dynamical due to urban area growth, illegal logging and forest clearing for agricultural purposes in many regions. A previous land cover project combined Landsat-ETM and RADARSAT-1 imagery in Central Mexico, where forest areas are frequently foggy. A current project involves testing the potential benefits of combining polarimetric radar and optical data for forest applications. RADARSAT-2 imagery will be used as part of the Science and Operational Applications Research Program. The project aims to evaluate combined optical/radar approaches to improve forest inventory at regional scales. As a first step the total forested area is determined from optical SPOT 5 images. We show preliminary results from the optical data which are being validated on the field. As RADARSAT-2 imagery become available, polarization signatures for forest parameters will be obtained. Further work will evaluate the complementarities with optical signatures in determining forest species. [C3026]

"The active-passive remote sensing for aerosol optical depth retrieval"

In this paper, a hybrid retrieval method of aerosol optical depth based on the combination of active and passive optical remote sensing is proposed. Two methods to retrieve the atmospheric optical depth are introduced: the so-called dark pixel method is used for retrieving the aerosol optical depth from MODIS; the other one is used by CALIPSO lidar data. After analyzing the two methods, the combined MODIS and CALIPSO method is applied for the aerosol optical depth, the primary experimental results show that these data are in agreement with each other in time-space evolution trend. [C3027]

"Robust measurement of glacier surface motion from multiscale speckle tracking using local constraints"

A grown importance in long-term operational glacier monitoring has emerged, mainly due to the connection of glacier recession to climate changes. Up to now, mainly two types of methods have been used for the estimation of glacier flow velocities: Image matching and differential interferometry (DInSAR). Although the principal potential of DInSAR for glacier velocity estimation has been shown in several case studies, its successful application is often limited by phase noise, described by the coherence. Additionally, the glacier velocity is often too large to be analysed by means of DInSAR since this method can be too sensitive to correctly track the large displacements occurring during a typical data acquisition interval of one month. SAR amplitude images are not limited by phase stability problems like in DInSAR and can reliably be acquired on a regular basis. In this work, a novel algorithm for computing the velocity field and motion parameters from a sequence of SAR amplitude images are presented. The algorithm is based on the vector relaxation combined with standardized cross-covariance matrix information and cross-correlation techniques. The cross-correlation is used to indicate the candidate motion vectors for each pixel. After this step, by a relaxation operation local smoothness constraints are introduced into the estimated flow pattern, leading to a more homogeneous velocity estimation. In order to handle fast motion and reduce the mismatches, the mentioned algorithms are applied in different scales and linked using anisotropic diffusion equation in case of multiscale cross-correlation. This significantly improves the reliability of the motion detection in the presence of noise, inherent in case of SAR data. [C3028]

"Passive microwave signatures of autumnal sea ice types from ship-based observation"

Surface-scale passive microwave signatures of newly formed sea ice were collected using ship-based radiometers in the Southern Beaufort Sea and Amundsen Gulf between mid October and mid November 2003. Sea ice in the region was highly spatially and temporally variable. Over a heterogeneous area of open water and thin ice, polarization ratios showed multimodal frequency distributions and the differences between surface and satellite radiometric data were large. However, differences were small over a homogeneous area of snow-covered first-year ice during late fall and the corresponding histograms showed unimodal distributions. Our results suggest that sub-pixel heterogeneity is a critical factor in characterizing the mixture rules used in passive microwave sea ice algorithms. [C3029]

"First steps towards multimodal georeferencing of 3D VHR optical and X-band SAR imagery"

With the advent of new, more widely available very high resolution (VHR) SAR and optical sensor satellite constellations, the issue of jointly exploiting the corresponding imaging data in the best possible way naturally arises. Our ultimate goal is the pixel-level fusion of these modalities and their visualization in a 3D context, i.e. draped over terrain data, itself obtained from interferometric SAR processing. In this paper, we investigate the issues associated with adapting tools originally developed for low-resolution C-band SAR imagery to high-resolution X-band SAR imagery (both spaceborne). Specifically, we consider the issues associated with SAR interferometry (InSAR) and more particularly those associated with complex interpolation and phase unwrapping. We found that the existing chirp-Z transform complex interpolator previously used at low resolution is perfectly suitable for handling VHR SAR data. We also found that, while the selected phase unwrapping procedure works well when the resolution is reduced by averaging, it is deficient at full resolution, in part due micro-reliefs and specific phase responses. [C3030]

"Lidar Approach for Measuring the CO2 Concentrations in the Troposphere from Space"

We report progress in assessing the feasibility of a new satellite-based laser-sounding instrument to measure CO₂ concentrations in the lower troposphere from space. [C3031]

"RADAR REMPI: A New Approach to Detection, Spectroscopy, and the Dynamics of Gases for Combustion, Fluid Dynamics and Homeland Defense"

Radar REMPI has the promise of remotely measuring atomic and molecular species with high sensitivity and high selectivity. High sensitivity is achieved through detection by microwave scattering. High selectivity is achieved through resonant enhanced ionization. [C3032]

"Utilization of LIDAR and NOAA's Vertical Datum Transformation Tool (VDatum) for Shoreline Delineation"

The National Oceanic and Atmospheric Administration (NOAA), an organization of the U.S. Department of Commerce, is mandated to map the United States' coastal boundary, defining the nation's legal shoreline. This paper presents a new methodology for extraction of shorelines from lidar data. The methodology incorporates NOAA's vertical datum transformation tool (VDatum) for transforming lidar data to a specified tidally-based datum for shoreline extraction. The VDatum utility comprises geoid models, fields representing departures of an orthometric datum from local mean sea level, and hydrodynamic models portraying tidal regimes for accurate demarcation of coastal lines. The procedure presented here minimizes the variability and subjectivity that have plagued more traditional shoreline delineation techniques. The semi-automated routine allows for consistent, non-interpreted shorelines to be derived, providing significant advantages over proxies such as the high water line, beach scarps, and dune lines. This technique is invariant to coastline type, and has provided good results for a range of margins, such as a sandy or rocky. Additional advantages include the ability to derive multiple tidally-based shorelines from a single dataset and greater flexibility in data acquisition. Perhaps most importantly, the lidar data can be collected in a manner to support a variety of Integrated Ocean and Coastal Mapping (10CM) applications, including nautical charting, storm surge/tsunami modeling, coral reef mapping, ecosystem monitoring, and coastal mapping. [C3033]

"Image quality analysis of the vibrating sparse MIMO antenna array of the airborne 3D imaging radar ARTINO"

ARTINO is a new radar system, integrated in a small mobile and dismountable experimental UAV. The side-looking geometry of usual SAR systems produces shading effects of the scene to be imaged. ARTINO overcomes this restriction with the ability to image the direct overflowed area (Nadir looking) in three dimensions. The effects caused by vibrations of the used sparse MIMO antenna array - which is embedded in the wings of the airplane - are discussed with respect to the 3D imaging quality. A correction approach within the image formation process is presented, too. [C3034]

"A three dimensional SAR system on an UAV"

Applications of small unmanned aerial vehicles (UAVs) have increased steadily over the past years. Applications are found in Earth observation, reconnaissance, monitoring, and surveillance missions using imaging systems. The big advantage of radar sensors is their all-weather capability. Especially imaging radars possess several benefits over optical systems, as they are not affected by rain, snow, fog, or the time of day. The advantages using small unmanned platforms come at the cost of having to deal with restrictions on weight and volume.

Hence, these parameters are the predominant design drivers for UAV sensor developments. This paper presents the concept, the technical realization and the status of a 3D imaging radar system suitable for small UAVs. ARTINO (Airborne Radar for Three dimensional Imaging and Nadir Observation) combines a real aperture, realized by a linear array of nadir pointing antennas, and a synthetic aperture, which is spanned by the moving airplane. [C3035]

"Implementation Issues of the Matched Field Processing Method of Refractivity Structure Sounding"

As the atmospheric conditions, expressed in terms of radio refractivity can considerably influence the performance of radio communication links and radar systems, there is a need for reliable prediction of refractivity structure in the lower atmosphere. The paper is focused on the remote sensing of refractivity structure in the lower atmosphere using Matched Field Processing method. The paper discusses the proper radio link set-up with respect to improving the performance of radio refractivity estimation using remote the sensing technique. [C3036]

"Radar Estimation of Building Layouts Using Jump-Diffusion"

Estimating buildings layouts using exterior radar measurements is a challenging task involving the electromagnetic modeling, many unknown parameters, and limited number of sensors. We propose using the jump-diffusion algorithm as a powerful stochastic tool that can be used to determine the number of walls, estimate their unknown positions and other parameters. We improve the convergence rate of the jump-diffusion algorithm by developing an iterative procedure that first finds low- resolution estimates, which are then used to initiate our more accurate estimation. Our efficient usage of the available frequency bandwidth, improves the computational speed that otherwise would be hampered by the forward electromagnetic modeling. [C3037]

"Application of Doppler Spectrum for Retrieval of Statistical Parameters of Sea Waves"

The experiment for studying of microwave backscatter by the rough water surface during the flight above the Gorky water storage basin was performed. A Doppler radar (10GHz) with a knife-like beam (1deg-16deg) was installed at a helicopter and was oriented vertically downward. The analysis of the experimental data has confirmed that the width of the Doppler spectrum depends on the direction of wave propagation. The new algorithm for determination the correlation coefficient between the vertical component of the orbital velocity and water surface slopes, as well as the variance of orbital velocity was developed using the width of the Doppler spectrum of the reflected radar signal for the case of moving radar. The experimental data processing has confirmed the effectiveness of retrieval algorithm and demonstrated the possibility to determine the average phase velocity of sea waves, the average wavelength, and the significant wave height. [C3038]

"A mid-IR DIAL System Using Interband Cascade Laser Diodes"

A compact, portable mid-IR differential absorption lidar system was built using interband cascade lasers operating at 3.38 μm and 3.54 μm and its operation was demonstrated by measuring absorption of vapor phase ethanol. [C3039]

"Building Corner Feature Extraction Based on Fusion Technique with Airborne LiDAR Data and Aerial Imagery"

Generally, automatic building corner or linear feature extraction from urban area aerial imagery is based on traditional computer vision corner or edge detection techniques. However, challenges and difficulties remained due to the complex characteristic of objects in urban images. Visually, the linear features in airborne LiDAR are much more distinct than those in aerial imagery, however, common criticisms arising from the low horizontal accuracy of LiDAR data. To overcome these difficulties, this study proposes a building corner extraction algorithm based on information fusion technology by integrating aerial imagery and airborne LiDAR data. According to experiment results, the proposed method can obtain the distinct building corners not only with the characteristics of uniform spatial distributed pattern based on Voronoi graph theory, but also with the shape, length, and height constrained conditions derived from LiDAR linear features. The proposed algorithm resolves the heterogeneous remote sensing data registration difficulties between LiDAR data and raw aerial imagery. [C3040]

"A low-cost imaging radar: DRIVE on board ONERA motorglider"

UAVs from different countries and with different payloads have proven their capabilities within military applications. Future UAV employment in the civilian areas of surveillance (pollution, natural risks prevention, fire

prevention), monitoring (traffic control, environmental monitoring, earth observation) and communication relays becomes unavoidable. Many payload configurations may be used in UAV operations, but compared to systems working in other spectral regions (such as optical or infrared sensors), radar has the main advantage to be able to operate in all-weather condition. A concept of low-cost imaging Ka-Band radar is presented in this paper. This radar is integrated into under-wings pods that are fixed on a STEMME S10VT motorglider. This radar concept combines real aperture in the cross-track direction, by the antennas geometrical aperture, and synthetic aperture in the along-track direction, realized with the aircraft motion. Radar front-end uses FMCW technique which allows to reduce the power emission to a few Watts. In addition, the use of the millimeter band induces antennas size reduction, and makes possible the radar integration into pods. Thus, radar particularities are a low-size, a low-weight and a low-cost basis, making this radar suitable for future integration on board small vehicles, such as UAV. The radar definition and specifications will be detailed, together with the first results obtained on Fall 2006. Two ways of operating the radar will be presented: An application as vertical sounder, using horn antennas, and an application as SAR radar, using rectangular antennas. The two cases will be illustrated by samples of acquisitions results. The DRIVE radar has been developed and built to fly on board an UAV vehicle. Indeed, this radar is designed and will be used by ONERA as a UAV radar test bench. Current airplane used for testing applications is a STEMME S10-VT motorglider as the geometry of this airplane may be representative of a MALE UAV-: wingspan is 23 m large and weigh is about 900 kilograms. DRIVE Project started at ONERA on January 2005, and first flights happened in the beginning of 2006. DRIVE radar uses FMCW techniques and operates in Ka Frequency Band: Central frequency is 35 GHz and bandwidth is about 800 MHz width. [C3041]

"Lidar, sun photometer and polar nephelometer measurements: Remote sensing of aerosol size distribution properties"

We are developing new sensors to measure aerosols using lidar, automated Sun photometers, and in situ polar nephelometers. The lidar measurements are based on a ground system using a 532 nm laser. The sun photometer are based on a custom Sun tracking design. The aerosol phase function measurements are based on a custom polar nephelometer system developed at the University of Hawaii. Results from our first joint field experiment using these new systems will be discussed. [C3042]

"A new type of lidar for atmospheric optical turbulence"

We are developing a new type of lidar for measuring range profiles of atmospheric optical turbulence. The lidar is based on a measurement concept that is immune to artifacts caused by effects such as vibration and defocus. Four different types of analysis and experiment have all shown that a turbulence lidar built from commercially-available components will attain a demanding set of performance goals. The lidar is currently being built for testing scheduled in 2007. [C3043]

"Lidar method for determination of quartz concentration in the tropospheric mineral aerosols"

We present a lidar method that enables the determination of quartz concentration in mineral aerosols. The method combines the Raman scattering lidar using a 466 cm⁻¹ quartz line with a high-spectral resolution lidar (HSRL). The methodology and experimental results are described. [C3044]

"Improved receiver architecture for future L-band radiometer missions"

Microwave radiometer measurements are viable technique for measurement of soil moisture and ocean salinity. Therefore, there is a strong interest in new L-band remote sensing radiometers. For example, European Space Agency's SMOS (soil moisture and ocean salinity) satellite is currently under development. SMOS applies Noise Injection Radiometer subsystem for the measurement of the average brightness temperature of the scene. This paper proposes the use of reference channel control method for the future L-band radiometer missions, e.g., for potential SMOS follow-on mission. According to analysis, significant improvement in radiometric resolution (up to 40%) would be achieved compared to traditional antenna channel noise injection architecture. The proposed system is based on the use of an active cold load (ACL) as cold reference. [C3045]

"Advances in real time lidar spectroscopy"

We summarize the resolution limits and potential sensitivity of existing Hoar-spectrometer systems. The spectral resolution of these systems is limited primarily by the phase space area (entendue), which depends on the width and convergence angle of the laser beam's image on the spectrometer input slit. Decreasing the beam's image width can be achieved with conventional optics at the expense of an increase in convergence angle, which often results in a loss in coupling efficiency due to mismatching with the spectrometer's phase space area. We describe how this limitation has been overcome using suitably designed optical fiber bundles. We also discuss both theoretical and computer modeling predictions of the variation in telescope-to-spectrometer coupling

efficiency with range for lidar spectrometers. Finally we compare the performance of photon counters and intensified CCD arrays and discuss methods of range-gating their outputs. [C3046]

"A space-time minimum cost flow phase unwrapping algorithm for the generation of persistent scatterers deformation time-series"

We have investigated the phase retrieval capability of the Extended Minimum Cost Flow (EMCF) phase unwrapping (PhU) approach in the framework of the Persistent Scatterers Interferometry (PSI) algorithms for the generation of deformation time-series. The presented technique exploits an appropriate selection of full resolution interferograms obtained via a triangulation step carried out in the Temporal/Perpendicular baseline plane, where the available SAR image sequence is represented. Moreover, the phase unwrapping procedure is implemented via the cascade of two steps, based on the conventional Minimum Cost Flow (MCF) algorithm, that allows us to exploit both the spatial characteristics and the temporal relationships among the produced interferograms. The presented experiments, carried out by analyzing a set of 43 ERS SAR images relevant to an area of the city of Rome (Italy), confirm the effectiveness of the exploited PhU approach. [C3047]

"A new framework for multi-pass SAR interferometry with distributed targets"

This paper focuses on multi-pass spaceborne synthetic aperture radar interferometry (InSAR) in presence of distributed scattering, paying particular attention to the role of target decorrelation in the estimation process. This phenomenon is accounted for by splitting the analysis into two steps. In the first step we estimate the interferometric phases from the data, while in the second step we use these phases to retrieve the physical parameters of interest, such as LOS displacement and residual topography. This approach is suited both to derive the performances of InSAR with different decorrelation models and for providing an actual estimate of LOS motion and DEM. Results achieved from Monte-Carlo simulations and a set of repeated pass ENVISAT images are shown. [C3048]

"New potentials of differential SAR tomography: Volumetric differential interferometry and robust DEM generation"

A new interferometric SAR mode has been recently introduced termed differential interferometry (Diff-Tomo). In this paper, two new potentials coming from the joint elevation- velocity resolution capability of Diff-Tomo are introduced. The first concerns differential measurements and elevation profiling of volumetric scatterers with non rigid motion and possible temporal decorrelation. The second concerns estimation of terrain elevations which is robust to some temporal decorrelation effects. Simulated results are reported as a first preliminary probing of performance and limits of these methods. [C3049]

"Multi baseline SAR acquisition concepts and phase unwrapping algorithms for the TanDEM-X mission"

The TanDEM-X (TerraSAR-X add-on for Digital Elevation Measurement) mission will start in 2009 with the aim of generating a global Digital Elevation Model with high accuracy corresponding to HRTI-3 specifications (12 m posting, 2 m relative point-to-point height accuracy for flat terrain). To achieve this goal, a second satellite similar to TerraSAR-X will fly close to TerraSAR-X in a controlled Helix configuration for 3 years to jointly acquire interferometric SAR data in bistatic mode. According to the current mission concept, there will be at least two complete coverages of the global land surface, each one running one year. The different coverages will have different heights of ambiguity to allow multi-baseline phase unwrapping. For the sake of a homogenous data quality the second acquisition will be shifted by half the swath width with respect to the first coverage. Finally difficult terrain will be covered two more times with different acquisition geometries (i.e. different look direction and/or incidence angles). This paper presents first study results of phase unwrapping algorithms foreseen to process SAR data from the bistatic TanDEM-X configuration. [C3050]

"Spaceborne multi-dimensional SAR imaging: Current status and perspectives"

Multi-Dimensional (MultiD) SAR imaging is a modern technique, based on coherent SAR data combination, aimed to space (full-3D) and space deformation-velocity (4D) analysis. It extends the concept of SAR interferometry and differential interferometry and offers new options for the analysis and monitoring of ground scenes. With this regard, we discuss the current status and the results obtained by processing ERS real data, we investigate perspectives related to the next generation multi-static satellite formations, and we show some sample results regarding 3D and 4D theoretical performance bounds. [C3051]

"Remote Sensing Signature Fields Reconstruction Via Robust Regularization of Bayesian Minimum

Risk Technique"

The robust numerical technique for high-resolution reconstructive imaging and scene analysis is developed as required for enhanced remote sensing with large scale sensor array radar/synthetic aperture radar. The problem-oriented modification of the previously proposed fused Bayesian-regularization (FBR) enhanced radar imaging method is performed to enable it to reconstruct remote sensing signatures (RSS) of interest alleviating problem ill-posedness due to system-level and model-level uncertainties. We report some simulation results of hydrological RSS reconstruction from enhanced real-world environmental images indicative of the efficiency of the developed method. [C3052]

"Inversion of residual errors to improve insar data acquisition, processing and interpretation"

The quality of the InSAR products has improved remarkably during the past few years. However, in order to further enhance the accuracy of the InSAR products and obtain results close to the real parameters further tuning of the InSAR processing is needed. In this work efforts have been made to improve upon the interpretation and analysis of the repeat pass space borne InSAR system data by quantifying and inverting the error sources. In an innovative way, error evaluation at every important step in the InSAR signal processing has been carried out and small algorithms have been incorporated to inverse the errors, thus fine tuning the InSAR signal processing. [C3053]

"The Gauss-Newton algorithm applied to track-while-scan radar"

The Gauss-Newton (GN) algorithm is the minimum-variance non-recursive estimation procedure invented by Gauss in 1809 [3, 4, 7]. Mathematicians refer to it by that name; statisticians refer to it as nonlinear regression; astronomers call it differential correction. In 1959 Swerling reworked Gauss' non-recursive algorithm into a recursive format [9], giving rise to the Bayes-Swerling filter. In 1960/61, Kalman and Bucy published their algorithm [5, 6], which, in the absence of process noise, can be derived from Swerling's recursive format [7]. The huge advances in computing power and affordability of RAM since the early 60's have made it desirable that we re-examine Gauss' original algorithm which avoids the problems and/or limitations incurred by either the Swerling or the Kalman recursive formats, and at the same time opens up tremendous flexibility in terms of access to internal filter values. This paper examines the GN algorithm and how it has been applied to Track-While-Scan (TWS) radar. A companion paper in these proceedings discusses the application of GN to Passive Coherent Location (PCL) radar [8]. [C3054]

"Optimisation of bistatic HF surface wave radar configurations"

HF surface wave radars are increasingly being deployed in bistatic configurations, usually via the mechanism of overlapping the coverage of two monostatic radars and sharing signals, but sometimes as intrinsically bistatic radar designs. In either case, the advantages which may attach to bistatic scattering geometries may easily be compromised by suboptimum positioning of the transmitting and receiving systems. Here we address the problem of finding the optimum spatial configuration for a given palette of radar missions, taking account of target signatures, clutter, noise, propagation and geographical constraints on the siting of the radar facilities. [C3055]

"Miniature wide-band microstrip patch antennas for GSM applications: A parametric study and optimum design"

Microstrip Antennas (MSAs) consist of a metallic radiating patch on one side of thin dielectric substrate and other side is ground plane. Most important advantages of MSAs are low profile, light weight and compatibility with integrated circuit technology. MSAs are used in mobile communication, satellite communication, radar, direct broadcasting, global positioning systems and remote sensing. The major limitations of microstrip antennas are their narrow impedance bandwidth, small gain and low power handling capability. In this paper, we designed full and half U slot MSAs (0.8 to 1.4 GHz) with shorting wall used between non radiating edge of MSAs and ground plane. The behavior of full and half structure is similar with slight change in center frequency. The feed is optimized in such a way to get the maximum bandwidth. We have studied effect of thickness of substrate, length, width and dielectric constant on the performance of full U slot MSAs. The U-slot and Half U-slot MSAs with shorting wall has been simulated in IE3D and experimental results are verified on Agilent VNA E5062A. [C3056]

"The Gauss-Newton algorithm in passive aircraft tracking using doppler and bearings"

Passive Coherent Location (PCL) radar systems capitalise on illuminators of opportunity such as TV broadcast stations, in order to obtain RF backscatter from targets such as aircraft. In this paper it is envisaged that an

array of receivers is available, each of which measures both the bearing to an airborne target as well as the Doppler shift of the signal induced by the target's motion. These bearing and Doppler values are then processed by the method invented by Gauss in 1809 called the Gauss-Newton (GN) algorithm [2, 3, 6], which is discussed in further detail in an accompanying paper in these proceedings [7]. Results are presented, based on an extensive simulation study for various target types and varying numbers of receivers. [C3057]

"Independent Component Analysis of POLSAR Images. Relative Newton-Based Approach"

We propose here a new method for POLSAR image analysis. The method is based on a new PCA-ICA model in which the relative Newton-based approach for performing ICA is developed. The basic idea of ICA with relative Newton method consists in approximating the negentropy by taking account of the orthogonality constraint of the extracted components. This concept is recognized for its robustness and gives consequently very good theoretical results. The approach is well justified from the mathematical point of view. However, its implementation requires being more flexible because of the number of the estimated parameters. The purpose of this paper is to try to open new issues, in future research, in the concern of working out a new method for SAR image analysis that accumulate the advantages of the proposed method while avoiding its disadvantages. [C3058]

"Brightness Temperature Maps Retrieval for the SMOS Space Mission: Regularized Inversion and Bias Reduction"

Synthetic aperture imaging radiometers (SAIR) are powerful sensors for high-resolution observations of the Earth at low microwaves frequencies. Within this context, the European Space Agency is currently developing the SMOS mission devoted to the monitoring of soil moisture and ocean salinity at global scale from L-band space borne radiometric observations obtained with a two-dimensional interferometer. This contribution is concerned with the reconstruction of radiometric brightness temperature maps from interferometric measurements provided by SMOS. [C3059]

"Determination of Earth Surface from TRMM Satellite Images"

The Precipitation Radar (PR), on board of the TRMM satellite, provides many information and measurements related to the weather above the Earth. Images are produced from reflectivity measurement of different particles and materials. Determination of Earth surface level is required when investigating detection methods using TRMM PR data, such as detection of oil and underground water below the Earth surface. In this paper, two techniques were proposed for detecting exact Earth location from TRMM satellite rays reflectivity. First technique is based on satellite reflectivity images and the second one is based on the reflectivity data itself. The former performed better than the latter in estimating the Earth surface level. This finding can facilitate oil and underground water detection. [C3060]

"TanDEM-X: A satellite formation for high-resolution SAR interferometry"

TanDEM-X (TerraSAR-X add-on for Digital Elevation Measurements) is an innovative spaceborne radar interferometer mission that was approved for full implementation by the German Space Agency in spring 2006. This paper gives an overview of the TanDEM-X mission concept, summarizes the basic products, illustrates the achievable performance, and provides some examples for new imaging modes and applications. [C3061]

"Multidimensional waveform encoding for synthetic aperture radar remote sensing"

This paper introduces and analyses the innovative concept of multidimensional waveform encoding for spaceborne synthetic aperture radar (SAR). The combination of this technique with digital beamforming on receive enables a new class of highly performant SAR systems employing novel and highly flexible radar imaging modes. Examples are adaptive high-resolution wide-swath SAR imaging with compact antennas, enhanced parameter estimation sensitivity for applications like along-track interferometry and moving object indication, and the implementation of hybrid SAR imaging modes that are well suited to satisfy the hitherto incompatible user requirements for frequent monitoring and detailed mapping. Further advantages arise for fully polarimetric operation where it becomes possible to reduce the PRF by a factor of two. Implementation specific issues will be discussed and examples demonstrate the potential of the new technique for different remote sensing applications. [C3062]

"Source localization in view of urban sensing applications"

An analysis of the effect of sensor positions and the number of sensors on source location estimates in urban environments is performed. The sensors are uniformly distributed on a circle around a building in which the

source is to be localized. Location estimates are obtained via trilateration and multilateration. Source location errors, as a function of the number and positions of sensors, are derived under equal range errors assumption, and the asymptotic behavior of location errors is observed. [C3063]

"Reconstruction of the Building Objects from Multi-Aspect High-Resolution SAR Images"

In this paper, an approach to the automatic reconstruction of 3D simple building objects from multi-aspect metric-resolution SAR images is proposed. The edge detector of constant false alarm rate (CFAR) and a parallel Hough transform technique are first employed to extract the parallelogram-like image of the building walls in SAR image. A set of probability density functions is presented to describe the extracted random wall-images and their multi-aspect coherence. Then the maximum-likelihood estimation of object is derived from its multi-aspect object-images. A hybrid priority criterion is defined to evaluate the reliability of reconstruction result, based on which, an automatic reconstruction algorithm is further devised to match object-images of different aspects and finally reconstruct the building objects. Four-aspect Pi-SAR images over Sendai, Japan are adopted for reconstruction. The results show the fidelity of the whole process chain and the feasibility of 3D objects automatic reconstruction from multi-aspect SAR images. [C3064]

"Electromagnetic Scattering Properties of Thin Curved Dielectric Surface and Cylinder"

Electromagnetic (EM) scattering from curved surface and cylinder is important in the area of propagation and remote sensing in order to determine EM properties of scatterers. The radar cross sections (RCS) of a dielectric thin curved surface and cylinder are obtained by employing a quasi-static approximation. The results are complemented by numerical calculations and their validity is presented by comparison with available exact results in literature. Excellent agreement is found for horizontal and vertical polarization. [C3065]

"Performance of a Developed Low-Power and High-Sensitivity Cloud Profiling Millimeter-wave Radar: FALCON-I"

We have developed a low-power and high-sensitivity cloud profiling radar, named FALCON-I, transmitting frequency modulated continuous wave (FM-CW) at 95 GHz for ground-based observations. Millimeter wave at 95 GHz is used to realize much higher sensitivity than lower frequencies to small cloud particles. An FM-CW type radar realizes similar sensitivity with much smaller output power to a pulse type radar. Two 1m-diameter parabolic antennas separated by 1.4 m each other are used for transmitting and receiving the wave. The direction of the antennas is fixed at the zenith at this moment. The radar can observe clouds up to 20 km in height with the range resolution of 15 m and the angular resolution of 0.2 degree. Simultaneous observations of FALCON-I and a pulse type radar, SPIDER, show good performance of FALCON-I. Sensitivity of FALCON-I is -32 dBZ in radar reflectivity factor at 5 km, which is only 3 dB worse than that of SPIDER although its output power is 1/3000 to SPIDER. Ranging resolution of 15 m is realized for FALCON-I, which is 1/10 of that of SPIDER. Using developed FALCON-I, we observed clouds in various regions and oceans in the last three years. [C3066]

"Stream Profile and Neotectonic Analysis in Hazara Kashmir Syntaxis using Shuttle Radar Digital Elevation Data"

Digital elevation models are replacing traditional topographic maps in geosciences with the advent of space technology. We used digital elevation models from SRTM data for neotectonic and stream profile analysis in Hazara Kashmir Syntaxis. Hazara Kashmir Syntaxis is a NNW-SSE complex tectonic zone and makes a hair pin like structure located in North Western Himalayan Fold and Thrust Belt. There is no distinct pattern of Hazara Kashmir Syntaxis and surrounding faults i.e. Main Boundary thrust, Main Central Thrust, etc. which marks loop around it. NW-SE trending Himalayan Frontal thrust starts from the core of the Syntaxis while other faults like Kotil thrust, Riasi thrust and Tanda fault runs along NS directed Jehlum Strike Slip Fault. Seismicity is distributed along all the parts of the Syntaxis i.e. in the core and along the outer loop but decreases southward. Major earthquakes like Kangra (1905) and Muzaffarabad Earthquake (2005) caused surface deformation in the area and gave motivation for this study. Streams network has been extracted from DEM; Choice of stream delineation algorithms can influence the stream parameters like contributing area, slope, elevation, downstream distance and Strahler order. This study focuses Kunhar River, Kishanganga Rivers and their tributaries. Both rivers and their tributaries come across many faults in this area at different locations which help us in understanding the tectonic activity in this region. We use stream power law to calculate steepness and concavity indices by making area slope plots. Tectonic and seismicity map also supports that the area is tectonically active showing thrust faulting. The results show high uplift eastern and western flanks of the Syntaxis and also along the loop while in the core it is comparatively less uplifted. [C3067]

"SAFIRE: A close range real time millimetre wave radar for public education"

Millimetre wave (MMW) imaging is a fast moving technological area which has seen major advances in the last few years and is now offering practical solutions across a wide spectrum of imaging applications. Despite this, the technology is largely unknown and poorly understood by the general public. Under a UK EPSRC partnership for public engagement grant, the millimetre wave group at the University of St Andrews has partnered with exhibit development company FifeX Ltd to construct a touring exhibition designed to showcase the alternative view of the world provided by MMW remote sensing, illustrating the science principles behind the technology. The group is providing the centrepiece of the programme, a 94 GHz FMCW radar named SAFIRE (St Andrews fast imaging radar equipment). SAFIRE uses a frequency multiplied 7G Hz source to provide a low power (+2.5 dBm) 94 GHz carrier with a 750 MHz modulation bandwidth (i.e. a radar range resolution of 0.2 m). SAFIRE has a single zenith-pointing antenna scanned in azimuth via a rotating mirror angled at 45 degrees to the antenna axis to generate a PPI display of the immediate scene surrounding the radar (the maximum range is 25 m). Since real time imagery is essential for a project of this type the PPI is refreshed at minimum rate of 4 Hz. We present an outline of the motivation for the radar design and the expected system performance. [C3068]

"Adaptive neuro-fuzzy inference system for speckle noise reduction in SAR images"

An adaptive neuro-fuzzy inference system (ANFIS) based method is proposed for speckle noise reduction in synthetic aperture radar (SAR) images. Before using active RADAR (radio detection and ranging) and SAR imageries, the very first step is to reduce the effect of speckle noise. Reduction of speckle noise is one of the most important processes to increase the quality of radar coherent images. Filtering is the common method which is used to reduce the speckle noise. For this purpose, two ANFISs are trained and outputs of these systems are converted to one output through a mean calculator in this work. Performance of the proposed method is compared with performances of state-of-the-art methods in the literature for speckle noise reduction. Results are presented by filtered images and a table. [C3069]

"Urban target classifications using time-frequency micro-Doppler signatures"

Moving target indicators (MTI) find important applications in urban sensing. While motion detection can be achieved using simple CW radars, characterization of moving targets can be provided by estimating the key parameters of the target micro-Doppler signature. For indoor sensing, this signature has underlying instantaneous frequency features, which may depend on the radar viewing angle. This paper considers typical animate and inanimate moving objects and presents time-frequency motion classifiers using quadratic time-frequency distributions. The distinctions between the different target micro-Doppler parameter values and bounds are delineated. [C3070]

"Forest monitoring by using L-band coherence"

Two ALOS/PALSAR polarimetry data taken in 2006 were used and examined the deforestation stage by using coherence value. Many trees were fallen by a typhoon hit on September 8, 2004 at a test site in Japan. Reforestation has started for the deforestation sites and several kinds of deforestation stages are appeared there. We classified the stands into four groups. 1) Only small stumps and branches are left. 2) Tree trunks have been carried out, but branches and stumps have been left. 3) The fallen trees have been left. 4) No trees were fallen by the typhoon (normal forest). Coherence values of HH-HH and VV-VV become ~0.39 for group 1 and ~0.30 for group 4, and show a significant difference. But the coherence values of group 2, and group 3 are ~0.3 and show almost same value as group 1. The coherence value of HH-VV and VV-HH are 0.1 lower than the one of the HH-HH and W-VV. The coherence values, which include cross polarization, such as HV-HV and HV-VV, show no difference for all groups and the value is 0.2 to 0.3. While coherence values show the difference between group 1 and group 4, sigma0HV shows wider dynamic range and is preferable to distinguish the deforested stands from forest stands. [C3071]

"Recent Advancements of Radar Remote Sensing; Air- and Space-borne Multimodal SAR Remote Sensing in Forestry & Agriculture, Geology, Geophysics (Volcanology and Tectonology): Advances in POL-SAR, IN-SAR, POLinSAR and POL-DIFF-IN-SAR Sensing and Imaging with Applications to Environmental and Geodynamic Stress-change Monitoring"

Radar Polarimetry Radar Interferometry and Polarimetric SAR Interferometry represent the current culmination in 'Microwave Remote Sensing' technology, but we still need to progress very considerably in order to reach the limits of physical realizability. Whereas with radar polarimetry the textural fine-structure, target orientation, symmetries and material constituents can be recovered with considerable improvement above that of standard 'amplitude-only' radar; by implementing 'radar interferometry' the spatial (in depth) structure can be explored.

With Polarimetric Interferometric Synthetic Aperture Radar (POL-IN-SAR) imaging, it is possible to recover such co-registered textural and spatial information from POL-IN-SAR digital image data sets simultaneously, including the extraction of Digital Elevation Maps (DEM) from either Polarimetric (scattering matrix) or Interferometric (dual antenna) SAR systems. Simultaneous Polarimetric plus Interferometric SAR Imaging offers the additional benefit of obtaining co-registered textural-plus-spatial three-dimensional POL-IN-DEM information, which when applied to Repeat-Pass Image-Overlay Interferometry provides differential background validation and environmental stress-change information with highly improved accuracy. Then, by either designing multiple dual polarization antenna POL-IN-SAR systems or by applying advanced POL-IN-SAR image compression techniques, will result in 'POLarimetric TOMOgraphic' (Multi-Interferometric) SAR or POL-TOMO-SAR imaging. By advancing these EWB-D-POL-IN/TOMO-SAR Imaging modes, we are slowly but steadily approaching the ultimate goal of eventually realizing air-borne and space-borne 'Geo-Environmental Background Validation, Stress Assessment, and Stress-Change Monitoring and Wide-area Military Surveillance of the Terrestrial and Planetary Covers'.

[C3072]

"Polarimetric SAR observation by ALOS"

The Japanese microwave remote sensing satellite ALOS/PALSAR was launched successfully in January 2006. We are carrying out polarimetric calibration of the PALSAR sensor, which has the full-polarimetric function of L-band SAR. We set corner reflectors in Ulaanbaatar in May and August 2006, and the acquired data was used to confirm the polarimetric calibration coefficients, which will be used for the data sets delivered from October 2006. In addition, the acquired polarimetric SAR data will provide new possibility in remote sensing. Since this is the world first satellite borne full-polarimetric SAR system, we cannot show many examples in this moment, but from airborne SAR data, which we have studied, we show some examples of polarimetric SAR, which include tree type classification, and estimation of the orientation angle of scattering targets. [C3073]

"Physical parameter extraction over urban areas using L-band POLSAR data and interferometric baseline diversity"

Estimating the number of backscattering sources is an important issue in analyzing multibaseline interferometric SAR data. This paper extends model order selection algorithms to process polarimetric multibaseline InSAR observations. These methods are applied to urban environments using fully polarimetric dual-baseline InSAR data of Dresden city acquired by DLR's E-SAR system. Experimental results for single polarization and polarimetric set-ups are presented and discussed. [C3074]

"Highly accurate DSM reconstruction using Ku-band airborne InSAR"

We present a newly developed airborne InSAR system incorporating a novel phase unwrapping algorithm, capable of retrieving a highly accurate Digital Surface Model (DSM). The SAR sensor system, with a spatial resolution of 30 cm, is carried on an airborne platform which has 2 antennas placed in a baseline length of 1 m. We have established a DSM reconstruction processing technique, which includes the new "Iterated Conditional Modes-Minimum Cost Flow" (ICM-MCF) phase-unwrapping algorithm. The ICM-MCF algorithm finds a locally optimal configuration of unwrapped phases under a well-characterized statistical model of the terrain and noise. An experimental field observation was carried out in Tsukuba, Japan. The DSM was generated, and the height accuracy of the SAR-DSM was evaluated by comparing with laser profiler data. For 50 cm x 50 cm mesh, an accuracy of better than 50 cm in height was confirmed. [C3075]

"Height dependent motion compensation and coregistration for airborne SAR tomography"

SAR tomography (SARTom) is an imaging technique that allows multiple phase centers separation in the vertical (height) direction. It is performed after standard 2D SAR repeat-pass processing and operates on a stack of coregistered SAR images. Theoretically, the coregistration between two images is height dependent and the use of a reference height (or a DEM) is needed, although not ideal in the case of volumetric target (multiple phase centers in one resolution cell). In this paper, the drawbacks related to the choice of this reference in a tomographic context are analysed and a height dependent coregistration approach is proposed. In order to do this, it is also necessary to remove processing corrections related to the reference height, such as motion compensation, and make them height dependent. The inclusion of the height dependency during the tomographic SAR processing results in a better quality of the final tomograms in terms of pseudo-power and phase centers separation. The results of the proposed approach are validated on real data acquired by the E-SAR system of the German Aerospace Centre-DLR. [C3076]

"Some polarimetric aspects of processing sea surface M-ATI SAR data"

A brief review is presented of published work on detection and imaging techniques based on matrix group theory

for the scalar non-polarimetric two channel along track interferometer and the vector polarimetric two channel across track interferometer. The relevance to ATI of the vector theory for the across track interferometer is discussed as is the problem of extending the theory to the case of the ATI with N beams. Difficulties in developing detection and imaging methods for the general case of N beams have lead to attempts to develop an alternative approach based on linear filtering. It is assumed that image modulations are a result of local fluctuations in mean intensity which can be described by a spherically invariant statistical process with a compound distribution. The unmodulated background consists of Gaussian scatterers. These scatterers and the modulated ones have different Doppler spectra and maximising the normalised standard deviation of the filtered image maximises the visibility of the image modulations. Polarimetric aspects of this approach are discussed and experimental results obtained with an airborne four beam M-ATI are presented illustrating aspects of the discussion. [C3077]

"A novel optimization approach to forest height reconstruction from multi-baseline data"

The paper deals with the problem of reconstructing the height of forests from polarimetric/multi-baseline SAR data. The approach consists of optimizing an objective functional defined as the distance between the measured data and the data predicted by the model at the actual estimate of the unknowns. We indicate the role of global optimization on the performance of the forest height reconstruction algorithm. As global optimizer, a multilevel single-linkage method, which incorporates a local optimization into the global search, is exploited, thus offering computational efficiency and reliability. The performance of the method are illustrated against numerically simulated data. [C3078]

"Status and perspectives of GNSS-R at ESA"

This paper presents an overview of the activities currently being undertaken by the European Space Agency in the field of GNSS reflectometry. Furthermore, the salient features of Europe's Galileo project with respect to the applicability of the signals for the purpose of GNSS-R are given. Furthermore, the prospects for the near future in terms of experiments and applications are given and finally there is a review of the potential for GNSS-R space missions. [C3079]

"Oceanpal®: Monitoring sea state with a GNSS-R coastal instrument"

Oceanpalreg is a coastal instrument developed at Starlab for operational remote sensing of the ocean surface, with potential direct applications to snow/ice mapping and soil moisture monitoring. The instrument is based on the exploitation of global navigation satellite systems (GNSS) and their augmentation systems (WAAS, EGNOS). The emitted signals provide an exceptional source of opportunity for passive remote sensing of the Earth. The use of GNSS reflections (GNSS-R) for sea-surface monitoring is a bistatic radar technique only requiring a receiving system. The concept has already been implemented for coastal platforms (few meters above the water), aircraft (1km to 10 km) and is being studied for space platforms (LEO, orbiting at 500-1000 km). The potential applications include sea-state, sea-surface altimetry and surface roughness, both for scientific and operational oceanography. We report on a recent long-term experimental and demonstration campaign, carried out at the Oceanpalreg Coeli station in the Barcelona Port during the period 2004-2007, with a real time web-based service. This campaign has been made possible through collaboration with the Barcelona Port Authority Environmental Monitoring Department (APB). The instrument was installed on a breakwater near the main entrance of the port, at 23 m over the sea-surface. We describe in this paper the successful long-term comparison between the data obtained by Oceanpal instrument and the observables recorded by two nearby buoys. Data used for this analysis cover a period of over one year, allowing a definitive evaluation of the performances of this GNSS-R based coastal instrument for SWH retrieval. We also review results from a weeklong phase altimetry campaign at the port of Vilagarcia. [C3080]

"High resolution millimeter wave SAR interferometry"

High resolution millimeter wave synthetic aperture radar (SAR) interferometry is presented using the MEMPHIS multi-baseline InSAR system. A complete processing chain is used to generate digital elevation models starting from the radar raw data. A deeper focus is laid on the phase unwrapping step, which is achieved using the multi-baseline properties of the system. In November 2006, an experiment was realized including two test sites in Switzerland; the actual results are presented and discussed. [C3081]

"Modeling and analyzing InSAR phase profiles at building locations"

The improved ground resolution of state-of-the-art synthetic aperture radar (SAR) sensors suggests utilizing SAR data for the analysis of urban areas. Even in the case of InSAR, for building recognition usually the analysis is triggered mainly from features detected in the magnitude images. However, considering InSAR data

significant phase profiles in range direction at building locations are observable. In this paper a simple model for these characteristic profiles in layover areas is proposed. The model takes into account that in layover areas a mixture of several signal sources contribute to the interferometric phase of a range cell. At building locations a combination of contributions from ground, wall, and roof is observed. The resulting phase profiles are characterized by sensor and illumination parameters as well as object parameters. In the first part of this paper, simulated phase images at building locations based on a given surface profile in range direction are presented. In the second part, real InSAR data sets of the airborne sensors AeS-1 (Intermap) and AER-II (FGAN-FHR) with a slant range resolution of 38 cm respectively 94 cm are used to calculate interferometric phase truth data which are then compared with the simulation results. [C3082]

"The repeat-pass interferometric SAR by Pi-SAR(L)"

This paper describes the system and experiment of Pi-SAR(L) repeat pass interferometric SAR. To obtain a high-quality interferometric image, it is necessary to make two flights on the same pass and observe in the same direction. We built a flight control system utilizing the preinstalled autopilot. This system measures position and altitude precisely with using a differential GPS, and controls the flight pass to be within virtual tube of 10 m diameter. The antenna rotation mechanism was also installed to control the observation direction. The repeat-pass flight has been conducted many times. The flights were stable and the deviation was within a few meters for both horizontal and vertical even in the gusty condition. The SAR data were processed in time domain based on range Doppler algorithm to make the complete motion compensation. The interferometric image processed after precise phase compensation is shown. [C3083]

"Using airborne laser altimetry to improve river flood extents delineated from SAR data"

Flood extent maps derived from SAR images are a useful source of data for validating hydraulic models of river flood flow. The accuracy of such maps is reduced by a number of factors, including changes in returns from the water surface caused by different meteorological conditions and the presence of emergent vegetation. The paper describes how improved accuracy can be achieved by modifying an existing flood extent delineation algorithm to use airborne laser altimetry (LiDAR) as well as SAR data. The LiDAR data provide an additional constraint that waterline (land-water boundary) heights should vary smoothly along the flooded reach. The method was tested on a SAR image of a flood for which contemporaneous aerial photography existed, together with LiDAR data of the un-flooded reach. Waterline heights of the SAR flood extent conditioned on both SAR and LiDAR data matched the corresponding heights from the aerial photo waterline significantly more closely than those from the SAR flood extent conditioned only on SAR data. [C3084]

"ICC's project for DInSAR terrain subsidence monitoring of the catalonian territory"

The Institut Cartogràfic de Catalunya (ICC) has initiated a project for continuous subsidence monitoring of the Catalan territory using an automatic advanced DInSAR processor (DISICC). Data used in this project are acquired by ERS-1/2, ENVISAT, and the future ALOS, TerraSAR-X and Radarsat 2 satellites. The processor performs the co-registration, interferogram generation, filtering, topographic cancellation, linear deformation model adjustment and non-linear displacement estimation, allowing the generation of classical and advanced DInSAR results combining information from different orbits and satellites. The project consists of the usage of 10 different ERS/ENVISAT frames, 5 descending and 5 ascending, completely covering the desired area, which is about 31.930 Km². The data temporal frame comprises images acquired from 1992 to 2006. [C3085]

"Numerical simulation of electromagnetic-wave propagation for land mine detection using GPR"

The ground penetrating radar (GPR) has demonstrated good potential for the remote imaging of surface-laid or shallow-buried landmine-like objects (typically ~ 5-30 cm) and its use is currently receiving much attention. It has turned out to be a promising alternative technology for low dielectric contrast objects, a difficult detection situation that is often encountered in practice (e.g. detection of plastic mines in dry or sandy soils environment). This paper examines numerically the imaging of buried objects using ultrawide-band (UWB) time domain radar. We develop a simplified model to characterize the system, air-ground-buried targets-antennas and simulate the electromagnetic wave propagation and scattering at a bandwidth of 0.5-2.5 GHz. All the elements need to be modelled simultaneously in order to obtain an accurate estimation of our radar performance and surface response to the incoming radar pulses. The final goal is to improve the detection rate of plastic antipersonnel mines, reducing the false alarm level. We show some simulated results in 2D and 3D assuming plane waves and afterwards we introduce a model for our GPR antennas to characterize the real source. [C3086]

"Disaster monitoring by extracting geophysical parameters from SAR data"

The fractal geometry proved to be the most appropriate mathematical instrument in describing natural scenes, by

means of few effective and reliable geophysical parameters. In this paper we use fractal concepts to model and to identify geometrical changes occurred in areas hit by disasters. We present an overall framework employing fractal based models, algorithms and tools to support identification of natural area changes due to natural or man-made disasters. The proposed framework includes a SAR raw signal simulator, which is of key importance to improve the comprehension of the mechanisms underlying SAR image formation. In addition, we consider, as a case study, the simulation and detection of lava flows in a volcanic scenario. The potentialities of our technique for the discrimination between different types of lava are presented and discussed. [C3087]

"Multidimensional radar waveforms a new paradigm for the design and operation of highly performant spaceborne synthetic aperture radar systems"

This paper introduces and analyses the innovative paradigm of multidimensional waveform encoding for spaceborne synthetic aperture radar (SAR). The combination of this technique with digital beamforming on receive enables a new class of highly performant SAR systems employing novel and highly flexible radar imaging modes. Examples are adaptive high-resolution wide-swath SAR imaging with compact antennas, enhanced parameter estimation sensitivity for applications like along-track interferometry and moving object indication, and the implementation of hybrid SAR imaging modes that are well suited to satisfy the hitherto incompatible user requirements for frequent monitoring and detailed mapping. Implementation specific issues will be discussed and examples demonstrate the potential of the new technique for different remote sensing applications. [C3088]

"SBRAS-an advanced simulator of spaceborne radar"

An application-oriented spaceborne radar advanced simulator (SBRAS) is presented in this paper. SBRAS is initiated by the technical and economical requirements to verify formation-flying distributed satellites synthetic aperture radar (SAR) scheme and simplify the instrument hardware design. The simulator develops a full flow of signal processing including formation design, SAR raw data simulation of nature scene, imaging, InSAR processing, digital elevation model (DEM) generation and performance analysis. A user-friendly GUI is provided. [C3089]

"The EarthCARE mission: Mission concept and lidar instrument pre-development"

The earth clouds, aerosols, and radiation explorer mission has been selected as the 6th earth explorer mission of ESA's living planet programme [1]. A suite of four instruments, active and passive, will be embarked on the same satellite to measure cloud and aerosol properties simultaneously with TOA radiances in order to derive TOA fluxes in relation to clouds and aerosols. [C3090]

"Initial CRAM aerosol retrievals from CALIPSO and supporting airborne HSRL measurements"

The successful launch of the Cloud-Aerosol Lidar and Infrared Pathfinder Satellite Observation (CALIPSO) and Cloud-Satellite (CloudSAT) satellites on April 28, 2006, placing two new active remote sensing systems (lidar and radar) in space, heralded a new era in spaceborne earth observations. Not only will they provide new information unique to active sensing satellites, but by positioning them in orbit with the A-Train constellation of satellites, joining the passive sensing satellites AURA, PARASOL and AQUA, this will enable myriad synergistic active-passive sensing opportunities. CALIPSO and CloudSAT have both successfully completed their payload checkouts and initial validations; some six months of data have already been collected and data are now beginning to be distributed to the scientific community (e.g., CALIPSO Level 1 and 2a data released on Dec. 8, 2006). Thus there are sufficient data, with more arriving daily, to fuel years of scientific studies addressing questions critical to more fully understanding the earth-atmosphere system and assessing weather-climate change issues. The Constrained Ratio Aerosol Model-fit (CRAM) technique for aerosol retrieval is examined in the context of CALIPSO data, and temporally/spatially coincident High Spectral Resolution Lidar (HSRL) data is studied with respect to its potential to provide external context to the retrievals and to verify aerosol models upon which the CRAM technique relies. [C3091]

"ADM-Aeolus: The first space-based high spectral resolution Doppler Wind Lidar"

The 'Living Planet Programme' of the European Space Agency (ESA) is gaining momentum. Six Earth Explorer missions are currently being implemented including ADM- Aeolus, ESA's Doppler Wind Lidar (DWL) mission. The Aeolus mission will demonstrate the capability of a space- borne high spectral resolution DWL to accurately measure wind profiles in the troposphere and the lower stratosphere (0- 30 km). The Mission thus addresses one of the main identified deficiencies of the current Global Observing System (GOS). From the backscattered frequency-shifted laser light it will be possible to obtain about 3,000 globally distributed horizontal line-of-sight (HLOS) wind profiles daily. The accuracy of the Aeolus winds, in cloud-free regions and above thick clouds, is expected to be comparable to that of radiosonde wind measurements. Additional geophysical products that will

be retrieved from the Aeolus measurements are cloud and aerosol optical properties. Aeolus HLOS wind profiles will find wide application in Numerical Weather Prediction (NWP) and climate studies, improving the accuracy of numerical weather forecasting, advancing our understanding of tropical dynamics and processes relevant to climate variability and climate modelling. Impact experiments, assimilating synthetic Aeolus wind data into operational NWP models, have already been performed. One focus has been the forecast performance in regions known to be particularly sensitive to the accuracy of the initial conditions. The tentative results show that the largest benefits from Aeolus HLOS winds can be expected over the oceans and in the Tropics. In view of other lidar missions in space, the potential of a long-term database of cloud and aerosol optical properties is being studied. An additional topic is the potential benefit of wind profile observations in the lower stratosphere. Ground-based and airborne campaigns are being prepared for the validation of the Aeolus Airborne Demonstrator (A2D)-a high spectral- resolution DWL instrument with technology very similar to Aeolus. This paper provides an overview of the Aeolus mission, the science and application activities being performed in support of the mission and the potential benefit of such observations in a wider context. [C3092]

"An efficient electromagnetic approach to train the SVM for depth estimation of shallow buried objects with microwave remote sensing data"

Present paper deals the fusion of image analysis with electromagnetic and support vector machine (SVM) optimization approach to estimate the depth of shallow buried metallic and dummy mine (i.e., without explosive) objects with microwave remote sensing data at X-band (i.e., 10 GHz). The objects were buried under dry and smooth sand. For this purpose, a monostatic scatterometer at X-band has been indigenously developed, which consists a transmitter and receiver mounted on the stand of the sand pit and when operated it moves over it in X- and Y- axis. An algorithm has been proposed for identification of suspected region first i.e., region of interest (ROI) that contains buried objects in the image by proposing a quantity "detection figure" (D), which further proceed for depth estimation of buried objects. Algorithm includes image processing, electromagnetic multi layer interaction and SVM approach. The convolution-using image processing techniques has been applied to avoid the overlapping of the return signal. The support vector machine (SVM) approach has been analyzed for estimation of depth and an efficient method based on electromagnetic multiplayer interaction concept has been proposed to train the SVM. The depth estimated for Al sheet gives better result than dummy landmine, but the estimated depths results for both objects are in good agreement with actual depths. The present approach may be quite helpful to develop an automatic satellite data based information systems to estimate the depth of various shallow buried objects with satellite or air-borne radar data. [C3093]

"Extinction-to-backscatter ratios of lofted aerosol layers observed during the first three months of CALIPSO measurements"

Case studies from the first three months of the Cloud and Aerosol Lidar and Infrared Pathfinder Spaceborne Observations (CALIPSO) measurements of lofted aerosol layers are analyzed using transmittance [Young, 1995] and two-wavelength algorithms [Vaughan et al, 2004] to determine the aerosol extinction-to-backscatter ratios at 532 and 1064 nm. The transmittance method requires clear air below the layer so that the transmittance through the layer can be determined. Suitable scenes are selected from the browse images and clear air below features is identified by low 532 nm backscatter signal and confirmed by low depolarization and color ratios. The transmittance and two-wavelength techniques are applied to a number of lofted layers and the extinction-to-backscatter ratios are compared with values obtained from the CALIPSO aerosol models [Omar et al, 2004]. The results obtained from these studies are used to adjust the aerosol models and develop observations based extinction-to-backscatter ratio look-up tables and phase functions. Values obtained by these techniques are compared to Sadeterminations using other independent methods with a goal of developing probability distribution functions of aerosol type-specific extinction to backscatter ratios. [C3094]

"Status of GNSS reflectometry related receiver developments and feasibility studies within the German Indonesian Tsunami Early Warning System"

In the frame of the German Indonesian Tsunami Early Warning System (GITEWS) project a multi-frequency Global Navigation Satellite System (GNSS) Occultation & Reflectometry & Scatterometry (GORS) space receiver is developed. It is based on commercial off-the-shelf (COTS) GNSS receiver technology, as the core instrument for a future tsunami detection constellation of small low Earth orbit (LEO) satellites. For use in reflectometry, scatterometry and radio-occultation measurements as well as high-precision navigation applications, specific adaptations of the GNSS receiver firmware are desirable, which require a close interaction between scientists and the receiver manufacturer. Within the GITEWS project GFZ has set up a team consisting of GFZ, DLR and JAVAD GNSS (JAVAD) to adapt and extend their new generation GNSS receivers for advanced scientific space applications. Specific adaptations address the improvement of the cold start time-to-first-fix, the selection of optimal tracking loop parameters and channel slaving for monitoring of reflected signals. Besides pseudorange,

phase and signal-to-noise measurements, the modified receiver allows output of in-phase (I) and quadrature-phase (Q) accumulations at 5 msec intervals (200 Hz). As a major step forward compared to current space receivers, the new receiver supports tracking of the civil L2C signal of the GPS constellation. An overview of the current status is given and first results are discussed. Within GITEWS the feasibility of a tsunami detection mission is studied, including the constellation mission design, the options for operating the system and the ways to develop an end-to-end system for the quick response to tsunami events. In parallel simulation studies of the GNSS signals reflected to a LEO satellite are carried out. This will be realised by a Zavorotny and Voronovich scattering model with a two-scale model approach using an Elfouhaily sea wave spectrum. An overview of the current activities is given and first results are discussed. [C3095]

"Performance Prediction and Verification for the Synchronization Link of TanDEM-X"

The paper describes the synchronization link of the two satellites of the TanDEM-X mission. The synchronization link is established to track the oscillator phase noise difference which- after appropriate processing-can be used to compensate the effect of oscillator phase noise. A signal model based on the synchronization link hardware is presented which is then used to derive an analytical expression for the compensation phase including effects such as instrument drift, Doppler, antennas, and receiver noise. Specifically the influence of the synchronization link RF hardware on the quality of the derived compensation signal is crucial for the performance. Therefore the synchronization link RF hardware of the TerraSAR-X satellite is characterized to obtain realistic data. These measurements will be used for the calibration of the synchronization link, i.e. to remove systematic errors due to temperature drifts of the instrument. [C3096]

"Prediction and detection of Faraday rotation in ALOS PALSAR data"

Faraday rotation can degrade the quality of low- frequency spaceborne SAR data, making an estimation and correction of these effects a prerequisite for data quality continuity. In this paper, methods for predicting and estimating Faraday rotation are presented and tested on ALOS/PALSAR data. A first example for unambiguous detection of Faraday rotation in SAR is shown. In addition, the improvement after correcting for FR is proven using a real data example. [C3097]

"Individual T/R module characterisation of the TerraSAR-X active phased array antenna by calibration pulse sequences with orthogonal codes"

TerraSAR-X is a high resolution synthetic aperture radar (SAR) satellite due for launch in 2007. Its active phased array X-Band antenna hosts 384 transmit/receive modules controlling the beam steering in azimuth and elevation direction. Precise modelling of the antenna is only possible if the actual characteristics of each individual transmit/receive module are known. TerraSAR-X has been equipped with an innovative characterisation mode based on the so-called PN Gating method. Individual and simultaneous characterisation of all transmit/receive modules is realised under most realistic conditions with the same power loads like in the nominal mode. This paper shows the results of PN Gating measurements on a satellite SAR system. [C3098]

"Inversion of soil moisture content from L- and P-band AIRSAR polarimetric SAR data"

Improvements of polarimetric inversion algorithms is presented in this paper. The confounding influence of roughness and vegetation cover on the estimation of the soil moisture contents is considered in the inversion algorithm that estimates volumetric moisture contents and roughness parameters simultaneously from the pertinent combination of polarization measurements. The estimation of the soil moisture contents from polarimetric SAR data is investigated using L- and P-band AIRSAR polarimetric SAR data collected over the Jeju Island, Korea. Results indicate that the estimation of the soil moisture contents can be expanded to a wider range of terrain types by using both L- and P-band polarimetric SAR data. [C3099]

"Full motion compensation for LFM-CW synthetic aperture radar"

Small, low-cost, high-resolution SAR systems, such as the Brigham Young University (BYU) muSAR, are made possible by using a linear frequency modulated continuous wave (LFM-CW) signal. SAR processing assumes that the sensor is moving in a straight line at a constant speed, but in actuality a UAV or airplane will deviate, often significantly, from this ideal. This non-ideal motion can seriously degrade the SAR image quality. In a continuous wave system this motion happens during the radar pulse which means that existing motion compensation techniques, which approximate the position as constant over a pulse, are limited for an LFM-CW SAR. In this paper, the LFM-CW SAR signal model is presented and processing algorithms are discussed. The effects of non-ideal motion during the SAR signal are derived and new methods for motion correction are developed which correct for motion during the pulse. These new motion correction algorithms are verified with simulated data and with actual data collected using the BYU muSAR system. [C3100]

"Characterization of local regularity in SAR Imagery by means of multiscale techniques: application to oil spill detection"

Thanks to their capability to cover large areas, in all weather conditions, during the day as well as during the night, spaceborne Synthetic Aperture Radar (SAR) techniques constitute an extremely promising alternative to traditional surveillance methods. Nevertheless, in order to assure further usability of SAR images, specific data mining tools are still to be developed to provide an efficient automatic interpretation of SAR data. The aim of this paper is to introduce texture analysis performed in the framework of time-frequency theory, as a means to detect oil spills in the sea surface. In particular, an algorithm permitting a precise quantitative characterization of the border between the oil spill candidate and the sea, will allow a novel classification of oil spills and look-alikes.

[C3101]

"Developing a GeoSTAR science mission"

The geostationary synthetic thinned aperture radiometer (GeoSTAR) is a new instrument design that has been under development at the Jet Propulsion Laboratory in the form of a proof-of-concept prototype. It is intended to fill a serious gap in our Earth remote sensing capabilities-namely the lack of a microwave atmospheric sounder in geostationary orbit. Such sensors have long been part of low-earth-orbiting (LEO) operational weather satellites and research satellites and have had a major impact ranging from numerical weather prediction to climate research. A similar capability in GEO is highly desired because of the advantageous observing point GEO offers, with continuous views of the entire visible Earth disc-crucial for the observation of hurricanes and other rapidly evolving atmospheric phenomena. GEO also enables full resolution of the diurnal cycle, which is particularly important in the study of atmospheric processes and climate variability where clouds and convection play a role, since those phenomena are known to have strong diurnal variability and are difficult to sample properly with sun synchronous LEO satellites. The GeoSTAR prototype produced the first interferometric radiometric images obtained at sounding frequencies in early 2005, and subsequent tests have demonstrated that the system exhibits excellent stability, accuracy and sensitivity and performs even better than predicted. This can be characterized as a breakthrough development. The technology required to implement GeoSTAR is at a level of maturity that a space mission can be contemplated. Such a mission is recommended by the U.S. National Research Council in its recent Decadal Survey of Earth missions and is being considered by both NASA and NOAA for the coming decade. Recent studies indicate that it is indeed feasible to implement a GeoSTAR mission in the 2014-16 time frame. We discuss possible mission scenarios as well as the science benefits that would ensue. The benefits are particularly significant in the area of tropical cyclones and severe storms, where there currently is a dearth of observations. With a geostationary microwave sounder it is possible to obtain the 3-dimensional distribution of temperature, water vapor and liquid water continuously and regardless of cloud cover, and atmospheric stability indices such as lifted index (LI) and convective available potential energy (CAPE) can be derived nearly everywhere. That will make it possible, for example, to detect severe-storm precursor conditions even if the area is under cloud cover. Recent progress in radiative transfer models now also makes it possible to obtain those parameters in the presence of moderate precipitation, and rain rates and snow rates can be derived as well. Aircraft based field campaign observations have also shown that a microwave sounder can be used to derive measures of convective intensity and precipitation in deep-convective systems from scattering due to ice particles formed by such systems. This can be used to estimate the intensity of tropical cyclones and can be used to detect sudden intensification and weakening in near-real time. [C3102]

"Analysis and improvement of polarimetric calibration techniques"

This work presents an analytical study of the Quegan's PolSAR data calibration algorithm. As it shall be demonstrated, the solution proposed by Quegan based on certain approximations, gives in certain situations, biased crosstalk ratios u , v , w and z . An improved Quegan's calibration algorithm is proposed and tested.

[C3103]

"ALOS PALSAR products verification"

ALOS, an enhanced successor of the Japanese Earth Resources Satellite 1 (JERS-1), was launched from JAXA's Tanegashima Space Center in January 2006. An important contribution to the ALOS mission is the verification of PALSAR products to be distributed by the European ADEN node using the PALSAR processor developed by JAXA. A total of 28 ALOS PALSAR products have been analysed with respect to radiometric, geometric and polarimetric quality (including effects of Faraday rotation caused by the ionosphere) and a summary of the results is shown in this paper. [C3104]

"Calibration of the SHARAD Instrument"

The Mars Shallow Radar Sounder (SHARAD) is an HF (20 MHz) Sounding Radar embarked onboard the Mars Reconnaissance Orbiter (MRO) spacecraft. SHARAD on-ground calibration activities have been limited to the characterization of the SEB (SHARAD Electronic Box), not having been possible to perform extensive characterization of the flight antenna nor end- to-end calibrations on ground. Scope of the present document is to define the activities to be carried out in-flight in order to ensure SHARAD products calibration. The calibration needs are assessed and an overall calibration strategy is then defined, leading to the identification of the data sets to be collected and relevant processing to be applied. The document also address how to exploit the available calibration data (from both on- ground and in-flight calibration) to correct SHARAD products, and the organization of the calibration database. [C3105]

"Subaperture analysis of polarimetric SAR imagery"

In this paper we investigate the nonstationary behavior of individual polarimetric parameters, e.g. entropy, anisotropy, alpha angle, orientation angle, helicity, etc. We distinguish between parameters that depend solely on the eigenvalues of the standard Cloude-Pottier polarimetric decomposition (span, entropy and anisotropy) and the others that depend on the scattering mechanisms, i.e. the Cloude-Pottier eigenvectors. After producing a series of azimuth subaperture polarimetric images, we apply the polarimetric decomposition to each subaperture frame and identify subaperture frames that show nonstationary scattering. Comparison of several specific targets, both discrete and distributed, will highlight aspects of polarimetric variability with respect to the SAR view angle. We illustrate our results using EMISAR L-band polarimetric SAR data. [C3106]

"Evaluation of the altimetric information from RADARSAT-1, ASTER and SRTM data for topographic mapping in the Amazon Region"

Brazilian Amazon is a vast territory rich in natural renewable and non-renewable resources. Due to the adverse environmental condition (rain, cloud, dense vegetation, poor access), topographic information is still poor, and when available needs to be up-dated or re-mapped. In this paper, the feasibility of using altimetric information for topographic mapping through orbital stereoscopic (ASTER, RADARSAT-1) and interferometric (SRTM-3) DEMs (digital elevation models) was investigated for two regions in the Brazilian Amazon: Tapajos National Forest (flat terrain) and Serra dos Carajas (mountainous relief). The quality of information produced from these data was evaluated regarding field altimetric measurements. Precise topographic field information acquired from differential global positioning system (DGPS) was used as Ground Control Points (GCPs) for the modeling of the stereoscopic DEMs and as independent check points (ICPs) for the calculation of altimetric accuracies of the products. The investigation has shown that the accuracy of the altimetric information derived from Fine RADARSAT-1, ASTER and SRTM-3 DEMs met the requirements for a semi-detailed (1:100,000-map) scale as requested by the Brazilian standard for cartographic accuracy. Furthermore, SRTM-3 DEM was more accurate than stereoscopic DEMs. The additional great advantage of using SRTM-3 is the free access data. However, up-dated planimetric information is also necessary for cartographic production. Thus it is suggested a combination of altimetry derived for SRTM-3 and planimetry from high-resolution SAR (Fine RADARSAT-1, PALSAR) or if possible optical data (ASTER, SPOT) for topographic mapping at semi-detailed scale in similar environments of the Brazilian Amazon, where terrain information is seldom available or presents low quality. [C3107]

"Joint time-frequency analysis for radar signal and imaging"

The Fourier transform has been widely used in SAR signal and image processing. In most cases, SAR signals exhibit time-varying behavior in the Doppler spectrum. Thus, a joint time-frequency analysis (JTFA) for SAR signals is more useful. In this paper, we introduce three important issues with JTFA for radar signal and imaging: (1) time-frequency based image formation; (2) time-frequency analysis of ground moving targets; and (3) time-frequency analysis of micro- Doppler signatures. [C3108]

"ALTICORE-A consortium serving european seas with coastal altimetry"

In this paper, we describe the ALTICORE (value added satellite ALTImetry in COastal REgions) initiative, a consortium aiming at providing high quality coastal altimetry over some European seas. Taking the Ligurian Sea in the NW Mediterranean as an example, which acts as a test zone for this work, we show the improvement in availability and quality of ENVISAT data, through our processing, when compared with the official altimetric products delivered by AVISO. We also introduce the building concepts of solutions for data search, extraction, update and delivery based on web-services. This grid-type infrastructure is being designed within ALTICORE. [C3109]

"TOGA, a prototype for an optimal orbiting GNSS-R instrument"

Remotely sensing the Earth's surface using GNSS (Global Navigation Satellite System) signals as bi-static radar sources is one of the most challenging applications for radiometric instrument design. As part of NASA's Instrument Incubator Program, our group at JPL is building a prototype instrument, TOGA (Time-shifted, Orthometric, GNSS Array), to address a variety of GNSS science needs. Observing GNSS reflections is major focus of the design/development effort. The TOGA design features an electronically steered antenna (ESA) array which forms simultaneous high-gain beams in multiple directions. Multiple FPGAs provide flexible digital signal processing logic to process both GPS and Galileo reflections. A Linux operating system based science processor serves as experiment scheduler and data post-processor. This paper outlines the TOGA design approach as it applies specifically to observing science quality GNSS-R signals from low Earth orbit. [C3110]

"Altimetric calibration experiences in the Western Mediterranean"

Since many years, space borne radar altimeters have brought a powerful contribution in monitoring the dynamic sea surface topography, and in understanding better the ocean circulation and its impact on the earth system. Today, altimetric satellites are observing the whole oceans, measuring the sea surface height with a rms precision of 3-4 cm at 1 Hz sampling, as demonstrated by TOPEX/POSEIDON, launched in 1992, by Jason-1, launched in 2001 and by ENVISAT, launched in 2002. Such a high level error budget was achieved thanks to the tremendous improvements which have been obtained in radar performances as well as in precise orbit determination. Indeed, applications of altimetry in oceanography and geodesy requires very precise measurements of the satellite-sea level range, along with appropriate environmental corrections, but also an accurate knowledge of the satellite position with respect to the Earth reference. One campaign has also been made in June 2003 at the Ibiza island area (Martinez-Benjamin et al., 2003). The marine geoid has been used to relate the coastal tide gauge data from Ibiza and San Antonio harbours to off-shore altimetric data. A technical Spanish contribution to the calibration experience has been the design of GPS buoys and GPS catamaran taking in account the University of Colorado at Boulder and Senetosa/Capraia designs. We present a synthesis of the sea level results results obtained from the altimeter calibration campaign at Ibiza island on June 2003 using the direct measurements from GPS buoys and the derived marine geoid. The main objective of the marine campaign was to check the value of Ibiza Island as a permanent calibration site in the western Mediterranean Sea, to complement the Corsica site in the network of altimeter calibration sites. [C3111]

"Complex scene analysis from Time-Frequency statistics of POLSAR data"

This article presents a statistical approach for the study of PolSAR images using Time-Frequency (TF) correlation properties. PolSAR information is analyzed using a linear time- frequency (TF) decomposition which permits to describe a scene polarimetric behavior for different azimuth angles of observation and frequencies of illumination. A TF signal model is proposed and studied using two statistical descriptors related to the signal stationary aspect and coherence in the time-frequency domain. These indicators are shown to provide complementary information for an enhanced description of the scene. [C3112]

"Characterization of scatterers by their anisotropic and dispersive behavior"

Synthetic Aperture Radar (SAR) images built from received signals are high-resolution maps of the spatial distribution of the reflectivity function of targets. Conventional radar imaging assumes that all the scatterers are considered as bright points (isotropic for all observation angles and white in the frequency band) [1]. Recent studies based on multidimensional Time-Frequency Analysis describe the angular and frequency behavior of scatterers and show that they are anisotropic and dispersive [2]. Another useful information source in radar imaging is the polarimetry. Studies based on multidimensional wavelet and coherent decompositions allow to represent the angular and frequency polarimetric behavior and show the non-stationarity of this behavior. The aim is to characterize scatterers by time-frequency analysis and polarimetry. [C3113]

"The cross Time-Frequency Distribution Series for Synthetic Aperture Radar (SAR) applications"

Joint Time Frequency Analysis (JTFA) is a powerful analysis tool in SAR image processing. At the heart of this process are the Time-Frequency Representations (TFR's) such as the Wigner-Ville distribution (WVD), which is difficult to use because of its large cross-product terms. The pseudo-WV TFR reduces the cross terms by smoothing the integration defining the WV transform. The Time-Frequency Distribution Series (TFDS) mitigates the unwanted cross product terms by averaging only those expansion terms close to the signal. The cross-Wigner-Ville Distribution (CWVD) is a generalization of the cross correlation function to the time-frequency (TF) plane. Likewise, the cross- pseudo-WV and the cross-TFDS can be defined and applied to pairs of signals. The cross-TFDS is shown to reduce the cross terms seen in the cross-WV distribution. Two examples are shown using SAR data. [C3114]

"An improved time-frequency phase adjustment technique for ISAR"

The time-frequency method is a promising phase adjustment technique for inverse synthetic aperture radar (ISAR). Usually, the time-frequency method estimates the translational Doppler frequency and thus the translational Doppler phase by detecting the peaks of the time-frequency representation at different times. Unfortunately, it has some defects, such as the sensitivity to noise and target scintillation, and the aliasing of the time-frequency representation due to undersampling. In order to remove these limitations, we develop an improved time-frequency method. It estimates the translational Doppler frequency from the envelope correlation of the instantaneous slices of the time-frequency representation. Compared with the traditional time-frequency method, this technique can estimate the translational Doppler frequency more accurately. Moreover, we develop a preprocessing method to avoid the aliasing of the time-frequency representation due to undersampling.

[C3115]

"The fractional Fourier transform and its application to high resolution SAR imaging"

The fractional Fourier transform (FrFT), which is a generalized form of the well-known Fourier transform, has opened up the possibility of a new range of potentially promising and useful applications including radar involving the use and detection of chirp signals, pattern recognition and Synthetic Aperture Radar (SAR) image processing. The Chirp Scaling Algorithm (CSA) is one of the most important and well-known radar imaging algorithms. It is attractive because of its excellent focusing ability and implementation simplicity. Benefiting from the inherent structure of the FrFT for non-stationary digital signal processing and analysis, especially for chirped-type signals, a new version of the CSA based on the Fractional Fourier Transform (FrFT) is developed. The introduced Fractional Chirp Scaling Algorithm (FrCSA) applied the Fast Fourier Transform (FFT) instead of the fractional Fourier transform (FrFT) in the azimuth direction for the analytical development tractability purposes only as it is numerically tractable in both dimensions. To demonstrate the resolution and focusing enhancement in the azimuth dimension using the FrCSA and also to be able to perform azimuth fractional filtering, noise removal and flight path nonlinearity compensation, a closed form expression for the azimuth fractional transformation is required. In this talk we present the mathematical derivation for a closed-form expression of the azimuth-fractional Fourier transform of the new FrCSA with application to high resolution imaging. Results to real SAR data images will show significantly enhanced features using the FrFT-based azimuth expression instead of the classical FFT-based one within the fractional chirp scaling algorithm or any other chirped-type SAR imaging algorithm. [C3116]

"Retrieval of ice thickness distribution in the seasonal ice zone from L-band SAR"

Airborne polarimetric and interferometric synthetic aperture radar (Pi-SAR) observation, conducted in the southern Sea of Okhotsk in February 2005, provided the opportunity to validate the retrieval of ice thickness distribution. In conjunction with the airborne SAR observation, in-situ ice thickness and ice-surface roughness measurements were carried out in the same area with ship-borne electromagnetic (EM) inductive sounding and supersonic profiling, respectively. Based on the analyzed results of data acquired in this experiment, this paper examines the possibility of ice thickness retrieval from the L-band SAR backscattering data in the seasonal ice zone (SIZ). [C3117]

"Perspective of remote optical measurement techniques (ROMTs)"

This article presents an intercomparison between four different ROMTs: differential optical absorption spectroscopy (DOAS), differential absorption LIDAR (DIAL), Fourier transform infrared spectroscopy (FTIR), and tunable diode laser absorption spectroscopy (TDLAS). The main focus is on the TDLAS technique, where the main laser-diode typologies and modulation schemes, namely, wavelength modulation spectroscopy (WMS) and frequency modulation spectroscopy (FMS), are reviewed. At present, new promising modulation schemes with range resolution capability are being investigated. Among them, analog frequency modulation (FM) and digital pseudo-random schemes are discussed. [C3118]

"Mapping subsidence in Tianjin area using ASAR images based on PS technique"

By identifying temporarily stable natural reflectors or persistent scatterers (PS), PSInSAR (Persistent Scatterers for SAR Interferometry) technique can analyze this subset of pixels in SAR images, even with long temporal and space baselines, to get high accuracy deformation measurements. We implement the PSInSAR process that is briefly summarized in this paper and apply this method in Tianjin area to detect the deformation phenomena using ENVISAT ASAR images. Calibration of ASAR images helps us select more PSC and using calibrated backscattering coefficient threshold we can discard the pixels whose amplitude are relatively stable while whose backscattered signals are weak and incoherent. Results obtained by processing 14 images show the distribution and the relative deformation value of the displacement field. The estimated linear velocities of PS are not

accurate enough because of the relatively small number of images. [C3119]

"ASAP, towards a PARIS instrument for space"

The technological aspects of the Altimetric and Scatterometric Applications of PARIS (ASAP) sensor are presented in this paper. This sensor is based on the PARIS concept, which makes use of GPS signals reflected on the ocean's surface in order to measure the surface's properties (altitude and roughness). The ASAP instrument is a hardware real-time PARIS receiver with the aim of being an intermediate step between the airborne GOLD-RTR receiver developed at our institute and a future spaceborne PARIS instrument. [C3120]

"Semi-automatic true orthophoto production by using LIDAR data"

Light Detection and Ranging (LIDAR) has been used for years with a variety of applications, including the efficient creation of digital terrain models (DTMs) for large-scale, high- accuracy mapping. LIDAR technology offers fast, real-time collection of 3-D points so that allows the production of higher-accuracy orthophotos than traditional stereo-compilation methods. The technology is moving quickly toward offering more efficient collection techniques for applications such as city modelling and true orthophoto production. Traditional orthophoto production suffers from the fact that buildings (and any other objects above ground) are not correctly placed in the orthophoto. True orthophoto production overcomes these deficiencies by taking the digital surface model (DSM) into account. However, the resulting true orthophotos still suffer from occluded areas and unsharp edges of buildings and roads. The experimental investigations with different data sets show that it is essential to use high quality DSMs to produce high quality true orthophotos. In this paper, aspects of the improvement of true orthophoto production will be discussed: (a) in the first approach which has been widely used in photogrammetry, the DSM is used for generating true orthophotos and (b) in comparison to the DSM based method, semi-automatically collected vector data of buildings are superimposed on DTM and are used as input data for generating true orthophotos in the second approach. The processes and problems of both true orthophoto production procedures will be investigated in detail and results include the comparison of true orthophoto productions based on DSM (from LIDAR data) and DTM plus vector data. For the experimental investigation, a LIDAR data set for downtown Stuttgart is used. [C3121]

"An airborne multi-angle power line inspection system"

This paper gives a brief description of an Airborne Multi-angle Power Line Inspection System (AMPLIS). AMPLIS is composed by 3 CCD cameras, a Position and Orientation System (POS), a stabilized platform, the data collection and control subsystem. It can be equipped on a helicopter and fly along the lines at a speed of about 100km/h at a relative height of 100 m over the power lines. AMPLIS is capable of detecting the distance between the power lines and the ground surface with an accuracy of less than 0.5 m. It can automatically find the dangerous objects beneath the lines which can greatly decrease the man power and cost in power line inspection. It has been successfully tested with good performance in Wuhan, China, 2005. [C3122]

"DInSAR monitoring of land subsidence in Orihuela City, Spain: Comparison with geotechnical data"

An advanced DInSAR technique called Coherent Pixels Technique (CPT) has been used to measure the subsidence existing in Orihuela city (Spain) during the period 1993-2001 due to ground water level fall. The estimated subsidence, with values lower than 7 cm, is highly influenced by soil geotechnical conditions like the deformable soil thickness. In addition, the wells location is an important subsidence factor because they are directly related to a decrease of the piezometric level. [C3123]

"Student developed meteorological radar network for the western part of Puerto Rico: First node"

This paper summarizes the work being done in developing a student designed radar network in western Puerto Rico. Modifications to a commercially available Raytheon MK2 marine radar are presented as well as the sensitivity expected. [C3124]

"3-D tsunami coastal hazard mapping in Sri Lanka by very-high resolution, airborne and spaceborne remote-sensing"

Following an inter-Government agreement established between Italy and Sri Lanka in the aftermath of the great 2004 Indian Ocean tsunami, the operational project 'HyperDEM' was designed for mapping in 3-D the coastal areas of Sri Lanka, aimed to easing and speeding-up emergency mapping in tsunami- prone areas. The work, based on integration of airborne Lidar and spaceborne Radar campaigns, started in autumn 2005 and was accomplished in summer 2006 after acquisition of the outstanding data volume of ca. 2.7 TeraBytes. Some

examples of results, and technical hints on methodological solutions adopted in solving operational problems are presented here. Upon completion of the work, the Government of Sri Lanka was provided with ca. 2'500 sq.km of Digital Elevation Models of the coastal areas, ca. 1'800 of which at the exceptional resolution of 1 metre and the elevation precision of 0.3 metres, and c.a. 700 at the resolution of 30 metres vs. an elevation precision of 2.6 metres. [C3125]

"Earthquake damage detection using remote sensing data"

In this study, we propose a new earthquake damage detection method based on a combination of the results estimated by using earthquake information (magnitude and location of source) and the change of the earth's surface observed by SAR. As a map produced by the detection method has less noise than a coherence ratio image, we found that the proposed method has better detection ability than that which only uses the change of coherence value. [C3126]

"Improvement and validation of MODIS performance in automated detection and extent estimate of wildfires"

Global MODIS Fire products (MOD14) are routinely generated by automated application of the Giglio algorithm (Giglio et al., 2003, Remote Sensing of Environment 87, 273-282) on daytime and night-time data collected up to four times a day. We present here the results and the validation of an Improved Giglio Algorithm for the Detection of Italian Fires (IGADIF). IGADIF presents substantial innovation in the computing of (two) physical parameter estimates at sub-pixel resolution: the top fractional temperature present in candidate Hot-Spot pixels, and the total area involved in the burnout. GIS validation of IGADIF and MOD-14 results are conducted considering two independent sets of ground truth data, the record of fire extinguishing operations carried out by the Italian National Firemen Corps (NFC), and the burn scars obtained from ASTER. [C3127]

"Retrieving 3D canopy structure from synergistic analysis of multi-angle and lidar data"

Recent empirical studies have shown that multi-angle data can be useful for predicting canopy height, but the physical reason for this correlation was not understood. The research presented here puts forth a physical explanation for this phenomenon. We employ the use of Radiative Transfer, more specifically canopy spectral invariants, which can decouple spectral and structural parameters in a vegetation canopy. As a case study we compare canopy heights predicted from a multivariate analysis of 28 (7 cameras* 4 bands) and LVIS canopy heights and a multivariate analysis of 7 directional escape probabilities and LVIS canopy heights. We find that the 7 directional escape probabilities can provide approximately the same amount of information about canopy height as 28 spectral/angular reflectances from AirMISR. Finally we speculate that multi-angle data does not allow for extraction of canopy height but in fact requires synergy between Lidar sensors. [C3128]

"Speed measurements with a continuous wave lidar prototype"

The UPC lidar group is developing a Doppler wind lidar based on the "edge-technique". Such systems use the slope of a high resolution optical filter as frequency discriminator. A laboratory prototype, able to measure the speed of solid targets emitting continuous wave radiation and using a Fabry-Perot interferometer as optical filter, has been built. A tuning control has been included to compensate drifts between the emitted frequency and the filter resonance frequencies in order to assure maximum sensitive measurements. The design of the system and different results concerning the performance of the tuning control system and speed measurements will be presented. [C3129]

"A wind speed and fluctuation simulator for characterizing the wind lidar correlation method"

Aerosol distribution in the atmosphere is used as a wind-tracer by lidars since it is drifted by the wind and responds to its changes. Two methods are used: the correlation and the Doppler method. This first one is easier and cheaper to implement than the latter. It makes it competitive for retrieving wind speed profiles or estimating wind turbulence. However, its accuracy decreases significantly as the distance from the optical radiation source increases, hence the need to characterize the method by means of wind field profile simulations and validate it by comparing the retrieval of real wind velocities with that of cooperative instruments such as radiosoundings. In this paper, the bases of a 2D lidar signal simulator are presented. The relationship between wind fields and the aerosol concentration dynamics, and the way they relate to lidar signal returns is explained. The first results of the application of the correlation method for the retrieval of wind velocities from real data at the UPC are presented and compared to radiosoundings measurements. [C3130]

"Statistical considerations on the extinction error variance for the raman lidar inversion algorithm"

At the basis of the Raman lidar extinction inversion algorithm is the derivative of the logarithm of the ratio between the atmospheric nitrogen number density and the range-corrected Raman power return. While its computation is straightforward under ideal (noiseless) conditions, this is not the case under low signal-to-noise ratios, for which the observation noise may lead the logarithm to singular values. This work presents an analytical-statistical overview of the inversion problem and related error bars, tentative noise limiting criteria, and justifies the approximations at play to estimate the inversion error by means of error-propagation techniques for high signal- to-noise ratios. Simulation examples consider a 532/607-nm elastic-Raman system. [C3131]

"Intercomparison of spanish advanced lidars in the framework of EARLINET"

To extend and reinforce the action of the EARLINET- ASOS project, a nucleus of Spanish advanced lidars was created. Four systems were intercompared satisfactorily in terms of backscatter coefficients at two elastic wavelengths. [C3132]

"Lidar determination of the frequency of variations of the boundary-layer top"

The frequency of thermals up- and downdraft, during the day, and that of gravity waves, during night, are retrieved by applying a fast Fourier transform to the temporal evolution of the boundary-layer height as obtained by lidar measurements. The principal components of each obtained spectrum of frequency are related to the dominant processes occurring at the convective and nocturnal boundary-layer tops. The formation of lee-waves systems during special meteorological conditions determined the oscillation of the boundary-layer height. Fluctuations at the nocturnal boundary-layer height can occur even if the conditions through the layer depth are statically stable. These oscillations are principally due to wind shear and buoyancy (gravity) waves at the altitude of the nocturnal boundary-layer top. [C3133]

"Comparison of SRTM-NED data to LIDAR derived canopy metrics"

Forest canopy height derived from the SRTM-NED were compared to three LIDAR vegetation metrics for the Sierra Nevada forest. Generally the SRTM-NED was found to under estimate the vegetation canopy height. The SRTM SAR signal was found to penetrate, on average, into 44% of the canopies. The residual errors as a function of LVIS canopy height and cover were found to generally increase with height and cover. Likewise, the RMSE was found to initially increase with canopy height and cover but saturates at 50 m height and 60% cover. [C3134]

"Extracting tree crown properties from ground-based scanning laser data"

The spatial organization of above-ground plant material plays an important role in controlling not only plant functional activities like photosynthesis and evapotranspiration, but also the photo-vegetation interactions. To improve our understanding of such interactions, the acquisition of highly detailed information about the 3D architecture of individual plants and communities of plants is required. Recently, Light detection and ranging (LiDAR) sensors, both at the ground and the airborne-level, have emerged as useful tools for mapping 3D plant structure. One such ground-based instrument is the Intelligent Laser Ranging and Imaging System (ILRIS 3D), which was developed at Optech Incorporated. This laser scanner, generates a 3D digital reconstruction of any scene, by actively emitting laser pulses and recording the time elapsed for the return of a pulse, thereby measuring the distance of any given object. It is the objective of this research to utilize the ILRIS 3D to measure structural, and biophysical information of individual trees for use as direct inputs into complex radiative transfer models. The key parameters under investigation are crown dimensions (i.e. shape, area, and volume), crown-level gap fraction (GF) and crown- level leaf area index (LAI). The ILRIS 3D was used to acquire 3D point clouds of an artificial 6' Ficus tree, in a controlled laboratory environment. Measured XYZ point cloud data was segmented to retrieve laser pulse return density profiles, which subsequently were used to estimate gap fraction and LAI . Gap fraction estimates were cross-validated with traditional methods of histogram thresholding of digital photographs ($r^2 = 0.96$). Crown LAI estimates were compared with the actual values ($r^2 = 0.95$, RMSE = 0.45). The next challenge was to implement the developed algorithms to real crowns, namely olive (*Olea europaea* L.) orchards in southern Spain. Individual tree-level ILRIS 3D data was collected from 24 structural- y diverse crowns. Crown dimensional profiles were extracted for ILRIS data that was collected from a horizontal view (i.e ground-based) and a nadir view (i.e from platform 12 meters above ground). Preliminary retrievals from the olive orchards dataset is described here, while current ongoing field measurements are being conducted to validate the findings. Successful demonstration of extracting crown-level structural parameters like gap fraction and LAI from ground-based LiDAR will be important new information that can be used for detailed radiative transfer modeling in olive orchards and likely lead to more robust inversion algorithms. [C3135]

"Intercomparison of Calibration techniques for the 1064nm channel on a Nd:YAG elastic lidar"

The need for accurate calibration is apparent for accurate retrievals of backscatter at 1064 nm. Due to the low molecular scattering in comparison to the aerosol component, it is not possible to use a Rayleigh calibration procedure which is suitable for the 355 and 532 nm channels and an alternative approach is needed. In particular, a modified cirrus cloud calibration method is considered which uses the fact that the cirrus cloud scatter is spectrally independent together with an approach to properly estimate the backscatter at cloud base. We find that the calibration accuracy can be taken within 15% which is reasonable agreement with the uncertainty in the backscatter color ratio between 532 nm and 1064 nm. [C3136]

"Numerical simulation of a heterodyne Doppler LIDAR for wind measurement in a turbulent atmospheric boundary layer"

This study concerns the modeling and the design of a monostatic heterodyne pulsed LIDAR. The heart of the system is constituted of a 1.55 μm able to produce high pulse repetition frequency. The aim of this work is to assess its efficiency to perform accurate wind speed measurements in the low atmospheric boundary layer, from a 2-D scanning pattern, in the presence of refractive turbulence. A complete LIDAR numerical simulation technique has been developed. Its main originality is the integration of both optical and fluid dynamics numerical methods to take into account the signal coherence loss due to refractive turbulence and speckle effect as well as the fine structures of the wind field. The wind speed profiles along each line-of-sight are retrieved from the return signal using a low-order autoregressive model. An adequate averaging model is then used estimate horizontal components of the wind speed for altitudes up to 150 m. [C3137]

"Coherent lidar modulated with frequency stepped pulse trains for unambiguous high duty cycle range and velocity sensing in the atmosphere"

Range unambiguous high duty cycle coherent lidars can be constructed based on frequency stepped pulse train modulation, even continuously emitting systems could be envisioned. Such systems are suitable for velocity sensing of dispersed targets, like the atmosphere, at fast acquisition rates. The lightwave synthesized frequency sweeper is a suitable generator yielding fast pulse repetition rates and stable equidistant frequency steps. Theoretical range resolution profiles of modulated lidars are presented. [C3138]

"An algorithm to improve the NEXRAD rain rate estimates"

A Doppler WSR-88D radar (NEXRAD) is currently operating in Cayey (East of PR, at 886 m). Reflectivity and rain rate (Z-R) relationships were developed using a dense network of rain gauges to validate radar estimates. These equations intent to correct the radar estimates for seasonal effects. Equations were derived for wet and dry seasons over Puerto Rico. To minimize the errors due to beam block and clutter, equations were derived with 20 rain gauges located 15 km or less from the radar location. [C3139]

"Use of tandem pairs of ERS-2 and ENVISAT SAR data for the analysis of oceanographic and atmospheric processes"

Currently the European satellites ERS-2 and ENVISAT are flying on the same orbit with a time separation of 30 minutes. In this presentation pairs of the respective synthetic aperture radar data are analyzed with respect to different atmospheric and oceanic processes. The presented results were obtained in the framework of the ESA AO project COTAR. The tandem configuration exists since the launch of ENVISAT in 2002. In the presentation an overview will be given of the available image pairs acquired over the ocean on a global scale. Combinations of ERS-2 SAR data with both image mode and wide swath mode scenes provided by the ENVISAT ASAR are considered. The two SAR images enable the analysis of the change of radar cross section within half an hour. This temporal separation is very interesting for oceanographic applications because there are many processes like atmospheric fronts, convective cells, ocean tides, etc., which are detectable on this time scale. In the presentation tandem pairs acquired over the research platform FINO west of the island Borkum in the North Sea will be presented. The area is of high practical interest because of the planned Offshore Windpark Borkum West. The platform provides wind measurements at different heights and additional oceanic information to support the planning activities for this windpark. The dynamics of atmospheric structures is analysed. It is well known that the near surface wind field is a dominating factor for the normalized radar cross section of the sea surface. For this reason SAR scenes are well suited to study atmospheric effects with high spatial resolution. It is shown that the use of tandem pairs enables the study of processes like the propagation of an atmospheric fronts or the evolution of convective cells. Both effects are illustrated with different examples using additional information from in situ measurements. Furthermore existing techniques for the estimation of the wind field in 10 m height from SAR data are applied to both images. The evolution of the spatial structure of both wind speed and wind direction is analysed. The observations are related to some theoretical issues like, e.g., the Taylor hypothesis. Particular emphasize is put on the connection between the spatial and the temporal structure of the wind field.

This topic is of high practical relevance, e.g., in the context of offshore windenergy exploitation. Additional applications like ship tracking, oil spill detection and the study of ocean wave field dynamics are briefly discussed as well. [C3140]

"Measurements of eddies in the ocean surface wind field by a mix of single and multiple-frequency HF radars on monterey bay california"

To properly assess the impact of global climate change and plan for remediation, accurate regional climate models are necessary, functioning on 10 km size scales rather than the typical 100 km scales. Examples of 10 km size scale phenomena are coastal wind eddies at 10-40 km scales, studied over Monterey Bay, California by Archer, Ludwig et al. using shore and buoy anemometers and satellite images. Most frequent in the evening and early morning hours, these, typically cyclonic, eddies are often responsible for fog in the Santa Cruz California area. We have previously demonstrated the ability of multifrequency HF radar (4.8 to 21.8 MHz) to map the ocean wind field. Observations over a year time span indicate standard errors of prediction of 1.7 m/s for wind speed and 25deg for direction with biases of 0.1 m/s and 0.3deg respectively. Combining HF radar wind vector estimates with shore based anemometer data in the WOCSS surface wind field model allows formation of detailed (3 to 5 km resolution) images of wind eddies over Monterey Bay and observation of their creation and decay. We discuss requirements for wind field observations with HF radars and demonstrate how multiple radar sites can be used to produce HF radar wind field maps. We report observations of 10-20 km cyclonic eddies in the northern and eastern parts of Monterey Bay. [C3141]

"Cantarell natural seep modelling using SAR derived ocean surface wind and meteo-oceanographic buoy data."

The Cantarell Seep is the most significant natural seep discovered in the Southern Gulf of Mexico. The trajectory of the oil seep, driven by sea surface winds and ocean currents, can sometimes impinge on the environmentally sensitive Mexican coast. For this reason it is necessary for the implementation of slick impact models to determine and track oil slick behaviour on sea surface as an aid to contingency planning. The focus of this study was to improve the confidence of the Cantarell natural seep impact model by utilizing SAR derived ocean surface wind field data and in situ meteo-oceanographic buoy data. The advantage of the SAR wind is that the data provides high resolution, wide-area coverage, up to 500 km by 500 km in the case of RADARSAT-1. The accuracies are +/- 2 m/s for wind speed and +/- 25deg for wind direction. The buoy is stationary and only provides wind data for that location but the instruments are more sensitive and provide higher accuracies than the SAR. The buoy information is recorded in one-minute intervals, transmitted to shore by microwave communication and the accuracies are +/- 0.7 m/s for wind speed and +/- 3deg for wind direction. Our approach was to combine the two data sources to provide better coverage and accuracy for oil slick modeling. [C3142]

"Morphological segmentation of Lidar Digital Elevation Models to extract stream channels in forested terrain"

Our paper proposes an approach for the extraction of stream channels from Airborne Laser Swath Mapping (ALSM) data. Recent advances in technology have led to high-resolution topographic data acquisition by means of airborne lidar (i.e. ALSM), which can yield Digital Elevation Model (DEM) datasets with horizontal resolutions of 1 m and vertical rms errors in the range of 10-15 cm. The extraction of a stream network from a DEM plays a fundamental role in modeling spatially distributed hydrological processes and flow routing. We apply morphological filtering to an ALSM DEM to detect and characterize stream channels in forested terrain. Since the size and shape of morphological Structuring Elements (SEs) is known to strongly affect filtered results, we test for accuracy by developing a set of error measures over simulated terrain. We subsequently apply the filter to actual ALSM data. For linking disconnected stream segments, a measure of pixel connectedness known as the Connectivity Number is used. The method presented is shown to enable systematic characterization and comparisons of streams, even in heavily forested terrain. [C3143]

"Study on inversion models for the severity of winter wheat stripe rust using hyperspectral remote sensing"

For Large-scale farming of agricultural crops, it is needed to detect diseases of crops in early time. After that, measurements can be taken to prevent and cure the diseases. Hyperspectral remote sensing data, of which spectrum resolution is less than 10 nm, include a mass of diagnosing spectrum information, which can be used to non-destructively detect disease stresses in green vegetation. In 2002-2003 and 2004-2005, a series of field experiments were conducted to collect the canopy spectral reflectance of winter wheat in the selected field. Canopy reflectance spectra were acquired by ASD FieldSpec Pro TM spectrometer in different severity regions of diseased winter wheat interval 7~10 days, meantime, in the same regions, the disease index (DI) were gained

by the field survey. The results showed that while DI increased, the spectral reflectance of the canopy gradually increased in the red valley region. The DI was highly correlative with the hyperspectral variables such as R672, vegetation indices (R553-R672)/ (R553+R672), (R808-R672)/ (R808+R672), (R808-R976)/ (R808+R976), slope of red edge (Dlambdared), sum of 1st derivative value within red edge(SDr), the vegetation indices $SDr/SDg, SDr/SDb, (SDr-SDg)/(SDr+SDg), (SDr-SDb)/(SDr+SDb)$. Here, R denotes reflectance. Number in subscript is wavelength (nm). SDb and SDg denote sum of 1st derivative value within blue edge and green edge respectively. The coefficient between vegetation index SDr/SDg and DI is the largest. Linear and non-linear regression methods were used to build the inversion models. Using 2002-2003 data to test all above models, the models consisted of the variable of SDr/SDg has the highest predicable precision. Therefore, the model is the best one for inversion about severity of winter wheat yellow rust by hyperspectra. The conclusion has important-mean to guide people to cure the disease of crops and increase yields of crops and ensure security of food supplies. [C3144]

"Validation of an X-Band SAR Wind Algorithm by SIR-C/X SAR Data"

Space borne radar systems are capable of providing wind field information over the ocean. Radar instruments are of high value for operational applications because of their all weather and daylight capabilities. Synthetic aperture radar (SAR) instruments as flown on the European satellites ERS-2, ENVISAT or the Canadian platform RADARSAT are of particular interest for applications where high resolution two- dimensional information on the near surface wind field is needed. All these operate in C-band. The respective wind field algorithm CMOD was tuned to this wavelength. New research focussed on high speed cases to be able to measure wind speeds above 20 m/sec and on the W to HH polarisation ratio. For future missions like TerraSAR-X, to be launched in May 2007 new wind field algorithms tuned to X-band are needed. The TerraSAR-X instrument has a spatial resolution of up to 1 m and additional features like multi polarisation which make it a very interesting tool for oceanographic applications. In this paper a new X band wind field algorithm, XMOD1.0 is introduced. The algorithm is based on the detection of wind streaks in the SAR images and scatterometer measurements of [1]. Data from the SRTM mission flown on the shuttle in February 2000 and SIR C/X SAR in 1994 are used to test the algorithm. Results are validated against in situ data and model data from ECMWF. The potential of SAR measurements to support the optimal siting, the design, as well as the operation of offshore wind parks is shown. Applications for offshore wind farming of the TerraSAR-X mission will be discussed. The platform FINO 1 was chosen as a primary test site to calibrate and validate wind fields for X band satellite images. For the development, optimisation and validation of the retrieval algorithms comparisons with in situ data, e.g., acquired at the FINO platform will be carried out. The respective calibration and validations strategies will be summarized. [C3145]

"Validation of a new empirical SAR algorithm"

A new empirical algorithm-CWAVE [1] was developed at the German aerospace center (DLR). A global dataset of two years (September 1998 to December 2000) of ERS SAR data was reprocessed to more than one million SAR imageries. Met ocean parameters like significant ocean wave height (Hs), wind speed (U10) and mean wave period (Tm-10) are derived from the SAR images using the CWAVE algorithm [1]. The results are compared to collocated ERS altimeter data and in situ measurements from NOAA buoys and observations taken onboard the vessel Polarstern. It is shown that the SAR derived Hsis comparable in quality to altimeter measurements and can thus be used for real time assimilation. [C3146]

"Global analysis of a 2 Year ERS-2 wavemode dataset over the oceans"

Starting in 1991, the ERS-1 and (later) ERS-2 satellites have collected wavemode data over the global oceans whenever no image mode data acquisition was requested. Wave- mode data are full resolution SAR data covering small areas of size 5 km times 10 km every 200 km along the orbits thus forming a dataset giving information from all global oceans daily. In the scope of the WAVEATLAS ESA AO Project, ESA provided two years (Sep. 1998-Nov. 2000) of raw ERS-2 wave mode data to DLR which were processed into more than one million single look complex images, so-called imageries, using DLR's BSAR processor. The algorithms CWAVE and LISE were applied to estimate wind and wave parameters such as significant wave height, wind speed and sea surface elevation fields together with several single wave parameters. The paper presents global statistics with emphasis on wave parameters, namely significant wave height, single wave crest height, and wave height. Areal and seasonal distribution of high sea states is discussed and the relevance of the analysis for extreme sea state mapping is pointed out. As far as possible, the results are related to existing theoretical knowledge and compared to observational data (Hogben atlas) as well as model results. The outcome of this processing will be compiled into a new unique atlas on global waves and extreme events. It is planned to extend the atlas back to 1991 when ERS-1 was launched and forward to present times thus covering a more than 15 years period. [C3147]

"A novel method for estimating offshore wind fields using synthetic aperture radar and meteorological model data"

Synthetic aperture radar (SAR) provides a promising method for offshore wind field estimation, particularly in the context of important for offshore wind farm development. This paper introduces an iterative maximum a posteriori probability (MAP) method for combining meteorological model output with synthetic aperture radar for offshore wind field estimation. The MAP approach is demonstrated for 40 ENVISAT ASAR scenes collected for 2004-2006 over the UK Irish Sea. Both the CMOD4 and CMOD5 geophysical model functions are implemented and retrievals using MAP and a simpler direction based windspeed algorithm are validated against insitu mast observations. The CMOD5 MAP algorithm in particular shows promising results with an estimates on average within 2 observations. [C3148]

"Computation of wind direction from SAR images without external a priori information"

We present here the follow-up of a previously published work [1], where we described a wavelet based method to characterize the sea surface backscatter structures present in the SAR images. The method relies on the ability of the two-dimensional continuous wavelet technique to detect the spatial structure of the marine atmospheric boundary layer and to isolate wind-related cells and features. The analysis of the cells' geometry, moulded by the radiometric characteristics of the sea surface, permits the identification of the wind direction inside the cells and thus the computation of the wind speed through standard algorithms. About twenty SAR images (ERS-2 and ASAR Wide Swath) over the Mediterranean Sea have been analyzed, and the results compared with NSCAT and QuikSCAT satellites wind fields. These images cover a wide range of meteorological conditions, from low (2 m/s) to moderate winds (12 m/s), presenting many kinds of signature, i.e. wind cells, atmospheric gravity waves, convective structures and radiometric flatness. The main difference of this method, with respect to the majority of those already proposed, is that it does not require a-priori information about the wind direction as well as any periodicity of the backscatter structures. The aliased wind directions are estimated from the texture of the SAR reconstructed map, while the dealiasing is possible due to the asymmetries present in the detected backscatter structures. The resulting SAR derived wind fields have been compared with those provided by satellite scatterometers. Results indicate a good score in detecting the wind direction (ap 70%). The developed methodology, once tested over an adequate quantity of images to derive statistically reliable results, could be routinely used to enrich SAR images with the wind field, as well as to characterize other backscatter structures displayed by SAR not depending directly on the wind. [C3149]

"Statistical classification methodology of SHOALS 3000 backscatter to mapping coastal benthic habitats"

The scanning hydrographic operational airborne LiDAR survey (SHOALS) consists of a bathymetric LiDAR system which provides high precision measurements of water depth. Even though the acquisition is focused on depth accuracy, the return signal, i.e. waveform, contains other relevant information because of integration signatures from the water surface, the water column and the sea-bed. This paper highlights the benthic characterization in extracting statistical parameters derived from the bottom backscatter. In applying multivariate analysis (K-means), it is significantly proven that signals derived from habitat, described as statistically homogeneous throughout ground-truth analysis, are (1) similar within an intra-habitat view, while they are (2) different between themselves. [C3150]

"Lidar application in selection and design of power line route"

Light detection and ranging is a relatively new technology, developed to complement traditional remote sensing technology. Digital aerial image provides reflectance information for land cover while LIDAR data provide more accurate geometrical information. There is much potential for fusing these two sources to achieve increased accuracy and utility for feature detection and classification. In order to assist Guangxi Electric Power Design Institute to improve their efficiency in power transmission line selection and design, field survey work, and reduce the cost, we have recently carried out the first power line project by using LIDAR and high resolution digital camera in China. The use of coloring LIDAR points by RGB of digital images makes it possible for obtaining high quality of in-room surveying, feature detection and classification. In addition, high quality and high resolution of DEM, DSM, DOM and visualization provides our customer not only with better selection and design of power line route, and reduced survey work, but also significant savings by 10 percent reduction of power line construction. [C3151]

"Comparison of measured scattering coefficient of dry soil at X-band with the scattering coefficient estimated using the dielectric constant"

The soil is one of the natural earth material which is produced by withering of rocks. The soil is mix of sand, silt and clay with air pores. The compactness of soil depends upon the percentage of these constituents and the pore size. The dry soil has its dielectric constant which is independent of frequency and so the scattering coefficient also will be independent of frequency for pure dry sand. But in nature it is not so, it always has some percentage of moisture in it. The moisture will be due to presence of water which will be a combination of bound water and free water. More the percentage of moisture more is the presence of free water. But for dry soil there is no water and for natural dry soil the free water is very small and mostly it is bound water. The scattering coefficient will be different although soil is close to dry and also will vary with frequency due to presence of small quantity of free water present. The scattering coefficient has been measured for HH, VV, HV, VH polarizations. Separately using the values of the soil constituents the dielectric constant is estimated for pure dry sand. Using this dielectric constant the scattering coefficient is estimated for different polarization. For estimation of scattering coefficient the small perturbation model is used which is applicable for slightly rough surface. The measured values of scattering coefficient is compared with estimated values of scattering and the error analysis is done.

[C3152]

"Object-based classification of multi-sensor optical imagery to generate terrain surface roughness information for input to wind risk simulation"

Geoscience Australia is conducting a series of national risk assessments for a range of natural hazards such as severe winds. The impact of severe wind varies considerably between equivalent structures located at different sites due to local roughness of the upwind terrain, shielding provided by upwind structures and topographic factors. Terrain surface roughness information is a critical spatial input to generate wind multipliers. It is generally the first spatial field to be evaluated, as it is utilised in both the generation of the terrain and topographic wind multiplier. Landsat imagery was employed to generate a terrain surface roughness product for six major metropolitan areas across Australia. It was necessary to investigate the applicability of multi-sensor approaches to generate a regional/national terrain surface roughness map based on the Australian/New Zealand wind loading standard (AS/NZS 1170.2). This paper discusses the methodology that developed a procedure to derive terrain surface roughness from various multi-source satellite images. MODIS, Landsat, and IKONOS imagery were acquired (from 12 September-26 November 2002) covering a significant portion of the New South Wales, Australia. An object-based image segmentation and classification technique was tested for seven bands of MODIS, six bands of Landsat Thematic Mapper, and four bands of IKONOS. Eleven terrain categories were identified using this technique which achieved classification accuracies of 79% and 93% over metropolitan (Sydney) and rural/urban areas respectively. It was revealed that the object-based image classification enhances the quality of the terrain product compared to traditional spectral- based maximum likelihood classification methods. To further improve the derivation of terrain roughness classification results, an integrated textural-spectral analysis merged Synthetic Aperture Radar and optical datasets provided in a study by [1]. A comparison with results derived from textual-spectral classification showed considerable improvement over the results from earlier classification techniques. [C3153]

"Reflectivity retrieval in a networked radar environment: Demonstration from the CASA IP1 radar network"

A network-based reflectivity retrieval technique has been developed within the Center for Collaborative Adaptive Sensing of the Atmosphere (CASA). The concept of a networked- radar system is simultaneous observations of the same precipitation event by multiple radars operating at the attenuating frequency such as X-band and scanning in a low elevation plane. This paper presents the preliminary demonstration of the network-based retrieval using data from the first Integration Project (IP1) radar network in Oklahoma. Electromagnetic waves backscattered from a common volume in a networked radar system are attenuated differently along the different paths. The CASA networked-retrieval method is based on a set of governing integral equations describing the backscatter and propagation of common volume with constraints of total path attenuation. The method has been implemented in a multiprocessor environment, which operate simultaneously and collaboratively to meet the real time requirement of CASA. The performance of the implemented retrieval algorithm such as computation requirement will be presented. Comparison of the CASA networked retrieval is made against the conventional attenuation correction based on the principle of coupling the specific attenuation, differential propagation phase and reflectivity. The preliminary results show good agreement with conventional differential phase base attenuation correction. [C3154]

"A study on optical and SAR data fusion for extracting flooded area"

This article proposes a method of fusing the optical data before the flood and SAR (synthetic aperture radar) data during the flood. The main goal of this study is to evaluate the capability of data fusion to combine the information from Landsat ETM image with Radarsat SAR image for water body and flooded area extraction. The

Landsat ETM data will basically provide the information of landform and background information which includes the normal water extent. The Radarsat SAR data however was taken during flood will provide information mainly on water body extent and flooded area. In the result image, flooded area was significantly enhanced. We can distinguish the flooded area and normal water area easily. [C3155]

"What optech's bathymetric LiDAR sees underwater"

This article presents early results of the FUDOTERAM project using bathymetric LiDAR data acquired with the SHOALS-3000, the latest bathymetric LiDAR system from Optech. The survey area is in the coastal zone along the northern shore of Chaleurs Bay, in the western Gulf of St. Lawrence, Canada. The project aimed to apply the SHOALS-3000 to geological mapping, sedimentary process monitoring and marine habitat mapping. This paper focuses on the sedimentological part of the study and presents the early raw data obtained to produce a bottom type classification based on some simple parameters, roughness, slope angle and direction. Two methods are evaluated for analysis of the SHOALS-3000 waveforms, the Moment Method and the Gaussian Mixture Model, and the latter is used as an approach to model the bottom type signal. [C3156]

"LIDAR detection of plankton in the ocean"

For a variety of oceanographic applications, airborne LIDAR is very attractive, because of its ability to cover large areas in a short amount of time and at low cost compared with traditional research vessel surveys. One application we have investigated is the detection of plankton in the ocean. We have found that zooplankton layers can be detected, structure within those layers can be tracked, and relative estimates of abundance can be made. This paper describes the NOAA LIDAR and some of the results related to detection of zooplankton in the upper ocean. [C3157]

"CALIPSO-AERONET Combined Application for Weather and Climate Research"

In this paper, a new method is proposed, which combine CALIPSO lidar data with AERONET data to acquire the unstable aerosol information in Taiwan. First, introduce a CALIPSO retrieval arithmetic to obtain the aerosol optical depth, and then compare the differences between CALIPSO and AERONET. By combining these two techniques we could not only have the precise site data from AERONET, but also own the change information of aerosol in southeast China from CALIPSO. Different from AERONET, we can also display the spatial properties of aerosol from CALIPSO lidar backscatter data, such as, the strength of aerosol in each layer and their change with time in the aerosphere. [C3158]

"Piece-wise variance method for signal-to-noise ratio estimation in elastic/Raman lidar signals"

A straightforward signal-to-noise ratio (SNR) estimator for elastic/Raman lidar channels and related noise-induced errorbars is presented. The estimator is based on piece-wise estimation of the mean signal power and noise variance component under analog detection. The piece-wise estimator results are compared with those obtained from a previously published SNR parametric estimator under high and low SNR scenarios. [C3159]

"Design methodology of a ceilometer lidar prototype"

This article presents step-by-step applied methodology to design a 905-nm 5-kHz rep. rate diode-laser biaxial lidar ceilometer prototype beginning from the definition of initial specs, and related trade-offs to the first measurement tests. It is shown how key variables such as the received and background power, the range-dependent signal-to-noise ratio (SNR), the integration time, and the overlap factor have been simulated and analysed by means of parameter tuning inside acceptable state-of-the-art goal intervals. Main emission and reception subsystems as well as some auxiliary mechanical subsystems (adjustment parts and protection/subject) are discussed. Finally, preliminary test measurements on topographic targets and storm clouds carried out with the ceilometer prototype are presented. Future improvements and trade-offs are also discussed. [C3160]

"Refocusing through single layer building wall using synthetic aperture radar"

Through-wall imaging using synthetic aperture array technique is studied by employing ultra-wideband antennas and for wide incidence angles. The effect of the building walls on the target image distortions is investigated by simulations and measurements. It is shown that using the idea of match filtering, the effect of the wall can be compensated for and point target response can be reconstructed. A controlled experiment within the laboratory environment is performed to verify the methods, presented. It is shown that for an ultra-wideband system operating over frequency band of 1-3 GHz highly distorted images of two point targets in close proximity of each other behind a wall can be resolved after refocusing. A dual-frequency synthetic method is also presented that

can improve the cross-range resolution of the refocused image. [C3161]

"Simulation studies of forest structure using 3D lidar and radar models"

The use of lidar and radar instruments to measure forest structure attributes such as height and biomass are being considered for future Earth Observation satellite missions. Large footprint lidar makes a direct measurement of the heights of scatterers in the illuminated footprint and can yield information about the vertical profile of the canopy. Synthetic Aperture Radar (SAR) is known to sense the canopy volume, especially at longer wavelengths and is useful for estimating biomass. Interferometric SAR (InSAR) has been shown to yield some forest canopy height information. There is much interest in exploiting these technologies separately and together to get important information for carbon cycle and ecosystem science. More detailed information of the electromagnetic radiation interactions within forest canopies is needed and backscattering models can be of much utility here. A three-dimensional (3D) coherent radar backscattering model and a 3D lidar backscatter models were used to investigate the use of large footprint lidar, SAR and InSAR for characterizing realistic forest scenes. The tree height indices derived from lidar waveform and heights of InSAR phase centers were compared. Results will address the possible synergies between lidar and radar data in terms of forest structural information. [C3162]

"Half-space born approximation modeling and inversion for cross-well radar sensing of contaminants in soil"

Detection of dense non-aqueous phase liquids (DNAPLs) is a practical interesting problem in geophysics. This problem involves forward modeling, subsurface sensing and object reconstruction. An analytical forward model-HSBA-in the frequency domain containing dyadic Green's function solution to describe the cross-well radar sensing in infinite soil media is developed. First order Born approximation is employed to linearize this inverse scattering problem. The forward model is validated by both frequency domain computational models and laboratory experiments that are collected using cross-well radar method that uses broadband antennas in subsurface to illuminate the inhomogeneous field and receive scattered electromagnetic (EM) waves. A shape-based inversion algorithm is proposed for contaminant pool localization and reconstruction, in which the shape of the object is assumed priori and represented by a low-order differentiable parametric function. The characteristics of the object-location, size and dielectric contrast to the background medium-are obtained by an iterative non-linear optimization. The inversion method using synthesized data by numerical experiments gives promising preliminary results. [C3163]

"ASCAT scatterometer ocean calibration"

The European Organisation for the Exploitation of Meteorological Satellites (EUMETSAT) is responsible for the absolute calibration of the new Advanced scatterometer (ASCAT), onboard MetOp-A, which mainly relies on the use of transponders. An alternative calibration method, which uses scatterometer measurements over the ocean, is presented here. The method is based on the knowledge of the backscatter signal modulation by the ocean surface, which is derived from previous C-band scatterometer missions, and on the use of numerical weather prediction wind output as calibration reference. The method proves to be very useful in providing guidance to EUMETSAT calibration efforts and provides continuity of the C-band scatterometers. Moreover, the ocean calibration results in very good quality winds. As such, within the framework of the EUMETSAT Ocean & Sea Ice Satellite Application Facility, the Royal Netherlands Meteorological Institute has released a demonstration ASCAT 25-km wind product, which is available at <http://www.knmi.nl/scatterometer> since 28 March 2007. [C3164]

"Scattering from sahelian grassland: a coherent modeling"

A coherent scattering formulation is developed for radar remote sensing of Sahelian grassland. This African vegetation is composed of shrubs and annual grass. The proposed model includes a vegetation generator tool in order to create vegetation structure with realistic architectures and botanical information. This is important in the development of the coherent scattering model, since the relative position of plant elements needs be preserved as accurately as possible. To correctly account for the coherent attenuation through the crown layer, the crown shape of shrubs must be considered. The crown shape is highly irregular, but for the most part can be encompassed in an ellipsoidal or cylindrical volume depending on the ground truth data. Thus, the extinction of the coherent wave is then calculated only when traveling within the crown volume. On the other hand, the grass generator models the grass as a set of cylindrical stalks and blade leaves arranged in a semi-deterministic fashion. Since grass blades are thin, multiple scattering among adjacent elements can be neglected at microwave frequencies. Backscatter statistics are acquired via a Monte Carlo simulation over a large number of realizations. Depending on the season, it is shown that contribution from soil and grass are the dominant

components of the overall backscatter. [C3165]

"Technique of remote sensing image processing in active faults survey"

The paper employed image fusion technology for SAR image and ETM+ multi-spectrum image, combined enhancement technology of multi-spectrum texture characters and spectrum characters to process SAR image, ETM+ image, SPOT-5 image and high precision DEM data. Then, with the help of high resolution image and three-dimensional image of the fault, the paper analyzed the characters of the active fault's remote sensing image. [C3166]

"Need for developing repeat-pass differential POLSAR interferometry"

Radar Polarimetry, Radar Interferometry and Polarimetric SAR Interferometry represent the current culmination in active 'Microwave Remote Sensing' technology, but we still need to progress very considerably in order to reach the limits of physical realizability. Whereas with radar polarimetry the textural fine-structure, target orientation, symmetries and material constituents can be recovered with considerable improvement above that of standard 'amplitude-only' radar; by implementing 'radar interferometry' the spatial (in depth) structure can be explored. With Polarimetric Interferometric Synthetic Aperture Radar (POL-IN-SAR) imaging, it is possible to recover such co-registered textural and spatial information from POL-IN-SAR digital image data sets simultaneously, including the extraction of Digital Elevation Maps (DEM) from either Polarimetric (scattering matrix) or Interferometric (dual antenna) SAR systems. Simultaneous Polarimetric-plus- Interferometric SAR Imaging offers the additional benefit of obtaining co-registered textural-plus-spatial three-dimensional POL-IN-DEM information, which when applied to Repeat-Pass Image-Overlay Interferometry provides differential background validation and environmental stress-change information with highly improved accuracy. However, hitherto only single-polarization-channel repeat-pass IN-SAR was developed and considered; and therefore the aim of this paper is to scrutinize and determine why and for what specific problems fully polarimetric differential RP-POL-IN-SAR imaging is required. [C3167]

"SAR-based estimation of the baltic sea ice motion"

The ice season in the northern part of the Baltic Sea varies from a few weeks up to 4-5 months depending on the location and the winter. As a long-term average the Baltic Sea is ice covered for about 45% of its surface area at the annual maximum. Due to the relatively narrow basins, the deformation rate remains rather high throughout the winter. The ice thickness measurements show that in the Bay of Bothnia over one third of the ice cover is thicker than 1 m in the later stages of the ice season during a typical winter. Modeling the state and development of the Baltic ice cover has been an active research area which have resulted in operative ice models. The current operative ice model run at the Finnish Ice Service (FIS) models the following parameters: ice motion and concentration, mean ice thickness, ridged ice thickness, ridged ice concentration, compressive region, and deformed ice fraction. Some case studies have been made to validate the results. However, a more systematic forecast evaluation is needed, the final goal being the data assimilation to integrate the EO data into the numerical ice model. In this paper we present an algorithm which estimates the ice motion field from two successive RADARSAT-1 SAR images. A large number of RADARSAT-1 ScanSAR Wide mode SAR images, usually over 100, is received at FIS every winter. The same sea areas are visible in the images with a time interval of 1-3 days. [C3168]

"Inversion model validation of ground emissivity. Contribution to the development of SMOS algorithm"

SMOS (Soil Moisture and Ocean Salinity), is the second mission of "Earth Explorer" to be developed within the program "Living Planet" of the European Space Agency (ESA). This satellite, containing the very first 1.4 GHz interferometric radiometer 2D, will carry out the first cartography on a planetary scale of the moisture of the grounds and the salinity of the oceans. The forests are relatively opaque, and the knowledge of moisture remains problematic. The effect of the vegetation can be corrected thanks a simple radiative model. Nevertheless simulations show that the effect of the litter on the emissivity of a system litter + ground is not negligible. Our objective is to highlight the effects of this layer on the total multi layer system. This will make it possible to lead to a simple analytical formulation of a model of litter which can be integrated into the calculation algorithm of SMOS. Radiometer measurements, coupled to dielectric characterizations of samples in laboratory can enable us to characterize the geological structure. The goal of this article is to present the step which we chose to validate this analytical model. [C3169]

"Change detection and analysis with radarsat-1 SAR image"

In the present paper, according to data analysis, the problem of change detection has been addressed with

unsupervised change detection with multi-temporal single-channel single-polarization RADARSAT-1 SAR images. Method proposed in this paper is based on four main steps: (1) Data preprocessing. SAR images are rectified and calibrated to Gauss-Kruger projection firstly. Moreover they are co-registered to ensure the condition of good accuracy of change detection. (2) Change detection. The window log-ratio approach is adopted to compare multi-temporal SAR data, because of the multiplicative speckle in the images. Then a proper window is selected to average pixels from the two SAR data in log-ratio process instead of pixel by pixel. (3) Selection of optimal threshold value. Minimum error threshold is applied to find the optimal threshold. (4) Change detection map can be obtained by segmentation of window log-ratio image. Experiments show the approach deal well with change detection in water area. [C3170]

"Dependency analysis of normalized radar cross section of ocean surface on ocean winds using an airborne dual-frequency polarimetric SAR"

The normalized radar cross section (NRCS) of ocean surface is measured from three directions of illumination by an airborne dual-frequency synthetic aperture radar (SAR) with L- and X-band, and the dependency of the NRCS and the polarimetric ratio on the relative wind direction is analyzed. In X-band, the NRCSs in parallel polarizations represent the dependency on the relative wind direction. The NRCS in HH polarization of X-band has difference between upwind and downwind condition, though that in VV polarization the NRCSs for upwind and downwind condition are almost same. The wind dependency of the NRCS in L-band is smaller than that of X-band. The polarimetric rate in X-band shows the wind dependency with small difference between upwind and downwind conditions, though that in L-band is not apparent. The results suggest the possibility of measurement of ocean winds only using the polarimetric SAR in X-band. Moreover, the small dependency of the NRCS in L-band suggests the possibility of the wind speed measurement over the ocean. [C3171]

"Exploiting full-waveform lidar data and multiresolution wavelet analysis for vertical object detection and recognition"

A current challenge in performing airport obstruction surveys using airborne lidar is lack of reliable, automated methods for extracting and attributing vertical objects from the lidar data. This paper presents a new approach to solving this problem, taking advantage of the additional data provided by full-waveform systems. The procedure entails first deconvolving and georeferencing the lidar waveform data to create dense, detailed point clouds in which the vertical structure of objects, such as trees, towers, and buildings, is well characterized. The point clouds are then voxelized to produce high-resolution volumes of lidar intensity values, and a 3D wavelet decomposition is computed. Vertical object detection and recognition is performed in the wavelet domain using a multiresolution template matching approach. The method was tested using lidar waveform data and ground truth collected for project areas in Madison, Wisconsin. Preliminary results demonstrate the potential of the approach. [C3172]

"Detection of foliage-obscured vehicle using a multiwavelength polarimetric lidar"

Foliage obscured man-made targets detection and identification is of great interest to many applications. In this paper, the backscattered laser signals from a multiwavelength polarimetric lidar were used to detect a vehicle hidden inside a vegetated area. The polarimetric reflectance data from the lidar at two separate laser wavelengths at 1064 nm and 532 nm revealed distinct target characteristics from both the vehicle and the vegetation. The results from this case study demonstrated the validity of the proposed lidar detection technique. Furthermore, the results could potentially lead to a lidar detection and identification technique for a wide variety of foliage-obscured man-made targets under various application scenarios. [C3173]

"Two-dimensional surface river flow patterns measured with paired riversondes"

Two RiverSondes were operated simultaneously in close proximity in order to provide a two-dimensional map of river surface velocity. The initial test was carried out at Threemile Slough in central California. The two radars were installed about 135 m apart on the same bank of the channel. Each radar used a 3-yagi antenna array and determined signal directions using direction finding. The slough is approximately 200 m wide, and each radar processed data out to about 300 m, with a range resolution of 15 m and an angular resolution of 1 degree. Overlapping radial vector data from the two radars were combined to produce total current vectors at a grid spacing of 10 m, with updates every 5 minutes. The river flow in the region, which has a maximum velocity of about 0.8 m/s, is tidally driven with flow reversals every 6 hours, and complex flow patterns were seen during flow reversal. The system performed well with minimal mutual interference. The ability to provide continuous, non-contact two-dimensional river surface flow measurements will be useful in several unique settings, such as studies of flow at river junctions where impacts to juvenile fish migration are significant. Additional field experiments are planned this year on the Sacramento River. [C3174]

"The Comparison of the V-Fold and the Monte-Carlo cross validation to estimate the number of clusters for the fully polarimetric sar data segmentation"

In this paper, the cross validation algorithm is used to estimate the number of clusters for the unsupervised classification of fully polarimetric SAR data. Three different cross validation algorithms are applied for comparison, which are the dispersion measure method, the V-fold cross validation (VFCV) and the Monte-Carlo cross validation (MCCV). Our current experiments show that the dispersion measure method appears generally unable to provide a reliable estimation. The VFCV and the MCCV algorithms seem to be more effective than the dispersion measure method. Moreover, the VFCV is much faster than the MCCV, but the MCCV may be able to provide better estimation than the VFCV. [C3175]

"Wetlands map of Alaska using L-Band radar satellite imagery"

We have used two seasons of L-band SAR imagery to produce a thematic map of wetlands throughout Alaska. The classification was developed using the Random Forests statistical decision tree algorithm. Input data included mosaics of summer and winter JERS-1 SAR imagery with associated image collection dates, summer and winter SAR backscatter texture, elevation, slope, proximity to water, and geographic latitude. The accuracy of the resulting thematic map was quantified using extensive ground reference data. The overall aggregate accuracy calculated based on all classified pixels was 89.5%, with individual per-tile aggregate accuracies ranging from 80% to 97%. As the first high-resolution large-scale synoptic wetlands map of Alaska, this product provides the basis for improved characterization of land-atmosphere CH₄ and CO₂ fluxes and climate change impacts associated with thawing soils and changes in extent and drying of wetland ecosystems. [C3176]

"A comparison of models for retrieving high wind speeds"

Based on polarization ratio from ENVISAT ASAR, we compared the wind vectors retrieved from CMOD5 with $\alpha = 0.6$, $\alpha = 0.5$, our polarization ratio, VV HWGMF with our polarization ratio and HH HWGMF with results from QuikSCAT and buoy, respectively. We found that CMOD5 with $\alpha = 0.5$ polarization ratio is best one for retrieving high wind speed from RADARSAT SAR; and error between QuikSCAT and HH HWGMF is the least. The polarization ratio and GMF for high wind need be improved. [C3177]

"On SAR hurricane wind speed ambiguities"

Radar backscattered signals over the ocean are dampened in extremely high winds, which leads to a wind speed ambiguity problem during the process of wind retrieval from synthetic aperture radar (SAR). This problem was firstly studied by Shen et al. (2007), where we proposed a wind speed ambiguity removal scheme for the two wind speed solutions that may exist for any given normalized radar cross section (NRCS) and wind direction. This approach is based on the operational geophysical model function (GMF) CMOD5. Recently, new C-band GMFs for high wind have been developed, among which, a HH polarized GMF was established for the first time. In this study, the wind speed ambiguity problem will be studied within the context of the available high wind GMFs, which are, CMOD5, CMOD4HW, HWGMF_V and HWGMF_H. For the wind retrieval from HH polarized SAR images, a hybrid empirical polarization ratio is generally adopted. To compare the different behavior of various GMF models, this polarization ratio is used to transform the HH polarized GMF into a W field. Although the wind speed ambiguity problem is found in most GMFs, the saturation wind speed where radar backscattered signals start to decrease is different for the various GMFs. We show that consideration of the wind speed ambiguity problem is important for high wind retrieval from SAR images, especially for category 5 hurricanes. [C3178]

"A geophysical model function for windsat polarimetric radiometer wind retrievals using linear polarizations"

In this paper, we develop a novel geophysical model function (GMF) for the WindSat radiometer relating the vertically (V-pol) and horizontally (H-pol) polarized brightness temperature (TB) to the ocean surface wind field. The brightness temperature data from the 10, 18 and 37 GHz channels were used in this analysis. The brightness temperature combination of the form (AV-H) is found to be mostly independent of the atmospheric variations, where A is a constant number for each frequency. The GMF was developed empirically using the collocated wind vectors from the QuikSCAT scatterometer retrieval as truth and the WindSat's (AV-H) TB's. We examined the characteristic of the GMF and explored the opportunity to improve our current WindSat wind direction retrieval that utilizes only 3rd and 4th Stokes measurements, by integrating this GMF. The strength of the wind directional signals is encouraging for moderate wind speed at 8 m/s and higher. [C3179]

"Automatic extraction of salient geometric entities from LIDAR point clouds"

This paper introduces a modularized tool for the processing of LIDAR data based on the analysis of neighbor relationships between LIDAR points with the goal to extract planes, lines, and points in 3D. The tool's functionalities will be exemplified by the application of reconstructing building roofs. Detecting buildings within digital surface models is one further step to enhance the results of fully- and semi-automatic software tools which handle huge LIDAR point clouds. The functionalities comprise the sorting of point coordinates to improve efficiency, the retrieval of LIDAR point topology by triangulation of points, the extraction of 3D planes by "plane growing" and the determination of lines, points and roof outlines based on the 3D planes by statistical estimation and hypothesis testing of their parameters. [C3180]

"Automatic feature extraction from airborne lidar measurements to identify cross-shore morphologies indicative of beach erosion"

Airborne lidar data were acquired along St. Augustine Beach, Florida six times between August 2003 and June 2006. To identify sub-aerial morphologies indicative to beach erosion, the data sets were mined extensively by extracting several morphological features using cross-shore profile sampling. For each profile, the features were grouped into erosion or accretion classes and their class-conditional probability density functions (PDFs) estimated via Parzen windowing. PDF separability was ranked using symmetric and normalized measures of relative entropy (i.e. divergence). Results were compared to a simple median metric. The more interclass separation provided by a feature, the greater its potential as an indicator for erosion or accretion. Over short time periods (>1 month), beach slope and beach width ranked highest by providing the most separation and therefore high potential as indicators for erosion. Over longer time periods (>1 year), deviation-from-trend, which is the shoreline's deviation from the natural strike of the beach, ranked highest. This is significant in that the pier region's deviation from the natural trend is believed by coastal researchers to be a strong contributing factor to it being an erosion "hot spot". The method we have developed provides a systematic framework to mine high-resolution airborne lidar data over beaches, detect erosion-prone areas, and numerically rank a feature's potential as an indicator for erosion. [C3181]

"Quad-polarimetry and interferometry from repeat-pass dual-polarimetric SAR imagery"

New space-borne polarimetric SAR systems employ, or will employ, dual-pol imaging modes as well as full quad-pol imaging, e.g. PALSAR, RADARSAT-2, TERRASAR-X. Therefore questions arise as to the capabilities (and limitations) of these various dual-pol SAR imaging modes. One novel offshoot of our work on dual-pol SAR image analysis and polarimetric decompositions of dual-pol data was the idea to collect two dual-pol images employing geometry appropriate for parallel repeat-pass interferometry. The polarizations of the dual-pol collections differ, e.g. one is (HH, HV) and the other (VV, VH). Using the example of transmitting either horizontal (H) or vertical (V) polarizations, one collects all four polarimetric channels, but only two per pass. Except for the interferometric repeat-pass nature of the SAR image collections the polarimetric information should be identical to standard quad-pol SAR imagery. The relevant open questions concern the interferometric baseline and temporal decorrelations between the repeat-pass dual-pol images. [C3182]

"Simulation of minimal infrastructure short-range radar networks"

Distributed networks of short-range radars offer the potential to observe winds and rainfall at high spatial resolution in volumes of the troposphere that are unobserved by today's long-range weather radars. One class of potential distributed radar network designs includes Off-the-Grid (OTG) weather radar networks. These are short-range radar nodes designed to be deployed as part of an ad-hoc network and to limit their reliance on existing infrastructure. Independence of the wired infrastructure (power or communications) would allow OTG networks to be deployed in specific regions where sensing needs are greatest, such as mountain valleys prone to flash-flooding, geographic regions where the infrastructure is susceptible to failure, and underdeveloped regions lacking urban infrastructure. This paper will present a system model and simulation framework for the design of OTG networks. The model estimates the energy requirements of the three major system functions, sensing, communicating and computing, as well as power generated from the solar panel. The simulation will be used to develop an energy cost function to be used in control decisions. [C3183]

"Implementation of a new refractivity estimation algorithm on a network of S-band radars"

The retrieval of the surface-layer moisture field can be obtained by estimating the refractive index of air, measured in parts per million and referred to as refractivity. A technique developed to estimate the refractivity using radar has been demonstrated with validated results from field experiments [1], [2]. This technique utilizes the measured change in phase from stationary ground targets, which will be primarily due to changes in refractivity at warmer temperatures given a stable radar frequency. While this technique has been successfully demonstrated on individual radars, there is no clearly defined method of combining multiple radar estimations

beyond gridding and averaging. Recently, however, a new algorithm was proposed as an alternative approach, especially when dealing with multiple radars [3]. The new algorithm uses a minimum least squared error approach, with a smoothing constraint and a method to address phase wrapping. This paper will explore the implementation of this constrained least squares (CLS) approach with data collected during a refractivity field experiment during the summer of 2006 in Colorado. It will also explore the implications of running the CLS algorithm in real-time, and briefly discuss future directions. [C3184]

"Radar network characterization"

The use of dense networks of small radars for weather sensing is being investigated by the Engineering Research Center for Collaborative Adaptive Sensing of the Atmosphere, with a first test-bed of this new paradigm well underway. The potential benefits of closely-deployed, overlapping, short-range weather radars are easy to see intuitively, and can be summarized as a greater ability to mitigate the effects of the Earth curvature and sense close the ground in all of the network domain, an increased spatial and temporal resolution, the capability of performing multiple-radar measurements, and the capability of adaptively tasking the individual radars according to the meteorological scene, while using less complex radar units. Virtually all of these potential benefits are governed by the trade-offs generated by the characteristics of the particular radar units employed and their spatial distribution, creating different data outcomes depending on the individual radar capabilities, the radar network layout, and the resulting number of radars with overlapping coverage. [C3185]

"Building characterisation in VHR SAR data acquired under controlled EMSL conditions"

The upcoming availability of new very high resolution SAR imagery from satellite sensors (e.g. Radarsat-2, TerraSAR-X, COSMOSkyMed) has renewed interest in extraction of scene parameters for the characterisation of urban areas. In order to properly face this problem, we have defined a structured and hierarchical research strategy that follows a systematic approach to 3-D building characterisation in VHR SAR data. This research strategy, starting from a theoretical analysis based on the literature, aims at a more depth understanding of the backscattering behaviour in VHR SAR urban images on the basis of empirical tests on different experimental setups. These setups include trials in the EMSL, with the outdoor Linear Synthetic Aperture radar (LISA) and a final validation and tuning of the results on VHR SAR from airborne and satellite platforms. This paper describes the proposed research framework in general, and presents the results obtained from the first set of EMSL experiments aimed at analysing the effect of the viewing and aspect angles, i.e. the orientation of the building structure with respect to the SAR's azimuthal direction. [C3186]

"Rainfall estimation and rain gauge comparison for x-band polarimetric CASA radars"

The Center for Collaborative and Adaptive Sensing of the Atmosphere (CASA) developed and deployed four polarimetric and Doppler-capable distributed, collaborative and adaptive X-band radars in Oklahoma with the capability to detect and track tornadoes and storms in the lower troposphere with high spatial and temporal resolution. This paper presents an analysis of the performance of X-band rainfall estimation composite algorithms and the conventional reflectivity-rainfall relationship. The polarimetric estimators are developed by different combinations of radar products including horizontal equivalent reflectivity (Z_h), differential reflectivity (Z_{dr}) and specific differential phase (K_{dp}). The Micronet Little Washita rain gauge network is used for validating rainfall estimates of the KCYR CASA radar. In addition, NEXRAD WSR-88D KFDR radar data are analyzed and compared with the rain gauge network and the CASA radar estimates. Fourteen hours of data collected during August 2006 from three different storms are analyzed. Both convective and stratiform events are represented in the radar data analysis. An accuracy of point radar measurement is assessed for different rain intensities. Results demonstrate an improvement in hourly rainfall accumulation estimation for average rainfall intensities beyond 5 mm/hr with the use of polarimetric estimators. An increase in absolute difference standard error with distance by the use of absolute difference in radar and rain gauges estimates is also evaluated. [C3187]

"Real-time three-dimensional radar mosaic in CASA IP1 testbed"

This paper reports on a real-time three-dimensional radar mosaic technique for Collaborative and Adaptive Sensing of the Atmosphere (CASA) Integrated Project 1 (IP1) testbed. The technique exploits the dual-polarization capability of the IP1 radar network for the improvement of multi-radar composite fields. In particular, the copolar correlation and the attenuation derived from the differential propagation phase are injected to the interpolation process to derive a weighting scheme and a data quality index field for the composite fields. This technique is also served as a front-end that drives the composite reflectivity fields to the CSU DART now-casting algorithm. [C3188]

"A grid based weather radar data retrieval and processing framework."

In this paper, we describe the implementation of a distributed data retrieval and processing strategy enabled by using grid computing technologies and applied to distributed collaborative adaptive sensing environments. Underlying the grid computing and storage infrastructure there is a data dispersion algorithm to guarantee pervasive data management. Experimental results show that the proposed framework integrates successfully radar networks to grid infrastructures, while providing higher resources utilization than typical storage strategies. [C3189]

"Phase shifter system using vector modulation for xband phased array radar applications"

This paper presents the design and implementation of a complete phase shifter system using vector (polar) modulation, suitable for solid-state phased array radar applications, providing a cost effective solution which overcomes the main constraints involved with traditional systems. The performance characteristics for three intermediate frequencies were measured. In addition, measurements at X- band were performed using frequency up-converters. Finally a four channel prototype was built to evaluate the network connectivity of the phase shifter. [C3190]

"Evaluation of first generation CASA radar waveforms in the IP1 testbed"

The Center for Collaborative Adaptive Sensing of the Atmosphere (CASA), an engineering research center (ERC) established by the National Science Foundation (NSF) deployed its first generation network of four low-power, short-range, X- band, dual-polarized Doppler weather radars known as NE- TRAD. The short range CASA radars will have range overlay and velocity folding problems with conventional pulse-pair processing. The first testbed of X-band radar systems (developed within the ERC) in central Oklahoma called IP-1 (Integrated Project 1) have a low unambiguous velocity due to their short wavelength, and increasing the PRF will result in multiple trip overlays since storms can extend over a large distance. In addition the radar observations at short ranges are contaminated by ground clutter. This paper describes the waveforms for the individual radar nodes based on NETRAD operational requirements such as scan speeds, volume coverage pattern and system/hardware limitations to resolve range and velocity ambiguities. A dual PRF waveform has been suggested for operational use based on a simulation study. This paper presents an evaluation of the waveform from data collected by the first generation CASA radars. [C3191]

"Low cross-polarization antenna array for CASA's student test bed radar"

A series-fed aperture-coupled antenna array is designed using a substrate with a relative permittivity of 1.2 and a thickness of 1.75 mm for the patch antenna. A substrate with a relative permittivity of 6.15 and a thickness of 0.625 mm is used for the feed lines. The array was designed to achieve a sidelobe level lower than 20 dB and a cross-polarization lower than 30 dB. The array presented is a center-fed array composed of two sub-arrays of 6 elements. This configuration makes the array a 4-port array, having two ports for horizontal polarization (H and H₁₈₀), and two for the vertical polarization (V and V₁₈₀). The cross-polarization and sidelobe levels achieved are -39.11 dB, and 19.3 dB respectively. The half power beam width (HPBW) is around 9deg and the front-to-back ratio (FBR) is -15.84 dB. Isolations SHV and SHV₁₈₀ are -26.61 dB and -23.08 dB respectively. [C3192]

"Radar imaging of urban areas by means of very high resolution SAR and interferometric SAR"

In remote sensing applications the monitoring of urban areas by means of SAR sensors has been grown to a valuable and indispensable tool. Whereas SAR imaging with a spatial resolution down to one meter is widespread, a resolution down to 10 cm and below is offered only by a very few SAR sensors worldwide. In this contribution the potential of high resolution and very high resolution radar imaging of urban areas by means of SAR and interferometric imaging will be demonstrated and discussed. Limits of these techniques and open problems will be addressed as well. The corresponding data were acquired with PAMIR, the X-band SAR/GMTI demonstrator of FGAN-FHR. [C3193]

"Application of Polarimetric SAR images acquired in square-loop flights"

We acquired several data sets of polarimetric SAR data in Sendai, Japan by airborne Pi-SAR system for fundamental research of radar polarimetry and interferometry. Among these data acquisitions, two data sets were acquired in multiple flight paths in a short time period, and polarimetric SAR image acquired from different angles are available. We found very clear azimuth incident angle dependency of the polarimetric SAR images. In addition, a square-loop flight was carried out in the same location in January 2004. The incident angle dependency of the SAR image in polarimetry in X-band is very clear in these SAR images. We found that the phase difference in orthogonal circular polarization has significant dependency on the azimuth incident angle. The data sets also has a very good potential for SAR radargrammetry. We discussed the possibility of application of polarimetric SAR data acquired from multiple directions. [C3194]

"Coherence dependency of the PALSAR POLInSAR on forest in japan and amazon"

PALSAR PolInSAR capability was evaluated. One of the important capabilities that the PolInSAR offers is to estimate the forest height. For one-year and more months after the launch of the ALOS on Jan. 24 2006, PALSAR observed several test areas using the polarimetry modes repeatedly. We applied the PolInSAR method to retrieve the forest heights of the four test sites in Japan and Amazon. In this paper, we introduce an applied method and results. The results show that the forest tree height can be estimated with good accuracy. [C3195]

"Disaster monitoring and environmental alert in taiwan by repeat-pass spaceborne SAR"

The prevailing complex geological and ecological conditions of Taiwan have drawn considerable attention from various geo-ecological communities because of their vulnerability to produce various natural hazards at different scales. Located in the tropical/subtropical zone of the Pacific Rim, its ecological and rugged mountainous properties are environmentally sensitive making monitoring and observations especially difficult because of the high population density. For example, in terms of natural hazard mitigation tectonically active regions are used for analyzing the cause of abundant risk events, such as earthquakes, landslides and land subsidence. In fact Taiwan is well suited as a test site for studying those geologically disastrous processes. Implementing novel techniques of space remote sensing has proved to be an effective means in recent years for greatly improving our understanding of these phenomena. In this paper we report on the monitoring of such events using multi-modal polarimetric and/or interferometric SAR images at C and L band from ERS, JERS-1, RADARSAT-1, ENVISAT, and from the recent ALOS satellite. For crustal and surface deformation, we used radar image pairs with long temporal baselines and large areas of coverage for investigating deformation over Western Taiwan. Pre-seismic and co-seismic deformation patterns are spatial-temporally analyzed. The other topic deals with the coastline changes observed from a sequence of ERS-1/2 SAR images within the years of 1996 to 2005. Waterlines were extracted using multi-scale procedures of edge detection and were corrected with tidal motion data. Substantial analyses were carried out in conjunction with ground surveys and lidar mapping. The topographic feature changes due to large scale landslides triggered by torrential rains were also monitored. In addition, the SAR interferograms were used to analyze the deposition changes along the riverbeds and riverbanks for short-intervals using optimal baselines. Summary and remarks on the implementation of such multi-modal polarimetric and/or interferometric SAR imagery for environmental monitoring are provided. [C3196]

"Multi-baseline polarimetrically optimised phases and scattering mechanisms for InSAR applications"

An interesting, but rarely used technique in polarimetric SAR interferometry is the enhancement of interferometric coherence by projection into an optimal polarimetric state. In particular, newly developed methods for polarimetric optimisation of multi-baseline coherences provide the possibility of simultaneous constrained coherence optimisation for more than one baseline. This technique can significantly improve the usefulness of long-term interferometric pairs and time-series, and appears, therefore, of interest to various fields of application. The aim of this paper is to discuss the correct derivation of multi-baseline differential interferograms with polarimetrically optimised coherence and to outline several possible areas of application, particularly in the field of differential interferometry and permanent scatterers. [C3197]

"Multibaseline POLInSAR coherence modelling and optimization"

This paper analyzes a POLInSAR coherence model with respect to polarization diversity. The coherence constituents are identified and examined. Extending POLInSAR to multiple baselines, two general multibaseline coherence optimization methods are introduced. The coherence model is utilized to discuss the advantages and applications of these newly developed multibaseline coherence optimization methods. [C3198]

"Building feature extraction via a deterministic approach: application to real high resolution SAR images"

Interpretation of high resolution SAR (synthetic aperture radar) images is still a hard task, especially when man-made objects crowd the scene under detection. This paper contributes to the analysis of this kind of data by adopting an approach, based on a scattering model, for the retrieval of buildings height from real SAR images and presenting first numerical results. [C3199]

"Mapping subsurface geology in Arid Africa using L-band SAR"

Using L-band SAR data from JERS-1 and ALOS, we produce regional mosaics of Sahara in order to map subsurface geology. A first mosaic of eastern Sahara using more than 1600 JERS-1 scenes allowed the

discovery of unknown paleo-rivers, faults, and impact craters. On-going work concerns a new L- band high-quality mosaic of the entire Sahara, based on ALOS/PALSAR data. [C3200]

"PolSAR image filtering based on feature detection using the wavelet transform"

This paper elucidates a new approach for speckle reduction in polarimetric synthetic aperture radar ("PolSAR") images based on the stationary wavelet transform. Noisy wavelet coefficients are thresholded using an entropic thresholding technique. Principal Component Analysis and Sum of Squared Coefficients methods are used to detect significant coefficients based on the entire polarimetric covariance matrix. [C3201]

"Estimation of physical properties of persistent scatterers using JERS-1 data"

The physical properties of persistence scatterers (PS) are estimated utilizing variety means. Two urban areas of Seoul and Busan in Korea are processed using L-band HH-polarization JERS-1 data. The linear and one-year periodic deformations are monitored. The size and brightness variation of PSs are also estimated. In addition, the concurrence of PSs and the point-like targets are examined and disagreement between the positions of both types of scatterers is identified. [C3202]

"Snow wetness monitoring using multi-temporal polarimetric ASAR data and multi-layer hybrid model"

This paper presents a method to characterize snow cover using multi-temporal dual polarization ASAR/ENVISAT data. At first, variations of electromagnetic backscattering of snowpack depending on melting are explained and validated by a multi-layer model. It is demonstrated that it is crucial to exactly model the distribution of Liquid Water Content inside snow pack in C-band. Consequently, a new mapping algorithm based on the French weather model CROCUS is proposed in order to estimate the spatial variability of layered snowpack profile. [C3203]

"IDRA: A new instrument for drizzle monitoring"

IRCTR is currently developing a high resolution radar aimed at the observation of rainfall and drizzle parameters for use in hydrological studies and in studies of the effect of the increase in anthropogenic aerosols in the radiation budget. Much effort has been done at obtaining a high sensitivity to be able to detect low reflectivity phenomena like drizzle. The radar is placed in the Cabauw meteorological super-site, allowing synergy with other instruments to further improve its capabilities. [C3204]

"A new tracker for ocean-land compatible radar altimeter"

Satellite radar altimeter is an active microwave remote sensor for obtaining ocean topography, as well as the marine and land ice mass fluxes at a global scale. Because the echo properties of ocean, land and pole ice are very different, the on-board tracker of radar altimeter should have the ability to handle the distinct signals automatically. In this paper, a new tracker for ocean land compatible, the model compatible tracker (MCT), is proposed. In MCT, two track algorithms, MLE (Maximum likelihood Estimate) and OCOG (off center of gravity), cooperate in parallel. Therefore, not only the good accuracy but also the robustness can be realized in real time on board. So MCT is very suitable for the ocean-land compatible radar altimeter. The principle of MCT, the cooperation strategy for the two algorithms, the adaptive bandwidth technique, and the realization of MCT are discussed in this paper. [C3205]

"An innovative algorithm for radar altimeter acceleration bias compensation"

In this paper, the characteristics of the alpha-beta filter in altimeter height loop are analyzed. The "acceleration lag bias" is firstly described and the previous approaches are reviewed, and then, an innovative algorithm is designed to compensate the error. Finally, a numerical simulation is presented to test the effectiveness. It is shown that bias can be almost totally compensated by the algorithm. [C3206]

"An interferometric imaging altimeter applied for both ocean and land observation"

This paper introduces an interferometric imaging altimeter system designed for both ocean and land observations. This sensor combines the functions of interferometric radar altimeter and SAR together and is aimed to provide centimeter- level accuracy of topography for ocean and meter-level accuracy of topography for land. With the interferometry technique, a wide swath of 80 km is achieved, and with the synthetic aperture technique, a resolution of 100 m for land observation is achieved. System design is outlined and some preliminary results are presented. [C3207]

"Microwave radar remote sensing of Plinian volcanic ash clouds for aviation hazard and civil protection applications"

The potential of ground-based microwave weather radar systems for volcanic ash cloud detection and quantitative retrieval is evaluated. A prototype algorithm for volcanic ash radar retrieval (VARR) is discussed. Starting from measured single-polarization reflectivity, the statistical inversion technique to retrieve ash concentration and fall rate is based on two cascade steps: i) classification of eruption regime and volcanic ash category; ii) estimation of ash concentration and fall rate. An application of the VARR technique is finally shown taking into consideration the eruption of the Grimsvotn volcano in Iceland on Nov. 2004. Volume scan data from a Doppler C-band radar, located at 260 km from the volcano vent, are processed by means of the VARR algorithm. Examples of the achievable VARR products are presented and discussed. [C3208]

"Lidar DEM for characterizing the volcanic landforms of tatun volcanoes in metropolitan taipei"

Tatun volcano group is a cluster of dormant volcanoes surrounding metropolitan Taipei. Rugged terrain, monotonic lithology and dense vegetation covers are adverse factors for mapping the geological structures. In this study, airborne lidar survey was conducted to obtain a bare ground DEM with 2 m grid and with an accuracy of decimeters. Shaded-relief images, pit-patterns and drainage networks are then derived from these DEMs for visual interpretation. 51 volcanoes are thus recognized. Two fissures running through the highest volcano in this area, namely Mount Seven-Stars, are extending 2000 m and 1000 m, respectively. The largest width and depth of the opening of the ruptures is located in the west flank of the volcanic cone. The slope angle of the east-wing of the volcanic cone is 36deg, whereas the angle of the west-wing is only 24.5deg. The opening of the west fissure is larger and its extension is longer than the east one. Thus, the west side can be subjected to an active extensional process of strain. The fissures could be resulted from the ongoing regional extension of the Tatun volcanic area due to the plate subduction and collision of the Eurasian plate and the Philippine sea plate.

[C3209]

"Integrating point, curve and area descriptors into geospatial databases for metric resolution SAR image analysis"

Image understanding and retrieval for metric SAR data needs to be tackled by specific algorithms in order to exploit the specific metric scale scene characteristics and the typical sensor phenomenology. A composite approach is developed to this end. Extraction, characterization and simplification/grouping algorithms are employed together with super-resolution for isolated bright scatterers, scatterer alignments and uniform backscatter and texture areas to populate a geospatial database. The generated descriptors can be navigated via different data viewers for scene understanding and data retrieval applications. Examples on real metric SAR data are given. [C3210]

"Multiscale filtering of SAR images using scale and space consistency"

A new approach for speckle reduction in SAR images based on the stationary wavelet transform is proposed. Noisy wavelet coefficients are reduced via a shrinkage function that depends on a statistical modeling of the normalized wavelet coefficient probability density functions. Consistencies between coefficients across scales and space are also reinforced using consistency rules. The approach is particularly robust in cases of correlated speckle noise. [C3211]

"Polarimetric analysis of maritime SAR data collected with the DSTO ingara X-Band radar"

Fine resolution spotlight synthetic aperture radar (SAR) imagery collected on a circular flight path is used to investigate the variation in ship detection performance with respect to three fundamental radar parameters: the transmit/receive polarisation combination, the incidence angle and the azimuth angle. The polarisation combinations examined are HH, HV, VV, RR and cross-slant 45deg. Three different incidence angles are considered-50deg, 60deg and 70deg-corresponding to collection geometries for high altitude maritime surveillance systems. Performance is assessed using a simple target-to-background contrast measure. Results are compared with preliminary results from a four component decomposition of the Mueller matrix. While the latter and cross-slant 45deg show promise, in general HH is shown to have the best performance. [C3212]

"Theoretic error analysis of split-gate tracker in satellite radar altimetry"

A theoretical analysis of the altimeter split-gate height tracker error is carried out in this paper. The principles of altimeter split-gate tracker are reviewed, and the discriminative curve of the tracker is derived. It is shown that the antenna parameters have little influence on the slope of discriminative curve. The height noise of the tracker

is analyzed, assuming there is no other noise in the instrument. It shows that the AGC gate noise contributes much in the overall tracker noise in high sea state condition, so a long AGC gate is preferable. Finally, the 1s-averaged height noise level in a typical sea state (SWH=4 m) is calculated, and the error specification (<2 cm) is proved to be met. [C3213]

"Very high resolution interferogram acquisition campaign and processing"

The ONERA RAMSES system is a flexible SAR system in constant evolution, developed mainly as a test bench for new technologies and to provide specific data for TDRI (Target Detection, Recognition and Identification) algorithm evaluation. It is flown on a Transall C160 platform operated by the CEV (Centre d'Essais en Vol). This paper gives an overview of the latest upgrading to acquire large data set without on board deramp-on-receive mode and then present the acquisition campaign at X band for very high resolution single pass interferometric multi-baseline mode. The multi-baseline mode used is a ping-pong mode where four antennas are used. The goal of this campaign was to acquire interferometric data in very high resolution mode, better than 0.3 m along slant range axis with a large slant range swath of 2400 m. [C3214]

"Snow avalanche detection and classification algorithm for GB-SAR imagery"

This paper presents an algorithm for the automatic detection and classification of snow avalanches using GB-SAR imagery. The algorithm has been validated extensively in two different test sites in Sion (CH) and Alagna (I), respectively. Results show an important reduction on the images to manually supervise and minimal false negative rate. The real-time availability of the location and extent of the avalanche events provided by this system has demonstrated to be of high interest to ski resort administrators, allowing a more efficient management of the resources available to prepare the tracks. [C3215]

"Effect of salinity on the dielectric properties of geological materials: implication for soil moisture detection by means of remote sensing"

This paper deals with the exploitation of dielectric properties of saline deposits for the detection and mapping of moisture in arid regions on both Earth and Mars. We then present a simulation and experimental study in order to assess the effect of salinity on the permittivity of geological materials and therefore on the radar backscattering coefficient in the [1-7 GHz] frequency range. Dielectric mixing models were first calibrated by means of experimental measurements before being used as input parameters of analytical scattering models (IEM, SPM). Simulation results will finally be compared to field measurements (Pyla dune, Death Valley, Mojave Desert) and will be used for the interpretation of SAR data (AIRSAR, PALSAR). [C3216]

"Potential of X-band spaceborne synthetic aperture radar for precipitation retrieval over land"

Numerous space-borne X-band Synthetic Aperture Radars (X-SAR) systems will be launched by European agencies in the coming decade commencing this year. Those X-SARs can measure precipitation over land, thereby significantly augmenting the sensors that comprise the Global Precipitation Mission (GPM). This will incur relatively little incremental cost because they have already been funded. X-SAR measurements are especially beneficial over land where rainfall is difficult to measure by means of microwave radiometers that depend on scattering by frozen hydrometeors associated with that rain. The improved horizontal resolution of the retrievals will match the higher spatial resolution of mesoscale and general circulation models that will become available in the coming decade. [C3217]

"Evaluation of the influence of land cover on the noise level of ERS-scatterometer backscatter"

In this study we assess the impact of different land cover types on the azimuthal noise of backscatter signal using multi-year ERS-scatterometer data. Results indicate a strong response of the azimuthal noise level to the different land cover types like rainforests, lakes, rivers, floodplains, coastal areas, permanent snow or ice, urban areas, and deserts as well as topography. Complex topography with high standard deviation in heights, ridge-shaped features oblique to the satellite track on the surface, and water-contaminated areas are the main causes of the high azimuthal noise in scatterometer measurements. The azimuthal noise fluctuations generally show a minimum over rain forests and maximum over sand deserts. Changes in the level of azimuthal noise of backscatter signal clearly reflect changes in land cover or surface roughness. [C3218]

"Polarimetric measurements of radar backscatters of a wet-land rice field throughout a growth period at L- and C-bands"

Backscattering coefficients and phase-difference statistics of a wet-land rice field in Suwon, Korea are measured using a ground-based polarimetric scatterometer at 1.9 and 5.3 GHz throughout a growth year from

transplanting period to harvest period (May to October in 2006). The ground truth data including bio-mass, plant height, and leaf-area index (LAI) are also collected for each measurement. The measured backscattering coefficients and phase difference statistics are analyzed based on the growth age for each polarization, frequency, and incidence angle. It is found that the hh-polarized backscattering coefficients have wider sensitivity region than the w-polarized backscattering coefficients with respect to the rice growth age. [C3219]

"A semi-empirical backscattering model for estimation of leaf area index (LAI) of rice in southern China"

Most paddy rice in southern China grows in warm, humid and rainy areas where it is hard to acquire optical remote sensing data. In this study, a semi-empirical backscattering model was proposed to estimate leaf area index (LAI) of rice in the area using ENVISAT Advanced Synthetic Aperture Radar (ASAR) alternating polarization data. Ground measurements of LAI, water content and height of rice in the test site were collected and the model fitted at the same time as the acquisition of ASAR data. LAI estimated from the model was compared with ground measurements to evaluate the accuracy of the model. The results showed that the model provides a promising alternative to optical remote sensing data for predicting LAI of rice in southern China. [C3220]

"ALOS PALSAR radar observation of tropical peat swamp forest as a monitoring tool for environmental protection and restoration"

Tropical peat swamp forests are threatened by large scale deforestation and canal drainage. Oxidation and forest fire cause enormous carbon emissions. Most remaining areas are located in Indonesia. Time series of historical JERS-1 SAR data reveal the extent and nature of recent disturbances, such as those caused by excess drainage and severe ENSO. Since the dynamics of flooding and drought events can be observed well by the recently launched ALOS PALSAR instrument, important information relevant for detection of ecosystem disturbance and evaluation of restoration efforts can be obtained. [C3221]

"Optimal configurations of bistatic radar for retrieving soil moisture and vegetation biomass"

The possible contribution of bistatic radar measurements to estimate bare soil moisture and vegetation biomass is investigated by a simulation study based on well established electromagnetic models (both coherent and incoherent components). The best system configuration, in terms of observation directions, polarisations and frequency has been singled out by predicting the retrieval accuracy. This has been evaluated using the Cramer-Rao lower bound to identify optimal configurations for single polarisation and multipolarisation receivers, as well as in case the bistatic measurements are complemented by monostatic ones. [C3222]

"Soil parameter estimation and analysis of bistatic scattering X-band controlled measurements"

In this paper, we will present well controlled experimental bistatic X-band measurements of rough surfaces, which have been recorded in the Bistatic Measurement Facility (BMF) at the DLR Oberpfaffenhofen, Microwaves and Radar Institute. The bistatic measurement sets are composed of soils with different statistical roughness and different moistures controlled by a TDR (Time Domain Reflectivity) system. The BMF has been calibrated using the Isolated Antenna Calibration Technique (IACT). The validation of the calibration was achieved by measuring the reflectivity of fresh water. In the second part, the first validation of the specular algorithm by estimating the soil moisture of two surfaces with different roughness scales will be reported. Additionally, a new technique using the coherent term of the Integral Equation Method (IEM) to estimate the soil roughness will be presented, as well as evaluation of the sensitivity of phase and reflectivity with regard to moisture variation in the specular direction. [C3223]

"Integration of L-band SAR data into land surface models"

Land surface process modelling might be limited due to lack of reliable model input data. Key surface variables as land cover information or soil moisture conditions have been proven to be observable by remote sensing systems. The integration of remote sensing data into land surface process models might therefore help to improve their simulations results. Longer wavelength SAR data has a higher sensitivity to soil moisture content than higher frequency systems. Recent (ALOS) and planned (e.g. TerraSAR-L) SAR systems are therefore expected to provide valuable information about soil moisture dynamics. The present study investigates the potential to retrieve land cover information and geophysical parameters from L-band SAR data. The retrieval results are assimilated into a state-of-the-art land surface model to evaluate the merit of L-band SAR data assimilation. [C3224]

"Application of C and Ku-Band scatterometer data for catchment hydrology in northern latitudes"

Spatially continuous soil moisture information is on high demand globally. A database which is available from active microwave data (ERS scatterometer, C-band, 50 km) has been assessed over two large basins (Mackenzie and Lena) in northern latitudes. This information was combined with snowmelt patterns which can be derived based on diurnal thaw-refreeze of the snow cover from a further scatterometer (Quikscat, Ku-band, 25 km). Relative soil water information has been averaged over each basin and compared to discharge measurements for the summer periods 1996-2000. A correlation (logarithmic function) of 0.78 is observed for the Lena basin. The Mackenzie is much more complex and thus the relationship is less obvious. This is also reflected in the snowmelt data. Whereas 80% of basin area undergoes melting at the same time in the Lena basin in 2000, at maximum 40% can be observed for the Mackenzie during the same year. Maximum runoff in the Lena basin is observed when snowmelt ceases for the entire basin. This is delayed by three weeks for the Mackenzie although increased runoff can be observed already after 70% of the basin is snow-free. [C3225]

"Robust change analysis of SAR data through information-theoretic multitemporal features"

Multi-temporal analysis of Synthetic Aperture Radar (SAR) images has gained an ever increasing attention due to the availability of several satellite platforms with different revisit times and to the intrinsic capability of the SAR system of producing all-weather observations. As a drawback, automated analysis in general and change detection in particular are made difficult by the inherent noisiness of SAR imagery. Even if a pre-processing step aimed at speckle reduction is adopted, most of algorithms borrowed from computer vision cannot be profitably used. In this work, a novel pixel feature suitable for change analysis is derived from information-theoretic concepts. It does not require preliminary de-speckling and capable of providing accurate change maps from a couple of SAR images. The rationale is that the negative of logarithm of the probability of an amplitude level in one image conditional to the level of the same pixel in the other image conveys an information on the amount of change occurred between the two passes. Experimental results carried out on two couples of multi-temporal SAR images demonstrate that the proposed IT feature outperform the Log-Ratio in terms of capability of discriminating changes. [C3226]

"TerraSAR-X value added image products"

The space mission TerraSAR-X is the first German space project implemented under a Public Private Partnership (PPP). Cooperation partners are the German Aerospace Centre (DLR) and EADS Astrium GmbH. Within this construct, DLR will be responsible for the scientific use of the TerraSAR-X data, whereas commercial marketing will be undertaken exclusively by Infoterra GmbH, a wholly-owned EADS Astrium subsidiary. In a co-operation between Infoterra GmbH and Joanneum Research, Value Added products and processors have been developed for TerraSAR-X data. These products are mainly oriented at the area of interest or are mapping products which represent a higher level of image processing in terms of radiometric correction and orthorectification, mosaics, subsets and merges. In this paper, these products are described. Further, an insight into the automated and semi-automated production chain is provided. [C3227]

"TerraSAR-X interferometry: report on a first assessment"

The German radar sensor TerraSAR-X will be launched by the middle of the year 2007 and will provide high-resolution data with also high radiometric and geometric accuracy. First interferometric results can be reported at the time of the conference. Various interferometric tests and a prediction on the performance of the monostatic interferometry will be described in the course of the presentation. Unfortunately, no data are available at the moment. [C3228]

"Quality of orthorectified TerraSAR-X products"

Summary form only given. The German Aerospace Center (DLR) has developed the TerraSAR-X Ground Segment. One part is the geocoding system that provides orthorectification capability for multi-resolution, multi-polarisation and multi-frequency data. Besides an ellipsoid corrected product a new product called Enhanced Ellipsoid Corrected (EEC) will be offered that considers digital elevation models (DEM) of a moderately coarser resolution than the 1 up to 3 m resolution of the TerraSAR-X modes. SRTM/X-band DEMs with approximately 25 m spacing will be the backbone for this operational and fully automated service. As optional product an geocoded incidence angle mask (GIM) is available providing information about the incidence angle of the radar beam, as well as about layover and shadow areas. High precision terrain correction using high resolution DEMs, tie-pointing and image adjustment will be implemented in an experimental processor. This paper gives detailed information on the image quality, which is examined in detail based on the first available geocoded TerraSAR-X products. Therefore radiometric and geometric aspects will be investigated. It is to be shown that the orthorectification step does not tamper the original radiometric properties. The geometric accuracy of the

orthorectification mainly depends on the quality of the used DEM. Besides the SRTM/X-band DEM additional elevation data like SRTM/C-band, ERS-derived and GLOBE data are used for EEC generation. The achieved pixel location accuracies will be presented. The quality characteristics of the Geocoded Incidence Angle Mask- depending also on the used DEM-are described. Moreover the high precision orthorectified image (called geocoded terrain corrected-GTC) will be examined with regard to pixel location accuracy. A high resolution laserscanning DEM, tie-points and image adjustment will be used for this analysis. Furthermore information regarding processing performance will be given. [C3229]

"TerraSAR-X calibration-first results"

As TerraSAR-X, due for launch in 2007, will be an operational scientific mission with commercial potential, product quality is of crucial importance. The success or failure of the mission essentially depends on the calibration of the TerraSAR- X system ensuring the product quality and the correct in-orbit operation of the entire SAR system. The paper describes the in- orbit calibration procedure for TerraSAR-X and dedicated activities performed during the commissioning phase. First results could not be described because TerraSAR-X was not launched up to the time of uploading the full paper. [C3230]

"TerraSAR-X payload data processing-First Experiences"

In February 2007 the German TerraSAR-X satellite will be launched and the TerraSAR-X mission will enter its approximately 5 months commissioning phase. At that time, the challenging developments on both sides, the advanced high- resolution multi-mode SAR instrument on the one hand and the corresponding sophisticated TerraSAR-X ground segment on the other hand will prove correct interaction and functioning. Screening and processing of the SAR data is the task of the DLR developed TerraSAR Multi Mode SAR Processor TMSP. Preceded by data reception, transcription including decryption and followed by archiving, cataloguing and product delivery, processing of the data by the TMSP is the central part of the SAR data workflow implemented in the Payload Ground Segment PGS. Space and ground segment have been subject to intense complete system testing on ground. Here, the compatibility of SAR instrument commanding, SAR instrument operations and subsequent SAR data processing has been successfully proven for the various acquisition modes of the sensor. Compliance of specified and measured product performance has been investigated as far as possible utilizing simulated point target SAR data. However, the real challenge will be the screening and SAR processing of TerraSAR-X data acquired in orbit and linked down to the receiving station. Therefore, the complete reception and processing chain will be properly tuned and adjusted to the properties of the received TerraSAR-X payload data. The TMSP algorithms have to be configured, e.g. thresholds for calibration pulse analysis, estimation window sizes for SAR data analysis, parameterization of estimation algorithms. Also the configuration of product variants with respect to resolution and radiometric quality will be checked and refined. This paper presents the very first experiences in reception, transcription, screening and processing of TerraSAR-X data with respect to performance, throughput and quality. During the TMSP checkout phase the compatibility of instrument commanding and SAR processing have to be verified and the accordance of SAR performance prediction and the obtained product performance and quality have to be investigated. First characteristics of the SAR data with respect to raw data statistics, calibration pulse analysis and Doppler centroid measurements will be shown. As far as available examples of SAR image products featuring the different image modes, Stripmap, ScanSAR and Spotlight at different incidence angles and polarizations will be displayed and a first estimate of product performance parameters will be given. [C3231]

"A new algorithm to calculate sea ice concentration from the SSM/I 85GHz observations"

A new algorithm has been developed to calculate sea ice concentration from any set of passive microwave observations. It was applied to estimate total ice concentration and partial concentration of three ice types using SSM/I 85 GHz observations. The essence of the algorithm is a mathematical optimization technique to determine the best solution from multi-channel observations of a heterogeneous footprint that contains ice types of highly complex and overlapped brightness temperature. Results were validated against ice concentrations from Radarsat image analysis; an operational product from the Canadian Ice Service (CIS). They have proven the successful performance of the algorithm. [C3232]

"Glacier volume changes using ASTER optical stereo. A test study in Eastern Svalbard"

Currently, one of the major methodological gaps in the observation of glaciers from space is the measurement of volume changes of mountain glaciers and small ice caps. Here, we present a case study of comparing a photogrammetric digital elevation model derived from ASTER satellite optical stereo to contour lines from a topographic map from the 1970s. For two small ice caps in Eastern Svalbard, Kvalpyntfonna and Digerfonna, we obtain an overall thickness change of about -0.5 m/yr between 1970 and 2002. From comparison of different

methods and quality checks we estimate the error of this number to be in the order of 5-10%. [C3233]

"Interpretation of C-band SAR backscattering coefficient time series for the Baltic Sea landfast sea ice using a 1-D thermodynamic snow/ice model"

We have compared time series of C-band HH-polarization backscattering coefficients (σ_{deg}) of the Baltic Sea land-fast level ice with results from a 1D high-resolution thermodynamic snow/ice model (HIGHTSI). The σ_{deg} time series were obtained from ENVISAT synthetic aperture radar (SAR) images acquired in February 3-April 7, 2004, and February 6-April 30, 2006. Typically the HIGHTSI results greatly helped to interpret the σ_{deg} behavior with changing weather conditions. There were some cases where detailed ground truth, combined with theoretical σ_{deg} modeling, would have been needed for interpretation of the σ_{deg} trends. From the point of view of operational Baltic Sea ice monitoring with SAR images, the most interesting observation was the large variation of level ice σ_{deg} with changing weather conditions. [C3234]

"First results of ground moving target analysis in TerraSAR-X data"

Summary form only given. The advanced high-resolution German SAR satellite TerraSAR-X is scheduled to be launched at the end of May 2007. Due to its daylight and weather independent applicability in combination with a large spatial coverage and a short acquisition time, SAR has become a promising tool for traffic monitoring in recent years. Ground moving target indication (GMTI) techniques shall be applied to TerraSAR-X data in order to demonstrate the capability of a space borne SAR sensor to monitor traffic flows on highways. A series of GMTI experiments were to be carried out during the commissioning phase of the TerraSAR-X satellite. In first trials, cars, which are equipped with special radar reflectors and GPS receivers, were to be used as moving target references that are imaged in TerraSAR-X data takes. In a follow on experiment, arbitrary cars on motorways were to be imaged simultaneously by TerraSAR-X and by an airborne high-resolution camera. Car tracks extracted from the series of the optical images shall serve as a reference for the evaluation of the TerraSAR-X moving target data in this case. The paper presents first results of the data evaluation. An experimental GMTI processing system is used to detect and measure moving targets in both single-channel and dual-channel data. The dual-channel data, which enable the application of well established GMTI methods like the along-track interferometry (ATI) or displaced phase centre array (DPCA) techniques, are acquired either in the so-called "aperture switching" mode with virtual multiple receiving channels or in the dual-receive antenna (DRA) mode with physically separated receiving channels. The paper reports on the analysis of the first experimental GMTI data by using different detection and measurement strategies. This includes the adapted processing of the SAR raw data with respect to the moving target signals, the incorporation of GIS data in the detection and measurement process and the application of different detectors for across- and along-track velocity components of the moving cars. The quality of the data is thoroughly analyzed and conclusions are drawn for the development and the performance of a fully automatic GMTI processing system for TerraSAR-X. Furthermore, an outlook on the planned experiments is given. [C3235]

"The TanDEM-X mission: Overview and status"

TanDEM-X opens a new era in space borne radar remote sensing. The first bistatic SAR mission, is formed by adding a second, almost identical spacecraft, to TerraSAR-X and flying the two satellites in a closely controlled formation with typical distances between 250 and 500 m. Primary mission objective is the generation of a consistent global digital elevation model with an unprecedented accuracy according to the HRTI-3 specifications. Beyond that, TanDEM-X provides a highly reconfigurable platform for the demonstration of new SAR techniques and applications. This paper gives an overview of the TanDEM-X mission concept, summarizes the capabilities of the system, illustrates the achievable performance, and provides some examples for new imaging modes and applications. The mission has been approved for full implementation by the German Space Agency with a planned launch in spring 2009. [C3236]

"In-orbit SAR performance of TerraSAR-X"

TerraSAR-X is the first German Radar satellite for scientific and commercial applications. The project is a public-private partnership between DLR and EADS Astrium GmbH. TerraSAR-X consists of a high resolution Synthetic Aperture Radar at X-Band. The radar antenna is based on active phased array technology that allows the control of many different instrument parameters and operational modes (Stripmap, ScanSAR and Spotlight) with various polarizations. Following the TerraSAR-X launch, it is planned a six month Commissioning Phase covering the characterization and verification of the SAR mission. Within this phase, the Overall SAR System Performance takes care of the correct working and interaction of all SAR system elements essential for obtaining an optimum SAR Performance. [C3237]

"Simultaneous radar observations of tropical cyclones by space-based and ground-based radar"

Megha 2700, S-band ground-based Doppler weather radar (DWR) located on the east coast of India, is capable of providing long range detection and characterization precipitation and severe storm such as tropical cyclone over Bay of Bengal. The location of the radar is in coverage area of Tropical Rainfall Measurement Mission (TRMM) satellite. Precipitation radar (PR) operating at Ku-band (13.8 GHz) aboard the TRMM has capability of providing vertical structure of tropical cyclones. Although tropical cyclones can be frequently observed by PR, and their vertical structure can be studied, it is not so frequent that they are observed by most existing Ground based weather Radars (GR). The authors take this opportunity for performing inter- comparison between the two radars and inter-compare vertical profile of reflectivity (VPR) of tropical cyclone which were simultaneously observed by the Megha 2700 DWR and PR This work can be useful not only in cross-monitoring severe tropical cyclone activity in a long range over Bay of Bengal, but also as ground validation study of TRMM, and even to the future global space based precipitation mission such as Global Precipitation Measurement (GPM), which is planned to fly over the globe in the near future. [C3238]

"Observational data set in support of falling snow retrieval algorithm development"

The Canadian CloudSat/CALIPSO Validation Program (C3VP) was a field campaign held during the winter of 2006-2007. The C3VP provided an opportunity for the Global Precipitation Measurement (GPM) mission team to participate in cold-season northern latitude data collection activities in advance of GPM's launch. The GPM team collaborated by providing instrumentation and scientists in order to advance the development of falling snow detection and snow rate retrieval algorithms. This paper will describe the field campaign, present some observations, and provide early analysis from the resulting measurements. [C3239]

"Linear versus non-linear analysis of relevant scatterers in high resolution SAR images"

With the increase of synthetic aperture radar (SAR) sensor resolution, SAR images could include a large variety of interesting real man-made structures. Therefore, a more detailed analysis and a finer description of SAR images of urban areas are needed for a better understanding of the scene. Nevertheless, recognizing scenes using high resolution SAR images requires the capability to identify relevant signal signatures (called also descriptors), depending on variable image acquisition geometry, arbitrary objects poses and configurations. Among feature extraction methods, we propose to use principal components analysis (PCA) and/or independent components analysis (ICA), in order to exploit deeper the nature of SAR signatures. In this paper, both a description of our work and a presentation of our preliminary classification performance results will be provided. [C3240]

"Stochastic models of SLC HR SAR images"

The paper presents two algorithms for texture primitive feature extraction on Single Look Complex (SLC) and Polarimetric Synthetic Aperture Radar (PolSAR) SLC data. We assume the data to be modeled by a Gauss-Markov Random Field (GMRF): a complex GMRF model for characterizing the spatial correlation in SLC data and an extension of the model for inter-band correlation characterization. The complex GMRF characterizes the spatial relationship of a two-dimensional complex signal, i.e. SLC SAR data. The extended model characterizes the spatial interaction and the inter-band pixels correlation between the polarimetric complex channels. The Bayesian approach permits to deal with model fitting and selection in a direct way. The results are presented on a polarimetric E-SAR L band scene of Mannheim, Germany. [C3241]

"Unsupervised segmentation of SAR images using Triplet Markov fields and fisher noise distributions"

This paper deals with SAR data segmentation in an unsupervised way. The model we propose is a combination of the nonstationary triplet Markov field recently introduced and the Fisher distributions. The first one allows modeling the different stationarities present in a given image. The second one has the advantage that is well adapted to this kind of data. We present an original technique based on Iterative Conditional Estimation method, to estimate the parameters of the model we propose. Application examples on simulated data and real SAR images are presented as well. [C3242]

"Comparison of NOWRAD, AMSU, AMSR-E, TMI, and SSM/I surface precipitation rate Retrievals over the united states great plains"

This paper compares surface precipitation rates retrieved for the United States Great Plains (USGP) during the summer of 2004 using the Advanced Microwave Sounding Unit (AMSU) aboard the United States NOAA-15 and

-16 satellites with similar precipitation products produced by AMSR-E aboard the NASA Aqua satellite, SSM/I aboard the United States DMSP F-13, -14, and -15 satellites, TMI aboard the NASA TRMM satellite, and a doppler radar product (NOWRAD) of the Weather Services International Corporation (WSI). AMSU surface precipitation rates were retrieved using neural network algorithms trained with either a cloud-resolving MM5 physical model for 106 global storms (the AMSU/MM5 algorithm), or summer NEXRAD radar data for the USGP (the AMSU/NR algorithm). Observed correlation coefficients between $\log_{10}(X + 0.01)$ for NOWRAD surface precipitation rates X (mm/h) at 0.25-degree resolution and those for other sensors were, in declining order, 0.82, 0.79, 0.78, 0.71, and 0.68 for TMI, SSM/I, AMSU/NR, AMSR-E, and AMSU/MM5, respectively. Higher correlation coefficients were obtained when TMI was regarded as truth: 0.86, 0.83, 0.82, 0.80, and 0.78 for SSM/I, AMSU/NR, NOWRAD, AMSU/MM5, and AMSR-E, respectively. Other sensor comparisons include false alarm statistics for all pairs of sensors, rms and mean differences with respect to NOWRAD, precipitation-rate distribution functions, and observed correlations between NOWRAD and AMSU/MM5 precipitation and hydrometeor water path retrievals. [C3243]

"TerraSAR-X Mission Status"

TerraSAR-X is Germany's first national remote sensing satellite being implemented in a public-private partnership between the German Aerospace Centre (DLR) and EADS Astrium GmbH, with a significant financial contribution from the industrial partner. This radar satellite, which is to be launched in June 2007 will supply high-quality radar data for purposes of scientific observation of the Earth for a period of at least five years. At the same time it is designed to satisfy the steadily growing demand of the private sector for remote sensing data in the commercial market. This contribution will describe first the public-private partnership scheme, the roles and responsibilities of the partners as well as the overall project organization. The mission and system design will then be described, followed by a brief overview of the satellite, the related Ground Segment and the applied data policy. The contribution will then focus on the actual mission status. Finally a brief outlook will be given on the activities to come. [C3244]

"Modification of the beam mismatch correction algorithm"

In August 2001, the orbit of the Tropical Rainfall Measuring Mission (TRMM) satellite has been boosted from the altitude of 350 km to 400 km to extend its life time. The time delay between transmission of pulses and reception from rain/surface echoes occurs by one inter pulse period (IPP) (Takahashi and Iguchi, 2004). Due to this time delay, one pulse transmitted at N-1th angle bin is received at the receiving time gate of the next angle bin N. So the mismatch occurs between the transmitting antenna beam direction and the receiving antenna beam direction. This causes antenna gain reduction by 6 dB and leakage of rain/surface echo from the N-1th angle bin to the Nth angle bin. In this paper, the modified beam mismatch correction algorithm is tested numerically, then it's applied to the standard algorithm of TRMM/precipitation radar to reduce the correction error of the current beam mismatch correction algorithm. [C3245]

"Adjustment of cross-track dependence of TRMM Precipitation Radar observation"

The Tropical Rainfall Measuring Mission (TRMM) is NASA's first mission dedicated to observing and understanding tropical rainfall and its effects on global climate. The Precipitation Radar in TRMM is the first spaceborne instrument designed to obtain three-dimensional maps of precipitation reflectivity. Such measurements yield information on the intensity and distribution of rain, rain type and storm depth. An advantage of space radar is that the scattering volume has similar size at any location. However, it has been a challenge to compare data to the one that is collected from the Tropical Rainfall Measuring Mission (TRMM) precipitation radar (PR) for varying scan angles. Intercomparisons between ground radar and spaceborne radar on a point-by-point basis can be a difficult task. Errors result from the mismatch between ground radar and spaceborne radar resolution volume, spatial alignment, and operating frequencies as well as the limited number of the data set collected instantaneously by both instruments. Differences in viewing aspects and resolution that result from the measurement of return signals from different volumes of the precipitation medium contribute to the intercomparison error. A study of the characteristics of the region of the bright band from TRMM-PR vertical profile measurements on a global scale indicates that while bright band height varies widely, the distribution of bright band structure does not vary around the globe. The results show that the average profile of the bright band vertical profile using bright band height as a reference point around the globe has unique profile and do not changes around the globe for large data set. This unique profile can be used to adjust the radar observation error due to different parameters. The TRMM-PR vertical resolution becomes poorer with increasing distance of the TRMM-PR samples from the nadir. Studying the model profile at the nadir profile and other profiles that are off-nadir ray can be used to build the statistical model that can be used to adjust the effect of the scanning cross-track at angle far from the nadir-ray, and the results are presented. [C3246]

"Analysis of densely observed TRMM/PR data during 180-degree yaw maneuver"

The Tropical Rainfall Measuring Mission (TRMM) satellite performs 180-degree yaw maneuver (yaw-around) when the solar beta angle which is the angle between the satellite orbit plane and the direction to the sun crosses the 0-degree. The yaw- maneuver is completed about 16 minutes (about 7000 km in flight length on the Earth) in the TRMM case. During the yaw-around, the precipitation radar (PR) onboard TRMM continues nominal observation (but data processing is limited to level-1 algorithms). Therefore very dense observation is realized during the yaw- around. Since nearly fixed target (rain echo and surface echo) is observed by different incident angles in a short time, new information can be obtained that cannot be obtained nominal observation. On the incident angle dependency of the sea surface echo, we can avoid the uncertainties comes from the changes in the target. Range profiles of the sea surface echo of different incident angles are compared with the long-term global average data. The same approach can be used to quantitative estimation of bright band structure such as blurring effect of the off-nadir incident angles. A case study on 24 January, 2000, which is the stratiform rainfall case over Borneo Island and the range of the incident angle is about +/- 6 degrees, shows that significant difference cannot be seen among data and that the echo strength of each height concentrate within 3-dB. However, the range profiles of the surface echo underneath the stratiform rainfall show quite different angle bin dependency from the reference echo profiles near the rain area. For convective echoes, the nonuniform beam filling (NUBF) effect can be estimated by the different incident angle data and the data which location is slightly offset from the center. More reliable path integrated attenuation (PIA) can be obtained from different incident angle data and the NUBF can be estimated both by the range profiles of surface echo of off-nadir angle bin data with an approach b- y Takahashi et al. (2006) and their change with the location within a footprint.

[C3247]

"QuikSCAT and SSM/I ocean surface winds for wind energy"

Ocean surface winds observed by satellite scatterometer (QuikSCAT) and passive microwave (SSM/I) provide valuable information for wind energy applications. In wind energy two long-term aspects on the offshore wind climate is of concern. One is the 20-year average necessary for the estimation of produced wind power during the life-time of a wind turbine (i.e. wind resource assessment); the other is the month-to-month variation in produced wind power (i.e. wind-indexing). In the present study, the offshore wind resource is estimated from QuikSCAT wind maps. The offshore wind climates at the North-European mid-latitudes and in the Atlantic trade belt zone are compared. Distinct differences are identified and these agree well with independent data from meteorological masts in the two regions. Seven years of twice daily observations from QuikSCAT are used for the offshore wind resource assessment. Wind-indexing is based on long-term trends observed in wind climate statistics. It is customary to observe winds and produced power in parallel in order to keep track of performance. Wind-indexing is based on long-term wind observations and the present study investigate variation in offshore and land-based variations during 18 years observed from SSM/I, other wind observations, model results and produced wind power. Very interestingly it is found that the offshore wind climate is different from wind climates over land in the North-European mid-latitudes. [C3248]

"Towards a high-resolution ASCAT scatterometer wind product"

In scatterometry, the wind vector retrieval problem is ambiguous, i.e., the inversion procedure does not result in a unique wind solution. To remove such ambiguity, a spatial filter is applied over the ambiguous wind field. Such filtering methods succeed in most of the cases. However, as the resolution increases both the noise and the direction ambiguity in retrieved winds increases, leading to arbitrary local minima wind solutions. Exploiting the full wind vector probability density function of the wind inversion, and adopting spatial meteorological balance constraints in a 2D-Var ambiguity removal (AR) alleviates the problem of arbitrary minima and noise, and provides a spatially consistent scatterometer wind field at high resolution. In other words, the method has the advanced filtering properties needed for maintaining small-scale meteorological information in scatterometers, while reducing noise. The method can be adopted in the context of 3D- or 4D-Var data assimilation systems. Moreover, these findings will be used to develop a high resolution (12.5-km sampled) coastal wind product from the new ASCAT scatterometer. [C3249]

"Oceanic Rainfall Retrievals using passive and active measurements from SeaWinds Remote Sensor"

The SeaWinds sensor was launched onboard two satellite missions. The first was the QuikSCAT mission launched in mid 1999 by NASA, and the second was the ADEOS II mission launched by JAXA in late 2002. SeaWinds operates at a ku-band frequency of 13.4 GHz, and was originally designed to measure the speed and direction of the ocean surface wind vector by relating the normalized radar backscatter measurements to the near surface wind vector through a geophysical model function. In addition to the backscatter measurement

capability, SeaWinds simultaneously measures the polarized radiometric emission from the surface and atmosphere, utilizing a ground signal processing algorithm known as the QuikSCAT / SeaWinds Radiometer (QRad / SRad). This paper presents an oceanic rainfall retrieval algorithm that combines the simultaneous active radar backscatter and the passive microwave brightness temperatures observed by the SeaWinds sensor. The retrieval algorithm is statistically based, and has been developed using collocated measurements from SeaWinds, the Tropical Rainfall Measuring Mission (TRMM) Microwave Imager (TMI) rain rates, and the National Center for Environmental Prediction (NCEP) wind fields. The rain is retrieved on a wind vector cell (WVC) measurement grid that has a spatial resolution of 25 km. Examples of the rain estimates from SeaWinds are presented, and comparisons are made with the standard TRMM 2A12 rain data product. Validation results demonstrate that SeaWinds rain measurements are in good agreement with the independent microwave rain observations obtained from TMI. Further, by applying a threshold on the retrieved rain rates, SeaWinds rain estimates can be utilized as a rain flag. In order to evaluate the performance of the SeaWinds flag, comparisons are made with the Impact based Multidimensional Histogram (IMUDH) rain flag developed by JPL. Results emphasize the powerful rain detection capabilities of the SeaWinds retrieval algorithm. Due to its broad swath coverage, SeaWinds affords additional independent sampling of the oceanic rainfall, which may contribute to the future NASA's Precipitation Measurement Mission (PMM) objectives of improving the global sampling of oceanic rain within 3 hour windows. Also, since SeaWinds is the only sensor onboard QuikSCAT, the SeaWinds rain estimates can be used to improve the flagging of rain-contaminated oceanic wind vector retrievals. The passive-only rainfall retrieval algorithm (QRad /SRad) has been implemented by JPL as part of the level 2B science data product, and can be obtained from the Physical Oceanography Distributed Data Archive (PO.DAAC). [C3250]

"Canadian Space Agency's Hurricane Watch Program: Archive contents, Data Access and improved planning strategies"

The Canadian Space Agency's Hurricane Watch program monitors tropical cyclones worldwide and acquires RADARSAT-1 Synthetic Aperture Radar imagery to provide experimental datasets to the scientific research community interested in surface wind field studies. The current HW archives spans from 1999 to 2006 and contain a variety of tropical cyclones from around the world. The images show various storm development stages, and morphological characteristics. To further promote the initiative, CSA is about to provide processed images to the scientific community through an Announcement of Opportunity. In this paper, we will demonstrate how simulations of extensive acquisition plans over the Atlantic basin can provide an improved planning strategy to increase the number of valuable images. [C3251]

"Simultaneous X-band radar and Ka -band radiometer observations of the ocean"

Simultaneous microwave radar and radiometer observations of the ocean were conducted from aircraft during the ShoWEx'99 experiment. Both radar and radiometer wind dependences show similar signal growth with wind speed increase (except for the radiometer at vertical polarization and a near-Brewster angle). Analysis of the low-wind data shows that wind speed is a poor characteristic of the sea surface state in calm conditions because the wind field itself is quite non-uniform in space and time. Under such conditions both radar and radiometer data show strong scatter versus mean wind speed, but they are still well correlated with each other. We conclude that both active and passive instruments respond to the local variations of the sea surface roughness, which are not related to the mean wind speed at low winds. Our comparison shows that the best correlation is between the radar looking at 40-60deg and the near-nadir looking radiometer, which agrees with the theory of scattering/emission from a rough surface. [C3252]

"The Sentinel-3 mission and its topography element"

In the frame of GMES Program, ESA is currently starting the implementation phase of Sentinel-3 mission, which is intended to provide sustained Ocean and Land observation data over a period of 15 to 20 years. The Topography element of this mission will serve primarily the marine operational users but will also allow the monitoring of sea ice and land ice, as well as inland water surfaces, using novel observation techniques. The launch date for this mission is currently foreseen mid 2012. [C3253]

"Re-tracking of SAR altimeter ocean power-waveforms and related accuracies of the retrieved sea surface height, significant wave height and wind speed"

This paper describes the simulation of the power- waveforms acquired in by a radar altimeter operating in SAR mode over ocean surfaces, including the effects of the radar transfer function and of the geophysical ocean parameters, namely the sea surface height(SSH), the sea surface wave height (SWH) and the surface wind speed (WS). The performances of the SAR mode with respect to the retrieval of the ocean geophysical variables (SSH, SWH, WS) are then computed using the Cramer-Rao estimation bounds. It is shown that the radar to

ocean range estimation provided by the SAR mode is improved by more than a factor of two compared with conventional Ku band altimeters. Improvements on SWH and wind speed are also discussed. [C3254]

"An assessment of the Ka band interferometric radar altimeter for monitoring rivers and lakes with the WatER mission"

The Water Elevation Recovery (WatER) satellite mission was recently proposed and supported by a large international scientific community. It is dedicated to the determination of land surface water extent, elevation and slope, and also ocean mesoscale and submesoscale phenomena, using a Ka band Radar Interferometer (KaRIN) as its primary instrument. This instrument is able to provide the appropriate space-time sampling required to observe full signatures of the parameters characterizing these phenomena. However, determining these parameters to the accuracy desired for hydrologic applications is challenging. [C3255]

"Statistical characterization of radar sea scatter for breaking wave detection"

Radar backscatter data are collected using a coherent, dual-polarized radar from a fixed tower in the ocean. Statistical analysis is performed to investigate the 1D and 2D probability density functions of backscatter intensity, Doppler frequency, coherence function and polarization ratio. The fraction of sea spike coverage generally increases with wind speed but the trend of increase is modified by the intensity of background swell condition. Parameterizations of sea spike coverage combining both wind and wave factors show some apparent advantage than parameterizations with wind or wave factors alone. [C3256]

"Wind jet transition and its localized impact on wave height distribution along the Pacific Coast of Northern Japan"

We present a case study of low-level wind jets induced in sequence by orographic effects off the Pacific coast of northern Japan during 7-11 June 2003, and demonstrate that the transition of the wind jets causes areal differences of the wave height variations along the coast. First, we analyze SeaWinds scatterometer wind measurements. Under the easterly wind, a strong wind jet formed after passing by Cape Erimo. As the wind shifted to the southeast, the wind jet started to decay. In turn, the southerly wind along the coast led to another wind jet in the lee of the easternmost tip of the Sanriku coast. Then, we identify onsets and decays of the wind jets from time series of wind speed at meteorological stations. Finally, we demonstrate that the transition of the wind jets has local impacts on wave height variations. Significant wave heights measured by altimeters were correlated positively with local wind energy, i.e., squares of wind speeds. Accompanying the wind jet formation/decline, significant differences of wave height variations became marked among wave observation stations located along the coast at intervals of up to 50 km. [C3257]

"A comparison of the methods for the urban land cover change detection by high-resolution SAR data"

The land cover change detection method using the standard deviation of the backscattering coefficient was suggested. Comparing with the previous method using spatial information such as correlation coefficients, it reduced the commission errors in the agricultural areas. It was found that the detection accuracy increased when the target area was large, but each changed target was difficult to detect for crowded and complex urban areas, even though high-spatial resolution airborne SAR data was used. [C3258]

"A time domain clutter filter for staggered PRT and dual- PRF measurements"

In this paper, a method for clutter filtering and the estimation of spectral moments from non-uniformly sampled Doppler weather radar signals is presented. The method uses a parametric model for the received signal. The spectral moments of both clutter and precipitation echoes are estimated using the maximum likelihood estimator. Unlike the current frequency domain techniques where non-uniformly sampled signals are zero-padded to be uniform sequences, the likelihood function used in this algorithm can be constructed directly from the non-uniformly sampled data. Therefore an accurate estimation of spectral moments even in case of clutter-to-signal ratio as high as 60 dB can be obtained. The proposed method is illustrated on simulated radar signal time series and measurements collected using the staggered pulse repetition time (PRT) and dual pulse repetition frequency (PRF) transmission schemes from the CSU- CHILL and collaborative adaptive sensing of atmosphere (CASA) IP1 radars. [C3259]

"Mapping and monitoring land cover in Corumbiara area, Brazilian Amazonia, using JERS-1 SAR multitemporal data"

This paper discusses the use of a JERS-1 synthetic aperture radar (SAR) time-series for mapping and monitoring land cover in a test site in the region of Corumbiara, Rondonia State, western Brazilian Amazonia. In order to support JERS-1 data analysis, land cover maps were obtained by digital classification of Landsat TM images acquired from 1993 to 1997 period, following a procedure based on image segmentation, unsupervised classification, and post-classification image edition. The comparison of these products with JERS-1 images shows that clean deforested areas are well identified presenting a low backscattering response as expected. However areas that have been cleared and even burned but with remaining forest material left on the ground present high backscattering response opposed to expected. Considering these observations and user interpretation expertise, JERS-1 SAR images can be used to map and monitor land cover changes in Amazonia.

[C3260]

"A new high-altitude airborne millimeter-wave radar for atmospheric research"

A high-altitude airborne millimeter-wave radar for atmospheric research is being developed by the National Center for Atmospheric Research. The radar will be mounted on the High-Performance Instrumented Airborne Platform for Environmental Research (HIAPER). We present simulations of the minimum detectable signal, the reflectivity accuracy, the polarimetric purity, and the expected accuracy of cloud liquid water retrievals to describe the expected performance of the radar. We also describe the phased approach to implementing the system which starts with a W-band Doppler radar, and through phases, adds pulse compression, polarimetric capability, and a second wavelength (Ka-band) radar. [C3261]

"Dual-polarization spectral decompositions: Application to radar parameter estimation and quality control"

Spectral decompositions of dual polarization observation allows for extending of analysis of polarimetric radar data to the new dimension, namely Doppler frequency domain. In this paper it is shown how this new paradigm can be used for improving quality of radar data. On an example of the CSU- CHILL observations it is demonstrated that this analysis can be used to design a spectral filter that allows for both ground clutter mitigation and radar sensitivity improvement. [C3262]

"Application of single drop scattering algorithms to rain related retrieval"

Since many years radars are known as valuable tools to retrieve rain. Applying well established relations for different types of radar allows accessing many rain parameters. For calculating the scattering function, the flattening of rain drops constitutes a non-negligible error source. In this contribution, different algorithms are applied to calculate the scattering function or the cross section of rain drops. Their results are compared to each other. A point matching algorithm serves as reference. To this reference, results from a Mie scattering algorithm, and-for backscatter-the Rayleigh approximation and an algorithm correcting the backscatter cross section according to the Rayleigh approximation for drop flattening are compared. The findings from this inter-comparison are presented for transmitting frequencies of 10 GHz, 24 GHz and 94 GHz. [C3263]

"Implementation of 3D discrete wavelet scheme for space-borne imagery classification and its application"

A three dimensional discrete wavelet transform (3D DWT) expands planes of the 2D DWT into volume data. The 3D DWT scheme has advantages of analyzing spectral characteristics in the order of frequency and analyzing changes of spatial information and spectral information simultaneously. Nonetheless, few researchers have attempted to classify multi-spectral images using the 3D DWT. This study aims to apply the 3D DWT to the classification of multi-spectral images and synthetic aperture radar image. To classify these images, we employ two numerical values: The 3D wavelet coefficients and the energy of each band. And then we evaluate their results quantitatively with those of traditional classification techniques including the 2D wavelet scheme. Therefore, the results show that the classification technique of the 3D DWT is more effective than that of traditional techniques, especially in complicated imagery. The accuracy of the 3D energy in SAR imagery is higher. This study provides new numerical values to classify images effectively. Furthermore, these values can be extended to the image retrieval and pattern recognition in high-resolution imagery and this scheme can be employed in image dataset obtained at other times. [C3264]

"Land use changes driven by 2008 beijing olympic playground constructions and depicted by landsat temporal data"

Landsat TM/ETM+ data in May or June are used to depict the land use changes from 1988,1994, 2001, 2003, 2005, 2006 respectively inner Beijing six ring express road and specially to watch the land use changes from the

beginning of Beijing Olympic playground area housebreaking in 2002. The great changes are identified in terms of land use change and usage replacements. [C3265]

"Application of a coherent modeling on Sahelian grassland"

The validity of a coherent Sahelian-grassland scattering model is determined by comparing the model predictions with satellite measurements of a representative site. This model considers the realistic botanical structure of grassland. The site Agoufou, located in the Northern Mali, was selected as the test target. This site is governed by a semi-arid tropical climate. Its vegetation is mainly composed of shrubs and annual grass. HH polarization backscattering data was collected over an entire growing season at different incidence angles by means of the ENVISAT ASAR. Simulations provided by the coherent model show a good agreement with measured data having a correlation coefficient equal to 0.92. Model predictions show that the HH polarization component is higher than the W polarization component during all growing season. Significant parameters are shown to be the grass density, the soil moisture content and the grass moisture content. The most sensitive parameter is the ground soil moisture content. Moreover, it is observed that the variation of the backscattering coefficient for all parameters can be represented by a linear regression function. [C3266]

"Land cover analysis at a regional scale exploiting low and medium resolution ENVISAT ASAR Data: Application to Poyang Lake Area (Jianxi Province, P.R. China)"

Located in Jiangxi Province, Poyang Lake is the largest freshwater lake in China and constitutes a major hydrological subsystem of the middle Yangtze river (Changjiang) basin in central China. An impressive amount of low to medium resolution ENVISAT data covering the Poyang Lake's 2004 and 2005 hydrologic years were acquired and analysed within the framework of the flood DRAGON project. Land cover mapping was realized synergistically using: 1) a land cover map derived from a colour composition containing seasonal ENVISAT ASAR Global Monitoring Mode image sums, and; 2) a land cover map derived from a colour composition containing filtered, seasonal ENVISAT ASAR wide swath mode image sums. Confronted and validated with the hydrodynamic characterization derived from Landsat reference data, these preliminary classifications lead to a land cover map with 13 classes covering 20,000 km² (170 km from north to south and 120 km from East to West) and was realized at a 1/200 000 scale, but can be used from 1/150 000 to 1/500 000. The results highlight the great potential of ASAR medium and low resolution products for wide-area mapping. Worldwide, large archives of such data already exist which should enable access to the prerequisite amount of data required for such large-scale, land cover characterization. [C3267]

"Adaptive bayesian algorithm for vegetated field parameters extraction by using multi-frequency and multi-polarimetric SAR images"

This paper proposes an alternative inversion algorithm for extracting soil and vegetation parameters from multi-frequency, multi-polarimetric SAR data. The alternative approaches aim at identifying a useful modelization of the soil and vegetation response to radar signal and then indicate a possible solution to the extraction of soil moisture and vegetation water content. The core of the algorithm is based on the determination of probability density functions (pdfs) through a Bayesian methodology and has been initially developed for bare soils and tested on numerous data sets. The purpose is to apply this inversion algorithm to fields that have different levels of vegetation cover and considering different theoretical and empirical approaches. In fact, as already stated, a single approach, theoretical or empirical model, cannot be often applied on a wide number of cases. This paper addresses a possible solution based on two alternative different modelizations. [C3268]

"An advanced concept of radar altimetry over oceans with improved performances and ocean sampling: AltiKa"

This paper describes the AltiKa project: the mission, the instrument design, the altimeter parameters, the anticipated performances, the key technologies involved, the whole payload design and budgets, and the micro-sat configuration. A status of AltiKa development is also given. [C3269]

"ALOS PALSAR for characterizing wooded savannas in Northern Australia"

With the successful launch of Japan's advanced land observing satellite (ALOS) phased array L-band SAR (PALSAR) and the recent provision of a Japanese earth resources satellite (JERS-1) synthetic aperture radar (SAR) mosaic for north Australia, significant opportunities for characterizing, mapping and monitoring the structural diversity and biomass of wooded savannas in Australia have been provided. This paper gives an overview of research undertaken and preparations being made to support such mapping in the state of Queensland. Preliminary observations on the integration of ALOS PALSAR and Landsat-derived foliage

projective cover (FPC) for mapping woody regrowth and dead standing trees are presented. [C3270]

"The ALOS Kyoto & Carbon Initiative"

The ALOS Kyoto & Carbon Initiative is an international collaborative project led by the JAXA Earth Observation Research Center (EORC). It forms the continuation of JAXA's on-going JERS-1 SAR Global Rain Forest and Global Boreal Forest Mapping project (GRFM/GBFM) into the era of the Advanced Land Observation Satellite (ALOS). The ALOS K & C Initiative has been set up to support the data and information needs required by international environmental Conventions; Carbon Cycle scientists and Environmental Conservation programs (referred below to as the CCCs). Led and coordinated by EORC JAXA, the Initiative is being undertaken by an international Science Team and focuses primarily on defining and optimizing the provision of data products and validated thematic information derived from in-situ and satellite sensors focusing on data acquired from the Phased Array L-band Synthetic Aperture Radar (PALSAR) on-board the Advanced Land Observing Satellite (ALOS). The objective of the ALOS K & C Initiative is to define, develop and validate thematic products derived from ALOS PALSAR data that can be used to meet specific information requirements relating to the CCCs. A key component of this work has been the development of a systematic data acquisition strategy for ALOS which comprises fixed, systematic global observation plans for PALSAR. The strategy is implemented as a top-level foreground mission and with a priority level second only to that of emergency observations. With emphasis on acquiring repetitive and consistent data over continental scales, it ensures that adequate data will be collected to allow the required thematic output products to be developed on a timely basis. The K & C Initiative is based on the three coordinated themes relating to global biomes; Forests, Wetlands, Deserts and Semi-Arid Regions, and a fourth theme dealing with the generation of regional ALOS PALSAR Mosaics. A key word for the Initiative is regional- scale applications and- product development, with data requirements in the order of hundreds or thousands of PALSAR scenes for each prototype area. Each theme has identified key products that can be generated from the PALSAR data including land cover, forest change mapping and forest biomass and structure analysis; global wetland inventory compilation and landscape change determination; and freshwater resources and desertification. Each of the products developed will be generated using a combination of PALSAR imagery, in situ measurements and ancillary datasets. An international Scientific Advisory Panel has been established to maintain the scientific relevance of project design and to ensure alignment with other relevant international efforts (e.g. GOFC/GOLD, IGOL, GTOS/TCO). The panel consists of scientists active in the fields of carbon modeling and biophysical parameter retrieval; SAR and image processing, as well as and representatives from GOFC, TCO, FAO, space agencies, universities and public research institutions. [C3271]

"Relationship between wind vectors and L-band radar cross sections examined using PALSAR"

The relationship between ocean wind vectors and L-band normalized radar cross sections (NRCS) is examined using the Phased-Array L-band Synthetic Aperture Radar (PALSAR). We used PALSAR ScanSAR images with a wide range of incidence angles from 17deg to 43deg. More than 6,000 match-ups, each consisting of the NRCS, incidence angles, wind speeds and wind directions, were collected. The NRCS exhibits a power-law relationship with respect to the wind speed. The coefficients of the power law can be derived as a function of the incidence angles. Based on this relation, the wind speeds are then inversely estimated from the NRCS and the incidence angles. A comparison with the truth winds reveals -0.23 m/s bias and 2.63 m/s rms error, demonstrating the feasibility of L-band scatterometry. Collecting more match-ups and further considering wind-direction dependence, which was not included in this study, would lead to the derivation of a robust L-band model function. [C3272]

"PALSAR CALVAL summary and update 2007"

This paper summarizes the geometric and radiometric calibration results of the PALSAR achieved during the ALOS initial calibration phase, which covers five months between May 16 2006 and October 23, 2006, and the half-year of the operational phase. All the PALSAR modes, FBS (fine beam single), FBD (Fine beam dual), SCANSAR, DSN (band limited SAR), and POL (Full polarimetry) were calibrated and validated using in-total 500 calibration points collected world widely and distributed target data from the Amazon. Through the characterization of the PALSAR, antenna pattern determination, and polarimetric calibration, we performed the adjustments of the PALSAR radiometric and geometric model installed on the SAR processor (SIGMA-SAR). Using the reference points, we finally confirmed that the geometric accuracy of the FBS, FBD, DSN, and POL modes is 9.3 m, that of SCANSAR is 70 m, and radiometric accuracy is 0.64 dB. Polarimetric calibration was successful that amplitude balance of VV/HH is 0.025 dB and the phase balance is 0.32 degrees. [C3273]

"Pol-InSAR Results from ALOS-PaISAR"

The launch of JAXA's ALOS in January 2006 provides-for the first time since the SIR-C/X-SAR mission's in the

80's-the opportunity to acquire Pol-InSAR data from space. Indeed, PalSAR (i.e. the SAR instrument onboard of ALOS) is able to operate in a quad-pol mode-declared by JAXA as an "experimental mode"-that allows the acquisition of Pol-InSAR data in a repeat- pass mode. In this sense, ALOS-PalSAR allows the application, validation and development of Pol-InSAR inversion techniques on a much wider range of sites distributed world-wide and accessible to a much wider scientific user community than possible with airborne sensors. In this paper we present the analysis of fully- and/or dual-polarimetric and interferometric data sets acquired by ALOS/PalSAR during its CAL-VAL and operational data acquisition phase and discuss the potential and the limitations for different polarimetric interferometric applications. More developed applications as forest height estimation from single- and multi-baseline Pol-InSAR ALOS-PalSAR data inversion-addressed in the frame of JAXA's Karbon & Kyoto initiative-as well as novel applications regarding coherent scatterer's detection and interpretation in urban environments are discussed. The impact of critical mission and operation design parameters as spatial coverage, repeat-pass time, observation scenario, and orbit control are evaluated and discussed. [C3274]

"Sensitivity of multi-temporal high resolution polarimetric C and L-band SAR to grapes in vineyards"

In the follow-up of the BACCHUS project, aimed at establishing a reference high quality geographic information system for vineyards, an airborne SAR survey has been carried out in fall 2005 in the Frascati area, near Rome (Italy) to investigate on the potential of radar remote sensing in vineyard monitoring. This contribution reports on the polarimetric very- high resolution C and L-band SAR data acquisition campaign supported by ESA and carried out by the DLR E-SAR on two dates in October 2005. The possible relation between the observed variations of backscattering at different polarizations and the harvest of the grapes is discussed. [C3275]

"Corn monitoring and crop yield using optical and RADARSAT-2 images"

In agriculture, soil and crop conditions change from day to day and throughout the growing season. Agricultural targets also vary spatially with differences observed from field to field, as well as within individual fields. The heterogeneity of corn-growing conditions in Mexico makes accurate data for crop type, crop condition and crop yield prediction difficult to obtain. Yield predictions are needed by the federal government to estimate, ahead of harvest time, the amount of corn required to be imported in order to meet the expected domestic shortfall. In this project a methodology for the estimation of corn yield ahead of harvest time is developed which uses radar and optical remote sensing and which specifically considers the corn-growing situation in Central Mexico. Radar based crop type classification requires data sets with multiple polarizations. Recent research to assess relative classification accuracies of multi-polarized combinations for target crops using airborne data has been reported. In addition to identifying crop type and variety, identifying crop growth stage is valuable. Crop condition, loosely defined as the vigor or health of a crop in a particular growth stage, is related to crop productivity and yield; however, the relationship is complex. Main crop condition indicators include biomass, height, leaf area and contents of plant water, chlorophyll and nitrogen. Crop-type and crop-condition mapping are among the applications that are expected to benefit the most from the technical enhancements embodied by RADARSAT-2. The potential of RADARSAT-1 data for these applications has been rated as "limited", whereas for RADARSAT-2 data this potential is anticipated to be "strong". The Science and Operational Applications Research for RADARSAT-2 Program (SOAR) is promoting the evaluation of Synthetic Aperture Radar (SAR) capabilities by providing images to selected research projects which include the present one. objectives of this project are: a) use RADA- RSAT-2 data and optical data to determine cultivated areas and monitor crop condition for obtaining better estimations of crop yield; b) obtain polarization signatures from RADARSAT-2 data for corn and relate these to Leaf Area Index and photosynthetic active radiation (PAR) crop parameters and vegetation indexes, to establish indicators of crop condition and produce estimates for crop yield; c) use field data collected for three key corn crop growth stages over 300 pilot plots during 2001-2006, and increase the number of plots to build a database to support accuracy studies using RADARSAT-2 data. The expected benefits of this project are: to obtain knowledge about crop type, crop condition and crop yield with better accuracy than with current methodologies; to support national corn farmers associations; to design agriculture related activities within State agriculture plans; to support the corn product industry and aid government decision making. Relevant results and economical impact will imply operational usage of RADARSAT- 2 data in the agricultural sector in Mexico.

[C3276]

"Remote sensing data assimilation for regional crop growth modelling in the region of Bonn (Germany)"

The study investigates the possibilities to improve the performance of CERES-Wheat crop growth model by assimilating information derived by optical and SAR Earth observation data. Biophysical parameter retrieval was done with the water cloud model for SAR data and the CLAIR model was applied to multispectral imagery. The CERES -Wheat model was calibrated using ground truth information. The re-initialization method with an adjustable planting date was selected as assimilation strategy. Modelling results generally improved by using all

different kind of remote sensing data. However, best results were achieved by using information of the optical sensors only and not by a synergetic time series of all available data. [C3277]

"Ground calibration of SMOS: NIR and CAS"

Ground calibration of the calibration subsystems of MIRAS (Microwave Imaging Radiometer using Aperture Synthesis) has been performed. The MIRAS instrument is the payload of European Space Agency's (ESA) Soil Moisture and Ocean Salinity (SMOS) mission. The calibration subsystems are Calibration Subsystem (CAS), which is a noise distribution network, and Noise Injection Radiometer (NIR), which measures the noise levels of CAS and the average incident brightness temperature. This paper presents the used measurement approaches, related uncertainties, and the calibration results for the NIR and CAS. The results show that in spite of uncertainties, the characterization methods allow accurate ground calibration of the two subsystems. The performance of both subsystems meet the requirements. [C3278]

"Some results of the MIRAS-SMOS demonstrator campaigns"

In this paper, some results of the MIRAS-SMOS demonstrator campaigns are presented. The follow two campaigns were held: an image validation campaign at IRTA side and a flight demonstrator campaign at Finland. The ultimate objective of the airborne demonstrator is to demonstrate its imaging capabilities by applying improved calibration and inversion algorithms to natural low-contrast targets. [C3279]

"Advanced land observing satellite (ALOS): On-orbit status and platform calibration"

The Advanced Land Observing Satellite (ALOS) was launched on January 24, 2006. Since then, it has been operated successfully on orbit, delivering a variety of high-resolution images in numerous quantities and contributing to disaster management support many times. This paper reviews the last 15 months' operations and on-orbit status of the ALOS spacecraft, with the flight data analysis of the bus subsystems and the mission subsystems. A particular emphasis is given to the assessment, calibration and validation of the mission-related platform performances such as orbit determination and control accuracies, attitude determination and control accuracies, attitude stability, and pixel geolocation determination accuracy. Efforts to improve these performances are also reported. [C3280]

"Rain microphysics estimation using X-band dual polarization radar measurements"

Rain microphysics retrieval has been proposed and demonstrated mainly at S-band where attenuation effects are usually negligible. Recent advances in attenuation correction techniques enable rain microphysics retrieval also using attenuating frequencies, such as X- and C-band. Most up to date attenuation correction methodologies are based on the use of a constraint represented by the total amount of the attenuation encountered along the path, which is distributed over each range bin contained in the path. The inner self-consistency of radar measurements can be exploited to improve the attenuation estimate obtained using those techniques. In fact, based on the self-consistency principle, an optimization procedure can be devised to obtain the best estimate of specific and cumulative attenuation as well as of specific and cumulative differential attenuation. The main goal of the study is the examination of the drop size distribution retrieval from X-band radar measurements after attenuation correction. The study is based both on simulated and measured data. Simulations based on the use of profiles of gamma drop size distribution parameters obtained from S-band observations are used for quantitative analysis. Examples of the DSD parameter retrievals using radar measurements corrected for attenuation and differential attenuation are also shown. [C3281]

"Surface clutter suppression for ice sounding radars by coherent combination of repeat-pass data"

This paper formulates a new approach for ambiguous surface clutter suppression for ice sounding radars. While surface clutter from the non-orthogonal direction is reduced by means of Doppler and/or SAR processing, the residual surface contributions from across-track may still mask the reflection of internal layers and the bedrock, both coming from the nadir direction. The suggested approach involves several repeated acquisitions separated by certain baselines. It uses a geometry model to derive a synthesized sparse array diagram with adaptive nulls in the direction of the ambiguities. Initial performance evaluations for a P-band space-borne mission indicates that clutter can be suppressed by 30-40 dB. The approach can potentially be demonstrated with airborne sounder data in case precise navigation and motion compensation is ensured. [C3282]

"Preliminary design of the spaceborne dual-frequency precipitation radar for the global precipitation measurement"

The dual-frequency precipitation radar (DPR) installed on the Global Precipitation Measurement (GPM) core

satellite is being developed by JAXA and NICT. This paper describes the results of preliminary design of the DPR instrument. [C3283]

"The RA-2 individual echoes processing description and some scientific results"

The RA-2 in its nominal operation provides averaged waveforms at the rate of 18 Hz (one averaged waveform over 100 individual echoes, every 0.0557 seconds). It has also the capability to provide limited bursts of individual, unaveraged echo sample data in phase (I) and quadrature (Q), at the full PRF rate. In this concept the full-rate data are stored, for a short burst, into an internal buffer memory, in parallel to the normal averaging and other functions of the instrument. The buffered data are subsequently read out at a much lower rate and appended to the normal science data. These Individual Echoes (IE) are, therefore, not processed onboard in the same way that the nominal RA-2 waveforms are. Recent studies have demonstrated that through the full rate data it is possible to discover some behaviour than cannot be seen with the averaged data. Moreover, it is the first time in altimetry that we have echoes that contain the information of the phase. This is a great potential for new science studies. This paper describes the algorithm applied on-ground to the IE of the RA-2 Burst Waveforms to reproduce the same process done by the instrument on-board (except for the averaging). Once this algorithm is applied to the IE they will be in the same condition than the normal RA-2 telemetred average waveform, but at 100 time higher surface sampling and with the phase information. The final objective of this work is the use of the IE fully processed and instrument calibrated for calibration, validation and science exploitation purposes. We will present results of studies carried out using these IE. The blurring on the averaged waveforms depends on the total movement of the range window [1], which in turn depends on slope of the terrain, the orbit slope and ultimately, how well the on-board tracker tracks that particular waveform shape. In early studies using ERS data, the blurring on the averaged waveforms has been estimated by simulating the ERS range window movement during-tracking. Using individual echoes there is no longer the need to do so, we can directly use these echoes. The IE will be averaged in the correct way and compared to the averaged waveform provided in the nominal RA-2 product. Changes on the retracked epoch and slope of the leading edge can be assessed for different type of waveforms over different surfaces. In particular we will present results of the analysis of the behaviour of IE over the "Salar D'Uyuni" in Bolivia, to better understand biases in retracking of specular echoes. The results can be used to improve the current understanding of retracked elevations over sea ice and help to improve tuning of current sea ice retracking schemes for the EnviSat RA-2 instrument. ESA has run a study on this topic to seed the use of individual echoes by scientists. This study is completed and reconstructed echoes will be made available for the first time to the scientific community. Final results from the technical and scientific application of individual echoes and S band data are described in [3]. [C3284]

"Prototype of NASA's global precipitation measurement mission ground validation system"

NASA is developing a Ground Validation System (GVS) as one of its contributions to the Global Precipitation Mission (GPM). The GPM GVS provides an independent means for evaluation, diagnosis, and ultimately improvement of GPM spaceborne measurements and precipitation products. NASA's GPM GVS consists of three elements: field campaigns/physical validation, direct network validation, and modeling and simulation. The GVS prototype of direct network validation compares Tropical Rainfall Measuring Mission (TRMM) satellite-borne radar data to similar measurements from the U.S. national network of operational weather radars. A prototype field campaign has also been conducted; modeling and simulation prototypes are under consideration. [C3285]

"Evaluation of X-band polarimetric radar estimates of drop size distributions from coincident S-band polarimetric estimates and measured raindrop spectra"

Recent research has demonstrated the value of polarimetric measurements for the correction of rain-path attenuation at X-band radar frequency and the estimation of rain parameters including drop size distributions (DSD). The issue this study is concerned with is to what degree uncertainties in attenuation correction can affect the estimation of DSD. Since attenuation correction uncertainty enhances with rain path our hypothesis is that DSD retrieval uncertainty at X-band may deteriorate with range. In this study we evaluate the relative accuracy of X-band DSD retrieval against DSD estimates from S-band radar observations and in-situ disdrometer spectra. We present comparisons of various techniques for estimating DSD model parameters from attenuation-corrected X-band dual-polarization radar data. Coincident X-band (XPOL) and S-band (S-Pol) dual-polarized radar measurements from the International H₂O experiment (IHOP) as well as coincident X-band polarimetric radar (MP-X) measurements over disdrometer during a Typhoon storm case in Japan are used to assess the accuracy of the different DSD retrieval algorithms applied to X-band radar. [C3286]

"Survey of bathymetry and current fields by radar image series acquired by shore based x-band radar"

The error source in assessing the bathymetry by the Dispersive Surface Classifier method is discussed in this paper. The accuracy of the method is high in the deeper areas and is reduced behind the slopes. The identification of systematic correlation of the absolute value of the error with the slope was not possible. The spatial correlation of the error illustrates that the direction of the wave field influences the two neighboring cells in the same direction. [C3287]

"Waveform coding for dual polarization weather radars"

Polarimetric variables are an essential part of algorithms for improved rainfall rate estimation, attenuation correction and hydrometeor identification. In such systems the transmit polarization state changes according to some fixed pattern that is repeated. The simultaneous mode and alternating mode waveforms are commonly used in weather radars. In the simultaneous mode of operation the horizontal and vertical polarization states are transmitted simultaneously and samples of both horizontal and vertical co-polar return are obtained. A drawback of the current implementation of simultaneous mode is its inability to measure cross-polar parameters such as linear depolarization ratio. In this paper a technique to estimate cross-polar signals with a simultaneous mode waveform is presented. In this method, the horizontally and vertically polarized transmit waveforms are coded with orthogonal phase sequences. The performance of the phase coded waveform is determined by the properties of the phase codes. This paper presents the performance of the cross-polar and co-polar parameter estimation based on the simulation as well as data collected from CSU- CHILL radar. [C3288]

"Synthetic range profile focusing via contrast optimization"

In stepped frequency radar, target motions produce range profile distortion. Specifically, the target radial velocity causes range profile shift, point spread function symmetric spreading and peak reduction, whereas the target radial acceleration is responsible for both asymmetric and symmetric point spread function spreading. This paper proposes a contrast-based technique for estimating the target motion parameters and therefore for reducing range profile distortions. [C3289]

"Wide area traffic monitoring with the PAMIR system"

This paper presents some Scan-MTI results, which were obtained with the SAR-GMTI system PAMIR developed at FGAN-FHR. The Scan-MTI mode was designed to rapidly monitor wide areas for ground moving targets. The scan operation enables detection of targets from different aspect angles with a high revisit rate. This mode is particularly adapted to perform an efficient traffic monitoring, as well. [C3290]

"Wavelets: a Versatile Tool for the High Frequency Surface Wave Radar"

Widely used in image processing, wavelets seem to be a promising versatile tool for the high frequency surface wave radar (HFSWR). HFSWR is based on the ability of HF waves (3 MHz to 30 MHz) to propagate along the earth curvature. HFSWR can detect targets up to few hundred kilometers beyond the horizon. The two main applications of the HFSWR are the maritime surveillance of the exclusive economic zone (EEZ) and the remote sensing of the sea. Beside the classical noise which affects all radar signals, the detection capabilities of HFSWR suffer from two limitations: the sea clutter and the ionospheric clutter which are target masks. However sea clutter can be used to perform remote sensing of the sea. In this paper we are studying how wavelets may contribute to the improvement of radar signal processing. We consider general de-noising feature for radar signals, we carry out a wavelet-based improvement of remote sensing of oceanographic parameters and we show the first results of a wavelet-based processing for ionospheric clutter mitigation. [C3291]

"Algorithm Overview Based On Image Processing with Electromagnetic (EM) Techniques in X Band and GA Approach for Depth Estimation of Shallow Buried Dummy Mines"

Detection of buried landmines and estimation of depth by modeling layered media is a complex and computationally intensive task. Microwave remote sensing with the capability to penetrate subsurface and its ability to resolve landmines as well as non-lethal targets can therefore be used for subsurface landmine detection. A model based on electromagnetic scattering and image analysis techniques at X-band frequency for sub-surface detection of dummy landmines buried under a sand layer and estimation of its depth has been proposed in this paper. An extensive set of lab experiments have been carried out using dummy landmines (without explosives) and backscatter observed at different depths. The raw data is processed through a series of image processing steps, the detection is carried out using Otsu's thresholding and the depth estimated by optimizing through a GA (genetic algorithm) based electromagnetic model developed. The method does not have any requirement of separate training and test data set to train the optimizer and validate the results. The results under laboratory conditions indicate that detection of dummy landmines is possible using thresholding techniques with data generated in X band and the proposed model is capable of estimating depth of the buried landmine to

a significant accuracy. [C3292]

"UWB Radars: Recent Technological Advances and Applications"

A number of challenging radar applications (such as anti-personnel mine detection and human being detection) is discussed. In these applications UWB technology has multiple advantages over the traditional narrow-band approach, in particular very high positioning accuracy, rigidity to multi-path propagation and target classification abilities. On a number of examples recent advances of UWB technology in radar have been demonstrated and remaining challenges have been discussed. [C3293]

"An Experimental Study on Using Electronically Scanning Microwave Radar Systems on Surface Mining Machines"

Using a series-model of an automotive short range radar sensor (SRR) and a recently completed experimental radar system, field tests have been performed in a surface mine. It was examined, to what extent low-cost electronically scanning radar sensors can provide useful data for assistance systems in large scale mining machines. The series SRR sensor using mono-pulse principles for cross range measurement, proved to be useful to supervise the safety zone of a bucket wheel excavator. The more complex and sophisticated experimental radar system using digital beam-forming for cross range processing, can clearly detect and map the contours of trenches and escarpments. The overall promising results refer to many more potential applications for electronically scanning radar in surface mining and motivate to adapt the experimental sensor for such applications. [C3294]

"Perspectives on Worldwide Spaceborne Radar Programs"

Radar technology and techniques were originally developed for land-based, maritime, and airborne applications. Spaceborne radar systems development began in the 1960s in the USSR for military purposes, and in the 1970s in the United States for civilian scientific purposes. NASA launched the SeaSAT satellite in 1978, carrying a synthetic aperture radar, a radar altimeter, a radar scatterometer, and a radiometer, ushering in the modern era of spaceborne radar observations. NASA embarked on a shuttle-based space radar program in the 1980s that was geared to advancing space radar technology and demonstrating scientific utility of multi-parameter synthetic aperture radar, culminating in the Shuttle Imaging Radar-C flights in 1994. With the launch of the European Space Agency ERS satellite and the Japanese JERS satellite in 1992, and the Canadian Radarsat satellite in 1995, international systems have had a persistent orbiting radar presence in space around the Earth, replenished with new systems with increasing emphasis on dual use capabilities, while the US has fielded only one Earth orbiting space radar system for a 10-day period in 2000, the Shuttle Radar Topography Mission. The US program has evolved differently, with emphasis on mapping SARs for the planet Venus and Saturn's moon Titan, and a series of targeted scientific platforms focusing on Earth system and climate studies: TOPEX altimetry and follow-ons for ocean topography, QuikScat scatterometer for global winds, and TRMM and Cloudsat for precipitation and cloud water content. Radar programs worldwide are flourishing as the technology advances and new scientific uses and applications are generated from the abundant globally acquired data from international systems. Questions of security and global competition are now complicating the development of highly capable systems, such as the SAR systems required for persistent surveillance in both the military and scientific arenas. [C3295]

"Developments in Modern Synthetic Aperture Radar"

Since their origins in the 1950s, the techniques of synthetic aperture radar have come a long way, and SAR is now routinely used, both from satellites for geophysical remote sensing and from aircraft for high-resolution surveillance. This paper presents a subjective and selective review of some developments in systems, techniques and results. [C3296]

"InSAR Remote Sensing Over Decorrelating Terrains: Persistent Scattering Methods"

Interferometric synthetic aperture radar, or InSAR, is a visual geodetic technique permitting detailed mapping of motion over wide areas. InSAR has been limited to regions without much vegetation, which shields the ground from the radar signals and contributes random motions to the observed deformation. The resulting "decorrelation" of the echoes precludes accurate displacement measurements in these areas. Decorrelation also occurs in interferograms with acquisitions separated too far in the sky. Yet certain points, denoted persistent scatterers, in a radar image are stable, do not decorrelate, and form a network of fiducial points that allow measurements in otherwise poor-quality interferograms. We have generalized an algorithm to find networks of stable points in natural terrain, rather than in urban areas, and applied the method to spaceborne satellite data.

Using modern information theory to optimize persistent scatterer detection, we can now find many, many more such points than previously possible. We have applied this improved algorithm to the San Francisco Bay segments of the San Andreas and Hayward faults, and in both cases find that a large number of stable points are seen in the vegetated areas that have to date resisted InSAR analysis. Our method of integrating information theoretic estimation and detection theory to all parts of the method, improves the identification, filtering, and phase unwrapping of the observations. Identification of stable true-ground scattering points permits mapping of subtle surface motions and deformations and also of "bare-Earth" topography. [C3297]

"A System for the Measurement of the Amazon"

The System for the Vigilance of the Amazon (SIVAM) is a \$1.4 billion dollar project of Brazil aimed at the development and deployment of a high-technology system-of-systems to perform monitoring, protection and control of the land, air and water resources of the Brazilian Amazon region. The primary challenge of the SIVAM project is to perform remote sensing and communications over a vast and undeveloped land area. The SIVAM network meets this challenge through an extensive network of air traffic control/surveillance radars, environmental sensors, communications systems, airborne sensor systems and coordination centers. Now fully operational, the SIVAM system is the world's largest fully integrated remote monitoring system of the environment and provides critical information on a timely basis to the Brazilian government, law enforcement agencies, and to commercial, educational and research groups. [C3298]

"Joint combination of point cloud and DSM for 3D building reconstruction using airborne laser scanner data"

More and more cities are looking for service providers able to deliver 3D city models in a short time. Airborne laser scanning techniques make it possible to acquire a three-dimensional point cloud leading almost instantaneously to digital surface models (DSM), but these models are far from a topological 3D model needed by geographers or land surveyors. The aim of this paper is to present the pertinence and advantages of combining simultaneously the point cloud and the normalized DSM (nDSM) in the main steps of a building reconstruction approach. This approach has been implemented in order to exempt any additional data and to automate the process. The proposed workflow firstly extracts the off-terrain mask based on DSM. Then, it combines the point cloud and the DSM for extracting a building mask from the off-terrain. At last, based on the previously extracted building mask, the reconstruction of 3D flat roof models is carried out and analyzed. [C3299]

"Simulation Tools for Interpretation of High Resolution SAR Images of Urban Areas"

New powerful spaceborne sensors for monitoring urban areas have been designed and are ready for launch. More detailed SAR images will be soon available and, consequently, new tools for their interpretation are needed, above all when urban scenes are illuminated. In this paper, the authors propose some tools for the study and the analysis of high resolution SAR images based on a SAR raw signal simulator for urban areas. Comparing simulated SAR images with the real one, interpretation of SAR data is improved and fundamental support of the employed tools is further assessed. [C3300]

"SAR measurement simulation on urban structures using a FDTD technique"

The purpose of this work is, starting from a close tracking of basic electromagnetic processes, to propose a simulator enabling a better understanding of the radar images of urban areas. An improved understanding of the radar images formation processes in this case should lead to a better knowledge of the potentialities of the SAR imagery of urban areas. With the rapid development of computer, numerical techniques with no physical approximation play more and more important role in some studies such as electromagnetic scattering from urban scene. We argue that finite-difference time domain method (FDTD) is a quite new and promising approach for the propagation in urban areas. In order to numerically evaluate its electromagnetic return to an active microwave sensor, a geometric and electromagnetic model of a typical element of urban structure is presented. It consists of a rectangular parallelepiped whose vertical walls form a generic angle with respect to the sensor line of flight. This parallelepiped is placed on an either smooth or rough surface, to take into account multiple scattering between buildings and terrain. Finally, the above model is used to analyze the field backscattered from a building, as a function of the main scene parameters. [C3301]

"Object-Oriented Classification of LIDAR-Fused Hyperspectral Imagery for Tree Species Identification in an Urban Environment"

The objective of the current study was to develop a methodology for the identification of tree species in an urban environment by using Quickbird multispectral data, AISA hyperspectral data, AISA Eagle hyperspectral

data and Leica ALS50 LiDAR data. For this research, object-oriented classification was performed using eCognition Professional. The classifications were performed on each of the images available with and without the aid of LiDAR. Elevation and intensity data was used to create images segments as well as user-defined class rules. Classes included honey locust, white pine, crab apple, sugar maple, white spruce, American basswood, pin oak and ash. Initial results indicate fusing LiDAR data with these imageries showed an increase in overall classification accuracy for all datasets. Increases in overall accuracy ranged from 12 to 24 percent over classifications based on spectral imagery alone. There were some more substantial increases in some individual species accuracies, particularly classes that consisted of smaller objects such as saplings or shrubbery. [C3302]

"Re-configurable Completely Unpowered Wireless Sensors"

A methodology for remotely and wirelessly reading any type of unpowered impedance varying sensor is described. Unpowered wireless sensors, in existence for a number of years, have been limited to low impedance sensors. Techniques for reading high impedance sensors are introduced here. The resulting methodology can be used to measure a wide range of different sensors, including temperature, pressure, light level, mechanical switch, acoustic emission, and acceleration. These sensors report physically measurable data in the same manner as do similar conventional sensors, but they do it remotely and without any local power source. The sensors are measured remotely using a radar-like interrogation device, and the sensors and their related communication electronics draw all of the power needed for communicating from the radar pulse. [C3303]

"Beam-Shaping of Planar Array Antennas Using Integrated Attenuators"

The use of planar integrated attenuators to shape the beam of a planar array antenna is investigated on a lightweight organic polymer ideal for satellite applications. The entire array is fabricated using a single type of liquid crystal polymer (LCP), reducing the cost of fabrication and simplifying the integration of the attenuators. A fabricated prototype was designed, fabricated, and measured revealing a sidelobe reduction of 12dB compared with a similar antenna using a uniform amplitude distribution, or an overall sidelobe level of -25dB. The 3dB beamwidth of the binomial array was measured to be 31 degrees, an increase of 3 degrees over the uniform amplitude case. [C3304]

"Cell Decomposition for Building Model Generation at Different Scales"

Usually, 3D building reconstruction is realized by systems, which either apply constructive solid geometry (CSG) or boundary representation (B-Rep) to model the respective buildings. We present an alternative approach based on cell decomposition, which can be used efficiently for building reconstruction at different scales. Firstly, building polyhedrons are constructed from airborne LIDAR data and given outlines of the respective buildings. In this context, cell decomposition is used to guarantee topological correct representations and the simple implementation of constraints between different building parts like co-planarity or right angles. As it will be demonstrated in the second part of the paper, cell decomposition is also advantageous if large scale building models have to be generated for example based on the analysis of terrestrial LIDAR data. [C3305]

"Fusion Of Remote Sensing Images via Lattice Filters"

A new image fusion algorithm based on the subband decomposition of the source images using 2-D separable lattice filters is presented. The method is used for the fusion of multispectral and SAR data. The source images are decomposed into subband images using separable lattice filters, these images are combined in the subband domain using a predefined rule, then the fused image is obtained by the inverse lattice filter. [C3306]

"Earth Observation Remote Sensing and GIS Services for Monitoring of Integration Systems"

Today availability of using the high resolution of space imagery creates a positive environment on application of space technology for monitoring of integrated systems in different areas of industry and commercial purposes. They are an airborne, unmanned aerial vehicles (UAV) and satellite Synthetic Aperture Radar and LIDAR multi-spectral and hyper-spectral sensors. One of the advance methods of feasibility study of appropriate services for monitoring of integration systems is based on remote sensing data and GIS developments. Objective of this approach is to improve safety, security aspects of integration systems, reduce survey costs and improve transportation and transmission efficiency through an increased monitoring frequency. Conceptually monitoring the integration system is structured into four main system components: (1) the Pipeline Operator System (POS), which is the part of the monitoring system which is used by the pipeline operator for delivery and handling of alarms and for specifying the monitoring characteristics for different parts of the pipeline network. (2) the Pipeline Information Management System (PEMS), which stores all relevant information on the pipeline network, the environment around it, and the integrity monitoring and which provides analyses and scheduling functionalities

for the pipeline operator. The PIMS also includes an alarm production system, which decides what hazards should be considered as alarms. (3) the Hazard Extraction System (HES), which extracts the hazard report information out of the basic remote sensing imagery layers, using advanced image interpretation techniques. (4) the imagery Collection System (ICS), which collects the required remote sensing imagery with a suit of both spaceborne and airborne platforms and different types of sensors, conform the monitoring priorities. In the ICS all these means are scheduled optimally conform the specified priorities of the pipeline operators and the weather and season conditions. Here also the data are pre-processed to remote sensing basic imagery layers. The four components in principle can be independent of each other so that maximal flexibility exists. Also each system component in itself is set up as much as possible in a modular and flexible way. By implementation of this above mentioned issues, new technologies on sensors, platforms, data processing, data storage and transfer can be integrated and the system easily can be extended to other operators or areas. The future integration systems monitoring scenarios can only be turned into reality if sufficient supply from spaceborne data will be available for reasonable economic conditions and with certain technical performance. Earth observation for appropriate investigation requires very high resolution optical and in most cases radar sensors. Very high resolution is here defined as a resolution of 1 meter and better. This scale is required to allow the detection of targets. Very high resolution satellite observation, formerly limited to national and strictly classified reconnaissance tasks, has become a commercial business in the recent years. However, national security users are still the basis for the commercial viability of that business. Affected by satellites losses and pioneered with Space Imaging's IKONOS satellite, better than 1 meter resolution optical data is now available for science and commercial use. [C3307]

"Spectral Predictors of Crop Development and Yield"

Remote sensing enters still wider into its application stage when the goal is to bring the up-to-now investigation results to an operational use. Agricultural monitoring is among the priorities of remote sensing observations supplying early information on crop growth. Interest is rapidly spreading over the past years in the application of hyperspectral data to precision farming. In this paper, we propose and investigate the performance of an approach for providing crop state assessment and yield forecasts. In order crop information to be obtained from remotely sensed data the approach comprised: development of models between plant spectral reflectance and biophysical parameters for estimation of crop state variables from radiometric data; development of yield forecasting models from single-date and time-series spectral data; verification of remote sensing predictions through comparison with estimations from yield relationships with crop agronomical parameters. The algorithm was realized on winter wheat. In-situ high-resolution visible and near-infrared reflectance data were acquired throughout the growing season, along with detailed datasets of crop parameters. Spectral-biophysical models were developed relating crop variables and yield to different spectral predictors. The algorithm was tested and validated using airborne remote sensing data. A good correspondence was found between predicted and actual yield. [C3308]

"GPS/TEC Estimation with IONOLAB Method"

Total Electron Content (TEC) is a key variable to measure the ionospheric characteristics and disturbances. The Global Positioning System (GPS) can be used for TEC estimation making use of the recorded signals at the GPS receiver. Reg-Est method that is developed by F. Ankan, C.B. Erol and O. Arikan can be used to estimate high resolution, robust TEC values combining GPS measurements of 30 s resolution obtained from the satellites which are above the 10deg elevation limit. Using this method, it is possible to estimate TEC values for a whole day or a desired time period both for quiet and disturbed days of the ionosphere. Reg-Est provides robust TEC estimates for high-latitude, mid-latitude and equatorial stations. In this study, some important parameters of Reg-Est such as ionospheric thin shell height, weighting function and receiver-satellite biases are investigated. By incorporating the results of the investigation, Reg-Est algorithm is developed into IONOLAB method. Thin shell model height is an important parameter for Single Layer Ionosphere Model (SLIM). In this study, it is shown that IONOLAB provides reliable and robust TEC estimates independent of the choice of the maximum ionization height. Signals from the low elevation satellites are prone to multipath effects. In order to reduce the distortion due to multipath signals, the optimum weighting function is implemented in IONOLAB, minimizing the non-ionospheric noise effects. GPS receivers record both pseudorange and phase data of signals. IONOLAB can input absolute TEC computed from the pseudorange measurements or phase-corrected low-noise TEC. The TEC estimates for both of these inputs are in good accordance with each other. Thus, taking either pseudorange or phase-corrected measurement data as input, high resolution, robust TEC estimates can be obtained from IONOLAB. Another important parameter for TEC estimation is satellite-receiver instrumental biases. The biases are the frequency dependent delays due- to satellite and receiver hardware. In order to compute TEC, satellite and receiver biases should be removed from GPS measurements correctly. However, the proper procedure of how to include them in the TEC computation is generally vaguely defined. IONOLAB suggests a technique for inclusion of the hardware biases obtained from the web for TEC estimates that are consistent with the results from the IGS analysis centers. [C3309]

"A Hyperspectral Imaging Mission for Small Satellites-Five Years Orbit Experience"

The ESA Proba-1 platform has now been in orbit since October 2001. Since that time significant value has been obtained from the CHRIS hyperspectral imager, with over 10,000 acquired images. To day CHRIS still offers the highest spatial resolution of any spaceborne hyperspectral instrument. The original intent of the CHRIS/Proba-1 programme was to acquire images of land areas particular to measure the bidirectional reflectance distribution function (BRDF) properties of selected targets using multi-angle observations. A secondary objective was to monitor aerosol properties of the atmosphere. This latter aspect has only recently been revisited and results are likely to be available later this year. This paper describes the instrument and provides an update of the associated hyperspectral mission. [C3310]

"TerraSAR-X and TanDEM-X: Reconnaissance Applications"

Commercially available imagery is and will remain indispensable to civilian and military organizations gathering intelligence information. Whether fulfilling international agreements, providing contingents in international peacekeeping or humanitarian missions, or conducting joint exercises with other countries-a reliable access to timely, high resolution remote sensing data is an essential basis for well-informed decision making, particularly in time-critical situations. Today, organizations with these needs customarily resort to high resolution data acquired by optical sensors -often a lengthy operation. TerraSAR-X, with it's complementary near-real time data acquisition capabilities, offers a whole new approach to the use of space-borne datasets in time-critical situations: TerraSAR-X delivers unique, novel quality SAR satellite image data with a resolution of up to 1 m, which can significantly augment the capabilities of armed forces and intelligence agencies, creating both tactical and strategic advantages. In order to close the information gap towards the third dimension TanDEM-X (TerraSAR-X Add on for Digital Elevation Measurements) is the new German mission of a sophisticated satellite generation operating at X-band in single pass SAR interferometry. The single pass SAR interferometric constellation is realized by two independent X-band satellites flying in a close formation and has the goal to deliver a global digital elevation model at HRTI-3 specification. The increasing demand of sophisticated geospatial data sets requires appropriate and precise planning documents in all the three dimensions. However, a continuous and up-to-date acquisition by optical sensors is strongly limited by unfavorable weather conditions. Therefore, the easy access to the high-resolution radar missions TerraSAR-X and TanDEM-X provides the possibility to participate in one of the most ambitious space programs to the global remote sensing community. [C3311]

"The TerraSAR-X and TanDEM-X Satellites"

TerraSAR-X is a multi-role SAR Satellite with active phased array antenna technology which will be the backbone of the next German national radar Earth observation mission. With its large variety of different SAR imaging modes and its high operational flexibility, TerraSAR-X will ideally serve both the scientific community and users from the industrial sector. The innovative satellite system design is based on the rich experience from past German and European SAR space missions like X-SAR, SRTM, ERS 1&2 and Envisat combined with state-of-the-art Earth Observation Bus technology as used e.g. on the CHAMP and GRACE satellites. In a preparatory effort co-funded by the national agency DLR and its industrial partner EADS Astrium, the main new, performance critical SAR features of TerraSAR-X were thoroughly studied, and a sound market analysis was undertaken to define individual system requirements concerning image product characteristics and availability. The paper describes the TerraSAR-X system design and performance, with emphasis on the SAR instrument and SAR-relevant features of the satellite bus. SAR product performance relevant elements of the satellite system architecture are discussed in particular. Also the additional payloads flying on TerraSAR-X -the Tracking, Occultation and Ranging experiment (TOR) furnished by the GeoForschungszentrum Potsdam (GFZ) and the Taser Communication Terminal (TCT) furnished by DLR with the industrial prime contractor Tesat-are briefly introduced. Moreover, a short description on the TanDEM-X mission is given to generate a global Digital Elevation Model (DEM) with an unprecedented accuracy. [C3312]

"Estimation of Electromagnetic of Libyan soil Properties by Stepped Frequency Radar"

A vector network analyzer was used to measure the electromagnetic properties of two types of Libyan soil. The vector network analyzer was used to act as a stepped frequency ground probing radar. The frequency that was covered is from 1 to 3 GHz. A TEM horn antenna was used for transmission and reception. From the experiments the attenuation and time delay was measured. Then conductivity, permittivity and moisture content were estimated from the measurements. The samples were taken before and after it rained by a week following a long dry season. The experiments gave a reasonable estimation of the parameters and showed that clay retained its moisture for a longer period than sandy soil. [C3313]

"A Wireless Location System for Sensing the Relative Position between Mining Vehicles"

In this paper a novel system and concept for sensing the relative position between mining vehicles is introduced. The localization is based on secondary radar like distance measurements between radar basestations on the excavator and transponders on the truck. Based on a novel geometry-matching algorithm it is possible to determine the relative position between truck and excavator precisely even in complex measurement and environmental conditions. The geometry-matching algorithm overcomes problems of usual triangulation based approaches because it efficiently reduces the risk to get an underdetermined set of geometric equations in conditions where measuring paths are shadowed or disturbed. The proposed concept allows for a steady and flexible control of all movements of the truck relative to an excavator and thus can contribute effectively to increase automation and productivity in future mining systems. The results of first full-scale experiments show the consistency and good performance of the proposed approach. [C3314]

"Spectral Signature Classification Using A Support Vector Classifier For Real-Time Instrumentation"

The research WSR-88D (weather surveillance radar) locally operated by the National Severe Storm Laboratory (NSSL) in Norman has the unique capability of collecting massive volumes of Level I time series data over many hours which provides a rich environment for evaluating our new post-processing algorithms. In this work, a Support Vector Machine (SVM) classifier is employed to identify tornado vortices based on their characteristic Doppler spectra and eigen analysis technique. A SVM-based classifier evades the pitfalls of the traditional statistical learning algorithms, such as neural networks, by setting up a convex optimization problem with a single global minimum. In addition, through the use of kernels and nonlinear mapping to higher dimensional spaces, the SVM classifier is able to effectively handle nonlinear classification problems. Finally, the SVM classifier has the added advantage of reducing overfitting by constructing a maximum margin separating hyperplane in a higher dimensional feature space which ensures a small generalization error bound. [C3315]

"Radar Scattering from Partially-Submerged Objects in Ducting Environments"

This paper describes the ducted ocean surface scattering integral equation routine (DOSSIER). DOSSIER is a numerically-efficient high-fidelity numerical model for calculating scattering from partially-submerged targets in ducting environments. The model is based on a hybrid 2D-3D integral equation formulation where the 2D formulation is used to propagate the radar energy to the target location, while the 3D model is used to calculate the backscattered field from the target and its proximity. The combined model effectively accounts for shadowing, multipath, and ducting effects on the effective target reflectivity in such a complex environment. [C3316]

"A 26GHz Short-Range UWB Vehicular-Radar Using 2.5Gcps Spread Spectrum Modulation"

A 26 GHz short-range radar (SRR) system has been developed based on a 2.5 Gcps direct sequence spread spectrum (DSSS) technique combined with simple homodyne detection. Separate frequency-triplers have been provided with transmitter (TX) and receiver (RX) chips to cut off the carrier-leakage path from local signal. By using this configuration, carrier-leakage in TX signal can be significantly suppressed falling into the satisfactory range of the UWB regulation. The present radar system achieved the maximum detection range of 14 m with the resolution of 6 cm. TX, RX, and PN generator chipset has been developed using InGaP/GaAs HBT process, where f_T/f_{max} of 65 GHz/ 83 GHz were attained. [C3317]

"Displaying LiDAR Data for Interactive Web-Based Modelling of the Environment"

The increasing commercial availability of highly accurate LiDAR scanning offers remote sensed data accurate enough for generalized and distant views of the environment. From this data, bare earth digital terrain models (DTMs) can be processed semi-automatically, then draped with aerial imagery. The paper describes an approach developed in the VEPs project that switches on the LiDAR data for trees and buildings removed from the DTM in the 3D Scene. This data can then be used to visually judge the appropriate height and form of buildings and trees. A set of web-based interactive tools have been developed to enable users to freely adjust the scale and mass of structures and vegetation to match the selected point cloud area, substantially improving the quality of presence and accuracy of the resulting model. Issues are raised in obtaining equally accurate data of what is proposed from Planners and Developers. [C3318]

"Multisource Data Processing for Semi-Automated Radiometrically-Correct Scene Simulation"

The digital imaging and remote sensing image generation (DIRSIG) model is an established, first-principles based scene simulation tool that produces synthetic multi-spectral and hyperspectral images from the visible to long wave infrared (0.4 to 20 microns). Significant enhancements such as spectral polarimetric and active light

detection and ranging (lidar) models have also been incorporated into the software, providing an extremely powerful tool for algorithm testing and sensor evaluation. However, the extensive time required to create large-scale scenes has limited DIRSIG's ability to generate scenes "on demand." To date, scene generation has been a laborious, time-intensive process, as the terrain model, CAD objects and background maps have to be created and attributed manually. To shorten the time required for this process, we have initiated a research effort that aims to reduce the man-in-the-loop requirements for several aspects of synthetic hyperspectral scene construction. Through a fusion of 3D lidar data with passive imagery, we are working to semi-automate several of the required tasks in the creation of high-resolution urban DIRSIG scenes. This paper reports on the progress made thus far in achieving these objectives. [C3319]

"600 GHz Imaging Radar with 2 cm Range Resolution"

We report the first submillimeter-wave imaging system that has radar ranging capabilities. By frequency-modulating the K-band synthesizers of a single-pixel 630 GHz scanning vector imager and applying a distortion compensation technique in software, we have achieved a range resolution of approximately 2 cm for targets at a range of several meters. Relief images of test objects obtained with our system demonstrate that three-dimensional THz imaging of scanned targets is feasible using a room temperature, all solid-state approach. [C3320]

"A Spatial Classification Model for Multicriteria Analysis"

This paper stresses that standard multicriteria aggregation procedures either do not assume any structure in data or this structure is in fact assumed linear. Nevertheless, many decision making problems are based upon a family of data with a well denned spatial structure, which is simply not taken into account. Hence, such aggregation procedures may be misleading. Therefore, we propose an alternative model where the aggregation of criteria assumes a certain structure, according to remote sensing data [C3321]

"Cognitive Dynamic Systems"

The first half of the paper addresses the rationale for why we need to study cognitive dynamic systems, with particular reference to two wireless applications: cogitative radio for communication, and cognitive radar for remote sensing. The second half of the paper discusses the issues involved in dynamic spectrum management and transmit-power control, which are of particular importance to cognitive radio. The iterative water-filling algorithm, in a noncooperative radio environment is discussed, and its virtues and limitations are highlighted. [C3322]

"Clustering Polarimetric SAR Image Under Deorientation Theory"

In natural complex terrain surfaces, scattering targets with random orientations produce random fluctuating echoes which lead to confused classifications by directly using target decomposition on polarimetric SAR (PolSAR) image. In order to reduce the influence, the target vector is transformed into the state with minimization of cross-polarization. Then a set of new parameters $u/v/w$ are used to characterize scattering mechanisms under the deorientation theory, and the fuzzy membership is adopted instead of "hard" division of parameter plan. Characterizing the sample coherency matrices as complex Wishart distribution, the PolSAR image is clustered based on Bayes maximum likelihood (ML) criteria. Experiment is carried out on an L-band NASA/JPL SIR-C PolSAR image over Danshui town, Guangdong, China. Comparison results with the popular used methods show that the proposed method provides a significant improvement in classification and the associated scattering mechanism of class is more accurate and beneficial for automatic terrain recognition. [C3323]

"Microwave Imaging Using Spread Spectrum Modulation"

An X-band Side Looking Airborne Radar is being developed and tested. It uses solid state electronics and phase modulated impulses. The first images show that rivers, lakes, buildings, roads, railroads and agricultural fields can be identified. [C3324]

"SAR and Optical Data Fusion for Change Detection"

In this work, we devise a change detection technique for urban areas based on the fusion of temporal series of SAR images with a single multi-band optical image. The proposed technique aims at exploiting both the high repetition observation rate available with the new generation of SAR systems and the high level of details available even in a single multiband optical image. The approach has been validated by using a multitemporal set of ENVISAT SAR images and a couple of Quick Bird optical images, that are also used to provide evidence

on the changes by visual inspection at high resolution. The preliminary results shown in the paper show the potentiality of the joint processing of SAR and optical images. [C3325]

"Urban area remote sensing from L-band PolSAR data using Time-Frequency techniques"

This article presents a new approach for the study of urban areas using polarimetric SAR (PolSAR) data. The PolSAR multidimensional information is analyzed using a linear time-frequency (TF) decomposition which permits to describe an urban area polarimetric behavior for different azimuth angles of observation and frequencies of illumination. A TF signal model, adapted to the case of urban areas is proposed and studied using two statistical descriptors related to the signal stationary aspect and coherence in the time-frequency domain. These indicators are shown to provide complementary information, adapted to the case of man made environments. A TF based classification is proposed and applied to fully polarimetric SAR data acquired by the ESAR sensor at L-band. Results demonstrate the efficiency of this method in terms of buildings location retrieval and response characterization. [C3326]

"3D Visualisation and Physical Feature Extraction of Urban Areas using Multibaseline POL-InSAR Data at L-Band"

This paper extends two single polarization multi-baseline interferometric SAR spectral analysis techniques to the fully polarimetric configuration. These new algorithms enhance the height estimation of scatterers by calculating optimal polarization combinations and allow to determine their physical characteristics. First experimental results show the retrieval of building height and their polarimetric properties by means of single-baseline polarimetric datasets. Dual-baseline observations permit the solution of the layover problem by separating two contributions within one resolution cell. The algorithms are tested using multibaseline Pol-InSAR data acquired by DLR's E-SAR system. [C3327]

"Blind Separation of Human Heartbeats and Breathing by the use of a Doppler Radar Remote Sensing"

The combined use of a Doppler radar with digital signal processing technique gives an effective non-invasive remote sensing of heart beat signals. Initial results have showed that the proposed technique is very promising in successfully isolating desired heart beat signals from other mobile objects and other distortion effects characterizing the wireless channel. We concentrate in this paper on the harder problem of separating at low SNR the signals from two subjects in the same room. We show that preliminary results obtained by the real analytical constant modulus algorithm (RACMA) and the independent component analysis (ICA) on experimental data are very promising into this goal. [C3328]

"Co-Boresighted Coherent Laser Velocimeter and Direct Detection Lidar for Dust Devil Characterization"

This paper describes recent work developing a mobile co-boresighted coherent laser velocimeter and direct detection Lidar for the characterization of dust devils. We also report on the field deployment of that system during the Summer of 2006. The Lidar consists of a large, scanning aperture direct detection elastic scattering Lidar operating at 355 nm, and a CW coherent heterodyne laser velocimeter operating at 1550 nm. The coherent system is not capable of ranging but provides azimuthal velocities in the dust devil. Spatial dimensions and azimuthal velocity are critical parameters for understanding the energetics of the dust devils. [C3329]

"Dual Polarized UHF/VHF Honeycomb Stacked-Patch Feed Array for a Large-Aperture Spaceborne Radar Antenna"

As penetration depth through vegetation and ground becomes more important in active remote sensing applications, there is a shift toward using lower frequencies. To facilitate imaging of ground water, soil moisture and composition, and penetrating through forest canopies, a dual-band synthetic aperture radar (SAR) has been proposed to operate at VHF and UHF frequencies. To accommodate weekly repeat observations from LEO, a swath of roughly 350 Km is needed, requiring a 30-m long antenna aperture from the SAR design point of view. The beams of the UHF and the VHF antennas must coincide in the cross-track direction, resulting in antenna widths of 3m and 11m, respectively. A stacked, linearly dual-polarized patch array feeding a 30 meter diameter parabolic reflector is proposed for this application, which synthesizes near-rectangular effective apertures on the reflector. Using a mesh reflector technology, the mass of such an antenna configuration is about ten times smaller than a corresponding phased-array antenna. A scaled-frequency version of the feed array was initially designed, built, and tested. It was also integrated with a scaled reflector antenna to verify the performance of the overall system. The actual frequency version was then designed, built, and tested. The design of the dual-band

stacked array and the power dividers will be discussed, the fabrication process explained, and the approaches used for optimizing the performance characteristics will be presented. The measurement results for return loss on both transmit and receive, isolation, and radiation pattern will be presented and shown to be in good agreement with the simulated results. [C3330]

"Future Mission Concept for 3-D Remote Sensing of Aerosols from Low Earth Orbit"

Aerosols are generated and transformed by myriad processes, affecting Earth's climate, hydrological cycle, air quality, and human health. In this paper, we describe the scientific rationale and mission architecture for a future aerosol mission concept, the Aerosol Global Interactions Satellite (AEGIS). Its payload is designed to eliminate ambiguities in aerosol microphysical retrievals and contribute to the next generation of atmospheric models. By combining several satellite-based approaches aimed at observing the 3D distribution of aerosol abundances, sizes, shapes, and absorption, AEGIS represents a major advance in our ability to monitor and characterize particulate matter from space, and comprises a logical next step beyond the Earth observing system, the "A-train," and Glory. [C3331]

"Technology Demonstration of Ka-band Digitally-Beam formed Radar for Ice Topography Mapping"

GLISTIN (Glacier and Land Ice Surface Topography Interferometer) is a spaceborne interferometric synthetic aperture radar for topographic mapping of ice sheets and glaciers. GLISTIN will collect ice topography measurements over a wide swath with sub-seasonal repeat intervals using a Ka-Band digitally-beamformed antenna. This paper will give an overview of the system design and key technology demonstrations including a 1m x 1m digitally-beamformed Ka-band waveguide slot antenna with integrated digital receivers. We will also detail the experimental scenario that we will use to demonstrate both the beamforming and interferometric performance of this system. [C3332]

"Concept for a High MEO InSAR Seismic Monitoring System"

Demonstration of a spaceborne system to image seismic surface waves dynamically (i.e. coseismically) would be the early steps of a future operational capability for monitoring earthquakes and discriminating clandestine underground nuclear tests. Complementing the global network of seismic instruments, such system would enable unprecedented global mapping of the velocity structure of the Earth's crust, thereby improving hypocentral location, understanding of rupture dynamics and wave propagation effects, and source characterization. Seismic wave measurement requirements include lower bounds on detectability of events and wave amplitude accuracy for different levels of analysis, such as source characterization and crustal tomography, with 10-100 μ m wave amplitude resolution for waves nominally traveling 5 km/s, an upper frequency bound based on earthquake surface displacement spectra, and minimum horizontal resolution (1-5 km) and areal coverage. Advanced radar technologies are keys to demonstrating a pre-operational system leading to a high MEO (10,400 km orbit altitude) constellation for continuous surveillance. [C3333]

"Soil Moisture Smart Sensor Web Concept Using Data Assimilation and Optimal Control"

We present a new concept for a smart sensor web technology for measurements of soil moisture that include spaceborne and in-situ assets. The objective of the technology is to enable a guided/adaptive sampling strategy for the in-situ sensor network to meet the measurement validation objectives of the spaceborne sensors with respect to resolution and accuracy. The sensor nodes are guided to perform as a macro-instrument measuring processes at the scale of the satellite footprint, hence meeting the requirements for the difficult problem of validation of satellite measurements. The science measurement considered is the surface-to-depth profiles of soil moisture estimated from satellite radars and radiometers, with calibration/validation using in-situ sensors. Satellites allow global mapping but with coarse footprints. The total variability in soil-moisture fields comes from variability in processes on various scales. Installing an in-situ network to sample the field for all ranges of variability is impractical. However, a sparser but smarter network can provide the validation estimates by operating in a guided fashion with guidance from its own sparse measurements. The feedback and control take place in the context of a data assimilation system. The design and demonstration of the smart sensor web including the control architecture, assimilation framework, and actuation hardware are the building blocks of this concept and will be introduced in the presentation. This technology, once developed, enables a guided/adaptive sampling strategy for generating optimal, statistically unbiased, calibration/validation data for space-based measurements. [C3334]

"Applications of MIMO Technique for Aerospace Remote Sensing"

Inspired by recent advances in multiple-input multiple-output (MIMO) radar, this paper introduces the MIMO synthetic aperture radar (SAR) concept. This concept differs substantially from current SARs in which closely

spaced antenna arrays are used. With closely spaced antenna elements, it is possible to coherent a beam toward a direction in space and to realize a coherent processing gain. However, these systems are prone to severe target fading, and hence they may suffer considerable performance degradation. The fundamental difference between MIMO SAR and other SAR is that the latter seek to maximize the coherent processing gain, while MIMO SAR capitalizes on the diversity of target scattering to improve radar performance. The superiority of MIMO SAR in many aspects over the conventional SAR, e.g., high resolution, good sensitivity, and counteracting target fluctuations is investigated. It is shown that, the use of MIMO SAR leads to solutions that previously thought to be out of reach for remote sensing scientists and customers. [C3335]

"An Integral Detection Scheme for Moving Object Indication in Dual-Channel High Resolution Spaceborne SAR Data"

Upcoming SAR satellite missions like TerraSAR-X or RADARSAT-2 will deliver high resolution dual channel SAR data with large coverage. These new missions-together with rising interest in area-wide traffic monitoring-motivate spaceborne GMTI as an attractive alternative to conventional traffic data acquisition. However, a moving object appears distorted in the SAR image since the well-known stationary world assumption in the SAR focusing process is violated. In this paper, a detection approach is presented, which considers simultaneously the effects of azimuthal and radial motion of an object. The mathematical framework of this detector combines information of the measured signal, the expected signal, and their variances. Furthermore, the performance of the proposed algorithm is analysed using experimental airborne SAR data. [C3336]

"3D Urban Models from Laser Radar Data"

Updated geographic information and 3D models of environments are becoming increasingly important for applications such as city planning, crisis management, visualisation, architecture, and landscaping. The task of producing detailed geospecific terrain databases or 3D city models has traditionally been manual and thus time-consuming, and the availability of appropriate source data has been limited. The use of available sensors such as airborne laser scanners (ALS) and digital cameras provides new opportunities to acquire detailed remote sensing data of the natural environment. This type of data is very suitable as the basis for the construction of high-fidelity 3D virtual environment models. To make use of this new type of data and to develop applications as mentioned above requires new methods for processing 3D sensor data and extracting geographic feature information from the data. In this paper we present recent results from the development of methods for processing ALS data and for transforming the data into geographic information and environment models, with the emphasis on urban environments. The long term objective of our work is the development of new methods for rapid and highly automated extraction of geographic information to support the construction of high-fidelity 3D virtual environment models from remote sensing data. As remote sensing data we use data from current high resolution ALS systems and digital cameras. [C3337]

"Urban Land Cover in Rome, Italy, monitored by single-parameter multi-temporal SAR images"

This paper reports on monitoring land cover in the urban and sub-urban area of Rome, Italy, by multi-temporal ERS 1-2 SLC SAR images. The identification of the SAR image parameters, including backscattering, degree of interferometric coherence and textural pixel-based features to be exploited in classification, is discussed. The information extracted from the SAR images is fused and processed by a Multi-Layer Perceptron (MLP) neural network (NN) to produce land cover maps. The network topology has been carefully designed, paying special attention to the number of hidden units. Once trained, the net's performance has been validated over a statistically significant ensemble of patterns independent of the learning set. The net has been used for the automatic classification of a large area in two different years, 1994 and 1999, thus obtaining a map of hot spots corresponding to areas where changes had occurred. [C3338]

"Perceptual Grouping for Building Recognition in High-resolution SAR Images using the GESTALT-System"

GESTALT is a production system interpreter designed for advanced automatic recognition from difficult pictorial data. Building recognition from leading edge high resolution SAR-data is a good example for such a challenge. This contribution explains the system itself and its application to this particular issue. Perceptual grouping paradigms are coded in the productions in order to discriminate man-made ordered structure from arbitrary clutter. In particular symmetry and repetitive similar structure render promising prospects for this application. [C3339]

"Applications of Multi-source Remote Sensing Information to Urban Environment Monitoring in Mining Industrial Cities"

Remote Sensing (RS) has been viewed as the one of the most effective tools for environment monitoring, urban resources and environment investigation, change detection and urban growth analysis in mining industrial cities. Firstly, the framework and structure of applying multi-source RS information to environment monitoring of mining industrial cities is proposed based on the general methodologies of RS applications and the characteristics of mining industrial cities. RS can be used to monitor land use/cover change, extract subsidence land because of underground mining, analyze the dynamic change and simulate the trends of mining industrial city growth, monitor the extension of mining contamination, analyze the impacts of mining to farmland and ground buildings, assess the feasibility and performance of land reclamation and ecological reconstruction, and so on. Land subsidence is a very serious environmental damage caused by mining, and that leads to more negative impacts to ecological system, even leads to geological disaster. Three methods to extract subsidence land from RS image: thematic information based on decision tree, object-oriented subsidence land extraction and target identification based on RS information, geographical data and domain knowledge are experimented. Multi-source and multi-temporal RS information fusion is used for environmental analysis in mining areas. By the fusion of Landsat TM and SAR image, both high spatial resolution and multi-spectral information can be integrated so high classification and target extraction accuracy can be got. IHS fusion algorithm is improved by considering the image content and adaptive IHS fusion is experimented. Multi-temporal RS information fusion is used for change detecting and dynamic monitoring. By the case study in Xuzhou city, it proves that remote sensing can play important roles in environmental analysis and assessment in mining industrial cities and serve as the efficient decision-making support tool for regional sustainable development. [C3340]

"Raster to Vector in 2D Urban Data"

The aim of this work is to propose a refined approach to urban object recognition and extraction exploiting a priori information about geometrical features of the urban objects. In particular, the proposed procedure shows that it is possible to improve the characterization of elements of the urban scene by assuming that they fit to some geometrical models. Advantages includes the possibility to manage urban object as vector files, to compare object presence and shapes in multi-temporal remotely sensed data sets, and finally to compare and fuse remotely sensed data with Geographic Information vector layers. [C3341]

"Detection and classification of urban structures based on high-resolution SAR imagery"

In this paper, several advanced methods for detecting and classifying urban structures in high-resolution SAR imagery are presented. The detection of man-made structures resp. the suppression of clutter, for example natural surfaces, can be accomplished by a coherent time-frequency analysis. These techniques can detect targets in the scene that behave like point-scatterers (such as edges, poles, etc.) by their high degree of correlation across sub-apertures of the scene. If polarimetric data are available, this approach can be extended by taking into account the frequently anisotropic polarimetric backscattering of man-made targets. As a third approach, a simple but powerful operator for detecting urban structures by analysing texture inhomogeneity in SAR images is developed. A second objective of this paper is the segmentation and classification of the detected urban structures. Based on the detected man-made structures, the characteristic structure size is investigated, using several approaches, to distinguishing between residential areas, industrial areas and dense city centres. The methods are evaluated using several real airborne SAR datasets. [C3342]

"Model Based Building Recognition from Multi-Aspect InSAR Data in Urban Areas"

The achievable ground resolution of state-of-the-art synthetic aperture radar (SAR) sensors enables the analysis of urban areas with industrial as well as residential character. In this paper, an approach is proposed to detect and reconstruct small as well as extended buildings from multi-aspect high resolution InSAR data sets. The recognition of buildings is supported by knowledge based analysis considering SAR-specific effects such as layover, radar shadow and multipath signal propagation. But especially in dense built up areas those effects can also lead to a reduction of the reconstruction quality e.g. in the case of adjacent trees or other buildings. In those cases the results can be significantly improved by a combined analysis of multi-aspect data. The presented approach exploits amplitude, phase, coherence data and classification results. That is demonstrated in an urban environment for an InSAR data set, which has a spatial resolution of about 30 cm and was taken from two orthogonal flight directions. [C3343]

"Using LIDAR Surface Deformation Mapping to Constrain Earthquake Magnitudes on the Seattle Fault in Washington State, USA"

Airborne laser swath mapping (ALSM) conducted by the Puget Sound LIDAR Consortium reveals uplift, folding, and faulting associated with earthquakes on the Seattle fault zone (SFZ) in Washington State, USA. The SFZ is a 5-to 7-km-wide, east-west trending zone of south-dipping thrust faults, north-dipping backthrust faults, and

folds that runs through the Seattle urban area. Marine terraces along the shoreline of the Puget Sound, visible in ALSM images, record uplift of a wave-cut platform about A.D. 900 during a large earthquake on the SFZ. Bald Earth digital elevation models (DEMs) with a 1.8-meter grid spacing document spatial patterns of terrace uplift, as measured from the elevation of shoreline angles at the landward edge of the uplifted platform. Shoreline angles were identified using profiles and slope images interactively generated from the DEMs. The bald Earth DEMs were produced by applying a virtual deforestation, despiking filtering algorithm to point clouds of laser data acquired by the TerraPoint ALTM instrument, a small-footprint, discrete-return system that records up to four returns per laser pulse. A data density of ~1 pulse per square meter was acquired using 50% sidelap between adjacent swaths. The elevations of the uplifted terraces provide a clear picture of earthquake deformation. On the east side of Puget Sound, marine terraces define a 5-km-wide, north-vergent geologic anticline with planar limbs. The fold amplitude is 6 meters, and the limbs dip more steeply north (0.25deg) than south (0.10deg). The fold hinge is located above the frontal thrust fault of the SFZ. Near Bainbridge Island, the anticline hinge is locally modified by backthrust faults producing a tightened, south-vergent fold with amplitude as large as 8 m. Terrace deformation patterns suggest that slip on the frontal thrust during the A.D. 900 earthquake produced the anticlinal folding and that lesser slip occurred at that time, or more recently, on structurally higher thrust faults and backthrust faults within the SFZ. Inverse modeling of slip on the Seattle fault, constrained by elevations of the uplifted marine terraces mapped in the ALSM images, provides a well-constrained estimate of the magnitude of the A.D. 900 Seattle fault earthquake. For each of several different Seattle fault subsurface geometry interpretations, we use a linear inversion algorithm to solve for distributed slip on the fault surfaces. We calculate moment magnitudes of 7.2 to 7.4 directly from the different slip solutions. This study represents the first known use of LIDAR-based coseismic deformation mapping in solving for earthquake source parameters. [C3344]

"RADARSAT Fine-Beam SAR Data for Land-Cover Mapping and Change Detection in the Rural-Urban Fringe of the Greater Toronto Area"

This research investigates the capability of the multitemporal RADARSAT Fine-Beam C-HH SAR imagery for land use/land-cover mapping and change detection in the rural-urban fringe of the Greater Toronto Area (GTA). Five-date RADARSAT fine-beam SAR images were acquired during May to August in 2002. One scene of Landsat TM imagery was acquired in 1988 for change detection. The major land use/land-cover classes were high-density built-up areas, low-density built-up areas, roads, forests, parks, golf courses, water and three types of agricultural lands. These ten classes were chosen to characterize the complex land use/land-cover types in the rural-urban fringe of the GTA. The results demonstrated that, for identifying land use/land-cover classes, five-date raw SAR imagery yielded very poor result due to speckles. Much better results were achieved with combined Mean, Standard Deviation and Correlation texture images using artificial neural networks (ANN) and with raw images using object-based classification. The change detection procedure was able to identify the areas of significant changes, for example, major new roads, new low-density and high-density built up areas and golf courses, even though the overall accuracy of the change detection was rather low. [C3345]

"Monitoring of Flooding in Urban Areas"

Urban areas are crowded environments, where a disaster can bring dramatic consequences, if not adequately forecasted and faced. Remote sensing instruments can be fruitfully used for both prediction and aid organization purposes. In particular, in this paper we present innovative synthetic aperture radar (SAR) techniques for the detection of a flooded area in urban settlements. A SAR raw signal simulator is presented and used, in order to improve the comprehension of the main physical phenomena and to plan the most adequate sensor characteristics for detection purposes. The single and multiple scattering phenomena, in conjunction with strong layover effects make the SAR images relative to urban areas extremely involved. The presented study is focused on a canonical environment, in order to provide a complete and powerful instrument for the comprehension of the complex texture of urban area SAR images. [C3346]

"Measurements of the Radius of Atmosphere Surface Layer Pollution near the Plant With Microwave"

Microwave technique and device for the measurements of the radius of atmosphere surface layer pollution near the plant with phase radar methods are presented. Uncertainty elimination of the phase measurements is discussed and one is achieved by frequency changing upon certain rule. That gives increasing of measurement accuracy. [C3347]

"Reconstruction of the 3D Stereo Buildings from Polarimetric SAR Images in Two Converse Flights"

The height and location of the three dimensional (3D) objects can be retrieved from polarimetric SAR images in

multidirectional flights, and the 3D stereo objects can then be reconstructed. Polarimetric SAR image describes the objects via polarization synthesis, and presents much richer information than mono-polarized SAR image. Furthermore, multi-aspect flights of polarimetric SAR can see the 3D stereo objects in different angles and become feasible to invert the height and location of the objects. This paper presents an attractive approach for reconstruction of the 3D stereo buildings from two converse flights of airborne PI-SAR images (at X band with spatial resolution 1.5 m). [C3348]

"New Methods for Understanding Intra-urban Contours at a Global Scale: An Application of Dense Sampling Methods of QuikSCAT Scatterometer with Population and Housing Data"

A global and consistent characterization of land use and land change in urban and suburban environments are crucial for many fundamental social and economic science studies and applications. Here, we present for the first time a dense sampling method (DSM) that uses satellite scatterometer data at a coarse resolution (~12 km) to delineate urban and intra-urban areas at a much higher resolution (~1 km). The trade-off is that the daily or near daily temporal resolution is reduced to yearly or multi-year time scale, which is still appropriate to map urban areas and to identify interannual changes in most cases. The DSM results will be analyzed together with information on population and housing censuses, with Spectral Mixture Analysis (SMA) of moderate and high spatial resolution optical satellite imagery, and with both DMSP night lights. [C3349]

"Use of high resolution optical and radar imagery for intelligence and situational awareness in urban areas"

We have used high resolution optical satellite stereo data to generate a digital surface model containing building heights, so that 3-dimensional information is available for the purpose of urban situational awareness. In addition we have applied change detection techniques to Radarsat fine beam imagery with a resolution of 10 meters to find infrastructural changes and to assess damages in order to obtain up-to-date infrastructural information. We show that the changes obtained from the radar data can be characterized using other data, such as high resolution optical imagery, maps, and data from GIS. Furthermore we show how these results can be combined with a digital surface model to produce an actual description of the urban area needed for urban situational awareness. [C3350]

"Advances in Lidar Transmitter Sources for Ocean-Atmosphere Remote Sensing"

Pulsed, tunable alexandrite lasers in combination with harmonic generators and Raman wavelength shifter form a powerful and versatile tool for lidar (light detection and ranging) remote sensing. Such an integrated laser system can generate any wavelength from ultraviolet to infrared with the necessary beam qualities required for lidar measurement. This paper presents the development of injection seeded alexandrite ring lasers and linear cavity alexandrite lasers that can be deployed in ocean-atmosphere lidar remote sensing. [C3351]

"Measurements of the Effect of Rain-induced Sea Surface Roughness on the Satellite Scatterometer Radar Cross Section"

Radar measurements of the sea surface, with satellite scatterometers that operate at Ku-band, will be affected by the presence of rain through modification of the sea surface roughness by rain impacts. This is in addition to wind driven roughness, atmospheric reflectivity and attenuation that affect the measured normalized radar cross section (NRCS). Numerous surface-based studies, using ocean platforms and wind-wave tanks, have shown the increase in the total NRCS can be significant and strongly dependent on radar frequency, incidence angle, polarization and wind speed [1], [2], [3]. Herein is the first study combining satellite based Ku-band data with high-resolution 3-D volumetric rain measurements, from simultaneous collocated NEXRAD data. The results to be presented were acquired during a significant rain event in the Gulf of Mexico just south of Houston, TX in May 2005. They are directly applicable to questions that are important to the interpretation of satellite derived wind vector estimates in the presence of rain of varying intensity and spatial distribution. This project is developing techniques to correct scatterometer derived wind-vector estimates. The acquisition of new knowledge on rain-splash effects is a necessary part of this effort. [C3352]

"New Application of Wavelet Transform for Internal Wave Detection SAR and Optical Image: A Case Study in Japan Waters"

We observed the internal wave features in ERS1/2 SAR and ASTER images data over Japan waters, during 1993-2004 period. The internal wave features were shown in the Tsushima Strait, coast of Izu Peninsula, coast of Ibaraki in east of Honshu, coast of Sado Island in west of Honshu, and southwest and south of Hokkaido. The internal wave feature characteristics in image suggest tidal generation source. At these places, packets of non-

linear internal waves were formed over shelf break areas such as ridge and sill. Various wavelet transform, e.g. Haar, Daubechies, Symlet, Coif, Biorthogonal, and Meyer wavelet, are tested comparably to study the internal wave detection in image using multi resolution analysis. Though all of wavelet families can be used for internal wave packet detection, the decomposed feature tends to follow the wavelet function, which compress the first wave crest. To solve this problem, we propose new wavelet function constructed from Damped Oscillation Function. So far this method show good result. Finally, we show the application of KdV model to calculate the nonlinear speed of the internal wave, which can be use to predict the generation of strong current when internal waves occur. [C3353]

"Remote Sensing of the Sea and Target Detection Improvement Using a Wavelet-based Extraction of Sea Echoes from High Frequency Radars"

High frequency radars (HFR) use HF waves (3 MHz to 30 MHz). They interact with the sea surface and are well-suited radars to perform remote sensing of the sea. Moreover, HFR coverage range is not limited by the radio horizon: it is possible to keep watch over the sea up to few hundred kilometers from the coast line (surface wave mode) or up to few thousands kilometers (space wave mode). Oceanographic parameters (i.e. wave height, surface current velocity, wind direction and wind velocity) are derived from the so-called sea spectrum. Moreover, HFR can be used for maritime surveillance of the Exclusive Economic Zone (EEZ). In that case, the sea spectrum is an unwanted signal because it can mask targets. So, sea spectrum extraction is an important topic of HFR signal processing since it is a key point for remote sensing accuracy and target detection features. Wavelet-based processing allows an efficient extraction. [C3354]

"Distributed and Layered Sensing: Relevant EMC Issues"

One can easily envision future military operations and emerging civilian requirements (e.g. intelligent unmanned vehicles for urban warfare, intelligent manufacturing plants) that will be both complex and stressing and will demand innovative sensors and sensor configurations. The goal of our research into distributed and layered sensing is to develop a cost effective and extendable approach for providing surveillance for a variety of applications in dynamically changing military and civilian environments. Within distributed and layered sensing, we foresee a new sensor archetype. In this paradigm, sensors and algorithms will be autonomously altered depending on the environment. Radars will use the same returns to perform detection and discrimination, to adjust the platform flight path and change mission priorities. The sensors will dynamically and automatically change waveform parameters to accomplish these goals. Disparate sensors will communicate and share data and instructions in real-time. Intelligent sensor systems will operate within and between sensor platforms such that the integration of multiple sensor data provides information needed to achieve dynamic goals and avoid electromagnetic fratricide. Intelligent sensor platforms working in partnership will increase information flow, minimize ambiguities, and dynamically change multiple sensors' operations based upon a changing environment. Concomitant with the current emphasis on more flexible defense structures, distributed and layered sensing will allow the appropriate incremental application of remote sensing assets by matching resources to the situation at hand. [C3355]

"Comparisons between HF radar and SAR current measurements in the Iroise Sea"

In coastal oceanography, currents are difficult to measure with a good temporal and spatial resolution. Nevertheless, precise knowledge of these currents is crucial for certain applications such as pollution monitoring. Up until now, very few instruments have been able to provide current measurements. Although techniques based on HF radar and satellite-based Synthetic Aperture Radar(SAR) are promising, comparisons between these two approaches must be carefully formulated since the approaches differ in terms of scattering geometry, radiation frequency, and antenna footprint. In this document, we present a brief review of these two approaches as well as a comparison between them using data acquired over the Iroise Sea in France. Since the dominant source of currents in this area is tidal in nature, we also compare the results to the currents predicted by the tidal model MARS2D. The results are encouraging: the SAR-derived currents (specifically, the component of the current in the radial direction along the SAR beam) are qualitatively similar to the equivalent projected radial components deduced from HF measurements and MARS2D output. It must be noted, however, that the HF radar results may be compromised by the presence of island, and the SAR results may be compromised owing to the sensitivity to wind waves. [C3356]

"Features and Limitations of the Modular Oceanography Radar System WERA"

The WERA system (wave radar) is a shore based remote sensing system to monitor ocean surface currents, waves and wind direction. This long range, high resolution monitoring system based on short radio wave radar technology. The vertical polarised electromagnetic wave is coupled to the conductive ocean surface and follows

the curvature of the earth. This over the horizon oceanography radar can pick up back-scattered signals from the rough ocean surface (Bragg effect) from ranges of up to 200 km. The physical background, technical concept and environmental boundary conditions are explained. Results for various installations from all over the world demonstrates the features and flexibility of the system: high resolution monitoring (range cell size of 300 m) over a range of 60 km or long range applications with 3 km range cell size, all generated with the typical high temporal resolution of 10 minutes. The technical performance depends on the site geometry, system configuration and the environmental conditions. These aspects will be discussed to enable interested users to estimate the potential of this technology for their specific application. [C3357]

"A Nested Multi-static HF Radar Testbed for the New York Bight and Beyond"

Surface currents are envisioned to be an integral component of the Integrated Ocean Observing System (IOOS) and High Frequency (HF) radar technologies provide the means to measure these data across multiple scales. The Rutgers University Coastal Ocean Observation Lab (COOL) has continuously operated a nested network of HF radars since 1998 as part of a sustained coastal observatory centered on the New York Bight. Components of this network include 25 MHz, 13MHz, and 5 MHz Tx /Rx shore stations and offshore buoy mounted Tx stations. These components are linked through GPS synchronization technology to provide fully nested multi-static surface current coverage. Data from these systems are supporting a growing number testbed activities and large science campaigns. Testbed activities focus on extending the present surface current mapping coverage closer to the beach with the development of new nearshore wave and current applications. Additional software and hardware modifications are beginning to extend the environmental monitoring to full maritime domain awareness by transitioning the sites to a dual-use mode that include hard target detection and tracking. The HF radar data has most recently supports two science campaigns, the Shallow Water 2006 (SW06) Joint Experiment supported by the Office of Naval Research and the Mid-shelf Front Experiment supported by the National Science Foundation (NSF). Both campaigns have used the HF radar as a resource for adaptive sampling. During the SW06 experiment, HF radar data was incorporated into daily reports along with other observation and forecast data to support the science fleet offshore. In addition to the adaptive sampling application, the mid-shelf front experiment takes advantage of the 5.5 year dataset within the study site. Long term means show a significant cross-shelf transport pathway south of the Hudson Shelf Valley that could possibly feed the mid-shelf front. These Rutgers systems fit into a larger effort across the entire Mid-Atlantic Bight (MAB) region from Cape Hatteras, NC to Cape Code, MA. HF radar groups across this region have now formed a consortium for the operation and maintenance of the entire network, including system hardware, data management, and product delivery. Through this consortium the existing pockets of systems, of which Rutgers is one, can be operated as one regional system that spans over 1000 km of coastline. This network consists of 11 long-range sites providing total vector coverage across a large portion of the region from Cape Hatteras NC to the apex of the New York Bight. Additional funded sites for Moriches, NY and Block Island, RI, will extend the coverage north to Cape Cod, MA and Nantucket MA. In addition there are four higher resolution sub-systems made up of 15 sites in operation in the Chesapeake Bay, New York Harbor, the Long Island Sound and the Delaware Bay estuaries. In addition to scientific research and education applications, the United States Coast Guard Research and Development Center has identified the Mid-Atlantic Bight as a testbed for the new search and rescue planning tool, SAROPS. [C3358]

"MARCOAST-Operational Marine Oil Spill and Water Quality Monitoring Services"

The MARCOAST partnership, supported by the European Space Agency (ESA) under the global monitoring for environment and security (GMES) service element programme is providing operational oil spill and water quality monitoring services, using products derived from satellite remote sensing data combined with models and in-situ measurements. This paper provides a brief overview of the ESA GMES service element programme, describes the services being offered by the MARCOAST partnership, and discusses how the MARCOAST project is meeting the key challenge of making the transition from research to operational application of satellite remote sensing data. The aim of this paper is twofold: To raise awareness of the purpose, aims and future plans of the ESA/EC GMES programme, in terms of the development and provision of marine services, and to provide a technical overview of the operational services offered by MARCOAST, so that Oceans '07 participants can take a view on their potential utility with regard to their own operational needs. [C3359]

"Mapping Ocean Currents With IKONOS"

The velocity of sea surface gravity waves depends on the wave wavenumber, k , and the surface current, U . The surface current can thus be inferred from the displacement of waves in a sequence of ocean surface images. This has been demonstrated using both marine radars and aerial video to image the ocean waves. In this paper we describe the implementation with IKONOS satellite images. We discuss special considerations for obtaining and processing satellite images: the need for precise co-registration of the images; the optimum sun angle for

imaging ocean waves; the optimum oceanographic conditions; and the use of multi-spectral bands to edit non wave surface features (e.g., whitecaps). In the test case a current velocity map was produced at 200 m grid spacing. The rms error in the velocity estimates is 10 cm/s. [C3360]

"Method of Compound Object Identification in Microwave Band by Scattered Field Interference Pattern"

There is proposed and investigated the method of compound object identification by scattered field amplitude and phase parameters in the made of coherent-pulse probing signal spectral scanning. [C3361]

"Coastal applications of X-band radar to achieve spatial and temporal surface wave monitoring"

In this paper wave data from two different coastal stations will be discussed with respect to spatial inhomogeneities in the wave field. Effects of the changes in the local topography and strong tidal currents are reproduced in the radar data. The discussion will focus on the potentials of these data to monitor spatial and temporal variabilities of the sea state in coastal approaches. As an example, dissipation, refraction, and reflection of waves will be analysed. [C3362]

"Radio Frequency Interference Suppression Techniques in FMCW Modulated HF Radars"

High-frequency (HF) radars are operated in the 3-30 MHz frequency range and need to share the frequency bands with other radio services. Due to their over-the-horizon (OTH) capabilities, HF radars play an important role in remote sensing and surveillance. The propagation conditions of the electromagnetic wave depend on the earth's ionosphere and mainly follow a daily cycle. Communication paths between the HF radar and other radio services, some thousands of kilometres off, open and close with a high variability. Special care must be taken to dynamically adapt the HF radar's characteristics to the varying electromagnetic environment. The impact of a frequency modulated continuous wave (FMCW) HF radar on other radio services is not very strong, because of its low transmit power and utilisation of the radio spectrum. However, strong signals from other radio services can significantly reduce the performance of the oceanographic measurements. Several radar control and signal processing steps are discussed in this paper. All together form an effective procedure to reduce the impact of Radio Frequency Interference (RFI) on the oceanographic measurements. [C3363]

"HF Radar Observation of Wave Directional Spectra in a Strong Current Regime"

Dual Wellen HF Radar (WERA) systems have been observing near-surface currents and wave parameters over the Southeast Florida shelf since June 2004 as a part of the Southeast Atlantic Coastal Ocean Observing System (SEACOOS). The region of coverage includes the Florida Straits and the Florida Current (FC) which typically has maximum surface velocities approaching 2 ms^{-1} . The echo-Doppler spectra are also routinely recorded and archived at both stations which allows post-processing to extract surface wave directional spectra using an iterative approach as implemented in Seaview Sensing reg software. Both WERA sites operated continuously during the passage of Hurricane Jeanne over the Florida Straits on 25 Sept 2004. Although it passed ~200 km to the north of the measurement domain, the local mean winds exceeded 20 ms^{-1} and rotated over 270° . The near-surface currents during the passage of Hurricane Jeanne reflected the influence of the wind as well as the Florida Current. The effect of the wind on the near surface flow was seen in easterly and southerly flow over the shallow shelves near Florida and the Bahamas respectively as well as relatively slow flow in the center of the Florida current. Maximum current velocities were only 130 cms^{-1} - 150 cms^{-1} less than typical values. The interaction of these wave fields from differing directions with the high lateral shear of the western edge of the Florida Current was observed every 10 minutes.. The wind-wave component of the spectrum was observed to respond rapidly to the rotating wind-field, but effects of the horizontal shear were observed in the off-wind angle of the wind-wave peak. Tower frequencies were often observed at large angles to the local wind. [C3364]

"Tsunami Monitoring by HF Ocean Radar: Time and Space Scales"

HF coastal ocean radars are ideal instruments for detection of surface currents in coastal waters and have had wide application for monitoring tidal and wind driven surface currents. This paper addresses the questions of spatial and temporal scales for optimal detection of tsunami properties by HF radar at the shelf break and on the continental shelf itself. Two approaches are used in this evaluation. One is a stylized tsunami wave approaching a shelf which has parallel bathymetry contours and a shelf with uniform depth. In this case the non-linear effects at the edge of the shelf are the same at all points along the shelf edge, and the subsequent wave train emerging onto the shelf has parallel wave fronts. The second approach is a case study of a real section of shelf-edge and shelf bathymetry. In this case numerical modelling indicates that there is a complex pattern of surface currents at the shelf break which varies in space and time. The subsequent wave train has a complex wave front which can

be considered to be generated from point sources along the shelf edge. These wave fronts are shaped by local shelf bathymetry as well as interference of waves from the originating source points at the shelf edge. In the case of real bathymetry there are complexities in the surface current field which will produce different outcomes for direction-finding and phased array types of HF radar facilities. Because of its ability to resolve spatially complex current patterns, the phased array system is preferred for tsunami observation networks. [C3365]

"Mining Induced Subsidence Monitoring in Urban Areas with a Ground-Based SAR"

Since June 2006 the Remote Sensing Laboratory (RSLab) of the Technical University of Catalonia is carrying on a subsidence monitoring activity in Salient, a village in the central Catalonia. The project, in collaboration with the Cartographic Institute of Catalonia (ICC), aims at studying the deformation phenomenon induced by salt mining extraction of the past years using a ground-based SAR sensor. Polarimetric data are being monthly acquired at X-Band in a perfect zero-baseline configuration. A detailed description of the on-going measuring campaign is here given. The advantages and drawbacks of using a terrestrial sensor are also stressed. Finally, first results carried out using a coherence approach are shown. [C3366]

"Application of the Coherent Pixels Technique (CPT) to urban monitoring"

During the past years, Remote Sensing has become a powerful tool for earth observation. In particular, SAR differential interferometry (DInSAR) has shown to be a very reliable technique for deformation phenomena monitoring, being able to achieve millimetric accuracies. It is the aim of this paper to present and show the potentials of the UPC's advanced DInSAR algorithm, the coherent pixels technique (CPT). Deformation results of different studied areas will be presented, revealing the performances of DInSAR for risk management as well as for the understanding of much geological processes. [C3367]

"Multipass SAR Processing for Urbanized Areas Imaging and Deformation Monitoring at Small and Large Scales"

A new processing chain that allows monitoring ground deformations, both at small scales and large scales, is discussed. Core of the chain is the spatial differencing (SD) algorithm that allows very quick estimation of the small scale (low resolution) mean deformations velocity and residual topography by means of the use of spatial differences between adjacent and non-adjacent pixels. Small scale deformation time series is then generated by using the Enhanced spatial differences (ESD) that permits separating atmospheric phase contribution, linear and non-linear deformation velocity and residual topography. Deformations and target localization at large scales (full resolution) is provided by the application of a multi-dimensional (4D) imaging (differential-tomography) that exploits the complex nature of the received signal to focus the data in the space-time domain. [C3368]

"Extraction of Bridge Features from high-resolution InSAR Data and optical Images"

Modern airborne SAR sensor systems provide geometric resolution in the order well below half a meter. By SAR interferometry from pairs of such images DEM of the same grid size can be obtained. In data of this kind many features of urban objects become visible, which were beyond the scope of radar remote sensing only a few years ago. However, because of the side-looking SAR sensor principle, layover and occlusion issues inevitably arise in undulated terrain or urban areas. Therefore, SAR data are difficult to interpret even for senior human interpreters. Furthermore, the quality of the InSAR DEM may vary significantly depending on the local topography. In order to support interpretation SAR data are often analyzed using additional complementary information provided by maps or other remote sensing imagery. In this paper a fusion of high-resolution InSAR data and one aerial image is discussed for the example of a scene containing bridges that are core elements of infrastructure. The aims are improvement of the 3D visualization of the scene and the extraction of the main parameters of the bridges' geometry. [C3369]

"Distributed and Layered Sensing"

One can easily envision future military operations and emerging civilian requirements (e.g. intelligent unmanned vehicles for urban warfare, intelligent manufacturing plants) that will be both complex and stressing and will demand innovative sensors and sensor configurations. The goal of our research into distributed and layered sensing is to develop a cost effective and extendable approach for providing surveillance for a variety of applications in dynamically changing military and civilian environments. Within distributed and layered sensing, we foresee a new sensor archetype. In this paradigm, sensors and algorithms will be autonomously altered depending on the environment. Radars will use the same returns to perform detection and discrimination, to adjust the platform flight path and change mission priorities. The sensors will dynamically and automatically change waveform parameters to accomplish these goals. Disparate sensors will communicate and share data

and instructions in real-time. Intelligent sensor systems will operate within and between sensor platforms such that the integration of multiple sensor data provides information needed to achieve dynamic goals and avoid electromagnetic fratricide. Intelligent sensor platforms working in partnership will increase information flow, minimize ambiguities, and dynamically change multiple sensors' operations based upon a changing environment. Concomitant with the current emphasis on more flexible defense structures, distributed and layered sensing will allow the appropriate incremental application of remote sensing assets by matching resources to the situation at hand. In this paper, we discuss the electromagnetic compatibility (EMC) issues that must be addressed and understood as part of the development of a futuristic intelligence, surveillance and reconnaissance concept utilizing distributed and layered sensing waveform diverse systems. These systems involve the innovative integration of cutting edge technologies such as: knowledge-based signal processing, robotics, wireless networking waveform diversity, the semantic web, advanced computer architectures and supporting software languages. This concept is projected as an autonomous constellation of air, space, and ground vehicles that would offer a robust paradigm to build toward future deployments. The goal is to develop waveform-time-space adaptive processing for distributed apertures that could reduce EMC issues. [C3370]

"Agenda-at-a-glance"

{no data available} [C3371]

"Long-Term and Seasonal Subidence Rates in Urban Areas from Persistent Scatterer Interferometry"

As it is well known, space-borne radar interferometry (InSAR) is an appealing and powerful technique to measure the earth's topography and surface deformation with high accuracy and high spatial coverage and sampling. Even though the potential of InSAR was extensively proven within the last years and has been widely recognized throughout the scientific community, its value and applicability to geodynamic monitoring problems is severely limited by the influence of temporal decorrelation and electromagnetic path delay variations. The invention of the multi-image Persistent Scatterer (PS) technique in the late 1990's was a big step forward towards a high accuracy observation of slow surface motion and object deformation over long temporal time spans as it enables the identification, isolation, and estimation of millimeter surface deformation processes from space. This approach proves to be particularly suitable for the observation of the deformation regimes of cities from wide (deformation of extended areas) to small scales (deformation of isolated buildings). In this paper the functionality and the basic workflow of the original PS technique is described. Starting from this overview, every processing step is explained in detail and recent advances are mentioned. Based on this the performance of Persistent Scatterer Interferometry to measure linear as well as nonlinear surface deformation with high accuracy and high spatial sampling is exemplified by a case study from the city of Munich. A summary and an outlook concludes the paper. [C3372]

"Phase Offset Estimation for DEM Reconstruction in Multi-Channel SAR Interferometry"

Multi-channel Interferometric SAR (InSAR) systems allow the estimation of the height profile of the Earth surface, exploiting the availability of multiple radar acquisitions, obtained via different baselines/frequencies. Maximum A Posteriori (MAP) statistical technique, and Markov random field image models, have shown to be effective for such estimation problem. However, real interferograms are affected from the presence of undetermined phase offsets, which makes impossible to get correct height estimation. In this paper we present a procedure to estimate phase offsets. The procedure is tested on simulated data, showing the effectiveness of the method. [C3373]

"Statistical Polygonal Snakes for 3D building reconstruction using High Resolution SAR data"

In this paper, the polygonal active contour method is adapted to the case of synthetic aperture radar (SAR) images of urban areas. The statistical criterion is modified to be able to deal with multiple images in order to improve the segmentation of buildings. A criterion is proposed and is then implemented and tested over real high resolution SAR images containing urban areas. A discussion about the benefits of this approach is done and further work about 3D statistical active contour is introduced. [C3374]

"Satellite SAR and Human Settlement Detection"

Due to the peculiar features of human settlement areas, with enormous variance of objects and the resulting variability and possibly also ambiguity of data, such areas represent the most demanding cases for information extraction from SAR data. This research is particularly aimed at human settlement mapping at a regional scale. Indeed, informal settlement monitoring is an important topic for the many national and international initiatives including GMES and the humanitarian and development aid policies of major countries. Also, monitoring

settlements is related to phenomena like illegal immigration that are very high on the list of policy makers; finally, SAR is still underestimated as a reliable source of data. From a technical point of view, this work is based on the integration of spatial information extracted from SAR data to reach a suitable mapping accuracy for urban areas. In particular, the use of co-occurrence textural features has been considered, and the role of the spatial scales in the images for determining different environment investigated. In particular, the procedure will be discussed for the Chinese region of Wuhan using ENVISAT SAR data. [C3375]

"Detection/Imaging of Buried Objects: Using Spatial/Angular Diversity with Distributed/Embedded Sub-Surface Sensors for Reduced Mutual Coupling and Suppressed EM Emissions"

The proliferation of strategic subsurface sanctuaries has increased the need for enhanced remote sensing techniques providing for the accurate detection and identification of deeply buried objects. A new RF Tomographic Technique is proposed in this concept paper for developing RF CAT Scans of buried objects using spectral, spatial/angular, and polarization diversity. This imaging technique uses an embedded ring of subsurface radiators, delivered by earth-penetrating, non-explosive, electronic "e-bombs", as the source of strong underground radiated transmissions and uses distributed surface-contact sensors to collect the tomographic data for relay to a circling UAV and transmission to a remote control site (using layered sensing). Three-dimensional imaging algorithms are being developed to detect, image, and characterize deeply buried targets. Distributed transmitters and receivers significantly increase unwanted mutual coupling and EM emissions that interfere with signal reception. However, by embedding the transmitters underground, reduced mutual coupling and EM emissions (and improved signal-to-noise ratios) can be achieved. Simple surface SAR experiments over deep mine shafts have been performed to validate the 3D processing algorithms using 2D surface SAR sensor data. WIPL-D models have also been used to simulate the embedded and distributed sensors and to verify the significant enhancement in the received signal-to-noise ratio obtained by burying the radiating ring under the surface sensors. [C3376]

"Road Extraction from SAR Multi-Aspect Data Supported by a Statistical Context-Based Fusion"

In this paper we describe a fusion approach for automatic object extraction from multi-aspect SAR images. The fusion is carried out by means of the Bayesian probability theory. The first step consists of a line extraction in each image, followed by attribute extraction. Based on these attributes the uncertainty of each line segment is estimated, followed by an iterative fusion of these uncertainties supported by context information and sensor geometry. On the basis of a resulting uncertainty vector each line obtains an estimation of the probability that the line really belongs to a road. [C3377]

"A land subsidence study via DInSAR technique over large urbanised areas"

The paper discusses the potential of a DInSAR (Differential Synthetic Aperture Radar Interferometry) technique for the study of subsidence phenomena over large areas. The validation tests of low resolution DInSAR data, spanning the period 1992-2001, were carried out at a "municipal scale" in the urban area of Sarno (Italy), affected by ground surface settlements ascribed to groundwater withdrawals. The analysis was then extended to the whole Campanian Plain, with the same stratigraphic and structural settings as Sarno area, in order to use the remote sensed data as a tool for detecting, at regional scale, the most critical areas in terms of rate of the recorded settlements. At least five highly urbanised areas were identified as "unstable", thus addressing further investigations to deepen the relationship between the causes and the effects of the detected phenomena. [C3378]

"Target recognition by means of spaceborne C-band SAR data"

The relative low resolution (~25 m times 5 m on the ground) of spaceborne C-band SAR data as acquired e.g. by ESA sensors ERS and Envisat can be significantly increased (up to sub-meter precisions (Perissin and Rocca, 2005)) by processing coherently long series of images. Moreover, by analyzing the amplitude of the radar signal, the main radar characteristics of urban targets can be estimated and a system for automatic recognition of a set of scattering structures can be developed. In this work, we present the methodology and the results obtained on the test-sites of Milan and Shanghai by combining data acquired from ascending and descending passes and from parallel satellite tracks. [C3379]

"Towards a Complete Processing Chain of Multibaseline Airborne InSAR Data for Layover Scatterers Separation"

Interest is continuing to grow in exploiting the advanced multibaseline operation of synthetic aperture radar interferometry (InSAR) to solve layover effects, that can degrade conventional InSAR topographic mapping. In

this work we report about experiments of the functionality of "layover-free" or "higher-order" interferometry with the dual-baseline single-pass SAR interferometer AER-II. Estimation of the number of multiple layover scatterers, i.e. of the interferometric order, and model-based spatial spectral estimation are integrated to process the three-antenna non uniform array data. Results are discussed for a bridge over the valley test site. [C3380]

"Characterization of the Temporal and Spatial Variability of Soil Moisture through Multi-Temporal Analysis of ASAR Observations"

In this paper, synthetic aperture radar (SAR) based soil moisture retrieval results are presented using observations acquired over the Tibetan Plateau. Two different time series based methods are used for the retrieval of soil moisture. With method I, soil moisture is retrieved through scaling of the backscatter (σ_{0}) observations between the maximum and minimum observed σ_{0} at a specific location. For method II, soil moisture is retrieved using the integral equation method (IEM, Fung et al. 1992), for which a site-specific effective surface roughness parameterization is obtained through model inversion using minimum observed σ_{0} . The retrievals are validated against ground measurements and showed that using method I and method II soil moisture can be estimated with accuracies up to 0.056 and 0.035 cm³cm⁻³, respectively. [C3381]

"Multi-Frequency Antenna design for Space-based Reconfigurable Satellite Sensor Node"

The paper investigates the antenna design to be applied in the ESPACENET sensor node. The project involves a network of autonomous pico satellites working at a large number of communication standards and as passive radar sensors for earth observation. They would form the next generation of "eyes in the skies"; looking out for natural disasters, helping in the survey and effective utilization of natural resources and also form a seamless network of global communication which will have the potential to evolve itself with the growing demands of tomorrow's world. We discuss the need for a multiple frequency broadband antenna which would help cover a larger range of microwave frequencies enabling the antenna to work as both a communications antenna and a sensor device. [C3382]

"A Knowledge-Based Target Recognition Method For Remote Sensing Image"

This paper proposed a knowledge-based target bridge detection method from remote sensing images. Firstly, the prior knowledge about bridge can supervise the low and middle image processing and analysis to detect the edges of bridges and riversides. Secondly, knowledge about the different characters of the bridge edges and riverside edges was used to wipe off the riverside edges and remain the lines of bridges, so that the purpose of recognition on bridge can be achieved. The method was tested on spot remote sensing images and the result shows it can detect the bridges exactly from images. [C3383]

"Robust Satellite Techniques (RST) for Oil Spill Detection and Monitoring"

Satellite remote sensing is an useful tool supporting the management of marine technological hazards, especially for what concern oil discharge. Nowadays, the most reliable satellite techniques are based on SAR (Synthetic Aperture Radar) active sensors operating in the microwave region of the electromagnetic (EM) spectrum. Such methods (even if not in whatever wind condition), assure good sensitivity for oil spill detection and high spatial resolution for a detailed description of the polluted area. Unfortunately, they cannot be used for real-time monitoring at all latitudes because of a revisiting cycles which ranges from few days up to 5 weeks moving from polar to equatorial zones respectively. Passive optical sensors on board meteorological satellites could be, in principle, also used for oil spill monitoring provided that suitable data analysis techniques (still lacking) are developed. In fact, thanks to a time resolution which is better than of few hours (up to few minutes) and despite their lower spatial resolution (not better than 250 m in the visible spectral range) they could represent the unique possibility when a timely detection is crucial in order to mitigate the damages. In this paper a new satellite technique for oil spill detection and monitoring is discussed. It is based on the general RST (Robust Satellite Techniques) approach applied to AVHRR1 observations in the Thermal Infrared (TIR) region of the EM spectrum. The proposed approach, which exploits the analysis of multi-temporal satellite records, seems able to detect the anomalous signals on the sea due to the oil polluted areas with excellent reliability (0% of false alarms) and good sensitivity in different observational conditions. It is applied in this paper to the "San George" Argentina -Uruguay oil spill event occurred in February 1997. Preliminary results so far achieved confirm the reliability of the proposed approach which promises to offer new (economically sustainable too) opportunities for building a real-time monitoring system for oil spill at the global scale. [C3384]

"Dynamical Analysis of Hydrological Indexes Extracted from Remote Sensing Imagery: An Introductory Study"

A new intelligent computational paradigm based on filtering techniques modified to enhance the quality of reconstruction of the physical characteristics of environmental electronic maps extracted from the large scale remote sensing imagery is proposed. First, the problem-oriented modification of the previously proposed fused Bayesian-regularization enhanced radar imaging method is performed to enable it to reconstruct remote sensing signatures of interest. Second, the extraction of the so-called hydrological electronic maps and the analysis of its dynamics are proposed. Finally, simulation results of hydrological remote sensing signatures reconstruction from enhanced real-world environmental images are reported to verify the efficiency of the proposed approach.

[C3385]

"Performance Estimation of Similarity Measures of Multi-Sensor Images for Change Detection Applications"

Change detection of remotely sensed images is a particularly challenging task when the available data come from different sensors. Indeed, many change indicators are based on radiometry measures, operating on them differences or ratios, that are no longer reliable when the data have been acquired by different instruments. For this reason, it is interesting to study the performance of those indicators that do not rely completely on radiometric values. A series of similarity measures for automatic change detection was investigated and their performance compared using optical and SAR images covering a period of several years. We could observe that the considered change detection algorithms perform differently but that none of them permits an "absolute" measure of the changes independent of the sensor. [C3386]

"A Novel Methodology for Parameter Retrieval from Multi-temporal Data Demonstrated for Forest Biomass Retrieval from C-band SAR Backscatter"

A methodology for parameter retrieval from multi-temporal Earth observation data is proposed and applied to forest biomass retrieval from C-band SAR backscatter. The potential of single observation C-band SAR data to map forest biomass is limited mainly due to a low sensitivity and the dependence of C-band scattering on many other parameters. In this contribution a methodology to retrieve forest biomass from multi-temporal C-band SAR observations is presented. The method was applied to map forest biomass over a large area in Central Siberia using significant stacks of ENVISAT ASAR Wide-Swath data. The resulting forest biomass map is assessed by comparison with available inventory data. The quality achieved appears very promising. [C3387]

"Finite Array Observations-Adapted Regularization Unified with Descriptive Experiment Design Approach for High-Resolution Spatial Power Spectrum Estimation with Application to Radar/SAR Imaging"

We address a new approach to solving array radar/SAR imaging problems stated and treated as uncertain ill-posed inverse problems of nonparametric estimation of the power spatial spectrum pattern (SSP) of the wavefield scattered from an extended remotely sensed scene via processing the discrete measurements of a finite number of independent observations of the degraded data signals (one realization of the trajectory signal in the case of SAR). The problem is treated in the framework of the worst-case statistical performance optimization-adapted regularization (WOR) method aggregated with descriptive experiment design (DED) paradigm. Our approach is based on the optimization of worst-case statistical performance of the resulting finite-dimensional fused WORDED estimator of the SSP. The DED-formalized projection schemes as well as the weighting "degrees of freedom" of the WOR strategy are incorporated into the optimization procedure subject to the statistical operational worst-case performance constraints imposed on the desired solution operator. [C3388]

"Simulation of Radar Backscattering Coefficients Using IEM-A Tool for Surface Soil Moisture Retrieval"

The present paper attempts to simulate the radar backscattering coefficients of bare surface at steep and shallow incidence angle applying the integral equation model (IEM). Using the simplified form of IEM with the known input parameters of incidence angle, dielectric constant of the surface soil and corresponding surface roughness parameters; the backscattering coefficients have been simulated. This model has been implemented on the bare and sparsely vegetated fields of alluvial plains of India. The two selected test sites are located at Batala (Punjab Plain) and Diamond Harbor (Kolkata, West Bengal). Synchronized with the RADARSAT 1 satellite overpass, the field campaigns have been carried out during September 2003 for Batala test site and two campaigns for Diamond Harbor test site in February and December 2005. Here, the terrain surface is assumed to be exponential in nature and the associated autocorrelation function of the surface has been computed. As both the study sites are characterized by gently sloping terrain, only the single scattering term of the model has been considered for the estimation of the backscattering coefficients. The modelled backscatter values for HH polarization is validated using RADARSAT 1 SAR (Synthetic Aperture Radar) data in order to evaluate the

performance of the simulation. The sensitivity experiments are performed considering the near, mid and far range of the incidence angle. Initially, the experiments are carried out for Batala test site using both steep (Extended Low) and shallow (Standard 5) incidence angle beam mode data. An rms error of 1.79 dB and 2.96 dB is achieved while comparing the simulated and observed backscattering coefficients for the extended low and standard beam modes respectively. The computation of the index of agreement is also revealed that the indices are 0.80 and 0.66 respectively for steep and shallow incidence angle. Hence, only the steep incidence angle beam mode data has been used subsequently for the model evaluation of Diamond Harbor coastal alluvial test site where the rms error is observed to be 1.98 dB with 0.79 index of agreement for the entire sampling dataset. The present study has utilized 102 point observation samples in the entire analysis. The overall results have demonstrated that about 76% of the simulated backscatter data are within the radiometric resolution of RADARSAT 1. It is observed that the model result provides consistently good agreement with the measured backscattering data which indicates a scope to retrieve the surface soil moisture using SAR observations.

[C3389]

"Comparison of DEM Accuracies Generated by Various Methods"

Presently, various different methods are being used for digital elevation model (DEM) generation. DEMs can be generated from topographic maps obtained with terrestrial measurements, photogrammetric flight data or remote sensing technologies. And also a question can be asked that which method is better than others that's why these DEM generation techniques have been analysed and the accuracies of DEMs have been compared in this study. For Zonguldak test field, three types of DEMs have been used. First DEM has been produced by digitized contour lines of 1:25000 scale topographic maps, second one has been produced by photogrammetric flight project data had been made by Zonguldak Municipality in 2005 and last one has been derived from Shuttle Radar Topography Mission (SRTM) X-band data which has used single-pass interferometric synthetic aperture radar (InSAR) technique for DEM generation. In the study, all these DEMs have been compared one by one based on selected reference. The DEM produced with Photogrammetric method has approximately 5.5 m better accuracy for open and flat, 6.5 m better accuracy for forest areas against the DEM generated from 1:25000 scale topographic maps. SRTM X-band DEM is 4 m less accurate for open, 4.5 m less accurate for forest areas against the DEM produced with photogrammetric method and 9.5 m less accurate for open, 11 m less accurate for forest areas against the DEM generated from 1:25000 scale topographic maps. And at the result, it has been clearly seen that the DEM produced by photogrammetric flight project in 2005 has better accuracy than the others. [C3390]

"Integral Solution for Oil Spill Detection using SAR Data"

Oil spill detection on sea surface is a very difficult and actual task. Oil and oil products spills may occur at any stage of the offshore oil production and transportation cycle. Therefore taking into account the current trends of oil production, system developing for shelf and tank fleet monitoring becomes very crucial today. The ScanEx R&D Center has developed an integral solution for the SAR data fast acquisition, processing and oil spill monitoring. This technology has combined the UniScan multimission station, the ScanEx SAR Processor and ScanEx Image Processor software. The UniScan station is capable to receive data from the 12 operating Earth observation satellites including the Radarsat-1 and Envisat-1. The SAR images were processed using the ScanEx SAR Processor software. The new version of the ScanEx Image Processor supports automatic and manual oil spill detection. The ScanEx SAR integral technology was successfully tested to detect oil spills in the Caspian Sea in May 2006 and in September 2007. The technology meets the customer's requirements for fast data processing. [C3391]

"Synthetic Aperture Radar Raw Data Simulation for Microwave Remote Sensing Applications"

To make proper feature extraction from SAR imagery is strictly deal with not only to understand imaging mechanism of SAR sensor, but also to take into account scattering mechanism of targets. In this work, a point scatterer model and a facet model based on synthetic aperture radar (SAR) simulators are presented. [C3392]

"Covers"

The following topics are dealt with: security and disaster management; near earth space environment; space benefits and opportunities for emerging countries; space and security; aerospace materials and characterization; aerospace structures; space surveillance; space propulsion and launch; remote sensing; SAR; satellite design; space communication; navigation and control; social benefits and education; space weather and space sciences. [C3393]

"The Eads Astrium Astrosat Product Line A New Generation of High Resolution Small and Micro

Satellites Embarking Innovative Technologies"

Homeland security and associated benefits obtained from satellite data are essential for a country. Even more important are the additional benefits gained by a country possessing its own satellite system, such as: i) independence and sovereignty acquired from immediately available and reliable data, ii) creation of dual services benefiting both the military and civilian community, iii) creation of new competencies in the highly educated population in various scientific fields (e.g. satellite design, satellite operation, satellite data processing, and image information extraction), iv) significant improvement of the local manufacturing capability by introducing some space design rules (no right for mistake after launch), v) creation/improvement of scientific cooperation at regional scale. From the late 90s, EADS Astrium has developed and improved several classes of high resolution optical Earth Observation satellites. The resulting product line ranges from micro-satellites (about 130 Kg) type to the large satellites (in the range of 1200 kg). They all make use of state of the art technologies for optical and SAR payloads, as well as for avionics. 3 classes of platforms have been defined and standardized: AS 100 for satellites up to 130 kg, allowing affordable but fully operational missions, AS500 for satellites up to 800 kg, allowing complex high resolution missions, and AS 1000 for satellites up to 1200 kg, providing very high resolution and outstanding imaging and agility capabilities. 2 Synthetic Radar satellites (TerraSAR-X for global applications and AstroSAR Lite (for regional applications) are also offered, both benefiting from long experience of radar payloads (ERS, SRTM, ENVISAT). The satellites are designed for simple flight operations, large data collection capability, and large versatility of payload and missions. They are adaptable to a large range of performances. Astrium satellites have already been selected by various customers worldwide. It now has a long and recognized experience to complement its system/satellite offer with a long term cooperation to support the Customer in reaching any of the goals identified above. [C3394]

"A High Performance EO Small Satellite Platform (SSTL-300)"

This paper describes a new high performance Earth Observation Platform, the SSTL-300, which has been developed to provide customers with a capability that has previously only been available at much higher cost and on larger platforms. This platform offers a 7-year mission lifetime with a very high operational availability. The main payload is a very high-resolution imager (VHRI) with a panchromatic 2.5 m ground sampling distance (GSD) channel and four multi-spectral channels offering 5 m GSD. The imager swath is 20 km in all channels. This imager is an extension of the 4 m GSD imager already flying on Beijing-1, which was launched in October 2005. Additional payloads can be accommodated, such as the Medium Resolution Imager (MRI), offering lower resolution of 22 m or 32 m GSD in four multiple spectral bands with 300 km swath width. The 32 m MRI has already flown on four previous Disaster Monitoring Constellation (DMC) Missions. High performance geo-location is provided, the performance of which is dependent on the chosen subsystem options. Simultaneous imaging is possible with the VHRI and the MRI and scenes can be as long as 2000 km. The image data is compressed on-board, using lossless data compression, for store-and-forward operations. Furthermore, switchable encryption is available, using the Data Encryption Standard (DES), on the TM/TC as well as switchable scrambling on payload data. Near real-time imaging & down-linking is possible for a range of targets close to the ground station. A range of imaging modes are available including: strip mapping, fast response scene capture, stereo imaging, with pitch angles between 10 and 45deg to provide digital elevation models, and increased area coverage to provide wide-swath high-resolution imagery of up to 85 km. The nominal orbit for the SSTL-300 will be sun-synchronous, with a 10.30 am node to provide repeatable global coverage and good lighting conditions. The platform will orbit at approximately 700 km, which provides good optimisation for single satellite and constellation revisits. On-board propulsion is included for orbit maintenance. [C3395]

"Interpretation of an Influence of the Transmitter and Receiver Bistatic SAR Tracks to Resolution"

Remote sensing of a surface by the bistatic model allows obtaining more information about surface conditions. Practically all remote sensing problems are solved on basis of ambiguity function analysis of a system. Here a qualitative variables of such system is determined by a resolution or by an ambiguity function width on the fixed level. The resolution of the bistatic SAR as the monostatic has an objects space discrimination in all directions even if is used unmodulated sounding signal and a selection degree mainly depends on a phase function variation rapidity where return signal is processed. [C3396]

"Ground-Based Noise Waveform SAR and Differential Interferometry for Remote Monitoring of Large Objects"

The work is dedicated to experimental investigation of parameters of this SAR. A brief overview of SAR system is given; measurement set-up and estimation results of both accuracy and phase stability are described. [C3397]

"Implementation of Noise Radar Technology in Ground Based SAR for Short Range Applications"

In this paper, results of implementation of noise radar technology in X-band narrowband ground based (GB) synthetic aperture radar (SAR) were presented. The radars under consideration use noise waveform (NW) as a probe signal and perform the range focusing by correlating the radar returns with a reference signal taken before transmission, while the way the azimuth compression is done is similar to that of the conventional SAR. Evaluation of the phase measurements precision with the help of GB NW SAR was carried out on the basis of the obtained interferograms. It has been shown that both NW SAR systems provide quite high precision of displacement measurements. It was also demonstrated that noise radar technology may provide rather high performance of radar designed for short range applications with interferometric capabilities including ground based SAR and d-InSAR systems. [C3398]

"Polarization-Spectral Indication of the Objects"

The experimental study of the features of the polarization-spectral structure of the signals scattered from the sea surface, hydrometeors, lots covered of flora and above-sea objects allowed to ascertain that for the acquiring signals of the object the appreciably high level of the correlation at orthogonal polarizations than for the noise is typical. This condition could be used for the indication of the low-speed objects against a background of lots covered of flora. Since the signal scattered from the object at the polarization orthogonal to the transmitted partially coherent to the signal at the matched polarization, the latter could be used as reference for the realization narrow-band tracking of the orthogonally polarized signal component. [C3399]

"Fractal Analysis of Sea Ices Images"

The use of methods of the fractal analysis of radar allowed to define the ice-sea, sea-land borders. The application of quantization of the range of the received values of fractal dimensions allowed to carry out preliminary segmentation of the analyzed image by the selection of clusters of the set range of values of fractal dimensions. The line analysis of the initial image fractal dimensions can be used for estimating the degree of heterogeneity of the sea surface and selecting the ice-sea, sea-coast borders. The fractal analysis of images can be used for the development of safe routes of ships in Arctic. [C3400]

"Possibilities of Surface Relief Determination by Photometric Method in Millimeter and Submillimeter Wavelength Range"

In this paper, possibilities of planet surface relief determination by photometric method in millimeter and submillimeter wavelength range were studied. Considered in this paper was the case where the initial images were acquired with a side-looking radar, focusing attention upon the issue of informativity of obtained image series relative to the relief desired. [C3401]

"Detection of the Stochastic Objects in Multiposition SAR"

Proposed detection method in multiposition SAR is a high-stable, allows to detect objects with high probability of true detection along with low probability of the false alarm in comparison with monostatic/bistatic SAR. Significant advantages of the multiposition SAR are possibility to detect objects hidden for some bistatic pairs; possibility to detect targets even if their backscattering diagram is "almost zero" for some receivers (stealth objects as well); possibility of detection and identification of objects, width of which is closer/smaller than resolution. Optimal and quasioptimal detection algorithms were derived for two kinds of the objects- given by distribution of the complex scattering coefficient and objects given by distribution of the statistical characteristics of the object complex scattering coefficient. [C3402]

"Damage mapping for the 2004 Niigata-ken Chuetsu earthquake using Radarsat images"

The building damage detection technique which we have developed has been successfully applied to past events such as the earthquakes in Kobe in 1995, India in 2001, and Bam in 2003 by using the compound index, z-value, a value derived from the correlation and difference in intensities between pre-and post-event SAR images. This technique was applied to the aJapan earthquakereas affected in the Niigata-ken Chuetsu, Japan earthquake of October 23, 2004 by using one pair of radarsat images taken before and after the earthquake. However, it was not possible to identify any significant distribution of damaged buildings. In this study, we examined the reasons for that and proposed a new technique that uses two pairs (pre-seismic and co-seismic) of SAR images to identify smaller building damage ratios in less densely built-up areas as compared to previous techniques. The main idea is to minimize the effects of signal noise and temporal changes of the earth's surface on building damage estimation by calculating the difference values of the two pre-event images and one post-event image. From a macroscopic point of view, the distributions of both difference values of the z-values and the correlation coefficients in built-up areas were in good agreement with damage reported in survey reports. In Yamakoshi village, located in the highlands, we could also identify large-scale landslides with accuracy as good

as that of interpretation from aerial photos. [C3403]

"Performance of Falcon-I: Developed Low-Power and High-Sensitivity Cloud Profiling FM-CW Radar at 95GHz"

We have developed a low-power and high-sensitivity cloud profiling radar, named FALCON-I, transmitting frequency modulated continuous wave (FM-CW) at 95 GHz for ground-based observations. Millimeter wave at 95 GHz is used to realize much higher sensitivity than lower frequencies to small cloud particles. An FM-CW type radar realizes similar sensitivity with much smaller output power to a pulse type radar. Two 1m-diameter parabolic antennas separated by 1.4 m each other are used for transmitting and receiving the wave. The direction of the antennas is fixed at the zenith at this moment. The radar can observe clouds up to 20 km in height with the range resolution of 15 m and the angular resolution of 0.2 degree. Simultaneous observations of FALCON-I and a pulse type radar, SPIDER, show good performance of FALCON-I. Sensitivity of FALCON-I is -32 dBZ in radar reflectivity factor at 5 km, which is only 3 dB worse than that of SPIDER although its output power is 1/3000 to SPIDER. Ranging resolution of 15 m is realized for FALCON-I, which is 1/10 of that of SPIDER. Using developed FALCON-I, we observed clouds in various regions and oceans in the last three years.

[C3404]

"Doppler-Polarimetric Approach to Microwave Remote Sensing of Precipitation"

This study has shown that considered Doppler and polarization parameters of radar signal contain information on rain microstructure and turbulence intensity in weather object. The differential Doppler velocity of raindrops carries the important information on microstructure of rain and can be used in order to measure the rain intensity. However turbulence decreases this effect and should be taken into consideration as well. Application of independent turbulence-related variables can improve the reliability and accuracy of radar measurements in rain. Measurements of weather objects by Doppler-polarimetric radar can be very useful to solve wave propagation problems for the tasks of microwave remote sensing, communications and the radar's ability to detect targets embedded in high clutter background. [C3405]

"Improved Classification of Building Infrastructure from Airborne Lidar Data Using Spin Images and Fusion with Ground-Based Lidar"

Over the last five to ten years, Airborne Laser Swath Mapping (ALSM) technology, also known simply as Lidar, has become widely available to the remote sensing research community. In that time, many fields of application have been proposed. The majority of the early successful applications were for terrain mapping and surveying, but the high resolution data delivered by this technology has allowed researchers to apply it to problems in forestry, civil engineering, urban planning, and many other fields. In urban planning for example, explicit three-dimensional (3D) building models are an important data product for estimating microwave line-of-sight communications and emergency responder plans. Such models can be extracted from the 3D ALSM point cloud data once the points are properly segmented into building and non-building classes. The work presented here focuses on improved segmentation of building points in the ALSM point cloud using a local subspace mapping known as a spin image. The ALSM data are then fused with ground-based laser scanner data to improve discriminability among complex building architectures, adjacent vegetation, and even rooftop infrastructure.

[C3406]

"Complex Wishart Distribution Based Analysis of Polarimetric Synthetic Aperture Radar Data"

Multi-look, polarimetric synthetic aperture radar (SAR) data are often worked with in the so-called covariance matrix representation. For each pixel this representation gives a 3 times 3 Hermitian, positive definite matrix which follows a complex Wishart distribution. Based on this distribution a test statistic for equality of two such matrices and an associated asymptotic probability for obtaining a smaller value of the test statistic are given and applied to change detection, edge detection and segmentation in polarimetric SAR data. In a case study EMISAR L-band data from 17 April 1998 and 20 May 1998 covering agricultural fields near Foulum, Denmark, are used. Soon the Japanese ALOS, the German TerraSAR-X and the Canadian RADARSAT-2 will acquire space-borne, polarimetric data making analysis based on these methods important. [C3407]

"Derivation of Soil Surface Roughness Dynamics from Multi-temporal and Multi-parametric Airborne PolSAR-data"

The dynamics of soil surface roughness is important to a number of land surface processes. The potential of multi-temporal and multi-parametric PolSAR-data for soil surface roughness estimation is investigated to determine its temporal development. The study is based on weekly quadpol L-Band E-SAR backscatter data,

which was collected over the agri-phenological cycle in the course of the AgriSAR 2006 campaign. For ground truthing, the soil surface roughness was measured using photogrammetric imaging techniques. Two ground truth roughness indices (rms-height s , tortuosity index TB) and three polarimetric roughness estimators (anisotropy A , circular polarization coherence γ_{RRLL} and the real part of the circular polarization coherence $\text{Re}[\gamma_{RRLL}]$) were compared. While most of the comparison outlined weak correlations, best and sufficient results were obtained between s and $\text{Re}[\gamma_{RRLL}]$. Multi-temporal roughness maps were derived from this relationship, which are further affected by the presence and development of particular plants. [C3408]

"Measurement of Wind Wave Slope Variance with the Radar Having a Knife-Like Antenna Pattern"

This paper deals on measuring backscattering from a moving platform. A Doppler radar with a knife-like beam was installed on a MI-8 helicopter and the measurements were carried out during a flight above the Gorky water storage basin. These were our first measurements performed from a moving platform. [C3409]

"SAR and optical remote sensing for urban damage detection and mapping: case studies"

Remote sensing techniques have revealed a suitable monitoring tool to provide data useful for disaster studies. They allow the quick detection of damage and building collapses due to earthquakes, especially in remote areas or where the infrastructures are not well developed to ensure the necessary communication exchanges. In particular, Synthetic Aperture Radar (SAR) sensor is widely used in environmental studies due to its characteristics which allow a fairly synoptic view in almost completely weather and time independent conditions. The spatial resolution of satellite optical sensors is rapidly increasing in the last few years, reaching less than 1 meter (IKONOS and QuickBird satellites) and thus becoming a reliable tool for detecting changes of individual buildings. The combined use of optical satellite images, either at medium and high spatial resolution, and SAR data has been investigated. The results concerning the case studies of Bam and Izmit earthquakes are reported in this paper. Moreover, a comparison between the damage assessment obtained by satellite image analysis and ground survey is also shown. [C3410]

СПИСОК ЛИТЕРАТУРЫ

C1664. Foucher S. SAR Image Filtering Via Learned Dictionaries and Sparse Representations. 2008. IGARSS 2008. IEEE International Geoscience and Remote Sensing Symposium. - Boston, MA, 7-11 July 2008. - Vol. 1. - P. I-229-I-232-229. ↑

C1665. Lounis B. Statistical Similarity Measure for Oil Slick Detection in SAR Image. / Lounis B., Belhadj-Aissa A., Mercier G. // 2008. IGARSS 2008. IEEE International Geoscience and Remote Sensing Symposium. - Boston, MA, 7-11 July 2008. - Vol. 1. - P. I-233-I-236-233. ↑

C1666. Wenju He. Comparison of Three Unsupervised Segmentation Algorithms for SAR Data in Urban Areas. / Wenju He, Jager M., Hellwich O. // 2008. IGARSS 2008. IEEE International Geoscience and Remote Sensing Symposium. - Boston, MA, 7-11 July 2008. - Vol. 1. - P. I-241-I-244-241. ↑

C1667. Palubinskas G. Change Detection for Traffic Monitoring in Terrasar-X Imagery. / Palubinskas G., Runge H. // 2008. IGARSS 2008. IEEE International Geoscience and Remote Sensing Symposium. - Boston, MA, 7-11 July 2008. - Vol. 1. - P. I-169-I-172-169. ↑

C1668. Dragosevic M.V. Extending Airborne SAR-ATI Algorithms to the RADARSAT-2 Moving Object Detection Experiment (MODEX). / Dragosevic M.V., Chiu S. // 2008. IGARSS 2008. IEEE International Geoscience and Remote Sensing Symposium. - Boston, MA, 7-11 July 2008. - Vol. 1. - P. I-165-I-168-165. ↑

C1669. Argenti F. SAR Image Despeckling in the Undecimated Contourlet Domain: A Comparison of Lmmse and Map Approaches. / Argenti F., Bianchi T., Scarfizzi G., Alparone L. // 2008. IGARSS 2008. IEEE International Geoscience and Remote Sensing Symposium. - Boston, MA, 7-11 July 2008. - Vol. 1. - P. I-225-I-228-225. ↑

C1670. Debes C. Target Detection in Multiple-Viewing Through-the-Wall Radar Imaging. / Debes C., Zoubir A.M., Amin M.G. // 2008. IGARSS 2008. IEEE International Geoscience and Remote Sensing Symposium. - Boston, MA, 7-11 July 2008. - Vol. 1. - P. I-173-I-176-173. ↑

- C1671.** Coatanhay A. Statistical Analysis of the Electromagnetic Field Scattered by the Ocean Surface in Various Weather Conditions: A Numerical Study in L-Band. 2008. IGARSS 2008. IEEE International Geoscience and Remote Sensing Symposium. - Boston, MA, 7-11 July 2008. - Vol. 1. - P. I-292-I-295-292. ↑
- C1672.** Xuetong Xie. Validation of QSCAT-1 Geophysical Model Function Using Seawinds Level 2 and Buoy Data. / Xuetong Xie, Qiming Zeng, Weidong Hu, Wenxian Yu, Kehai Chen, Yu Fang. // 2008. IGARSS 2008. IEEE International Geoscience and Remote Sensing Symposium. - Boston, MA, 7-11 July 2008. - Vol. 1. - P. I-339-I-342-339. ↑
- C1673.** Tison C. A Spaceborne Radar for Directional Wave Spectrum Estimation: First Performance Simulations. / Tison C., Carayon G., Lambin J., Castilian P., Souyris J.C., Hauser D. // 2008. IGARSS 2008. IEEE International Geoscience and Remote Sensing Symposium. - Boston, MA, 7-11 July 2008. - Vol. 1. - P. I-347-I-350-347. ↑
- C1674.** Laupattarakasem P. SeaWinds Hurricane Wind Retrievals and Comparisons with H* Wind Surface Winds Analyses. / Laupattarakasem P., Jones W.L., Hennon C.C. // 2008. IGARSS 2008. IEEE International Geoscience and Remote Sensing Symposium. - Boston, MA, 7-11 July 2008. - Vol. 1. - P. I-284-I-287-284. ↑
- C1675.** Lang M.W. Radar Monitoring of Wetland Hydrology: Dynamic Information for the Assessment of Ecosystem Services. / Lang M.W., McCarty G.W., Ritchie J.C., Sadeghi A.M., Hively W.D., Eckles S.D. // 2008. IGARSS 2008. IEEE International Geoscience and Remote Sensing Symposium. - Boston, MA, 7-11 July 2008. - Vol. 1. - P. I-261-I-264-261. ↑
- C1676.** D'Addio S. Performance Assessment of GNSS-R Space Based Scatterometry by Means of Delay-Doppler Map. / D'Addio S., Buck C. // 2008. IGARSS 2008. IEEE International Geoscience and Remote Sensing Symposium. - Boston, MA, 7-11 July 2008. - Vol. 1. - P. I-280-I-283-280. ↑
- C1677.** Xiaolong Dong. System design and performance simulation of a spaceborne Ku-band rotation fan-beam scatterometer. / Xiaolong Dong, Wenming Lin. // 2008. IGARSS 2008. IEEE International Geoscience and Remote Sensing Symposium. - Boston, MA, 7-11 July 2008. - Vol. 1. - P. I-355-I-358-355. ↑
- C1678.** Salvia M. Monitoring Inundation Dynamics in ParanΓfBŸ River, Argentina, by C and L Band SAR. / Salvia M., Grings F., Karszenbaum H., Ferrazzoli P., Kandus P., Soldano A., Guerriero L. // 2008. IGARSS 2008. IEEE International Geoscience and Remote Sensing Symposium. - Boston, MA, 7-11 July 2008. - Vol. 1. - P. I-102-I-105-102. ↑
- C1679.** Atlas R. A New Cross-Calibrated, Multi-Satellite Ocean Surface Wind Product. / Atlas R., Hoffman R.N., Ardizzone J., Leidner M., Jusem J.C. // 2008. IGARSS 2008. IEEE International Geoscience and Remote Sensing Symposium. - Boston, MA, 7-11 July 2008. - Vol. 1. - P. I-106-I-109-106. ↑
- C1680.** Alsweiss S. A Ku-Band Active/Passive Wind Vector Retrieval Over the Ocean. / Alsweiss S., Laupattarakasem P., Jones W.L., Roeder R. // 2008. IGARSS 2008. IEEE International Geoscience and Remote Sensing Symposium. - Boston, MA, 7-11 July 2008. - Vol. 1. - P. I-110-I-113-110. ↑
- C1681.** Attema E. The European GMES Sentinel-1 Radar Mission. / Attema E., Snoeij P., Davidson M., Floury N., Levrini G., Rommen B., Rosich B. // 2008. IGARSS 2008. IEEE International Geoscience and Remote Sensing Symposium. - Boston, MA, 7-11 July 2008. - Vol. 1. - P. I-94-I-97-94. ↑
- C1682.** Franceschetti G. Electromagnetic Modelling for Information Extraction from High Resolution SAR Images of Urban Areas. / Franceschetti G., Guida R., Iodice A., Riccio D. // 2008. IGARSS 2008. IEEE International Geoscience and Remote Sensing Symposium. - Boston, MA, 7-11 July 2008. - Vol. 1. - P. I-78-I-81-78. ↑
- C1683.** Datcu M. Automated Information Extraction from TerraSAR-X Data: The Content Map. / Datcu M., Cerra D., Chaabouni H., de Miguel A., Molina D.E., Schwarz G., Soccorsi M. // 2008. IGARSS 2008. IEEE International Geoscience and Remote Sensing Symposium. - Boston, MA, 7-11 July 2008. - Vol. 1. - P. I-82-I-85-82. ↑
- C1684.** Schwarz G. Optimized Multilooking for Robust SAR Image Indexing. / Schwarz G., Molina D.E., Breit H., Datcu M. // 2008. IGARSS 2008. IEEE International Geoscience and Remote Sensing Symposium. - Boston, MA, 7-11 July 2008. - Vol. 1. - P. I-86-I-89-86. ↑

- C1685.** Eisenburger D. Stepped-Frequency Radar System in Gating Mode: An Experiment as a New Helicopter-Borne GPR System for Geological Applications. / Eisenburger D., Krellmann Y., Lentz H., Trilitzsch G. // 2008. IGARSS 2008. IEEE International Geoscience and Remote Sensing Symposium. - Boston, MA, 7-11 July 2008. - Vol. 1. - P. I-153-I-156-153. ↑
- C1686.** Sjogren T.K. Moving Target Relative Speed Estimation in the Presence of Strong Stationary Surrounding Using a Single Antenna UWB SAR System. / Sjogren T.K., Vu V.T., Pettersson M.I. // 2008. IGARSS 2008. IEEE International Geoscience and Remote Sensing Symposium. - Boston, MA, 7-11 July 2008. - Vol. 1. - P. I-157-I-160-157. ↑
- C1687.** Vu V.T. Moving Target Detection by Focusing for Frequency Domain Algorithms in UWB Low Frequency SAR. / Vu V.T., Sjogren T.K., Pettersson M.I. // 2008. IGARSS 2008. IEEE International Geoscience and Remote Sensing Symposium. - Boston, MA, 7-11 July 2008. - Vol. 1. - P. I-161-I-164-161. ↑
- C1688.** Tiwari S. Texture Feature Selection for Buried Mine Detection in Airborne Multispectral Imagery. / Tiwari S., Agarwal S., Trang A. // 2008. IGARSS 2008. IEEE International Geoscience and Remote Sensing Symposium. - Boston, MA, 7-11 July 2008. - Vol. 1. - P. I-145-I-148-145. ↑
- C1689.** Stoffele A. High-Resolution ASCAT Scatterometer Winds Near the Coast. / Stoffele A., Portabella M., Verhoef A., Verspeek J., Vogelzan J. // 2008. IGARSS 2008. IEEE International Geoscience and Remote Sensing Symposium. - Boston, MA, 7-11 July 2008. - Vol. 1. - P. I-114-I-117-114. ↑
- C1690.** Soisuvann S. Validation of NOAA's Near Real-Time Ascat Ocean Vector Winds. / Soisuvann S., Jelenak Z., Chang P.S., Qi Zhu, Sindic-Rancic G. // 2008. IGARSS 2008. IEEE International Geoscience and Remote Sensing Symposium. - Boston, MA, 7-11 July 2008. - Vol. 1. - P. I-118-I-121-118. ↑
- C1691.** Surussavadee C. Global Observations of Precipitation Using Satellite Passive Millimeter-Wave Sensors. 2008. IGARSS 2008. IEEE International Geoscience and Remote Sensing Symposium. - Boston, MA, 7-11 July 2008. - Vol. 1. - P. I-126-I-129-126. ↑
- C1692.** Hoffman R.N. All Data are Useful, but not All Data are Used! What'S Going on Here?. / Hoffman R.N., Moncet J.-L. // 2008. IGARSS 2008. IEEE International Geoscience and Remote Sensing Symposium. - Boston, MA, 7-11 July 2008. - Vol. 2. - P. II-1-II-4-1. ↑
- C1693.** Pieraccini M. The Orfeus Project (Optimised Radar for Finding Every Utility in the Street). / Pieraccini M., Parrini F., de Pasquale G., Scott H. // 2008. IGARSS 2008. IEEE International Geoscience and Remote Sensing Symposium. - Boston, MA, 7-11 July 2008. - Vol. 2. - P. II-9-II-12-9. ↑
- C1694.** Gurbuz A.C. GPR Imaging Using Compressed Measurements. / Gurbuz A.C., McClellan J.H., Scott W.R. // 2008. IGARSS 2008. IEEE International Geoscience and Remote Sensing Symposium. - Boston, MA, 7-11 July 2008. - Vol. 2. - P. II-13-II-16-13. ↑
- C1695.** Kye-Lim Kim. A Study on the Characteristics of the Sedimentary Environments by Using SAR Data in the Ganghwa Tidal Flat. / Kye-Lim Kim, Sang-Wan Kim, Joo-Hyung Ryu, Sang-Hoon Hong. // 2008. IGARSS 2008. IEEE International Geoscience and Remote Sensing Symposium. - Boston, MA, 7-11 July 2008. - Vol. 1. - P. I-480-I-483-480. ↑
- C1696.** Yu-Chang Tzeng. Integration of Spatial Chaotic Model and Type-2 Fuzzy Sets to Coastline Detection in SAR Images. / Yu-Chang Tzeng, Dana Chen, Kun-Shan Chen. // 2008. IGARSS 2008. IEEE International Geoscience and Remote Sensing Symposium. - Boston, MA, 7-11 July 2008. - Vol. 1. - P. I-430-I-433-430. ↑
- C1697.** Chan-Su Yang. Comparison of Ship Detectability Using SAR Polarization Data: Envisat ASAR AP Mode. / Chan-Su Yang, Ouchi K. // 2008. IGARSS 2008. IEEE International Geoscience and Remote Sensing Symposium. - Boston, MA, 7-11 July 2008. - Vol. 1. - P. I-450-I-453-450. ↑
- C1698.** Kaiguo Fan. Simulation Study on the Optimal Conditions for Shallow Water Bathymetry Observation by SAR. / Kaiguo Fan, Weigen Huang, Bin Fu, Mingxia He. // 2008. IGARSS 2008. IEEE International Geoscience and Remote Sensing Symposium. - Boston, MA, 7-11 July 2008. - Vol. 1. - P. I-454-I-457-454. ↑
- C1699.** Baumgartner S.V. SAR Traffic Monitoring Using Time-Frequency Analysis for Detection and Parameter Estimation. / Baumgartner S.V., Krieger G. // 2008. IGARSS 2008. IEEE International Geoscience and Remote Sensing Symposium. - Boston, MA, 7-11 July 2008. - Vol. 2. - P. II-25-II-28-25. ↑

- C1700.** Niamsuwan N. Low Frequency Sea and Ice Sheet Impulse Responses Acquired by the Global Ice Sheet Mapping Orbiter (GISMO) Demonstrator. / Niamsuwan N., Johnson J.T. // 2008. IGARSS 2008. IEEE International Geoscience and Remote Sensing Symposium. - Boston, MA, 7-11 July 2008. - Vol. 2. - P. II-53-II-56-53. ↑
- C1701.** Longepe N. Toward an Operational Method for Refined Snow Characterization Using Dual-Polarization C-Band SAR Data. / Longepe N., Allain S., Pottier E. // 2008. IGARSS 2008. IEEE International Geoscience and Remote Sensing Symposium. - Boston, MA, 7-11 July 2008. - Vol. 2. - P. II-57-II-60-57. ↑
- C1702.** Macon C. Seafloor and Land Cover Classification Through Airborne Lidar and Hyperspectral Data Fusion. / Macon C., Wozencraft J., Joong Yong Park, Tuell G. // 2008. IGARSS 2008. IEEE International Geoscience and Remote Sensing Symposium. - Boston, MA, 7-11 July 2008. - Vol. 2. - P. II-77-II-80-77. ↑
- C1703.** Padmanabhan S. Retrieval of 3-D Water Vapor Field Using a Network of Scanning Compact Microwave Radiometers. / Padmanabhan S., Reising S.C., Vivekanandan J. // 2008. IGARSS 2008. IEEE International Geoscience and Remote Sensing Symposium. - Boston, MA, 7-11 July 2008. - Vol. 2. - P. II-49-II-52-49. ↑
- C1704.** Thayaparan T. S-Method-Based Approach for Image Formation, Motion Compensation, and Image Enhancement of Moving Targets in ISAR and SAR. / Thayaparan T., Stankovic L., Dakovic M. // 2008. IGARSS 2008. IEEE International Geoscience and Remote Sensing Symposium. - Boston, MA, 7-11 July 2008. - Vol. 2. - P. II-29-II-32-29. ↑
- C1705.** Yimin Zhang. Localization of Inanimate Moving Targets Using Dual-Frequency Synthetic Aperture Radar and Time-Frequency Analysis. / Yimin Zhang, Amin M., Ahmad F. // 2008. IGARSS 2008. IEEE International Geoscience and Remote Sensing Symposium. - Boston, MA, 7-11 July 2008. - Vol. 2. - P. II-33-II-36-33. ↑
- C1706.** Kersten P.R. Estimating Surface Water Speeds using Time-Frequency Analysis. / Kersten P.R., Jansen R.W., Ainsworth T.L., Toporkov J.V., Sletten M.A. // 2008. IGARSS 2008. IEEE International Geoscience and Remote Sensing Symposium. - Boston, MA, 7-11 July 2008. - Vol. 2. - P. II-37-II-40-37. ↑
- C1707.** Wei Chen. Estimation of Surface Velocity from Infrared Image Using the Global Optimal Solution to an Inverse Model. / Wei Chen, Mied R.P., Shen C.Y. // 2008. IGARSS 2008. IEEE International Geoscience and Remote Sensing Symposium. - Boston, MA, 7-11 July 2008. - Vol. 1. - P. I-383-I-386-383. ↑
- C1708.** Sajjad N. An Improved Two-Scale Model for the Ocean Surface Bistatic Scattering. / Sajjad N., Khenchaf A., Coatanhay A., Awada A. // 2008. IGARSS 2008. IEEE International Geoscience and Remote Sensing Symposium. - Boston, MA, 7-11 July 2008. - Vol. 1. - P. I-387-I-390-387. ↑
- C1709.** Xuetong Xie. A Study on Geophysical Model Function Modeling with Water Surface Temperature as One of the Input Parameters. / Xuetong Xie, Kehai Chen, Wenxian Yu, Weidong Hu, Qiming Zeng, Yu Fang. // 2008. IGARSS 2008. IEEE International Geoscience and Remote Sensing Symposium. - Boston, MA, 7-11 July 2008. - Vol. 1. - P. I-398-I-401-398. ↑
- C1710.** Li Haiyan. Polarimetric Scattering Mechanisms of Ocean Surface from Wave Breaking or at Large Incident Angles. / Li Haiyan, Zhang Shufang, Shen Hui, He Yijun. // 2008. IGARSS 2008. IEEE International Geoscience and Remote Sensing Symposium. - Boston, MA, 7-11 July 2008. - Vol. 1. - P. I-379-I-382-379. ↑
- C1711.** Nadai A. Dependency of NRCS of Ocean Surface on Wind Direction Using an Airborne Dual-Frequency Polarimetric SAR Observation. / Nadai A., Umehara T., Matsuoka T., Kobayashi T., Uratsuka S. // 2008. IGARSS 2008. IEEE International Geoscience and Remote Sensing Symposium. - Boston, MA, 7-11 July 2008. - Vol. 1. - P. I-367-I-370-367. ↑
- C1712.** Arakelyan A. Preliminary Polarimetric Measurements of Ruffled Water Surface Radar Backscattering Coefficients and Brightness Temperatures Angular Dependences at 15GHz. / Arakelyan A., Darbinyan S., Grigoryan M., Hakobyan I., Hambaryan A., Hambaryan V., Karyan V., Manukyan M., Hovhannisyan G. // 2008. IGARSS 2008. IEEE International Geoscience and Remote Sensing Symposium. - Boston, MA, 7-11 July 2008. - Vol. 1. - P. I-371-I-374-371. ↑
- C1713.** Forget P. Monitoring of Surface Ocean Circulation in the Gulf of Lions (North-West Mediterranean Sea) Using WERA HF Radars. / Forget P., Barbin Y., Andre G. // 2008. IGARSS 2008. IEEE International Geoscience

and Remote Sensing Symposium. - Boston, MA, 7-11 July 2008. - Vol. 1. - P. I-375-I-378-375. ↑

C1714. Satake M. Ocean Surface Observation by C-Band Polarimetric Weather Radar in Okinawa Island. / Satake M., Nakagawa K., Kojima S., Satoh S., Shusse Y. // 2008. IGARSS 2008. IEEE International Geoscience and Remote Sensing Symposium. - Boston, MA, 7-11 July 2008. - Vol. 1. - P. I-402-I-404-402. ↑

C1715. Qing Xu. SAR Measurement of Ocean Surface Wind Using A Physics Model. / Qing Xu, Hui Lin, Liming Jiang, Xiaobin Yin, Quanan Zheng, Yuguang Liu. // 2008. IGARSS 2008. IEEE International Geoscience and Remote Sensing Symposium. - Boston, MA, 7-11 July 2008. - Vol. 1. - P. I-420-I-423-420. ↑

C1716. Biao Zhang. A Parametric Algorithm to Retrieve Ocean Wave Spectra from Interferometric Synthetic Aperture Radar. / Biao Zhang, Yijun He. // 2008. IGARSS 2008. IEEE International Geoscience and Remote Sensing Symposium. - Boston, MA, 7-11 July 2008. - Vol. 1. - P. I-424-I-427-424. ↑

C1717. Bourgeau-Chavez L.L. Remotely Monitoring Great Lakes Coastal Wetlands with Multi-Sensor, Multi-Temporal SAR and Multi-Spectral Data. / Bourgeau-Chavez L.L., Riordan K., Miller N., Nowels M., Powell R. // 2008. IGARSS 2008. IEEE International Geoscience and Remote Sensing Symposium. - Boston, MA, 7-11 July 2008. - Vol. 1. - P. I-428-I-429-428. ↑

C1718. Chan-Su Yang. Extraction of Wind and Wave Information Using SAR Images. / Chan-Su Yang, Moon-Kyung Kang. // 2008. IGARSS 2008. IEEE International Geoscience and Remote Sensing Symposium. - Boston, MA, 7-11 July 2008. - Vol. 1. - P. I-417-I-419-417. ↑

C1719. Vesecky J.F. Monitoring of Coastal Vessels Using Surface Wave HF Radars: Multiple Frequency, Multiple Site and Multiple Antenna Considerations. / Vesecky J.F., Laws K., Paduan J.D. // 2008. IGARSS 2008. IEEE International Geoscience and Remote Sensing Symposium. - Boston, MA, 7-11 July 2008. - Vol. 1. - P. I-405-I-408-405. ↑

C1720. Kaiguo Fan. Simulation Study on the Effect of Wind Direction on SAR Imaging Shallow Water Bathymetry. / Kaiguo Fan, Weigen Huang, Mingxia He, Bin Fu, Xilin Gan. // 2008. IGARSS 2008. IEEE International Geoscience and Remote Sensing Symposium. - Boston, MA, 7-11 July 2008. - Vol. 1. - P. I-409-I-412-409. ↑

C1721. Moon-Kyung Kang. Estimation of Ocean Current Velocity in Coastal Area Using Radarsat-1 SAR Images and HF-Radar Data. / Moon-Kyung Kang, Hoonyol Lee, Chan-Su Yang, Wang-Jung Yoon. // 2008. IGARSS 2008. IEEE International Geoscience and Remote Sensing Symposium. - Boston, MA, 7-11 July 2008. - Vol. 1. - P. I-413-I-416-413. ↑

C1722. Vasile G. Normalized Coherency Matrix Estimation Under the SIRV Model. Alpine Glacier PolSAR Data Analysis. / Vasile G., Ovarlez J.-P., Pascal F., Tison C., Bombrun L., Gay M., Trouve E. // 2008. IGARSS 2008. IEEE International Geoscience and Remote Sensing Symposium. - Boston, MA, 7-11 July 2008. - Vol. 1. - P. I-74-I-77-74. ↑

C1723. Samsonov S. Deformations occurring in the city of Auckland, New Zealand as mapped by the differential synthetic aperture radar. / Samsonov S., Tiampo K., Manville V., Jolly G. // 2008. USEReST 2008. Second Workshop on Use of Remote Sensing Techniques for Monitoring Volcanoes and Seismogenic Areas. - Naples, 11-14 Nov. 2008. - P. 1-4. ↑

C1724. Shahzad F. Remote sensing analysis of ongoing deformation in Hazara Kashmir Syntaxis in Northern Pakistan. / Shahzad F., Mahmood S.A., Gloaguen R. // 2008. USEReST 2008. Second Workshop on Use of Remote Sensing Techniques for Monitoring Volcanoes and Seismogenic Areas. - Naples, 11-14 Nov. 2008. - P. 1-4. ↑

C1725. Xiaoying Cong. Ground deformation measurement with radar interferometry in Exupry. / Xiaoying Cong, Hinz S., Eineder M., Parizzi A. // 2008. USEReST 2008. Second Workshop on Use of Remote Sensing Techniques for Monitoring Volcanoes and Seismogenic Areas. - Naples, 11-14 Nov. 2008. - P. 1-4. ↑

C1726. Marzano F.S. Ground-based radar remote sensing of explosive volcanic ash eruptions: Numerical models and quantitative applications. / Marzano F.S., Marchiotto S., Barbieri S., Schneider D., Textor C., Giuliani G. // 2008. USEReST 2008. Second Workshop on Use of Remote Sensing Techniques for Monitoring Volcanoes and Seismogenic Areas. - Naples, 11-14 Nov. 2008. - P. 1-5. ↑

C1727. Minet C. Requirements for an L-band SAR-mission for global monitoring of tectonic activities. / Minet C., Eineder M., Bamler R., Friedrich A., Hajnsek I. // 2008. USEReST 2008. Second Workshop on Use of Remote Sensing Techniques for Monitoring Volcanoes and Seismogenic Areas. - Naples, 11-14 Nov. 2008. - P. 1-3. ↑

C1728. Calla O.P.N. Study of scattering coefficient of flooded soil, semi dry soil and natural dry soil at CJ, X and Ku band of microwave frequencies. / Calla O.P.N., Vyas R., Bohra D., Harit K.C., Ranjan A., Kumar R., Mittal S.K. // 2008. MICROWAVE 2008. International Conference on Recent Advances in Microwave Theory and Applications. - Jaipur, 21-24 Nov. 2008. - P. 692-694. ↑

C1729. Puglisi G. Definition of the deformation pattern of Sicily (Italy) through DInSAR techniques and studies on its integration with geodetic data. / Puglisi G., Guglielmino F., Bonforte A., Nunnari G., Spata A. // 2008. USEReST 2008. Second Workshop on Use of Remote Sensing Techniques for Monitoring Volcanoes and Seismogenic Areas. - Naples, 11-14 Nov. 2008. - P. 1-4. ↑

C1730. Boerner W.-M. Recent advances of POL-SAR, POL-IN-SAR & RP-POL-IN-SAR imagery for remotely sensing natural habitats: Desert and wetlands remote sensing. 2008. MICROWAVE 2008. International Conference on Recent Advances in Microwave Theory and Applications. - Jaipur, 21-24 Nov. 2008. - P. 205-206. ↑

C1731. Boerner W.-M. Recent advances in RP-POL-IN-SAR Hazard monitoring of tectonic stress and land-slides. 2008. MICROWAVE 2008. International Conference on Recent Advances in Microwave Theory and Applications. - Jaipur, 21-24 Nov. 2008. - P. 423-426. ↑

C1732. Ya-Qiu Jin. SAR Imaging Simulation for an Inhomogeneous Undulated Lunar Surface Based on Triangulated Irregular Network. / Ya-Qiu Jin, Wenzhe Fa, Feng Xu. // 2008 China-Japan Joint Microwave Conference. - Shanghai, 10-12 Sept. 2008. - P. 333-336. ↑

C1733. Di Martino G. Volcano monitoring via fractal modeling of lava flows. / Di Martino G., Iodice A., Riccio D., Ruello G. // 2008. USEReST 2008. Second Workshop on Use of Remote Sensing Techniques for Monitoring Volcanoes and Seismogenic Areas. - Naples, 11-14 Nov. 2008. - P. 1-5. ↑

C1734. Proietti C. Photogrammetric and LIDAR surveys on the Sciara del Fuoco to monitor the 2007 Stromboli eruption. / Proietti C., Coltelli M., Marsella M., Sonnessa A., Bernardo E. // 2008. USEReST 2008. Second Workshop on Use of Remote Sensing Techniques for Monitoring Volcanoes and Seismogenic Areas. - Naples, 11-14 Nov. 2008. - P. 1-6. ↑

C1735. Joyce K. Satellite remote sensing of volcanic activity in New Zealand. / Joyce K., Samsonov S., Jolly G. // 2008. USEReST 2008. Second Workshop on Use of Remote Sensing Techniques for Monitoring Volcanoes and Seismogenic Areas. - Naples, 11-14 Nov. 2008. - P. 1-4. ↑

C1736. Fernandez J. DInSAR, GPS and gravity observation results in La Palma, Canary islands. / Fernandez J., Gonzalez P.J., Camacho A.G., Rodriguez-Velasco G., Arjona A., Pallero J.L.G., Prieto J.F., Perlock P.A., Tiampo K.F., Seco A., Aparicio A., Rundle J.B. // 2008. USEReST 2008. Second Workshop on Use of Remote Sensing Techniques for Monitoring Volcanoes and Seismogenic Areas. - Naples, 11-14 Nov. 2008. - P. 1-5. ↑

C1737. Gupta V.K. Roughness effect of the soil of Alwar on passive and active microwave remote sensing. / Gupta V.K., Jangid R.A. // 2008. MICROWAVE 2008. International Conference on Recent Advances in Microwave Theory and Applications. - Jaipur, 21-24 Nov. 2008. - P. 207-210. ↑

C1738. Zhu Yaping. Detection of Deep Convective Clouds Using AMSU-B and GOES-9 Data. / Zhu Yaping, Liu Jianwen, Cheng Zhoujie. // 2008 China-Japan Joint Microwave Conference. - Shanghai, 10-12 Sept. 2008. - P. 278-281. ↑

C1739. Sharma S.B. Antenna technologies for microwave sensors: A review. 2008. MICROWAVE 2008. International Conference on Recent Advances in Microwave Theory and Applications. - Jaipur, 21-24 Nov. 2008. - P. 69. ↑

C1740. Calla O.P.N. Microwave remote sensing using space borne sensors. 2008. MICROWAVE 2008. International Conference on Recent Advances in Microwave Theory and Applications. - Jaipur, 21-24 Nov. 2008. - P. 422. ↑

- C1741.** Boerner W.-M. Recent advances in microwave multi-modal SAR remote sensing of the terrestrial covers. 2008. MICROWAVE 2008. International Conference on Recent Advances in Microwave Theory and Applications. - Jaipur, 21-24 Nov. 2008. - P. 201-204. ↑
- C1742.** Yanan Xie. Research in the Spaceborne Meteorological Radar Equation. / Yanan Xie, Jianping Huan. // 2008 China-Japan Joint Microwave Conference. - Shanghai, 10-12 Sept. 2008. - P. 13-16. ↑
- C1743.** Rahman M.S. A new digital signal processor for Doppler radar cardiopulmonary monitoring system. / Rahman M.S., Byung-Jun Jang, Ki-Doo Kim. // 2008. ICECE 2008. International Conference on Electrical and Computer Engineering. - Dhaka, 20-22 Dec. 2008. - P. 76-79. ↑
- C1744.** Boerner W.-M. Basics of microwave radar & SAR polarimetry and its applications. 2008. MICROWAVE 2008. International Conference on Recent Advances in Microwave Theory and Applications. - Jaipur, 21-24 Nov. 2008. - P. 1-2. ↑
- C1745.** Singh G. LOS PALSAR data analysis of snow cover area in Himalayan region using four component scattering decomposition technique. / Singh G., Venkataraman G. // 2008. MICROWAVE 2008. International Conference on Recent Advances in Microwave Theory and Applications. - Jaipur, 21-24 Nov. 2008. - P. 772-774. ↑
- C1746.** Pant T. Multifractal analysis of SAR images for unsupervised classification. / Pant T., Singh D., Srivastava T. // 2008. MICROWAVE 2008. International Conference on Recent Advances in Microwave Theory and Applications. - Jaipur, 21-24 Nov. 2008. - P. 427-430. ↑
- C1747.** Prakash R. Microwave sensitivity analysis of soil texture at C-band with bistatic scatterometer for remote sensing. / Prakash R., Singh D. // 2008. MICROWAVE 2008. International Conference on Recent Advances in Microwave Theory and Applications. - Jaipur, 21-24 Nov. 2008. - P. 211-213. ↑
- C1748.** Singh G. Snow density estimation using polarimetric ASAR data. / Singh G., Venkataraman G. // 2008. MICROWAVE 2008. International Conference on Recent Advances in Microwave Theory and Applications. - Jaipur, 21-24 Nov. 2008. - P. 463-466. ↑
- C1749.** Agrawal N. Investigation of SAR compression technique for point target. / Agrawal N., Venugopalan K. // 2008. MICROWAVE 2008. International Conference on Recent Advances in Microwave Theory and Applications. - Jaipur, 21-24 Nov. 2008. - P. 217-219. ↑
- C1750.** Srivastava P. Design and development of multi-frequency comb generator for space borne microwave active sensors. / Srivastava P., Kumar P.P., Rao C.V.N. // 2008. MICROWAVE 2008. International Conference on Recent Advances in Microwave Theory and Applications. - Jaipur, 21-24 Nov. 2008. - P. 445-447. ↑
- C1751.** Calla O.P.N. Measurement of soil moisture using microwave radiometer. / Calla O.P.N., Bohra D., Vyas R., Purohit B.S., Prasher R., Loomba A., Kumar N. // 2008. MICROWAVE 2008. International Conference on Recent Advances in Microwave Theory and Applications. - Jaipur, 21-24 Nov. 2008. - P. 621-624. ↑
- C1752.** Bonforte A. A decade of applying Differential SAR Interferometry on Mount Etna volcano: Analysis at different time and space scales. / Bonforte A., Guglielmino F., Puglisi G., Palano M. // 2008. USEReST 2008. Second Workshop on Use of Remote Sensing Techniques for Monitoring Volcanoes and Seismogenic Areas. - Naples, 11-14 Nov. 2008. - P. 1-3. ↑
- C1753.** D'Oreye N. Systematic InSAR monitoring of African active volcanic zones: What we have learned in three years, or an harvest beyond our expectations. / D'Oreye N., Fernandez J., Gonzalez P., Kervyn F., Wauthier C., Frischknecht C., Calais E., Heleno S., Cayol V., Oyen A., Marinkovic P. // 2008. USEReST 2008. Second Workshop on Use of Remote Sensing Techniques for Monitoring Volcanoes and Seismogenic Areas. - Naples, 11-14 Nov. 2008. - P. 1-6. ↑
- C1754.** Prata F. Support to Aviation for Volcanic Ash Avoidance (SAVAA). / Prata F., Buongiorno F., Eckhardt S., Seibert P., Stohl A., Richter A. // 2008. USEReST 2008. Second Workshop on Use of Remote Sensing Techniques for Monitoring Volcanoes and Seismogenic Areas. - Naples, 11-14 Nov. 2008. - P. 1-7. ↑
- C1755.** Peltier A. Eruptive cycles inferred from ground deformation at Piton de La Fournaise-a case study for the Globvolcano project. / Peltier A., Kaminski E., Komorowski J.C. // 2008. USEReST 2008. Second Workshop on Use of Remote Sensing Techniques for Monitoring Volcanoes and Seismogenic Areas. - Naples, 11-14 Nov. 2008. - P. 1-2. ↑

2008. - P. 1-5. ↑

C1756. Alipour S. InSAR time series investigation of land subsidence due to groundwater overexploitation in Tehran, Iran. / Alipour S., Motgah M., Sharifi M.A., Walter T.R. // 2008. USEReST 2008. Second Workshop on Use of Remote Sensing Techniques for Monitoring Volcanoes and Seismogenic Areas. - Naples, 11-14 Nov. 2008. - P. 1-5. ↑

C1757. Casu F. SBAS-DInSAR GRID processing on-demand: A case study. / Casu F., Manunta M., Lanari R., Sansosti E., Guarino S., Cossu R., Fusco L., Mazzarella G. // 2008. USEReST 2008. Second Workshop on Use of Remote Sensing Techniques for Monitoring Volcanoes and Seismogenic Areas. - Naples, 11-14 Nov. 2008. - P. 1-5. ↑

C1758. Casu F. Surface deformation analysis of the Mauna Loa and Kīlauea volcanoes, Hawai'i, based on InSAR displacement time series. / Casu F., Solaro G., Tizzani P., Poland M., Miklius A., Sansosti E., Lanari R. // 2008. USEReST 2008. Second Workshop on Use of Remote Sensing Techniques for Monitoring Volcanoes and Seismogenic Areas. - Naples, 11-14 Nov. 2008. - P. 1-4. ↑

C1759. O'Neill P. Microwave Soil Moisture Retrieval Under Trees. / O'Neill P., Lang R., Kurum M., Joseph A., Cosh M., Jackson T. // 2008. IGARSS 2008. IEEE International Geoscience and Remote Sensing Symposium. - Boston, MA, 7-11 July 2008. - Vol. 1. - P. I-37-I-40-37. ↑

C1760. Comer D.C. Wide-Area, Planning Level Archaeological Surveys Using SAR and Multispectral Images. 2008. IGARSS 2008. IEEE International Geoscience and Remote Sensing Symposium. - Boston, MA, 7-11 July 2008. - Vol. 1. - P. I-45-I-47-45. ↑

C1761. Cantalloube H.M.J. Physic and Experimental Issues on High Resolution SAR Imaging of Urban Area. / Cantalloube H.M.J., Oriot H., ColinKoeniger E. // 2008. IGARSS 2008. IEEE International Geoscience and Remote Sensing Symposium. - Boston, MA, 7-11 July 2008. - Vol. 1. - P. I-70-I-73-70. ↑

C1762. Isoguchi O. Polarization Dependence of L-Band Measurements Over the Ocean on Surface Wind at 23-25 Incidence Angles. / Isoguchi O., Shimada M. // 2008. IGARSS 2008. IEEE International Geoscience and Remote Sensing Symposium. - Boston, MA, 7-11 July 2008. - Vol. 1. - P. I-25-I-28-25. ↑

C1763. Miyagi Y. ALOS emergency observations by JAXA for monitoring earthquakes and volcanic eruptions in 2008. / Miyagi Y., Shimada M., Tadono T., Isoguchi O., Ohki M. // 2008. USEReST 2008. Second Workshop on Use of Remote Sensing Techniques for Monitoring Volcanoes and Seismogenic Areas. - Naples, 11-14 Nov. 2008. - P. 1-5. ↑

C1764. Shimada M. Palsar Calval and Generation of the Continent Scale Mosaic Products for Kyoto and Carbon Projects. / Shimada M., Isoguchi O., Rosenqvist A. // 2008. IGARSS 2008. IEEE International Geoscience and Remote Sensing Symposium. - Boston, MA, 7-11 July 2008. - Vol. 1. - P. I-17-I-20-17. ↑

C1765. Touzi R. Polarimetric PALSAR System Model Assessment and Calibration. / Touzi R., Nedelcu S., Shimada M. // 2008. IGARSS 2008. IEEE International Geoscience and Remote Sensing Symposium. - Boston, MA, 7-11 July 2008. - Vol. 1. - P. I-21-I-24-21. ↑

C1766. Akbari V. Land subsidence monitoring using InSAR time series, case study: Mashhad, Iran (2004-2007). / Akbari V., Motagh M., Rajabi M.A., Djamour Y., Seddighi M. // 2008. USEReST 2008. Second Workshop on Use of Remote Sensing Techniques for Monitoring Volcanoes and Seismogenic Areas. - Naples, 11-14 Nov. 2008. - P. 1-4. ↑

C1767. Elton B.H. A Scalability Study on Multicore Cluster Systems of an AFRL Radar Frequency Tomography Imaging Code Written in MATLAB(r) for Parallel Execution Using Star-P(r). / Elton B.H., Magde K.M. // 2008. DOD HPCMP UGC DoD HPCMP Users Group Conference. - Seattle, WA, 14-17 July 2008. - P. 459-467. ↑

C1768. Ul-Ann Q. A point target reference spectrum based on Loffeld's bistatic formula (LBF) for hybrid configurations. / Ul-Ann Q., Loffeld O., Nies H., Wang R. // 2008. ICET 2008. 4th International Conference on Emerging Technologies. - Rawalpindi, 18-19 Oct. 2008. - P. 74-77. ↑

C1769. Ghoneim E. Mapping Water Basins in the Eastern Sahara by SRTM Data. / Ghoneim E., El-Baz F. // 2008. IGARSS 2008. IEEE International Geoscience and Remote Sensing Symposium. - Boston, MA, 7-11 July 2008. - Vol. 1. - P. I-1-I-4-1. ↑

- C1770.** Rincon R.F. Reconfigurable L-band radar. 2008. EuRAD 2008. European Radar Conference. - Amsterdam, 30-31 Oct. 2008. - P. 104-107. ↑
- C1771.** Zhao Heng-kai. Synthetic Digital Correlation for Combined Polarimetric Microwave Remote Sensing. / Zhao Heng-kai, Chen Hui-min, Chen Yi-feng, Wu You-yong. // 2008 China-Japan Joint Microwave Conference. - Shanghai, 10-12 Sept. 2008. - P. 669-672. ↑
- C1772.** Agrawal N. On-board SAR compression system based on back-propagation neural network. / Agrawal N., Venugopalan K. // 2008. EuRAD 2008. European Radar Conference. - Amsterdam, 30-31 Oct. 2008. - P. 380-383. ↑
- C1773.** Pieraccini M. Monitoring of bridges using coherent radar: Detection of longitudinal and torsional modes. / Pieraccini M., Fratini M., Parrini F., Atzeni C. // 2008. EuRAD 2008. European Radar Conference. - Amsterdam, 30-31 Oct. 2008. - P. 176-179. ↑
- C1774.** Armbrrecht G. Obstacle Based Concept for Compact Mode-Preserving Waveguide Transitions for High-Precision Radar Level Measurements. / Armbrrecht G., Denicke E., Pohl N., Musch T., Rolfes I. // 2008. EuMC 2008. 38th European Microwave Conference. - Amsterdam, 27-31 Oct. 2008. - P. 472-475. ↑
- C1775.** Shen Chiu. Radarsat-2 Moving Object Detection Experiment (MODEX). / Shen Chiu, Livingstone C., Sikaneta I., Gierull C., Beaulne P. // 2008. IGARSS 2008. IEEE International Geoscience and Remote Sensing Symposium. - Boston, MA, 7-11 July 2008. - Vol. 1. - P. I-13-I-16-13. ↑
- C1776.** Usman M. Acquisition of reflected GPS signals for remote sensing applications. / Usman M., Armitage D.W. // 2008. ICAST 2008. 2nd International Conference on Advances in Space Technologies. - Islamabad, 29-30 Nov. 2008. - P. 131-136. ↑
- C1777.** Feil P. Foreign Objects Debris Detection (FOD) on Airport Runways Using a Broadband 78 GHz Sensor. / Feil P., Menzel W., Nguyen T.P., Pichot C., Migliaccio C. // 2008. EuMC 2008. 38th European Microwave Conference. - Amsterdam, 27-31 Oct. 2008. - P. 1608-1611. ↑
- C1778.** Cote S. Twelve Years of Radarsat-1 Calibration: Operations Experience and Lessons Learned. / Cote S., Srivastava S.K., Hawkins R.K. // 2008. IGARSS 2008. IEEE International Geoscience and Remote Sensing Symposium. - Boston, MA, 7-11 July 2008. - Vol. 1. - P. I-5-I-8-5. ↑
- C1779.** Flett D. Initial Evaluation of Radarsat-2 for Operational Sea Ice Monitoring. / Flett D., de Abreu R., Arkett M., Gauthier M.-F. // 2008. IGARSS 2008. IEEE International Geoscience and Remote Sensing Symposium. - Boston, MA, 7-11 July 2008. - Vol. 1. - P. I-9-I-12-9. ↑
- C1780.** Agrawal N. Back propagation neural network approach for SAR raw data compression. / Agrawal N., Venugopalan K. // 2008. MILCOM 2008. IEEE Military Communications Conference. - San Diego, CA, 16-19 Nov. 2008. - P. 1-4. ↑
- C1781.** Sugimoto N. Lidar Network for Monitoring Asian Dust and Air Pollution Aerosols. / Sugimoto N., Matsui I., Shimizu A., Nishizawa T. // 2008. IGARSS 2008. IEEE International Geoscience and Remote Sensing Symposium. - Boston, MA, 7-11 July 2008. - Vol. 2. - P. II-573-II-576-573. ↑
- C1782.** Tebaldini S. Model Based SAR Tomography of Forested Areas. / Tebaldini S., Rocca F., Guarneri A.M. // 2008. IGARSS 2008. IEEE International Geoscience and Remote Sensing Symposium. - Boston, MA, 7-11 July 2008. - Vol. 2. - P. II-593-II-596-593. ↑
- C1783.** Reigber A. Multi-baseline coherence optimisation in partial and compact polarimetric modes. / Reigber A., Neumann M., Ferro-Famil L., Jager M., Prats P. // 2008. IGARSS 2008. IEEE International Geoscience and Remote Sensing Symposium. - Boston, MA, 7-11 July 2008. - Vol. 2. - P. II-597-II-600-597. ↑
- C1784.** McPherson C.J. Analysis of Sararan Dust Observations by Calipso in the Context of CRAM. / McPherson C.J., Reagan J.A. // 2008. IGARSS 2008. IEEE International Geoscience and Remote Sensing Symposium. - Boston, MA, 7-11 July 2008. - Vol. 2. - P. II-570-II-572-570. ↑
- C1785.** Dubois-Fernandez P. Polinsar at Low Frequency and Ionospheric Effects. / Dubois-Fernandez P., Angelliaume S., My-Linh truong-Loi, Freeman A., Pottier E. // 2008. IGARSS 2008. IEEE International Geoscience and Remote Sensing Symposium. - Boston, MA, 7-11 July 2008. - Vol. 2. - P. II-545-II-548-545. ↑

- C1786.** Chen Jie. Image Formation Algorithm for Topside Ionosphere Sounding with Spaceborne HF-SAR System. / Chen Jie, Li Zhuo, Liu Wei, Li Chunsheng, Zhou Yinqing. // 2008. IGARSS 2008. IEEE International Geoscience and Remote Sensing Symposium. - Boston, MA, 7-11 July 2008. - Vol. 2. - P. II-549-II-552-549. ↑
- C1787.** Reagan J.A. Using Combined 532 NM HSRL and 1064 NM Elastic-Scatter Lidar Observations to Verify and Update CRAM Dual-Wavelength Aerosol Retrieval Models. / Reagan J.A., McPherson C.J., Ferrare R., Hostetler C., Hair J. // 2008. IGARSS 2008. IEEE International Geoscience and Remote Sensing Symposium. - Boston, MA, 7-11 July 2008. - Vol. 2. - P. II-567-II-569-567. ↑
- C1788.** Fukuda S. Forest Spatial Structure Enhancing Non-Gaussian Texture in Airborne L-Band Polsar Images. 2008. IGARSS 2008. IEEE International Geoscience and Remote Sensing Symposium. - Boston, MA, 7-11 July 2008. - Vol. 2. - P. II-637-II-640-637. ↑
- C1789.** Angiuli E. Towards Complex-Valued Neural Algorithms for Forest Parameters Estimation from Polinsar Data. / Angiuli E., del Frate F., Polsinelli B., Solimini D. // 2008. IGARSS 2008. IEEE International Geoscience and Remote Sensing Symposium. - Boston, MA, 7-11 July 2008. - Vol. 2. - P. II-641-II-644-641. ↑
- C1790.** Sung-Hyun Kim. W-band 2-D Scanning Fully Polarimetric Radiometer System for Remote Sensing Applications. / Sung-Hyun Kim, Jin-Taek Seong, Hyuk Park, Ho-Jin Lee, Yong-Hoon Kim, Valeriy O., Alexander D. // 2008. IGARSS 2008. IEEE International Geoscience and Remote Sensing Symposium. - Boston, MA, 7-11 July 2008. - Vol. 2. - P. II-645-II-648-645. ↑
- C1791.** Wei Shunjun. Robust vegetation height Extraction using maximum likelihood estimation for Dual-baseline PolInSAR. / Wei Shunjun, Zhang Xiaoling, Han Di. // 2008. IGARSS 2008. IEEE International Geoscience and Remote Sensing Symposium. - Boston, MA, 7-11 July 2008. - Vol. 2. - P. II-633-II-636-633. ↑
- C1792.** Margarit G. A Public Database of Simulated Multidimensional SAR Data for Techniques Validation. / Margarit G., Mallorqui J.J., Corney I., Lopez-Martinez C. // 2008. IGARSS 2008. IEEE International Geoscience and Remote Sensing Symposium. - Boston, MA, 7-11 July 2008. - Vol. 2. - P. II-601-II-604-601. ↑
- C1793.** Wollersheim M. Extraction of Forest Biophysical Parameters Using Polarimetric SAR. / Wollersheim M., Collins M.J. // 2008. IGARSS 2008. IEEE International Geoscience and Remote Sensing Symposium. - Boston, MA, 7-11 July 2008. - Vol. 2. - P. II-625-II-628-625. ↑
- C1794.** Lopez-Martinez C. Analysis and Correction of Speckle Noise Effects on Polinsar Data Based on Coherent Modeling. / Lopez-Martinez C., Pipia L., Papathanassiou K.P. // 2008. IGARSS 2008. IEEE International Geoscience and Remote Sensing Symposium. - Boston, MA, 7-11 July 2008. - Vol. 2. - P. II-629-II-632-629. ↑
- C1795.** Quegan S. Quantifying and Correcting Ionospheric Effects on P-Band SAR Images. / Quegan S., Green J., Zandona-Schneider R., Scheiber R., Papathanassiou K. // 2008. IGARSS 2008. IEEE International Geoscience and Remote Sensing Symposium. - Boston, MA, 7-11 July 2008. - Vol. 2. - P. II-541-II-544-541. ↑
- C1796.** Neumann M. Modeling and Interpretation of the Multitemporal and Multibaseline Polinsar Coherence. / Neumann M., Ferro-Famil L., Reigber A. // 2008. IGARSS 2008. IEEE International Geoscience and Remote Sensing Symposium. - Boston, MA, 7-11 July 2008. - Vol. 2. - P. II-477-II-480-477. ↑
- C1797.** Ahmed R. Temporal Decorrelation Studies for Vegetation Parameter Estimation with Space-Borne Radars. / Ahmed R., Siqueira P., Hensley S., Chapman B., Bergen K. // 2008. IGARSS 2008. IEEE International Geoscience and Remote Sensing Symposium. - Boston, MA, 7-11 July 2008. - Vol. 2. - P. II-481-II-484-481. ↑
- C1798.** Brusch S. SAR Derived Wind Fields of Mesoscale Cyclones. / Brusch S., Lehner S., Reppucci A. // 2008. IGARSS 2008. IEEE International Geoscience and Remote Sensing Symposium. - Boston, MA, 7-11 July 2008. - Vol. 2. - P. II-489-II-492-489. ↑
- C1799.** Yong-sheng Zhou. Analysis of Temporal Decorrelation in Dual-Baseline Polinsar Vegetation Parameter Estimation. / Yong-sheng Zhou, Wen Hong, Fang Cao, Yan-ping Wang, Yi-rong Wu. // 2008. IGARSS 2008. IEEE International Geoscience and Remote Sensing Symposium. - Boston, MA, 7-11 July 2008. - Vol. 2. - P. II-473-II-476-473. ↑
- C1800.** Fornaro G. Detection of Single and Multiple Scatterers in Multibaseline Multitemporal SAR Data. / Fornaro G., Pauciuolo A., Lombardini F., Pardini M. // 2008. IGARSS 2008. IEEE International Geoscience and

Remote Sensing Symposium. - Boston, MA, 7-11 July 2008. - Vol. 2. - P. II-453-II-456-453. ↑

C1801. Lombardini F. 3D Tomographic and Differential Tomographic Response to Partially Coherent Scenes. / Lombardini F., Cai F. // 2008. IGARSS 2008. IEEE International Geoscience and Remote Sensing Symposium. - Boston, MA, 7-11 July 2008. - Vol. 2. - P. II-457-II-460-457. ↑

C1802. Praks J. SAR Coherence Tomography for Boreal Forest with Aid of Laser Measurements. / Praks J., Kugler F., Hyypä J., Papathanassiou K., Hallikainen M. // 2008. IGARSS 2008. IEEE International Geoscience and Remote Sensing Symposium. - Boston, MA, 7-11 July 2008. - Vol. 2. - P. II-469-II-472-469. ↑

C1803. Danklmayer A. Analysis of Atmospheric Propagation Effects in TerraSAR-X Images. / Danklmayer A., Doring B., Schwerdt M., Chandra M. // 2008. IGARSS 2008. IEEE International Geoscience and Remote Sensing Symposium. - Boston, MA, 7-11 July 2008. - Vol. 2. - P. II-533-II-536-533. ↑

C1804. Nicoll J.B. Mapping the Ionosphere Using L-Band SAR Data. / Nicoll J.B., Meyer F.J. // 2008. IGARSS 2008. IEEE International Geoscience and Remote Sensing Symposium. - Boston, MA, 7-11 July 2008. - Vol. 2. - P. II-537-II-540-537. ↑

C1805. Tomas S. Overview of Wind Lidar Techniques and Current Related Developments at the Technical University of Catalonia. / Tomas S., Munoz C., Sicard M., Rocabenbosch F., Rodriguez A., Comeron A. // 2008. IGARSS 2008. IEEE International Geoscience and Remote Sensing Symposium. - Boston, MA, 7-11 July 2008. - Vol. 2. - P. II-1120-II-1123-1120. ↑

C1806. Wegmuller U. Initial Assessment of the Applicability of TerraSAR-X for Repeat-Track Interferometry. / Wegmuller U., Werner C., Wiesmann A., Strozzi T., Santoro M. // 2008. IGARSS 2008. IEEE International Geoscience and Remote Sensing Symposium. - Boston, MA, 7-11 July 2008. - Vol. 2. - P. II-529-II-532-529. ↑

C1807. Congling Nie. RADARSAT ScanSAR Wind Retrieval and Rain Effects on ScanSAR Measurements Under Hurricane Conditions. / Congling Nie, Long D.G. // 2008. IGARSS 2008. IEEE International Geoscience and Remote Sensing Symposium. - Boston, MA, 7-11 July 2008. - Vol. 2. - P. II-493-II-496-493. ↑

C1808. Nguyen C.M. Gaussian model adaptive time domain filter (GMAT) for weather radars. / Nguyen C.M., Chandrasekar V., Moiseev D.N. // 2008. IGARSS 2008. IEEE International Geoscience and Remote Sensing Symposium. - Boston, MA, 7-11 July 2008. - Vol. 2. - P. II-509-II-512-509. ↑

C1809. Pasolli E. Automatic Detection and Classification of Buried Objects in GPR Images Using Genetic Algorithms and Support Vector Machines. / Pasolli E., Melgani F., Donelli M., Attoui R., de Vos M. // 2008. IGARSS 2008. IEEE International Geoscience and Remote Sensing Symposium. - Boston, MA, 7-11 July 2008. - Vol. 2. - P. II-525-II-528-525. ↑

C1810. Yamaki R. Singular Unit Restoration Based on Complex-Valued Markov Random Field Model for InSAR Interferograms. / Yamaki R., Hirose A. // 2008. IGARSS 2008. IEEE International Geoscience and Remote Sensing Symposium. - Boston, MA, 7-11 July 2008. - Vol. 2. - P. II-1076-II-1079-1076. ↑

C1811. Poulain V. High Resolution Remote Sensing Image Analysis with Exogenous Data: A Generic Framework. / Poulain V., Inglada J., Spigai M. // 2008. IGARSS 2008. IEEE International Geoscience and Remote Sensing Symposium. - Boston, MA, 7-11 July 2008. - Vol. 2. - P. II-1025-II-1028-1025. ↑

C1812. Jalobeanu A. Inferring Deformation Fields from Multisatellite Images. / Jalobeanu A., Fitzenz D. // 2008. IGARSS 2008. IEEE International Geoscience and Remote Sensing Symposium. - Boston, MA, 7-11 July 2008. - Vol. 2. - P. II-962-II-965-962. ↑

C1813. Lidicky L. Fourier Array Processing for Buried Victims Detection Using Ultra Wide Band Radar with Uncalibrated Sensors. 2008. IGARSS 2008. IEEE International Geoscience and Remote Sensing Symposium. - Boston, MA, 7-11 July 2008. - Vol. 2. - P. II-831-II-834-831. ↑

C1814. Das N.N. Characterization of Backscatter by Surface Features in L-Band Active Microwave Remote Sensing of Soil Moisture. / Das N.N., Mohanty B.P., Njoku E.G. // 2008. IGARSS 2008. IEEE International Geoscience and Remote Sensing Symposium. - Boston, MA, 7-11 July 2008. - Vol. 2. - P. II-817-II-820-817. ↑

C1815. Qiang Yin. Analysis of Valid Ranges in Soil Inversion Models Based on the Cloude-Pottier Decomposition. / Qiang Yin, Fang Cao, Wen Hong. // 2008. IGARSS 2008. IEEE International Geoscience and Remote Sensing Symposium. - Boston, MA, 7-11 July 2008. - Vol. 2. - P. II-821-II-824-821. ↑

Remote Sensing Symposium. - Boston, MA, 7-11 July 2008. - Vol. 2. - P. II-821-II-823-821. ↑

C1816. Xiaohui Yuan. An Adaptive Method for the Construction of Digital Terrain Model from Lidar Data. / Xiaohui Yuan, Liangmei Hu, Buckles B.P., Steinberg L., Sarma V. // 2008. IGARSS 2008. IEEE International Geoscience and Remote Sensing Symposium. - Boston, MA, 7-11 July 2008. - Vol. 2. - P. II-828-II-830-828. ↑

C1817. Lambers M. Automatic Point Target Detection for Interactive Visual Analysis of SAR Images. / Lambers M., Kolb A. // 2008. IGARSS 2008. IEEE International Geoscience and Remote Sensing Symposium. - Boston, MA, 7-11 July 2008. - Vol. 2. - P. II-903-II-906-903. ↑

C1818. Bangsen Tian. Non-Parameter Correlation Analysis in Polarimetric Signature and its Application to Change Detection in Polarimetric SAR. / Bangsen Tian, Zhen Li, Yongqian Wang. // 2008. IGARSS 2008. IEEE International Geoscience and Remote Sensing Symposium. - Boston, MA, 7-11 July 2008. - Vol. 2. - P. II-891-II-894-891. ↑

C1819. Amolins K. Classification of Lidar Data Using Standard Deviation of Elevation and Characteristic Point Features. / Amolins K., Yun Zhang, Dare P. // 2008. IGARSS 2008. IEEE International Geoscience and Remote Sensing Symposium. - Boston, MA, 7-11 July 2008. - Vol. 2. - P. II-871-II-874-871. ↑

C1820. Huan Ruohong. SAR Target Recognition Based on MRF and Gabor Wavelet Feature Extraction. / Huan Ruohong, Yang Ruliang. // 2008. IGARSS 2008. IEEE International Geoscience and Remote Sensing Symposium. - Boston, MA, 7-11 July 2008. - Vol. 2. - P. II-907-II-910-907. ↑

C1821. Hu De-yong. Texture Analysis and its Application for Single-Band SAR Thematic Information Extraction. / Hu De-yong, Li Xiao-juan, Zhao Wen-ji, Gong Hui-li. // 2008. IGARSS 2008. IEEE International Geoscience and Remote Sensing Symposium. - Boston, MA, 7-11 July 2008. - Vol. 2. - P. II-935-II-938-935. ↑

C1822. Bagan H. Extended Subspace Method for Remote Sensing Image Classification. / Bagan H., Takeuchi W., Aosier B., Kaneko M., Xiaohui Wang, Yasuoka Y. // 2008. IGARSS 2008. IEEE International Geoscience and Remote Sensing Symposium. - Boston, MA, 7-11 July 2008. - Vol. 2. - P. II-927-II-930-927. ↑

C1823. Bin Zou. Super-Resolution of Polarimetric SAR Images Based on Target Decomposition and Polarimetric Spatial Correlation. / Bin Zou, Huijun Hao, Xingjie Guo. // 2008. IGARSS 2008. IEEE International Geoscience and Remote Sensing Symposium. - Boston, MA, 7-11 July 2008. - Vol. 2. - P. II-911-II-914-911. ↑

C1824. Ruijing Sun. A New Method to Retrieve Soil Moisture at Bare Soil Surface Using ERS Scatterometer Data. / Ruijing Sun, Jinyang Du, Jiancheng Shi, Lingmei Jiang. // 2008. IGARSS 2008. IEEE International Geoscience and Remote Sensing Symposium. - Boston, MA, 7-11 July 2008. - Vol. 2. - P. II-813-II-816-813. ↑

C1825. Xin Li. An Airborne Remote Sensing Experiment for Catchment-Scale Water Cycle Study in a Typical Inland River Basin of China. / Xin Li, Jian Wang, Mingguo Ma, Zeyong Hu, Tao Che, Peixi Su, Rui Jin, Weizhen Wang, Qiang Liu, Qing Xiao, Qinhua Liu. // 2008. IGARSS 2008. IEEE International Geoscience and Remote Sensing Symposium. - Boston, MA, 7-11 July 2008. - Vol. 2. - P. II-699-II-702-699. ↑

C1826. Trudel M. Surface Roughness Classification with Multipolarized C-Band SAR Data. / Trudel M., Charbonneau F., Leconte R. // 2008. IGARSS 2008. IEEE International Geoscience and Remote Sensing Symposium. - Boston, MA, 7-11 July 2008. - Vol. 2. - P. II-727-II-730-727. ↑

C1827. Niang M.A. Potential of C-Band Multipolarized and Polarimetric SAR for Soil Drainage Classification and Mapping. / Niang M.A., Nolin M.C., Bernier M., Perron I. // 2008. IGARSS 2008. IEEE International Geoscience and Remote Sensing Symposium. - Boston, MA, 7-11 July 2008. - Vol. 2. - P. II-734-II-737-734. ↑

C1828. Liu W.T. High Wind and Power Density Over Global Oceans. / Liu W.T., Wenqing Tang, Xiaosu Xie. // 2008. IGARSS 2008. IEEE International Geoscience and Remote Sensing Symposium. - Boston, MA, 7-11 July 2008. - Vol. 2. - P. II-672-II-675-672. ↑

C1829. Pichel W.G. High-Velocity Wind Measurements Using Synthetic Aperture Radar. / Pichel W.G., Xiaofeng Li, Monaldo F., Sikora T., Jackson C. // 2008. IGARSS 2008. IEEE International Geoscience and Remote Sensing Symposium. - Boston, MA, 7-11 July 2008. - Vol. 2. - P. II-661-II-663-661. ↑

C1830. Williams B.A. Rain and Wind Estimation from Seawinds in Hurricanes at Ultra High Resolution. / Williams B.A., Long D.G. // 2008. IGARSS 2008. IEEE International Geoscience and Remote Sensing Symposium. - Boston, MA, 7-11 July 2008. - Vol. 2. - P. II-661-II-663-661. ↑

Symposium. - Boston, MA, 7-11 July 2008. - Vol. 2. - P. II-664-II-667-664. ↑

C1831. Bourassa M.A. Scatterometer-Derived Wind Fields for Mid-Latitude Storms. 2008. IGARSS 2008. IEEE International Geoscience and Remote Sensing Symposium. - Boston, MA, 7-11 July 2008. - Vol. 2. - P. II-668-II-671-668. ↑

C1832. Heitz S. Active and Passive Microwave Sensors as a Tool to Monitor Soil Moisture Over Winter. / Heitz S., Matgen P., Schumann G., Pfister L. // 2008. IGARSS 2008. IEEE International Geoscience and Remote Sensing Symposium. - Boston, MA, 7-11 July 2008. - Vol. 2. - P. II-773-II-776-773. ↑

C1833. Mladenova I. KU-Band Sensitivity to Soil Moisture. An Evaluation Study for Monitoring Temporal Soil Moisture Change Detection Over the NAFE06 Study Area. / Mladenova I., Lakshmi V., Jackson T., Walker J. // 2008. IGARSS 2008. IEEE International Geoscience and Remote Sensing Symposium. - Boston, MA, 7-11 July 2008. - Vol. 2. - P. II-805-II-808-805. ↑

C1834. Quan Chert. Soil Moisture Change Retrieval Using S-Band Radar Data During SGP99 and SMEX02. / Quan Chert, Zhen Li, Lei Wang, Yun Shao, Tianhai Cheng. // 2008. IGARSS 2008. IEEE International Geoscience and Remote Sensing Symposium. - Boston, MA, 7-11 July 2008. - Vol. 2. - P. II-809-II-812-809. ↑

C1835. Scipal K. Error Estimation of Soil Moisture Derived from Active and Passive Microwave Satellite Observations and Model Data. / Scipal K., Holmes T., de Jeu R., Naeimi V., Wagner W. // 2008. IGARSS 2008. IEEE International Geoscience and Remote Sensing Symposium. - Boston, MA, 7-11 July 2008. - Vol. 2. - P. II-761-II-764-761. ↑

C1836. Shao Yun. SAR Remote Sensing Data for Subsurface Targets Detection and Lop Nur Lake Evolution and Extinction Study. / Shao Yun, Gong Huaze, Dong Qing. // 2008. IGARSS 2008. IEEE International Geoscience and Remote Sensing Symposium. - Boston, MA, 7-11 July 2008. - Vol. 2. - P. II-738-II-741-738. ↑

C1837. Susaki J. Calibration of IEM Model for the Soil Moisture Mapping of Non-Inundated Paddy Fields Using ALOS/PALSAR Data. 2008. IGARSS 2008. IEEE International Geoscience and Remote Sensing Symposium. - Boston, MA, 7-11 July 2008. - Vol. 2. - P. II-753-II-756-753. ↑

C1838. Arakelyan A. Preliminary Polarimetric Measurements of Bare and Vegetated Soils Radar Backscattering Coefficients and Brightness Temperatures Angular Dependences at 15GHz. / Arakelyan A., Grigoryan M., Hakobyan I., Hambaryan A., Karyan V., Manukyan M., Hovhannisyan G. // 2008. IGARSS 2008. IEEE International Geoscience and Remote Sensing Symposium. - Boston, MA, 7-11 July 2008. - Vol. 2. - P. II-757-II-760-757. ↑

C1839. Costantini M. A New Method for Identification and Analysis of Persistent Scatterers in Series of SAR Images. / Costantini M., Falco S., Malvarosa F., Minati F. // 2008. IGARSS 2008. IEEE International Geoscience and Remote Sensing Symposium. - Boston, MA, 7-11 July 2008. - Vol. 2. - P. II-449-II-452-449. ↑

C1840. Schwerdt M. TerraSAR-X Calibration Results. / Schwerdt M., Brautigam B., Bachmann M., Doring B., Schrank D., Gonzalez J.H. // 2008. IGARSS 2008. IEEE International Geoscience and Remote Sensing Symposium. - Boston, MA, 7-11 July 2008. - Vol. 2. - P. II-205-II-208-205. ↑

C1841. Breit H. TerraSAR-X Payload Data Processing: Results from Commissioning and Early Operational Phase. / Breit H., Schattler B., Fritz T., Damerow H., Schwarz E., Balss U. // 2008. IGARSS 2008. IEEE International Geoscience and Remote Sensing Symposium. - Boston, MA, 7-11 July 2008. - Vol. 2. - P. II-209-II-212-209. ↑

C1842. Tello M. A Novel Strategy for Radar Imaging Based on Compressive Sensing. / Tello M., Lopez-Dekker P., Mallorqui J.J. // 2008. IGARSS 2008. IEEE International Geoscience and Remote Sensing Symposium. - Boston, MA, 7-11 July 2008. - Vol. 2. - P. II-213-II-216-213. ↑

C1843. Mittermayer J. TerraSAR-X Instrument, SAR System Performance & Command Generation. / Mittermayer J., Metzger R., Steinbrecher U., Gonzalez C., Polimeni D., Boer J., Younis M., Marquez J., Wollstadt S., Schulze D., Meta A., Tous-Ramon N., Ortega-Miguez C. // 2008. IGARSS 2008. IEEE International Geoscience and Remote Sensing Symposium. - Boston, MA, 7-11 July 2008. - Vol. 2. - P. II-201-II-204-201. ↑

C1844. Kangwook Kim. Thermal Noise Analysis on the Resistive Vee Dipole Antenna for Ground-Penetrating Radar Applications. / Kangwook Kim, Chang Won Jung. // 2008. IGARSS 2008. IEEE International Geoscience

and Remote Sensing Symposium. - Boston, MA, 7-11 July 2008. - Vol. 2. - P. II-185-II-188-185. ↑

C1845. Gunnala S.K. Subsurface Sensing of Near Surface Object Using Cavity Backed Slot (CBS) Antenna. / Gunnala S.K., Mingyu Lu, Bredow J.W., Tjuatja S. // 2008. IGARSS 2008. IEEE International Geoscience and Remote Sensing Symposium. - Boston, MA, 7-11 July 2008. - Vol. 2. - P. II-189-II-192-189. ↑

C1846. Mittermayer J. TerraSAR-X Commissioning Phase Execution and Results. / Mittermayer J., Schattler B., Younis M. // 2008. IGARSS 2008. IEEE International Geoscience and Remote Sensing Symposium. - Boston, MA, 7-11 July 2008. - Vol. 2. - P. II-197-II-200-197. ↑

C1847. Dongryeol Ryu. Soil Moisture Retrieval Using an L-Band Synthetic Aperture Radiometer During the Soil Moisture Experiments 2003 (SMEX03) and 2004 (SMEX04). / Dongryeol Ryu, Thomas J.J., Bindlish R., Le Vine D.M., Haken M. // 2008. IGARSS 2008. IEEE International Geoscience and Remote Sensing Symposium. - Boston, MA, 7-11 July 2008. - Vol. 2. - P. II-233-II-236-233. ↑

C1848. Bindlish R. Combined Passive and Active Soil Moisture Observations During CLASIC. / Bindlish R., Jackson T., Cosh M., Ruijing Sun, Yueh S., Dinardo S. // 2008. IGARSS 2008. IEEE International Geoscience and Remote Sensing Symposium. - Boston, MA, 7-11 July 2008. - Vol. 2. - P. II-237-II-240-237. ↑

C1849. Yueh S. Passive and Active L-Band System and Observations during the 2007 CLASIC Campaign. / Yueh S., Dinardo S., Chan S., Njoku E., Jackson T., Bindlish R. // 2008. IGARSS 2008. IEEE International Geoscience and Remote Sensing Symposium. - Boston, MA, 7-11 July 2008. - Vol. 2. - P. II-241-II-244-241. ↑

C1850. Kohlleppe R. Enhancement of Along-Track Interferometry for Ground Moving Target Indication. / Kohlleppe R., Gierull C.H. // 2008. IGARSS 2008. IEEE International Geoscience and Remote Sensing Symposium. - Boston, MA, 7-11 July 2008. - Vol. 2. - P. II-229-II-232-229. ↑

C1851. Tao Xiong. Volume Coherence Estimation for Random Forest Height Retrieval Based on Polinsar Data. / Tao Xiong, Guangyi Zhou, Jian Yang, Weijie Zhang. // 2008. IGARSS 2008. IEEE International Geoscience and Remote Sensing Symposium. - Boston, MA, 7-11 July 2008. - Vol. 2. - P. II-217-II-220-217. ↑

C1852. Junghyo Kim. Investigation of a New Multifunctional High Performance SAR System Concept Exploiting MIMO Technology. / Junghyo Kim, Wiesbeck W. // 2008. IGARSS 2008. IEEE International Geoscience and Remote Sensing Symposium. - Boston, MA, 7-11 July 2008. - Vol. 2. - P. II-221-II-224-221. ↑

C1853. Nunziata F. On the Use of Dual-Polarized SAR Data for Oil Spill Observation. / Nunziata F., Gambardella A., Migliaccio M. // 2008. IGARSS 2008. IEEE International Geoscience and Remote Sensing Symposium. - Boston, MA, 7-11 July 2008. - Vol. 2. - P. II-225-II-228-225. ↑

C1854. Sato M. Dual Sensor ALIS for Humanitarian Demining and its Evaluation Test in Mine Fields in Croatia. 2008. IGARSS 2008. IEEE International Geoscience and Remote Sensing Symposium. - Boston, MA, 7-11 July 2008. - Vol. 2. - P. II-181-II-184-181. ↑

C1855. Eineder M. High Bandwidth Spotlight SAR Interferometry with TerraSAR-X. / Eineder M., Adam N., Brcic R., Yague-Martinez N., Fritz T. // 2008. IGARSS 2008. IEEE International Geoscience and Remote Sensing Symposium. - Boston, MA, 7-11 July 2008. - Vol. 2. - P. II-113-II-116-113. ↑

C1856. Adam N. High Resolution Interferometric Stacking with TerraSAR-X. / Adam N., Eineder M., Yague-Martinez N., Bamler R. // 2008. IGARSS 2008. IEEE International Geoscience and Remote Sensing Symposium. - Boston, MA, 7-11 July 2008. - Vol. 2. - P. II-117-II-120-117. ↑

C1857. Moon Y. Precise Orbit and Baseline Determination for TerraSAR-X and TanDEM-X. / Moon Y., Koenig R., Michalak G., Rothacher M. // 2008. IGARSS 2008. IEEE International Geoscience and Remote Sensing Symposium. - Boston, MA, 7-11 July 2008. - Vol. 2. - P. II-121-II-124-121. ↑

C1858. Denis L. A Regularization Approach for InSAR and Optical Data Fusion. / Denis L., Tupin F., Darbon J., Sigelle M. // 2008. IGARSS 2008. IEEE International Geoscience and Remote Sensing Symposium. - Boston, MA, 7-11 July 2008. - Vol. 2. - P. II-97-II-100-97. ↑

C1859. Cossio T. Performance Prediction for Low-SNR Lidar Sensors. / Cossio T., Slatton K.C., Shrestha K., Carter W.E. // 2008. IGARSS 2008. IEEE International Geoscience and Remote Sensing Symposium. - Boston, MA, 7-11 July 2008. - Vol. 2. - P. II-81-II-84-81. ↑

- C1860.** Lach S.R. Robust Extraction of Exterior Building Boundaries from Topographic Lidar Data. / Lach S.R., Kerekes J.P. // 2008. IGARSS 2008. IEEE International Geoscience and Remote Sensing Symposium. - Boston, MA, 7-11 July 2008. - Vol. 2. - P. II-85-II-88-85. ↑
- C1861.** Cho P. 3D Organization of 2D Urban Imagery. 2008. IGARSS 2008. IEEE International Geoscience and Remote Sensing Symposium. - Boston, MA, 7-11 July 2008. - Vol. 2. - P. II-89-II-92-89. ↑
- C1862.** Frankford M.T. Compensation of Faraday Rotation in Multi-Polarization Scatterometry. / Frankford M.T., Johnson J.T. // 2008. IGARSS 2008. IEEE International Geoscience and Remote Sensing Symposium. - Boston, MA, 7-11 July 2008. - Vol. 2. - P. II-169-II-172-169. ↑
- C1863.** Bartalis Z. Validation of Coarse Resolution Microwave Soil Moisture Products. / Bartalis Z., Wagner W., Anderson C., Bonekamp H., Naeimi V., Hasenauer S. // 2008. IGARSS 2008. IEEE International Geoscience and Remote Sensing Symposium. - Boston, MA, 7-11 July 2008. - Vol. 2. - P. II-173-II-176-173. ↑
- C1864.** Yuksel S.E. Hierarchical Methods for Landmine Detection with Wideband Electro-Magnetic Induction and Ground Penetrating Radar Multi-Sensor Systems. / Yuksel S.E., Ramachandran G., Gader P., Wilson J., Ho D., Gyeongyong Heo. // 2008. IGARSS 2008. IEEE International Geoscience and Remote Sensing Symposium. - Boston, MA, 7-11 July 2008. - Vol. 2. - P. II-177-II-180-177. ↑
- C1865.** Weissman D.E. The Effect of Rain on Satellite Sensor Estimates of Surface Roughness Conditions and on the Air-Sea Momentum Flux. / Weissman D.E., Bourassa M.A. // 2008. IGARSS 2008. IEEE International Geoscience and Remote Sensing Symposium. - Boston, MA, 7-11 July 2008. - Vol. 2. - P. II-165-II-168-165. ↑
- C1866.** Bachmann C.M. Very Shallow Water Bathymetry Retrieval from Hyperspectral Imagery at the Virginia Coast Reserve (VCR'07) Multi-Sensor Campaign. / Bachmann C.M., Montes M.J., Fusina R.A., Parrish C., Sellars J., Weidemann A., Goode W., Nichols C.R., Woodward P., McIlhany K., Hill V., Zimmerman R., Korwan D., Truitt B., Schwarzschild A. // 2008. IGARSS 2008. IEEE International Geoscience and Remote Sensing Symposium. - Boston, MA, 7-11 July 2008. - Vol. 2. - P. II-125-II-128-125. ↑
- C1867.** Goodenough D.G. Comparison of Aviris and AISA Airborne Hyperspectral Sensing for Above-Ground Forest Carbon Mapping. / Goodenough D.G., Niemann K.O., Dyk A., Hobart G., Gordon P., Loisel M., Hao Chen. // 2008. IGARSS 2008. IEEE International Geoscience and Remote Sensing Symposium. - Boston, MA, 7-11 July 2008. - Vol. 2. - P. II-129-II-132-129. ↑
- C1868.** Manninen T. Subarctic Boreal Forest Albedo Estimation Using Envisat ASAR for BRDF Determination. / Manninen T., Riihela A. // 2008. IGARSS 2008. IEEE International Geoscience and Remote Sensing Symposium. - Boston, MA, 7-11 July 2008. - Vol. 2. - P. II-145-II-148-145. ↑
- C1869.** Bernhardt P. Detection of Ionospheric Structures with L-Band Synthetic Aperture Radars. / Bernhardt P., Ainsworth T., Groves K., Beach T., Caton R.G., Carrano C.S., Alcalá C.M., Sponseller D.D. // 2008. IGARSS 2008. IEEE International Geoscience and Remote Sensing Symposium. - Boston, MA, 7-11 July 2008. - Vol. 2. - P. II-395-II-397-395. ↑
- C1870.** Joseph A.T. A Vegetation Correction Methodology Applied for Soil Moisture Retrieval from C-Band Radar Observations. / Joseph A.T., O'Neill P.E., van der Velde R., Lang R., Gish T. // 2008. IGARSS 2008. IEEE International Geoscience and Remote Sensing Symposium. - Boston, MA, 7-11 July 2008. - Vol. 2. - P. II-398-II-401-398. ↑
- C1871.** Yisok Oh. Inversion Algorithm for Soil Moisture Retrieval from Polarimetric Backscattering Coefficients of Vegetation Canopies. / Yisok Oh, Seung-Gun Jung. // 2008. IGARSS 2008. IEEE International Geoscience and Remote Sensing Symposium. - Boston, MA, 7-11 July 2008. - Vol. 2. - P. II-402-II-405-402. ↑
- C1872.** Meyer F.J. The Impact of the Ionosphere on Interferometric SAR Processing. / Meyer F.J., Nicoll J. // 2008. IGARSS 2008. IEEE International Geoscience and Remote Sensing Symposium. - Boston, MA, 7-11 July 2008. - Vol. 2. - P. II-391-II-394-391. ↑
- C1873.** Buckreuss S. Status Report on the TerraSAR-X Mission. / Buckreuss S., Roth A. // 2008. IGARSS 2008. IEEE International Geoscience and Remote Sensing Symposium. - Boston, MA, 7-11 July 2008. - Vol. 2. - P. II-379-II-382-379. ↑
- C1874.** Lisini G. Rapid Land Mapping by TerraSAR-X VHR Data. / Lisini G., Acqua D., Gamba P. // 2008.

IGARSS 2008. IEEE International Geoscience and Remote Sensing Symposium. - Boston, MA, 7-11 July 2008. - Vol. 2. - P. II-383-II-386-383. ↑

C1875. Shimada M. Discovery of Anomalous Stripes Over the Amazon by the PALSAR onboard ALOS satellite. / Shimada M., Muraki Y., Otsuka Y. // 2008. IGARSS 2008. IEEE International Geoscience and Remote Sensing Symposium. - Boston, MA, 7-11 July 2008. - Vol. 2. - P. II-387-II-390-387. ↑

C1876. Bockmann C. From EARLINET-ASOS Raman-Lidar Signals to Microphysical Aerosol Properties Via Advanced Regularizing Software. / Bockmann C., Muller D., Osterloh L., Pornsawad P., Papayannis A. // 2008. IGARSS 2008. IEEE International Geoscience and Remote Sensing Symposium. - Boston, MA, 7-11 July 2008. - Vol. 2. - P. II-422-II-425-422. ↑

C1877. Nannini M. On the Minimum Number of Tracks for SAR Tomography. / Nannini M., Scheiber R., Moreira A. // 2008. IGARSS 2008. IEEE International Geoscience and Remote Sensing Symposium. - Boston, MA, 7-11 July 2008. - Vol. 2. - P. II-441-II-444-441. ↑

C1878. Frey O. Combining Time-Domain Back-Projection and Capon Beamforming for Tomographic SAR Processing. / Frey O., Meier E. // 2008. IGARSS 2008. IEEE International Geoscience and Remote Sensing Symposium. - Boston, MA, 7-11 July 2008. - Vol. 2. - P. II-445-II-448-445. ↑

C1879. Mitev V. Backscatter Lidar Measurement in the Atmospheric Boundary Layer: Data Analysis and Interpretation Capabilities. / Mitev V., Matthey R., Martucci G., Frioud M. // 2008. IGARSS 2008. IEEE International Geoscience and Remote Sensing Symposium. - Boston, MA, 7-11 July 2008. - Vol. 2. - P. II-418-II-421-418. ↑

C1880. Daniel S. Surface Parameter Estimation Over Periodic Surfaces Using a Time-Frequency Approach. / Daniel S., Allain S., Ferro-Famil L., Pottier E. // 2008. IGARSS 2008. IEEE International Geoscience and Remote Sensing Symposium. - Boston, MA, 7-11 July 2008. - Vol. 2. - P. II-406-II-409-406. ↑

C1881. Rocadenbosch F. The European Aerosol Research Lidar Network (EARLINET): An Overview. / Rocadenbosch F., Mattis I., Ansmann A., Wandinger U., Bockmann C., Pappalardo G., Amodeo A., Bosenberg J., Alados-Arboledas L., Apituley A., Balis D., Chaikovskiy A., Comeron A., Munoz C., Sicard M., Freudenthaler V., Wiegner M., Gustafsson O., Hansen G., Mamouri R.-E., Papayannis A., Mitev V., Nicolae D., Perez C., Perrone M.R., Pietruczuk A., Pujadas M., Putaud J.-P., Ravetta F., Rizi V., Simeonov V., Spinelli N., Stoyanov D., Trickl T. // 2008. IGARSS 2008. IEEE International Geoscience and Remote Sensing Symposium. - Boston, MA, 7-11 July 2008. - Vol. 2. - P. II-410-II-413-410. ↑

C1882. Apituley A. Earlinet Approach to Optimisation of Individual Network Instruments with the Aim of Homogenisation of Aerosol Data Products and Increased Data Coverage. / Apituley A., Freudenthaler V., Comeron A., Rocadenbosch F. // 2008. IGARSS 2008. IEEE International Geoscience and Remote Sensing Symposium. - Boston, MA, 7-11 July 2008. - Vol. 2. - P. II-414-II-417-414. ↑

C1883. Frigui H. Context-Dependent Multi-Sensor Fusion for Landmine Detection. / Frigui H., Lijun Zhang, Gader P. // 2008. IGARSS 2008. IEEE International Geoscience and Remote Sensing Symposium. - Boston, MA, 7-11 July 2008. - Vol. 2. - P. II-371-II-374-371. ↑

C1884. Goodenough D.G. Data Fusion Study Between Polarimetric SAR, Hyperspectral and Lidar Data for Forest Information. / Goodenough D.G., Hao Chen, Dyk A., Hobart G., Richardson A. // 2008. IGARSS 2008. IEEE International Geoscience and Remote Sensing Symposium. - Boston, MA, 7-11 July 2008. - Vol. 2. - P. II-281-II-284-281. ↑

C1885. Touzi R. Scattering type phase for wetland classification using C-band polarimetric SAR. / Touzi R., Deschamps A., Rother G. // 2008. IGARSS 2008. IEEE International Geoscience and Remote Sensing Symposium. - Boston, MA, 7-11 July 2008. - Vol. 2. - P. II-285-II-288-285. ↑

C1886. Sato R. Seasonal Change Monitoring of Wetlands by Using Airborne and Satellite PolSAR Sensing. / Sato R., Yamaguchi Y., Yamada H., Boerner W.-M. // 2008. IGARSS 2008. IEEE International Geoscience and Remote Sensing Symposium. - Boston, MA, 7-11 July 2008. - Vol. 2. - P. II-289-II-292-289. ↑

C1887. Bruzzone L. A Novel Protocol for Accuracy Assessment in Classification of Very High Resolution Multispectral and SAR Images. / Bruzzone L., Persello C. // 2008. IGARSS 2008. IEEE International Geoscience and Remote Sensing Symposium. - Boston, MA, 7-11 July 2008. - Vol. 2. - P. II-265-II-268-265. ↑

- C1888.** Disney M.I. Quantifying Surface Reflectivity for Spaceborne Lidar Missions. / Disney M.I., Lewis P., Bouvet M. // 2008. IGARSS 2008. IEEE International Geoscience and Remote Sensing Symposium. - Boston, MA, 7-11 July 2008. - Vol. 2. - P. II-249-II-252-249. ↑
- C1889.** Belkhouche M.Y. A Preprocessing Method for Automatic Break Lines Detection. / Belkhouche M.Y., Buckles B.P., Xiaohui Yuan, Steinberg L. // 2008. IGARSS 2008. IEEE International Geoscience and Remote Sensing Symposium. - Boston, MA, 7-11 July 2008. - Vol. 2. - P. II-253-II-256-253. ↑
- C1890.** Baker B.J. Fourier Error Analysis of Ray Tracing on a Geospatial Polygonal Model. 2008. IGARSS 2008. IEEE International Geoscience and Remote Sensing Symposium. - Boston, MA, 7-11 July 2008. - Vol. 2. - P. II-257-II-260-257. ↑
- C1891.** Mityagina M. Dynamic Phenomena in the Coastal Waters of the North-Eastern Black Sea Retrieved from Satellite Data. / Mityagina M., Lavrova O. // 2008. IGARSS 2008. IEEE International Geoscience and Remote Sensing Symposium. - Boston, MA, 7-11 July 2008. - Vol. 2. - P. II-347-II-350-347. ↑
- C1892.** Mitnik L.M. Advanced Land Observing Satellite PALSAR Observations of the Oceanic Dynamic Phenomena in the Coastal Zone. 2008. IGARSS 2008. IEEE International Geoscience and Remote Sensing Symposium. - Boston, MA, 7-11 July 2008. - Vol. 2. - P. II-351-II-354-351. ↑
- C1893.** Torrione P. Statistical Models for Landmine Detection in Ground Penetrating Radar: Applications to Synthetic Data Generation and Pre-Screening. / Torrione P., Collins L. // 2008. IGARSS 2008. IEEE International Geoscience and Remote Sensing Symposium. - Boston, MA, 7-11 July 2008. - Vol. 2. - P. II-367-II-370-367. ↑
- C1894.** Bourassa M.A. The Influence of Air Density on Scatterometer Retrievals of Surface Turbulent Stress. / Bourassa M.A., Weissman D.E. // 2008. IGARSS 2008. IEEE International Geoscience and Remote Sensing Symposium. - Boston, MA, 7-11 July 2008. - Vol. 2. - P. II-343-II-346-343. ↑
- C1895.** Boerner W.-M. Recent Advances in POL-SAR & POL-IN-SAR Imaging of Natural Habitats and Wetland Remote Sensing. / Boerner W.-M., Yamaguchi Y. // 2008. IGARSS 2008. IEEE International Geoscience and Remote Sensing Symposium. - Boston, MA, 7-11 July 2008. - Vol. 2. - P. II-293-II-294-293. ↑
- C1896.** Freedman A.P. The Detection and Mitigation of RFI with the Aquarius L-Band Scatterometer. / Freedman A.P., Piepmeier J.R., Fischman M.A., McWatters D.A., Spencer M.W. // 2008. IGARSS 2008. IEEE International Geoscience and Remote Sensing Symposium. - Boston, MA, 7-11 July 2008. - Vol. 2. - P. II-319-II-322-319. ↑
- C1897.** Ebuchi N. Cross-Validation of Wind Products from Seawinds and AMSR on ADEOS-II. 2008. IGARSS 2008. IEEE International Geoscience and Remote Sensing Symposium. - Boston, MA, 7-11 July 2008. - Vol. 2. - P. II-339-II-342-339. ↑
- C1898.** Ferretti A. Volcanic Deformation Mapping using PSInSARTM: Piton de la Fournaise, Stromboli and Vulcano test sites for the Globvolcano project. / Ferretti A., Bianchi M., Novali F., Tamburini A., Rucci A. // 2008. USEReST 2008. Second Workshop on Use of Remote Sensing Techniques for Monitoring Volcanoes and Seismogenic Areas. - Naples, 11-14 Nov. 2008. - P. 1-5. ↑
- C1899.** Ying Li. Remote sensing image fusion based on fast discrete curvelet transform. / Ying Li, Xing Xu, Ben-Du Bai, Yan-Ning Zhang. // 2008 International Conference on Machine Learning and Cybernetics. - Kunming, 12-15 July 2008. - Vol. 1. - P. 106-109. ↑
- C1900.** Kohut J. The Mid-Atlantic Regional Coastal Ocean Observing System: Serving coast guard needs in the mid-atlantic bight. / Kohut J., Roarty H., Lichtenwalner S., Glenn S., Barrick D., Lipa B., Allen A. // 2008 IEEE/OES US/EU-Baltic International Symposium. - Tallinn, 27-29 May 2008. - P. 1-5. ↑
- C1901.** Klemas V. Remote sensing of coastal ecosystems. 2008 IEEE/OES US/EU-Baltic International Symposium. - Tallinn, 27-29 May 2008. - P. 1-11. ↑
- C1902.** Yue X.J. Multi-photo combined adjustment with airborne SAR images based on a few ground control points. / Yue X.J., Huang G.M. // 2008. EORSA 2008. International Workshop on Earth Observation and Remote Sensing Applications. - Beijing, June 30 2008-July 2 2008. - P. 1-4. ↑
- C1903.** Yong Liang. Road tracking by Parallel Angular Texture Signature. / Yong Liang, Jing Shen, Xiangguo

Lin, Junfang Bi, Ying Li. // 2008. EORSA 2008. International Workshop on Earth Observation and Remote Sensing Applications. - Beijing, June 30 2008-July 2 2008. - P. 1-6. ↑

C1904. Li H.T. Object-oriented classification of polarimetric SAR imagery based on Statistical Region Merging and Support Vector Machine. / Li H.T., Gu H.Y., Han Y.S., Yang J.H. // 2008. EORSA 2008. International Workshop on Earth Observation and Remote Sensing Applications. - Beijing, June 30 2008-July 2 2008. - P. 1-6. ↑

C1905. Xiaoye Liu. Ground truth extraction from LiDAR data for image orthorectification. / Xiaoye Liu, Zhenyu Zhang. // 2008. EORSA 2008. International Workshop on Earth Observation and Remote Sensing Applications. - Beijing, June 30 2008-July 2 2008. - P. 1-6. ↑

C1906. Migliaccio M. Ship detection over single-look complex SAR images. / Migliaccio M., Gambardella A., Nunziata F. // 2008 IEEE/OES US/EU-Baltic International Symposium. - Tallinn, 27-29 May 2008. - P. 1-4. ↑

C1907. Migliaccio M. Polarimetric signature for oil spill observation. / Migliaccio M., Nunziata F., Gambardella A. // 2008 IEEE/OES US/EU-Baltic International Symposium. - Tallinn, 27-29 May 2008. - P. 1-5. ↑

C1908. Alias A.N. EASI Modelling Algorithms for Aerosol-Cloud Distribution Analysis. / Alias A.N., MatJafri M.Z., Lim H.S., Abdullah K., Saleh N.M. // 2008. CGIV '08. Fifth International Conference on Computer Graphics, Imaging and Visualisation. - Penang, 26-28 Aug. 2008. - P. 193-196. ↑

C1909. Uiboupin R. Detection of oil spills on SAR images, identification of polluters and forecast of the slicks trajectory. / Uiboupin R., Raudsepp U., Sipelgas L. // 2008 IEEE/OES US/EU-Baltic International Symposium. - Tallinn, 27-29 May 2008. - P. 1-5. ↑

C1910. Kaitala S. Recent advances in ferrybox monitoring on board Finnmaid ferry. / Kaitala S., Seppala J., Raateoja M., Hallfors S., Fleming-Lehtinen V., Maunula P., Helminen J., Ylostalo P. // 2008 IEEE/OES US/EU-Baltic International Symposium. - Tallinn, 27-29 May 2008. - P. 1-5. ↑

C1911. Ambjorn C. Seatrack Web forecasts and backtracking of oil spills-an efficient tool to find illegal spills using AIS. 2008 IEEE/OES US/EU-Baltic International Symposium. - Tallinn, 27-29 May 2008. - P. 1-9. ↑

C1912. Ermakov S.A. Possibilities of identification of oil films using radar probing of the sea surface. 2008 IEEE/OES US/EU-Baltic International Symposium. - Tallinn, 27-29 May 2008. - P. 1-6. ↑

C1913. Wenyu Gong. Detecting ground deformation with Permanent scatterer of Suzhou region. / Wenyu Gong, Jixian Zhang, Yonghong Zhang. // 2008. EORSA 2008. International Workshop on Earth Observation and Remote Sensing Applications. - Beijing, June 30 2008-July 2 2008. - P. 1-5. ↑

C1914. Xiaofei Wang. Registration of remote sensing images based on Gaussian fitting. / Xiaofei Wang, Junping Zhang, Ye Zhang. // 2008. ICIEA 2008. 3rd IEEE Conference on Industrial Electronics and Applications. - Singapore, 3-5 June 2008. - P. 378-381. ↑

C1915. Knoechel R. Correlation processing of noise-like signals from coherent radar. / Knoechel R., Tepliuk A.L., Khlopov G.I., Shuenemann K. // 2008 International Radar Symposium. - Wroclaw, 21-23 May 2008. - P. 1-4. ↑

C1916. Pepyne D. Distributed Collaborative Adaptive Sensor networks for remote sensing applications. / Pepyne D., Westbrook D., Philips B., Lyons E., Zink M., Kurose J. // 2008 American Control Conference. - Seattle, WA, 11-13 June 2008. - P. 4167-4172. ↑

C1917. Yanovsky F. Classification algorithms for weather radar. / Yanovsky F., Marchuk V., Ostrovsky Y., Averyanova Y. // 2008. MMET 2008. 12th International Conference on Mathematical Methods in Electromagnetic Theory. - Odesa, June 29 2008-July 2 2008. - P. 366-368. ↑

C1918. Schneebeli M. X-band opacity of a tropical tree canopy and its relation to intercepted rain, eddy fluxes and other meteorological variables. / Schneebeli M., Matzler C., Wolf S., Eugster W. // 2008. MICRORAD 2008 Microwave Radiometry and Remote Sensing of the Environment. - Firenze, 11-14 March 2008. - P. 1-4. ↑

C1919. Monerris A. Radiometric observations of vines from the green period to the withering. / Monerris A., Vall-Ilossera M., Camps A., Piles M. // 2008. MICRORAD 2008 Microwave Radiometry and Remote Sensing of

the Environment. - Firenze, 11-14 March 2008. - P. 1-4. ↑

C1920. Golikov V. CFAR robust detection of moving target in presence of fluctuating background. / Golikov V., Castillejos A., Lebedeva O., Ponomaryov V., Cruz-Irisson M. // 2008. MMET 2008. 12th International Conference on Mathematical Methods in Electromagnetic Theory. - Odesa, June 29 2008-July 2 2008. - P. 144-146. ↑

C1921. Yu-Jiun Ren. A dual-frequency dual-polarized planar airborne array antenna. / Yu-Jiun Ren, Shih-Hsun Hsu, Ming-Yi Li, Kai Chang. // 2008. AP-S 2008. IEEE Antennas and Propagation Society International Symposium. - San Diego, CA, 5-11 July 2008. - P. 1-4. ↑

C1922. Dogaru T. Recent investigations in sensing through the wall radar modeling. / Dogaru T., Calvin Le. // 2008. AP-S 2008. IEEE Antennas and Propagation Society International Symposium. - San Diego, CA, 5-11 July 2008. - P. 1-4. ↑

C1923. Bayraktar Z. GA optimized reconfigurable frequency selective surfaces for passive standoff detection of chemical agents. / Bayraktar Z., Bray M.G., Werner D.H. // 2008. AP-S 2008. IEEE Antennas and Propagation Society International Symposium. - San Diego, CA, 5-11 July 2008. - P. 1-4. ↑

C1924. Sun Xiaokun. Polarization filtering enhancement of buried landmine. / Sun Xiaokun, Zhou Zhimin. // 2008. ICIA 2008. International Conference on Information and Automation. - Changsha, 20-23 June 2008. - P. 646-649. ↑

C1925. Matei B.C. Building segmentation for densely built urban regions using aerial LIDAR data. / Matei B.C., Sawhney H.S., Samarasekera S., Kim J., Kumar R. // 2008. CVPR 2008. IEEE Conference on Computer Vision and Pattern Recognition. - Anchorage, AK, 23-28 June 2008. - P. 1-8. ↑

C1926. Min Ding. Automatic registration of aerial imagery with untextured 3D LiDAR models. / Min Ding, Lyngbaek K., Zakhor A. // 2008. CVPR 2008. IEEE Conference on Computer Vision and Pattern Recognition. - Anchorage, AK, 23-28 June 2008. - P. 1-8. ↑

C1927. Schulz F. Post-doppler space-time filtering for suppressing moving target signals in multi-channel SAR data. 2008. SAM 2008. 5th IEEE Sensor Array and Multichannel Signal Processing Workshop. - Darmstadt, 21-23 July 2008. - P. 468-472. ↑

C1928. Nosich A.A. Comparison of two configurations of a four-reflector beam-waveguide for a large space communication facility. / Nosich A.A., Sauleau R., Gandel Y.V. // 2008. MRRS 2008 Microwaves, Radar and Remote Sensing Symposium. - Kiev, 22-24 Sept. 2008. - P. 26-29. ↑

C1929. Priimenko S.D. On realization of the transition radiation antenna. / Priimenko S.D., Bondarenko L.A. // 2008. MRRS 2008 Microwaves, Radar and Remote Sensing Symposium. - Kiev, 22-24 Sept. 2008. - P. 30-33. ↑

C1930. Wasyliwskyj W. Coherent scattering from distributed targets. / Wasyliwskyj W., Alatishe J. // 2008. MRRS 2008 Microwaves, Radar and Remote Sensing Symposium. - Kiev, 22-24 Sept. 2008. - P. 36-41. ↑

C1931. Debogovic T. Dual band reconfigurable slot antenna with high frequency ratio. / Debogovic T., Karabelj A., Bartolic J. // 2008. MRRS 2008 Microwaves, Radar and Remote Sensing Symposium. - Kiev, 22-24 Sept. 2008. - P. 22-25. ↑


C1932. Immoreev I. Remote monitoring of human cardiorespiratory system parameters by radar and its applications. / Immoreev I., Ivashov S. // 2008. UWBUSIS 2008. 4th International Conference on Ultrawideband and Ultrashort Impulse Signals. - Sevastopol, Crimea, 15-19 Sept. 2008. - P. 34-38. ↑


C1933. Goshi D. Integrated hardware reduction schemes for retrodirective array architectures. / Goshi D., Itoh T. // 2008. MRRS 2008 Microwaves, Radar and Remote Sensing Symposium. - Kiev, 22-24 Sept. 2008. - P. 12-15. ↑


C1934. Sorrentino R. Reconfigurable reflectarrays based on RF MEMS technology. 2008. MRRS 2008 Microwaves, Radar and Remote Sensing Symposium. - Kiev, 22-24 Sept. 2008. - P. 16-21. ↑


C1935. Khaikin V.B. A compact highly sensitive radiometer for thermal sounding of atmosphere in 5 MM band. / Khaikin V.B., Radzikhovskiy V.N., Kuzmin S.E., Shlenzin S.V., Shaposhnikov A.V. // 2008. MRRS 2008
↑


Microwaves, Radar and Remote Sensing Symposium. - Kiev, 22-24 Sept. 2008. - P. 66-70. 


C1936. Radionov S. Interactive-mode X-band direction-finder. / Radionov S., Ivanchenko I., Korolev A., Popenko N. // 2008. MRRS 2008 Microwaves, Radar and Remote Sensing Symposium. - Kiev, 22-24 Sept. 2008. - P. 71-74. 


C1937. Malanowski M. PaRaDe-PAssive RADar DEmonstrator family development at Warsaw University of Technology. / Malanowski M., Kulpa K., Misiurewicz J. // 2008. MRRS 2008 Microwaves, Radar and Remote Sensing Symposium. - Kiev, 22-24 Sept. 2008. - P. 75-78. 


C1938. Bezousek P. Coherent multilateration systems. / Bezousek P., Schejbal V. // 2008. MRRS 2008 Microwaves, Radar and Remote Sensing Symposium. - Kiev, 22-24 Sept. 2008. - P. 60-65. 


C1939. Greving G. Status of advanced scattering distortion system analysis for nav aids and radar-examples of A380 and wind turbines. / Greving G., Biermann W.-D., Mundt R. // 2008. MRRS 2008 Microwaves, Radar and Remote Sensing Symposium. - Kiev, 22-24 Sept. 2008. - P. 42-47. 


C1940. Nagy L. Material parameter measurements for microwave anti reflection coating development. 2008. MRRS 2008 Microwaves, Radar and Remote Sensing Symposium. - Kiev, 22-24 Sept. 2008. - P. 48-53. 


C1941. Savenkov S.N. Analysis of generalized polarimetric measurement equations for Stokes polarimetry techniques. / Savenkov S.N., Oberemok Y.A., Klimov A.S. // 2008. MRRS 2008 Microwaves, Radar and Remote Sensing Symposium. - Kiev, 22-24 Sept. 2008. - P. 54-57. 


C1942. Wang Min. Fusion of Multi-band SAR Images Based on Nonsubsampled Contourlet and PCNN. / Wang Min, Peng Dongliang, Yang Shuyuan. // 2008. ICNC '08. Fourth International Conference on Natural Computation. - Jinan, 18-20 Oct. 2008. - Vol. 5. - P. 529-533. 


C1943. Schatz V. Synchronised data acquisition for sensor data fusion in airborne surveying. 2008 11th International Conference on Information Fusion. - Cologne, June 30 2008-July 3 2008. - P. 1-6. 


C1944. Suri S. Application of generalized partial volume estimation for mutual information based registration of high resolution SAR and optical imagery. / Suri S., Reinartz P. // 2008 11th International Conference on Information Fusion. - Cologne, June 30 2008-July 3 2008. - P. 1-8. 


C1945. Hafner N. Underwater motion and physiological sensing using UHF doppler radar. / Hafner N., Massagram W., Lubecke V.M., Boric-Lubecke O. // 2008 IEEE MTT-S International Microwave Symposium Digest. - Atlanta, GA, 15-20 June 2008. - P. 1501-1504. 

C1946. Kwong K.M. Using LIDAR doppler velocity data and chaotic oscillatory-based neural network for the forecast of meso-scale wind field. / Kwong K.M., Liu J.N.K., Chan P.W., Lee R. // 2008. CEC 2008. (IEEE World Congress on Computational Intelligence). IEEE Congress on Evolutionary Computation. - Hong Kong, 1-6 June 2008. - P. 2012-2019. 

C1947. Ghazali J.N. A Real Time Simulation of Flood Hazard. / Ghazali J.N., Kamsin A. // 2008. CGIV '08. Fifth International Conference on Computer Graphics, Imaging and Visualisation. - Penang, 26-28 Aug. 2008. - P. 393-397. 

C1948. Ligthart L.P. Multi-frequency polarimetric radar earth observations. / Ligthart L.P., Kuzuza B. // 2008. MIKON 2008. 17th International Conference on Microwaves, Radar and Wireless Communications. - Wroclaw, 19-21 May 2008. - P. 1-7. 

C1949. Prudyus I. Noise-robust data fusion on a pixel level. / Prudyus I., Lazko L., Semenov S. // 2008. MIKON 2008. 17th International Conference on Microwaves, Radar and Wireless Communications. - Wroclaw, 19-21 May 2008. - P. 1-3. 

C1950. Smirnova E.I. Design and fabrication of a 100 GHz channel-drop filter. / Smirnova E.I., Earley L.M., Heath C.E., Shchegolkov D.Yu. // 2008. IRMMW-THz 2008. 33rd International Conference on Infrared, Millimeter and Terahertz Waves. - Pasadena, CA, 15-19 Sept. 2008. - P. 1-2. 

C1951. Huilong Li. Multispectral Land Cover Classification Using Averaged Learning Subspace Method. / Huilong Li, Yonghui Yang, Bagan H. // 2008. ICNC '08. Fourth International Conference on Natural Computation.



- Jinan, 18-20 Oct. 2008. - Vol. 4. - P. 182-186.

C1952. Yang Shuyuan. SAR Image Compression Based on Bandelet Network. / Yang Shuyuan, Peng DongLiang, Wang Min. // 2008. ICNC '08. Fourth International Conference on Natural Computation. - Jinan, 18-20 Oct. 2008. - Vol. 4. - P. 559-563. ↑

C1953. Ceccarelli M. A texture based approach for ocean surface wind detection in SAR images. / Ceccarelli M., De Filippo M., Di Bisceglie M., Galdi C. // 2008. IST 2008. IEEE International Workshop on Imaging Systems and Techniques. - Crete, 10-12 Sept. 2008. - P. 193-197. ↑

C1954. Zhang B. Application of artificial neural computation in topex waveform data: A case study in water ratio regression. / Zhang B., Schwartz F.W., Tong D. // 2008. ICCI 2008. 7th IEEE International Conference on Cognitive Informatics. - Stanford, CA, 14-16 Aug. 2008. - P. 232-238. ↑

C1955. Galin N. 2-8 GHz FMCW radar for estimating snow depth on antarctic sea ice. / Galin N., Worby A., Massom R., Brooker G., Leuschen C., Gogineni S.P., Jansen P. // 2008 International Conference on Radar. - Adelaide, SA, 2-5 Sept. 2008. - P. 276-281. ↑

C1956. Li Kaiming. A new separation method for Micro-Doppler information of a target with rotating parts. / Li Kaiming, Luo Ying, Chi Long, Zhang Qun. // 2008. ICCAS 2008. International Conference on Communications, Circuits and Systems. - Fujian, 25-27 May 2008. - P. 1365-1369. ↑

C1957. Shalina E.V. Multi year sea ice concentration mapping using passive and active microwave satellite data. / Shalina E.V., Johannessen O.M. // 2008. MICRORAD 2008 Microwave Radiometry and Remote Sensing of the Environment. - Firenze, 11-14 March 2008. - P. 1-4. ↑

C1958. Wilson J.C. Using Airborne Hydrographic LiDAR To Support Mapping of California's Waters. OCEANS 2008-MTS/IEEE Kobe Techno-Ocean. - Kobe, 8-11 April 2008. - P. 1-8. ↑

C1959. Wang X.B. High-Resolution Inverse Synthetic Aperture Radar Imaging Based on the Shooting and Bouncing Ray Method. / Wang X.B., Zhou X.Y., Cui T.J., Tao Y.B., Lin H. // 2008. GSMM 2008. Global Symposium on Millimeter Waves. - Nanjing, 21-24 April 2008. - P. 1-3. ↑

C1960. Chen Qian. Z-R Relationship from the Particle Size and Velocity (Parsivel) Optical Disdrometer and its Application in Estimating Areal Rainfall. / Chen Qian, Niu Shengjie, Zhang Yu, Xu Feng. // 2008. ICBBE 2008. The 2nd International Conference on Bioinformatics and Biomedical Engineering. - Shanghai, 16-18 May 2008. - P. 4637-4640. ↑

C1961. Takatsu N. Ocean Observing System in the East China Sea. OCEANS 2008-MTS/IEEE Kobe Techno-Ocean. - Kobe, 8-11 April 2008. - P. 1-7. ↑

C1962. Hilliard L.M. Development of Coherent, Expandable, Reconfigurable Instrument Node (ERIN) for Web Sensor Applications. 2008 IEEE Aerospace Conference. - Big Sky, MT, 1-8 March 2008. - P. 1-8. ↑

C1963. Nsaibi M. Image fusion of radar and optical remote sensing data for land cover classification. / Nsaibi M., Chaabane F. // 2008. ICTTA 2008. 3rd International Conference on Information and Communication Technologies: From Theory to Applications. - Damascus, 7-11 April 2008. - P. 1-4. ↑

C1964. Walsh J. A Monostatic Ocean Scattering Cross Section for the Case of Surface Wave Radar Operating from a Floating Barge. / Walsh J., Gill E., Weimin Huang. // OCEANS 2008-MTS/IEEE Kobe Techno-Ocean. - Kobe, 8-11 April 2008. - P. 1-4. ↑

C1965. Khalili R. Practical Algorithms for Gathering Stored Correlated Data in a Network. / Khalili R., Kurose J. // 2008. SECON '08. 5th Annual IEEE Communications Society Conference on Sensor, Mesh and Ad Hoc Communications and Networks. - San Francisco, CA, 16-20 June 2008. - P. 487-496. ↑

C1966. Norgard J. Three-dimensional Microwave Tomography: Waveform diversity and distributed sensors for detecting and imaging buried objects with suppressed electromagnetic interference. / Norgard J., Musselman R., Drozd A. // 2008. APEMC 2008. Asia-Pacific Symposium on Electromagnetic Compatibility and 19th International Zurich Symposium on Electromagnetic Compatibility. - Singapore, 19-23 May 2008. - P. 371-374. ↑

C1967. Hinz S. Detection and velocity estimation of moving vehicles in high-resolution spaceborne synthetic aperture radar data. / Hinz S., Weihsing D., Suchandt S., Bamler R. // 2008. CVPRW '08. IEEE Computer Society

Conference on Computer Vision and Pattern Recognition Workshops. - Anchorage, AK, 23-28 June 2008. - P. 1-6. ↑

C1968. Yeary M. Compact Digital Receiver Development for Radar Based Remote Sensing. / Yeary M., Kelley R., Meier J., Ong S., Palmer R. // 2008. IMTC 2008. IEEE Instrumentation and Measurement Technology Conference Proceedings. - Victoria, BC, 12-15 May 2008. - P. 1761-1765. ↑

C1969. Qingxia Li. An aperture synthesis radiometer at millimeter wave band. / Qingxia Li, Ke Chen, Wei Guo, Liang Lang, Fangmin He, Liangbing Chen. // 2008. ICMMT 2008. International Conference on Microwave and Millimeter Wave Technology. - Nanjing, 21-24 April 2008. - Vol. 4. - P. 1699-1701. ↑

C1970. Xinhua Mao. An overlapped subaperture polar format algorithm based on sub-chirp signals. / Xinhua Mao, Daiyin Zhu, Zhaoda Zhu. // 2008. ICMMT 2008. International Conference on Microwave and Millimeter Wave Technology. - Nanjing, 21-24 April 2008. - Vol. 4. - P. 2073-2076. ↑

C1971. Atoche A.C. FPGA based radar image enhanced: A robust evolutionary controlled filter approach. / Atoche A.C., Aguilar J.O., Castillo J.V. // 2008. ICCDCS 2008. 7th International Caribbean Conference on Devices, Circuits and Systems. - Cancun, 28-30 April 2008. - P. 1-5. ↑

C1972. Carswell J.R. A High Altitude Airborne Wind Mapping Radar. / Carswell J.R., Heymsfield G., Lihua Li, Schaubert D., Creticos J. // 2008 IEEE Aerospace Conference. - Big Sky, MT, 1-8 March 2008. - P. 1-7. ↑

C1973. Teague C.C. Dual-RiverSonde Measurements of Two-Dimensional River Flow Patterns. / Teague C.C., Barrick D.E., Lilleboe P.M., Cheng R.T., Stumpner P., Burau J.R. // 2008. CMTC 2008. IEEE/OES 9th Working Conference on Current Measurement Technology. - Charleston, SC, 17-19 March 2008. - P. 258-263. ↑

C1974. Kostis T. G. Simulator Implementation of an Inverse Synthetic Aperture Radar System for an Extended Naval Target in a Three Dimensional Synthetic Environment. 2008. UKSIM 2008. Tenth International Conference on Computer Modeling and Simulation. - Cambridge, UK, 1-3 April 2008. - P. 366-371. ↑

C1975. Fritz J. Enhancements of an Adaptive Neighborhood Speckle Filtering Algorithm to Improve Analysis of Polarimetric SAR Imagery. / Fritz J., Tabb M., Chandrasekar V. // 2008. SSIAI 2008. IEEE Southwest Symposium on Image Analysis and Interpretation. - Santa Fe, NM, 24-26 March 2008. - P. 81-84. ↑

C1976. Kohut J. Surface current and wave validation of a nested regional HF radar Network in the Mid-Atlantic Bight. / Kohut J., Roarty H., Lichtenwalner S., Glenn S., Barrick D., Lipa B., Allen A. // 2008. CMTC 2008. IEEE/OES 9th Working Conference on Current Measurement Technology. - Charleston, SC, 17-19 March 2008. - P. 203-207. ↑

C1977. Hwang P.A. A conceptual design for simultaneous measurements of 3D surface wave field and ocean surface current vector using the InSAR technology. / Hwang P.A., Toporkov J.V., Sletten M.A. // 2008. CMTC 2008. IEEE/OES 9th Working Conference on Current Measurement Technology. - Charleston, SC, 17-19 March 2008. - P. 160-164. ↑

C1978. Romeiser R. Current Measurements in Coastal Waters and Rivers by TerraSAR-X Along-Track InSAR. 2008. CMTC 2008. IEEE/OES 9th Working Conference on Current Measurement Technology. - Charleston, SC, 17-19 March 2008. - P. 165-167. ↑

C1979. Perkovic D. Marine Doppler Radar Surface Current Measurements in the Surf Zone. / Perkovic D., Frasier S.J., Lippmann T.C. // 2008. CMTC 2008. IEEE/OES 9th Working Conference on Current Measurement Technology. - Charleston, SC, 17-19 March 2008. - P. 194-202. ↑

C1980. Re E. Millimeter Wave Technology for Moon and Mars Exploration. / Re E., Ruggeri M., Dainelli V., Ferri M. // 2008 IEEE Aerospace Conference. - Big Sky, MT, 1-8 March 2008. - P. 1-11. ↑

C1981. Wen-Qin Wang. Models and Signal Processing for Millimeter-Wave LFM CW SAR Imaging. / Wen-Qin Wang, Jingye Cai, Qicong Peng. // 2008 IEEE Aerospace Conference. - Big Sky, MT, 1-8 March 2008. - P. 1-10. ↑

C1982. Wen-Qin Wang. Baseline Estimation in Distributed Spaceborne Interferometry SAR Systems. 2008 IEEE Aerospace Conference. - Big Sky, MT, 1-8 March 2008. - P. 1-8. ↑

- C1983.** Shen Lin. A wireless network based on the combination of Zigbee and GPRS. / Shen Lin, Shixiangquan, Ling Ming. // 2008. ICNSC 2008. IEEE International Conference on Networking, Sensing and Control. - Sanya, 6-8 April 2008. - P. 267-270. ↑
- C1984.** Capozzoli A. The radon transform for the tomography of vegetated areas. / Capozzoli A., Curcio C., D'Elia G., Liseno A., Mele A. // 2008. LAPC 2008. Loughborough Antennas and Propagation Conference. - Loughborough, 17-18 March 2008. - P. 321-324. ↑
- C1985.** Zheng Xiang. A new DEM reconstruction method based on an accurate flattening algorithm in interferometric SAR. / Zheng Xiang, Kaizhi Wang, Xingzhao Liu. // 2008. ICASSP 2008. IEEE International Conference on Acoustics, Speech and Signal Processing. - Las Vegas, NV, March 31 2008-April 4 2008. - P. 1093-1096. ↑
- C1986.** Eunyoung Seok. A 410GHz CMOS Push-Push Oscillator with an On-Chip Patch Antenna. / Eunyoung Seok, Changhua Cao, Dongha Shim, Arenas D.J., Tanner D.B., Chin-Ming Hung, O K.K. // 2008. ISSCC 2008. Digest of Technical Papers. IEEE International Solid-State Circuits Conference. - San Francisco, CA, 3-7 Feb. 2008. - P. 472-629. ↑
- C1987.** Westwater E.R. Deployments of microwave and millimeterwave radiometers in the Arctic. / Westwater E.R., Cimini D., Mattioli V., Gasiewski A.J., Klein M., Leuski V., Turner D.D. // 2008. MICRORAD 2008 Microwave Radiometry and Remote Sensing of the Environment. - Firenze, 11-14 March 2008. - P. 1-4. ↑
- C1988.** Okamoto K. High precision and high resolution global precipitation map from satellite data. / Okamoto K., Takahashi N., Iwanami K., Shige S., Kubota T. // 2008. MICRORAD 2008 Microwave Radiometry and Remote Sensing of the Environment. - Firenze, 11-14 March 2008. - P. 1-4. ↑
- C1989.** Kurum M. Estimation of canopy attenuation for active/passive microwave soil moisture retrieval algorithms. / Kurum M., Lang R.H., O'Neill P.E., Joseph A., Jackson T., Cosh M. // 2008. MICRORAD 2008 Microwave Radiometry and Remote Sensing of the Environment. - Firenze, 11-14 March 2008. - P. 1-4. ↑
- C1990.** Imperatore P. Perturbative solution for the scattering from multilayered structure with rough boundaries. / Imperatore P., Iodice A., Riccio D. // 2008. MICRORAD 2008 Microwave Radiometry and Remote Sensing of the Environment. - Firenze, 11-14 March 2008. - P. 1-4. ↑
- C1991.** Khazaal A. On the reduction of the systematic error in imaging radiometry by aperture synthesis: a new approach for the SMOS space mission. / Khazaal A., Carfantan H., Anterrieu E. // 2008. MICRORAD 2008 Microwave Radiometry and Remote Sensing of the Environment. - Firenze, 11-14 March 2008. - P. 1-4. ↑
- C1992.** {no data available}. Remote Sensing. 2008. CMTC 2008. IEEE/OES 9th Working Conference on Current Measurement Technology. - Charleston, SC, USA, 17-19 March 2008. - P. 129. ↑
- C1993.** Pinkel R. The development of Doppler sonar technology at SIO. 2008. CMTC 2008. IEEE/OES 9th Working Conference on Current Measurement Technology. - Charleston, SC, 17-19 March 2008. - P. 11-18. ↑
- C1994.** Shige S. On the use of microwave sounder data for high-temporal rainfall maps based on microwave radiometers. / Shige S., Yamamoto T., Kida S., Tsukiyama T., Kubota T., Okamoto K. // 2008. MICRORAD 2008 Microwave Radiometry and Remote Sensing of the Environment. - Firenze, 11-14 March 2008. - P. 1-4. ↑
- C1995.** Pospelov M.N. Air-sea interaction monitoring by remote and contact measurements: The results of the CAPMOS'05 and CAPMOS'07 experiments on an oceanographic platform in the Black Sea. / Pospelov M.N., Goryachkin Y.N., Komarova N.Y., Kuzmin A.V., Kuznetsov A.S., Pampaloni P., Repina I.A., Smirnov M.T., Zecchetto S. // 2008. MICRORAD 2008 Microwave Radiometry and Remote Sensing of the Environment. - Firenze, 11-14 March 2008. - P. 1-4. ↑
- C1996.** Pospelov M.N. Dynamics of short waves spectrum measured by remote and contact sensors from an oceanographic platform. / Pospelov M.N., Antonov V.S., Kuzmin A.V., Sadovsky I.N. // 2008. MICRORAD 2008 Microwave Radiometry and Remote Sensing of the Environment. - Firenze, 11-14 March 2008. - P. 1-4. ↑
- C1997.** Bobylev L.P. Neural-Network based algorithm for ice concentration retrievals from satellite passive microwave data. / Bobylev L.P., Zabolotskikh E.V., Mitnik L.M., Johannessenn O.M. // 2008. MICRORAD 2008 Microwave Radiometry and Remote Sensing of the Environment. - Firenze, 11-14 March 2008. - P. 1-4. ↑

- C1998.** Smith D.F. An anisotropic ocean surface emissivity model based on WindSat polarimetric brightness observations. / Smith D.F., Weber B.L., Gasiewski A.J. // 2008. MICRORAD 2008 Microwave Radiometry and Remote Sensing of the Environment. - Firenze, 11-14 March 2008. - P. 1-4. ↑
- C1999.** Bobak J.P. On the correlation of area-extensive measurement of fractional area whitecap coverage with microwave brightness temperatures. / Bobak J.P., Asher W.E., Dowgiallo D.J., Anguelova M.D. // 2008. MICRORAD 2008 Microwave Radiometry and Remote Sensing of the Environment. - Firenze, 11-14 March 2008. - P. 1-4. ↑
- C2000.** Johnson B.T. Combined passive and active microwave retrieval of falling snow during the 2003 Wakasa Bay field experiment. / Johnson B.T., Skofronick-Jackson G., Petty G.W. // 2008. MICRORAD 2008 Microwave Radiometry and Remote Sensing of the Environment. - Firenze, 11-14 March 2008. - P. 1-4. ↑
- C2001.** Jirousek M. High-resolution spectral radiometer imaging system. / Jirousek M., Peichl M., Suess H. // 2008. MICRORAD 2008 Microwave Radiometry and Remote Sensing of the Environment. - Firenze, 11-14 March 2008. - P. 1-4. ↑
- C2002.** Hughes E.J. Investigation into the utility of using CFAR cluster size information in target track association. / Hughes E.J., Izzawati I. // 2008 IET Seminar on Target Tracking and Data Fusion: Algorithms and Applications. - Birmingham, 15-16 April 2008. - P. 5. ↑
- C2003.** Mudroch M. An Experimental Study of the Lowest Troposphere Layers at 10 GHz-First Results. / Mudroch M., Grabner M., Kvicera V., Hudec P., Bedrna P., Pechac P. // 2008. COMITE 2008. 14th Conference on Microwave Techniques. - Prague, 23-24 April 2008. - P. 1-4. ↑
- C2004.** Toth C. Terrain-based navigation: Trajectory recovery from LiDAR data. / Toth C., Grejner-Brzezinska D.A., Young-Jin Lee. // 2008 IEEE/ION Position, Location and Navigation Symposium. - Monterey, CA, 5-8 May 2008. - P. 760-765. ↑
- C2005.** Zhang Huapeng. Performance Assessment of IHS Fusion for Remote Sensing Images Based on Multiple Attribute Decision Making. / Zhang Huapeng, Du Peijun, Yin Zuoxia. // 2008. CISP '08. Congress on Image and Signal Processing. - Sanya, China, 27-30 May 2008. - Vol. 4. - P. 768-772. ↑
- C2006.** Hu Wendong. Texture Analysis on Weather Radar Images of Severe Convective Precipitation in the Arid Area of Ningxia. / Hu Wendong, Huang Xiaoyu, Li Yanchun. // 2008. CISP '08. Congress on Image and Signal Processing. - Sanya, China, 27-30 May 2008. - Vol. 2. - P. 150-154. ↑
- C2007.** Zhang Suoping. Application of Ridgelet Transform to Wave Direction Estimation. / Zhang Suoping, Zhang Chuntian. // 2008. CISP '08. Congress on Image and Signal Processing. - Sanya, China, 27-30 May 2008. - Vol. 2. - P. 690-693. ↑
- C2008.** Lin Yi. Adaptive Balancing of Edge Extraction in LADAR-Referenced Navigation over Plain Area. / Lin Yi, Yan Lei, Liu Yuefeng, Jiang Miao, Tong Qingxi. // 2008. CISP '08. Congress on Image and Signal Processing. - Sanya, China, 27-30 May 2008. - Vol. 4. - P. 348-351. ↑
- C2009.** Marzano F.S. FLORAD: Micro-satellite flower constellation of millimeter-wave radiometers for atmospheric remote sensing. / Marzano F.S., Cimini D., Montopoli M., Memmo A., Ferretti R., Rossi T., De Sanctis M., Lucente M., Mortari D., Oricchio D., Varchetta S., Pavia P., Nassisi A., Balduccini M., Scorzolini A., Reboa L., Tozzi P., Bruno A., Greco F., Perrotta G., Giuliani G., Giusto R., Di Michele S. // 2008. MICRORAD 2008 Microwave Radiometry and Remote Sensing of the Environment. - Firenze, 11-14 March 2008. - P. 1-4. ↑
- C2010.** Zribi M. Combined airborne radio-instruments for ocean and land studies (CAROLS). / Zribi M., Hauser D., Parde M., Fanise P., Leroy P., Dechambre M., Boutin J., Reverdin G., Calvet J.C., Weill A., Wigneron J.P., Skou N., Sobjaerg S.S., Ruis A., Cadareche E. // 2008. MICRORAD 2008 Microwave Radiometry and Remote Sensing of the Environment. - Firenze, 11-14 March 2008. - P. 1-4. ↑
- C2011.** Pazmany A.L. A compact airborne G-band (183 GHz) water Vapor Radiometer and retrievals of liquid cloud parameters from coincident radiometer and millimeter wave radar measurements. / Pazmany A.L., Wolde M. // 2008. MICRORAD 2008 Microwave Radiometry and Remote Sensing of the Environment. - Firenze, 11-14 March 2008. - P. 1-4. ↑
- C2012.** Le Vine D.M. The Aquarius/SAC-D mission and status of the Aquarius instrument. / Le Vine D.M.,

Lagerloef G., Pellerano F., Colomb F.R. // 2008. MICRORAD 2008 Microwave Radiometry and Remote Sensing of the Environment. - Firenze, 11-14 March 2008. - P. 1-4. ↑

C2013. Mitnik L.M. Microwave characteristics of organized mesoscale convection over the ocean. / Mitnik L.M., Mitnik M.L. // 2008. MICRORAD 2008 Microwave Radiometry and Remote Sensing of the Environment. - Firenze, 11-14 March 2008. - P. 1-4. ↑

C2014. Shutko A.M. Microwave radiometry of land, vegetation and water bodies: More than 30 years of modeling, conducting experiments and practical applications. 2008. MICRORAD 2008 Microwave Radiometry and Remote Sensing of the Environment. - Firenze, 11-14 March 2008. - P. 1-4. ↑

C2015. Haarbrink R.B. Simultaneous multi-sensor data for global information management system. / Haarbrink R.B., Shutko A.M. // 2008. MICRORAD 2008 Microwave Radiometry and Remote Sensing of the Environment. - Firenze, 11-14 March 2008. - P. 1-4. ↑

C2016. Snoeij P. Sentinel-1, the GMES radar mission. / Snoeij P., Attema E., Davidson M., Floury N., Levrini G., Rosich B., Rommen B. // 2008. RADAR 08. IEEE Radar Conference. - Rome, 26-30 May 2008. - P. 1-5. ↑

C2017. Cumming I.G. Current interferometry results in Canada. / Cumming I.G., Rabus B., Mercer B. // 2008. RADAR 08. IEEE Radar Conference. - Rome, 26-30 May 2008. - P. 1-6. ↑

C2018. Iorio M. Mars north polar cup subsurface materials property estimation using GPR SHallow RADar data. / Iorio M., Fois F., Mecozzi R., Catallo C., Picardi G., Seu R., Flamini E. // 2008. RADAR 08. IEEE Radar Conference. - Rome, 26-30 May 2008. - P. 1-6. ↑

C2019. Yueh S. Airborne Ku-band polarimetric radar remote sensing of terrestrial snow cover. / Yueh S., Cline D., Elder K. // 2008. RADAR 08. IEEE Radar Conference. - Rome, 26-30 May 2008. - P. 1-6. ↑

C2020. Xinhua Mao. A two dimension overlapped subaperture polar format algorithm based on stepped-chirp signal. / Xinhua Mao, Daiyin Zhu, Ling Wang, Zhaoda Zhu. // 2008. ICIP 2008. 15th IEEE International Conference on Image Processing. - San Diego, CA, 12-15 Oct. 2008. - P. 1872-1875. ↑

C2021. Silveira M. Water/land segmentation in SAR images using level sets. / Silveira M., Heleno S. // 2008. ICIP 2008. 15th IEEE International Conference on Image Processing. - San Diego, CA, 12-15 Oct. 2008. - P. 1896-1899. ↑

C2022. Chehata N. Terrain modeling from lidar data: Hierarchical K-means filtering and Markovian regularization. / Chehata N., Bretar F. // 2008. ICIP 2008. 15th IEEE International Conference on Image Processing. - San Diego, CA, 12-15 Oct. 2008. - P. 1900-1903. ↑

C2023. Shkvarko Y.V. Descriptive experiment design unified with worst-case performance optimization-adapted regularization for high-resolution radar/SAR imaging. 2008. RADAR 08. IEEE Radar Conference. - Rome, 26-30 May 2008. - P. 1-6. ↑

C2024. Papathanassiou K.P. Recent advances in Polarimetric SAR Interferometry for forest parameter estimation. / Papathanassiou K.P., Kugler F., Seungkuk Lee, Marotti L., Hajnsek I. // 2008. RADAR 08. IEEE Radar Conference. - Rome, 26-30 May 2008. - P. 1-6. ↑

C2025. Pottier E. Advances in SAR Polarimetry applications exploiting polarimetric spaceborne sensors. / Pottier E., Ferro-Famil L. // 2008. RADAR 08. IEEE Radar Conference. - Rome, 26-30 May 2008. - P. 1-6. ↑

C2026. Anderson S. Multiple scattering of HF skywave radar signals: Physics, interpretation and exploitation. 2008. RADAR 08. IEEE Radar Conference. - Rome, 26-30 May 2008. - P. 1-5. ↑

C2027. Picardi G. Subsurface sounding in Northern hemisphere for Mars by MARSIS: Mars express mission. / Picardi G., Biccari D., Cartacci M., Cicchetti A., Iorio M., Masdea A., Seu R., Plaut J.J., Johnson W.T.K., Jordan R.L., Safaeinili A., Frigeri A., Melacci P.T., Orosei R., Bombaci O., Calabrese D., Zampolini E. // 2008. RADAR 08. IEEE Radar Conference. - Rome, 26-30 May 2008. - P. 1-6. ↑

C2028. Muellerschoen R. Real-time autonomous disturbance detection and monitoring system with L-band UAVSAR. / Muellerschoen R., Yunling Lou, Chien S., Saatchi S. // 2008. RADAR 08. IEEE Radar Conference. - Rome, 26-30 May 2008. - P. 1-6. ↑

- C2029.** Buckreuss S. The German satellite mission TerraSAR-X. / Buckreuss S., Werninghaus R., Pitz W. // 2008. RADAR 08. IEEE Radar Conference. - Rome, 26-30 May 2008. - P. 1-5. ↑
- C2030.** Dey C. Decision Fusion for Reliable Flood Mapping Using Remote Sensing Images. / Dey C., Xiuping Jia, Fraser D. // 2008. DICTA '08. Digital Image Computing: Techniques and Applications. - Canberra, ACT, 1-3 Dec. 2008. - P. 184-190. ↑
- C2031.** Yatsevich S.Ye. The fractal analysis of radar images of tropical cyclones. / Yatsevich S.Ye., Yefimov V.B., Ivanov V.K., Pashchenko R.E., Tsymbal V.N. // 2008. CriMiCo 2008. 2008 18th International Crimean Conference Microwave & Telecommunication Technology. - Sevastopol, Crimea, 8-12 Sept. 2008. - P. 901-902. ↑
- C2032.** Atroshenko L.M. Providing basic data for the wood segment of GEOUA-information service system "leskosmos" (Forest-UA). / Atroshenko L.M., Gorobets N.N., Kostjashkin S.I., Kostjashkina T.D., Safronova L.P. // 2008. CriMiCo 2008. 2008 18th International Crimean Conference Microwave & Telecommunication Technology. - Sevastopol, Crimea, 8-12 Sept. 2008. - P. 907-908. ↑
- C2033.** Korolyov S.V. Analysis of relative permits depending on signal-noise ratio at the use of optimal on minimum error average square in signal processing algorithms. 2008. CriMiCo 2008. 2008 18th International Crimean Conference Microwave & Telecommunication Technology. - Sevastopol, Crimea, 8-12 Sept. 2008. - P. 911-912. ↑
- C2034.** Roenko A.N. Experimental investigations of flat reflector influence on the signal in Fresnel zone. / Roenko A.N., Velichko D.A., Levantovsky V.Yu., Odnovolik E.V. // 2008. CriMiCo 2008. 2008 18th International Crimean Conference Microwave & Telecommunication Technology. - Sevastopol, Crimea, 8-12 Sept. 2008. - P. 734-735. ↑
- C2035.** Kostina S.S. Organization of computer experiment for Radar research. 2008. MRRS 2008 Microwaves, Radar and Remote Sensing Symposium. - Kiev, 22-24 Sept. 2008. - P. 340-343. ↑
- C2036.** Hao Chen. Hybrid Algorithms for Electromagnetic Detection Satellites Scheduling. / Hao Chen, Jun Li, Ning Jing, Yu Tang. // 2008. ICTAI 08. 20th IEEE International Conference on Tools with Artificial Intelligence. - Dayton, OH, 3-5 Nov. 2008. - Vol. 1. - P. 411-418. ↑
- C2037.** Stikhiy S.V. Modelling of SAR transceiver as a complex system. / Stikhiy S.V., Chikachev V.S. // 2008. CriMiCo 2008. 2008 18th International Crimean Conference Microwave & Telecommunication Technology. - Sevastopol, Crimea, 8-12 Sept. 2008. - P. 419-420. ↑
- C2038.** Heikenfeld J. A novel electrowetting approach for optical phased arrays invited talk-EOSS. / Heikenfeld J., Smith N., Hou L., Zhang J. // 2008. LEOS 2008. 21st Annual Meeting of the IEEE Lasers and Electro-Optics Society. - Acapulco, 9-13 Nov. 2008. - P. 577-578. ↑
- C2039.** Mengling Liu. A hierarchical boosting algorithm based on feature selection for Synthetic Aperture Radar image retrieval. / Mengling Liu, Chu He, Chao Qian, Hong Sun. // 2008. ICSP 2008. 9th International Conference on Signal Processing. - Beijing, 26-29 Oct. 2008. - P. 981-984. ↑
- C2040.** Wen-Qin Wang. Azimuth signal processing for near-space high-resolution and wide-swath SAR imaging. / Wen-Qin Wang, Qicong Peng, Jingye Cai, Lin Wang. // 2008. ICSP 2008. 9th International Conference on Signal Processing. - Beijing, 26-29 Oct. 2008. - P. 2330-2333. ↑
- C2041.** Hu Donghong. Snail Identification Based on Fourier Transformation. / Hu Donghong, Chen Wei, Wang Hao, Zhang Ling, Wang Ying. // 2008. ICINIS '08. First International Conference on Intelligent Networks and Intelligent Systems. - Wuhan, 1-3 Nov. 2008. - P. 543-547. ↑
- C2042.** Lutsenko V.I. Use doppler radars for studying turbulence of air weights in storm clouds. / Lutsenko V.I., Lutsenko I.V. // 2008. CriMiCo 2008. 2008 18th International Crimean Conference Microwave & Telecommunication Technology. - Sevastopol, Crimea, 8-12 Sept. 2008. - P. 913-914. ↑
- C2043.** {no data available}. Title page. 2008. CriMiCo 2008. 2008 18th International Crimean Conference Microwave & Telecommunication Technology. - Sevastopol, Crimea, 8-12 Sept. 2008. - P. I. ↑
- C2044.** Buonanno S. Wind map retrieval from SAR data for offshore wind turbines positioning. / Buonanno S.,

Cuozzo G., Fusco A. // 2008. ISIE 2008. IEEE International Symposium on Industrial Electronics. - Cambridge, June 30 2008-July 2 2008. - P. 2311-2316. ↑

C2045. Cong Chen. Electromagnetic modelling of ship classification in OTHR. / Cong Chen, Huotao Gao. // 2008. ISAPE 2008. 8th International Symposium on Antennas, Propagation and EM Theory. - Kunming, 2-5 Nov. 2008. - P. 717-720. ↑

C2046. Wen-Qin Wang. Digital beamforming for near-space wide-swath SAR imaging. / Wen-Qin Wang, Qicong Peng, Jingye Cai. // 2008. ISAPE 2008. 8th International Symposium on Antennas, Propagation and EM Theory. - Kunming, 2-5 Nov. 2008. - P. 1270-1273. ↑

C2047. Chaojian Shi. Architecture of vision enhancement system for maritime search and rescue. / Chaojian Shi, Kaiyu Xu, Jing Peng, Lei Ren. // 2008. ITST 2008. 8th International Conference on ITS Telecommunications. - Phuket, 24-24 Oct. 2008. - P. 12-17. ↑

C2048. Jee-Hoon Lee. Doppler radar sensing system of respiration and heart rate. / Jee-Hoon Lee, Yun-Taek Im, Seong-Ook Park. // 2008. ISAPE 2008. 8th International Symposium on Antennas, Propagation and EM Theory. - Kunming, 2-5 Nov. 2008. - P. 706-708. ↑

C2049. Wanlan Wu. Classification for polarimetric SAR images based on subaperture decomposition. / Wanlan Wu, Haijiang Wang, Yiming Pi. // 2008. ISAPE 2008. 8th International Symposium on Antennas, Propagation and EM Theory. - Kunming, 2-5 Nov. 2008. - P. 381-384. ↑

C2050. Feng Zhu. A new method of camouflage jamming against ISAR based on compensating modulation. / Feng Zhu, You-qian Feng, You-qing Bai, Qun Zhang, Ying Luo. // 2008. ISAPE 2008. 8th International Symposium on Antennas, Propagation and EM Theory. - Kunming, 2-5 Nov. 2008. - P. 422-425. ↑

C2051. Wang Qin. Range sidelobes suppression for HF surface wave radar with discontinuous spectra. / Wang Qin, Yang Zijie, Wan Xianrong, Xiong Junzhi. // 2008. ISAPE 2008. 8th International Symposium on Antennas, Propagation and EM Theory. - Kunming, 2-5 Nov. 2008. - P. 645-648. ↑

C2052. Currenti G. Automated procedure for InSAR data inversion using Finite Element Method. / Currenti G., Del Negro C., Scandura D., Williams C.A. // 2008. USEReST 2008. Second Workshop on Use of Remote Sensing Techniques for Monitoring Volcanoes and Seismogenic Areas. - Naples, 11-14 Nov. 2008. - P. 1-5. ↑

C2053. Samsonov S. Surface deformation studies of Tenerife Island, Spain from joint GPS-DInSAR observations. / Samsonov S., Tiampo K., Gonzalez P.J., Prieto J., Camacho A.G., Fernandez J. // 2008. USEReST 2008. Second Workshop on Use of Remote Sensing Techniques for Monitoring Volcanoes and Seismogenic Areas. - Naples, 11-14 Nov. 2008. - P. 1-6. ↑

C2054. Zarah S. Preliminary results of lava flow mapping using remote sensing in Piton de la Fournaise, La Réunion island. / Zarah S., Nicolas V., Minoru U., Thomas S., Astrid G. // 2008. USEReST 2008. Second Workshop on Use of Remote Sensing Techniques for Monitoring Volcanoes and Seismogenic Areas. - Naples, 11-14 Nov. 2008. - P. 1-4. ↑

C2055. Borgstrom S. GlobVolcano project overview. / Borgstrom S., Seifert F.M., Tampellini L., Ratti R. // 2008. USEReST 2008. Second Workshop on Use of Remote Sensing Techniques for Monitoring Volcanoes and Seismogenic Areas. - Naples, 11-14 Nov. 2008. - P. 1-6. ↑

C2056. {no data available}. Proceedings of the 2008 second workshop on USE of remote sensing techniques for monitoring volcanoes and seismogenic areas USEReST 2008. 2008. USEReST 2008. Second Workshop on Use of Remote Sensing Techniques for Monitoring Volcanoes and Seismogenic Areas. - Naples, 11-14 Nov. 2008. - P. 1-3. ↑

C2057. Crippa B. Coupling geophysical modelling and geodesy to unravel the physics of active faults. / Crippa B., Sabadini R., Chersich M., Barzaghi R., Panza G. // 2008. USEReST 2008. Second Workshop on Use of Remote Sensing Techniques for Monitoring Volcanoes and Seismogenic Areas. - Naples, 11-14 Nov. 2008. - P. 1-5. ↑

C2058. Antonello G. Microwave interferometric sensors as a tool for space and time analysis of active volcano deformations: The Stromboli case. / Antonello G., Fortuny J., Tarchi D., Casagli N., Del Ventisette C., Guerri L., Luzi G., Mugnai F., Leva D. // 2008. USEReST 2008. Second Workshop on Use of Remote Sensing Techniques

for Monitoring Volcanoes and Seismogenic Areas. - Naples, 11-14 Nov. 2008. - P. 1-6. ↑

C2059. Zhijiang Li. Dynamic Range Compression and Pseudo-color Presentation Based on Retinex for SAR Images. / Zhijiang Li, Jianping Liu, Jing Huang. // 2008 International Conference on Computer Science and Software Engineering. - Wuhan, Hubei, 12-14 Dec. 2008. - Vol. 6. - P. 257-260. ↑

C2060. Venturini R. Experimental verification of COSMO-SkyMed SAR capabilities. / Venturini R., Fois F., Sirocchi G., Bauleo A., Bazzoni A., Borgarelli L., Capece P., Cereoli L., Croci R., Farina C., Pepe P., Scarchilli C., Torre A., Capuzi A., Caltagirone F. // 2008. RADAR 08. IEEE Radar Conference. - Rome, 26-30 May 2008. - P. 1-5. ↑

C2061. Nghiem S.V. Arctic sea ice mapping with satellite radars. / Nghiem S.V., Clemete-Colon P. // 2008. RADAR 08. IEEE Radar Conference. - Rome, 26-30 May 2008. - P. 1-3. ↑

C2062. Allen C. Ground-based multi-channel synthetic-aperture radar for mapping the ice-bed interface. / Allen C., Paden J., Dunson D., Gogineni P. // 2008. RADAR 08. IEEE Radar Conference. - Rome, 26-30 May 2008. - P. 1-6. ↑

C2063. Jara V.A. Portable temperate ice depth sounder radar (TIDSoR). / Jara V.A., Player K.M., Abi D., Rodriguez-Morales F., Gogineni S., Harish A.R., Leuschen C. // 2008. RADAR 08. IEEE Radar Conference. - Rome, 26-30 May 2008. - P. 1-5. ↑

C2064. Lanari R. ERS Differential SAR Interferometry: A powerful tool for surface deformation analysis. / Lanari R., Sansosti E. // 2008. RADAR 08. IEEE Radar Conference. - Rome, 26-30 May 2008. - P. 1-6. ↑

C2065. Hanssen R.F. Monitoring water defense structures using radar interferometry. / Hanssen R.F., van Leijen F.J. // 2008. RADAR 08. IEEE Radar Conference. - Rome, 26-30 May 2008. - P. 1-4. ↑

C2066. Krieger G. Advanced synthetic aperture radar based on digital beamforming and waveform diversity. / Krieger G., Gebert N., Younis M., Moreira A. // 2008. RADAR 08. IEEE Radar Conference. - Rome, 26-30 May 2008. - P. 1-6. ↑

C2067. Giudici D. Analysis of antenna pointing errors on SAR image quality. / Giudici D., D'Aria D., Guarnieri A.M., Bazzoni A., Venturini R. // 2008. RADAR 08. IEEE Radar Conference. - Rome, 26-30 May 2008. - P. 1-6. ↑

C2068. Calabrese D. COSMO-SkyMed: Calibration & validation resources and activities. / Calabrese D., Cricenti A., Grimaldi V., Scaranari D., Vigliotti R., Covello F., Marano G. // 2008. RADAR 08. IEEE Radar Conference. - Rome, 26-30 May 2008. - P. 1-6. ↑

C2069. Kononov A.A. Maximum likelihood estimation of the forest stem volume from VHF SAR data at the individual tree level. / Kononov A.A., Min-Ho Ka. // 2008. RADAR 08. IEEE Radar Conference. - Rome, 26-30 May 2008. - P. 1-6. ↑

C2070. Nieto-Borge J.C. Analysis of sea state parameters and ocean currents from temporal sequences of marine radar images of the sea surface. / Nieto-Borge J.C., Hessner K., Jarabo-Amores P., de la Mata Moya D. // 2008. RADAR 08. IEEE Radar Conference. - Rome, 26-30 May 2008. - P. 1-5. ↑

C2071. Kumar Mishra A. Multipolar SAR ATR: Experiments with the GTRI dataset. / Kumar Mishra A., Mulgrew B. // 2008. RADAR 08. IEEE Radar Conference. - Rome, 26-30 May 2008. - P. 1-5. ↑

C2072. Alberti G. Preliminary performance analysis and design for a distributed P-band synthetic aperture radar. / Alberti G., Fasano G., D'Errico M., Cesare S., Sechi G., Cosmo M., Formaro R., Rioli Q. // 2008. RADAR 08. IEEE Radar Conference. - Rome, 26-30 May 2008. - P. 1-6. ↑

C2073. Chuhong Fei. Development of a polarimetric CFAR detector using Markov Chains. / Chuhong Fei, Anastassopoulos V., Ting Liu, Lampropoulos G.A., Murnaghan K., Sabry R. // 2008. RADAR 08. IEEE Radar Conference. - Rome, 26-30 May 2008. - P. 1-6. ↑

C2074. Balajti I. Performance measurements of the radar "in situ". 2008. MRRS 2008 Microwaves, Radar and Remote Sensing Symposium. - Kiev, 22-24 Sept. 2008. - P. 334-339. ↑

C2075. Prokopenko I.G. Spectral estimation by the model of Autoregressive Moving Average and its resolution

power. / Prokopenko I.G., Churina A.J. // 2008. MRRS 2008 Microwaves, Radar and Remote Sensing Symposium. - Kiev, 22-24 Sept. 2008. - P. 162-165. ↑

C2076. Kawalec A. Radar pulse trains classification. / Kawalec A., Pieniezny A. // 2008. MRRS 2008 Microwaves, Radar and Remote Sensing Symposium. - Kiev, 22-24 Sept. 2008. - P. 166-169. ↑

C2077. Bokal Z.M. Nonparametric method for estimating spoken language sound multivariate probability density function. / Bokal Z.M., Sinitsyn R.B. // 2008. MRRS 2008 Microwaves, Radar and Remote Sensing Symposium. - Kiev, 22-24 Sept. 2008. - P. 170-171. ↑

C2078. Alexin S.G. Modification of Newton-Kantorovich iteration procedure for piecewise-constant real permittivity profile reconstruction. / Alexin S.G., Drobakhin O.O., Tkachenko V.O. // 2008. MRRS 2008 Microwaves, Radar and Remote Sensing Symposium. - Kiev, 22-24 Sept. 2008. - P. 158-161. ↑

C2079. Antropov O.S. Edge-preserving piecewise-constant image restoration via method of minimum of extension. 2008. MRRS 2008 Microwaves, Radar and Remote Sensing Symposium. - Kiev, 22-24 Sept. 2008. - P. 143-146. ↑

C2080. Antropov O.S. Microwave Fourier-holography approach improvement via minimum duration amplitude multifrequency data extrapolation. / Antropov O.S., Borulko V.F., Drobakhin O.O., Vovk S.M. // 2008. MRRS 2008 Microwaves, Radar and Remote Sensing Symposium. - Kiev, 22-24 Sept. 2008. - P. 147-150. ↑

C2081. Kulpa K. The CLEAN type algorithms for radar signal processing. 2008. MRRS 2008 Microwaves, Radar and Remote Sensing Symposium. - Kiev, 22-24 Sept. 2008. - P. 152-157. ↑

C2082. Yanovsky F.J. Recent researches in the field of weather radar at the National Aviation University. 2008. MRRS 2008 Microwaves, Radar and Remote Sensing Symposium. - Kiev, 22-24 Sept. 2008. - P. 190-193. ↑

C2083. Boriskin A.V. 2-D analysis and synthesis of dielectric lens antennas with boundary integral equations. / Boriskin A.V., Sauleau R., Nosich A.I. // 2008. MRRS 2008 Microwaves, Radar and Remote Sensing Symposium. - Kiev, 22-24 Sept. 2008. - P. 196-200. ↑

C2084. Pasternak M. Quasi-loop antenna for SAW RFID device. / Pasternak M., Pietrasinski J. // 2008. MRRS 2008 Microwaves, Radar and Remote Sensing Symposium. - Kiev, 22-24 Sept. 2008. - P. 201-203. ↑

C2085. Ostrovsky Y. Multivariate algorithms for dangerous turbulence detection in weather formations. 2008. MRRS 2008 Microwaves, Radar and Remote Sensing Symposium. - Kiev, 22-24 Sept. 2008. - P. 186-189. ↑

C2086. Zrnic D. Weather radar-recent developments and trends. 2008. MRRS 2008 Microwaves, Radar and Remote Sensing Symposium. - Kiev, 22-24 Sept. 2008. - P. 174-178. ↑

C2087. Averyanova Yu. The estimate of instantaneous power of polarization spectrum components in polarimetric weather radar. / Averyanova Yu., Averyanov A., Yanovsky F. // 2008. MRRS 2008 Microwaves, Radar and Remote Sensing Symposium. - Kiev, 22-24 Sept. 2008. - P. 179-181. ↑

C2088. Marchuk V. Use of spectral differential reflectivity at remote sensing of precipitation. / Marchuk V., Yanovsky F.J. // 2008. MRRS 2008 Microwaves, Radar and Remote Sensing Symposium. - Kiev, 22-24 Sept. 2008. - P. 182-185. ↑

C2089. Lukin V.V. An automatic approach to lossy compression of images corrupted by Poisson noise. / Lukin V.V., Zriakhov M.S., Ponomarenko N.N., Kaarna A. // 2008. MRRS 2008 Microwaves, Radar and Remote Sensing Symposium. - Kiev, 22-24 Sept. 2008. - P. 139-142. ↑

C2090. Grimalsky V. Amplification of space charge waves of millimeter wave range in transversely inhomogeneous n-GaN Films. / Grimalsky V., Koshevaya S., Diaz-A F., Hernandez-P J.A. // 2008. MRRS 2008 Microwaves, Radar and Remote Sensing Symposium. - Kiev, 22-24 Sept. 2008. - P. 98-101. ↑

C2091. Moroz I. Simulation of electromagnetic wave propagation through dielectric waveguide with p-i-n control element. / Moroz I., Koshevaya S., Grimalsky V., Kotsarenko A., Escobedo-A J. // 2008. MRRS 2008 Microwaves, Radar and Remote Sensing Symposium. - Kiev, 22-24 Sept. 2008. - P. 102-104. ↑

- C2092.** Antyufeyeva M.S. Microwave oscillations in a cavity with dispersive double negative medium. / Antyufeyeva M.S., Butrym A.Yu., Tretyakov O.A. // 2008. MRRS 2008 Microwaves, Radar and Remote Sensing Symposium. - Kiev, 22-24 Sept. 2008. - P. 105-107. ↑
- C2093.** Cherpak N.T. Quasi-optical sapphire resonators for millimeter wave impedance characterization of high-TC superconducting thin films. / Cherpak N.T., Barannik A.A., Bunyaev S.A. // 2008. MRRS 2008 Microwaves, Radar and Remote Sensing Symposium. - Kiev, 22-24 Sept. 2008. - P. 94-97. ↑
- C2094.** Falie D. Wide range Time of Flight camera for outdoor surveillance. / Falie D., Buzuloiu V. // 2008. MRRS 2008 Microwaves, Radar and Remote Sensing Symposium. - Kiev, 22-24 Sept. 2008. - P. 79-82. ↑
- C2095.** Konchenko I. Availability analysis of the multilateration surveillance system in Kiev (Boryspil) airport. 2008. MRRS 2008 Microwaves, Radar and Remote Sensing Symposium. - Kiev, 22-24 Sept. 2008. - P. 83-85. ↑
- C2096.** Poplavko Y. Microwave study of ferroelectrics in waveguide. / Poplavko Y., Molchanov V., Pashkov V., Prokopenko Y., Kazmirenko V., Yermenko A., Carru J.-C., Fasquelle D., Mascot M. // 2008. MRRS 2008 Microwaves, Radar and Remote Sensing Symposium. - Kiev, 22-24 Sept. 2008. - P. 88-93. ↑
- C2097.** Shutenko T.A. Quantum interference in transistors. / Shutenko T.A., Aleiner I.L., Altshuler B.L. // 2008. MRRS 2008 Microwaves, Radar and Remote Sensing Symposium. - Kiev, 22-24 Sept. 2008. - P. 126-129. ↑
- C2098.** Jung-Young Son. Comparisons of 3 dimensional temperature distributions of mm and IR images. / Jung-Young Son, Guschin V.P., Denisov A.G., Seok-Won Yeom, Dae-Hyun Jung. // 2008. MRRS 2008 Microwaves, Radar and Remote Sensing Symposium. - Kiev, 22-24 Sept. 2008. - P. 132-135. ↑
- C2099.** Drobakhin O.O. Microwave multifrequency radar images of electrodynamic objects. / Drobakhin O.O., Alekseev V.V., Chekh A.I. // 2008. MRRS 2008 Microwaves, Radar and Remote Sensing Symposium. - Kiev, 22-24 Sept. 2008. - P. 136-138. ↑
- C2100.** Korotash I.V. High-temperature superconductor-films microstrip band-pass filters for extreme working conditions. / Korotash I.V., Rudenko E.M. // 2008. MRRS 2008 Microwaves, Radar and Remote Sensing Symposium. - Kiev, 22-24 Sept. 2008. - P. 122-125. ↑
- C2101.** Chamor T.G. Hybrid oscillations in composite resonators with uniaxial hexaferites. / Chamor T.G., Chevnyuk L.V., Gorpynyuk A.Yu., Kostenko V.I. // 2008. MRRS 2008 Microwaves, Radar and Remote Sensing Symposium. - Kiev, 22-24 Sept. 2008. - P. 108-109. ↑
- C2102.** Brebels S. System-in-a-package technology for 3D integration of radar modules. / Brebels S., Sun X., Carchon G., Posada G., Dussopt L., Dubois M.-A., Vandenbosch G., De Raedt W. // 2008. MRRS 2008 Microwaves, Radar and Remote Sensing Symposium. - Kiev, 22-24 Sept. 2008. - P. 112-115. ↑
- C2103.** Malyshev S. High-speed photodiodes for microwave and millimeter-wave systems. / Malyshev S., Chizh A., Vasileuski Y. // 2008. MRRS 2008 Microwaves, Radar and Remote Sensing Symposium. - Kiev, 22-24 Sept. 2008. - P. 116-121. ↑
- C2104.** Pitertsev A. Radar determination of probable icing-in-flight. 2008. MRRS 2008 Microwaves, Radar and Remote Sensing Symposium. - Kiev, 22-24 Sept. 2008. - P. 293-295. ↑
- C2105.** Korchemkina E.N. Regional analytical algorithm of sea chlorophyll concentrations retrieving from sea reflectance. / Korchemkina E.N., Shybanov E.B., Lee M.E. // 2008. MRRS 2008 Microwaves, Radar and Remote Sensing Symposium. - Kiev, 22-24 Sept. 2008. - P. 296-299. ↑
- C2106.** Assiri A. Using ASTER imagery for massive sulphide deposits exploration. / Assiri A., Mousa H. // 2008. MRRS 2008 Microwaves, Radar and Remote Sensing Symposium. - Kiev, 22-24 Sept. 2008. - P. 300-303. ↑
- C2107.** Khlopov G.I. Remote sensing for systems of active impact on clouds. / Khlopov G.I., Sirota N.V., Khomenko S.I., Morozov V.E., Vojtovich O.A. // 2008. MRRS 2008 Microwaves, Radar and Remote Sensing Symposium. - Kiev, 22-24 Sept. 2008. - P. 289-292. ↑
- C2108.** Mozhyrovskiy M.V. Bandwidth suppression in MM-Wave photonic structure with magnetic "defect". / Mozhyrovskiy M.V., Oliynyk V.V. // 2008. MRRS 2008 Microwaves, Radar and Remote Sensing Symposium. -

Kiev, 22-24 Sept. 2008. - P. 276-278. ↑

C2109. Vishnevsky A.V. Computation method of mutual impact coefficient of the quarter-wave wire antennas placed on airplane wire-grid model. 2008. MRRS 2008 Microwaves, Radar and Remote Sensing Symposium. - Kiev, 22-24 Sept. 2008. - P. 279-282. ↑

C2110. Hernandez C.C. Design and performance assessment of an airborne ice sounding radar front-end. / Hernandez C.C., Krozer V., Vidkjaer J., Dall J. // 2008. MRRS 2008 Microwaves, Radar and Remote Sensing Symposium. - Kiev, 22-24 Sept. 2008. - P. 284-288. ↑

C2111. Aznakayev E. Mathematical modeling of the cardiac electrical signals formation. / Aznakayev E., Melnikov E. // 2008. MRRS 2008 Microwaves, Radar and Remote Sensing Symposium. - Kiev, 22-24 Sept. 2008. - P. 321-323. ↑

C2112. Naidenko V.I. Application of microwave radiation in incinerator. / Naidenko V.I., Shumakov D.S. // 2008. MRRS 2008 Microwaves, Radar and Remote Sensing Symposium. - Kiev, 22-24 Sept. 2008. - P. 326-328. ↑

C2113. Karpovich V. Electromagnetic energy application for soil infectious diseases sterilization. / Karpovich V., Ermolovich A., Volinets G., Kostukevich I. // 2008. MRRS 2008 Microwaves, Radar and Remote Sensing Symposium. - Kiev, 22-24 Sept. 2008. - P. 329-331. ↑

C2114. Khraisat Y.S.H. Multi-switch Satellite Digital System (MSDS). 2008. MRRS 2008 Microwaves, Radar and Remote Sensing Symposium. - Kiev, 22-24 Sept. 2008. - P. 317-320. ↑

C2115. Al-Qawasmi A.-R. The effect of amplitude fades on a forward transmission system using a DS CDMA. / Al-Qawasmi A.-R., Al-lawama A. // 2008. MRRS 2008 Microwaves, Radar and Remote Sensing Symposium. - Kiev, 22-24 Sept. 2008. - P. 306-309. ↑

C2116. Kasperovych N. Noise modeling for global satellite aeronavigation systems. / Kasperovych N., Shvets V., Ostrovsky Y. // 2008. MRRS 2008 Microwaves, Radar and Remote Sensing Symposium. - Kiev, 22-24 Sept. 2008. - P. 310-313. ↑

C2117. Borodin V.A. Organization of software for dynamic scenes visualization and analysis in real-time geoinformation complexes. 2008. MRRS 2008 Microwaves, Radar and Remote Sensing Symposium. - Kiev, 22-24 Sept. 2008. - P. 314-316. ↑

C2118. Vizitiu I.-C. More efficient ATR system using the decision fusion between HRR and video imagery. / Vizitiu I.-C., Nicolaescu I. // 2008. MRRS 2008 Microwaves, Radar and Remote Sensing Symposium. - Kiev, 22-24 Sept. 2008. - P. 272-275. ↑

C2119. Ferro-Famil L. Remote sensing of urban areas from polarimetric SAR data using Time-Frequency and spectral analysis methods. / Ferro-Famil L., Leducq P., Sauer S. // 2008. MRRS 2008 Microwaves, Radar and Remote Sensing Symposium. - Kiev, 22-24 Sept. 2008. - P. 220-225. ↑

C2120. Vavriv D.M. High-accuracy Doppler measurements for airborne SAR imaging. / Vavriv D.M., Bezvesilnyi O.O., Vynogradov V.V. // 2008. MRRS 2008 Microwaves, Radar and Remote Sensing Symposium. - Kiev, 22-24 Sept. 2008. - P. 226-231. ↑

C2121. Kulpa K. Multilook technique for dominant scatterer removal in SAR images. / Kulpa K., Misiurewicz J., Samczynski P., Smolarczyk M. // 2008. MRRS 2008 Microwaves, Radar and Remote Sensing Symposium. - Kiev, 22-24 Sept. 2008. - P. 232-235. ↑

C2122. Khraisat Y.S.H. Analysis of the parameters of asymmetrical dual feeding full wave dipole antenna. / Khraisat Y.S.H., Hmood K.A., Anwar A. // 2008. MRRS 2008 Microwaves, Radar and Remote Sensing Symposium. - Kiev, 22-24 Sept. 2008. - P. 215-217. ↑

C2123. Chernobrovkin R. Test results of a compact smooth-walled spline-profile horn at 30-38 GHz for radio astronomy application. / Chernobrovkin R., Popenko N., Khaikin V., Granet C. // 2008. MRRS 2008 Microwaves, Radar and Remote Sensing Symposium. - Kiev, 22-24 Sept. 2008. - P. 204-207. ↑

C2124. Khruslov M. Monopole antenna with plug-shape ground plane. / Khruslov M., Ivanchenko I., Popenko

N. // 2008. MRRS 2008 Microwaves, Radar and Remote Sensing Symposium. - Kiev, 22-24 Sept. 2008. - P. 208-210. ↑

C2125. Ivanchenko I. Near-field measurements in the microwave and millimetre ranges. / Ivanchenko I., Ivanchenko D., Korolev A., Khruslov M., Popenko N. // 2008. MRRS 2008 Microwaves, Radar and Remote Sensing Symposium. - Kiev, 22-24 Sept. 2008. - P. 211-214. ↑

C2126. Karwatka J. Target tracking using radar and direction finder. 2008. MRRS 2008 Microwaves, Radar and Remote Sensing Symposium. - Kiev, 22-24 Sept. 2008. - P. 256-260. ↑

C2127. Van Tho Dang. An adaptive Kalman filter for radar tracking application. 2008. MRRS 2008 Microwaves, Radar and Remote Sensing Symposium. - Kiev, 22-24 Sept. 2008. - P. 261-264. ↑

C2128. Suarez A. Global stability analysis and stabilization of power amplifiers. / Suarez A., Jeon S., Rutledge D. // 2008. MRRS 2008 Microwaves, Radar and Remote Sensing Symposium. - Kiev, 22-24 Sept. 2008. - P. 266-271. ↑

C2129. Nicolaescu I. Procedures to improve the performances of a Sfcw radar used for landmine detection. / Nicolaescu I., van Genderen P. // 2008. MRRS 2008 Microwaves, Radar and Remote Sensing Symposium. - Kiev, 22-24 Sept. 2008. - P. 250-255. ↑

C2130. Dukhopelnikova I.V. New difference Doppler centroid estimation method with high space resolution. 2008. MRRS 2008 Microwaves, Radar and Remote Sensing Symposium. - Kiev, 22-24 Sept. 2008. - P. 236-239. ↑

C2131. Samczynski P. The Coherent MapDrift technique robustness to low SNR SAR data. 2008. MRRS 2008 Microwaves, Radar and Remote Sensing Symposium. - Kiev, 22-24 Sept. 2008. - P. 240-243. ↑

C2132. Beasley P. Advances in millimetre wave FMCW radar. 2008. MRRS 2008 Microwaves, Radar and Remote Sensing Symposium. - Kiev, 22-24 Sept. 2008. - P. 246-249. ↑

C2133. Reale D. 3D Imaging of Ground based SAR Data. / Reale D., Pascasio V., Schirinzi G., Serafino F. // 2008. IGARSS 2008. IEEE International Geoscience and Remote Sensing Symposium. - Boston, MA, 7-11 July 2008. - Vol. 4. - P. IV-1280 - IV - 1283-1280. ↑

C2134. Vu V.T. A Comparison between Fast Factorized Backprojection and Frequency-Domain Algorithms in UWB Lowfrequency SAR. / Vu V.T., Sjogren T.K., Pettersson M.I. // 2008. IGARSS 2008. IEEE International Geoscience and Remote Sensing Symposium. - Boston, MA, 7-11 July 2008. - Vol. 4. - P. IV-1284 - IV - 1287-1284. ↑

C2135. Fan Ye. Radar Signal Level Fusion Imaging. / Fan Ye, Feng He, Zaoyu Sun. // 2008. IGARSS 2008. IEEE International Geoscience and Remote Sensing Symposium. - Boston, MA, 7-11 July 2008. - Vol. 4. - P. IV-1288 - IV - 1291-1288. ↑

C2136. Xinwu Li. Land Cover Characterization and Classification using Polarimetric ALOS PALSAR. / Xinwu Li, Touzi R., Huadong Guo. // 2008. IGARSS 2008. IEEE International Geoscience and Remote Sensing Symposium. - Boston, MA, 7-11 July 2008. - Vol. 4. - P. IV-1276 - IV - 1279-1276. ↑

C2137. Garcia-Pineda O. Synthetic Aperture Radar Image Processing using the Supervised Textural-Neural Network Classification Algorithm. / Garcia-Pineda O., MacDonald I., Zimmer B. // 2008. IGARSS 2008. IEEE International Geoscience and Remote Sensing Symposium. - Boston, MA, 7-11 July 2008. - Vol. 4. - P. IV-1265 - IV - 1268-1265. ↑

C2138. Wei Jie. A Nonlinear Refined Extended Chirp Scaling Algorithm for Spaceborne ScanSAR. / Wei Jie, Chen Houjin, Zhong Xiaofeng. // 2008. IGARSS 2008. IEEE International Geoscience and Remote Sensing Symposium. - Boston, MA, 7-11 July 2008. - Vol. 4. - P. IV-1269 - IV - 1271-1269. ↑

C2139. Zaugg E.C. Along-Track Resolution Enhancement Forwide-Bandwidth, Low-Frequency SAR by Accounting for the Wavelength Change over the Bandwidth. / Zaugg E.C., Long D.G. // 2008. IGARSS 2008. IEEE International Geoscience and Remote Sensing Symposium. - Boston, MA, 7-11 July 2008. - Vol. 4. - P. IV-1272 - IV - 1275-1272. ↑

- C2140.** Fengli Zhang. Oil Spill Identification based on Textural Information of SAR Image. / Fengli Zhang, Yun Shao, Wei Tian, Shiang Wang. // 2008. IGARSS 2008. IEEE International Geoscience and Remote Sensing Symposium. - Boston, MA, 7-11 July 2008. - Vol. 4. - P. IV-1308 - IV - 1311-1308. ↑
- C2141.** Yong Li. Study on the Geometric Distortion Correction Algorithm for Circular-Scanning SAR Imaging. / Yong Li, Daiyin Zhu, Ling Wang. // 2008. IGARSS 2008. IEEE International Geoscience and Remote Sensing Symposium. - Boston, MA, 7-11 July 2008. - Vol. 4. - P. IV-1312 - IV - 1315-1312. ↑
- C2142.** Sun Bing-Zhang. A New Interference Elimination Method for Multi-Satellite SAR System. / Sun Bing-Zhang, Li Jing-Wen. // 2008. IGARSS 2008. IEEE International Geoscience and Remote Sensing Symposium. - Boston, MA, 7-11 July 2008. - Vol. 4. - P. IV-1316 - IV - 1319-1316. ↑
- C2143.** Li Ran. Precise Simulation of Spaceborne Synthetic Aperture Radar and Its Evaluation. / Li Ran, Li Jing-wen. // 2008. IGARSS 2008. IEEE International Geoscience and Remote Sensing Symposium. - Boston, MA, 7-11 July 2008. - Vol. 4. - P. IV-1304 - IV - 1307-1304. ↑
- C2144.** Lihua Jin. Adaptive Subaperture Approach for Spotlight SAR Azimuth Processing. / Lihua Jin, Xingzhao Liu, Junfeng Wang. // 2008. IGARSS 2008. IEEE International Geoscience and Remote Sensing Symposium. - Boston, MA, 7-11 July 2008. - Vol. 4. - P. IV-1292 - IV - 1295-1292. ↑
- C2145.** Shi Jun. A New LASAR Fast 3-D Imaging Method via Wavelet Approximation. / Shi Jun, Zhang Xiaoling, Yang Jianyu. // 2008. IGARSS 2008. IEEE International Geoscience and Remote Sensing Symposium. - Boston, MA, 7-11 July 2008. - Vol. 4. - P. IV-1296 - IV - 1299-1296. ↑
- C2146.** WeiXian Tan. Airborne Spotlight SAR Imaging with Super High Resolution based on Back-Projection and Autofocus Algorithm. / WeiXian Tan, DaoJing Li, Wen Hong. // 2008. IGARSS 2008. IEEE International Geoscience and Remote Sensing Symposium. - Boston, MA, 7-11 July 2008. - Vol. 4. - P. IV-1300 - IV - 1303-1300. ↑
- C2147.** Santoro M. Thematic Applications of ERS-ENVISAT Cross-Interferometry. / Santoro M., Wegmuller U., Strozzi T., Werner C., Wiesmann A., Lengert W. // 2008. IGARSS 2008. IEEE International Geoscience and Remote Sensing Symposium. - Boston, MA, 7-11 July 2008. - Vol. 4. - P. IV-1225 - IV - 1228-1225. ↑
- C2148.** Qingsong Wang. A Novel Method of InSAR Processing Performance Evaluation based on Ideal Interferometric Factors. / Qingsong Wang, Haifeng Huang, Zhen Dong. // 2008. IGARSS 2008. IEEE International Geoscience and Remote Sensing Symposium. - Boston, MA, 7-11 July 2008. - Vol. 4. - P. IV-1229 - IV - 1232-1229. ↑
- C2149.** Wdowinski S. Evaluation of TerraSAR-X Observations for Wetland InSAR Application. / Wdowinski S., Sang-Hoon Hong, Sang-Wan Kim. // 2008. IGARSS 2008. IEEE International Geoscience and Remote Sensing Symposium. - Boston, MA, 7-11 July 2008. - Vol. 4. - P. IV-1233 - IV - 1236-1233. ↑
- C2150.** Ballatore P. Effect of the Unwrapping Process on the Correlations Among InSAR Differences for the Same Area. / Ballatore P., Wasowski J. // 2008. IGARSS 2008. IEEE International Geoscience and Remote Sensing Symposium. - Boston, MA, 7-11 July 2008. - Vol. 4. - P. IV-1221 - IV - 1224-1221. ↑
- C2151.** Zhang Xiaoling. Trajectory Optimization of Sparse LASAR 3-D SAR Via Lagrange Multiplier Method. / Zhang Xiaoling, Shi Jun, Yang Jianyu. // 2008. IGARSS 2008. IEEE International Geoscience and Remote Sensing Symposium. - Boston, MA, 7-11 July 2008. - Vol. 4. - P. IV-1209 - IV - 1212-1209. ↑
- C2152.** Nies H. Phase Unwrapping using 2D-Kalman Filter-Potential and Limitations. / Nies H., Loffeld O., Wang R. // 2008. IGARSS 2008. IEEE International Geoscience and Remote Sensing Symposium. - Boston, MA, 7-11 July 2008. - Vol. 4. - P. IV-1213 - IV - 1216-1213. ↑
- C2153.** Martinez-Espla J.J. InSAR Phase Unwrapping by Means of a Particle Filter. / Martinez-Espla J.J., Martinez-Marin T., Ballester-Berman J.D., Lopez-Sanchez J.M. // 2008. IGARSS 2008. IEEE International Geoscience and Remote Sensing Symposium. - Boston, MA, 7-11 July 2008. - Vol. 4. - P. IV-1217 - IV - 1220-1217. ↑
- C2154.** Zengguo Sun. Heavy-Tailed Rayleigh Distribution: A New Tool for the Modeling of SAR Amplitude Images. / Zengguo Sun, Chongzhao Han. // 2008. IGARSS 2008. IEEE International Geoscience and Remote Sensing Symposium. - Boston, MA, 7-11 July 2008. - Vol. 4. - P. IV-1253 - IV - 1256-1253. ↑

- C2155.** Junfeng Wang. Automatic Range-Migration Correction in SAR Imaging. / Junfeng Wang, Xingzhao Liu. // 2008. IGARSS 2008. IEEE International Geoscience and Remote Sensing Symposium. - Boston, MA, 7-11 July 2008. - Vol. 4. - P. IV-1257 - IV - 1260-1257. ↑
- C2156.** Qulin Tan. Imaging Experiments from Phase-Corrupted Airborne L-SAR Data. 2008. IGARSS 2008. IEEE International Geoscience and Remote Sensing Symposium. - Boston, MA, 7-11 July 2008. - Vol. 4. - P. IV-1261 - IV - 1264-1261. ↑
- C2157.** Martorella M. Automatic Target Recognition by Means of Polarimetric ISAR Images and Neural Networks. / Martorella M., Giusti E., Capria A., Berizzi F., Bates B. // 2008. IGARSS 2008. IEEE International Geoscience and Remote Sensing Symposium. - Boston, MA, 7-11 July 2008. - Vol. 4. - P. IV-1249 - IV - 1252-1249. ↑
- C2158.** Ballatore P. Application of Independent Component Analysis on ERS SAR Interferograms for the Elimination of Spurious Artifacts. 2008. IGARSS 2008. IEEE International Geoscience and Remote Sensing Symposium. - Boston, MA, 7-11 July 2008. - Vol. 4. - P. IV-1237 - IV - 1240-1237. ↑
- C2159.** Fukuchi H. Extraction of Area Averaged Urban Parameters from POLSAR Measurement. / Fukuchi H., Aso Y., Takeshiro A., Komatsu Y., Satake M. // 2008. IGARSS 2008. IEEE International Geoscience and Remote Sensing Symposium. - Boston, MA, 7-11 July 2008. - Vol. 4. - P. IV-1241 - IV - 1244-1241. ↑
- C2160.** Sant'Anna S. Analysis of Simulated Polarimetric SAR Images Generated by a Multilayer Electromagnetic Scattering Model. / Sant'Anna S., da S. Lacava J.C., Fernandes D. // 2008. IGARSS 2008. IEEE International Geoscience and Remote Sensing Symposium. - Boston, MA, 7-11 July 2008. - Vol. 4. - P. IV-1245 - IV - 1248-1245. ↑
- C2161.** Sang-Hoon Lee. Adaptive SAR Despeckling using a Proximity Measure to Boundary. 2008. IGARSS 2008. IEEE International Geoscience and Remote Sensing Symposium. - Boston, MA, 7-11 July 2008. - Vol. 4. - P. IV-1320 - IV - 1323-1320. ↑
- C2162.** Naenna P. Monte Carlo Simulation of Altimeter Pulse Returns and Electromagnetic Bias. / Naenna P., Johnson J.T. // 2008. IGARSS 2008. IEEE International Geoscience and Remote Sensing Symposium. - Boston, MA, 7-11 July 2008. - Vol. 5. - P. V-120 - V - 123-120. ↑
- C2163.** Santoro M. Automatic Model Inversion of Multi-Temporal C-band Coherence and Backscatter Measurements for Forest Stem Volume Retrieval. / Santoro M., Askne J., Beer C., Cartus O., Schmullius C., Wegmuller U., Wiesmann A. // 2008. IGARSS 2008. IEEE International Geoscience and Remote Sensing Symposium. - Boston, MA, 7-11 July 2008. - Vol. 5. - P. V-124 - V - 127-124. ↑
- C2164.** Moghaddam M. A Soil Moisture Smart Sensor Web using Data Assimilation and Optimal Control: Formulation and First Laboratory Demonstration. / Moghaddam M., Entekhabi D., Goykhman Y., Liu M., Mahajan A., Nayyar A., Shuman D., Teneketzis D. // 2008. IGARSS 2008. IEEE International Geoscience and Remote Sensing Symposium. - Boston, MA, 7-11 July 2008. - Vol. 5. - P. V-140 - V - 143-140. ↑
- C2165.** Hwang P.A. An Empirical Study of Breaking Wave Contribution to Radar Backscatter from the Ocean Surface at Low Grazing Angle. / Hwang P.A., Sletten M.A., Toporkov J.V. // 2008. IGARSS 2008. IEEE International Geoscience and Remote Sensing Symposium. - Boston, MA, 7-11 July 2008. - Vol. 5. - P. V-113 - V - 116-113. ↑
- C2166.** Venkatesh V. The UMass X-Pol Mobile Doppler Radar: Description, Recent Observations, and New System Developments. / Venkatesh V., Palreddy S., Hopf A., Hardwick K., Tsai P.-S., Frasier S.J., Bluestein H., Hauser J., French M., Snyder J., Tanamachi R. // 2008. IGARSS 2008. IEEE International Geoscience and Remote Sensing Symposium. - Boston, MA, 7-11 July 2008. - Vol. 5. - P. V-101 - V - 104-101. ↑
- C2167.** McLinden M. Calibration of the UMass Advanced Multi-Frequency Radar (AMFR). / McLinden M., Siqueira P., Majurec N. // 2008. IGARSS 2008. IEEE International Geoscience and Remote Sensing Symposium. - Boston, MA, 7-11 July 2008. - Vol. 5. - P. V-105 - V - 108-105. ↑
- C2168.** George J. Considerations in Pulse Compression Design for Weather Radars. / George J., Bharadwaj N., Chandrasekar V. // 2008. IGARSS 2008. IEEE International Geoscience and Remote Sensing Symposium. - Boston, MA, 7-11 July 2008. - Vol. 5. - P. V-109 - V - 112-109. ↑

- C2169.** Junghyo Kim. Experimental Performance Investigation of Digital Beamforming on Synthetic Aperture Radar. / Junghyo Kim, Younis M., Wiesbeck W. // 2008. IGARSS 2008. IEEE International Geoscience and Remote Sensing Symposium. - Boston, MA, 7-11 July 2008. - Vol. 5. - P. V-176 - V - 179-176. ↑
- C2170.** Tao Lai. Achieving HRWS Images with Space-borne Bistatic SAR with Multiple Phase Centers. / Tao Lai, Zhen Dong, Dian-nong Liang, Feng He. // 2008. IGARSS 2008. IEEE International Geoscience and Remote Sensing Symposium. - Boston, MA, 7-11 July 2008. - Vol. 5. - P. V-180 - V - 183-180. ↑
- C2171.** Back D. Analysis of C-band Polarimetric Signatures of Arctic Lead Ice using Data from AIRSAR and RADARSAT-1. / Back D., Holt B., Ron Kwok. // 2008. IGARSS 2008. IEEE International Geoscience and Remote Sensing Symposium. - Boston, MA, 7-11 July 2008. - Vol. 5. - P. V-184 - V - 187-184. ↑
- C2172.** Stasolla M. Semi-Automated Extraction of Human Settlement Extent in HR SAR Images. / Stasolla M., Gamba P. // 2008. IGARSS 2008. IEEE International Geoscience and Remote Sensing Symposium. - Boston, MA, 7-11 July 2008. - Vol. 5. - P. V-168 - V - 171-168. ↑
- C2173.** Chandrasekar V. Evaluation of Distributed Collaborative Adaptive Sensing in a Four-Node Radar Network: Integrated Project 1. / Chandrasekar V., McLaughlin D., Brotzge J., Zink M., Philips B., Yanting Wang. // 2008. IGARSS 2008. IEEE International Geoscience and Remote Sensing Symposium. - Boston, MA, 7-11 July 2008. - Vol. 5. - P. V-148 - V - 151-148. ↑
- C2174.** Zink M. Meteorological Command & Control: Architecture and Performance Evaluation. / Zink M., Lyons E., Westbrook D., Pepyne D., Pilips B., Kurose J., Chandrasekar V. // 2008. IGARSS 2008. IEEE International Geoscience and Remote Sensing Symposium. - Boston, MA, 7-11 July 2008. - Vol. 5. - P. V-152 - V - 155-152. ↑
- C2175.** Philips B. User Evaluations of Adaptive Scanning Patterns in the CASA Spring Experiment 2007. / Philips B., Westbrook D., Pepyne D., Brotzge J., Bass E.J., Rude D. // 2008. IGARSS 2008. IEEE International Geoscience and Remote Sensing Symposium. - Boston, MA, 7-11 July 2008. - Vol. 5. - P. V-156 - V - 159-156. ↑
- C2176.** Dogrul M. Simulation of Improved Bandwidth Conformal Bow-Tie Antennas for Remote Sensing Printed on Multi-Scale Triangular-Patch High-Impedance Ground Planes. / Dogrul M., Collins P.J., Saville M., Sertel K., Terzuoli A.J. // 2008. IGARSS 2008. IEEE International Geoscience and Remote Sensing Symposium. - Boston, MA, 7-11 July 2008. - Vol. 4. - P. IV-1402 - IV - 1405-1402. ↑
- C2177.** Xiaolong Dong. Compromise and Trade-Off between Signal-to-Noise Ratio and Number of Independent Samples for Radar Scatterometers with Pulse Compression. / Xiaolong Dong, Wenming Lin, Shuyan Lang, Heguang Liu, Jingshan Jiang. // 2008. IGARSS 2008. IEEE International Geoscience and Remote Sensing Symposium. - Boston, MA, 7-11 July 2008. - Vol. 4. - P. IV-1410 - IV - 1413-1410. ↑
- C2178.** Guo J. Wave Parameters Estimated from Scatterometer Data. / Guo J., He Y., Perrie W. // 2008. IGARSS 2008. IEEE International Geoscience and Remote Sensing Symposium. - Boston, MA, 7-11 July 2008. - Vol. 4. - P. IV-1414 - IV - 1417-1414. ↑
- C2179.** Bernardi G. Fractal based Modeling of Altimeter Data. / Bernardi G., Franceschetti G., Iodice A., Riccio D. // 2008. IGARSS 2008. IEEE International Geoscience and Remote Sensing Symposium. - Boston, MA, 7-11 July 2008. - Vol. 4. - P. IV-1398 - IV - 1401-1398. ↑
- C2180.** Du Lei. Analysis of 3D-SAR based on Angle Compression Principle. / Du Lei, Wang Yanping, Hong Wen, Wu Yirong. // 2008. IGARSS 2008. IEEE International Geoscience and Remote Sensing Symposium. - Boston, MA, 7-11 July 2008. - Vol. 4. - P. IV-1324 - IV - 1327-1324. ↑
- C2181.** Shkvarko Y. Towards the Virtual Remote Sensing Laboratory: Intelligent Experiment Design Paradigm. / Shkvarko Y., Perez-Meana H.M., Castillo-Atoche A. // 2008. IGARSS 2008. IEEE International Geoscience and Remote Sensing Symposium. - Boston, MA, 7-11 July 2008. - Vol. 4. - P. IV-1328 - IV - 1331-1328. ↑
- C2182.** Fan Zhang. SAR Image Simulation of Man-Made Scenes based on Computer Graphics. / Fan Zhang, Wen Hong, Daojing Li. // 2008. IGARSS 2008. IEEE International Geoscience and Remote Sensing Symposium. - Boston, MA, 7-11 July 2008. - Vol. 4. - P. IV-1395 - IV - 1397-1395. ↑
- C2183.** Kontu A. Simulation of Spaceborne Microwave Radiometer Measurements of Snow Cover using In-Situ Data and Emission Models. / Kontu A., Pulliainen J. // 2008. IGARSS 2008. IEEE International Geoscience and

Remote Sensing Symposium. - Boston, MA, 7-11 July 2008. - Vol. 5. - P. V-37 - V - 40-37. ↑

C2184. Nakatsuka H. System Design of Cloud Profiling Radar for Earthcare. / Nakatsuka H., Okada K., Horie H., Kimura T., Iida Y., Kojima M., Sato K., Ohno Y., Takahashi N., Kumagai H. // 2008. IGARSS 2008. IEEE International Geoscience and Remote Sensing Symposium. - Boston, MA, 7-11 July 2008. - Vol. 5. - P. V-93 - V - 96-93. ↑

C2185. Vedantham H. A Ka-band Interferometer for Cryospheric Applications-Instrument Description and First Results. / Vedantham H., Siqueira P.R., Srinivasan K., Insanic E. // 2008. IGARSS 2008. IEEE International Geoscience and Remote Sensing Symposium. - Boston, MA, 7-11 July 2008. - Vol. 5. - P. V-97 - V - 100-97. ↑

C2186. Yingni Hou. The Thinned Array Time Division Multiple Phase Center Aperture Synthesis and Application. / Yingni Hou, Daojing Li, Wen Hong. // 2008. IGARSS 2008. IEEE International Geoscience and Remote Sensing Symposium. - Boston, MA, 7-11 July 2008. - Vol. 5. - P. V-25 - V - 28-25. ↑

C2187. McManus J.J. Implementation of Pulse Compression on an Airborne Scatterometer. / McManus J.J., Frasier S.J., Carswell J.R. // 2008. IGARSS 2008. IEEE International Geoscience and Remote Sensing Symposium. - Boston, MA, 7-11 July 2008. - Vol. 4. - P. IV-1418 - IV - 1421-1418. ↑

C2188. Klare J. Digital Beamforming for a 3D MIMO SAR-Improvements through Frequency and Waveform Diversity. 2008. IGARSS 2008. IEEE International Geoscience and Remote Sensing Symposium. - Boston, MA, 7-11 July 2008. - Vol. 5. - P. V-17 - V - 20-17. ↑

C2189. Gebert N. Ultra Wide Swath Imaging with Multi-Channel ScanSAR. / Gebert N., Krieger G., Younis M., Bordoni F., Moreira A. // 2008. IGARSS 2008. IEEE International Geoscience and Remote Sensing Symposium. - Boston, MA, 7-11 July 2008. - Vol. 5. - P. V-21 - V - 24-21. ↑

C2190. Yan Wang. Surface Subsidence Monitoring with Coherent Point Target SAR Interferometry. / Yan Wang, Daqing Ge, Qiong Hu, Xiaofang Guo. // 2008. IGARSS 2008. IEEE International Geoscience and Remote Sensing Symposium. - Boston, MA, 7-11 July 2008. - Vol. 4. - P. IV-1205 - IV - 1208-1205. ↑

C2191. Bierman P. Understanding Phytoplankton Variability Throughout Spencer Gulf, South Australia, via Satellite Derived Chlorophyll-A. / Bierman P., Lewis M., Tanner J., Ostendorf B. // 2008. IGARSS 2008. IEEE International Geoscience and Remote Sensing Symposium. - Boston, MA, 7-11 July 2008. - Vol. 4. - P. IV-902 - IV - 905-902. ↑

C2192. Huili Gong. Modeling Atmospheric Effects of InSAR Measurements based on Meris and GPS observations. / Huili Gong, Youquan Zhang, Xiaojuan Li, Angsheng Li, Beibei Chen, Huan Zhou, Yonghua Sun. // 2008. IGARSS 2008. IEEE International Geoscience and Remote Sensing Symposium. - Boston, MA, 7-11 July 2008. - Vol. 4. - P. IV-978 - IV - 981-978. ↑

C2193. Melsheimer C. Integrated Retrieval of Surface and Atmospheric Parameters over the Arctic from AMSR-E Satellite Microwave Radiometer Data using Inverse Methods. / Melsheimer C., Heygster G., Pedersen L.T. // 2008. IGARSS 2008. IEEE International Geoscience and Remote Sensing Symposium. - Boston, MA, 7-11 July 2008. - Vol. 4. - P. IV-986 - IV - 989-986. ↑

C2194. Kim J. Comparison of Surface Roughness Parameters of Tidal Flat Estimated from AIRSAR and ALOS Observations. / Kim J., Park S.-E., Moon W.M. // 2008. IGARSS 2008. IEEE International Geoscience and Remote Sensing Symposium. - Boston, MA, 7-11 July 2008. - Vol. 4. - P. IV-894 - IV - 897-894. ↑

C2195. Dupuis X. Very High Resolution Interferogram Acquisition Campaign and Analysis. / Dupuis X., Oriot H., Angelliaume S. // 2008. IGARSS 2008. IEEE International Geoscience and Remote Sensing Symposium. - Boston, MA, 7-11 July 2008. - Vol. 4. - P. IV-810 - IV - 813-810. ↑

C2196. Kyung-Tak Kim. Analysis of Flood Inundated Area using Hydrological Model and Radarsat SAR Imagery. / Kyung-Tak Kim, Jung-Sool Park, Joo-Hun Kim. // 2008. IGARSS 2008. IEEE International Geoscience and Remote Sensing Symposium. - Boston, MA, 7-11 July 2008. - Vol. 4. - P. IV-874 - IV - 877-874. ↑

C2197. Teague C.C. Two-Dimensional Flow Patterns Observed at Threemile Slough Using Two RiverSondes. 2008. IGARSS 2008. IEEE International Geoscience and Remote Sensing Symposium. - Boston, MA, 7-11 July 2008. - Vol. 4. - P. IV-890 - IV - 893-890. ↑

- C2198.** Junyent F. Weather Radar Network Design. / Junyent F., Chandrasekar V. // 2008. IGARSS 2008. IEEE International Geoscience and Remote Sensing Symposium. - Boston, MA, 7-11 July 2008. - Vol. 4. - P. IV-1022 - IV - 1025-1022. ↑
- C2199.** Longepe N. Capabilities of Full-Polarimetric PALSAR/ALOS for Snow Extent Mapping. / Longepe N., Shimada M., Allain S., Pottier E. // 2008. IGARSS 2008. IEEE International Geoscience and Remote Sensing Symposium. - Boston, MA, 7-11 July 2008. - Vol. 4. - P. IV-1026 - IV - 1029-1026. ↑
- C2200.** Sheng Chang. The Radiation Behavior Analysis of Thin Snow Cover based on Field Measurements by a Multi-Frequency Microwave Radiometer. / Sheng Chang, Lixin Zhang, Jiancheng Shi, Lingmei Jiang. // 2008. IGARSS 2008. IEEE International Geoscience and Remote Sensing Symposium. - Boston, MA, 7-11 July 2008. - Vol. 4. - P. IV-1038 - IV - 1041-1038. ↑
- C2201.** Hopf A.P. Scalable Multifunction Dense Radar Network. / Hopf A.P., Knapp E.J., McLaughlin D.J. // 2008. IGARSS 2008. IEEE International Geoscience and Remote Sensing Symposium. - Boston, MA, 7-11 July 2008. - Vol. 4. - P. IV-1018 - IV - 1021-1018. ↑
- C2202.** Klugmann D. Mie versus Point Matching Algorithm for Radar Rain Properties Retrieval. / Klugmann D., Fiser O. // 2008. IGARSS 2008. IEEE International Geoscience and Remote Sensing Symposium. - Boston, MA, 7-11 July 2008. - Vol. 4. - P. IV-1002 - IV - 1005-1002. ↑
- C2203.** Bharadwaj N. Networked Waveform System for Range Velocity Ambiguity Mitigation. / Bharadwaj N., Chandrasekar V. // 2008. IGARSS 2008. IEEE International Geoscience and Remote Sensing Symposium. - Boston, MA, 7-11 July 2008. - Vol. 4. - P. IV-1010 - IV - 1013-1010. ↑
- C2204.** Carswell J. A Novel Solid-State, Dual-Polarized, Dual Wavelength Precipitation Doppler Radar/Radiometer. / Carswell J., Bidwell S., Meneghini R. // 2008. IGARSS 2008. IEEE International Geoscience and Remote Sensing Symposium. - Boston, MA, 7-11 July 2008. - Vol. 4. - P. IV-1014 - IV - 1017-1014. ↑
- C2205.** Rank R.H. Experiences Developing OAIS-RM Recommended Submission Agreements. / Rank R.H., Cremidis C., McCormick S., Throwe J. // 2008. IGARSS 2008. IEEE International Geoscience and Remote Sensing Symposium. - Boston, MA, 7-11 July 2008. - Vol. 4. - P. IV-617 - IV - 620-617. ↑
- C2206.** Yu-Chang Tzeng. Integration of Spatial Chaotic Model and Type-2 Fuzzy Sets for SAR Images Change Detection. / Yu-Chang Tzeng, Dana Chen, Kun-Shan Chen. // 2008. IGARSS 2008. IEEE International Geoscience and Remote Sensing Symposium. - Boston, MA, 7-11 July 2008. - Vol. 4. - P. IV-655 - IV - 658-655. ↑
- C2207.** Xi Chen. Change Detection with Multi-Polarization SAR Imagery. / Xi Chen, Fan Wu, Chao Wang, Hong Zhang, Bo Zhang, Yixian Tang. // 2008. IGARSS 2008. IEEE International Geoscience and Remote Sensing Symposium. - Boston, MA, 7-11 July 2008. - Vol. 4. - P. IV-659 - IV - 662-659. ↑
- C2208.** Litovchenko K. Monitoring of Oil Spills in the North Caspian Sea using SAR Imagery and Multi-Sensor Satellite Data. / Litovchenko K., Ivanov A. // 2008. IGARSS 2008. IEEE International Geoscience and Remote Sensing Symposium. - Boston, MA, 7-11 July 2008. - Vol. 4. - P. IV-605 - IV - 608-605. ↑
- C2209.** Fritz J. The Impact of Adaptive Speckle Filtering on Multi-Channel SAR Change Detection. / Fritz J., Chandrasekar V. // 2008. IGARSS 2008. IEEE International Geoscience and Remote Sensing Symposium. - Boston, MA, 7-11 July 2008. - Vol. 4. - P. IV-561 - IV - 564-561. ↑
- C2210.** Chien-ping Kao. Design and Analysis of UWB TEM Horn Antenna for Ground Penetrating Radar Applications. / Chien-ping Kao, Jing Li, Liu R., Yu Cai. // 2008. IGARSS 2008. IEEE International Geoscience and Remote Sensing Symposium. - Boston, MA, 7-11 July 2008. - Vol. 4. - P. IV-569 - IV - 572-569. ↑
- C2211.** Nunziata F. A BPM Two-Scale Contrast Model. / Nunziata F., Migliaccio M., Sobieski P. // 2008. IGARSS 2008. IEEE International Geoscience and Remote Sensing Symposium. - Boston, MA, 7-11 July 2008. - Vol. 4. - P. IV-593 - IV - 596-593. ↑
- C2212.** Chaabane F. Interferometric Data Fusion for Topographic Profile Reconstruction. 2008. IGARSS 2008. IEEE International Geoscience and Remote Sensing Symposium. - Boston, MA, 7-11 July 2008. - Vol. 4. - P. IV-798 - IV - 801-798. ↑

- C2213.** Yi Yang. A Markov Random Field Model-based Fusion Approach to Segmentation of SAR and Optical Images. / Yi Yang, Chongzhao Han, Deqiang Han. // 2008. IGARSS 2008. IEEE International Geoscience and Remote Sensing Symposium. - Boston, MA, 7-11 July 2008. - Vol. 4. - P. IV-802 - IV - 805-802. ↑
- C2214.** Xilong Sun. Approximation Error in Differential SAR Interferometry. / Xilong Sun, Anxi Yu, Bin Cai, Diannong Liang. // 2008. IGARSS 2008. IEEE International Geoscience and Remote Sensing Symposium. - Boston, MA, 7-11 July 2008. - Vol. 4. - P. IV-806 - IV - 809-806. ↑
- C2215.** Dabboor M. Land Cover Segmentation of ALOS Polarimetric SAR Data. / Dabboor M., Karathanassi V., Braun A. // 2008. IGARSS 2008. IEEE International Geoscience and Remote Sensing Symposium. - Boston, MA, 7-11 July 2008. - Vol. 4. - P. IV-790 - IV - 793-790. ↑
- C2216.** Russell K. Integration of RADARSAT-2 Dual and Quad Polarization Data into Pipeline Third Party Encroachment Monitoring. / Russell K., Howell C., Bobby P., McHugh S., Power D., Rizkalla M. // 2008. IGARSS 2008. IEEE International Geoscience and Remote Sensing Symposium. - Boston, MA, 7-11 July 2008. - Vol. 4. - P. IV-675 - IV - 678-675. ↑
- C2217.** Amano Y. A study on the classification of urban region using Hyper-spectrum data at AVIRIS. / Amano Y., Takagi N., Getz A. // 2008. IGARSS 2008. IEEE International Geoscience and Remote Sensing Symposium. - Boston, MA, 7-11 July 2008. - Vol. 4. - P. IV-687 - IV - 690-687. ↑
- C2218.** Borgeaud M. Analysis of Temporal Land Cover Change using the ESA Rolling Archives. / Borgeaud M., Tschudi M., Jeanbourquin D. // 2008. IGARSS 2008. IEEE International Geoscience and Remote Sensing Symposium. - Boston, MA, 7-11 July 2008. - Vol. 4. - P. IV-778 - IV - 781-778. ↑
- C2219.** Chou Xie. A Permanent Scatterers Method for Analysis of Deformation over Permafrost Regions of Qinghai-Tibetan Plateau. / Chou Xie, Zhen Li, Xinwu Li. // 2008. IGARSS 2008. IEEE International Geoscience and Remote Sensing Symposium. - Boston, MA, 7-11 July 2008. - Vol. 4. - P. IV-1050 - IV - 1053-1050. ↑
- C2220.** Awada A. Correlation between the NRCS and the Wind Speed over Sea in Both Monostatic and Bistatic Configurations. / Awada A., Khenchaf A., Coatanhay A. // 2008. IGARSS 2008. IEEE International Geoscience and Remote Sensing Symposium. - Boston, MA, 7-11 July 2008. - Vol. 4. - P. IV-1149 - IV - 1152-1149. ↑
- C2221.** Qiuzhao Dong. Microwave Subsurface Crosswell Imaging using Finite Difference Frequency Domain Modeling. / Qiuzhao Dong, Rappaport C.M. // 2008. IGARSS 2008. IEEE International Geoscience and Remote Sensing Symposium. - Boston, MA, 7-11 July 2008. - Vol. 4. - P. IV-1157 - IV - 1160-1157. ↑
- C2222.** Yunhua Zhang. Layered Subsurface Radar Profiling with Combined ESPRIT and SVA Algorithms. / Yunhua Zhang, Xiang Gu, Wenshuai Zhai, Jingshan Jiang. // 2008. IGARSS 2008. IEEE International Geoscience and Remote Sensing Symposium. - Boston, MA, 7-11 July 2008. - Vol. 4. - P. IV-1161 - IV - 1164-1161. ↑
- C2223.** Sant'Anna S.J.S. Polarimetric Characterization of Magnetic Flat Dipole Embedded in Multilayer Structures. / Sant'Anna S.J.S., da S. Lacava J.C., Fernandes D. // 2008. IGARSS 2008. IEEE International Geoscience and Remote Sensing Symposium. - Boston, MA, 7-11 July 2008. - Vol. 4. - P. IV-1145 - IV - 1148-1145. ↑
- C2224.** Pinel N. Forward Propagation over Thick Oil Spills on Sea Surfaces for a Coastal Coherent Radar. / Pinel N., Bourlier C. // 2008. IGARSS 2008. IEEE International Geoscience and Remote Sensing Symposium. - Boston, MA, 7-11 July 2008. - Vol. 4. - P. IV-1125 - IV - 1128-1125. ↑
- C2225.** Pinel N. Modeling of Height Spectrum and Radar Cross Section of Oil Slicks on Sea Surfaces. / Pinel N., Bourlier C. // 2008. IGARSS 2008. IEEE International Geoscience and Remote Sensing Symposium. - Boston, MA, 7-11 July 2008. - Vol. 4. - P. IV-1129 - IV - 1132-1129. ↑
- C2226.** Brelet Y. Bistatic Scattering from a Sea-Like One-Dimensional Rough Surface with the Perturbation Theory in HF-VHF Band. / Brelet Y., Bourlier C. // 2008. IGARSS 2008. IEEE International Geoscience and Remote Sensing Symposium. - Boston, MA, 7-11 July 2008. - Vol. 4. - P. IV-1137 - IV - 1140-1137. ↑
- C2227.** Cuizhen Wang. Biophysical Estimation of Paddy Rice with Canopy Scattering Model and ALOS/PALSAR Imagery in Southeast China. / Cuizhen Wang, Jiaping Wu, Yuan Zhang. // 2008. IGARSS 2008.

IEEE International Geoscience and Remote Sensing Symposium. - Boston, MA, 7-11 July 2008. - Vol. 4. - P. IV-1185 - IV - 1188-1185. ↑

C2228. Bin Cai. Very Large Baseline Interferometry based On Distributed SAR Satellites For High Resolution DEM. / Bin Cai, Haifeng Huang, Jiying Liu, Zhen Dong. // 2008. IGARSS 2008. IEEE International Geoscience and Remote Sensing Symposium. - Boston, MA, 7-11 July 2008. - Vol. 4. - P. IV-1197 - IV - 1200-1197. ↑

C2229. Daqing Ge. Using Small Baseline SAR Interferometry to Investigate Land Subsidence Induced by Underground Coal Mining. / Daqing Ge, Yan Wang, Qiong Hu, Junhai Gao, Xiaofang Guo. // 2008. IGARSS 2008. IEEE International Geoscience and Remote Sensing Symposium. - Boston, MA, 7-11 July 2008. - Vol. 4. - P. IV-1201 - IV - 1204-1201. ↑

C2230. Contreras R. The Imaging Wind and Rain Airborne Profiler (IWRAP) Data Archive. / Contreras R., Frasier S., Chu T., Perkovic D., McManus J., Chang P., Jelenak Z., Carswell J., Esteban-Fernandez D. // 2008. IGARSS 2008. IEEE International Geoscience and Remote Sensing Symposium. - Boston, MA, 7-11 July 2008. - Vol. 4. - P. IV-1181 - IV - 1184-1181. ↑

C2231. Xiaobin Yin. An Ocean Wave Spectrum Derived from Polarimetric Microwave Radiometer Data. / Xiaobin Yin, Zhenzhan Wang, Lei Han, Qing Xu. // 2008. IGARSS 2008. IEEE International Geoscience and Remote Sensing Symposium. - Boston, MA, 7-11 July 2008. - Vol. 4. - P. IV-1169 - IV - 1172-1169. ↑

C2232. Eltoft T. Analysis of SAR Images in the Framework of Scale Mixture of Gaussian Models. 2008. IGARSS 2008. IEEE International Geoscience and Remote Sensing Symposium. - Boston, MA, 7-11 July 2008. - Vol. 4. - P. IV-1173 - IV - 1176-1173. ↑

C2233. Xiaoyang Wen. The High Resolution Radar Image Simulation of Target on Rough Surface. / Xiaoyang Wen, Chao Wang, Yanzhao Wu, Hong Zhang. // 2008. IGARSS 2008. IEEE International Geoscience and Remote Sensing Symposium. - Boston, MA, 7-11 July 2008. - Vol. 4. - P. IV-1177 - IV - 1180-1177. ↑

C2234. Singh G. InSAR Coherence Measurement Techniques for Snow Cover Mapping in Himalayan Region. / Singh G., Venkataraman G., Rao Y.S., Kumar V., Snehmami. // 2008. IGARSS 2008. IEEE International Geoscience and Remote Sensing Symposium. - Boston, MA, 7-11 July 2008. - Vol. 4. - P. IV-1077 - IV - 1080-1077. ↑

C2235. Singh G. The H/A/Alpha Polarimetric Decomposition Theorem and Complex Wishart Distribution for Snow Cover Monitoring. / Singh G., Venkataraman G., kumar V., Rao Y.S., Snehmami. // 2008. IGARSS 2008. IEEE International Geoscience and Remote Sensing Symposium. - Boston, MA, 7-11 July 2008. - Vol. 4. - P. IV-1081 - IV - 1084-1081. ↑

C2236. Kumar V. Spaceborne InSAR Technique for Study of Himalayan Glaciers using ENVISAT ASAR and ERS Data. / Kumar V., Venkataraman G., Rao Y.S., Singh G., Snehmami. // 2008. IGARSS 2008. IEEE International Geoscience and Remote Sensing Symposium. - Boston, MA, 7-11 July 2008. - Vol. 4. - P. IV-1085 - IV - 1088-1085. ↑

C2237. Norland R. Observations of Small Deviations in Glacier Velocity Measurements. 2008. IGARSS 2008. IEEE International Geoscience and Remote Sensing Symposium. - Boston, MA, 7-11 July 2008. - Vol. 4. - P. IV-1073 - IV - 1076-1073. ↑

C2238. Zhen Li. The Glacier Identification using SAR Interferometric and Polarimetric Information in Qinghai-Tibetan Plateau. / Zhen Li, Jianmin Zhou, Bangsen Tian, Chou Xie. // 2008. IGARSS 2008. IEEE International Geoscience and Remote Sensing Symposium. - Boston, MA, 7-11 July 2008. - Vol. 4. - P. IV-1054 - IV - 1056-1054. ↑

C2239. Jianmin Zhou. Estimation the Movement of Glacier IN Qinhai-Tibetan Plateau Using Satellite Radar Interferometry. / Jianmin Zhou, Zhen Li. // 2008. IGARSS 2008. IEEE International Geoscience and Remote Sensing Symposium. - Boston, MA, 7-11 July 2008. - Vol. 4. - P. IV-1057 - IV - 1060-1057. ↑

C2240. Pieraccini M. Digital elevation models by a GBSAR interferometer for monitoring glaciers: the case study of Belvedere Glacier. / Pieraccini M., Noferini L., Mecatti D., Macaluso G., Luzi G., Atzeni C. // 2008. IGARSS 2008. IEEE International Geoscience and Remote Sensing Symposium. - Boston, MA, 7-11 July 2008. - Vol. 4. - P. IV-1061 - IV - 1064-1061. ↑

- C2241.** Yamanokuchi T. Development of Grounding Line Database using ERS-1/2 Data by InSAR Technique. / Yamanokuchi T., Doi K., Shibuya K., Aoki S. // 2008. IGARSS 2008. IEEE International Geoscience and Remote Sensing Symposium. - Boston, MA, 7-11 July 2008. - Vol. 4. - P. IV-1109 - IV - 1112-1109. ↑
- C2242.** Bellez S. Integral Representation of the Electromagnetic Field for the Description of the Main Mechanisms Appearing in Forested Area for Monostatic Radar Configurations. / Bellez S., Dahon C., Roussel H. // 2008. IGARSS 2008. IEEE International Geoscience and Remote Sensing Symposium. - Boston, MA, 7-11 July 2008. - Vol. 4. - P. IV-1113 - IV - 1116-1113. ↑
- C2243.** Susaki J. Decomposition of Polarimetric Scattering of Paddy Rice. / Susaki J., Kawatani Y. // 2008. IGARSS 2008. IEEE International Geoscience and Remote Sensing Symposium. - Boston, MA, 7-11 July 2008. - Vol. 4. - P. IV-1117 - IV - 1120-1117. ↑
- C2244.** Puthalapat D. Conjunctive Radar and Laser Altimetry Data Processing to Measure Snow Thickness. / Puthalapat D., Leuschen C., Markus T., Cavalieri D., Krabill W., Sonntag J., Sturm M., Maslanik J. // 2008. IGARSS 2008. IEEE International Geoscience and Remote Sensing Symposium. - Boston, MA, 7-11 July 2008. - Vol. 4. - P. IV-1105 - IV - 1108-1105. ↑
- C2245.** Wakabayashi H. A Study on Sea Ice Observation in the Sea Okhotsk by Polarimetric SAR. / Wakabayashi H., Nakamura K., Nishio F. // 2008. IGARSS 2008. IEEE International Geoscience and Remote Sensing Symposium. - Boston, MA, 7-11 July 2008. - Vol. 4. - P. IV-1089 - IV - 1092-1089. ↑
- C2246.** Karvonen J. Sea Ice SAR Feature Extraction by Non-Negative Matrix and Tensor Factorization. / Karvonen J., Kaarna A. // 2008. IGARSS 2008. IEEE International Geoscience and Remote Sensing Symposium. - Boston, MA, 7-11 July 2008. - Vol. 4. - P. IV-1093 - IV - 1096-1093. ↑
- C2247.** Simila M. Comparison Between Envisat SAR and 3-D Laser Scanner Statistics for the Baltic Sea Ice. / Simila M., Makynen M., Heiler I., Hallikainen M. // 2008. IGARSS 2008. IEEE International Geoscience and Remote Sensing Symposium. - Boston, MA, 7-11 July 2008. - Vol. 4. - P. IV-1097 - IV - 1100-1097. ↑
- C2248.** Arnett M. Evaluating ALOS-PALSAR for Ice Monitoring-What Can L-band do for the North American Ice Service?. / Arnett M., Flett D., De Abreu R., Clemente-Colon P., Woods J., Melchior B. // 2008. IGARSS 2008. IEEE International Geoscience and Remote Sensing Symposium. - Boston, MA, 7-11 July 2008. - Vol. 5. - P. V-188 - V - 191-188. ↑
- C2249.** Di Zhu. Predistortion Arithmetic on Low Sidelobe Pulse Compression Signal for Spaceborne Weather Radar. / Di Zhu, Xiaolong Dong. // 2008. and 2008 International Workshop on Geoscience and Remote Sensing. ETT and GRS 2008. International Workshop on Education Technology and Training. - Shanghai, 21-22 Dec. 2008. - Vol. 1. - P. 476-478. ↑
- C2250.** Jun Ji. A TSVM Based Semi-Supervised Approach to SAR Image Segmentation. / Jun Ji, Fengjing Shao, Rencheng Sun, Neng Zhang, Guanfeng Liu. // 2008. and 2008 International Workshop on Geoscience and Remote Sensing. ETT and GRS 2008. International Workshop on Education Technology and Training. - Shanghai, 21-22 Dec. 2008. - Vol. 1. - P. 495-498. ↑
- C2251.** Lining Liu. SIFT Based Automatic Tie-Point Extraction for Multitemporal SAR Images. / Lining Liu, Yunhong Wang, Yiding Wang. // 2008. and 2008 International Workshop on Geoscience and Remote Sensing. ETT and GRS 2008. International Workshop on Education Technology and Training. - Shanghai, 21-22 Dec. 2008. - Vol. 1. - P. 499-503. ↑
- C2252.** Changwei Wang. Study on Point Spread Function of Optical Synthetic Aperture. / Changwei Wang, Yuesong Jiang, Haiyang Wang. // 2008. and 2008 International Workshop on Geoscience and Remote Sensing. ETT and GRS 2008. International Workshop on Education Technology and Training. - Shanghai, 21-22 Dec. 2008. - Vol. 1. - P. 414-416. ↑
- C2253.** Yanhong Tang. Ocean Surface Currents Determination from X-Band Radar Image Sequences. / Yanhong Tang, Yanling Hao, Zhizhong Lu. // 2008. and 2008 International Workshop on Geoscience and Remote Sensing. ETT and GRS 2008. International Workshop on Education Technology and Training. - Shanghai, 21-22 Dec. 2008. - Vol. 1. - P. 320-323. ↑
- C2254.** Zhang De-xiang. Improving PWF Method of Despeckle in Polarimetric SAR Image by Fusion Based on Nonsampled Contourlet Transform. / Zhang De-xiang, Wu Xiao-pei, Gao Qing-wei, Guo Xiao-jing. // 2008.

and 2008 International Workshop on Geoscience and Remote Sensing. ETT and GRS 2008. International Workshop on Education Technology and Training. - Shanghai, 21-22 Dec. 2008. - Vol. 1. - P. 328-331. ↑

C2255. Yiding Wang. Optimal Mismatch Network in Active Radar Reflector. / Yiding Wang, Hai Wang. // 2008. and 2008 International Workshop on Geoscience and Remote Sensing. ETT and GRS 2008. International Workshop on Education Technology and Training. - Shanghai, 21-22 Dec. 2008. - Vol. 1. - P. 389-392. ↑

C2256. Fei Ding. A ZigBee Based Mesh Network for Home Control System. / Fei Ding, Guangming Song, Jianqing Li, Aiguo Song. // 2008. and 2008 International Workshop on Geoscience and Remote Sensing. ETT and GRS 2008. International Workshop on Education Technology and Training. - Shanghai, 21-22 Dec. 2008. - Vol. 1. - P. 744-748. ↑

C2257. Ling-zhi Zhong. Evaluation of a 35-GHz Radar for Cloud and Precipitation Research in SCHeREX-Experiment. / Ling-zhi Zhong, Li-ping Liu, Run-sheng Ge, Lin Chen. // 2008. and 2008 International Workshop on Geoscience and Remote Sensing. ETT and GRS 2008. International Workshop on Education Technology and Training. - Shanghai, 21-22 Dec. 2008. - Vol. 2. - P. 103-106. ↑

C2258. Wang Zhan-feng. Numerical Study for Backscattering Enhancement of Concrete Specimens with FRP-TriCR Buried and Its Compatibility with Infrared Camouflage. / Wang Zhan-feng, Lv Xu-liang, Jia Qi. // 2008. and 2008 International Workshop on Geoscience and Remote Sensing. ETT and GRS 2008. International Workshop on Education Technology and Training. - Shanghai, 21-22 Dec. 2008. - Vol. 2. - P. 129-132. ↑

C2259. Zhaoquan Huang. Monitoring Land Subsidence by Using Multi-temporal Differential SAR Interferometry: A Use Case in Jiading, China. / Zhaoquan Huang, Fan Wang, Bin Xie, Le Yu, Dengrong Zhang. // 2008. and 2008 International Workshop on Geoscience and Remote Sensing. ETT and GRS 2008. International Workshop on Education Technology and Training. - Shanghai, 21-22 Dec. 2008. - Vol. 1. - P. 591-595. ↑

C2260. Xiaoting Wang. Validation of Two Soil Moisture Products from ERS Scatterometer Data over East China. / Xiaoting Wang, Weidong Guo, Zhong Zhong. // 2008. and 2008 International Workshop on Geoscience and Remote Sensing. ETT and GRS 2008. International Workshop on Education Technology and Training. - Shanghai, 21-22 Dec. 2008. - Vol. 1. - P. 528-531. ↑

C2261. Jian-Zhong Huang. Research and Application on Network Update of Land Survey Spatial Data Based on Embedded GIS and GPS. / Jian-Zhong Huang, Yao-Lin Liu, Yan-Fang Liu, Jian-Hua He, Dan Chen. // 2008. and 2008 International Workshop on Geoscience and Remote Sensing. ETT and GRS 2008. International Workshop on Education Technology and Training. - Shanghai, 21-22 Dec. 2008. - Vol. 1. - P. 532-535. ↑

C2262. Ruan Zheng. A Study of Drop-Size Distribution in Precipitation Cloud from Wind Profile Radar. / Ruan Zheng, Wang Xiaolei. // 2008. and 2008 International Workshop on Geoscience and Remote Sensing. ETT and GRS 2008. International Workshop on Education Technology and Training. - Shanghai, 21-22 Dec. 2008. - Vol. 1. - P. 571-574. ↑

C2263. Bera R. Modeling and Implementation Of Wireless Embedded System For Intelligent Transport System Application. / Bera R., Dhar S., Kandar D., Sinha N.B., Mitra M. // 2008. ICIIIS 2008. IEEE Region 10 and the Third international Conference on Industrial and Information Systems. - Kharagpur, 8-10 Dec. 2008. - P. 1-6. ↑

C2264. Walli K. Automated image registration to 3-D scene models. / Walli K., Rhody H. // 2008. AIPR 08. 37th IEEE Applied Imagery Pattern Recognition Workshop. - Washington DC, 15-17 Oct. 2008. - P. 1-8. ↑

C2265. Shifeng Kang. Propagation environments of radiowave information systems. / Shifeng Kang, Hongguang Wang. // 2008. APMC 2008. Asia-Pacific Microwave Conference. - Macau, 16-20 Dec. 2008. - P. 1-4. ↑

C2266. Xia Yuan. Road-surface abstraction using ladar sensing. / Xia Yuan, Chun-xia Zhao, Yun-fei Cai, Haofeng Zhang, De-bao Chen. // 2008. ICARCV 2008. 10th International Conference on Control, Automation, Robotics and Vision. - Hanoi, 17-20 Dec. 2008. - P. 1097-1102. ↑

C2267. O'Hagan D.W. Passive Bistatic Radar (PBR) using FM radio illuminators of opportunity. / O'Hagan D.W., Baker C.J. // 2008 New Trends for Environmental Monitoring Using Passive Systems. - Hyeres, French Riviera, 14-17 Oct. 2008. - P. 1-6. ↑

C2268. Thomas J.M. HF passive bistatic radar potential and applications for remote sensing. / Thomas J.M.,

Baker C.J., Griffiths H.D. // 2008 New Trends for Environmental Monitoring Using Passive Systems. - Hyeres, French Riviera, 14-17 Oct. 2008. - P. 1-5. ↑

C2269. Li Q. Beach soil moisture measurement with a land reflected GPS bistatic radar technique. / Li Q., Reboul S., Boutoille S., Choquel J.B., Benjelloun M., Gardel A. // 2008 New Trends for Environmental Monitoring Using Passive Systems. - Hyeres, French Riviera, 14-17 Oct. 2008. - P. 1-6. ↑

C2270. Biao Chen. Internal Wave Detection and Parameter Estimation from SAR Images Based on a Novel Radon Transform Method. / Biao Chen, Jie Chen, Jiyin Sun. // 2008. and 2008 International Workshop on Geoscience and Remote Sensing. ETT and GRS 2008. International Workshop on Education Technology and Training. - Shanghai, 21-22 Dec. 2008. - Vol. 1. - P. 234-237. ↑

C2271. Rui-Bin Zhao. Synthesizing Large-Scale Virtual Terrain from Image Atlas. / Rui-Bin Zhao, Ming-Yong Pang. // 2008. and 2008 International Workshop on Geoscience and Remote Sensing. ETT and GRS 2008. International Workshop on Education Technology and Training. - Shanghai, 21-22 Dec. 2008. - Vol. 1. - P. 242-246. ↑

C2272. Yanwei Li. Radar Echo Characteristics of Convective and Stratiform Mixed Clouds during Their Formation in a Mountainous Region. / Yanwei Li, Shengjie Niu, Ning Luo, Jifen Wen, Haojun Huang. // 2008. and 2008 International Workshop on Geoscience and Remote Sensing. ETT and GRS 2008. International Workshop on Education Technology and Training. - Shanghai, 21-22 Dec. 2008. - Vol. 1. - P. 265-268. ↑

C2273. Jie Chen. The Turbulent Wake Detection and Beam Estimation of a Ship in SAR Images. / Jie Chen, Biao Chen, Jifeng Yang. // 2008. and 2008 International Workshop on Geoscience and Remote Sensing. ETT and GRS 2008. International Workshop on Education Technology and Training. - Shanghai, 21-22 Dec. 2008. - Vol. 1. - P. 230-233. ↑

C2274. Ya-Qiu Jin. Research on scattering and imaging simulation from the object and randomly rough surface. 2008. APMC 2008. Asia-Pacific Microwave Conference. - Macau, 16-20 Dec. 2008. - P. 1-4. ↑

C2275. Jae-Hyung Park. 0.18um CMOS receiver front-end for non-invasive cardiopulmonary monitoring. / Jae-Hyung Park, Byung-Jun Jang, Jong-Gwan Yook. // 2008. APMC 2008. Asia-Pacific Microwave Conference. - Macau, 16-20 Dec. 2008. - P. 1-4. ↑

C2276. Xiang Gu. Radar altimeter echo simulation based on PO method. / Xiang Gu, Qingshan Yang, Yunhua Zhang. // 2008. APMC 2008. Asia-Pacific Microwave Conference. - Macau, 16-20 Dec. 2008. - P. 1-4. ↑

C2277. Xu Chunliang. Measuring the Microwave Backscattering Coefficient of Paddy Rice Using FM-CW Ground-Based Scatterometer. / Xu Chunliang, Chen Yan, Tong Ling, Jia Mingquan, Liu Zhengchan, Lu Haiping. // 2008. and 2008 International Workshop on Geoscience and Remote Sensing. ETT and GRS 2008. International Workshop on Education Technology and Training. - Shanghai, 21-22 Dec. 2008. - Vol. 2. - P. 194-198. ↑

C2278. Silva S.R. Shallow water height mapping with interferometric synthetic aperture sonar. / Silva S.R., Cunha S., Matos A., Cruz N. // OCEANS 2008. - Quebec City, QC, 15-18 Sept. 2008. - P. 1-7. ↑

C2279. Garelo R. The MODENA project: Modeling and simulation of the maritime environment remotely sensed by radar. OCEANS 2008. - Quebec City, QC, 15-18 Sept. 2008. - P. 1-5. ↑

C2280. Pettigrew N.R. Retrospective and prospective views of the Ocean Observing System in the Gulf of Maine. / Pettigrew N.R., Wallinga J.P., Mangum L., Neville F. // OCEANS 2008. - Quebec City, QC, Canada, 15-18 Sept. 2008. - P. 1-9. ↑

C2281. Forand J.L. Surveillance of Canada's high Arctic. / Forand J.L., Larochelle V., Brookes D., Lee J.P.Y., MacLeod M., Dao R., Heard G.J., McCoy N., Kollenberg K. // OCEANS 2008. - Quebec City, QC, 15-18 Sept. 2008. - P. 1-8. ↑

C2282. Hongling Shi. 2003-2008 Ice Sheet Elevation Change on the Lake Vostok, Antarctica, From ICESat. / Hongling Shi, Yang Lu, Lifeng Bao, Zongliang Du, Zizhan Zhang. // 2008. and 2008 International Workshop on Geoscience and Remote Sensing. ETT and GRS 2008. International Workshop on Education Technology and Training. - Shanghai, 21-22 Dec. 2008. - Vol. 2. - P. 561-564. ↑

- C2283.** Assilzadeh H. Oil Spill emergency response mapping for coastal area using SAR imagery and GIS. / Assilzadeh H., Gao Y. // OCEANS 2008. - Quebec City, QC, 15-18 Sept. 2008. - P. 1-6. ↑
- C2284.** Costes C. Convective clouds modelling and tracking by an airborne radar. / Costes C., Garelo R., Mercier G., Artis J.-P., Bon N. // OCEANS 2008. - Quebec City, QC, 15-18 Sept. 2008. - P. 1-5. ↑
- C2285.** Zuguang Guan. LIDAR technique for remote gas analysis in solid scattering media. / Zuguang Guan, Lewender M., Gronlund R., Lundberg H., Svanberg S. // 2008. AOE 2008. Asia Optical Fiber Communication & Optoelectronic Exposition & Conference. - Shanghai, Oct. 30 2008-Nov. 2 2008. - P. 1-3. ↑
- C2286.** Zubkov A. Microwave imaging systems: Achievements and improvement prospects. 2008 Proceedings of International Conference on Modern Problems of Radio Engineering, Telecommunications and Computer Science. - Lviv-Slavsko, 19-23 Feb. 2008. - P. 9-11. ↑
- C2287.** Prudyus I. Sparse antenna array geometry synthesis for remote sensing systems. / Prudyus I., Lazko L. // 2008 Proceedings of International Conference on Modern Problems of Radio Engineering, Telecommunications and Computer Science. - Lviv-Slavsko, 19-23 Feb. 2008. - P. 333. ↑
- C2288.** Jayalaksahmi U. Difference patterns from continuous line sources. / Jayalaksahmi U., Raju G.S.N. // 2008. INCEMIC 2008. 10th International Conference on Electromagnetic Interference & Compatibility. - Bangalore, 26-27 Nov. 2008. - P. 341-345. ↑
- C2289.** Jianjun Zhang. High frequency (HF) radar cross sections of the ocean surface incorporating a continuous wave frequency modulated source. / Jianjun Zhang, Gill E.W., Walsh J. // OCEANS 2008. - Quebec City, QC, 15-18 Sept. 2008. - P. 1-5. ↑
- C2290.** Parenthoen M. Autonomy based modeling for the simulation of ocean remote sensing. / Parenthoen M., Belemalem Z. // OCEANS 2008. - Quebec City, QC, 15-18 Sept. 2008. - P. 1-7. ↑
- C2291.** Weissman D.E. Measurements of the effect of rain-induced sea surface roughness on the QuikSCAT scatterometer radar cross section and wind stress. / Weissman D.E., Bourassa M.A. // OCEANS 2008. - Quebec City, QC, 15-18 Sept. 2008. - P. 1-4. ↑
- C2292.** Hong-yin Shi. Performance Analysis and Improved Method for Airborne Three-Channel SAR/GMTI System. / Hong-yin Shi, Yin-qing Zhou. // 2008. and 2008 International Workshop on Geoscience and Remote Sensing. ETT and GRS 2008. International Workshop on Education Technology and Training. - Shanghai, 21-22 Dec. 2008. - Vol. 2. - P. 336-339. ↑
- C2293.** Chen Jiongfeng. Soil Moisture Mapping in Typical Semi-Arid Regions of China by Using Envisat ASAR Data. / Chen Jiongfeng, Zhang Wanchang. // 2008. and 2008 International Workshop on Geoscience and Remote Sensing. ETT and GRS 2008. International Workshop on Education Technology and Training. - Shanghai, 21-22 Dec. 2008. - Vol. 2. - P. 360-363. ↑
- C2294.** Bi Xuemei. Long Term Analyses on Spatial and Temporal Evaluation of Snow Covers in Northern China by Using RS and Meteorological data. / Bi Xuemei, Zhang Wanchang. // 2008. and 2008 International Workshop on Geoscience and Remote Sensing. ETT and GRS 2008. International Workshop on Education Technology and Training. - Shanghai, 21-22 Dec. 2008. - Vol. 2. - P. 368-371. ↑
- C2295.** Xiaoguang Deng. Linking Geospatial Datasets with Different Scales by Conflation. / Xiaoguang Deng, Huayi Wu, Zhihui Yu. // 2008. and 2008 International Workshop on Geoscience and Remote Sensing. ETT and GRS 2008. International Workshop on Education Technology and Training. - Shanghai, 21-22 Dec. 2008. - Vol. 2. - P. 328-331. ↑
- C2296.** Zhang Y. Mapping Paddy Rice Biomass Using ALOS/PALSAR Imagery. / Zhang Y., Huang H., Chen X., Wu J., Wang C. // 2008. and 2008 International Workshop on Geoscience and Remote Sensing. ETT and GRS 2008. International Workshop on Education Technology and Training. - Shanghai, 21-22 Dec. 2008. - Vol. 2. - P. 207-210. ↑
- C2297.** Jiaxiang Feng. Quality Evaluation of Spatial Point-Cloud Data Collected by Vehicle-Borne Laser Scanner. / Jiaxiang Feng, Ruofei Zhong, Yong Yang, Wenji Zhao. // 2008. and 2008 International Workshop on Geoscience and Remote Sensing. ETT and GRS 2008. International Workshop on Education Technology and Training. - Shanghai, 21-22 Dec. 2008. - Vol. 2. - P. 320-323. ↑

- C2298.** Jing Xu. Design and Application of In-Vehicle Terminal for Car Network System Based on ARM9. / Jing Xu, Tao Lu, Lingling Gao. // 2008. and 2008 International Workshop on Geoscience and Remote Sensing. ETT and GRS 2008. International Workshop on Education Technology and Training. - Shanghai, 21-22 Dec. 2008. - Vol. 2. - P. 324-327. ↑
- C2299.** Hongdong Fan. Study on the Methods of InSAR Baseline Estimation. / Hongdong Fan, Kazhong Deng, Guoman Huang. // 2008. and 2008 International Workshop on Geoscience and Remote Sensing. ETT and GRS 2008. International Workshop on Education Technology and Training. - Shanghai, 21-22 Dec. 2008. - Vol. 2. - P. 453-455. ↑
- C2300.** Lei Pang. DGPS-Supported Flight Track Processing and Direct Geo-location from High Resolution Airborne SAR Images. / Lei Pang, Qin Yan, Jujie Wei, Kui Yang. // 2008. and 2008 International Workshop on Geoscience and Remote Sensing. ETT and GRS 2008. International Workshop on Education Technology and Training. - Shanghai, 21-22 Dec. 2008. - Vol. 2. - P. 456-459. ↑
- C2301.** Li Yanwen. Quad Polarimetry SAR Target Recognition Based on Parametric Statistics and Multidimensional Analysis. / Li Yanwen, Yang Yingbao, Zhang Yonghong. // 2008. and 2008 International Workshop on Geoscience and Remote Sensing. ETT and GRS 2008. International Workshop on Education Technology and Training. - Shanghai, 21-22 Dec. 2008. - Vol. 2. - P. 549-552. ↑
- C2302.** Jia Mingquan. Land-Based Scatterometer Measurements and Retrieval of Surface Parameters Using Neural Networks. / Jia Mingquan, Chen Yan, Tong Ling, Liu Zengcan, Xu Chunliang, Lu Haiping. // 2008. and 2008 International Workshop on Geoscience and Remote Sensing. ETT and GRS 2008. International Workshop on Education Technology and Training. - Shanghai, 21-22 Dec. 2008. - Vol. 2. - P. 448-452. ↑
- C2303.** Shao Yuehong. Analysis of Quantitative Estimation of Precipitation Using Different Algorithms with Doppler Radar Data. / Shao Yuehong, Zhang Wanchang, Liu Yonghe, Zhang Jingying. // 2008. and 2008 International Workshop on Geoscience and Remote Sensing. ETT and GRS 2008. International Workshop on Education Technology and Training. - Shanghai, 21-22 Dec. 2008. - Vol. 2. - P. 372-375. ↑
- C2304.** Yuehong Shao. Application of Back-Propagation Neural Network to Estimate Precipitation with Doppler Radar in Yishuhe Watershed of China. / Yuehong Shao, Wanchang Zhang, Yonghe Liu. // 2008. and 2008 International Workshop on Geoscience and Remote Sensing. ETT and GRS 2008. International Workshop on Education Technology and Training. - Shanghai, 21-22 Dec. 2008. - Vol. 2. - P. 376-379. ↑
- C2305.** Jie Chen. Typical Ocean Features Detection in SAR Images. / Jie Chen, Jiyin Sun, Jifeng Yang. // 2008. and 2008 International Workshop on Geoscience and Remote Sensing. ETT and GRS 2008. International Workshop on Education Technology and Training. - Shanghai, 21-22 Dec. 2008. - Vol. 2. - P. 425-428. ↑
- C2306.** Clausi D.A. MAGIC: MAP-Guided Ice Classification system for operational analysis. / Clausi D.A., Qin A.K., Chowdhury M.S., Yu P., Maillard P. // 2008 IAPR Workshop on Pattern Recognition in Remote Sensing (PRRS 2008). - Tampa, FL, 7-7 Dec. 2008. - P. 1-4. ↑
- C2307.** Donovan B.C. Western Massachusetts Off-the-Grid Radar Technology Testbed. / Donovan B.C., McLaughlin D.J., Zink M., Kurose J. // 2008. IGARSS 2008. IEEE International Geoscience and Remote Sensing Symposium. - Boston, MA, 7-11 July 2008. - Vol. 5. - P. V-314 - V - 317-314. ↑
- C2308.** Salazar J.L. Phase-Tilt Array Antenna Design for Dense Distributed Radar Networks for Weather Sensing. / Salazar J.L., Medina R., Knapp E.J., McLaughlin D.J. // 2008. IGARSS 2008. IEEE International Geoscience and Remote Sensing Symposium. - Boston, MA, 7-11 July 2008. - Vol. 5. - P. V-318 - V - 321-318. ↑
- C2309.** Yanting Wang. Development of Scan Strategy for Dual Doppler Retrieval in a Networked Radar System. / Yanting Wang, Chandrasekar V., Dolan B. // 2008. IGARSS 2008. IEEE International Geoscience and Remote Sensing Symposium. - Boston, MA, 7-11 July 2008. - Vol. 5. - P. V-322 - V - 325-322. ↑
- C2310.** Lim S. Real-time implementation of the network-based reflectivity retrieval for CASA. / Lim S., Chandrasekar V., Lee P., Jayasumana A.P. // 2008. IGARSS 2008. IEEE International Geoscience and Remote Sensing Symposium. - Boston, MA, 7-11 July 2008. - Vol. 5. - P. V-310 - V - 313-310. ↑
- C2311.** Schwabisch M. Early Results using Single-Pass L-band Pol-InSAR. / Schwabisch M., Gopal S., Mercer B., Qiaoping Zhang, Ming Wei. // 2008. IGARSS 2008. IEEE International Geoscience and Remote

Sensing Symposium. - Boston, MA, 7-11 July 2008. - Vol. 5. - P. V-286 - V - 289-286. ↑

C2312. Viergever K.M. Sar Interferometry For Estimating Above-Ground Biomass Of Savanna Woodlands In Belize. / Viergever K.M., Woodhouse I.H., Marino A., Brolley M., Stuart N. // 2008. IGARSS 2008. IEEE International Geoscience and Remote Sensing Symposium. - Boston, MA, 7-11 July 2008. - Vol. 5. - P. V-290 - V - 293-290. ↑

C2313. Cheong B.L. Real-Time Refractivity Retrieval using the Magnetron-based CASA X-band Radar Network During the Spring 2008 Campaign. / Cheong B.L., Palmer R., Chandrasekar V., Junyent F. // 2008. IGARSS 2008. IEEE International Geoscience and Remote Sensing Symposium. - Boston, MA, 7-11 July 2008. - Vol. 5. - P. V-306 - V - 309-306. ↑

C2314. Yisok Oh. Classification of Polarimetric SAR Images using the Degree of Polarization and the Co-Polarized Phase Difference. / Yisok Oh, Geba Chang. // 2008. IGARSS 2008. IEEE International Geoscience and Remote Sensing Symposium. - Boston, MA, 7-11 July 2008. - Vol. 5. - P. V-362 - V - 365-362. ↑

C2315. Narvekar P.S. Analysis of WindSat Data over Arctic Sea Ice. / Narvekar P.S., Heygster G., Tonboe R., Jackson T.J. // 2008. IGARSS 2008. IEEE International Geoscience and Remote Sensing Symposium. - Boston, MA, 7-11 July 2008. - Vol. 5. - P. V-369 - V - 372-369. ↑

C2316. Burini A. TerraSAR-X/SPOT-5 Fused Images for Supervised Land Cover Classification. / Burini A., Putignano C., Del Frate F., Licciardi G., Pratola C., Schiavon G., Solimini D. // 2008. IGARSS 2008. IEEE International Geoscience and Remote Sensing Symposium. - Boston, MA, 7-11 July 2008. - Vol. 5. - P. V-373 - V - 376-373. ↑

C2317. Fei C. A Markov Chain CFAR Detector for Polarimetric Data using Adaptive Linear Discriminant Analysis. / Fei C., Liu T., Lampropoulos G.A., Sabry R., Murnaghan K. // 2008. IGARSS 2008. IEEE International Geoscience and Remote Sensing Symposium. - Boston, MA, 7-11 July 2008. - Vol. 5. - P. V-358 - V - 361-358. ↑

C2318. Gamba P. Anisotropic Rotation Invariant Built-Up Presence Index: Applications to SAR Data. / Gamba P., Pesaresi M., Molch K., Gerhardinger A., Lisini G. // 2008. IGARSS 2008. IEEE International Geoscience and Remote Sensing Symposium. - Boston, MA, 7-11 July 2008. - Vol. 5. - P. V-338 - V - 341-338. ↑

C2319. Bombrun L. Segmentation of Polarimetric SAR Data based on the Fisher Distribution for Texture Modeling. / Bombrun L., Beaulieu J.-M. // 2008. IGARSS 2008. IEEE International Geoscience and Remote Sensing Symposium. - Boston, MA, 7-11 July 2008. - Vol. 5. - P. V-350 - V - 353-350. ↑

C2320. Lavigne D.A. Enhanced Military Target Discrimination using Active and Passive Polarimetric Imagery. / Lavigne D.A., Breton M., Pichette M., Laroche V., Simard J.-R. // 2008. IGARSS 2008. IEEE International Geoscience and Remote Sensing Symposium. - Boston, MA, 7-11 July 2008. - Vol. 5. - P. V-354 - V - 357-354. ↑

C2321. Wiesmann A. Mobile X- to Ku-band Scatterometer in Support of the CoRe-H2O Mission. / Wiesmann A., Werner C., Matzler C., Schneebeil M., Strozzi T., Wegmüller U. // 2008. IGARSS 2008. IEEE International Geoscience and Remote Sensing Symposium. - Boston, MA, 7-11 July 2008. - Vol. 5. - P. V-244 - V - 247-244. ↑

C2322. Verspeek J. ASCAT Scatterometer Ocean Calibration. / Verspeek J., Stoffelen A., Portabella M., Verhoef A., Vogelzang J. // 2008. IGARSS 2008. IEEE International Geoscience and Remote Sensing Symposium. - Boston, MA, 7-11 July 2008. - Vol. 5. - P. V-248 - V - 251-248. ↑

C2323. Di Zhu. Pulse Compression with Very Low Sidelobes in a Spaceborne Weather Radar. / Di Zhu, Xiaolong Dong, Wenming Lin. // 2008. IGARSS 2008. IEEE International Geoscience and Remote Sensing Symposium. - Boston, MA, 7-11 July 2008. - Vol. 5. - P. V-252 - V - 255-252. ↑

C2324. Torres O. Retrieval of Reflected Direct Broadcast Satellite (DBS) Signals for Earth Science Applications. / Torres O., Lawrence R. // 2008. IGARSS 2008. IEEE International Geoscience and Remote Sensing Symposium. - Boston, MA, 7-11 July 2008. - Vol. 5. - P. V-240 - V - 243-240. ↑

C2325. Stuart K.M. Analysis of Antarctic Iceberg and Sea Ice Melting Patterns using QuikSCAT. / Stuart K.M., Long D.G. // 2008. IGARSS 2008. IEEE International Geoscience and Remote Sensing Symposium. - Boston, MA, 7-11 July 2008. - Vol. 5. - P. V-192 - V - 195-192. ↑

- C2326.** Shorter N. Autonomous Registration of LiDAR Data to Single Aerial Image. / Shorter N., Kasparis T. // 2008. IGARSS 2008. IEEE International Geoscience and Remote Sensing Symposium. - Boston, MA, 7-11 July 2008. - Vol. 5. - P. V-216 - V - 219-216. ↑
- C2327.** Enjolras V. SWIM: A Multi-Incidence Beams Ku-band Real Aperture Radar for the Observation of the Ocean Wave Field Spectra. / Enjolras V., Caubet E., Richard J., Lorenzo J., Carayon G., Castillanr P. // 2008. IGARSS 2008. IEEE International Geoscience and Remote Sensing Symposium. - Boston, MA, 7-11 July 2008. - Vol. 5. - P. V-236 - V - 239-236. ↑
- C2328.** Cloude S.R. Forest Vertical Structure Estimation using Coherence Tomography. / Cloude S.R., Papathanassiou K.P. // 2008. IGARSS 2008. IEEE International Geoscience and Remote Sensing Symposium. - Boston, MA, 7-11 July 2008. - Vol. 5. - P. V-275 - V - 278-275. ↑
- C2329.** Dubois-Fernandez P. Compact Polarimetry Mode for a Low Frequency SAR in Space. / Dubois-Fernandez P., Angelliaume S., My-Linh Truong-Loi, Souyris J.-C. // 2008. IGARSS 2008. IEEE International Geoscience and Remote Sensing Symposium. - Boston, MA, 7-11 July 2008. - Vol. 5. - P. V-279 - V - 282-279. ↑
- C2330.** Eriksson L.E.B. Temporal Decorrelation for Forested Areas Observed in Spaceborne L-band SAR Interferometry. / Eriksson L.E.B., Santoro M., Fransson J. // 2008. IGARSS 2008. IEEE International Geoscience and Remote Sensing Symposium. - Boston, MA, 7-11 July 2008. - Vol. 5. - P. V-283 - V - 285-283. ↑
- C2331.** Imperatore P. Small Perturbation Method for Scattering From Rough Multilayers. / Imperatore P., Iodice A., Riccio D. // 2008. IGARSS 2008. IEEE International Geoscience and Remote Sensing Symposium. - Boston, MA, 7-11 July 2008. - Vol. 5. - P. V-271 - V - 274-271. ↑
- C2332.** Ya-Qiu Jin. SAR Imaging Simulation for an Inhomogeneous Undulated Lunar Surface based on Triangulated Irregular Network. / Ya-Qiu Jin, Wenzhe Fa, Feng Xu. // 2008. IGARSS 2008. IEEE International Geoscience and Remote Sensing Symposium. - Boston, MA, 7-11 July 2008. - Vol. 5. - P. V-256 - V - 259-256. ↑
- C2333.** Bourlier C. Scattering from a Scatterer Near a Large Random Rough Surface with the Extended PILE Method. / Bourlier C., Kubicke G. // 2008. IGARSS 2008. IEEE International Geoscience and Remote Sensing Symposium. - Boston, MA, 7-11 July 2008. - Vol. 5. - P. V-260 - V - 263-260. ↑
- C2334.** Kung-Hau Ding. Amplitude and Phase Statistics for Bistatic Scattering from Rough Surfaces. / Kung-Hau Ding, Stevens W.G. // 2008. IGARSS 2008. IEEE International Geoscience and Remote Sensing Symposium. - Boston, MA, 7-11 July 2008. - Vol. 5. - P. V-264 - V - 267-264. ↑
- C2335.** Molinier M. Comparison of Polarimetric Change Detection Methods on ALOS PALSAR Images over Finland. / Molinier M., Lonnqvist A., Rauste Y. // 2008. IGARSS 2008. IEEE International Geoscience and Remote Sensing Symposium. - Boston, MA, 7-11 July 2008. - Vol. 5. - P. V-377 - V - 380-377. ↑
- C2336.** Mouri M. Improvement of Earthquake Prediction by using Global Signal Elimination from Environmental Electromagnetic Signals. / Mouri M., Funase A., Takumi I., Cichocki A., Yasukawa H., Hata M. // 2008. IGARSS 2008. IEEE International Geoscience and Remote Sensing Symposium. - Boston, MA, 7-11 July 2008. - Vol. 5. - P. V-566 - V - 569-566. ↑
- C2337.** Yuhong Yi. Validation of Multilayered Cloud Properties using A-Train Satellite Measurements. / Yuhong Yi, Minnis P., Jianping Huang, Sun-Mack S., Yan Chen, Ayers K. // 2008. IGARSS 2008. IEEE International Geoscience and Remote Sensing Symposium. - Boston, MA, 7-11 July 2008. - Vol. 5. - P. V-574 - V - 577-574. ↑
- C2338.** Yoshikawa E. Development and Observation of the Ku-band Broad-Band Radar for Meteorological Application. / Yoshikawa E., Mega T., Morimoto T., Ushio T., Kawasaki Z. // 2008. IGARSS 2008. IEEE International Geoscience and Remote Sensing Symposium. - Boston, MA, 7-11 July 2008. - Vol. 5. - P. V-578 - V - 581-578. ↑
- C2339.** Lulu Tan. Investigation on Tree Height Retrieval with Polarimetric SAR Interferometry. / Lulu Tan, Ruliang Yang. // 2008. IGARSS 2008. IEEE International Geoscience and Remote Sensing Symposium. - Boston, MA, 7-11 July 2008. - Vol. 5. - P. V-546 - V - 549-546. ↑

- C2340.** Gherboudj I. Understanding of the interaction of the radar response with the river ice cover. / Gherboudj I., Bernier M., Leconte R. // 2008. IGARSS 2008. IEEE International Geoscience and Remote Sensing Symposium. - Boston, MA, 7-11 July 2008. - Vol. 5. - P. V-526 - V - 529-526. ↑
- C2341.** Siqueira P. Combining Lidar and InSAR Observations over the Harvard and Duke Forests for Making Wide Area Maps of Vegetation Height. / Siqueira P., Hensley S., Chapman B., Ahmed R. // 2008. IGARSS 2008. IEEE International Geoscience and Remote Sensing Symposium. - Boston, MA, 7-11 July 2008. - Vol. 5. - P. V-538 - V - 541-538. ↑
- C2342.** Zhifeng Guo. The Potential of Combined Lidar and SAR Data in Retrieving Forest Parameters using Model Analysis. / Zhifeng Guo, Guoqing Sun, Ranson K.J., Wenjian Ni, Wenhan Qin. // 2008. IGARSS 2008. IEEE International Geoscience and Remote Sensing Symposium. - Boston, MA, 7-11 July 2008. - Vol. 5. - P. V-542 - V - 545-542. ↑
- C2343.** Wei Yao. Automatic vehicle extraction from airborne LiDAR data of urban areas using morphological reconstruction. / Wei Yao, Hinz S., Stilla U. // 2008 IAPR Workshop on Pattern Recognition in Remote Sensing (PRRS 2008). - Tampa, FL, 7-7 Dec. 2008. - P. 1-4. ↑
- C2344.** Yu P. Combining AMSR-E and QuikSCAT image data to improve sea ice classification. / Yu P., Clausi D.A., De Abreu R., Agnew T. // 2008 IAPR Workshop on Pattern Recognition in Remote Sensing (PRRS 2008). - Tampa, FL, 7-7 Dec. 2008. - P. 1-4. ↑
- C2345.** Thomas M. Streamline regularization for large discontinuous motion of sea ice. / Thomas M., Geiger C.A., Kannan P., Kambhamettu C. // 2008 IAPR Workshop on Pattern Recognition in Remote Sensing (PRRS 2008). - Tampa, FL, 7-7 Dec. 2008. - P. 1-4. ↑
- C2346.** Yang Cao. Optimization algorithms in FMRF model-based segmentation for LIDAR data and co-registered bands. / Yang Cao, Hong Wei, Huijie Zhao. // 2008 IAPR Workshop on Pattern Recognition in Remote Sensing (PRRS 2008). - Tampa, FL, 7-7 Dec. 2008. - P. 1-4. ↑
- C2347.** Ebert R. Applications for remote laser vibration sensing. / Ebert R., Lutzmann P., Hebel M. // 2008. IPGC 2008. IEEE PhotonicsGlobal@Singapore. - Singapore, 8-11 Dec. 2008. - P. 1-5. ↑
- C2348.** Wong A. Automatic registration of inter-band and inter-sensor images using robust complex wavelet feature representations. / Wong A., Clausi D. // 2008 IAPR Workshop on Pattern Recognition in Remote Sensing (PRRS 2008). - Tampa, FL, 7-7 Dec. 2008. - P. 1-4. ↑
- C2349.** Michaelsen E. Extraction of building polygons from SAR images: Grouping and decision-level in the GESTALT System. / Michaelsen E., Stilla U., Soergel U., Doktorski L. // 2008 IAPR Workshop on Pattern Recognition in Remote Sensing (PRRS 2008). - Tampa, FL, 7-7 Dec. 2008. - P. 1-4. ↑
- C2350.** Guifu Zhang. Phased Array Radar Polarimetry for Weather Sensing: Challenges and Opportunities. / Guifu Zhang, Doviak R., Zrnic D., Crain J. // 2008. IGARSS 2008. IEEE International Geoscience and Remote Sensing Symposium. - Boston, MA, 7-11 July 2008. - Vol. 5. - P. V-449 - V - 452-449. ↑
- C2351.** Aydin K. Ice Water Content Estimation in Clouds Using Radar Reflectivity and Dual-Frequency Ratio at 94 and 220 GHz. / Aydin K., Walsh T.M. // 2008. IGARSS 2008. IEEE International Geoscience and Remote Sensing Symposium. - Boston, MA, 7-11 July 2008. - Vol. 5. - P. V-453 - V - 454-453. ↑
- C2352.** Gorgucci E. Reflectivity and Differential Reflectivity Rainfall Algorithm Performance at X-band. / Gorgucci E., Baldini L., Chandrasekar V., Le M. // 2008. IGARSS 2008. IEEE International Geoscience and Remote Sensing Symposium. - Boston, MA, 7-11 July 2008. - Vol. 5. - P. V-459 - V - 462-459. ↑
- C2353.** Fritz J. Ground Scattering Analysis to Identify Targets for Refractivity Field Estimation. / Fritz J., Chandrasekar V. // 2008. IGARSS 2008. IEEE International Geoscience and Remote Sensing Symposium. - Boston, MA, 7-11 July 2008. - Vol. 5. - P. V-429 - V - 432-429. ↑
- C2354.** van Zyl J.J. Requirements for Model-based Polarimetric Decompositions. / van Zyl J.J., Yunjin Kim, Arii M. // 2008. IGARSS 2008. IEEE International Geoscience and Remote Sensing Symposium. - Boston, MA, 7-11 July 2008. - Vol. 5. - P. V-417 - V - 420-417. ↑
- C2355.** Wenjian Ni. Effect of Forest Structure on Scattering Center Height from Model and SAR Data. /

Wenjian Ni, Guoqing Sun, Zhifeng Guo, Wenhan Qin. // 2008. IGARSS 2008. IEEE International Geoscience and Remote Sensing Symposium. - Boston, MA, 7-11 July 2008. - Vol. 5. - P. V-421 - V - 424-421. ↑

C2356. Yurchak B.S. Radar Volume Backscatter from Spatially Extended Geophysical Targets in "Slice" Approach. 2008. IGARSS 2008. IEEE International Geoscience and Remote Sensing Symposium. - Boston, MA, 7-11 July 2008. - Vol. 5. - P. V-425 - V - 428-425. ↑

C2357. Edwards M. microASAR: A Small, Robust LFM-CW SAR for Operation on UAVs and Small Aircraft. / Edwards M., Madsen D., Stringham C., Margulis A., Wicks B., Long D.G. // 2008. IGARSS 2008. IEEE International Geoscience and Remote Sensing Symposium. - Boston, MA, 7-11 July 2008. - Vol. 5. - P. V-514 - V - 517-514. ↑

C2358. Auer S. Ray Tracing for Simulating Reflection Phenomena in SAR Images. / Auer S., Hinz S., Bamler R. // 2008. IGARSS 2008. IEEE International Geoscience and Remote Sensing Symposium. - Boston, MA, 7-11 July 2008. - Vol. 5. - P. V-518 - V - 521-518. ↑

C2359. Peichl M. Radar Signature Analysis of Urban Structures. / Peichl M., Kempf T., Dill S. // 2008. IGARSS 2008. IEEE International Geoscience and Remote Sensing Symposium. - Boston, MA, 7-11 July 2008. - Vol. 5. - P. V-522 - V - 525-522. ↑

C2360. Nouvel J.F. Along Track Interferometry on Rhone River. / Nouvel J.F., Dubois-Fernandez P., Kosuth P., Lasne Y. // 2008. IGARSS 2008. IEEE International Geoscience and Remote Sensing Symposium. - Boston, MA, 7-11 July 2008. - Vol. 5. - P. V-495 - V - 497-495. ↑

C2361. Denis L. Joint Filtering of SAR Interferometric and Amplitude Data in Urban Areas by TV Minimization. / Denis L., Tupin F., Darbon J., Sigelle M. // 2008. IGARSS 2008. IEEE International Geoscience and Remote Sensing Symposium. - Boston, MA, 7-11 July 2008. - Vol. 5. - P. V-471 - V - 474-471. ↑

C2362. Fornaro G. 4D SAR Focusing: A Tool for Improved Imaging and Monitoring of Urban Areas. / Fornaro G., Reale D., Serafino F. // 2008. IGARSS 2008. IEEE International Geoscience and Remote Sensing Symposium. - Boston, MA, 7-11 July 2008. - Vol. 5. - P. V-475 - V - 478-475. ↑

C2363. Cadario E. Change Detection for Bridges over Water in Airborne and Spaceborne SAR Data. / Cadario E., Gross H., Hammer H., Schulz K., Thiele A., Thoennessen U., Soergel U., Weydahl D.J. // 2008. IGARSS 2008. IEEE International Geoscience and Remote Sensing Symposium. - Boston, MA, 7-11 July 2008. - Vol. 5. - P. V-479 - V - 482-479. ↑

C2364. Perissin D. Comparison between SAR Atmospheric Phase Screens at 30' by Means of ERS and Envisat Data. / Perissin D., Prati C. // 2008. IGARSS 2008. IEEE International Geoscience and Remote Sensing Symposium. - Boston, MA, 7-11 July 2008. - Vol. 4. - P. IV-557 - IV - 560-557. ↑

C2365. Riris H. Laser Sounder for Global Measurement of CO₂ Concentrations in the Troposphere. / Riris H., Abshire J.B., Allan G., Xiaoli Sun, Chen S.J., Kawa R., Jian-Ping Mao, Stephen M., Burris J., Wilson E., Krainak M.A. // 2008. IGARSS 2008. IEEE International Geoscience and Remote Sensing Symposium. - Boston, MA, 7-11 July 2008. - Vol. 3. - P. III-519 - III - 521-519. ↑

C2366. Alasset P.-J. InSAR Monitoring of Permafrost Activity in the Lower Mackenzie Valley, Canada. / Alasset P.-J., Poncos V., Singhroy V., Couture R. // 2008. IGARSS 2008. IEEE International Geoscience and Remote Sensing Symposium. - Boston, MA, 7-11 July 2008. - Vol. 3. - P. III-530 - III - 533-530. ↑

C2367. Del Frate F. Automatic Retrieval of Tectonic Parameters with Neural Networks and SAR Interferometry: An Assessment with Experimental Data. / Del Frate F., Schiavon G., Stramondo S. // 2008. IGARSS 2008. IEEE International Geoscience and Remote Sensing Symposium. - Boston, MA, 7-11 July 2008. - Vol. 3. - P. III-534 - III - 537-534. ↑

C2368. Apituley A. Construction of Satellite Derived PM_{2.5} Maps using the Relationship between AOD and PM_{2.5} at the Cabauw Experimental Site for Atmospheric Research (CESAR)-The Netherlands. / Apituley A., Schaap M., Koelemeijer R., Timmermans R., Schoemaker R., de Leeuw G. // 2008. IGARSS 2008. IEEE International Geoscience and Remote Sensing Symposium. - Boston, MA, 7-11 July 2008. - Vol. 3. - P. III-507 - III - 510-507. ↑

C2369. Pottier E. PolSARpro v3.3: The Educational Toolbox for Polarimetric and Interferometric Polarimetric

SAR Data Processing. / Pottier E., Ferro-Famil L., Allain S., Cloude S., Hajnsek I., Papathanassiou K., Moreira A., Williams M., Minchella A., Desnos Y.-L. // 2008. IGARSS 2008. IEEE International Geoscience and Remote Sensing Symposium. - Boston, MA, 7-11 July 2008. - Vol. 3. - P. III-471 - III - 474-471. ↑

C2370. Lange H. Leaf Area Index Estimation using Lidar and Forest Reflectance Modelling of Airborne Hyperspectral Data. / Lange H., Solberg S. // 2008. IGARSS 2008. IEEE International Geoscience and Remote Sensing Symposium. - Boston, MA, 7-11 July 2008. - Vol. 3. - P. III-475 - III - 478-475. ↑

C2371. Thoonen G. Spatial Classification of Hyperspectral Data of Dune Vegetation along the Belgian Coast. / Thoonen G., De Backer S., Provoost S., Kempeneers P., Scheunders P. // 2008. IGARSS 2008. IEEE International Geoscience and Remote Sensing Symposium. - Boston, MA, 7-11 July 2008. - Vol. 3. - P. III-483 - III - 486-483. ↑

C2372. Skriver H. Comparison between Multitemporal and Polarimetric SAR Data for Land Cover Classification. 2008. IGARSS 2008. IEEE International Geoscience and Remote Sensing Symposium. - Boston, MA, 7-11 July 2008. - Vol. 3. - P. III-558 - III - 561-558. ↑

C2373. Martinez-Benjamin J.J. Monitoring Sea Level by Radar Altimeter and CGPS in the North-Western Mediterranean. / Martinez-Benjamin J.J., Davila J.M., Garate J., Bonnefond P., Garcia M.M., Castellon M., Talaya J., Velasco G.R., Perez B. // 2008. IGARSS 2008. IEEE International Geoscience and Remote Sensing Symposium. - Boston, MA, 7-11 July 2008. - Vol. 3. - P. III-577 - III - 580-577. ↑

C2374. Wang R. Analysis and Processing of Spaceborne/Airborne Bistatic SAR Data. / Wang R., Loffeld O., Nies H., Ul-Ann Q., Medrano-Ortiz A., Knedlik S., Samarah A. // 2008. IGARSS 2008. IEEE International Geoscience and Remote Sensing Symposium. - Boston, MA, 7-11 July 2008. - Vol. 3. - P. III-597 - III - 600-597. ↑

C2375. Sanjuan M.-J. Microwave Scattering Profiles of a Rice Sample by Means of Polarization Coherence Tomography. / Sanjuan M.-J., Lopez-Sanchez J.M., Ballester-Berman J.D. // 2008. IGARSS 2008. IEEE International Geoscience and Remote Sensing Symposium. - Boston, MA, 7-11 July 2008. - Vol. 3. - P. III-554 - III - 557-554. ↑

C2376. Elmozoughi A. InSAR Phase Unwrapping based on a Combination of Markov Random Fields and Hypergeometric Phase Pdf Models. / Elmozoughi A., Maalij A., Abdelfattah R., Belhadj Z. // 2008. IGARSS 2008. IEEE International Geoscience and Remote Sensing Symposium. - Boston, MA, 7-11 July 2008. - Vol. 3. - P. III-538 - III - 541-538. ↑

C2377. Hajnsek I. Soil Moisture Estimation in time with D-InSAR. / Hajnsek I., Prats P. // 2008. IGARSS 2008. IEEE International Geoscience and Remote Sensing Symposium. - Boston, MA, 7-11 July 2008. - Vol. 3. - P. III-546 - III - 549-546. ↑

C2378. Sang-Hoon Hong. Small Temporal Baseline Subset (STBAS): A New InSAR Technique for Multi-Temporal Monitoring Wetland's Water Level Changes. / Sang-Hoon Hong, Wdowski S., Sang-Wan Kim. // 2008. IGARSS 2008. IEEE International Geoscience and Remote Sensing Symposium. - Boston, MA, 7-11 July 2008. - Vol. 3. - P. III-550 - III - 553-550. ↑

C2379. Wang Yinbo. A new bistatic-based sparse linear array 3D imaging SAR model. / Wang Yinbo, Zhang Xiaoling, Li Weihua, Shi Jun. // 2008. IGARSS 2008. IEEE International Geoscience and Remote Sensing Symposium. - Boston, MA, 7-11 July 2008. - Vol. 3. - P. III-463 - III - 466-463. ↑

C2380. Khaldoune J. An Approach for Mapping Frozen Soil of Agricultural Land under Snow Cover using RADARSAT-1 and RADARSAT-2. / Khaldoune J., van Bochove E., Bernier M., Nolin M.C. // 2008. IGARSS 2008. IEEE International Geoscience and Remote Sensing Symposium. - Boston, MA, 7-11 July 2008. - Vol. 3. - P. III-382 - III - 385-382. ↑

C2381. Watanabe M. Simultaneous field experiments with PALSAR observations for soil moisture estimation. / Watanabe M., Fukuda M., Kadosaki G., Sato M. // 2008. IGARSS 2008. IEEE International Geoscience and Remote Sensing Symposium. - Boston, MA, 7-11 July 2008. - Vol. 3. - P. III-386 - III - 389-386. ↑

C2382. Loew A. Analysis and Surface Parameter Retrieval from Multitemporal Airborne and Satellite Data During AGRISAR 2006. / Loew A., Osenstetter S. // 2008. IGARSS 2008. IEEE International Geoscience and Remote Sensing Symposium. - Boston, MA, 7-11 July 2008. - Vol. 3. - P. III-390 - III - 393-390. ↑

- C2383.** Jiali Shang. Contribution of Multi-Frequency, Multi-Sensor, and Multi-Temporal Radar Data to Operational Annual Crop Mapping. / Jiali Shang, McNairn H., Champagne C., Xianfeng Jiao. // 2008. IGARSS 2008. IEEE International Geoscience and Remote Sensing Symposium. - Boston, MA, 7-11 July 2008. - Vol. 3. - P. III-378 - III - 381-378. ↑
- C2384.** Raney R.K. Pathfinder Advanced Radar Ice Sounder: PARIS. / Raney R.K., Leuschen C., Jose M. // 2008. IGARSS 2008. IEEE International Geoscience and Remote Sensing Symposium. - Boston, MA, 7-11 July 2008. - Vol. 3. - P. III-346 - III - 349-346. ↑
- C2385.** Dobbs M. A Multi-Functional Fiber Laser Lidar for Earth Science & Exploration. / Dobbs M., Krabill W., Cisewski M., Harrison F.W., Shum C.K., McGregor D., Neal M., Stokes S. // 2008. IGARSS 2008. IEEE International Geoscience and Remote Sensing Symposium. - Boston, MA, 7-11 July 2008. - Vol. 3. - P. III-350 - III - 353-350. ↑
- C2386.** Lihua Li. High-Altitude Imaging Wind and Rain Airborne Radar (HIWRAP). / Lihua Li, Heymsfield G., Carswell J., Schaubert D., Creticos J., Vega M. // 2008. IGARSS 2008. IEEE International Geoscience and Remote Sensing Symposium. - Boston, MA, 7-11 July 2008. - Vol. 3. - P. III-354 - III - 357-354. ↑
- C2387.** Rodriguez-Cassola M. Bistatic spaceborne-airborne experiment TerraSAR-X/F-SAR: data processing and results. / Rodriguez-Cassola M., Baumgartner S.V., Krieger G., Nottensteiner A., Horn R., Steinbrecher U., Metzger R., Limbach M., Prats P., Fischer J., Schwerdt M., Moreira A. // 2008. IGARSS 2008. IEEE International Geoscience and Remote Sensing Symposium. - Boston, MA, 7-11 July 2008. - Vol. 3. - P. III-451 - III - 454-451. ↑
- C2388.** Ul-Ann Q. Optimizing the Individual Azimuth Contribution of Transmitter and Receiver Phase terms in Loffeld's Bistatic Formula (LBF) for Bistatic SAR Processing. / Ul-Ann Q., Loffeld O., Nies H., Wang R., Knedlik S. // 2008. IGARSS 2008. IEEE International Geoscience and Remote Sensing Symposium. - Boston, MA, 7-11 July 2008. - Vol. 3. - P. III-455 - III - 458-455. ↑
- C2389.** Knedlik S. GPS/INS Integration for Footprint Chasing in Bistatic SAR Experiments. / Knedlik S., Edwan E., Zhou J., Dai Z., Uboldosold P., Loffeld O. // 2008. IGARSS 2008. IEEE International Geoscience and Remote Sensing Symposium. - Boston, MA, 7-11 July 2008. - Vol. 3. - P. III-459 - III - 462-459. ↑
- C2390.** Yang-Lang Chang. Multisource Image Classification Based on Parallel Minimum Classification Error Learning. / Yang-Lang Chang, Jyh-Peng Fang, Wen-Yew Liang, Lena Chang, Kun-Shan Chen. // 2008. IGARSS 2008. IEEE International Geoscience and Remote Sensing Symposium. - Boston, MA, 7-11 July 2008. - Vol. 3. - P. III-443 - III - 446-443. ↑
- C2391.** Sang-Eun Park. Analysis of Polarimetric Surface Scattering in High Resolution SAR. / Sang-Eun Park, Ferro-Famil L., Allain S., Pottier E. // 2008. IGARSS 2008. IEEE International Geoscience and Remote Sensing Symposium. - Boston, MA, 7-11 July 2008. - Vol. 3. - P. III-394 - III - 397-394. ↑
- C2392.** Hallikainen M. Results from Microwave Radiometer Campaign of Seasonal Snow and Comparison with Emission Models. / Hallikainen M., Lahtinen P., Piepponen T., Honkavaara L., Schafer A. // 2008. IGARSS 2008. IEEE International Geoscience and Remote Sensing Symposium. - Boston, MA, 7-11 July 2008. - Vol. 3. - P. III-402-402. ↑
- C2393.** Vignudelli S. Reprocessing Altimeter Data Records along European Coasts: Lessons Learned from the Altice Project. / Vignudelli S., Kostianoy A., Ginzburg A., Sheremet N., Lebedev S., Sirota A., Snaith H.M., Bouffard J., Roblou L., Cipollini P. // 2008. IGARSS 2008. IEEE International Geoscience and Remote Sensing Symposium. - Boston, MA, 7-11 July 2008. - Vol. 3. - P. III-419 - III - 422-419. ↑
- C2394.** Benveniste J. Basic Radar Altimetry Toolbox. / Benveniste J., Rosmorduc V., Niemeijer S., Picot N. // 2008. IGARSS 2008. IEEE International Geoscience and Remote Sensing Symposium. - Boston, MA, 7-11 July 2008. - Vol. 3. - P. III-895 - III - 898-895. ↑
- C2395.** Jinye Zhang. Study of Atmospheric Correction in the Remote Sensing based on Multifunctional Raman/Mie Lidar System and Sunphotometer. / Jinye Zhang, Wei Gong, Jun Li, Feiyue Mao, Rongliang Zeng, Zhenluan Hu, Liangpei Zhang, Pingxiang Li. // 2008. IGARSS 2008. IEEE International Geoscience and Remote Sensing Symposium. - Boston, MA, 7-11 July 2008. - Vol. 3. - P. III-899 - III - 902-899. ↑
- C2396.** Apituley A. Overview of Research and Networking with Ground based Remote Sensing for

Atmospheric Profiling at the Cabauw Experimental Site for Atmospheric Research (CESAR)-The Netherlands. / Apituley A., Russchenberg H., van der Marel H., Bosveld F., Boers R., ten Brink H., de Leeuw G., Uijlenhoet R., Arbresser-Rastburg B., Rockmann T. // 2008. IGARSS 2008. IEEE International Geoscience and Remote Sensing Symposium. - Boston, MA, 7-11 July 2008. - Vol. 3. - P. III-903 - III - 906-903. ↑

C2397. Bourgeau-Chavez L.L. Monitoring Fuel Moisture and Improving the Prediction of Wildfire Potential in Boreal Alaska with Satellite C-Band Imaging Radar. / Bourgeau-Chavez L.L., Riordan K., Garwood G. // 2008. IGARSS 2008. IEEE International Geoscience and Remote Sensing Symposium. - Boston, MA, 7-11 July 2008. - Vol. 3. - P. III-864 - III - 866-864. ↑

C2398. Katoh M. Comparison of individual crowns among species in Japanese conifer plantations using airborne data for leaf-on and leaf-off conditions. 2008. IGARSS 2008. IEEE International Geoscience and Remote Sensing Symposium. - Boston, MA, 7-11 July 2008. - Vol. 3. - P. III-800 - III - 803-800. ↑

C2399. Pairman D. Pasture Monitoring from Polarimetric TerraSAR-X Data. / Pairman D., McNeill S., Belliss S., Dalley D., Dynes R. // 2008. IGARSS 2008. IEEE International Geoscience and Remote Sensing Symposium. - Boston, MA, 7-11 July 2008. - Vol. 3. - P. III-820 - III - 823-820. ↑

C2400. Maosong Xu. Polarimetric SAR Data for Forest and Deforestation Mapping in Guizhou Province, Southwest of China. / Maosong Xu, Fengli Zhang, Zhongsheng Xia, Huaze Gong. // 2008. IGARSS 2008. IEEE International Geoscience and Remote Sensing Symposium. - Boston, MA, 7-11 July 2008. - Vol. 3. - P. III-852 - III - 855-852. ↑

C2401. Jun Li. Retrieval of Aerosol Optical Properties based on Measurements of Lidar, Sun-Photometer, and CALIPSO at Wuhan, China. / Jun Li, Wei Gong, Yingying Ma, Zhongmin Zhu, Pingxiang Li, Liangpei Zhang. // 2008. IGARSS 2008. IEEE International Geoscience and Remote Sensing Symposium. - Boston, MA, 7-11 July 2008. - Vol. 3. - P. III-969 - III - 972-969. ↑

C2402. Yingying Ma. Aerosol Character Comparison of CALIPSO and Sunphotometer in Hubei Province, China. / Yingying Ma, Wei Gong, Jun Li, Zhongmin Zhu, Liangpei Zhang, Pingxiang Li. // 2008. IGARSS 2008. IEEE International Geoscience and Remote Sensing Symposium. - Boston, MA, 7-11 July 2008. - Vol. 3. - P. III-984 - III - 987-984. ↑

C2403. Gouinaud C. SAR Image Fusion in Multi Sensor Context for Small Urban Area Detection. 2008. IGARSS 2008. IEEE International Geoscience and Remote Sensing Symposium. - Boston, MA, 7-11 July 2008. - Vol. 3. - P. III-988 - III - 991-988. ↑

C2404. Xinli Hu. Retrieval of Spectral Aerosol Optical Thickness over Land Surface from Multi-Wavelength Polarization Space-Borne Sensors. / Xinli Hu, Liangfu Chen, Xingfa Gu. // 2008. IGARSS 2008. IEEE International Geoscience and Remote Sensing Symposium. - Boston, MA, 7-11 July 2008. - Vol. 3. - P. III-950 - III - 953-950. ↑

C2405. Frasier S.J. Vertical Velocity Turbulence Observed with FMCW Radar. / Frasier S.J., Muschinski A., Tsai P.-S., Behn M. // 2008. IGARSS 2008. IEEE International Geoscience and Remote Sensing Symposium. - Boston, MA, 7-11 July 2008. - Vol. 3. - P. III-911 - III - 914-911. ↑

C2406. Sicard M. Planetary Boundary Layer Height and Wind Field Characterization by Means of a Lidar at the Teide Observatory in the Canary Islands. / Sicard M., Tomas S., Comeron A., Rocadenbosch F., Rodriguez A., Muoz C., Batet O. // 2008. IGARSS 2008. IEEE International Geoscience and Remote Sensing Symposium. - Boston, MA, 7-11 July 2008. - Vol. 3. - P. III-915 - III - 918-915. ↑

C2407. Zhongting Wang. Retrieval of Aerosol from Space-Borne Polarimetric Data in Beijing. / Zhongting Wang, Liangfu Chen, Xingfa Gu. // 2008. IGARSS 2008. IEEE International Geoscience and Remote Sensing Symposium. - Boston, MA, 7-11 July 2008. - Vol. 3. - P. III-946 - III - 949-946. ↑

C2408. Susaki J. Three-Dimensional Digitizing of Paddy Rice and Modeling for the Scattering Simulation. / Susaki J., Tamura M., Koura A. // 2008. IGARSS 2008. IEEE International Geoscience and Remote Sensing Symposium. - Boston, MA, 7-11 July 2008. - Vol. 3. - P. III-782 - III - 785-782. ↑

C2409. Chini M. The SIGRIS Project: A Remote Sensing System for Seismic Risk Management. / Chini M., Bignami C., Atzori S., Brunori C.A., Kyriakopoulos C., Moro M., Salvi S., Stramondo S., Tolomei C., Trasatti E., Zoffoli S. // 2008. IGARSS 2008. IEEE International Geoscience and Remote Sensing Symposium. - Boston,

MA, 7-11 July 2008. - Vol. 3. - P. III-624 - III - 627-624. ↑

C2410. Paradzayi C. Field Surveys for Biomass Assessment in African Savanna Woodlands. / Paradzayi C., Annegarn H.J., Matsika R., Erasmus B. // 2008. IGARSS 2008. IEEE International Geoscience and Remote Sensing Symposium. - Boston, MA, 7-11 July 2008. - Vol. 3. - P. III-632 - III - 635-632. ↑

C2411. Burini A. TerraSAR-X Imaging for Unsupervised Land Cover Classification and Fire Mapping. / Burini A., Putignano C., Del Frate F., Lazzarini M., Licciardi G., Schiavon G., Solimini D., De Biasi F., Manunta P. // 2008. IGARSS 2008. IEEE International Geoscience and Remote Sensing Symposium. - Boston, MA, 7-11 July 2008. - Vol. 3. - P. III-660 - III - 663-660. ↑

C2412. Ortiz A.M. Second-Order Motion Compensation in Bistatic Airborne SAR based on the Windowed Fourier-Transformation. / Ortiz A.M., Loffeld O., Nies H., Wang R. // 2008. IGARSS 2008. IEEE International Geoscience and Remote Sensing Symposium. - Boston, MA, 7-11 July 2008. - Vol. 3. - P. III-613 - III - 616-613. ↑

C2413. Duque S. Back and Forward Bistatic Interferometry. / Duque S., Lopez-Dekker P., Mallorqui J.J., Merlano J.C. // 2008. IGARSS 2008. IEEE International Geoscience and Remote Sensing Symposium. - Boston, MA, 7-11 July 2008. - Vol. 3. - P. III-601 - III - 604-601. ↑

C2414. Ya-Qiu Jin. Polarimetric BISAR Image Simulation and Analysis. / Ya-Qiu Jin, Feng Xu. // 2008. IGARSS 2008. IEEE International Geoscience and Remote Sensing Symposium. - Boston, MA, 7-11 July 2008. - Vol. 3. - P. III-605 - III - 608-605. ↑

C2415. Merlano-Duncan J.C. Airborne Bistatic SAR Receiver with the Capability of Use Different Opportunity Transmitters. / Merlano-Duncan J.C., Lopez-Dekker P., Mallorqui J.J., Duque S. // 2008. IGARSS 2008. IEEE International Geoscience and Remote Sensing Symposium. - Boston, MA, 7-11 July 2008. - Vol. 3. - P. III-609 - III - 612-609. ↑

C2416. Wright W.C. Predicting L-band Microwave Attenuation through Forest Canopy using Directional Structuring Elements and Airborne Lidar. / Wright W.C., Liu P.W., Slatton K.C., Shrestha R.L., Carter W.E., Lee H. // 2008. IGARSS 2008. IEEE International Geoscience and Remote Sensing Symposium. - Boston, MA, 7-11 July 2008. - Vol. 3. - P. III-688 - III - 691-688. ↑

C2417. Buckley J.R. Polarimetric Classification of Vegetation in Prairie Landscapes. 2008. IGARSS 2008. IEEE International Geoscience and Remote Sensing Symposium. - Boston, MA, 7-11 July 2008. - Vol. 3. - P. III-704 - III - 707-704. ↑

C2418. Odagawa S. Development of Rice Yield Estimation Method based on Spaceborne Hyperspectral Data: Preliminary Study using Airborne Hyperspectral Data. / Odagawa S., Kato M., Suhami T., Sasaki J., Uto K., Kosugi Y., Saito G. // 2008. IGARSS 2008. IEEE International Geoscience and Remote Sensing Symposium. - Boston, MA, 7-11 July 2008. - Vol. 3. - P. III-716 - III - 719-716. ↑


C2419. Hancock S. Extracting Tree Heights over Topography with Multi-Spectral Spaceborne Waveform Lidar. / Hancock S., Lewis P., Foster M., Disney M., Muller J.-P. // 2008. IGARSS 2008. IEEE International Geoscience and Remote Sensing Symposium. - Boston, MA, 7-11 July 2008. - Vol. 3. - P. III-684 - III - 687-684. ↑


C2420. Lach S.R. Atmospheric Compensation using a Geometrically-Compensated Empirical Line Method. / Lach S.R., Kerekes J.P. // 2008. IGARSS 2008. IEEE International Geoscience and Remote Sensing Symposium. - Boston, MA, 7-11 July 2008. - Vol. 3. - P. III-664 - III - 667-664. ↑


C2421. Neuenschwander A. Signal Processing Techniques for Feature Extraction and Classification using Small-Footprint Full-Waveform Airborne LIDAR. / Neuenschwander A., Magruder L., Gutierrez R. // 2008. IGARSS 2008. IEEE International Geoscience and Remote Sensing Symposium. - Boston, MA, 7-11 July 2008. - Vol. 3. - P. III-676 - III - 679-676. ↑


C2422. Jung J. A Two-Stage Approach for Decomposition of ICESat Waveforms. / Jung J., Crawford M.M. // 2008. IGARSS 2008. IEEE International Geoscience and Remote Sensing Symposium. - Boston, MA, 7-11 July 2008. - Vol. 3. - P. III-680 - III - 683-680. ↑


C2423. Halem M. A Semi-Decadal Multi-Sensor Gridded Data Record of Outgoing Longwave Radiation (OLR) from Aqua. / Halem M., Chapman D., Nguyen P. // 2008. IGARSS 2008. IEEE International Geoscience and Remote Sensing Symposium. - Boston, MA, 7-11 July 2008. - Vol. 3. - P. III-690 - III - 693-690. ↑


Remote Sensing Symposium. - Boston, MA, 7-11 July 2008. - Vol. 3. - P. III-334 - III - 337-334. 


C2424. Wada Y. A Land-Cover Monitoring for Volcanoes by using ALOS-PALSAR Quad-Pol. Data. / Wada Y., Ukawa M., Yamaguchi Y., Ohkura H. // 2008. IGARSS 2008. IEEE International Geoscience and Remote Sensing Symposium. - Boston, MA, 7-11 July 2008. - Vol. 3. - P. III-19 - III - 22-19. 


C2425. Mermoz S. River Ice Mapping from PolSAR Images. / Mermoz S., Allain S., Bernier M., Pottier E. // 2008. IGARSS 2008. IEEE International Geoscience and Remote Sensing Symposium. - Boston, MA, 7-11 July 2008. - Vol. 3. - P. III-23 - III - 26-23. 


C2426. Watanabe M. GB-SAR/PiSAR simultaneous experiment for a trial of flood area detection. / Watanabe M., Shimada M., Matsumoto M., Sato M. // 2008. IGARSS 2008. IEEE International Geoscience and Remote Sensing Symposium. - Boston, MA, 7-11 July 2008. - Vol. 3. - P. III-27 - III - 30-27. 


C2427. Boerner W.-M. Recent Advances in RP-POL-In-SAR Hazard Monitoring of Tectonic Stress and Land-Slides. / Boerner W.-M., Kun-Shan Chen. // 2008. IGARSS 2008. IEEE International Geoscience and Remote Sensing Symposium. - Boston, MA, 7-11 July 2008. - Vol. 3. - P. III-16 - III - 18-16. 


C2428. Zhao Q. A High performance Communication Program for a GPS-based Vehicle Tracing Mobile Platform. / Zhao Q., Fan H., Qinhan L. // 2008. IGARSS 2008. IEEE International Geoscience and Remote Sensing Symposium. - Boston, MA, 7-11 July 2008. - Vol. 2. - P. II-1345-II-1348-1345. 


C2429. Entekhabi D. The Soil Moisture Active/Passive Mission (SMAP). / Entekhabi D., Njoku E., O'Neill P., Spencer M., Jackson T., Entin J., Im E., Kellogg K. // 2008. IGARSS 2008. IEEE International Geoscience and Remote Sensing Symposium. - Boston, MA, 7-11 July 2008. - Vol. 3. - P. III-1 - III - 4-1. 


C2430. Donnellan A. Deformation, Ecosystem Structure, and Dynamics of Ice (DESDynI). / Donnellan A., Rosen P., Ranson J., Zebker H. // 2008. IGARSS 2008. IEEE International Geoscience and Remote Sensing Symposium. - Boston, MA, 7-11 July 2008. - Vol. 3. - P. III-5 - III - 8-5. 


C2431. Ray R.L. Landslide Susceptibility Mapping using Remotely Sensed Soil Moisture. / Ray R.L., Jacobs J.M. // 2008. IGARSS 2008. IEEE International Geoscience and Remote Sensing Symposium. - Boston, MA, 7-11 July 2008. - Vol. 3. - P. III-47 - III - 50-47. 


C2432. Chu P.C. Weibull Distribution for the Global Surface Current Speeds Obtained from Satellite Altimetry. 2008. IGARSS 2008. IEEE International Geoscience and Remote Sensing Symposium. - Boston, MA, 7-11 July 2008. - Vol. 3. - P. III-59 - III - 62-59. 

C2433. Richard J. Space Altimetry from Nano-Satellites: Payload Feasibility, Missions and System Performances. / Richard J., Enjolras V., Rys L., Vallon J., Nann I., Escudier P. // 2008. IGARSS 2008. IEEE International Geoscience and Remote Sensing Symposium. - Boston, MA, 7-11 July 2008. - Vol. 3. - P. III-71 - III - 74-71. 

C2434. Jinyang Du. Development of a Parameterized Snow Scattering Model. / Jinyang Du, Jiancheng Shi. // 2008. IGARSS 2008. IEEE International Geoscience and Remote Sensing Symposium. - Boston, MA, 7-11 July 2008. - Vol. 3. - P. III-43 - III - 46-43. 

C2435. Rott H. Scientific Preparations for CoRe-H2 O, a Dual Frequency SAR Mission for Snow and Ice Observations. / Rott H., Cline D., Duguay C., Essery R., Haas C., Kern M., Macelloni G., Malnes E., Pulliainen J., Rebhan H., Yueh S. // 2008. IGARSS 2008. IEEE International Geoscience and Remote Sensing Symposium. - Boston, MA, 7-11 July 2008. - Vol. 3. - P. III-31 - III - 34-31. 

C2436. Yueh S. POLSCAT Ku-band Radar Remote Sensing of Terrestrial Snow Cover. / Yueh S., Cline D., Elder K. // 2008. IGARSS 2008. IEEE International Geoscience and Remote Sensing Symposium. - Boston, MA, 7-11 July 2008. - Vol. 3. - P. III-35 - III - 38-35. 

C2437. Ding Liang. Modeling Active Microwave Remote Sensing of Multilayer Dry Snow using Dense Media Radiative Transfer Theory. / Ding Liang, Leung Tsang, Simon Yueh, Xiaolan Xu. // 2008. IGARSS 2008. IEEE International Geoscience and Remote Sensing Symposium. - Boston, MA, 7-11 July 2008. - Vol. 3. - P. III-39 - III - 42-39. 

C2438. Yang Li. Estimation of Terrain Slope Using a Compensation-Lambertian Method from Single-Pass

Polsar Data. / Yang Li, Wen Hong, Fang Cao, Yan-ping Wang, Yi-rong Wu. // 2008. IGARSS 2008. IEEE International Geoscience and Remote Sensing Symposium. - Boston, MA, 7-11 July 2008. - Vol. 2. - P. II-1310-II-1313-1310. ↑

C2439. Collin A. The use of the SHOALS waveforms to mapping habitat within the seamless benthoscape. / Collin A., Long B., Archambault P. // 2008. IGARSS 2008. IEEE International Geoscience and Remote Sensing Symposium. - Boston, MA, 7-11 July 2008. - Vol. 2. - P. II-1144-II-1147-1144. ↑

C2440. Zhaonan Zhang. Dual-643 GHz and 874 GHz Airborne Radiometers for Ice Cloud Measurements. / Zhaonan Zhang, Monosmith B. // 2008. IGARSS 2008. IEEE International Geoscience and Remote Sensing Symposium. - Boston, MA, 7-11 July 2008. - Vol. 2. - P. II-1172-II-1175-1172. ↑

C2441. Kim S.-B. Brightness temperature retrieval with scale-model antenna patterns of the aquarius I-band radiometer. / Kim S.-B., Wentz F.J. // 2008. IGARSS 2008. IEEE International Geoscience and Remote Sensing Symposium. - Boston, MA, 7-11 July 2008. - Vol. 2. - P. II-1184-II-1187-1184. ↑

C2442. Li Hui. Laser Intensity Used in Classification of Lidar Point Cloud Data. / Li Hui, Liping Di, Huang Xianfeng, Deren L. // 2008. IGARSS 2008. IEEE International Geoscience and Remote Sensing Symposium. - Boston, MA, 7-11 July 2008. - Vol. 2. - P. II-1140-II-1143-1140. ↑

C2443. Zaccheo T.S. Simulations of Space-Based CO2 Measurements: Measurement Impacts on Mesoscale Transport Modeling. / Zaccheo T.S., Connor T., Eluszkiewicz J., Dobbs M., Snell H.E. // 2008. IGARSS 2008. IEEE International Geoscience and Remote Sensing Symposium. - Boston, MA, 7-11 July 2008. - Vol. 2. - P. II-1124-II-1127-1124. ↑

C2444. Martinez-Benjamin J.J. Space Borne Laser and Airborne Lidar Experiences at L'Estartit (Spain). / Martinez-Benjamin J.J., Schutz B., Urban T., Castellon M. // 2008. IGARSS 2008. IEEE International Geoscience and Remote Sensing Symposium. - Boston, MA, 7-11 July 2008. - Vol. 2. - P. II-1128-II-1131-1128. ↑

C2445. Ling Z. Study on the Resolution of Laser Scanning Point Cloud. / Ling Z., Yuqing M., Ruoming S. // 2008. IGARSS 2008. IEEE International Geoscience and Remote Sensing Symposium. - Boston, MA, 7-11 July 2008. - Vol. 2. - P. II-1136-II-1139-1136. ↑

C2446. Xia Y. CR-Based SAR-Interferometry for Landslide Monitoring. 2008. IGARSS 2008. IEEE International Geoscience and Remote Sensing Symposium. - Boston, MA, 7-11 July 2008. - Vol. 2. - P. II-1239-II-1242-1239. ↑

C2447. Youquan Zhang. Insar Analysis of Land Subsidence Caused by Groundwater Exploitation in Changping, Beijing, China. / Youquan Zhang, Huili Gong, Xiaojuan Li, Taiguang Liu, Wen Yang, Beibei Chen, Angsheng Li, Yaoming Su. // 2008. IGARSS 2008. IEEE International Geoscience and Remote Sensing Symposium. - Boston, MA, 7-11 July 2008. - Vol. 2. - P. II-1247-II-1250-1247. ↑

C2448. Joyce K.E. Using Remote Sensing for Mapping the Effects of Natural Hazards in New Zealand. / Joyce K.E., Samsonov S., Jongens R., Lee J.M., Glassey P.J. // 2008. IGARSS 2008. IEEE International Geoscience and Remote Sensing Symposium. - Boston, MA, 7-11 July 2008. - Vol. 2. - P. II-1251-II-1254-1251. ↑

C2449. Daqing Ge. Land Subsidence Investigation Along Railway Using Permanent Scatterers SAR Interferometry. / Daqing Ge, Yan Wang, Xiaofang Guo, Yi Wang, Ye Xia. // 2008. IGARSS 2008. IEEE International Geoscience and Remote Sensing Symposium. - Boston, MA, 7-11 July 2008. - Vol. 2. - P. II-1235-II-1238-1235. ↑

C2450. Zribi M. Combined Airborne Radio-instruments for Ocean and Land Studies (CAROLS). / Zribi M., Hauser D., Parde M., Fanise P., Leroy P., Dechambre M., Weill A., Boutin J., Reverdin G., Calvet J.C., Wigneron J.P., Skou N., Sobjaerg S.S., Reul N., Ruis A., Cardellach E. // 2008. IGARSS 2008. IEEE International Geoscience and Remote Sensing Symposium. - Boston, MA, 7-11 July 2008. - Vol. 2. - P. II-1200-II-1203-1200. ↑

C2451. Parde M. Carols Campaign, Scientific Data Analysis Results. / Parde M., Zribi M., Fanise P., Leroy P., Hauser D., Leduc-Leballeur M., Boutin J., Reul N., Tenerelli J. // 2008. IGARSS 2008. IEEE International Geoscience and Remote Sensing Symposium. - Boston, MA, 7-11 July 2008. - Vol. 2. - P. II-1204-II-1207-1204. ↑

C2452. Jin-King Liu. The Geomorphometry of Rainfall-Induced Landslides in Alishan Area Obtained by

Airborne Lidar and Digital Photography. / Jin-King Liu, Tian-Yuan Shih, Zu-Yi Liao, Chi-Chung Lau, Pai-Hui Hsu. // 2008. IGARSS 2008. IEEE International Geoscience and Remote Sensing Symposium. - Boston, MA, 7-11 July 2008. - Vol. 2. - P. II-1220-II-1223-1220. ↑

C2453. Wade U.B. Airborne Measurement of Snow Thickness over Sea Ice. 2008. IGARSS 2008. IEEE International Geoscience and Remote Sensing Symposium. - Boston, MA, 7-11 July 2008. - Vol. 3. - P. III-222 - III - 225-222. ↑

C2454. Genong Yu. Downscaling of Global Soil Moisture using Auxiliary Data. / Genong Yu, Liping Di, Wenli Yang. // 2008. IGARSS 2008. IEEE International Geoscience and Remote Sensing Symposium. - Boston, MA, 7-11 July 2008. - Vol. 3. - P. III-230 - III - 233-230. ↑

C2455. Severini J. Bayesian Estimation of Altimeter Echo Parameters. / Severini J., Mailhes C., Thibaut P., Tourneret J.-Y. // 2008. IGARSS 2008. IEEE International Geoscience and Remote Sensing Symposium. - Boston, MA, 7-11 July 2008. - Vol. 3. - P. III-238 - III - 241-238. ↑

C2456. Macelloni G. Impact of Vegetation in the Retrieval of Snow Parameters from Backscattering Measurements at the X- and Ku-bands. / Macelloni G., Pettinato S., Santi E., Rott H., Cline D., Rebhan H. // 2008. IGARSS 2008. IEEE International Geoscience and Remote Sensing Symposium. - Boston, MA, 7-11 July 2008. - Vol. 3. - P. III-218 - III - 221-218. ↑

C2457. Howell C. Dual Polarization Detection of Ships and Icebergs-Recent Results with ENVISAT ASAR and Data Simulations of RADARSAT-2. / Howell C., Power D., Lynch M., Dodge K., Bobby P., Randell C., Vachon P., Staples G. // 2008. IGARSS 2008. IEEE International Geoscience and Remote Sensing Symposium. - Boston, MA, 7-11 July 2008. - Vol. 3. - P. III-206 - III - 209-206. ↑

C2458. Werner C. A Real-Aperture Radar for Ground-Based Differential Interferometry. / Werner C., Strozzi T., Wiesmann A., Wegmuller U. // 2008. IGARSS 2008. IEEE International Geoscience and Remote Sensing Symposium. - Boston, MA, 7-11 July 2008. - Vol. 3. - P. III-210 - III - 213-210. ↑

C2459. Luoju K. Development of SAR-Based Snow-Covered Area Estimation Method for Boreal Forest Zone. / Luoju K., Pulliainen J., Metsamaki S., Molera G., Nakari R., Karna J.-P., Hallikainen M. // 2008. IGARSS 2008. IEEE International Geoscience and Remote Sensing Symposium. - Boston, MA, 7-11 July 2008. - Vol. 3. - P. III-214 - III - 217-214. ↑

C2460. Gabele M. GMTI Performance of a High Resolution Wide Swath SAR Operation Mode. / Gabele M., Krieger G. // 2008. IGARSS 2008. IEEE International Geoscience and Remote Sensing Symposium. - Boston, MA, 7-11 July 2008. - Vol. 3. - P. III-282 - III - 285-282. ↑

C2461. Lavalley M. PolInSAR for Forest Biomass Retrieval: PALSAR Observations and Model Analysis. / Lavalley M., Solimini D., Pottier E., Desnos Y.-L. // 2008. IGARSS 2008. IEEE International Geoscience and Remote Sensing Symposium. - Boston, MA, 7-11 July 2008. - Vol. 3. - P. III-302 - III - 305-302. ↑

C2462. Pavlic G. Satellite Data Fusion Techniques for Terrain and Surficial Geological Mapping. / Pavlic G., Singhroy V., Duk-Rodkin A., Alasset P.-J. // 2008. IGARSS 2008. IEEE International Geoscience and Remote Sensing Symposium. - Boston, MA, 7-11 July 2008. - Vol. 3. - P. III-314 - III - 317-314. ↑

C2463. Younis M. Smart Multi-Aperture Radar Techniques for Spaceborne Remote Sensing. / Younis M., Bordoni F., Gebert N., Krieger G. // 2008. IGARSS 2008. IEEE International Geoscience and Remote Sensing Symposium. - Boston, MA, 7-11 July 2008. - Vol. 3. - P. III-278 - III - 281-278. ↑

C2464. Martin-Puig C. Theoretical Model of SAR Altimeter over Water Surfaces. / Martin-Puig C., Ruffini G., Marquez J., Cotton D., Srokosz M., Challenor P., Raney K., Benveniste J. // 2008. IGARSS 2008. IEEE International Geoscience and Remote Sensing Symposium. - Boston, MA, 7-11 July 2008. - Vol. 3. - P. III-242 - III - 245-242. ↑

C2465. Maussang F. Multistatic Scenarios for a GPS SAR System. / Maussang F., Daout F., Ginolhac G., Schmitt F. // 2008. IGARSS 2008. IEEE International Geoscience and Remote Sensing Symposium. - Boston, MA, 7-11 July 2008. - Vol. 3. - P. III-270 - III - 273-270. ↑

C2466. Evangelista A. Reflectivity and DEM Estimation from Multi-baseline Complex SAR Signals. / Evangelista A., Meglio F., Schirinzi G. // 2008. IGARSS 2008. IEEE International Geoscience and Remote

Sensing Symposium. - Boston, MA, 7-11 July 2008. - Vol. 3. - P. III-274 - III - 277-274. ↑

C2467. Singhroy V. InSAR Monitoring of Landslides in Canada. / Singhroy V., Alasset P.-J., Couture R., Froese C. // 2008. IGARSS 2008. IEEE International Geoscience and Remote Sensing Symposium. - Boston, MA, 7-11 July 2008. - Vol. 3. - P. III-202 - III - 205-202. ↑

C2468. Wessel B. TanDEM-X: DEM Calibration Concept. / Wessel B., Gruber A., Gonzalez J.H., Bachmann M., Wendleder A. // 2008. IGARSS 2008. IEEE International Geoscience and Remote Sensing Symposium. - Boston, MA, 7-11 July 2008. - Vol. 3. - P. III-111 - III - 114-111. ↑

C2469. Gonzalez J.H. TanDEM-X DEM Calibration and Processing Experiments with E-SAR. / Gonzalez J.H., Bachmann M., Scheiber R., Andres C., Krieger G. // 2008. IGARSS 2008. IEEE International Geoscience and Remote Sensing Symposium. - Boston, MA, 7-11 July 2008. - Vol. 3. - P. III-115 - III - 118-115. ↑

C2470. Wen Zhang. Automatic Forest Species Classification using Combined LIDAR Data and Optical Imagery. / Wen Zhang, Baoxin Hu, Linhai Jing, Woods M.E., Courville P. // 2008. IGARSS 2008. IEEE International Geoscience and Remote Sensing Symposium. - Boston, MA, 7-11 July 2008. - Vol. 3. - P. III-134 - III - 137-134. ↑

C2471. Younis M. Determining the optimum compromise between SAR data compression and radiometric performance -An approach based on the analysis of TerraSAR -X data-. / Younis M., Boer J., Ortega C., Schulze D., Huber S., Mittermayer J. // 2008. IGARSS 2008. IEEE International Geoscience and Remote Sensing Symposium. - Boston, MA, 7-11 July 2008. - Vol. 3. - P. III-107 - III - 110-107. ↑

C2472. Tournet J.-Y. Classification of Altimetric Signals using Linear Discriminant Analysis. / Tournet J.-Y., Mailhes C., Amarouche L., Steunou N. // 2008. IGARSS 2008. IEEE International Geoscience and Remote Sensing Symposium. - Boston, MA, 7-11 July 2008. - Vol. 3. - P. III-75 - III - 78-75. ↑

C2473. Soccorsi M. TerraSAR-X: Complex Image Inversion for Feature Extraction. / Soccorsi M., Datcu M., Gleich D. // 2008. IGARSS 2008. IEEE International Geoscience and Remote Sensing Symposium. - Boston, MA, 7-11 July 2008. - Vol. 3. - P. III-99 - III - 102-99. ↑

C2474. Hahmann T. Automatic Extraction of Water Bodies from TerraSAR-X Data. / Hahmann T., Roth A., Martinis S., Tuele A., Gruber A. // 2008. IGARSS 2008. IEEE International Geoscience and Remote Sensing Symposium. - Boston, MA, 7-11 July 2008. - Vol. 3. - P. III-103 - III - 106-103. ↑

C2475. Haimov S. Multi-Doppler Measurements of Atmospheric Rotors and Turbulent Mountain Waves. / Haimov S., Grubisic V., French J., Oolman L. // 2008. IGARSS 2008. IEEE International Geoscience and Remote Sensing Symposium. - Boston, MA, 7-11 July 2008. - Vol. 3. - P. III-182 - III - 185-182. ↑

C2476. Brancaccio A. Linear Inversion of PEC Scatterers. / Brancaccio A., Di Dio C., Leone G. // 2008. IGARSS 2008. IEEE International Geoscience and Remote Sensing Symposium. - Boston, MA, 7-11 July 2008. - Vol. 3. - P. III-194 - III - 197-194. ↑

C2477. Robinson C.A. Understanding the Distribution of Groundwater Resources using Synthetic Aperture Radar Data over Southwest Egypt. 2008. IGARSS 2008. IEEE International Geoscience and Remote Sensing Symposium. - Boston, MA, 7-11 July 2008. - Vol. 3. - P. III-198 - III - 201-198. ↑

C2478. Wiltshire B. Combining CALIPSO and Meteosat Images to Study the Distribution of Atmospheric Dust. / Wiltshire B., Govindan R., Astin I., Evans A.N. // 2008. IGARSS 2008. IEEE International Geoscience and Remote Sensing Symposium. - Boston, MA, 7-11 July 2008. - Vol. 3. - P. III-178 - III - 181-178. ↑

C2479. Mercier G. Change Detection with Misregistration Errors. / Mercier G., Inglada J. // 2008. IGARSS 2008. IEEE International Geoscience and Remote Sensing Symposium. - Boston, MA, 7-11 July 2008. - Vol. 3. - P. III-154 - III - 157-154. ↑

C2480. Bovolo F. An Adaptive Technique based on Similarity Measures for Change Detection in Very High Resolution SAR Images. / Bovolo F., Bruzzone L. // 2008. IGARSS 2008. IEEE International Geoscience and Remote Sensing Symposium. - Boston, MA, 7-11 July 2008. - Vol. 3. - P. III-158 - III - 161-158. ↑

C2481. Hongtao Yu. A DCT-based Change Detection Method for Multi-Temporal SAR Images. / Hongtao Yu, Zhiping Lin, Geok Ling Chai, Chye Hwang Yan, Raman N. // 2008. IGARSS 2008. IEEE International

Geoscience and Remote Sensing Symposium. - Boston, MA, 7-11 July 2008. - Vol. 3. - P. III-166 - III - 169-166.



C2482. Meyer F. A Comparative Analysis of Tropospheric Water Vapor Measurements from MERIS and SAR. / Meyer F., Bamler R., Leinweber R., Fischer J. // 2008. IGARSS 2008. IEEE International Geoscience and Remote Sensing Symposium. - Boston, MA, 7-11 July 2008. - Vol. 4. - P. IV-228 - IV - 231-228.

C2483. Ferraioli G. Bayesian DEM Reconstruction from SAR and Optical Data. / Ferraioli G., Baselice F., Pascasio V. // 2008. IGARSS 2008. IEEE International Geoscience and Remote Sensing Symposium. - Boston, MA, 7-11 July 2008. - Vol. 4. - P. IV-232 - IV - 235-232.

C2484. Gudipati K. Time Series Analysis of Scansar Interferograms using the Small Baseline Subset Technique. / Gudipati K., Buckley S.M. // 2008. IGARSS 2008. IEEE International Geoscience and Remote Sensing Symposium. - Boston, MA, 7-11 July 2008. - Vol. 4. - P. IV-236 - IV - 239-236.

C2485. Ho P.-G.P. Multivariate AR Model based Support Vector Machine for Multispectral Remote Sensing Image Classification. / Ho P.-G.P., Chen C.H. // 2008. IGARSS 2008. IEEE International Geoscience and Remote Sensing Symposium. - Boston, MA, 7-11 July 2008. - Vol. 4. - P. IV-208 - IV - 211-208.

C2486. Doulgeris A.P. Analysis and Classification of high Arctic Glaciers with ASAR Data. / Doulgeris A.P., Langley K., Eltoft T. // 2008. IGARSS 2008. IEEE International Geoscience and Remote Sensing Symposium. - Boston, MA, 7-11 July 2008. - Vol. 4. - P. IV-181 - IV - 184-181.

C2487. Monaldo F.M. Cross Comparison of ALOS PALSAR L-Band Retrieval Model Functions. / Monaldo F.M., Thompson D.R. // 2008. IGARSS 2008. IEEE International Geoscience and Remote Sensing Symposium. - Boston, MA, 7-11 July 2008. - Vol. 4. - P. IV-201 - IV - 203-201.

C2488. Plagge A.M. Validation and Evaluation of QuikSCAT Ultra-High Resolution Wind Retrieval in the Gulf of Maine. / Plagge A.M., Vandemark D.C., Long D.G. // 2008. IGARSS 2008. IEEE International Geoscience and Remote Sensing Symposium. - Boston, MA, 7-11 July 2008. - Vol. 4. - P. IV-204 - IV - 207-204.

C2489. Chandrasekar V. Hybrid Neural Network Technique to Estimate Rainfall from TRMM Measurements. / Chandrasekar V., Alqudah A., Yanting Wang. // 2008. IGARSS 2008. IEEE International Geoscience and Remote Sensing Symposium. - Boston, MA, 7-11 July 2008. - Vol. 4. - P. IV-291 - IV - 294-291.

C2490. Ahmad K. An Improved Oceanic Rainfall Retrieval Algorithm and Results from Seawinds. / Ahmad K., Jones W.L., Kasparis T. // 2008. IGARSS 2008. IEEE International Geoscience and Remote Sensing Symposium. - Boston, MA, 7-11 July 2008. - Vol. 4. - P. IV-295 - IV - 298-295.

C2491. Owen M.P. Progress Toward Validation of Quikscat Ultra-High-Resolution Rain Rates using TRMM PR. / Owen M.P., Long D.G. // 2008. IGARSS 2008. IEEE International Geoscience and Remote Sensing Symposium. - Boston, MA, 7-11 July 2008. - Vol. 4. - P. IV-299 - IV - 302-299.

C2492. Wojcik M.D. Lidar based Particulate Flux Measurements of Agricultural Field Operations. / Wojcik M.D., Bingham G.E., Marchant C.C., Zavyalov V.V., Ahlstrom D.J., Moore K., Wilkerson T.D., Hipps L.E., Martin R.S., Hatfield J.L., Prueger J.H. // 2008. IGARSS 2008. IEEE International Geoscience and Remote Sensing Symposium. - Boston, MA, 7-11 July 2008. - Vol. 4. - P. IV-263 - IV - 266-263.

C2493. Hoonyol Lee. An Experiment of GB-SAR Interferometric Measurement of Target Displacement and Atmospheric Correction. / Hoonyol Lee, Jae-Hee Lee, Seong-Jun Cho, Nak-Hoon Sung, Jung-Ho Kim. // 2008. IGARSS 2008. IEEE International Geoscience and Remote Sensing Symposium. - Boston, MA, 7-11 July 2008. - Vol. 4. - P. IV-240 - IV - 243-240.

C2494. Jianying Jia. Scansar Differential Interferometry and Wet Delay Correction: Case Studies in Dangxiong, Tibet. / Jianying Jia, Qiming Zeng, Jian Jiao, Ying Li, Xia Cui. // 2008. IGARSS 2008. IEEE International Geoscience and Remote Sensing Symposium. - Boston, MA, 7-11 July 2008. - Vol. 4. - P. IV-244 - IV - 247-244.

C2495. Junping Zhang. Spaceborne Hyperspectral Image Generation based on Airborne Hyperspectral Image. / Junping Zhang, Wenjie Zhang, Haibin Jiao, Ye Zhang. // 2008. IGARSS 2008. IEEE International Geoscience and Remote Sensing Symposium. - Boston, MA, 7-11 July 2008. - Vol. 4. - P. IV-259 - IV - 262-259.

C2496. Tagawa T. Derivation of sub-footprint scale σ_{Spl} observed by TRMM Precipitation Radar. /

Tagawa T., Shimizu S., Oki R. // 2008. IGARSS 2008. IEEE International Geoscience and Remote Sensing Symposium. - Boston, MA, 7-11 July 2008. - Vol. 4. - P. IV-137 - IV - 140-137. ↑

C2497. Brunner D. Extraction of Building Heights from VHR SAR Imagery using an Iterative Simulation and Match Procedure. / Brunner D., Lemoine G., Bruzzone L. // 2008. IGARSS 2008. IEEE International Geoscience and Remote Sensing Symposium. - Boston, MA, 7-11 July 2008. - Vol. 4. - P. IV-141 - IV - 144-141. ↑

C2498. Sauer S. 3D Urban Remote Sensing using Dual-baseline POL-InSAR Images at L-Band. / Sauer S., Ferro-Famil L., Reigber A., Pottier E. // 2008. IGARSS 2008. IEEE International Geoscience and Remote Sensing Symposium. - Boston, MA, 7-11 July 2008. - Vol. 4. - P. IV-145 - IV - 148-145. ↑

C2499. Shimizu S. Evaluation of the Effect of the Orbit Boost of the TRMM Satellite on the PR Rain Estimates. / Shimizu S., Iguchi T., Oki R., Hirose M., Tagawa T. // 2008. IGARSS 2008. IEEE International Geoscience and Remote Sensing Symposium. - Boston, MA, 7-11 July 2008. - Vol. 4. - P. IV-133 - IV - 136-133. ↑

C2500. Shimada M. PALSAR SCANSAR SCANSAR Interferometry. 2008. IGARSS 2008. IEEE International Geoscience and Remote Sensing Symposium. - Boston, MA, 7-11 July 2008. - Vol. 4. - P. IV-93 - IV - 96-93. ↑

C2501. Villard L. Bistatic Pol-InSAR Scenario and Evaluation by Forest Scattering Simulations. / Villard L., Borderies P., Hajnsek I. // 2008. IGARSS 2008. IEEE International Geoscience and Remote Sensing Symposium. - Boston, MA, 7-11 July 2008. - Vol. 4. - P. IV-97 - IV - 100-97. ↑

C2502. Frankenberger J.R. Low-Altitude Digital Photogrammetry Technique to Assess Ephemeral Gully Erosion. / Frankenberger J.R., Huang C., Nouwakpo K. // 2008. IGARSS 2008. IEEE International Geoscience and Remote Sensing Symposium. - Boston, MA, 7-11 July 2008. - Vol. 4. - P. IV-117 - IV - 120-117. ↑

C2503. Honglei Chen. Performance Analysis of Multivariate Super-resolution Processing of Polarimetric Synthetic Aperture Radar Tomography. / Honglei Chen, Kasilingam D. // 2008. IGARSS 2008. IEEE International Geoscience and Remote Sensing Symposium. - Boston, MA, 7-11 July 2008. - Vol. 4. - P. IV-169 - IV - 172-169. ↑

C2504. Karvonen J. Baltic Sea Ice Thickness Charts based on Thermodynamic Snow/Ice Model, C-band SAR Classification and Ice Motion Detection. / Karvonen J., Bin Cheng, Simila M., Hallikainen M. // 2008. IGARSS 2008. IEEE International Geoscience and Remote Sensing Symposium. - Boston, MA, 7-11 July 2008. - Vol. 4. - P. IV-173 - IV - 176-173. ↑

C2505. Brandt O. Comparison of Airborne Radar Altimeter and Ground-based Ku-band Radar Measurements on the Ice Cap Austfonna, Svalbard. / Brandt O., Hawley R.L., Dunse T., Kohler J., Hagen J.O., Morris E., Scott J., Eiken T. // 2008. IGARSS 2008. IEEE International Geoscience and Remote Sensing Symposium. - Boston, MA, 7-11 July 2008. - Vol. 4. - P. IV-177 - IV - 180-177. ↑

C2506. Dreuillet P. The New ONERA Multispectral Airborne SAR System. / Dreuillet P., Bonin G., du Plessis O.R., Angelliaume S., Cantalloube H., Dubois-Fernandez P., Dupuis X., Coulombeix C., team R. // 2008. IGARSS 2008. IEEE International Geoscience and Remote Sensing Symposium. - Boston, MA, 7-11 July 2008. - Vol. 4. - P. IV-165 - IV - 168-165. ↑

C2507. Yinghua Wang. Building Detection from High Resolution PolSAR Data by combining Region and Edge Information. / Yinghua Wang, Tupin F., Chongzhao Han, Nicolas J.-M. // 2008. IGARSS 2008. IEEE International Geoscience and Remote Sensing Symposium. - Boston, MA, 7-11 July 2008. - Vol. 4. - P. IV-153 - IV - 156-153. ↑

C2508. Chaabouni-Chouayakh H. Geometrical and Topological Urban Areas Characterization using TerraSAR-X Data. / Chaabouni-Chouayakh H., Datcu M. // 2008. IGARSS 2008. IEEE International Geoscience and Remote Sensing Symposium. - Boston, MA, 7-11 July 2008. - Vol. 4. - P. IV-157 - IV - 160-157. ↑

C2509. Yamaguchi Y. Coherent Decomposition of Fully Polarimetric Radar Data. / Yamaguchi Y., Nakamura J., Aoyama K., Yamada H. // 2008. IGARSS 2008. IEEE International Geoscience and Remote Sensing Symposium. - Boston, MA, 7-11 July 2008. - Vol. 4. - P. IV-161 - IV - 164-161. ↑

C2510. Chu D.A. Developing Aerosol Height Product from MODIS and Synergy of MODIS and CALIPSO Measurements for Global Application. / Chu D.A., Szykman J., Kittaka C., Chin M., Liu H.-C., Remer L., Al-Saadi

J., Winker D. // 2008. IGARSS 2008. IEEE International Geoscience and Remote Sensing Symposium. - Boston, MA, 7-11 July 2008. - Vol. 4. - P. IV-303 - IV - 306-303. ↑

C2511. Sato R. Polarimetric Scattering Analysis for Simplified Man-Made Structure Model on Rough and/or Inclined Ground Plane. / Sato R., Yamaguchi Y., Yamada H. // 2008. IGARSS 2008. IEEE International Geoscience and Remote Sensing Symposium. - Boston, MA, 7-11 July 2008. - Vol. 4. - P. IV-483 - IV - 486-483. ↑

C2512. Anfinson S.N. Estimation of the Equivalent Number of Looks in Polarimetric SAR Imagery. / Anfinson S.N., Doulgeris A.P., Eltoft T. // 2008. IGARSS 2008. IEEE International Geoscience and Remote Sensing Symposium. - Boston, MA, 7-11 July 2008. - Vol. 4. - P. IV-487 - IV - 490-487. ↑

C2513. Raney R.K. Hybrid-Quad-Pol SAR. 2008. IGARSS 2008. IEEE International Geoscience and Remote Sensing Symposium. - Boston, MA, 7-11 July 2008. - Vol. 4. - P. IV-491 - IV - 493-491. ↑

C2514. Dekker R.J. Road Extraction and Network Building from Synthetic Aperture Radar Images using A-Priori Information. 2008. IGARSS 2008. IEEE International Geoscience and Remote Sensing Symposium. - Boston, MA, 7-11 July 2008. - Vol. 4. - P. IV-471 - IV - 474-471. ↑

C2515. Nies H. Image Registration of TerraSAR-X Data using Different Information Measures. / Nies H., Loffeld O., Domnez B., Ben Hammadi A., Wang R. // 2008. IGARSS 2008. IEEE International Geoscience and Remote Sensing Symposium. - Boston, MA, 7-11 July 2008. - Vol. 4. - P. IV-419 - IV - 422-419. ↑

C2516. Khajonrat D. Simulation of Spaceborne Radar Observations of Precipitation: Application to GPM-DPR. / Khajonrat D., Chandrasekar V. // 2008. IGARSS 2008. IEEE International Geoscience and Remote Sensing Symposium. - Boston, MA, 7-11 July 2008. - Vol. 4. - P. IV-455 - IV - 458-455. ↑

C2517. Hedman K. Evaluation of a Statistical Fusion of Linear Features in SAR Data. / Hedman K., Stefan Hinz, Stilla U. // 2008. IGARSS 2008. IEEE International Geoscience and Remote Sensing Symposium. - Boston, MA, 7-11 July 2008. - Vol. 4. - P. IV-467 - IV - 470-467. ↑

C2518. Sang-Wan Kim. X-band InSAR Observations in New Orleans, Louisiana. / Sang-Wan Kim, Wdowinski S., Amelung F., Dixon T., Sang-Hoon Hong. // 2008. IGARSS 2008. IEEE International Geoscience and Remote Sensing Symposium. - Boston, MA, 7-11 July 2008. - Vol. 4. - P. IV-514 - IV - 517-514. ↑

C2519. Chamundeeswari V.V. A Critical Analysis to Generate Change Detection Map using SAR Interferometry for Land Subsidence Monitoring of New Orleans City of USA. / Chamundeeswari V.V., Singh D., Singh K., Wiesbeck W. // 2008. IGARSS 2008. IEEE International Geoscience and Remote Sensing Symposium. - Boston, MA, 7-11 July 2008. - Vol. 4. - P. IV-518 - IV - 521-518. ↑

C2520. Kim Y.-h. Radar Backscattering Measurement of a Paddy Rice Field using Multi-frequency(L, C and X) and Full-polarization. / Kim Y.-h., Hong S.Y., Lee H. // 2008. IGARSS 2008. IEEE International Geoscience and Remote Sensing Symposium. - Boston, MA, 7-11 July 2008. - Vol. 4. - P. IV-553 - IV - 556-553. ↑

C2521. Makynen M. Simulation of ASIRAS Multilooked Echoes for Snow Covered Sea Ice. / Makynen M., Hallikainen M. // 2008. IGARSS 2008. IEEE International Geoscience and Remote Sensing Symposium. - Boston, MA, 7-11 July 2008. - Vol. 4. - P. IV-506 - IV - 509-506. ↑

C2522. Dall J. P-band Polarimetric Ice Sounder: Concept and First Results. / Dall J., Hernandez C.C., Kristensen S.S., Krozer V., Kusk A., Vidkjoer J., Balling J., Skou N., Sobjerg S.S., Christensen E.L. // 2008. IGARSS 2008. IEEE International Geoscience and Remote Sensing Symposium. - Boston, MA, 7-11 July 2008. - Vol. 4. - P. IV-494 - IV - 497-494. ↑

C2523. Blake W. A VHF Radar for Deployment on a UAV for Basal Imaging of Polar Ice. / Blake W., Ledford J., Allen C., Leuschen C., Gogineni S., Rodriguez-Morales F., Lei Shi. // 2008. IGARSS 2008. IEEE International Geoscience and Remote Sensing Symposium. - Boston, MA, 7-11 July 2008. - Vol. 4. - P. IV-498 - IV - 501-498. ↑

C2524. Uppuluri A.V. SAR Image Analysis to Estimate Freeze-Thawdates for a High Latitude Lake in Alaska. / Uppuluri A.V., Jost R.J., Luecke C., White M.A. // 2008. IGARSS 2008. IEEE International Geoscience and Remote Sensing Symposium. - Boston, MA, 7-11 July 2008. - Vol. 4. - P. IV-502 - IV - 505-502. ↑

- C2525.** Yamada H. Polarimetric Scattering Model Decomposition for Pol-InSAR Data. / Yamada H., Yamaguchi Y., Sato R. // 2008. IGARSS 2008. IEEE International Geoscience and Remote Sensing Symposium. - Boston, MA, 7-11 July 2008. - Vol. 4. - P. IV-331 - IV - 334-331. ↑
- C2526.** Lambert B. Monitoring Changes in the Antarctic Ice Sheet from 1978 to 2007. / Lambert B., Long D.G. // 2008. IGARSS 2008. IEEE International Geoscience and Remote Sensing Symposium. - Boston, MA, 7-11 July 2008. - Vol. 4. - P. IV-335 - IV - 338-335. ↑
- C2527.** Yonghong Li. Decadal Mass Balance of the Greenland and Antarctic Ice Sheets from High Resolution Elevation Change Analysis of ERS-2 and Envisat Radar Altimetry Measurements. / Yonghong Li, Davis C.H. // 2008. IGARSS 2008. IEEE International Geoscience and Remote Sensing Symposium. - Boston, MA, 7-11 July 2008. - Vol. 4. - P. IV-339 - IV - 342-339. ↑
- C2528.** Pipia L. Polarimetric Deformation Maps Retrieval of Urban Areas using Ground-Based SAR Acquisitions. / Pipia L., Fabregas X., Aguasca A., Duque S., Mallorqui J.J., Lopez-Martinez C. // 2008. IGARSS 2008. IEEE International Geoscience and Remote Sensing Symposium. - Boston, MA, 7-11 July 2008. - Vol. 4. - P. IV-327 - IV - 330-327. ↑
- C2529.** Chuen-Meei Gan. Analysis of the Interaction of Aerosol Transport Layers on Local Air Quality. / Chuen-Meei Gan, Charles L., Gross B., Moshary F., Ahmed S. // 2008. IGARSS 2008. IEEE International Geoscience and Remote Sensing Symposium. - Boston, MA, 7-11 July 2008. - Vol. 4. - P. IV-307 - IV - 310-307. ↑
- C2530.** Dubois-Fernandez P. Review of Polarimetric Indicators for Forest Characterisation over Several Sites. / Dubois-Fernandez P., Angelliaume S., Champion I., Ulander L. // 2008. IGARSS 2008. IEEE International Geoscience and Remote Sensing Symposium. - Boston, MA, 7-11 July 2008. - Vol. 4. - P. IV-319 - IV - 322-319. ↑
- C2531.** Hajnsek I. Agricultural Vegetation Parameter Estimation using Pol-SAR: Retrieval of Soil Moisture. / Hajnsek I., Jagdhuber T., Schon H., Papathanassiou K.P. // 2008. IGARSS 2008. IEEE International Geoscience and Remote Sensing Symposium. - Boston, MA, 7-11 July 2008. - Vol. 4. - P. IV-323 - IV - 326-323. ↑
- C2532.** Zhang P. A New Superresolution SAR Imaging Algorithm based on Extrapolation. / Zhang P., Ruliang Yang. // 2008. IGARSS 2008. IEEE International Geoscience and Remote Sensing Symposium. - Boston, MA, 7-11 July 2008. - Vol. 4. - P. IV-407 - IV - 410-407. ↑
- C2533.** Giacobazzo V.M. Identification of Coherent Scatterers: Spectral Correlation vs. Multi-Chromatic Phase Analysis. / Giacobazzo V.M., Refice A., Bovenga F., Veneziani N. // 2008. IGARSS 2008. IEEE International Geoscience and Remote Sensing Symposium. - Boston, MA, 7-11 July 2008. - Vol. 4. - P. IV-411 - IV - 414-411. ↑
- C2534.** Frey O. Focusing SAR Data Acquired from Non-Linear Sensor Trajectories. / Frey O., Magnard C., Ruegg M., Meier E. // 2008. IGARSS 2008. IEEE International Geoscience and Remote Sensing Symposium. - Boston, MA, 7-11 July 2008. - Vol. 4. - P. IV-415 - IV - 418-415. ↑
- C2535.** Wesson J. Aircraft and in Situ Salinity and Ocean Color Measurements and Comparisons in the Gulf of Mexico. / Wesson J., Burrage D., Osburn C., Maisonet V., Howden S., Chen X. // 2008. IGARSS 2008. IEEE International Geoscience and Remote Sensing Symposium. - Boston, MA, 7-11 July 2008. - Vol. 4. - P. IV-383 - IV - 386-383. ↑
- C2536.** Koch M. Application of ALOS PALSAR and Landsat ETM+ Data for the Study of Periglacial Features and Permafrost within the South Shetland Islands, Western Antarctica. / Koch M., Lopez-Martinez J., Schmid T., Serrano E., Gumuzzio J. // 2008. IGARSS 2008. IEEE International Geoscience and Remote Sensing Symposium. - Boston, MA, 7-11 July 2008. - Vol. 4. - P. IV-343 - IV - 346-343. ↑
- C2537.** Floricioiu D. Velocities of Major Outlet Glaciers of the Patagonia Icefield Observed by TerraSAR-X. / Floricioiu D., Eineder M., Rott H., Nagler T. // 2008. IGARSS 2008. IEEE International Geoscience and Remote Sensing Symposium. - Boston, MA, 7-11 July 2008. - Vol. 4. - P. IV-347 - IV - 350-347. ↑
- C2538.** Frison P.-L. Radar Polar Decomposition for Natural Surfaces Cartography. / Frison P.-L., Lardeux C., Souyris J.-C., Tison C., Stoll B., Rudant J.-P. // 2008. IGARSS 2008. IEEE International Geoscience and Remote Sensing Symposium. - Boston, MA, 7-11 July 2008. - Vol. 4. - P. IV-363 - IV - 366-363. ↑

- C2539.** Bin Zou. Moving Targets Detection and Analysis on Multi-Look Polarimetric SAR Images using PWF Method. / Bin Zou, Tao Wei, Lamei Zhang. // 2008. IGARSS 2008. IEEE International Geoscience and Remote Sensing Symposium. - Boston, MA, 7-11 July 2008. - Vol. 3. - P. III-1190 - III - 1193-1190. ↑
- C2540.** Li Lin-lin. Computation of Optimum Azimuth Sampling Time for Dual-Channel DPCA System based on Signal-to-Noise Ratio. / Li Lin-lin, Li Jing-wen. // 2008. IGARSS 2008. IEEE International Geoscience and Remote Sensing Symposium. - Boston, MA, 7-11 July 2008. - Vol. 3. - P. III-1186 - III - 1189-1186. ↑
- C2541.** Bing Sun. GMTI Performance Analysis for Circular Scanning SAR Equipped on Slow Platform. / Bing Sun, Yinqing Zhou, Jie Chen. // 2008. IGARSS 2008. IEEE International Geoscience and Remote Sensing Symposium. - Boston, MA, 7-11 July 2008. - Vol. 3. - P. III-1198 - III - 1200-1198. ↑
- C2542.** Guo Wei. A New Method of SAR Image Target Recognition based on AdaBoost Algorithm. / Guo Wei, Qi Qingwen, Jiang Lili, Zhang Ping. // 2008. IGARSS 2008. IEEE International Geoscience and Remote Sensing Symposium. - Boston, MA, 7-11 July 2008. - Vol. 3. - P. III-1194 - III - 1197-1194. ↑
- C2543.** D'Addio S. Rain Impact on Sensitivity of Ka-band Scan-on-Receive Synthetic Aperture Radars. / D'Addio S., Ludwig M. // 2008. IGARSS 2008. IEEE International Geoscience and Remote Sensing Symposium. - Boston, MA, 7-11 July 2008. - Vol. 3. - P. III-1174 - III - 1177-1174. ↑
- C2544.** Yonezawa C. Comparison of Atmospheric Phase Delay on ALOS PALSAR Interferogram and Cloud Distribution Pattern on Simultaneously Observed AVNIR-2 Images. / Yonezawa C., Yamanokuchi T., Tomiyama N., Oguro Y. // 2008. IGARSS 2008. IEEE International Geoscience and Remote Sensing Symposium. - Boston, MA, 7-11 July 2008. - Vol. 3. - P. III-1170 - III - 1173-1170. ↑
- C2545.** Yu Zuo. Doppler Parameter Estimation for Single-Channel SAR Moving Target based on a Novel Model in Complex Image Domain. / Yu Zuo, Jia Xu, Yingning Peng. // 2008. IGARSS 2008. IEEE International Geoscience and Remote Sensing Symposium. - Boston, MA, 7-11 July 2008. - Vol. 3. - P. III-1182 - III - 1185-1182. ↑
- C2546.** Budillon A. Moving Target Detection in along Track SAR Interferometry from In-Phase and Quadrature Components Data. / Budillon A., Pascasio V., Schirizzi G. // 2008. IGARSS 2008. IEEE International Geoscience and Remote Sensing Symposium. - Boston, MA, 7-11 July 2008. - Vol. 3. - P. III-1178 - III - 1181-1178. ↑
- C2547.** Makido Y. Revealing Intra-Urban Features using Optical and SAR Images. / Makido Y., Yamagata Y., Dhakal S. // 2008. IGARSS 2008. IEEE International Geoscience and Remote Sensing Symposium. - Boston, MA, 7-11 July 2008. - Vol. 3. - P. III-1220 - III - 1223-1220. ↑
- C2548.** Yanping Wang. Imaging Geometry Analysis of 3D SAR using Linear Array Antennas. / Yanping Wang, Bin Wang, Wen Hong, Lei Du, Yirong Wu. // 2008. IGARSS 2008. IEEE International Geoscience and Remote Sensing Symposium. - Boston, MA, 7-11 July 2008. - Vol. 3. - P. III-1216 - III - 1219-1216. ↑
- C2549.** Gernhardt S. Advanced Displacement Estimation for PSI using High Resolution SAR Data. / Gernhardt S., Hinz S. // 2008. IGARSS 2008. IEEE International Geoscience and Remote Sensing Symposium. - Boston, MA, 7-11 July 2008. - Vol. 3. - P. III-1276 - III - 1279-1276. ↑
- C2550.** Onana V.P. A Flood Hazard Risk Assessment Map in Growing Urban Areas by Integrating Remote Sensing and DEM Data. / Onana V.P., Rudant J.P., Trouve E., Mauris G., Laporte N.T., Walker W. // 2008. IGARSS 2008. IEEE International Geoscience and Remote Sensing Symposium. - Boston, MA, 7-11 July 2008. - Vol. 3. - P. III-1268 - III - 1271-1268. ↑
- C2551.** Xiaolan Qiu. Influence and Dependent Parameters of Terrain Undulation to Bistatic SAR Imaging. / Xiaolan Qiu, Donghui Hu, Chibiao Ding, Daojing Li. // 2008. IGARSS 2008. IEEE International Geoscience and Remote Sensing Symposium. - Boston, MA, 7-11 July 2008. - Vol. 3. - P. III-1205 - III - 1208-1205. ↑
- C2552.** Yang K.F. Compensation of the Range Variant Bistatic Deformation Term for LBF. / Yang K.F., He F., Liang D.N. // 2008. IGARSS 2008. IEEE International Geoscience and Remote Sensing Symposium. - Boston, MA, 7-11 July 2008. - Vol. 3. - P. III-1201 - III - 1204-1201. ↑
- C2553.** WeiXian Tan. 3-D Range Stacking Algorithm for Forward-Looking SAR 3-D Imaging. / WeiXian Tan, Wen Hong, YanPing Wang, YiRong Wu. // 2008. IGARSS 2008. IEEE International Geoscience and Remote Sensing Symposium. - Boston, MA, 7-11 July 2008. - Vol. 3. - P. III-1212 - III - 1215-1212. ↑

- C2554.** Lei Ling. Synchronization of Geo Spaceborne-Airborne Bistatic SAR. / Lei Ling, Zhou Yinqing, Li Jingwen, Sun Bing. // 2008. IGARSS 2008. IEEE International Geoscience and Remote Sensing Symposium. - Boston, MA, 7-11 July 2008. - Vol. 3. - P. III-1209 - III - 1211-1209. ↑
- C2555.** Jackson J.A. Estimation Performance for Canonical Shape Features. / Jackson J.A., Moses R.L. // 2008. IGARSS 2008. IEEE International Geoscience and Remote Sensing Symposium. - Boston, MA, 7-11 July 2008. - Vol. 3. - P. III-1111 - III - 1114-1111. ↑
- C2556.** Insanic E. Velocity Unfolding in Networked Radar System. / Insanic E., Siqueira P. // 2008. IGARSS 2008. IEEE International Geoscience and Remote Sensing Symposium. - Boston, MA, 7-11 July 2008. - Vol. 3. - P. III-1103 - III - 1106-1103. ↑
- C2557.** Insanic E. Use of Vector Velocity Estimate Accuracy for Improved Resource Allocation in a Network of Doppler Radars. / Insanic E., Siqueira P. // 2008. IGARSS 2008. IEEE International Geoscience and Remote Sensing Symposium. - Boston, MA, 7-11 July 2008. - Vol. 3. - P. III-1123 - III - 1126-1123. ↑
- C2558.** Monsivais-Huertero A. Sahelian-Grassland Parameter Estimation from Backscattered Radar Response. / Monsivais-Huertero A., Chenierie I., Sarabandi K. // 2008. IGARSS 2008. IEEE International Geoscience and Remote Sensing Symposium. - Boston, MA, 7-11 July 2008. - Vol. 3. - P. III-1119 - III - 1122-1119. ↑
- C2559.** Sato T. Detection of Anomalous Environmental Electromagnetic Wave by Statistical Property in Magnetic Field Azimuth. / Sato T., Takumi I., Hata M., Yasukawa H. // 2008. IGARSS 2008. IEEE International Geoscience and Remote Sensing Symposium. - Boston, MA, 7-11 July 2008. - Vol. 3. - P. III-1024 - III - 1027-1024. ↑
- C2560.** Burini A. Fusion of High Resolution Polarimetric SAR and Multi-Spectral Optical Data for Precision Viticulture. / Burini A., Schiavon G., Solimini D. // 2008. IGARSS 2008. IEEE International Geoscience and Remote Sensing Symposium. - Boston, MA, 7-11 July 2008. - Vol. 3. - P. III-1000 - III - 1003-1000. ↑
- C2561.** Rocadenbosch F. Comparison between the Kalman and the Non-Linear Least-Squares Estimators in Low Signal-to-Noise Ratio Lidar Inversion. / Rocadenbosch F., Sicard M., Comeron A., Reba M. // 2008. IGARSS 2008. IEEE International Geoscience and Remote Sensing Symposium. - Boston, MA, 7-11 July 2008. - Vol. 3. - P. III-1083 - III - 1086-1083. ↑
- C2562.** Chu P.C. Optimal Spectral Decomposition (OSD) for Remotely Sensed Ocean Data Assimilation. 2008. IGARSS 2008. IEEE International Geoscience and Remote Sensing Symposium. - Boston, MA, 7-11 July 2008. - Vol. 3. - P. III-1048 - III - 1051-1048. ↑
- C2563.** Guccione P. Motion Compensation Processing of Airborne SAR Data. / Guccione P., Cafforio C. // 2008. IGARSS 2008. IEEE International Geoscience and Remote Sensing Symposium. - Boston, MA, 7-11 July 2008. - Vol. 3. - P. III-1154 - III - 1157-1154. ↑
- C2564.** Sveinsson J.R. Combined Wavelet and Contourlet Denoising of SAR Images. / Sveinsson J.R., Benediktsson J.A. // 2008. IGARSS 2008. IEEE International Geoscience and Remote Sensing Symposium. - Boston, MA, 7-11 July 2008. - Vol. 3. - P. III-1150 - III - 1153-1150. ↑
- C2565.** Keming Chen. Unsupervised Change Detection in SAR Image using Graph Cuts. / Keming Chen, Chunlei Huo, Zhixin Zhou, Hanqing Lu. // 2008. IGARSS 2008. IEEE International Geoscience and Remote Sensing Symposium. - Boston, MA, 7-11 July 2008. - Vol. 3. - P. III-1162 - III - 1165-1162. ↑
- C2566.** Sveinsson J.R. Speckle Reduction of SAR Images in the Bandlet Domain. / Sveinsson J.R., Semar Z., Benediktsson J.A. // 2008. IGARSS 2008. IEEE International Geoscience and Remote Sensing Symposium. - Boston, MA, 7-11 July 2008. - Vol. 3. - P. III-1158 - III - 1161-1158. ↑
- C2567.** Bin Wang. Application of Spatial Spectrum Estimation Technique in Multibaseline SAR for Layover Solution. / Bin Wang, Yanping Wang, Wen Hong, Yirong Wu. // 2008. IGARSS 2008. IEEE International Geoscience and Remote Sensing Symposium. - Boston, MA, 7-11 July 2008. - Vol. 3. - P. III-1139 - III - 1142-1139. ↑
- C2568.** Benito E. Inversion of Backscatter Ionograms Optimization by using Simulated Annealing and Genetic Algorithms. / Benito E., Saillant S., Molinie J.P., Rannou V., Bourdillon A. // 2008. IGARSS 2008. IEEE International Geoscience and Remote Sensing Symposium. - Boston, MA, 7-11 July 2008. - Vol. 3. - P. III-1127

- III - 1130-1127. ↑

C2569. Feng Xu. Region Feature Extraction Based on Improved Regularization Method in SAR Image. / Feng Xu, Shirong Chen, Yida Fan, Chao Wang. // 2008. IGARSS 2008. IEEE International Geoscience and Remote Sensing Symposium. - Boston, MA, 7-11 July 2008. - Vol. 3. - P. III-1147 - III - 1149-1147. ↑

C2570. Di Martino G. The Effects of Finite Resolution on Radar Images of Fractal Profiles. / Di Martino G., Iodice A., Riccio D., Ruello G. // 2008. IGARSS 2008. IEEE International Geoscience and Remote Sensing Symposium. - Boston, MA, 7-11 July 2008. - Vol. 3. - P. III-1143 - III - 1146-1143. ↑

C2571. Jong-Sen Lee. Speckle Filtering of Dual-Polarization and Polarimetric SAR Data based on Improved Sigma Filter. / Jong-Sen Lee, Ainsworth T.L., Kun-Shan Chen. // 2008. IGARSS 2008. IEEE International Geoscience and Remote Sensing Symposium. - Boston, MA, 7-11 July 2008. - Vol. 4. - P. IV-21 - IV - 24-21. ↑

C2572. Liming Jiang. Monitoring Crustal Deformation along the Xianshuihe Fault in the Eastern Tibetan Margin Area with Envisat ScanSAR Interferometry. / Liming Jiang, Hui Lin, Qing Zhao, Fang Liu. // 2008. IGARSS 2008. IEEE International Geoscience and Remote Sensing Symposium. - Boston, MA, 7-11 July 2008. - Vol. 4. - P. IV-9 - IV - 12-9. ↑

C2573. Beaulieu J.-M. Classification of Polarimetric SAR Images using Radiometric and Texture Information. / Beaulieu J.-M., Touzi R. // 2008. IGARSS 2008. IEEE International Geoscience and Remote Sensing Symposium. - Boston, MA, 7-11 July 2008. - Vol. 4. - P. IV-29 - IV - 32-29. ↑

C2574. Farage G. Turbo Speckle Filtering applied to PolSAR Data. / Farage G., Foucher S., Lopez-Martinez C., Benie G.B. // 2008. IGARSS 2008. IEEE International Geoscience and Remote Sensing Symposium. - Boston, MA, 7-11 July 2008. - Vol. 4. - P. IV-25 - IV - 28-25. ↑

C2575. Rodriguez F.R. A Tool to Query and Visualize the Complete SRTM Data Set Indexed by the Q-tree in an Open GIS. / Rodriguez F.R., Pinero J.J.H., Garcia M.B. // 2008. IGARSS 2008. IEEE International Geoscience and Remote Sensing Symposium. - Boston, MA, 7-11 July 2008. - Vol. 3. - P. III-1410 - III - 1413-1410. ↑

C2576. Duk-jin Kim. Observation of Crude Oil Spill Off the West Coast of Korea using TerraSAR-X, ENVISAT ASAR and ALOS PALSAR. / Duk-jin Kim, Jinho Kang, Boyeol Yoon, Younsoo Kim, Yongseung Kim. // 2008. IGARSS 2008. IEEE International Geoscience and Remote Sensing Symposium. - Boston, MA, 7-11 July 2008. - Vol. 3. - P. III-1398 - III - 1401-1398. ↑

C2577. Teng Wang. Deformation Monitoring by Long Term D-InSAR Analysis in Three Gorges Area, China. / Teng Wang, Perissin D., Mingsheng Liao, Rocca F. // 2008. IGARSS 2008. IEEE International Geoscience and Remote Sensing Symposium. - Boston, MA, 7-11 July 2008. - Vol. 4. - P. IV-5 - IV - 8-5. ↑

C2578. Sharma N.C.P. Data Analysis System Design for Lidar Experimentation. / Sharma N.C.P., Parikh J.A. // 2008. IGARSS 2008. IEEE International Geoscience and Remote Sensing Symposium. - Boston, MA, 7-11 July 2008. - Vol. 3. - P. III-1418 - III - 1420-1418. ↑

C2579. Ferro-Famil L. Analysis of Natural Scenes using Polarimetric and Interferometric SAR Data Statistics in Particular Configurations. / Ferro-Famil L., Neumann M., Lopez-Martinez C. // 2008. IGARSS 2008. IEEE International Geoscience and Remote Sensing Symposium. - Boston, MA, 7-11 July 2008. - Vol. 4. - P. IV-33 - IV - 36-33. ↑

C2580. Plant W.J. Measuring and Modeling the NRCS of the Sea for Backscatter. / Plant W.J., Keller W.C., Hayes K., Chatham G. // 2008. IGARSS 2008. IEEE International Geoscience and Remote Sensing Symposium. - Boston, MA, 7-11 July 2008. - Vol. 4. - P. IV-65 - IV - 68-65. ↑

C2581. Tao Chu. The Impact of Surface Scattering on Ocean Atmospheric Boundary Layer (ABL) Wind Profile Estimates from an Airborne Doppler Radar. / Tao Chu, Frasier S.J., Fernandez D.E., Chang P.S., Carswell J.R. // 2008. IGARSS 2008. IEEE International Geoscience and Remote Sensing Symposium. - Boston, MA, 7-11 July 2008. - Vol. 4. - P. IV-61 - IV - 64-61. ↑

C2582. Gaetano R. Region-Based Classification of Multisensor Optical-SAR Images. / Gaetano R., Moser G., Poggi G., Scarpa G., Serpico S.B. // 2008. IGARSS 2008. IEEE International Geoscience and Remote Sensing Symposium. - Boston, MA, 7-11 July 2008. - Vol. 4. - P. IV-81 - IV - 84-81. ↑

- C2583.** Sedlacek S. Sediment Modeling based on Radar Observed Surface Hydrodynamics. / Sedlacek S., Ziemer F., Cysewski M. // 2008. IGARSS 2008. IEEE International Geoscience and Remote Sensing Symposium. - Boston, MA, 7-11 July 2008. - Vol. 4. - P. IV-69 - IV - 72-69. ↑
- C2584.** Guerra J.B. Evaluating the Potential of L Band PolSAR Data to Discriminate Deforestation Increment Areas in Amazon Rain Forest. / Guerra J.B., da Costa Freitas C., Mura J.C. // 2008. IGARSS 2008. IEEE International Geoscience and Remote Sensing Symposium. - Boston, MA, 7-11 July 2008. - Vol. 4. - P. IV-45 - IV - 48-45. ↑
- C2585.** Forster R.R. Alaskan Glaciology from Space. / Forster R.R., Michishita R., VanLooy J., Hall D.K. // 2008. IGARSS 2008. IEEE International Geoscience and Remote Sensing Symposium. - Boston, MA, 7-11 July 2008. - Vol. 4. - P. IV-37 - IV - 40-37. ↑
- C2586.** Alpers W. Investigation of Atmospheric Gravity Waves and Rotors in the Marine Boundary Layer using Spaceborne Synthetic Aperture Radar Images. 2008. IGARSS 2008. IEEE International Geoscience and Remote Sensing Symposium. - Boston, MA, 7-11 July 2008. - Vol. 4. - P. IV-57 - IV - 60-57. ↑
- C2587.** Ebuchi N. Subinertial Variations in the Soya Warm Current Revealed by HF Ocean Radars, Coastal Tide Gauges, and Bottom-Mounted ADCP. / Ebuchi N., Fukamachi Y., Ohshima K.I., Wakatsuchi M. // 2008. IGARSS 2008. IEEE International Geoscience and Remote Sensing Symposium. - Boston, MA, 7-11 July 2008. - Vol. 4. - P. IV-53 - IV - 56-53. ↑
- C2588.** Wei Tian. A System for Automatic Identification of Oil Spill in ENVISAT ASAR Images. / Wei Tian, Yun Shao, Shiang Wang. // 2008. IGARSS 2008. IEEE International Geoscience and Remote Sensing Symposium. - Boston, MA, 7-11 July 2008. - Vol. 3. - P. III-1394 - III - 1397-1394. ↑
- C2589.** Zhan H. Effectiveness of 2D FDTD Ground Penetrating Radar Modeling for Bridge Deck Deterioration Evaluated by 3D FDTD. / Zhan H., Belli K., Wadia-Fascetti S., Rappaport C. // 2008. IGARSS 2008. IEEE International Geoscience and Remote Sensing Symposium. - Boston, MA, 7-11 July 2008. - Vol. 3. - P. III-1330 - III - 1333-1330. ↑
- C2590.** Yun Shao. Oil spill monitoring using multi-temporal SAR and microwave scatterometer data. / Yun Shao, Wei Tian, Shiang Wang, Fengli Zhang. // 2008. IGARSS 2008. IEEE International Geoscience and Remote Sensing Symposium. - Boston, MA, 7-11 July 2008. - Vol. 3. - P. III-1378 - III - 1381-1378. ↑
- C2591.** Gambardella A. On the Mathematical Formulation of the SAR Oil-Spill Observation Problem. / Gambardella A., Giacinto G., Migliaccio M. // 2008. IGARSS 2008. IEEE International Geoscience and Remote Sensing Symposium. - Boston, MA, 7-11 July 2008. - Vol. 3. - P. III-1382 - III - 1385-1382. ↑
- C2592.** Daiyong Wei. Traffic Spatial Measures and Interpretation of Road Network Using Aerial Remotely Sensed Data. / Daiyong Wei, Guoqing Zhou. // 2008. IGARSS 2008. IEEE International Geoscience and Remote Sensing Symposium. - Boston, MA, 7-11 July 2008. - Vol. 3. - P. III-1319 - III - 1322-1319. ↑
- C2593.** Hong Zhang. Surface deformation retrieval of Yongcheng City(China) based on small baseline DInSAR technique. / Hong Zhang, Hong'an Wu, Chao Wang, Yixian Tang, Tao Wu. // 2008. IGARSS 2008. IEEE International Geoscience and Remote Sensing Symposium. - Boston, MA, 7-11 July 2008. - Vol. 3. - P. III-1316 - III - 1318-1316. ↑
- C2594.** Shafri H. Optimization of Ground Penetrating Radar (GPR) Mixture Model in Road Pavement Density Data Analysis. / Shafri H., Abdullah R.R., Roslee M., Muniandy R. // 2008. IGARSS 2008. IEEE International Geoscience and Remote Sensing Symposium. - Boston, MA, 7-11 July 2008. - Vol. 3. - P. III-1326 - III - 1329-1326. ↑
- C2595.** Morales D.I. Detection of Oil Slicks in SAR Images using Hierarchical MRF. / Morales D.I., Moctezuma M., Parmiggiani F. // 2008. IGARSS 2008. IEEE International Geoscience and Remote Sensing Symposium. - Boston, MA, 7-11 July 2008. - Vol. 3. - P. III-1390 - III - 1393-1390. ↑
- C2596.** Monaldo F.M. Retrieval of wind speed using an L-band synthetic aperture radar. / Monaldo F.M., Thompson D.R., Christiansen M.B. // 2007. IGARSS 2007. IEEE International Geoscience and Remote Sensing Symposium. - Barcelona, 23-28 July 2007. - P. 1338-1341. ↑
- C2597.** Hauser D. Probability density function of ocean surface slopes from radar observations. / Hauser D.,

Caudal G., Guimbard S., Mouche A. // 2007. IGARSS 2007. IEEE International Geoscience and Remote Sensing Symposium. - Barcelona, 23-28 July 2007. - P. 1346-1349. ↑

C2598. Malinovsky V.V. Identification of oil spills based on ratio of alternating polarization images from ENVISAT. / Malinovsky V.V., Sandven S., Mironov A.S., Korinenko A.E. // 2007. IGARSS 2007. IEEE International Geoscience and Remote Sensing Symposium. - Barcelona, 23-28 July 2007. - P. 1326-1329. ↑

C2599. Pelizzari S. Oil spill segmentation of SAR images via graph cuts. / Pelizzari S., Bioucas-Dias J. // 2007. IGARSS 2007. IEEE International Geoscience and Remote Sensing Symposium. - Barcelona, 23-28 July 2007. - P. 1318-1321. ↑

C2600. Migliaccio M. A physically consistent stochastic model to observe oil spills and strong scatterers on SLC SAR images. / Migliaccio M., Ferrara G., Gambardella A., Nunziata F., Sorrentino A. // 2007. IGARSS 2007. IEEE International Geoscience and Remote Sensing Symposium. - Barcelona, 23-28 July 2007. - P. 1322-1325. ↑

C2601. Cereoli L. The role of performance modelling in active phased array SAR. / Cereoli L., Torre A. // 2007. IGARSS 2007. IEEE International Geoscience and Remote Sensing Symposium. - Barcelona, 23-28 July 2007. - P. 1569-1572. ↑

C2602. Hallikainen M. Use of quikscat ku-band scatterometer data for retrieval of seasonal snow characteristics in Finland. / Hallikainen M., Sievinen P., Yuanzhi Zhang, Halme P. // 2007. IGARSS 2007. IEEE International Geoscience and Remote Sensing Symposium. - Barcelona, 23-28 July 2007. - P. 1228. ↑

C2603. Vachon P.W. Ship signatures in synthetic aperture radar imagery. / Vachon P.W., English R.A., Wolfe J. // 2007. IGARSS 2007. IEEE International Geoscience and Remote Sensing Symposium. - Barcelona, 23-28 July 2007. - P. 1393-1396. ↑

C2604. Zavorotny V.U. Comparison of geometric optics and diffraction effects in radar scattering from steep and breaking waves. / Zavorotny V.U., Voronovich A.G. // 2007. IGARSS 2007. IEEE International Geoscience and Remote Sensing Symposium. - Barcelona, 23-28 July 2007. - P. 1350-1353. ↑

C2605. Girard R. The RADARSAT constellation payload design. / Girard R., Plourde P., Seguin G. // 2007. IGARSS 2007. IEEE International Geoscience and Remote Sensing Symposium. - Barcelona, 23-28 July 2007. - P. 1387-1392. ↑

C2606. Cuozzo G. The role of spatial interactions for prediction of the spectral structure of the atmospheric phase screen. / Cuozzo G., di Bisceglie M., Fusco A. // 2007. IGARSS 2007. IEEE International Geoscience and Remote Sensing Symposium. - Barcelona, 23-28 July 2007. - P. 1287-1290. ↑

C2607. Plant W.J. X-band backscatter from the ocean at low-grazing angles. / Plant W.J., Keller W.C., Hayes K. // 2007. IGARSS 2007. IEEE International Geoscience and Remote Sensing Symposium. - Barcelona, 23-28 July 2007. - P. 1303-1306. ↑

C2608. Abhyankar A.A. Qualitative approaches to rapidly identify completely submerged rice due to tropical cyclone using satellite data. / Abhyankar A.A., Patwardhan A., Inamdar A. // 2007. IGARSS 2007. IEEE International Geoscience and Remote Sensing Symposium. - Barcelona, 23-28 July 2007. - P. 1283-1286. ↑

C2609. Carrao H. Retrieving land cover information from MERIS and MODIS Data: a comparative study for landscape characterization in Portugal. / Carrao H., Sarmento P., Araujo A., Caetano M. // 2007. IGARSS 2007. IEEE International Geoscience and Remote Sensing Symposium. - Barcelona, 23-28 July 2007. - P. 1271-1274. ↑

C2610. Karlsen S.R. Mapping and modelling the snowmelt and greening pattern in southern norway by combining microwave and optical remote sensing sensors. / Karlsen S.R., Malnes E., Haarpaintner J., Solberg R. // 2007. IGARSS 2007. IEEE International Geoscience and Remote Sensing Symposium. - Barcelona, 23-28 July 2007. - P. 1279-1282. ↑

C2611. Alpers W. Bora events over the adriatic sea and black sea studied by multi-sensor satellite imagery. / Alpers W., Ivanov A.Yu., Horstmann J. // 2007. IGARSS 2007. IEEE International Geoscience and Remote Sensing Symposium. - Barcelona, 23-28 July 2007. - P. 1307-1313. ↑

C2612. Hasager C.B. Satellite eye for the galathea 3 ship expedition: global tour 2006-2007. / Hasager C.B.,

Christiansen M.B., Sorensen P.B., Lichtenegger J., Pedersen L.T., Andersen O.B., Hoyer J.L., Jorgensen P.V., Hojerslev N.K., Nielsen R.M., Rasmussen M.S., Nyborg L. // 2007. IGARSS 2007. IEEE International Geoscience and Remote Sensing Symposium. - Barcelona, 23-28 July 2007. - P. 1232-1237. ↑

C2613. Yamanokuchi T. Combined use of InSAR and ICESat / GLAS data for high accuracy DEM generation on antarctica. / Yamanokuchi T., Doi K., Shibuya K. // 2007. IGARSS 2007. IEEE International Geoscience and Remote Sensing Symposium. - Barcelona, 23-28 July 2007. - P. 1229-1231. ↑

C2614. Karvonen J. Polarview@FIMR: WWW-based delivery of baltic sea ice products to end-users. / Karvonen J., Haapala J., Lehtiranta J., Seina A. // 2007. IGARSS 2007. IEEE International Geoscience and Remote Sensing Symposium. - Barcelona, 23-28 July 2007. - P. 1242-1245. ↑

C2615. Danisi A. SAR simulation of ocean scenes covered by oil slicks with arbitrary shapes. / Danisi A., Di Martino G., Iodice A., Riccio D., Ruello G., Tello M., Mallorqui J.J., Lopez-Martinez C. // 2007. IGARSS 2007. IEEE International Geoscience and Remote Sensing Symposium. - Barcelona, 23-28 July 2007. - P. 1314-1317. ↑

C2616. Waser L.T. Extraction of forest parameters in a mire biotope using high-resolution digital surface models and airborne imagery. / Waser L.T., Ginzler C., Kuechle M., Thee P., Baltsavias E., Eisenbeiss H. // 2007. IGARSS 2007. IEEE International Geoscience and Remote Sensing Symposium. - Barcelona, 23-28 July 2007. - P. 1265-1270. ↑

C2617. O'Neill P. ComRAD active / passive microwave measurement of tree canopies. / O'Neill P., Joseph A., Nelson R., Lang R., Kurum M., Cosh M., Jackson T., Spicknall M. // 2007. IGARSS 2007. IEEE International Geoscience and Remote Sensing Symposium. - Barcelona, 23-28 July 2007. - P. 1420-1423. ↑

C2618. Vecchia A.D. A statistical and theoretical study about radar sensitivity to crop growth from S to X band. / Vecchia A.D., Ferrazzoli P., Guerriero L., Strozzi T., Wegmuller U. // 2007. IGARSS 2007. IEEE International Geoscience and Remote Sensing Symposium. - Barcelona, 23-28 July 2007. - P. 1424-1427. ↑

C2619. Christoulas G. The use of ASAR data for class cover identification from small swatches. / Christoulas G., Anastassopoulos V., Petrou M. // 2007. IGARSS 2007. IEEE International Geoscience and Remote Sensing Symposium. - Barcelona, 23-28 July 2007. - P. 1513-1516. ↑

C2620. Niemann K.O. Integration of first and last return LiDAR with hyperspectral data to characterize forested environments. / Niemann K.O., Frazer G., Loos R., Visintini F., Stephen R. // 2007. IGARSS 2007. IEEE International Geoscience and Remote Sensing Symposium. - Barcelona, 23-28 July 2007. - P. 1537-1540. ↑

C2621. Pinheiro A. Evaluation of ASAR and optical data synergy for high resolution land cover mapping in portugal. / Pinheiro A., Carrao H., Caetano M. // 2007. IGARSS 2007. IEEE International Geoscience and Remote Sensing Symposium. - Barcelona, 23-28 July 2007. - P. 1517-1520. ↑

C2622. Peng Xu. Emissivities of rough surface over layered media in microwave remote sensing of snow. / Peng Xu, Leung Tsang, Li Li, Kun Shan Chen. // 2007. IGARSS 2007. IEEE International Geoscience and Remote Sensing Symposium. - Barcelona, 23-28 July 2007. - P. 1436-1439. ↑

C2623. Luzi G. Ground-based microwave interferometric measurements over a snow covered slope:an experimental data collection in Tyrol (Austria). / Luzi G., Pieraccini M., Noferini L., Mecatti D., Macaluso G., Atzeni C., Joerg P., Sailer R. // 2007. IGARSS 2007. IEEE International Geoscience and Remote Sensing Symposium. - Barcelona, 23-28 July 2007. - P. 1452-1455. ↑

C2624. Stankov B.B. Empirical SWE retrieval using airborne microwave and in situ snow measurements. / Stankov B.B., Cline D., Tedesco M. // 2007. IGARSS 2007. IEEE International Geoscience and Remote Sensing Symposium. - Barcelona, 23-28 July 2007. - P. 1444-1447. ↑

C2625. Piles M. Deconvolution algorithms in image reconstruction for aperture synthesis radiometers. / Piles M., Camps A., Vall-Ilossera M., Monerris A., Talone M., Perez J.L.A. // 2007. IGARSS 2007. IEEE International Geoscience and Remote Sensing Symposium. - Barcelona, 23-28 July 2007. - P. 1460-1463. ↑

C2626. Munoz-Mari J. Combination of one-class remote sensing image classifiers. / Munoz-Mari J., Camps-Valls G., Gomez-Chova L., Calpe-Maravilla J. // 2007. IGARSS 2007. IEEE International Geoscience and Remote Sensing Symposium. - Barcelona, 23-28 July 2007. - P. 1509-1512. ↑

- C2627.** Karasakal G. Speckle noise reduction in SAR imaging using lattice filters based subband decomposition. / Karasakal G., Erer I. // 2007. IGARSS 2007. IEEE International Geoscience and Remote Sensing Symposium. - Barcelona, 23-28 July 2007. - P. 1476-1480. ↑
- C2628.** Lenz R. Overview of the active TerraSAR-X calibrators and first results. / Lenz R., Wiesbeck W. // 2007. IGARSS 2007. IEEE International Geoscience and Remote Sensing Symposium. - Barcelona, 23-28 July 2007. - P. 1581-1584. ↑
- C2629.** Falzini S. COSMO-SkyMed active calibrator: A sophisticated tool for SAR image calibration. / Falzini S., Speziale V., De Viti E. // 2007. IGARSS 2007. IEEE International Geoscience and Remote Sensing Symposium. - Barcelona, 23-28 July 2007. - P. 1577-1580. ↑
- C2630.** Ferrer P.J. Transpolarizing surfaces for polarimetric SAR systems calibration. / Ferrer P.J., Lopez-Martinez C., Fabregas X., Gonzalez-Arbesu J.M., Romeu J., Aguasca A., Craeye C. // 2007. IGARSS 2007. IEEE International Geoscience and Remote Sensing Symposium. - Barcelona, 23-28 July 2007. - P. 1585-1588. ↑
- C2631.** Fukuchi H. New polarimetric calibration proposal and its evaluation using ALOS PALSAR calibration campaign measurements. / Fukuchi H., Furuya T., Noda H., Satake M. // 2007. IGARSS 2007. IEEE International Geoscience and Remote Sensing Symposium. - Barcelona, 23-28 July 2007. - P. 1593-1595. ↑
- C2632.** Eriksson L.E.B. ALOS PALSAR Calibration and Validation Results from Sweden. / Eriksson L.E.B., Sandberg G., Ulander L.M.H., Smith-Jonforsen G., Hallberg B., Folkesson K., Fransson J.E.S., Magnusson M., Olsson H., Gustavsson A., Flood B. // 2007. IGARSS 2007. IEEE International Geoscience and Remote Sensing Symposium. - Barcelona, 23-28 July 2007. - P. 1589-1592. ↑
- C2633.** McNairn H. The value of SAR Multi-polarization data in delivering annual crop inventories. / McNairn H., Champagne C., Jiali Shang. // 2007. IGARSS 2007. IEEE International Geoscience and Remote Sensing Symposium. - Barcelona, 23-28 July 2007. - P. 1397-1400. ↑
- C2634.** Jingsong Yang. Error analysis of Envisat ASAR level 2 algorithm based on simulation technique. / Jingsong Yang, He Wang, Weigen Huang, Qingmei Xiao. // 2007. IGARSS 2007. IEEE International Geoscience and Remote Sensing Symposium. - Barcelona, 23-28 July 2007. - P. 1409-1411. ↑
- C2635.** Bachmann C.M. Bathymetric retrieval from manifold coordinate representations of hyperspectral imagery. / Bachmann C.M., Ainsworth T.L. // 2007. IGARSS 2007. IEEE International Geoscience and Remote Sensing Symposium. - Barcelona, 23-28 July 2007. - P. 1548-1551. ↑
- C2636.** Caspar C. Generation of ENVISAT ASAR Mosaics accessible on-line. / Caspar C., Colin O., Laur H., Rosich Tell B., Tandurella G., Mathot E., Goncalves P., Brito F. // 2007. IGARSS 2007. IEEE International Geoscience and Remote Sensing Symposium. - Barcelona, 23-28 July 2007. - P. 1405-1408. ↑
- C2637.** Tell B.R. ASAR instrument performance and product quality evolution. / Tell B.R., Monti-Guarnieri A., Meadows P.J., D'Aria D., Tranfaglia M., Santuari M., Traver I.N. // 2007. IGARSS 2007. IEEE International Geoscience and Remote Sensing Symposium. - Barcelona, 23-28 July 2007. - P. 1401-1404. ↑
- C2638.** Yu Wang. A comparison of internal calibration schemes for spaceborne single-pass InSAR applications. / Yu Wang, Xing-dong Liang, Yi-rong Wu. // 2007. IGARSS 2007. IEEE International Geoscience and Remote Sensing Symposium. - Barcelona, 23-28 July 2007. - P. 1573-1576. ↑
- C2639.** Lawrence R. Differential absorption microwave radar measurements for remote sensing of atmospheric pressure. / Lawrence R., Fralick D., Harrah S., Bing Lin, Yongxiang Hu, Hunt P. // 2007. IGARSS 2007. IEEE International Geoscience and Remote Sensing Symposium. - Barcelona, 23-28 July 2007. - P. 1045-1048. ↑
- C2640.** Alados-Arboledas L. Detection of May 2006 Saharan dust outbreak over Granada, Spain, by combination of active and passive remote sensing. / Alados-Arboledas L., Guerrero-Rascado J.L., Lyamani H., Gil J.E., Cazorla A., Olmo F.J. // 2007. IGARSS 2007. IEEE International Geoscience and Remote Sensing Symposium. - Barcelona, 23-28 July 2007. - P. 1055-1058. ↑
- C2641.** Meta A. Sampling quantization analysis and results for FMCW SAR. / Meta A., Hoogeboom P., Ligthart L.P. // 2007. IGARSS 2007. IEEE International Geoscience and Remote Sensing Symposium. - Barcelona, 23-28 July 2007. - P. 1029-1032. ↑

- C2642.** Ehler I. Determine the location of a thermal front in the Iroise Sea by using HF radar data and tide model results. / Ehler I., Schlick T., Gurgel K.-W., Seille B. // 2007. IGARSS 2007. IEEE International Geoscience and Remote Sensing Symposium. - Barcelona, 23-28 July 2007. - P. 997-999. ↑
- C2643.** Demarty Y. Exact electromagnetic modeling of the scattering of realistic sea surfaces for HFSWR applications. / Demarty Y., Gobin V., Thirion L., Guinvarc'h R., Lesturgie M. // 2007. IGARSS 2007. IEEE International Geoscience and Remote Sensing Symposium. - Barcelona, 23-28 July 2007. - P. 1004-1007. ↑
- C2644.** Gherboudj I. Validation of a backscatter model of a river ice covers using Radarsat-1 images. / Gherboudj I., Bernier M., Leconte R. // 2007. IGARSS 2007. IEEE International Geoscience and Remote Sensing Symposium. - Barcelona, 23-28 July 2007. - P. 1087-1090. ↑
- C2645.** Ng A.H.-M. Application of persistent scatterer InSAR and GIS for urban subsidence monitoring. / Ng A.H.-M., Linlin Ge. // 2007. IGARSS 2007. IEEE International Geoscience and Remote Sensing Symposium. - Barcelona, 23-28 July 2007. - P. 1091-1094. ↑
- C2646.** Williams B.A. Hurricane wind field estimation from seawinds at ultra high resolution. / Williams B.A., Long D.G. // 2007. IGARSS 2007. IEEE International Geoscience and Remote Sensing Symposium. - Barcelona, 23-28 July 2007. - P. 1075-1078. ↑
- C2647.** Frontoso M.G. The vertical distribution of Saharan dust over the western and central Mediterranean through dust modelling and lidar observations. / Frontoso M.G., Sicard M., Comeron A., Perez C., Baldasano J.M. // 2007. IGARSS 2007. IEEE International Geoscience and Remote Sensing Symposium. - Barcelona, 23-28 July 2007. - P. 1059-1062. ↑
- C2648.** Vladutescu D.V. Examination of hygroscopic properties of aerosols using a combined multiwavelength elastic-Raman lidar. / Vladutescu D.V., Yonghua Wu, Gross B., Charles L., Moshary F., Ahmed S. // 2007. IGARSS 2007. IEEE International Geoscience and Remote Sensing Symposium. - Barcelona, 23-28 July 2007. - P. 1063-1066. ↑
- C2649.** Gambardella A. Wavelet polarimetric SAR signature analysis of sea oil spills and look-alike features. / Gambardella A., Migliaccio M., De Grandi G. // 2007. IGARSS 2007. IEEE International Geoscience and Remote Sensing Symposium. - Barcelona, 23-28 July 2007. - P. 983-986. ↑
- C2650.** Zhang Yafei. Distributed target detection in SAR images using improved chaos-based method. / Zhang Yafei, Zhu Minhui, Chong Jinsong. // 2007. IGARSS 2007. IEEE International Geoscience and Remote Sensing Symposium. - Barcelona, 23-28 July 2007. - P. 929-932. ↑
- C2651.** Jingsong Yang. Simulation of SAR image cross spectra from mixed ocean waves. / Jingsong Yang, He Wang, Qingmei Xiao, Weigen Huang. // 2007. IGARSS 2007. IEEE International Geoscience and Remote Sensing Symposium. - Barcelona, 23-28 July 2007. - P. 952-954. ↑
- C2652.** Bentz C.M. Automatic recognition of coastal and oceanic environmental events with orbital radars. / Bentz C.M., Politano A.T., Ebecken N.F.F. // 2007. IGARSS 2007. IEEE International Geoscience and Remote Sensing Symposium. - Barcelona, 23-28 July 2007. - P. 914-916. ↑
- C2653.** Reppucci A. Extreme wind conditions in tropical cyclones observed from synthetic aperture radar images. / Reppucci A., Lehner S., Schulz-Stellenfleth J., Breit H. // 2007. IGARSS 2007. IEEE International Geoscience and Remote Sensing Symposium. - Barcelona, 23-28 July 2007. - P. 894-897. ↑
- C2654.** Xiao-Ming Li. Measurement of extreme wave height by ERS-2 SAR and numerical wave model (WAM). / Xiao-Ming Li, Koenig T., Lehne S., Schulz-Stellenfleth J. // 2007. IGARSS 2007. IEEE International Geoscience and Remote Sensing Symposium. - Barcelona, 23-28 July 2007. - P. 905-908. ↑
- C2655.** Jian Sun. A case study on swell modulation caused by surface winds using spaceborne Synthetic Aperture Radar. / Jian Sun, Kawamura H. // 2007. IGARSS 2007. IEEE International Geoscience and Remote Sensing Symposium. - Barcelona, 23-28 July 2007. - P. 975-978. ↑
- C2656.** Kojima S. Wave measurements under the typhoon by 9.25MHz ocean radar. / Kojima S., Kashima M. // 2007. IGARSS 2007. IEEE International Geoscience and Remote Sensing Symposium. - Barcelona, 23-28 July 2007. - P. 979-982. ↑

- C2657.** Gauthier M.-F. Integrated satellite tracking of pollution: A new operational program. / Gauthier M.-F., Weir L., Ziqiang Ou, Arkett M., De Abreu R. // 2007. IGARSS 2007. IEEE International Geoscience and Remote Sensing Symposium. - Barcelona, 23-28 July 2007. - P. 967-970. ↑
- C2658.** Bertacca M. A FEXP model Short Range Dependence analysis for improving oil slicks and low-wind areas discrimination in sea SAR imagery. 2007. IGARSS 2007. IEEE International Geoscience and Remote Sensing Symposium. - Barcelona, 23-28 July 2007. - P. 959-962. ↑
- C2659.** Essen H. High resolution millimeterwave SAR for the remote sensing of wave patterns. / Essen H., Fuchs H.-H., Pagels A. // 2007. IGARSS 2007. IEEE International Geoscience and Remote Sensing Symposium. - Barcelona, 23-28 July 2007. - P. 963-966. ↑
- C2660.** Sauer S. Multibaseline POL-InSAR analysis of urban scenes for 3D modeling and physical feature retrieval at L-band. / Sauer S., Ferro-Famil L., Reigber A., Pottier E. // 2007. IGARSS 2007. IEEE International Geoscience and Remote Sensing Symposium. - Barcelona, 23-28 July 2007. - P. 1098-1101. ↑
- C2661.** Crosetto M. Uncertainty analysis in advanced differential interferometric SAR processing. / Crosetto M., Monserrat O., Agudo M., Crippa B., Rossi G. // 2007. IGARSS 2007. IEEE International Geoscience and Remote Sensing Symposium. - Barcelona, 23-28 July 2007. - P. 1171-1173. ↑
- C2662.** Rott H. Increased export of grounded ice after the collapse of northern Larsen ice shelf, Antarctic Peninsula, observed by Envisat ASAR. / Rott H., Rack W., Nagler T. // 2007. IGARSS 2007. IEEE International Geoscience and Remote Sensing Symposium. - Barcelona, 23-28 July 2007. - P. 1174-1176. ↑
- C2663.** Perissin D. ASAR parallel-track PS analysis in urban sites. / Perissin D., Prati C., Rocca F. // 2007. IGARSS 2007. IEEE International Geoscience and Remote Sensing Symposium. - Barcelona, 23-28 July 2007. - P. 1167-1170. ↑
- C2664.** Berardino P. Surface deformation analysis of the Campi Flegrei caldera, Italy, by exploiting the ENVISAT ASAR data with the SBAS-DInSAR technique. / Berardino P., Casu F., Fornaro G., Lanari R., Manunta M., Manzo M., Pepe A., Pepe S., Sansosti E., Serafino F., Solaro G., Tizzani P., Zeni G. // 2007. IGARSS 2007. IEEE International Geoscience and Remote Sensing Symposium. - Barcelona, 23-28 July 2007. - P. 1159-1162. ↑
- C2665.** Blanco-Sanchez P. Optimizing interferogram generation, pixel selection and data processing for high non-linear deformation monitoring with Orbital DInSAR. / Blanco-Sanchez P., Duque S., Mallorqui J.J., Monells D. // 2007. IGARSS 2007. IEEE International Geoscience and Remote Sensing Symposium. - Barcelona, 23-28 July 2007. - P. 1163-1166. ↑
- C2666.** Jinyang Du. A multi-scattering and multi-layer snow model and its validation. / Jinyang Du, Shi J., Tjuatja S., Chen K.S. // 2007. IGARSS 2007. IEEE International Geoscience and Remote Sensing Symposium. - Barcelona, 23-28 July 2007. - P. 1219-1222. ↑
- C2667.** Wiesmann A. Microwave remote sensing of alpine snow. / Wiesmann A., Strozzi T., Werner C., Wegmuller U., Santoro M. // 2007. IGARSS 2007. IEEE International Geoscience and Remote Sensing Symposium. - Barcelona, 23-28 July 2007. - P. 1223-1227. ↑
- C2668.** Yuen S. Airborne Ku-band radar remote sensing of terrestrial snow cover. / Yuen S., Cline D., Elder K. // 2007. IGARSS 2007. IEEE International Geoscience and Remote Sensing Symposium. - Barcelona, 23-28 July 2007. - P. 1211-1214. ↑
- C2669.** Rott H. CoRe-H2 O-A dual frequency SAR mission for hydrology and climate research. / Rott H., Pulliainen J., Cline D., Rebhan H., Nagler T., Yueh S. // 2007. IGARSS 2007. IEEE International Geoscience and Remote Sensing Symposium. - Barcelona, 23-28 July 2007. - P. 1204-1206. ↑
- C2670.** Morrison K. The SARALPS-2007 measurement campaign on Xand Ku-Band Backscatter of snow. / Morrison K., Rott H., Nagler T., Rebhan H., Wursteisen P. // 2007. IGARSS 2007. IEEE International Geoscience and Remote Sensing Symposium. - Barcelona, 23-28 July 2007. - P. 1207-1210. ↑
- C2671.** Haiyan Li. Ship detection with the fuzzy c-mean clustering algorithm using fully polarimetric SAR. / Haiyan Li, Yijun He, Hui Shen. // 2007. IGARSS 2007. IEEE International Geoscience and Remote Sensing Symposium. - Barcelona, 23-28 July 2007. - P. 1151-1154. ↑

- C2672.** Minnis P. Characterizing the radiation fields in the atmosphere using a cloud-aerosol-radiation product from integrated CERES, MODIS, CALIPSO and CloudSat data. / Minnis P., Wielicki B., Trepte C.A., Kato S., Sun-Mack S., Yan Chen, Gibson S., Stephens G. // 2007. IGARSS 2007. IEEE International Geoscience and Remote Sensing Symposium. - Barcelona, 23-28 July 2007. - P. 1122-1125. ↑
- C2673.** Praks J. X-band extinction in boreal forest: Estimation by using E-SAR POLInSAR and HUTSCAT. / Praks J., Hallikainen M., Kugler F., Papathanassiou K.P. // 2007. IGARSS 2007. IEEE International Geoscience and Remote Sensing Symposium. - Barcelona, 23-28 July 2007. - P. 1128-1131. ↑
- C2674.** Im E. Cloud Profiling Radar Performance Eastwood Im. / Im E., Tanelli S., Durden S.L., Kyung Pak. // 2007. IGARSS 2007. IEEE International Geoscience and Remote Sensing Symposium. - Barcelona, 23-28 July 2007. - P. 5061-5064. ↑
- C2675.** Jumani K. An investigation of PN sequences for multistatic SAR/InSAR applications. / Jumani K., Sarabandi K. // 2007. IGARSS 2007. IEEE International Geoscience and Remote Sensing Symposium. - Barcelona, 23-28 July 2007. - P. 1102-1105. ↑
- C2676.** Arnold-Bos A. Obtaining a ship's speed and direction from its Kelvin wake spectrum using stochastic matched filtering. / Arnold-Bos A., Martin A., Khenchaf A. // 2007. IGARSS 2007. IEEE International Geoscience and Remote Sensing Symposium. - Barcelona, 23-28 July 2007. - P. 1106-1109. ↑
- C2677.** Lopez-Sanchez J.M. Volume and double-bounce decorrelation effects in the OVoG model for Single-Tx PolInSAR. / Lopez-Sanchez J.M., Ballester-Berman J.D., Marquez-Moreno Y. // 2007. IGARSS 2007. IEEE International Geoscience and Remote Sensing Symposium. - Barcelona, 23-28 July 2007. - P. 1143-1146. ↑
- C2678.** Sharma J.J. Vertical profile reconstruction with Pol-InSAR data of a subpolar glacier. / Sharma J.J., Hajsek I., Papathanassiou K.P. // 2007. IGARSS 2007. IEEE International Geoscience and Remote Sensing Symposium. - Barcelona, 23-28 July 2007. - P. 1147-1150. ↑
- C2679.** Cantalloube H. POLINSAR for FOPEN using flashlight mode images along circular trajectories. / Cantalloube H., Colin E.K. // 2007. IGARSS 2007. IEEE International Geoscience and Remote Sensing Symposium. - Barcelona, 23-28 July 2007. - P. 1139-1142. ↑
- C2680.** Florian K. Potential of forest height estimation using X band by means of two different inversion scenarios. / Florian K., Kostas P., Irena H., Angelo C. // 2007. IGARSS 2007. IEEE International Geoscience and Remote Sensing Symposium. - Barcelona, 23-28 July 2007. - P. 1132-1135. ↑
- C2681.** Angelliaume S. Compact PolInSAR for vegetation characterisation. / Angelliaume S., Dubois-Fernandez P., Souyris J.-C. // 2007. IGARSS 2007. IEEE International Geoscience and Remote Sensing Symposium. - Barcelona, 23-28 July 2007. - P. 1136-1138. ↑
- C2682.** Satake M. Polarimetric Calibration Experiment of ALOS PALSAR with Polarization-Selective Dihedrals. / Satake M., Matsuoka T., Umehara T., Fukuchi H. // 2007. IGARSS 2007. IEEE International Geoscience and Remote Sensing Symposium. - Barcelona, 23-28 July 2007. - P. 1596-1598. ↑
- C2683.** Raney R.K. Comments on hybrid-polarity SAR architecture. 2007. IGARSS 2007. IEEE International Geoscience and Remote Sensing Symposium. - Barcelona, 23-28 July 2007. - P. 2229-2231. ↑
- C2684.** Jager M. Unsupervised classification of polarimetric SAR data using graph cut optimization. / Jager M., Reigber A., Hellwich O. // 2007. IGARSS 2007. IEEE International Geoscience and Remote Sensing Symposium. - Barcelona, 23-28 July 2007. - P. 2232-2235. ↑
- C2685.** Foucher S. Application of bootstrap techniques for the estimation of Target Decomposition parameters in RADAR polarimetry. / Foucher S., Farage G., Benie G.B. // 2007. IGARSS 2007. IEEE International Geoscience and Remote Sensing Symposium. - Barcelona, 23-28 July 2007. - P. 2224-2228. ↑
- C2686.** Torres F. MERIT Erasmus Mundus: an opportunity for international cooperation in Remote Sensing education in Europe. / Torres F., Wiesbeck W., Beccari C., Macq B. // 2007. IGARSS 2007. IEEE International Geoscience and Remote Sensing Symposium. - Barcelona, 23-28 July 2007. - P. 2209-2210. ↑
- C2687.** Spies T. Remote sensing information visualization using volume based objects in world wind. / Spies T., Moorhead R., Brill M. // 2007. IGARSS 2007. IEEE International Geoscience and Remote Sensing Symposium. - Barcelona, 23-28 July 2007. - P. 2211-2212. ↑

Symposium. - Barcelona, 23-28 July 2007. - P. 2213-2216. ↑

C2688. Aydin K. Dual-polarization and dual-frequency radar scattering from ice crystals. / Aydin K., Santiago E. // 2007. IGARSS 2007. IEEE International Geoscience and Remote Sensing Symposium. - Barcelona, 23-28 July 2007. - P. 2264. ↑

C2689. Eloranta E.W. Cloud particle size measurements in Arctic clouds using lidar and radar data. / Eloranta E.W., Uttal T., Shupe M. // 2007. IGARSS 2007. IEEE International Geoscience and Remote Sensing Symposium. - Barcelona, 23-28 July 2007. - P. 2265-2267. ↑

C2690. Loew A. Impact of surface heterogeneity on surface soil moisture retrievals from passive microwave data. 2007. IGARSS 2007. IEEE International Geoscience and Remote Sensing Symposium. - Barcelona, 23-28 July 2007. - P. 2252-2255. ↑

C2691. Mercier G. The use of multidimensional copulas to describe amplitude distribution of polarimetric SAR data. / Mercier G., Bouchemakh L., Smara Y. // 2007. IGARSS 2007. IEEE International Geoscience and Remote Sensing Symposium. - Barcelona, 23-28 July 2007. - P. 2236-2239. ↑

C2692. Ersahin K. Segmentation of polarimetric SAR data using contour information via spectral graph partitioning. / Ersahin K., Cumming I.G., Ward R.K. // 2007. IGARSS 2007. IEEE International Geoscience and Remote Sensing Symposium. - Barcelona, 23-28 July 2007. - P. 2240-2243. ↑

C2693. Lewis C. Multi-waveform radar for ice sheet measurements and classroom demonstration. / Lewis C., Owen H., Abi D., Hecker J., Sulzen J. // 2007. IGARSS 2007. IEEE International Geoscience and Remote Sensing Symposium. - Barcelona, 23-28 July 2007. - P. 2202-2205. ↑

C2694. Ossowska A. Influence of mechanical antenna distortions on the performance of the HRWS SAR system. / Ossowska A., Jung Hyo Kim, Wiesbeck W. // 2007. IGARSS 2007. IEEE International Geoscience and Remote Sensing Symposium. - Barcelona, 23-28 July 2007. - P. 2152-2155. ↑

C2695. Nico G. Performance analysis of bistatic SAR configurations. / Nico G., Tesauro M. // 2007. IGARSS 2007. IEEE International Geoscience and Remote Sensing Symposium. - Barcelona, 23-28 July 2007. - P. 2156-2159. ↑

C2696. Cantalloube H.M.J. Elevation-dependent motion compensation for frequency-domain bistatic SAR image synthesis. / Cantalloube H.M.J., Krieger G. // 2007. IGARSS 2007. IEEE International Geoscience and Remote Sensing Symposium. - Barcelona, 23-28 July 2007. - P. 2148-2151. ↑

C2697. Shi jun. Translational variant bistatic SAR signal space-time feature and processing method. / Shi jun, Zhang Xiaoling, Yang Jianyu. // 2007. IGARSS 2007. IEEE International Geoscience and Remote Sensing Symposium. - Barcelona, 23-28 July 2007. - P. 2140-2143. ↑

C2698. Walterscheid I. Performance analysis of a hybrid bistatic SAR system operating in the double sliding spotlight mode. / Walterscheid I., Espeter T., Ender J.H.G. // 2007. IGARSS 2007. IEEE International Geoscience and Remote Sensing Symposium. - Barcelona, 23-28 July 2007. - P. 2144-2147. ↑

C2699. Ito Y. Development of web-based SAR processor for education. / Ito Y., Teramoto Y., Abe K. // 2007. IGARSS 2007. IEEE International Geoscience and Remote Sensing Symposium. - Barcelona, 23-28 July 2007. - P. 2185-2187. ↑

C2700. Marques P. A low cost testbed for synthetic aperture techniques. / Marques P., Dias I., Fernandes E. // 2007. IGARSS 2007. IEEE International Geoscience and Remote Sensing Symposium. - Barcelona, 23-28 July 2007. - P. 2195-2198. ↑

C2701. Gimmetstad G.G. Lidar education at Georgia Tech. / Gimmetstad G.G., West L.L. // 2007. IGARSS 2007. IEEE International Geoscience and Remote Sensing Symposium. - Barcelona, 23-28 July 2007. - P. 2174-2176. ↑

C2702. Espeter T. Synchronization techniques for the bistatic spaceborne/airborne SAR experiment with TerraSAR-X and PAMIR. / Espeter T., Walterscheid I., Klare J., Ender J.H.G. // 2007. IGARSS 2007. IEEE International Geoscience and Remote Sensing Symposium. - Barcelona, 23-28 July 2007. - P. 2160-2163. ↑

- C2703.** Huang Yulin. Vehicleborne bistatic synthetic aperture radar imaging. / Huang Yulin, Yang Jianyu, Xian Li, Yang Haiguang, Tian Zhong. // 2007. IGARSS 2007. IEEE International Geoscience and Remote Sensing Symposium. - Barcelona, 23-28 July 2007. - P. 2164-2166. ↑
- C2704.** Montopoli M. Processing disdrometer raindrop spectra time series from various climatological regions using estimation and autoregressive methods. / Montopoli M., Vulpiani G., Anagnostou M.N., Anagnostou E.N., Marzano F.S. // 2007. IGARSS 2007. IEEE International Geoscience and Remote Sensing Symposium. - Barcelona, 23-28 July 2007. - P. 2268-2271. ↑
- C2705.** Villard L. Bistatic border effects modelling in forest scattering. / Villard L., Borderies P., Dubois-Fernandez P., Nouvel J.-F. // 2007. IGARSS 2007. IEEE International Geoscience and Remote Sensing Symposium. - Barcelona, 23-28 July 2007. - P. 2354-2357. ↑
- C2706.** Alberga V. Comparison of similarity measures of multi-sensor images for change detection applications. / Alberga V., Idrissa M., Lacroix V., Inglada J. // 2007. IGARSS 2007. IEEE International Geoscience and Remote Sensing Symposium. - Barcelona, 23-28 July 2007. - P. 2358-2361. ↑
- C2707.** Fransson J.E.S. Mapping of wind-thrown forests using VHF/UHF SAR images. / Fransson J.E.S., Magnusson M., Folkesson K., Hallberg B., Sandberg G., Smith-Jonforsen G., Gustavsson A., Ulander L.M.H. // 2007. IGARSS 2007. IEEE International Geoscience and Remote Sensing Symposium. - Barcelona, 23-28 July 2007. - P. 2350-2353. ↑
- C2708.** dos Santos J.R. Analysis of airborne SAR data (L-band) for discrimination land use/land cover types in the Brazilian Amazon region. / dos Santos J.R., Goncalves F.G., Dutra L.V., Mura J.C., Paradella W.R. // 2007. IGARSS 2007. IEEE International Geoscience and Remote Sensing Symposium. - Barcelona, 23-28 July 2007. - P. 2342-2345. ↑
- C2709.** Viergever K.M. backscatter and interferometry for estimating above- ground biomass in tropical savanna woodland. / Viergever K.M., Woodhouse I.H., Stuart N. // 2007. IGARSS 2007. IEEE International Geoscience and Remote Sensing Symposium. - Barcelona, 23-28 July 2007. - P. 2346-2349. ↑
- C2710.** Mercier G. Conditional copula for change detection on heterogeneous SAR data. / Mercier G., Moser G., Serpico S. // 2007. IGARSS 2007. IEEE International Geoscience and Remote Sensing Symposium. - Barcelona, 23-28 July 2007. - P. 2394-2397. ↑
- C2711.** Bosch-Lluis X. Calibration and performance analysis of the PAU- RAD instrument. / Bosch-Lluis X., Camps A., Marchan-Hernandez J.F., Ramos-Perez I., Rodriguez-Alvarez N., Banque X., Guerrero M.A. // 2007. IGARSS 2007. IEEE International Geoscience and Remote Sensing Symposium. - Barcelona, 23-28 July 2007. - P. 2419-2422. ↑
- C2712.** Molinier M. Detecting changes in polarimetric SAR data with content-based image retrieval. / Molinier M., Laaksonen J., Rauste Y., Hame T. // 2007. IGARSS 2007. IEEE International Geoscience and Remote Sensing Symposium. - Barcelona, 23-28 July 2007. - P. 2390-2393. ↑
- C2713.** Andreoli R. Large scale change detection techniques dedicated to flood monitoring using ENVISAT wide swath mode data. / Andreoli R., Yesou H. // 2007. IGARSS 2007. IEEE International Geoscience and Remote Sensing Symposium. - Barcelona, 23-28 July 2007. - P. 2382-2385. ↑
- C2714.** Molinier M. Comparison and evaluation of polarimetric change detection techniques in aerial SAR data. / Molinier M., Rauste Y. // 2007. IGARSS 2007. IEEE International Geoscience and Remote Sensing Symposium. - Barcelona, 23-28 July 2007. - P. 2386-2389. ↑
- C2715.** Riihela A. Estimation of the bidirectional reflectance distribution function of subarctic boreal forest using C-band SAR. / Riihela A., Manninen T. // 2007. IGARSS 2007. IEEE International Geoscience and Remote Sensing Symposium. - Barcelona, 23-28 July 2007. - P. 2334-2337. ↑
- C2716.** Marotti L. Analysis of the temporal behavior of coherent scatterers (CSs) in ALOS PalsAR data. / Marotti L., Zandona-Schneider R., Papathanassiou K.P. // 2007. IGARSS 2007. IEEE International Geoscience and Remote Sensing Symposium. - Barcelona, 23-28 July 2007. - P. 2473-2476. ↑
- C2717.** Singhroy V. InSAR monitoring of landslides on permafrost terrain in Canada. / Singhroy V., Couture R., Alasset P.-J., Poncos V. // 2007. IGARSS 2007. IEEE International Geoscience and Remote Sensing Symposium. - Barcelona, 23-28 July 2007. - P. 2473-2476. ↑

Symposium. - Barcelona, 23-28 July 2007. - P. 2451-2454. ↑

C2718. Angiuli E. Inversion algorithms comparison using L-band simulated polarimetric interferometric data for forest parameters estimation. / Angiuli E., Del Frate F., Vecchia A.D., Lavallo M., Solimini D., Licciardi G. // 2007. IGARSS 2007. IEEE International Geoscience and Remote Sensing Symposium. - Barcelona, 23-28 July 2007. - P. 2477-2480. ↑

C2719. Ince T. Preliminary quantitative analysis of S-band FNCW radar data from atmospheric observation. 2007. IGARSS 2007. IEEE International Geoscience and Remote Sensing Symposium. - Barcelona, 23-28 July 2007. - P. 2280-2283. ↑

C2720. Waser L.T. Modeling fractional shrub/tree cover and multi-temporal changes in mire ecosystems using high-resolution digital surface models and CIR aerial images. / Waser L.T., Ginzler C., Kuechler M., Baltsavias E., Eisenbeiss H. // 2007. IGARSS 2007. IEEE International Geoscience and Remote Sensing Symposium. - Barcelona, 23-28 July 2007. - P. 2288-2293. ↑

C2721. Watanabe M. Forest monitoring with JERS-1/SAR and ALOS/PALSAR. / Watanabe M., Shimada M., Ouchi K., Haipeng Wang, Matsuoka M., Sato M. // 2007. IGARSS 2007. IEEE International Geoscience and Remote Sensing Symposium. - Barcelona, 23-28 July 2007. - P. 2326-2329. ↑

C2722. Fransson J.E.S. Detection of forest changes using ALOS PALSAR satellite images. / Fransson J.E.S., Magnusson M., Olsson H., Eriksson L.E.B., Sandberg G., Smith-Jonforsen G., Ulander L.M.H. // 2007. IGARSS 2007. IEEE International Geoscience and Remote Sensing Symposium. - Barcelona, 23-28 July 2007. - P. 2330-2333. ↑

C2723. Garestier F. Vegetation modelling for height inversion using InSAR/Pol-InSAR data. / Garestier F., Thuy Le Toan. // 2007. IGARSS 2007. IEEE International Geoscience and Remote Sensing Symposium. - Barcelona, 23-28 July 2007. - P. 2322-2325. ↑

C2724. Anderson L.O. Spatial patterns of the canopy stress during 2005 drought in Amazonia. / Anderson L.O., Malhi Y., Aragao L.E.O., Saatchi S. // 2007. IGARSS 2007. IEEE International Geoscience and Remote Sensing Symposium. - Barcelona, 23-28 July 2007. - P. 2294-2297. ↑

C2725. Ranson K.J. Using MODIS and GLAS data to develop timber volume estimates in central Siberia. / Ranson K.J., Nelson R., Kimes D., Guoqing Sun, Kharuk V., Montesano P. // 2007. IGARSS 2007. IEEE International Geoscience and Remote Sensing Symposium. - Barcelona, 23-28 July 2007. - P. 2306-2309. ↑

C2726. Arakelyan A.K. Ku-band, polarimetric, combined, short pulse scatterometer-radiometer system for stationary fixed platform, vessel and airborne applications. / Arakelyan A.K., Arakelyan A.A., Darbinyan S.A., Grigoryan M.L., Hakobyan I.K., Hambaryan A.K., Karyan V.V., Manukyan M.R., Hovhannisyan G.G., Poghosyan N.G., Clifford S.F. // 2007. IGARSS 2007. IEEE International Geoscience and Remote Sensing Symposium. - Barcelona, 23-28 July 2007. - P. 1832-1834. ↑

C2727. Dongryeol Ryu. Two-dimensional synthetic aperture radiometry over land surface during soil moisture experiment in 2003 (SMEX03). / Dongryeol Ryu, Jackson T.J., Bindlish R., Le Vine D.M., Haken M. // 2007. IGARSS 2007. IEEE International Geoscience and Remote Sensing Symposium. - Barcelona, 23-28 July 2007. - P. 1842-1845. ↑

C2728. Edwards M.A. Assessing pine barrens soil moisture regimes using Synthetic Aperture Radar (SAR) techniques. / Edwards M.A., Winslow M. // 2007. IGARSS 2007. IEEE International Geoscience and Remote Sensing Symposium. - Barcelona, 23-28 July 2007. - P. 1828-1831. ↑

C2729. Contreras R.F. Return from insects in the clear-air convective boundary layer. / Contreras R.F., Frasier S.J. // 2007. IGARSS 2007. IEEE International Geoscience and Remote Sensing Symposium. - Barcelona, 23-28 July 2007. - P. 1677-1679. ↑

C2730. Guerrero-Rascado J.L. Atmospheric vertical profiles obtained by Lidar over Évora during CAPEX project. / Guerrero-Rascado J.L., Lyamani H., Alados-Arboledas L., Silva A.M., Wagner F., Pereira S. // 2007. IGARSS 2007. IEEE International Geoscience and Remote Sensing Symposium. - Barcelona, 23-28 July 2007. - P. 1709-1712. ↑

C2731. Romero R. Usage of multitemporal filtering of SAR images for change detection. / Romero R., Marcos

J.S., Carrasco D., Moreno V., Valero J.L., Lafitte M. // 2007. IGARSS 2007. IEEE International Geoscience and Remote Sensing Symposium. - Barcelona, 23-28 July 2007. - P. 1955-1958. ↑

C2732. Junghum Yu. Accuracy comparison of Differential Interferometric Synthetic Aperture Radar using LiDAR Digital Elevation Model. / Junghum Yu, Linlin Ge, Sungheuk Jung, Lee Jeakee. // 2007. IGARSS 2007. IEEE International Geoscience and Remote Sensing Symposium. - Barcelona, 23-28 July 2007. - P. 1970-1973. ↑

C2733. Tzeng Y.C. Change detections from sar images for damage estimation based on a spatial chaotic model. / Tzeng Y.C., Chiu S.H., Chen D., Chen K.S. // 2007. IGARSS 2007. IEEE International Geoscience and Remote Sensing Symposium. - Barcelona, 23-28 July 2007. - P. 1926-1930. ↑

C2734. Ruijing Sun. A method to retrieve soil moisture using ERS Scatterometer data. / Ruijing Sun, Jiancheng Shi, Lingmei Jiang. // 2007. IGARSS 2007. IEEE International Geoscience and Remote Sensing Symposium. - Barcelona, 23-28 July 2007. - P. 1857-1860. ↑

C2735. Perez-Gutierrez C. Modeling of soil roughness using terrestrial laser scanner for soil moisture retrieval. / Perez-Gutierrez C., Martinez-Fernandez J., Sanchez N., Alvarez-Mozos J. // 2007. IGARSS 2007. IEEE International Geoscience and Remote Sensing Symposium. - Barcelona, 23-28 July 2007. - P. 1877-1880. ↑

C2736. Tatarov B. Stratospheric ozone layer observations over tsukuba, Japan by NIES ozone DIAL. / Tatarov B., Chan Bong Park, Nakane H., Sugimoto N., Matsui I., Sasano Y. // 2007. IGARSS 2007. IEEE International Geoscience and Remote Sensing Symposium. - Barcelona, 23-28 July 2007. - P. 1673-1676. ↑

C2737. Croci R. SHARAD design and operation. / Croci R., Fois F., Calabrese D., Zampolini E.M., Seu R., Picardi G., Flamini E. // 2007. IGARSS 2007. IEEE International Geoscience and Remote Sensing Symposium. - Barcelona, 23-28 July 2007. - P. 1611-1615. ↑

C2738. Iwashita A. Study of ground surface displacement estimation using ALOS/PALSAR D-InSAR interferometry. / Iwashita A., Kudo M., Baba H., Morohoshi T., Hara M., Yu-Feng Lin, Wen-Qing Jiang. // 2007. IGARSS 2007. IEEE International Geoscience and Remote Sensing Symposium. - Barcelona, 23-28 July 2007. - P. 1616-1617. ↑

C2739. da Silva Narvaes I. Evaluation of the interaction between SAR L-band signal and structural parameters of forest cover. / da Silva Narvaes I., de Queiroz da Silva A., dos Santos J.R. // 2007. IGARSS 2007. IEEE International Geoscience and Remote Sensing Symposium. - Barcelona, 23-28 July 2007. - P. 1607-1610. ↑

C2740. Jung C.H. Parameter based SAR simulator for image quality evaluation. / Jung C.H., Choi M.S., Kwag Y.K. // 2007. IGARSS 2007. IEEE International Geoscience and Remote Sensing Symposium. - Barcelona, 23-28 July 2007. - P. 1599-1602. ↑

C2741. Xi Chen. Robust forest height extraction using polarimetric SAR interferometry. / Xi Chen, Chao Wang, Hong Zhang. // 2007. IGARSS 2007. IEEE International Geoscience and Remote Sensing Symposium. - Barcelona, 23-28 July 2007. - P. 1603-1606. ↑

C2742. Vicente A.M.P. Classification of satellite images applied to geological mapping (Douro Region-Northeastern Portugal). / Vicente A.M.P., Rabaca T., Pereira A.J.S. // 2007. IGARSS 2007. IEEE International Geoscience and Remote Sensing Symposium. - Barcelona, 23-28 July 2007. - P. 1661-1664. ↑

C2743. Lopes F.C.C. Recognizing salt-structures on the basis of geophysical and remote sensing data: the case of monte real salt-structure (onshore west-central portugal). / Lopes F.C.C., Pereira A.S.C., Vicente A.M.P. // 2007. IGARSS 2007. IEEE International Geoscience and Remote Sensing Symposium. - Barcelona, 23-28 July 2007. - P. 1665-1668. ↑

C2744. Pereira A.J.S. Structural lineaments in a volcanic island evaluated through remote sensing techniques The case of Santiago Island (Cape Verde). / Pereira A.J.S., Victoria S., Vicente A.M.P., Neves L.J.P. // 2007. IGARSS 2007. IEEE International Geoscience and Remote Sensing Symposium. - Barcelona, 23-28 July 2007. - P. 1632-1635. ↑

C2745. Rauste Y. Ortho-rectification and terrain correction of polarimetric SAR data applied in the ALOS/Palsar context. / Rauste Y., Lonnqvist A., Molinier M., Henry J.-B., Hame T. // 2007. IGARSS 2007. IEEE International Geoscience and Remote Sensing Symposium. - Barcelona, 23-28 July 2007. - P. 1618-1621. ↑

- C2746.** Wobbe F. Uplift rates from river profiles: methodology and case study, Oriente, Cuba. / Wobbe F., Stanek K., Gloaguen R. // 2007. IGARSS 2007. IEEE International Geoscience and Remote Sensing Symposium. - Barcelona, 23-28 July 2007. - P. 1629-1631. ↑
- C2747.** Takaku J. High resolution DSM generation from ALOS PRISM. / Takaku J., Futamura N., Iijima T., Tadono T., Shimada M. // 2007. IGARSS 2007. IEEE International Geoscience and Remote Sensing Symposium. - Barcelona, 23-28 July 2007. - P. 1974-1977. ↑
- C2748.** Qiang Chen. Evaluation of accuracy in PS-based radar interferometry with simulated data. / Qiang Chen, Xiaoli Ding, Guoxiang Liu, Yongshu Li. // 2007. IGARSS 2007. IEEE International Geoscience and Remote Sensing Symposium. - Barcelona, 23-28 July 2007. - P. 2110-2113. ↑
- C2749.** Fornaro G. Deformation monitoring over a large area via the ESD technique with data takes on adjacent tracks. / Fornaro G., Serafino F., Pauciuolo A. // 2007. IGARSS 2007. IEEE International Geoscience and Remote Sensing Symposium. - Barcelona, 23-28 July 2007. - P. 2114-2117. ↑
- C2750.** Poncos V. Point target interferometry for natural and artificial scatterers. / Poncos V., Mei S., Singhroy V. // 2007. IGARSS 2007. IEEE International Geoscience and Remote Sensing Symposium. - Barcelona, 23-28 July 2007. - P. 2106-2109. ↑
- C2751.** Prats P. Glacier displacement field estimation using airborne SAR interferometry. / Prats P., Andres C., Scheiber R., Reigber A., Camara de Macedo K.A., Fischer J. // 2007. IGARSS 2007. IEEE International Geoscience and Remote Sensing Symposium. - Barcelona, 23-28 July 2007. - P. 2098-2101. ↑
- C2752.** van Leijen F.J. Persistent scatterer density improvement using adaptive deformation models. / van Leijen F.J., Hanssen R.F. // 2007. IGARSS 2007. IEEE International Geoscience and Remote Sensing Symposium. - Barcelona, 23-28 July 2007. - P. 2102-2105. ↑
- C2753.** Duque S. A bistatic SAR interferometric simulator for fixed receiver configurations. / Duque S., Lopez-Dekker P., Mallorqui J.J., Martinez C.L. // 2007. IGARSS 2007. IEEE International Geoscience and Remote Sensing Symposium. - Barcelona, 23-28 July 2007. - P. 2130-2133. ↑
- C2754.** Fois F. Comparison between MARSIS & SHARAD results. / Fois F., Mecozzi R., Iorio M., Calabrese D., Bombaci O., Catallo C., Croce A., Croci R., Guelfi M., Zampolini E., Ravasi D., Molteni M., Ruggeri P., Ranieri A., Ottavianelli M., Flamini E., Picardi G., Seu R., Biccari D., Orosei R., Cartacci M., Cicchetti A., Masdea A., Giacomoni E., Cutigni M., Provenziani M., Fuga O., Alberti G., Mattei S., Papa C., Marras P., Tattarletti B., Vicari D., Bonaventura F., Paterno T., Di Placido A., Morlupi A. // 2007. IGARSS 2007. IEEE International Geoscience and Remote Sensing Symposium. - Barcelona, 23-28 July 2007. - P. 2134-2139. ↑
- C2755.** Ortiz A.M. Second-order motion compensation in bistatic airborne SAR based on a geometrical approach. / Ortiz A.M., Loffeld O., Nies H., Knedlik S. // 2007. IGARSS 2007. IEEE International Geoscience and Remote Sensing Symposium. - Barcelona, 23-28 July 2007. - P. 2126-2129. ↑
- C2756.** Xilong Sun. Research on differential interferometry for spaceborne bistatic SAR. / Xilong Sun, Anxi Yu, Zhen Dong, Diannong Liang. // 2007. IGARSS 2007. IEEE International Geoscience and Remote Sensing Symposium. - Barcelona, 23-28 July 2007. - P. 2118-2121. ↑
- C2757.** Deguchi T. Monitoring of mining induced land subsidence using L- and C-band SAR interferometry. / Deguchi T., Kato M., Akcin H., Kutoglu H.S. // 2007. IGARSS 2007. IEEE International Geoscience and Remote Sensing Symposium. - Barcelona, 23-28 July 2007. - P. 2122-2125. ↑
- C2758.** Damoah-Afari P. Six years of land subsidence in shanghai revealed by JERS-1 SAR data. / Damoah-Afari P., Xiao-li Ding, Zhiwei Li, Zhong Lu, Omura M. // 2007. IGARSS 2007. IEEE International Geoscience and Remote Sensing Symposium. - Barcelona, 23-28 July 2007. - P. 2093-2097. ↑
- C2759.** Fulong Chen. SAR images classification using case-based reasoning method. / Fulong Chen, Chao Wang, Hong Zhang, Bo Zhang, Fan Wu. // 2007. IGARSS 2007. IEEE International Geoscience and Remote Sensing Symposium. - Barcelona, 23-28 July 2007. - P. 2048-2051. ↑
- C2760.** Pop G. Combining modern techniques for urban 3D modelling. / Pop G., Bucksch A. // 2007. IGARSS 2007. IEEE International Geoscience and Remote Sensing Symposium. - Barcelona, 23-28 July 2007. - P. 2067-2070. ↑

- C2761.** Bolton J. Application of random set-based clustering to landmine detection with hyperspectral imagery. / Bolton J., Gader P. // 2007. IGARSS 2007. IEEE International Geoscience and Remote Sensing Symposium. - Barcelona, 23-28 July 2007. - P. 2022-2025. ↑
- C2762.** Almeida-Filho R. The mega capture of the negro river, central amazonia, brazil: a novel feature revealed by SRTM data. / Almeida-Filho R., Miranda F.P., Beisl C.H. // 2007. IGARSS 2007. IEEE International Geoscience and Remote Sensing Symposium. - Barcelona, 23-28 July 2007. - P. 1978-1981. ↑
- C2763.** Pacifici F. Urban land cover classification: potential of high and very-high resolution SAR imagery. / Pacifici F., Del Frate F., Solimini D., Burini A. // 2007. IGARSS 2007. IEEE International Geoscience and Remote Sensing Symposium. - Barcelona, 23-28 July 2007. - P. 1982-1985. ↑
- C2764.** Qiming Zeng. Correction of tropospheric water vapour effect on ASAR interferogram using synchronous MERIS data. / Qiming Zeng, Ying Li, Xiaofan Li. // 2007. IGARSS 2007. IEEE International Geoscience and Remote Sensing Symposium. - Barcelona, 23-28 July 2007. - P. 2086-2089. ↑
- C2765.** Hsing-Chung Chang. Radar interferometry for 3-D mining deformation monitoring. / Hsing-Chung Chang, Linlin Ge, Hua Wang, Rizos C., Milne T. // 2007. IGARSS 2007. IEEE International Geoscience and Remote Sensing Symposium. - Barcelona, 23-28 July 2007. - P. 2090-2092. ↑
- C2766.** Gernhardt S. A stability analysis of the lambda estimator for solving the ambiguity problem in persistent scatterer interferometry. / Gernhardt S., Meyer F., Bamler R., Adam N. // 2007. IGARSS 2007. IEEE International Geoscience and Remote Sensing Symposium. - Barcelona, 23-28 July 2007. - P. 2082-2085. ↑
- C2767.** Sirui Tian. A wavelet based targets detection method for high resolution airborne SAR data. / Sirui Tian, Chao Wang, Hong Zhang, Bo Zhang, Fan Wu. // 2007. IGARSS 2007. IEEE International Geoscience and Remote Sensing Symposium. - Barcelona, 23-28 July 2007. - P. 2071-2073. ↑
- C2768.** Zhang Shiyu. Urban subsidence observed by InSAR in Tianjin Region. / Zhang Shiyu, Li Tao, Liu Jingnan, Xia Ye, Jiang Yanxiang, Lu Xu. // 2007. IGARSS 2007. IEEE International Geoscience and Remote Sensing Symposium. - Barcelona, 23-28 July 2007. - P. 2078-2081. ↑
- C2769.** Parmiggiani F. Surface signature of ocean convection in the greenland sea as detected by SAR and enhanced by statistical pattern analysis. / Parmiggiani F., Morales D., Moctezuma M. // 2007. IGARSS 2007. IEEE International Geoscience and Remote Sensing Symposium. - Barcelona, 23-28 July 2007. - P. 879-881. ↑
- C2770.** Liu Hui. A simple implementation of multi-baseline INSAR. / Liu Hui, Zhou Yinqing, Xu Huaping, Li Chunsheng. // 2007. APSAR 2007. 1st Asian and Pacific Conference on Synthetic Aperture Radar. - Huangshan, 5-9 Nov. 2007. - P. 747-750. ↑
- C2771.** Hongjun Cai. Parameter inversion models based on PolInSAR images. / Hongjun Cai, Bin Zou, Maoliu Lin. // 2007. APSAR 2007. 1st Asian and Pacific Conference on Synthetic Aperture Radar. - Huangshan, 5-9 Nov. 2007. - P. 751-754. ↑
- C2772.** Jinshan Ding. Modified phase history model for high resolution spaceborne bistatic SAR. / Jinshan Ding, Mengdao Xing, Zheng Bao. // 2007. APSAR 2007. 1st Asian and Pacific Conference on Synthetic Aperture Radar. - Huangshan, 5-9 Nov. 2007. - P. 646-649. ↑
- C2773.** Dong Yin. Multi-scale feature analysis method for bridge recognition in SAR images. / Dong Yin, Yuqing Miao, Guiqin Li, Bin Cheng. // 2007. APSAR 2007. 1st Asian and Pacific Conference on Synthetic Aperture Radar. - Huangshan, 5-9 Nov. 2007. - P. 517-520. ↑
- C2774.** Zhang Lei. The propagation of orbital errors in the 3-Pass DInSAR processing. / Zhang Lei, Wu Jicang, Ding Xiaoli, Xiao Feng. // 2007. APSAR 2007. 1st Asian and Pacific Conference on Synthetic Aperture Radar. - Huangshan, 5-9 Nov. 2007. - P. 550-554. ↑
- C2775.** Trivero P. High resolution COSMO-SkyMed SAR images for oil spills automatic detection. / Trivero P., Biamino W., Nirchio F. // 2007. IGARSS 2007. IEEE International Geoscience and Remote Sensing Symposium. - Barcelona, 23-28 July 2007. - P. 2-5. ↑
- C2776.** Boni G. High resolution COSMO/SkyMed SAR data analysis for civil protection from flooding events. / Boni G., Castelli F., Ferraris L., Pierdicca N., Serpico S., Siccardi F. // 2007. IGARSS 2007. IEEE International

Geoscience and Remote Sensing Symposium. - Barcelona, 23-28 July 2007. - P. 6-9. ↑

C2777. Wang Kai-bin. Radar image segmentation using active contour. / Wang Kai-bin, Yu Bian-zhang, Xi Wei. // 2007. APSAR 2007. 1st Asian and Pacific Conference on Synthetic Aperture Radar. - Huangshan, 5-9 Nov. 2007. - P. 806-810. ↑

C2778. Huibin Peng. An improved model of HF-SAR for estimating surface current velocity. / Huibin Peng, Wenhui Xue, Sanwen Zhu, Guishui Yu. // 2007. APSAR 2007. 1st Asian and Pacific Conference on Synthetic Aperture Radar. - Huangshan, 5-9 Nov. 2007. - P. 760-765. ↑

C2779. Li Fei. Internal wave parameters retrieval from SAR image: based on EMD filter and parameterized buoyancy frequency. / Li Fei, Chong Jongsong, Ouyang Yue. // 2007. APSAR 2007. 1st Asian and Pacific Conference on Synthetic Aperture Radar. - Huangshan, 5-9 Nov. 2007. - P. 766-769. ↑

C2780. Feng Wanpeng. Uncertainty of the 2003 BAM Mw =6.4 earthquake fault model inverted from ENVISAT SAR interferometric data. 2007. APSAR 2007. 1st Asian and Pacific Conference on Synthetic Aperture Radar. - Huangshan, 5-9 Nov. 2007. - P. 462-464. ↑

C2781. Lu Wang. Semiautomatic registration between ground-level panoramas and an orthorectified aerial image for building modeling. / Lu Wang, Suyu You, Neumann U. // 2007. ICCV 2007. IEEE 11th International Conference on Computer Vision. - Rio de Janeiro, 14-21 Oct. 2007. - P. 1-8. ↑

C2782. Li Dao-jing. Airborne MMW cross-track InSAR System Analysis. / Li Dao-jing, Qiao Ming, Yin Jian-feng, Zhu Jin-biao, Xi Ying. // 2007. APSAR 2007. 1st Asian and Pacific Conference on Synthetic Aperture Radar. - Huangshan, 5-9 Nov. 2007. - P. 32-36. ↑

C2783. Ting Liu. Change detection methodology based on region classification fusion. / Ting Liu, Gigli G., Lampropoulos G.A. // 2007 10th International Conference on Information Fusion. - Quebec, Que., 9-12 July 2007. - P. 1-7. ↑

C2784. Gonzalez J.H. Development of TanDEM-X DEM calibration concept. / Gonzalez J.H., Bachmann M., Fiedler H., Huber S., Krieger G., Wessel B., Zink M. // 2007. European Microwave Conference. - Munich, 9-12 Oct. 2007. - P. 1743-1746. ↑

C2785. Xiao-lei Wei. Multi-band SAR Images Fusion Using the EM Algorithm in Contourlet Domain. / Xiao-lei Wei, Yong-an Zheng, Zhan-zhong Cui, Quan-li Wang. // 2007. FSKD 2007. Fourth International Conference on Fuzzy Systems and Knowledge Discovery. - Haikou, 24-27 Aug. 2007. - Vol. 1. - P. 502-506. ↑

C2786. Li Maokuan. Pixel level image fusion based on ICA and wavelet transform. / Li Maokuan, Guan Jian. // 2007. APSAR 2007. 1st Asian and Pacific Conference on Synthetic Aperture Radar. - Huangshan, 5-9 Nov. 2007. - P. 229-231. ↑

C2787. Sun Junping. The fusion arithmetic of multi-resolution remote sense image based on a modified fast independent component analysis. / Sun Junping, Liu Yang. // 2007. APSAR 2007. 1st Asian and Pacific Conference on Synthetic Aperture Radar. - Huangshan, 5-9 Nov. 2007. - P. 342-346. ↑

C2788. Xinzhen Zhang. Data fusion of multiple polarimetric SAR images based on combined curvelet and wavelet transform. / Xinzhen Zhang, Peikang Huang, Ping Zhou. // 2007. APSAR 2007. 1st Asian and Pacific Conference on Synthetic Aperture Radar. - Huangshan, 5-9 Nov. 2007. - P. 225-228. ↑

C2789. Wen-Qin Wang. Near-space SAR: A revolutionary microwave remote sensing mission. / Wen-Qin Wang, Jingye Cai, Qicong Peng. // 2007. APSAR 2007. 1st Asian and Pacific Conference on Synthetic Aperture Radar. - Huangshan, 5-9 Nov. 2007. - P. 127-131. ↑

C2790. Yin Qiang. A validation method for bare soil surface parameters inverted by Oh empirical model using integral equation method. / Yin Qiang, Cao Fang, Hong Wen. // 2007. APSAR 2007. 1st Asian and Pacific Conference on Synthetic Aperture Radar. - Huangshan, 5-9 Nov. 2007. - P. 211-214. ↑

C2791. Berardino P. The SBAS-DInSAR technique as a tool for the observation of active volcanic areas: Results and future perspectives. / Berardino P., Casu F., Fornaro G., Lanari R., Manunta M., Manzo M., Pepe A., Pepe S., Sansosti E., Serafino F., Solaro G., Tizzani P., Zeni G. // 2007. IGARSS 2007. IEEE International Geoscience and Remote Sensing Symposium. - Barcelona, 23-28 July 2007. - P. 10-13. ↑

- C2792.** Fois F. Performance results of the SHARAD instrument. / Fois F., Croci R., Seu R., Picardi G., Flamini E. // 2007. IGARSS 2007. IEEE International Geoscience and Remote Sensing Symposium. - Barcelona, 23-28 July 2007. - P. 119-124. ↑
- C2793.** Nashashibi A.Y. Bistatic SAR imaging: A novel approach using a stationary receiver. / Nashashibi A.Y., Ulaby F.T. // 2007. IGARSS 2007. IEEE International Geoscience and Remote Sensing Symposium. - Barcelona, 23-28 July 2007. - P. 125-128. ↑
- C2794.** Weiss M. Position and orientation estimation of two airborne platforms towards each other. / Weiss M., Marino G. // 2007. IGARSS 2007. IEEE International Geoscience and Remote Sensing Symposium. - Barcelona, 23-28 July 2007. - P. 115-118. ↑
- C2795.** Lopez-Dekker P. Bistatic SAR interferometry using ENVISAT and a ground based receiver: Experimental results. / Lopez-Dekker P., Merlano J.C., Duque S., Sanz-Marcos J., Aguasca A., Mallorqui J.J. // 2007. IGARSS 2007. IEEE International Geoscience and Remote Sensing Symposium. - Barcelona, 23-28 July 2007. - P. 107-110. ↑
- C2796.** Jung-Hyo Kim. Experimental investigation of Digital Beamforming SAR Performance using a ground-based demonstrator. / Jung-Hyo Kim, Ossowska A., Wiesbeck W. // 2007. IGARSS 2007. IEEE International Geoscience and Remote Sensing Symposium. - Barcelona, 23-28 July 2007. - P. 111-114. ↑
- C2797.** Cantalloube H.M.J. Merging of the stereogrammetry and interferometry techniques as relative bandwidth grows. Illustration with VHF Carabas SAR images. / Cantalloube H.M.J., Colin-Koeniguer E., Frolind P.O., Ulander L.M.H. // 2007. IGARSS 2007. IEEE International Geoscience and Remote Sensing Symposium. - Barcelona, 23-28 July 2007. - P. 141-143. ↑
- C2798.** Walterscheid I. Evaluation of the Bistatic Range migration processor. / Walterscheid I., Brenner A.R., Ender J.H.G., Loffeld O. // 2007. IGARSS 2007. IEEE International Geoscience and Remote Sensing Symposium. - Barcelona, 23-28 July 2007. - P. 144-147. ↑
- C2799.** D'Aria D. Delay/Doppler altimeter data processing. / D'Aria D., Guccione P., Rosich B., Cullen R. // 2007. IGARSS 2007. IEEE International Geoscience and Remote Sensing Symposium. - Barcelona, 23-28 July 2007. - P. 137-140. ↑
- C2800.** Santoro M. Improvement of interferometric SAR coherence estimates by slope-adaptive range common-band filtering. / Santoro M., Werner C., Wegmuller U., Cartus O. // 2007. IGARSS 2007. IEEE International Geoscience and Remote Sensing Symposium. - Barcelona, 23-28 July 2007. - P. 129-132. ↑
- C2801.** Martorella M. Polarimetric phase gradient autofocus. / Martorella M., Preiss M., Haywood B., Bates B. // 2007. IGARSS 2007. IEEE International Geoscience and Remote Sensing Symposium. - Barcelona, 23-28 July 2007. - P. 133-136. ↑
- C2802.** Ender J.H.G. Space-based moving target positioning using radar with a switched aperture antenna. / Ender J.H.G., Gierull C.H., Cerutti-Maori D. // 2007. IGARSS 2007. IEEE International Geoscience and Remote Sensing Symposium. - Barcelona, 23-28 July 2007. - P. 101-106. ↑
- C2803.** Kovalenko V. Polarimetric feature fusion in GPR for landmine detection. / Kovalenko V., Yarovoy A., Ligthart L.P. // 2007. IGARSS 2007. IEEE International Geoscience and Remote Sensing Symposium. - Barcelona, 23-28 July 2007. - P. 30-33. ↑
- C2804.** Galletti M. Concept design of a near-space radar for tsunami detection. / Galletti M., Krieger G., Borner T., Marquart N., Schultz-Stellenfleth J. // 2007. IGARSS 2007. IEEE International Geoscience and Remote Sensing Symposium. - Barcelona, 23-28 July 2007. - P. 34-37. ↑
- C2805.** Mazhar R. Use of an application-specific dictionary for matching pursuits discrimination of landmines and clutter. / Mazhar R., Wilson J.N., Gader P.D. // 2007. IGARSS 2007. IEEE International Geoscience and Remote Sensing Symposium. - Barcelona, 23-28 July 2007. - P. 26-29. ↑
- C2806.** Milisavljevic N. Possibilistic multi-sensor fusion for humanitarian demining. / Milisavljevic N., Bloch I. // 2007. IGARSS 2007. IEEE International Geoscience and Remote Sensing Symposium. - Barcelona, 23-28 July 2007. - P. 14-17. ↑

- C2807.** Sato M. Hand held dual sensor ALIS and its evaluation test in Cambodia. / Sato M., Takahashi K., Fujiwara J. // 2007. IGARSS 2007. IEEE International Geoscience and Remote Sensing Symposium. - Barcelona, 23-28 July 2007. - P. 18-21. ↑
- C2808.** Pietra G.D. Feasibility of spaceborne bistatic radar missions for land applications. / Pietra G.D., Capobianco F., Falzini S., Pierdicca N., De Titta L. // 2007. IGARSS 2007. IEEE International Geoscience and Remote Sensing Symposium. - Barcelona, 23-28 July 2007. - P. 93-96. ↑
- C2809.** Lopez-Dekker P. Phase and temporal synchronization in bistatic SAR systems using sources of opportunity. / Lopez-Dekker P., Mallorqui J.J., Serra-Morales P., Sanz-Marcos J. // 2007. IGARSS 2007. IEEE International Geoscience and Remote Sensing Symposium. - Barcelona, 23-28 July 2007. - P. 97-100. ↑
- C2810.** Wenjian Ni. Improvement of 3D radar backscatter model by matrix-doubling methods. / Wenjian Ni, Zhifeng Guo, Guoqing Sun, Fang Wang. // 2007. IGARSS 2007. IEEE International Geoscience and Remote Sensing Symposium. - Barcelona, 23-28 July 2007. - P. 85-88. ↑
- C2811.** Weissman D.E. Measurements of the effect of rain-induced sea surface roughness on the satellite scatterometer radar cross section. / Weissman D.E., Bourassa M.A. // 2007. IGARSS 2007. IEEE International Geoscience and Remote Sensing Symposium. - Barcelona, 23-28 July 2007. - P. 46-49. ↑
- C2812.** Brogioni M. Bistatic scattering from bare soils: Sensitivity to soil moisture and surface roughness. / Brogioni M., Macelloni G., Paloscia S., Pampaloni P., Pettinato S., Ticconi F. // 2007. IGARSS 2007. IEEE International Geoscience and Remote Sensing Symposium. - Barcelona, 23-28 July 2007. - P. 77-80. ↑
- C2813.** Kidder C.C. Design Considerations For An Atmospheric Imaging Radar. / Kidder C.C., Yeary M.B., Palmer R.D. // 2007 IEEE Region 5 Technical Conference. - Fayetteville, AR, 20-22 April 2007. - P. 97-101. ↑
- C2814.** Edwards W.C. Laser Technology Development at NASA Langley Research Center for Space based Applications. 2007. LEOS 2007. The 20th Annual Meeting of the IEEE Lasers and Electro-Optics Society. - Lake Buena Vista, FL, 21-25 Oct. 2007. - P. 384. ↑
- C2815.** Christophe E. Robust Road Extraction for High Resolution Satellite Images. / Christophe E., Inglada J. // 2007. ICIP 2007. IEEE International Conference on Image Processing. - San Antonio, TX, Sept. 16 2007-Oct. 19 2007. - Vol. 5. - P. V-437 - V - 440-437. ↑
- C2816.** Konjovic Z. Land Use Management Based on GPS Technology, and Satellite and Ground Remote Sensing Technologies. / Konjovic Z., Petrovacki D., Govedarica M. // 2007. TELSIKS 2007. 8th International Conference on Telecommunications in Modern Satellite, Cable and Broadcasting Services. - Serbia, 26-28 Sept. 2007. - P. 369-384. ↑
- C2817.** Imaizumi S. Collusion Attack-Resilient Hierarchical Encryption of JPEG 2000 Codestreams with Scalable Access Control. / Imaizumi S., Fujiyoshi M., Abe Y., Kiya H. // 2007. ICIP 2007. IEEE International Conference on Image Processing. - San Antonio, TX, Sept. 16 2007-Oct. 19 2007. - Vol. 2. - P. II-137 - II - 140-137. ↑
- C2818.** Shkvarko Y.V. Unification of Descriptive Experiment Design and Worst-Case Performance Optimization-Adapted Regularization Paradigms for High-Resolution Reconstruction of Radar Imagery. 2007. ICEAA 2007. International Conference on Electromagnetics in Advanced Applications. - Torino, 17-21 Sept. 2007. - P. 340-343. ↑
- C2819.** Norgard J. Distributed/Embedded Sub-Surface Sensors for Imaging Buried Objects with Reduced Mutual Coupling and Suppressed Electromagnetic Emissions. / Norgard J., Wicks M., Drozd A. // 2007. ICEAA 2007. International Conference on Electromagnetics in Advanced Applications. - Torino, 17-21 Sept. 2007. - P. 427-430. ↑
- C2820.** Somekawa T. Simultaneous Three-wavelength Depolarization Lidar Using a Coherent White Light Continuum. / Somekawa T., Yamanaka C., Fujita M., Galvez M.C.D. // 2007 and the International Quantum Electronics Conference. CLEOE-IQEC 2007. European Conference on Lasers and Electro-Optics. - Munich, 17-22 June 2007. - P. 1-2. ↑
- C2821.** Lisinetskii V.A. Efficient high-energy Raman laser for troposphere ozone lidar. / Lisinetskii V.A., Shpak P.V., Grabtchikov A.S., Orlovich V.A. // 2007 and the International Quantum Electronics Conference. CLEOE-

IQEC 2007. European Conference on Lasers and Electro-Optics. - Munich, 17-22 June 2007. - P. 1. ↑

C2822. Cassel-Engquist M. Remote Gas Detection in Solid Scattering Media using Differential Absorption Lidar. / Cassel-Engquist M., Gronlund R., Andersson M., Persson L., Svanberg S. // 2007 and the International Quantum Electronics Conference. CLEOE-IQEC 2007. European Conference on Lasers and Electro-Optics. - Munich, 17-22 June 2007. - P. 1. ↑

C2823. Gonzalez L. Improving oil slick detection by SAR imagery using ancillary data. / Gonzalez L., Palenzuela J.M.T. // 2007. ISIE 2007. IEEE International Symposium on Industrial Electronics. - Vigo, 4-7 June 2007. - P. 1657-1662. ↑

C2824. Yuan Guo. Genetic Algorithm and Region Growing Based Road Detection in SAR Images. / Yuan Guo, Zhengyao Bai, Yue Li, Yang Liu. // 2007. ICNC 2007. Third International Conference on Natural Computation. - Haikou, 24-27 Aug. 2007. - Vol. 4. - P. 330-334. ↑

C2825. Ling Kuang. The Influence of Random motion Errors on Bistatic SAR Resolution. / Ling Kuang, Qun Wan, Wan-lin Yang. // 2007. ICCAS 2007. International Conference on Communications, Circuits and Systems. - Kokura, 11-13 July 2007. - P. 863-866. ↑

C2826. Khoor S. Heart Rate Analysis and Telemedicine: New concepts & Maths. / Khoor S., Kecskes I., Kovacs I., Verner D., Remete A., Jankovich P., Bartus R., Stanko N., Schramm N., Domijan M., Domijan E. // 2007. SISY 2007. 5th International Symposium on Intelligent Systems and Informatics. - Subotica, 24-25 Aug. 2007. - P. 39-43. ↑

C2827. Krieger G. Multidimensional waveform encoding for spaceborne synthetic aperture radar systems. / Krieger G., Gebert N., Moreira A. // 2007. International Waveform Diversity and Design Conference. - Pisa, 4-8 June 2007. - P. 282-286. ↑

C2828. Xujing Guo. Speckle Reduction for Remote Sensing Images Based on Nonsubsampled Contourlet. / Xujing Guo, Zulin Wang. // 2007. WiCom 2007. International Conference on Wireless Communications, Networking and Mobile Computing. - Shanghai, 21-25 Sept. 2007. - P. 2927-2930. ↑

C2829. Guerrero L.G. Simulation Study of the SAR Imaging with the Virtual Remote Sensing Laboratory. / Guerrero L.G., Gutierrez J., Jalisco C. // 2007. CERMA 2007 Electronics, Robotics and Automotive Mechanics Conference. - Morelos, 25-28 Sept. 2007. - P. 563-567. ↑

C2830. Pustovoytenko V.V. Remote Probing of Sea Waters. Stages and Development; (to the 30-years Anniversary of Native Satellite Oceanology). / Pustovoytenko V.V., Teryokhin Yu.V., Korotayev G.K., Tsimbal V.N., Yefimov V.B., Kurekin A.S., Dranovsky V.I., Kavelin S.S., Saltykov Yu.D., Yermolov P.P. // 2007. CriMiCo 2007. 17th International Crimean Conference Microwave & Telecommunication Technology. - Crimea, 10-14 Sept. 2007. - P. 15-25. ↑

C2831. Qingguo Zhou. Test bed for Remote Environmental Monitoring in Northwestern China. / Qingguo Zhou, Guanghui Cheng, Tzu-Han Kao, Wenzhong Wu, Lian Li. // 2007. ICPCA 2007. 2nd International Conference on Pervasive Computing and Applications. - Birmingham, 26-27 July 2007. - P. 705-708. ↑

C2832. Zhou Peng. Geometry and System Aspects of Spaceborne/Airborne Hybrid Bistatic SAR. / Zhou Peng, Pi Yiming. // 2007. ICCAS 2007. International Conference on Communications, Circuits and Systems. - Kokura, 11-13 July 2007. - P. 867-871. ↑

C2833. Massagram W. Feasibility of Heart Rate Variability Measurement from Quadrature Doppler Radar Using Arctangent Demodulation with DC Offset Compensation. / Massagram W., Hafner N.M., Byung-Kwan Park, Lubecke V.M., Host-Madsen A., Boric-Lubecke O. // 2007. EMBS 2007. 29th Annual International Conference of the IEEE Engineering in Medicine and Biology Society. - Lyon, 22-26 Aug. 2007. - P. 1643-1646. ↑

C2834. Yamaguchi Y. Development of an imaging lidar for aerosol monitoring using a wide field-of-view, high-resolution telescope. / Yamaguchi Y., Kouga I., Shinomiya K., Takeuchi N., Kuze H., Sasaki M., Asaka Y., Ogawa S. // 2007. CLEO/Pacific Rim 2007. Conference on Lasers and Electro-Optics-Pacific Rim. - Seoul, 26-31 Aug. 2007. - P. 1-2. ↑

C2835. Brooker G. Millimetre wave radar visualisation in mines. / Brooker G., Widzyk-Capehart E., Scheduling S., Hennessy R., Lobsey C. // 2007. EuRAD 2007. European Radar Conference. - Munich, 10-12 Oct. 2007. - P. 1. ↑

417-420. ↑

C2836. Khraisat Y.S.H. Joint influence of rain rate and turbulence on radar signal spectrum width. / Khraisat Y.S.H., Yanovsky F.J. // 2007. EuRAD 2007. European Radar Conference. - Munich, 10-12 Oct. 2007. - P. 429-432. ↑

C2837. Pitertsev A.A. Polarimetric approach to detection of probable aircraft icing zones. icing detection algorithms. / Pitertsev A.A., Yanovsky F.J. // 2007. EuRAD 2007. European Radar Conference. - Munich, 10-12 Oct. 2007. - P. 271-274. ↑

C2838. Lievers C.M. Digital beamforming and multidimensional waveform encoding for spaceborne radar remote sensing. / Lievers C.M., van Rossum W.L., Maas A.P.M., Huizing A.G. // 2007. EuRAD 2007. European Radar Conference. - Munich, 10-12 Oct. 2007. - P. 43-46. ↑

C2839. Pinel N. Spectrum of rough sea surfaces covered in oil: consequences on the radar cross section. / Pinel N., Bourlier C., Dechamps N. // 2007. EuRAD 2007. European Radar Conference. - Munich, 10-12 Oct. 2007. - P. 267-270. ↑

C2840. Khraisat Y.S.H. Joint influence of rain rate and turbulence on radar signal spectrum width. / Khraisat Y.S.H., Yanovsky F.J. // 2007. European Microwave Conference. - Munich, 9-12 Oct. 2007. - P. 1708-1711. ↑

C2841. Zakeri B. Statistical distribution for scattering mechanism of targets based on eigenvector decomposition in Polarimetric Radars. / Zakeri B., Ghorbani A., Galletti M. // 2007. European Microwave Conference. - Munich, 9-12 Oct. 2007. - P. 1712-1714. ↑

C2842. Pitertsev A.A. Polarimetric approach to detection of probable aircraft icing zones. Icing detection algorithms. / Pitertsev A.A., Yanovsky F.J. // 2007. European Microwave Conference. - Munich, 9-12 Oct. 2007. - P. 1550-1553. ↑

C2843. Zakeri B. Statistical distribution for scattering mechanism of targets based on eigenvector decomposition in polarimetric radars. / Zakeri B., Ghorbani A., Galletti M. // 2007. EuRAD 2007. European Radar Conference. - Munich, 10-12 Oct. 2007. - P. 433-435. ↑

C2844. Hueso Gonzalez J. Development of TanDEM-X DEM calibration concept. / Hueso Gonzalez J., Bachmann M., Fiedler H., Huber S., Krieger G., Wessel B., Zink M. // 2007. EuRAD 2007. European Radar Conference. - Munich, 10-12 Oct. 2007. - P. 464-467. ↑

C2845. Peichl M. Passive microwave remote sensing for security applications. / Peichl M., Dill S., Jirousek M., Suess H. // 2007. EuRAD 2007. European Radar Conference. - Munich, 10-12 Oct. 2007. - P. 32-35. ↑

C2846. Chia-Chuen Kao. Buoy and Radar Observation Network around Taiwan. / Chia-Chuen Kao, Kuo-Ching Jao, Dong-Jiing Doong, Hui-Lin Chen, Chwen-Ling Kuo. // OCEANS 2006-Asia Pacific. - Singapore, 16-19 May 2007. - P. 1-7. ↑

C2847. Trizna D.B. Monitoring Coastal Processes and Ocean Wave Directional Spectra Using a Marine Radar. OCEANS 2006-Asia Pacific. - Singapore, 16-19 May 2007. - P. 1-4. ↑

C2848. Boerner W.-M. Recent Advancements of Multi-modal Radar & SAR Imaging. 2007 International Symposium on Microwave, Antenna, Propagation and EMC Technologies for Wireless Communications. - Hangzhou, 16-17 Aug. 2007. - P. 1485-1488. ↑

C2849. Chan Bong Park. Characterization of dust aerosols with dual wavelengths (532 nm/1064 nm) polarization lidar. / Chan Bong Park, Choo Hie Lee, Sugimoto N. // 2007. CLEO/Pacific Rim 2007. Conference on Lasers and Electro-Optics-Pacific Rim. - Seoul, 26-31 Aug. 2007. - P. 1-2. ↑

C2850. Kliamis N.H.H. Determination of the Melting Layer from Meteorological Radar Data in Malaysia. / Kliamis N.H.H., Sharif O.A.R., Hanzaz Z., Baharom A. // 2007 International Symposium on Microwave, Antenna, Propagation and EMC Technologies for Wireless Communications. - Hangzhou, 16-17 Aug. 2007. - P. 1467-1470. ↑

C2851. Sinitsyn R. Signal Detection Algorithms Based on Non-Parametric Estimates of Density Function. / Sinitsyn R., Yanovsky F. // 2007 European Conference on Wireless Technologies. - Munich, 8-10 Oct. 2007. - P. ↑

201-204. ↑

C2852. Krozer V. Development of an airborne ice sounding radar front-end. / Krozer V., Hernandez C.C., Vazquez Roy J.L., Vidkjaer J., Dall J. // 2007. EuRAD 2007. European Radar Conference. - Munich, 10-12 Oct. 2007. - P. 5-8. ↑

C2853. Chih-hao Kuo. Electromagnetic scattering from multilayer rough surfaces with arbitrary dielectric profiles for remote sensing of subsurface soil moisture. / Chih-hao Kuo, Moghaddam M. // 2007 IEEE Antennas and Propagation Society International Symposium. - Honolulu, HI, 9-15 June 2007. - P. 4797-4800. ↑

C2854. Heron M.L. VHF PortMap Sea Surface Radar Observations in a Shipping Channel. / Heron M.L., Prytz A., Page G., Mazzoldi A., Cosoli S., Gacic M., Kovacevic V. // OCEANS 2006-Asia Pacific. - Singapore, 16-19 May 2007. - P. 1-4. ↑

C2855. Massagram W. Feasibility of HRV measurement from single-channel doppler radar. / Massagram W., Hafner N.M., Yamada S., Lubecke V.M., Boric-Lubecke O. // 2007 IEEE Antennas and Propagation Society International Symposium. - Honolulu, HI, 9-15 June 2007. - P. 269-272. ↑

C2856. Prats P. A SAR processing algorithm for TOPS imaging mode based on extended chirp scaling. / Prats P., Scheiber R., Mittermayer J., Meta A., Moreira A., Sanz-Marcos J. // 2007. IGARSS 2007. IEEE International Geoscience and Remote Sensing Symposium. - Barcelona, 23-28 July 2007. - P. 148-151. ↑

C2857. Zahn R. A high resolution SAR sensor for space and airborne applications. / Zahn R., Weidman K., Boukamp J. // 2007. IGARSS 2007. IEEE International Geoscience and Remote Sensing Symposium. - Barcelona, 23-28 July 2007. - P. 596-599. ↑

C2858. Xiuhong Sun. An advanced airborne multisensor imaging system for fast mapping and change detection applications. / Xiuhong Sun, Chen W., Fischer R.L., Jones M., Eichholz J.C., Richards J.E., Shu P., Jhabvala M., Anh La, Kahle D., Adams J. // 2007. IGARSS 2007. IEEE International Geoscience and Remote Sensing Symposium. - Barcelona, 23-28 July 2007. - P. 600-605. ↑

C2859. Wenling Xuan. A combined sensor system of digital camera with LiDAR. / Wenling Xuan, Zhaoqiang Huang, Xiuwan Chen, Zongjian Lin. // 2007. IGARSS 2007. IEEE International Geoscience and Remote Sensing Symposium. - Barcelona, 23-28 July 2007. - P. 589-592. ↑

C2860. Reigber A. A distributed approach to efficient time-domain SAR processing. / Reigber A., Jager M., Dietzsch A., Hansch R., Weber M., Przybyl H., Prats P. // 2007. IGARSS 2007. IEEE International Geoscience and Remote Sensing Symposium. - Barcelona, 23-28 July 2007. - P. 582-585. ↑

C2861. Jie Wei. Effects of attitude error on spaceborne ScanSAR mosaic. 2007. IGARSS 2007. IEEE International Geoscience and Remote Sensing Symposium. - Barcelona, 23-28 July 2007. - P. 586-588. ↑

C2862. Xiaolong Dong. Surface clutter analysis and ranging sidelobe level requirements for spaceborne meteorological radars. / Xiaolong Dong, Honggang Yin, Di Zhu, Huguang Liu, Jingshan Jiang. // 2007. IGARSS 2007. IEEE International Geoscience and Remote Sensing Symposium. - Barcelona, 23-28 July 2007. - P. 626-629. ↑

C2863. Roth A. Scientific use of TerraSAR-X. / Roth A., Marschall U. // 2007. IGARSS 2007. IEEE International Geoscience and Remote Sensing Symposium. - Barcelona, 23-28 July 2007. - P. 630. ↑

C2864. Jiang Xiao. Optimum design of antenna pattern for spaceborne SAR performance using improved NSGA-II. / Jiang Xiao, Yongqiang Chen, Xiaoqing Wang, Minhui Zhu, Liu Xiao. // 2007. IGARSS 2007. IEEE International Geoscience and Remote Sensing Symposium. - Barcelona, 23-28 July 2007. - P. 615-618. ↑

C2865. Chih-Tien Wang. Disaster monitoring and environmental alert in Taiwan by repeat-pass spaceborne SAR. / Chih-Tien Wang, Kun-Shen Chen, Hong-Wei Lee, Jong-Sen Lee, Boerner W.-M., Ruei-Yuan Wang, Hong-Sen Wan. // 2007. IGARSS 2007. IEEE International Geoscience and Remote Sensing Symposium. - Barcelona, 23-28 July 2007. - P. 609-612. ↑

C2866. Xingsong Hou. Investigation of H.264 intra coding for SAR image. / Xingsong Hou, Yujie Dun, Rongjing Ji. // 2007. IGARSS 2007. IEEE International Geoscience and Remote Sensing Symposium. - Barcelona, 23-28 July 2007. - P. 613-614. ↑

- C2867.** Bhattacharya C. Dyadic resolution multilook image generation by wavelet packettransform correlation of complex SAR signals. 2007. IGARSS 2007. IEEE International Geoscience and Remote Sensing Symposium. - Barcelona, 23-28 July 2007. - P. 578-581. ↑
- C2868.** Giusti E. The equivalence of Cameron's unit disc and Poincaré's sphere for symmetric scattering characterisation and classification. / Giusti E., Martorella M., Berizzi F., Petronio C. // 2007. IGARSS 2007. IEEE International Geoscience and Remote Sensing Symposium. - Barcelona, 23-28 July 2007. - P. 551-554. ↑
- C2869.** Ya-Qiu Jin. Reconstruction of the building objects from multi-aspect high-resolution SAR images. / Ya-Qiu Jin, Feng Xu. // 2007. IGARSS 2007. IEEE International Geoscience and Remote Sensing Symposium. - Barcelona, 23-28 July 2007. - P. 555-558. ↑
- C2870.** Chamundeeswari V.V. Unsupervised land cover classification of SAR images by contour tracing. / Chamundeeswari V.V., Singh D., Singh K. // 2007. IGARSS 2007. IEEE International Geoscience and Remote Sensing Symposium. - Barcelona, 23-28 July 2007. - P. 547-550. ↑
- C2871.** Liu Hui. The analysis and compensation for the unwrapped phase error raised by the dynamic baseline of DSS-INSAR. / Liu Hui, Zhou Yinqing, Xu Huaping, Li Chunsheng, Sun Muhan, Liu Guohui. // 2007. IGARSS 2007. IEEE International Geoscience and Remote Sensing Symposium. - Barcelona, 23-28 July 2007. - P. 540-542. ↑
- C2872.** Yunhua Zhang. A new method for Doppler centroid estimation for spaceborne SAR based on chirp scaling algorithm. / Yunhua Zhang, Wenshuai Zhai. // 2007. IGARSS 2007. IEEE International Geoscience and Remote Sensing Symposium. - Barcelona, 23-28 July 2007. - P. 543-546. ↑
- C2873.** Xu Feng. Region feature extraction based on improved regularization method in SAR image. / Xu Feng, Wang Chao, Zhang Hong. // 2007. IGARSS 2007. IEEE International Geoscience and Remote Sensing Symposium. - Barcelona, 23-28 July 2007. - P. 571-573. ↑
- C2874.** Ghaleb A. Fine micro-Doppler analysis in ISAR imaging. / Ghaleb A., Vignaud L., Nicolas J.-M. // 2007. IGARSS 2007. IEEE International Geoscience and Remote Sensing Symposium. - Barcelona, 23-28 July 2007. - P. 574-577. ↑
- C2875.** Yu Wang. Spotlight-mode SAR data focusing using a modified wavenumber domain algorithm. / Yu Wang, Loffeld O., Knedlik S. // 2007. IGARSS 2007. IEEE International Geoscience and Remote Sensing Symposium. - Barcelona, 23-28 July 2007. - P. 567-570. ↑
- C2876.** Wellig P. Clutter analysis of high resolution millimeter-wave SAR-data in the spatial and wavelet domain. / Wellig P., Schmid K., Essen H., Kurz A., Schimpf H., Brehm T. // 2007. IGARSS 2007. IEEE International Geoscience and Remote Sensing Symposium. - Barcelona, 23-28 July 2007. - P. 559-562. ↑
- C2877.** Radius A. A velocity vector estimation algorithm tested on simulated SAR raw data. / Radius A., Solimini D. // 2007. IGARSS 2007. IEEE International Geoscience and Remote Sensing Symposium. - Barcelona, 23-28 July 2007. - P. 563-566. ↑
- C2878.** Kwag Y.K. UAV based collision avoidance radar sensor. / Kwag Y.K., Chung C.H. // 2007. IGARSS 2007. IEEE International Geoscience and Remote Sensing Symposium. - Barcelona, 23-28 July 2007. - P. 639-642. ↑
- C2879.** Chang Zheng Ma. ISAR imaging of helicopter. / Chang Zheng Ma, Tat Soon Yeo, Hwee Siang Tan, Zhoufeng Liu, Xiujie Dong, Bin Zou. // 2007. IGARSS 2007. IEEE International Geoscience and Remote Sensing Symposium. - Barcelona, 23-28 July 2007. - P. 838-841. ↑
- C2880.** Zhe Liu. Frequency domain imaging algorithm for spaceborne/airborne hybrid bistatic SAR. / Zhe Liu, Jianyu Yang, Xiaoling Zhang, Yiming Pi. // 2007. IGARSS 2007. IEEE International Geoscience and Remote Sensing Symposium. - Barcelona, 23-28 July 2007. - P. 842-845. ↑
- C2881.** Ghayourmanesh S. Shape from shading of SAR imagery in fourier space. / Ghayourmanesh S., Yun Zahng. // 2007. IGARSS 2007. IEEE International Geoscience and Remote Sensing Symposium. - Barcelona, 23-28 July 2007. - P. 835-837. ↑
- C2882.** Yijun He. The effect of polarization ratio on RADARSAT wind vector retrievals. / Yijun He, Biao Zhang,

Hui Shen, Perrie W., Jie Guo. // 2007. IGARSS 2007. IEEE International Geoscience and Remote Sensing Symposium. - Barcelona, 23-28 July 2007. - P. 790-792. ↑

C2883. Gong Zhenqiang. Automobile-based Bistatic SAR processing and experimental results. / Gong Zhenqiang, Zhang Xiaoling, Tian Zhong. // 2007. IGARSS 2007. IEEE International Geoscience and Remote Sensing Symposium. - Barcelona, 23-28 July 2007. - P. 831-834. ↑

C2884. Pedroso E.C. A multi-sensor approach and ranking analysis procedure for oil seeps detection in marine environments. / Pedroso E.C., de Miranda F.P., Bannerman K., HenriqueBeisl C., Rodriguez M.H., Caceres R.G. // 2007. IGARSS 2007. IEEE International Geoscience and Remote Sensing Symposium. - Barcelona, 23-28 July 2007. - P. 865-870. ↑

C2885. Xiaoqing Wang. Bistatic SAR Raw Data Simulation for Ocean. / Xiaoqing Wang, Yin Yu, Yongqiang Chen, Jiang Xiao, Minhui Zhu. // 2007. IGARSS 2007. IEEE International Geoscience and Remote Sensing Symposium. - Barcelona, 23-28 July 2007. - P. 871-874. ↑

C2886. Isoguchi O. Kuroshio-induced cold eddy streets in the lee of isolated islands. / Isoguchi O., Shimada M., Sakaida F., Kawamura H. // 2007. IGARSS 2007. IEEE International Geoscience and Remote Sensing Symposium. - Barcelona, 23-28 July 2007. - P. 858-861. ↑

C2887. Cantalloube H.M.J. High resolution SAR imaging along circular trajectories. / Cantalloube H.M.J., Colin-Koeniguer E., Oriot H. // 2007. IGARSS 2007. IEEE International Geoscience and Remote Sensing Symposium. - Barcelona, 23-28 July 2007. - P. 850-853. ↑

C2888. Xu Sanyuan. A quadtree algorithm for high squint SAR imaging. / Xu Sanyuan, Wang Jianguo. // 2007. IGARSS 2007. IEEE International Geoscience and Remote Sensing Symposium. - Barcelona, 23-28 July 2007. - P. 854-857. ↑

C2889. Nunziata F. A simulator for SAR sea surface waves imaging. / Nunziata F., Gambardella A., Migliaccio M. // 2007. IGARSS 2007. IEEE International Geoscience and Remote Sensing Symposium. - Barcelona, 23-28 July 2007. - P. 786-789. ↑

C2890. Mironov V.L. Dielectric spectroscopic model for tussock and shrub tundra soils. / Mironov V.L., Savin S.V. // 2007. IGARSS 2007. IEEE International Geoscience and Remote Sensing Symposium. - Barcelona, 23-28 July 2007. - P. 726-731. ↑

C2891. Braham K.A. Scattering from 2D-dielectric random surfaces effect of roughness and moisture of seedbed surfaces upon the bistatic scattering coefficient. / Braham K.A., Dusseaux R., Vannier E., Taconet O., Granet G. // 2007. IGARSS 2007. IEEE International Geoscience and Remote Sensing Symposium. - Barcelona, 23-28 July 2007. - P. 746-748. ↑

C2892. Sant'Anna S.J.S. Closed form expressions for scattering matrix of simple targets in multilayer structures. / Sant'Anna S.J.S., da S. Lacava J.C., Fernandes D. // 2007. IGARSS 2007. IEEE International Geoscience and Remote Sensing Symposium. - Barcelona, 23-28 July 2007. - P. 714-717. ↑

C2893. Blake W. A UAV avionics system to facilitate VHF depth sounding and SAR. / Blake W., Siegele K., Burns R. // 2007. IGARSS 2007. IEEE International Geoscience and Remote Sensing Symposium. - Barcelona, 23-28 July 2007. - P. 643-646. ↑

C2894. Bartolomeo V. Cassini RADAR: investigation of titan's surface parameters by means of Bayesian inversion technique and gravity-capillary waves modelling of liquid hydrocarbons surfaces. / Bartolomeo V., Domenico C., Claudia N., Francesco P. // 2007. IGARSS 2007. IEEE International Geoscience and Remote Sensing Symposium. - Barcelona, 23-28 July 2007. - P. 706-709. ↑

C2895. Komarov S.A. Pulse electromagnetic sounding of the petroleum- containing layered medium. / Komarov S.A., Mironov V.L., Muzalevsky K.V. // 2007. IGARSS 2007. IEEE International Geoscience and Remote Sensing Symposium. - Barcelona, 23-28 July 2007. - P. 766-768. ↑

C2896. Rangwala M. Study of millimeter-wave radar for helicopter assisted landing system. / Rangwala M., Feinian Wang, Sarabandi K. // 2007. IGARSS 2007. IEEE International Geoscience and Remote Sensing Symposium. - Barcelona, 23-28 July 2007. - P. 777-780. ↑

- C2897.** Narvekar P.S. Polarimetric microwave emission from snow surfaces: 4th Stokes component analysis. / Narvekar P.S., Heygster G., Jackson T.J., Bindlish R. // 2007. IGARSS 2007. IEEE International Geoscience and Remote Sensing Symposium. - Barcelona, 23-28 July 2007. - P. 762-765. ↑
- C2898.** Mironov V.L. Validation of the soil dielectric spectroscopic models with input parameters based on soil composition. / Mironov V.L., Kosolapova L.G., Fomin S.V. // 2007. IGARSS 2007. IEEE International Geoscience and Remote Sensing Symposium. - Barcelona, 23-28 July 2007. - P. 749-753. ↑
- C2899.** Morgenthaler A. Semi-Analytic Mode Matching (SAMM) algorithm for efficient computation of nearfield scattering in lossy ground from borehole sources. / Morgenthaler A., He Zhan, Rappaport C. // 2007. IGARSS 2007. IEEE International Geoscience and Remote Sensing Symposium. - Barcelona, 23-28 July 2007. - P. 754-757. ↑
- C2900.** Rostan F. The C-SAR instrument for the GMES sentinel-1 mission. / Rostan F., Riegger S., Pitz W., Torre A., Torres R. // 2007. IGARSS 2007. IEEE International Geoscience and Remote Sensing Symposium. - Barcelona, 23-28 July 2007. - P. 215-218. ↑
- C2901.** Le Roy Y. SRAL SAR radar altimeter for sentinel-3 mission. / Le Roy Y., Deschaux-Beaume M., Mavrocordatos C., Aguirre M., Heliere F. // 2007. IGARSS 2007. IEEE International Geoscience and Remote Sensing Symposium. - Barcelona, 23-28 July 2007. - P. 219-222. ↑
- C2902.** Saunier S. The contribution of the european space agency to the ALOS PRISM / commissioning phase. / Saunier S., Santer R., Goryl P., Gruen A., Wolf K., Bouvet M., Viallefont F. // 2007. IGARSS 2007. IEEE International Geoscience and Remote Sensing Symposium. - Barcelona, 23-28 July 2007. - P. 208-211. ↑
- C2903.** Schneider R.Z. Pol-dinSAR: polarimetric SAR differential interferometry using coherent scatterers. / Schneider R.Z., Papathanassiou K. // 2007. IGARSS 2007. IEEE International Geoscience and Remote Sensing Symposium. - Barcelona, 23-28 July 2007. - P. 196-199. ↑
- C2904.** Sato R. Classification of stricken residential houses by the mid niigata prefecture earthquake based on POLSAR image analysis. / Sato R., Soma K., Yajima Y., Yamaguchi Y., Yamada H. // 2007. IGARSS 2007. IEEE International Geoscience and Remote Sensing Symposium. - Barcelona, 23-28 July 2007. - P. 200-203. ↑
- C2905.** Thiele A. Feature extraction of gable-roofed buildings from multi-aspect high-resolution InSAR data. / Thiele A., Cadario E., Schulz K., Thoennessen U., Soergel U. // 2007. IGARSS 2007. IEEE International Geoscience and Remote Sensing Symposium. - Barcelona, 23-28 July 2007. - P. 262-265. ↑
- C2906.** D'Hondt O. Quantitative analysis of texture parameter estimation in SAR images. / D'Hondt O., Lopez-Martinez C., Ferro-Famil L., Pottier E. // 2007. IGARSS 2007. IEEE International Geoscience and Remote Sensing Symposium. - Barcelona, 23-28 July 2007. - P. 274-277. ↑
- C2907.** Padmanabhan S. Estimation of 3-D Water vapor distribution using a network of compact microwave radiometers. / Padmanabhan S., Reising S.C., Iturbide-Sanchez F., Vivekanandan I.J. // 2007. IGARSS 2007. IEEE International Geoscience and Remote Sensing Symposium. - Barcelona, 23-28 July 2007. - P. 251-254. ↑
- C2908.** Christensen J. GAS: the Geostationary Atmospheric Sounder. / Christensen J., Carlstrom A., Ekstrom H., de Maagt P., Colliander A., Emrich A., Embretsen J. // 2007. IGARSS 2007. IEEE International Geoscience and Remote Sensing Symposium. - Barcelona, 23-28 July 2007. - P. 223-226. ↑
- C2909.** Ramos-Perez I. Synthetic Aperture PAU: a new instrument to test potential improvements for future SMOSops. / Ramos-Perez I., Camps A., Bosch-Lluis X., Marchan-Hernandez J.F., Rodriguez-Alvarez N., Valencia E., Frascella F., Campigotto P., Donadio M. // 2007. IGARSS 2007. IEEE International Geoscience and Remote Sensing Symposium. - Barcelona, 23-28 July 2007. - P. 247-250. ↑
- C2910.** Pipia L. Polarimetric temporal information for urban deformation map retrieval. / Pipia L., Fabregas X., Aguasca A., Lopez-Martinez C., Mallorqui J.J., Moraline O. // 2007. IGARSS 2007. IEEE International Geoscience and Remote Sensing Symposium. - Barcelona, 23-28 July 2007. - P. 192-195. ↑
- C2911.** Ainsworth T.L. Classification comparisons between dual-pol and quad-pol SAR imagery. / Ainsworth T.L., Lee J.-S., Chang L.W. // 2007. IGARSS 2007. IEEE International Geoscience and Remote Sensing Symposium. - Barcelona, 23-28 July 2007. - P. 164-167. ↑

- C2912.** Cao Fang. Analysis of fully polarimetric SAR data based on the Cloude-Pottier decomposition and the complex Wishart classifier. / Cao Fang, Hong Wen, Wu Yirong, Pottier E. // 2007. IGARSS 2007. IEEE International Geoscience and Remote Sensing Symposium. - Barcelona, 23-28 July 2007. - P. 168-171. ↑
- C2913.** Doulgeris A. Analysis of non-Gaussian POLSAR data. / Doulgeris A., Anfinson S.N., Eltoft T. // 2007. IGARSS 2007. IEEE International Geoscience and Remote Sensing Symposium. - Barcelona, 23-28 July 2007. - P. 160-163. ↑
- C2914.** Meta A. Investigations on the TOPSAR acquisition mode with TerraSAR-X. / Meta A., Mittermayer J., Steinbrecher U., Prats P. // 2007. IGARSS 2007. IEEE International Geoscience and Remote Sensing Symposium. - Barcelona, 23-28 July 2007. - P. 152-155. ↑
- C2915.** Frey O. Tomographic processing of multi-baseline P-band SAR data for imaging of a forested area. / Frey O., Morsdorf F., Meier E. // 2007. IGARSS 2007. IEEE International Geoscience and Remote Sensing Symposium. - Barcelona, 23-28 July 2007. - P. 156-159. ↑
- C2916.** Landes T. Monitoring temperate glaciers by high resolution Pol-InSAR data: First analysis of Argentine E-SAR acquisitions and in-situ measurements. / Landes T., Gay M., Trouve E., Nicolas J.-M., Bombrun L., Vasile G., Hajsek I. // 2007. IGARSS 2007. IEEE International Geoscience and Remote Sensing Symposium. - Barcelona, 23-28 July 2007. - P. 184-187. ↑
- C2917.** Nouvel J.F. Sub-band interferometry on polarimetric SAR dataset. / Nouvel J.F., Dubois-Fernandez P., Angelliaume S., Mimoun D. // 2007. IGARSS 2007. IEEE International Geoscience and Remote Sensing Symposium. - Barcelona, 23-28 July 2007. - P. 188-191. ↑
- C2918.** Boerner W.-M. Review of existing monographs and books on radar polarimetry and polarimetric SAR with the aim of justifying the need of updates. / Boerner W.-M., Jong-Sen Lee. // 2007. IGARSS 2007. IEEE International Geoscience and Remote Sensing Symposium. - Barcelona, 23-28 July 2007. - P. 180-183. ↑
- C2919.** Jong-Sen Lee. Evaluation and bias removal of multi-look effect on entropy/alpha/anisotropy. / Jong-Sen Lee, Ainsworth T.L., Kelly J., Lopez-Martinez C. // 2007. IGARSS 2007. IEEE International Geoscience and Remote Sensing Symposium. - Barcelona, 23-28 July 2007. - P. 172-175. ↑
- C2920.** Lopez-Martinez C. Multidimensional speckle noise reduction in synthetic aperture radar images. / Lopez-Martinez C., Fabregas X. // 2007. IGARSS 2007. IEEE International Geoscience and Remote Sensing Symposium. - Barcelona, 23-28 July 2007. - P. 176-179. ↑
- C2921.** Solimene R. Localizing metallic small spheres by a linear distributional approach. / Solimene R., Buonanno A., Pierri R., Leone G. // 2007. IGARSS 2007. IEEE International Geoscience and Remote Sensing Symposium. - Barcelona, 23-28 July 2007. - P. 350-353. ↑
- C2922.** Gras V. Phase distortion modelling due to motion in wave scattering mechanism applied to SAR images analysis. / Gras V., Sintès C., Garello R. // 2007. IGARSS 2007. IEEE International Geoscience and Remote Sensing Symposium. - Barcelona, 23-28 July 2007. - P. 511-515. ↑
- C2923.** Zhihua He. Spaceborne SAR raw signal simulation of ocean scene. / Zhihua He, Zhen Dong, Haifeng Huang, Anxi Yu. // 2007. IGARSS 2007. IEEE International Geoscience and Remote Sensing Symposium. - Barcelona, 23-28 July 2007. - P. 516-519. ↑
- C2924.** Moon-Kyung Kang. The extraction of ocean wind, wave, and current parameters using SAR imagery. / Moon-Kyung Kang, Hoonyol Lee, Moonjin Lee, Yong-Wook Park, Wang-Jung Yoon. // 2007. IGARSS 2007. IEEE International Geoscience and Remote Sensing Symposium. - Barcelona, 23-28 July 2007. - P. 507-510. ↑
- C2925.** Hwee Siang Tan. ISAR imaging of targets with moving parts using micro-doppler detection on the range profile image. / Hwee Siang Tan, Changzheng Ma, Tat Soon Yeo, Qun Zhang, Chun Sum Ng, Bin Zou. // 2007. IGARSS 2007. IEEE International Geoscience and Remote Sensing Symposium. - Barcelona, 23-28 July 2007. - P. 499-502. ↑
- C2926.** Sveinsson J.R. Combined wavelet and curvelet denoising of SAR images using TV segmentation. / Sveinsson J.R., Benediktsson J.A. // 2007. IGARSS 2007. IEEE International Geoscience and Remote Sensing Symposium. - Barcelona, 23-28 July 2007. - P. 503-506. ↑

- C2927.** Chaomin Shen. Variational-based speckle noise removal of SAR imagery. / Chaomin Shen, Yaxin Peng, Ling Pi, Zhibin Li. // 2007. IGARSS 2007. IEEE International Geoscience and Remote Sensing Symposium. - Barcelona, 23-28 July 2007. - P. 532-535. ↑
- C2928.** Kalkuhl M. Parallel computation of synthetic SAR raw data. / Kalkuhl M., Droste P., Wiechert W., Nies H., Loffeld O., Lambers M. // 2007. IGARSS 2007. IEEE International Geoscience and Remote Sensing Symposium. - Barcelona, 23-28 July 2007. - P. 536-539. ↑
- C2929.** Meglio F. Three dimensional SAR image focusing from non-uniform samples. / Meglio F., Panariello G., Schirinz G. // 2007. IGARSS 2007. IEEE International Geoscience and Remote Sensing Symposium. - Barcelona, 23-28 July 2007. - P. 528-531. ↑
- C2930.** Tzong-Dar Wu. Geological lineament and shoreline detection in SAR images. / Tzong-Dar Wu, Lee M.T. // 2007. IGARSS 2007. IEEE International Geoscience and Remote Sensing Symposium. - Barcelona, 23-28 July 2007. - P. 520-523. ↑
- C2931.** Andres C. A multiprocessing framework for SAR image processing. / Andres C., Keil T., Herrmann R., Scheiber R. // 2007. IGARSS 2007. IEEE International Geoscience and Remote Sensing Symposium. - Barcelona, 23-28 July 2007. - P. 524-527. ↑
- C2932.** Aboutanios E. Evaluation of the single and two data set STAP detection algorithms using measured data. / Aboutanios E., Mulgrew B. // 2007. IGARSS 2007. IEEE International Geoscience and Remote Sensing Symposium. - Barcelona, 23-28 July 2007. - P. 494-498. ↑
- C2933.** Uschkerat U. Application of 3D-SAR nearfield imaging algorithms to GPR data. 2007. IGARSS 2007. IEEE International Geoscience and Remote Sensing Symposium. - Barcelona, 23-28 July 2007. - P. 452-455. ↑
- C2934.** Tison C. Target recognition in SAR images with Support Vector Machines (SVM). / Tison C., Pourthie N., Souyris J.-C. // 2007. IGARSS 2007. IEEE International Geoscience and Remote Sensing Symposium. - Barcelona, 23-28 July 2007. - P. 456-459. ↑
- C2935.** Sipelgas L. Elimination of oil spill like structures from radar image using MODIS data. / Sipelgas L., Uiboupin R. // 2007. IGARSS 2007. IEEE International Geoscience and Remote Sensing Symposium. - Barcelona, 23-28 July 2007. - P. 429-431. ↑
- C2936.** Cuinas I. Measurement and analysis of depolarization generated by scattering over constructive obstacles at 5.8 GHz. / Cuinas I., Sanchez M.G., Alejos A.V. // 2007. IGARSS 2007. IEEE International Geoscience and Remote Sensing Symposium. - Barcelona, 23-28 July 2007. - P. 354-357. ↑
- C2937.** Qi Li. Steerable filter based multiscale registration method for JERS-1 SAR and ASTER images. / Qi Li, Sato I., Murakami Y. // 2007. IGARSS 2007. IEEE International Geoscience and Remote Sensing Symposium. - Barcelona, 23-28 July 2007. - P. 381-384. ↑
- C2938.** Schulz F. Design of GMTI combining networks. / Schulz F., Saalman O. // 2007. IGARSS 2007. IEEE International Geoscience and Remote Sensing Symposium. - Barcelona, 23-28 July 2007. - P. 486-489. ↑
- C2939.** Yixian Tang. CAESAR-XInSAR: A new software for interferometric SAR processing. / Yixian Tang, Hong Zhang, Chao Wang, Tao Wu. // 2007. IGARSS 2007. IEEE International Geoscience and Remote Sensing Symposium. - Barcelona, 23-28 July 2007. - P. 490-493. ↑
- C2940.** Jie Wei. Relationship between antenna pointing stability and spaceborne ScanSAR scalloping calibration. 2007. IGARSS 2007. IEEE International Geoscience and Remote Sensing Symposium. - Barcelona, 23-28 July 2007. - P. 482-485. ↑
- C2941.** Bemad G.P. Semi-automatic fast recognition of areas of interest for SAR image interpretation. / Bemad G.P., Denise L., Refregier P. // 2007. IGARSS 2007. IEEE International Geoscience and Remote Sensing Symposium. - Barcelona, 23-28 July 2007. - P. 464-467. ↑
- C2942.** Thompson P. Target separation in SAR image with the MUSIC algorithm. / Thompson P., Nannini M., Scheiber R. // 2007. IGARSS 2007. IEEE International Geoscience and Remote Sensing Symposium. - Barcelona, 23-28 July 2007. - P. 468-471. ↑

- C2943.** Ketelaar G. Multi-track PS-InSAR datum connection. / Ketelaar G., van Leijen F., Marinkovic P., Hanssen R. // 2007. IGARSS 2007. IEEE International Geoscience and Remote Sensing Symposium. - Barcelona, 23-28 July 2007. - P. 2481-2484. ↑
- C2944.** Andreoli R. Inland lake monitoring using low and medium resolution ENVISAT ASAR and optical data: Case study of Poyang Lake (Jiangxi, P.R. China). / Andreoli R., Yesou H., Li J., Desnos Y.-L. // 2007. IGARSS 2007. IEEE International Geoscience and Remote Sensing Symposium. - Barcelona, 23-28 July 2007. - P. 4578-4581. ↑
- C2945.** Renzong Ruan. Identification of inland fresh water wetland using SAR and ETM+ data. / Renzong Ruan, Liliang Ren. // 2007. IGARSS 2007. IEEE International Geoscience and Remote Sensing Symposium. - Barcelona, 23-28 July 2007. - P. 4592-4595. ↑
- C2946.** Esch T. Analysis of urban land use pattern based on high resolution radar imagery. / Esch T., Roth A., Dech S. // 2007. IGARSS 2007. IEEE International Geoscience and Remote Sensing Symposium. - Barcelona, 23-28 July 2007. - P. 4525. ↑
- C2947.** Meglio F. DEM estimation from multi-Baseline ENVISAT- ASAR interferometric data through maximum likelihood techniques. / Meglio F., Schirizzi G. // 2007. IGARSS 2007. IEEE International Geoscience and Remote Sensing Symposium. - Barcelona, 23-28 July 2007. - P. 4517-4520. ↑
- C2948.** Norland R. Improving interferometric radar measurement accuracy using local meteorological data. // 2007. IGARSS 2007. IEEE International Geoscience and Remote Sensing Symposium. - Barcelona, 23-28 July 2007. - P. 4521-4524. ↑
- C2949.** Yunqing Jiao. Uncertainty analysis of flood disaster assessment using radar imagery. / Yunqing Jiao, Shixin Wang, Yi Zhou, Litao Wang. // 2007. IGARSS 2007. IEEE International Geoscience and Remote Sensing Symposium. - Barcelona, 23-28 July 2007. - P. 4729-4732. ↑
- C2950.** Taejung Kim. Semiautomatic reconstruction of building height and footprints from single satellite images. / Taejung Kim, Javzandulam T., Tae-Yoon Lee. // 2007. IGARSS 2007. IEEE International Geoscience and Remote Sensing Symposium. - Barcelona, 23-28 July 2007. - P. 4737-4740. ↑
- C2951.** Chen Yun. Typhoon monitoring/operational forecasting and services 2005 in China. / Chen Yun, Li Qiang, Li Zechun, Xu zhi-fang. // 2007. IGARSS 2007. IEEE International Geoscience and Remote Sensing Symposium. - Barcelona, 23-28 July 2007. - P. 4675-4678. ↑
- C2952.** Elias P. Small scale surface deformation detection of the Gulf of Corinth (Hellas) using Permanent Scatterers technique. / Elias P., Kontoes C., Papoutsis I., Kotsis I. // 2007. IGARSS 2007. IEEE International Geoscience and Remote Sensing Symposium. - Barcelona, 23-28 July 2007. - P. 4659-4662. ↑
- C2953.** Lee C.-W. SAR measurements of surface displacements at Augustine volcano, Alaska from 1992 to 2005. / Lee C.-W., Lu Z., Kwoun O.-I. // 2007. IGARSS 2007. IEEE International Geoscience and Remote Sensing Symposium. - Barcelona, 23-28 July 2007. - P. 4671-4674. ↑
- C2954.** Ferraioli G. Offset Phase Estimation in Multi-Channel InSAR DEM Reconstruction. / Ferraioli G., Pascasio V., Ferraiuolo G. // 2007. IGARSS 2007. IEEE International Geoscience and Remote Sensing Symposium. - Barcelona, 23-28 July 2007. - P. 4513-4516. ↑
- C2955.** Gonzalez J.H. DEM calibration concept for TanDEM-X. / Gonzalez J.H., Bachmann M., Fiedler H., Huber S., Krieger G., Zink M. // 2007. IGARSS 2007. IEEE International Geoscience and Remote Sensing Symposium. - Barcelona, 23-28 July 2007. - P. 4487-4490. ↑
- C2956.** Darizhapov D. Investigation of creation methods of digital elevation model. / Darizhapov D., Leonov A. // 2007. IGARSS 2007. IEEE International Geoscience and Remote Sensing Symposium. - Barcelona, 23-28 July 2007. - P. 4491-4492. ↑
- C2957.** Boncori J.P.M. Statistical description of tropospheric delay for InSAR: Overview and a new model. / Boncori J.P.M., Mohr J.J. // 2007. IGARSS 2007. IEEE International Geoscience and Remote Sensing Symposium. - Barcelona, 23-28 July 2007. - P. 4483-4486. ↑
- C2958.** Duro J. Impact of SAR impulse response function in interferometric measurement. / Duro J., Miranda

N., Cooksley G., Biescas E., Arnaud A. // 2007. IGARSS 2007. IEEE International Geoscience and Remote Sensing Symposium. - Barcelona, 23-28 July 2007. - P. 4474-4478. ↑

C2959. Abdelfattah R. Mixture model for the segmentation of the InSAR coherence map. / Abdelfattah R., Nicolas J.M. // 2007. IGARSS 2007. IEEE International Geoscience and Remote Sensing Symposium. - Barcelona, 23-28 July 2007. - P. 4479-4482. ↑

C2960. Zheng-Shu Zhou. Development of a baseband signal ATI-SAR simulator for ground moving target indication. / Zheng-Shu Zhou, Bates B.D., Yunhan Dong. // 2007. IGARSS 2007. IEEE International Geoscience and Remote Sensing Symposium. - Barcelona, 23-28 July 2007. - P. 4505-4508. ↑

C2961. Jie Li. A multi-baseline InSAR DEM reconstruction approach without ground control points. / Jie Li, Haifeng Huang, Diannong Liang. // 2007. IGARSS 2007. IEEE International Geoscience and Remote Sensing Symposium. - Barcelona, 23-28 July 2007. - P. 4509-4512. ↑

C2962. Mecatti D. Remote sensing of glacier by ground-based radar interferometry. / Mecatti D., Noferini L., Macaluso G., Pieraccini M., Luzzi G., Atzeni C., Tamburini A. // 2007. IGARSS 2007. IEEE International Geoscience and Remote Sensing Symposium. - Barcelona, 23-28 July 2007. - P. 4501-4504. ↑

C2963. Selva J. Image coregistration in SAR interferometry only by means of arithmetic operations. / Selva J., Lopez-Sanchez J.M. // 2007. IGARSS 2007. IEEE International Geoscience and Remote Sensing Symposium. - Barcelona, 23-28 July 2007. - P. 4493-4496. ↑

C2964. Martinez-Espla J.J. Introduction of a grid-based filter approach for InSAR phase filtering and unwrapping. / Martinez-Espla J.J., Martinez-Marin T., Lopez-Sanchez J.M. // 2007. IGARSS 2007. IEEE International Geoscience and Remote Sensing Symposium. - Barcelona, 23-28 July 2007. - P. 4497-4500. ↑

C2965. Hieu Duong. Error analysis of ICESat waveform processing by investigating overlapping pairs over Europe. / Hieu Duong, Lindenbergh R., Pfeifer N., Vosselman G. // 2007. IGARSS 2007. IEEE International Geoscience and Remote Sensing Symposium. - Barcelona, 23-28 July 2007. - P. 4753-4756. ↑

C2966. Tao Wu. Ground deformation retrieval of urban and suburb areas based on multi-baseline DInSAR algorithm: A case study in Cangzhou City (China). / Tao Wu, Hong Zhang, Chao Wang. // 2007. IGARSS 2007. IEEE International Geoscience and Remote Sensing Symposium. - Barcelona, 23-28 July 2007. - P. 4898-4901. ↑

C2967. Teichrieb V. Enhancement of radar based DEMs using 3D techniques. / Teichrieb V., Kelner J. // 2007. IGARSS 2007. IEEE International Geoscience and Remote Sensing Symposium. - Barcelona, 23-28 July 2007. - P. 4902-4905. ↑

C2968. Marinkovic P. Dynamic persistent scatterers interferometry. / Marinkovic P., Hanssen R. // 2007. IGARSS 2007. IEEE International Geoscience and Remote Sensing Symposium. - Barcelona, 23-28 July 2007. - P. 4894-4897. ↑

C2969. de Macedo K.A.C. An autofocus approach for residual motion errors with application to airborne repeat-pass SAR interferometry. / de Macedo K.A.C., Scheiber R., Moreira A. // 2007. IGARSS 2007. IEEE International Geoscience and Remote Sensing Symposium. - Barcelona, 23-28 July 2007. - P. 4886-4889. ↑

C2970. Li Z.T. DEM alignment and registration in interferometric SAR processing and evaluation. / Li Z.T., Bethel J. // 2007. IGARSS 2007. IEEE International Geoscience and Remote Sensing Symposium. - Barcelona, 23-28 July 2007. - P. 4890-4893. ↑

C2971. Faller N. TerraSAR-X and TanDEM-X: Revolution in spaceborne radar. / Faller N., Weber M. // 2007. IGARSS 2007. IEEE International Geoscience and Remote Sensing Symposium. - Barcelona, 23-28 July 2007. - P. 4924-4928. ↑

C2972. Mittermayer J. Verification of the TerraSAR-X system. / Mittermayer J., Younis M., Brautigam B., Fritz T., Kahle R., Metzger R., Schattler B. // 2007. IGARSS 2007. IEEE International Geoscience and Remote Sensing Symposium. - Barcelona, 23-28 July 2007. - P. 4929-4932. ↑

C2973. Fischman M.A. Advanced control and processing capabilities in the aquarius scatterometer flight electronics. / Fischman M.A., McWatters D.A., Berkun A.C., Cheetham C.M., Chu A.J., Duong V.A., Freedman A.P., Hausmann R.W., Jourdan M.N., Kang E.C., Kobzeff P.A., Paller M. // 2007. IGARSS 2007. IEEE

International Geoscience and Remote Sensing Symposium. - Barcelona, 23-28 July 2007. - P. 4920-4923. ↑

C2974. Blom R. Genesis of a new NASA InSAR mission concept, and natural hazards applications. / Blom R., Donnellan A., Fielding E., Freeman A., Hensley S., Johnson W.T.K., Loverro A., Lundgren P., Rosen P., Saatchi S. // 2007. IGARSS 2007. IEEE International Geoscience and Remote Sensing Symposium. - Barcelona, 23-28 July 2007. - P. 4912-4915. ↑

C2975. Rincon R. RadSTAR L-band imaging scatterometer- performance assessment. / Rincon R., Hildebrand P.R., Hilliard L. // 2007. IGARSS 2007. IEEE International Geoscience and Remote Sensing Symposium. - Barcelona, 23-28 July 2007. - P. 4916-4919. ↑

C2976. Zolotarev I.D. Research of influence of transients, non-equidistance of the taken readings, divergence of beams on characteristics of interferometric SAR. / Zolotarev I.D., Pozharsky T.O., Miller Ya.E. // 2007. IGARSS 2007. IEEE International Geoscience and Remote Sensing Symposium. - Barcelona, 23-28 July 2007. - P. 4882-4885. ↑

C2977. Di Bisceglie M. Multiband CFAR detection of thermal anomalies using principal component analysis. / Di Bisceglie M., Episcopo R., Galdi C., Ullo S.L. // 2007. IGARSS 2007. IEEE International Geoscience and Remote Sensing Symposium. - Barcelona, 23-28 July 2007. - P. 4822-4825. ↑

C2978. Waske B. Fusion of support vector machines for classifying SAR and multispectral imagery from agricultural areas. / Waske B., Menz G., Benediktsson J.A. // 2007. IGARSS 2007. IEEE International Geoscience and Remote Sensing Symposium. - Barcelona, 23-28 July 2007. - P. 4842-4845. ↑

C2979. Weihing D. Detecting moving targets in dual-channel high resolution spaceborne SAR images with a compound detection scheme. / Weihing D., Hinz S., Meyer F., Suchandt S., Bamler R. // 2007. IGARSS 2007. IEEE International Geoscience and Remote Sensing Symposium. - Barcelona, 23-28 July 2007. - P. 4818-4821. ↑

C2980. Lidicky L. A new method for moving target indication and detection in multi-channel SAR data. 2007. IGARSS 2007. IEEE International Geoscience and Remote Sensing Symposium. - Barcelona, 23-28 July 2007. - P. 4802-4805. ↑

C2981. Lugan S. Simulation of LIDAR-based aircraft wake vortex detection using a bi-gaussian spectral model. / Lugan S., Bricteux L., Macq B., Sobieski P., Winckelmans G., Douchamps D. // 2007. IGARSS 2007. IEEE International Geoscience and Remote Sensing Symposium. - Barcelona, 23-28 July 2007. - P. 4806-4809. ↑

C2982. Prats P. Advanced D-InSAR techniques applied to a time series of airborne SAR data. / Prats P., Scheiber R., Moreira A., Reigber A., Mallorqui J.J. // 2007. IGARSS 2007. IEEE International Geoscience and Remote Sensing Symposium. - Barcelona, 23-28 July 2007. - P. 4874-4877. ↑

C2983. Perna S. X-band airborne differential interferometry over the Perugia area. / Perna S., Wimmer C., Moreira J., Fornaro G. // 2007. IGARSS 2007. IEEE International Geoscience and Remote Sensing Symposium. - Barcelona, 23-28 July 2007. - P. 4878-4881. ↑

C2984. Vasile G. Coherent-stable scatterers detection in SAR multi-interferograms: Feature fuzzy fusion in Alpine glacier geophysical context. / Vasile G., Trouve E., Valet L., Nicolas J.-M., Bombrun L., Gay M., Petillot I., Bolon P., Buzuloiu V. // 2007. IGARSS 2007. IEEE International Geoscience and Remote Sensing Symposium. - Barcelona, 23-28 July 2007. - P. 4862-4865. ↑

C2985. Moser G. Unsupervised change detection by multichannel SAR data fusion. / Moser G., Serpico S.B. // 2007. IGARSS 2007. IEEE International Geoscience and Remote Sensing Symposium. - Barcelona, 23-28 July 2007. - P. 4854-4857. ↑

C2986. Shabou A. Similarity measures between SAR and optic data. / Shabou A., Tupin F., Chaabane F. // 2007. IGARSS 2007. IEEE International Geoscience and Remote Sensing Symposium. - Barcelona, 23-28 July 2007. - P. 4858-4861. ↑

C2987. Goh A.S. Comparison of parameter estimation accuracy of distributed-target polarimetric calibration techniques. / Goh A.S., Preiss M., Gray D.A., Stacy N.J.S. // 2007. IGARSS 2007. IEEE International Geoscience and Remote Sensing Symposium. - Barcelona, 23-28 July 2007. - P. 4175-4178. ↑

- C2988.** Kurz A. The problem of parameter estimation for spatially correlated polarimetric ground clutter at millimeterwave frequencies. / Kurz A., Schimpf H. // 2007. IGARSS 2007. IEEE International Geoscience and Remote Sensing Symposium. - Barcelona, 23-28 July 2007. - P. 4179-4182. ↑
- C2989.** Li Xiaowei. A ship detection method for dual polarization SAR data based on whitening filtering. / Li Xiaowei, Chong Jinsong, Zhu Minhui. // 2007. IGARSS 2007. IEEE International Geoscience and Remote Sensing Symposium. - Barcelona, 23-28 July 2007. - P. 4171-4174. ↑
- C2990.** Burini A. A neural approach to unsupervised classification of very-high resolution polarimetric SAR data. / Burini A., Putignano C., Del Frate F., Del Greco M., Schiavon G., Solimini D. // 2007. IGARSS 2007. IEEE International Geoscience and Remote Sensing Symposium. - Barcelona, 23-28 July 2007. - P. 4164-4166. ↑
- C2991.** Ya-Qiu Jin. Retrieval of fully polarimetric mueller matrix under Faraday rotation effect at P band in space-borne polarimetric SAR observation. / Ya-Qiu Jin, Ren-Yuan Qi. // 2007. IGARSS 2007. IEEE International Geoscience and Remote Sensing Symposium. - Barcelona, 23-28 July 2007. - P. 4167-4170. ↑
- C2992.** Skriver H. Signatures of polarimetric parameters and their implications on land cover classification. 2007. IGARSS 2007. IEEE International Geoscience and Remote Sensing Symposium. - Barcelona, 23-28 July 2007. - P. 4195-4198. ↑
- C2993.** de Souza Soler L. An approach to classify polarimetric P-band SAR images for land use and land cover mapping in the. / de Souza Soler L., Joao S., Sant'Anna S. // 2007. IGARSS 2007. IEEE International Geoscience and Remote Sensing Symposium. - Barcelona, 23-28 July 2007. - P. 4199-4201. ↑
- C2994.** Colin E.K. Polarimetric optical tools and decompositions applied to SAR images. 2007. IGARSS 2007. IEEE International Geoscience and Remote Sensing Symposium. - Barcelona, 23-28 July 2007. - P. 4191-4194. ↑
- C2995.** Rangwala M. Design of FMCW millimeter-wave radar for helicopter assisted landing. / Rangwala M., Juseop Lee, Sarabandi K. // 2007. IGARSS 2007. IEEE International Geoscience and Remote Sensing Symposium. - Barcelona, 23-28 July 2007. - P. 4183-4186. ↑
- C2996.** Galletti M. Degree of polarization for weather radars. / Galletti M., Chandra M., Borner T., Bebbington D.H.O. // 2007. IGARSS 2007. IEEE International Geoscience and Remote Sensing Symposium. - Barcelona, 23-28 July 2007. - P. 4187-4190. ↑
- C2997.** Margarit G. Grecosar, a SAR simulator for complex targets: Application to urban environments. / Margarit G., Mallorqui J.J., Lopez-Martinez C. // 2007. IGARSS 2007. IEEE International Geoscience and Remote Sensing Symposium. - Barcelona, 23-28 July 2007. - P. 4160-4163. ↑
- C2998.** Redadaa S. Focusing problems of subsurface imaging by a low-frequency SAR. / Redadaa S., Le Caillec J.-M., Solaiman B., Benslama M. // 2007. IGARSS 2007. IEEE International Geoscience and Remote Sensing Symposium. - Barcelona, 23-28 July 2007. - P. 4101-4104. ↑
- C2999.** Soldovieri F. Experimental validation of a Kirchhoff based shape reconstruction algorithm in realistic conditions: a test case for buried pipes. / Soldovieri F., Brancaccio A., Prisco G., Sglavo D., Pierri R., Leone G. // 2007. IGARSS 2007. IEEE International Geoscience and Remote Sensing Symposium. - Barcelona, 23-28 July 2007. - P. 4105-4108. ↑
- C3000.** Iorio M. GPR missions on mars. / Iorio M., Fois F., Mecozzi R., Seu R., Picardi G. // 2007. IGARSS 2007. IEEE International Geoscience and Remote Sensing Symposium. - Barcelona, 23-28 July 2007. - P. 4095-4100. ↑
- C3001.** Lambers M. Gpu-based framework for interactive visualization of SAR data. / Lambers M., Kolb A., Nies H., Kalkuhl M. // 2007. IGARSS 2007. IEEE International Geoscience and Remote Sensing Symposium. - Barcelona, 23-28 July 2007. - P. 4076-4079. ↑
- C3002.** Huneycutt B. Active remote sensing applications to disaster management with implications to spectrum management. 2007. IGARSS 2007. IEEE International Geoscience and Remote Sensing Symposium. - Barcelona, 23-28 July 2007. - P. 4091-4094. ↑
- C3003.** Schimpf H. Properties of polarimetric sea clutter at 35 GHz. / Schimpf H., Fuchs H.-H. // 2007. IGARSS

2007. IEEE International Geoscience and Remote Sensing Symposium. - Barcelona, 23-28 July 2007. - P. 4152-4155. ↑

C3004. Marzano F.S. Bayesian classification of hydrometeors from polarimetric radars at S- and X- bands: algorithm design and experimental comparisons. / Marzano F.S., Scaranari D., Montopoli M., Vulpiani G., Anagnostou M.N., Anagnostou E.N. // 2007. IGARSS 2007. IEEE International Geoscience and Remote Sensing Symposium. - Barcelona, 23-28 July 2007. - P. 4156-4159. ↑

C3005. Zuberbuhler L. The dependence of polarimetric decomposition parameters on biophysical forest parameters, frequency and methodology. / Zuberbuhler L., Meier E. // 2007. IGARSS 2007. IEEE International Geoscience and Remote Sensing Symposium. - Barcelona, 23-28 July 2007. - P. 4148-4151. ↑

C3006. Villard L. Bistatic foliage penetration modelling. / Villard L., Borderies P. // 2007. IGARSS 2007. IEEE International Geoscience and Remote Sensing Symposium. - Barcelona, 23-28 July 2007. - P. 4109-4112. ↑

C3007. Souyris J.-C. Multi-look polar decomposition of polarimetric SAR images. / Souyris J.-C., Tison C. // 2007. IGARSS 2007. IEEE International Geoscience and Remote Sensing Symposium. - Barcelona, 23-28 July 2007. - P. 4144-4147. ↑

C3008. Luoju K. Assimilating spaceborne radar and ground-based weather station data for operational snow-covered area estimation. / Luoju K., Pulliainen J., Metsamäki S., Anttila S., Hallikainen M. // 2007. IGARSS 2007. IEEE International Geoscience and Remote Sensing Symposium. - Barcelona, 23-28 July 2007. - P. 4202-4205. ↑

C3009. Hanna R. Brightness temperature validation for SeaWinds radiometer using Advanced Microwave Scanning Radiometer on ADEOS-II. / Hanna R., Jones W.L. // 2007. IGARSS 2007. IEEE International Geoscience and Remote Sensing Symposium. - Barcelona, 23-28 July 2007. - P. 4419-4421. ↑

C3010. Cabot F. Calibration of SMOS geolocation biases. / Cabot F., Kerr Y.H., Waldteufel P. // 2007. IGARSS 2007. IEEE International Geoscience and Remote Sensing Symposium. - Barcelona, 23-28 July 2007. - P. 4448-4450. ↑

C3011. Molero F. New inversion algorithm for raman lidar without derivative of the inelastic signal. / Molero F., Pujadas M. // 2007. IGARSS 2007. IEEE International Geoscience and Remote Sensing Symposium. - Barcelona, 23-28 July 2007. - P. 4379-4382. ↑

C3012. Rocadenbosch F. Morphological tools for range-interval segmentation of elastic lidar signals. / Rocadenbosch F., Sicard M., Reba M.N.M., Tomas S. // 2007. IGARSS 2007. IEEE International Geoscience and Remote Sensing Symposium. - Barcelona, 23-28 July 2007. - P. 4372-4375. ↑

C3013. Tabatabaeenejad A. Inversion of a layered rough surface model: maximizing the number of retrievable parameters for the design of future subsurface sensing radar systems. / Tabatabaeenejad A., Moghaddam M. // 2007. IGARSS 2007. IEEE International Geoscience and Remote Sensing Symposium. - Barcelona, 23-28 July 2007. - P. 4376-4378. ↑

C3014. Xiaolong Dong. Accuracy and resolution analysis of the pencil beam radar scatterometer onboard China's HY-2 satellite. / Xiaolong Dong, Shuyan Lang, Tao Wang, Huguang Liu. // 2007. IGARSS 2007. IEEE International Geoscience and Remote Sensing Symposium. - Barcelona, 23-28 July 2007. - P. 4467-4470. ↑

C3015. Hambaryan A.K. Polarimetric, combined, short pulse scatterometer-radiometer system at 5.6GHz. / Hambaryan A.K., Arakelyan A.K., Arakelyan A.A., Darbinyan S.A., Grigoryan M.L., Hakobyan I.K., Karyan V.V., Manukyan M.R., Hovhannisyan G.G., Poghosyan T.N., Poghosyan N.G. // 2007. IGARSS 2007. IEEE International Geoscience and Remote Sensing Symposium. - Barcelona, 23-28 July 2007. - P. 4471-4473. ↑

C3016. Contreras R.F. The effect of rain on retrieval of C- and Ku-band scatterometer surface winds during Hurricanes Lili (2002) and Isabel (2003). / Contreras R.F., Frasier S.J., Esteban-Fernandez D., Chang P. // 2007. IGARSS 2007. IEEE International Geoscience and Remote Sensing Symposium. - Barcelona, 23-28 July 2007. - P. 4463-4466. ↑

C3017. Congling Nie. Simultaneous wind and rain retrieval for ERS scatterometer measurements. / Congling Nie, Long D.G. // 2007. IGARSS 2007. IEEE International Geoscience and Remote Sensing Symposium. - Barcelona, 23-28 July 2007. - P. 4455-4458. ↑

- C3018.** Awada A. Frequency impact on the bistatic radar scattering from an ocean surface. / Awada A., Khenchaf A., Coatanhay A. // 2007. IGARSS 2007. IEEE International Geoscience and Remote Sensing Symposium. - Barcelona, 23-28 July 2007. - P. 4459-4462. ↑
- C3019.** Fayard F. Matching stereoscopic SAR images for radargrammetric applications. / Fayard F., Meric S., Pottier E. // 2007. IGARSS 2007. IEEE International Geoscience and Remote Sensing Symposium. - Barcelona, 23-28 July 2007. - P. 4364-4367. ↑
- C3020.** Dall J. P-sounder: an airborne P-band ice sounding radar. / Dall J., Skou N., Kusk A., Kristensen S.S., Krozer V. // 2007. IGARSS 2007. IEEE International Geoscience and Remote Sensing Symposium. - Barcelona, 23-28 July 2007. - P. 4225-4228. ↑
- C3021.** Strozzi T. Potential of a C-band SAR mission with 12-day repeat cycle to derive ice surface velocity with interferometry and offset tracking. / Strozzi T., Wegmuller U., Werner C., Wiesmann A., Santoro M. // 2007. IGARSS 2007. IEEE International Geoscience and Remote Sensing Symposium. - Barcelona, 23-28 July 2007. - P. 4229-4232. ↑
- C3022.** Cea C. An improved methodology to map Snow Cover by means of Landsat and MODIS imagery. / Cea C., Cristobal J., Pons X. // 2007. IGARSS 2007. IEEE International Geoscience and Remote Sensing Symposium. - Barcelona, 23-28 July 2007. - P. 4217-4220. ↑
- C3023.** Hudier E. Diurnal SAR variability due to ice and snow air interface wetness overnight changes. / Hudier E., Gosselin J.-S., Febres D. // 2007. IGARSS 2007. IEEE International Geoscience and Remote Sensing Symposium. - Barcelona, 23-28 July 2007. - P. 4206-4208. ↑
- C3024.** Nakamura K. Ice flow estimation of Shirase Glacier by using JERS-1/SAR image correlation. / Nakamura K., Wakabayashi H., Doi K., Shibuya K. // 2007. IGARSS 2007. IEEE International Geoscience and Remote Sensing Symposium. - Barcelona, 23-28 July 2007. - P. 4213-4216. ↑
- C3025.** Magnusson M. Estimation of forest stem volume using ALOS PALSAR satellite images. / Magnusson M., Fransson J.E.S., Eriksson L.E.B., Sandberg G., Smith-Jonforsen G., Ulander L.M.H. // 2007. IGARSS 2007. IEEE International Geoscience and Remote Sensing Symposium. - Barcelona, 23-28 July 2007. - P. 4343-4346. ↑
- C3026.** Fernandez-Ordonez Y. Forest inventory applications using optical and RADARSAT-2 images in Mexico. / Fernandez-Ordonez Y., Soria-Ruiz J., Woodhouse I.H. // 2007. IGARSS 2007. IEEE International Geoscience and Remote Sensing Symposium. - Barcelona, 23-28 July 2007. - P. 4350-4353. ↑
- C3027.** Zhongmin Zhu. The active-passive remote sensing for aerosol optical depth retrieval. / Zhongmin Zhu, Wei Gong, Pingxiang Li, Liangpei Zhang, Qianqing Qin, Yingying Ma, Shalei Song, Jun Li, Mengyu Liu, Zhongyu Hao. // 2007. IGARSS 2007. IEEE International Geoscience and Remote Sensing Symposium. - Barcelona, 23-28 July 2007. - P. 4291-4294. ↑
- C3028.** Erten E. Robust measurement of glacier surface motion from multiscale speckle tracking using local constraints. / Erten E., Reigber A., Jaeger M., Hellwich O. // 2007. IGARSS 2007. IEEE International Geoscience and Remote Sensing Symposium. - Barcelona, 23-28 July 2007. - P. 4237-4240. ↑
- C3029.** Byong Jun Hwang. Passive microwave signatures of autumnal sea ice types from ship-based observation. / Byong Jun Hwang, Ehn J.K., Galley R., Barber D.G. // 2007. IGARSS 2007. IEEE International Geoscience and Remote Sensing Symposium. - Barcelona, 23-28 July 2007. - P. 4245-4248. ↑
- C3030.** Belmonte A. First steps towards multimodal georeferencing of 3D VHR optical and X-band SAR imagery. / Belmonte A., Derauw D., Barbier C., Verly J.G. // 2007. IGARSS 2007. IEEE International Geoscience and Remote Sensing Symposium. - Barcelona, 23-28 July 2007. - P. 4933-4936. ↑
- C3031.** Abshire J.B. Lidar Approach for Measuring the CO2 Concentrations in the Troposphere from Space. / Abshire J.B., Riris H., Xiaoli Sun, Krainak M.A., Kawa R., Jian-Ping Mao, Pey-Schuan Jian, Burris J.F. // 2007. CLEO 2007. Conference on Lasers and Electro-Optics. - Baltimore, MD, 6-11 May 2007. - P. 1-2. ↑
- C3032.** Miles R.B. RADAR REMPI: A New Approach to Detection, Spectroscopy, and the Dynamics of Gases for Combustion, Fluid Dynamics and Homeland Defense. / Miles R.B., Zhili Zhang, Shneider M.N., Zaidi S.H. // 2007. CLEO 2007. Conference on Lasers and Electro-Optics. - Baltimore, MD, 6-11 May 2007. - P. 1-2. ↑

- C3033.** White S. Utilization of LIDAR and NOAA's Vertical Datum Transformation Tool (VDatum) for Shoreline Delineation. OCEANS 2007. - Vancouver, BC, Sept. 29 2007-Oct. 4 2007. - P. 1-6. ↑
- C3034.** Klare J. Image quality analysis of the vibrating sparse MIMO antenna array of the airborne 3D imaging radar ARTINO. / Klare J., Cerutti-Maori D., Brenner A., Ender J. // 2007. IGARSS 2007. IEEE International Geoscience and Remote Sensing Symposium. - Barcelona, 23-28 July 2007. - P. 5310-5314. ↑
- C3035.** Weiss M. A three dimensional SAR system on an UAV. / Weiss M., Peters O., Ender J. // 2007. IGARSS 2007. IEEE International Geoscience and Remote Sensing Symposium. - Barcelona, 23-28 July 2007. - P. 5315-5318. ↑
- C3036.** Valtr P. Implementation Issues of the Matched Field Processing Method of Refractivity Structure Sounding. / Valtr P., Pechac P., Kvicera V., Grabner M. // 2007. EuCAP 2007. The Second European Conference on Antennas and Propagation. - Edinburgh, 11-16 Nov. 2007. - P. 1-4. ↑
- C3037.** Nikolic M.M. Radar Estimation of Building Layouts Using Jump-Diffusion. / Nikolic M.M., Ortnier M., Nehorai A., Djordjevic A.R. // 2007. CAMPSAP 2007. 2nd IEEE International Workshop on Computational Advances in Multi-Sensor Adaptive Processing. - St. Thomas, VI, 12-14 Dec. 2007. - P. 177-180. ↑
- C3038.** Yu K.V. Application of Doppler Spectrum for Retrieval of Statistical Parameters of Sea Waves. / Yu K.V., Kanevsky M.B., Meshkov E.M. // 2007. EuCAP 2007. The Second European Conference on Antennas and Propagation. - Edinburgh, 11-16 Nov. 2007. - P. 1-6. ↑
- C3039.** Schuetz M. A mid-IR DIAL System Using Interband Cascade Laser Diodes. / Schuetz M., Bufton J., Prasad C.R. // 2007. CLEO 2007. Conference on Lasers and Electro-Optics. - Baltimore, MD, 6-11 May 2007. - P. 1-2. ↑
- C3040.** Liang-Hwei Lee. Building Corner Feature Extraction Based on Fusion Technique with Airborne LiDAR Data and Aerial Imagery. / Liang-Hwei Lee, Shyue S.-W., Ming-Jer Huang. // 2007. IIHMSP 2007. Third International Conference on Intelligent Information Hiding and Multimedia Signal Processing. - Kaohsiung, 26-28 Nov. 2007. - Vol. 1. - P. 43-46. ↑
- C3041.** Nouvel J.F. A low-cost imaging radar: DRIVE on board ONERA motorglider. / Nouvel J.F., Roques S., du Plessis O.R. // 2007. IGARSS 2007. IEEE International Geoscience and Remote Sensing Symposium. - Barcelona, 23-28 July 2007. - P. 5306-5309. ↑
- C3042.** Porter J. Lidar, sun photometer and polar nephelometer measurements: Remote sensing of aerosol size distribution properties. / Porter J., Bates D., Walterspiel J. // 2007. IGARSS 2007. IEEE International Geoscience and Remote Sensing Symposium. - Barcelona, 23-28 July 2007. - P. 5266-5267. ↑
- C3043.** Gimmestad G.G. A new type of lidar for atmospheric optical turbulence. / Gimmestad G.G., Roberts D.W., Stewart J.M., Wood J.W. // 2007. IGARSS 2007. IEEE International Geoscience and Remote Sensing Symposium. - Barcelona, 23-28 July 2007. - P. 5268-5271. ↑
- C3044.** Tatarov B. Lidar method for determination of quartz concentration in the tropospheric mineral aerosols. / Tatarov B., Sugimoto N., Matsui I. // 2007. IGARSS 2007. IEEE International Geoscience and Remote Sensing Symposium. - Barcelona, 23-28 July 2007. - P. 5262-5265. ↑
- C3045.** Lahtinen J. Improved receiver architecture for future L-band radiometer missions. / Lahtinen J., Piironen P., Colliander A. // 2007. IGARSS 2007. IEEE International Geoscience and Remote Sensing Symposium. - Barcelona, 23-28 July 2007. - P. 5247-5250. ↑
- C3046.** Lienert B. Advances in real time lidar spectroscopy. / Lienert B., Sharma S.K., Teng Chen, Madey M.J. // 2007. IGARSS 2007. IEEE International Geoscience and Remote Sensing Symposium. - Barcelona, 23-28 July 2007. - P. 5258-5261. ↑
- C3047.** Pepe A. A space-time minimum cost flow phase unwrapping algorithm for the generation of persistent scatterers deformation time-series. / Pepe A., Manunta M., Mazzarella G., Lanari R. // 2007. IGARSS 2007. IEEE International Geoscience and Remote Sensing Symposium. - Barcelona, 23-28 July 2007. - P. 5285-5288. ↑
- C3048.** Guarnieri A.M. A new framework for multi-pass SAR interferometry with distributed targets. / Guarnieri

A.M., Tebaldini S. // 2007. IGARSS 2007. IEEE International Geoscience and Remote Sensing Symposium. - Barcelona, 23-28 July 2007. - P. 5289-5293. ↑

C3049. Lombardini F. New potentials of differential SAR tomography: Volumetric differential interferometry and robust DEM generation. 2007. IGARSS 2007. IEEE International Geoscience and Remote Sensing Symposium. - Barcelona, 23-28 July 2007. - P. 5281-5284. ↑

C3050. Lachaise M. Multi baseline SAR acquisition concepts and phase unwrapping algorithms for the TanDEM-X mission. / Lachaise M., Eineder M., Fritz T. // 2007. IGARSS 2007. IEEE International Geoscience and Remote Sensing Symposium. - Barcelona, 23-28 July 2007. - P. 5272-5276. ↑

C3051. Fornaro G. Spaceborne multi-dimensional SAR imaging: Current status and perspectives. / Fornaro G., Lombardini F., Pardini M., Serafino F., Soldovieri F., Costantini M. // 2007. IGARSS 2007. IEEE International Geoscience and Remote Sensing Symposium. - Barcelona, 23-28 July 2007. - P. 5277-5280. ↑

C3052. Shkvarko Y.V. Remote Sensing Signature Fields Reconstruction Via Robust Regularization of Bayesian Minimum Risk Technique. / Shkvarko Y.V., Villalon-Turrubiates I.E., Leyva-Montiel J.L. // 2007. CAMPSAP 2007. 2nd IEEE International Workshop on Computational Advances in Multi-Sensor Adaptive Processing. - St. Thomas, VI, 12-14 Dec. 2007. - P. 237-240. ↑

C3053. Bawar Zahid Hasan. Inversion of residual errors to improve insar data acquisition, processing and interpretation. / Bawar Zahid Hasan, Long Teng, Tao Zeng. // 2007 IET International Conference on Radar Systems. - Edinburgh, UK, 15-18 Oct. 2007. - P. 1-4. ↑

C3054. Morrison N. The Gauss-Newton algorithm applied to track-while-scan radar. / Morrison N., Lord R.T., Inggs M.R. // 2007 IET International Conference on Radar Systems. - Edinburgh, UK, 15-18 Oct. 2007. - P. 1-5. ↑

C3055. Anderson S.J. Optimisation of bistatic HF surface wave radar configurations. 2007 IET International Conference on Radar Systems. - Edinburgh, UK, 15-18 Oct. 2007. - P. 1-4. ↑

C3056. Nandgaonkar A.B. Miniature wide-band microstrip patch antennas for GSM applications: A parametric study and optimum design. / Nandgaonkar A.B., Deosarkar S.B., Shirbahadurkar S.D. // 2007 IEEE Sarnoff Symposium. - Nassau Inn, Princeton, NJ, April 30 2007-May 2 2007. - P. 1-5. ↑

C3057. Morrison N. The Gauss-Newton algorithm in passive aircraft tracking using doppler and bearings. / Morrison N., Lord R.T., Inggs M.R. // 2007 IET International Conference on Radar Systems. - Edinburgh, UK, 15-18 Oct. 2007. - P. 1-5. ↑

C3058. Chitroub S. Independent Component Analysis of POLSAR Images. Relative Newton-Based Approach. / Chitroub S., Hachemi R. // 2007. ICSPC 2007. IEEE International Conference on Signal Processing and Communications. - Dubai, 24-27 Nov. 2007. - P. 684-687. ↑

C3059. Khazaal A. Brightness Temperature Maps Retrieval for the SMOS Space Mission: Regularized Inversion and Bias Reduction. / Khazaal A., Anterrieu E. // 2007. ICSPC 2007. IEEE International Conference on Signal Processing and Communications. - Dubai, 24-27 Nov. 2007. - P. 1323-1326. ↑

C3060. Al Suwaidi A.R. Determination of Earth Surface from TRMM Satellite Images. / Al Suwaidi A.R., Dawood A., Mubarak K., Matar G., Al Hammadi H. // 2007. ICSPC 2007. IEEE International Conference on Signal Processing and Communications. - Dubai, 24-27 Nov. 2007. - P. 580-583. ↑

C3061. Krieger G. TanDEM-X: A satellite formation for high-resolution SAR interferometry. / Krieger G., Fiedler H., Zink M., Hajnsek I., Younis M., Huber S., Bachmann M., Hueso Gonzalez J., Werner M., Moreira A. // 2007 IET International Conference on Radar Systems. - Edinburgh, UK, 15-18 Oct. 2007. - P. 1-5. ↑

C3062. Krieger G. Multidimensional waveform encoding for synthetic aperture radar remote sensing. / Krieger G., Gebert N., Moreira A. // 2007 IET International Conference on Radar Systems. - Edinburgh, UK, 15-18 Oct. 2007. - P. 1-5. ↑

C3063. Shoeb M. Source localization in view of urban sensing applications. / Shoeb M., Ahmad F., Amin M. // 2007. ISSPA 2007. 9th International Symposium on Signal Processing and Its Applications. - Sharjah, 12-15 Feb. 2007. - P. 1-4. ↑

- C3064.** Ya-Qiu Jin. Reconstruction of the Building Objects from Multi-Aspect High-Resolution SAR Images. / Ya-Qiu Jin, Feng Xu. // 2007. APMC 2007. Asia-Pacific Microwave Conference. - Bangkok, 11-14 Dec. 2007. - P. 1-4. ↑
- C3065.** Seker S.S. Electromagnetic Scattering Properties of Thin Curved Dielectric Surface and Cylinder. / Seker S.S., Apaydin G. // 2007. APMC 2007. Asia-Pacific Microwave Conference. - Bangkok, 11-14 Dec. 2007. - P. 1-4. ↑
- C3066.** Takano T. Performance of a Developed Low-Power and High-Sensitivity Cloud Profiling Millimeter-wave Radar: FALCON-I. / Takano T., Nakanishi Y., Abe H., Yamaguchi J., Yokote S.-I., Futaba K.-I., Kawamura Y., Kumagai H., Ohno Y., Takamura T., Nakajima T. // 2007. APMC 2007. Asia-Pacific Microwave Conference. - Bangkok, 11-14 Dec. 2007. - P. 1-4. ↑
- C3067.** Shahzad F. Stream Profile and Neotectonic Analysis in Hazara Kashmir Syntaxis using Shuttle Radar Digital Elevation Data. / Shahzad F., Mahmood S.A., Gloaguen R. // 2007. ICET 2007. International Conference on Emerging Technologies. - Islamabad, 12-13 Nov. 2007. - P. 84-88. ↑
- C3068.** Macfarlane D.G. SAFIRE: A close range real time millimetre wave radar for public education. / Macfarlane D.G., Robertson D.A. // 2007 and the 2007 15th International Conference on Terahertz Electronics. IRMMW-THz. Joint 32nd International Conference on Infrared and Millimeter Waves. - Cardiff, 2-9 Sept. 2007. - P. 924-925. ↑
- C3069.** Basturk A. Adaptive neuro-fuzzy inference system for speckle noise reduction in SAR images. / Basturk A., Emin Yuksel M. // 2007. ISSPA 2007. 9th International Symposium on Signal Processing and Its Applications. - Sharjah, 12-15 Feb. 2007. - P. 1-4. ↑
- C3070.** Setlur P. Urban target classifications using time-frequency micro-Doppler signatures. / Setlur P., Amin M., Ahmad F. // 2007. ISSPA 2007. 9th International Symposium on Signal Processing and Its Applications. - Sharjah, 12-15 Feb. 2007. - P. 1-4. ↑
- C3071.** Watanabe M. Forest monitoring by using L-band coherence. / Watanabe M., Sato M., Ouchi K., Shimada M., Haipeng Wang. // 2007. APMC 2007. Asia-Pacific Microwave Conference. - Bangkok, 11-14 Dec. 2007. - P. 1-4. ↑
- C3072.** Boerner W.-M. Recent Advancements of Radar Remote Sensing; Air- and Space-borne Multimodal SAR Remote Sensing in Forestry & Agriculture, Geology, Geophysics (Volcanology and Tectonology): Advances in POL-SAR, IN-SAR, POLinSAR and POL-DIFF-IN-SAR Sensing and Imaging with Applications to Environmental and Geodynamic Stress-change Monitoring. 2007. APMC 2007. Asia-Pacific Microwave Conference. - Bangkok, 11-14 Dec. 2007. - P. 1-4. ↑
- C3073.** Sato M. Polarimetric SAR observation by ALOS. / Sato M., Watanabe M., Iribe K. // 2007. APMC 2007. Asia-Pacific Microwave Conference. - Bangkok, 11-14 Dec. 2007. - P. 1-4. ↑
- C3074.** Sauer S. Physical parameter extraction over urban areas using L-band POLSAR data and interferometric baseline diversity. / Sauer S., Ferro-Famil L., Reigber A., Pottier E. // 2007. IGARSS 2007. IEEE International Geoscience and Remote Sensing Symposium. - Barcelona, 23-28 July 2007. - P. 5045-5048. ↑
- C3075.** Okada Y. Highly accurate DSM reconstruction using Ku-band airborne InSAR. / Okada Y., Hirao C., Horiuchi T., Hara Y., Yedidia J.S., Azarbayejani A., Oishi N. // 2007. IGARSS 2007. IEEE International Geoscience and Remote Sensing Symposium. - Barcelona, 23-28 July 2007. - P. 5049-5052. ↑
- C3076.** Nannini M. Height dependent motion compensation and coregistration for airborne SAR tomography. / Nannini M., Scheiber R. // 2007. IGARSS 2007. IEEE International Geoscience and Remote Sensing Symposium. - Barcelona, 23-28 July 2007. - P. 5041-5044. ↑
- C3077.** Barber B.C. Some polarimetric aspects of processing sea surface M-ATI SAR data. 2007. IGARSS 2007. IEEE International Geoscience and Remote Sensing Symposium. - Barcelona, 23-28 July 2007. - P. 5032-5036. ↑
- C3078.** Capozzoli A. A novel optimization approach to forest height reconstruction from multi-baseline data. / Capozzoli A., D'Elia G., Liseno A., Moreira A., Papathanassiou K.P. // 2007. IGARSS 2007. IEEE International Geoscience and Remote Sensing Symposium. - Barcelona, 23-28 July 2007. - P. 5037-5040. ↑

- C3079.** Buck C. Status and perspectives of GNSS-R at ESA. / Buck C., D'Addio S. // 2007. IGARSS 2007. IEEE International Geoscience and Remote Sensing Symposium. - Barcelona, 23-28 July 2007. - P. 5076-5079. ↑
- C3080.** Caparrini M. Oceanpal@: Monitoring sea state with a GNSS-R coastal instrument. / Caparrini M., Egido A., Soulat F., Germain O., Farres E., Dunne S., Ruffini G. // 2007. IGARSS 2007. IEEE International Geoscience and Remote Sensing Symposium. - Barcelona, 23-28 July 2007. - P. 5080-5083. ↑
- C3081.** Magnard C. High resolution millimeter wave SAR interferometry. / Magnard C., Meier E., Ruegg M., Brehm T., Essen H. // 2007. IGARSS 2007. IEEE International Geoscience and Remote Sensing Symposium. - Barcelona, 23-28 July 2007. - P. 5061-5064. ↑
- C3082.** Thiele A. Modeling and analyzing InSAR phase profiles at building locations. / Thiele A., Cadario E., Schulz K., Thoennessen U., Soergel U. // 2007. IGARSS 2007. IEEE International Geoscience and Remote Sensing Symposium. - Barcelona, 23-28 July 2007. - P. 5053-5056. ↑
- C3083.** Nohmi H. The repeat-pass interferometric SAR by Pi-SAR(L). / Nohmi H., Shimada M., Miyawaki M. // 2007. IGARSS 2007. IEEE International Geoscience and Remote Sensing Symposium. - Barcelona, 23-28 July 2007. - P. 5057-5060. ↑
- C3084.** Mason D.C. Using airborne laser altimetry to improve river flood extents delineated from SAR data. / Mason D.C., Dall'Amico J.T., Scott T.R., Horritt M.S., Bates P.D. // 2007. IGARSS 2007. IEEE International Geoscience and Remote Sensing Symposium. - Barcelona, 23-28 July 2007. - P. 5017-5020. ↑
- C3085.** Mora O. ICC's project for DInSAR terrain subsidence monitoring of the catalonian territory. / Mora O., Arbiol R., Pala V. // 2007. IGARSS 2007. IEEE International Geoscience and Remote Sensing Symposium. - Barcelona, 23-28 July 2007. - P. 4953-4956. ↑
- C3086.** Gonzalez-Huici M.A. Numerical simulation of electromagnetic-wave propagation for land mine detection using GPR. / Gonzalez-Huici M.A., Uschkerat U., Hoerdet A. // 2007. IGARSS 2007. IEEE International Geoscience and Remote Sensing Symposium. - Barcelona, 23-28 July 2007. - P. 4957-4960. ↑
- C3087.** Di Martino G. Disaster monitoring by extracting geophysical parameters from SAR data. / Di Martino G., Iodice A., Riccio D., Ruello G. // 2007. IGARSS 2007. IEEE International Geoscience and Remote Sensing Symposium. - Barcelona, 23-28 July 2007. - P. 4949-4952. ↑
- C3088.** Krieger G. Multidimensional radar waveforms a new paradigm for the design and operation of highly performant spaceborne synthetic aperture radar systems. / Krieger G., Gebert N., Moreira A. // 2007. IGARSS 2007. IEEE International Geoscience and Remote Sensing Symposium. - Barcelona, 23-28 July 2007. - P. 4937-4941. ↑
- C3089.** Min Wang. SBRAS-an advanced simulator of spaceborne radar. / Min Wang, Diannong Liang, Haifeng Huang, Zhen Dong. // 2007. IGARSS 2007. IEEE International Geoscience and Remote Sensing Symposium. - Barcelona, 23-28 July 2007. - P. 4942-4944. ↑
- C3090.** Heliere A. The EarthCARE mission: Mission concept and lidar instrument pre-development. / Heliere A., Lefebvre A., Wehr T., Bezy J.-L., Durand Y. // 2007. IGARSS 2007. IEEE International Geoscience and Remote Sensing Symposium. - Barcelona, 23-28 July 2007. - P. 4975-4978. ↑
- C3091.** Reagan J.A. Initial CRAM aerosol retrievals from CALIPSO and supporting airborne HSRL measurements. / Reagan J.A., McPherson C.J., Hostetler C.A., Hair J.W., Ferrare R.A. // 2007. IGARSS 2007. IEEE International Geoscience and Remote Sensing Symposium. - Barcelona, 23-28 July 2007. - P. 4979-4982. ↑
- C3092.** Straume-Lindner A.G. ADM-Aeolus: The first space-based high spectral resolution Doppler Wind Lidar. / Straume-Lindner A.G., Ingmann P. // 2007. IGARSS 2007. IEEE International Geoscience and Remote Sensing Symposium. - Barcelona, 23-28 July 2007. - P. 4969-4974. ↑
- C3093.** Singh D. An efficient electromagnetic approach to train the SVM for depth estimation of shallow buried objects with microwave remote sensing data. 2007. IGARSS 2007. IEEE International Geoscience and Remote Sensing Symposium. - Barcelona, 23-28 July 2007. - P. 4961-4964. ↑
- C3094.** Omar A. Extinction-to-backscatter ratios of lofted aerosol layers observed during the first three months

of CALYPSO measurements. / Omar A., Vaughan M., Liu Z., Hu Y., Reagan J., Winker D. // 2007. IGARSS 2007. IEEE International Geoscience and Remote Sensing Symposium. - Barcelona, 23-28 July 2007. - P. 4965-4968. ↑

C3095. Helm A. Status of GNSS reflectometry related receiver developments and feasibility studies within the German Indonesian Tsunami Early Warning System. / Helm A., Stosius R., Beyerle G., Montenbruck O., Rothacher M. // 2007. IGARSS 2007. IEEE International Geoscience and Remote Sensing Symposium. - Barcelona, 23-28 July 2007. - P. 5084-5087. ↑

C3096. Younis M. Performance Prediction and Verification for the Synchronization Link of TanDEM-X. / Younis M., Metzger R., Krieger G., Bachmann M., Klein R. // 2007. IGARSS 2007. IEEE International Geoscience and Remote Sensing Symposium. - Barcelona, 23-28 July 2007. - P. 5206-5209. ↑

C3097. Nicoll J. Prediction and detection of Faraday rotation in ALOS PALSAR data. / Nicoll J., Meyer F., Jehle M. // 2007. IGARSS 2007. IEEE International Geoscience and Remote Sensing Symposium. - Barcelona, 23-28 July 2007. - P. 5210-5213. ↑

C3098. Brautigam B. Individual T/R module characterisation of the TerraSAR-X active phased array antenna by calibration pulse sequences with orthogonal codes. / Brautigam B., Schwerdt M., Bachmann M., Stangl M. // 2007. IGARSS 2007. IEEE International Geoscience and Remote Sensing Symposium. - Barcelona, 23-28 July 2007. - P. 5202-5205. ↑

C3099. Sang-Eun Park. Inversion of soil moisture content from L- and P-band AIRSAR polarimetric SAR data. / Sang-Eun Park, Moon W.M. // 2007. IGARSS 2007. IEEE International Geoscience and Remote Sensing Symposium. - Barcelona, 23-28 July 2007. - P. 5194-5197. ↑

C3100. Zaugg E.C. Full motion compensation for LFM-CW synthetic aperture radar. / Zaugg E.C., Long D.G. // 2007. IGARSS 2007. IEEE International Geoscience and Remote Sensing Symposium. - Barcelona, 23-28 July 2007. - P. 5198-5201. ↑

C3101. Tello M. Characterization of local regularity in SAR Imagery by means of multiscale techniques: application to oil spill detection. / Tello M., Lopez-Martinez C., Mallorqui J.J., Danisi A., Di Martino G., Iodice A., Ruello G., Riccio D. // 2007. IGARSS 2007. IEEE International Geoscience and Remote Sensing Symposium. - Barcelona, 23-28 July 2007. - P. 5228-5231. ↑

C3102. Lambrigtsen B. Developing a GeoSTAR science mission. / Lambrigtsen B., Tanner A., Gaier T., Kangaslahti P., Brown S. // 2007. IGARSS 2007. IEEE International Geoscience and Remote Sensing Symposium. - Barcelona, 23-28 July 2007. - P. 5232-5236. ↑

C3103. Lopez-Martinez C. Analysis and improvement of polarimetric calibration techniques. / Lopez-Martinez C., Cortes A., Fabregas X. // 2007. IGARSS 2007. IEEE International Geoscience and Remote Sensing Symposium. - Barcelona, 23-28 July 2007. - P. 5224-5227. ↑

C3104. Borner T. ALOS PALSAR products verification. / Borner T., Papathanassiou K.P., Marquart N., Zink M., Meininger M., Meadows P.J., Rye A.J., Wright P., Rosich Tell B. // 2007. IGARSS 2007. IEEE International Geoscience and Remote Sensing Symposium. - Barcelona, 23-28 July 2007. - P. 5214-5217. ↑

C3105. Croci R. Calibration of the SHARAD Instrument. / Croci R., Fois F., Guelfi M., Noschese P., Mecozzi R., Seu R. // 2007. IGARSS 2007. IEEE International Geoscience and Remote Sensing Symposium. - Barcelona, 23-28 July 2007. - P. 5218-5223. ↑

C3106. Kelly J. Subaperture analysis of polarimetric SAR imagery. / Kelly J., Ainsworth T.L., Lee J.-S. // 2007. IGARSS 2007. IEEE International Geoscience and Remote Sensing Symposium. - Barcelona, 23-28 July 2007. - P. 5190-5193. ↑

C3107. Paradella W.R. Evaluation of the altimetric information from RADARSAT-1, ASTER and SRTM data for topographic mapping in the Amazon Region. / Paradella W.R., de Oliveira C.G. // 2007. IGARSS 2007. IEEE International Geoscience and Remote Sensing Symposium. - Barcelona, 23-28 July 2007. - P. 5134-5137. ↑

C3108. Chen V.C. Joint time-frequency analysis for radar signal and imaging. 2007. IGARSS 2007. IEEE International Geoscience and Remote Sensing Symposium. - Barcelona, 23-28 July 2007. - P. 5166-5169. ↑

- C3109.** Vignudelli S. ALTICORE-A consortium serving european seas with coastal altimetry. / Vignudelli S., Roblou L., Snaith H.M., Cipollini P., Venuti F., Kostianoy A., Ginzburg A., Lyard F., Cretaux J.F., Birol F., Lebedev S., Sirota A., Medvedev D., Khlebnikova S., Mamedov R., Ismatova K., Alyev A., Nabiyeu T. // 2007. IGARSS 2007. IEEE International Geoscience and Remote Sensing Symposium. - Barcelona, 23-28 July 2007. - P. 5125-5128. ↑
- C3110.** Meehan T.K. TOGA, a prototype for an optimal orbiting GNSS-R instrument. / Meehan T.K., Esterhuizen S., Franklin G.W., Lowe S., Munson T.N., Robison D., Spitzmesser D.J., Tien J.Y.T., Young L.E. // 2007. IGARSS 2007. IEEE International Geoscience and Remote Sensing Symposium. - Barcelona, 23-28 July 2007. - P. 5109-5112. ↑
- C3111.** Martinez-Benjamin J.J. Altimetric calibration experiences in the Western Mediterranean. / Martinez-Benjamin J.J., Garcia M.M., Davila J.M., Garate J., Castellon M.A.O., Talaya J., Baron A., Velasco G.R., Bonnefond P., Perez B. // 2007. IGARSS 2007. IEEE International Geoscience and Remote Sensing Symposium. - Barcelona, 23-28 July 2007. - P. 5121-5124. ↑
- C3112.** Ferro-Famil L. Complex scene analysis from Time-Frequency statistics of POLSAR data. / Ferro-Famil L., Reigber A. // 2007. IGARSS 2007. IEEE International Geoscience and Remote Sensing Symposium. - Barcelona, 23-28 July 2007. - P. 5182-5185. ↑
- C3113.** Duquenoy M. Characterization of scatterers by their anisotropic and dispersive behavior. / Duquenoy M., Ovarlez J.-P., Ferro-Famil L., Pottier E., Vignaud L. // 2007. IGARSS 2007. IEEE International Geoscience and Remote Sensing Symposium. - Barcelona, 23-28 July 2007. - P. 5186-5189. ↑
- C3114.** Kersten P.R. The cross Time-Frequency Distribution Series for Synthetic Aperture Radar (SAR) applications. / Kersten P.R., Jansen R.W., Ainsworth T.L. // 2007. IGARSS 2007. IEEE International Geoscience and Remote Sensing Symposium. - Barcelona, 23-28 July 2007. - P. 5178-5181. ↑
- C3115.** Mengmeng Zhu. An improved time-frequency phase adjustment technique for ISAR. / Mengmeng Zhu, Junfeng Wang, Xingzhao Liu. // 2007. IGARSS 2007. IEEE International Geoscience and Remote Sensing Symposium. - Barcelona, 23-28 July 2007. - P. 5170-5173. ↑
- C3116.** Amein A.S. The fractional Fourier transform and its application to high resolution SAR imaging. / Amein A.S., Soraghan J.J. // 2007. IGARSS 2007. IEEE International Geoscience and Remote Sensing Symposium. - Barcelona, 23-28 July 2007. - P. 5174-5177. ↑
- C3117.** Toyota T. Retrieval of ice thickness distribution in the seasonal ice zone from L-band SAR. / Toyota T., Ohshima K.I., Ebuchi N., Nakamura K., Uto S. // 2007. IGARSS 2007. IEEE International Geoscience and Remote Sensing Symposium. - Barcelona, 23-28 July 2007. - P. 3997-4000. ↑
- C3118.** Gregorio E. Perspective of remote optical measurement techniques (ROMTs). / Gregorio E., Rocadenbosch F. // 2007. IGARSS 2007. IEEE International Geoscience and Remote Sensing Symposium. - Barcelona, 23-28 July 2007. - P. 2955-2958. ↑
- C3119.** Jinghui Fan. Mapping subsidence in Tianjin area using ASAR images based on PS technique. / Jinghui Fan, Xiaofang Guo, Huadong Guo, Zhengmin He, Daqing Ge, Shengwei Liu. // 2007. IGARSS 2007. IEEE International Geoscience and Remote Sensing Symposium. - Barcelona, 23-28 July 2007. - P. 2975-2978. ↑
- C3120.** Ribo S. ASAP, towards a PARIS instrument for space. / Ribo S., Arco J.C., Cardellach E., Nogues-Correig O., Rius A., Alvarez M.T., Tabero J. // 2007. IGARSS 2007. IEEE International Geoscience and Remote Sensing Symposium. - Barcelona, 23-28 July 2007. - P. 2916-2919. ↑
- C3121.** Gunay A. Semi-automatic true orthophoto production by using LIDAR data. / Gunay A., Arefi H., Hahn M. // 2007. IGARSS 2007. IEEE International Geoscience and Remote Sensing Symposium. - Barcelona, 23-28 July 2007. - P. 2873-2876. ↑
- C3122.** Guangjian Yan. An airborne multi-angle power line inspection system. / Guangjian Yan, Junfa Wang, Qiang Liu, Lin Su, Pengxin Wang, Junming Liu, Wuming Zhang, Zhiqiang Xiao. // 2007. IGARSS 2007. IEEE International Geoscience and Remote Sensing Symposium. - Barcelona, 23-28 July 2007. - P. 2913-2915. ↑
- C3123.** Tomas R. DInSAR monitoring of land subsidence in Orihuela City, Spain: Comparison with geotechnical data. / Tomas R., Lopez-Sanchez J.M., Delgado J., Vicente F., Cuenca A., Mallorqui J.J., Blanco

P., Duque S. // 2007. IGARSS 2007. IEEE International Geoscience and Remote Sensing Symposium. - Barcelona, 23-28 July 2007. - P. 3027-3030. ↑

C3124. Vega M.A. Student developed meteorological radar network for the western part of Puerto Rico: First node. / Vega M.A., Colom J.G. // 2007. IGARSS 2007. IEEE International Geoscience and Remote Sensing Symposium. - Barcelona, 23-28 July 2007. - P. 3057-3059. ↑

C3125. Ferrucci F. 3-D tsunami coastal hazard mapping in Sri Lanka by very-high resolution, airborne and spaceborne remote-sensing. / Ferrucci F., Rocca F., Calabretta G., Savio G., Coren F., Sterzai P., Hirn B. // 2007. IGARSS 2007. IEEE International Geoscience and Remote Sensing Symposium. - Barcelona, 23-28 July 2007. - P. 3018-3021. ↑

C3126. Hosokawa M. Earthquake damage detection using remote sensing data. / Hosokawa M., Byeong-pyo Jeong. // 2007. IGARSS 2007. IEEE International Geoscience and Remote Sensing Symposium. - Barcelona, 23-28 July 2007. - P. 2989-2991. ↑

C3127. Hirn B. Improvement and validation of MODIS performance in automated detection and extent estimate of wildfires. / Hirn B., Di Bartola C., Ferrucci F. // 2007. IGARSS 2007. IEEE International Geoscience and Remote Sensing Symposium. - Barcelona, 23-28 July 2007. - P. 3004-3007. ↑

C3128. Schull M. Retrieving 3D canopy structure from synergistic analysis of multi-angle and lidar data. / Schull M., Ganguly S., Samanta A., Jenkins J., Knyazikhin Y., Myneni R.B., Dong Huang. // 2007. IGARSS 2007. IEEE International Geoscience and Remote Sensing Symposium. - Barcelona, 23-28 July 2007. - P. 2833-2835. ↑

C3129. Munoz C. Speed measurements with a continuous wave lidar prototype. / Munoz C., Rodriguez A., Comeron A., Batet O., Garcia D., Rocadenbosch F., Sicard M. // 2007. IGARSS 2007. IEEE International Geoscience and Remote Sensing Symposium. - Barcelona, 23-28 July 2007. - P. 2775-2778. ↑

C3130. Tomas S. A wind speed and fluctuation simulator for characterizing the wind lidar correlation method. / Tomas S., Sicard M., Masjuan J., Reba M.N.M., Munoz C., Rocadenbosch F. // 2007. IGARSS 2007. IEEE International Geoscience and Remote Sensing Symposium. - Barcelona, 23-28 July 2007. - P. 2779-2782. ↑

C3131. Rocadenbosch F. Statistical considerations on the extinction error variance for the raman lidar inversion algorithm. / Rocadenbosch F., Comeron A., Sicard M., Reba M.N.M. // 2007. IGARSS 2007. IEEE International Geoscience and Remote Sensing Symposium. - Barcelona, 23-28 July 2007. - P. 2771-2774. ↑

C3132. Sicard M. Intercomparison of spanish advanced lidars in the framework of EARLINET. / Sicard M., Reba M.N.M., Rocadenbosch F., Gregorio E., Kumar D., Tomas S., Comeron A., Molero F., Pujadas M., Guerrero-Rascado J.L., Pedros R., Martinez J.A. // 2007. IGARSS 2007. IEEE International Geoscience and Remote Sensing Symposium. - Barcelona, 23-28 July 2007. - P. 2763-2766. ↑

C3133. Martucci G. Lidar determination of the frequency of variations of the boundary-layer top. / Martucci G., Matthey R., Mitev V., Richner H. // 2007. IGARSS 2007. IEEE International Geoscience and Remote Sensing Symposium. - Barcelona, 23-28 July 2007. - P. 2767-2770. ↑

C3134. Kenyi L. Comparison of SRTM-NED data to LIDAR derived canopy metrics. / Kenyi L., Dubayah R., Hofton M., Blair J.B., Schardt M. // 2007. IGARSS 2007. IEEE International Geoscience and Remote Sensing Symposium. - Barcelona, 23-28 July 2007. - P. 2825-2829. ↑

C3135. Moorthy I. Extracting tree crown properties from ground-based scanning laser data. / Moorthy I., Miller J.R., Berni J.A.J., Zarco-Tejada P.J., Qingmou Li. // 2007. IGARSS 2007. IEEE International Geoscience and Remote Sensing Symposium. - Barcelona, 23-28 July 2007. - P. 2830-2832. ↑

C3136. Shuki Chaw. Intercomparison of Calibration techniques for the 1064nm channel on a Nd:YAG elastic lidar. / Shuki Chaw, Yonghua Wu, Gross B., Moshary F., Ahmed S. // 2007. IGARSS 2007. IEEE International Geoscience and Remote Sensing Symposium. - Barcelona, 23-28 July 2007. - P. 2791-2794. ↑

C3137. Brousmiche S. Numerical simulation of a heterodyne Doppler LIDAR for wind measurement in a turbulent atmospheric boundary layer. / Brousmiche S., Bricteux L., Sobieski P., Macq B., Winckelmans G. // 2007. IGARSS 2007. IEEE International Geoscience and Remote Sensing Symposium. - Barcelona, 23-28 July 2007. - P. 2783-2786. ↑

- C3138.** Lindelow P. Coherent lidar modulated with frequency stepped pulse trains for unambiguous high duty cycle range and velocity sensing in the atmosphere. / Lindelow P., Mohr J.J. // 2007. IGARSS 2007. IEEE International Geoscience and Remote Sensing Symposium. - Barcelona, 23-28 July 2007. - P. 2787-2790. ↑
- C3139.** Ramirez N.D. An algorithm to improve the NEXRAD rain rate estimates. / Ramirez N.D., Cruz-Pol S., Xiomara Ortiz, Castro J.M., Kuliwoski R. // 2007. IGARSS 2007. IEEE International Geoscience and Remote Sensing Symposium. - Barcelona, 23-28 July 2007. - P. 3060-3064. ↑
- C3140.** Schulz-Stellenfleth J. Use of tandem pairs of ERS-2 and ENVISAT SAR data for the analysis of oceanographic and atmospheric processes. / Schulz-Stellenfleth J., Lehner S., Konig T., Reppucci A., Brusch S. // 2007. IGARSS 2007. IEEE International Geoscience and Remote Sensing Symposium. - Barcelona, 23-28 July 2007. - P. 3265-3268. ↑
- C3141.** Vesecky J.F. Measurements of eddies in the ocean surface wind field by a mix of single and multiple-frequency HF radars on monterey bay california. / Vesecky J.F., Drake J., Laws K., Ludwig F.L., Teague C.C., Paduan J.D., Sinton D. // 2007. IGARSS 2007. IEEE International Geoscience and Remote Sensing Symposium. - Barcelona, 23-28 July 2007. - P. 3269-3272. ↑
- C3142.** Rodriguez M.H. Cantarell natural seep modelling using SAR derived ocean surface wind and meteo-oceanographic buoy data. / Rodriguez M.H., Bannerman K., Caceres R.G., de Miranda F.P., Pedroso E.C. // 2007. IGARSS 2007. IEEE International Geoscience and Remote Sensing Symposium. - Barcelona, 23-28 July 2007. - P. 3257-3260. ↑
- C3143.** Hyun-chong Cho. Morphological segmentation of Lidar Digital Elevation Models to extract stream channels in forested terrain. / Hyun-chong Cho, Kampa K., Slatton K.C. // 2007. IGARSS 2007. IEEE International Geoscience and Remote Sensing Symposium. - Barcelona, 23-28 July 2007. - P. 3182-3185. ↑
- C3144.** Jiang Jinbao. Study on inversion models for the severity of winter wheat stripe rust using hyperspectral remote sensing. / Jiang Jinbao, Chen Yunhao, Gong Adu, Li Jing. // 2007. IGARSS 2007. IEEE International Geoscience and Remote Sensing Symposium. - Barcelona, 23-28 July 2007. - P. 3186-3189. ↑
- C3145.** Lehner S. Validation of an X-Band SAR Wind Algorithm by SIR-C/X SAR Data. / Lehner S., Schulz-Stellenfleth J., Brusch S., Eineder M. // 2007. IGARSS 2007. IEEE International Geoscience and Remote Sensing Symposium. - Barcelona, 23-28 July 2007. - P. 3285-3288. ↑
- C3146.** Guiting Song. Validation of a new empirical SAR algorithm. / Guiting Song, Lehner S., Schulz-Stellenfleth J., Breit H., Grassl H. // 2007. IGARSS 2007. IEEE International Geoscience and Remote Sensing Symposium. - Barcelona, 23-28 July 2007. - P. 3289-3292. ↑
- C3147.** Konig T. Global analysis of a 2 Year ERS-2 wavemode dataset over the oceans. / Konig T., Lehner S., Schulz-Stellenfleth J. // 2007. IGARSS 2007. IEEE International Geoscience and Remote Sensing Symposium. - Barcelona, 23-28 July 2007. - P. 3281-3284. ↑
- C3148.** Cameron I.D. A novel method for estimating offshore wind fields using synthetic aperture radar and meteorological model data. / Cameron I.D., Woodhouse I.H., Walker N. // 2007. IGARSS 2007. IEEE International Geoscience and Remote Sensing Symposium. - Barcelona, 23-28 July 2007. - P. 3273-3276. ↑
- C3149.** Zecchetto S. Computation of wind direction from SAR images without external a priori information. / Zecchetto S., De Biasio F., Trivero P. // 2007. IGARSS 2007. IEEE International Geoscience and Remote Sensing Symposium. - Barcelona, 23-28 July 2007. - P. 3277-3280. ↑
- C3150.** Collin A. Statistical classification methodology of SHOALS 3000 backscatter to mapping coastal benthic habitats. / Collin A., Cottin A., Long B., Archambault P., Kuus P., Clarke J.H., Sohn G., Miller J. // 2007. IGARSS 2007. IEEE International Geoscience and Remote Sensing Symposium. - Barcelona, 23-28 July 2007. - P. 3178-3181. ↑
- C3151.** Lijun Zhang. Lidar application in selection and design of power line route. / Lijun Zhang, Qiu Li, Zizheng Wang, Huijie Liu, Zhongsheng Li, Yao Gui, Kletzli R., Xiaodong Yang, Shuming Chen, Yanjing Liu. // 2007. IGARSS 2007. IEEE International Geoscience and Remote Sensing Symposium. - Barcelona, 23-28 July 2007. - P. 3109-3111. ↑
- C3152.** Calla O.P.N. Comparison of measured scattering coefficient of dry soil at X-band with the scattering

coefficient estimated using the dielectric constant. / Calla O.P.N., Harit K.C., Vyas R., Bohra D., Mishra S.K. // 2007. IGARSS 2007. IEEE International Geoscience and Remote Sensing Symposium. - Barcelona, 23-28 July 2007. - P. 3135-3137. ↑

C3153. Forghani A. Object-based classification of multi-sensor optical imagery to generate terrain surface roughness information for input to wind risk simulation. / Forghani A., Cechet B., Nadimpalli K. // 2007. IGARSS 2007. IEEE International Geoscience and Remote Sensing Symposium. - Barcelona, 23-28 July 2007. - P. 3090-3095. ↑

C3154. Lim S. Reflectivity retrieval in a networked radar environment: Demonstration from the CASA IP1 radar network. / Lim S., Chandrasekar V., Lee P., Jayasumana A.P. // 2007. IGARSS 2007. IEEE International Geoscience and Remote Sensing Symposium. - Barcelona, 23-28 July 2007. - P. 3065-3068. ↑

C3155. Sun Yonghua. A study on optical and SAR data fusion for extracting flooded area. / Sun Yonghua, Li Xiaojuan, Gong Huili, Zhao Wenji, Gong Zhaoning. // 2007. IGARSS 2007. IEEE International Geoscience and Remote Sensing Symposium. - Barcelona, 23-28 July 2007. - P. 3086-3089. ↑

C3156. Long B. What optech's bathymetric LiDAR sees underwater. / Long B., Cottin A., Collin A. // 2007. IGARSS 2007. IEEE International Geoscience and Remote Sensing Symposium. - Barcelona, 23-28 July 2007. - P. 3170-3173. ↑

C3157. Churnside J.H. LIDAR detection of plankton in the ocean. 2007. IGARSS 2007. IEEE International Geoscience and Remote Sensing Symposium. - Barcelona, 23-28 July 2007. - P. 3174-3177. ↑

C3158. Wei Gong. CALIPSO-AERONET Combined Application for Weather and Climate Research. / Wei Gong, Yingying Ma, Zhongmin Zhu, Pingxiang Li, Shalei Song, Mengyu Liu, Zhongyu Hao. // 2007. IGARSS 2007. IEEE International Geoscience and Remote Sensing Symposium. - Barcelona, 23-28 July 2007. - P. 3166-3169. ↑

C3159. Md Reba M.N. Piece-wise variance method for signal-to-noise ratio estimation in elastic/Raman lidar signals. / Md Reba M.N., Rocadenbosch F., Sicard M., Munoz C., Tomas S. // 2007. IGARSS 2007. IEEE International Geoscience and Remote Sensing Symposium. - Barcelona, 23-28 July 2007. - P. 3158-3161. ↑

C3160. Gregorio E. Design methodology of a ceilometer lidar prototype. / Gregorio E., Rocadenbosch F., Comeron A. // 2007. IGARSS 2007. IEEE International Geoscience and Remote Sensing Symposium. - Barcelona, 23-28 July 2007. - P. 3162-3165. ↑

C3161. Dehmollaian M. Refocusing through single layer building wall using synthetic aperture radar. / Dehmollaian M., Sarabandi K. // 2007. IGARSS 2007. IEEE International Geoscience and Remote Sensing Symposium. - Barcelona, 23-28 July 2007. - P. 2558-2561. ↑

C3162. Guoqing Sun. Simulation studies of forest structure using 3D lidar and radar models. / Guoqing Sun, Ranson K.J., Dawei Liu, Koetz B. // 2007. IGARSS 2007. IEEE International Geoscience and Remote Sensing Symposium. - Barcelona, 23-28 July 2007. - P. 2562-2565. ↑

C3163. He Zhan. Half-space born approximation modeling and inversion for cross-well radar sensing of contaminants in soil. / He Zhan, Morgenthaler A., Qiuzhao Dong, Rappaport C., Miller E. // 2007. IGARSS 2007. IEEE International Geoscience and Remote Sensing Symposium. - Barcelona, 23-28 July 2007. - P. 2550-2553. ↑

C3164. Portabella M. ASCAT scatterometer ocean calibration. / Portabella M., Stoffelen A., Verspeek J., Verhoef A., Vogelzang J. // 2007. IGARSS 2007. IEEE International Geoscience and Remote Sensing Symposium. - Barcelona, 23-28 July 2007. - P. 2539-2542. ↑

C3165. Monsivais-Huertero A. Scattering from sahelian grassland: a coherent modeling. / Monsivais-Huertero A., Chenerie I., Sarabandi K. // 2007. IGARSS 2007. IEEE International Geoscience and Remote Sensing Symposium. - Barcelona, 23-28 July 2007. - P. 2543-2545. ↑

C3166. Aixia Dou. Technique of remote sensing image processing in active faults survey. / Aixia Dou, Xiaoqing Wang, Guoyan Wang, Dongliang Wang. // 2007. IGARSS 2007. IEEE International Geoscience and Remote Sensing Symposium. - Barcelona, 23-28 July 2007. - P. 2609-2612. ↑

C3167. Boerner W.-M. Need for developing repeat-pass differential POLSAR interferometry. / Boerner W.-M.,

Kun-Shan Chen. // 2007. IGARSS 2007. IEEE International Geoscience and Remote Sensing Symposium. - Barcelona, 23-28 July 2007. - P. 2613-2615. ↑

C3168. Karvonen J. SAR-based estimation of the baltic sea ice motion. / Karvonen J., Simila M., Lehtiranta J. // 2007. IGARSS 2007. IEEE International Geoscience and Remote Sensing Symposium. - Barcelona, 23-28 July 2007. - P. 2605-2608. ↑

C3169. Demontoux F. Inversion model validation of ground emissivity. Contribution to the development of SMOS algorithm. / Demontoux F., Le Crom B., Ruffle G., Wigneron J.P., Grant J., Hernandez D.M. // 2007. IGARSS 2007. IEEE International Geoscience and Remote Sensing Symposium. - Barcelona, 23-28 July 2007. - P. 2570-2573. ↑

C3170. Fan Wu. Change detection and analysis with radarsat-1 SAR image. / Fan Wu, Chao Wang, Hong Zhang, Bo Zhang. // 2007. IGARSS 2007. IEEE International Geoscience and Remote Sensing Symposium. - Barcelona, 23-28 July 2007. - P. 2601-2604. ↑

C3171. Nadai A. Dependency analysis of normalized radar cross section of ocean surface on ocean winds using an airborne dual-frequency polarimetric SAR. / Nadai A., Umehara T., Matsuoka T., Satake M., Uratsuka S. // 2007. IGARSS 2007. IEEE International Geoscience and Remote Sensing Symposium. - Barcelona, 23-28 July 2007. - P. 2535-2538. ↑

C3172. Parrish C.E. Exploiting full-waveform lidar data and multiresolution wavelet analysis for vertical object detection and recognition. 2007. IGARSS 2007. IEEE International Geoscience and Remote Sensing Symposium. - Barcelona, 23-28 July 2007. - P. 2499-2502. ↑

C3173. Songxin Tan. Detection of foliage-obscured vehicle using a multiwavelength polarimetric lidar. / Songxin Tan, Stoker J., Greenlee S. // 2007. IGARSS 2007. IEEE International Geoscience and Remote Sensing Symposium. - Barcelona, 23-28 July 2007. - P. 2503-2506. ↑

C3174. Teague C.C. Two-dimensional surface river flow patterns measured with paired riversondes. / Teague C.C., Barrick D.E., Lilleboe P.M., Cheng R.T. // 2007. IGARSS 2007. IEEE International Geoscience and Remote Sensing Symposium. - Barcelona, 23-28 July 2007. - P. 2491-2494. ↑

C3175. Cao Fang. The Comparison of the V-Fold and the Monte-Carlo cross validation to estimate the number of clusters for the fully polarimetric sar data segmentation. / Cao Fang, Hong Wen, Wu Yirong, Pottier E. // 2007. IGARSS 2007. IEEE International Geoscience and Remote Sensing Symposium. - Barcelona, 23-28 July 2007. - P. 2485-2486. ↑

C3176. Whitcomb J. Wetlands map of Alaska using L-Band radar satellite imagery. / Whitcomb J., Moghaddam M., McDonald K., Podest E., Kelndorfer J. // 2007. IGARSS 2007. IEEE International Geoscience and Remote Sensing Symposium. - Barcelona, 23-28 July 2007. - P. 2487-2490. ↑

C3177. Yijun He. A comparison of models for retrieving high wind speeds. / Yijun He, Hui Shen, Jie Guo, Perrie W. // 2007. IGARSS 2007. IEEE International Geoscience and Remote Sensing Symposium. - Barcelona, 23-28 July 2007. - P. 2527-2530. ↑

C3178. Hui Shen. On SAR hurricane wind speed ambiguities. / Hui Shen, Perrie W., Yijun He. // 2007. IGARSS 2007. IEEE International Geoscience and Remote Sensing Symposium. - Barcelona, 23-28 July 2007. - P. 2531-2534. ↑

C3179. Soisuvann S. A geophysical model function for windsat polarimetric radiometer wind retrievals using linear polarizations. / Soisuvann S., Jelenak Z., Chang P.S. // 2007. IGARSS 2007. IEEE International Geoscience and Remote Sensing Symposium. - Barcelona, 23-28 July 2007. - P. 2523-2526. ↑

C3180. Auer S. Automatic extraction of salient geometric entities from LIDAR point clouds. / Auer S., Hinz S. // 2007. IGARSS 2007. IEEE International Geoscience and Remote Sensing Symposium. - Barcelona, 23-28 July 2007. - P. 2507-2510. ↑

C3181. Starek M.J. Automatic feature extraction from airborne lidar measurements to identify cross-shore morphologies indicative of beach erosion. / Starek M.J., Vemula R.K., Slatton K.C., Shrestha R.L., Carter W.E. // 2007. IGARSS 2007. IEEE International Geoscience and Remote Sensing Symposium. - Barcelona, 23-28 July 2007. - P. 2511-2514. ↑

- C3182.** Ainsworth T.L. Quad-polarimetry and interferometry from repeat-pass dual-polarimetric SAR imagery. / Ainsworth T.L., Preiss M., Stacy N., Lee J.-S. // 2007. IGARSS 2007. IEEE International Geoscience and Remote Sensing Symposium. - Barcelona, 23-28 July 2007. - P. 2616-2619. ↑
- C3183.** Donovan B.C. Simulation of minimal infrastructure short-range radar networks. / Donovan B.C., McLaughlin D.J., Zink M., Kurose J. // 2007. IGARSS 2007. IEEE International Geoscience and Remote Sensing Symposium. - Barcelona, 23-28 July 2007. - P. 2734-2737. ↑
- C3184.** Fritz J. Implementation of a new refractivity estimation algorithm on a network of S-band radars. / Fritz J., Chandrasekar V. // 2007. IGARSS 2007. IEEE International Geoscience and Remote Sensing Symposium. - Barcelona, 23-28 July 2007. - P. 2738-2741. ↑
- C3185.** Junyent F. Radar network characterization. / Junyent F., Chandrasekar V. // 2007. IGARSS 2007. IEEE International Geoscience and Remote Sensing Symposium. - Barcelona, 23-28 July 2007. - P. 2730-2733. ↑
- C3186.** Brunner D. Building characterisation in VHR SAR data acquired under controlled EMSL conditions. / Brunner D., Lemoine G., Fortuny J., Bruzzone L. // 2007. IGARSS 2007. IEEE International Geoscience and Remote Sensing Symposium. - Barcelona, 23-28 July 2007. - P. 2694-2697. ↑
- C3187.** Trabal J.M. Rainfall estimation and rain gauge comparison for x-band polarimetric CASA radars. / Trabal J.M., McLaughlin D.J. // 2007. IGARSS 2007. IEEE International Geoscience and Remote Sensing Symposium. - Barcelona, 23-28 July 2007. - P. 2726-2729. ↑
- C3188.** Yuxiang Liu. Real-time three-dimensional radar mosaic in CASA IP1 testbed. / Yuxiang Liu, Yanting Wang, Chandrasekar V., Bringi V.N. // 2007. IGARSS 2007. IEEE International Geoscience and Remote Sensing Symposium. - Barcelona, 23-28 July 2007. - P. 2754-2757. ↑
- C3189.** Arias D. A grid based weather radar data retrieval and processing framework. / Arias D., Sanabria J., Rivera W. // 2007. IGARSS 2007. IEEE International Geoscience and Remote Sensing Symposium. - Barcelona, 23-28 July 2007. - P. 2758-2762. ↑
- C3190.** Colom J.G. Phase shifter system using vector modulation for xband phased array radar applications. / Colom J.G., Giraldo Castaneda L., Knapp E. // 2007. IGARSS 2007. IEEE International Geoscience and Remote Sensing Symposium. - Barcelona, 23-28 July 2007. - P. 2750-2753. ↑
- C3191.** Bharadwaj N. Evaluation of first generation CASA radar waveforms in the IP1 testbed. / Bharadwaj N., Chandrasekar V., Junyent F. // 2007. IGARSS 2007. IEEE International Geoscience and Remote Sensing Symposium. - Barcelona, 23-28 July 2007. - P. 2742-2745. ↑
- C3192.** Marrero-Fontanez V.J. Low cross-polarization antenna array for CASA's student test bed radar. / Marrero-Fontanez V.J., Rodriguez-Solis R.A. // 2007. IGARSS 2007. IEEE International Geoscience and Remote Sensing Symposium. - Barcelona, 23-28 July 2007. - P. 2746-2749. ↑
- C3193.** Brenner A.R. Radar imaging of urban areas by means of very high resolution SAR and interferometric SAR. / Brenner A.R., Roessing L. // 2007. IGARSS 2007. IEEE International Geoscience and Remote Sensing Symposium. - Barcelona, 23-28 July 2007. - P. 2689-2693. ↑
- C3194.** Sato M. Application of Polarimetric SAR images acquired in square-loop flights. / Sato M., Iribe K., Hamasaki T. // 2007. IGARSS 2007. IEEE International Geoscience and Remote Sensing Symposium. - Barcelona, 23-28 July 2007. - P. 2632-2635. ↑
- C3195.** Shimada M. Coherence dependency of the PALSAR POLinSAR on forest in japan and amazon. 2007. IGARSS 2007. IEEE International Geoscience and Remote Sensing Symposium. - Barcelona, 23-28 July 2007. - P. 2636-2639. ↑
- C3196.** Chih-Tien Wang. Disaster monitoring and environmental alert in taiwan by repeat-pass spaceborne SAR. / Chih-Tien Wang, Kun-Shen Chen, Hong-Wei Lee, Jong-Sen Lee, Boerner Wolfgang M., Ruei-Yuan Wang, Hong-Sen Wan. // 2007. IGARSS 2007. IEEE International Geoscience and Remote Sensing Symposium. - Barcelona, Spain, 23-28 July 2007. - P. 2628-2631. ↑
- C3197.** Reigber A. Multi-baseline polarimetrically optimised phases and scattering mechanisms for InSAR

applications. / Reigber A., Neumann M., Erten E., Jager M., Prats P. // 2007. IGARSS 2007. IEEE International Geoscience and Remote Sensing Symposium. - Barcelona, 23-28 July 2007. - P. 2620-2623. ↑

C3198. Neumann M. Multibaseline POLInSAR coherence modelling and optimization. / Neumann M., Ferro-Famil L., Reigber A. // 2007. IGARSS 2007. IEEE International Geoscience and Remote Sensing Symposium. - Barcelona, 23-28 July 2007. - P. 2624-2627. ↑

C3199. Franceschetti G. Building feature extraction via a deterministic approach: application to real high resolution SAR images. / Franceschetti G., Guida R., Iodice A., Riccio D., Ruello G., Stilla U. // 2007. IGARSS 2007. IEEE International Geoscience and Remote Sensing Symposium. - Barcelona, 23-28 July 2007. - P. 2681-2684. ↑

C3200. Paillou P. Mapping subsurface geology in Arid Africa using L-band SAR. / Paillou P., Lopez S., Lasne Y., Rosenqvist A., Farr T. // 2007. IGARSS 2007. IEEE International Geoscience and Remote Sensing Symposium. - Barcelona, 23-28 July 2007. - P. 2685-2688. ↑

C3201. Farage G. PolSAR image filtering based on feature detection using the wavelet transform. / Farage G., Foucher S., Benie G.B. // 2007. IGARSS 2007. IEEE International Geoscience and Remote Sensing Symposium. - Barcelona, 23-28 July 2007. - P. 2648-2652. ↑

C3202. Jun-su Kim. Estimation of physical properties of persistent scatterers using JERS-1 data. / Jun-su Kim, Moon W.M. // 2007. IGARSS 2007. IEEE International Geoscience and Remote Sensing Symposium. - Barcelona, 23-28 July 2007. - P. 2640-2643. ↑

C3203. Longepe N. Snow wetness monitoring using multi-temporal polarimetric ASAR data and multi-layer hybrid model. / Longepe N., Allain S., Pottier E. // 2007. IGARSS 2007. IEEE International Geoscience and Remote Sensing Symposium. - Barcelona, 23-28 July 2007. - P. 2644-2647. ↑

C3204. Figueras i Ventura J. IDRA: A new instrument for drizzle monitoring. / Figueras i Ventura J., Russchenberg H.W.J. // 2007. IGARSS 2007. IEEE International Geoscience and Remote Sensing Symposium. - Barcelona, 23-28 July 2007. - P. 3301-3304. ↑

C3205. Ke Xu. A new tracker for ocean-land compatible radar altimeter. / Ke Xu, Jingshan Jiang, Huguang Liu. // 2007. IGARSS 2007. IEEE International Geoscience and Remote Sensing Symposium. - Barcelona, 23-28 July 2007. - P. 3825-3828. ↑

C3206. Xu Xi-Yu. An innovative algorithm for radar altimeter acceleration bias compensation. / Xu Xi-Yu, Liu He-Guang. // 2007. IGARSS 2007. IEEE International Geoscience and Remote Sensing Symposium. - Barcelona, 23-28 July 2007. - P. 3829-3831. ↑

C3207. Yunhua Zhang. An interferometric imaging altimeter applied for both ocean and land observation. / Yunhua Zhang, Xiangkun Zhang, Xin Meng, Wei Luo, Zhixin Zhou, Jingshan Jiang. // 2007. IGARSS 2007. IEEE International Geoscience and Remote Sensing Symposium. - Barcelona, 23-28 July 2007. - P. 3821-3824. ↑

C3208. Marzano F.S. Microwave radar remote sensing of Plinian volcanic ash clouds for aviation hazard and civil protection applications. / Marzano F.S., Barbieri S., Picciotti E., Vulpiani G. // 2007. IGARSS 2007. IEEE International Geoscience and Remote Sensing Symposium. - Barcelona, 23-28 July 2007. - P. 3748-3751. ↑

C3209. Jin-King Liu. Lidar DEM for characterizing the volcanic landforms of tatan volcanoes in metropolitan taipei. / Jin-King Liu, Yu-Chang Chan, Tian-Yuan Shih, Yu-Chung Hsieh. // 2007. IGARSS 2007. IEEE International Geoscience and Remote Sensing Symposium. - Barcelona, 23-28 July 2007. - P. 3752-3755. ↑

C3210. Avolio S. Integrating point, curve and area descriptors into geospatial databases for metric resolution SAR image analysis. / Avolio S., Galli L., Passaro D., Quartulli M., Sagona M., Sinatra G., Zelli C. // 2007. IGARSS 2007. IEEE International Geoscience and Remote Sensing Symposium. - Barcelona, 23-28 July 2007. - P. 3874-3877. ↑

C3211. Foucher S. Multiscale filtering of SAR images using scale and space consistency. 2007. IGARSS 2007. IEEE International Geoscience and Remote Sensing Symposium. - Barcelona, 23-28 July 2007. - P. 3878-3882. ↑

C3212. Crisp D.J. Polarimetric analysis of maritime SAR data collected with the DSTO ingara X-Band radar. / Crisp D.J., Stacy N.J.S., Hudson D.A., Pincus P.B., Goh A.S. // 2007. IGARSS 2007. IEEE International

Geoscience and Remote Sensing Symposium. - Barcelona, 23-28 July 2007. - P. 3870-3873. ↑

C3213. Liu He-Guang. Theoretic error analysis of split-gate tracker in satellite radar altimetry. / Liu He-Guang, Xu Xi-Yu, Xu Ke. // 2007. IGARSS 2007. IEEE International Geoscience and Remote Sensing Symposium. - Barcelona, 23-28 July 2007. - P. 3832-3835. ↑

C3214. Dupuis X. Very high resolution interferogram acquisition campaign and processing. / Dupuis X., Angelliaume S., Oriot H., Dubois-Fernandez P., Cantalloube H., Coulombeix C., du Plessis O., Fromage P., Bonin G., Heuze D. // 2007. IGARSS 2007. IEEE International Geoscience and Remote Sensing Symposium. - Barcelona, 23-28 July 2007. - P. 3866-3869. ↑

C3215. Martinez-Vazquez A. Snow avalanche detection and classification algorithm for GB-SAR imagery. / Martinez-Vazquez A., Fortuny-Guasch J. // 2007. IGARSS 2007. IEEE International Geoscience and Remote Sensing Symposium. - Barcelona, 23-28 July 2007. - P. 3740-3743. ↑

C3216. Lasne Y. Effect of salinity on the dielectric properties of geological materials: implication for soil moisture detection by means of remote sensing. / Lasne Y., Paillou P., Ruffle G., Serradilla C., Demontoux F., Freeman A., Farr T., McDonald K., Chapman B., Malezieux J.-M. // 2007. IGARSS 2007. IEEE International Geoscience and Remote Sensing Symposium. - Barcelona, 23-28 July 2007. - P. 3689-3693. ↑

C3217. Marzano F.S. Potential of X-band spaceborne synthetic aperture radar for precipitation retrieval over land. / Marzano F.S., Poccia G., Cantelmi R., Pierdicca N., Weinman J.A., Chandrasekar V., Mugnai A. // 2007. IGARSS 2007. IEEE International Geoscience and Remote Sensing Symposium. - Barcelona, 23-28 July 2007. - P. 3694-3697. ↑

C3218. Naeimi V. Evaluation of the influence of land cover on the noise level of ERS-scatterometer backscatter. / Naeimi V., Kuenzer C., Hasenauer S., Bartalis Z., Wagner W. // 2007. IGARSS 2007. IEEE International Geoscience and Remote Sensing Symposium. - Barcelona, 23-28 July 2007. - P. 3685-3688. ↑

C3219. Jin-Young Hong. Polarimetric measurements of radar backscatters of a wet-land rice field throughout a growth period at L- and C-bands. / Jin-Young Hong, Yisok Oh, Sukyoung Hong. // 2007. IGARSS 2007. IEEE International Geoscience and Remote Sensing Symposium. - Barcelona, 23-28 July 2007. - P. 3663-3666. ↑

C3220. Jinsong Chen. A semi-empirical backscattering model for estimation of leaf area index (LAI) of rice in southern China. / Jinsong Chen, Hui Lin, Aixia Liu, Yun Shao, Limin Yang. // 2007. IGARSS 2007. IEEE International Geoscience and Remote Sensing Symposium. - Barcelona, 23-28 July 2007. - P. 3667-3680. ↑

C3221. Hoekman D. ALOS PALSAR radar observation of tropical peat swamp forest as a monitoring tool for environmental protection and restoration. / Hoekman D., Vissers M. // 2007. IGARSS 2007. IEEE International Geoscience and Remote Sensing Symposium. - Barcelona, 23-28 July 2007. - P. 3710-3714. ↑

C3222. Pierdicca N. Optimal configurations of bistatic radar for retrieving soil moisture and vegetation biomass. / Pierdicca N., Pulvirenti L., Guerriero L., Della Pietra G. // 2007. IGARSS 2007. IEEE International Geoscience and Remote Sensing Symposium. - Barcelona, 23-28 July 2007. - P. 3715-3718. ↑

C3223. Khadhra K.B. Soil parameter estimation and analysis of bistatic scattering X-band controlled measurements. / Khadhra K.B., Boerner T., Chandra M., Zink M., Hounam D. // 2007. IGARSS 2007. IEEE International Geoscience and Remote Sensing Symposium. - Barcelona, 23-28 July 2007. - P. 3706-3709. ↑

C3224. Loew A. Integration of L-band SAR data into land surface models. / Loew A., Hoekman D., Hajnsek I., Davison M. // 2007. IGARSS 2007. IEEE International Geoscience and Remote Sensing Symposium. - Barcelona, 23-28 July 2007. - P. 3698-3701. ↑

C3225. Bartsch A. Application of C and Ku-Band scatterometer data for catchment hydrology in northern latitudes. / Bartsch A., Wagner W., Rupp K., Kidd R. // 2007. IGARSS 2007. IEEE International Geoscience and Remote Sensing Symposium. - Barcelona, 23-28 July 2007. - P. 3702-3705. ↑

C3226. Alparone L. Robust change analysis of SAR data through information-theoretic multitemporal features. / Alparone L., Aiazzi B., Baronti S., Garzelli A., Nencini F. // 2007. IGARSS 2007. IEEE International Geoscience and Remote Sensing Symposium. - Barcelona, 23-28 July 2007. - P. 3883-3886. ↑

C3227. Schmidt N. TerraSAR-X value added image products. / Schmidt N., Janoth J., Raggam J., Gutjahr K.,

Wimmer A. // 2007. IGARSS 2007. IEEE International Geoscience and Remote Sensing Symposium. - Barcelona, 23-28 July 2007. - P. 3938-3941. ↑

C3228. Adam N. TerraSAR-X interferometry: report on a first assessment. / Adam N., Eineder M., Schattler B., Bamler R. // 2007. IGARSS 2007. IEEE International Geoscience and Remote Sensing Symposium. - Barcelona, 23-28 July 2007. - P. 3942. ↑

C3229. Huber M. Quality of orthorectified TerraSAR-X products. / Huber M., Wessel B., Habermeyer M., Roth A. // 2007. IGARSS 2007. IEEE International Geoscience and Remote Sensing Symposium. - Barcelona, 23-28 July 2007. - P. 3937. ↑

C3230. Schwerdt M. TerraSAR-X calibration-first results. / Schwerdt M., Brautigam B., Bachmann M., Doring B. // 2007. IGARSS 2007. IEEE International Geoscience and Remote Sensing Symposium. - Barcelona, 23-28 July 2007. - P. 3932-3935. ↑

C3231. Breit H. TerraSAR-X payload data processing-First Experiences. / Breit H., Fritz T., Schattler B., Borner E., Lachaise M., Niedermeier A., Eineder M., Balss U. // 2007. IGARSS 2007. IEEE International Geoscience and Remote Sensing Symposium. - Barcelona, 23-28 July 2007. - P. 3936. ↑

C3232. Shokr M. A new algorithm to calculate sea ice concentration from the SSM/I 85GHz observations. / Shokr M., Lambe A., Agnew T. // 2007. IGARSS 2007. IEEE International Geoscience and Remote Sensing Symposium. - Barcelona, 23-28 July 2007. - P. 3987-3990. ↑

C3233. Kaab A. Glacier volume changes using ASTER optical stereo. A test study in Eastern Svalbard. 2007. IGARSS 2007. IEEE International Geoscience and Remote Sensing Symposium. - Barcelona, 23-28 July 2007. - P. 3994-3996. ↑

C3234. Makynen M. Interpretation of C-band SAR backscattering coefficient time series for the Baltic Sea landfast sea ice using a 1-D thermodynamic snow/ice model. / Makynen M., Bin Cheng, Simila M., Vihma T., Hallikainen M. // 2007. IGARSS 2007. IEEE International Geoscience and Remote Sensing Symposium. - Barcelona, 23-28 July 2007. - P. 3983-3986. ↑

C3235. Suchandt S. First results of ground moving target analysis in TerraSAR-X data. / Suchandt S., Runge H., Eineder M., Breit H., Kotenkov A., Balss U. // 2007. IGARSS 2007. IEEE International Geoscience and Remote Sensing Symposium. - Barcelona, 23-28 July 2007. - P. 3943. ↑

C3236. Zink M. The TanDEM-X mission: Overview and status. / Zink M., Krieger G., Fiedler H., Moreira A. // 2007. IGARSS 2007. IEEE International Geoscience and Remote Sensing Symposium. - Barcelona, 23-28 July 2007. - P. 3944-3947. ↑

C3237. Marquez-Martinez J. In-orbit SAR performance of TerraSAR-X. / Marquez-Martinez J., Gonzalez C., Younis M., Wollstadt S., Metz R. // 2007. IGARSS 2007. IEEE International Geoscience and Remote Sensing Symposium. - Barcelona, 23-28 July 2007. - P. 3931. ↑

C3238. Khajonrat D. Simultaneous radar observations of tropical cyclones by space-based and ground-based radar. / Khajonrat D., Chandrasekar V., Viswanathan G., Shellar V. // 2007. IGARSS 2007. IEEE International Geoscience and Remote Sensing Symposium. - Barcelona, 23-28 July 2007. - P. 3899-3902. ↑

C3239. Jackson G.S. Observational data set in support of falling snow retrieval algorithm development. / Jackson G.S., Johnson B., Tokay A., Petersen W. // 2007. IGARSS 2007. IEEE International Geoscience and Remote Sensing Symposium. - Barcelona, 23-28 July 2007. - P. 3903-3906. ↑

C3240. Chaabouni-Chouayakh H. Linear versus non-linear analysis of relevant scatterers in high resolution SAR images. / Chaabouni-Chouayakh H., Datcu M. // 2007. IGARSS 2007. IEEE International Geoscience and Remote Sensing Symposium. - Barcelona, 23-28 July 2007. - P. 3895-3898. ↑

C3241. Soccorsi M. Stochastic models of SLC HR SAR images. / Soccorsi M., Datcu M. // 2007. IGARSS 2007. IEEE International Geoscience and Remote Sensing Symposium. - Barcelona, 23-28 July 2007. - P. 3887-3890. ↑

C3242. Benboudjema D. Unsupervised segmentation of SAR images using Triplet Markov fields and fisher noise distributions. / Benboudjema D., Tupin F., Pieczynski W., Sigelle M., Nicolas J.-M. // 2007. IGARSS 2007.

IEEE International Geoscience and Remote Sensing Symposium. - Barcelona, 23-28 July 2007. - P. 3891-3894.



C3243. Surussavadee C. Comparison of NOWRAD, AMSU, AMSR-E, TMI, and SSM/I surface precipitation rate Retrievals over the united states great plains. / Surussavadee C., Staelin D.H., Chadarong V., McLaughlin D., Entekhabi D. // 2007. IGARSS 2007. IEEE International Geoscience and Remote Sensing Symposium. - Barcelona, 23-28 July 2007. - P. 3923-3926.

C3244. Werninghaus R. TerraSAR-X Mission Status. / Werninghaus R., Buckreuss S., Pitz W. // 2007. IGARSS 2007. IEEE International Geoscience and Remote Sensing Symposium. - Barcelona, 23-28 July 2007. - P. 3927-3930.

C3245. Tagawa T. Modification of the beam mismatch correction algorithm. / Tagawa T., Shimizu S., Oki R. // 2007. IGARSS 2007. IEEE International Geoscience and Remote Sensing Symposium. - Barcelona, 23-28 July 2007. - P. 3920-3922.

C3246. Zafar B. Adjustment of cross-track dependence of TRMM Precipitation Radar observation. / Zafar B., Chandrasekar V. // 2007. IGARSS 2007. IEEE International Geoscience and Remote Sensing Symposium. - Barcelona, 23-28 July 2007. - P. 3907-3909.

C3247. Takahashi N. Analysis of densely observed TRMM/PR data during 180-degree yaw maneuver. / Takahashi N., Iguchi T. // 2007. IGARSS 2007. IEEE International Geoscience and Remote Sensing Symposium. - Barcelona, 23-28 July 2007. - P. 3914-3919.

C3248. Hasager C.B. QuikSCAT and SSM/I ocean surface winds for wind energy. / Hasager C.B., Astrup P., Nielsen P. // 2007. IGARSS 2007. IEEE International Geoscience and Remote Sensing Symposium. - Barcelona, 23-28 July 2007. - P. 3507-3512.

C3249. Portabella M. Towards a high-resolution ASCAT scatterometer wind product. / Portabella M., Stoffelen A., Vogelzang J., Verhoef A., Verspeek J. // 2007. IGARSS 2007. IEEE International Geoscience and Remote Sensing Symposium. - Barcelona, 23-28 July 2007. - P. 3513-3516.

C3250. Ahmad K.A. Oceanic Rainfall Retrievals using passive and active measurements from SeaWinds Remote Sensor. / Ahmad K.A., Jones W.L., Kasparis T. // 2007. IGARSS 2007. IEEE International Geoscience and Remote Sensing Symposium. - Barcelona, 23-28 July 2007. - P. 3502-3506.

C3251. Banal S. Canadian Space Agency's Hurricane Watch Program: Archive contents, Data Access and improved planning strategies. / Banal S., Iris S., Saint-Jean R. // 2007. IGARSS 2007. IEEE International Geoscience and Remote Sensing Symposium. - Barcelona, 23-28 July 2007. - P. 3494-3497.

C3252. Irisov V. Simultaneous X-band radar and Ka -band radiometer observations of the ocean. / Irisov V., Plant W.J. // 2007. IGARSS 2007. IEEE International Geoscience and Remote Sensing Symposium. - Barcelona, 23-28 July 2007. - P. 3498-3501.

C3253. Mavrocordatos C. The Sentinel-3 mission and its topography element. / Mavrocordatos C., Berruti B., Aguirre M., Drinkwater M. // 2007. IGARSS 2007. IEEE International Geoscience and Remote Sensing Symposium. - Barcelona, 23-28 July 2007. - P. 3529-3532.

C3254. Phalippou L. Re-tracking of SAR altimeter ocean power-waveforms and related accuracies of the retrieved sea surface height, significant wave height and wind speed. / Phalippou L., Enjolras V. // 2007. IGARSS 2007. IEEE International Geoscience and Remote Sensing Symposium. - Barcelona, 23-28 July 2007. - P. 3533-3536.

C3255. Enjolras V. An assessment of the Ka band interferometric radar altimeter for monitoring rivers and lakes with the WatER mission. / Enjolras V., Rodriguez E. // 2007. IGARSS 2007. IEEE International Geoscience and Remote Sensing Symposium. - Barcelona, 23-28 July 2007. - P. 3525-3528.

C3256. Hwang P.A. Statistical characterization of radar sea scatter for breaking wave detection. / Hwang P.A., Sletten M.A., Toporkov J.V. // 2007. IGARSS 2007. IEEE International Geoscience and Remote Sensing Symposium. - Barcelona, 23-28 July 2007. - P. 3517-3520.

C3257. Shimada T. Wind jet transition and its localized impact on wave height distribution along the Pacific Coast of Northern Japan. / Shimada T., Kawamura H. // 2007. IGARSS 2007. IEEE International Geoscience

and Remote Sensing Symposium. - Barcelona, 23-28 July 2007. - P. 3521-3524. ↑

C3258. Nonaka T. A comparison of the methods for the urban land cover change detection by high-resolution SAR data. / Nonaka T., Shibayama T., Umakawa H., Uratsuka S. // 2007. IGARSS 2007. IEEE International Geoscience and Remote Sensing Symposium. - Barcelona, 23-28 July 2007. - P. 3470-3473. ↑

C3259. Nguyen C.M. A time domain clutter filter for staggered PRT and dual- PRF measurements. / Nguyen C.M., Moiseev D.N., Chandrasekar V. // 2007. IGARSS 2007. IEEE International Geoscience and Remote Sensing Symposium. - Barcelona, 23-28 July 2007. - P. 3325-3328. ↑

C3260. Shimabukuro Y.E. Mapping and monitoring land cover in Corumbiara area, Brazilian Amazonia, using JERS-1 SAR multitemporal data. / Shimabukuro Y.E., Almeida-Filho R., Kuplich T.M., de Freitas R.M. // 2007. IGARSS 2007. IEEE International Geoscience and Remote Sensing Symposium. - Barcelona, 23-28 July 2007. - P. 3370-3373. ↑

C3261. Farquharson G. A new high-altitude airborne millimeter-wave radar for atmospheric research. / Farquharson G., Loew E., Vivekanandan J., Wen-Chau Lee. // 2007. IGARSS 2007. IEEE International Geoscience and Remote Sensing Symposium. - Barcelona, 23-28 July 2007. - P. 3313-3316. ↑

C3262. Chandrasekar V. Dual-polarization spectral decompositions: Application to radar parameter estimation and quality control. / Chandrasekar V., Moiseev D.N., George J. // 2007. IGARSS 2007. IEEE International Geoscience and Remote Sensing Symposium. - Barcelona, 23-28 July 2007. - P. 3305-3308. ↑

C3263. Klugmann D. Application of single drop scattering algorithms to rain related retrieval. / Klugmann D., Fiser O. // 2007. IGARSS 2007. IEEE International Geoscience and Remote Sensing Symposium. - Barcelona, 23-28 July 2007. - P. 3309-3312. ↑

C3264. Hee-Young Yoo. Implementation of 3D discrete wavelet scheme for space-borne imagery classification and its application. / Hee-Young Yoo, Kiwon Lee, Byung-Doo Kwon. // 2007. IGARSS 2007. IEEE International Geoscience and Remote Sensing Symposium. - Barcelona, 23-28 July 2007. - P. 3437-3440. ↑

C3265. Ma Jianwen. Land use changes driven by 2008 beijing olympic playground constructions and depicted by landsat temporal data. / Ma Jianwen, Chen Xue, Dai Qin, Li Liwei. // 2007. IGARSS 2007. IEEE International Geoscience and Remote Sensing Symposium. - Barcelona, 23-28 July 2007. - P. 3456-3457. ↑

C3266. Monsivais-Huertero A. Application of a coherent modeling on Sahelian grassland. / Monsivais-Huertero A., Chenerie I., Sarabandi K., Baup F. // 2007. IGARSS 2007. IEEE International Geoscience and Remote Sensing Symposium. - Barcelona, 23-28 July 2007. - P. 3405-3407. ↑

C3267. Andreoli R. Land cover analysis at a regional scale exploiting low and medium resolution ENVISAT ASAR Data: Application to Poyang Lake Area (Jianxi Province, P.R. China). / Andreoli R., Yesou H., Shifeng H., Li J., Desnos Y.-L. // 2007. IGARSS 2007. IEEE International Geoscience and Remote Sensing Symposium. - Barcelona, 23-28 July 2007. - P. 3374-3377. ↑

C3268. Notarnicola C. Adaptive bayesian algorithm for vegetated field parameters extraction by using multi-frequency and multi-polarimetric SAR images. / Notarnicola C., Ventura B., Posa F. // 2007. IGARSS 2007. IEEE International Geoscience and Remote Sensing Symposium. - Barcelona, 23-28 July 2007. - P. 3401-3404. ↑

C3269. Richard J. An advanced concept of radar altimetry over oceans with improved performances and ocean sampling: ALtiKa. / Richard J., Phalippou L., Robert F., Stenou N., Thouvenot E., Sengenès P. // 2007. IGARSS 2007. IEEE International Geoscience and Remote Sensing Symposium. - Barcelona, 23-28 July 2007. - P. 3537-3540. ↑

C3270. Lucas R.M. ALOS PALSAR for characterizing wooded savannas in Northern Australia. / Lucas R.M., Armston J.D. // 2007. IGARSS 2007. IEEE International Geoscience and Remote Sensing Symposium. - Barcelona, 23-28 July 2007. - P. 3610-3613. ↑

C3271. Rosenqvist A. The ALOS Kyoto & Carbon Initiative. / Rosenqvist A., Shimada M., Milne A.K. // 2007. IGARSS 2007. IEEE International Geoscience and Remote Sensing Symposium. - Barcelona, 23-28 July 2007. - P. 3614-3617. ↑

C3272. Isoguchi O. Relationship between wind vectors and L-band radar cross sections examined using

PALSAR. / Isoguchi O., Shimada M. // 2007. IGARSS 2007. IEEE International Geoscience and Remote Sensing Symposium. - Barcelona, 23-28 July 2007. - P. 3598-3601. ↑

C3273. Shimada M. PALSAR CALVAL summary and update 2007. / Shimada M., Isoguchi O., Tadono T., Higuchi R., Isono K. // 2007. IGARSS 2007. IEEE International Geoscience and Remote Sensing Symposium. - Barcelona, 23-28 July 2007. - P. 3593-3596. ↑

C3274. Papathanassiou K.P. Pol-InSAR Results from ALOS-PaLSAR. / Papathanassiou K.P., Marotti L., Schneider R.Z., Hajnsek I. // 2007. IGARSS 2007. IEEE International Geoscience and Remote Sensing Symposium. - Barcelona, 23-28 July 2007. - P. 3597. ↑

C3275. Schiavon G. Sensitivity of multi-temporal high resolution polarimetric C and L-band SAR to grapes in vineyards. / Schiavon G., Solimini D., Burini A. // 2007. IGARSS 2007. IEEE International Geoscience and Remote Sensing Symposium. - Barcelona, 23-28 July 2007. - P. 3651-3654. ↑

C3276. Soria-Ruiz J. Corn monitoring and crop yield using optical and RADARSAT-2 images. / Soria-Ruiz J., McNairn H., Fernandez-Ordóñez Y., Bugden-Storie J. // 2007. IGARSS 2007. IEEE International Geoscience and Remote Sensing Symposium. - Barcelona, 23-28 July 2007. - P. 3655-3658. ↑

C3277. Heinzl V. Remote sensing data assimilation for regional crop growth modelling in the region of Bonn (Germany). / Heinzl V., Waske B., Braun M., Menz G. // 2007. IGARSS 2007. IEEE International Geoscience and Remote Sensing Symposium. - Barcelona, 23-28 July 2007. - P. 3647-3650. ↑

C3278. Colliander A. Ground calibration of SMOS: NIR and CAS. / Colliander A., Lemmetyinen J., Uusitalo J., Suomela J., Veijola K., Kontu A., Kempainen S., Pihlflyckt J., Rautiainen K., Hallikainen M., Lahtinen J. // 2007. IGARSS 2007. IEEE International Geoscience and Remote Sensing Symposium. - Barcelona, 23-28 July 2007. - P. 3631-3634. ↑

C3279. Duffo N. Some results of the MIRAS-SMOS demonstrator campaigns. / Duffo N., Torres F., Corbella I., Gonzalez V., Blanch S., Camps A., Vall-Ilossera M., Alvarez J.L., Ribo S., Martin-Neira M. // 2007. IGARSS 2007. IEEE International Geoscience and Remote Sensing Symposium. - Barcelona, 23-28 July 2007. - P. 3639-3642. ↑

C3280. Iwata T. Advanced land observing satellite (ALOS): On-orbit status and platform calibration. 2007. IGARSS 2007. IEEE International Geoscience and Remote Sensing Symposium. - Barcelona, 23-28 July 2007. - P. 3583-3588. ↑

C3281. Gorgucci E. Rain microphysics estimation using X-band dual polarization radar measurements. / Gorgucci E., Baldini L., Chandrasekar V. // 2007. IGARSS 2007. IEEE International Geoscience and Remote Sensing Symposium. - Barcelona, 23-28 July 2007. - P. 3555-3558. ↑

C3282. Scheiber R. Surface clutter suppression for ice sounding radars by coherent combination of repeat-pass data. / Scheiber R., Prats P. // 2007. IGARSS 2007. IEEE International Geoscience and Remote Sensing Symposium. - Barcelona, 23-28 July 2007. - P. 3559-3562. ↑

C3283. Furukawa K. Preliminary design of the spaceborne dual-frequency precipitation radar for the global precipitation measurement. / Furukawa K., Hanado H., Hyakusoku Y., Ishii Y., Kojima M., Takahashi N., Iguchi T., Okumura M. // 2007. IGARSS 2007. IEEE International Geoscience and Remote Sensing Symposium. - Barcelona, 23-28 July 2007. - P. 3551-3554. ↑

C3284. Roca M. The RA-2 individual echoes processing description and some scientific results. / Roca M., Martinez D., Reche M. // 2007. IGARSS 2007. IEEE International Geoscience and Remote Sensing Symposium. - Barcelona, 23-28 July 2007. - P. 3541-3546. ↑

C3285. Schwaller M.R. Prototype of NASA's global precipitation measurement mission ground validation system. / Schwaller M.R., Morris K.R., Petersen W.A. // 2007. IGARSS 2007. IEEE International Geoscience and Remote Sensing Symposium. - Barcelona, 23-28 July 2007. - P. 3547-3550. ↑

C3286. Anagnostou M.N. Evaluation of X-band polarimetric radar estimates of drop size distributions from coincident S-band polarimetric estimates and measured raindrop spectra. / Anagnostou M.N., Anagnostou E.N., Vulpiani G., Montopoli M., Vivekanandan J. // 2007. IGARSS 2007. IEEE International Geoscience and Remote Sensing Symposium. - Barcelona, 23-28 July 2007. - P. 3575-3578. ↑

- C3287.** Flampouris S. Survey of bathymetry and current fields by radar image series acquired by shore based x-band radar. / Flampouris S., Ziemer F., Seemann J. // 2007. IGARSS 2007. IEEE International Geoscience and Remote Sensing Symposium. - Barcelona, 23-28 July 2007. - P. 3579-3582. ↑
- C3288.** Chandrasekar V. Waveform coding for dual polarization weather radars. / Chandrasekar V., Bharadwaj N., George J. // 2007. IGARSS 2007. IEEE International Geoscience and Remote Sensing Symposium. - Barcelona, 23-28 July 2007. - P. 3571-3574. ↑
- C3289.** Berizzi F. Synthetic range profile focusing via contrast optimization. / Berizzi F., Martorella M., Cacciavano A. // 2007. IGARSS 2007. IEEE International Geoscience and Remote Sensing Symposium. - Barcelona, 23-28 July 2007. - P. 3563-3566. ↑
- C3290.** Cerutti-Maori D. Wide area traffic monitoring with the PAMIR system. / Cerutti-Maori D., Klare J., Burger W., Brenner A.R., Ender J.H.G. // 2007. IGARSS 2007. IEEE International Geoscience and Remote Sensing Symposium. - Barcelona, 23-28 July 2007. - P. 3567-3570. ↑
- C3291.** Jangal F. Wavelets: a Versatile Tool for the High Frequency Surface Wave Radar. / Jangal F., Saillant S., Helier M. // 2007 IEEE Radar Conference. - Boston, MA, 17-20 April 2007. - P. 497-502. ↑
- C3292.** Tiwari K.C. Algorithm Overview Based On Image Processing with Electromagnetic (EM) Techniques in X Band and GA Approach for Depth Estimation of Shallow Buried Dummy Mines. / Tiwari K.C., Singh D., Arora M. // 2007 IEEE Radar Conference. - Boston, MA, 17-20 April 2007. - P. 331-336. ↑
- C3293.** Yarovoy A.G. UWB Radars: Recent Technological Advances and Applications. / Yarovoy A.G., Ligthart L.P. // 2007 IEEE Radar Conference. - Boston, MA, 17-20 April 2007. - P. 43-48. ↑
- C3294.** Nienhaus K. An Experimental Study on Using Electronically Scanning Microwave Radar Systems on Surface Mining Machines. / Nienhaus K., Winkel R., Mayer W., Gronau A., Menzel W. // 2007 IEEE Radar Conference. - Boston, MA, 17-20 April 2007. - P. 509-512. ↑
- C3295.** Rosen P.A. Perspectives on Worldwide Spaceborne Radar Programs. / Rosen P.A., Buccolo G.M. // 2007 IEEE Radar Conference. - Boston, MA, 17-20 April 2007. - P. 740-745. ↑
- C3296.** Griffiths H.D. Developments in Modern Synthetic Aperture Radar. 2007 IEEE Radar Conference. - Boston, MA, 17-20 April 2007. - P. 734-739. ↑
- C3297.** Zebker H. InSAR Remote Sensing Over Decorrelating Terrains: Persistent Scattering Methods. / Zebker H., Shankar P., Hooper A. // 2007 IEEE Radar Conference. - Boston, MA, 17-20 April 2007. - P. 717-722. ↑
- C3298.** Ferraro P.B. A System for the Measurement of the Amazon. / Ferraro P.B., Bauersachs M., Bums J., Battaler G. // 2007 IEEE Radar Conference. - Boston, MA, 17-20 April 2007. - P. 28-36. ↑
- C3299.** Tarsha-Kurdi F. Joint combination of point cloud and DSM for 3D building reconstruction using airborne laser scanner data. / Tarsha-Kurdi F., Landes T., Grussenmeyer P. // 2007 Urban Remote Sensing Joint Event. - Paris, 11-13 April 2007. - P. 1-7. ↑
- C3300.** Franceschetti G. Simulation Tools for Interpretation of High Resolution SAR Images of Urban Areas. / Franceschetti G., Guida R., Iodice A., Riccio D., Ruello G., Stilla U. // 2007 Urban Remote Sensing Joint Event. - Paris, 11-13 April 2007. - P. 1-5. ↑
- C3301.** Delliére J. SAR measurement simulation on urban structures using a FDTD technique. / Delliére J., Maitre H., Maruani A. // 2007 Urban Remote Sensing Joint Event. - Paris, 11-13 April 2007. - P. 1-8. ↑
- C3302.** Sugumaran R. Object-Oriented Classification of LIDAR-Fused Hyperspectral Imagery for Tree Species Identification in an Urban Environment. / Sugumaran R., Voss M. // 2007 Urban Remote Sensing Joint Event. - Paris, 11-13 April 2007. - P. 1-6. ↑
- C3303.** Brocato R.W. Re-configurable Completely Unpowered Wireless Sensors. / Brocato R.W., Wouters G.A., Heller E., Blaich J., Palmer D.W. // 2007. ECTC 07. Proceedings. 57th Electronic Components and Technology Conference. - Reno, NV, May 29 2007-June 1 2007. - P. 179-183. ↑

- C3304.** Horst S. Beam-Shaping of Planar Array Antennas Using Integrated Attenuators. / Horst S., Anagnostou D.E., Ponchak G.E., Tentzeris E., Papapolymerou J. // 2007. ECTC 07. Proceedings. 57th Electronic Components and Technology Conference. - Reno, NV, May 29 2007-June 1 2007. - P. 165-168. ↑
- C3305.** Haala N. Cell Decomposition for Building Model Generation at Different Scales. / Haala N., Becker S., Kada M. // 2007 Urban Remote Sensing Joint Event. - Paris, 11-13 April 2007. - P. 1-6. ↑
- C3306.** Kaplan N.H. Fusion Of Remote Sensing Images via Lattice Filters. / Kaplan N.H., Erer I., Kent S. // 2007. RAST '07. 3rd International Conference on Recent Advances in Space Technologies. - Istanbul, 14-16 June 2007. - P. 285-288. ↑
- C3307.** Kurnaz S. Earth Observation Remote Sensing and GIS Services for Monitoring of Integration Systems. / Kurnaz S., Rustamov R.B. // 2007. RAST '07. 3rd International Conference on Recent Advances in Space Technologies. - Istanbul, 14-16 June 2007. - P. 268-270. ↑
- C3308.** Kancheva R. Spectral Predictors of Crop Development and Yield. / Kancheva R., Borisova D., Georgiev G. // 2007. RAST '07. 3rd International Conference on Recent Advances in Space Technologies. - Istanbul, 14-16 June 2007. - P. 247-251. ↑
- C3309.** Nayir H. GPS/TEC Estimation with IONOLAB Method. / Nayir H., Arıkan F., Arıkan O., Erol C.B. // 2007. RAST '07. 3rd International Conference on Recent Advances in Space Technologies. - Istanbul, 14-16 June 2007. - P. 29-34. ↑
- C3310.** Cutter M. A Hyperspectral Imaging Mission for Small Satellites-Five Years Orbit Experience. / Cutter M., Sweeting M. // 2007. RAST '07. 3rd International Conference on Recent Advances in Space Technologies. - Istanbul, 14-16 June 2007. - P. 355-360. ↑
- C3311.** Weber M. TerraSAR-X and TanDEM-X: Reconnaissance Applications. 2007. RAST '07. 3rd International Conference on Recent Advances in Space Technologies. - Istanbul, 14-16 June 2007. - P. 299-303. ↑
- C3312.** Ochs S. The TerraSAR-X and TanDEM-X Satellites. / Ochs S., Pitz W. // 2007. RAST '07. 3rd International Conference on Recent Advances in Space Technologies. - Istanbul, 14-16 June 2007. - P. 294-298. ↑
- C3313.** Elkhetafi S. I. Estimation of Electromagnetic of Libyan soil Properties by Stepped Frequency Radar. / Elkhetafi S. I., Salem K. A. // 2007 4th International Workshop on Advanced Ground Penetrating Radar. - Aula Magna Partenope, 27-29 June 2007. - P. 110-113. ↑
- C3314.** Khrebto P. A Wireless Location System for Sensing the Relative Position between Mining Vehicles. / Khrebto P., Pottkeir A., Max S. // 2007. IMTC 2007. IEEE Instrumentation and Measurement Technology Conference Proceedings. - Warsaw, 1-3 May 2007. - P. 1-5. ↑
- C3315.** Nemati S. Spectral Signature Classification Using A Support Vector Classifier For Real-Time Instrumentation. / Nemati S., Yeary M., Yu T.-Y., Wang Y., Zhai Y., Fagg A.H. // 2007. IMTC 2007. IEEE Instrumentation and Measurement Technology Conference Proceedings. - Warsaw, 1-3 May 2007. - P. 1-4. ↑
- C3316.** Awadallah R.S. Radar Scattering from Partially-Submerged Objects in Ducting Environments. / Awadallah R.S., Ku H.C., Sprouse C.R. // 2007 IEEE Radar Conference. - Boston, MA, 17-20 April 2007. - P. 932-937. ↑
- C3317.** Fukuda T. A 26GHz Short-Range UWB Vehicular-Radar Using 2.5Gcps Spread Spectrum Modulation. / Fukuda T., Negoro N., Ujita S., Nagai S., Nishijima M., Sakai H., Tanaka T., Ueda D. // 2007. IEEE/MTT-S International Microwave Symposium. - Honolulu, HI, 3-8 June 2007. - P. 1311-1314. ↑
- C3318.** Counsell J. Displaying LiDAR Data for Interactive Web-Based Modelling of the Environment. / Counsell J., Smith S. // 2007. IV 07. 11th International Conference Information Visualization. - Zurich, 4-6 July 2007. - P. 573-578. ↑
- C3319.** Lach S.R. Multisource Data Processing for Semi-Automated Radiometrically-Correct Scene Simulation. / Lach S.R., Kerekes J.P. // 2007 Urban Remote Sensing Joint Event. - Paris, 11-13 April 2007. - P. 1-10. ↑
- C3320.** Dengler R.J. 600 GHz Imaging Radar with 2 cm Range Resolution. / Dengler R.J., Cooper K.B.,

Chattopadhyay G., Mehdi I., Schlecht E., Skalare A., Chen C., Siegel P.H. // 2007. IEEE/MTT-S International Microwave Symposium. - Honolulu, HI, 3-8 June 2007. - P. 1371-1374. ↑

C3321. Del Amo A. A Spatial Classification Model for Multicriteria Analysis. / Del Amo A., Garmendia L., Gomez D., Montero J. // IEEE Symposium on Computational Intelligence in Multicriteria Decision Making. - Honolulu, HI, 1-5 April 2007. - P. 348-353. ↑

C3322. Haykin S. Cognitive Dynamic Systems. 2007. ICASSP 2007. IEEE International Conference on Acoustics, Speech and Signal Processing. - Honolulu, HI, 15-20 April 2007. - Vol. 4. - P. IV-1369-IV-1372-1369. ↑

C3323. Xin Kang. Clustering Polarimetric SAR Image Under Deorientation Theory. / Xin Kang, Chongzhao Han, Feng Xu. // 2007. ICASSP 2007. IEEE International Conference on Acoustics, Speech and Signal Processing. - Honolulu, HI, 15-20 April 2007. - Vol. 1. - P. I-877-I-880-877. ↑

C3324. Horvath M. Microwave Imaging Using Spread Spectrum Modulation. / Horvath M., Seller R. // 2007. 17th International Conference Radioelektronika. - Brno, 24-25 April 2007. - P. 1-3. ↑

C3325. Orsomando F. SAR and Optical Data Fusion for Change Detection. / Orsomando F., Lombardo P., Zavagli M., Costantini M. // 2007 Urban Remote Sensing Joint Event. - Paris, 11-13 April 2007. - P. 1-9. ↑

C3326. Ferro-Famil L. Urban area remote sensing from L-band PolSAR data using Time-Frequency techniques. / Ferro-Famil L., Pottier E. // 2007 Urban Remote Sensing Joint Event. - Paris, 11-13 April 2007. - P. 1-6. ↑

C3327. Sauer S. 3D Visualisation and Physical Feature Extraction of Urban Areas using Multibaseline POL-InSAR Data at L-Band. / Sauer S., Ferro-Famil L., Pottier E., Reigber A. // 2007 Urban Remote Sensing Joint Event. - Paris, 11-13 April 2007. - P. 1-5. ↑

C3328. Petrochilos N. Blind Separation of Human Heartbeats and Breathing by the use of a Doppler Radar Remote Sensing. / Petrochilos N., Rezk M., Host-Madsen A., Lubecke V., Boric-Lubecke O. // 2007. ICASSP 2007. IEEE International Conference on Acoustics, Speech and Signal Processing. - Honolulu, HI, 15-20 April 2007. - Vol. 1. - P. I-333-I-336-333. ↑

C3329. Beck S.M. Co-Boresighted Coherent Laser Velocimeter and Direct Detection Lidar for Dust Devil Characterization. / Beck S.M., Wright T.J., Linares J.R., Kozlowski D.A. // 2007 IEEE Aerospace Conference. - Big Sky, MT, 3-10 March 2007. - P. 1-11. ↑

C3330. Moghaddam M. Dual Polarized UHF/VHF Honeycomb Stacked-Patch Feed Array for a Large-Aperture Space-borne Radar Antenna. / Moghaddam M., Rahmat-Samii Y., Partridge P., Van Nieuwstadt L., Vitaz J., Haynes M., Huang J., Cable V. // 2007 IEEE Aerospace Conference. - Big Sky, MT, 3-10 March 2007. - P. 1-10. ↑

C3331. Diner D.J. Future Mission Concept for 3-D Remote Sensing of Aerosols from Low Earth Orbit. / Diner D.J., Boland S.W., Davis E.S., Kahn R.A., Hostetler C.A., Ferrare R.A., Hair J.W., Cairns B., Torres O. // 2007 IEEE Aerospace Conference. - Big Sky, MT, 3-10 March 2007. - P. 1-9. ↑

C3332. Sadowy G. Technology Demonstration of Ka-band Digitally-Beam formed Radar for Ice Topography Mapping. / Sadowy G., Heavey B., Moller D., Rignot E., Zawadzki M., Rengarajan S. // 2007 IEEE Aerospace Conference. - Big Sky, MT, 3-10 March 2007. - P. 1-10. ↑

C3333. Tralli D.M. Concept for a High MEO InSAR Seismic Monitoring System. / Tralli D.M., Foxall W., Schultz C. // 2007 IEEE Aerospace Conference. - Big Sky, MT, 3-10 March 2007. - P. 1-7. ↑

C3334. Moghaddam M. Soil Moisture Smart Sensor Web Concept Using Data Assimilation and Optimal Control. / Moghaddam M., Entekhabi D., Mingyan Liu, Teneketzis D. // 2007 IEEE Aerospace Conference. - Big Sky, MT, 3-10 March 2007. - P. 1-6. ↑

C3335. Wenqin Wang. Applications of MIMO Technique for Aerospace Remote Sensing. 2007 IEEE Aerospace Conference. - Big Sky, MT, 3-10 March 2007. - P. 1-10. ↑

C3336. Weihing D. An Integral Detection Scheme for Moving Object Indication in Dual-Channel High Resolution Spaceborne SAR Data. / Weihing D., Hinz S., Meyer F., Suchandt S., Bamler R. // 2007 Urban

Remote Sensing Joint Event. - Paris, 11-13 April 2007. - P. 1-6. ↑

C3337. Tolt G. 3D Urban Models from Laser Radar Data. / Tolt G., Soderman U., Ahlberg S. // 2007 Urban Remote Sensing Joint Event. - Paris, 11-13 April 2007. - P. 1-5. ↑

C3338. Del Frate F. Urban Land Cover in Rome, Italy, monitored by single-parameter multi-temporal SAR images. / Del Frate F., Pacifici F., Solimini D. // 2007 Urban Remote Sensing Joint Event. - Paris, 11-13 April 2007. - P. 1-5. ↑

C3339. Michaelsen E. Perceptual Grouping for Building Recognition in High-resolution SAR Images using the GESTALT-System. / Michaelsen E., Doktorski L., Soergel U., Stilla U. // 2007 Urban Remote Sensing Joint Event. - Paris, 11-13 April 2007. - P. 1-6. ↑

C3340. Du Peijun. Applications of Multi-source Remote Sensing Information to Urban Environment Monitoring in Mining Industrial Cities. / Du Peijun, Zhang Huapeng, Pan Chen, Liu Pei. // 2007 Urban Remote Sensing Joint Event. - Paris, 11-13 April 2007. - P. 1-12. ↑

C3341. Gamba P. Raster to Vector in 2D Urban Data. / Gamba P., Dell'Acqua F., Lisini G. // 2007 Urban Remote Sensing Joint Event. - Paris, 11-13 April 2007. - P. 1-6. ↑

C3342. Reigber A. Detection and classification of urban structures based on high-resolution SAR imagery. / Reigber A., Jager M., He W., Ferro-Famil L., Hellwich O. // 2007 Urban Remote Sensing Joint Event. - Paris, 11-13 April 2007. - P. 1-6. ↑

C3343. Thiele A. Model Based Building Recognition from Multi-Aspect InSAR Data in Urban Areas. / Thiele A., Cadario E., Schulz K., Thoennessen U., Soergel U. // 2007 Urban Remote Sensing Joint Event. - Paris, 11-13 April 2007. - P. 1-6. ↑

C3344. Muller J.R. Using LIDAR Surface Deformation Mapping to Constrain Earthquake Magnitudes on the Seattle Fault in Washington State, USA. / Muller J.R., Harding D.J. // 2007 Urban Remote Sensing Joint Event. - Paris, 11-13 April 2007. - P. 1-7. ↑

C3345. Yifang Ban. RADARSAT Fine-Beam SAR Data for Land-Cover Mapping and Change Detection in the Rural-Urban Fringe of the Greater Toronto Area. / Yifang Ban, Hongtao Hu. // 2007 Urban Remote Sensing Joint Event. - Paris, 11-13 April 2007. - P. 1-7. ↑

C3346. Di Martino G. Monitoring of Flooding in Urban Areas. / Di Martino G., Iodice A., Riccio D., Ruello G. // 2007 Urban Remote Sensing Joint Event. - Paris, 11-13 April 2007. - P. 1-5. ↑

C3347. Shirokov I.B. Measurements of the Radius of Atmosphere Surface Layer Pollution near the Plant With Microwave. 2007 Urban Remote Sensing Joint Event. - Paris, 11-13 April 2007. - P. 1-5. ↑

C3348. Ya-Qiu Jin. Reconstruction of the 3D Stereo Buildings from Polarimetric SAR Images in Two Converse Flights. / Ya-Qiu Jin, Eryan Dai. // 2007 Urban Remote Sensing Joint Event. - Paris, 11-13 April 2007. - P. 1-5. ↑

C3349. Balk D. New Methods for Understanding Intra-urban Contours at a Global Scale: An Application of Dense Sampling Methods of QuikSCAT Scatterometer with Population and Housing Data. / Balk D., Nghiem S.V., Rodriguez E., Small C. // 2007 Urban Remote Sensing Joint Event. - Paris, 11-13 April 2007. - P. 1-4. ↑

C3350. van den Broek B. Use of high resolution optical and radar imagery for intelligence and situational awareness in urban areas. / van den Broek B., Dekker R., Gutjahr K., Raggam H. // 2007 Urban Remote Sensing Joint Event. - Paris, 11-13 April 2007. - P. 1-8. ↑

C3351. Thevar T. Advances in Lidar Transmitter Sources for Ocean-Atmosphere Remote Sensing. / Thevar T., Boczar B., Rousseva I., Walling J.C., Heller D.F. // OCEANS 2007-Europe. - Aberdeen, 18-21 June 2007. - P. 1-4. ↑

C3352. Weissman D.E. Measurements of the Effect of Rain-induced Sea Surface Roughness on the Satellite Scatterometer Radar Cross Section. / Weissman D.E., Bourassa M.A. // OCEANS 2007-Europe. - Aberdeen, 18-21 June 2007. - P. 1-4. ↑

C3353. Arvelyna Y. New Application of Wavelet Transform for Internal Wave Detection SAR and Optical

Image: A Case Study in Japan Waters. / Arvelyna Y., Oshima M. // OCEANS 2007-Europe. - Aberdeen, 18-21 June 2007. - P. 1-6. ↑

C3354. Jangal F. Remote Sensing of the Sea and Target Detection Improvement Using a Wavelet-based Extraction of Sea Echoes from High Frequency Radars. / Jangal F., Saillant S., Dorey P., Helier M. // OCEANS 2007-Europe. - Aberdeen, 18-21 June 2007. - P. 1-5. ↑

C3355. Wicks M.C. Distributed and Layered Sensing: Relevant EMC Issues. / Wicks M.C., Moore W. // 2007. EMC 2007. IEEE International Symposium on Electromagnetic Compatibility. - Honolulu, HI, 9-13 July 2007. - P. 1-7. ↑

C3356. Danilo C. Comparisons between HF radar and SAR current measurements in the Iroise Sea. / Danilo C., Chapron B., Mouche A., Garello R., Collard F. // OCEANS 2007-Europe. - Aberdeen, 18-21 June 2007. - P. 1-5. ↑

C3357. Helzel T. Features and Limitations of the Modular Oceanography Radar System WERA. / Helzel T., Kniephoff M., Petersen L. // OCEANS 2007-Europe. - Aberdeen, 18-21 June 2007. - P. 1-4. ↑

C3358. Kohut J.T. A Nested Multi-static HF Radar Testbed for the New York Bight and Beyond. / Kohut J.T., Glenn S.M., Roarty H.J., Schofield O.M. // OCEANS 2007-Europe. - Aberdeen, 18-21 June 2007. - P. 1-3. ↑

C3359. Cotton D. MARCOAST-Operational Marine Oil Spill and Water Quality Monitoring Services. OCEANS 2007-Europe. - Aberdeen, 18-21 June 2007. - P. 1-5. ↑

C3360. Abileah R. Mapping Ocean Currents With IKONOS. OCEANS 2007-Europe. - Aberdeen, 18-21 June 2007. - P. 1-5. ↑

C3361. Anatoliy. Method of Compound Object Identification in Microwave Band by Scattered Field Interference Pattern. / Anatoliy, Lobur M. // 2007. CADSM '07. 9th International Conference-The Experience of Designing and Applications of CAD Systems in Microelectronics. - Lviv-Polyana, 19-24 Feb. 2007. - P. 106-108. ↑

C3362. Reichert K. Coastal applications of X-band radar to achieve spatial and temporal surface wave monitoring. / Reichert K., Hessner K., Lund B. // OCEANS 2007-Europe. - Aberdeen, 18-21 June 2007. - P. 1-6. ↑

C3363. Gurgel K.-W. Radio Frequency Interference Suppression Techniques in FMCW Modulated HF Radars. / Gurgel K.-W., Barbin Y., Schlick T. // OCEANS 2007-Europe. - Aberdeen, 18-21 June 2007. - P. 1-4. ↑

C3364. Haus B.K. HF Radar Observation of Wave Directional Spectra in a Strong Current Regime. / Haus B.K., Mei Wang, Shay L.K., Wyatt L.R. // OCEANS 2007-Europe. - Aberdeen, 18-21 June 2007. - P. 1-5. ↑

C3365. Heron M.L. Tsunami Monitoring by HF Ocean Radar: Time and Space Scales. OCEANS 2007-Europe. - Aberdeen, 18-21 June 2007. - P. 1-5. ↑

C3366. Pipia L. Mining Induced Subsidence Monitoring in Urban Areas with a Ground-Based SAR. / Pipia L., Aguasca A., Fabregas X., Mallorqui J.J., Lopez-Martinez C., Marturia J. // 2007 Urban Remote Sensing Joint Event. - Paris, 11-13 April 2007. - P. 1-5. ↑

C3367. Duque S. Application of the Coherent Pixels Technique (CPT) to urban monitoring. / Duque S., Mallorqui J.J., Blanco P., Monells D. // 2007 Urban Remote Sensing Joint Event. - Paris, 11-13 April 2007. - P. 1-7. ↑

C3368. Fornaro G. Multipass SAR Processing for Urbanized Areas Imaging and Deformation Monitoring at Small and Large Scales. / Fornaro G., Paucillo A., Serafino F. // 2007 Urban Remote Sensing Joint Event. - Paris, 11-13 April 2007. - P. 1-7. ↑

C3369. Soergel U. Extraction of Bridge Features from high-resolution InSAR Data and optical Images. / Soergel U., Thiele A., Gross H., Thoennessen U. // 2007 Urban Remote Sensing Joint Event. - Paris, 11-13 April 2007. - P. 1-6. ↑

C3370. Wicks M.C. Distributed and Layered Sensing. / Wicks M.C., Moore W. // 2007. International Waveform Diversity and Design Conference. - Pisa, 4-8 June 2007. - P. 233-239. ↑

- C3371.** {no data available}. Agenda-at-a-glance. 2007. International Waveform Diversity and Design Conference. - Pisa, Italy, 4-8 June 2007. - P. vi. ↑
- C3372.** Meyer F. Long-Term and Seasonal Subidence Rates in Urban Areas from Persistent Scatterer Interferometry. / Meyer F., Gernhardt S., Adam N. // 2007 Urban Remote Sensing Joint Event. - Paris, 11-13 April 2007. - P. 1-6. ↑
- C3373.** Ferraioli G. Phase Offset Estimation for DEM Reconstruction in Multi-Channel SAR Interferometry. / Ferraioli G., Ferraiuolo G., Pascasio V., Schirinz G. // 2007 Urban Remote Sensing Joint Event. - Paris, 11-13 April 2007. - P. 1-6. ↑
- C3374.** Le Moigne V. Statistical Polygonal Snakes for 3D building reconstruction using High Resolution SAR data. / Le Moigne V., Tupin F. // 2007 Urban Remote Sensing Joint Event. - Paris, 11-13 April 2007. - P. 1-5. ↑
- C3375.** Gamba P. Satellite SAR and Human Settlement Detection. / Gamba P., Dell'Acqua F., Trianni G. // 2007 Urban Remote Sensing Joint Event. - Paris, 11-13 April 2007. - P. 1-4. ↑
- C3376.** Norgard J. Detection/Imaging of Buried Objects: Using Spatial/Angular Diversity with Distributed/Embedded Sub-Surface Sensors for Reduced Mutual Coupling and Suppressed EM Emissions. / Norgard J., Magde K., Wicks M., Drozd A., Musselman R. // 2007. EMC 2007. IEEE International Symposium on Electromagnetic Compatibility. - Honolulu, HI, 9-13 July 2007. - P. 1-5. ↑
- C3377.** Hedman K. Road Extraction from SAR Multi-Aspect Data Supported by a Statistical Context-Based Fusion. / Hedman K., Hinz S., Stilla U. // 2007 Urban Remote Sensing Joint Event. - Paris, 11-13 April 2007. - P. 1-6. ↑
- C3378.** Cascini L. A land subsidence study via DInSAR technique over large urbanised areas. / Cascini L., Ferlisi S., Peduto D., Di Nocera S., Fornaro G., Serafino F. // 2007 Urban Remote Sensing Joint Event. - Paris, 11-13 April 2007. - P. 1-7. ↑
- C3379.** Perissin D. Target recognition by means of spaceborne C-band SAR data. / Perissin D., Prati C. // 2007 Urban Remote Sensing Joint Event. - Paris, 11-13 April 2007. - P. 1-5. ↑
- C3380.** Lombardini F. Towards a Complete Processing Chain of Multibaseline Airborne InSAR Data for Layover Scatterers Separation. / Lombardini F., Rossing L., Ender J., Viviani F. // 2007 Urban Remote Sensing Joint Event. - Paris, 11-13 April 2007. - P. 1-6. ↑
- C3381.** van der Velde R. Characterization of the Temporal and Spatial Variability of Soil Moisture through Multi-Temporal Analysis of ASAR Observations. / van der Velde R., Rientjes T., Yao-ming Ma, Yizhou Zhao, Su B. // 2007. MultiTemp 2007. International Workshop on the Analysis of Multi-temporal Remote Sensing Images. - Leuven, 18-20 July 2007. - P. 1-6. ↑
- C3382.** Haridas N. Multi-Frequency Antenna design for Space-based Reconfigurable Satellite Sensor Node. / Haridas N., El-Rayis A., Erdogan A.T., Arslan T. // 2007. AHS 2007. Second NASA/ESA Conference on Adaptive Hardware and Systems. - Edinburgh, 5-8 Aug. 2007. - P. 14-19. ↑
- C3383.** Zhenli Ma. A Knowledge-Based Target Recognition Method For Remote Sensing Image. / Zhenli Ma, Huibin Wang, Xinyao Lao, Min Tang, Fengchen Huang. // 2007. ICIT '07. IEEE International Conference on Integration Technology. - Shenzhen, 20-24 March 2007. - P. 414-417. ↑
- C3384.** Casciello D. Robust Satellite Techniques (RST) for Oil Spill Detection and Monitoring. / Casciello D., Lacava T., Pergola N., Tramutoli V. // 2007. MultiTemp 2007. International Workshop on the Analysis of Multi-temporal Remote Sensing Images. - Leuven, 18-20 July 2007. - P. 1-6. ↑
- C3385.** Villalon-Turrubiates I.E. Dynamical Analysis of Hydrological Indexes Extracted from Remote Sensing Imagery: An Introductory Study. 2007. MultiTemp 2007. International Workshop on the Analysis of Multi-temporal Remote Sensing Images. - Leuven, 18-20 July 2007. - P. 1-4. ↑
- C3386.** Alberga V. Performance Estimation of Similarity Measures of Multi-Sensor Images for Change Detection Applications. / Alberga V., Idrissa M., Lacroix V., Inglada J. // 2007. MultiTemp 2007. International Workshop on the Analysis of Multi-temporal Remote Sensing Images. - Leuven, 18-20 July 2007. - P. 1-5. ↑

- C3387.** Wegmuller U. A Novel Methodology for Parameter Retrieval from Multi-temporal Data Demonstrated for Forest Biomass Retrieval from C-band SAR Backscatter. / Wegmuller U., Santoro M., Wiesmann A. // 2007. MultiTemp 2007. International Workshop on the Analysis of Multi-temporal Remote Sensing Images. - Leuven, 18-20 July 2007. - P. 1-6. ↑
- C3388.** Shkvarko Y. Finite Array Observations-Adapted Regularization Unified with Descriptive Experiment Design Approach for High-Resolution Spatial Power Spectrum Estimation with Application to Radar/SAR Imaging. 2007 15th International Conference on Digital Signal Processing. - Cardiff, 1-4 July 2007. - P. 79-82. ↑
- C3389.** Sujata Dash. Simulation of Radar Backscattering Coefficients Using IEM-A Tool for Surface Soil Moisture Retrieval. / Sujata Dash, Prusty G. // 2007. RAST '07. 3rd International Conference on Recent Advances in Space Technologies. - Istanbul, 14-16 June 2007. - P. 383-388. ↑
- C3390.** Sefercik U.G. Comparison of DEM Accuracies Generated by Various Methods. 2007. RAST '07. 3rd International Conference on Recent Advances in Space Technologies. - Istanbul, 14-16 June 2007. - P. 379-382. ↑
- C3391.** Gershenzon O.N. Integral Solution for Oil Spill Detection using SAR Data. / Gershenzon O.N., Gershenzon V.E., Osheyko S.V. // 2007. RAST '07. 3rd International Conference on Recent Advances in Space Technologies. - Istanbul, 14-16 June 2007. - P. 361-365. ↑
- C3392.** Kent S. Synthetic Aperture Radar Raw Data Simulation for Microwave Remote Sensing Applications. / Kent S., Kartal M., Kasapoglu N.G., Kargin S. // 2007. RAST '07. 3rd International Conference on Recent Advances in Space Technologies. - Istanbul, 14-16 June 2007. - P. 389-392. ↑
- C3393.** {no data available}. Covers. 2007. RAST '07. 3rd International Conference on Recent Advances in Space Technologies. - Istanbul, 14-16 June 2007. - P. 1. ↑
- C3394.** Lambert H. The Eads Astrium Astrosat Product Line A New Generation of High Resolution Small and Micro Satellites Embarking Innovative Technologies. / Lambert H., Limouzin G. // 2007. RAST '07. 3rd International Conference on Recent Advances in Space Technologies. - Istanbul, 14-16 June 2007. - P. 9-13. ↑
- C3395.** Cutter M. A High Performance EO Small Satellite Platform (SSTL-300). / Cutter M., Davies P., Baker A., Sweeting M. // 2007. RAST '07. 3rd International Conference on Recent Advances in Space Technologies. - Istanbul, 14-16 June 2007. - P. 453-457. ↑
- C3396.** Volosuk V.K. Interpretation of an Influence of the Transmitter and Receiver Bistatic SAR Tracks to Resolution. / Volosuk V.K., Voloschuk R.P. // 2007. MSMW '07. The Sixth International Kharkov Symposium on Physics and Engineering of Microwaves, Millimeter and Submillimeter Waves and Workshop on Terahertz Technologies. - Kharkov, 25-30 June 2007. - Vol. 1. - P. 458-460. ↑
- C3397.** Lukin K.A. Ground-Based Noise Waveform SAR and Differential Interferometry for Remote Monitoring of Large Objects. / Lukin K.A., Mogila a.A.A., Vyplavin P.L. // 2007. MSMW '07. The Sixth International Kharkov Symposium on Physics and Engineering of Microwaves, Millimeter and Submillimeter Waves and Workshop on Terahertz Technologies. - Kharkov, 25-30 June 2007. - Vol. 1. - P. 445-447. ↑
- C3398.** Tarchi D. Implementation of Noise Radar Technology in Ground Based SAR for Short Range Applications. / Tarchi D., Lukin K., Leva D., Fortuni J., Mogila A., Vyplavin P., Sieber A. // 2007. MSMW '07. The Sixth International Kharkov Symposium on Physics and Engineering of Microwaves, Millimeter and Submillimeter Waves and Workshop on Terahertz Technologies. - Kharkov, 25-30 June 2007. - Vol. 1. - P. 442-444. ↑
- C3399.** Lutsenko V.I. Polarization-Spectral Indication of the Objects. / Lutsenko V.I., Popov I.V. // 2007. MSMW '07. The Sixth International Kharkov Symposium on Physics and Engineering of Microwaves, Millimeter and Submillimeter Waves and Workshop on Terahertz Technologies. - Kharkov, 25-30 June 2007. - Vol. 1. - P. 461-463. ↑
- C3400.** Ivanov V.K. Fractal Analysis of Sea Ices Images. / Ivanov V.K., Paschenko R.E., Yatsevich S.Ye., Yefimov V.B., Tsybal V.N., Vovk A.I. // 2007. MSMW '07. The Sixth International Kharkov Symposium on Physics and Engineering of Microwaves, Millimeter and Submillimeter Waves and Workshop on Terahertz Technologies. - Kharkov, 25-30 June 2007. - Vol. 2. - P. 989-991. ↑
- C3401.** Dulova I.A. Possibilities of Surface Relief Determination by Photometric Method in Millimeter and

Submillimeter Wavelength Range. / Dulova I.A., Kornienko Yu.V., Skuratovskiy S.I. // 2007. MSMW '07. The Sixth International Kharkov Symposium on Physics and Engineering of Microwaves, Millimeter and Submillimeter Waves and Workshop on Terahertz Technologies. - Kharkov, 25-30 June 2007. - Vol. 2. - P. 766-768. ↑

C3402. Ksendzuk A.V. Detection of the Stochastic Objects in Multiposition SAR. 2007. MSMW '07. The Sixth International Kharkov Symposium on Physics and Engineering of Microwaves, Millimeter and Submillimeter Waves and Workshop on Terahertz Technologies. - Kharkov, 25-30 June 2007. - Vol. 1. - P. 481-483. ↑

C3403. Matsuoka M. Damage mapping for the 2004 Niigata-ken Chuetsu earthquake using Radarsat images. / Matsuoka M., Yamazaki F., Ohkura H. // 2007 Urban Remote Sensing Joint Event. - Paris, 11-13 April 2007. - P. 1-5. ↑

C3404. Takano T. Performance of Falcon-I: Developed Low-Power and High-Sensitivity Cloud Profiling FM-CW Radar at 95GHz. / Takano T., Nakanishi Y., Abe H., Yamaguchi J., Yokote S.-I., Futaba K.-I., Kawamura Y., Kumagai H., Ohno Y., Takamura T., Nakajima T. // 2007. MSMW '07. The Sixth International Kharkov Symposium on Physics and Engineering of Microwaves, Millimeter and Submillimeter Waves and Workshop on Terahertz Technologies. - Kharkov, 25-30 June 2007. - Vol. 1. - P. 427-429. ↑

C3405. Yanovsky F.J. Doppler-Polarimetric Approach to Microwave Remote Sensing of Precipitation. 2007. MSMW '07. The Sixth International Kharkov Symposium on Physics and Engineering of Microwaves, Millimeter and Submillimeter Waves and Workshop on Terahertz Technologies. - Kharkov, 25-30 June 2007. - Vol. 1. - P. 436-438. ↑

C3406. Caceres J.J. Improved Classification of Building Infrastructure from Airborne Lidar Data Using Spin Images and Fusion with Ground-Based Lidar. / Caceres J.J., Slatton K.C. // 2007 Urban Remote Sensing Joint Event. - Paris, 11-13 April 2007. - P. 1-7. ↑

C3407. Nielsen A.A. Complex Wishart Distribution Based Analysis of Polarimetric Synthetic Aperture Radar Data. / Nielsen A.A., Skriver H., Conradsen K. // 2007. MultiTemp 2007. International Workshop on the Analysis of Multi-temporal Remote Sensing Images. - Leuven, 18-20 July 2007. - P. 1-6. ↑

C3408. Marzahn P. Derivation of Soil Surface Roughness Dynamics from Multi-temporal and Multi-parametric Air-borne PolSAR-data. / Marzahn P., Kruger K., Ludwig R. // 2007. MultiTemp 2007. International Workshop on the Analysis of Multi-temporal Remote Sensing Images. - Leuven, 18-20 July 2007. - P. 1-5. ↑

C3409. Karaev V. Measurement of Wind Wave Slope Variance with the Radar Having a Knife-Like Antenna Pattern. / Karaev V., Kanevsky M., Meshkov E., Titov V.I., Balandina G. // 2007. MSMW '07. The Sixth International Kharkov Symposium on Physics and Engineering of Microwaves, Millimeter and Submillimeter Waves and Workshop on Terahertz Technologies. - Kharkov, 25-30 June 2007. - Vol. 1. - P. 424-426. ↑

C3410. Stramondo S. SAR and optical remote sensing for urban damage detection and mapping: case studies. / Stramondo S., Bignami C., Pierdicca N., Chini M. // 2007 Urban Remote Sensing Joint Event. - Paris, 11-13 April 2007. - P. 1-6. ↑